REMARKABLE MEN - UNUSUAL GLASSES

Harold Rawson
Emeritus Professor of Glass Technology, University of Sheffield, UK.

Abstract

The subject of this paper is innovation. The formation of new associations takes place for a variety of reasons, some economic, some political or, in the case of ICG, a need to share information and experience. The factors giving rise to technical innovations are even more diverse. Examples are given in both categories.

This article is mainly about making new things: new materials, new devices, new processes, new institutions. Sometimes this may seem easy in retrospect, but usually it is very difficult. There has to be a large driving force to carry the activity through and some reward, or the prospect of reward at the end.

1. INSTITUTIONS AND ASSOCIATIONS

'*It is better to hang together than to hang separately.*' Anon.

In much of what I say, I shall be quoting from Turner and from a close associate of his, Edward Meigh. I do this partly because Turner was our co-founder but also because he was a great writer of survey articles and historical commentaries, which are readily available, for anyone interested, in the pages of the Journal of the Society of Glass Technology. The quality of the man is perhaps more evident there than in his purely scientific papers.[1]

The student of Business Studies is often urged to review his position by taking two pieces of paper. On one he should write a list under the heading: 'Threats and Problems.' On the second, the heading is 'Opportunities and Challenges.' This seems to be a fine idea, provided one can decide what to do next.

In the UK, perhaps the first example of a group of people responding to an opportunity in the glass field was that involving the collaboration between the Worshipful Company of Glass Sellers and George Ravenscroft who was responsible for the development of lead crystal glass. Although this happened more than 300 years ago, there is some point in reminding ourselves of the story, especially now when the State of California seems concerned about the risk of lead poisoning from liquids which have been in contact with Ravenscroft's glass. The Company was established in 1664 and is what we now call one of the Livery Companies of the City of London. Ravenscroft carried out his development work between 1673 and 1678, some years after the Company had been formed. His first glass contained no lead. However he was using especially pure materials and so his glass was particularly clear and colourless. The Company was delighted with his products and soon signed contracts to take his glass and

[1] V.C. Hender (1977), then chairman of United Glass, attempts to summarise Turner's character in a few words in one of the Turner Memorial Lectures. Since he did not know Turner himself, he could only repeat the comments of others. One said 'He had charisma.' Another said 'He could open a Yorkshireman's purse.' Hender believes that these were merely two ways of saying the same thing.

market it. His glass seemed infinitely better than the glass of Venice. It later became clear to Ravenscroft that his glass was not especially durable and he took the unusual step of introducing increasing amounts of lead. The Company was even more delighted and continued their association with Ravenscroft until he had changed his line of interest to the manufacture of flat glass. (Moody 1988,1989; Watts 1990).

I understand that many of the present members of the Company are lawyers. Maybe they should be encouraged to bring their legal experience to bear in defence of the product which was so influential in their early history and which is probably less life-threatening than the atmosphere of Los Angeles.

Now we jump more than 200 years to the closing years of the nineteenth century, when mechanisation of glass making processes was developing rapidly, especially in the US. By 19O3, the six-arm A-type Owens machine was in commercial use and by 1911 more than 100 Owens machines were installed with a capacity of more than four million bottles a year.

Libbey and Owens set up the Owens European Bottle Company and built a factory in NW England with two Owens machines. British and continental container manufacturers were invited to view the machines in operation and were given the choice between buying the European patents for £600 000 (£30 million at current values) or having to compete against two more machines which the Libbey-Owens Company would immediately instal. I am sure that such an offer would go on the list as a threat. It seems that negotiations were not unduly long. The British manufacturers, joined together as the British Association of Glass Bottle Manufacturers Ltd., agreed to pay £120 000 as their share of the licence fee. By 1920 16 Owens machines were installed in UK factories.

I remember in 1945 as a student seeing one of the last of these machines in operation. To me machines have character. I remember the Owens machine for its impression of power and dignity, rather like Queen Victoria. Its present day replacement is rather nervy. It reminds me more of a team of noisy conjurors.

The next major challenge to the UK industry as a whole came with the outbreak of World War I. At that time the UK industry was poorly equipped to meet the needs of the economy. Most of the optical glass required for military instruments came from Germany or France and the industry as a whole was not able to meet the many other needs of a country at war. Edward Meigh, in his book ‘The Making of a Federation' (1975) gives an excellent account of the tremendous amount of effort that was applied, mainly by the Ministry of Munitions of War, to resolve these problems and the support given by the Government of the time to encourage manufacturers to strengthen their technological base.

It was at this time that Turner came into the picture. At the beginning of the war, he was happily carrying out basic research in physical chemistry at Sheffield University. He was almost completely ignorant of the nature of the industries within a few miles of Sheffield. However he had heard of metallurgy and was chairman of the Sheffield Society of Applied Metallurgy, so clearly he had some knowledge of and interest in industry. Somehow he became vaguely aware that there was a glass industry on his doorstep and he was soon to realise that the greater part of the UK glass bottle industry almost surrounded him. He soon recognised that the scientific understanding in the industry was practically non-existent (Turner, 1937).

I am sure he didn't regard the situation as a threat, rather than as an opportunity and I believe the story is well known how he persuaded the industry and the University to set up the Department of Glass Technology at the University, followed only a few months later by the Society of Glass Technology.

2. COLLABORATIVE RESEARCH

What is less well known is Turner's role in establishing within the Department of Glass Technology a body called the Glass Delegacy. This organisation was open to all manufacturers who were prepared to make a financial contribution towards running the Department and its research programme. The financial contribution was assessed on the basis of the tonnage of glass melted.

This arrangement was very common in many UK industries between the wars. The various organisations for collaborative research were known as Research Associations, but, so far as I am aware, only that for the glass industry operated within a University Department.

Initially I'm sure this was an excellent arrangement. The industry was not able to carry out many of the simplest methods of quality control: analysis of batch materials and glasses, measurement of chemical durability and of physical properties such as density, viscosity and thermal expansion. Much effort went into the development of the necessary measuring techniques and into the systematic study of the effects of composition of simple silicate glasses on their properties.

The system also had great value to the students. The academic staff of the Department were in close touch with the manufacturers and their problems. They were thus in an ideal position to teach the glass technology (if not the glass science) of that time to students.

The Department continued to serve both as a University teaching and research Department and as a Research Association for the glass industry until 1955, when the Glass Delegacy was replaced by a separate organisation, the British Glass Research Association, eventually occupying a new building on a site next to the University Department (Anon 1955).

Collaborative research in glass has also had a long history in other countries. For example, Schaeffer (1995) has recently outlined the history of the HVG from its origins in 1920.

I find it interesting that only a few years ago the US glass community took the step of establishing at Alfred University in New York State the NSF Industry-University Center for Glass Research - an organisation very similar, it seems to me, to our own Glass Delegacy. I assume that this became possible following relaxation of what had previously been extremely strict anti-trust legislation.

3. THE GLASS MANUFACTURERS' FEDERATION AND THE BRITISH GLASS MANUFACTURERS' CONFEDERATION

Now let us look at another major challenge to the UK industry and the consequence of that challenge. The story reminds one of some of the present day conflicts between the UK government and the EEC and discussions about opting out of bits of the Maastricht Treaty which one doesn't like.

Briefly, the International Labour Organisation was asked in 1923 to consider a proposal from the French Government that all glass factories should be required to cease production for 24 hours each Sunday and to provide a period of ‘collective rest’ for all workers. Apparently the move was prompted by the increasing competition which the French glass industry faced from Belgium where the manufacture of flat glass had been largely mechanised. Thus the motive was economic rather than social. The UK objections came mainly from the container manufacturers, who pointed out that the interests of British workers were already taken care of, since the average working week of the British bottle maker was 42 hours compared with 48, 56 and, in some cases 60 hours per week, in some countries supporting the Convention. Like the French, they too were not primarily concerned about the welfare of their workers. However they did not feel inclined to let the ILO and/or the French government prevent them from running their Owens machines 24 hours a day and seven days a week. These discussions

which went on for several years led to the formation of the Glass Manufacturers Federation in 1926 (Meigh 1975). The flavour of the GMF's field of operation can be judged from the following statement of its principle aim.

'To watch over and keep members informed regarding the operation of existing laws and practices, the activities of Government Committees and all legislative proposals which may affect or tend to affect the interests of members.'

The ILO attempted on several later occasions to impose the 'Six Day Rule' right up to the outbreak of World War II - a tribute to the outstanding tenacity of bureaucratic organisations and of those who oppose them.

The Federation still exists, of course, operating under the name 'British Glass Manufacturers Confederation.' It now shares a building with the British Glass Industry Research Association in Sheffield.

4. INTERNATIONAL COLLABORATION

It is hardly necessary now to explain or to emphasise the value of international collaboration by glass scientists and engineers. Nowadays overseas visits by staff of glass companies are almost a daily event and there are many occasions when scientists from Universities and research institutes meet to discuss progress in particular fields. I have in mind in particular the 'Sol-Gel' glass workshops. In the 1930's and before, such contacts were far less common, and it is to the credit of Turner and his contemporaries in other countries that they saw a need for an organisation in which international co-operation could be fostered. The International Commission on Glass was founded in 1933 and two Congresses were held before World War II. Turner's account of the early years of the Commission is quoted *in extenso* in Pierre Gilard's book '50 Years ICG' (1983). The present structure and activities of the ICG Technical Committees have been reviewed by Yaraman (1995).

It was some years after World War II that the ICG began to operate on a scale and in a manner with which we are familiar today. Not only would International Congresses be held at three yearly intervals, but the Commission also developed an ongoing technical programme of work through its Technical Committees.

An early initiative of the Commission after World War II was to try to remedy the difficult situation which existed in Germany where the Control Commission allowed the HVG to operate only in the Land of Hesse and the DGG not at all. In spite of representations made to the Allied Control Commission, no speedy relaxation resulted (Turner 1948).

An interesting discussion, which took place as the ICG began to re-establish itself, arose from a proposal from Professor Stevels that there should be an International Journal of Glass Technology. Turner was clearly not in favour of the proposal. He considered that the language skills of most glass specialists, especially in the U.K. and the USA, would make the proposal impractical. However Stevels' proposal did have one productive result. It led to the foundation by the ICG of the Pool of Abstracts, although, in my opinion, language problems have acted as a brake on this enterprise also (Stevels, 1950).

5. INNOVATION AND INVENTION.

'*Necessity is the mother of invention.*' Anon.

'*If you can write a better book, preach a better sermon, or make a better mousetrap than your neighbour, then though your house be in a wood, the world will make a beaten track to your door.*'

Attributed (probably incorrectly) to Emerson.

Turner (1908) makes the following observations about inventions and inventors:

'The present century so far has been noteworthy for some of its mechanical contrivances. I have sometimes said that some of these contrivances exist despite the chemist and the physicist. The inventor is sometimes a man led on by a vision he has seen, and though he often sees the end but not the means. he is prepared to hammer these out by infinite labour.

The physicist or chemist comes along later to work out the conditions under which the process once invented is capable of success.'

These comments may be true for all the inventions one can think of involving the development of new glass manufacturing processes. I doubt, however, if they are true of inventions in general [2].

Remember that Edison tried more than 1000 organic fibrous materials, which, when carbonised, would provide a suitable carbon filament for his incandescent filament lamp. He eventually chose a particular variety of Japanese bamboo. Here is Mike Owens slaving away at the development of suction feeding, which was soon to engulf the entire glass container industry (Figure 1). These two people knew quite clearly what they wished to attain, but neither physics nor chemistry could tell them how to get there. They just had to proceed on a trial and error basis. These two inventions appear to fit in with Turner's analysis.

It is commonly believed that inventions occur as a result of an accident. I suspect that the basis for that belief is wish fulfilment i.e. accidents can happen to anyone, to me for example, so I too could be lucky and become famous. It is true that accidental discoveries are sometimes made, but they are only developed into something useful if the person experiencing the accident is sufficiently knowledgeable and intelligent to see its significance. The discovery of penicillin by Alexander Fleming was largely the result of an accident, but the observation of the killing of bacteria around the chance contamination of a glass plate by the penicillin mould was made by a man who was a Professor of Bacteriology. He could see the implications of the accident and apply it.

Indeed the first discovery of glass must have been as the result of an accident- a happy accident, some might say. It could hardly have been otherwise. The nature of the accident is the subject of speculation. One suggestion is that it was the result of the cooling of a slag, produced during the smelting of bronze. The other is a fanciful, but plausible account by Pliny of sailors, who transporting blocks of natron, put in on a sandy beach to cook a meal. They supported their cooking vessels on blocks of their cargo, natron and lit a fire. This caused the natron and the silica from the beach, to react, melt and on cooling produce a glass. If nothing else, this shows that Pliny had some knowledge of glass technology. However the story I like best, if only because it puts the discovery of glass in the category of one of the Great British Inventions which did not come to anything, is told by the archaeologist Colin Renfrew (1973). He first points out that in the islands of Orkney off the north coast of Scotland, cremation sites often contain a glassy slag, simply because seaweed was used as a fuel. A glass would be produced if the cremation were carried out on a sandy shore. It is interesting also that a small number of partly glassy beads have been discovered in beach sites in Scotland and Northern

[2]Any reader interested in the general circumstances which lead to inventions being made and in reading the case histories of many inventions of the present century will find the book by Jewkes, Sawers and Stillerman (1969) of great interest.

Ireland, indicating that the people of those parts had some knowledge of shaping glassy materials. We should not be surprised at these discoveries. The main thesis of Renfrew's book is that many of the important discoveries of prehistoric man were made by accident and that similar accidents occurred in different parts of the world. It is not reasonable to believe that all these important discoveries were made in the middle east and were introduced to Europe through the Roman Empire. This may have been the most important route, but it is not the only one.

In our own time, there are at least two recent examples of the beneficial role of accidents. One is the 'Mystery of the Fractured Spout' - a good title for a Sherlock Holmes story. This is told by Alistair Pilkington in his accounts in 'Glass Technology' and the Proceedings of the Royal Society of the development of the float process (1969,1971,1976). If that accident had not happened and if its significance had not been thoroughly studied, it is doubtful if Pilkington would have been first in what turned out to be a race to develop the float process.

Often one invention leads on to others. To fully exploit the potentialities of flat glass in buildings and in road transport, it is necessary to be able to control the spectral transmission of the material throughout the solar spectrum. This is done by colouring additions to the glass itself, by surface coatings or by a combination of the two.

On-line coating of float glass is a possibility in principle, but would not have been so for ground and polished plate. Until relatively recently, probably the most widely used coating process used on float glass was magnetron sputtering using a series of cathode bars made from different metals and mounted in the same chamber. The equipment is large and expensive, but once established, a range of transmission characteristics can be achieved using the same plant. However the coatings made in this way are fairly sensitive to mechanical and chemical attack. Moreover they will not withstand conventional thermal tempering schedules. Pilkington have shown that certain products can be made quite satisfactorily on-line in the float process by chemical vapour deposition processes. These are much more robust than the sputtered coatings and will withstand thermal tempering.

At least two products are made in this way: a low emissivity coated glass, 'K glass,' for reducing heat losses through double- and multiple glazed windows, and a mirror product 'Reflex' produced by depositing controlled thickness films of silica and silicon.

Another example of the role of lady luck is the discovery of the so-called heavy metal fluoride glasses by Michel Poulain in 1974. He was trying to make a crystal by heating a complicated mixture of fluorides, including zirconium tetrafluoride in a nickel tube. The 'crystal' turned out to be largely glassy. Further work was carried out to determine regions of glass formation and to study glass properties. The most important property is their transparency over a wide range of wavelengths from the UV to the mid-IR. They have been widely studied, in particular for possible application in fibre optic communication systems. Unfortunately they are dreadful glasses to work with and much ingenuity has been spent in attempting to make fibres from them.

However Turner would have been wrong, I believe, to suggest that engineers working head down and with little understanding are the most common form of inventor. This picture becomes less true with the elapse of time. I worked for some time in the early 50's in the next lab to the man who in 1948 invented holography. His name was Dennis Gabor and hanging on the corridor wall outside his lab. was a series of rather fuzzy photographic images of the names 'Newton, Huyghens, Fermat etc. - all names famous for their contributions to Optics. The photographs had a title which was something like 'Image Re-construction by Wave Front Interference.' Nobody had coined the word Holography at that time and, even more remarkable, no-one had made a laser. Gabor was not interested in what we now recognise as the more important applications of holograms. What he was trying to do was to improve the

resolving power of the electron microscope. I am quite sure that Gabor did not produce his invention by messing around blindly with pin holes, lenses and photographic plates. Rather he worked the whole system out on paper first, and then made the equipment himself. (He had a small lathe in his laboratory.) Not surprisingly, he finished up as a Fellow of the Royal Society.

The laboratory where Gabor and I worked was on the top floor of an aesthetically challenged three storey building which looked across a very large factory site toward the green fields of Warwickshire. Most of that factory area housed some very large machine tools for making steam turbines, large motors and other items of electrical equipment. Early in World War II, the company built for Frank Whittle the Mark I version of his jet engine. To get so far, he had had to overcome great engineering and materials problems. But he had also to overcome scepticism and disbelief from many quarters. He was a serving officer in the Air Force. His fellow officers, no doubt, were not taken by the idea of being pushed along by a stream of hot air. Also as a serving officer he was not able to approach financial institutions for backing. When he had almost won his battle, our steam turbine engineers who built his Mark I engine heaped on him further insults by being very critical of his blade designs. His story is one of perseverance of the highest order. Like Gabor, he too finished up as a Fellow of the Royal Society.

In my view Whittle doesn't fit into Turner's category. He was an academically trained engineer and knew better than our turbine engineers the type of blade design that was necessary for his engine. He knew very clearly where he was going, but organisational and financial problems made it difficult for him to get there.

Recently Brian Moody, in an article in ‘Glass Technology’ (1988) has pointed out an interesting connection between glass science and the development of the jet engine. All students of glass science and fracture mechanics will know the name of A.A.Griffith, the man who introduced us to the worrying idea that the surface of all-glass products is severely flawed and to the relationship between glass strength and flaw depth.

Griffith was not especially interested in glass. He used it in his experiments because it was ideally elastic and also because it was readily available. He was an engineer (initially working at the Royal Aircraft Establishment where his work on the strength of glass was carried out) who became increasingly involved in the development of aircraft engines. Independently of Whittle, he became interested in the idea of jet propulsion and had developed a prototype engine as early as 1929. Shortly afterwards, he was moved to another post where he did not have the facilities to continue his work. He and Whittle knew of each others' work but did not attempt to cooperate, perhaps because neither was in a position to do so.

It was only late in the war when Griffith had joined the Rolls Royce company that he became involved in jet engines again. By then Whittle had in effect been sidelined and the whole development was put in the hands of the major engine manufacturers. Griffith's later contributions were considerable. As Head of Engine Development at Rolls Royce, he was responsible for many of the famous engines of the post war period.

Here is another invention, this time one involving glass. In 1966 a paper was published by two members of the STC laboratory at Harlow, Essex. They were Kao and Hockham. They were the first to put forward the idea of an extremely high capacity communication system, based on glass fibre (Figure 2). This was a purely paper exercise, although it was well worked out. Nothing had been made. They showed that it would be necessary to develop glasses with very much lower contents of transition metal ion impurities that any then known.

A few months after this paper was published, we had a visit in Sheffield from a Mr. Roberts of the Post Office Research Laboratory, as it then was, and Mr. Don Williams of the Ministry

of Defence. They told us that they had been unsuccessful in interesting any UK glass company in attempting to make high purity glasses and we were asked to help. Since none of our money was at risk, we didn't take much persuading.

There was some initial disagreement between us. I would have preferred to use a vapour phase route but we were told that for the defence application pairs of glasses with significantly different refractive indices were needed. We could not be sure that this could be done using the vapour phase method. So we were deflected at the outset from investigating the type of process which is now universally used. Nevertheless our efforts led us along some interesting paths and provided UK engineers with fibre on which they could experiment. Our initial target was to produce glasses with a loss of less than 100 dB/km. Sufficiently pure raw materials were developed, at great expense, by the suppliers of laboratory chemicals. We soon reached the target figure, which, of course, was promptly moved to 20 dB/km. Slowly we reached 50 dB/km and couldn't see how we might improve on that. We decided that we needed to consider radically new methods of melting. Up to then we had been melting in platinum and although the glass melt could only see >99% pure, impervious alumina refractories, we believed that some transition metal impurities were being transferred to the melt by vapour phase transport from the refractories.

I remembered seeing a paper in Verres et Refractaires, published about 1946 on melting glass in a refractory pot by dielectric heating, so that the heat was developed in the glass batch rather than in the pot. We contacted the main supplier of such equipment in the UK, a firm which also supplied RF heating equipment. Trials were carried out and it was quickly shown that the best results were obtained using a 5 MHz RF generator. The only limitation was that the crucible containing the batch had first to be heated to about 500^{o}C to make it sufficiently conducting to accept power from the RF field (Rawson and Scott, 1973). Melting was carried out in semiconductor grade vitreous silica and the crucible was air cooled (Figure 3).

We adopted a Pilkington idea for producing cladded rod for fibre drawing. After melting the core glass as described, we poured onto it a layer of a lower melting point glass, which had been melted separately. This was transferred to a rig, where we had set up a miniature version of the Fourcault process. A bait was lowered onto the melt surface and was then slowly pulled upwards (Figure 4). This produced cladded rod, perhaps 3 metres long. The rods were then sent to Professor Gambling at Southampton University for drawing into fibre. I believe we eventually reached a loss of about 5 dB/km before the project at Sheffield was closed and the work transferred to British Telecom (Figure 3).

Now I will tell you a story with a moral. The moral is ‘Never argue about someone else's experimental results, if your reasons for arguing are based on a rather vague understanding of theory.’

In the early 1950's John Stanworth and I were involved together in attempts to make glasses not previously thought to be glass formers. We both doubted the reasons behind Zachariesen's rules for glass formation. Stanworth had produced aluminate glasses and later tellurite glasses. In general, the latter group of glasses had unusually high values of refractive index, approaching that of diamond. They also had very high thermal expansion coefficients. l won't tell you the sad story of a colleague from Czechoslovakia who asked us to let him try to make huge gem stones from these glasses. This is what he had done at home. It nearly broke his heart.

At this stage I got the bit between my teeth and began a survey of about all the possible glass-forming oxides, including the most unlikely. (How about potassium selenite glass for example?) However the most interesting new glass systems that came from this work were the vanadate glasses. We made them on a scale of tens of grams and measured their properties.

We found; not to our surprise, that they were semiconductors. I presented a paper on these glasses at the 1956 Glass Congress in Paris (Baynton, Rawson and Stanworth, 1956,1957).

In the discussion, a most eminent glass chemist commented:

‘You can't be right. A material can be a glass or it can be a semiconductor. It can't be both.’

Well he was wrong. The well known semiconductor materials at that time were silicon and germanium. Both are crystalline. Also in the text books of the day, one could read about the band theory of solids, as developed in the context of crystalline materials. This explains why some materials are insulators, some are conductors and others semi-conductors.

The problem was that at that time no-one had considered what a band theory for a non-crystalline material might be. But just because you can't do the necessary mathematics, it doesn't follow that your observations are wrong.

It was some years later that the phenomenon of semiconductivity in amorphous solids was worked out theoretically by Professor Mott at Cambridge and Dr. Anderson of Bell Labs (Mott and Davis 1979). They were jointly awarded the Nobel Prize in Physics. That's the nearest we ever got to glory - helping make possible for someone else to win a Nobel prize.

Most of us working in or with the glass industry are concerned with a limited range of glass compositions and technical improvement depends on more and more exact control of the melting and forming processes. However there are some engineers using glasses who would like to be able to specify glasses which may not be commercially available. They do not wish to order a pot melt and they would like the dimensions to be under better control than can be obtained by hand working. Here is one possible solution to their problems - extrusion of the glass at a relatively high viscosity, say $1O^6$ Pas. Quite complicated cross sections can be produced (Figure 5) (Roeder 1971,1972). This process was developed by Professor Roeder when he was working at the Philips laboratory in Aachen. I like to think of this process as the converse of the float process. As you know, in the float process, surface tension and gravity forces are large compared with viscous forces. Hence surface irregularities in the glass are smoothed out fairly rapidly whilst the glass is on the tin bath. In the extrusion process, viscous forces are dominant whilst surface tension forces are negligible by comparison. Consequently the profile produced in the extrusion die is retained. In Sheffield, we have recently built such an extruder, (Figs 6 and 7) with Professor Roeder's help and guidance. We are not especially interested at present in producing tubing with unusual cross sections but rather with making circular section tubing from less common oxide glasses (Furniss, Shephard and Seddon, 1996).

A second circumstance in which relatively small quantities of glass are needed is in the studio glass field. A hundred years ago men like Frederick Carder, Tiffany and Gallé produced wonderful pieces of art glass. They were working either in or closely associated with glass works. Young glass artists today would find it diffícult to set up similar relationships. The situation changed in the early 1960's when Harvey Littleton (who I believe is the son of ‘Softening Point’ Littleton) working with Dominick Labino showed how to build quite a small furnace and to gather relatively good quality glass from it. This meant that young glass artists could build and operate their own furnace and do their own thing with the glass. Maybe even now their work is not of the standard of Carder, Tiffany and Gallé but then few modern painters can reach the standard of Michelangelo.

It may be worth noting that a student of Littleton and Labino, Sam Herman, introduced studio glass making to England after studying some time in Edinburgh with Helen Munro Turner, Professor Turner's widow, who was a very talented glass engraver.

So innovation and invention are difficult tasks, especially when the invention or even improvement of a process is involved. It is a task which can test the abilities of the most able scientist. This point is well brought out by the following quotation from a paper presented by Michael Faraday in 1830. For the previous five years he had been engaged in work on a UK government contract to make a high lead glass of improved quality for use in telescope objectives (Faraday 1830).

'It may be said that a long time has elapsed since the first experiments were first instituted; and that if anything could be done, it should have been effected in so long a period.

But be it remembered that it is not a mere analysis or even the development of mathematical reasoning that is required. It is the foundation and development of a manufacturing process, not in principle only, but through all the difficulties of practice until it is competent to give constant success; and I may be allowed to plead the acknowledged difficulty of the subject as a reason, both why it may not yet have obtained perfection and why it should still be pursued.

Within a year of his finishing his work on glass, and just to make his point, he had published his first paper on electromagnetic induction !

When I started to think about this talk, I toyed with the idea of giving it the same title as a novel by a well-known English poet, John Masefield. This novel is called ODTAA. This is an acronym and means 'One Damned Thing After Another', implying a random flow of ideas. It is only cowardice, and some consideration for those who have to chose key words that led me to settle on a more orthodox title.

REFERENCES.

Anon 'The British Glass Industry Research Association,' J. Soc. Glass. Technol. 39 (1955) N26-27.

Baynton, P.L.; Rawson, H.; Stanworth, J.E.: 'New glasses based on the oxides of Te, V, Mo and W,' Proc. IVth Internat. Congr. Glass. (1956) 52-61.

Baynton, P.L.; Rawson, H.; Stanworth, J.E., 'The semi-conducting properties of some vanadate glasses.' Trans. Electrochem. Soc.104 (1957) 237-240.

Hender, V.C.: 'Glass Technology. The challenge of change.' Glass Technol.18 (2) (1977) 35-42.

Faraday, M.: 'On the manufacture of glass for optical purposes.' Phil. Trans. R. Soc. (1830) 1-57.

Furniss, D.; Shephard, J.D.; Seddon, A.B.: 'A novel apporach for producing optical fibre with halide core and oxide cladding.' To be presented at Conference on Non- oxide glasses. Corning June 1996.

Gilard, P.: 'Fifty Years ICG' (1983)

Jewkes,J.; Sawers, D.; Stillerman, R.: 'The Sources of Invention,' Second Edition. Macmillan 1969.

Kao, K.C.; Hockham, G.A.: ‘Dielectric-film surface waveguides for optical frequencies,’ Proc. I.E.E.113 (1966) 1151-1158.

Meigh, E.: ‘The Making of a Federation.’ 1975.

Moody, B.E.: ‘Griffith and cracks,’ Glass Technol. 29(1988) 73-77.

Moody, B.E. ‘The life of George Ravenscroft,’ Glass Technol. 29 (1988) 198-210.

Moody, B.E. ‘The life of George Ravenscroft: an addition,’ Glass Technol. 30 (1989) 191-2.

Mott, N.F.; Davis, E.A.: ‘Electronic processes in non-crystalline solids,’ 2nd. Edn. Clarendon Press, Oxford (1979).

Newton, R. and Davison, S. ‘Conservation of Glass,’ Butterworth-Macmillan (1989) 318 pp.

Pilkington, L.A.B.: ‘The float process,’ Proc. R. Soc. A314 (1969) 1-25.

Pilkington, L.A.B.: ‘Float-an application of science, analysis and judgement,’ Glass technol.12 (1971) 76-83.

Pilkington, L.A.B.: ‘The flat glass industry: evolution and revolution over 60 years,’ Glass Technol.17 (5) (1976) 182-193.

Rawson, H.; Scott, B.: 'Techniques for producing low loss glasses for optical fibre commmunications.' Glass Technol.14 (1973) 115-124.

Renfrew, C. ‘Before Civilisation,’ Jonathan Cape (1973).

Rider, D. ‘The Glass Manufacturers Federation and its work,’ J. Soc. Glass. Technol. 38 (1954) N87-95.

Roeder, E.: ‘Extrusion of glass,’ J. Non-Cryst. Solids 5 (1971) 377-288.

Roeder, E.: ‘Flow behaviour of glass during extrusion,’ J. Non-Cryst. Solids 7 (1972) 203-220.

Schaeffer, H.A.: ‘Industry-University Cooperative Research on Glass Technology in Germany,’ Ceram. Eng. Sci. Proc. (1995) 16 216-220.

Stevels, J.M. ‘Some thoughts on the present situation of scientific periodicals on glass,’ J. Soc. Glass Technol. 34 (1950) NR 134-138.

Turner, W.E.S.T: ‘The Department. Its foundation and work since 1915,’ J Soc Glass Technol. 21 (1937) T5-43.

Turner, W.E.S.T: ‘Twenty one years. A professor looks out at the glass industry,’ J Soc Glass Technol. 22 (1938) T99-164.

Turner, W.E.S.T: ‘The International Commission and the Deutsche Glastechnische Gesellschaft,’ J. Soc. Glass Technol. 32 (1948) NR 18-19.

Turner, W.E.S.T: ‘The International Commission on Glass. Its programme of work,’ J. Soc Glass Technol. (1950) 34 132-133.

Watts, D.C. ‘Why George Ravenscroft introduced lead oxide into crystal glass,’ Glass Technol. 31 (1990) 208-212.

Yaraman, A.: ‘The International Commission on Glass and the Glass World,’ Ceram. Eng. Sci. Proc. (1995) 16 228-238.

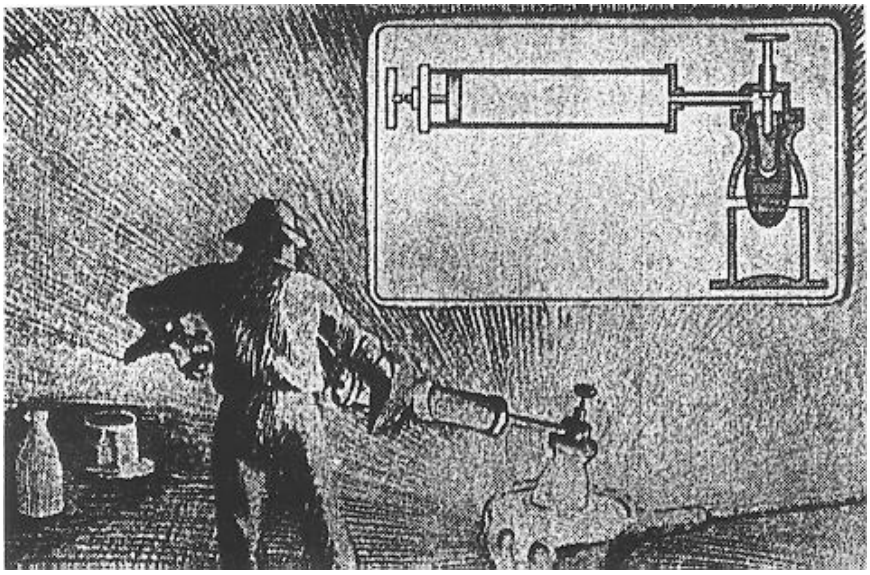

Figure 1. Artist's impression of Mike Owens developing the suction feed principle.

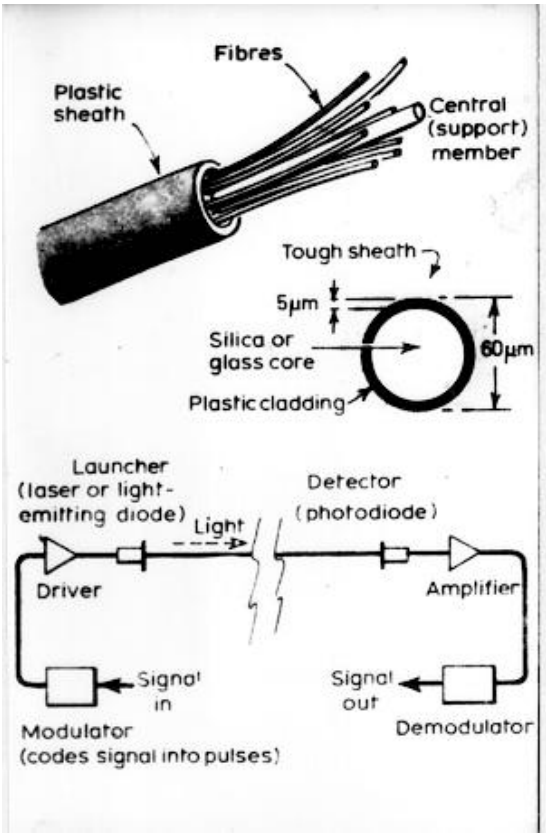

Figure 2. Diagram illustrating the principle of the fibre optic communication system.

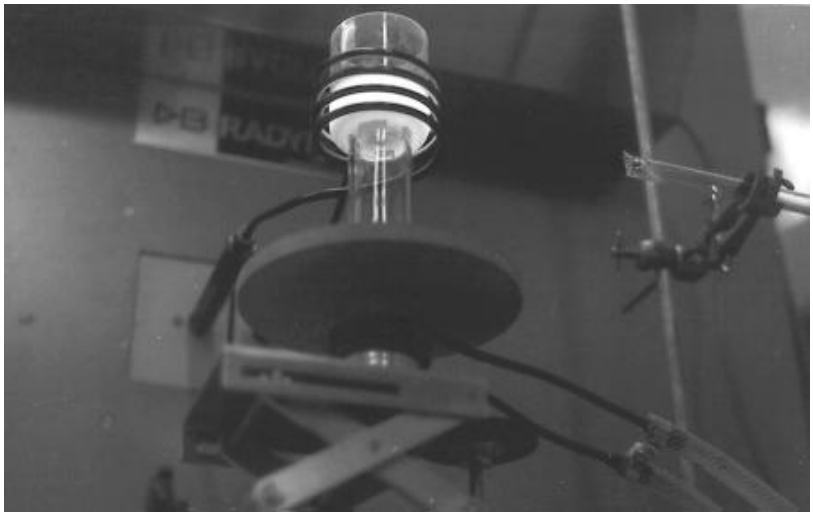

Figure 3. Glass melting in a silica crucible by direct RF heating

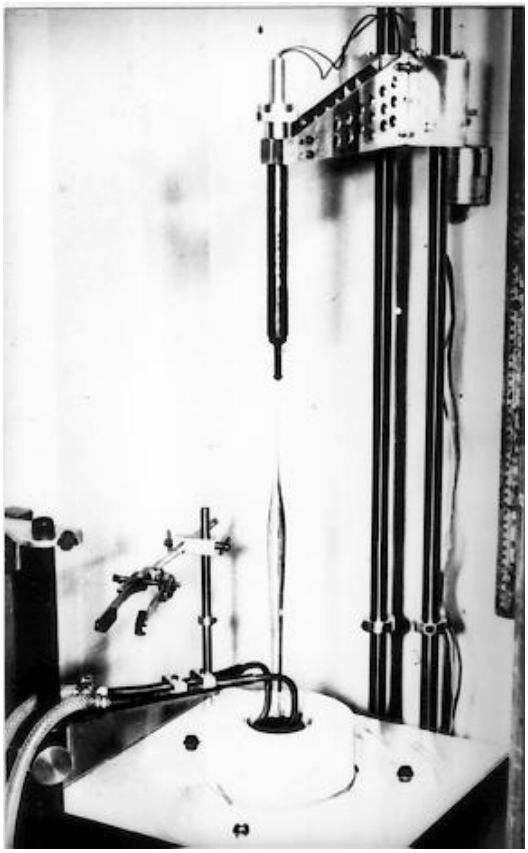

Figure 4. Drawing cladded rod from the surface of the melt

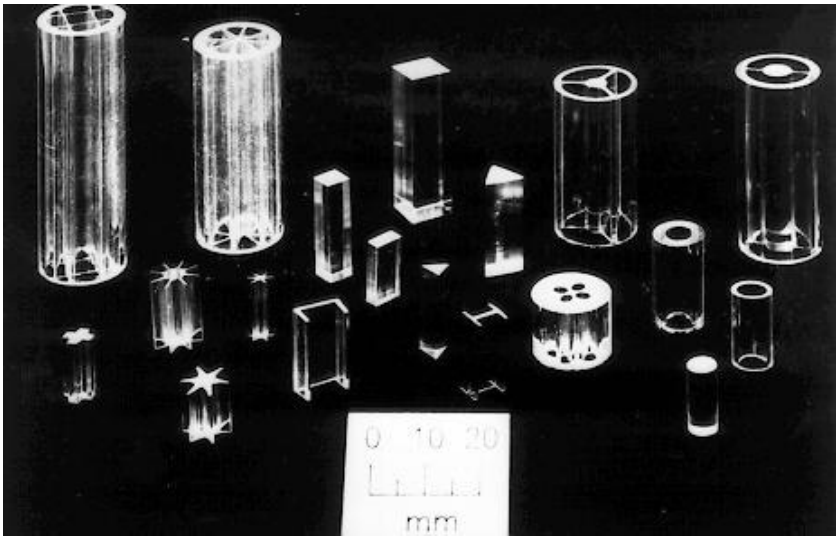

Figure 5. Complex sections produced by extrusion. (Professor E Roeder, University of Kaiserslautern.)

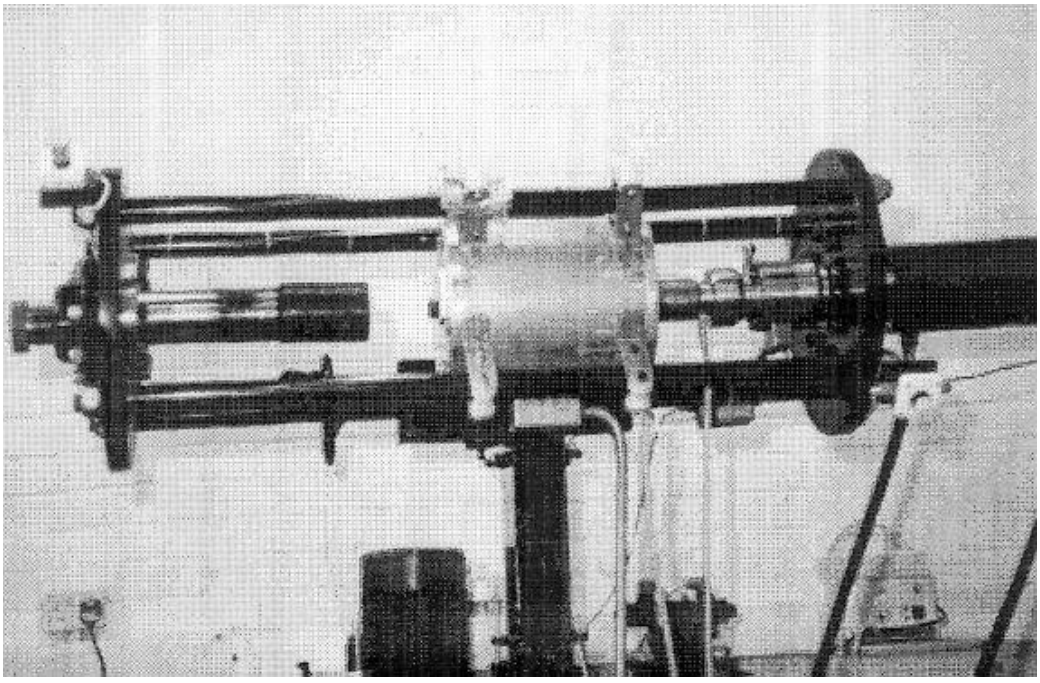

Figure 6. Sheffield version of Roeder's extruder. Extrusion can be carried out either vertically or horizontally.

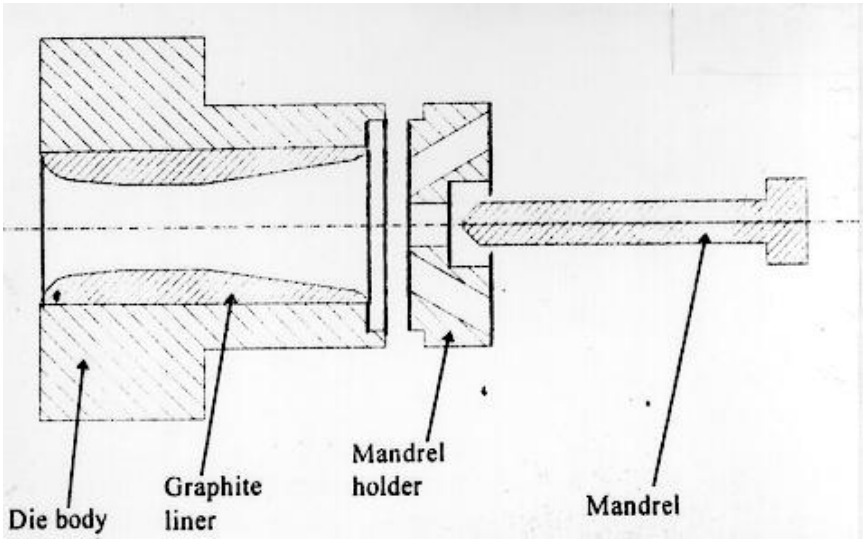

Figure 7. Diagram of an extruder nozzle. The graphite liner is to reduce die swell.

GLASSES WITH MOLECULAR OR TRANSITIONAL STRUCTURES AND THEIR FORMING BEHAVIOR

William C. LaCourse, Wesley King, Alexis Clare and **Chanqing Shen**
Center for Glass Research, NYS College of Ceramics at Alfred University, USA

Extended Abstract

The effect of melt structure on forming behavior is a topic of considerable technological importance. Unfortunately, we generally know less about the structure of melts than we do the corresponding glasses since characterization techniques used at low temperatures are not always applicable at elevated temperatures. It is clear however that melt structure has important influences on forming, particularly under "extreme" conditions. Such conditions are extant when a forming stress is coupled with a continuously cooling glass, as is the case in fiber drawing and some blowing and pressing operations. As shown by Brückner and coworkers[1,2] melt fracture can occur if forming stresses are too high relative and/or the viscosity is too high Simmons et al[3] as well as Brückner's group have also shown that at lower viscosities non-Newtonian flow effects (shear thinning) predominate.

Melt structure is important in both cases. Simmons suggests that a "high cohesive" strength of the liquid shifts shear thinning to higher draw rates. On the other hand, Brückner has shown that the tendency for melt fracture is enhanced when the melt structure becomes more "brittle". Structures typically considered weak, such as chain structure phosphates, are less prone to melt fracture than are those with more three dimensional structures. The ability the chain structure to orient under the applied forming stress, and the inability of the network type silicates is apparently related to this behavior.

Work in our laboratory has recently centered on the behavior of oxide glasses[4,5] having a range of structures, and chalcogenide glasses[5,6] particularly As_2Se_3 which has a two-dimensional layered structure in the solid state, and presumably in the forming range. The oxide compositions under investigation (Na_2O - x Al_2O_3 - (3-x)SiO_2 and Na_2O - xB_2O_3 - (3-x)SiO_2) have been chosen to cover a range of structures. Property measurements such as T_g, Young's modulus, ionic conductivity and fracture toughness indicate that when $x<0.2$ the melt structure is one in which the properties are controlled by a continuous alkali-NBO rich network[7]. Silica rich regions are locally isolated by such regions. This structure is commonly referred to as a "modified random network"[8]. The non-directional bonding in such regions is such that the ability of the structure to respond to drawing stresses is similar to that of the phosphate (chain) and As_2Se_3 (layer) structures. When x is large (> about 0.4) the structure can be considered 3-dimensional with a continuous Al- or B-silicate network. Between $x = 0.2$ and $x = 0.4$ the structures are "transitional".

It is the transitional region that is of most interest, since the structure and properties change rapidly in this compositional range and several commercial glasses apparently are in this region.

Results of neutron scattering studies indicate that, like the phosphates, As_2Se_3 fibers orient during drawing, particularly under extreme draw conditions. Previous studies of these fibers indicated that the strength was initially increased by the orientation but that a maximum strength occurred at the same conditions in which DSC and EPR studies suggested that shear thinning

conditions had been reached and that "depolymerization" of the structure was occurring. DSC studies of the pre-T_g exotherm of freshly formed fibers apparently signal the onset of shear thinning. The magnitude of the exotherm decreases abruptly in the shear thinning region. Recent Nuclear Quadruple Resonance results also show that such extreme conditions can lead to permanent changes in the structure, and that annealing does not lead to a single metastable structure for fibers formed under conditions leading to orientation and/or shear thinning.

For oxide glasses, similar strength behaviors were observed for the Al-silicate glasses with x = 0. No such maxima have been observed for glasses with 3-dimensional network structures. On the other hand, DSC results on a 3-dimensional glass show similar decreases in the magnitude of the pre-T_g exotherm at high draw rates, and structural studies of these fibers also indicate a depolymerized structure which does not anneal to the same state as fibers formed under less severe conditions. However, results for oxide glasses are complicated by the fact that the chemical reactivity of the fibers is extremely high when continuous NBO rich regions are present.

REFERENCES

1. R. Brückner, in Advances in The Fusion and Processing of Glass, eds., A. Varshneya, D. Bickford and P. Bihuniak, Am. Ceram. Society (1993). pp 3-24.

2. R. Brückner and Y. Yue, J. Non-Cryst. Solids, **175** 118-28 (1994).

3. J. Simmons, T. Swiler and C. Simmons, in Advances in The Fusion and Processing of Glass, eds., A. Varshneya, D. Bickford and P. Bihuniak, Am. Ceram. Society (1993). pp 27-34.

4. C.T. Ho, W. C. LaCourse, R.A. Condrate, Sr., and A. Jillavenkatesa, A Raman Spectral Investigation of Structural Variations in Thin Silicate Glass Fibers. Mat. Lett. 23 237-40 (1995).

5. W. C. LaCourse, C. T. Ho, K. Cerqua-Richardson, R. K. MacCrone, P. Hari and P.C. Taylor, "Effects of Forming Conditions on Glass Fiber Structures and Properties" Glastech. Ber. Glas. Sci. Technol. 68 C2, 4-13 (1995).

6. W. A. King, A. G. Clare, W.C. LaCourse, P. Hari and C. Taylor, Proc. Intl. Conf. on Non-Oxide Glasses, Corning NY (1996) (J. Non-Cryst. Solids, (in press) See also P. Hari, P.C. Tayor, K. A. Cerqua-Richardson and W. C. LaCourse, "Nuclear-quadrupole-resonance studios of As_2Se_3 fibers" Phys. Rev. B 51 [4] 2347-51 (1995)

7. William C. LaCourse, V. Malot and W. Mason, Structural Implications of Elastic Properties, Fracture Toughness and Fracture Surface Energy of R_2O-Al_2O_3-SiO_2 Glasses, in Ceramic Trans. Am. Ceram. Soc. eds. J. Varner and V. Frechette (1996)

8. Y. Cao and A.N. Cormack, A Structural Model for Interpretation of an Anomaly in Alkali Aluminosilicate Glasses at Al/Alkali = 0.2 - 0.4, pp 137-152 in: Diffusion in Amorphous Materials, eds. H. Jain and D. Gupta, TMS, Warrendale, PA (1994)

BARRIER-RELATED ANHARMONICITY OF INTERATOMIC INTERACTIONS IN INORGANIC GLASSES

V. N. Sanin
State Technical University, Russia
B. G. Varshal
State Institute of Glass, Russia

Abstract

The concept of barrier-related anharmonicity as a special kind of anharmonicity due to the presence of barriers in the potential energy of atomic interactions is introduced. Based on a numerical solution of the Schroedinger equation, it is demonstrated that anomalous anharmonic effects manifest themselves in the excess heat capacity, negative coefficient of thermal expansion, and increase in elastic moduli with increase of temperature and decrease of pressure are due to structural units of glass (atoms and clusters of atoms), which experience vibrations in two-well potentials (TWP). These structural units residing in symmetric or slightly asymmetric TWPs constitute two-level systems at temperatures of the order of several Kelvin and give rise to anomalous increase in the ultrasound velocity at about 4 K and to resonance absorption of ultrasound. The changes in properties of glasses due to the barrier-related anharmonicity at higher temperatures are determined by the parameters of TWP. In the case of high barriers, the barrier-related anharmonicity in glasses is similar to that in crystals.

1. INTRODUCTION

A great many physical phenomena in solids are difficult to interpret adequately in terms of a purely harmonicity-based theory, because these phenomena are completely due to the higher (anharmonic) terms in the expansion of interaction energy in terms of coordinates.

The anharmonic effects in the majority of crystalline solids exhibit a similar pattern and can be described to a good accuracy in a quasi-harmonic approximation or in terms of the perturbation theory [1]. These methods are applicable to the weakly anharmonic solids, i.e., when the assumption that the amplitudes of atomic vibrations are small is realistic.

With highly anharmonic solids (quantum-mechanical crystals and the systems with structural phase transitions), all or a fraction of atoms experience vibrations about their equilibrium positions with large amplitudes and are subjected to appreciably anharmonic forces from the surrounding atoms; moreover, the latter cannot be considered as rigidly fixed. In this case, the motion of atoms is governed by effective potentials and effective force constants [2].

Glasses also should be assigned to the class of highly anharmonic solids. Various experiments demonstrate [3, 4] that a fraction of the total number of ions and larger structural fragments (tetrahedra and clusters of tetrahedra) in glasses can be displaced to distances of about 0.1 nm even at low temperatures. The model of two-level systems (TLS) successfully implemented to

describe a number of anomalous properties of glasses at low temperatures [5, 6] also assumes large displacements of atoms or clusters of atoms as a result of tunneling under a barrier which separates the equilibrium sites of the species in motion.

At the same time, there are a number of quantitative discrepancies between the theory and experiment; in our opinion, the main drawback of the TLS theory is that it failed to provide an answer to the question as to why the vitreous materials feature a remarkable uniformity of some of their properties (heat capacity, thermal conductivity, low-temperature peaks in the sound-absorption spectra, and increase in the elastic moduli with temperature in the region up to about 4 K), while the other properties (thermal expansion and dependencies of elastic moduli on temperature and pressure) often differ radically from glass to glass.

In our opinion, these deficiencies of the theory are due to the fact that the possibilities of the theory have been constrained by phenomenological approach to the TLS, which has been employed in the majority of studies. At the same time, the attempts of microscopic analysis have been restricted to a treatment only of the motion either under or above the barrier because of the lack of an analytical solution to the Schroedinger equation for the motion of particles in two-well potentials (TWP) and have been reduced to consideration of particular cases of the low- and high-temperature dependencies. The microscopic model of soft atomic potentials (configurations) [7] suggested for implementation within a wide temperature range abounds with various approximations and estimated quantities to such an extent that the usefulness of this model turns out to be questionable.

A quantum-mechanical analysis of the motion of structural units of a glass in the TWP potential substantially contributed to an understanding of anomalous properties of glasses [8]. In this paper, we determine more accurately (as compared to [8]) certain features of the motion of particles in a TWP potential and take also into account the effects of asymmetry of the potential.

2. MICROSCOPIC MODEL

We will consider the model for a silica glass; we state beforehand that the microscopic models for the glasses of other types will be probably not much different from the one under consideration. Experimental data [9] indicate that the structures of the silica glass and high-temperature cristobalite are similar; these data and the results of X-ray diffraction studies of [β-cristobalite [10] suggest that a fraction of oxygen atoms involved in the Si-O-Si bridge bonds can occupy several equilibrium sites in the silica glass structure, which are located about the Si-Si axis and are separated with barriers of various (sometimes, of moderate) heights.

By separating two most accessible sites from the total number of feasible ones, we obtain the TWP that controls the motion of oxygen atom in its rotation about the Si-Si axis. Since the equilibrium sites correspond generally to different angles θ of the Si-O-Si bond, this rotation may be considered as the motion of the oxygen atom in the TWP with the Si-Si distance as a variable.

The potentials of pairwise Si-O interactions do not change with transition from a crystal to a glass. Contrastingly, the Si-Si interaction potentials change in that case substantially. It is noteworthy that a compession of all the $Si0_2$ modifications is accompanied, in general, with variations in the angle θ [11, 12]; i.e., the elastic moduli of such structures depend to a larger extent on the resistance of the valence-bond angles to deformation rather than on the valence-bond rigidity. Therefore, the Si-Si interaction potentials are of no less importance than the Si-O potentials. However, the Si-Si potentials do not account for the interaction of only this pair of

atoms (Si-Si designation is taken merely for convenience). These potentials are considerably more complex; they represent the model of changes in the Si-O-Si angles and Si-Si distances as a result of rotational motion of the bridge-oxygen atoms with account taken of the interaction of the latter with the atoms from the next-neighbor coordination shells. These are essentially effective potentials which account for the long-range forces and the structure of material. Due to the density fluctuations and topological disorder, the Si-Si potentials in glasses feature a double-well configuration, while in crystals these potentials are of a single-well type (at least at temperatures up to those corresponding to phase transitions).

We will assume to a first approximation that the potentials of pairwise Si-O interactions are sufficiently harmonic; therefore, we may exclude them from consideration and concentrate on the TWPs. Owing to this approach, the problem is reduced to a one-dimensional one and, thus, is considerably simplified. Instead of dealing with the chain of several Si-O-Si bonds, we consider just a separate bridge bond having the average parameters of potential in the chain.

We represent a TWP as the sum of a harmonic term U_1 and a Gaussian function U_2 that simulates the potential barrier, i.e.,

$$U= U_1 + U_2 ; U_1 = (1/2)\, f_\theta\, x^2; U_2 = A \exp[-d(x- b)^2], \qquad (1)$$

where;

f_θ is the force constant that corresponds to changes in the angle;

x is the excursion of oxygen atom from the equilibrium site that corresponds to the harmonic approximation;

A, d, and b determine, respectively, the height, shape, and asymmetry of the potential barrier.

We call attention to the bond force constant f_θ. A variation in the angle θ of a Si-O-Si bond can be accomplished by rotating the oxygen atom about the Si-Si axis but it can occur also without rotation, in a Si-O-Si plane. Since the different force constants correspond to the above-mentioned types of motion and our one-dimensional model includes only a single parameter f_θ, the value of f_θ should be chosen beforehand. The parameter f_θ must be greater than (or equal to) the force constant for rotation, but less than (or equal to) the force constant for changes of the angle θ in the Si-O-Si plane. The absolute value of f_θ does not affect profoundly the results of calculations; therefore, we assume f_θ to be equal to the force constant for rotation (f_θ = 3.5 N/m [11]). However, we take into consideration in discussion that an increase in f_θ is plausible with the rise of temperature when the thermal motion obliterates the effects of rotation on θ in the case of the above-barrier motion of atom.

Calculations were also performed for alternative microscopic models. The rigidity of $Si0_4$ tetrahedra and certain experimental data [3,7] indicate that the rotation of a tetrahedron or even a cluster of tetrahedra is quite probable at low temperatures. Because of this, we considered the motion of a $Si0_4$ tetrahedron and a cluster of five tetrahedra in the TWP as alternatives in order to compare the results of calculations and determine, if possible, the number of particles involved in the formation of TLS. The TWPs for these alternative models are also described by a formula of the form (1); however, the force constant f is, respectively, 4 and 12 times greater than f_θ (the factors account for the number of Si-O-Si bridges which link these clusters with the rest of the structural network of a glass).

3. A SYMMETRIC TWO-WELL POTENTIAL

Figure 1 shows the potential profiles, energy-level positions, and wave functions for lowest four energy levels when oxygen atom moves in the TWP. The values of effective force constants f_n for the corresponding energy levels are also indicated in Fig. 1. A similarity is observed between the results shown in Fig. 1 and those reported in [8] for the case of a $Si0_4$ tetrahedron in the TWP. It is appropriate to point out that the separation of the zeroth and the first energy levels decreases with increase in the particle mass and the height and width of the barrier, in accordance with the laws of quantum mechanics.

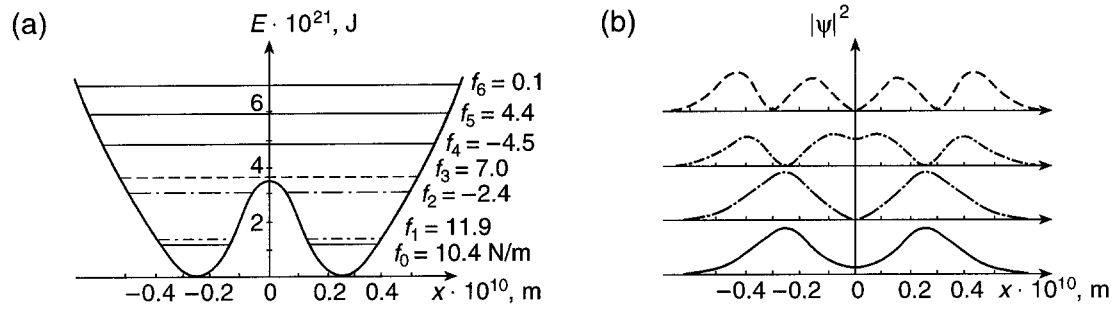

Figure 1. The profile of a TWP, energy levels (a) and wave functions for the lowest energy levels (b) of an oxygen atom. The TWP has the following parameters: f = 3.5 N/m, d = 4 $\cdot 10^{21}$ m^{-2}, A = 5 $\cdot 10^{-21}$J, and b = 0.

Figure 2 shows the temperature dependence of average force constant <f> and heat capacity C_v for the barrier height in the TWP as a variable parameter. While emphasizing a similar temperature behavior of <f> in Fig. 2 to the data in [8], we point out below certain specific features of the results obtained, which were not reported in [8].

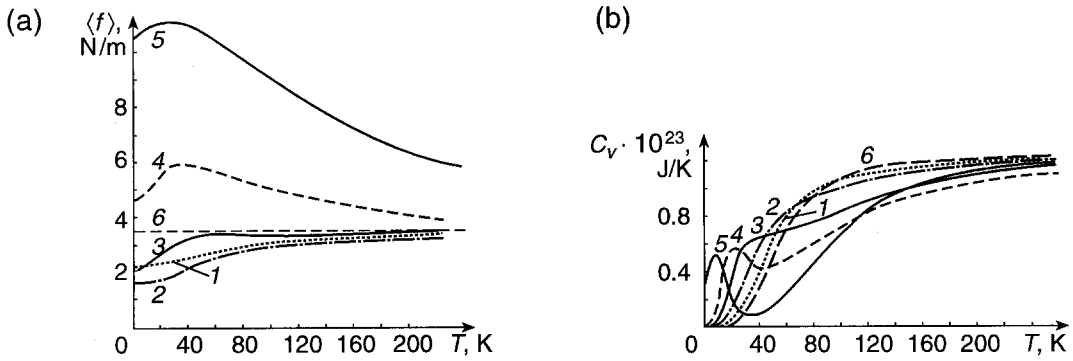

Figure 2. Changes in the temperature dependencies of the average force constants (a) and heat capacity (b) with increase in the barrier height A for oxygen atom in the TWP that has the following parameters: f = 3.5 N/m, d = 4 .10^{21} m^{-2} , b = 0, and A = (1) 0.5 · 10^{-21} J, (2) 1 · 10^{-21} J, (3) 2 · 10^{-21} J, (4) 3 · 10^{-21} J, and (5) 5 · 10^{-21} J. Curve (6) corresponds to the case of harmonic oscillator.

The temperature range and the amount of increase in <f> at the lowest temperatures (from 0 to about 30 K) depend on the particle mass and also on the height and width of the barrier, which is related to the tunneling ability of the particle. The heavier the particle and the higher and wider the barrier, the lower the probability of finding the particle in the barrier region and the narrower the temperature range and the smaller the amount of increase in <f>. With very high barriers, the temperature behavior of <f> at low temperatures is the same as in crystalline solids; this asymptotic behavior of <f> lends support to the correctness of calculations.

The temperature behavior of <f> at temperatures above about 30 K depends on the relation between the parameters of the barrier and those of parabolic potential. With relatively low or gently sloping barriers (this condition is defined by the approximate inequality $A \cdot d$. 4f), a further increase in <f> with temperature is observed (see curves 1 and 2 in Fig. 2). In the case of such TWPs, an external pressure induces an increase in the height of barriers and, consequently, decrease in <f> (the transition from curve 1 to curve 2 in Fig. 2), which corresponds to negative derivatives of <f> with respect to pressure and to negative Grüneisen parameters for acoustic modes. This characteristic behavior, i.e., the increase of elastic moduli with temperature (and decrease of them with increase in pressure) and negative acoustic-mode Grüneisen parameters, are typical of the silica glass and also of vitreous BeF_2, $Ge0_2$ and $Zn(P0_3)_2$.

With relatively high or steep barriers ($A \cdot d$ / 5f), a decrease in <f> with temperature is observed (curves 4 and 5 in Fig. 2). An increase in the barrier height in such TWPs under an external pressure is accompanied by increase in <f>, which corresponds to positive derivatives of elastic moduli with respect to pressure and to positive acoustic-mode Grüneisen parameters; these properties are characteristic of crystals and a wide range of glasses.

Thus, the results of numerical calculations indicate that the presence of a barrier in the TWP can result not only in softening of the potential as it was assumed in the model of soft potentials [7], but can also harden the potential. Such a model may be referred to as the model of soft and hard potentials or, to be more precise, as the model of the barrier-related anharmonicity characteristic of amorphous solids.

Conceivably, the dependence of <f> on the parameters of TWPs, as determined in this study, might make it possible to separate all glasses into two broad classes; i.e., with common nature of vitreous state and the presence of TWPs in all the glasses, a difference in some of the properties of glasses is determined merely by diversity of the parameters of TWPs with due account taken also of the pairwise interatomic potentials.

Figure 2 also shows the data (somewhat more comprehensive than in [8]) on the influence of the barrier-induced anharmonicity on the vibrational heat capacity. In all the cases considered, the presence of a barrier in the TWP gave rise to a low-temperature excess heat capacity as compared to the case of harmonic oscillators (curve 6 in Fig. 2). The relative excess of heat capacity is as high as 10 orders of magnitude for certain types of TWPs at selected temperatures; this fact indicates that even a small fraction of particles residing in the symmetric TWPs can give rise to the excess heat capacity observed experimentally in glasses at low temperatures. It is noteworthy that the heavier is the particle and the higher and wider is the barrier in the TWP, the less is the separation between the E_o and E_1 levels; as a result, a maximum of excess heat capacity is observed at lower temperatures. In addition to the excess of heat capacity, a deficit of heat capacity is observed at higher temperatures.

4. THE EFFECTS OF ASYMMETRY IN THE TWO-WELL POTENTIAL

It is quite evident that the symmetric TWPs comprise only a fraction of the total number of TWPs in a glass. The asymmetry of the TWPs profoundly affects the positions of energy levels, the wave functions, and the temperature dependencies of (f) and C_v.

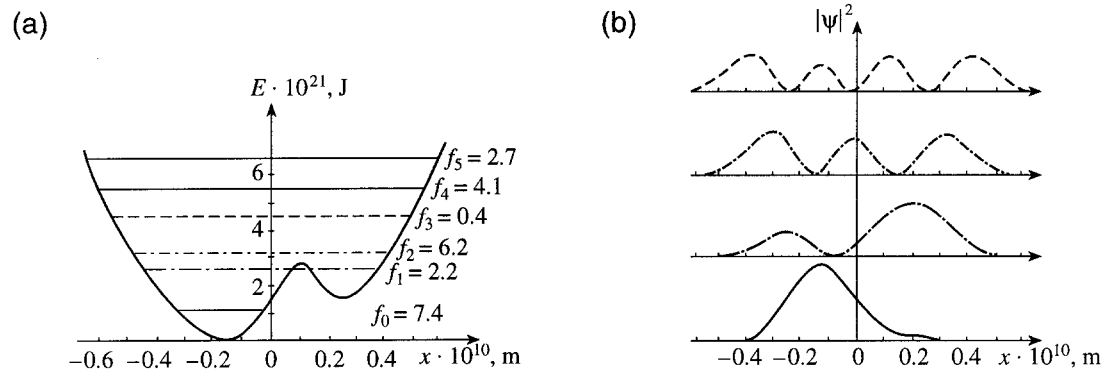

Figure 3. The influence of asymmetry in the TWP on the energy levels (a) and wave functions (b) of oxygen atom. The following parameters of the TWP were used: f = 3.5 N/m, $d = 4 \cdot 10^{21}$ m^{-2}, $A = 3 \cdot 10^{-21}$ J, and $b = 1 \cdot 10^{-11}$ m.

Figure 3 illustrates the energy levels and corresponding wave functions for oxygen atoms residing in the asymmetric TWF. As is evident from Fig. 3, the TLS ceased to exist and, as a result, the characteristic TLS properties, namely, an increase in <f> at temperatures up to about 30 K and a large magnitude of excess heat capacity at low temperatures, were no more observed (Fig. 4). Figure 4 also shows the sequence of variations in the temperature dependence of <f> and C_v with increase in the shift of the barrier. Numerous computations performed for various parameters of the TWP have demonstrated that the characteristic increase in <f> at low temperatures and the low-temperature excess heat capacity occur only with the magnitudes of asymmetry being no greater than about 0.2 - 0.3 £ ω_o (ω_o is the angular eigenfrequency of the particle in a parabolic potential). With larger asymmetry, even if the barriers are relatively low, <f> and C_v vary with temperature almost in the same way as they do in the case of a single-well potential that has the conventional cubic anharmonicity. A similar pattern for the effects of asymmetry was also observed on consideration of $Si0_4$ tetrahedron and a cluster of five tetrahedra in the TWP. We may infer that the high-asymmetry TWPs exhibit properties similar to those in the case of conventional anharmonicity and only the symmetric or slightly asymmetric TWPs impart to the glasses their specific features.

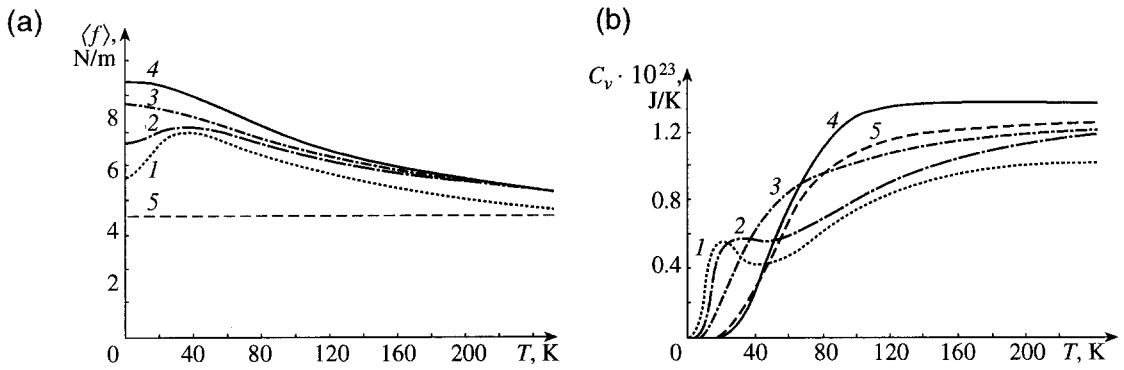

Figure 4. The temperature dependence of the average force constants (a) and heat capacities (b) for oxygen atom in the asymmetric TWP that has the following parameters: f = 3.5 N/m; d = $4 \cdot 10^{21}$ m^{-2}; A = $3 \cdot 10^{-21}$ J; and b = (1) 0, (2) $0.2 \cdot 10^{-11}$ m, (3) $0.5 \cdot 10^{-11}$m, and (4) $1 \cdot 10^{-11}$ m. Curve (5) corresponds to the case of harmonic oscillator.

5. CONCLUSION

Thus, a comprehensive treatment of the motion of structural units of glass in the TWPs demonstrated that an inherent characteristic of glasses is a particular kind of anharmonicity, namely, the barrier-related anharmonicity, brought about by the presence of barriers in the potential of atomic interactions; the sign and magnitude of the effect of the barrier-related anharmonicity on the properties of glasses depend on the parameters of TWPs. The barriers are also present in the atomic interaction potentials of crystals, though in that case they are considerably higher than in glasses and, as such, become evident only at high temperatures. As we already observed in the case of high barriers, the effects of such potentials are similar to those of conventional cubic anharmonicity; it is possible that, for this reason, the effects of different types of anharmonicity have not been separated so far. The experimental data indicating that the TLSs are present in polymers and in the amorphous semiconductors and metals suggest that the barrier-related anharmonicity is characteristic of all amorphous solids.

The performed computations have given no way so far of identifying the species involved in the formation of TLS; however, it was demonstrated that these species may be both atoms and larger structural fragments.

REFERENCES

1. G. Leibfried and W. Ludwig, Theory of Anharmonic Effects in Crystals, New York: Academic,1961, p. 231.
2. H. Boettiger, Principles of the Theory of Lattice Dynamics, Berlin: Akademie Verlag, 1983, p. 382.
3. U. Buchenau, H. M. Zhou, et al., Phys. Rev. Lett.,1988, vol. 60, no.13, p.1318.
4. S. A. Brawer, Phys. Rev. Lett.,1981, vol. 46, no.12, p. 778.
5. P.W. Anderson, B. Halperin, and C. M. Varma, Philos. Mag., 1972, vol.25, no.l,p.l.
6. W. A. Phillips, J. Low-Temp. Phys.,1972, vol. 7, no. 2-3, p. 351.

7. U. Buchenau et al., Phys. Rev. B,1991, vol. 43, p. 5039.
8. V. N. Sanin and B. G. Varshal, Proc. XVII Int. Congress on Glass, Beijing, 1995, vol. 2, p. 268.
9. A. J. Leadbetter, J. Chem. Phys.,1969, vol. 51, no. 2, p. 779.
10. A. F Wright and A. J. Leadbetter, Philos. Mag.,1975, vol. 31, no. 6, p.1391.
11. B. Bridge, N. D. Patel, and N. D. Waters, Phys. Status Solidi A,1983, vol. 77, no. 2, p. 655.
[12] L. Levien,. C. T. Prewitt, and D. J. Weidner, Am. Mineral., 1980, vol. 65, no. 9-10, p. 920.

GLASS FORMATION CHARACTERISTICS OF FLUOROPHOSPHATE GLASSES

Abdullah Ozturk
Middle East Technical University, Turkey

Abstract

Glass formation characteristics of glasses from the system AlF_3-MF_2-$Ba(PO_3)_2$ (M=Ca, Mg, Sr, Ba) have been studied as a function of $Ba(PO_3)_2$. Glass formation tendency increased with increasing concentrations of $Ba(PO_3)_2$. The critical cooling rate for glass formation decreased from 98±7 °C/s to 4±1 °C /s when $Ba(PO_3)_2$ concentration increased from 0 to 1 mole %. The improvement in glass formation caused by $Ba(PO_3)_2$ was due to linking the broken chains present in the structure of fluoride glass. The infrared transmission spectra of these glasses and their crystallization products suggested that the structure changed from short chains of AlF_6 groups to long chains of PO_3F and $Ba(Ca,Mg,Sr)P_20_7$ groups with increasing $Ba(PO_3)_2$ content. X-ray diffraction analysis revealed that $CaAlF_5$, $SrAlF_5$, $CaAlF_7$, and $CaSrAlF_7$, crystallize from these glasses.

I. INTRODUCTION

The discovery and development of fluorophosphate glasses have attracted considerable attention in recent years because of their potential use as host materials in high energy laser systems[1]. These glasses possess superior optical properties such as low refractive index with high Abbe number, large anomalous partial dispersion, low nonlinear refractive index, and high transmittance in near UV and IR regions[1-6]. They also have low melting and forming temperature[1-3]. Utilization of these glasses in special applications such as IR domes, mid-IR optical fibers, and polarizing substrates have been reported[5,7].

The fabrication of bulk samples for optics requires slow cooling rates to achieve suitable optical quality and convenient size. For this purpose, cooling rate of the melt must be as low as possible. However, small cooling rates promotes devitrification. Therefore the compositional dependence of the minimum cooling rate for glass formation must be known precisely. Otherwise glassy preforms may crystallize during processing or service. A good understanding of the glass formation characteristics in these glasses appears thus as a fundamental condition for their technological development. In spite of some investigations[8-11] on the formation and structure of fluorophosphate glasses, the data are sparse compared to silicate, borate, and phosphate glasses. Hence, studies on fluorophosphate glasses have both scientific and practical significance.

The purpose of this study was to determine the effect of a small amount of glass former additions on the formation characteristics and structure of fluorophosphate glasses.

II. EXPERIMENTAL PROCEDURES

A) Sample Preparation: On the basis of studies on the formation of fluorophosphate glasses, composition #1 in Table I was selected as the starting composition. In addition to this composition, six other compositions of progressively higher $Ba(PO_3)_2$ content were prepared in this study. The raw materials were certified reagent grade $BaHPO_4$, $NH_4H_2PO_4$, AlF_3, MF_2, CaF_2, SrF_2, and BaF_2. The $Ba(PO_3)_2$ was obtained by reacting $BaHPO_4$ and $NH_4H_2PO_4$ in the batch. The batch materials were carefully weighed to form a batch of desired glass compositions and dry mixed in a glass jar prior to melting. Glasses were prepared by melting 0.5 g (±0.0001 g) of the premixed powder in a strip furnace. Melting took place in a platinum boat at approximately 900 °C for 2 to 3 min in dry nitrogen atmosphere. Each composition was melted approximately 30 °C above its liquidus temperature and then cooled at various rates. The glass was recovered by unfolding the platinum boat.

Table I. Batch composition of the glasses investigated in this study.

Glass	Composition (mole %)					
No	$Ba(PO_3)_2$	AlF_3	CaF	MgF_2	SrF_2	BaF_2
1	0.0	42.10	31.58	10.53	10.53	5.26
2	0.1	42.06	31.55	10.52	10.52	5.25
3	0.2	42.03	31.52	10.50	10.50	5.25
3	0.25	42.00	31.50	10.50	10.50	5.25
4	0.5	41.90	31.43	10.47	10.47	5.23
5	0.75	41.78	31.35	10.45	10.45	5.22
6	1.0	41.69	31.26	10.42	10.42	5.21
7	1.5	41.48	31.10	10.37	10.37	5.18

B) Determination of Critical Cooling Rate: The critical cooling rate, R_c, for glass formation is defined as the minimum rate at which a melt can be cooled without crystallizing. R_c of various glass compositions was determined by inserting a Pt-Pt/13%Rh thermocouple bead in the platinum boat during melting the batch materials. The thermocouple bead was completely submerged in the melt without touching the boat. The thermocouple was connected to a chart recorder so as to obtain a record (cooling curve) of the temperature as a function of time. Cooling rates <50 °C /s were controlled by gradually decreasing the power to the strip furnace. Cooling rates from 50 to 100 °C /s were produced by simultaneously turning the power off and blowing helium gas over the sample.

C) Infrared (IR) Transmission: In order to measure the IR spectrum 3 mg of powdered glass and 300 mg potassium bromide was dry mixed and pressed in a vacuum die into pellets. The pellets were used to measure the IR spectrum from wavenumber 4000 to 200 cm^{-1} (2.5 to 50 μm wavelength).
D) X-Ray Diffraction (XRD): Glass samples and the corresponding devitrified products were analyzed by powder XRD. Powder patterns were obtained using Cu-Kα radiation. Each sample was scanned from 10 to 70 degrees two theta at 2 degrees per minute.

III. RESULTS AND DISCUSSION

As-quenched samples containing >0.5 mole % $Ba(PO_3)_2$ yielded a good glass, but it was difficult to obtain glass for compositions containing less $Ba(PO_3)_2$ than that value. The glassiness of the as-quenched samples were confirmed using X-raydiffraction and scanning electron microscopy techniques. Samples cooled at a rate slightly less than critical cooling rate yielded a mixture of glass and crystal when quenched in air. These compositions contained crystals adjacent to the sides of the platinum boat indicating heterogeneous crystallization.

No exothermic peak, corresponding to crystallization of the melt, was observed on the cooling curve since the heat of crystallization of fluorophosphate glasses is apparently low. When the cooling rate, R, was less than R_c the sample crystallized or contained a trace of crystalline material. The melt was then cooled at slightly higher rates until it was free from crystallinity. The cooling curve for which the sample became completely free from crystals was used to calculate the cooling rate which was taken as R_c.

R_c was determined for all compositions. The determination of the value is based on at least five individual experiments. The variation of R_c as a function of $Ba(PO_3)_2$ content for fluorophosphate glass is shown in Table II and in Figure 1. The results indicate that R_c decreases, that is glass formation becomes easier, with increasing $Ba(PO_3)_2$ content.

*Table II. The critical cooling rate, Rc, for glass formation for fluorophosphate compositions * of varying $Ba(PO_3)_2$ content*

Mole % $Ba(PO_3)_2$	R_c (C/s)
0.0	98±7
0.1	80±6
0.2	69±5
0.25	63±5
0.5	43±3
0.75	19±2
1.0	4±1

* Mole % composition is given in Table I.

The decrease in R_c with small amount of $Ba(PO_3)_2$ incorporation is due to linking the broken chains present in the structure of fluoride glasses and hence, increasing the ability for glass formation. The structure of fluoride glasses containing AlF_3, CaF_2, MgF_2, SrF_2,

and BaF_2 consists of a mixture of linear and branched AlF_6 octahedral chains of various length connected by Ca^{2+}, Mg^{2+} , Sr^{2+} , and Ba^{2+} ions [12,13]. The strongly charged Al^{3+} cation may link two or several chains, playing the role of a bridge[14]. Other cations (Ca, Mg, Sr and Ba) fill the interspace between the short chains and gather the short chains by electrostatic attraction between the cations and fluorine. Al^{3+} and Mg^{2+} may also form (AlF_4) and (MgF_4) tetrahedras and then reconnect the chains to one another, so that the ease of glass formation increases[10]. A schematic model for the structure of these glasses is shown in Figure 2

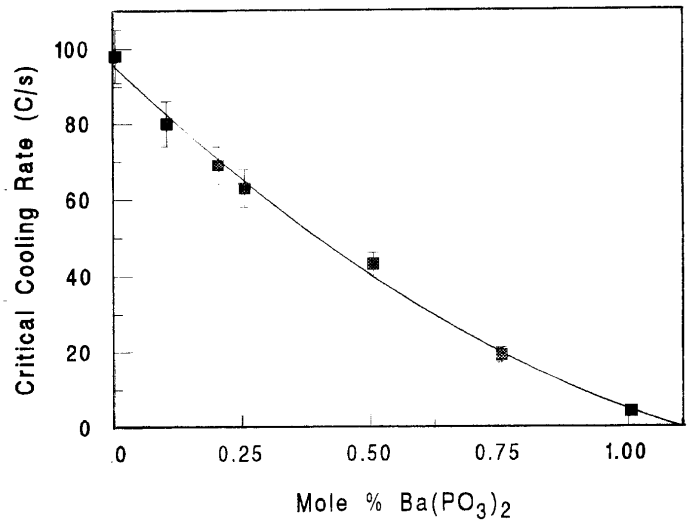

Figure 1. Variation of critical cooling rate for glass formation as a function of $Ba(PO_3)_2$ content for fluorophosphate glasses.

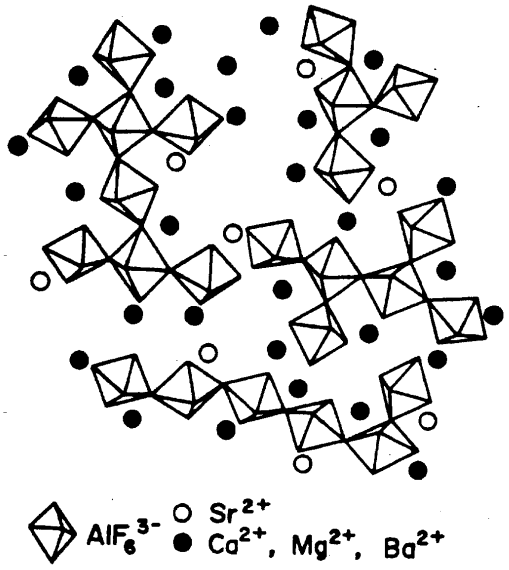

Figure 2. Schematic model for structure of fluoride glass containing AlF_3, CaF_2, MgF_2, SrF_2, and BaF_2. [12]

The improvement in glass formation caused by $Ba(PO_3)_2$ may be explained by the formation of long PO_4 chains in the glass structure. When $Ba(PO_3)_2$, which has a structure of long chains of PO_4, is introduced into the glass M-F bonds are disrupted and P-F bonds are formed as oxygen replaces fluorine[10]. This results in the formation of PO_3F tetrahedra which functions as terminal groups of the chains. With increasing $Ba(PO_3)_2$ content the chains become increasingly longer forming P-O-P bonds gradually. The formation of long P-O-P bonds modifies the glass network structure. The direct bonding of PO_4 groupings with the AlF_6 octahedral chains impedes the crystallization process.

The IR spectrum of the glass samples and the corresponding devitrified samples were measured to determine the basic structural groups. A portion of the IR spectra of selected fluorophosphate glasses and their crystallization products suggested that the structure changed gradually from short AlF_6 groups to long PO_3F and Ba(Ca, Mg, Sr)P_2O_7, the complex phosphate groups, as seen in Figure 3. Other phosphate groups such as $(P_2O_6F)^{3-}$ $(P_3O_9F)^{4-}$, $(P_4O_{11}\ F)^{5-}$, and $(P_5O_{15}F)^{6-}$ are reported to form as phosphate content of the glass increases[11].This confirms the effect of increasing $Ba(PO_3)_2$ on lengthening the PO_4 chains.

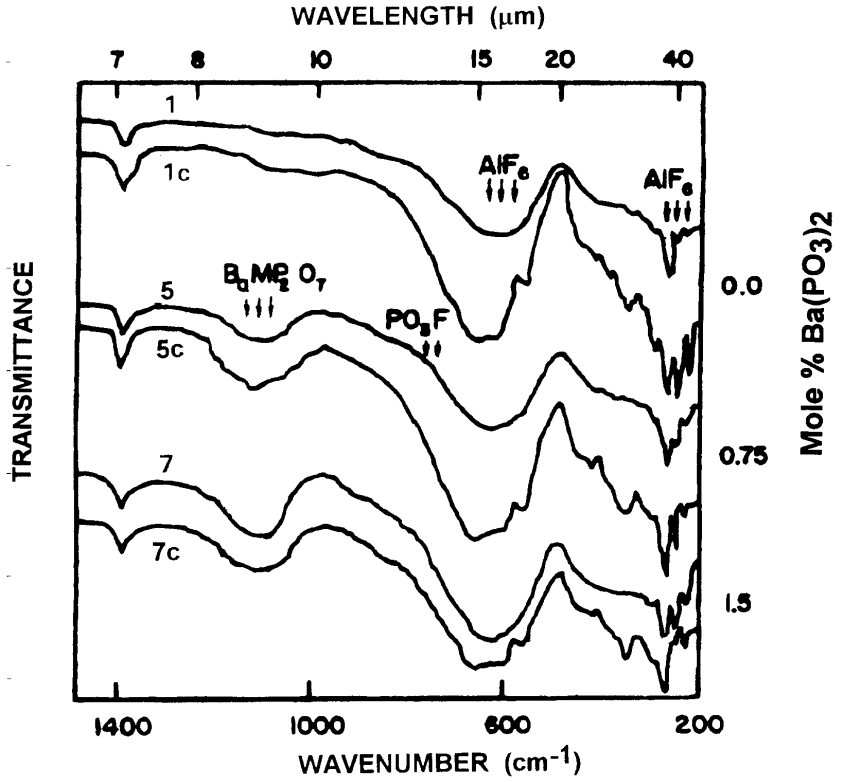

Figure 3. IR transmission spectra of selected fluorophosphate glasses (1, 5, 7) and their crystallization products (1c, 5c, 7c). Mole % compositions are given in Table 1. Curves are arbitrarily displaced along vertical axis for clearity.

As shown in Figure 3, the IR spectra of the glasses resemble those of the corresponding devitrified products although the absorption peaks for the glasses are not as sharp as those of crystallized products. This implies that the basic structural groups remain unchanged during crystallization[15]. A comparison of the spectra for the crystallization products

from glasses containing 1.5 mole % $Ba(PO_3)_2$ and no $Ba(PO_3)_2$ revealed that the IR spectrum of the crystallization products changed, i.e., the number of bands in the spectrum increased, with increasing $Ba(PO_3)_2$. This might be due to the formation of the pyrophosphate structural groups, and gradual symmetrization of the structural units of the phosphates[15]. The linking of PO_4 groupings within the AlF_6 octohedral chains impeded the crystallization process.

The IR spectra of the glass #1, containing no $Ba(PO_3)_2$ and corresponding devitrification product have no absorption peak at the high frequency bands, but absorption peaks appear at 240, 260, 285, 320, 380, 410 cm^{-1}, and in the region of 520-780 cm^{-1}, which have been previously attributed to the vibration of $(AlF_6)^{3-}$ groups[10,15]. With increasing $Ba(PO_3)_2$ content $(PO_3F)^{2-}$ and mixed pyrophosphates, $BaMP_2O_7$ (M=Ca, Mg, Sr) form[10,15-17]. However, the absorption peaks of $(PO_3F)^{2-}$, which is associated with the formation of P-F bonds, are overlapped with those of $(AlF_6)^{3-}$ and pyrophosphate groups[10,17]. In the region of the stretching vibrations, 800-1500 cm^{-1}, the spectrum does not contain any other bands apart from those characteristics of pyrophosphates. The absorption peak appears at 1130 cm^{-1}, which are due to asymmetric stretching vibrations, characteristics of pyrophosphates[10,15-17].

The XRD of the devitrified glasses had many peaks of nearly the same intensity and which overlapped or were close to each other. The presence of several compounds made identification of the crystalline phases difficult. Despite this difficulties, $CaAlF_5$ is determined as the chief crystalline compound. Other compounds crystallizing are $SrAlF_5$, $CaAlF_7$, and $CaSrAlF_7$.

IV. CONCLUSIONS

1) Incorporation of small amount of $Ba(PO_3)_2$ improved the glass formation tendency of fluorophosphate glasses. The critical cooling rate, R_c, for glass formation decreased from 98±7 to 4±1 °C/s when $Ba(PO_3)_2$ content increased from 0 to 1 mole %.

2) The basic structural groups in fluorophosphate glasses are mixed pyrophosphates, $BaMP_2O_7$ (M=Ca, Mg, Sr), phosphoromonofluoridate, $(PO_3F)^{2-}$ and $(AlF_6)^{3-}$. The additions of $Ba(PO_3)_2$ changed the network structure from short chains of AlF_6 octahedra to the long chains of PO_3F and $BaMP_2O_7$. The M-F bonds were disrupted and P-F and /or P-O-P bonds were formed gradually.

3) The IR transmission analysis of selected fluorophosphate glasses and their crystallization products revealed that the basic structural groups remain unchanged during crystallization

4) The XRD analysis revealed that $CaAlF_5$, $SrAlF_5$, $CaAlF_7$, and $CaSrAlF_7$, crystallize from these glasses.

REFERENCES

1. J.T. WENZEL, D.H. BLACKBURN, W.K. HALLER, S. STOWSKI and M.J. WEBER, "*Development of fluorophosphate optical glasses*" Soc. Photo-Opt. lnstrum. Eng., SPIE Vol. 204 59-66 (1979).
2. B. KUMAR and R. HARRIS, *"Synthesis and properties of fluorophosphate glasses*" Phys. and Chem. of Glasses, 25 155-58 (1984).
3. P.A. TICK, *"Durability and properties in alkali aluminofluorophosphate glasses*" J. Am. Cer. Soc. 66 716-19 (1983).
4. J. YASI, J. FUSONG and G. FUXI, *"Optical and other physical properties of fluorophosphate glasses*" Chin. Phys. 3 162-68 (1983).
5. B. KUMAR, *"Formation and properties of glasses in the CaF2-AIF3-P205 system*" Mat. Res. Bull.16 179-86 (1981).
6. L.V. FEDOROVA, V.S. MOLCHANOV, L.N. URUSOVSKAYA, and A.N. VENIGORODSKAYA, "*Moisture resistance and certain other properties of fluorophosphate multialkali glasses*" Sov. J. Opt. Technol. 50 429-30 (1983).
7. R. K. SANDWICK, R:J: SCHELLER and K.H. MADER, "*Production of homogenous fluorophosphate glass*" Soc. Photo-Opt. Instrum. Eng. SPIE Vol.171 161-64 (1979).
8. M. SAMMET and R. BRUCKNER, *" Characterization and structural aspects of fluorophosphate glasses*" Glastech. Ber. 58 106-15 (1985).
9. S. TAKEDA, K. SUGIYAMA, Y. WASEDA, and K. MORINAGA, *Structural study of tin fluorophosphate glasses by X-ray diffraction*" J. of Mat. Sci. Lett 12 291-93 (1993).
10. G. FUXI, J. YASI and J. FUSONG, *" Formation and structure of AI(P03)3 - containing fluorophosphate glasses*" J. Non-Cryst. Sol. 52 263-73(1982).
11. S. STEVIC, S. RADOSAVLJEVIC, and D. POLETI*" Structural study of fluorophosphate glasses by thin layer chromatography*" Rev. Chim. Miner 19 192-98 (1982).
12. D. EHRT, H. ERDMANN, and W. WOGEL, *" Fluoroaluminate glasses: System CaF2-SrF2-AIF3*" Z. Chem, 23 37-38 (1983).
13. D. EHRT and W. WOGEL, " *Fluoroaluminate glasses: Influence of phosphates on the glass formation in the system MgF2-CaF2-SrF2-AIF3*" Z. Chem, 23111-12 (1982).
14. J.J. VIDEAU, and J. PORTIER, "*Fluoride Glasses*" Ed. P. HAGENMULLER Academic Press, 309-29 (1985).
15. V.P. KOLOBKOV and V.I. VAKHRAMEEV, *"IR spectroscopy and X-ray phase analysis of alkali-free fluorophosphate glasses and their crystallization products*" Sov. J. Glass Phys. and Chem., 4 34-38 (1978).
16. G.P. NIKOLINA, "*The interaction of barium metaphosphate with fluorides*" Russ. J. Inorg. Chem. 21 180-82 (1976).
17. V.A. KOLESOVA, *"The vibrational spectra of some crystalline and vitreous phosphates*" Opt. Spectrosk., 2 165-67 (1957).

GLASS STRUCTURE BY THE IR SPECTROSCOPY: THE ADVANTAGES OF THE QUANTITATIVE APPROACH*

A. M. Efimov
Vavilov State Optical Institute, Russia

Abstract

The obtaining of information on glass structure based on the raw experimental IR spectra is often hindered by well-known obstacles of methodological and/or physical nature; hence the tentative character of the resultant conclusions. At the same time, the IR spectra of oxide glasses are, as a rule, much more rich in spectrum features revealing subtle characteristics of glass structure than their Raman spectra; examples will be given. This makes the IR spectroscopy more promising for studying thoroughly glass structure than the Raman spectroscopy. In view of the above, this advantage of the IR spectroscopy can only be put into practice by means of the quantitative treatment of the experimental IR reflection spectra aimed to their description in terms of individual band frequencies and intensities. Based on data obtained, many qualitative structural interpretations of the IR spectra of silicate, germanate, phosphate, and tellurite glasses available in literature can be reconsidered or refined. Examples will be given that concern topics as follows:

(i) the actual origin of the high-frequency shoulder in the IR spectrum of vitreous silica;

(ii) the question whether the low-frequency and high frequencycomponents of the doublet in the 900 to 1100 cm^{-1} range characteristic of the IR spectra of silicate glasses are related to the stretches of the $Si\text{-}O^-$ terminal group and SiOSi bridge, respectively, or vice versa;

(iii) the occurrence of the $(P_3O_9)^{3-}$ ring anions rather than the linear chain anions in the structures of some phosphate glasses;

(iv) the validity of some IR band assignments and corresponding structural models of tellurite glasses available in literature.

---

* Full manuscript not available at the time of printing

MEDIUM-RANGE ORDER AROUND CATIONS IN GLASSES, USING ANOMALOUS WIDE ANGLE X-RAY SCATTERING. RELATION WITH GLASS TRANSMITTIVITY PERFORMANCES

Sophie Creux

Universités Paris 6 et 7, and Saint-Gobain Recherche, France

Abstract

Medium-range structure around strontium and iron in silicate glasses has been investigated, using anomalous wide angle X-ray scattering. In simple silicate glasses Sr is concentrated in 2D domains of the nanometre scale, whereas in an aluminosilicate glass with Sr/Al = 0.5 Sr-Sr correlations are much weaker. Preliminary results on iron in a reduced $CaFeSi_2O_6$ glass indicate short Fe-Fe distances. These results show that Fe^{2+} and Sr can have a well-organized environment in silicate glasses. This helps to understand the chemical dependence of optical properties of Fe-bearing glasses.

I. INTRODUCTION

Detailed knowledge of the structure of glasses is a key to control their macroscopic properties. X-ray absorption spectroscopy has shown that most cations, including weakly bonded ones, have a well-defined coordination shell. However this method fails to give quantitative information on further shells. A well-organized medium-range environment of Ca has been revealed in $CaSiO_3$ glass, using sophisticated neutron scattering techniques [1]. Another method which can give direct structural information on a selected species up to distances of about 1 nanometre is Anomalous Wide Angle X-ray Scattering (AWAXS). This method was chosen to investigate the environment of Sr in silicate and aluminosilicate glasses and that of Fe^{2+} in a pyroxene-like glass.

II. ANOMALOUS WIDE ANGLE X RAY SCATTERING (AWAXS)

AWAXS can be used to investigate the short and medium-range environment of a selected element in multicomponent glasses. It uses variations of the atomic scattering factor of an element when the incident energy is close to its absorption edges.

In multicomponent glasses, the elastically scattered intensity consists of a superposition of all pair-correlations. This results in mixing and loss of information. AWAXS allows to cancel the correlations which are not centered on the element of interest (say, Sr). The scattered intensity is recorded for one incident energy, usually well below the absorption edge of Sr. A second measurement is made a few eV below the absorption edge. Then only the scattering factor of Sr has changed significantly. Subtraction of one normalized intensity to the other cancels pair correlations which are

not associated with Sr. Then only the structural information about Sr remains (differential functions).

The elastically scattered intensity, as a function of k (scattering vector amplitude) can be expressed as :

$$I_{EI}(k,E) = \left\langle |f|^2 \right\rangle + \left| \langle f \rangle^2 \right| (S(k) - 1) \qquad (1)$$

where <f> is the composition-weighted average of the atomic scattering factors f(k,E) over the elements in the sample. S(k) is the total structure factor. The reduced radial distribution function G(r), is related to S(k) via :

$$G(r) = \frac{2}{\pi} \int_0^\infty k(S(k) - 1)\sin(kr)\,dk \qquad (2)$$

Peaks in G(r) indicate atomic shells, which are broader at large distances. With the differential elastic intensity, a differential structure factor DS(k) can be calculated, as well as a differential reduced radial distribution function DG(r).

All the experiments we report here were carried out at the LURE synchrotron radiation facility (Orsay, France) on the wiggler beamline DW31B. Synchrotron radiation allows high flux on the sample and easy tuning of the incident energy. Analysis of the data includes corrections for geometry and absorption, subtraction of parasitic signals such as resonant Raman and Compton scattering, normalization to an absolute scale.

III. RESULTS ON SR-BEARING SILICATE AND ALUMINOSILICATE GLASSES

Three glasses were synthesized for this study, two silicates and one aluminosilicate. They were melted in platinum crucible, quenched and crushed into fine powder. Due to high melting point and ease of crystallization, the metasilicate composition $SrO\text{-}SiO_2$ could not be achieved. Therefore two compositions with a minor element, Na for glass S and Al for glass SAI, were melted (see Table 1 for composition). In the aluminosilicate glass, called A, $SrO/Al_2O_3=1$, which corresponds to a full charge-compensation of Al^{3+} by Sr^{2+}.

	SiO_2 (mol %)	**Al_2O_3 (mol %)**	**SrO (mol %)**	**Na_2O (mol %)**
Glass S	62	0	32	6
Glass SAl	58	3	39	0
Glass A	66	17	17	0

Table 1 : Molar composition (according to microprobe analysis) of the Sr-glasses.

For each glass, X-ray scattering diagrams were recorded at two energies, one about 1000 eV below the Sr K-absorption edge and one a few eV below the edge (measured

value 16100 eV). The available k-range at these energies is 0-13Å^{-1}. Qualitative comparison of the total structure factors S(k) for the three glasses (Fig.1) shows similarities between glasses S and SAI. However these similarities are difficult to interpret structurally at this stage. In the G(r) functions (Fig.1) peaks around 1.6 and 2.6Å can be assigned to Si/Al-O and O-O pairs. Sr-O pairs are expected around 2.6Å, they are therefore partially masked by strong O-O correlations. Differentiation is needed to isolate the structural information related to Sr.

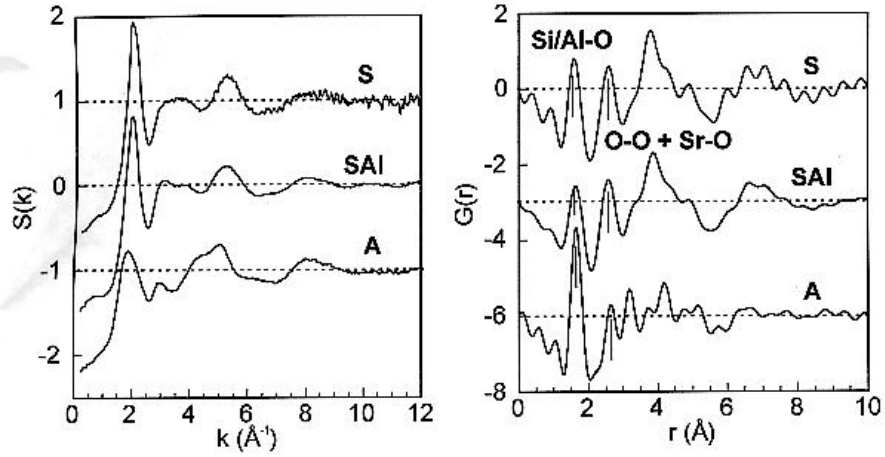

Fig. 1 : (left) S(k) for the three Sr-glasses. (right) G(r) functions for the same glasses.

Glasses S and SAI have similar DS(k), with a sharp and intense peak around 2 Å^{-1}. DS(k) for glass A is quite different, with a relatively low intensity on the whole k-range.

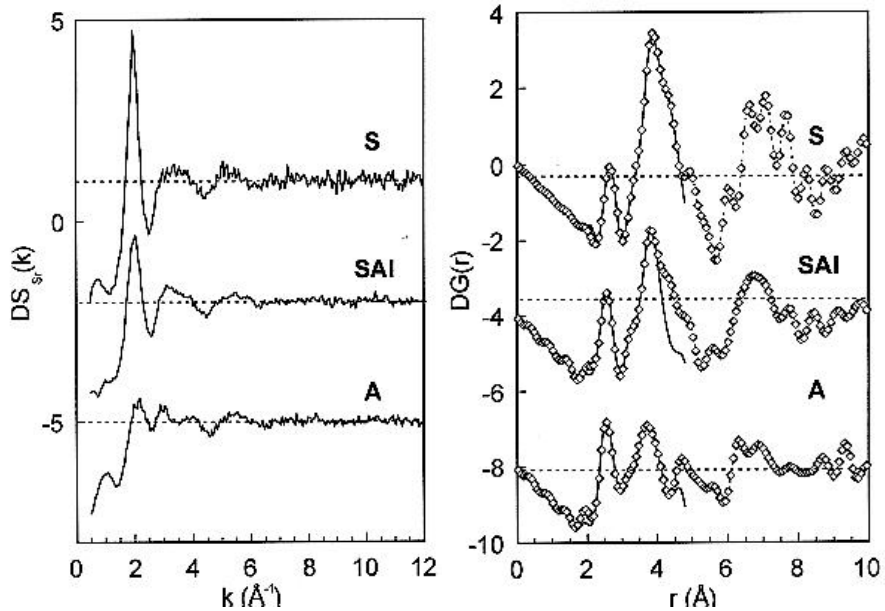

Fig. 2 : (left) DS(k) for the three Sr-glasses. (right) DG(r) experimental functions (symbols) and adjustments for the first shells (full line).

Modelling of the first shells in the DG(r) functions can give quantitative structural information. However only the first peak, due to Sr-O correlations, is isolated (Fig.2). Overlap of further atomic shells make structural models useful. Crystalline silicate and aluminosilicate were used as references. For the silicate glasses we used α-$SrSiO_3$ [2], where SrO_8 polyhedra are edge-connected to form sheets. 6 Sr-Sr pairs occurs at 4.116Å. For the aluminosilicate glass we used a feldspar, $SrAl_2Si_2O_8$ [3]. Sr is 7- or 9-fold coordinated and weak Sr-Sr correlations occur at 4.084Å. Experimental DG(r) functions were modelled with gaussian distributions up to 4Å. A broad oxygen distribution was added at higher distances. Results are given in Table 2. The quality of the adjustments can be judged from Fig.2.

	Sr-O R(Å)	**N**	**Sr-Si/Al R(Å)**	**N**	**Sr-Si/Al R(Å)**	**N**	**Sr-Sr R(Å)**	**N**
S	2.68	4	3.42	4.7	3.74	4.2	4.04	3.8
SAl	2.58	6.3	3.3	4	3.71	4	3.95	3.4
A	2.56	6	3.22	4.5	3.68	4	4.04	<1.5

Table 2 : Modelling of the environment of Sr. N is the number of neighbors for each shell.

For glasses SAl and A the first oxygen shell can be modelled by about 6 oxygens at 2.58Å. The coordination polyhedron for these glasses would then be smaller than in crystals. Another possibility is that the oxygen shell is asymmetric and that there is a broad contribution at higher distances. However none of these two models can be favored. For glass S the adjustment of the first oxygen shell is questionable, because of the higher distance and lower number of neighbors. It is known that distortion of the signal in reciprocal space results in peaks in real space which superimpose on structural features. In favorable cases however these errors are concentrated at low r values and do not distort higher shells.

Major Sr-Sr correlations arise at short distances in the silicate glasses whereas such correlations, if present, are much weaker in the aluminosilicate glass A. In the silicate glasses the Sr coordination polyhedron and Sr-Sr distances at 4Å and (most probably) 7Å are consistent with 2D-domains of edge-sharing octahedra. The environment of Sr in these simple silicates is similar to that of Ca in $CaSiO_3$ glass [4].

This AWAXS study of Sr-bearing silicate and aluminosilicate glasses reveals a well-defined short-range structure around Sr for all glasses. Evidence of medium-range organization around Sr is found to about 8Å in the aluminosilicate and 10Å or more in the silicates. In the aluminosilicate glass this medium-range organization is not dominated by Sr-Sr correlations but probably by relations with the aluminosilicate sub-network. This contrast in the medium-range structure of Sr in the silicate and aluminosilicate glasses reflects the different role played by this cation in the structure : in the simple silicates Sr acts as a "modifier" whereas in the aluminosilicate glass it compensates the charge of Al^{3+}.

IV. PRELIMINARY RESULTS ON A FE^{2+} -BEARING SILICATE GLASS

The local environment of Fe^{2+} in silicate glasses is still a matter of controversy, in spite of numerous studies (optical, Mössbauer and X-ray absorption spectroscopies mainly). AWAXS was used to clarify the medium-range environment of Fe^{2+}. A hedenbergite $CaFeSi_2O_6$ composition was chosen, which allows comparison with already studied $CaSiO_3$ and $Ca_2NiSi_3O_9$ compositions.

The first step of the synthesis was to prepare a gel with Fe- and Ca-nitrates and TEOS [5]. The gel was dessicated and calcined at 900K. The glass was melted in a vertical furnace with CO/CO_2 atmosphere to control oxygen fugacity ($fO_2=1O^{-7.5}$, T=1623K). Alloying of Pt-crucibles with Fe in iron-bearing reduced melts [6] was overcome by use of Pt-loops and enrichment of the gel with 2 wt% of metallic iron. The average composition of the final glass is $Ca_{0.047}$ $Fe_{0.045}$ $Si_{0.207}$ $O_{60.36}$.The green color of the material indicates that the majority of iron is in the reduced form.

AWAXS on iron is more difficult than on strontium : first the low energy of the iron K-edge (7111 eV) allows only a small k-range (0-6 $Å^{-1}$) to be explored. The major drawback of this limited k-range is the poor resolution in real space. Second, correlations due to Fe-Fe and Fe-Ca pairs will be hard to identify because of similar weights for these pairs in the differential functions.

The differential structure factor is of relatively poor quality (Fig.3), which results in a high non-structural peak around 1.8Å (Fig.3). This artefact precludes any information on the coordination polyhedron in this silicate glass. However Fe-Fe distances around 3.2 and 5.8Å are probable. This short Fe-Fe distance is almost the same as in the crystalline structure, hedenbergite (3.1Å) where pairs of Fe-centered octahedra share edges.

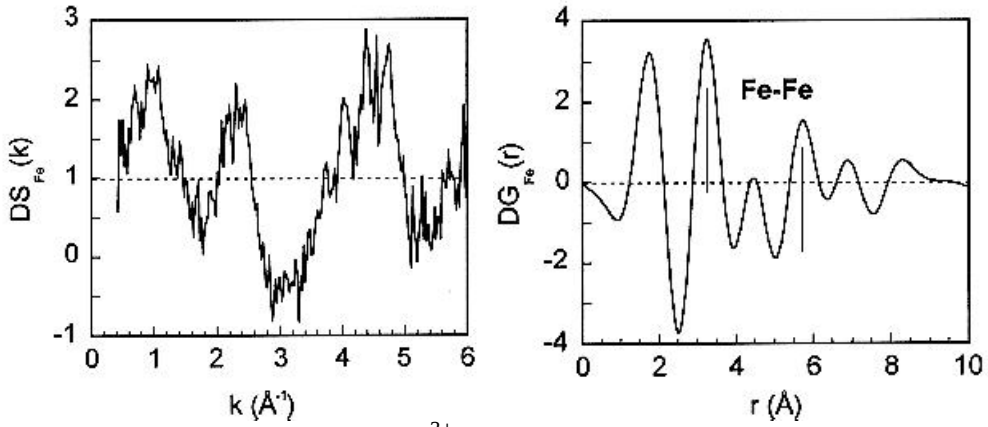

Fig. 3 : (left) DS(k) for Fe^{2+} in $CaFeSi_2O_6$ glass. (right) DG(r).

V. IMPACT ON THE OPTICAL PROPERTIES OF IRON IN SILICATE GLASSES

Recent studies of medium-range structure in silicate glasses reveal extended order around non-network forming cations such as Ca^{2+}, Sr^{2+}, Ni^{2+} and probably Fe^{2+} . These results have two implications for optical properties. First, an extended medium-range order implies that the short-range order (site) is well-defined and not very much distorted.

Second it implies that the second neighbor shell is not random. Optical properties of cations such as Fe^{2+} and Fe^{3+} are known to be determined by the site of the absorbing element. However these properties are also influenced by medium-range structure, through the effective charge carried by oxygens. Indeed huge modifications of the broad absorption band of Fe^{2+} around 10000 cm^{-1} were observed in various silicate glasses [7]. The position of the maximum absorption of this band is related to the silica content (that is to the average number of non-bridging oxygens) and to the type of cations in the composition. Not only the position, but also the shape of this broad, most probably non-unique band change with the matrix composition.

Ferrous iron is expected to act as a modifying element. However the smaller absorption band around 5000 cm^{-1} has been assigned to a tetrahedral site [8]. Then in silicate glasses, part of the ferrous iron might be modifier, and part of it could substitute for silicon. According to the traditional view ferric iron is expected to substitute for silicon and therefore to act mainly as network-former. A mixture of tetrahedral and octahedral sites has sometimes been proposed for Fe^{3+} in silicate glasses [9]. Such results indicate that (i) the site each species can occupy is not unique (ii) one species could play several roles in a given composition (for example network-former and network-modifier).

Ferric and ferrous iron might then have two types of environment, depending on which sub-network they belong to. Within the silica-rich network, cations can substitute for Si, if there is adequate charge compensation. Local charge balance on oxygens makes Fe-O-Fe links unlikely. Iron may also be concentrated within modifier-rich domains, such as those which have been observed for Ca and Sr. Short Fe-Fe distances could account for changes in the molar absorption coefficient.

VI. CONCLUSION

AWAXS shows that in simple silicate glasses "modifying" cations such as Sr^{2+} and Fe^{2+} can have well-organized local environments (up to distances of about 1 nm). The environment of these cations is different when they act as charge-compensator in aluminosilicate compositions. Spectroscopic studies of dilute Fe^{2+} and Fe^{3+} in complex matrices show a variety of sites for each species. The influence of the matrix composition on optical spectra can be accounted for by modifications of these sites' populations and of the charge on the oxygens.

ACKNOWLEDGMENTS

This work represents part of the doctoral research project of S. Creux at the Université Paris 6. We wish to thank B. Bouchet (LURE) and P.H. Gaskell (Cavendish Lab.) for help and advice.

BIBLIOGRAPHY

1. Eckersley, M.C., et al., Structural ordering in a calcium silicate glass. Nature, 1988. 335: p. 525-527.
2. Machida, K.-I., et al., Structure and high-pressure polymorphism of strontium metasilicate. Acta Cryst. B,1982. 38: p. 386-389.
3. Chiari, G., M. Calleri, and E. Bruno, The structure of a partially disordered, synthetic strontium feldspar. Am. Mineral.,1975. 60: p.111-119.
4. Gaskell, P.H., et al., Medium-range order in the cation distribution of a calcium silicate glass. Nature,1991. 350: p. 675-677.
5. Biggar, G.M. and M.J. O'Hara, A comparison of gels and glass starting materials for phase equilibrium studies. Mineral. Mag.,1969. 37: p.198-205.
6. Donaldson, C.H., Composition changes in a basalt melt contained in a wire loop of $Pt_{80}Rh_{20}$: effects of temperature, time, and oxygen fugacity. Mineral. Mag.,1979. 43: p.115-119.
7. Combes, J.-M., G. Calas, and S. Creux. Influence of field strength parameters on the optical spectra of iron-containing silicate glasses. in XVII International Congress on Glass 1995. Beijing, China.
8. Calas, G., et al., Etude de l'ordre local autour du fer dans les verres silicatés naturels et synthétiques à l'aide de la spectrométrie d'absorption X. Rev. Phys. Appl.,1980.15: p.1161-1167.
9. Virgo, D. and B.O. Mysen, The structural state of iron in oxidized vs reduced glasses at 1 atm : a ^{57}Fe Mössbauer study. Phys. Chem. Minerals,1985.12: p. 65-76.

RHEOCONDUCTOMETRIC MEASUREMENTS IN CONTINUOUS CURRENT, FOR STANDARD VISCOMETER FIXED POINTS, CRYSTALLISATION RANGE AND ALKALI CONTENT DETERMINATIONS IN GLASS

V.Cazan-Corbasca, C.G>rlescu and **R.Nastase**
Institutul National de Sticla, Rumania

Abstract

The work presents a new conductometric method of measurement, using the c.c. resulted from a global cation flux of Na_2O, K_2O, Li_2O, moving in molten glass structure, under a standard electrical potential. This method is able to measure viscosities, crystal growth, and alkali content in glass.

I. METHOD FOR VISCOMETER FIXED POINTS MEASUREMENTS THEORETICAL APPROACH

If we consider n_i cations separately or n_i aggregates of cations, under the form of vacancies (fixed negative charges) [1], in potential gaps, the general relationship of the conductivity, is [2] :

$$\sigma = nq\alpha = \frac{nq^2\delta^2\nu}{6KT}\exp(-\frac{U}{KT}) \qquad (1)$$

where σ is the electrical conductivity in c.c., n the number of cations in the ionical current, q the electrical charge of the cation, δ the lenght of the jump (hop) from one potential gap to another, in the next proximity, $\nu \approx (K/h)T$, K Boltzmann's constant, h Planck's constant, T the absolute temperature of the phenomenon and α the cation mobility (as interstitalcy).

The general condition for the cation moving, jumping over the potential barrier U_{st} is:

$$KT >> U_{st} \qquad (2)$$

In this conditions, the (1) relationship of conductivity is:

$$\sigma = \frac{nq^2\delta^2\nu}{6KT} \qquad (3)$$

The (3) relationship is typical to Arhenius' plots, for the molten soda-silicate glass [3].·The conclusion is that for every number n_i; of cations, being in the potential gap U_i

there is a particular contribution σ_i; in the total conductivity σ, of the ionical current, corresponding with:

$$\sigma(T) = \sum_{i=1}^{n} \sigma_i(T_i) = \frac{q^2}{6K}\left[\frac{\delta_1^2 v_1 n_1}{T_1} + \ldots + \frac{\delta_n^2 v_n n_n}{T_n}\right] \tag{4}$$

If the n_o is the total number of cations aggregates, one by one, in the unity of volume, between n_o and n_i it is:

$$n_O = n_1 + \ldots + n_n = \beta_1 n_O + \ldots + \beta_n n_O \tag{5}$$

$$\sum_{i=1}^{n} \beta_i = \beta_1 + \ldots + \beta_n = 1 \tag{6}$$

β_i (i=1,2,...,n) being the distribution function, attached to σ(T) function:

$$\sigma(T) = \frac{q^2}{6K}\left[\sum_{i=1}^{n} A_i \beta_i \frac{n_O}{T_i}\right] \tag{7}$$

$$A_i = \delta_i^2 v_i \tag{8}$$

Developing (7) we have:

$$\sigma(T_1) = \left(\frac{q^2}{6K}\right) A_1 n_O \left(\frac{\beta_1}{T_1}\right)$$

.....

$$\sigma(T_n) = \left(\frac{q^2}{6K}\right)(A_1 + \ldots A_n) n_O \left(\frac{\beta_1}{T_1} + \ldots + \frac{\beta_n}{T_n}\right) \tag{9}$$

and for the conductivity σ (T), as addition of all the contributions σ_i, we have:

$$\sigma(T) = \sum_{i=1}^{n} \sigma_i(T_i) = n_o \frac{q^2}{6K} \sum_{i=1}^{n} A_i \left(\frac{\beta_i}{T_i} \right) \tag{10}$$

where T_i can reach a particular value T_{tot}, corresponding with the temperature at which the total number of cations, one by one, form the ionical current.

If we must utilise the resistivity ρ, instead of the conductivity σ, (9) becomes:

$$\left.\begin{aligned} \rho_1(T_1) &= \frac{6K}{q^2}\left(\frac{1}{A_1}\right)\left(\frac{T_1}{\beta_1 n_o}\right) = \frac{6K}{q^2}\left(\frac{B_1}{n_o}\right)\left(\frac{T_1}{\beta_1}\right) \\ &\cdots\cdots\cdots\cdots\cdots\cdots\cdots\cdots\cdots\cdots\cdots\cdots \\ \rho_n(T_n) &= \frac{6K}{q^2}\left[\frac{(B_1+\ldots+B_n)}{n_o}\right]\left(\frac{T_1}{\beta_1}+\ldots+\frac{T_n}{\beta_n}\right) \end{aligned}\right\} \tag{11}$$

And for the resistivity ρ(T), and the totality of the n_o cations contribution, we have:

$$\rho(T) = \sum_{i=1}^{n} \rho_i(T_i) = \frac{6K}{q^2} \frac{1}{n_o} \sum_{i=1}^{n} \frac{B_i T_i}{\beta_i} \tag{12}$$

We must separate the conductivity or resistance phenomenon versus temperature in five distinct ranges, as follows:

- the first range includes the cationic aggregates, fixed in potential gaps (solid state range);
- the second range includes the cationic aggregates, entering gradually, in the ionic current (approximate 20% of the n_o aggregates per unity of volume) (transformation range). In this range the resistance of the ionical current decreases spectacularly, in a little interval of temperature and time;
- the third range includes the aggregates entered in the free volume V_f, of glass structure, in great number, forming a barrier in the way of the current and rejecting each other; in this range the resistance rises spectacularly, in a very little interval of temperature and time;
- the fourth range includes a more complex aspect, regarding that the resistance changes (decrease or increase) are influenced by two phenomena: the barrier of potential formed with accumulation of cations, or of the continuous increase of the n_o number of cations aggregates;
- the fifth range includes only cations circulating, in the free volume, one by one. In this range, the aggregates of cations (e.g. interstitalicis) are disaggregated by the thermal agitation of the glass structure in the liquid state.

ll. EXPERIMENTAL RELATIONS AND RESULTS

It is necessary, sometime, for measurement problems, to utilise directly, the ohmical resistance in c.c., function of temperature.

Beginning with the general relationship:

$$R = \rho\left(\frac{l}{S}\right) = \left(\frac{1}{\sigma}\right)\left(\frac{l}{S}\right) \tag{13}$$

where l is the distance between the electrodes of measurement, and S is the surface of the electrodes. It is possible to exprime the function β, substituting (1) in (13):

$$R = \frac{1}{n_O q\alpha}\frac{l}{S} = \frac{1}{\left(\sum_{i=1}^{n} n_i\right)q\alpha}\frac{l}{S} \tag{14}$$

Developing the conductivity σ from (14), we have:

$$\left.\begin{aligned} &\sigma(T_1) = \frac{q^2}{6K} A_1 n_O\left(\frac{\beta_1}{T_1}\right) = \left[\frac{1}{R(T_1)}\right]\left(\frac{l}{S}\right) \\ &\cdots\cdots\cdots\cdots\cdots\cdots\cdots\cdots\cdots\cdots\cdots\cdots\cdots\cdots\cdots\cdots \\ &\sigma(T_n) = \frac{q^2}{6K} n_O(A_1+\ldots+A_n)\left(\frac{\beta_1}{T_1}+\ldots+\frac{\beta_n}{T_n}\right) = \left[\frac{1}{R(T_1)}+\ldots+\frac{1}{R(T_n)}\right]\left(\frac{l}{S}\right) \end{aligned}\right\} \tag{15}$$

finally the capital group of relationships being:

$$\beta_1 = \frac{T_1}{R(T_1)};\ \ldots\ ;\ \beta_n = \frac{T_n}{R(T_n)} \tag{16}$$

The distribution function β_i is applicable in the range between the ambient temperature and T_{tot}. But with the (16) it is possible to determine the annealing point (ν_{13}), in the transformation range, plotting β function versus temperature. Plotting R = f(T) in the transformation range, the method obtains also the other viscometer fixed points ν_{14} and t_g. There have been realised measurements with this method on a reference glass N.B.S. 710 (soda-lime-silica glass). The results are presented in Table 1 (The measured values are the average of 8 results)

Table 1

V.F.P		Values Buletin	Measured values	Error
		^{o}C	^{o}C	%
Annealing Point	ν_{13}	546	542.5	- 0.64
Transf. temp.	t_g	537	538	0.19
Strain point	ν_{14}	504	505	0.19

III. CONDUCTOMETRIC MEASUREMENTS, IN C.C. FOR CRYSTALLIZATION (DEVITRIFICATION) RANGE. THEORETICAL APPROACH

Thurnbull and Cohen[5] give a dependence of the viscosity η, of free volume V_f, with the relationship:

$$\eta = A\exp\left(\frac{DV_o}{V_f}\right) \quad (17) \qquad \text{where } V_O = V - V_f,\ D = const. \tag{18}$$

V_o being the occupied volume of the glass structure, V the total volume. The resistivity ρ is related to the viscosity:

$$\rho = \frac{\eta\delta}{n_o q^2} = A\left(\frac{\delta}{n_o q^2}\right)\exp\frac{D(V - CV_f)}{CV_f} \tag{19}$$

$V_\rho = CV_f (0 < C < 1)$, V_ρ being the circulation volume of the cations, and expressing that not the entire V_f is entering in the cations circulation. For more precision we have:

$$C = f\left(\frac{1}{n_o}\right) \quad (20) \qquad \text{and} \qquad V_f = \varphi(T) \tag{21}$$

and in conclusion:

$$V \approx f\left(\frac{1}{n_o}\right)\varphi(T) \tag{22}$$

The free volume V_f and V_ρ increase in continuous manner, with the temperature rising, C decreases with the n_o increasing. But in the second range of the resistivity, C decreases more abruptly, the circulation volume touching the value ($V_\rho \approx 0$). The result in an agglomeration of cations in the free volume V_f and an abrupt rise of R.

In the third range of conductivity the circulation volume V_ρ decreases modestly with the crystal growth due to the little density increasing of the glass structure. It results an increasing of R, due to the same decreasing value of C.

IV. EXPERIMENTAL RESULTS

In the table 2 it is given an experimental determination of the crystallisation range with the value of $T_{low.c}$, $T_{max.c}$. and $T_{upp.c}$, for three glasses. The crystals formation at the three temperatures, are verified by microscope observations. The rate of the crystal growth versus T, at $T_{max.c}$. is expressed by the rate of the resistance rise versus time.

Table 2a *Table 2b*

Glass	**Cryst. rate at $T_{max.c.}$**	**$T_{low.c}$.**	**$T_{max.c.}$**	**$T_{upp.c.}$**	**T**/t
	W/**min**	**°C**	**°C**	**°C**	**°C/min**
White ind. so-li-si	0.06	848	890	930	5
Brown ind. so-li-si	0	1090	1170	1235	3
Optical filter UV	0	1042	1046	1050	3

V. METHOD FOR ALKALI CONTENT MEASUREMENTS IN MOLTEN GLASS: THEORETICAL APPROACH

From the (13) relationship, we have:

$$R = \rho\left(\frac{l}{S}\right) = \left(\frac{6h}{n_o q^2 \delta^2}\right)\left(\frac{l}{S}\right) \tag{23}$$

and

$$n_o = \left(\frac{6h}{Rq^2\delta^2}\right)\left(\frac{l}{S}\right) \tag{24}$$

For obtaining δ, we proceed, as follows:

$$\eta = \frac{6KT}{\left(\frac{K}{h}\right)T\delta^3}; \qquad \delta = \left(\frac{6h}{\eta}\right)^{1/3} \quad \text{[see (2)]} \tag{25}$$

being considered as the ionic hop (jump) of Anderson-Stuart's model [6], and substituting in (24):

$$n_o = \left(\frac{\eta^{2/3}}{R}\right)\left(\frac{l}{S}\right)\left[\frac{(6h)^{1/3}}{q^2}\right] \tag{26}$$

We have:

$$\left[\frac{(6h)^{1/3}}{q^2}\right]\left(\frac{I}{S}\right)=C' \qquad (27) \quad \text{and} \quad n_O = C'\left(\frac{\eta^{2/3}}{R}\right)$$

(28)

VI. PRACTICAL FORMULA FOR ALKALI CONTENT DETERMINATIONS IN GLASS.

The method is described for a glass with two alkali (Na_2O and K_2O). Considering ρ_{st} the density of glass at the temperature of measurement, the molecular mass M_{Na2O} and M_{K2O} and N Avogadro's number, the capital relationship for the alkali content measurement, resulted from (26) is:

$$m_{(Na_2O+K_2O)} = \left[\frac{50M_{(Na_2O+K_2O)}}{q^2}\frac{(6h)^{1/3}}{N}\frac{I}{S}\right]\frac{\eta^{2/3}}{R\rho_{st}} \qquad (29)$$

VII. PRACTICAL RESULTS

In the table 3 are shown values of global alkali content (Na_2O+K_2O) in a reference glass NBS-710 (soda-lime-silica). The I/S was determinated geometrically.

Table 3

Temperature	m value bulletin	m* measured value	Error
^oC	%	%	%
1345	16.4	16.27	-0.8

VIII. CONCLUSIONS

Excepting the practical purposes of the work, it is possible to assume a theoretical aspect: that the (29) relationship is valid, only for a temperature at which the alkali cations are moving in the glass structure, one by one, interstitialcies being destroyed by thermal agitation.

REFERENCES

1. Charles R.F. (1962) J.Am.Cer.Soc. 45,105
2. Hench L.L. and Schaake H.F. Electrical Properties of Glass in Introduction to Glass Science edited by L.D.Pye, H.J.Stevens, W.C.LaCourse Plenum Press N.Y.London 1972
3. Ingram M.D. (1985) Physics and Chemistry of Glasses Vol.28, No.6, December 1987
4. Certificate of Viscosity Values Standard Sample No.710 Soda-lime-silica glass N.B.S. Dep.of.Com.Nat.Bureau of Standard Washington 25 D.C.
5. Thurnbull D. and Cohen M.M. (1959) J.Chim.Phys 31.116
6. Anderson O.L. and Stuart D.A. (1954) J.Am.Cer.Soc.37.573

STRUCTURAL CLASSIFICATION OF OXIDE GLASS MELTS

G. Herms, W. Gerike and **J. Sakowski**
Rostock University, Germany

Abstract

A few selected experimental results are presented in order to show that there are different types of oxide glass melts. An outline of order is proposed supporting on 4 basic types of melts.

I. INTRODUCTION

In 1968 Riebling stated, "The structures, or distributions of different polyhedral species, of an oxide melt and its corresponding glass are not very different" [1]. This opinion on the short range order (SRO) of molten glasses seems to be widely held up to now. The condition SRO(glass) = SRO(melt) has even been considered to be a suitable definition of the vitreous state [2].

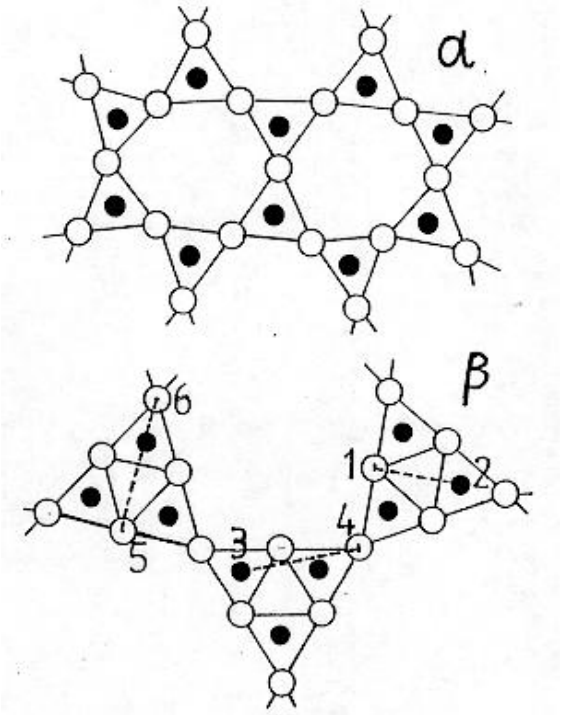

Fig.1: Structure models for vitreous B_2O_3
a) random continuous network of BO_3 units (O oxygen, · boron).
b) network of boroxol groups 1,2: BO distance of 2.74 Å
3,4: BO distance of 3.6 Å
5,6: OO distance of 4.1 Å

Of course, the whole discussion depends on what is associated with the notation "SRO". Some authors restrict "SRO" to the first coordination shells sometimes even to the shortest distances and coordination numbers only. This view, however, is obviously too narrow because in that case the two structures, shown in Fig, 1, would have to be described as structures with the same SRO. This would be at least inexpedient as actual distinctions would then be disguised. On average all oxygen atoms in structure α have the same neighbourhood while in structure β 67 % of the oxygens see their B neighbours at an angle of exactly 120^o and 33 % at an angle of about 180^o. (The immediate neighbourhood of the borons is obviously the same in both structures.) In order to be able to differentiate one has to include the angular relationships or else to use "SRO" in a broader sense. If we include larger distances, we will find distinct differences between the two structures in Fig. 1. Structure β has a sharp and frequent BO distance of 2.74 A, which does not at all exist in structure α. Besides this, well-defined distances in structure β (e.g. OB = 3.6 A and OO = 4.1 A) have corresponding counterparts in structure α only by chance. This means, the corresponding peaks in the radial distribution function (RDF) of structure α are very much lower and broader.

Bearing this example in mind it should be clear that "SRO" is more than the inner coordination shell. From a utilitarian point of view all that should be considered as SRO what can be derived from RDF. At least the distance range up to 5 or 6 A should be classified as SRO. This would go well together with the fact that structure features "existing on a length scale of, say, 5-20 A" are considered to be medium range order (MRO) [3].

After clarifying the term "SRO" we turn towards the question of what kind of structural changes can be expected if a glass is liquified by heating. The viscous flow is the main point in which solid glass and melt differ. Especially in case of a typical network glass (e.g. SiO_2 or B_2O_3) the visualizing of the melting process is not so easy. In the vitreous state there is a very extended random continuous network, rigidly held together by strong Si-O or B-O bonds, respectively. With increasing temperature the network separates into network fragments, the size of which decreases with increasing temperature. In case of B_2O_3 possible mechanisms were suggested by Mackenzie (—B=O grouping) and by Sperry and Mackenzy as well as Riebling (edge sharing BO_3 triangles) [4-6]. In this connection it must be stated that the idea of constant fragments, being distinctly separated from each other and always made up of the same atoms, is surely wrong. As pointed out by Krogh-Moe it is not necessary to postulate really unattached network pieces to account for a comparatively low viscosity [7]. It might be sufficient that accessible activated states exist and that this way a flow process becomes possible. The mentioned —B=O groupings and boron atoms with mechanically induced coordination change [7-8] could serve as such states.

Neither the activated states nor the separation into unattached pieces might have a great effect on the SRO parameters (even if a very extreme and unrealistic idea of "separation" is used). As stressed by Krogh-Moe the equilibrium concentration of the activated states is small, so that they are not discernible by structural investigations. But also the network decomposing (the splitting into pieces) has no chance to be reflected in the radial distribution functions unless the pieces become extremely small. As far as the scattering curve is concerned, however, an effect can be expected. It has been shown by

model calculation [9] that already 3 or 4 anion polyhedra, connected in the right manner, are sufficient to reproduce the typical shape of the scattering curve apart from the main peak. This means, on the other hand, that the far-reaching connection of the polyhedra within the network, the boundaries of the network pieces, the voids between them, and similar features reveal themselves in the main peak. The whole is a matter of MRO.

II. EXPERIMENTAL

Using modern X-ray diffraction equipments and an unconventional heating technique we have studied a selection of binary borate and phosphate glasses in the liquid state. The glasses were prepared at the Otto-Schott-Institute, Jena.

The measurements were accomplished in 3 different ways. At first a rotating anode and a conventional counter diffractometer with transmission geometry was used [10]. Shorter measuring times could be attained by means of a bent position sensitive detector and later on by using synchrotron radiation in connection with image plates.

The heating device excels in the fact that the primary X-ray beam is scattered by the melt only, in other words, parasitic scattering of windows, container walls etc. is avoided. Besides the device is rather universally applicable to normal glass melts and allows high heating- and cooling-rates [11].

III. RESULTS

The few earlier high-temperature diffraction studies seemed to show that both the scattering curves and the RDF curves indicate no changes caused by melting, leaving aside the main peak of the scattering curves. Just vitreous B_2O_3 is an example of a glass the scattering curve of which seems to show no alterations with rising temperature, excluding however the main peak. This peak is more and more increased and shifted to lower scattering angles if the temperature is increased. It is reasonable to suppose that the structural changes are limited to the decomposing of the network without altering the SRO. Although it is true that the scattering curve and the RDF contain the same information, such far-reaching conclusions on the structure require the consideration of the RDF too. Since Misawa [12] found no changes in the RDF of vitreous B_2O_3 this glass has seemed to be a textbook example of Riebling's view on melt structure. Recently accomplished measurements [13] show, however, that in actual fact the SRO is altered in a sense illustrated in Fig. 1. A change from structure β to structure α takes place during melting. In other words, in addition to the decomposing the network is altered in its topology too. This result confirms relatively unknown findings by Strong [14] and is in accordance with the results of NMR measurements [15-16] and Raman studies [17]. For the solid glass the boroxol group model seems to be well established [18-21].

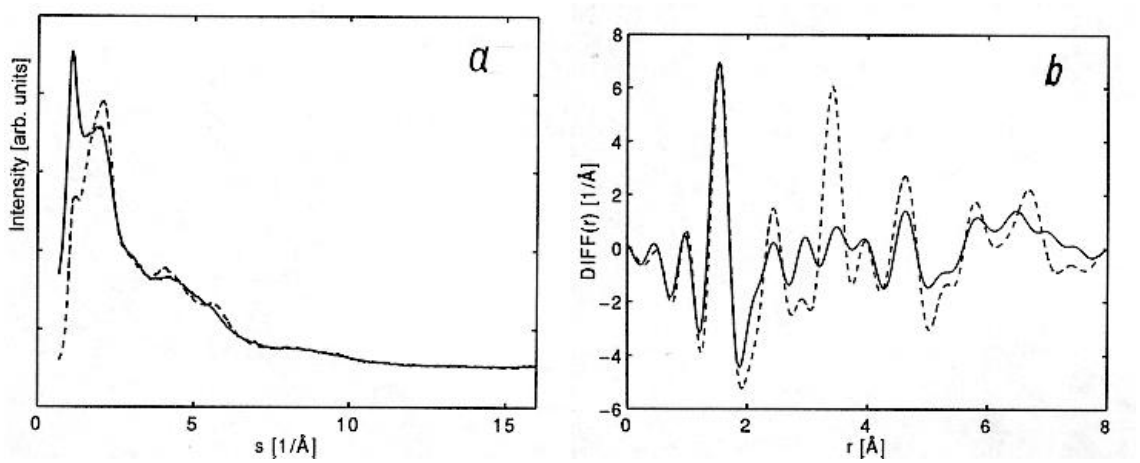

Fig. 2: Sodium metaphosphate glass (dashed line: room temperature, solid Iine:1020 K)
a) scattering curve
b) difference distribution function

As can be seen the supposed similarity between solid glass and melt turns out to be a consequence of inaccurate measurements. The question arises whether there are any glasses at all which meet the condition SRO(glass) = SRO(melt). To all appearances vitreous SiO_2 seems to be such a glass, and perhaps several of the silicate glasses studied by Waseda [22]. In any case glasses of such kind seem to be rarer than commonly assumed. E.g., in spite of nearly unchanged diffraction patterns, binary borate glasses with a low modifier content (approximately 12 mol % Na_2O or Li_2O, respectively) show a temperature-dependent change of the SRO, which is similar to the change in vitreous B_2O_3.

A drastic change of the SRO takes place in sodium metaphosphate glass. In this case already the scattering curve (Fig. 2a) shows remarkable alterations with increasing temperature. The one is the generation of a strong first sharp diffraction peak during heating up and is produced by changes of the MRO [23]. The other alteration occurs in that part of the scattering curve which is determined by the SRO. Two well separated diffraction maxima were replaced by one broad maximum if the glass becomes liquid. The RDF reveals that a very frequent atomic distance of 3.5 A disappears during melting (see Fig. 2b). It is known from model calculations that the structure of the solid glass can be described as a distorted version of Kurrol's salt and that the peak at 3.5 A reflects Na-P and Na-Na distances [24]. In the course of the melting process the sodium ions obviously move into other sites. The increased vibrational and diffusive motion of the sodium ions due to elevated temperature requires more space and probably leads to an increased separation distance or to an stretching of the PO_4 tetrahedra chains in the melt [23]. The result is a structure which has no resemblance to any crystalline form of sodium metaphosphate. A similar kind of behaviour is found with related glasses, e. g. with calcium metaphosphate glass.

Another kind of structural change seems to occur if borate glass with a higher content of modifier oxide is liquified. In Fig. 3 the scattering curves of solid and molten sodium borate glass with 29 mol% Na_2O are shown.

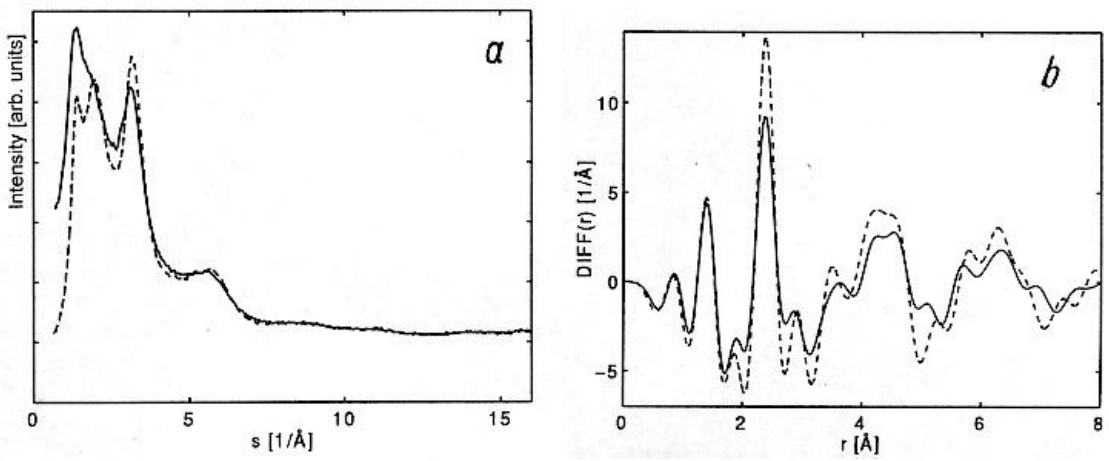

Fig. 3: Sodium borate glass, 29 mol% Na_2O (solid line :1120 K, otherwise like Fig.1)

The curves differ not only at smaller scattering angles, where the first sharp diffraction peak increases with temperature, but also in the further course. This indicates changes of the SRO. In contrast with sodium metaphosphate the RDFs show no big differences in the distance range 3 A up to 5 A. In the melt the BO peak at 1.4 A and the OO peak at 2.4 A is somewhat lowered, which could be interpreted as a sign of a decrease of NBO_4, the fraction of 4-coordinated boron atoms, with increasing temperature. This would be in accordance with convincing arguments by Visser and Stevels [25] and Araujo (26]. However, the conclusiveness of our measurements is still insufficient. A much higher expenditure is necessary to prove the supposition. Recent in situ, high temperature NMR studies give no insights into the problem [16, 27].

IV. DISCUSSION

Our wide angle X-ray studies on molten oxide glasses show that it is necessary to differentiate between several types of glass melts. There seem to be 4 basic types:

1. Type I is characterized by the fact that the mutual connection between the anion polyhedra remains unchanged in the course of melting and that the change of the network is mainly confined to the process of decomposing.
2. For type II the decomposing of the network is coupled with an alteration of its topology.
3. For type III it is essential that the spatial connections between modifier ions and surrounding anion polyhedra are distinctly changed during the melting process.
4. The essential feature of type IV is a conversion of the smallest network units simultaneously occurring during the network decomposing.

to 1) Type I should be called "Riebling's type" because it fully corresponds to Riebling's idea of melt structure. Perhaps vitreous silica belong to this type. We must bear in mind, however, that for this glass T_g is very high and that the accuracy of the diffraction results, which have been existing up to now, is still insufficient at the required temperatures.

to 2) For pure glass formers or glasses with a very small content of network modifying oxides bond breaking and new tying represent the one and only way to change markedly the SRO.

to 3) This kind of change might be the main way for glasses with a higher content of modifier oxide. Bond breaking within the loose network or within the polyhedral chains or rings is relatively unimportant. In interaction with the network modifier ions the polyhedral chains alter their shape (by straightening or puckering) or the space between themselves.

to 4) This type is connected with a transition in first coordination and, in all probability, limited to glasses containing B_20_3 or GeO_2.. Type IV should be denoted as "Dietzel's type" because he was the first to assume a coordination change due to temperature increase in borate melts [28].

In general a given glass is a mixed type. To quote an example: A binary borate glass with a low content of modifying oxide (let us say 10 mol%) is of the mixed type II/IV.

Acknowledgement

The authors are grateful to Mrs. Prof. D. Stachel, Jena, for preparing the glasses and to BMBF for financial support (FKZ 03-HE4ROK-0).

REFERENCES

[1] E. F. Riebling, J. Amer. Ceram. Soc.**51**, (1968) 143
[2] P. K. Gupta, J. Non-Cryst. Solids **195,** (1996) 158
[3] S. R. Elliot, Physics of Amorphous Materials, Longman, London 1990, p.139
[4] J.D. Mackenzie, J. Phys. Chem.**63,** (1959) 1875
[5] L. L. Sperry a. J. D. Mackenzie, Phys. Chem. Glasses **9,** (1968) 91
[6] E. F. Riebling, J. Amer. Ceram. Soc.**49,** (1966) 19
[7] J. Krogh-Moe, J. Non-Cryst. Solids **1,** (1969) 269
[8] A. Feltz, Amorphous Inorganic Materials and Glasses, VCH Weinheim 1993, p.197
[9] R. Strauch, Phasentrennung in SiO_x, Diploma Thesis, Rostock 1985
[10] G. Herms a. F. Hajdu, J. Appl. Cryst.**17,** (1984) 140
[11] G. Herms, W. Gerike, J. Sakowski a. S. Weyer, Meas. Sci. Technol.**7**, (1996) 627
[12] M. Misawa, J. Non-Cryst. Solids **122,** (1990) 33
[13] G. Herms, W. Gerike a. J. Sakowski, HASYLAB Jahresbericht 1995, Vol.**2**, p.1041
[14] S. L. Strong, Ph. D. Thesis, MIT 1965/66, cited in [7]
[15] M. Rubinstein, Phys. Rev. B **14**, (1976) 2778
[16] J. F. Stebbins, S. Sen a. A. M. George, J. Non-Cryst. Solids **192** & **193** (1995) 298
[17] G. E. Walrafen, S. R. Samanta a. P. N. Krishnan, J. Chem. Phys.**72**, (1980) 113
[18] R. L. Mozzi a. B. E. Warren, J. Appl. Cryst.**3,** (1970) 251
[19] R. N. Sinclair, J. A. E. Desa, G. Etherington, P. A. V. Johnson a. A. C. Wright, J. Non-Cryst. Solids **42**(1980) 107

[20] G. E. Jr. Jellison, L. W. Panek, P. J. Bray a. G. B. Jr. Rouse, J. Chem, Phys. **66** (1977) 802
[21] R. E. Youngman, S. T. Haubrich, J. W. Zwanziger, M. T. Janicke a. B. Chmelka, Science **269**, (1995) 1416
[22] Y. Waseda, The Structure of Non-Crystalline Materials, New York 1980
[23] U. Hoppe, G. Herms, J. Sakowski a. W. Gerike, submitted to J. Phys.: Condens. Matter
[24] G. Herms, U. Hoppe, W. Gerike, J. Sakowski a. S. Weyer, Proceedings of XVII Internat. Congress on Glass, Beijing 1995, Vol.**2**, p.110
[25] T. J. M. Visser a. J. M. Stevels, J. Non-Cryst. Solids **7,** (1972) 376
[26] R. J. Araujo, Phys. Chem. Glasses **20,** (1979) 115
[27] Y. Inagaki, H. Maekawa a. T. Yokokawa, Phys. Rev. B **47,** (1993) 674
[28] A, Dietzel, Glastechn. Ber.**22,** (1948) 12

STRUCTURE of K_2O-TiO_2-SiO_2-F-Cl GLASSES

James E. Dickinson Jr.
Corning Incorporated, U.S.A.

Abstract

Raman spectra have been collected for a series of glasses in the (20-x) K_2O*xTiO_2*80SiO_2 ± $K_2F_2(Cl_2)$ system to understand the structural role of Ti in alkali silicate glasses and to investigate the role of F and Cl in modifying the structure of these glasses. The effect of Ti substitution in the base glass is to develop strong bands at 914 cm^{-1} and 990 cm^{-1}. Based on comparison with spectra of alkali titanate crystals and the systematic spectral changes observed for other highly charged cations in alkali silicate glasses, these two bands are assigned to short Ti-O bonds in 5-coordinated polyhedra and Q_3 (Si-O-Ti) species, respectively. Substitution of F for O decreases the intensity of the 914 cm^{-1} band and results in a new band as a shoulder at ~870 cm^{-1}, indicating that F preferentially replaces the short Ti-O bonds. Substitution of Cl for O primarily increases intensity in the 440 cm^{-1} region, indicating that the glass is becoming more polymerized.

1. INTRODUCTION

Titanium is frequently added to glasses to act as a nucleating agent for the production of glass-ceramics. Fundamentally, the effectiveness of Ti as a nucleating agent depends on its structural role in the glass of interest, which is, in turn, governed by its interactions with other components of the glass. In this regard, there have been numerous studies of the structural role of Ti in silicate glasses of various compositions [1,2 and references therein]. Nevertheless, these studies are not always in agreement and, in addition, provide no information on how the incorporation of other anionic species (F and Cl) affect the structural role of titanium. This study will first present new data on the structural role of Ti in F and Cl-free alkali silicate glasses and then will follow with data on the effects of the substitution of F and Cl for oxygen.

2. EXPERIMENTAL

Glasses without F and Cl were synthesized by ball-milling the appropriate mixtures of oxides and carbonates. The mixtures were charged into Pt crucibles, covered, and melted for 8 hours at 1500^oC. The melts were poured onto steel plates and allowed to cool. The F and Cl bearing glasses were prepared in a similar manner except that part of the K_2O was batched using KF or KCl. This is equivalent to batching the halides as $K_2F_2(Cl_2)$ and assures a direct F(Cl) for O substitution. Nominal compositions are given in Table 1.

Raman spectra were collected from polished rectangular pieces of glass using a SPEX 1403 double monochromator and a 90^o scattering geometry. The excitation source was the 514 nm line of an Ar^+ laser operating at about 500 mW. The power at the sample was about 10 mW. Entrance

and exit slits were adjusted to give 3 cm^{-1} resolution and spectra were taken by stepping in 2 cm^{-1} increments and counting for 2 seconds at each step. Parallel (HH) and perpendicularly (HV) polarized spectra were taken for each sample by rotating a polarizer placed between the sample and monochromator. There was no further manipulation of the data.

*Table 1. Nominal compositions of (20-x)K_2O*x$Ti_{1/2}$ O*8OSiO_2±K_2F_2(Cl_2) glasses*

Sample	K_2O (mole%)	$Ti_{1/2}O$ (mole%)	SiO_2 (mole%)	K_2F_2 (mole%)	K_2Cl_2 (mole%)
NTi	20.0	----	80.0	----	----
4Ti	16.0	4.0	80.0	----	----
8Ti	12.0	8.0	80.0	----	----
12Ti	8.0	12.0	80.0	----	----
4Ti2F	14.0	4.0	80.0	2.0	----
4Ti4F	12.0	4.0	80.0	4.0	----
4Ti4Cl	12.0	4.0	80.0	----	4.0

3. RESULTS

Glasses without F and Cl

Raman spectra of glasses with TiO_2 substituted for K_2O on a constant oxygen basis (i.e. $Ti_{1/2}O$ for K_2O) are shown in Fig.1. This substitution preserves the Si/O ratio and directly measures the "competition" or distribution of K and Ti over the available non-bridging oxygens (NBO's). As the figure indicates, NTi glass is characterized by strong polarized bands at 1100 cm^{-1} and 520 cm^{-1}, with weaker polarized bands at 592 cm^{-1} and 770 cm^{-1}. With substitution of $Ti_{1/2}$ O for K_2O a partially polarized band appears at 990 cm^{-1}, along with a polarized band at 914 cm^{-1}. In addition, a weak shoulder begins to develop at 380 cm^{-1}. As the Ti concentration is increased the bands at 914 cm^{-1} and 990 cm^{-1} increase in intensity relative to those characteristic of the Ti-free glass. The 990 cm^{-1} band shows no change in frequency while the 914 cm^{-1} band jumps in frequency from 914 cm^{-1} to 922 cm^{-1} between glasses 8Ti and 12Ti. The band at 770 cm^{-1} shifts to 820 cm^{-1} with increasing substitution of $Ti_{1/2}$ O for K_2O, and the weak shoulder originally present at 380 cm^{-1} continues to increase in intensity. In addition to the development of the band at 380 cm^{-1}, new bands are seen to develop in the 440-460 cm^{-1} region. Finally, there is a decrease in the relative intensity of the band at 1100 cm^{-1} with increasing TiO_2 content.

Glasses with F and Cl

Spectra of glasses with F and Cl substituted for oxygen are shown in Fig. 2. The original halide free composition is analogous to glass 4Ti. With a 2 mole % substitution of K_2F_2 for K_2O the relative intensity of the band at 914 cm^{-1} decreases and a shoulder develops to the low frequency side of this band at about 874 cm^{-1}. With increasing F for O substitution the 914 cm^{-1} band continues to decrease in intensity and the shoulder at 874 cm^{-1} becomes more well resolved. There are no other significant changes in the spectra.

In contrast to the effect of F for O substitution, Cl for O does not dramatically effect the intensity of the 914 cm^{-1} and there is no evidence of a new band at lower frequency as in the F-bearing glasses. The most noticeable changes that are observed are that the shoulder of the 1100

cm^{-1} band at 1150 cm^{-1} becomes more well resolved and there is a distinct shoulder developed to the low frequency side of the 520 cm^{-1} band at about 440 cm^{-1}.

4. DISCUSSION

This spectrum of the TiO_2-free glass is similar to previously published data (e.g. [3]), with the 1100 cm^{-1} band being assigned to a symmetric vibration from tetrahedra with one NBO (i.e. a Q_3 species, where the subscript indicates the number of bridging oxygens per tetrahedra). The 520 cm^{-1} band is assigned to symmetric stretching motions associated with Si-BO motions within an extended network of Q_3 species. As $Ti_{1/2}$ O is substituted for K_2O the predominant effect is to produce the partially polarized band at 990 cm^{-1} and the polarized band at 914 cm^{-1}. The band at 914 cm^{-1} has no counterpart in any spectrum of a silicate glass and, therefore, is due to formation of species involving Ti. The assignment of this band follows from Fig. 3 which shows the Raman spectrum of crystalline $K_2Ti_2O_5$, a compound in which Ti is 5-coordinated [4]. Individual polyhedra are connected together forming infinite Ti_2O_5 "sheets", with K atoms occupying interlayer positions. Interestingly, the Ti polyhedron is pyramidal with one short Ti-O bond at 1.57A and 4 longer Ti-O bonds between 1.91-1.99A. The short bond is to the interlayer K atoms, and is, effectively, a double bond. Factor group analysis of the vibrational modes of this compound show that the strong band at 900 cm^{-1} of the crystal is totally due to a symmetric motion of the short Ti-O bonds to the interlayer K atoms. The strong similarity of this band to that observed in the glasses, suggests a similar origin, i.e. a mode localized on Ti atoms with short Ti-O bonds. Also by analogy, it is likely that these short Ti-O bonds are to K atoms instead of forming, for example, Ti-O-Si linkages.

The band at 990 cm^{-1} falls in the range commonly assigned to Q_2 silicate species in glasses with divalent cation modifiers [5]. However, in glasses with divalent cation modifiers, this band is completely polarized, not partially polarized as observed here. Ellison and Hess and Ellison et al. [6,7] make a convincing argument based on spectra for other highly charged cations (Zr, Y, rare earths, and Nb) that this band is from a Q_3 species, with the "non-bridging oxygen" being connected to the highly charged cation (in this case Ti). Alkalis may also be located nearby to preserve local charge balance. In particular, Fig. 4 shows the spectrum of an alkali silicate glass with $Nb_{2/5}$ O substituted for K_2O. Except for the frequency difference of the strong polarized band at 874 cm^{-1}, it is quite apparent that there is a strong similarity between the spectra of Ti and Nb bearing glasses. In fact, Ellison et al. [7] conclude that Nb has a dual role, occurring as a discrete hexaniobate anion and as a more "traditional" network modifier. A similar conclusion is possible for Ti.

That is, Ti occurs both as a discrete titanate anion (although of unknown stoichiometry) as indicated by the 914 cm^{-1} band and as a "network-modifying" cation, forming Q_3 species as indicated by the partially polarized band at 990 cm^{-1} · With this in mind and with reference to the spectrum of $K_2Ti_2O_5$, the band at 380 cm^{-1} is likely to be due to Ti-O-Ti motions within the titanate anions. The presence of bands in the region near 440cm^{-1} and the shift in frequency of the 770 cm^{-1} band to 816 cm^{-1} are consistent with an increase in Q_4 species present in an extended silicate framework [3,5]. These changes are consistent with the idea that Ti is using K as a charge balancing cation, stripping it from its non-bridging position and forcing polymerization of the remaining silicate framework.

When F is substituted for O the decrease in intensity of the band at 914 cm^{-1} can be interpreted to indicate that F is preferentially replacing the short Ti-O bonds of the anionic titanate clusters. Furthermore, because of the charge difference between F and O, the overall cluster charge will decrease, leading to an overall decrease in the average polarizability of the cluster. This will also result in an intensity decrease. The new band at 874 cm^{-1} is assigned to Ti-F bonds formed by replacement of the short Ti-O bonds. Of interest also is the observation that F for O substitution does not effect the 990 cm^{-1} band. This indicates that the oxygens of the Q_3 (Si-O-Ti) type are stable against this substitution.

In contrast, Cl for O has little effect on either the titanate anionic clusters or Q_3 (Si-O-Ti) type species as indicated by the lack of change of these bands. The Cl for O substitution apparently effects the basic structure of the silicate glass. The increase in intensity near 440 cm^{-1} signifies the presence of an extended framework of Q_4 species, and while not well understood, the change in the spectrum in the 1150 cm^{-1} region is consistent with the conclusion that Cl is preferentially coordinating K, again striping it from its non-bridging position and resulting in an increase in the overall polymerization of the silicate framework. This interpretation is further born out by the observation that when attempts are made to add more Cl to the base composition, phase separation occurs.

5. CONCLUSIONS

Raman spectra of glasses with $Ti_{1/2}$ O substituted for K_2O at constant molar silica (a constant oxygen substitution) show that Ti forms anionic titanate clusters terminated by short Ti-O bonds. In addition, this substitution results in the formation of silicate Q_3 species, indicating that Ti also plays a role as a more "traditional" network modifying cation. This dual role behavior is remarkably similar to that observed for Nb in alkali silicate glasses [7].

The substitution of F for O preferentially replaces the short terminal Ti-O bonds of the anionic titanate clusters, but does not affect the oxygens of Q_3 (Si-O-Ti) species. In contrast, substitution of Cl for O primarily effects the alkali silicate framework, resulting in polymerization and eventual phase separation.

REFERENCES

[1] B. Mysen and D. Neuville, Geochim. et Cosmochim. Acta 59, (1995) 325.
[2] F. Farges, G.E. Brown, A. Navrotsky, H. Gan and J. Rehr, Geochim. et Cosmochim. Acta (1996) in press.
[3]D.W. Matson, S.K. Sharma and J.A. Philpotts, J. Non-Cryst. Solids 58, (1983) 323.
[4] S. Andersson and A.D. Wadsley, Acta Cryst.15 (1961) 663.
[5] P. McMillan, Amer. Mineral. 69, (1984) 645.
[6] A. Ellison and P.C. Hess, Geochim. et Cosmochim. Acta 58 (1994) 1877.
[7] A. Ellison, P.C. Hess and J.E. Dickinson, Phys. Chem. Minerals, (1996) in press.

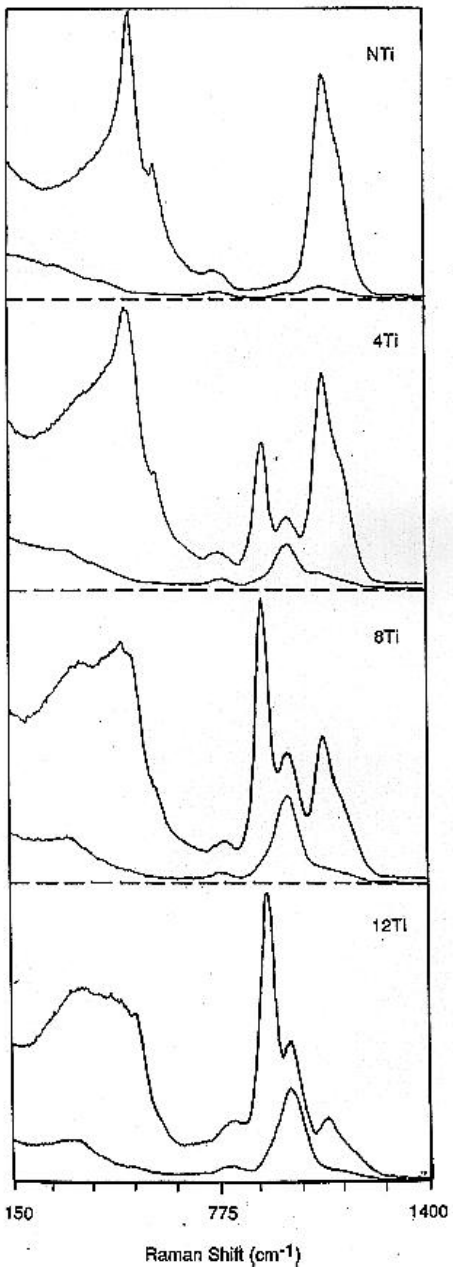

Figure 1. Parallel (upper) and perpendicularly (lower) polarized Raman spectra of alkali titanium silicate glasses. Compositions given in Table 1.

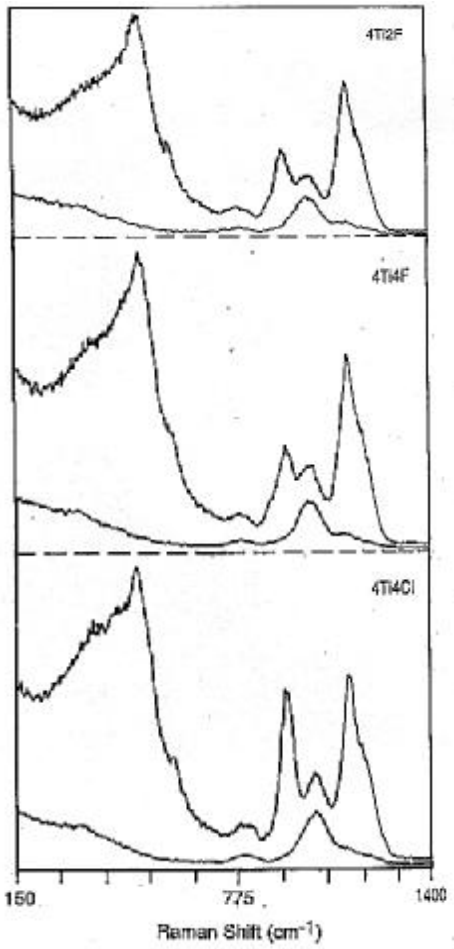

Figure 2. Parallel (upper) and perpendicularly (lower) polarized Raman spectra of alkali titanium silicate glasses with F and Cl substituted for oxygen. Compositions given in Table 1

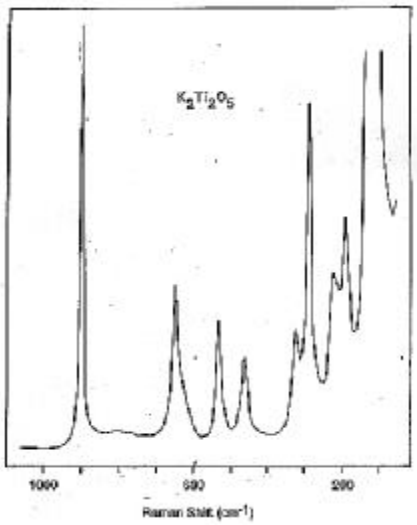

Figure 3. Raman spectrum of crystalline $K_2Ti_2O_5$.

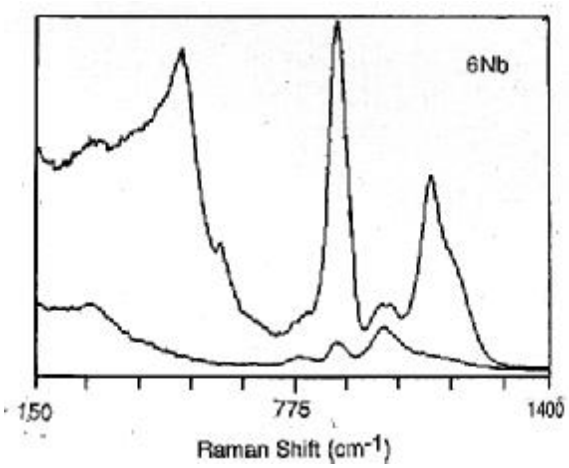

Figure 4. Parallel (upper) and perpendicularly (lower) polarized Raman spectra of a potassium nabium silicate glass with 6 mole % $Nb_{2/5}$ O substituted for K_2O

DEVELOPMENT AND PRODUCTION of 8.2 m ZERODUR MIRROR BLANKS FOR ESO'S VERY LARGE TELESCOPE (VLT)

Jürgen Petzoldt, Rudolf Müller, Hartmut Höness, and **Wolfgang Pannhorst**
Schott Glaswerke Mainz, Germany

Abstract

Since 1970, the glass ceramic Zerodur has demonstrated that it is a material of excellent choice for telescope mirror blanks, because of its near zero expansion, high homogeneity, besides other tailor-made properties for this application. In 1988, Schott Glaswerke received an order from ESO to deliver four Zerodur mirror blanks with 8.2 m in diameter, in the form of thin menisci. To produce such large monolithic pieces of glass ceramic, new melting, forming, ceramizing and machining processes had to be developed. Thanks to a new spin casting technology, the specification targets of ESO could be achieved. Today, production of all the blanks is completed. Three blanks are delivered to REOSC, where the finishing operation takes place. These three blanks have been accepted by ESO. The last blank will be delivered in summer this year. The results achieved were impressive: The mean value of the coefficient of thermal expansion was $-0.043 \times 10^{-6}\ K^{-1}$, with an uniformity of $0.0009 \times 10^{-6}\ K^{-1}$.

I. THE PROGRESS OF TERRESTERIAL TELESCOPE TECHNOLOGY

A driving force for the development of new terrestrial astro-telescopes is increasing the light intensity of the rays from space by enlarging the area of the light-collecting primary mirror. To achieve light-collecting areas of up to 50 m^2, three approaches are being realized:

1. Light-weighted mirrors with honeycomb support structure made from boro-silicate glass, where enforced cooling is supplied. Several telescopes are on the construction.

2. The Keck-telescopes are composed of 10 m primary mirrors consisting of 36 mirror segments each. Each segment measures 1.8 m in diameter and 90 mm in thickness. The problem is that an off-axis polishing method has to be applied, which means spherical polishing under bending stress. After polishing and moving the stress, an aspherical surface of the mirror blank is the result. The Mirror material of these telescopes is Zerodur. The two Keck-telescopes are operated by the University of California and the California Institute of Technology at the Maunia Kea volcano in Hawaii. It is planned to combine these two telescopes to achieve the performance of a 14 m instrument. The European Southern Observatory operates with a concept of four operative single telescopes with monolithic primary mirrors. Four telescopes with an aperture of 8.2 m are under construction. It is expected that, due to interferometric combination of beams collected by these four telescopes, the highest resolution ever known can be achieved. To realize this concept, the main problem was to get a rigid and sufficiently stiff mirror substrate 8.2 m in diameter, not deforming under its own

weight. For monolithic mirror blanks used for telescopes up to 4 m in diameter, a thickness:diameter ratio of 1:6 is needed. So, for an 8.2 m blank a thickness of 1.4 m would be necessary, which means a weight per piece of about 150 t. Construction of telescopes with such high-weighted mirror substrates are not economically feasible. With concept of active optics, ESO overcame this problem.

Numerous actuators support thin Zerodur menisci which at the same time adjust the contour of the mirror as closely as possible to its ideal shape.This concept allows thicknesses of the 8.2 m mirror blanks of 177 mm only, which is equivalent to a weight reduction of more than 85 %.This concept has been realized in ESO's 3.5 m New Technology Telescope with excellent results. To produce such relatively thin Zerodur menisci by machining thick-cast plane plates is mechanically and economically not feasible. So, a spin casting technology had to be developed by Schott Glaswerke. Application of the spin casting technology allows a yield improvement of nearly 100 %, which reduces production costs accordingly.

II. MATERIALS REQUIREMENTS FOR TELESCOPE MIRROR BLANKS

A material suitable for telescope mirror blanks has to meet the following specifications:

· Low thermal expansion within the temperature range of application (-30 - *70^{o}C), to avoid distortions due to temperature changes.

· Temperature dependence of the coefficient of thermal expansion within the temperature range of application must be extremely low.

· High natural stability and low specific weight must avoid mechanical deformations.

· Heat transfer coefficient should be high to avoid temperature gradients within the blanks.

· The material has to be ground and polished in order for optical surfaces with mean deviations of $\pm 1.3 \times 10^{-5}$ mm (NTT-Specification) to be achieved.

· Corrosion resistance and chemical durability must be high to apply aluminum coating to the mirror substrates. Aluminum coatings are the mirror material, to be removed from time to time to guarantee a high performance of the Aluminum mirror. The mirror substrate material has to withstand leaching, cleaning and drying processes, without development of any defects on its high-quality optical surfaces.

· Melting, casting, forming and ceramizing processes have to result in high-volume blanks of high homogeneity and an extremely low level of inclusions and striae. The homogeneity of the coefficient of thermal expansion within an 8.2m blank has to be lower than 0.05×10^{-6} K^{-1} .

· Material must be a transparent one for the wavelengths of visible light, to allow economical quality control of the material. Comparison of the properties of the glass ceramic Zerodour with alternative materials shows that TiO_2-doped silica (ULE) nearly has similar properties. Silicon carbide, with its relatively low coefficient of thermal expansion, its low specific weight, and its higher heat transfer coefficient could be an alternative material to glass ceramics or ULE, but until now pieces with high volume and high homogeneity are technically not yet feasible. The following results of our material development are important for meeting the specification targets for large mirror blanks: The glass ceramic production process starts with melting, followed by forming, annealing, nucleation, and crystallization of the material. Controlled crystallization is possible if the Tamman-Curves of the nucleation rate and

the crystal growth rate do not overlap. Zerodur glass ceramic consists of 70 % crystal and 30 % glassy phase. To achieve transparency, mean crystal sizes of about 500 A should be derived. Therefore, at least 10^{13} nuclei per mm^3 must be developed, with a nucleation rate of 10^5 nuclei per mm - 3 per second - to ensure economical ceramizing times. Metastable, high-quartz-solid solutions containing Li_20, ZnO, MgO, $AIPO_4$ and $Si0_2$ grow epitactically onto $TiZrO_4$ - nuclei. Transmission electron microscopy and X-ray analysis have shown evidence for this crystallization sequence. Nucleation temperatures are in the region of 600 - 620°C, and crystallization takes place from 680°C upwards. Within the crystallization process, of the high-quartz-solid solution they show a zonary growth. The inner volume of the crystals is lower in $Si0_2$ content than the outer areas. So, the composition of the glassy matrix and the outer areas of the crystals are similar. This result is important for the application of Zerodur for mirror blanks. Due to these results, chemical durability and hardness of glassy and crystalline phases are similar. This avoids unwanted roughness of polished surfaces due to micro-hardness differences and destruction of the optical surface within the AI-removing process, due to selective etching. The coefficient of thermal expansion of the high-quartz-solid solution phase changes very sensitively with its chemical composition. For instance the substitution of $LiAlO_2$ for 10 Mol % of $Si0_2$ decreases the phase transition temperature from low quartz modification to high quartz modification from 573°C to about 200°C. The relative length change of glass ceramic consisting of high-quartz-solid solution crystals can be very sensitively adjusted by ZnO, Li_20 and Mg0-content.Li_20 and Zn0 decreases the values, and Mg0 increases the values of thermal expansion. The $AlPO_4$-content of the crystals controls the characteristic of the curves of the relative length change with temperature. Because high-quartz-solid solution crystals are metastable, they steadily change their chemical composition at temperatures above 800°C. At about 800°C, a transition to Keatite-solid solution phase occurs. Both effects can be used to adjust the coefficient of the thermal expansion of the mirror material by thermal treatments. To get material with thermal expansions as near as possible to zero, a chemical composition is used leading to slightly negative expansion coefficients after crystallization. With thermal treatment of 800°C within 100 - 200 hours, lowest expansion coefficients can be achieved. With these results, the most important fundamentals of crystal chemistry, structure and texture are described.

III. THE PRODUCTION PROCESS OF THE 8.2 m MIRROR BLANKS

As reported at the beginning, a spin casting technology had to be developed to achieve thin Zerodur menisci with 8.2 m in diameter, thicknesses of 177 mm, and a radius of 28.97 m. In 1984, the development started with a feasibility study. Pilot runs with 1.8 m and 4.1 m blanks were carried out successfully in 1987. ESO placed in September 1988, the order for four 8.2 m Zerodur mirror blanks. A new 2700 m^2 facility, with a 70 t discontinuous melting tank, casting, spinning, annealing, ceramizing facilities, storing sites, lifting and turning devices, an 8 m grinding machine, and quality inspection facilities were planned and erected within 21 months. The whole project started in September 1988, and it will be completed with the delivery of the fourth blank this year. To produce a blank with 8.6 m in diameter, 32 cm in thickness, and a curvature of 29 m, it takes 30 days for melting, 5 hours for casting and spinning, 3 months for rough-annealing, 2 months for rough machining, 8 months for ceramizing. Machining to specified dimensions and quality inspection take

another 5 months. This results in a total production time of about 2 years. Melting and homogenizing 70 t of Zerodur glass in a discontinuous tank was not a problem for Schott, because ever since 1970, 4 m blanks had been produced in massive form, which required about 45 t of glass. The raising to 70 t created no problems. To get an homogeneous blank it is important to control temperatures in the tank, the feeder, and the mold very carefully. To minimize inhomogeneities and uncontrolled crystallization, the pouring and spinning processes have to be carried out as fast as possible. Nevertheless, it takes 5 hours to cool down the melt from about 1300 ^{o}C to 900^{o}C, where the glass maintains its shape. Within this period of time, the glass passes through the temperature region with maximum crystal growth velocity. Crystals grow on inclusions within the glass volume and at the reaction layer between the glass and the mold. It is impossible to avoid uncontrolled crystallization completely. The following measures lower the risk: Before pouring the melt into the mold, which is temperature-controlled, the tank feeder is heated up. Within the start-up phase of the powering process, the contaminated melt flows through an orifice in the bottom of the mold. When the melt is free from inclusions and striae, a stopper is pressed against the bottom of the mold, which now is filled with glass melt. Within the filled mold resting on a rotating support, the spinning process starts with typically 5 revolutions per minute to ensure that no surface glass is entrapped and transported into the interim volume. So the meniscus is formed. To accelerate the cooling process the mold cover is replaced by a cooling hood, which is cooled by sprinkling high amounts of water into its bottom steel plate. The forced cooling is stopped when the glass has reached a temperature of 900 ^{o}C. Further cooling to a safe temperature above the glass transition temperature proceeds by radiation. The mold, with the casting, is then transferred into an annealing lehr where a precise 3-month cooling program is applied. Stress formation during cooling-down to room temperature is particularly critical. The most dangerous stresses are caused by a crystalline reaction layer at the bottom side of the blank. It has a significantly lower CTE value than the glass, which is why this side will be put under tensile stresses. Taking the convex shape of the bottom side into account and applying the tools of fracture mechanics, FE-simulations indicated that tensile stresses on the bottom side should not exceed 2 MPa. With optimized production parameters, crystal layers < 0.5 mm thickness were obtained, which caused tensile stresses not more critical for the process. During the annealing process, the huge meniscus passes the glass transition region. Now, it behaves like a rigid body and does not adjust itself anymore to the mold, it did as viscous glass. To avoid breakage of the meniscus under its own weight, the latter has be supported actively by hydraulic elements. FE-simulations indicated that maximum tensile stresses introduced by the support system during cooling are 0.13 MPa. Because of the very slow annealing cycle, only small compressive stresses due to temperature gradients between surface and bulk volume elements, are expected. FE-simulation resulted in -4,8 MPa for the top surface and, -1.2 MPa for the bottom surface. When all measures derived from computer simulations and from test castings were applied to the production castings, no more failures of the glass blanks occurred anymore. After annealing, the crystal layer has to be removed from the blank to stop any subcritical growth of cracks which may take place. All of the handling and machining procedures with gigantic blanks are critical, too. Flexible support systems designed on the basis of FE simulation results were constructed and applied with success. The nucleation and crystallization processes takes 8 months. During this transformation, linear shrinkage of the body is about 1 %, which means the diameter reduces by about

8 cm. If the body stuck to the surface of the support system, breakage would be the result. To avoid this, the blank is put on a support plate with several thousands of small sand piles which allow the blank to move free from stress during the shrinking process. After ceramization, the blank is ready for machining to its final shape. Handling and supporting devices used for the glassy blank were used again for the glass ceramic blank. After drilling a central hole into the blank and achieving the specified dimensions, the blank was ready for inspection.

IV. PROPERTIES OF THE FOUR 8.2 m ZERODUR MIRROR BLANKS

As a result of quality inspection measurements on all four blanks, it can be reported that all specified values given by ESO were exceeded significantly. The inner quality of the blank material was specified by number and sizes of inclusions. The delivered blanks contained less than 20 % of the specified numbers. Stresses within the blank due to striae were not existent. Specified stresses were less than 25 nm. Stresses due to the annealing process were about 60 % of the given values (~6.2 - 7 nm/cm). Mean CTE was $-0.043 \times 10^{-6} \times K^{-1}$. Specification values were $0 \pm 0.15 \times 10^{-6} \times K^{-1}$ whereby the achieved CTE-homogeneity was $0.009 \times 10^{-6}\ K^{-1}$ The specification value was $< 0.05 \times 10^{-6} \times K^{-1}$. All blanks were and will be delivered in time. For land and sea-transportation to REOSC, where the blanks receive their optical finishing, both companies, REOSC and SCHOTT, developed a transportation device. Again, all results of the material stability derived from FE-simulation were taken into account. The transportation procedures were carried out without failures.

During these days, the 8.2 m project at SCHOTT is coming to a successful end, thanks to the outstanding performance by Dr. Rudolf Müller, Dr. Hartmut Höness, and their project team.

ADVANCED ION-EXCHANGEABLE GLASSES FOR WAVEGUIDE APPLICATIONS

Nikonorov Nikolai
Vavilov State Optical Institute, Russia

Abstract

New possibilities of oxide glasses for integrated optics have been shown. The new silicate and phosphate ion-exchangeable glass matrices were developed. Mechanisms of waveguide refractive index formation during the ion exchange have been studied. Optical waveguide characteristics are described to demonstrate the broad range of waveguide applications.

1. INTRODUCTION

Glasses are of the advanced optical materials for integrated optics and optoelectronics. For the development of waveguide structures, many researchers often use traditional commercial glasses. These glasses can transmit (uncolored BK7, Russian R8), record images (photosensitive DS, FKhS 2-7), and control light flux (laser - Hoya LHG 5, magneto-optical-MOS 12, semiconductor-doped color-filters glasses). The advantages of using these commercial glasses include availability and relatively low price. However there have been designed for purposes unrelated to integrated, and ion exchange technique, and often are pore for use in waveguide technology due to losses and active characteristics. Lately, new kind of special glasses (BGG21 and BGG31 [1], E0095 and E0184 [2]) with good ion exchange characteristics for integrated optics were developed. The design of new glasses with good optical, spectral, chemical, and mechanical characteristics suitable for effective waveguide processing for integrated optics has been the focus of our research. Our paper presents results of design and processing of new ion-exchangeable oxide glasses for waveguide applications.

2. MECHANISMS OF WAVEGUIDE REFRACTIVE INDEX

The increase of the refractive index in glass surface layers during ion exchange are governed by two mechanisms: 1) glass composition change (difference of exchanging ion's polarizabilities), 2) development and relaxation of diffusion stresses due to difference in exchanging ion radii and elasticity of glass matrix. In the low temperature ion exchange process, the extent of alkali ion diffusion, i.e. the number of ions exchanged, will dictate the magnitude of the refractive index change, Δn. The exchange conditions (temperature -T_{exch}, time -t) will dictate the depth of the modified layer (h), the
corresponding stress birefringence resulting from the mismatch ion-hole size, and the resulting compressive stress layer and its ability to undergo relaxation during the exchange period. In case $K^+ \Leftrightarrow Na^+$ ion exchange, the diffusion compressive stresses (the second mechanism) play a key role in formation of refractive index. Diffusion stresses between layer and substrate (macrostresses), and stresses between the exchanging ion and the surrounding matrix

(microstresses) can relax when the glass loses elastic properties while at the exchange temperature. For long exchange time and/or high exchange temperature (T_{exch} Close to T_g), stress relaxation occurs quickly and results in non-monotonic dependence of refractive index and birefringrnce in the exchanged layer [3]. We used this relaxation effect to create waveguide with "buried" refractive index profile. Modification of glass composition leads to a change in the transition temperature, T_g, which will affect the extent of relaxation in the layer. For example, the addition of ZrO_2, TiO_2, Nb_2O_5 on the base alkali-silicate and phosphate glasses lead to increase in T_g. This increase, ΔT, ($\Delta T = T_g - T_{exch}$), leads to a corresponding decrease in the rate of relaxation and increase Δn and δn. So, for development of ion-exchangeable glasses we used this effect.

3. ION-EXCHANGEABLE GLASSES FOR WAVEGUIDES

We have formulated next requirements for ion-exchangeable glasses for waveguide applications. The glasses must to combine good optical, spectral (low scattering and absorption, high homogeneity) and active properties with good ion exchange facility (high diffusion coefficients of alkaline ions). Besides, the glasses should have the improved mechanical, thermal, optical strength, and chemical stability, and enhanced glass transition temperature, which allows to safe a perfect optical quality of glass substrates, and to fabricate waveguides with small losses.

We have developed special glasses which answer these requirements. To enhanced T_g and improve chemical stability, we used some special modifiers as ZrO_2, Nb_2O_5, TiO_2, and others.

We have synthesized new ion-exchangeable glasses for waveguides. The characteristics of these glasses are better then ones for commercial glasses. For example, for zirconiumsilicate glasses (T_g = 700°C), the characteristics of K^+-waveguides are: $\Delta n = 120 \cdot 10^{-4}$, h =60 μm, α= 0.1 dB/cm, $D_{K\text{-}Na} = 7 \cdot 10^{-9}$ cm^2/s (T_{exch}=500°C, t= 1h); the characteristics of Cs^+-waveguides are: $\Delta n = 400 \cdot 10^{-4}$, h= 8 μm, α= 0.1 dB/cm, (T_{exch} 500°C, t= 2h). For phosphate glasses, the characteristics of Cs^+- waveguides are: $\Delta n = 360 \cdot 10^{-4}$, h= 7 μm, α= 0.1 dB/cm, $D_{Cs\text{-}Na} = 10^{-9}$ cm^2/s (T_{exch} - 450°C, t= 0.5h). For commercial K8 glass (T_g = 560°C), the characteristics of K^+-waveguides are: $\Delta n = 50 \cdot 10^{-4}$, h= 15 μm, α= 0.5 dB/cm, $D_{K\text{-}Na} = 7 \cdot 10^{-11}$ cm^2/s (T_{exch}= 500°C, t= 8h). To fabricate Cs^+-waveguides in K8 glass is not possible because of a small diffusion coefficient. So, the waveguides in special glasses have a small losses, high Δn, and depth.

The ion-exchangeable phosphate glass matrices are advanced materials for development of active waveguide structures. For example, we have doped the phosphate glass with Nd^{3+} [4] and studied optical, spectral, and ion-exchangeable properties. The phosphate glass matrices have high solubility of II-VI semiconductors phase and are more flexible to increase the content of CdS, CdSe semiconductors in glass, and to improve non-linear properties. For example, we have developed special phosphate glasses doped with high concentration of CdS microcrystals [5]. The non-linear refractive index of these
glasses is about $2 \cdot 10^{-9}$ esu.

4. ION EXCHANGEABLE GLASSES FOR WAVEGUIDE DIFFRACTION GRATINGS

The main idea for creating waveguide diffraction gratings is modulation of refractive index and glass surface relief (volume change) during ion-exchanged process. We have developed special silicate glasses which allowed to produce the gratings with high refractive index increase ($\Delta n = 350 \cdot 10^{-4}$) and very strong surface relief change (Δh= 0.1-0.6 μm) by $K^+ \Leftrightarrow Na^+$, $Rb^+ \Leftrightarrow Na^+$,

and $Cs^+ \Leftrightarrow Na^+$ ion exchange. The ion-exchanged treatment was produced through aluminum periodic (5-10 μm) masks. We created a combined structures of waveguides with gratings which can be used for different waveguide applications. The diffraction efficiency these waveguide gratings is about 20-30%.

5. ION EXCHANGEABLE GLASSES FOR WAVEGUIDE HOLOGRAMS

We have created special photothermorefractive (PTR) glass for hologram recording [6]. The main idea of PTR process is a growth of microcrystals after UV exposure and thermal development (T~520^{o}C). Difference between refractive index of microcrystalline phase and glass matrix, $5 \cdot 10^{-4}$, allows to record 3-D phase holograms with high diffraction efficiency (about 90%). The optical and spectral properties of these holograms are stable over wide temperature range (20-450^{o}C). This feature allowed to use ion-exchanged technique ($K^+ \Leftrightarrow Na^+$ ion exchange, T_{exch} = 400^{o}C for creation of waveguides on surface of holographic structure. So, PRT glasses can be used for fabrication of varied holographic waveguide multifunctional elements (like waveguide multiplexers and demultiplexers for telecommunication, etc.).

6. CONCLUSION

We have developed new ion-exchangeable silicate and phosphate glasses which are advanced materials for multifunctional waveguides. These glasses allow to create passive
and active waveguides with varied and improved characteristics, and to develop different waveguide diffraction gratings and holographic elements.

REFERENCES

1. L.Ross. *Glastechn. Berichte,* Vo1.62, N8, pp.285-297, (1989).
2. J.L.Jackel, E.M.Vogel, J.S.Aitchison. *Appl. Opt*., Vol.29, N21, pp.3126-3129, (1990).
3. N.V.Nikonorov, L.B.GIebov, G.T.Petrovsky, K.A.Cerqua-Richardson. *Proceedings of SPIE,* Vo1.2287, pp.200-212. (1994).
4. N.V.Nikonorov, D.A.Palagin, O.S.Shavelev, and O.A.Golovina. *Glass Physics and Chemistry*. Vo1.19, N1, pp.48-51, (1993).
5. E.V.Kolobkova, A.A.Lipovskii, and N.V.Nikonorov. Phys. Stat. Sol. (a), Vol.147, pp.K65-68, (1995).
6. L.B.GIebov, N.V.Nikonorov, E.I.Panysheva, G.T.Petrovskii, et.al. *Optics and Spectroscopy*. Vol.73, pp.237-241, (1992).

EVALUATION OF METHODS FOR THE DETERMINATION OF THERMAL RADIATION PROPERTIES OF MOLTEN GLASS

Peter A. van Nijnatten
TNO Institute of Applied Physics, The Netherlands

Abstract

In order to predict glass quality through glass tank modelling, reliable glass data is necessary. Thermal radiation properties play an important role in glass tank modelling since radiation is the dominant mode of heat transfer at melting temperatures. Therefore, optical properties of glasses at melting temperatures need to be determined accurately. Different measuring techniques can be found in literature, based upon either emittance measurement, transmittance measurement or reflectance measurement. The paper discusses the various methods and gives an overview of the problems involved with each method. Error analysis reveals their limitations and the reliability of the measurement results obtained with each method. A new method is proposed which promises superior photometrical accuracy, as compared with the existing methods.

1 INTRODUCTION

Accurate modelling of the processes in the glass tank results not only in a better understanding of the melting process, but is also an important tool in the optimalisation of the furnace design. One of the problems that have to be solved in order to improve the quality of the glass tank model predictions is the accurate calculation of the radiative heat transfer in the melt. Radiation heat-exchange is a dominant form of heat-transfer in glass melts and depends not only on glass composition and temperature, but also on the redox state.

For the measurement of high-temperature absorption coefficients of glass, three measurement principles can be found in literature: reflection- [1,2] , transmission- [3,8] and emission [9-12] spectroscopy. The accuracy with which the absorption coefficient of the glass can be determined using these methods, depends on the choice of the reference measurement. All three measurement principles are based on determining the ratio of two radiation intensities I_{SAMPLE} and $I_{REFERENCE}$, measured for instance before and after interaction with the sample.

Within the framework of a project which aims to improve the modelling of heat-transfer in molten glass, the TNO Institute of Applied Physics is developing an optical testing facility for the measurement of the spectral absorption coefficient of glass as function of the oxygen activity (redox state) at melting temperatures.

The work presented in this paper is the result of a preliminary study which aims to find the best measurement solution. The reliability of the measurement results obtained with

each of the three methods for different choices of the reference measurement are investigated by uncertainty analysis, using as input for the calculations an absorption spectrum of TV glass measured at 1450°C by Mazurin and Prokhorenko [8] (see Fig.1).

2 REFLECTION SPECTROSCOPY

In case of the reflection method [1,2] , a flat platinum mirror is submerged in the molten glass, having its surface parallel to that of the glass. The internal transmittance τ of the glass slab above the mirror is related to the reflectance through

$$R = \rho_g + \frac{(1-\rho_g)^2}{1-\rho_g\rho_p\tau^2}\rho_p\tau^2 \qquad (1)$$

where ρ_g and ρ_p are respectively the power reflectances of the air-glass and glass-platinum reflection interfaces, determined from the refractive indices of platinum and glass by Fresnel's equations [13] . For the present research, a constant and real refractive index of $n_g = 1.5$ is assumed for the glass ($\rho_g = 0.04$) and literature values are used for the spectrally dependent complex refractive index n_p of platinum (ρ_p = 0.5 -0.9). The reflectances for various thicknesses of the glass slab according to Eq.(1) are shown in Fig.2 for the TV-glass at a temperature of 1450°C.

An obvious method for obtaining the reflectance is by measuring the intensities of the incoming and reflecting beams and calculating their ratio. Then, the absorption coefficient can be calculated using the formula

$$\alpha = \frac{1}{2d}\left[\ln\left(\frac{(1-\rho_g)^2}{R-\rho_g}+\rho_g\right)+\ln(\rho_p)\right] \qquad (2)$$

which has been derived by inverting Eq.(1) and substituting $\tau=\exp\{-\alpha d\}$.

The parameters in this equation are known with limited accuracy, which results in an error in α. We will consider the effect of the various error components. An error δd in d causes an error $\delta(d)$ of equal size in α. The errors $\delta\rho_g$, $\delta\rho_p$ and δR in ρ_g, ρ_p and R respectively, cause corresponding error components $\delta(\rho_g)$, $\delta(\rho_p)$ and $\delta(R)$ in α. The total error δ_{tot} can be found by taking the square root of the sum of the squared error components (summing variances). In the error analysis, the following estimated values have been used: $\delta\rho_g$ = 5%, $\delta\rho_p$ = 2% and δR = 0.5%. These values are based upon practical experience with transmission spectroscopy at room temperature.

The effect on the total error of each of the parameter errors is investigated. As demonstrated by the upper graphs in Fig.3, a large error is caused by the uncertainty in ρ_p, which is not well known at high temperatures.

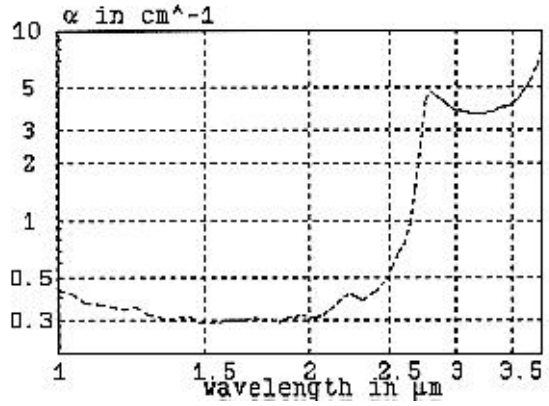

Figure 1. Absorption coefficient of TV glass at 1450°C [8]

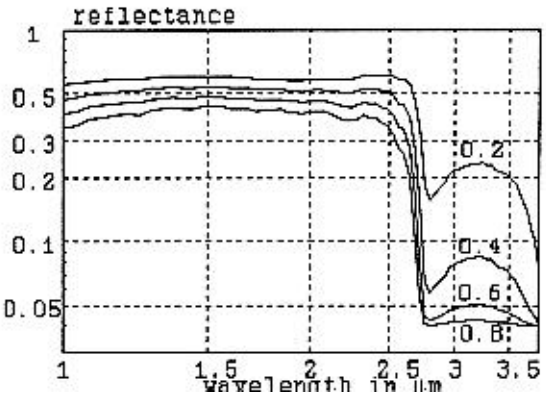

Figure 2. Sample reflectance for d = 0.2, 0.4, 0.6 and 0.8 cm

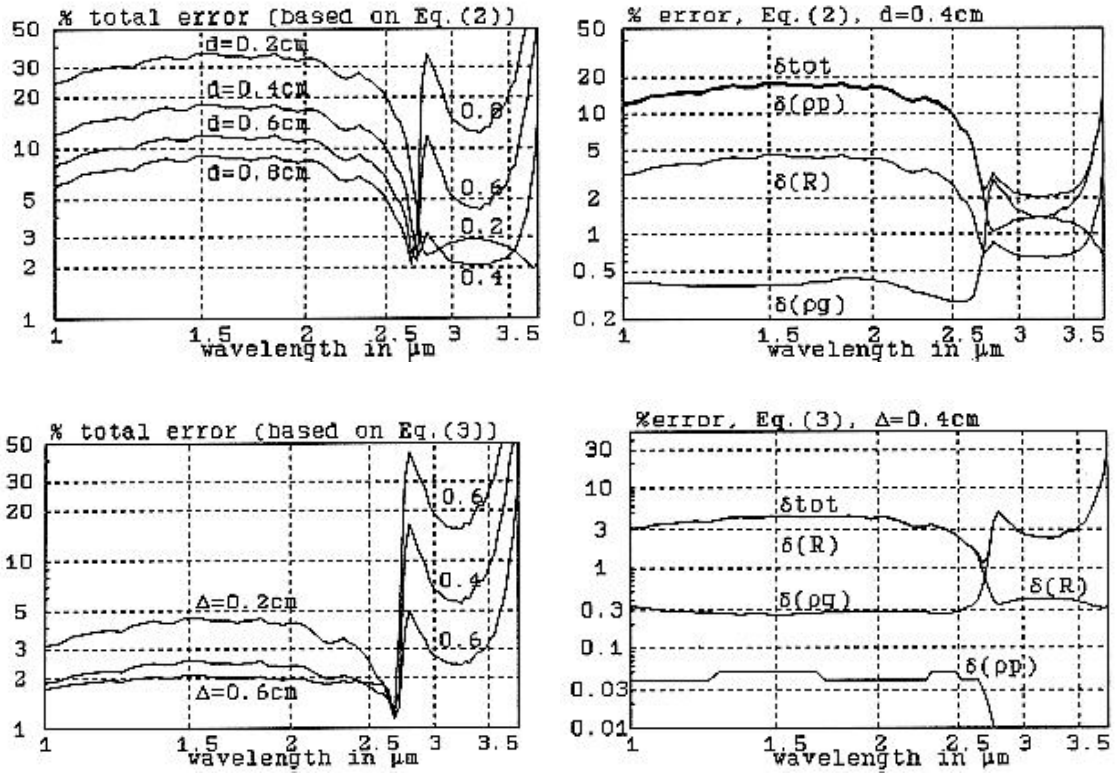

Figure 3 Result of the error analysis of the absorption coefficient of TV glass at 1450°C based on Eq. (2) (top graphs) on Eq. (3) (bottom graphs). The left graphs show the total error for different sample thicknesses, the right graphs show the effect of the individual error components in the case of d (or D) = 0.4 cm.

An alternative method, successfully used by Von Genzel [1] and Neuroth [2] , is based on performing measurements of the reflected signal with the mirror emerged at different

depths. From the reflectances R_1, and R_2 obtained with emersion depths d_1 and d_2 respectively, the absorption coefficient is determined by iteration with

$$\alpha = \frac{1}{2\Delta}\left[\ln\left(\frac{R_1 - \rho_g}{R_2 - \rho_g}\right) + \ln\left(\frac{1 - \rho_g\rho_p\exp(-2\alpha d_1)}{1 - \rho_g\rho_p\exp(-2\alpha d_2)}\right)\right] \tag{3}$$

where the parameter $\Delta = d_2 - d_1$. The second term between the brackets, which contains α, can be neglected to obtain a first approximation of α.

The result of an error analysis based upon this method is shown in the lower graphs of Fig.3. With this method, the total error is dominated by $\delta\rho_g$ and is much lower than the total error obtained with the first method according to Eq.(2). The results also demonstrate that for an accurate determination of low as well as of high absorption values, samples with different thicknesses have to be measured.

3 TRANSMISSION SPECTROSCOPY

In case of the transmission method, the molten glass is positioned between two parallel sapphire windows. The internal transmittance of the glass slab above the mirror is related to the transmittance through

$$T = \frac{T_s^2\tau}{1 - R_s^2\tau^2}, \tag{4}$$

where T_s and R_s are respectively the transmittance through the sapphire and reflectance from glass to sapphire given by

$$T_s = \frac{(1 - \rho_{gs})(1 - \rho_s)\tau_s}{1 - \rho_{gs}\rho_s\tau_s^2} \quad \text{and} \quad R_s = \rho_{gs} + \frac{(1 - \rho_{gs})^2\rho_s\tau_s^2}{1 - \rho_{gs}\rho_s\tau^2} \tag{5}$$

The coefficients ρ_g and ρ_s are respectively the power reflectances of the glass-sapphire and sapphire-air interfaces, determined from the refractive indices n_g and n_s using Fresnel's equations [13] and τ_s is the internal transmittance of the sapphire window. A suitable reference measurement will be the measurement of a parameter, that, as a denominator in the ratio $I_{SAMPLE}/I_{REFERENCE}$ will reduce the uncertainty in α caused by the uncertainties in T_s and R_s.

We will investigate the effect on the accuracy, of each of the following possible choices of the reference measurement: (i) 100% transmission obtained with the sample removed, (ii) transmission through 1 sapphire window with twice the thickness as the windows used in the sample measurement, and (iii) measurement of the same sample with a different thickness.

In the analysis, the following estimated values are used: δn_g =1 %, δn_p =1 % and δT = 0.2% (+ 0.0005 in T due to noise). These estimates are based upon practical experience with transmission spectroscopy at room temperature.Using reference measurement (i), α is obtained by evaluating

$$\alpha = -\frac{1}{d}\ln\left(\sqrt{\frac{T_s^4}{4T^2R_s^4} + \frac{1}{R_s^2}} - \frac{T_s^2}{2TR_s^2}\right) \tag{6}$$

In the case of reference measurement (ii), T_s^2 in Eq. (6) has to be replaced by

$$T_s^2 = T_o(1 - \rho_{gs}\rho_s\tau_s^4)\left(\frac{1-\rho_{gs}}{1-\rho_{gs}\rho_s\tau_s^2}\right)^2 \tag{7}$$

which T_o is the reference measurement (T is the sample measurement in this case, not the sample transmittance!).

If the same sample can be measured at a different thickness (reference measurement (iii)), the absorption coefficient is determined by iteration with

$$\alpha = \frac{1}{d_2 - d_1}\left[\ln\left(\frac{T_1}{T_2}\right) + \ln\left(\frac{1 - R_s^2\exp\{-2\alpha d_1\}}{1 - R_s^2\exp\{-2\alpha d_2\}}\right)\right] \tag{8}$$

An advantage of transmission spectroscopy is that all optical interfaces are flat and their position (and sample thickness) well defined. A disadvantage is the possibility of deterioration of the sapphire-glass interface due to chemical reactions. This may result in optical scattering which effects the measurement. In the error analysis, of which the result is shown in Fig.4, this effect is not considered. Fig.4 shows that the lowest accuracy is obtained with method (i) which is used by most researchers [3-8] . Using a reference measurement on a single sapphire window, having twice the thickness as those used in the sample holder, allows for compensation of δn_s (method (ii)), thereby improving the result significantly.

The total error in α in the case of method (iii), which gives the best results, depends mostly on the error in T (δ(T) and δ_{tot}) coincide in the graph. By making the distance between the windows variable, Δ can be measured accurately (better than 0.02 mm) using a calibrated displacement transducer. An extra advantage of using the same sample holder is that the effect of deterioration of the sapphire-glass interface, which adds to the error in ρ_g is mostly cancelled out in Eq.(8).

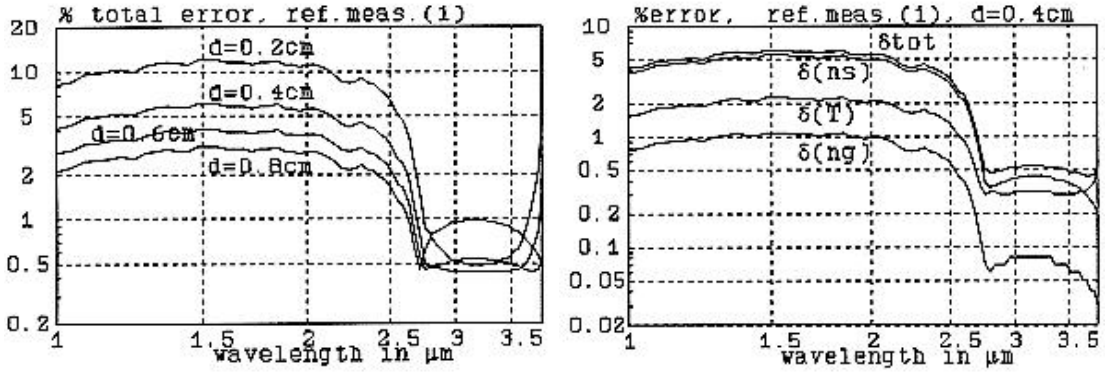

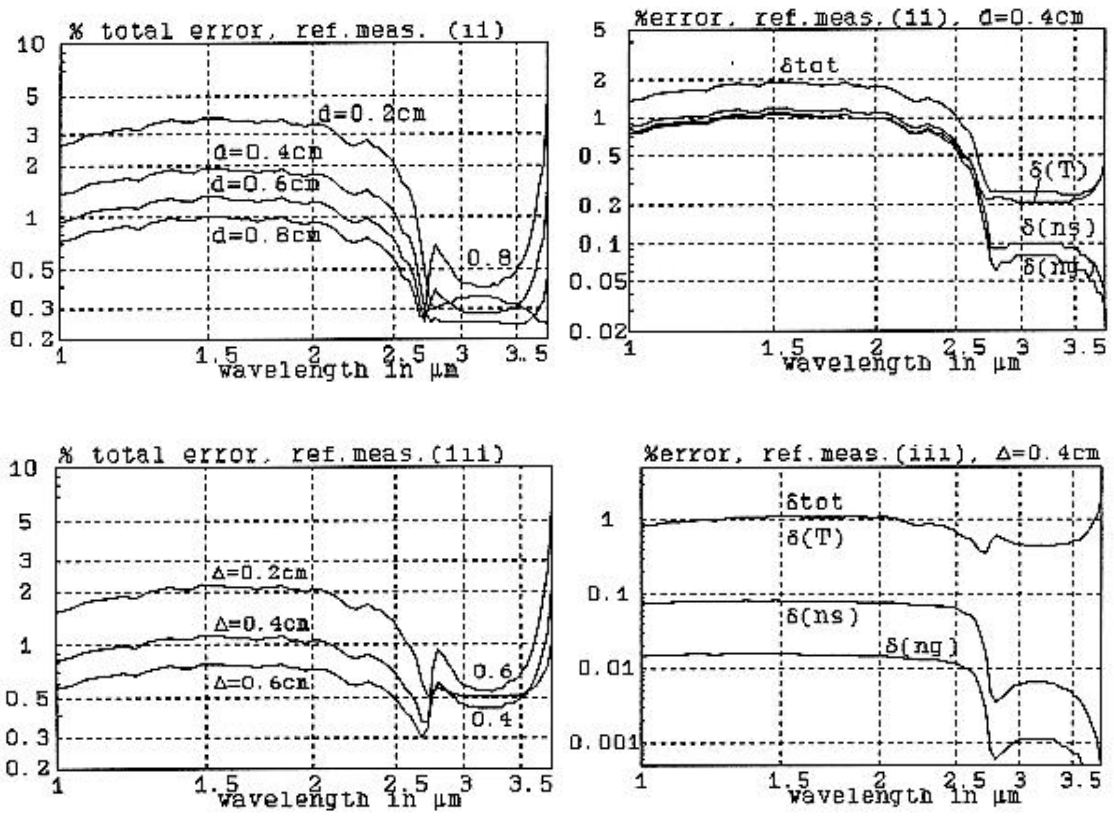

Fig. 4 Result of an error analysis for TV glass at 1450°C based on transmission spectroscopy for different reference measurements (i), (ii) and (iii). The left graphs show the total error for different sample thicknesses, the right graphs show the effect of the individual error components in the case of d (or D) = 0.4 cm.

4 EMISSION SPECTROSCOPY

Using emission spectroscopy, the optical interfacing is relatively simple because radiation is only directed from the sample to the spectrophotometer. Also, the problem of separating sample self-radiation from source radiation is eliminated.

Emission spectroscopy is generally performed in the same measurement geometry as used in reflection spectroscopy. In this case, the sample consists of a flat glass plate having a platinum-glass interfaces a mirror on the bottom [9-12] and the same reference measurements and equations as for reflectance spectroscopy are valid (ε=1-R), including the results of the error analysis shown in Fig.3.

An alternative way of measuring the emittance, is by using the facility for transmission spectroscopy and measuring only the sample self-radiation. Using a black body radiator at the same temperature as a reference, the emittance ε can be obtained with an accuracy of 0.5%. In this case, the following equation is valid:

$$\varepsilon = 1 - R'_s - T_s^2 \frac{1 + R_s\tau}{1 - R_s^2\tau^2}\tau \,, \tag{9}$$

from which an equation for α can be derived, similar to Eq.(2) and Eq.(6). The parameter R'_s is the total reflectance of the sapphire window at the sapphire-air interface (including the reflection of the back-side).

The result of an error analysis, based upon δn_g = 1 %, δn_p = 1 % and $\delta\varepsilon$ =0.5% is shown in Fig.5. The error in the optical measurement ($\delta\varepsilon$) proves to be dominant. Compared to the results which can be achieved by reflection and transmission spectroscopy, this method promises superior accuracy.

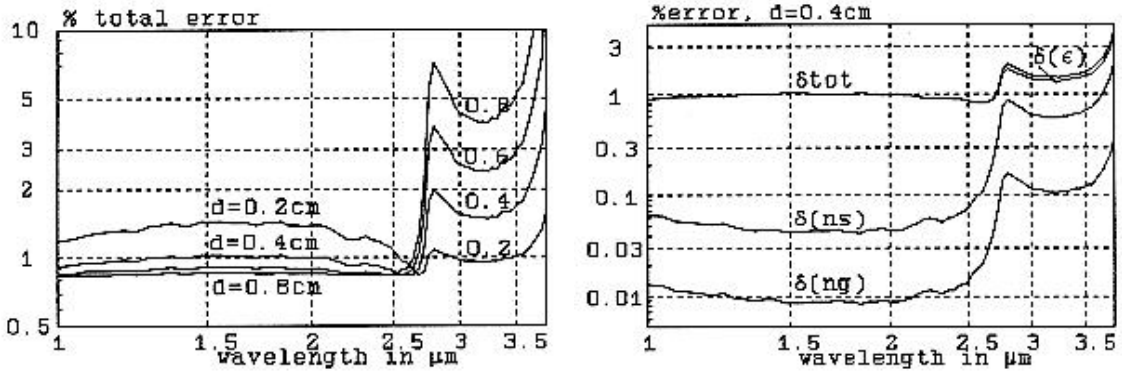

Figure 5 Result of an error analysis for TV glass at 1450°C based on emission spectroscopy. The left graph shows the total error for different sample thicknesses, the right graph shows the effect of the individual error components in the case of d = 0.4 cm.

5 CONCLUSION

The photometrical accuracy which can be achieved using different techniques for determining the high-temperature absorption in glass has been investigated. In all methods, the optimal sample thickness depends on value of the absorption coefficient. If accurate data has to be obtained for a wide range of absorption coefficients, the use of several thicknesses is required.

It has been shown that the reliability of the measurement results depends on the type of reference measurement. New methods, based on convenient choices for the reference measurement have been presented in this paper. The results of the error analysis demonstrates that these new methods lead to significant improvements in the accuracy of the determination of α. It has been demonstrated that the highest photometrical accuracy can be expected using a new method which is based upon emission spectroscopy.

ACKNOWLEDGMENTS

The work presented in this paper has been partly funded by NOVEM (The Netherlands Organisation for Energy and Environment) and the NCNG (the Dutch Glass Industry).

REFERENCES

[1] Genzel, L Von, Messung der Ultraror - Absorption von Glas zwische 20 und 1360°C, Glastech. Ber., 24 (1951), p.55-63
[2] Neuroth, N., Der TemperatureinfluB auf die optischen Konstanten von Glas im Gebiet starker Absorption, Glastech. Ber., 28 (1955), p.411-422.
[3] Grove, F.J. and Jellyman, P.E., Infrared Transmission of Glass in the Range Room Temperature to 1400^{o}, J. Soc. Glass Technol., 39 (1955), p.
[4] Grove, F.J., Spectal Transmission of Glass at High Temperature and its Application to Heat-Transfer Problems, J. Am. Cer. Soc., 44 (1961), p.317-320.
[5] Franz, H., Infrared absorption of molten soda-lime-silica glasses containing transition metal oxides,
[6] Blazek, A, et. al., Strahlungswarmeleitfahigkeit van Glas - EinfIuB det Glaszusammensetzung auf seine Warmedurchlassigkeit-, Glastechnische Berichte, 49 (1976), p.75-81.
[7] Wedding, B, Measurements of High-Temperature Absorption Coefficients of Glasses, J. Am. Cer. Soc., 58 (1975), p.102-105.
[8] Mazurin, O.V., Prokhorenko, O.A., Measurements of Transmission Spectra of Molten Glasses,
[9] Goldman, D.S. and Berg, J.I., Spectral Study of Ferrous Iron in Ca-Al- Borosilicate Glass at Room and Melt Temperatures, J. Non-Cryst. Sol., 38 & 39 (1980) p.183-188.
[10] Berg, J.I., Near Infrared Absorption Coefficient of Molten Glass by Emission Spectroscopy, Int. J. Thermophysics, 2 (1981), p.381-394.
[11] Banner, D. and Klarsfeld, S., High Temperature Infrared Spectra of Silicate Melts, from: The Physics of Non-Crystalline Solids,1992.
[12] Fabris, R. and Hucin, J.C., Identification method for infrared absorption spectra of semitransparent media by their emission data. Application to lime-aluminosilicate glasses at high temperatures, Glastech. Ber. Glass Sci.Technol., 67 (1994), p.81-86.
[13] Born, M. and Wolf, E., Principles of Optics, Pergamon, Oxford, 1980.

FORMATION OF METAL NANOCLUSTERS IN SILICATE GLASSES FOR NONLINEAR OPTICAL APPLICATIONS

G. Battaglin
INFM, Dipartimento di Chimica Fisica, Venezia, Italy
G. De Marchi, F. Caccavale, F. Gonella, G. Mattei, P. Mazzoldi, F. Spizzo
INFM, Dipartimento di Fisica, Padova, Italy
A. Quaranta
INFM Unita di Padova, Università di Trento, Italy
F. Garrido
CSNSM, IN2P3-CNRS, France 91405
G. De
Sol-Gel Laboratory, CGCRI, India

Abstract

Silver nanoclusters have been formed in light waveguides obtained by Ag^+-Na^+ ion-exchange process in glass, by either irradiating with low-mass ion beams or by heating in hydrogen atmosphere at temperatures varying in the range 100-250 ^oC. Metal nanocluster-silica composites have been also obtained by the sol-gel technique. Nanocluster modifications induced by pulsed laser irradiation have been investigated, and annealing behavior of nanoclusters synthesized by the sol-gel has been studied. Composites were characterized by Secondary Ion Mass Spectrometry and Rutherford Backscattering Spectrometry, in order to determine concentration depth-profiles, and by Transmission Electron Microscopy for the nanocluster detection and size evaluation. Optical analyses were performed to evidence linear and nonlinear properties.

I. INTRODUCTION

Nonlinear optical materials are essential components of functional photonic devices for optical communications, sensing, and computing [1-3], as -for example- all-optical switching devices [2]. Understanding the correlation between material processing and nonlinear optical properties is especially critical for the development of advanced nonlinear optical materials for photonic devices. The material properties for applications in such devices include picosecond or shorter response times, low power switching threshold, wavelength tunability, thermal stability, low two-photon absorption, high threshold for laser-induced damage, and THz recycling frequency.

In the last few years, composite glasses formed by embedding semiconductor or metal nanoclusters in glass have attracted much attention as promising materials for optoelectronics. In particular, metal nanocluster-doped glasses, i. e., glasses which contain crystallites of metals, show an enhanced third-order susceptibility, whose real

part is related to the intensity-dependent refractive index [2]. This technological interest is strengthened by the general interest in strongly quantum-confined electronic systems which exhibit quite a number of striking effects deriving from the increased electronic density of states near the conduction-band edges. This suggested the introduction for metal nanoclusters-doped composites of the term metal quantum-dot composites (MQDC) in analogy to multiple-quantum-well devices. Glass researchers have employed various ways to prepare metal nanocluster-doped glasses, namely, sol-gel processes, quenching and heat-treatments and processes which use porous glasses. More recently, ion implantation has attracted a large interest for the possibility to pattern the materials, to overcome the doping solubility limits, and to introduce virtually any element in the glass substrate [4-8). Several material-related aspects of the above mentioned metal colloids have been studied and we believe that, in addition to the development of the preparation techniques and of the chemical, structural and optical characterization, we should begin to consider the so-called architecture of systems for optical information processing.

In this paper we present the results obtained by our group, in cooperation with external laboratories, on metal (particularly silver) nanocluster formation in glasses obtained by sol-gel as well as low-mass ion irradiation or annealing in hydrogen atmosphere of light waveguides prepared by the ion-exchange technique. Results on thermal stability and modifications induced by pulsed-laser irradiation will be also reported.

II. EXPERIMENTAL

The composition of the glass utilized for the fabrication of ion-exchanged waveguides is (wt %): 69.6 $Si0_2$, 15.2 Na_20, 1.8 Al_20_3, 6.5 CaO, 5.1 MgO, 1.1 K_20, 0.4 $S0_3$, 0.2 $Ti0_2$ with trace-amounts of Fe_20_3, As_20_3 and Cs_20. Glass samples were ion-exchanged in a molten salt bath of 0.1 % mol. $AgNO_3$ in $NaNO_3$. Exchange temperature of 320 ^oC and processing time of 30 minutes were set to obtain penetration depths of about 5 μm. Two different experiments were performed on ion-exchanged samples. Some waveguides were irradiated by He^+ or N^+ ions at energies varying from 100 keV to 2 MeV. Other waveguides were heat-treated in a quartz tube with H_2 flux at a pressure slightly greater than atmospheric one. Treatments times were between 2 hours and 12 hours and temperatures in the range 120 ^oC to 250 ^oC. Furthermore, some samples, as-exchanged and after He^+ irradiation, were irradiated by using a Q-switched Nd:YAG laser operated at both 1064 nm and 532 nm of wavelength. Pulse duration was about 10 ns.

The sol-gel method was used for the synthesis of metal (copper or silver or copper-silver mixture) doped silica films deposited on silica glass substrates with a procedure described in [9-10). The sol-gel coatings were heat-treated in different atmospheres (argon, air, 5%H_2-95%N_2) at different temperatures, in the range 500-1100°C, using soaking periods for each step in a cumulative heating procedure.

In the case of ion-exchanged waveguides, subsequently treated with the above described methodologies, silver and sodium profiles were determined by Rutherford Backscattering Spectrometry (RBS), while the hydrogen profile was obtained by

Elastic Recoil Detection Analysis (ERDA). In both techniques, a $^4He^+$ beam at the energy of 2.2 MeV was used at National Laboratories INFN-Legnaro. Secondary lon Mass Spectrometry (SIMS) analyses were also performed, using a CAMECA IMS-4f spectrometer. Refractive index profiles of the waveguides were reconstructed by an inverse WKB method from the set of effective indices corresponding to the guided modes. The effective indices were determined by m-lines spectroscopy. Optical absorption spectra were recorded in the wavelength region from 250 to 600 nm, by a Cary UV-VIS-NIR dual-beam spectrophotometer. Samples for transmission electron microscopy (TEM) were prepared by cutting 3 mm diameter discs with a slurry drill, mechanical grinding of the disc from the backside to a thickness of about 20 mm. The final thinning to the electron transparency was achieved by planar backthinning by ion milling with an Ar gun at 5 keV. To minimize ion damage, samples were cryogenically cooled during ion milling. The prepared samples were examined in a Philips CM3O TEM, operating at 300kV. Finally, nonlinear refractive index was obtained by Z-scan measurements, performed using a mode-locked cavity-dumped dye laser with pulse duration of 6 ps and in the wavelength range from 570 to 590 nm.

III. RESULTS AND DISCUSSION

A. Annealing of waveguides in hydrogen atmosphere

Annealing causes a near-surface precipitation of metallic silver to form nanometer-size clusters with good uniformity in size and spatial distribution, as shown in Figure 1, where we reported the cross-sectional TEM photograph of the sample annealed at 250 ^oC for 5 hours. Here, from the surface to a depth of about 270 nm, it is evident the presence of silver clusters, of spheroidal shape, with fcc structure, randomly oriented with diameters in the range 4-6 nm. The optical absorption spectra of annealed samples display a band peaked at about 410 nm, typical of absorption in metallic silver nanoclusters, due to the surface plasmon resonance (SPR) [11-13]. The SPR frequency depends on metal-particle size through the dielectric response function of the metal, and in this case the absorption band is consistent with predictions of the Mie theory for silver nanoclusters having radius of the order of a few nanometers.

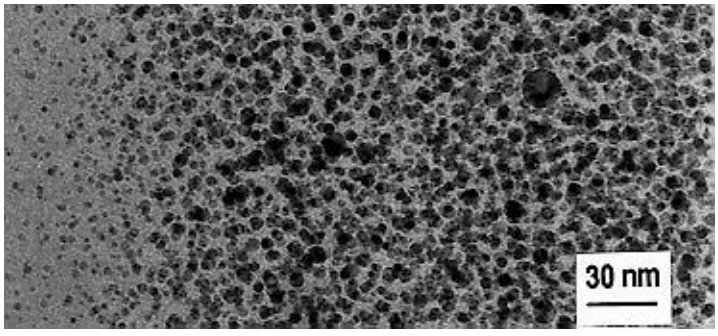

Figure 1. TEM micrographs (cross section) of silver nanoclusters, formed after annealing in hydrogen atmosphere for 5 hours at 250 ^oC.

In Figure 2 the hydrogen and silver concentration profiles are reported after annealing in hydrogen atmosphere for 5 hours at 180°C, together with a corresponding typical absorption spectrum, showing the characteristic peak due to metallic silver nanoclusters. In a study of this process [14] we reached the conclusion that the hydrogen permeation and ion-exchange between hydrogen and sodium (remaining in the glass matrix after silver-for-sodium exchange) are steps of annealing process. A further step is the diffusion of silver towards the surface, with an activation energy, 22 kcal/mole, close to that measured for silver-sodium interdiffusion in glasses of similar composition. Silver migration cannot be simply ascribed to a direct interaction with hydrogen, but to a more complex process involving a charge balancing mechanism during hydrogen-sodium ion-exchange. An activation energy of about 15 kcal/mole was obtained for the hydrogen permeation in the glass.

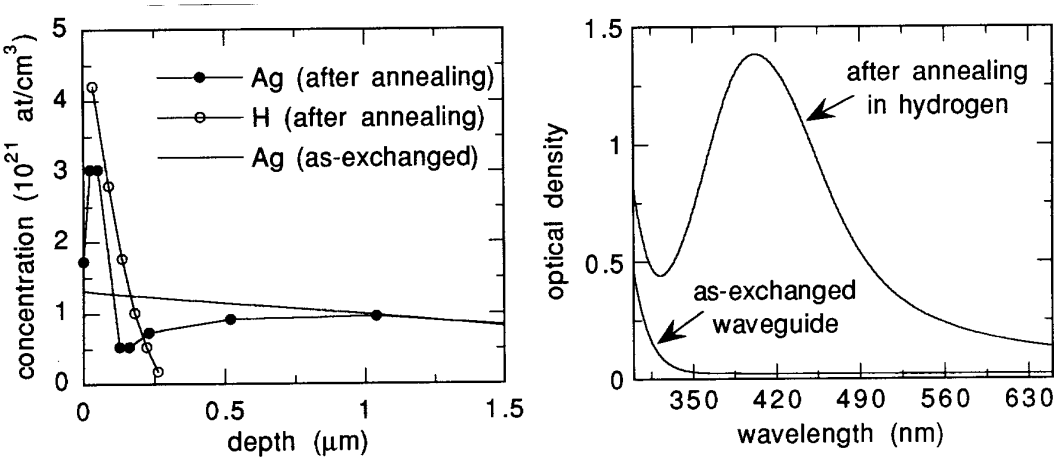

Figure 2. Hydrogen and silver depth concentration profiles (left) and:optical absorption spectrum (right) for samples annealed at 180 °C.

B. Low-mass ion irradiation of ion-exchanged waveguides

The formation of silver nanoclusters was also obtained by irradiation of ion-exchanged samples with He^+ or N^+ ions. The irradiation current and time were varied in order to study the role of deposited energy rate and processing time [15].

TEM micrograph for a 100 keV, $2x10^{16}$ cm^{-2} nitrogen-irradiated sample is reported in Figure 3. The inset shows the selected area electron diffraction pattern indicating the presence of randomly oriented silver crystals. The clusters radius in the irradiated region is about 2-3 nm.

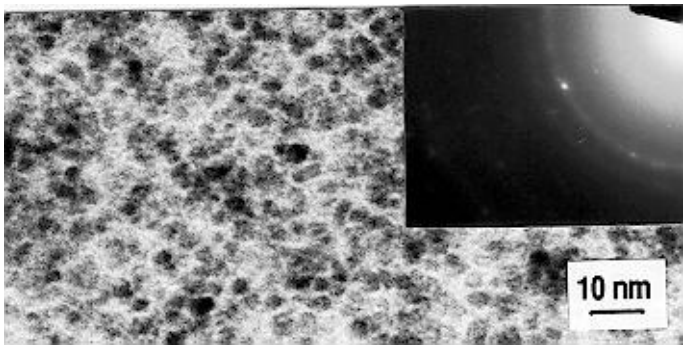

Figure 3. TEM micrograph (cross section) of silver nanoclusters, formed after 100 keV, 2x10^{16} cm^{-2} nitrogen irradiation of an ion-exchanged waveguide.

We have reported elsewere [16] that the irradiation current density is a critical parameter for the precipitation process. At present, it is not possible to separate the contributions to the silver precipitation, of thermal effects due to local heating, and of radiation-enhanced diffusion. Certainly the silver diffusivity, the deposited energy distribution and defect migration would play an important role in determining the final concentration distribution of precipitates.

Third-order susceptibility measurements for these samples gave positive values of the intensity-dependent refractive index n_2 up to 10^{-13} cm^2/W, that turn into negative values after repeated measurements. This peculiar behavior indicates that, when exposed to high optical power densities, silver in the nanoclusters tends to modify the chemical environment, possibly changing permanently its oxidation state. Ion-irradiated samples were laser-treated by using a Q-switched Nd:YAG laser operated at both 1064 and 532 nm of wavelength, with a pulse duration of about 10 ns. After a single pulse irradiation above a threshold value of 0.3±0.1 J/cm^2 for λ=532 nm and 5±1 J/cm^2 for λ=1064 nm, the irradiated region becomes nearly transparent and the SPR optical absorption peak is dramatically reduced. The TEM micrograph of a helium irradiated silver-exchanged soda-lime glass sample, before and after irradiation by a laser pulse at λ=532 nm and E= 0.5 J/cm^2, is reported in Figure 4.

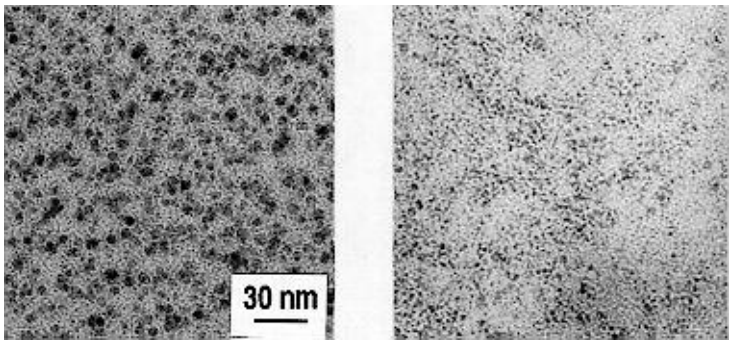

Figure 4. TEM views of an ion-exchanged/ion-irradiated sample before (left) and after (right) laser irradiation with 0.5 J/cm^2 at λ=532 nm.

A reduction of the cluster diameter from the value of about 5 nm before to a value of about 2.5 nm after laser irradiation is evident. This is accompanied by a corresponding increase in the number of clusters, being the total silver concentration constant, as determined by RBS analysis. The increasing ratio between the number of surface and bulk atoms with decreasing cluster size favours the formation of silver-oxygen interactions with respect to silver-silver bonds. This was evidenced by X-ray photoelectron spectroscopy (XPS) and X-ray excited Auger-electron spectroscopy (XE-AES) measurements [17]. After laser irradiation the silver α parameter (binding energy of XPS $Ag3d_{5/2}$ and kinetic energy of AES AgM_5NN peak) changes from 720.3±0.2 eV, close to the value of metallic silver (720.5±0.2 eV). to 719.1±0.2 eV, in agreement with the value measured for an Ag_2O standard. Besides the fragmentation of the silver clusters formed in the ion-irradiated region, we observe that the laser irradiation is also effective in promoting cluster formation in as-exchanged region, where are present few small clusters with a mean diameter of about 1.5 nm. In these regions the laser irradiation causes the formation of small nanocluster, about 2.5 nm in diameter. In this case, laser light induces nucleation and growth depending on different mechanisms [18].

C. Metal nanoclusters in silica matrix synthesized by the sol-gel technique

Metal (copper or silver or copper-silver mixture) doped silica films were deposited on silica glass substrates by the sol-gel dip-coating method [9-10]. In the case of silver nanocrystal-doped silica films, two types of clusters with different diameters were observed in the coatings heat-treated at 300 and 450 ^oC, with respective average diameter of about 1 nm and 15 nm, the latter composed by much few clusters, both with an fcc structure. At 500 ^oC and 550 ^oC, the densification of the silica matrix favours a new precipitation step for silver, with a final particle diameter distribution of 3±1 nm. The clusters formed at and above 500^oC are stable and do not exhibit any degradation of their optical properties with aging. The copper-containig films were first heated in air up to 550 ^oC to burn out organic compounds. A broad absorption band at about 740 nm indicate the presence of Cu^{2+} ions. Subsequent annealing in reducing atmosphere ($5\%H_2$-$95\%N_2$) induces the formation of Cu nanoclusters, evidenced by a broad Cu-SPR absorption band at about 570 nm, at 700 ^oC; however, the absorption band in the range 600-800 nm indicates that Cu^{2+} was not yet completely reduced. As the temperature rised at 800 ^oC, a clear SPR absorption peak grew at about 568 nm. At this temperature, the increase of the annealing time causes a sharpening of the SPR absorption band and its blue-shift to 562 nm. TEM analysis shows nearly spherical particles with an average diameter of about 8 nm and an fcc structure. In the case of Ag and Cu co-doped silica films, films were prepared with Cu/Ag molar ratio of 1,2 and 3 at constant $(Ag+Cu)/SiO_2$ molar ratio of 0.175. After annealing in reducing atmosphere, at 700 ^oC, separated Ag and Cu nanoclusters are formed in the silica matrix, with clearly visible SPR bands of both Ag and Cu. Both Ag and Cu SPR peaks are shifted with respect to SPR of single-metal doped silica. The size of the clusters and their distribution turn out to be dependent on the film

composition. Bright-field TEM of lAg3Cu sample, annealed at 700 ^{o}C, is shown in Figure 5.

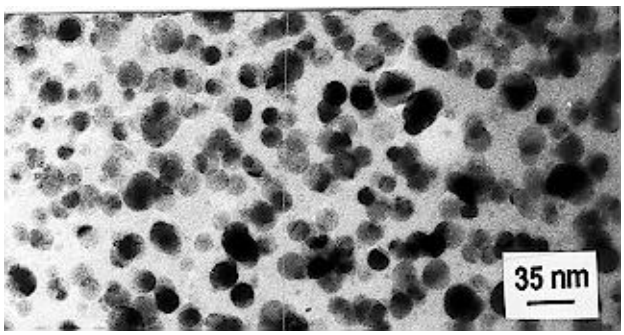

Figure 5. TEM micrograph of the lAg3Cu coating annealed at 700 ^{o}C in 5%H_2-95%N_2 atmosphere.

In the lAglCu sample small clusters of about 5 nm in diameter and bigger clusters of 40-50 nm in diameter coexist. A narrower size distribution with diameters from 5 to 35 nm is observed in the lAg2Cu film. Clusters become spherical with a more homogeneous distribution (5-20 nm in diameter) in the case of 1Ag3Cu sample. Z-scan measurements [10] were performed for a laser pulse duration of 6 ps and in the wavelength range from 570 to 590 nm. For sample 1Ag1Cu and pure Cu the measured value of nonlinear refractive index are both of the order of 10^{-13} m^2/W at λ=590 nm. A study of nanocluster annealing behavior has been performed in different annealing atmospheres. Cluster growth and dissolution, as well as migration of metal atoms towards the sample surface, with a subsequent evaporation, were observed to occur at temperatures which depend on the annealing atmosphere. In particular, in the mixed silver-copper system, the formation of Ag-Cu phase separated clusters was observed.

IV. CONCLUSIONS

Metal nanoclusters are formed in silica and soda-lime glasses by using different methods. From the point of view of nonlinear optical material fabrication, the investigated techniques promise to be suitable for designing nonlinear devices with performances based on nonlinear metal-doped glasses. Extended research activity is necessary in particular for reaching the control of the cluster size uniformity and of the cluster stability during high-power laser irradiation.

REFERENCES

[1] T. Kobayashi, Nonlinear Optics 1, 91 (1991).
[2] E. M. Vogel, J. Am. Ceram. Soc. 72, 719 (1989).
[3] G. I. Stegeman and R. H. Stolen, J. Opt. Soc. Am. B6, 652 (1989).
[4] G. W. Arnold, in: Homage to Galileo (Invited Paper at the International Conference "From Galileo's 'Occhialino' to Optoelectronics: Frontiers of Optical

Systems and Materials", Padova, Italy,1992), ed. P. Mazzoldi (CLEU P, Padova, 1992) p. 3 and references therein.
[5] P. D. Townsend, in: Modifications Induced by Irradiation of Glasses, ed. P. Mazzoldi (Elsevier, Amsterdam,1992) p. 73 and references therein.
[6] A. P. Webb and P. D. Townsend, J. Phys. D8,1567 (1975).
[7] P. Mazzoldi, G. W. Arnold, G. Battaglin, R. Bertoncello and F. Gonella, Nucl. Instr. Meth. B91, 478 (1994).
[8]R. F. Haglund, Jr., L. Yang, R. H. Magruder, C. W. White, R. A. Zuhr, Lena Yang, R. Dorsinville and R. R. Alfano, Nucl. lnstr. Meth. B91, 493 (1994).
[9] G. De, A. Licciulli, C. Massaro, L. Tapfer, M. Catalano, G. Battaglin, C. Meneghini and P. Mazzoldi, J. Non-Cryst. Solids 194, 225 (1996).
[10] G. De, L. Tapfer, M. Catalano, G. Battaglin, F. Caccavale, F. Gonella, P. Mazzoldi and R. F. Haglund, Jr., Appl. Phys. Lett., (1996) in press.
[11] G. W. Arnold and J.A. Borders, J. Appl. Phys. 48,1488 (1977).
[12] P. Mazzoldi, L. Tramontin, A. Boscolo-Boscoletto, G. Battaglin and G.W. Arnold, Nucl. Instr. Meth. B80/81,1192 (1993).
[13) G. W. Arnold, P. Mazzoldi, L. Tramontin, A. Boscolo-Boscoletto and G. Battaglin, Mat. Res. Soc. Symp. Proc. 279, 285 (1993).
[14] G. De Marchi, F. Caccavale, F. Gonella, G. Mattei, P. Mazzoldi, G. Battaglin and A. Quaranta, Appl. Phys. A, (1996) in press.
[15] F. Caccavale, G. De Marchi, F. Gonella, P. Mazzoldi, C. Meneghini, A. Quaranta, G. W. Arnold, G. Battaglin and G. Mattei, Nucl. Instr. Meth. B96, 382 (1995).
[16] G. Battaglin, G. De Marchi, F. Gonella, G. Mattei, P. Mazzoldi, C. Meneghini,A. Quaranta and F. Garrido, Proc. of the XVII International Congress on Glass, Beijing, China, October 1995, Vol. 4, Chinese Ceramic Society (Beijing 1995) 96.
[17] F. Gonella, G. Mattei, P. Mazzoldi, E. Cattaruzza, G. W. Arnold, G. Battaglin, P. Calvelli, R. Polloni, R. Bertoncello and R. F. Haglund, Jr, Appl. Phys. Lett., (1996) in press.
[18] A. A. Ahmed, N. A. Sharaf, E. W. Abd Allah and F. M. Ezz-Eldin, Phys. Chem. Glasses 34,168 (1993).

ON THE MULTIFARIOUS RESULTS OF INTERACTION BETWEEN AMORPHOUS MATERIALS AND IRRADIATION OF DIFFERENT ENERGIES - A SPECTROSCOPIC STUDY

Marianne Nofz[1], Reinhard Stosser[2], Christian Reich[1] and **Eberhard Janata[3]**
[1]Federal Institution of Material Science and Testing, Germany
[2]Humboldt-University, Institute of Chemistry, Germany
[3]Hahn-Meitner-Institute, Germany

Abstract

The interaction of UV- (excimer laser, 248 nm), $\gamma(^{60}Co)$ - radiation and high energy electrons with various silicate glasses was studied using ESR and time resolved optical techniques (absorption and emission). The parameters of irradiation, for example the radiation energy and repetition rate of the laser pulses, and the chemical composition of the glasses were varied. The latter was done in order to change the amount of hole and electron traps by altering the number of non-bridging oxygens and by replacing Ca by Cd or Zn. Thus, it was possible to distinguish between long lived deep and shallow trapped electrons and holes and to detect fast recombining species.

I. INTRODUCTION

Interaction between radiation and glasses or glassy-crystalline materials causes a variety of changes of microscopic and macroscopic properties. The extent of these changes depends on the composition and structure of the materials as well as on the irradiation parameters (energy, dose, dose rate, temperature). One of the essential processes occuring during irradiation of the samples by γ-rays or fast electrons is the formation of electron-hole pairs. These free carriers can move and recombine, or were trapped at structural defects or impurities [1]. Recombination rates and competetive trapping of holes and electrons depend on the physical state of the glass including the manifactoring history. The influence of the composition concerns the glass system itself and dopants/impurities as well. In alkaline earth aluminosilicate glasses [2,3], paramagnetic hole centres could be detected and assigned to different defect types. The simultaneous trapping of electrons by traces of Fe^{3+} forms the basis for the stability of the hole centres [4]. Since trapping of charge carriers by redox pairs like Fe^{2+}/Fe^{3+} leeds to a defect structure stable at room temperature, the physical and chemical action of electron traps like Zn^{2+} and Cd^{2+} is less understood: (i) The resulting Zn^{+} or Cd^{+} centres are well detectable at 77K but less stable at room temperature, and (ii) competetive trapping of electrons by Fe^{3+} and Zn^{2+}/Cd^{2+}, which depends on the polymerization of the glassy network [4], has to be considered.

It is the aim of this paper to get a deeper insight into the competing electron and hole trapping as well as their recombination processes and subsequent reactions in

aluminosilicate glasses. Therefore, samples of different composition were studied by means of ESR and optical spectroscopy before and after irradiation at 300 and 77 K respectively. The suitability of ESR was recently outlined in [5]. Coupling an excimer laser to an X-band ESR spectrometer allows to follow the interaction of laser light with the samples in situ. Electron irradiation induced emission and changes in optical transmission were registered on the microsecond domain.

II. EXPERIMENTAL

Table 1 shows the compositions of all glasses studied here. They were prepared by melting the respective carbonates and oxides (1 kg batches) at 1550 ^{o}C in Pt/Rh crucibles as described before [2,4].

Table 1: Compositions (Mol%) of the samples under investigation

Sample	Composition Mol%	Sample	Composition Mol%
Ca1	$33CaO/18Al_2O_3/49SiO_2$	Cd1	$33CdO/18Al_2O_3/49SiO_2$
Ca2	$21\ CaO/21Al_2O_3/58SiO_2$	Cd2	$21\ CdO/21\ Al_2O_3/58SiO_2$
Ca3	$33CaO/5Al_2O_3/62SiO_2$	Cd3	$24CdO/14Al_2O_3/62SiO_2$
CCAS	$29CaO/13Al_2O_3/58SiO_2$	Cd4	$33CdO/22Al_20_3/45SiO_2$
CdCAS	$8CdO/21\ CaO/13Al_2O_3/58SiO_2$	Zn	$20ZnO/15Al_2O_3/65SiO_2$
ZnCAS	$8ZnO/21\ CaO/13Al_2O_3/58SiO_2$		

A ^{60}Co source was used for γ-irradiation with a maximum dose of 3000 Gy. Irradiation of the samples was carried out at 300 K and 77 K respectively.

The pulse radiolysis facility ELBENA [6] was utilized to perform irradiations with 3.8 MeV electrons and to follow the induced changes in optical absorption and induced emission on the microsecond time scale. The shown emission spectra were not corrected for the wavelength dependent sensitivity of the detection system.

ESR spectra were measured at X-band frequencies as described before [2,4], using small samples (3 x 3 x 5 mm^3).

Optically polished samples (thickness: 0.5 mm) were used for the recording of UV/NIS transmission spectra.

III. RESULTS AND DISCUSSION

Fig. 1 summarizes characteristic ESR observations caused by hole and electron trapping in Cd or Ca containing aluminosilicate glasses.

The ESR spectra show the signals of trapped holes ($Si\text{-}O^-/h^+$; $Si\text{-}O\text{-}Al/h^+$) and electrons ($Cd^+$) as well (the different patterns are assigned in fig. 2). Comparing all spectra, the following results should be emphasized: (i) The paramagnetic centres in the Cd containing glasses are less stable than those in the Ca containing ones, (ii) if the content of CdO exceeds that of Al_2O_3, no Cd^+ centres are observable in these ternary aluminosilicate glasses. But, for $CdO=Al_2O_3$ a large signal due to Cd^+ centres was detected. The last observation can be explained by the role of Fe^{3+} ions, which are impurities of the Al^{3+} compound used for the sample preparation. Cd^+ centres are only

observable if Fe^{3+} cannot compete for electrons. For sample Cd2, the ESR signal at g'~4.3 did not decrease after irradiation as was observed for all other samples (not shown here). Then, in a simplified manner, a part of the radiation induced redox reactions can be summarized as follows:

(a) For all glasses it can be assumed:

$$X\text{-}O \overset{\Delta E}{\rightleftarrows} X\text{-}O/h^+ + e^- \quad (1)$$

$$Fe^{3+} + e^- \rightleftarrows Fe^{2+} \quad (2)$$

$$Fe^{3+} \overset{\Delta E'}{\rightleftarrows} Fe^{2+} + h^+ \quad (3)$$

$$Si\text{-}O^- + h^+ \rightleftarrows \{Si\text{-}O^- / h^+\} \quad (4)$$

$$Si\text{-}O\text{-}Al + h^+ \rightleftarrows \{Si\text{-}O\text{-}Al / h^+\} \quad (5)$$

(b) The following reaction additionally must be taken into account, if the content of CdO is equal to Al_2O_3:

$$Cd^{2+} + Fe^{2+} \rightleftarrows Cd^+ + Fe^{3+} \quad (6)$$

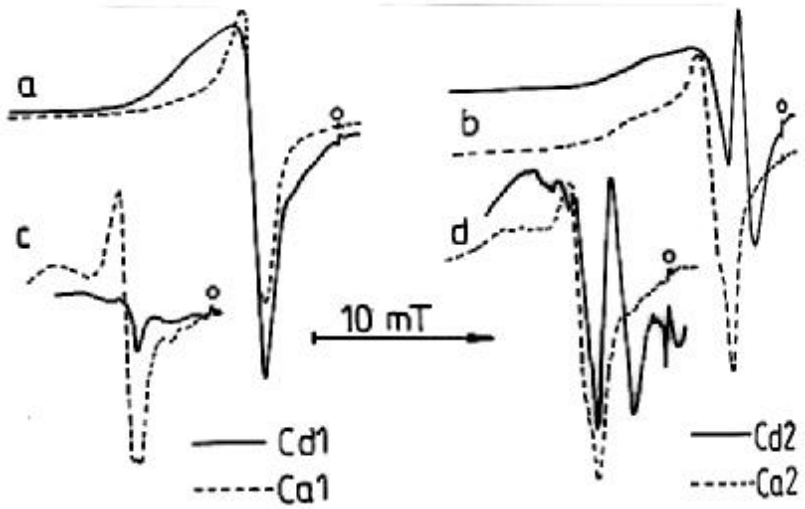

Fig. 1: ESR spectra (10 mW; 77 K) of the samples Cd1/Ca1 (left) and Cd2/Ca2 (right) taken a,b) immediately after γ-irradiation at 77 K, and c,d) after storing the samples at 300 K for some hours. O indicates the signal of a standard at g'=1.9796,which can be used to calibrate the field positions and the signal intensities respectively.

Figs. 2 and 3 show competitive electron and hole trapping under the action of γ- and UV-irradiation for another group of glassy samples. Though the content of Al_2O_3 is smaller than (CdO/ZnO + CaO), Cd^+/Zn^+ centres are formed while the content of Fe^{3+} decreases. As can be deduced from fig. 2, the UV-irradiation used here is not sufficient to trap holes at Si-O-Al bridges. Otherwise (fig. 3), the ratio between the paramagnetic hole and electron centres being detectable, depends on the repetition rate of the laser, indicating different thermal and radiation stabilities of these two types of centres.

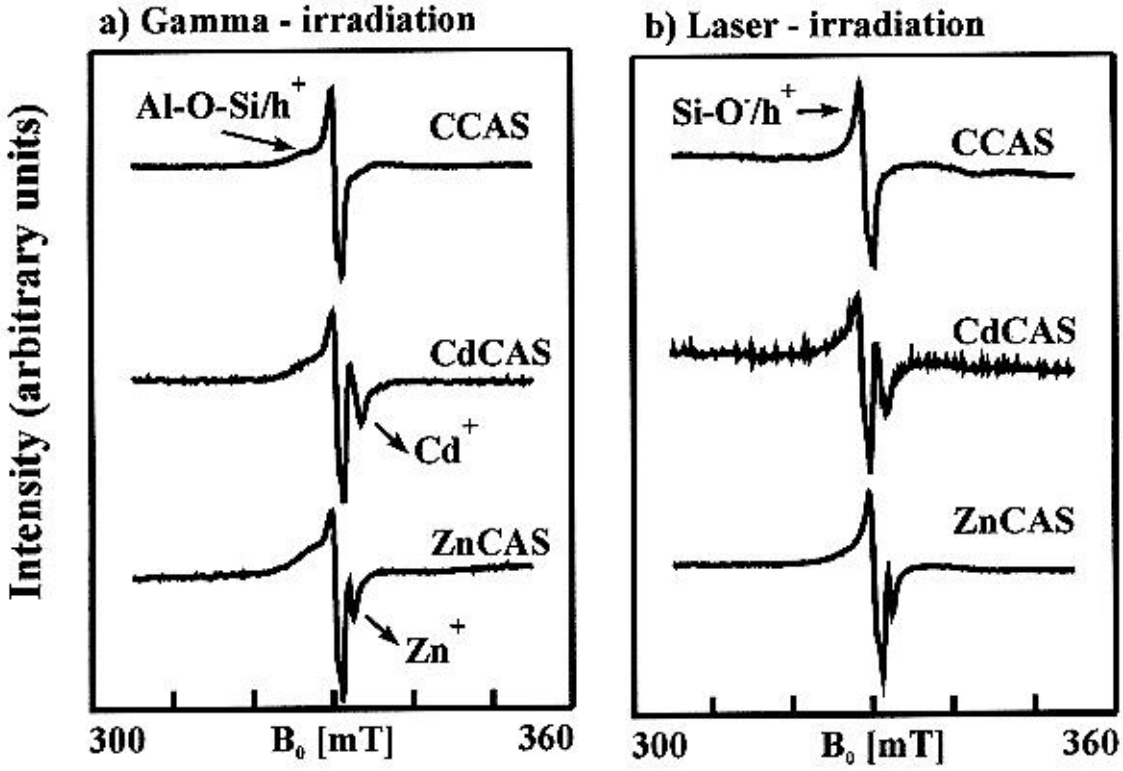

Fig. 2: Comparison of the ESR spectra (20 mW; 77 K) obtained after g-irradiation at 300 K (a) and in situ laser excitation (b); 77 K; 248 nm) respectively

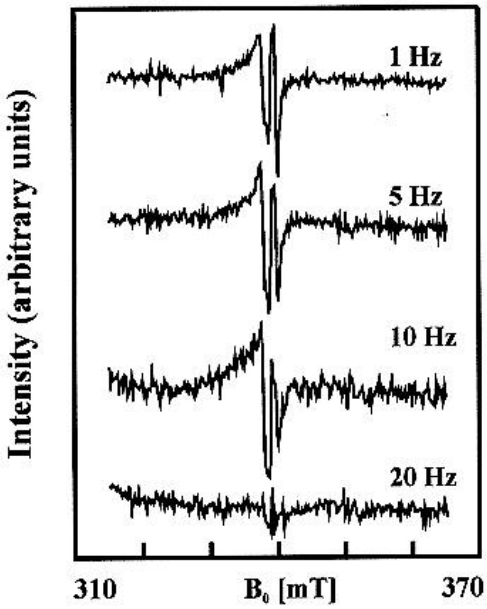

Fig. 3: ESR spectra (20 mW; 300 K) of sample ZnCAS taken after in situ laser excitation (300 K; 248 nm) at the repetition rates indicated

Fig. 4 shows γ- and electron-irradiation induced changes of Ca and Cd/Zn containing samples. These observations are stable at room temperature for some days.

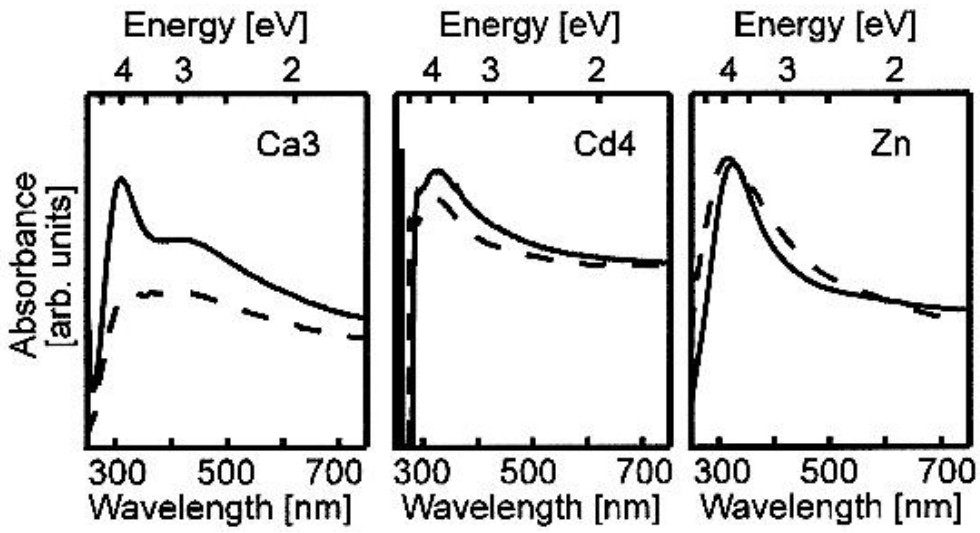

Fig. 4: UV/Vis spectra of the samples indicated taken days after g- (-) and electron (- - - -) irradiations respectively

The study of the time dependence of the radiation induced changes of the optical transmission exhibits more details of the processes responsible for the long-time stable changes of the optical and magnetic properties (fig. 5). As the comparison of the difference spectra (i.e., absorption after irradiation referenced to that of an unirradiated or bleached sample) shows, the color centres initially formed and absorbing in the visible

range of the spectrum, tend to rapidly recombine or transform to stable subunits, which have their absorption bands at shorter wavelength.

Fig. 6 shows the time dependence of the optical emission observed for three different glass compositions after irradiation with electrons. Obviously, the Zn^{2+} and Cd^{2+} ions interfere with defect formation and decay processes by locally trapping electrons. As a consequence, there is no remarkable shift in the emission spectra caused by the interactions with recombination centres and the radiation induced absorption decays faster than in the case of Ca aluminosilicate glasses.

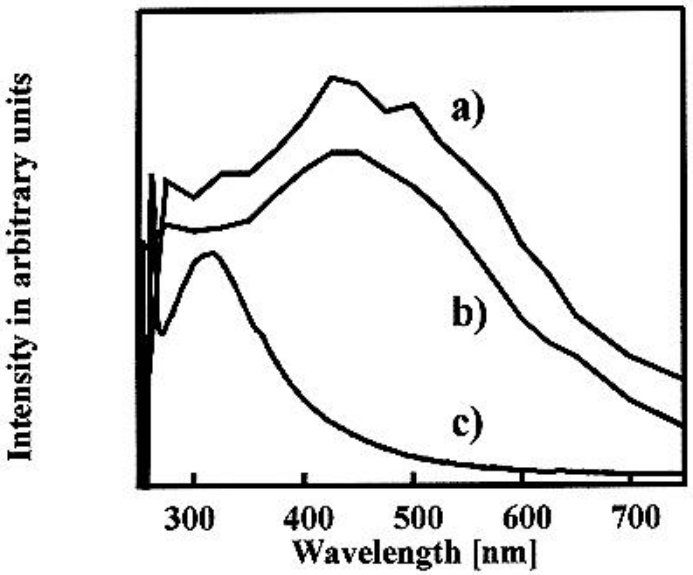

Fig. 5: Optical absorption difference spectra of sample Cd3 at a) $4.8 \cdot 10^{-7}$ s, b) $5.0 \cdot 10^{-6}$ s, and c) several days (amplified relative to a, b) after interaction with 3.8 MeV electrons at 300 K.

IV. CONCLUSIONS

The interaction of high-energy irradiation (excimer-laser operating at 248 nm, γ-radiation and electrons) with glasses of suitably selected compositions show different spectral responses on the short- (μs) and long-time (days) scales. Deep and shallow traps in the glasses were populated by electrons and holes in dependence on the kind, dose and repetition time of the action of irradiation. The types of electronic defects including their spinrelaxation behaviour were evidenced by ESR.

Time resolved optical absorption and emission measurements reveal similar effects in the short-time range after excitation of the glasses. But, at time intervals of some seconds, the optical phenomena depend on the composition and microstructure of the glasses, indicating different structural relaxation processes.

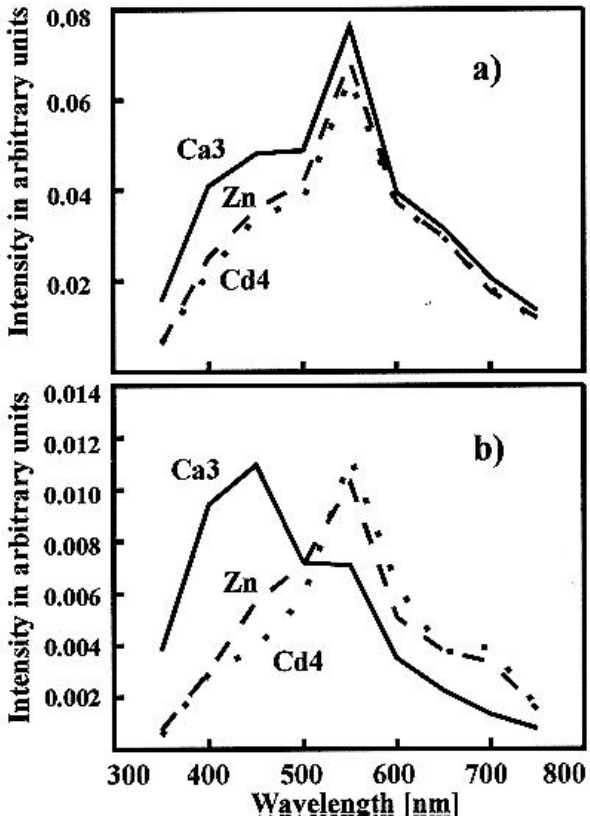

Fig. 6: Optical emission spectra of the samples indicated taken a) $3.36 \cdot 10^{-7}$ s at maximum of the electron pulse), and b) $5.05 \cdot 10^{-7}$ s after interaction with 3.8 MeV electrons

Acknowledgment

We wish to thank the Deutsche Forshungsgemeinschaft (Sto 301/1-1; Ha 1799/2-3) and the Fonds der Chemischen Industrie for financial support.

REFERENCES

[1] D.L. Griscom: SPIE 541(1985) 38
[2] M. Nofz, R. Stösser, F.G. Wihsmann: Phys. Chem. Glasses 31(1990) 57
[3] D.A. Dutt, P. L. Highby, C.I. Merzbacher, D. L. Griscom: Ceram. Trans. 28 (1992)111
[4] M. Nofz, R. Stösser, F.G. Wihsmann: J. Non-Cryst. Solids 129(1991) 249
[5] R. Stösser, M. Nofz: Glastech. Ber. Glass Sci. Technol.67(1994) 156
[6] E. Janata: Radiat. Phys. Chem.47(1996) 29

OPERATION PROPERTIES OF THE GLASSY OPTICAL GLUE

Ya. S•tina and **Yu. Auz~ns**
Riga Technical University, Latvia

Abstract

Easily melting glasses on the base of tetrafluorborates with the low refractive index n_D from 1.41 to 1.45, transparency region of spectra from 200 to 2700 nm and dispersion coefficient √=95-60 have been obtained. These glasses enable to substitute polymeric materials (optical glues) for assemble of the multimode optical quartz fiber into connectors.

The results of measurements of optical properties are presented with the respect to glass structure investigations that will be discussed in some details. As a rule, the refractive index decreases drastically, but dispersion coefficient increases with increasing of total amount of fluorine ion in compositions. To use the easily melting fluorine containing borophosphate (FBP) glasses as optical glues for connectors, it is essential that the microanalysis shows formation of the reaction zone of 2μm. This diffusion of chemical components of FBP glass and quartz glass provides necessary strength of coupling of fiber and FBP glass.

1. Introduction

The low refractive index of glasses needed for the construction knots with quartz fiber is provided by high content of fluorine. The easily melting fluorine containing borophosphate glasses (FBP), therefore, have been obtained and investigated within the system LiF - BPO_4 - RBF_4 (R=K,Na). The previous papers have presented glass structure investigations; however, some results concerning refractive index, spectral transparency region, and temperature application range have been reported [1,2].

The main objective of the current investigation is to present optical properties as well as some operation properties of glasses obtained. Generally, these properties can be controlled by changing the concentration of glass forming units. The previous investigations show that tetrafluorborate groupings and oxidation products participate in glass structure forming process during glass melting.

2. Experimental

Glasses were prepared using analytical reagent grades of chemicals, LiF, BPO_4, KBF_4 and $NaBF_4$. The mixtures of 10g for compositions under research were melted at 1000^oC for 0.15h in air. The alumina crucibles were used. Melt was poured onto a brass plate. To obtain the sample of 10 mm thickness the amount of 50g was melted and cast into a vitreous carbon mould.

Optical constants were determinated for glass samples annealed few degrees below transition temperature (T_g). T_g was determined on the base of dilatometric measurements. The optical

transmission was measured with СФ-26 spectrophotometer for well polished glass samples of 1.0 mm thickness. The refraction index (n_D) was determined for all the set of glass samples obtained by standard immersion liquid method. The dispersion coefficient was calculated on the basis of data obtained on Pullric refractometer PR-2. Raman spectra were measured on 10X10X10 mm well-polished samples using DFF-24 and OMAR-89 spectrometers. Spectra were exited by argon laser irradiation (λ=488 nm; power 1 W). Infrared absorption spectra (IR) within range 400-1600 cm^{-1} were measured with Specord-75 IR spectrophotometer. The contact zone between the optical glue (FBP glass) and quartz was investigated using scanning electron microscope STEPEOSCA 250 M K-3.

3. Results and discussion

The glassforming area for investigated system LiF-BPO_4-RBF_4 (R=K,Na) is limited by the content of KBF_4 40-65 and $NaBF_4$ 35-70 mol.%. This wide glassforming area is determined by presence of two glassformers: boron and phosphorus as well as by the possibility to form P-O-B structural groupings. Simultaneously fluorine ion can take part both in the formation of common glass network and in the depolymerization process of borophosphate frame. Within the melting process fluorine moves from the boron coordination sphere in BF_4 groups to the phosphorus coordination sphere in PO_3F groups. The main glassforming groupings of FBP glasses prove to be B(III)-O, B(IV)-O, P-O-B, PO_3F, or $PO_{(4-x)}F_x$ [3-6].

The phase equilibrium set up in the region with F^- content 25-35 mas.% and the ratio B/P = 2/1.2; and synthesized glasses have stabile operation properties, i.e., stabile to crystallization and resistant in air.

By variation of the ratio of borate to fluorphosphate groupings, the glass compositions with high fluorine content (up to 25-35 mas.%) reach the lowest values of the refractive index (n_D=1.41-1.43). For all glass compositions under research, the value of the refractive index decreases as the total content of fluorine within compositions increases (Fig.1 a,b).

Figures 2 a,b show n_D values of the particular cross-sections of the systems where content of BPO_4 is constant. Generally, n_D values of glasses in KBF_4 system are lower than those in $NaBF_4$ system. Depending on composition, these values change from 1.498 to 1.420 in KBF_4 system and from 1.512 to 1.448 in $NaBF_4$ system. It is remarkable that n_D is lower than 1.43 for the glass compositions where KBF_4 initially introduced is $\geq$ 65 mol.%. The tuming points in the curves $n_D=f(c_{F^-})$ occur for compositions when the amount of RBF_4 (R=Na, K) reaches 50 mol.%. Up to this, n_D values decrease constantly with the amount of fluorine. Regarding structural investigations, these changes of physical properties appear because of significant structural changes of glasses. Up to 50 mol.% of RBF_4 , it is assumed that fluorine is distributed within borophosphate frame without participation in forming of borophosphate groupings. When fluorine content exceeds some concentration, groupings containing fluorine were formed. Borophosphate frame become more open with shorter chains containing PO_3F^- ($PO_{4-x}F_x$) groupings. The formation of another fluorine containing groupings are possible as fluorine content raises.

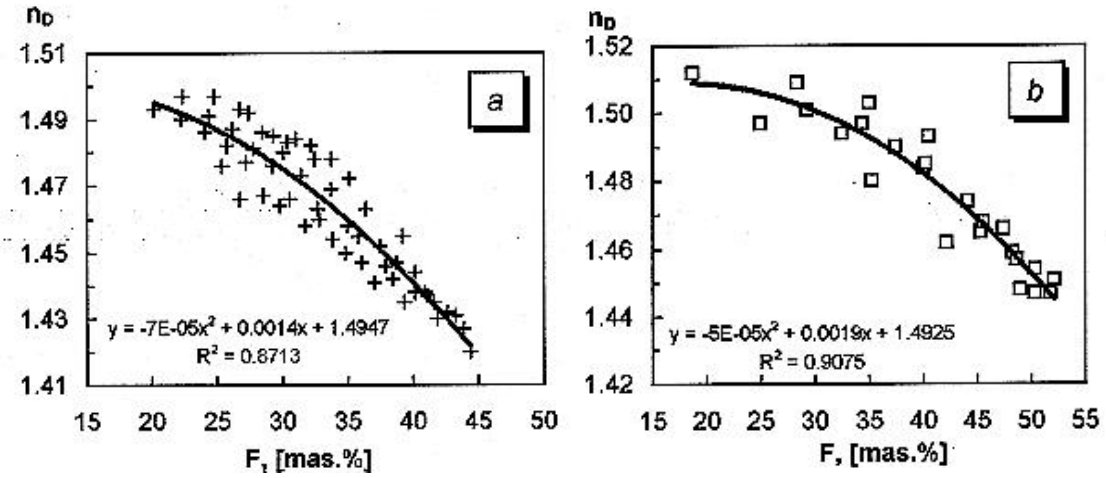

Fig.1 The sample set of refractive indexes of glasses in system a - LiF-BPO_4-KBF_4 and b - LiF-BPO_4-$NaBF_4$ depending on fluorine content.

The values of the principal optical properties for same glasses of both tetraborate systems are shown in Table 1. The Refractive indexes have corresponds to wavelength of spectra as follow: n_g - 435.8 nm, $n_{F'}$ - 480.0 nm, n_e - 546.1 nm, n_d - 587.6 nm, and $n_{c'}$ - 643.8 nm. The principal dispersion n_F-n_c and Abbe values $\sqrt{D}$ were calculated.

As follows from Table 1, the glasses in KBF_4 and $NaBF_4$ systems have particular optical constants. These characteristics combine low refractive index, principal dispersion n_F-n_c=0,0038÷0,0070, and high dispersion coefficient ν_D=68÷123. The Abbe values obtained glasses may exceed conventional values of optical glasses $\Delta\nu_D$ ~30. These glasses should be found in the left light crown region of Abbe diagram. Besides, like fluorphosphate crown glasses the low particular dispersion within blue region of spectra have been founded for these glasses $\gamma_{g\text{-}F'}$=0, 0049÷0, 0107.

The glasses of RBF_4 (Na,K) systems have start of UV transmitance (λ_0) in the region from 220 to 260 nm. The transmission for all glasses at 300 nm have the values 20%<T<67%. the maximal values of UV transmission are 80÷90%, generally starting from 320 nm. λ_0 for some glasses in KBF_4 system is shifted to the lower frequency region and reaches even 30 % transmission at 200 nm (Fig.3) [7-11].

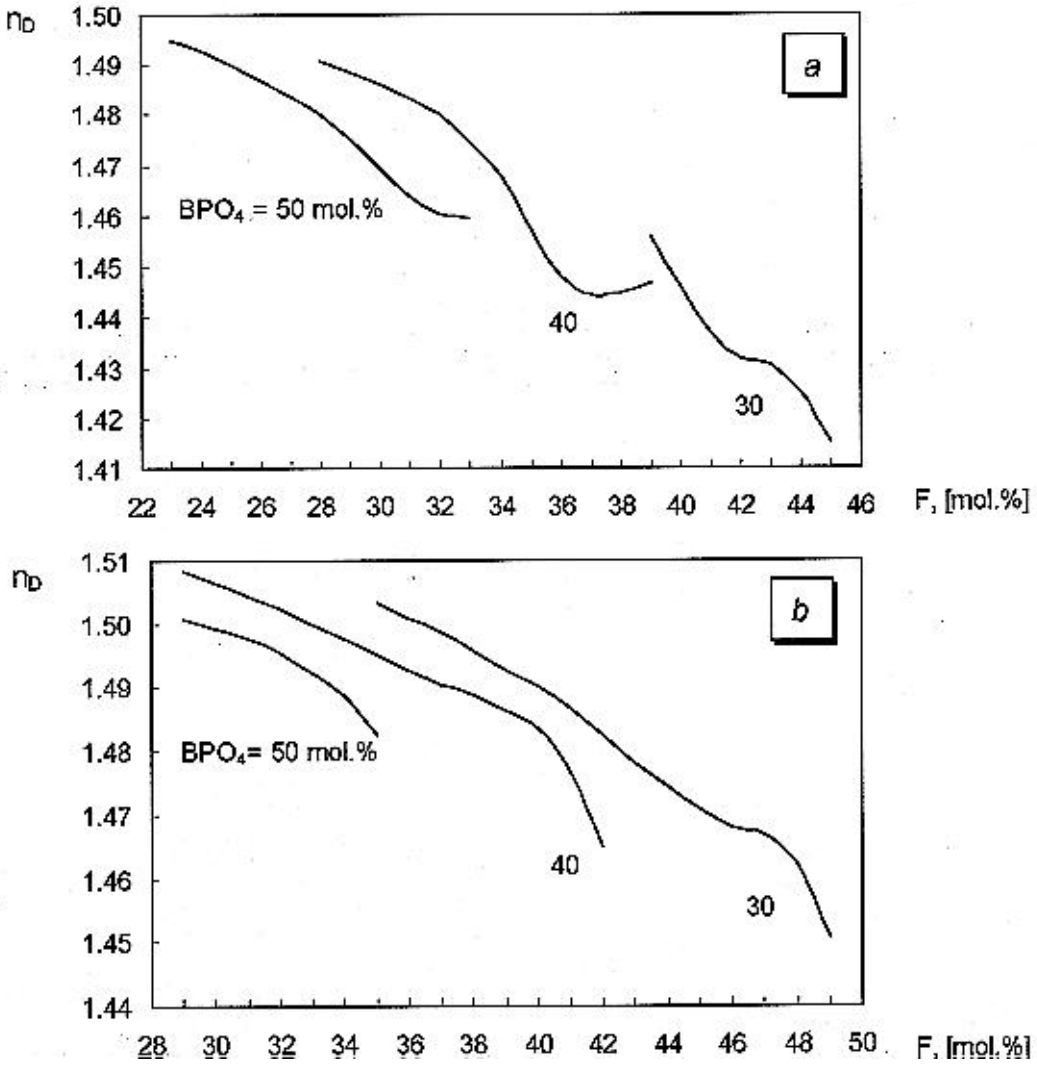

Fig. 2 The dependence of refractive index in the system KBF_4 (a) and $NaBF_4$ (b) glasses upon fluorine introduced for the cross-sections with the constant amount of BPO_4

In order to estimate a mechanism of coupling, microanalysis of the contact zone between FBP glass layer and quartz was carried out [12,13]. Formation of the reaction zone in depth of 2 μm was observed after the thermal treatment at temperature 600^0C (the temperature that corresponds to temperature of assembling of optical quartz fiber into connector). The reaction zone, which is responsible for the strength of coupling, was formed by mutual diffusion of chemical elements of FBP glass and quartz glass.

Table 1. Compositions, principal optical properties of glasses

Comp. No.	Composition (mol.%)				Refractive index						
	LiF	BPO_4	KBF_4	$NaBF_4$	n_g	n_F	n_e	n_d	n_C	n_F-n_C	$\sqrt{}_D$
A-19	30	50	20	-		1,4958	1,4916	1,4905	1,4890	0,0063	78
A-42	20	50	30	-		1,4878	1,4852	1,4826	1,4812	0,0066	73
A-40	30	40	30	-		1,4775	1,4741	1,4722	1,4702	0,0070	67
A-61	10	50	40	-		1,4733	1,4702	1,4692	1,4676	0,0050	94
A-59	20	40	40	-		1,4713	1,4678	1,4667	1,4656	0,0052	90
A-57	30	30	40	-		1,4578	1,4527	1,4517	1,4507	0,0054	84
A-76	-	50	50	-	1,4580	1,4541	1,4510	1,4497	1,4490	0,0048	94
A-74	10	40	50	-	1,4576	1,4550	1,4519	1,4508	1,4480	0,0054	83
B-72	20	30	-	50	1,4815	1,4708	1,4674	1,4657	1,4641	0,0067	70
B-85	-	40	-	60	1,4768	1,4719	1,4704	1,4681	1,4665	0,0058	81

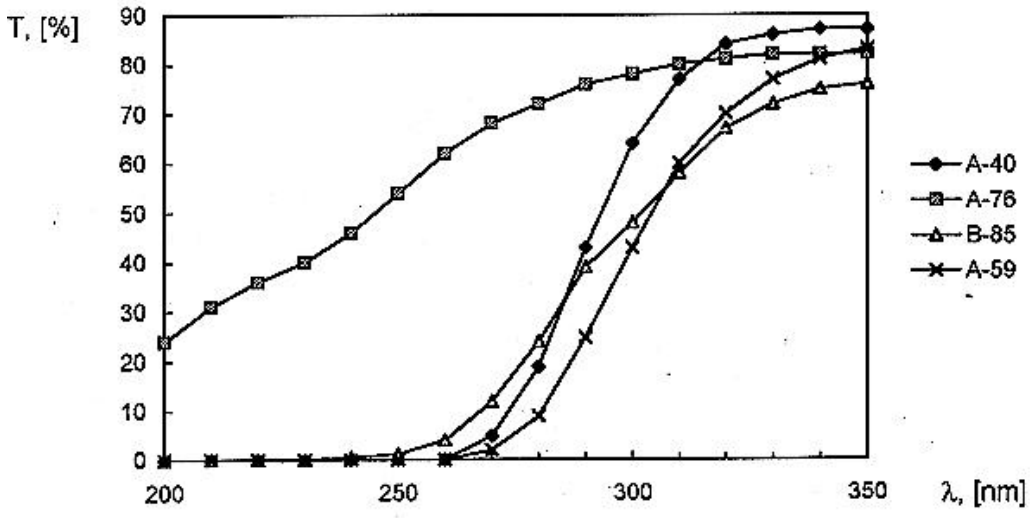

Fig. 3 UV transmission for some glasses investigated.

Fig. 4 shows that at the border of quartz glass (point 1) the distribution of Si, P, and K is regular, but microanalysis of quartz glass within the depth of 1 μm from contact surface (point 2) indicates only the presence of silicium. The diffusion of Si from quartz glass at the border of FBP glass and reaction zone (point 3) does not exceed the amount of 10 %. The results well agreed with the results of corrosion of quartz glass within fluorine containing glass melts [14]. To use FBP glasses as the optical glues for connectors of optical quartz glass fiber, it is important that the diffusion of chemical components and corrosion of quartz glass occurs within the contact layer of 2μm.

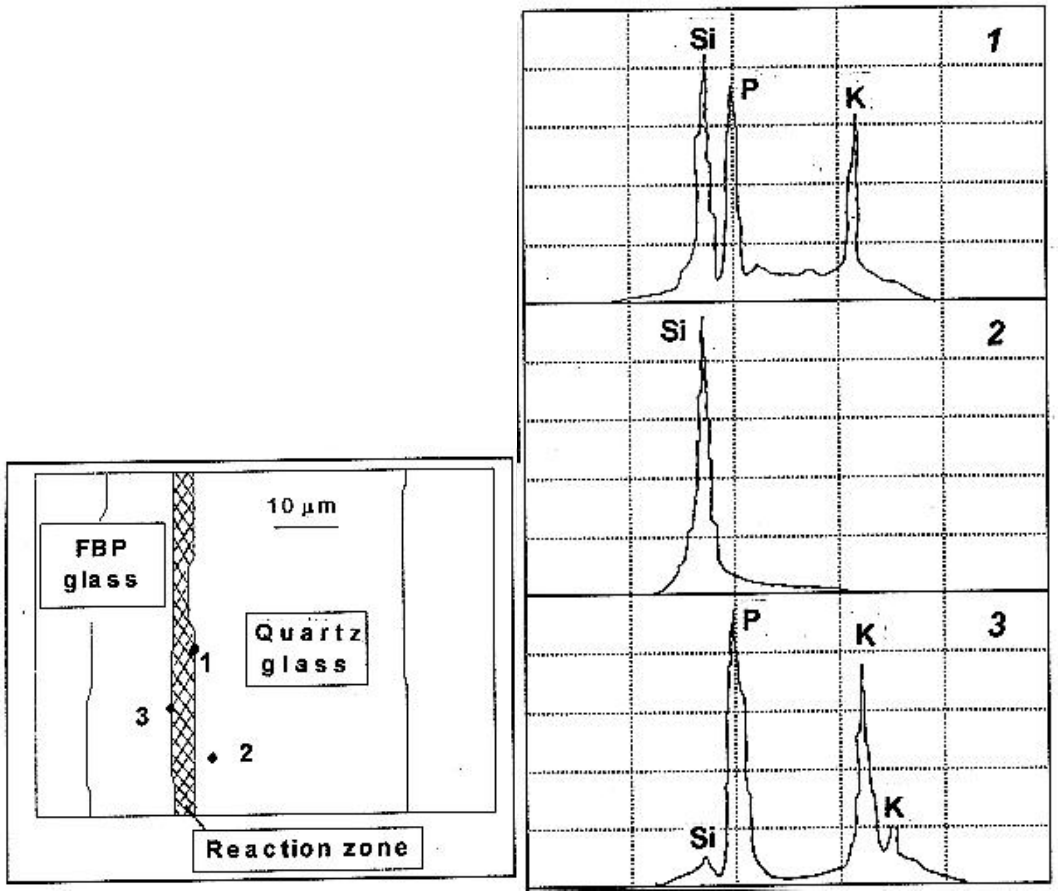

Fig. 4 Distribution of chemical elements in situ points: 1- quartz glass - reaction zone, 2 - quartz glass 1 mm depth, 3 - reaction zone-FBP glass

References

[1] S tina Ya., Auz~ns Yu., Sedmalis U., Glass structure formation procedure within the system LiF-8P0$_4$-KBF$_4$(NaBF$_4$). Glastechn. Ber.Glass Sci. Technol. C1 (1995), 91-96.
[2] S tina Ya., Auz~ns Yu., Sedmalis U., Fluorine containing borophosphate glasses for optoelectronics. Proc. of XVII International Congress on Glass, Vol. 5, Special Glasses (1995),115-120.
[3] Tian F. and Pan L., NMR studies of lithium borophosphate glasses, J Non-Cryst Solids,112(1-3)(1989),142-146.
[4] Massot M., Haro E., Oueslati M., et al, Structural investigation of doped lithium borate glasses, Mater Sci and Eng, 3 (1-2) (1989), 57-63.
(5] Smith R.A.., Boron in glass and glass making, J Non-Cryst Solids, 84 (1986), 421-432.
[6] Scagliotti M, Villa M., and Chiodelli G., Short range oder in the network of the borophosphate glasses: Raman results, J Non-Cryst Solids, 93 (1987), 350-360.

[7] Schmidt Günther, Optisches Glas-Eigenschaften und Applikation, Silikattechnik, 35 (11) (1984), 337-340.
[8] Ehrt D., Atzrodt R., Vogel W., Struktur-Eigeschaftsbeziehungen optischer Glaser mit anomaler Teildispersion, Wissenschaftliche Zeitschrift der Friedfich-Schiller Universit≅t, 2. Internationales Otto-Schott Kolloquim. Heft 2\3, (1983), 509-526.
[9] Kentaro Terashima, Sae-Hoon Kim, Toshinobu Yoko, Nonlinear optical properties of B_20_3-based glasses: M_20-B_2O_3 (M = Li, Na, K, Rb, Cs,and Ag) binary borate glasses, J. Am. Ceram. Soc., 78 (6) (1995),1601-1605.
[10] Dologudina V., Lebedeva R., Glass Physics and Chemistry,19 {1) (1993), 49-58 lin Russian/.
[11] Verweij H., Buster J.H.J.M., Remmers G.F., Refractive index and density of Li- Na- and K-germanosilicate glasses, J. of Materials Science,14 (1979), 931-940.
[12] Peters P.W.M., Albertsen H., The influence of fibre surface treatment on the formation of an interphase in CFRP, J. of Materials Science, 28 {1993), 1059-1066.
[13] Lemoine P., Salvo M., Ferraris M., Montorsi M., Reaction of SiCf\SiC composites with a zinc borate glass, J. Am. Ceram. Soc., 78 (6) (1995),1691-1694.
[14] S tina Ya., Auz~ns Yu., and Zolatorjova Y., Easily melting glass for assembly of optical fiber into connectors, Proc.SPIE, 2290 (1994), 366-377.

RAYLEIGH AND MANDEL'SHTAM-BRILLOUIN SCATTERING SPECTROSCOPY OF GLASS RELATED TO ITS INHOMOGENEOUS NATURE

Leonid Maksimov
State Optical Institute, Russia

Abstract

Results of glass nature investigation by means of Rayleigh and Mandel'shtam-Brillouin scattering (RMBS) spectroscopy have been generalized. Joint analysis of RMBS, acoustic and Raman scattering data for glasses of simple and complex compositions showed that the major part of Rayleigh scattering in glasses was due to "frozen-in" concentration fluctuations. The latter consist of constant composition groupings which can be determined from Raman scattering spectra. Doped ions presumably enter into concentration fluctuations of a matrix. Ion-ion interactions can be controlled by alteration of glass former/modifier ratio in a glass matrix.

1. INTRODUCTION

As is well-known, glass microinhomogeneity determines such properties of glasses as light scattering losses, optical breakdown threshold, spatial distribution of doped ions in a glassy matrix, etc. (1)

Therefore, the development of a direct structure sensitive method seems to be necessary to study the alteration of glass structure microinhomogeneities as a function of glass composition.

Taking into account that Rayleigh and Mandel'shtam-Brillouin scattering (RMBS) spectroscopy was developed for liquids and crystals earlier we can hope to resolve the problem of relationship between glass inhomogeneities and properties of a glass significant for its application.

It should be emphasized that Rayleigh scattering in glasses is more intensive than that in liquids and crystals. It seems to be an obstacle not only to glass structure investigation but to the development of low-scattering optical media for fiber optics.

The paper is aimed at consideration of RMBS spectroscopy data for both simple glasses and multicomponent commercial ones jointly with the data of high temperature acoustics and Raman scattering spectroscopy.

The sources of Rayleigh scattering losses in glasses and dependences of glass microstructure as a function of glass composition, impurity concentration and outer conditions may be studied by RMBS spectroscopy. As a result, the rating of glass systems and glass composition areas based on RMBS data may be established.

2. THEORETICAL BACKGROUND

As is well-known, Rayleigh scattering follows the Eq.(1):

$$I_{sc} \sim I_{inc} \frac{1}{\lambda^4} \langle \Delta n^2 \rangle (1 + \cos^2 \theta), \tag{1}$$

where I_{sc}, I_{inc} are the intensities of scattered and incident light, correspondingly, l is the light wavelength, q is the scattering angle, $\langle Dn2 \rangle$ is the mean square index fluctuations which are caused both vibrational and translational motion of atoms. The latter causes elastic (Rayleigh) scattering -RS- while the former leads to modulation of light wave of $n=1/l$ frequency with a longitudinal hypersonic wave and appearance of Mandelshtam-Brillouin scattering (RMBS) doublet at $n \pm Dn_l$ frequencies.

In the case of isotropic solids there are two doublets in a spectrum of Rayleigh and Mandelshtam-Brillouin scattering (RMBS) because of non-zero shear modulus in solids. The shifts may be found from Eq.(2,3):

$$\Delta \nu_l / \nu = 2n \, (v_l / c) \, \sin(\theta / 2), \tag{2}$$

$$\Delta \nu_t / \nu = 2n \, (v_t / c) \, \sin(\theta / 2), \tag{3}$$

where *nl, nt* are the velocities of longitudinal and transverse hypersonic waves, correspondingly, c is the light velocity.

As a result, the ratio of RS and MBS components (the so-called Landau-Placzek ratio) may be expressed from medium parameters as follows:

$$R = \frac{I^{RS}}{2I^{MBS}} = \frac{\beta_T}{\beta_S} - 1, \tag{4}$$

where b_T and b_S are the isothermal and adiabatic compressibilities[2].

Eq. (4) works poorly for liquids because relaxation properties of a liquid should be taken into account.

It should be emphasized that $R_{L\text{-}P}$ of a glass exceeds that of a liquid or a crystal significantly. This fact was explained in terms of "freezing-in" fluctuations theory in accordance of which the index fluctuations determining RS intensity correspond the temperatures close to the glass transition temperature T_g[3,4].

It means

$$R_{L\text{-}P} = R_\rho + R_c + R_{an} = \frac{I_\rho + I_c + I_{an}}{2I^{MBS}}, \tag{5}$$

where R_ρ, R_C, R_{an}, I_ρ, I_C, I_{an} are the contributions into $R_{L\text{-}P}$ from "frozen-in" density, concentration, and anisotropy fluctuations.

R_{an} may be estimated from depolarization coefficients with typical values of 0.02-0.10. R_ρ may be calculated from high-temperature acoustic data by means of Eq(5):

$$R = (T_g/T)\,(\beta_{Tg}^{0}\rho v_i^2 - 1), \qquad (6)$$

where $b_{Tg}^{\circ} = (\,r n_0^2)^{-1}$ is the static isothermal compressibility at T_g, n_i and n_{Tg}° are the high frequency and static sound velocities at T and T_g, correspondingly.

Hence, a RMBS spectrum gives us an opportunity to separately estimate contributions into RS losses, a_s and study of chemical inhomogeneity of glasses.

3. RESULTS AND DISCUSSION

3.1. LOW-SCATTERING GLASSES

As follows from RMBS spectra and results of high-temperature acoustic studies, sodium-silicate and sodium-borate glasses are characterized by the contribution of "frozen-in" concentration fluctuations into Rayleigh scattering losses not less than 50%.

Fig.1 shows multicomponent commercial glasses which are more scattering than a silica glass. As shown in Table 1, it is caused by the contribution of concentration fluctuations R_c as high as 93%.

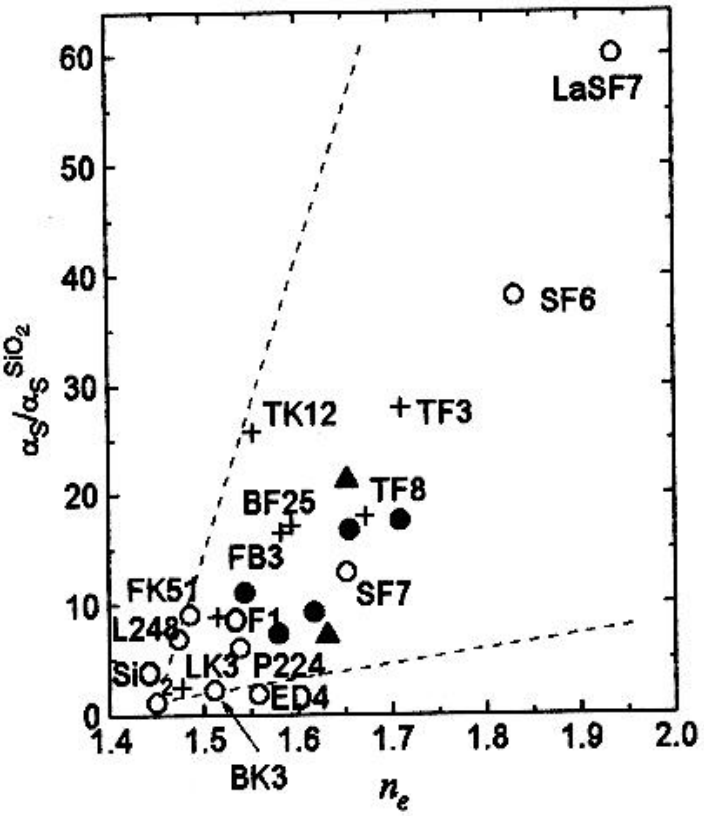

Fig.1. Relative scattering losses, $a_s/a_s^{SiO_2}$, of commercial glasses as a function of their indices.

Table.1. Landau-Placzek ratios and the contributions of frozen in" density and concentration fluctuations for some Russian commercial glasses.

Glass	R_r*	$R_{L\text{-}P}$	R_C	$R_C/R_{L\text{-}P}$
F1	9±2	130±10	120±10	0.92
K15	8±1	30.0±0.5	22±1	0.73
K8	15±3	50±1	35±4	0.70
TF1	7±1	150±10	140±10	0.93

*Note: Calculated from the data of Dr.V.Bogdanov.

If R_ρ is negligible,

$$R_{L\text{-}P} \sim \left(\frac{\partial n}{\partial C}\right)^2_{PT} <\Delta C^2>.$$

It means that low-scattering glass compositions should be sought among highly chemically homogeneous glasses or in the vicinity of extreme points of *n-C* curves. Indeed, the latter path may be followed in phosphate glass systems and low-scattering glass compositions have been found in alkalialuminaphosphate systems. RS losses of phosphate glasses may be reduced to 60% of that of silicate glass [5].

In the case of Na_2O-B_2O_3, Na_2O-SiO_2, Na_2O-GeO_2, K_2O-GeO_2, NaF-GeO_2, KF-GeO_2 glassy systems we showed that "frozen-in" concentration fluctuations are the fluctuations not of oxides or atoms, but of constant composition groupings (CCGs) which play a role of actual components of glass forming systems and may be determined from Raman scattering spectra. Therefore, low values of $<DC^2>$ characterize glasses consisting of CCGs of a single type without or with a minor amount of CCGs of another type. On the contrary, glasses containing CCG of two types of comparable contents are characterized by high Rayleigh scattering intensity [1]. Such behavior of Rayleigh scattering is similar to that in two component solutions [6].

3.2. DOPED IONS SEGREGATION

In 60s G. Karapetyan put forward the idea of non-random distribution of rare-earth ions in glassy matrices (activator segregation phenomenon). As a result, the glass composition dependencies of quantum yield of luminescence, life time of excited states, efficiency of ion-ion interaction, etc. have been explained by selective entering of doped ions into glass matrix inhomogeneities [7]. If so, we can expect correlation between RMBS and luminescence spectroscopy data.

As shown in Fig.2, segregation of rare-earths leads to an increase in $R_{L\text{-}P}$ as compared to undoped glasses ("decoration" of microinhomogeneities) because of the growth of index difference between a microinhomogeneity and its surrounding. Meanwhile, the segregation causes concentration quenching of Yb^{3+} luminescence and enhance of cooperative interaction between Yb^{3+} and Tb^{3+} ions [8].

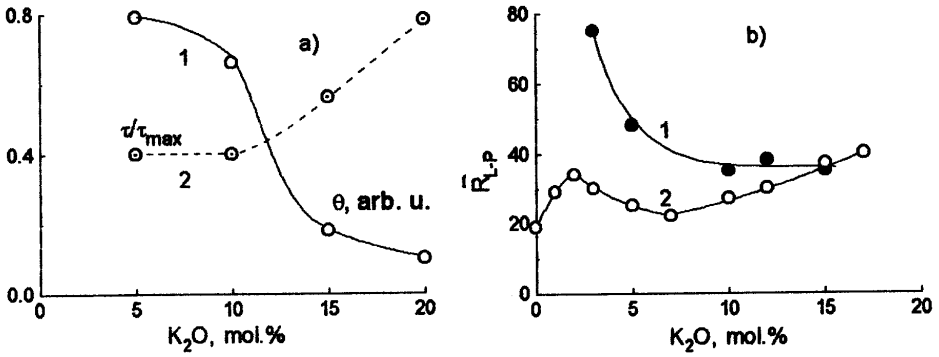

Fig.2. Composition dependencies of potassium-germanate glasses doped by 1 mol% Tb_2O_3 and 1 mol% Yb_2O_3: (a) efficiency of cooperative sensibilization of Tb^{3+} ions by Yb^{3+} ions (1), decay time of Yb^{3+} luminescence (2) [8]; (b) Landau-Placzek ratio for doped (1) and undoped (2) glasses.

Segregation of lead into potassium silicate microinhomogeneities of K_2O-PbO-SiO_2 glasses explains RS losses as a function of potassium oxide on flint glasses [9]. Segregation of niobium into alkali borate microinhomogeneities of alkaliborosilicate glasses leads to their "decoration" that is an increase in both Landau-Placzek ratio and light scattering losses [7]. Accumulation of niobium ions into alkali enriched microinhomogeneities of alkali silicate glassy matrix causes the growth of segnetoelectric microcrystals under the influence of heat treatment [10].

4. CONCLUSIONS

1. Analysis of RMBS spectroscopy results and high-temperature acoustics data makes it possible to separate the contributions into Rayleigh scattering intensity by glasses from those “frozen-in” density, concentration, and anisotropy fluctuations.
2. Low scattering glass compositions may be found on the basis of RMBS data.
3. Being controlled by RMBS spectroscopy the spatial distribution of doped ions are varied by alteration of glass matrix composition.

ACKNOWLEDGMENTS

The research was partially supported by Grant No U12300 from the International Science Foundation and Grant No 93-1316 from the International Association for the Promotion of Cooperation with the Scientists of the former Soviet Union. The author is grateful to Dr. A.Anan'ev and Mrs. E.Maksimova for help in the paper preparation.

REFERENCES

1. Karapetyan G.O., Maksimov L.V., Yanush O.V.J. Non-Crystalline Solids, 1990, v.126, n 1-2, p.93-102.
2. Fabelinskii I.L., Molecular Scattering of Light, New York. N.Y. 1968.
3. Schroeder, J., Light Scattering of Glass. In: Treatise on Materials Science and Technology. V.12, Glass 1. New York, N.Y., 1977, p.157-222.
4. Bogdanov V.N., Nemilov S.V., Solovyev V.A. et al. Fizika I Khimiya Stekla, 1978, v.4, n.4, p.47-55.
5. Karapetyan G.O., Maksimov L.V. Low Scattering Fiber Optics Glasses. First Intern. Sov. Fibre Optics Conf. Proc., V.1, Boston MS, 1991, p.197-222.
6. Vuks M.F. Light Scattering in Gases, Liquids, and Solutions. Leningrad, 1977
7. Karapetyan G.O., Maksimov L.V. Bol.Soc.Esp.Ceram.Vid. 1992, v.31C, n.6, p.495-496.
8. Dmitryuk A.V., Karapetyan G.O., Manenkov A.A., et al. Kvantovaya Elektronika, 1977, v.8, n.4, p.1661-1665.
9. Karapetyan G.O., Maksimov L.V., Yanush O.V. Sov.J.Glass Phys.Chem. 1992, v.18, n.6, p.412-422.
10.Koorolyov Yu. G., Berezhnoi A.A. Glassy-Crystalline Materials with Electrooptic Properties. Poc. XV Intern. Congress on Glass. V.3b, Leningrad. 1989, p.302-305 (in Russian).

THE INFLUENCE OF MINOR COMPONENTS ON COPPER COLOURING OF A SODA-LIME GLASS

Leena Hupa and **Raija Siikamäki***
Åbo Akademi University,
*University of Art and Design, Finland

Abstract

The typical turquoise colour of a commercial glass is due to cupric ions. The hue of the colour depends on the melting temperature of the glass, the concentration of copper and the content of minor ingredients such as iron oxide and refining agent in the glass. The influence of these factors on the colour intensity and hue was tested by melting a soda-lime glass in an electric laboratory furnace. Decreasing the melting temperature changes the hue slightly towards the blue region of the visible spectrum. The intensity of the colour fades with an increased melting temperature. The blue hue of the colour fades also with increased iron as well as antimony oxide content of the batch. Thus, changes in the thermal history of the glass or in content of refining agent or other minor components like impurities in the raw materials affect the colour intensity and hue.

1. BACKGROUND

Calculating a batch to give a glass with a desired colour still requires experiments performed according to the laborious trial and error method. On the other hand, modelling the colour generation in commercial systems containing several components is a tremendous task as the factors influencing the colour intensity and hue depend on many different variables. Fortunately, the overall trends for colouring are well known and applied in glass melting practice. The most important colouring factor states that the colour intensity and hue depend on the amount and properties of the colouring agents, often transition metal ions, added to the glass. Changes in base glass composition or melting parameters like furnace atmosphere and temperature are known to affect the colour. Most colouring agents also interact with reducing or oxidizing agents, i.e. other minor components, in the melt. However, the effect of some minor changes on a specific colour is not explicitly given in literature.

The goal of this work is study how the blue copper colour a particular commercial base glass is affected by changes in the melting parameters like temperature or by other redox ions present in the glass. The results are reported both as the absorption caused by the cupric ion and the colour sensation observed. Some of the absorbance values measured can be used to calculate the extinction coefficient of the cupric ion and the cuprous-cupric equilibrium in the base glass according to an optical method recently published by Cable et al (1989,1992,1992). However, their model is valid for glasses containing only one redox ion. This condition is seldom satisfied by commercial glasses.

2. EXPERIMENTAL

The experimental glass used was a commercial soda-lime pelletized batch available as Philips Brilliant 2500. For the colouring experiments the pellets were ground and the colouring oxide added to this pulverized mixture before melting. The chemical composition for the glass is given in Table 1 both as reported by the manufacturer and as analysed.

Table 1. The chemical composition of the base glass in weight-%. A) according to the manufacturer, B) analysed.

Oxide	A	B
$Si0_2$	65	64.50
B_20_3	-	0.30
Al_20_3	1	1.43
Li_20	-	0.46
Na_20	12	11.70
K_20	4	3.80
Mg0	2	1.94
Ca0	6	5.00
Zn0	1	2.81
Ba0	7	6.40
Fe_20_3	-	0.038
Sb_20_3	0.9	0.60

The commercial batch with different additions of copper oxide was melted in an electric laboratory furnace. The size of the melts was about 250 g and the melting time 4 hours. The commercial batch was melted at three different temperatures, 1353, 1400 and 1450^{o}C. The temperatures were chosen according to the experiments by Cable et al in order to enable a comparison between different glass systems if desired. The glasses were poured into a graphite mould to form rectangular samples of a thickness of roughly 1 cm. In order to estimate the effect of antimony oxide on the colour a batch based on the theoretical composition but without antimony oxide was mixed using commercial raw materials. The influence of iron oxide on the copper colour was studied by glasses with more iron but no antimony oxide. All antimony-free glasses were melted at 1400 ^{o}C.

The absorbance of the carefully annealed glass disks was analysed spectrophotometerically (Perkin Elmer Lambda 2 UV/NIS Spectrometer) using an integrating sphere (RSA-PE-20). All the measured values are calculated to correspond to 1 cm glass thickness. The glass colours were compared both photometrically in terms of colour coordinates and visually. The photometeric determination was done from the transmission spectrum for 1 cm thick glasses. The colour coordinates were measured according to the CIE system using illuminant D6500 corresponding the average daylight conditions. These data were drawn in a CIE (x,y) -chromaticity diagram, from which the dominating wavelength of the colour for each glass was determined graphically.

3. RESULTS AND DISCUSSION

I. Cupric absorption

The typical turquoise colour of glasses containing copper is due to the cupric ion absorbing visible wavelength with a maximum value at roughly 780 nm. Also in oxidized glasses copper can exist as cuprous ions having no visible absorption. The colour intensity of the glass depends on the total copper content and the ratio between the two copper ions in the glass. The influence of the melting temperature as well as the total copper content on the cupric absorption for the glass melted from the commercial pellets is given in Figure 1. The figure shows that the intensity increases with decreasing melting temperature at a specified total copper content. This same trend was observed also by Cable et al when using three component systems. However, for the commercial batch the increase in the maximum absorbance is not linear like was found for the ternary systems by Cable. This difference probably depends on the effect of the other redox ions present in the commercial batch, i.e. the refining agent antimony oxide and the iron impurity in the batch materials used.

Eliminating antimony oxide from the glasses drastically increases the cupric absorption at a specified total copper content, cf. Figure 2. The maximum absorption increases roughly by a factor of four when the refining agent is eliminated. In other words, four times more copper oxide is needed to achieve the same colour strength when the glass contains 0.6 per cent antimony oxide. Naturally this result is valid only at 1400 ^{o}C for the glass composition used.

The difference in the cupric absorption between the two glasses in Figure 2 is due to the reaction of antimony oxide with copper oxide. All other possible factors like glass basicity and structure were equal but for minor additions. The reaction between the two redox ions can be described as

$$2\ Cu^{2+} + Sb^{3+} = 2\ Cu^{+} + Sb^{5+} \qquad (1)$$

giving that one mole antimony (III) ions is needed to reduce two moles cupric ions. A stoichiometric calculation for a complete reduction of cupric to cuprous by antimony oxide gives that the amount available, 0.60 weight-% Sb_20_3, is capable to reduce 0.66 weight-% CuO. However, Figure 2 shows that the cupric absorbance increases also at lower total copper contents than 0.66 %. This means that reaction (1) is an equilibrium reaction. At higher copper contents all the antimony oxide is used up meaning that the cupric absorbance should increase with the total copper content analogously to the base glass. So far compositions with higher total copper contents have not been tested. However, the supposed trends in cupric absorbance will be limited to a certain total copper range.

Figures 2 also shows that glasses with no copper oxide have a relative absorbance value of about 0.1. This value depends on the bulk glass absorbance and the surface reflection losses at the glass-air interfaces. According to Cable (1992) surface reflection losses made the main contribution in three component soda-lime-silica glasses. The absorbances for the commercial glass systems both with and without antimony oxide increase with the copper content at roughly the same manner up to some 0.12 % CuO. At greater total copper the glass without antimony

oxide shows a steep and roughly linear increase in the maximum absorbance. The delayed onset of the cupric absorbance is assumed to depend on the iron impurities in the raw materials.

The effect of iron was examined by different copper-iron combinations in a batch without antimony oxide. Some results from these experiments are given in Figure 3. The figure also gives the absorbance maximum for the glass containing antimony oxide and different copper oxide additions.

Iron oxide clearly depresses the cupric absorption peak. At a total copper content of 0.1 weight-% the two lower iron contents used, 0.038 and 0.098 weight-% are already sufficient to reduce all cupric to cuprous according to reaction (2).

$$Cu^{2+} + Fe^{2+} = Cu^{+} + Fe^{3+} \qquad (2)$$

At higher copper contents the maximum absorbance is likely to increase for both glasses linearly with the total copper content. The glass containing a higher iron content, 0.63 % Fe_20_3, has somewhat smaller maximum absorption than the antimony glass containing the same amount of copper oxide. When stoichiometrically compared to each other, this iron content is found to be about 4 % less than the antimony content of the commercial batch. Thus the iron can be assumed to have a slightly higher reducing power than antimony in the glass examined. This result agrees with the series for the metals in order of increasing ease of oxidation where antimony is located just below iron (Bamford 1977). In the series referred copper oxide is located below the two other redox ions, which means that it is easily reduced by them.

It should be pointed out that for none of the examined glasses the maximum absorption for cupric ion was overlapped by the absorption of ferrous iron in the near infra-red region of the spectrum. Thus, the measured absorption maximum is a direct measure of the relative amount of cupric ion present in the glass. However, the total sensation of the colour is the result from the interaction between the glass and light within the whole visible spectrum together with near UV and IR.

II. Glass colour

Despite the fact that the cupric maximum absorbance at a certain total copper content hardly shifted the colour of the glass is clearly different for glasses containing either antimony or iron oxide. The location of the experimental glasses in a CIE-Chromaticity Diagram are given in Figure 4. At a first glance all but the glass with the highest iron content have roughly the same colour albeit a different colour intensity. However a more careful examination of the colour coordinates and also a bare visual subjective sensation of the glasses states that there are clear differences between the glass colours.

The glass with the lowest iron content and no antimony has the bluest colour of all corresponding to 485-480 nm in terms of dominating wavelength. The colour changes towards the shorter wavelengths, i.e. more blue region, when the total copper is increased. This change is likely to depend on a slight shift of the cupric absorption towards shorter wavelengths. The colour of these glasses is clearly stronger than of the glasses containing a corresponding amount of copper together with antimony or iron. Antimony containing glasses are blue-green with a dominating wavelength of roughly 485-488 nm. The shorter wavelengths are typical for glasses melted at a lower temperature and with a higher total copper content. Small amounts of iron only

slightly change the dominating wavelength of the colour compared to antimony glasses. A value of 488-489 nm is typical for the glasses studied. However, the colour of the glass with the highest iron content has a clear green hue typical to iron but still with a slight trace of copper blue in it. The dominating wavelength of the colour is just below 520 nm, i.e. in the green region of the visible spectrum.

4. CONCLUSIONS

The maximum absorption of cupric ion giving the typical blue-green colour in a commercial soda-lime glass depends on the amount of total copper in the glass, but also on the other redox ions simultaneously present. The maximum absorption caused by a given total copper content decreases when the glass also contains antimony or iron oxide. Also the hue of the colour changes towards more turquoise from the original bluer one in glasses with antimony or iron present simultaneously. At higher iron contents the cupric absorption still is close to the values typical for the other glasses with two redox ions but the colour is drastically changed.

REFERENCES

Bamford, C. R. (1977) Colour Generation and Control in Glass, Glass Science and Technology 2, Elsevier, Amsterdam.
Cable, M. and Xiang, Z. (1989) Glastech. Ber. 62,11, 382-388.
Cable, M. and Xiang, Z. (1992) Phys. Chem. Glasses, 33, 4,154-160.
Cable, M. and Meghirditchian, J. J. (1992) Bol. Soc. Esp. Ceram. Vid. 31-C, 4, 175-180.

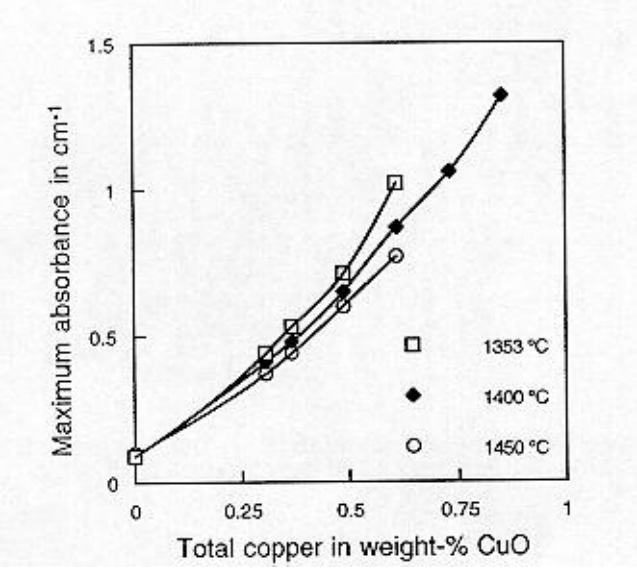

Figure 1. Cupric absorbance vs. total Cu0 for glasses containing 0.60 wt-% Sb_2O_3.

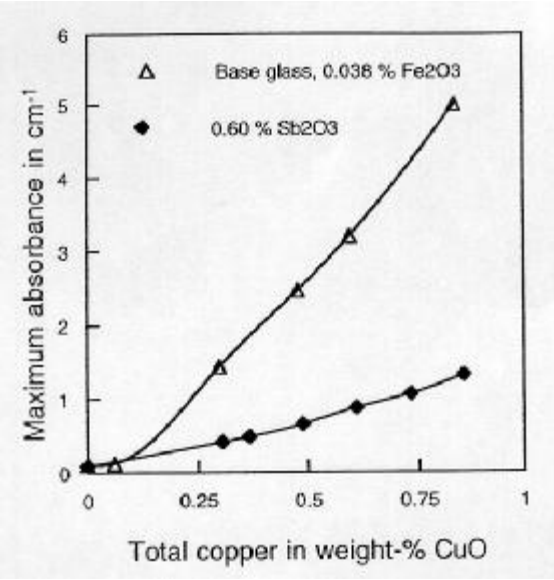

Figure 2. Cupric absorption vs. total copper for glasses melted at 1400 °C.

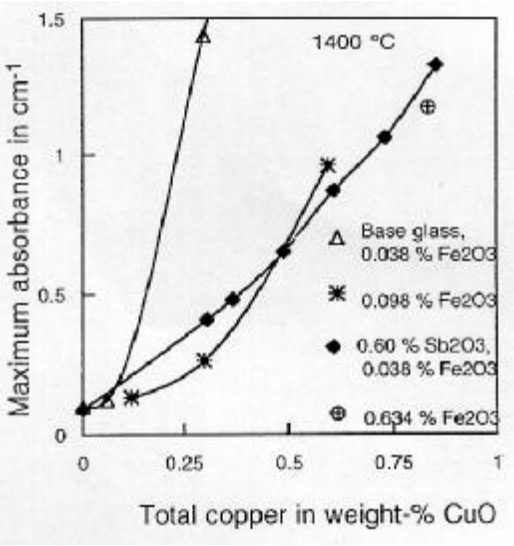

Figure 3. Cupric absorption vs. total copper for glasses containing antimony or iron oxide as specified. Melting at 1400 °C.

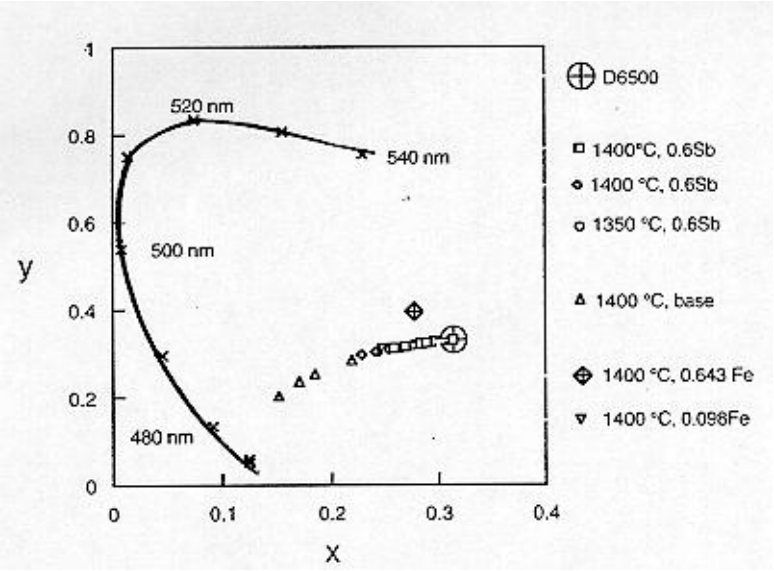

Figure 4. Colour coordinates for the experimental glasses.

CHEMISTRY OF GLASS SURFACES

Helmut Franz
PPG Industries, Inc., U.S.A.

Abstract

The physical and chemical properties of glass are to a great extent determined by composition, method of forming and the condition of the glass surface. During manufacturing processes, chemical reactions will occur on the freshly formed glass surface through interaction with the environment and by contact with forming equipment and process related aids. During secondary glass treatments and processes for improvements in mechanical, optical or chemical properties, chemical reactions at the glass surface as well as diffusion and ion exchange processes in the surface layer of the glass will take place. Reaction mechanism and methods for prevention of surface defects, protection of glass surfaces and modification of glass surface properties through applied surface chemistry will be discussed.

I. INTRODUCTION

The physical and chemical properties of glass are to a great extent determined by composition, method of forming and the condition of the glass surface. In all four major sectors of commercial glass products, i.e. flat glass, container glass, fiberglass and specialty glass, the condition of the glass surface will be a decisive factor for the quality and performance of the glass product with regard to optical transparency, mechanical strength and chemical durability. During manufacturing processes, chemical reactions will occur on the freshly formed glass surface through interaction with the environment and by contact with forming equipment and process related aids. During secondary glass treatments and processes for modifications or for improvements in mechanical, optical or chemical properties, chemical reactions at the glass surface as well as diffusion and ion exchange processes in the surface layer of the glass will take place. Large scale technologies have been developed for reduction of surface defects and protection of the glass surface as well as for surface modification by chemical reaction or thin film deposition [1].

II. SURFACE REACTIONS ON GLASS.

1. Float Glass - Hot End Reactions

In the float process, a continuous ribbon of glass is being formed on a bath of molten tin [2]. A reducing atmosphere must be maintained in the bath to protect the metallic tin against oxidation. Schematically the float bath can be described as a chemical reactor consisting of four stratified layers of materials or reaction zones in the following order from top to bottom:

Zone I : Reducing - bath atmosphere hydrogen/nitrogen.
Zone II : Oxidizing - molten glass in an oxidized state from melting.

Zone III : Reducing - molten tin metal in contact with hydrogen.
Zone IV : Oxidizing - refractory oxides in contact with outside air.

In the horizontal dimension, the temperature decreases gradually from approximately 1100^{o}C at the bath entry to 600^{o}C at the bath exit. The decrease in temperature is associated with an increase in viscosity of the glass by several orders of magnitude, which will slow down diffusion and ion exchange processes in the glass.

The formation of a continuous ribbon of molten glass in the hot end sector of the float bath is associated with a drastic change in redox conditions [3]. Entering the bath from oxidizing conditions in melting and refining, the glass suddenly gets exposed to strong reducing conditions both from the hydrogen in the bath atmosphere and the molten tin metal in contact with the bottom surface of the glass. Consequently, a number of ion exchange and redox reaction will take place, particularly at the glass/ molten tin interface, which can lead to significant changes in composition and condition of the glass surface [4].

In the first stage of reactions at the hot end section of the bath, iron oxide migrating from the interior of the glass to the bottom surface will be reduced at the glass / tin interface to metallic Fe^{O}, thereby oxidizing metallic Sn^{O} to SnO. Assuming that molten metals are insoluble in oxides and vica versa, oxides are insoluble in molten metals, it follows that the reduced iron will dissolve in the tin bath, and the oxidized tin will be
picked up by the molten glass:

$$FeO_{[Glass]} + Sn^{o}_{[Molten\ Tin]} \rightarrow Fe^{o}_{[Molten\ Tin]} + SnO_{[Glass]} \quad (1)$$

As the tin bath containing dissolved iron moves downstream with the flow of the glass ribbon, it will react with ingressing oxygen:

$$Fe^{o}/Sn^{o}_{[Molten\ Tin]} + O_2 \rightarrow FeO/SnO_{[Glass]} \quad (2)$$

Iron has a lower oxidation potential than tin and therefore will act as a ,scavenger for oxygen. The oxidation products FeO and SnO are insoluble in the molten metal, but will dissolve readily in the glass surface, where they can enter the soda-lime-silica structure either as silica network modifiers or in an ion exchange reaction with calcium:

$$(Fe/Sn)^{2+}_{[Surf]} + Ca^{2+}_{[Struct]} \rightarrow (Fe/Sn)^{2+}_{[Struct]} + Ca^{2+}_{[Surf]} \quad (3)$$

In the divalent ion exchange process depicted in Equation (3), calcium oxide will be displaced from its network modifier position and will be forced to the surface. Since CaO is insoluble in the molten tin, it will be trapped at the glass/tin interface as a deposit on the bottom surface of the float ribbon. As the glass is leaving the protective atmosphere of the bath, CaO will react immediately with the environment, especially with CO_2, SO_3 and H_2O, to form a hazy film commonly referred to as "calcium scum". Removal of the calcium scum, consisting mainly of crystalline $CaCO_3$, requires the addition of an acid, typically acetic acid, to the line washer.

Removal of the "bottom surface haze or scum" by acidic washing is only a corrective and somewhat costly procedure. Prevention of that defect must begin with the control of oxygen infiltrating the float bath atmosphere, causing oxidation of molten tin/iron to the respective

oxides, by providing tight seals and sufficient hydrogen levels in the atmosphere to maintain reducing conditions throughout the float bath.

2. Corrosion and Protection of Flat Glass Surfaces

Corrosion of flat glass is to a large extent a function of the environment to which it is exposed [5]. At the installation site, flat glass will usually face dynamic rain or condensation run-off or evaporation conditions. As a result, a rather uniform dealkalized surface layer will develop which will protect the glass against severe corrosion. In package, however, i.e. from wareroom through transit and storage, static conditions prevail in which condensate trapped in capillary spaces between adjacent glass surfaces can reach high pH levels and consequently will cause severe corrosion.

In alkaline media with pH above 9.0, the glass corrosion will proceed by hydroxyl ion attack on siloxane bonds, leading to a breakdown of the silicate network and extraction of silica:

$$\equiv Si\text{-}O\text{-}Si\equiv + OH^- \rightarrow \equiv Si\text{-}OH + \equiv SiO^- \qquad (4)$$

The key to prevention of flat glass corrosion in package is the neutralization of extracted alkali to keep the condensate between glass sheets below the critical pH of 9. At higher pH, alkaline attack on the silicate structure (Eqn.4) will cause severe corrosion and permanent damage to the glass surface known as "stain". Uniform coverage of the glass surface with the neutralizer for extracted alkali is another critical requirement for stain prevention. Condensation accumulating in an area without coverage, particularly around particles applied for mechanical separation, will cause a spotty corrosion pattern known as "measles".

The PPG W-Interleaving system provides superior stain protection for flat glass in package through a uniform coverage of the more vulnerable top surface with a layer of crystallized mixed organic acids with a buffering range between pH 3 and 7 [6].

3. Non-Wetting Coatings on Glass

Clean glass is wetted by water due to the hydrophilic character of the oxide glass surface. In order to make the glass surface water repellent, the surface energy of the glass substrate must be reduced by blocking reactive sites at the surface with molecular layers of paraffinic, olefinic or fluorinated hydrocarbons, or by deposition of thin films of hydrophobic substances such as waxes or organic polymers or organopolysiloxanes.

The most critical factor for the efficiency of water repellent surface treatments by molecular or polymeric films is the development of durable bonding to the glass substrate. The main reactive sites on the glass surface are silanol groups, single bonded negatively charged oxygens and, to a lesser degree, double bonded network forming oxygens. Due to the partial negative charge of the surface, cationic surfactants are known for relatively strong adsorption on the glass surface. More durable bonding can be achieved by adsorbing multivalent cations such as chromium or tin on the glass surface, then treating the surface with aqueous solutions of water soluble stearates, oleates or fluorosurfactants which develop chemical bonding with the adsorbed multivalent cations and form water-insoluble films at the surface [7].

Organosilicone or siloxanes, organotin and organotitania compounds with reactive or hydrolyzable groups (-Cl, -OR) do not require adsorbed cationic "anchors" but attach directly to the glass surface through hydrogen bonding and condensation with surface silanol groups. These

films can provide long lasting repellency and lubricity to the glass surface for protection against scratches and other mechanical damage.

The most durable water repellent glass surface can be produced by treatment with reactive fluorinated silanes [8]. Whereas adhesion of silicone coatings depends on weak chemical bonding of a highly cross-linked polymer film to the glass substrate, the strong adhesion of these repellent coatings on glass is the result of strong reaction bonding of monomeric fluorinated silanes. The high contact angle (115^{o}) of water on the treated surface indicates an outward orientation of the perfluoro-chain so that the most repellent -CF_3 groups are lined up in the outmost layer facing the water. Surface preparation of the glass substrate is very critical, because any contamination would reduce bond density and with it not only efficiency but also the durability of the repellent coating.

In addition to weather resistance, rain repellency and soil release properties, the treated glass exhibits a smooth surface finish that will improve scratch resistance and chemical durability of the glass without affecting hardness, strength, color or other optical properties.

REFERENCES

[1] Franz, H."Glass Surface Improvements by Chemical Reactions and Thin Film Deposition," Glastech. Ber.60,1987, Nr.5, p.182- 186.

[2] Edge, C.K."The Handbook of Glass Manufacture," 3rd ed., T.V. Tooley, Editor, Ashlee, New York,1984, Vol. II, p.714-1- 714-21.

[3] Franz, H."Surface Chemistry of Commercial Glasses," 55th Conf. Glass Problems 1994, p.221- 227.

[4] Franz, H. "lon Exchange and Redox Reactions in the Float Bath " Glastech. Ber.,3rd Glass Sci. Technol. Conf.,1995,68 C1, p.15- 20.

[5] Franz, H."Durability and Corrosion of Silicate Glass Surfaces," J. Non-Cryst. Solids 42,1980, p.529- 534.

[6] Duffer, P.F., Kelly, J.D., Franz, H."Mixed Acid Stain Inhibitor," U.S. Patent No.4,487,807, Dec.11,1984.

[7] Franz, H."Fluorocarbon Treatment for Reducing the Reactivity of a Glass Surface and Product, U.S. Patent No.4,276,350, Jun.30,1981.

[8] Franz, H., Goodwin, G.B."Chemically Reacted Glass Surface," U.S. Patent No.4,983,459, Jan.8,1991.

ACID-BASE INTERACTION IN SODIUM-CONTAINING GLASSFORMING OXIDE MELTS

E.L.Kozhina and **M.M.Shultz**
Russian Academy of Sciences, Russia

Abstract

EMF investigation of Na_2O-RaOb (R=P, Si, B, Ge) and Na_2O-Q_2O_3-SiO_2 (Q=B, Al) melts is carried out over a glassforming range. Temperature range under study is 800-1400 K. A complete set of thermodynamic properties, both partial and integral, is calculated being referred to the corresponding properties of the pure oxides. The results is discussed in terms of acid-base interaction in melt. Chemical structure of the melts is simulated from the ideal associated mixture model. On this basis an account for "germanate" and "borate anomalies" is proposed.

1. INTRODUCTION

During last several years we have been performing a systematic thermodynamic investigation of a great variety of slag and glassforming melts. We have summarised a valuable experimental information about electrochemical processes and thermodynamic properties of alkali-borate, -silicate, -germanate, -phosphate, -borosilicate and-alumosilicate melts. The comprehensive thermodynamic and acid-base information is very important both in theoretical and practical terms. The results obtained being interpreted from the acid-base interaction theory is the basis to describe such an important aspects of properties and structure of melts, as chemical properties, association phenomena, polymerisation and Red-Ox equilibrium. Reliable information is reached from the experiments by EMF technique over the temperature range 800 -1400 K:

- a complete set of the thermodynamic properties, both partial and integral, for the melt of the following systems: M_2O-SiO_2 (M=Li, Na, K, Cs), M_2O-GeO_2 (M=Li, Na), M_2O-B_2O_3 (M=Li,Na, Cs), M_2O-B_2O_3-SiO_2 (M= Li,Na, Cs), M_2O- Al_2O_3-SiO_2 (M=Li, Na), Na_2O-P_2O_5
- identification of a devitrification phenomena and an evaluation of its area for the metastable oxide melts
- identification of the melt crystallisation raising and evaluation of the crystal phase amount.

On practical term these results contribute a lot to an extension of the Thermodynamic Data Bank. Moreover, the results discussed in terms of acid-base interaction conception enable us to develop the theory of melt mixture structure. On the other hand these data allow us to evaluate conditions of glass, ceramic and glass-ceramic manufacture from raw materials for the construction of buildings.

GeO_2 - and P_2O_5-containing glasses seem to be very promising to develop new materials using for non-linear optic, computers, fibers and waveguides. Employment of natural sodium products is of importance for a cleaner environment.

2.EXPERIMENTAL

The aim of this paper is to collate the results of the thermodynamic study of Na_2O-RaOb (R=P, Si, B, Ge) [1-5] and Na_2O-Q_2O_3-SiO_2 (Q=B, Al) [6] melts which we have done by electro-motive force technique over a glass-forming range. An unconventional variant of a concentration galvanic cell with a transfer has been worked out, two air platinum electrodes and direct contact between the reference melt and the melt under study being employed:

(O_2) Pt| test melt : reference melt| Pt (O_2)

As a reference system, $31.95Na_2O \cdot 16.82Al_2O_3 \cdot 51.23SiO_2$ precrystallized glass has been used for all the experiments in order to results for various melts could be easily comparable.

Taking into account a reversibility of the platinum electrode with respect to oxygen according to the reaction:

$O^{2-} = 1/2O_2 + 2e$

and a conductivity due to the only alkali cation, the EMF values of the cell is given by:

$$E = R\,T/2F\,(a_{Na_2O}' - a_{Na_2O}'') = 1/2\,\xi\,(\mu_{Na_2O}' - \mu_{Na_2O}'')$$

From the temperature dependencies of the EMF values relative partial properties of sodium oxide has been calculated. Using Gibbs-Duhem's equation a complete set of the thermodynamic properties (partial properties of a glass-forming oxide and integral ones) has been calculated as well.

We have developed an unconventional way to normalise these thermodynamic data to the corresponding properties of pure oxides, while the common way is the only comparison to a reference melt [7-9]. A good agreement is noted between our normalised data and that of [7-9] recalculated according a schema proposed by us [1-5]. To normalise the data for Na_2O-SiO_2 and Na_2O-B_2O_3 melts the thermodynamic properties of sodium metasilicate and sodium metaborate have been used, which are known from a current reference literature. Thermodynamic properties for any compound of other above Na_2O-containing melts not being available in the literature, we have transformed the data obtained to the pure oxides according to formula cited in [3,4]. The accuracy of the chemical potentials, partial entropies and enthalpies of the components determined has not been worse than ±0.6 kcal/mol, ±1.3cal/(K· mol) and ±2.0 kcal/mol, respectively. Figures 1-3 compare the chemical potentials and partial entropies values for various melts.

3. RESULTS and DISCUSSION

It is established that the formation of all above melts from the initial oxides is accompanied by a considerable negative deviation from the ideal behaviour of Gibbs free energies and enthalpies. Table compares Gibbs free energies and enthalpies of various sodium-containing oxide melt formation.

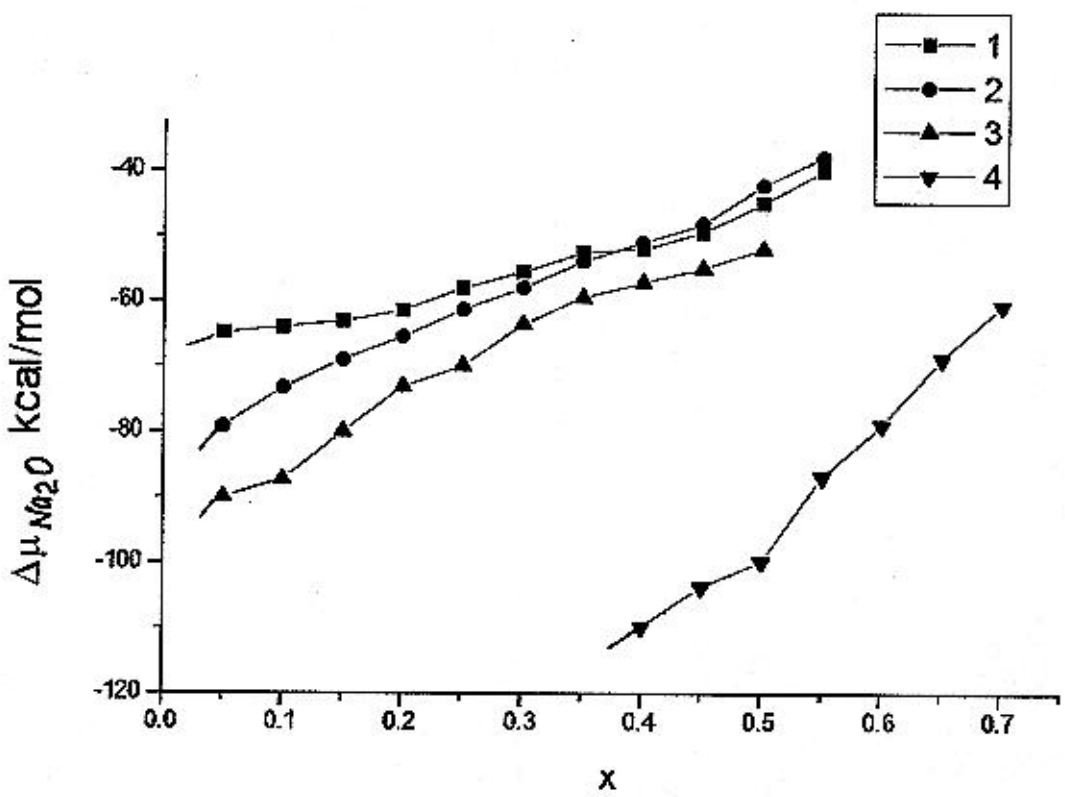

Figure 1. Chemical potentials of Na_2O in various oxide melts at 1300 K.
1- Na_2O - SiO_2 2-Na_2O - GeO_2 3-Na_2O - B_2O_3 4-Na_2O - P_2O_5 (1073K)

This gives evidence for a strong chemical interaction between Na_2O and above acid oxides, which being considerably different in their chemical nature follows the patterns seen in acid-base interaction. This negative deviation is found to increase in order: sodium- silicates <germanates < alumosilicates < borosilicates < borates< phosphates. This is due to the strong chemical interaction between initial oxides resulting in the formation of salt-like groupings constituting the melt. The latter are most likely similar in their stoichiometry and thermal effects of formation and to some extent in structure to those of the crystalline compounds available in the system according to the phase diagram. The experimental data show that sodium oxide is almost entirely bound into compounds even at high temperature(800-1400K). For example, in the sodium metagermanate melt the Na_2O activity is found to be less than 10^{-8}, and in sodium metaphosphate melt this value does not exceed 10^{-21}. So, chemical structure of the melts is suggested to be determined by equilibrium coexistence of the compounds which formation is most relevant in the melt at given composition. These are the reasons for choosing the ideal associated mixture model to simulate the thermodynamic properties and chemical structure of above melts. On the basis of extensive results accumulated in our earlier studies [1-6] we have concluded that this model provides the most adequate description of the thermodynamic behaviour of the systems formed by components which are different in their nature, remaining rather simple in computation without the adjustable parameters. According to an assumption made in this model the melts of such systems can be considered as ideal solutions of the above mentioned compounds.

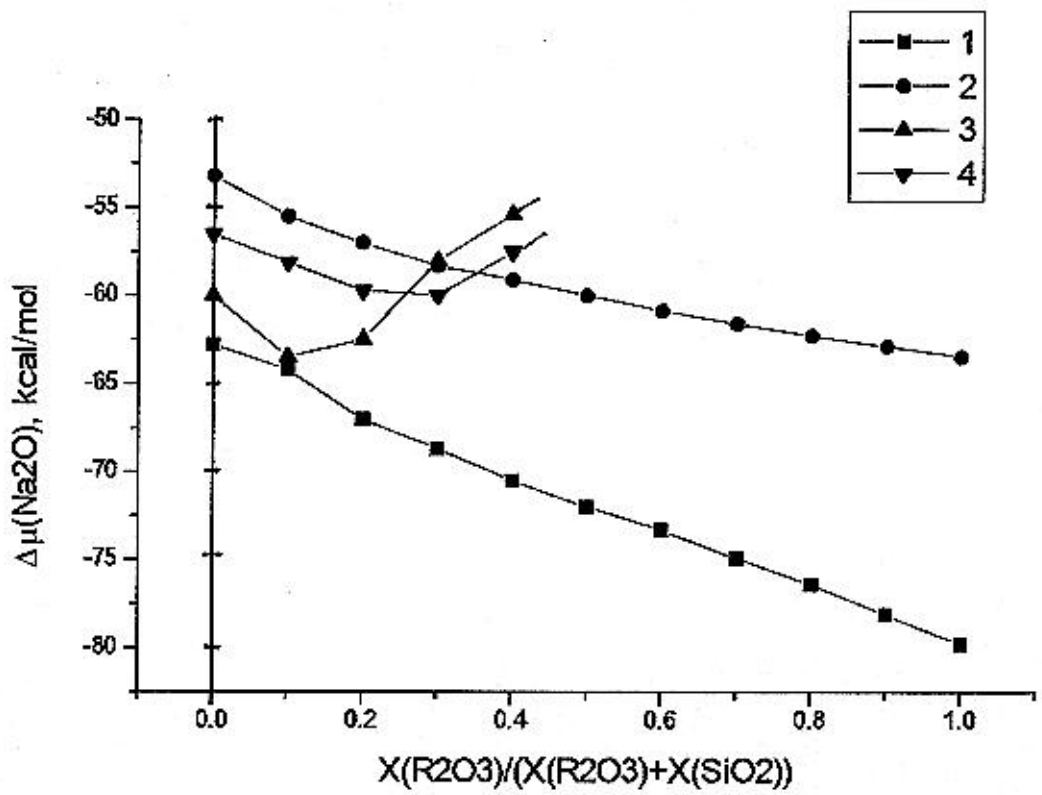

Figure 2. Chemical potential of Na_2O in borosilicate (1,2) and alumosilicate (3,4) melts. X(Na_2O):1-0.33, 2-0.15, 3-0.20, 4-0.30. T=1300 K.

Table. Enthapy of formation of sodium-containing melts at 1300 K in kcal/mol

X (Na_2O)	**Na - Si**	**Na - B**	**Na - Ge**	**Na - P (1073K)**
0.1	-4.4	-9.3	-6.6	
0.2	-10.3	-18.2	-13.3	
0.3	-17.5	-23.6	-19.5	
0.4	-23.7	-26.3	-25.6	-44.6
0.5	-28.8	-27.2	-31.0	-53.7
0.6			-32.8	-60.6
0.7				-64.7

We have applied to each of reactions of any compound formation in all above melts both the mass action law and equations of material balance for given composition of the melts. It yields to the

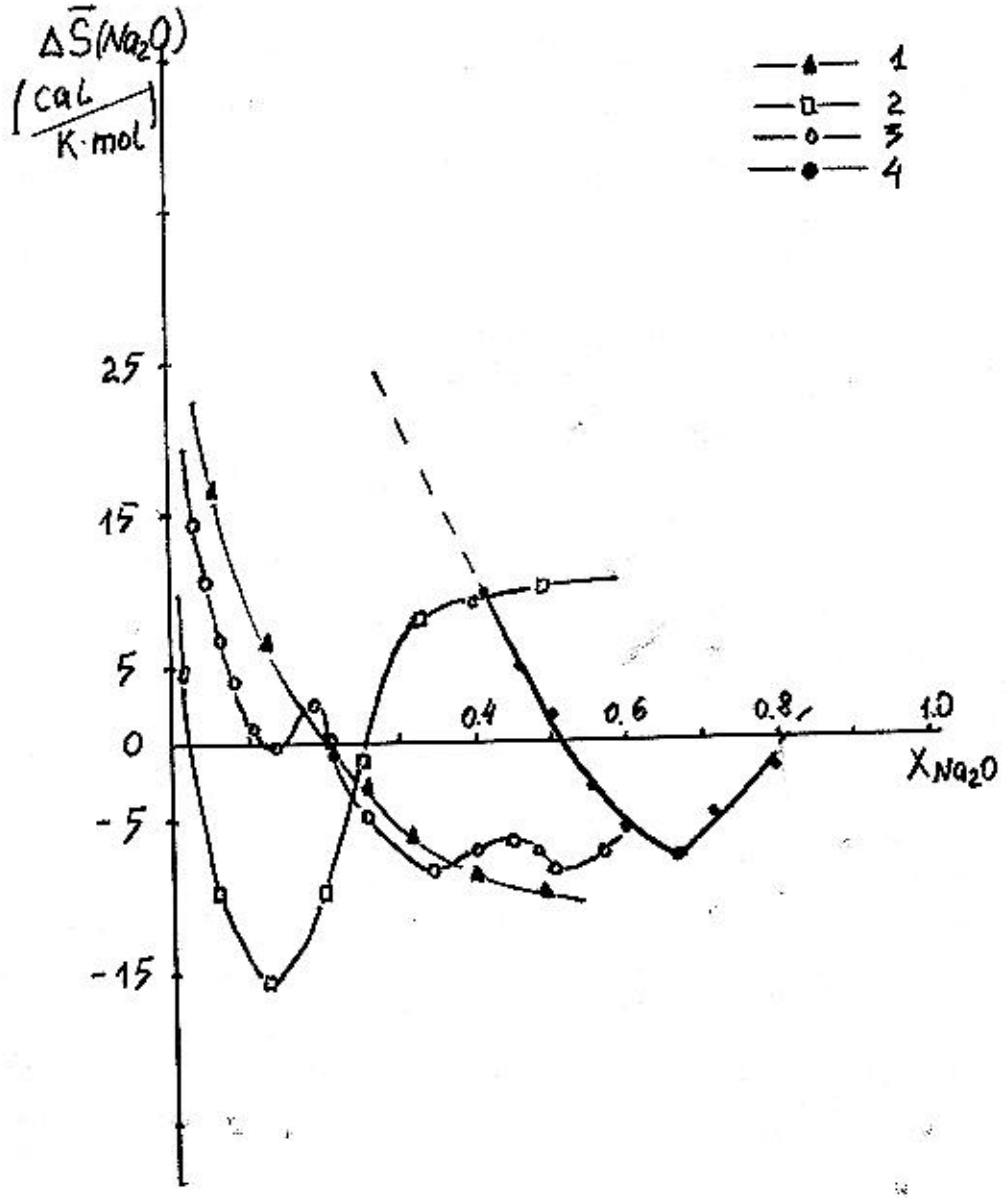

Figure 3. Partial molar entropy of Na_2O in { x Na_2O + (1-x) RaOb }.
1- 3 at 1300 K, 4 - at 1073 K. R:1- Si; 2 - B; 3 - Ge; 4 - P.

system of equations for each oxide melt, which solution using the data on the equilibrium constants of reactions permitted "the true molar fractions" of reaction participants to be calculated. For each compound a range of existence and maximal content within the limits of the range are estimated. Figure 4 shows the abundance of various compounds at given composition in the melt. The good agreement between the experimental data and simulated ones confirms a relevancy of the model to describe adequately melt chemical structure and properties. Moreover, computer simulated data correspond well to that calculated from NMR and Raman spectroscopy data [10].

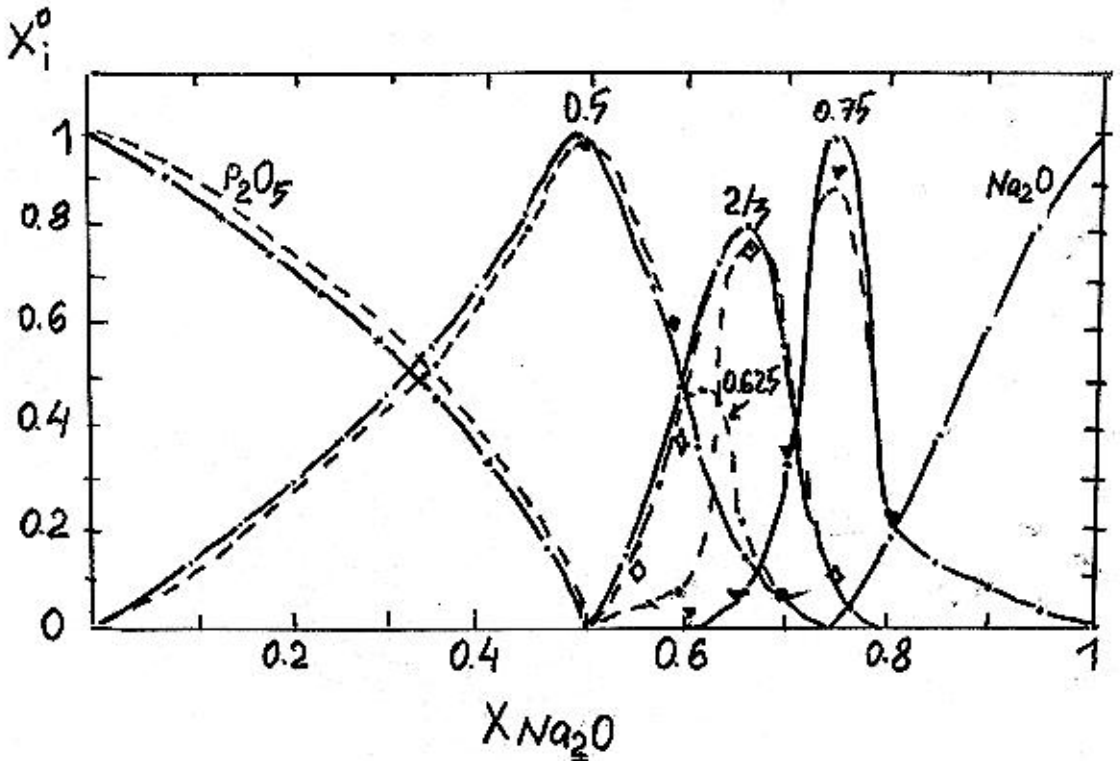

Figure 4. Simulation of the chemical structure of { x Na_2O+(1-x) P_2O_5}
-T=1073K; - - - T=873K ; •, ◊, ♥- results from reference [10] at T=298K:
• - x=0.5; ◊ - x=0.666; ♥ - x=0.75.

In Na_2O-B_2O_3-SiO_2 melts an equilibrium between sodium borate and sodium silicate structural units is observed. But the equilibrium is shifted to sodium borates formation. It is due to more negative meanings of ΔG_{form} values for sodium borate compounds than for silicate ones. Taking into consideration the differences in Na_2O chemical potential and Gibbs free energy values for silicate and borate subnetwork (Fig.2, Table), one may propose, that the first step of the process is the sodium tetraborate grouping's formation. Di-, metaborates and di- and metasilicates are formed when Na_2O content increases. By contrast, in Na_2O-Al_2O_3-SiO_2 melts the equilibrium between sodium aluminates and sodium borates is dramatically shifted to the formation of latter ones. Some decrease in chemical potential values when Al_2O_3 substitutes B_2O_3 (Fig.2) results from the equilibrium shift of the reaction occurring in the melt towards the formation of more stable compound. In a given composition range it is a ternary compound $Na_2O{\cdot}Al_2O_3$ $nSiO_2$.

A complicated character of the entropies concentration dependencies is noted for binary sodium oxide systems, as seen in Fig.3. We have attempted to account for this non-monotone behaviour by the change in relative content of compounds, available in the melts. As seen from Fig.4, the chemical structure of sodium phosphate melt changes with Na_2O content increase. It varies from the chains of PO_4 tetrahedra in pure P_2O_5 to metaphosphates (tetrahedra with one non-bridging oxygen atoms) and than to pyro- and orthophosphates (two and three non-bridging oxygen, respectively). The contributions from different compounds to the chemical constituents of partial and integral entropies are in accordance with the above structural changes in melts. We have derived in [3] an equation for the partial entropy of the components, the number of moles of

arisen compounds and the entropies of their formation from oxides being involved. In sodium-borate and -germanate melts the occurrence is established of the compounds in which the co-ordination numbers of boron and germanium atoms vary as follows: $B^3 \rightarrow B^4$, $Ge^4 \rightarrow Ge^6$. These compounds provide a considerable negative contribution to partial entropies of alkali oxides. This fact accounts for availability of minima in the curves of the dependencies $\Delta S(Na_2O) = f(X(Na_2O))$ in the low alkali regions where the number of such groupings is large. Such a non-monotone behaviour of a number of physical and chemical properties appropriate to alkali-borate and alkali-germanate systems is called "borate" and "germanate anomaly".

The same idea outlines the consideration of the chemical potential values dependencies seen in Fig.1. Bends of the curves are obsenred which fall out the limits of error. These data present evidence for a concentration fluctuation. There is no reason to relate this to miscibility gap. They are most probably due to the change in chemical structure of the melts. The curve is comparatively flat in the region where any compound just arises. But it becomes steeper when the greatest amount of the given compound is reached.

REFERENCES

1. Shakhmatkin B.A., Shultz M.M. Russ.Phys.Chem.Glass **1980**, 6,129.
2. Shakhmatkin B.A., Shultz M.M. Russ.Phy.Chem.Glass **1982**, 8, 270.
3. Kozhina E.L., Shultz M.M. Glass Physics and Chemistry **1995**, 21,186.
4. Kozhina E. L., Shultz M.M., l.Chem. Thermodyn.**1996**, to be published.
5. Shultz M.M. Trans.lndian Ceramic Soc.**1987**, 46, 95.
6. Shultz M.M., Kozhina E.L. Russ.Phys.Chem.Glass.**1989**,15, 500.
7. Iton M., Sasahira A., Maekawa T., Yokokawa T.,l.Chem.Soc.; Faraday Trans.l, **1984**, 80, 473.
8 .Yokokawa T., Kohsaka S. ,l.Chem.Fng.Data,**1979**, 24,167.
9. Yokokawa T., Tamura M., Sato S., Niwa K. Phys.Chem.Glass,**1974**,15,113.
10.Martin S.W. Eur.J.Solid.State Inorg.Chem.**1991**, 28,163.

APPLICATIONS OF ESR-SPECTROSCOPY IN GLASS INDUSTRY

B. Hahn and **R. Weibmann**
University of Erlangen, Germany

Abstract

Many macroscopic properties of glasses are strongly influenced by the microstructures. To use these structure-property correlations for quality control and the development of new glasses, powerful analytical methods are needed. The investigation of industrial glasses has shown that electron spin resonance (ESR) is a sensitive tool to detect oxidation states and defects including the corresponding microstructures in glass products. First comparisons between ESR parameters and chemical analysis of glasses containing chromium and iron in different oxidation states confirm the chemical analysis and show the potential of a quantitative species determination by ESR.

1. Introduction

Macroscopic properties of glasses not only depend on their main chemical

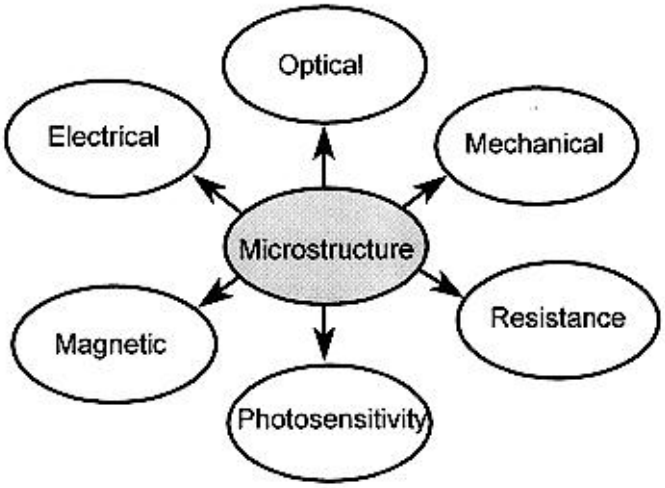

Fig.1 Structure-property correlation

composition but also on the minor components, oxidation states (species), defects and related microstructures. This is called structure-property correlation (Fig.1). At the moment routine characterization of glasses concentrates on the analysis of the elements. To benefit from the structure-property correlation new analytical methods focusing on the species and microstructures have to be introduced.

Table 1 shows the potential of several important methods that can be used for analyzing transition metals and microstructures in glasses.

Table 1: Overview of some important characterization methods and their power for the analysis of oxidation states; - poor, 0 fair, + good, ++ excellent

Method	**Species**	**Defects**	**Structure**	**Sensitivity**
NMR	-	-	+	-
Mössbauer	+	-	+	-
ESCA	+	-	0	-
Optical	++	+	+	++
ESR	++	++	+	++

Optical spectroscopy and ESR are very important methods due to their wide application range and sensitivity. Fig 2 shows the possible applications of ESR for analyzing glasses. All glass products, ceramics, advanced ceramics and raw materials can be analyzed by ESR if they have relevant paramagnetic centers like transition metals [1-3] and defects [4,5]. Carbon and its modifications usually contain unpaired electrons. We use these centers as so-called structural probes for the analysis of carbon phases in SiOC-glasses [6]. If a product does not naturally contain such paramagnetic centers, radiation treatment or doping with transition metals is necessary to obtain structural probes. Main group species such as Sb^{5+} and Pb^{4+} can be detected after radiation treatment. Surface analysis are performed by ESR with spin labels, i.e. paramagnetic molecules interacting with the surface of a material.

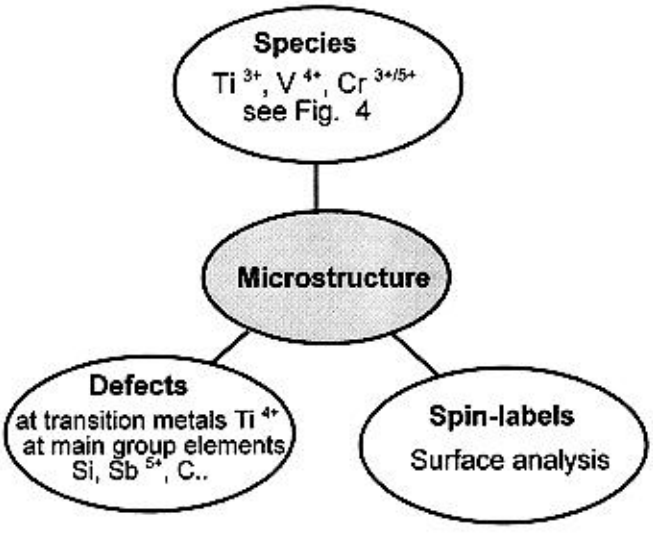

Fig 2 Application of ESR in glass analysis

As transition metals are present in most industrial glasses, this paper focuses on the analysis of these species. Fig. 3 summarizes the most important oxidation states that can be detected by ESR. They are introduced as impurities with the raw materials or added to obtain specific properties. In the past chemical methods have already been developed for the analysis of polyvalent elements [7,8]. At the moment research activities concentrate on improving these methods [9]. Major disadvantage of these chemical methods is that all structural information is lost during the analysis. In addition to that, the analysis of species by chemical methods are uncertain due to possible redox reactions during the decomposition. Therefore physical methods which can directly detect species in the glass get more and more important to confirm, improve or even substitute chemical methods. It is important to keep in mind that the widely used optical routine measurements must be calibrated by chemical methods and therefore needs confirmation, as well.

Ti^{3+}	**V^{4+}**	**$Cr^{3+/5+}$**	**Mn^{2+}**	**Fe^{3+}**	**Co^{2+}**	**Ni^{2+}**	**Cu^{2+}**
Zr^{3+}	**Nb**	**$Mo^{3+/5+}$**	**Tc**	**Ru**	**Rh**	**Pd**	**Ag**
Hf	**Ta**	**$W^{3+/5+}$**	**Re**	**Os**	**Ir**	**Pt**	**Au**

Ce^{3+}	**Pr^{3+}**	**Nd^{3+}**	**Pm^{3+}**	**Sm^{3+}**	**Eu^{2+}**	**Gd^{3+}**	**Tb^{3+}**

Fig.3. Important oxidation states that can be analyzed by ESR. The dark-shaded species can usually be detected at room temperature. For analyzing the grey marked elements low temperature measurements have to be conducted.

Although many ESR analyses have been carried out on laboratory melts [1-3, 10-16], only few industrial glasses have yet been analyzed [17, 18]. Concerning quantitative measurements no comparison between ESR results and chemical analysis of species have been published. This paper discusses the possible application of ESR in glass industry focusing on routine interpretation, the correlation to chemical procedures and quantitative analysis.

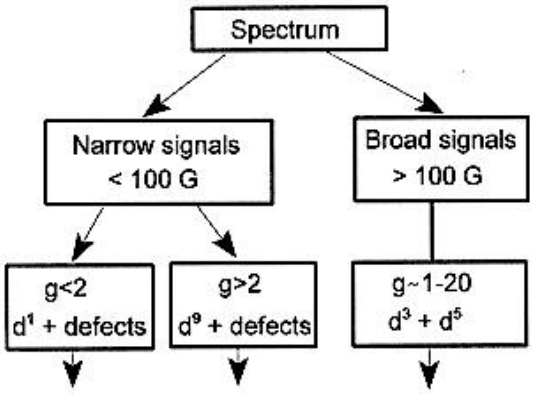

Fig. 4 Flow chart for interpretation of ESR-spectra

2. Measurement and interpretation

Applying the common X-band spectrometer bulk or powdered samples up to a diameter of 10 mm can be measured. Since ESR is a very sensitive method, results can be obtained from samples weighting only a few milligrams. The detection limit of V^{4+} for example, is below 1 ppm. Routine measurements can be done very quickly (~30-300s). Most ESR spectra are performed at room temperature. Low temperature measurements have to be used for analyzing rare earth elements (Fig. 3) and profound characterization of certain centers [16]. For some analysis, e.g. cooling of melts [12], high temperature measurements are done. Major advantage of the method compared to optical methods, is the simple preparation of glass samples. At the moment, no interpretation routines or data bases are available for the interpretation of ESR spectra of glasses. The reason for this is lack of demand as well as the problem that some glass spectra are still not completely understood. Industrial glasses usually contain several species, sometimes even in different environments. To simplify the interpretation of the resulting complicated spectra (Fig. 6) we propose to structurize the interpretation as shown in the flow chart (Fig. 4).

The two main groups can be separated mathematically by applying a fourier transformation technique. After that the spectrum of frequencies is divided in a low and high frequency part. These two parts are each transformed back. One back transformed spectrum contains the narrow, the other the broad signals. In many cases the resulting spectra of the significant narrow signals resulting from the d^1, d^9 elements and defects can be characterized by the line position and the hyperfine interaction. For the broad signals and many superimposed narrow signals further deconvolution, peak fitting and simulation of the integrated spectra is necessary. It is important to note that the d^5 element Fe^{3+} not only contains broad but also a characteristic narrow signal.

3. Quantification of paramagnetic centers

ESR-spectroscopy for quality control and development of new glasses needs quantitative measurements. For practical reasons, quantitative ESR spectroscopy is done by comparing an ESR signal with an appropriate standard [1,19]. At the moment ESR-researchers carry out first interlaboratory comparisons on simple paramagnetic centers [20]. Castner [1] tried already at the beginning of ESR investigations in glasses to apply this technique for the quantification of the characteristic Fe^{3+} signal at g~4,3. However, it has to be considered that this signal only represents a part of Fe^{3+}. Furthermore several workers showed that the ESR parameters line width and intensity depend in a complicated way on the matrix [10,11] as well as the total iron content [13-15]. As the redox ratio can change with composition [21, 22] ESR-parameters are better correlated with the species. That is the reason why we melted several glasses containing $Fe^{3+}$and compared the chemical analyzed Fe^{3+} concentration with the ESR parameters. The chemical analysis were done by our inhouse method [21]. These analysis exhibited, that the ESR parameters are also a difficult function of Fe^{3+} content. However, the comparison with the chemical analysis confirmed that within small concentration ranges the linewidth and intensity of this significant signal can be used as an indicator for changes in redox states and microtructures. An accurate correlation between the ESR and chemical analysis of d^5 element need a complete understanding of spectra.

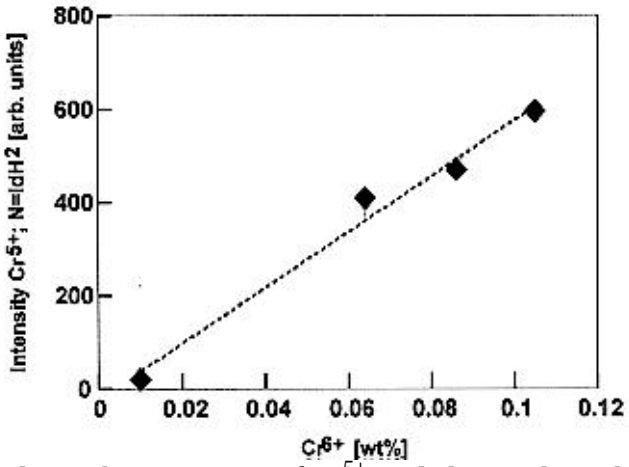

Fig. 5 Correlation between ESR of Cr^{5+} and chemical analysis of Cr^{6+}

As examples for species giving narrow signals we chose Cr^{5+} (d^1) for comparison with the chemical analysis. The chromium species are important for the colouring of glass and for health reasons. As packaging glass is in contact with food it is necessary to make sure that these glasses do not loose Cr^{6+} or better do not contain Cr^{6+}.ESR is the only method that detects the unusual oxidation state Cr^{5+} . We melted several glasses containing chromium and analyzed them by ESR and a chemical method [23]. All glasses contain Cr^{5+} and Cr^{6+}. This is in accordance with literature [24]. Fig 5 shows the excellent correlation between the intensity of the ESR signal of Cr^{5+} and the chemical determined Cr^{6+} amount.

These indicates that ESR can be applied together with chemical methods for the analysis of d^1 and d^9 species i.e. Ti^{3+} , Zr^{3+} , V^{4+} , Cr^{5+} , Mo^{5+} ,W^{5+} and Cu^{2+} . In limited ranges the narrow Fe^{3+} signal can be used as indicator for the Fe^{3+} content. Our further work will focus on the improvement of the method for the d^1 and d^9 elements and an enlargement to the d^3 and d^5 elements. Last but not least we plan quantitative measurement independent of chemical analysis of glass.

4. ESR-spectra of some industrial glass products

All spectra are recorded at room temperature on 100 mg powdered samples with an X-band spectrometer (ESP 300 Bruker, Rheinstetten, Germany). Fig. 6 shows the ESR spectrum of an olive container glass. The broad signals at 1500 and 3450 G are due to Cr^{3+} that can also be detected by optical spectroscopy. In addition the characteristic narrow Fe^{3+} signal at 1610 G and a hyperfine structure at 3450 G due to V^{4+} is visible. These narrow signals are very sensitive probes to changes of redox state and microstructures.

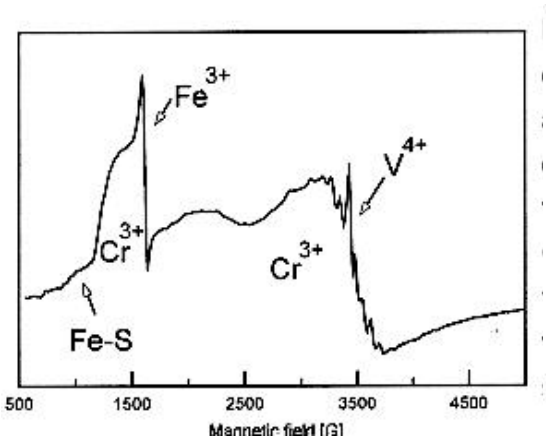

Fig 6. ESR Spectrum of olive container glass

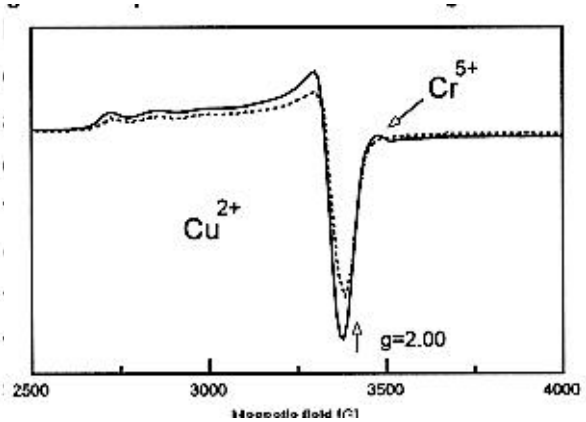

Fig 7. ESR Spectra of green flat glasses

Fig. 7 shows two green flat glasses, one of them melted under strong oxidizing condition (full line). This glass contains besides a large Cu^{2+}amount also Cr^{5+} and Cr^{6+} . In contrast to that the analysis of several container glasses from the European market showed neither Cr^{5+} nor Cr^{6+} . This can be explained by redox reactions between $Cr^{5+/6+}$ and oxidable species like Fe^{2+} during the production.

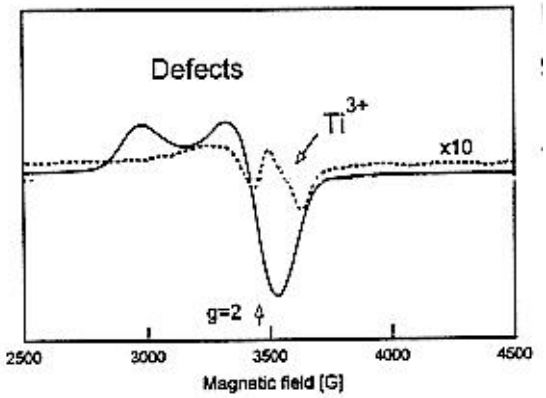

Fig 8. Silica glasses doped with Al, Ce and Ti

Fig. 8 shows the ESR spectra of two silica glasses doped with Al, Ti and Ce. The full line represents the raw glass showing a lot of defects at g>2. Heat treatment of this sample leads to the dotted spectrum. The amount of defects decreases drastically and a characteristic signal at g<2 arises. It can be attributed to a Ti^{3+} center. These defects are associated with the interesting fluorescence behaviour of such glasses.

5. Conclusion:

The analysis of several laboratory and industrial glasses showed that ESR spectroscopy is a powerful method to analyze species, defects and the corresponding microstructures. In cooperation with chemical methods it allows reliable quantitative analysis of many oxidation states.

6. References

1) T. Castner, G.S. Newell, W.C. Holton, C.P. Slichter, Note on the paramagnetic resonance of iron in glass, J. Chem. Phys. 32 (1960) 668-673.
2) D.L. Griscom, Electron Spin Resonance in Glasses, J. Non-Cryst. Solids 40 (1980) 211-272.
3) R. Stösser, M. Nofz, ESR spectroscopy on glasses and glassy-crystalline materials - New opportunities for material scientists, Glastech. Ber. Glass Sci. Technol. 67 (1994) 156-170.
4) A. Bishay, Radiation induced color centers in multi component glasses, J. Non-Cryst. Solids 3 (1970) 54-114.
5) G. Kordas, H.J.Oel, Structure of radiation-induced hole centres in alkali silicate glasses, Phys. Chem. Glasses 23 (1982) 179-183.
6) B. Hahn, R. Weissmann, P. Greil, EPR-Investigation of Carbon Distribution in SiOC-glasses, accepted for publication in J. Mat. Sci. Lett.1996.
7) P. Close, F.C. Raggon, W.E.L. Smith, Chemical analysis of soda-lime-silica glasses for trace quantities of several colorants, J. Am. Ceram. Soc. 33 (1950) 345-352.
8) P. Close, H.M. Shepherd, C.H. Drummond, Determination of several valences of iron, arsenic and antimony and selenium in glass, J. Am. Ceram. Soc. 41 (1958) 455-460.
9) E. Guadagnino, O. Corumluoglu, Indirect determination of sulphide-sulphur in glass by flame atomic absorption spectrometry, to be published.
10) B. Camara, Einbau von Eisen in Glas, Glastechn. Ber. 51 (1978) 87-95.
11) C. Russel, Iron oxide-doped alkali-lime-silica glasses, Glastech. Ber.66(1993) 68-75.
12) G. Gravanis, C. Rüssel, Redox rreactions in Fe_20_3, As_20_5 and Mn_20_3 doped soda-lime-silica glasses during cooling - A high-temperature ESR investigation, Glastech. Ber.62 (1989) 345-350.
13) S.K. Mendiratta, E.G. de Sousa, Clustering and g= 4.3 signal peak in iron-containing glasses, J. Mat. Sci. Lett.7(1988) 733-734.
14) D.W. Moon, J.M. Aitken, R.K. MacCrone, G.S. Cieloszyk, Magnetic properties and structure of xFe_20_3,$(1-x)[BaO\ 4B_20_3]$ glasses, Phys. Chem. Glasses 16(1975) 91-102.
15) C.S. Sunandana, R. Jagannathan, ESR and Mössbauer studies of Fe^{3+} ion in calcium boro-aluminate glasses, Solid St. Com.53(1985) 985-988.
16) M.M. Mestdagh, C. Dauby, L. Van Cangh, C. Dupont,Optical and electron paramagnetic resonance investigation of colour instabilities in amber glass as a function of melting temperature and batch redox conditions, Glass Techn.24(1983) 184-191.
17) C.R. Kurkjian, G.E. Peterson, An EPR study of Ti^{3+} - Ti^{4+} in $Ti0_2Si0_2$ glasses, Phys.Chem. Glasses 15(1974) 12-17.

18) H.D. Witzke, W. Göbke, I. Ebert, Zur Untersuchung von Schwarzungs erscheinungen an Kieselglas, Silikattechnik 29(1978) 79-82.
19) N.D.Yordanov, Quantitative EPR spectroscopy- “State of the Art”, Appl. Man.Reason.6(1994) 241-257.
20) N.D. Yordanov, M. Ivanova, The present state of quantitative EPR spectrometry: The results from an international experiment, Appl. Man. Reason.6(1994) 333-340.
21) H.D. Schreiber, B.K. Kochanowski, C.W. Schreiber, Compositional Effects on the Iron Redox State in Soda-Lime-Silica Glasses, Advances in Fusion & Processing of Glass, 4th Internat. Conf.1995, Glastech. Ber. Glass Sci. Technol.,68 C2(1995) 233-240.
22) B. Hahn, P. Buhler, R. Weißmann, Influence of the total iron content on the redox ratio, Supplement to 'Rivista della Stazione Sperimentale del Vetro' 23(1993) 205-210.
23) Inhouse method University Erlangen based on diphenylcarbazide.
24) H. Hirashima, T. Yoshida R. Bruckner, Redox equilibria and constitution of polyvalent ions in oxide melts and glasses, Glastech. Ber 61(1988) 283-292.

CORROSION BEHAVIOUR OF FLOAT GLASS IN AQUEOUS SOLUTIONS

Alec Helebrant and **Josef Matoucek**
Institute of Chemical Technology, Czech Republic

Abstract

The chemical durability of tin (bottom) and top side of float glass was tested in three different aqueous solutions: HCl (pH=3), distilled water (pH=5.2) and NaOH (pH=12). The tin side was found to be more durable against all three solutions. The corrosion of both tin and top side was minimal in distilled water. A comparison of the experimental results with a mathematical model shows that surface structure changes play an important role in the case of acid corrosion. The creation of secondary layers on the glass surface has to be taken into account in the case of NaOH corrosion.

I. INTRODUCTION

The chemical composition of float glass surface differs on the tin (bottom) and on the top side. This difference is considered to be responsible for increased chemical durability of tin side [1-3].

The glass corrosion generally consists of three simultaneous processes:

1. SiO_2-matrix dissolution involving surface reaction and eventually transport of reaction products through the precipitated layer.
2. SiO_2 back precipitation in the form of silica and/or silicates.
3. Na^+-H_3O^+ interdiffusion in glass.

These processes are usually strongly influenced by the pH-value of corrosion solution. The glass matrix dissolution could be often neglected in acid solutions especially for the glasses with high content of SiO_2 [4-7]. This opinion is supported by the constant silica solubility in the acid region. Also the precipitation of silicates is small in this region due to the low activity of silicate anions [8]. Then, only moveable ions leaching takes place in acid solutions. However, many authors reported that the glass matrix dissolution can influence the corrosion results in broad extent of solution pH. Perera and Doremus [9] found the increasing rate of dissolution of Pyrex glass from pH Õ 0 to pH=13.9. Other authors [10-14] have found the minimum of dissolution and leaching rates in the neutral and weak acid region.

The aim of this work is to compare the corrosion behaviour of tin and top side of float glass in solutions with different pH and to discuss the experimental results using a mathematical model of corrosion.

II. EXPERIMENTAL

The two float glass samples of the dimension 3 cmx2 cm and the thickness of 4 mm were glued together with tin or top side and hung into the polyethylene bottle with corroding solution. The corrosion experiments were performed at 96°C in three different solutions: HCl (pH=3), distilled water (pH=5.2) and NaOH (pH=12). Glass surface to solution volume ratio S/V was be the same in all experiments and amounted 60 m^{-1}. The time dependence of SiO_2 and Na^+ concentration in the solution was determined using spectrophotometry and flame photometry respectively. The pH values were constant during the experiments and did not differ more then ±0.02. The experimental procedures were described in detail in [15].

III. RESULTS AND DISCUSSION

The experimental results are depicted in figures 1-3 in the form of time dependence of SiO_2 and Na^+ amounts transferred into the solution through the glass surface unit ($Q_{SÝ}$, Q_A). The mathematical model considering the glass matrix dissolution, back precipitation and interdiffusion was used to describe the experimental results. This model was discussed in detail in our previous work [16].

The first process i.e. the glass matrix dissolution is described using the parameter a, i.e. the rate at which the boundary between the glass and solution moves toward the bulk glass ($m.s^{-1}$). This rate is generally time dependent. The value of a can decrease as the consequence of the saturation of corrosion solution by SiO_2 or due to the growth of the precipitated secondary layers on the glass surface. The products of the surface reaction diffuse through this layer. Thus the overall rate of glass matrix dissolution becomes lower. This process is characterised by the ratio D/I, where D is the diffusion coefficient of surface reaction products in the precipitated layer (m^2s^{-1}) and l is the layer thickness (m). The rate of dissolution could be also influenced by the rate of surface reaction e.g. if structure changes occurs in the glass surface or if the pH-value increases or decreases during the interaction.

The second process i.e. the back precipitation is in the model characterised by the dimensionless parameter k^-. This parameter represents the ratio of precipitated SiO_2 (in the form of SiO_2 and/or silicates) to the SiO_2 dissolved.

The third process i.e. the Na^+-H_3O^+ interdiffusion is characterised by the interdiffusion coefficient D_A (m^2s^{-1}). This coefficient could be concentration or time dependent. The initial sodium concentration profile which is needed as the initial condition in the model was obtained experimentally by X-ray microanalysis of uncorroded glass. This profile was fitted by the empirical equation

$$(X_A)_{t=0} = 9[1-\exp(-k_A y)] \qquad (1)$$

where x_A is the Na^+ concentration in weight %, y is the perpendicular distance from the glass surface. The value of constant k_A was 0.5 μm^{-1} for the tin side and 0.9μm^{-1} for the top side (fig.1).

The output of the model are the time dependencies of Q_{si} and Q_A which are calculated numerically using finite difference method.

Corrosion in distilled water (pH=5.2)

The comparison of experimental results with the model is depicted in fig.2. The constant rate of glass matrix dissolution was be used in modelling. This rate is slightly higher in the case of top side corrosion in comparison with the tin side corrosion (fig.5). The linear time dependence of Q_{si} means that no retardation of glass matrix dissolution occurs and therefore the back precipitation could be neglected in the modelling of an interaction in distilled water. However, after longer time of interaction or if the value of S/V ratio would be higher, the decrease of a due to the solution saturation takes place.

The Na^+-H_3O^+ interdiffusion can be described mathematically by using constant interdiffusion coefficient. The D_A value was found to be the same for both tin and top side according to the model calculation.

Corrosion in HCl (pH=3)

The experimental results and the results of the model are compared in fig.3. The glass matrix dissolution rate decreases with time in the case of HCl corrosion. As follows from the model, this decrease cannot be explained by the solution saturation only (fig.3). The precipitation of silicates is also not probable in the case of strong acid. The figure 2 shows a good agreement with the model assuming the exponential decrease of the rate of surface reaction between the solution and SiO_2 matrix. This time dependence of surface reaction can be explained due to the reactions

$$\text{Si-O-Na} + H^+ = \text{Si-O-H} + Na^+$$

$$\text{Si-O-H} + \text{H-O-Si} = \text{Si-O-Si} + H_2O$$

indicating that the surface layer with higher durability could be created during the corrosion. The rate of dissolution is again slightly higher in the case of top side (figs.3,5).

The time dependence of interdiffusion coefficient must be considered in the case of leaching in HCl (fig.5). This fact can be explained by the structure changes of glass surface layer during the interaction as mentioned above. The value of D_A was found to be slightly higher for the top side.

Corrosion in NaOH (pH=12)

The results of interaction between float glass and NaOH are summarised in fig.4 indicating that the rate of glass dissolution decreases with time. Also this decrease cannot be explained by the solution saturation, because the silica solubility rapidly increases at pH>9. The possible explanation could be the protective function of the precipitated silicates layer. The products of the surface reaction must be transported through this layer which grows and/or is less permeable with increasing time of interaction. In such a case

the D/I ratio decreases with time. The differences between the tin and top side durability against NaOH are more important than in previous cases. Although the rates of the SiO_2 dissolution are almost the same in the initial state of the interaction, the time dependence of a is different (fig.5). This difference could be explained by precipitation of hardly soluble tin compound (e.g. tin hydroxides)in a layer which is formed on tin side and retards SiO_2 dissolution.

The back precipitation plays an important role during the interaction with NaOH and cannot be neglected in the model. This fact is in agreement with the higher activity of SiO_3^{-2} at higher pH. The value of k^- used in the model was 0.4 for tin side and 0.3 for top side.

The interdiffusion can be neglected during the interaction between glass and NaOH. In this case the glass matrix dissolution is very fast and the sodium amount transferred into the solution by diffusion is negligible in comparison with the amount transferred by dissolution.

Influence of pH

The initial rate of SiO_2 dissolution a_o decreases in order NaOH>HCl>distilled water for both tin and top side. The rate of matrix dissolution changed during the interaction due to the changes described above so that this rate at steady state decreases in order NaOH>distilled water>HCl (fig.5).

The Na^+-H_3O^+ interdiffusion coefficient is higher in the case of corrosion in HCl solution then in the case of corrosion in distilled water. This fact can be explained by the higher activity of H_3O^+ ions in strong acid. During the interaction the values of D_A for HCl corrosion decreases and after 21 days are close to the ones for distilled water corrosion (fig.5). The interdiffusion is negligible in the case of NaOH corrosion.

IV. CONCLUSIONS

The durability again distilled water, HCl and NaOH is higher on the tin side of float glass in comparison with the top one. This effect is most pronounced in the case of NaOH corrosion. The comparison of the model and experimental results allows to explain the decreasing rate of glass matrix dissolution in HCl and in NaOH. The surface structural changes must be taken into account by modelling the corrosion in HCl. The protective secondary layers on the glass surface are to be expected during the corrosion in NaOH. The initial glass matrix dissolution decrease in order NaOH>HCl>distilled water. In steady state the rate of dissolution in HCl is lower than the one in distilled water.

Acknowledgement

This study was supported by the Grant Agency of the Czech Republic under the project No. GA R 106/960/0560.

REFERENCES

1. Shelby J.E., Vitko J.jr.: J. Non-Cryst. Solids 38&39, 631-636 (1980)
2. Gao M., Zhang Z., Li L. et al.: J. Non-Cryst. Solids 80, 319-323 (1986)
3. Matousek J., Maryska M., Helebrant A.: Glastech. Ber. Glass. Sci. Technol. 69, 7-11 (1996)
4. Dunken H.H.: Physikalische Chemie der Glasoberfläche, pp.325-330, VEB Deutscher Verlag fur Grundstoffindustrie, Leipzig 1981
5. Smets B.M.J., Tholen M.G.W.: Phys. Chem. Glasses 26, 60-63 (1985)
6. EI-Shamy T.M., Lewins J., Douglas R.W.: Glass Technology 13, 81-87 (1972)
7. Hench L.L.: J. Non-Cryst. Solids 28, 83 (1978)
8. Paul A.: J. Mater. Sci.12, 2246-68 (1977)
9. Perera G., Doremus R. H.: J. Am. Ceram. Soc. 74,1554-58 (1991)
10. Conradt R.: Berichte der Bunsengesselschaft fur Physikalische Chemie (in print).
11. Stone J.A.: Nuclear and Chemical Waste Management 2,113-118 (1981)
12. Chandler G.T., Wicks G.G., Wallace R.M.: Advances in Ceramics 20, 455 (1986)
13. Michajlovic J., Skrovankova D., Hlavac J.: Ceramics-Silikaty 37,137 (1993)
14. Helebrant A., Pekarkova I.: Berichte der Bunsengesselschaft für Physikalische Chemie (in print).
15. Tichankova J., Matousek J.: in Proc. 9th Conference on Glass (ed.: Kasa S.), pp.162-163, Czech Glass Society, Hradec Kralove 1994
16. Helebrant A., Matousek J.: Glastech. Ber. Glass Sci. Technol. 68C1, 207-214 (1995)

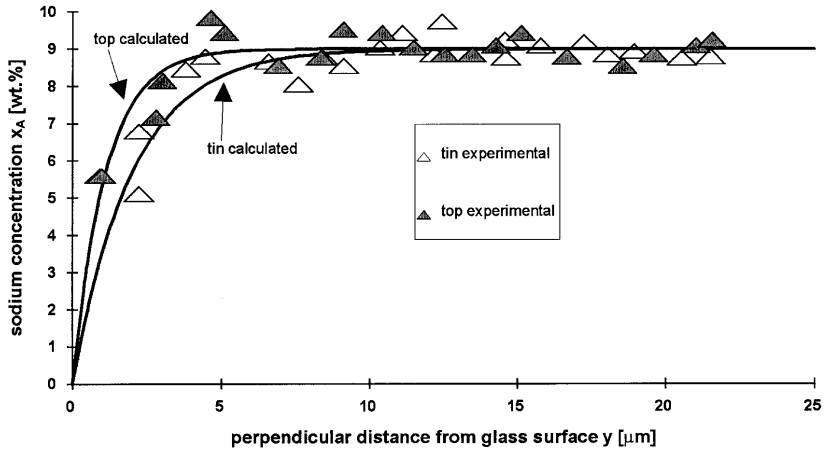

Fig.1. The sodium concentration profiles in tin and top side of uncorroded float glass. The lines represents the best fit of experimental data according to equation (1).

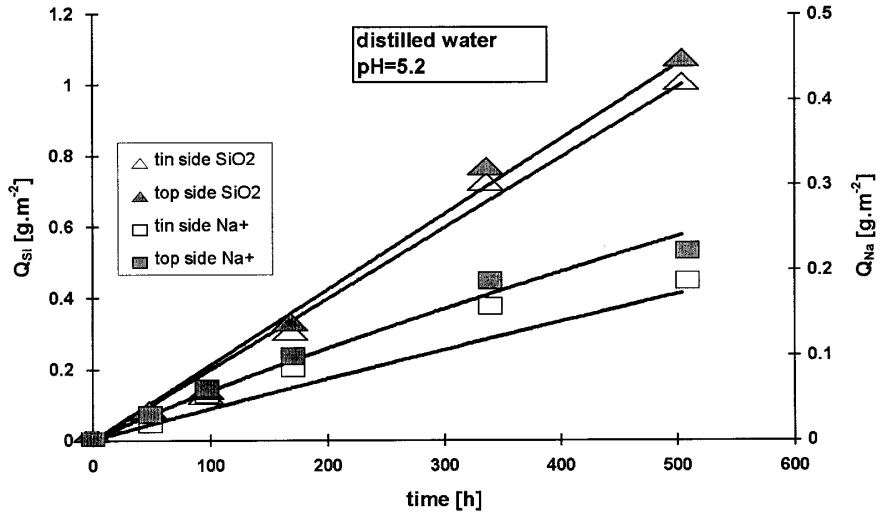

Fig.2. Comparison of the model solution with the experimental data. Corrosion in distilled water (pH=5.2)

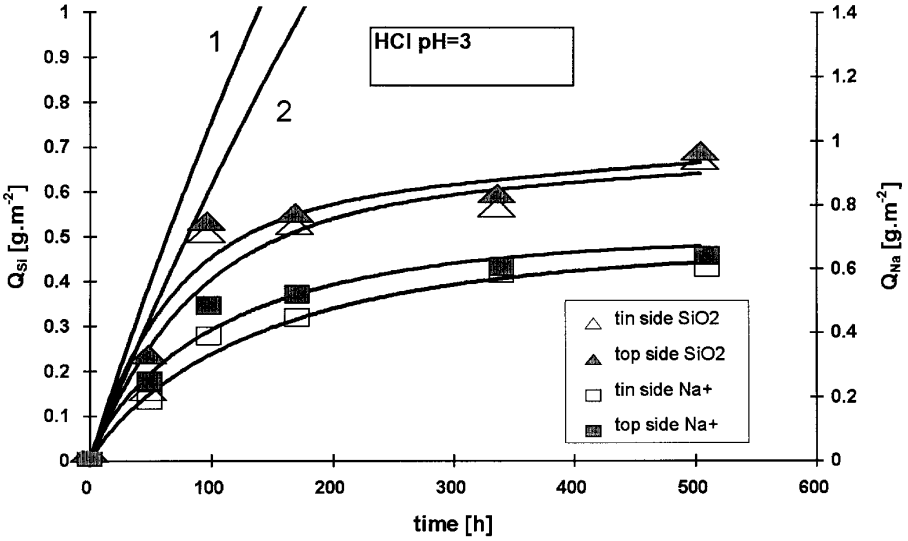

Fig.3. Comparison of the model solution with the experimental data. Corrosion in HCl (pH=3). Curves 1 and 2 represents calculated time dependencies of $Q_{SÝ}$ for top and tin side, respectively, if only saturation effect is considered.

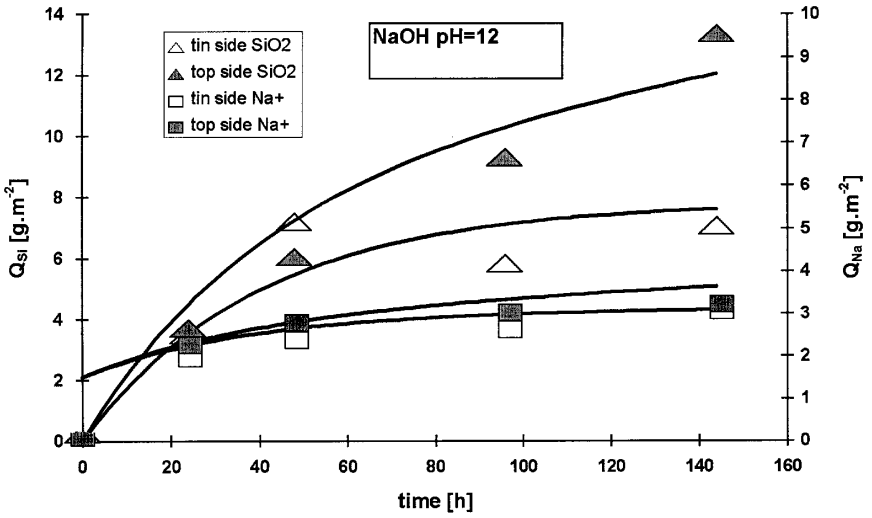

Fig.4. Comparison of the model solution with the experimental data. Corrosion in NaOH (pH=12)

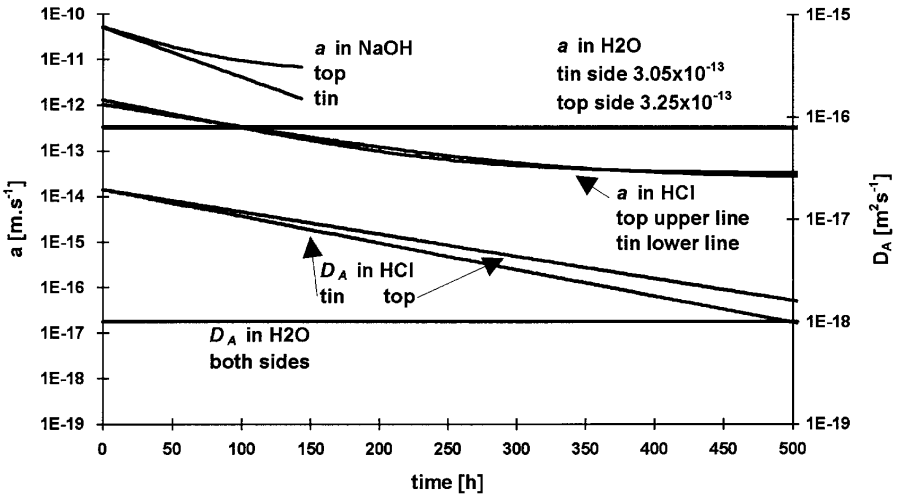

Fig.5. The time dependencies of the rate of glass matrix dissolution a and interdiffusion coefficient D_A used in the model.

CORRUSION MECHANISM IN TeO_2- BASED OXYCHLORIDE GLASS

M.R Sahar and **A.K. Jehbu**
Faculty of Science University Technology of Malaysia, Malaysia

Abstract

Some oxychloride glasses based on the TeO_2-ZnO-$ZnCl_2$ has been prepared and their corrosion mechanism was studied. It was observed that the corrosion is a diffusion controlled process which is strongly dependent on the acidity of the environment.

1.0 INTRODUCTION

It has been reported earlier that the TeO_2 -based oxychloride glass exhibits interesting physical, thermal and optical properties which can be use for a longer wavelength applications [1,2]. The introduction of metal halides has improved their stability [3], a factor which is very important in fibre production route. However, their corrosion mechanism is not well describe. In the present work, the current information on the corrosion mechanism of TeO_2-ZnO-$ZnCl_2$ glass will be reported.

2.0 EXPERIMENTAL

2.1 Sample preparation

Glasses were prepared from approximately 20 g batches using reagent grade TeO_2 (purity 99.99%), ZnO (99.99 %) and $ZnCl_2$ (99.8%). Detail on the glass preparation method has been described elsewhere [1]. EDAX (energy dispersive x-ray analysis) technique has been applied to analyse the glass composition.

2.2 Corrosion rates

The well polished flat surface of the cylindrical glass samples with known surface area are weighed before and after an immersion in 100 ml of distilled water, pH = 5.3 at 25^{o}C for 7 days. Samples were dried at 80 ^{o}C in the oven before being re-weighed. The corrosion rate was then determined using a relation

$$\text{Corrosion rate} = \Delta W/tA \quad gd^{-1}\ cm^{-2}$$

where W is the weight loss(g), t is the exposed time and A is the known surface area. The corrosion rates were then plotted against the $ZnCl_2$ content.

2.3 Leaching rate

A portion of glass sample was crushed into a powder form with a particle size of about 500 micron. About 1 g of the powder was then immersed in 100 ml of distilled water, pH 5.3 at 25 ^{o}C. The concentration of Zn^{2+} ions in a solution was determined using a camplexometric titration method [4]. The reading was taken for every 24 hrs up to 164 hrs. The values of Zn^{2+} concentrations were then plotted against the time taken (hours).

2.4 Effect of solution pH

Some of the glass sample as in (2.1) were put in solution pH of 1, 2, 4, 7 and 10 at 25^{o}C. The effect of solution pH was measured after 7 days. The corrosion rates were then plotted against the solution pH.

2.5 IR spectroscopy

The IR spectra for some of the corroded glasses as in (2.4) were carried out using a Perkin-Elmer IR Spectrophotometer. This method enable us to measured the relative quantitative amount of OH bonds that exist in the glass.

3.0 RESULTS

Table 1: The composition of nominal and analysed samples.

Sample No:	**Composition**					
	Nominal			**Analyzed by EDAX**		
	TeO_2	**ZnO**	**$ZnCl_2$**	**TeO_2**	**ZnO**	**$ZnCl_2$**
s_1	50	40	10	51.16	43.60	5.24
s_2	50	30	20	50.49	43.80	5.71
s_3	50	20	30	58.13	33.54	8.33
s_4	50	10	40	56.86	38.08	5.06
s_5	60	20	20	57.87	34.39	7.74
s_6	70	20	10	71.39	24.87	3.74

Table 1 shows the nominal and analysed (by EDAX) composition of the experimental glasses (mol %) while Figure 1 represents the dependence of corrosion rates of the glass in distilled water with $ZnCl_2$.. An almost linear relationship between corrosion rate an $ZnCl_2$ can be observed.. When a glass powder sample was immersed in distilled water, the variation in an amount of Zn^{2+}which leached from the sample with time can be seen in Figure 2. It can be seen that the Zn^{2+} leached almost linearly at the early stages before becomes constant after a certain period of time.

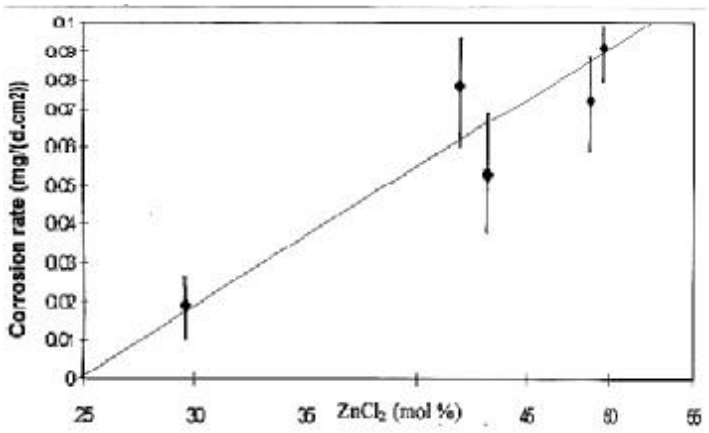

Figure 1: Corrosion rate against $ZnCl_2$ content

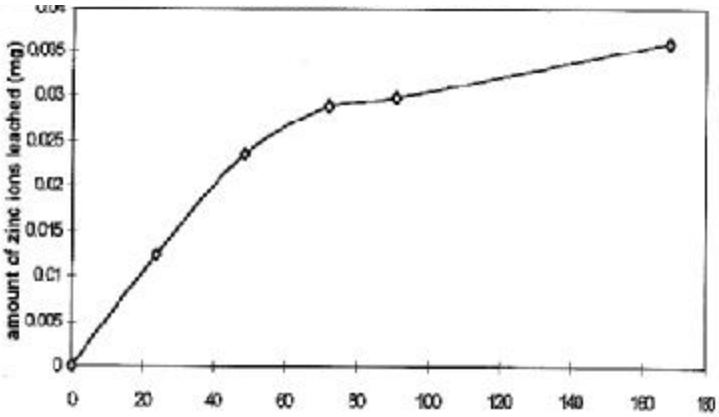

Figure 2: Amount of Zn^{2+} leached against time(h)

The effect of solution pH for some glasses are presented in Figure 3 while Figure 4 shows the IR spectra for the corroded glass sample (S_4).

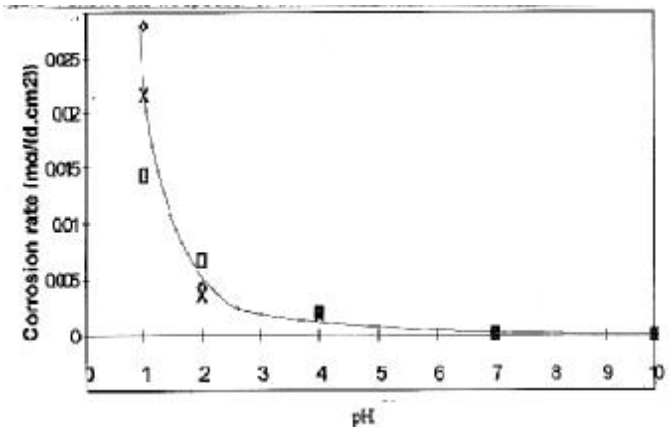

Figure 3 : Corrosion rate against the solution pH

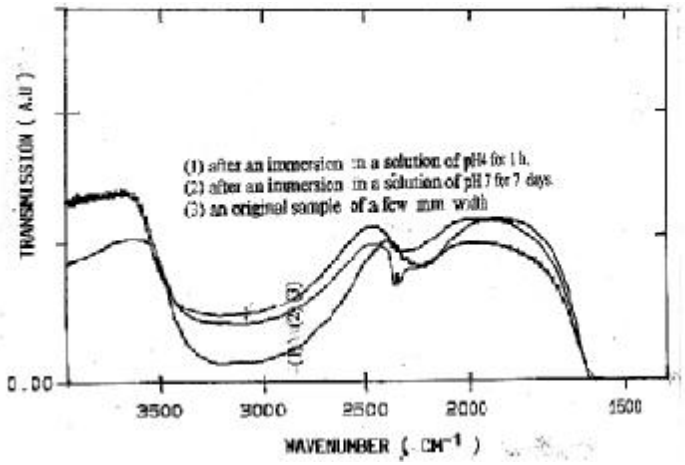

Figure 4: IR spectra for the corroded glass sample (S_4).

4.0 DISCUSSION

From table 1, it can clearly be seen that there are a significant loss of chorines during the melting process thus increasing the percentage amount of TeO_2 and ZnO. This is quite understandable because of the low melting point of the halide compounds. However, this losses might be suppressed by preparing the sample in nitrogen environment or in dried air.

4.1 Corrosion rate

Results from Figure 1 indicate, that most of the samples experienced weight loss in the presence of water. The higher the chlorine content, the faster the reactivity occurs. This is true since most of the metal halides containing $ZnCl_2$ always exhibits higher solubility in water [5].

4.2 Leaching rate

Results from Figure 2 indicate that the concentration of Zn^{2+} that leached from the sample into the solution increases as the time increases. However, after about 60 hours of an immersion time, the rates become almost constant. If this concentrations were plotted against $t^{1/2}$, then a result as shown in Figure 5 may be obtained.

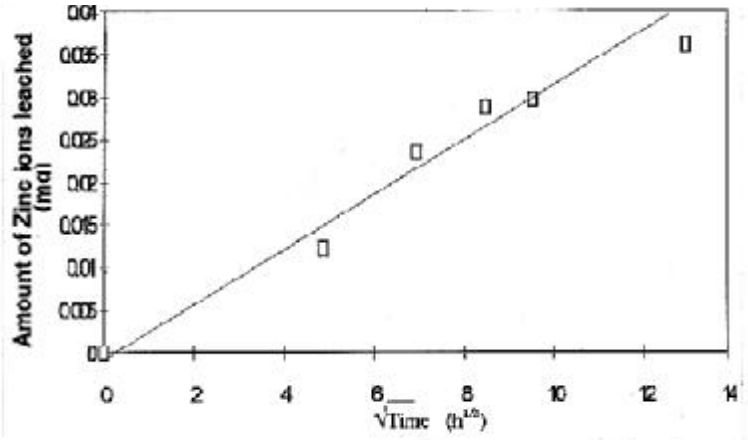

Figure 5: Zinc concentration leached against $t^{1/2}$

A linear relationship between concentration and $t^{1/2}$ strongly suggest that the corrosion is a diffusion control process. Such process would promotes further corrosion activity an will only be delayed by a creation of a diffusion barrier on front of a glass surface.

4. 3 Effect of solution pH

Results from Figure 3 show that most glasses are more effectively corroded in an acidic solution rather than in the alkaline. This might be due to the ion exchange process between the proton H^+ in the solution and cation (most probably Zn^{2+} ions) in the glass matrix [6]. This argument is also supported by the result shown in Figure 2 which indicates that the Zn^{2+} ions do leached from the sample.

4.4 lR spectroscopy

Results from Figure 4 indicate that the absorption peaks occurs around 3.2 μm which correspond to the vibration of OH bonds [6]. It should however important to be noted that the OH peaks in this area is becoming larger when the samples were put in acidic solution. This results indeed in agreement with the above argument.

4.5 Corrosion mechanism

It has been shown by previous work that the TeO_2-ZnO-$ZnCl_2$ oxychloride glasses were dominated by the presence of TeO_3 trigonal pyramid of $ZnTeO_3$ [1]. It could then be suggested that the corrosion process must involves the destruction of those units. Based on the experimental evidence that has been discussed above, the schematic corrosion mechanism may be expressed as,

$$\equiv TeO^{-}Zn^{2+}_{(g)} + H^{+}_{(s)} \rightarrow \equiv TeOH_{(g)} + Zn^{2+}_{(s)}$$

For glasses containing higher amount of chlorides, an additional equation may be required i.e.

$$\equiv TeO^{-}Cl^{-}_{(g)} + H^{+}_{(s)} \rightarrow \equiv TeOH_{(g)} + Cl^{-}_{(s)}$$

The existence of bonded OH is well observed in the IR spectra. However the exact corrosion mechanism needs the data on the qualitative ratio of Zn^{+} : CI^{-} : H^{+} and this surely needs more experiments to carried out.

5.0 CONCLUSION

The corrosion mechanism of oxychloride glasses based on TeO_2-ZnO-$ZnCl_2$ were shown to be a diffusion control process, which strongly dependent on the acidity of the environment.

The authors would like to thank UTM for their financial support under the research vot 61530.

REFERENCES

[1] M.R. Sahar and N.Noordin, J. Non-cryst. Sol 184(1995)137-140
[2] M.R. Sahar and R. Isahak, J.Fiz.Mal.15,21(1994)21-26
[3] M. R. Sahar, in Fundamentals of glass Science and Technology-ESG 1993,Venice p327-332
[4] A. I. Vogel, Quantitative inorganic Analysis, 3rd Ed.(longmans, 1981)
[5] L. E. Gorre and R. C. Postor, Mater. Res. Bull.18(1983) 1391
[6] H.SchoIze,J .Non-Cryst. Sol.52(1982)91

IMPROVING THE CHEMICAL DURABILITY OF LEAD CRYSTAL GLASS

Hande Sengel, Gülçin Albayrak and **Orhan Çorumluoglu**
SISECAM Research Center, Turkey

Tahir Cebecioglu
Paþabahçe Cam San. A. S., SISECAM, Turkey

Abstract

In a recent presentation (*), we have reported about the improvements that have been achieved in lead release levels of crystal glassware by altering the chemical composition of the basic glass. However, the PbO content of the glass obtained in the first industrial trials did not fulfill the requirements of the EEC Directive (69/493-EEC). Therefore, further studies were required.

The work persented here is the report of factory trials where the PbO content of the glass is slightly greater than 24%. The glass articles obtained in these trials were tested for their lead release characteristics, both before and after surface treatment. The physical properties of the glass which affect the melting-forming-annealing characteristics and which are cited in the EEC directive are also reported.

1. INTRODUCTION

Lead leaching from crystal glassware is an ion exchange process, largely determined by the basic glass composition, surface chemistry, nature of the liquid in contact with glass and the ratio of the interior surface of the glass item to the volume of the liquid contained by it.

The previous studies on basic glass composition revealed that decreasing the PbO content to a limiting value, reducing the alkali oxides (Na_2O, K_2O), adjusting the weight percent ratio Na_2O/K_2O and addition and/or removal of certain oxides (ZnO, Li_2O, etc.) significantly improve the chemical durability of lead crystal glass (1).

Application of surface treatments such as acid polishing, ammonium sulphate fuming, rinse treatment, sol-gel coating, ion exchange and polymer coating, all of which aim to reduce the lead content of the surface getting into contact with the liquid, have also proved to be methods that resulted in reduced lead migration.

Under the light of this basic information and due to the growing public interest, in lead release from lead crystal glassware since 1991, ÞÝÞECAM conducted a series of laboratory scale experimental studies and pioneering industrial trials, the results of which were reported elsewhere (2). The present work reports the results of the industrial trials of decisive importance

(*) Proceedings of the Seventh Technical Exchange Conference of International Crystal Federation..

2. REVIEW OF THE PREVIOUS WORK

As reported in(2), the previous work on this subject covered the following topics:

- The chemical compositions, physical properties and lead release characteristics (as determined by ISO 7086) of our previous lead crystal glass (SC-1) and samples of imported crystal glassware, which have considerable shares in the domestic market, were investigated.
- An industrial trial melt of 800 kg, which has a chemical composition similar to that of one of the imported glasses (SC-2), has been prepared, and from this melt, two types of glass item and a decanter were formed, annealed, cut and acid polished under the same conditions as those applied to SC-1. These items were then examined for their lead release characteristics and some physical properties.

The results obtained in the above-mentioned studies are summarized in Table 1 and Table 2. As can be seen from Table 2, the wine and champagne glasses made from SC-2 composition demonstrated far superior lead release characteristics, both in the polished and unpolished samples, when compared with the results of SC-1 glass. For decanters, $(NH_4)_2SO_4$ treatment improved this characteristic even more.

Table 1, shows the chemical compositions and some physical properties of the said glasses. It can be seen that SC-2 glass, although superior in lead release characteristics, did not comply with the requirements for lead crystal glass, as described by the EEC Directive (69/493-EEC).

Table 1

The chemical compositions and physical properties of SC-1 and SC-2 glasses, and the definition of lead crystal glass as given by EEC Directive (69/493-EEC)

Glass Type / Property	SC-1	SC-2	EEC Directive (69/493-EEC)
Chemical Composition* (% by weight):			
SiO_2	58.56	61.26	
B_2O_3	0.28	1.19	
PbO	24.59	23.65	≥24
ZnO	-	0.17	
Na_2O	2.16	5.06	
K_2O	13.58	7.78	
Physical Properties:			
Density (g/cm^3)	2.9388	2.9172	≥2.90
Refractive index, n_D	1.5460	1.5432	≥ 1.545

** SiO_2 and PbO were determined by gravimetry. The other constituents were analyzed by Inductively Coupled Plasma Emission Spectrometer (ICP).*

Table 2

The mean values of lead release (µg Pb/l) from SC-1 and SC-2 glasses and permissible limits according to ISO 7086 Standard and revision Draft No:2 of ISO 7086 Standard

Item	SC-1		SC-2			ISO 7086 limits	ISO 7086 Draft No:2 limits
	Unpolished	Polished	Unpolished	Polished	$(NH_4)_2SO_4$ treated		
Wine glass (FV*= 150 ml)	1135	242	143	34		5000	1500
Champagne glass (FV*= 184 ml)	790	210	139	16			
Whiskey decanter (FV*= 750 ml)			308	43	29		750

****** FV: Fill Volume*

3. REPORT ON THE PRESENT WORK

In an attempt to investigate the melting, forming characteristics and physical and chemical properties of a lead crystal glass which would comply with the EEC Directive (69/493-EEC), a second trial in industrial scale was conducted.

The theoretical glass composition of the second trial melt (SC-3) is given in Table 3. Note that in general, the chemical composition is the same as that of SC-2 glass, with the exception of the increased PbO content.

As in the previous trial, a melt of 800 kg SC-3 glass was prepared in an industrial pot furnace. The melting process was conducted under the same conditions as those applied to SC-1 and SC-2 glasses.

Again, 3 different items, similar in shape and volume to those in the first industrial trial were formed, and from each, the following sets of samples were taken:

- Whiskey decanter (710 ml. capacity)
  . 6 decanters, annealed
  . 6 decanters, annealed, decorated an acid polished
  . 6 decanters, $(NH_4)_2SO_4$ treated before annealing
- Wine glass:
  . 6 glasses, annealed, decorated and acid polished.
- Champagne glass:
  . 6 glasses, annealed, decorated and acid polished.

The above-mentioned samples were examined for their lead release characteristics, and the results were compared with those obtained from the previous trial (Table 4).

Table 3

The Chemical compositions and physical properties of SC-1 and SC-3 glasses and the values defining lead crystal glass as given in EEC Directive (69/493 EEC).

Property \ Glass Type	SC-1 (analysis)[1]	SC-3		EEC Directive (69/493-EEC)
		Theoretical	Analysis[1]	
Chemical Composition (% by weight):				
SiO_2	58.56	61.0	60.84	
B_2O_3	0.28	1.0	0.97	
PbO	24.59	25.0	24.04	≥24
ZnO	-	0.20	0.21	
Na_2O	2.16	5.0	5.00	
K_2O	13.58	8.0	8.04	
Physical Properties:				
T, C				
log = 2.5[2]	1353		1336	
=3.5[2]	1180		1171	
=4.5[2]	1051		1049	
=7.65[3]	628	-	640	
=13.0[4]	447	-	456	
= 14.5	407	-	415	
Density (g/cm^3)[5]	2.9388		2.9245	≥2.90
Refractive index, n_D[6]	1.5460		1.5484	≥1.545
Micro hardness (Vickers)	399		486	

(1) SiO_2 and PbO were determined by gravimetry. The other components were analyzed by ICP.
(2) ISO 7884-2 1987 (E)
(3) ASTM C338-73 (Reapproved 1983)
(4) ASTM C336-71 (Reapproved 1986)
(5) ASTM C693-84 (Reapproved 1986)
(6) Determined by Abbe Refractometer

Table 4: *Mean values of lead release (µg Pb/l) from SC-1, SC-2 and SC-3 glasses*

Item	SC-1		SC-2			SC-3**			ISO 7086 Draft No:2
	Un-polished	Polished	Un-polished	Polished	$(NH_4)SO_4$ treated	Un-polished	Polished	(NH4)SO4 treated	
Wine glass (FV*= 150 ml)	1135	242	143	34			38		1500
Champagne glass (FV*= 184 ml)	790	210	139	16			40		
Whiskey decanter (FV*= 750 ml)			308	43	29	270	42	18	750

***** *FV = Fill volume*

****** *Fill volume of the decanter = 710 ml*

The chemical composition and some physical properties of the glass, which are important for the melting, forming and annealing of the ware and for the quality of the finished glass article, were also determined experimentally with respect to those of the SC-1 glass (Table 3).

When the data in Table 3 and 4 are examined, the following conclusions can be drawn:

1. The PbO content of SC-3 glass is higher than that of SC-1 glass and is greater than 24%. The K_2O content is also slighly higher.
2. The high temperature viscosity of SC-3 (log =2.0-4.0) is lower and the low temperature viscosity is higher (T_S, T_{Ann}) than those of SC-1;
3. The density and the refractive index of SC-3 glass are lower than those of SC-1, but fulfill the requirements of EEC Directive given for 24% lead crystal glass; and
4. The hardness SC-3 glass is higher than that of SC-1.
5. The lead release levels given in Table 4 are far below the limits required by ISO 7086 (Draft 2), which is expected to replace the existing ISO 7086 soon. Acid polishing and $(NH_4)_2SO_4$ application for decanters drastically improved the lead release characteristics of the ware.

The data obtained during the trial melting and forming in the industrial scale confirmed the following results, which were speculated after the previous industrial trial:

1. As expected from the high temperature viscosity data, SC-3 glass was easier to refine than SC-1. Thus the inferior melting characteristics, as detemined experimentally in former laboratory studies, seems to be compensated by the ease in refining, resulting in comparable total "melting+fining" time for the SC-3 glass.
2. SC-3 glass is "shorter" than the SC-1 glass. However, with slight adjustments in the forming conditions, there were no complaints from the forming department.
3. The cutting and acid polishing conditions were kept unchanged, and the SC-3 glass items were cut and polished with the same success as SC-1 glass.

4. CONCLUSION

In view of the growing public interest in lead release from lead crystal glassware, ÞÝÞECAM conducted a series of experimental and industrial trials, aiming to obtain a glass with superior lead release properties and which fulfill the requirements of the EEC Directive (69/493-EEC) for 24% PbO, lead crystal glass. Among the many alternatives, we have chosen to modify the basic glass composition and to apply $(NH_4)_2SO_4$ treatment to decanters to reduce lead release. The major modifications in the basic glass composition were:

. reducing PbO to the lowest possible value (i.e. very close to 24%)
. reducing the total R_2O but adjusting the K_2O/Na_2O ratio,
. increasing B_2O_3 to compensate for the reduction in total R_2O, and
. adding ZnO.

This modification in the basic glass composition resulted in decreasing the lead release to 40 ppb, 1/5th of its original value, for acid polished wine and champagne glasses. This is far below the limiting values of any public discussion.

For decanters of 710 ml fill volume, the lead release results obtained after acid polishing were as low as 40 ppb, which is below the requirements of ISO 7086 Draft No: 2. $(NH_4)_2SO_4$ treatment reduced this value even more.

From the above-mentioned results, it can be concluded that by applying SC-3 as the basic glass composition and by acid polishing the items, it is possible to obtain lead crystal glassware

which have satisfactory lead release characteristics and which fulfill the requirements for lead crystal glass, as defined in the EEC Directive (69/493-EEC).

REFERENCES

1. Kennedy, J.; Review of Past Technical Conferences, Proceedings of the 4th Technical Exchange Conference of the International Crystal Federation, p. 19, 1993.

2. Proceedings of the Seventh Technical Exchange Conference of the International Crystal Federation, p. 163, 1995.

IS THERE AN ALTERNATIVE TO LEAD CRYSTAL GLASS ?

Miroslav Rada and **Ladislav** Òa Ó**ek**
Institute of Chemical Technology, Czech Republic

Abstract

An array of problems associated with the migration of lead from lead crystal glass into the liquid is surveyed in the introductory part of the paper. The effect on human beings as well as on the environment is assessed briefly.

Major attention is devoted to the possibility of substituting unleaded glasses based on various oxides (CaO, SrO, BaO, ZnO, Bi_2O_3, TiO_2, ZrO_2, etc.) for lead crystal glass. The importance of individual properties is analyzed from several viewpoints and the optimum values of such properties are assessed.

Some selected parameters of lead-containing and unleaded glasses are compared in the last part of the paper and the results obtained during the practical trials aimed at producing lead-free glass on the basis of ZrO_2 are given.

I. INTRODUCTION

The publication of a paper by Graziano and Blum in 1991[1] dealing with the increased lead leaching in beverages kept for a long period of time in lead crystal glass articles started a new era for the crystal glass industry.

In particular, an intense investigation aimed at reducing the amount of lead leached from lead crystal was initiated and the results demonstrate that there are essentially two basic approaches : the surface treatment of finished glass articles and the change of the chemical composition of base glass. Using various techniques the amount of lead leached out of the glass can be brought below a very safe limit of 0.1 mg per liter with the aid of both processes.

All lead compounds are toxic and their effect on the environment and human living also became a major topic in addition to lead migrated into the beverages. The standards specifying the amount of lead in the air, effluents from industrial plants, drinking water and human blood, the standards indicating the categories of various types of waste and the possibilities of their disposal as well as the development trends focusing on the above standards show that it will be ever more difficult to meet the standards in the future and that more money will have to be expended in this field.

Under these circumstances a question arises whether it may not be easier and better to substitute toxic lead oxide in the crystal glass for less toxic or non-toxic components. Of course, the new lead-free crystal glass should possess the same properties as lead crystal glass produced so far.

II. RESULTS AND DISCUSSION

1. Possible alternatives of substitution of lead crystal glass

The directive of the European Union EC 1969 (Table I) divides the lead crystal glass into several categories in dependence on the PbO content, its density and refractive index. In addition to this definition, the lead crystal glass is also characterized by a variety of other properties : a high dispersion, suitable melting and glass forming temperatures, a wide glass forming range, a good chemical durability, etc. This type of glass can also be easily cut and polished by exposure to acids.

Table 1 : Definition of crystal glass - EC Directive 1969

Type of glass	**% oxides by weight**	**Density [g/cm^3]**	**Refractive index**
Full lead crystal	PbO≥30	≥3.00	≥1.545
Lead crystal	PbO≥24	≥2.90	≥1.545
Crystalline	ZnO+BaO+PbO +K_2O≥10	≥2.45	≥1.520

The patents filed in this field (see Table II and III) show that major attention was primarily paid to the refractive index and the density whereas the mean dispersion and other properties were regarded as less important.

Except for Ba ion which is toxic in all soluble compounds, all the remaining compounds and components mentioned in patent applications possess a low toxicity or they are not toxic at all. It is obvious from the survey that PbO was most often substituted by MgO, CaO, SrO, BaO, ZnO, La_2O_3,Bi_2O_3, TiO_2, ZrO_2, HfO_2, SnO_2, Nb_2O_5 and Ta_2O_5.

The glass compositions aimed at achieving a density superior or equal to 2.7 g/cm3 and a refractive index superior or equal to 1.545 are listed in Table II.

The glasses mentioned in the patents filed by British Glass and Baccarat do not contain any toxic BaO. The glasses patented by British Glass are based on Bi_2O_3 , TiO_2 and SrO whereas Baccarat developed a glass on the basis of ZnO, SrO and CaO. BaO-containing glasses are mentioned in the patent application of Toyo Glass as well as in two patents filed by Corning. The glass composition filed by Toyo Glass is based on BaO, TiO_2 and ZnO, those filed by Corning contain BaO, SrO and ZnO. Furthermore, the Abbe number of the glasses developed by British Glass and Toyo Glass approaches the respective value of lead crystal glass in the best way.

The compositions of the glasses with a density superior or equal to 2.45 g/cm^3 and a refractive index superior or equal to 1.52 are given in Table III.

The glasses mentioned in the patents filed by Inn Crystal, Schott and by the Prague Institute of Chemical Technology (VSCHT) do not contain toxic BaO. However, another patent filed by Schott refers to a BaO-containing glass. The glass patented by Inn Crystal is based on ZnO, ZrO_2, and/or TiO_2 and CaO. The glass developed by Schott is based on CaO, and further on TiO_2 , ZrO_2, Nb_2O_5 and Ta_2O_5 and their combinations.

The Prague Institute of Chemical Technology (VSCHT) patented a glass based on ZrO_2, CaO, ZnO and HfO_2. The BaO-containing glass patented by Schott was derived from the patent filed for BaO-free crystal glass.

For the sake of clarity, the tables do not include decolorizing and fining agents.

Table 2 : Survey of glasses possessing a density r ³ 2.7 g/cm³ and a refractive index n_D ³ 1.545

Oxide /Firm	**Brit.Glass[2]**	**Baccarat[3]**	**Toyo Gl. [4]**	**Corning[5][c]**	**Corning[6][e]**
SiO_2	50-65	53-58	50-60	54-64	51-63
Li_2O	M_2O 12-23	0-0.3	0-1[b]	0-3	0-3
Na_2O		4.5-7.5	3-10	0-6.5	0-8
K_2O		6-10	5-13	0-7	0-12
MgO	-	-	-	0-3[d]	0-3
CaO	0-15[a]	0-9	1-5	0-3[d]	0-5
SrO	1-20	0-12	-	8-13	0-<8
BaO	-	-	10-15	8-13	>13-21
ZnO	0-15[a]	16-21	5-10	5.5-9	5-15
B_2O_3	0-15[a]	0-1.2	1-2[b]	0-3[d]	0-3
Al_2O_3	0-15[a]	0-1.5	-	0-3[d]	0-5
La_2O_3	0-15[a]	0-3	-	-	0-8
Bi_2O_3	1-20	-	-	0-3[d]	-
TiO_2	1-15	0-2	5-8	0-3[d]	0-3
ZrO_2	0-15[a]	-	0-2[b]	0-3[d]	0-6
HfO_2	-	-	-	-	-
SnO_2	-	0-2.5	-	-	-
Nb_2O_5	-	-	-	-	-
Ta_2O_5	-	-	-	-	-
Guaranteed values of parameters					
ρ[g/cm²]	≥ 2.7	≥ 2.9	≥ 2.9	≥ 2.75	≥ 2.9
n_D	≥ 1.55	≥ 1.545	≥ 1.55	-	≥1.545
Abbe num.	< 52	-	≤ 47	-	-

[a] a glass additionally containing one or more ..., in total amount up to 15% by weight
[b] a glass composition further comprising
[c] $Li_2O+Na_2O+K_2O$ = 8-15, BaO+SrO+ZnO = 22-33
[d] a glass also containing up to 5% total at least one metal oxide from the group
[e] $Li_2O+Na_2O+K_2O$ = 7-15, SrO+BaO+ZnO = 27-34, $SiO_2+Al_2O_3+ZrO_2$=55-66

2.Criteria for the selection of some of the alternatives aimed at substituting lead crystal glass

The selection of the glass from the survey of alternative compositions should be made by taking into consideration the following aspects.

1. Physical aspects

The new glass should meet the definition of crystal glass although even this definition will certainly be a subject of further evolution, i.e. especially the density and the refractive index. The latter property is closely associated with other optical parameters as

the mean dispersion, respectively the Abbe number, and the transmittance; this group of parameters is usually understood as characterizing the glass brilliance.

Table 3 : Survey of glasses possessing a density r ³ 2.45 g /cm³ and a refractive index n_D ³ 1.52

Oxide/ Firm	**InnCrystal [7]**	**Schott [8]**	**VSCHT [9]**	**Schott[10]**
SiO_2	65-70	50-75	50-75	50-75
Li_2O	-	0-5	0.001-1.5[b]	0-5
Na_2O	4-12	2-15	5-16	2-15
K_2O	4-12	5-15	0.1-10	1-15
MgO	-	0-5	0.001-6	0-5
CaO	6-9	3-12	2-9	3-12
SrO	-	0-7	-	0-7
BaO	-	-	0.05-6[b]	1-10
ZnO	4-7	0-7	0.05-10	0-7
B_2O_3	0.5-5	0-10	0.001-5[b]	0-10
Al_2O_3	-	0-5	0.05-10	0-5
La_2O_3	-	-	0.05-2[c]	-
Bi_2O_3	-	-	0.05-10[c]	-
TiO_2	1-6	0-8[a]	0.01-5	0-8[d]
ZrO_2	1-6	0-5[a]	0.05-15	0-5[d]
HfO_2	-	-	0.001-2.5	-
SnO_2	-	-	0.005-5[c]	-
Nb_2O_5	-	0-5[a]	-	0.5[d]
Ta_2O_5	-	0-5[a]	-	0.5[d]
Guaranteed values of parameters				
ρ [g/cm³]	-	≥ 2.45	-	≥ 2.45
n_D	≥ 1.52	> 1.52	>1.52	>1.52

[a] the sum of TiO_2+ZrO_2+Nb_2O_5+Ta_2O_5= 0.3-12
[b] a glass further with the content at least of one oxide from the group comprising Li_2O, BaO, B_2O_5 and 0.001-1.5 P_2O_5
[c] a glass further with the content at least of one oxide from the group comprising La_2O_3, Bi_2O_3, SnO_2 and 0.001-0.1 MoO_3 and 0.001-0.5 WO_3
[d] the sum of TiO_2+ZrO_2+Nb_2O_5+Ta_2O_5 = 0.3-12

2. Technological aspects

The processes taking place before the shaping of the glass articles are of paramount importance, i.e. the glass melting temperature, the glass working temperature and the glass working range. Also the corrosion of the refractory by molten glass is of great importance because this parameter may affect the total yield.

Also the subsequent processes, i.e. the glass cutting and polishing, are important; this is particularly true in the manufacture of lead crystal glass.

3. Aspects associated with the use of glass articles

The chemical durability of the glass articles as well as their resistance to the corrosion by acids and alkalis, the resistance to thermal shocks and the sound emitted during the clinking of glass articles are of importance.

4. Economic aspects

The batch cost, the energy costs, the cost of cutting tools, the operating costs of the acid polishing plant, etc. are the most important cost items influencing the overall economy of the glass making process.

3. Suggested values of individual parameters characterizing lead-free crystal glasses

1. Physical aspects

The density of the glass in which lead oxide has been replaced grows in the following sequence :

$MgO < TiO_2 < CaO < ZrO_2 < ZnO < SrO < BaO < La_2O_3 < Bi_2O_3.$

In the writer's opinion, however, the glass density is not important because "the feel" of article heaviness can also be obtained by changing the wall thickness. In this case, the density would not restrict the range of solutions of other problems which could be tackled technically or technologically in a much more difficult way.

The refractive index drops in the following sequence :

$TiO_2 > ZrO_2 > CaO > Bi_2O_3 > La_2O_3 > SnO_2 > SrO > BaO > ZnO > MgO > HfO_2.$

The mean dispersion diminishes in the following sequence :

$TiO_2 > Bi_2O_3 > ZrO_2 > CaO > La_2O_3 > ZnO > SnO_2 > SrO > HfO_2 > BaO > MgO.$

It seems that the refractive index of 1.52 would probably be quite acceptable for plain glass articles which are not subjected to further decorating. However, the refractive index of luxury glass items decorated by cutting and acid polished afterwards should be 1.545.

The mean dispersion of lead crystal glass ranges approximately from 1100 to1300 x 10^{-5}. The authors of some patents tried to achieve the above values by introducing suitable oxides into the glass but such glasses are either expensive (Bi_2O_3) or difficult to cut and polish (TiO_2). The experience has shown that - at the same refractive index and at a smaller value of the mean dispersion - the impression of a perfect brilliance can be obtained by an "excellent" colorlessness and a high transmittance of glass articles.

2. Technological aspects

The substitution of lead oxide for selected oxides usually results in a narrower glass working range. The glass melting temperatures should range approximately from 1380 to 1430 ^{o}C and the glass working temperatures should be in the range from 1160 to 1190 ^{o}C; these ranges correspond approximately to the temperatures of strengthened lead crystal

glasses exhibiting lower lead leaching. There should not be any difficulties even if the glass working range is narrower.

We should bear in mind the fact that a high content of bivalent oxides and, in particular, ZnO, SrO and BaO (in excess of 20 percent by weight) accompanied by an increased K_2O content may lead to considerable difficulties associated with the refractory corrosion.

The ease of cutting with the aid of diamond-impregnated wheels improves for the individual oxides in the following sequence :

$$TiO_2 < CaO \approx MgO < BaO \approx SrO < ZrO_2 \approx HfO_2 \approx ZnO \approx Bi_2O_3.$$

This parameter should be comparable to that characterizing lead crystal glass.

With all the above mentioned parameters satisfied, the glass ability to be polished in acids plays a key role. Our results have shown that the favorable effect of individual oxides on acid polishing grows in the following sequence :

$$TiO_2 < BaO < SrO < CaO < Bi_2O_3 < MgO < ZnO < ZrO_2 \ HfO_2.$$

It is not sufficient to achieve the same quality of acid polishing as that of lead crystal glass but the unleaded glass articles should be polished within the same (or shorter) period of time and - if possible - under the same polishing conditions.

3. Aspects associated with the use of glass articles

As regards the chemical durability of the articles made of lead crystal glass, they belong mostly to the 3 rd group. This value should be preserved. Also the values of other above mentioned properties should be comparable. The mean linear coefficient of thermal expansion of unleaded glasses could be slightly larger than that of the lead crystal glass (the expansion of lead glass is relatively low).

4. Economic aspects

The production costs of lead-free glasses would be given by the cost of the batch if the technological and operating parameters do not change significantly. It has been assumed that the cost of the batch required for making unleaded glasses would not be more than twice (including the cost of decolorizing agents) the present-day cost of lead crystal. The increased cost would be offset partially by the savings in the field of the pollution control, environment protection and work hygiene. It is obvious that the batch cost will grow with the increasing value of the refractive index.

4. Some results obtained during plant tests with unleaded crystal glasses on the basis of ZrO_2

Selected parameters of lead crystal glasses (L) are compared with lead free-glasses (LF) on the basis of ZrO_2 in Table IV.

The plant tests with the LF-1 glass were carried out in an electric pot furnace. The articles made of this type are earmarked for grinding by a loose SiC abrasive and

corundum wheels; cut articles are then polished by hand. This kind of glass is also suitable for decorating by other techniques (engraving, gilding, etching). However, it is not suitable for cutting by diamond-impregnated wheels or for acid polishing. The preliminary results of the tests are promising.

Table 4 : Selected parameters of lead (L-1, L-2) and lead-free (LF-1, LF-2) crystal glasses

Parameter	L-1	L-2	LF-1	LF-2
ρ_{20^oC} [g/cm^3]	2.9368	2.9339	2.5076	2.6911
Refractive index at 20^{o}C	1.5451	1.5496	1.5204	1.5517
Mean dispersion at20^{o}Cx10^5	1160	1197	908	1020
$t_{log\eta=2}$ [^{o}C]	1478	1423	1475	1425
$t_{log\eta=3}$ [^{o}C]	1174	1128	1189	1184
$t_{log\eta=4}$ [^{o}C]	991	951	1015	1034
$t_{log\eta=7.65}$ [^{o}C]	659	629	695	750
$t_{log\eta=13}$ [^{o}C]	453	430	508	565
t_{liq} [^{o}C]	740	848	830	945
Hydrolytic durability [1]	0.80	0.76	0.70	0.29
$\alpha_{20\text{-}300^oC}$ x10^6 [K^{-1}]	9.03	10.13	9.59	9.58

[1] hydrolytic durability at 98 oC (ISO 719) - consumption in ml [C = 0.01 mol/l] HCl

The LF-2 glass was developed especially for cutting with diamond-impregnated wheels and acid polishing. LF-2 glass samples prepared in laboratory were cut and acid polished under standard factory conditions used for lead crystal glass and the results are very good as well.

III. CONCLUSION

The necessity of replacing lead crystal by a new type of lead-free glass becomes ever more urgent because of the increased criticism of this kind of glass, i.e. the migration of lead into beverages, the harmful effect on environment and human health.

The above criteria should be observed when choosing from various alternatives.

The general assessment of individual criteria has demonstrated that the introduction of ecologically harmless unleaded crystal glasses might be restricted by their ability to be cut and, in particular, acid polished easily. If the values comparable with those characterizing lead crystal glass are to be achieved in this field, some other parameters will have to be sacrificed (especially the density and the mean dispersion).

REFERENCES

1. Graziano, J., Blum, C. : The Lancet 331,141 (1991)
2. UK Patent Application GB 2280432 A
3. European Patent Application 0553586 A1
4. European Patent Application 0594422 A1

5. European Patent Application 0575758 A1
6. European Patent Application 0657391 A1
7. European Patent Application 0547263 A1
8. European Patent Application 0564802 A2
9. PCT Patent Application WO 95/13993 A1
10. European Patent Application 0616984 A1

KINETIC ASPECTS OF REDOX EQUILIBRIUM IN GLASS

Petru Baltà
University "Politehnica" of Bucharest, Rumania

Abstract

A method was established for evidencing the evolution in time of the oxidised/reduced ratio for copper ions in given melting conditions. In this aim were recorded the electronic spectra, the peak corresponding to the d-d electron transition being used for Cu^{2+} ion concentration estimation. The obtained results are discussed in comparison with existing data. The problem of the glass basicity influence upon the redox equilibrium is approached too.

I. INTRODUCTION

Redox equilibrium in glass is always of interest for coloured glasses and for many today's applications in optics and in opto-electronics.

The chemical equilibrium studies at high temperatures meet with many difficulties and this is why, in spite of the accumulated data, new information is useful for more deeply understanding the chemical processes and the influence of different factors.

In the well known book of Weyl [1] works in this field, published in 1929, are cited. However the interest resisted during the time, some of the new results being comprised in the References [2-13].

Useful ideas and data are accumulated about the distortion of the coordination polyhedron of copper in glasses and the manner of interpreting the recorded spectra (2, 5-7, 9].

Thermodynamic aspects and mechanisms of processes involved in the establishment of equilibrium between Cu^{2+} and Cu^{+} and the influence of temperature upon the resulted Cu^{2+}/Cu^{+} ratio were treated in many works [3-6, 7, 9, 10].

An interesting discussion is in course, with experimental [6, 7, 10, 11] and theoretical [12, 13] controversial arguments, about the glass composition (basicity) influence upon the Cu^{2+}/Cu^{+} ratio. It seems that in the case of copper ions the increase of basicity does not always favours the higher oxidation state as happens with many other elements.

In this paper some kinetic aspects of the redox equilibrium establishment in copper containing sodium-borate glasses are presented, in correlation with glass composition.

II EXPERIMENTAL

Three base compositions of sodium borate glasses were used, containing. 1) 11.15 mole % Na_2O, 2) 19.95 and 3) 29.66 mole % Na_2O. The intention was to obtain glasses with quite exact pB (basicity) values of 50 %, 55 % and 60 %. Actually, using the revised data on B4 content function of Na2O concentration, published by Zhong and Bray [14], the following pB values were calculated. 1) 50.02 %, 2) 54.4 % and 3) 59.7 %. The calculation method is described elsewhere

[15]. The mentioned values correspond with the experimental ones, obtained using Cu^{2+} as indicator ion [16] or Pb^{2+} [17] and a conversion equation from **7** to pB, within ±1.5 %.

The glasses were melted in platinum crucible at temperatures respecting the condition $T_{melting}=T_{liquidus}$ + 200°C. The samples used for pB determination were annealed at Tg [16]. The glass samples used for kinetic study were cooled rapidly in air, on ceramic plates, without annealing, to avoid the influence of this heath treatment on redox process.

The electronic spectra of copper ions, between 200 and 1100 nm were recorded by means of a double beam spectrophotometer Shimadzu V-160 A, using glass disks of 1 mm thick and pure glass (without copper) as reference.

In figure 1 the spectrum of copper in glass No. 3 is presented, containing 0.1 atomic percents Cu, equilibrated for three hours in normal atmosphere. Three peaks are clearly visible: a d-d transition of Cu^{2+} at about 800 nm, charge transfer transitions of Cu^{2+} at 294 and of Cu^{+} at about 252 nm.

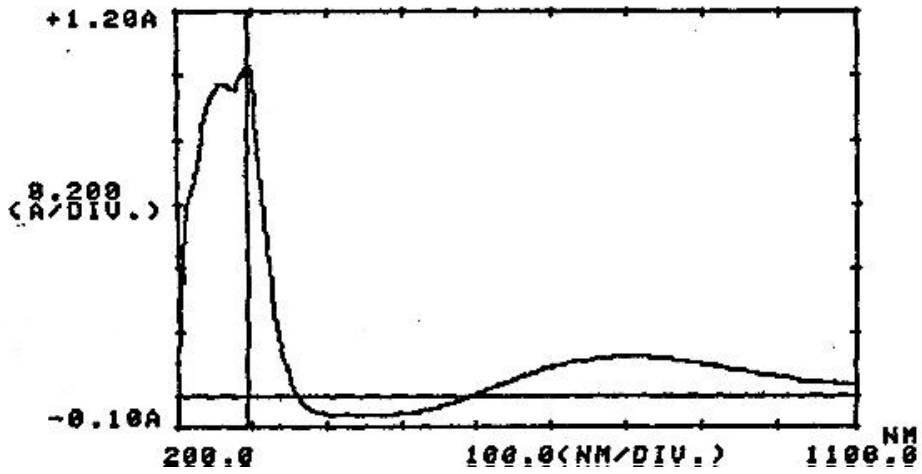

Fig. 1 The electronic spectrum of copper in the glass No.3, containing 0.1 atomic percents Cu, after three hours of melting and annealing in normal atmosphere

The charge transfer peaks position is sensible to glass composition changes and usually the envelope evidences only one peak and a shoulder or even a single peak when the amount of Cu^{2+} is small enough. Thus, in the present stage of our work, these peaks seems to be not suitable for quantitative determination of respective copper ions.

In spite of the fact that the envelope contains three peaks [6,7], the amplitude at 800 nm is determined principally by the $^2B_{lg}$-$^2_{Eg}$ transition, the next transition being centered at about 1,250 nm. So, this peak is convenient for Cu^{2+} concentration measurement.

For oxidation kinetic studies were prepared samples with majority of copper, if not all, in the lower oxidation state. In this aim Cu_2O was used and a quantity of carbon black was added, to avoid the oxidation of Cu^{+}. Additionally the oxygen from the furnace atmosphere was consumed by means of carbon black contained in a ceramic crucible. In such conditions the spectrum of the glass had no maximum in the visible region, confirming the absence of Cu^{2+}. Such glass samples were then maintained at the same melting temperature for time intervals between 5 minutes and three hours, in the normal, oxidising atmosphere.

The recorded spectra showed the rise of the amplitude of the maximum at about 800 nm, i.e. the increase of Cu^{2+} content.

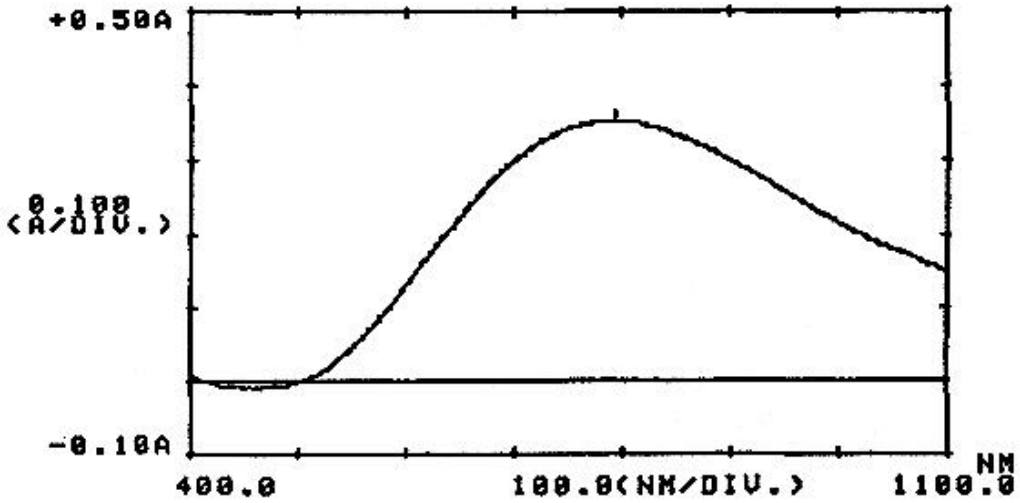

Fig. 2 The d-d transition spectrum of copper in the glass No. 3, containing 0.3 atomic percents copper, after reduction and three hours of oxidising melting, without annealing.

As an example, in figure 2 the d-d absorption maximum for the glass No.3 is shown, after three hours of melting-oxidation. In this case the peak is at 793 nm and the absorptivity 0.354.

III KINETIC ASPECTS

The results obtained after the above described treatment for the three glass compositions are presented in figure 3, in coordinates. optical absorptivity at about 800 nm function of time of oxidising treatment.

The influence of glass composition upon the curves position is obvious. The absorption increases together with the Na_2O content in glasses, i.e. together with glass basicity.

Having no possibility to determine experimentally the actual Cu^{2+} concentration a calculation method was used, by means of published ε values [6, 7]. The existing differences between the two cited sources make this tentative quite approximate. Were preferred the values from [7], being a little newer. Resulted that the increase in the absorption amplitude with the basicity of glasses is, among others, the consequence of Cu^{2+} concentration increase. It is clear that, at least up to a basicity of about 58 % (about 26 mole % Na_2O), corresponding to the maximum on the curve of e variation with glass composition [7], the increase in basicity favours the upper oxidation state of copper. In the basicity interval defined by the synthesized glasses, Cu^{2+} concentration varies from about 65 %, from total copper (at pB = 50 %), up to about 83 % (at pB = 60 %).

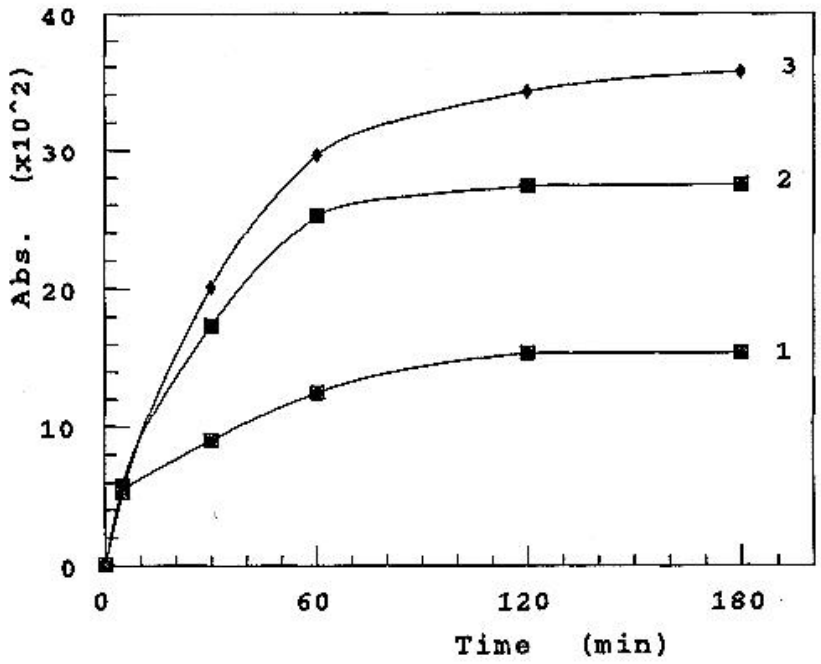

Fig. 3 The evolution of absorptivity at about 800 nm with time of oxidising treatment, for three studied glass compositions.

The tendency towards equilibrium, which is practically attained after about three hours, is clearly evidenced.

The presented results are in agreement with the known [18] conception that the oxidation process is related to the atmospheric oxygen diffusion in glass.

To underline this idea, in figure 4 the rate of oxygen penetration is presented, together with the absorption intensity at about 800 nm. The quantity of oxygen was calculated on the basis of the amount of Cu^{2+} and expressed in weight percents in a minute.

It must be mentioned that the above results were obtained in static conditions, that is, in the absence of any artificial convection in glass melt.

The importance of convection was evidenced when the glass samples were obtained from the same crucible, by putting it out of the furnace, pouring the glass melt quantity necessary for a disk and reintroducing the crucible with the rest of glass in the furnace. This procedure was repeated for three times at intervals of 5 minutes ant then for three more times at intervals of ten minutes.

The equilibrium optical absorptivity was obtained after only 45 minutes, the oxygen penetration rate being of $6.1 \cdot 10^{-3}$ grams per minute for 100 grams of glass melt, i.e. higher by a factor of ten.

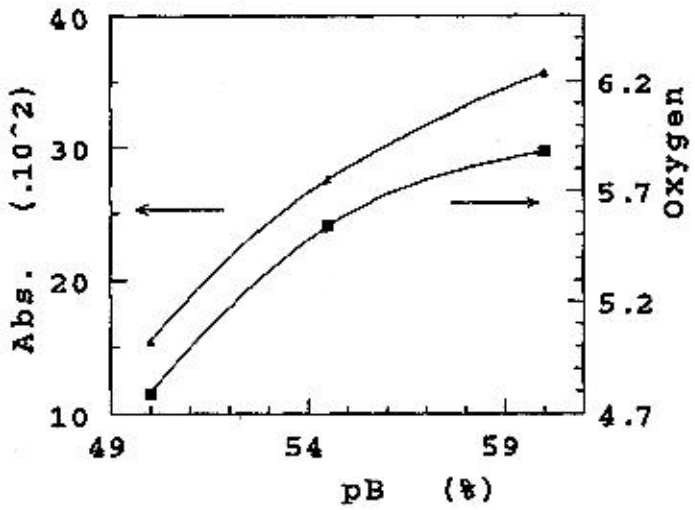

Fig. 4 Absorption at about 800 nm and rate of oxygen penetration in glass, (expressed in wt.%·min^{-1}·10^{4}), function of glass basicity.

The possibility of treating this oxidation process like a relaxation one was suggested. Using the simplest relaxation equation [19, 20] of the type.

$$M = \frac{A_e - A_t}{A_e - A_0} = e^{-\frac{t}{\tau}} \qquad (1)$$

where A_e is the absorptivity at equilibrium, A_O at the initial moment (practically zero), and At the current time, one obtain a satisfactory fit of experimental data (figure 5) for glasses No. 2 and 3. The experimental points corresponding to glass No. 1 are more scattered. For the mentioned glasses, values of relaxation time of 22 minutes (for glass 2) and respectively 35

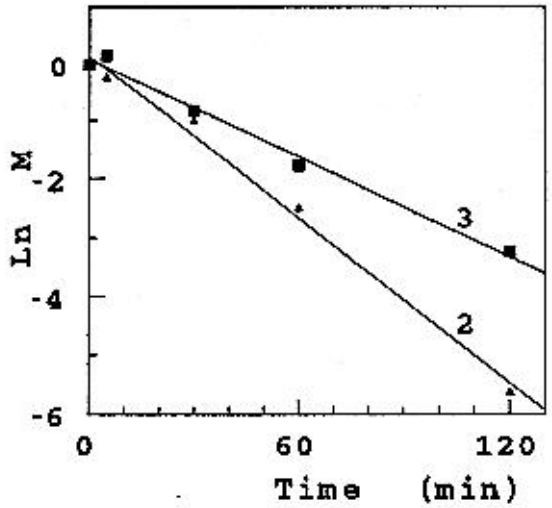

Fig. 5 Experimental data and the straight lines corresponding to the equation (1), considering the copper oxidation like a relaxation process.

minutes were obtained by means of equation (1). For the glass No.1 t seems to have the lowest value.

In this way the influence of glass composition upon the kinetics of the oxidation process is evidenced. A more basic glass (No. 3), diminishes the oxygen diffusion because of the blocking effect of the alkali ions, occupying the interstices and determining a contraction of the doorways used by the oxygen. This is in agreement with the increase in glass density too.

VI DISCUSSION AND CONCLUSIONS

It is well established the fact that the redox processes in glass depend on redox substances present in glass and in the atmosphere, on glass composition and temperature and, in normal conditions, on oxygen diffusion in and out of glass [18].

In this work were followed especially the oxygen diffusion and the glass composition influence.

When the redox system is put out of equilibrium then the reoxidation process maybe treated like a relaxation one. In this way was evidenced one of the aspects of glass composition and structure influence, namely the influence on the time necessary to attain the redox equilibrium, that is on oxygen diffusion.

The problem of basicity influence on the Cu^{2+}/Cu^{+} rate is more complex. Our results does not evidence a tendency of this rate to diminish at least up to a pB value of 58 % (Na_2O content of about 26 mole %). Taking into account the discrepancies between the ε values determined by different authors it seems that new efforts are necessary for new data accumulation and for better understanding the reality.

The experimented method of study seems to be a promising one, even the presented data being not fully exploited.

ACKNOWLEDGMENT

The contribution of Engineer Claudiu Mazilu in the synthesis of glasses, in the frame of his Diploma work, directed by the author, is kindly acknowledged.

REFERENCES

[1] W. A. Weyl "Coloured Glasses", Soc. of Glass Technology., Sheffield 1951, p.154-167, 420-435.

[2] H. G. Hecht, Phys. Chem: Glasses, 9, 6, (1968), p.l79-183.

[3] S.Banerje, A. Paul,J. Amer. Ceram. Soc. 57, 7, (1974), p.286-290.

[4] E. E. Pogarova, V. A. Tsehomskii, Phys. Chem. Glasses (Russian), 8, 1, (1982), p.93-97.

[5] A. A. Ahmed, in Proc. XIIIth I.C.G.,Hamburg 1983, p.1005-10.

[6] J. H. Lee, "Struktureller einbau von Co^{2+}, Ni^{2+} und Cu^{2+} ionen und ihre indikatoreigenschaften für die basizit@t von alkaliborat-germanat und silicatgl@sern", Dissertation, Berlin 1983, p.75-88.
[7] A. Duran, J. M. Fernandez Navarro, Phys. Chem. Glasses, 26, 4, (1985), p. 126-131.
[8] A. Paul, J. Non-Cryst. Solids, 71, (1985), p. 269-278.
[9] S.P.Singh, G. Prasad, P. Nath, J. Amer.Ceram.Soc. 61, 9-10 (1987), p· 377-379.
[10] M. Cable, Z. D. Xiang, Phys.Chem.Glasses, **30**, 6, (1989), p.273-242.
[11] S. P. Singh, A. Kumar, Phys. Chem. Glasses, **34**, 2, (1993), p. 45-51.
[12] G. Jedeloch, Phys. Chem. Glasses, 25, 6, (1984), p.163-164.
[13] R. Araujo, Phys. Chem. Glasses, 36, 3, (1995), p.131-135.
[14] J. Zhong, P. J. Bray, J. Non-Cryst. Solids, 111, (1989), p. 67-76.
[15] P. Balt┃, XVIIth I.C.G., Beijing 1995, vol. 3, p. 27-32.
[16] P. Balt┃, XVth I.C.G., Leningrad 1989, vol. 1b, p. 211-214.
[17] J. A. Duffy, M. D. Ingram, J.Amer.Chem.Soc. (1971),6448-54.
[18] H. D. Schreiber, S. J. Kozak, A. L. Fritchamn, D. S. Goldman, H. A. Schaeffer, Phys. Chem. Glasses, 27, 4, (1986), 152-177.
[19] O. V. Mazurin, "Steklovanie", Nauka,Leningrad, 1986, p.7-12
[20] S. Brawer "Relaxation in Viscous Liquids and Glasses", The American Ceramic Society, Inc.,Columbus, Ohio, 1985, p. 185-203.

LEAD-FREE GLASS FOR TABLEWARE

Fehiman Akmaz and **Hande Sengel**
SISECAM Research Center, Turkey

Abstract

Due to the physical properties it imparts to glass, lead oxide is a vital component of crystal glass compositions. However lead is toxic to the human body if taken in large enough quantities. This issue has gained public attention in the last few years, and resulted in directing research efforts towards;

- Decreasing lead release from lead crystal glassware by modifying the basic glass composition, and
- Developing new glass compositions which do not include lead oxide but are compatible with lead crystal glass in terms of their physical properties.

The work presented here is dedicated to a new glass composition, which has similar physical properties to lead crystal glass, but which does not contain lead oxide. The glass composition, melting-fining-forming behaviour and physical and chemical properties of the glass is reported.

1. INTRODUCTION

Crystal glass is primarily defined by its lead oxide content which adds to its brilliance and develops the melting and working properties thereby simplifying the glass processing. Glassware is often sold as lead crystal if it contains at least 24% lead oxide. It is this high lead content that gives the crystal glass its properties, but can cause trouble due to the lead leach from articles designed to contain food or beverages.

In order to eliminate this problem, research projects, both in modification of the chemical composition of lead crystal glass to reduce lead release[(1)] and the development of a new lead-free composition, are carried out in ÞÝÞECAM.

The steps and obtained results in one of the above mentioned studies which includes the development of a lead-free composition, will be reported here.

2. FOREWORD

As defined by the European standard EC-69, glasses can be labeled as crystal glass according to their chemical composition and two important physical properties which are density and refractive index. The range of compositions and physical properties for the types of crystal glasses are presented in Table 1.

Table 1: *Crystal glass categories according to EC-69.*

Type of glass	Oxides	Density (gr/cm^3)	Refractive Index, n_D	Label
Full lead crystal	PbO≥30%	≥3.00	≥1.545	Gold colour
Lead crystal	PbO≥24%	≥2.90	≥1.545	Gold colour
Crystalline	$ZnO+PbO+K_2O+BaO$≥10%	≥2.45	≥1.52	Silver colour

As can be seen in Table 1, to gain the gold coloured label, a crystal glass has to have a density of minimum 2.9 gr/cm^3 and a refractive index of minimum 1.545. By simply recalling the density and refractive index values of a typical soda-lime-silica glass, which are around 2.5 gr/cm^3 for the density and 1.50 for the refractive index, the importance of these properties imposed by lead oxide become more emphasized.

Optical dispersion is another important property that makes crystal glass different than the other types of glasses. Dispersion is a measure of how well white light is split into its components by a material. Although it is not mentioned in the European Standard, this is in fact, the effect that gives crystal glass its brilliance.

Optical dispersion differences between container and crystalware are much more easily perceived. Abbe number is a measure of dispersion of glass and is determined by measuring refractive index differences at specific wavelengths. The lower the Abbe number, the greater the dispersion, the more desirable the effect.
Container glass has an optical dispersion value of 6×10^{-3} ,whereas 24 % lead oxide containing crystal glass has an dispersion value of 12×10^{-3}. As can be seen from these values, the difference is obvious.

3. DEVELOPING A NEW LEAD-FREE COMPOSITION

In this type of a study, the most important point is that one can rarely reach the ideal composition which will have properties exactly the same with the glass to be replaced. So, the most suitable composition for the production has to be reached with the help of modelling, experimental studies, and small scale applications.

In this work, all possible oxides to replace PbO, including Bi_2O_3, SrO, ZnO, BaO, TiO_2 known as strongly affecting the density, refractive index and optical dispersion of glass, were examined experimentally.[2,3]

The silver colour labeled crystalline composition of ÞÝÞECAM was taken as the base composition. Various levels of above mentioned oxides were added to this composition, and the effects of them to the physical properties of glass were determined comparatively with the 24% PbO containing crystal composition of ÞÝÞECAM.

After these compositional studies, a new, optimum, lead-free composition is reached having the properties listed in Table 2.

Table 2: *Properties of new lead-free glass.*

Properties	**ÞÝÞECAM crystalline glass**	**ÞÝÞECAM crystal glass**	**Experimental Lead-free glass**
Melting temp. (Log η=2)	1424	1461	1395
Gob temp. (Log η=3)	1168	1172	1157
Working temp. (Log η=4)	1004	986	998
Softening point (Log η=7.65)	707	654	697
Annealing point (Log η=13)	536	463	521
Working Range ($T_{log\eta=3}$ -$T_{log\eta=7.65}$)	461	518	460
Liquidus temp.	966		923
Density (gr/cm^3)	2.5141	2.9365	2.7674
Refractive Index	1.5205	1.5487	1.5414
Optical Dispersion (x 10^{-3})	8.79	11.62	10.10
Hardness	Hardest	Third	Second
Acid Polishing	%1HF+%70H_2SO_4 +H_2O 90 min.	%2HF+%70 H_2SO_4 +H_2O 35 min.	%1HF+%70H_2SO_4+H_2O 50 min.

The developed lead-free composition, which has the properties listed in Table 2, contains TiO_2, ZnO and BaO. Although barium is also toxic, it can be considered as a better alternative than lead from the environmental point of view. The advantages are that vaporisation can be neglected and the metal leaching from a barium containing glass is considered to be lower than the leaching levels from lead crystal glasses.[4] Another important point to be mentioned here, is that BaO content of this lead-free composition is less than 6 %, so this level can be considered too low when compared to lead crystal.

As can be seen from Table 2, melting temperature of lead-free composition is lower than both crystal and crystalline compositions. A little difference appeared in working properties, due to eliminating lead oxide from the composition. Besides increasing the density, refractive index and optical dispersion of glass, lead oxide typically makes glass longer means i.e. the glass cools down slower and therefore in hand made production, gives longer period of time to work with it. The working range difference between lead crystal and lead-free composition is around 58^{o}C. Although the difference is not so small, working range value of lead-free composition is almost similar to that of the crystalline composition of ÞÝÞECAM. The small scale factory application has also proved this result.

Hardness and acid polishing behaviour of the lead-free glass do not also resemble those of lead crystal, but the obtained values are close to the crystalline glass, so these are not considered as disadvantages.

The only disadvantage appeared in refractory corrosion tests. Results showed 2-3 times higher corrosion rate of pot materials compared to the 24% lead oxide containing crystal glass. However suitable adjustments of the melting technique or other choices for the pot material can compensate a more aggressive glass.

For the chemical decolorization of the lead-free composition Ce-concentrate was used as the oxidizing agent.

In conventional applications, the oxidation of iron was obtained by adding arsenic oxide or antimony oxide with sodium nitrate to batch, but in recent years cerium oxide or materials containing cerium oxide such as cerium concentrate, have replaced arsenic and antimony to eliminate the health hazardous materials from the glass batch. In view of the above mentioned aspects, experimental glasses were melted from batches containing commercial grade raw materials. Ce-concentrate was used as the oxidizing agent and cobalt oxide as the physical decolorant.

As a result of the experimental decolorization study, the optimum amounts of decolorizing agent were obtained.

5. CONCLUSION

Because of the regulations for lead release from the tableware made of lead crystal glass, numerous research studies are carried out by the tableware industry worldwide. Main topics of these research efforts are :

. surface modifications or compositional modifications to decrease the lead release from the article,

. development of new lead-free compositions having similar physical properties with the lead crystal glass.

After the work presented here, was completed, the main opinion appeared that several combinations of various types of oxides can be prepared to give a glass with physical properties close to crystal glass. However the ideal composition, having the properties exactly the same as those of the lead crystal glass, while having no environmentally toxic components, seems very difficult to be reached. So, in order not to face the environmental problems in the future, the tableware glass industry has to compromise a little from the properties of lead crystal glass.

REFERENCES

1. Sengel H., Albayrak G., Çorumluoðlu O., ‘Improvement of Chemical Durability of Lead Crystal Glass’, Proceedings of the Seventh Technical Exchange Conference of ICF.
2. Volf M. B., ‘Chemical Approach to Glass’ Elsevier Science Publishers,1984.
3. Johansson L.G., Jonson B., ‘Development of Non-Lead Compositions’, Glass Tech.,Vol 34(3),1993.
4. Dalton D.A., ‘The Future of Crystal’, Glass Tech.,Vol34(3),1993.

MECHANISM OF CARBONACEOUS STAINS ON FLOAT GLASS SURFACES

O. Akif Özcan
SISECAM Research Center, Turkey

Abstract

The de-alkalization of commercial silicate glasses culminate in the formation of a calcium rich layer on the surface of the glass, which has secondary protective influence along with silica rich layer on the glass surface. The effect of high humidity and the presence of CO_2 in the atmosphere during transport and storage, may result in unwanted stains which is related to the presence of Ca-rich layer on the surface of the glass.

Float glass surfaces are particularly prone to the formation of Ca-rich layers. In the float process, the glass goes from the oxidizing atmosphere of the furnace to the severely reducing atmosphere of the tin-bath. This results in the diffusion of alkali and alkali-earth oxides towards the surface of the glass. Especially during sea transport of float glass, Ca-carbonate stains form on the top surfaces of clear float glass and the bottom surfaces of green float glass.

The formation patterns of these stains appear to be similar to the orientation of the acrylic interleaving beads put in between the float glass sheets. Electron microprobe analysis has shown that the Ca-rich layers, dissolved by water films of acidic character, agglomerates around the acrylic beads and later forms stable carbonates.

The study has employed a variety of surface analysis techniques to investigate the behaviour of different Ca-rich layers, forming on the top and bottom surfaces of float glass, the influence of bath conditions on the character of Ca-rich films.

Introduction

Market conditions characterized particularly by architectural aesthetics and performance needs require high quality, low-cost and wide range of products in the flat glass productions. The construction sector tends towards multi-layered and coated glasses instead of monolithic applications. However, the importance of surface defects, which can not be easily detectable in a single glass sheet, increases in multi-layered and coated glass productions. This fact leads to more narrow (stringent?) quality limits requiring better storage and transport conditions to preserve the pristine surface quality of glass as much as possible.

Surface Characteristics of Soda-Lime-Silicate Glasses and Weathering

Commercial soda-lime-silicate glasses which are resistant chemically react only with water in static conditions. When the glass contacts with water, an ion exchange process is initiated between Na^+ ions in glass and H^+ or H_3O ions in water during the fist stage of corrosion. In the second stage, the total dissolution takes place while the pH of the solution increases.

In the first stage, mostly Na and Ca compounds are aim to formed as reaction products. Different kinds of interleaving agents commonly used by glassmakers prevent corrosion of the glass surfaces. But, in long periods of storage and transports, carbonaceous stains may cause some surface cleaning difficulties with ordinary machines.

The chemistry of glass surface has been progressively studied by many researchers since the beginning of last century. Fundamental investigations are published after 1950's. The work published in 1977 by Hench[1] is an important milestone among these. He described the five types of surfaces which are characteristic of a silicate glass at any time in its history. The five characteristic types of glass surface are shown below.

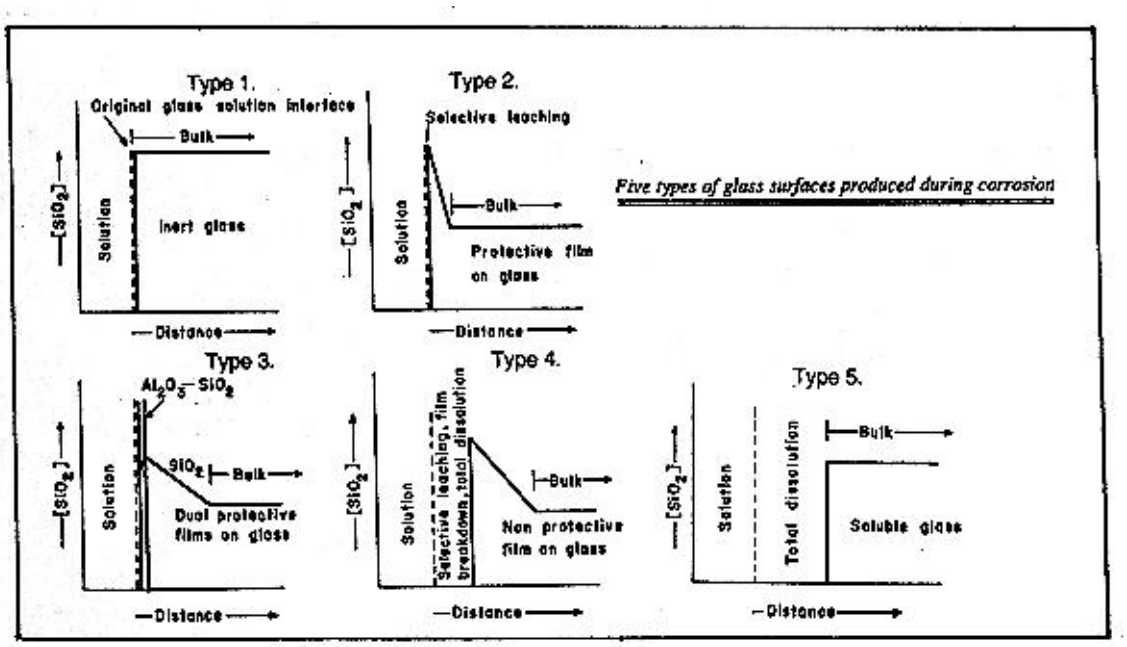

Nowadays, the commercial float glasses display the characteristic of third type which have dual protective film on their surfaces. Ca-rich layer of 10-15 nm thickness overlies the Si-rich layer. Although the Ca-rich layer increase the chemical durability of the glass surface, in some cases, such as long transportations, it may cause "obstinate" surface stains which cannot be cleaned by ordinary machines. Surface compositional profiles of typical soda-lime-silica glass were carried out by Hench & Clark[2] using AES-ion milling and SIMS techniques. The schematic compositional profiles after Hench & Clark are seen in the following figures.

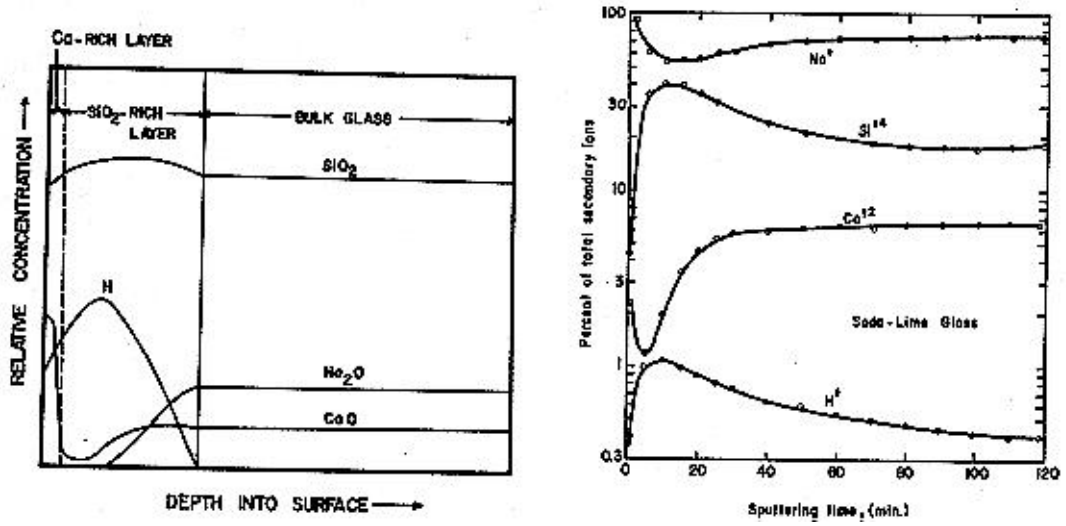

Float glass surfaces are particularly prone to the formation of Ca-rich layers. In the float process, the molten glass entering the tin bath from oxidizing conditions in refining, it is suddenly exposed to strong reducing conditions from both the metallic tin and the hydrogen atmosphere. In the bath, extensive diffusion processes and some exchange reactions take place depending upon temperature and duration. The amount and the direction of diffusions were given as schematic representation of the elements by Swift[3] as follows.

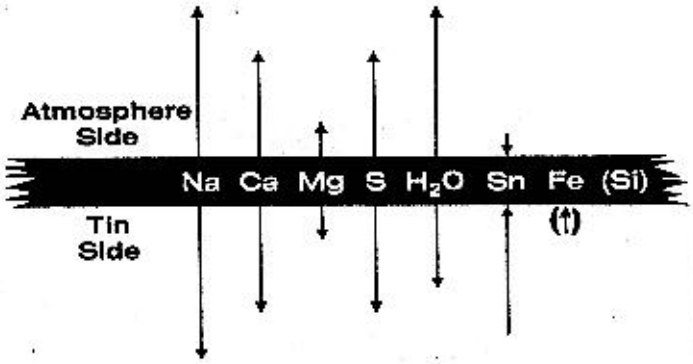

Experimental Studies

During the exchange operations of spout block in a float line, the glass pull was stopped for several days. During those operations, some glass sheets remained for 12 and 24 hours in tin bath. Those glass samples were taken for detail electron microprobe analysis. The depth profiles of Ca and Sn contents from both surfaces were taken. The intensities of Ca counts reached to 15 000 cps on both surfaces and the thickness of Ca-rich layers 3 000 to 6 000 nm on atmosphere and tin side surfaces respectively. Tin counts of the surface of atmosphere side were about 9 000 cps, while the tin counts of the bottom surface were in the order of 22 000 cps. Therefore the movements of CaO towards to

surfaces are dominantly related to the diffusion mechanism instead of exchange reactions. The following figures show the Ca and Sn line-profiles along the depth.

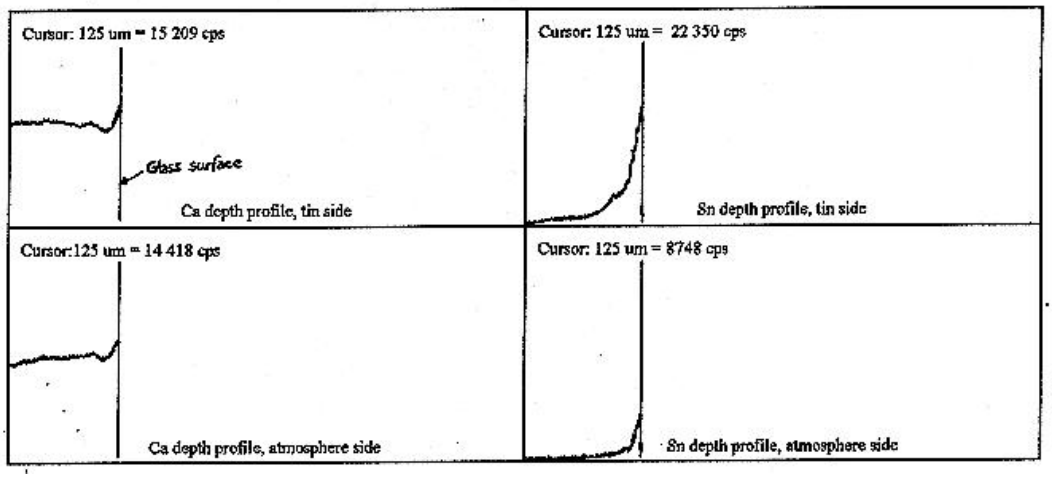

The Mechanism of the Formation of Carbonaceous Stains

Especially, during the sea transport of float glass, carbonaceous stains form on the top surfaces of clear glass and bottom surfaces of green float glass in practice. When these formations were analysed in electron microprobe, their distribution patterns, shapes and forms resemble volcanic crater were to be meaningful (Photo 1). The craters of $CaCO_3$ formations may have occurred as described figuratively below.

High humidity during transport, the condensed water in acidic character dissolves the Ca-rich films on the glass surfaces. The solutions are accumulated around the interleaving PMMA beads and precipitated. Those precipitates give a reaction with CO_2 in environment to stabilize as carbonates in a short period of time.

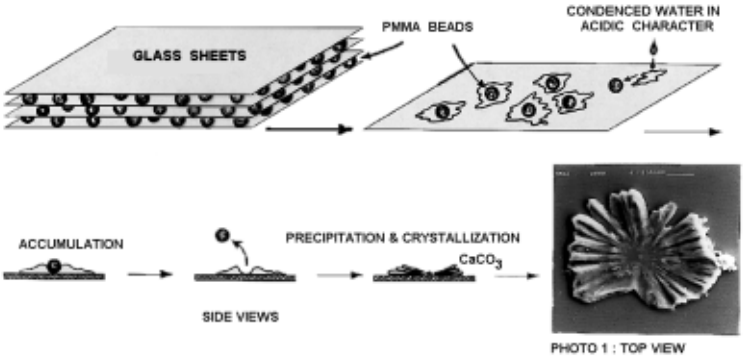

References

1) Hench, L.L., Proc. XI Int. Cong. Glass, Prague, Survey Papers, 11 (July 1977) 343-369.
2) Hench, L.L. and Clark, D.E., "Physical Chemistry of Glass Surfaces", J. Non-Crystalline Solids, 28 (1978) 83-105.
3) Swift, H.R., "How Surface Chemistry Affects Float Glass Properties", Glass Industry, (May 1994) 27-30.

MODELS OF WATER DIFFUSION IN SILICA GLASS

Valery A. Kreisberg
Chemistry Department, Moscow State University, Russia

Abstract

The diffusive transport of water in silica glass affect many important properties and working parameters of this material and its products. The known models of water diffusion based only on kinetic scheme of water interaction with silica matrix forming hydroxyl groups cannot explain the concentration dependence of water diffusion coefficient and some other features of diffusion behaviour of water in glass. The structural-geometric factor should be taken into account as well. During the process of diffusion into glass structure and fast hydroxylation, the breaking of silicon-oxygen bonds occurs, the rings formed by silicon-oxygen tetrahedra disclose, the mean effective diameter of the rings increases, and the water diffusion coefficient rises. The structural-geometric model interprets why crystalline quartz with more dense structure but with straight diffusion channels possesses higher water diffusion coefficients at high temperatures than silica glass.

I. INTRODUCTION

The gas incorporation into high purity silica glasses forms a defective structure of these materials. Water as a primary impurity in silica glass appears to be of importance in affecting many properties of glass and working parameters of glass products. For example, a decrease of water and gas content in silica glass crucibles for silicon crystal growth as well as a decrease of diffusion coefficients prevents explosive character of gas evolution out of crucible glass at working temperature near 1400^{o}C with crucible failure at the beginning of the silicon crystal growth and increases duration of the crucible use [1].

Gas diffusion coefficients in silica glass are controlled by a number of factors: temperature, size and nature of diffusing molecule, concentration of impurities and structural defects in silica glass, interaction of gas with silica matrix. Water diffusion in silica glass is accompanied by hydroxylation and dehydroxylation of silica. In general case the velocity of entry or removal of water depends on the velocities of many different processes. At high temperature the total velocity of the transport process is limited by the diffusion stage. Thus the water diffusion coefficients can be determined simpler at temperatures higher than 800^{o}C

Diffusion coefficients of water in silica glasses are usually determined either from kinetics of change in mean water concentration in silica glass or from "in-depth" profiling water concentration by layer-by-layer grinding of the glass surface. Such determinations for noncrushed and transparent glasses are most commonly performed by monitoring the hydroxyl water band at 3660-3670 cm^{-1} the infrared (IR) spectrum. IR-spectral method has some restrictions. Some other forms of water, as a rule, are not taken into consideration. In particular, the study of molecular water in silica glass presents a considerable challenge. High temperature limit of diffusion

investigations is close to the softening temperature of glass because of the demand to support the shape of sample with the strictly parallel planes. It is difficult to reproduce the same location of the sample in relation to beam after each of heat treatments. Moreover, heating of silica glass in water vapor at high temperature causes the substantial change in structure of the near-surface layer of glass and, consequently, the measurements of diffusion-in coefficients, i.e. for diffusion into glass, may be incorrect, particularly if the coefficients are determined from the concentration profile of water. It is known [2] that water and some other substances produce an appreciable catalytic effect on crystallization of amorphous silica even at relatively moderate temperatures.

These limitations are prevented by using kinetic thermodesorption mass spectral method [1,3] which enables to measure diffusion-out coefficients, e.g. for diffusion out of glass, from isothermal kinetics of liberating water into vacuum or (what is the same) from kinetics of decreasing mean water concentration in glass. For the particles of the spherical shape the corresponding equation is:

$$I = \frac{2mC_0 s^2 \rho^2 D}{3B} \sum_{n=1}^{\infty} \exp\left(-\frac{n^2 \pi^2 s^2 \rho^2 Dt}{9}\right)$$

or the equation valid for initial and middle stages of diffusion:

$$I = \frac{mC_0 s\rho \ D}{B}\left[\frac{1}{(\pi Dt)^{0,5}} - \frac{s\rho}{3}\right]$$

where ρ - density, s - specific surface of quartz grain, m - mass of quartz, C_o - initial concentration of gas impurity, B - sensitivity coefficient of the mass spectrometer with respect to the gas current, I - intensity of ion current of water peak in mass spectrum, t - time. This method can be applied to the particles of any shape. For cube, for example, the diffusion kinetics is described by the equation:

$$I = \frac{128mC_0 s^2 \rho^2 D}{3\pi^4 B} \sum_{i=0}^{\infty}\sum_{j=0}^{\infty}\sum_{k=0}^{\infty} \frac{\exp\left(-\frac{\left[(2i+1)^2 + (2j+1)^2 + (2k+1)^2\right]\pi^2 s^2 \rho^2 Dt}{36}\right)}{(2j+1)^2 (2k+1)^2}$$

Diffusivities of polydispertional materials, e.g. of nontransparent ceramics, with known dispersion function of particles size can be measured as well.

The use of mass spectral and IR spectral methods to determine water diffusion coefficients for the same transparent glasses under the same conditions has been proved to provide almost identical results (Fig.1).

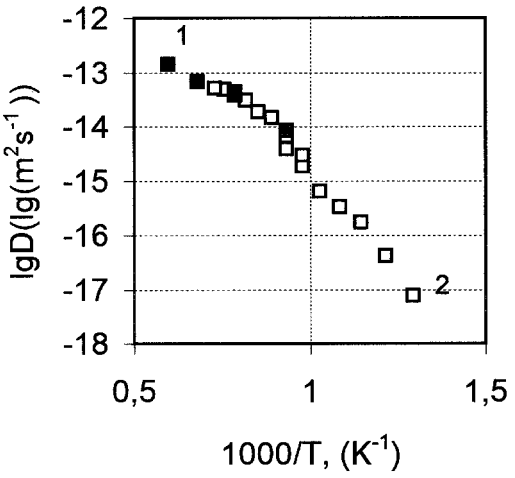

Fig.1. Arrhenius plot of the water diffusion-out coefficient for silica glasses of standard type III: 1 - Russian silica glass KU-1; 2 - data for Suprasil-I from Ref. [4].

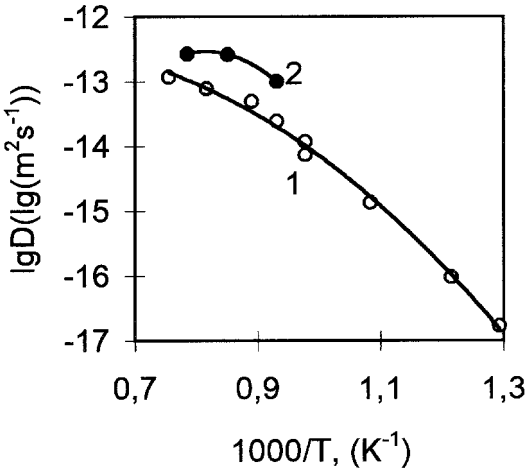

Fig.2. Arrhenius plot of the water diffusion coefficient for the removal (1) and the entry (2) of water in silica glass CGW-7940 of type III (Ref.[4]).

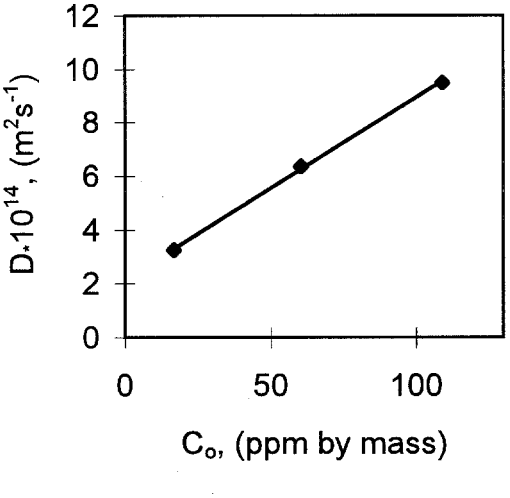

Fig.3. Relationship between water diffusion coefficient at 1400°C and initial water concentration in silica glass obtained by hydrolysis of in H_2-O_2-flame in three stages: deposition of SiO_2 on the form, thermal vacuum vitrification and heating in H_2-O_2 flame.

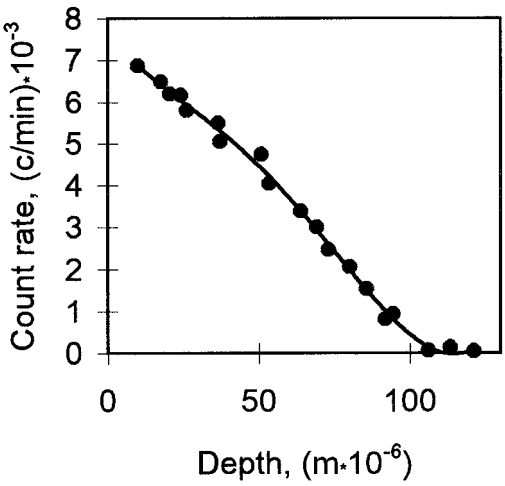

Fig.4. Tritiated water diffusion profile in silica glass I.R.Vitreosil (initially water-free) at 1200 °C, 92.1 kPa (700 mm Hg), 5 h (Ref.[5]).

II. SOME SPECIAL FEATURES OF WATER DIFFUSION IN SILICA GLASSES

Volume diffusion of water in silica glass at high temperatures is characterized by the certain features. The diffusion coefficient for the entry of water is several times greater than that for the water removal (Fig.2) [4]. The diffusion coefficient depends on water concentration (Fig.3)[1]. The concentration profile of diffusing water does not coincide with the error function profile at high temperatures (Fig.4) [5].

III. MODELS OF WATER DIFFUSION IN SILICA GLASS

Roberts and Roberts [6] supposed that the diffusion flux was controlled by the concentration gradient of SiOH groups which were produced by the reaction of water molecule with silica:

$$2 \equiv Si{-}OH + \equiv Si\text{-}O\text{-}Si\equiv \rightarrow 2 \equiv Si\text{-}O\text{-}Si\equiv + H2O \rightarrow \equiv Si\text{-}O\text{-}Si\equiv + 2 \equiv SiOH$$

Such a "lattice-breaking" mechanism which involves permanent breaking and forming silicon-oxygen bonds should exhibit a high activation energy that is not observed experimentally.

Doremus [7] suggested that molecular water diffused and reacted with silica network to form immobile hydroxyls. The effective diffusion constant D_{eff} depends on the diffusion coefficient of molecular water D_{H_2O}, on the concentration of hydroxyl [SiOH] and on the equilibrium constant $K = [SiOH]^2/[H_20]$. In a more refined version [8] this dependence can be given as:

$$D_{eff} = \frac{4D_{H_2O}[SiOH]}{K}$$

According to this model, the diffusion coefficient should be extrapolated to zero for silica glass with zero hydroxyl content what contradicts experimental data.

Tomozawa [9] made an attempt to overcome this discrepancy by assuming that both molecular water and hydroxyl water could diffuse. Then according to [10],

$$D_{eff} = D_{SiOH} + \frac{4D_{H_2O}[SiOH]}{K}$$

Equations (1) and (2) can explain the linear dependence of D_{eff} on the hydroxyl content when hydroxyl and water concentrations are low. At high water content the effective water diffusion coefficient for silica glass tends to a steady value what is not governed by Eqs.(1) and (2).

The kinetic scheme has been advanced to describe the water diffusion everywhere over the concentration range. From

$$\frac{d[H_2O]_{total}}{dt} = D_{H_2O}\frac{d[H_2O]}{dx} + \frac{1}{2}D_{SiOH}\frac{d[SiOH]}{dx}$$

$$[H_2O]_{total} = [H_2O] + \frac{1}{2}[SiOH]$$

we can realize

$$D_{eff} = \frac{\frac{4D_{H_2O}[SiOH]}{K} + D_{SiOH}}{\frac{4[SiOH]}{K} + 1}$$

When [SiOH] rises, dependence D_{eff} on [SiOH] becomes nonlinear, Deff tends to the upper limit, D_{H_2O}. For low [SiOH] ($4[SiOH]/K << 1$), Eq.(3) transforms to the known Eq.(2) and even to Eq.(1) if $D_{SiOH} << D_{H_2O}[SiOH]/K$.

The kinetic models discussed above state that D_{eff} at low [SiOH] is very small or zero (D_{SiOH} is assumed to be very small). What actually happens is that the effective water diffusion coefficient at low water content is high enough in experiments with silica glass. Besides, it is not clear from these models why the effective diffusion-in coefficient is higher than the diffusion-out one at the same mean concentration of water in glass.

IV. STRUCTURAL-GEOMETRIC CONSIDERATION OF DIFFUSION PROCESS

From the stated above it follows that the models of water diffusion based only on kinetic scheme of water interaction with silica matrix forming hydroxyl groups cannot completely explain the concentration dependence of water diffusion coefficient and some other features of diffusion behaviour of water in glass. It is likely that the structural-geometric factor should be taken into account as well. Water diffuses into glass structure by the pipe diffusion mechanism. During fast hydroxylation, the breaking of silicon-oxygen bonds occurs, the rings formed by silicon-oxygen tetrahedra disclose (Fig.5), the mean effective diameter of the rings increases, and the water diffusion coefficient rises. Water removal leads to reverse processes: to decreasing effective diameter of the rings and to decreasing water diffusion coefficient. This structural-geometric model can explain many features of diffusion behaviour of water in silica glass: concentration dependence of water diffusion coefficient is derived from the concentration dependence of diffusion channel diameter; concentration depletion or enrichment of near-surface layer at the initial stage of diffusion-out or diffusion-in explains why the effective diffusion coefficient is higher for entry than for removal at the same mean concentration of water in glass and why the concentration profile of diffusing water is convex up and not coincided with the error function profile.

The structural-geometric model is supported by the fact that crystalline quartz with a more dense structure but with straight diffusion channels possesses higher water diffusion coefficients than silica glass (Fig.6) [11]. It is consistent with the sensitivity of water diffusion coefficient to the method of silica glass production.

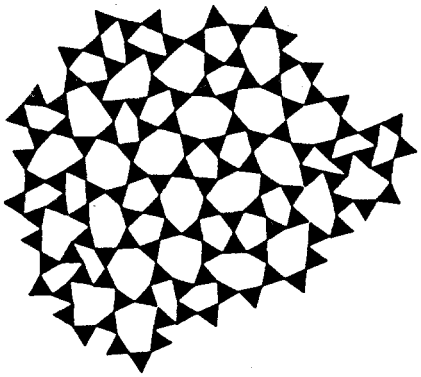

Fig.5. Structure of silica glass silicon-oxygen tetrahedra form and diffusion channels (Ref. [12]).

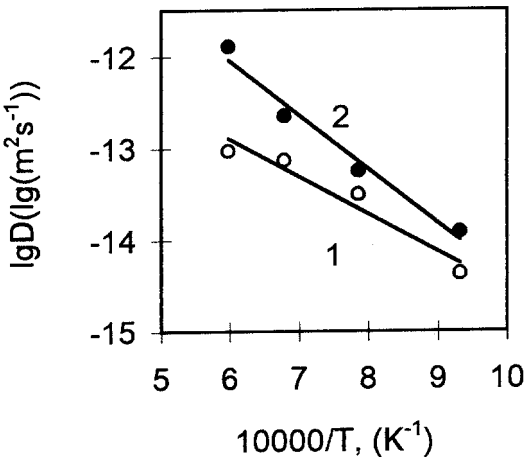

Fig.6. Arrhenius plot of the water diffusion-out coefficient for silica glass obtained by hydrolysis of $SiCl_4$ in H_2-O_2 flame in three stages (1) and for crystalline quartz (2) with initial water concentration 109 and 44.5 ppmm respectively.

V. CONCLUSION

The structural-geometric consideration does not eliminate the influence of kinetic factors connected with reaction of molecular water with silica on water diffusion. However at high temperatures when the rate-determing stage is volume diffusion, the contribution of the structural-geometric factors in diffusive transport of water should be prevalent.

REFERENCES

[1] V.A.Kreisberg, N.Y.Spivakova, *Diffusion in glasses used for production of silicon*, in: Proc. XVII Intern. Congress on Glass. Beijing,1995, v.3, pp.51-56.
[2] M. N. Danchevskaya, V.A. Kreisberg, V. P. Rakcheev, *Mechanism of the effect of surface-active substances on structure formation in silica*, Russian J. Phys. Chem.,1988, 62(1), 61-64.
[3] V.A.Kreisberg, M.N.Danchevskaya, *Investigation of gases in glass by kinetic mass spectrometry*, in: Proc. XVI Intern. Congress on Glass. Madrid,1992, v.6, pp.571-576.
[4] P.B.McGinnis, J.E.Shelby, *Diffusion of water in vitreous silica*, J. Non-Cryst. Solids, 1994, 179, 185-193.
[5] I. Burn, J. P. Roberts, *Influence of hydroxyl content on the diffusion of water in silica glass*, Phys. Chem. Glasses,1970, 11 (4), 106-114.
[6] G.J.Roberts, J:P.Roberts, *An oxygen tracer investigation of the diffusion of "water" in silica glass*, Phys. Chem. Glasses, 1966, 7(3), 82-89.
[7] R.H.Doremus, *The diffusion of water in fused silica*, in: Reactivity of Solids, ed. J.W.Mitchell, R.C. DeVries, R.W.Roberts and P.Cannon. Wiley, New York, 1969, pp.667-673.

[8] K.M.Davis, M.Tomozawa, *Water diffusion into silica glass: structural changes in silica glass and their effect on water solubility and diffusivity*, J. Non-Cryst. Solids, 1995, 185, 203-220.
[9] M.Tomozawa, *Concentration dependence of the diffusion coefficient of water in SiO_2 glass*, J. Am. Ceram. Soc.,1985, 68(9), C251-C252.
[10] Y.Zhang, E.M.Stolper, G.J.Wasserburg, *Diffusion of a multi-species component and its role in oxygen and water transport in silicates*, Earth Planet. Sci. Lett., 1991, 103 (1/4), 228-240.
[11] V.A. Kreisberg, M. N. Danchevskaya, V. P. Rakcheev, *Quality of natural quartz for producing high-purity silica glass*, in: Proc. XVII Intern. Congress on Glass. Beijing, 1995, v.3, pp.590-595.
[12] C.S.Marians, L.W.Hobbs, *A language for the study of network silica glasses*, Diffusion Defect Data, 1987, 53-54, 31-36.

PHYSICO-CHEMICAL PROPERTIES OF GLASS CONTAINERS TREATED BY ACTIVE GASES*

Sharagov V.A.
Beltsy State University, Republic of Moldova

Abstract

The thermochemical treatment of glass containers by acid gases is well-known to be used for glass maintenance properties improvement. The results of complex study of this process are presented in the paper.

The procedure of the experiments consists in the followings. Different types of bottles made from colorless, orange and deep-green glasses were treated by gases either at the final blowing or immediately after container's formation or in the stage of annealing. The treatment of jars was the same. The experiments were carried out both in the laboratory an at the plant. The next properties of glass containers were determined: mechanical strength, the internal hydrostatic pressure resistance, microhardness, chemical durability, thermoresistance. As a treating agent the oxides of sulphur, nitrogen and carbon, hydrogen fluoride and chloride as well as mixture of the gases were used.

Thermochemical treatment of glass by active gases was found to improve the water and acid resistance of glass in 1...2 orders of value, strength - on 20...30%, thermoresistance and microhardness being raised up to 5...10%.

The factors having an effect upon the improvement of physicochemical properties of glass containers under treatment by active gases are discussed.

To improve the thermochemical treatment method under industrial conditions the practical recommendations are proposed.

The results of joint treatment (treatment by gases, ion exchange, electromagnetic treatment, oxide-metal coating) are given.

The probable mechanism of interaction of different gases with glass surface is discussed.

---

* Full manuscript not available at the time of printing

PREPARATION AND CHARACTERIZATION OF NEW LEAD FREE GLASSES

H. Satha, M. Remram, J.Simons*

Universite de Guelma, B. P 401, Guelma, Algeria
*I. N. V, Bd. Defontaine,10- 6000- Charleroi, Belgium

Abstract

New glasses based on the use of oxides of barium, strontium and zinc have been prepared using the data from CD-ROM-INTERGLAD to replace the crystal lead. Physical and chemical studies have been undertaken by the measure of viscosity, thermal expansion, density, refractive index, and optical transmission. Results obtained from the experimental work were very close to those of a crystal lead. Very satisfactory coefficients of correlation were obtained by the modeling of physical parameters using multiple regression. They can be used to elaborate new compositions of glasses having equivalent physical and chemical properties as a crystal lead.

I. INTRODUCTION

Recently, research work in the glass domain has been oriented towards replacing crystal lead to overcome the related environmental problems [1/5]. The actual study aims to elaborate new lead free glasses having the same characteristics as crystal; i.e. brightness, density, mechanical resistance and the working range. Basing ourselves on the INTERGLAD database [6], several compositions have been chosen using multiple regressions on density, softening and melting temperatures using the relation: (property = Σ (content) x (factor) [7]. Physical and chemical analysis of these glasses have been carried out by way of measuring the high temperature viscosity, thermal expansion, density, microhardness, refraction index and optical transmission. Experimental results have been compared with those obtained with calculations by multiple regression [8] and models of HUGGINS [9] and HORMADAL Y [10].

II. EXPERIMENTAL

II.l. Preparation of glasses

II.1.1. Glasses compositions

The glasses are melted as described in Table 1.

II.1. 2. Melted batches

The raw materials used for the preparation of samples are shown in Table 2.

Sample	SiO_2	Al_2O_3	Na_2O	K_2O	BaO	SrO	ZnO	PbO	As_2O_3	total(%)
1	62.10	00	00	12.3	00	00	00	25	0.6	100
2	55.70	05	05	08.7	25	00	00	00	0.6	100
3	61.40	03	05	10	20	00	00	00	0.6	100
4	51.40	03	05	10	30	00	00	00	0.6	100
5	55.90	05	05	15	00	00	18.5	00	0.6	100
6	60.40	03	05	15	00	00	16	00	0.6	100
7	52.00	04	6.4	07	30	00	00	00	0.6	100
8	57.00	04	6.4	07	25	00	00	00	0.6	100
9	59.00	05	7.4	08	20	00	00	00	0.6	100
10	56.80	05	05	05	25	00	2.6	00	0.6	100
11	51.80	05	05	05	30	00	2.6	00	0.6	100
12	53.80	03	10	10	00	20	2.6	00	0.6	100
13	50.80	03	10	08	00	25	2.6	00	0.6	100
14	50.00	03	08	07	00	29	2.4	00	0.6	100
15	55.40	05	05	08	20	00	06	00	0.6	100
16	55.40	05	05	08	14	00	12	00	0.6	100
17	55.40	05	05	08	08	00	18	00	0.6	100
18	51.40	05	05	08	06	00	24	00	0.6	100
19	51.40	04	04	07	29	00	04	00	0.6	100
20	55.40	05	05	08	00	14	12	00	0.6	100
21	55.40	05	05	08	00	08	18	00	0.6	100
22	55.40	05	05	08	08	08	10	00	0.6	100
23	55.40	05	05	08	11	11	04	00	0.6	100

Table 1: Glass compositions (wt %)

Sample	Sable	$Al(OH)_3$	Na_2CO_3	K_2CO_3	KNO_3	$BaCO_3$	$SrCO_3$	ZnO	As_2O_3	Total (g)
1	139.13	00	00	34.37	8.96	*	00	00	1.34	240
2	111.73	14.15	19.19	21.25	8.01	64.47	00	00	1.20	240
3	125.13	09.24	19.50	24.36	8.14	52.40	00	00	1.22	239.99
4	102.30	09.04	19.00	24.36	07.95	76.75	00	00	1.19	240.02
5	116.25	15.80	19.86	23.79	08.31	00	00	38.43	1.25	240.03
6	126.74	09.51	20.86	40.13	08.38	00	00	33.53	1.26	239.99
7	101.30	11.82	21.30	40.49	29.28	75.13	00	00	1.17	240
8	112.35	11.95	21.55	00	29.63	63.35	00	00	1.18	240.01
9	115.38	14.84	24.72	00	33.60	50.28	00	00	1.17	239.99
10	114.55	15.30	17.22	00	21.65	64.81	00	05.24	1.21	239.98
11	103.23	15.14	17.02	00	21.39	79.85	00	05.24	1.19	240.02
12	100.38	08.47	31.87	00	40.07	00	53.25	04.85	1.12	240.01
13	94.90	08.48	31.91	00	32.09	00	66.64	04.85	1.12	240
14	94.03	08.54	25.70	00	28.27	00	77.83	04.51	1.13	240.01
15	109.87	15.06	16.94	00	34.07	50.99	00	11.89	1.19	241.01
16	111.45	15.27	17.18	00	34.56	36.20	00	24.11	1.21	239.98
17	113.08	15.49	17.43	00	35.07	20.99	00	36.70	1.22	239.98
18	105.44	15.58	17.51	00	35.24	15.82	00	49.17	1.23	239.99
19	101.77	12.01	13.527	00	29.76	73.81	00	07.91	1.19	239.98
20	109.63	15.05	16.90	00	34.00	00	39.53	23.72	1.19	239.99
21	112.01	15.35	17.27	00	34.73	00	23.08	36.35	1.21	240
22	109.88	15.06	16.94	00	34.07	20.39	22.64	19.81	1.19	239.96
23	107.96	14.79	16.64	00	33.48	27.56	30.60	07.78	1.17	239.98

*56.20 Pb_3O_4

Table 2: Melted batches

II.l.2. Melting conditions

The used crucibles are made from silica alumina refractory (almost 240 g). First the electric furnace is heated up to 1450 ^{o}C and then the crucibles are loaded in with the mixed batch. The melting and refining remain at constant temperature during 4 hours. The glass is poured on a steel plate, and then cooled slowly from 580 ^{o}C to 20^{o}C in order to remove the permanent stresses.

II.2. Analysis of glasses

II.2.l. VISCOSlTY

The viscosimeter ROTOVlSCO DV HAAKE was used to determine the viscosity curves using a step of 70 ^{o}C (Figure 1). The different values taken out of these curves are presented in Table 5.

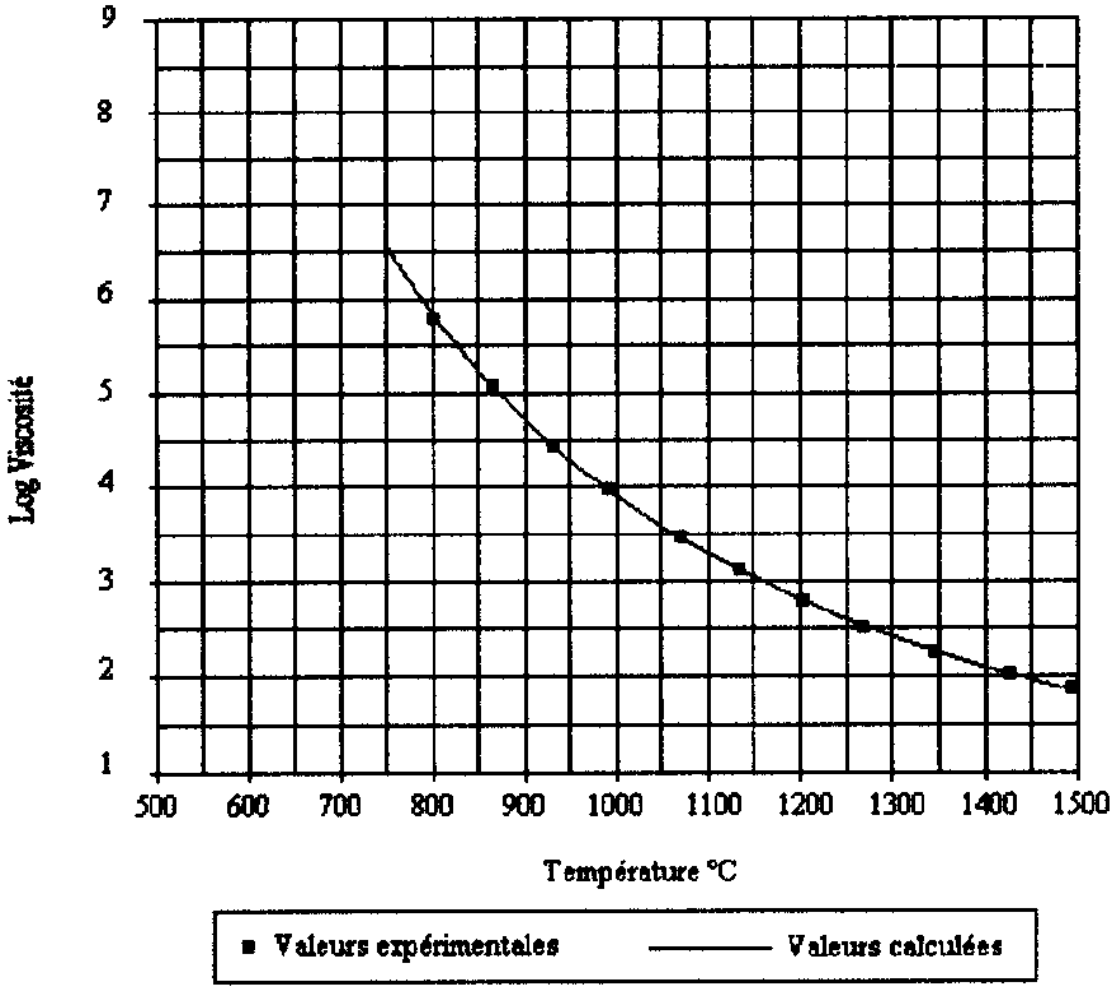

Figure 1: viscosity versus temperature

II.2.2 Thermal expansion

Thermal expansion tests were carried out on an ADAMEL LHOMARGY type dilatometer with a heating speed of 1.5°C/min for 40 mm test tubes {Figure 2). Thermal expansion coefficient is presented in Table 3.

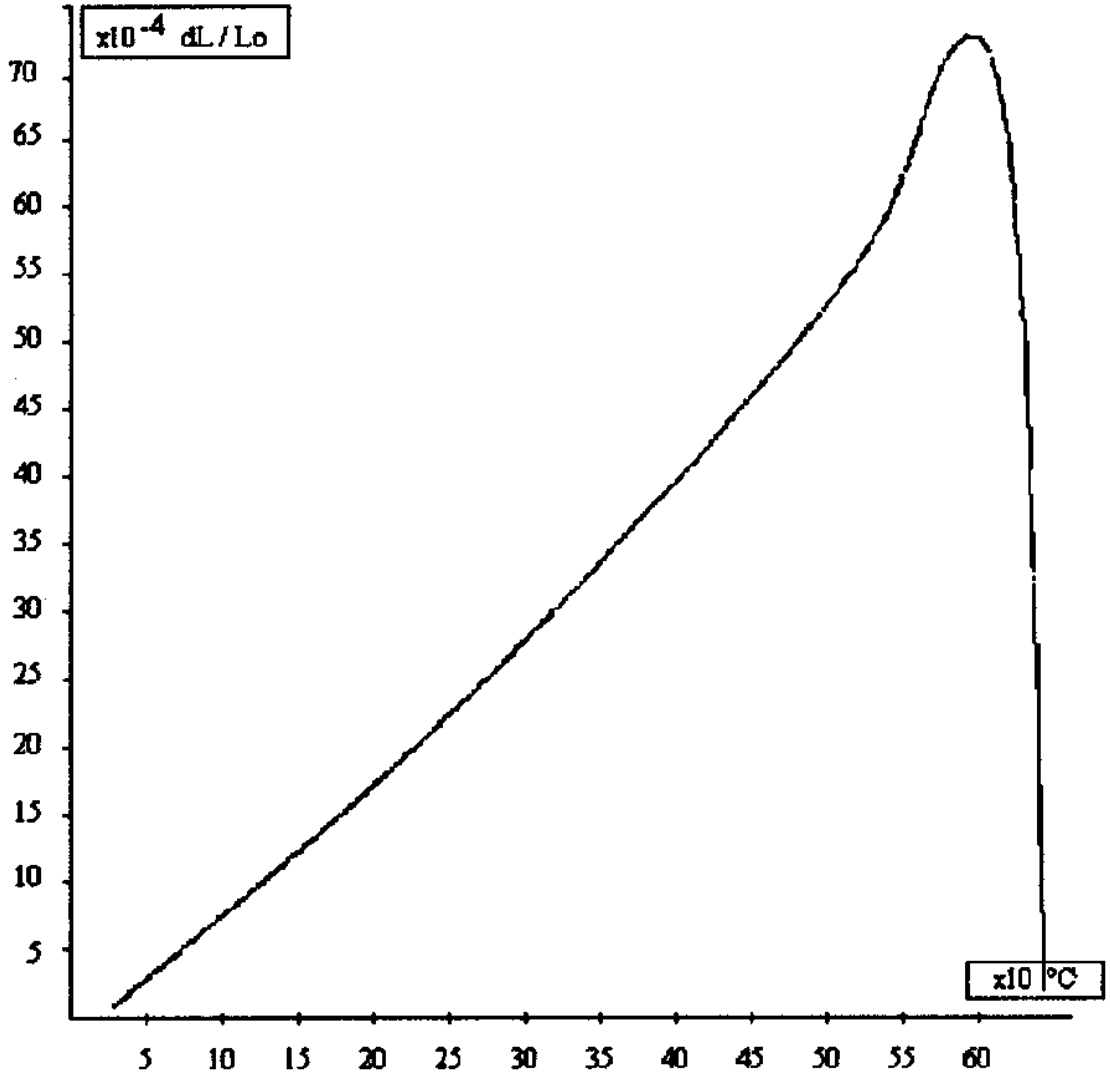

Figure 2: Thermal expansion curve

Sample	α.mes.10^{-7}	α.cal.10^{-7}(Hormadaly)	α.cal.10^{-7}(reg)
1	81.36	97.46	-
2	106.20	113.02	103.95
3	100.10	111.88	103.70
4	114.30	124.08	112.97
5	104.50	110.67	104.53
6	105.20	109.68	103.99
7	107.50	117.68	106.39
8	109.40	114.25	101.78
9	102.00	111.76	104.94
10	88.80	100.91	89.23
11	93.57	106.95	94.17
12	118.10	139.92	119.21
13	113.90	142.09	115.50
14	109.40	141.05	107.95
15	95.45	106.51	96.21
16	90.29	101.49	90.30
17	84.95	96.72	84.40
18	81.36	96.31	82.17
19	92.80	110.13	96.86
20	93.26	116.50	89.06
21	82.19	106.69	83.68
22	92.22	112.52	91.56
23	94.32	119.80	97.20

Table 3: Thermal expansion coefficient

II.2.3 Density

Density values presented in table 5 have been obtained with ACCUPYC 1330 PYCNOMETER.

II.2.4 Microhardness

The Knoop microhardness readings taken on the MATSUZAWA MXT 50 microhardness tester by applying a 100g load for 25 sec. are shown in Table 5.

II.2.5 Refractive index.

The measured results obtained with a dipping refractometer in visible light are presented in Table 4.

II.2.6. Optical transmission

In order to see the optical behaviour of glasses, the light transmission curves through them, have been carried out by spectrophotometer LAMBDA 19 UVNIS/NlR. An

example of these curves is presented in figure 3. The optical parameter (Brightness: L%) obtained out of these curves by computer programs, as shown in Table 5.

Sample	n. measured	n.cal(Huggins)	n.cal(reg)
1	1.542	1.568	-
2	1.539	1.558	1.539
3	1.526	1.547	1.527
4	1.554	1.576	1.552
5	1.528	1.554	1.528
6	1.523	1.549	1.522
7	1.553	1.569	1.551
8	1.541	1.556	1.539
9	1.531	1.546	1.530
10	1.542	1.555	1.542
11	1.555	1.569	1.555
12	1.541	1.560	1.541
13	1.551	1.568	1.552
14	1.558	1.574	1.558
15	1.541	1.558	1.541
16	1.538	1.556	1.540
17	1.537	1.555	1.540
18	1.550	1.563	1.549
19	1.552	1.574	1.554
20	1.543	1.556	1.541
21	1.545	1.555	1.540
22	1.540	1.557	1.541
23	1.541	1.558	1.541

Table 4: refraction index

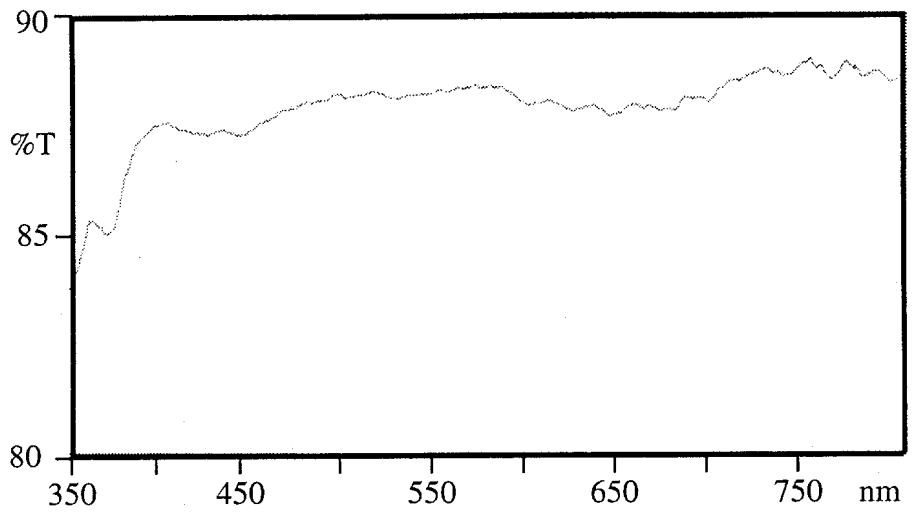

Figure 3: Optical transmission curve

III. DISCUSSION

The experimental results compared to those of crystal lead [11/13] are shown in Table 5. The followings are to be noted: the density varies from 2.84 to 3.05 g/cm^3, the refraction index from 1.52 to 1.56, the optical transmission (brightness) from 85 to 90 %, the thermal expansion coefficient from 8 to 11 x10-6 $^oC^{-1}$ and microhardness from 500 to 530. The properties linked to viscosity; i.e. the melting temperature varies from 1310 to 1540^{o}C, the transformation temperature varies from 490 to 570 ^{o}C and the glass's working stage ranges from between 240 to 330 ^{o}C.

Physical properties	prepared glasses		Lead
	mes.values	cal.values	
Density (g/cm^3)	2.84 - 3.05	2.85 - 3.06	2.95 - 3.15
Refractive index	1.52 - 1.56	1.54 - 1.57	1.55 - 1.57
Colour brightness %	87 - 90	-	90
Melting temp ^{o}C (Log η=2)	1310 - 1540	-	1400 - 1440
softening temp T_s ^{o}C	552 - 644	565 - 646	-
Transition temp T_g ^{o}C	492 - 576	508 - 568	450 - 480
W.range ^{o}C (ΔT:Log η=3-5)	238 - 330	235 - 327	290 - 310
$\alpha_{20\text{-}300}$ $^oC^{-1}$	8 - 11.8x10^{-6}	8 - 11.9x10^{-6}	8 - 9x10^{-6}
Young modulus (GN/m^2)	60 - 68$^{\#}$	-	62 - 64

Microhardness Knoop	505 - 538	506 - 534	440 - 450

Measured values by Grindo-Sonic

Table 5: Summary of the physical properties

In looking through this table, it may be seen that taken separately, the preparation of a lead free crystal having the same value as a lead crystal is possible.

We have carried out multiple regression for our experimental values with a view to finding the best possible formulation. The results show good coherence between the measured values and calculated values (Table 5) and consequently, correlation coefficients: satisfactory properties/formulations which can be used to calculate the best formulation. An example of calculated values using the relation: (Property)=Σ(content)x(factor) based on the derived correlation coefficients for both refraction index and thermal expansion coefficient is given below.

Example 1: Refraction index of composition 1.

$n_{composition1} = n_o + \Sigma C_i \times F_i$

with: C_i; = composition 1 : C_1, ($Si0_2$) = 52, C_2 (Al_20_3) = 4, C_3 (Na_20) = 6.4, C_4 (K_20)=7, C_5 (Ba0) = 30.

n_o and F_i obtained from regressions:

n_o =1.439, F, = 0.000245, F_2 = 0.000603, F_3= 0.001592, F_4 = 0.001151, F_5 =0.002614

$n_{composition}$ =1.439+52x0.000245+4x0.000603+6.4x0.001592+7x0.001151 +30x0.002614

$n_{composition\ ý}$ =1.551

Example 2: Thermal expansion coefficient of composition 1.

$\alpha_{composttion\ 1} = \alpha_0 + \Sigma C_i \times F_i$

with α_0 = -686.305, F_1 = 7.409, F_2 = 6.325, F_3 =10.241, F_4 =10.832, F_5 = 8.020.

$\alpha_{composition}$ = -686.305 + 52x7.409 + 4x6.325 + 6.4x10.241 + 7x10.832 + 30x8.020.

$\alpha_{composition\ 1}=106.388x10^{-7}\ ^oC^{-1}$

The whole computed values of all compositions are presented in table 4. More details may be found in reference [14]. Moreover, computation of the refractive index and the thermal expansion coefficient using HUGGINS and HORMADALY models respectively have been performed for all compositions. The obtained results (c.f. Tables 3 and 4) confirm the coherence between the measured values and the calculated values.

IV. CONCLUSION

Mixtures based on barium, strontium and zinc oxides have been melted at 1450^{o}C and the glasses analysed by different physical and chemical methods. The measured properties, i.e. viscosity, thermal expansion coefficient, density, refractive index and optical transmission have shown very close values to those of crystal lead.

Application of the multiple regression approach on the physical parameters has led to satisfactory results, i.e. correlation coefficients which may be used for the calculation of new compositions having the same characteristics as the lead crystal.

To conclude, the present study leads as to the interesting alternative consisting of the possibility of using new compositions in stead of the lead crystal. However, additional work will have to be carried out; glass refining and decolorising still have to be examined in order to reach a good quality of the product.

REFERENCES

[1] DALTON, D.A. The future of crystal. Glass technology, 1993, Vol.34, P.88-90

[2] JOHANSSON, L.G., JONSON, B. Development of non lead compositions. Glass technology,1993, Vol.34, P.91-93.

[3] JOHANSSON, L.G., JONSON, B. No lead, no barium.....no crystal ?. Glass December 1993, P.480-482.

[4] SEDDON, A.B, WHALL, M.E. The extraction of lead from lead crystalware. Glass Technology, (1993), Vol.34, P.71-73.

[5] BESSADA, C., MASSIOT, D.T., COUTURES, J. Si MAS-NMR in lead silicates. Journal of non-crystalline solids,1994, Vol.l68, P.76-85.

[6] SUZUKI, Y. A Glass Database System For Compact Disk. Am. Ceram. Soc. Bull., 1991, Vol. 70, P. 22-219.

[7] YASUI, I.; UTSUNO, F. Designing Glass Material Systems Using a Database. Feature,1993, Vol. 72, P. 65-71.

[8] STATISTICA. Multiple regression, Copyright StatSoft,1994.

[9] HUGGINS, M.L. Calculation of Density and Optical Constants of a Glass from its Compositions in Weight Percentage, Journal of the American Ceramic Society, 1943, Vol.26, P. 4-11.

[10] HORMADALY,J. Empirical Methods for Estimating the Linear Coefficient of Expansion of Oxide Glasses from their Composition Glasses from their Composition. Journal of non-Crystalline Solids,1986, Vol. 79, P. 311-324.

[11] SHAND, E.B. Glass engineering handbook, Ed: Mc.Graw Hill, N.Y,1958.

[12] TOOLY, F.V. Handbook of glass manufacture, Ed: Ogden, N.Y,1961.

[13] WEYL, W.A. Coloured glasses, Ed: Society of glass technology,1976.

[14] SIMONS, J.; SATHA, H.; REMRAM, M. Lead free crystal, International glass review, June 1996.

THE ALKALI RESISTANCE OF GLASSES PRODUCED IN THE SrO-MgO-ZrO_2-SiO_2 SYSTEM

B. KARASU* and **M. CABLE**
University of Sheffield, United Kingdom

Abstract

The earliest extensive study on was made by Ghanbari-Ahari (1989) who reported that there was a region of glass formation with 50 % SiO_2 content and the lowest eutectic temperature of the system is unexpectedly low, about 1000 °C this suggested that it may be possible to produce glasses within the system, which could be of interest to the glass industries. Ghanbari has mainly studied phase relationship in the system and detailed study on glass formation was not conducted. Consequently, the present study was firstly based on the discovery of easily melted glasses and the determination of the glass forming region of the system. Furthermore, all the glasses produced have been undertaken for the determination of some physical and chemical properties. It has been seen that some of glasses showed high resistance to highly alkaline environment and hereby chemical endurance of these glasses in the system is mentioned and discussed.

INTRODUCTION

The term "chemical durability" has been used conventionally to express the resistance offered by a glass towards attack by aqueous solutions and atmospheric agents.

Glass is often thought of as an 'inert' material. Most glasses have high corrosion resistance but one must take note that all glass products are chemically reactive to some degree. It is often important to know how glass alters a solution that it contacts or how the glass product is altered by the solution. The prediction of such effects, even when the conditions are well specified, is an inexact process; there are no neat formulas to account for the numerous variables. However, given a knowledge of the glass and its proposed environment, it is possible to make extremely useful comparisons and often to make good predictions.

All silicate glasses become particularly susceptible to decomposition above pH=9-10. This happens because strongly alkaline solutions decompose & dissolve the silicate network itself. Since the present system is free from alkali, which make silicate glasses vulnerable to alkali solution attack causing the total dissolution of glass eventually, and has zirconia as one of the major glass constituent whose positive effect on the improvement of durability in different kind of solutions with changing pH values is very well known it was thought that glasses in the SrO-MgO-ZrO_2-SiO_2 quaternary system might show better durability when exposed to an alkaline environment. Therefore a variety of glass compositions have been investigated for different time lengths. Durability experiments involved glasses with different level of silica, from maximum to minimum content, as well as with different ratios of the other constituents.

EXPERIMENTAL PROCEDURE

Glass compositions were coded in the form of $SiO_2/ZrO_2/SrO/MgO$ (in weight % and all the values were rounded of the nearest whole number) throughout the study. When other oxides such as Al_2O_3 and TiO_2 were added glass compositions were then named with the symbol of Al+Ti at the end of their codes, such as $SiO_2/ZrO_2/SrO/MgO$/Al+Ti. When a glass ceramic product was prepared from a glass GC sign was added at the end of code. Firstly, SrO, MgO and ZrO_2 were kept constant at the relative proportions as ZrO_2/SiO_2, SrO/SiO_2 and MgO/SiO_2 and the amount of silica in glasses was increased. Consequently, wide range of glass compositions with silica content of 35 to 62 % have been undertaken and called as first set of glasses. At the later stage of the present study more than 50 glass compositions at different silica level without having any ratio between their constituents were prepared and called as second set of glasses.

Glasses with different levels of silica varying from 40 to 60 % and some glass ceramics produced were taken to determine their resistance to NaOH attack. Firstly rectangular shaped specimens of size about 27 x

8 x 2.5 mm were prepared and their large faces polished in order to decrease the effect of surface roughness. 1 Molar NaOH solution was prepared, 40 g NaOH in 1 liter deionized water. The specimens were weighed to ± 0.0001 g accuracy and suspended in a 300 ml capacity plastic bottle containing 300 ml of solution. A water bath was heated to 75 °C and set at that temperature. The plastic bottles were sealed and immersed in the bath for a certain period of time. During the experiments the alkaline solutions were not replaced. A propeller was employed in water bath to ensure homogeneous temperature throughout. After taking the samples out of the bath they were washed, cleaned using acetone and glass ceramics were dried above 140 °C for 15 or 20 min in an autoclave to remove gel like phase on their surface then weighed. The difference in weights were inspected. After each durability experiment all the solutions chemically analyzed.

Some of the glasses which proved resistant to strong alkali solutions were also tested in a model cement extract. with pH value of 12.5-13. Two identical rectangular glass samples were prepared for each different glass to be examined and polished to decrease the effect of surface roughness. For the preparation of the cement extract 250 g of Portland cement was added to 1.25 liter of distilled water in each of two plastic containers. AR grade $CaSO_4.2H_2O$ was also added to the cement extract to give the equivalent of a half saturated solution (1.2 g $CaSO_4.2H_2O$ / liter). Those two containers were then rolled at 70 rev/min. continuously for 18 days. After that the solid and liquid phases were separated by vacuum filtration in a nitrogen atmosphere. Soon after filtration glass samples were inserted into 200 ml capacity plastic bottles and well sealed under the same atmosphere and the experiment carried for 35 days at 17 °C.

RESULTS

At the beginning, 13 different glass compositions from first set with different level of silica content were taken for their chemical durability against NaOH attack in 1M NaOH solutions with pH values of 14 for 33 days at 75 °C. In order to compare the durability of those 13 glasses with that of commercially available microscope slides all these glasses were studied under the same conditions (Table 1).

Effect of high silica content on durability can be seen for the 55/4.2/33.9/6.9 glass (Table 1) which has given one of the highest weight loss value in the MgO-SrO-ZrO_2-SiO_2 system after being exposed to alkaline attack for 228 days (Fig. 1A). After a gradual increase in weight loss values the glass has reached to a point where weight loss value was stabilized as 215 mg after 221 days. In order to see if this occurred because the attacking solution reached saturation, the solution was twice replaced by fresh solution and each time the glass has again started to dissolve. Those new conditions of the 55/4.2/33.9/6.9 glass are numbered as II and III and the results in terms of weight loss (in mg) are shown in Fig. 1. It has been seen that after replacing solution the glass started dissolving again.

Table 1: *Durability results for the first set of glasses with different silica levels in 1 M NaOH solution at 75 °C for 33 days.*

Composition	Weight Loss (mg)	Weight Loss / Total Surface Area (g/mm^2)	Composition	Weight Loss (mg)	Weight Loss / Total Surface Area (g/mm^2)
Glasses with 40 wt % silica			Glasses with 55 wt % silica		
40/10/39.3/10.7	12.05	14.83	55/7.5/29.4/8.1	36.85	45.25
40/10/42.2/7.8	11.75	15.03	55/7.5/31.7/5.8	42.60	51.22
40/7.8/45.5/6.7	14.95	20.36	55/5.8/34.2/5.0	45.35	62.95
40/5.6/45.2/9.3	22.10	29.88	55/4.2/33.9/6.9	48.50	120.44
Glasses with 45 wt % silica			Glass with 61 wt % silica		
45/9.2/36.0/9.8	15.55	17.66	61.5/8.5/23.5/6.3	64.55	83.32

45/9.2/38.7/7.1	20.50	25.18	Microscope slides	227.35	236.58
45/7.1/41.8/6.1	31.85	36.07			
45/5.1/41.4/8.5	35.20	43.12			

Table 2: *The durability results of the glasses investigated.*

Composition	Weight Loss (mg)	Time (days)	Final Weight Loss (mg)	Time For Final Weight Loss (days)
40/14/26/20	4.65	28	4.65	28
40/14.5/32/13.5	5.40	28	5.40	21
40/12.5/35/12.5	6.00	25	7.40	44
40/14.5/25/20.5	8.30	28	8.30	28
40/14/33/13	8.30	28	8.50	35
40/14/31/15	8.75	28	8.75	35
40/14/29/17	6.20	28	9.50	56
40/13.5/34/12.5	8.40	28	10.20	49
40/14.5/23/22.5	11.90	28	13.75	42
40/8/40/12	15.70	29	23.30	78
40/6/34.3/10.7/Al+Ti	21.70	29	28.90	113
40/4/35/12/Al+Ti	18.80	29	32.50	113
40/6/50/4	21.75	29	301.25	244*
40/15/35/10	8.00	25	32.60	253
40/5/35/20	26.80	29	49.30	113
40/5/35/20 (GC)	20.00	35	27.90	98
55/4.2/33.9/6.9	20.70	27	215.00	221*
Commercial Glasses				
G1	2.00	28	16.80	138
G2	30.60	28	126.40	105
CR-G	17.45	28	37.10	84*

For most of the glasses whose durability results are given in the Table 2 the column headed as time for final weight loss refers to the time that a constant weight loss value was given. Therefore time values in this column do not show the total duration for exposure of these glasses. The experiments were carried out further to ensure that these constant values did not change. Glasses shown with a (*) denotes full duration of experiment. Since they carried dissolving continuously the experiments were stopped in that case.

Glasses with 40 wt % silica from both first and second set showed better durability results against alkali attack (Table 1 & 2). Introducing ZrO_2 into the glass is much easier for those glasses as far as melting temperature is concerned. As a result, detailed study of durability is based on this group and improved durability is also expected with higher ZrO_2 contents.

Even a small amount of alumina is well known to improve the durability of many silicate glasses. For that reason, 5 wt % Al_2O_3 was added to some glass compositions (Table 2) Addition of 4 wt % TiO_2 was also made to see its effect on crystallization behavior. Chemical durability results of these glasses in 1 M NaOH showed the positive effect of Al_2O_3 on chemical durability of the glasses in the present system (Figure 1B).

Figure 1C shows the comparison between the 40/15/35/10 & 40/12.5/35/12.5 glasses with high level of zirconia. The 40/15/35/10 glass unexpectedly carried on dissolving without reaching a constant weight loss value after a long period of time. Since this particular glass had melting difficulties and consisted some amount of undissolved zirconia after melting it is expected that the zirconia content of the final glass is less than 15 %. Consequently, the continuous weight loss can be counted on such fact. As a result, the study of maximum zirconia addition to this glass system was carried out at this stage of the study and finally it has been found that 14.5 % zirconia could easily be introduced into glass compositions with 40 % silica content.

A comparison of durability behavior for the 40/5/35/20 glass and its glass ceramic product was also made. The result is given in Fig. 2A. Final weight loss value of 49.3 mg after 113 days was given by the glass whereas its glass ceramic product gave a constant weight loss value of 27.9 mg after 98 days. Such a high weight loss value of the glass ceramic may be caused by the dissolution of residual glass phase which can remain after heat treatment.

The Comparison of The Durability of The System with Other Alkali Resistant Glasses

Majumdar (1) & Ryder (1968) made a study on the alkali resistance of glass fibres made of the compositions coded G1 and G2 (Table 3). They indicated that alkali resistant glass fibres could reinforce Portland cement effectively and that such composites may be durable over a long period of time. Glasses having compositions in the system Na_2O-ZrO_2-SiO_2 in certain areas of the CaO-Al_2O_3-MgO-SiO_2 system have given promising results.

Table 3: *The commercially available glass compositions (weight %) used in the study:*

Glass	SiO_2	Al_2O_3	ZrO_2	CaO	MgO	Na_2O	Li_2O	K_2O
G1	71.0	1.00	16	-	-	11	1	-
G2	64.5	15.5	-	10	10	-	-	-
CR-G	71.3	-	15.8	0.1	0.1	11.5	0.8	1

Larner et al. (2) (1976) studied G1, A and E-glass fibres in an ordinary Portland cement (OPC) extract at different temperatures for certain period of time. According to their study the corrosion of zircono-silicate glass fibres, such as those made from the G1 composition, in alkaline cement extracts proceeds at a very much slower rate than either of the other two glasses studied, namely A and E-glass fibres.

In order to make a comparison between commercially available alkali resistant glasses (G1, 2, & CR-G) and glasses in the quaternary system which showed high chemical durability in alkali environment, these commercially available glasses have been prepared and melted. CR-G was produced and reported as an alkali resistant glass in 1968 (Table 3). The 40/13.5/34/12.5 glass, which is one of the glasses with high level of zirconia and gave higher weight loss value when compared to the other glasses containing higher zirconia in composition, has been chosen for the comparison with G1 & G2. The results are shown in Fig. 2B. The 40/13.5/34/12.5 glass has given the better chemical durability results than the other two. The sudden big jump of the weight loss value for G2 was because of the lose surface layer which came off. In another experiment Corning glass (CR-G) was compared to the glasses which gave the lowest weight loss values in the quaternary system. Results showed that all the glasses with 40 wt % silica have lower weight losses than Corning glass (Table 2). After these durability experiments it can be suggested that the glasses with high level of magnesia and zirconia at constant silica level of 40 % can be used for cement reinforcement in the form of fibres.

In another durability experiment G2 & the 40/13.5/34/12.5 glass were taken for an investigation in a model cement extract solution with the pH value of 12.5-13 for 35 days at 17 °C. Two identical glass samples were prepared for each different glass. Details of preparing the extract solution have been given before. According to this experiment 40/13.5/34/12.5 glass has had less mean weight loss (0.2 mg) than G2 (0.3 mg)

DISCUSSION

If we look at the literature to see the effect of glass composition on durability it can be noticed that a number of investigations have been made in this field. Dimbleby & Turner (3) (1926) reported the high resistance of zirconia containing glasses.

Larner et al. (2) (1976) who used the Portland cement extract in their study showed that the Zr concentration was much greater at the surface than in the bulk glass and Zr/Si ratio increased as a result of attack by Portland cement extract.

Makisma et al. (4) (1983) who established the characterization of insoluble layers formed by NaOH attack on the surface of a zirconia containing silicate glass (G1) was reported the positive effect of zirconia in silicate glasses and that dissolution rate decreases with time. According to this study the formation of an insoluble reaction product layer formed an adherent film and effectively blocked the reaction. He also reported that the Zr concentration was greater in the insoluble reaction product layer than in the unattacked glass. The same G1 glass was used by Makisma et al. (4) (1983) & Larner et al. (2) (1976) but both the type of alkali and the experimental procedure differed.

In the present system the effect of zirconia on durability was examined. Using the glass compositions containing 40 wt % silica the best result has been achieved with the 40/14/26/20 glass (Fig. 2C). Although zirconia content increased to 14.5 % decrease in MgO content (about 7 %) to 13.5 % may have caused to have higher weight loss value than the 40/14/26/20 glass. Further decrease in zirconia content to 12.5 % made the 40/12.5/35/12.5 glass give a weight loss value of 7.4 mg after 44 days. When we compare these results it will be quite obvious that at constant level of zirconia content as 14 % decrease in magnesia content from 20 % to 17 % caused a higher weight loss value as 6.2 mg after 28 days for the 40/14/29/17 glass. Further increase in both magnesia and zirconia level up to 22.5 & 14.5 % respectively did not improve durability as much as expected for the 40/14.5/23/22.5 glass having a weight loss value of 13.75 mg after 42 days. Although some of these glasses with high level of zirconia and magnesia seem to give high weight loss values they are superior when compared to soda-lime-silica glasses.

According to the weight loss versus time and square root of time diagrams of the glasses examined for their chemical durability it can be said that in the early stages of attack weight loss increases linearly as $t^{1/2}$ but at long times the rate of loss becomes almost linear, of course, as already pointed out, the solution can sometimes become saturated and attack ceases. This can be explained as that in the early stages ($t^{1/2}$ dependence) the reaction is a diffusion controlled ion exchange involving Sr and Na & H moving in opposite directions through a siliceous surface film and the Si is likely to be more or less direct dissolution of the glass at the interface, whilst later (t dependence) the surface film has attained a constant thickness. This thickness is probably determined by a balance between the diffusion of Zr, Si & Sr ions through the film, which thickens it, and the rate of removal of Si & Sr at the film-solution interface which has the opposite effect.

Paul (5) (1982) reported that MgO, SrO & BaO also improve the durability but the effects depend on such things as the temperature of the test and the radius of cation. Furthermore, when one moves up in the group of alkali earth metals Sr is expected to be better than Mg at high temperature since it has larger radius than Mg.

In the present system it has been found that up to a certain limit (~20 wt %) Mg silica has more positive effect than Sr on durability of glass of 40 wt %. This may suggest that higher amount of strontia in glass composition increases the possibility of its ionic movement to the glass surface like silicon ions, after Sr-O and Si-O bonds being broken by either sodium or hydrogen ion from the aqueous solution. On the other hand, Sr with larger radius can accommodate more oxygen than Mg therefore having lower bond strength and Mg may be strongly bonded with oxygen atoms than Sr in the glass structure.

Some of durability samples have been investigated by X-ray diffraction, SEM and EDX after durability experiment in order to examine the surface layer occurred during exposure. The x-ray diffraction pattern given by the 40/6/50/4 glass, after 244 days in NaOH, was thoroughly examined for hydrated compounds which may possibly have formed during exposure. Only the Joint Committee for Powder Diffraction Standards (JCPDS) data of $NaHSi_2O_4(OH)_2$, sodium hydrogen silicate hydroxide. These crystals may be embedded in the hydrated zirconia surface layer. In order to confirm the presence of Na in the glass surface SEM and EDS analysis were also made. The presence of Na was not so clear through SEM pictures but EDS analysis showed that as Si & Zr peaks as well as Na were given by protective surface layer, whilst the glass part, which had no protective layer, on the surface have shown Zr, Sr & Si peaks but no peak belonging to Mg or Na. This suggests that there may be ion transfer of Zr, Sr & Si towards the first surface layer which is in contact with attacking solution. From this layer dissolution of Sr & Si may take place. At the same time it is possible to think that a hydrated zirconia protective layer forms and finally decreases the dissolution of Sr & Si from the surface layer where glass is in contact with the solution and also prevent further diffusion of Na into the bulk glass. Since there was no sign of Mg either on glass surface or in the glass near to the surface, it has also been concluded that Mg must be tightly bonded by oxygen ions in the

glass structure therefore its ionic movement towards the surface of the glass is prevented. However, the glass examined had only small amount of MgO, 4 %, therefore it might avoid detection. The other possibility is that there may be diffusion inwards rather than glass surface. The 40/8/40/12 glass sample 6 mm thick after being exposed to NaOH solution for 15 days has also been examined by SEM and EDS. Similar results to that of the 40/6/50/4 glass have been achieved. Cracks of the protective surface layer have also been observed.

Tomozowa et al. (6) (1981) investigated the effect of alkali earth elements in hot alkaline solutions on silica microscope slide glasses in order to examine retarded dissolution behavior caused by a minor concentration of various ions in alkaline solution. They have seen that when solution contained a small amount of heavy alkaline earth elements such as Ba & Sr, sharp cracks formed on the glass surface. and the crack caused a drastic reduction in mechanical strength of the glass.

In the present work the attacking solution soon contains some of Sr during exposure of the glasses. Sr may be causing this sort of cracking of the protective layer.

CONCLUSIONS

1. The glasses with 40 wt % silica content in the SrO-MgO-ZrO_2-SiO_2 system have given high chemical resistance to alkaline solutions.
2. Increasing silica content in glass compositions decreases chemical durability of all glasses produced. On the other hand, as well as zirconia, up to a certain value magnesia has positive effect on chemical durability.
3. It is believed that in the early stages, the reaction between glass and attacking reagent is a diffusion controlled ion exchange, later the surface film has attained a constant thickness. This thickness is probably determined by a balance between the diffusion of Zr, Si & Sr ions through the film, which thickens it, and the rate of removal of Si & Sr at the film-solution interface which has the opposite effect.
4. It can be suggested that the glasses with high level of magnesia and zirconia at constant silica level of 40 % can be used for cement reinforcement in the form of fibres.

REFERENCES

1. Majumdar, A.. & Ryder T. F., 'Glass Fibre Reinforcement of Cement Products', Glass Tech., Vol. 9, No.3, June 1968.
2. Larner, L. J., Speakman, K., and Majumdar, A. J., ‘Chemical Interactions Between Glass Fibres and Cement', Journal of Non-Crystalline Solids, 20 pp. 43-74, 1976.
3. Dimbleby, V. and Turner, W. E. S., Glass Tech., Vol. 10, pp. 304-363, 1926.
4. Makisma, A., Tsutsumi, M., Shimohira, T. Communication of The American Ceramic Soc., C-139, August 1983.
5. Paul, A., 'Chemistry of Glasses', Chapman & Hall, London, 1982.
6. Tomozawa, M., Oka, Y. & Wahl, J. M, Communication of The Amer. Ceram. Soc., C-52, February 1981.

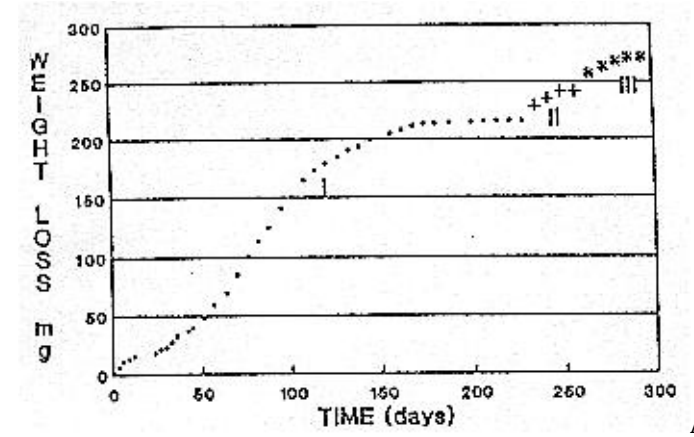

A

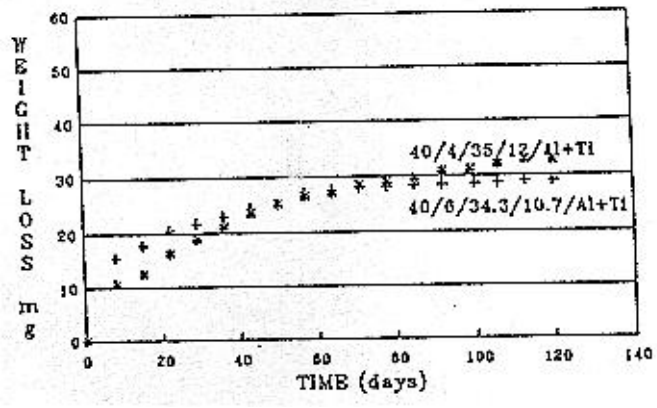

B

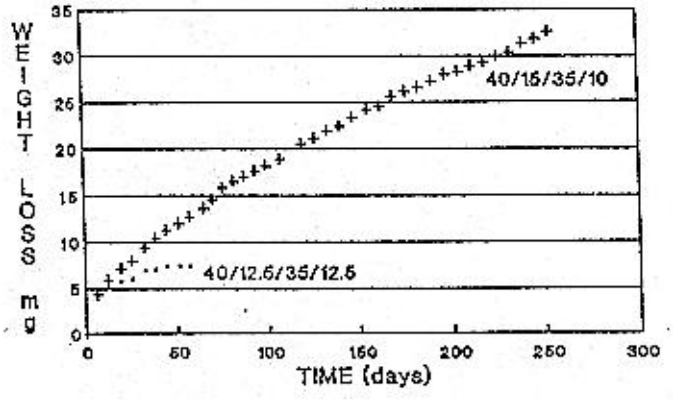

C

Figure 1: *A. Chemical durability results of the 55/4.2/33.9/6.9 glass in 1 M NaOH at 75°C and the effect of replacing solution on this glass B. Chemical durability results of the 40/6/34.3/10.7/Al+Ti and 40/4/35/12/ Al+Ti glasses 1 M NaOH at 75 °C C. Chemical durability results of the 40/15/35/10 and 40/12.5/35/12.5 glasses 1 M NaOH at 75 °C*

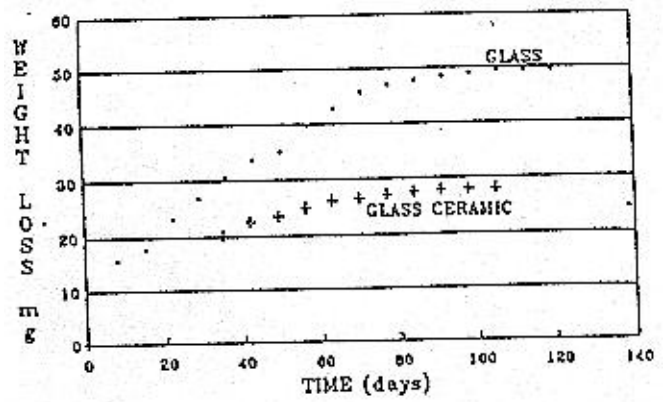

A

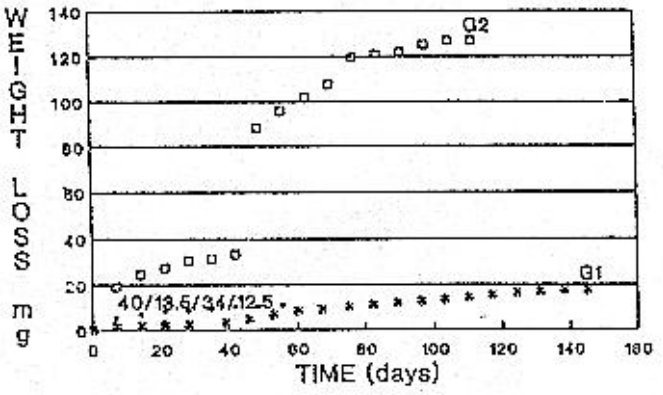

B

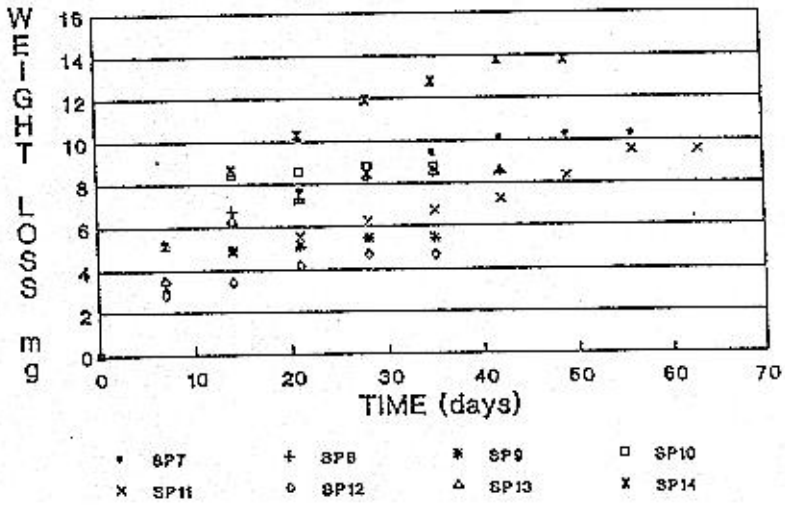

C

***Figure 2**: A. Chemical durability results of the 40/5/35/20 glass and its glass ceramic product in 1 M NaOH at 75°C B. Chemical durability results of the G1 G2 and 40/13.5/34/12.5 glasses in 1 M NaOH at 75 °C C. Chemical durability results of the 40/13.5/34/12.5 (SP7), 40/14/33/13 (SP8), 40/14/31/15 (SP10), 40/14/29/17 (SP11), 40/14/26/20 (SP12), 40/14.5/25/20.5 (SP13) and 40/14.5/23/22.5 (SP14) glasses in 1M NaOH at 75 °C*

X-RAY INDUCED PHOTO AND AUGER ELECTRON SPECTROSCOPIC INVESTIGATION OF FLOAT GLASSES

Sefik Süzer
Bilkent University, Turkey

Abstract

Surfaces of float glasses have been analysed using UV-Reflectance and electron spectroscopic techniques. UV-reflectance can distinguish the Sn-bath surface but can not give quantitative information. X-ray induced photo and Auger electron spectroscopic techniques reveal that Sn has a very high concentration (up to 0.2 Sn/Si atomic ratio) on the Sn-bath side and approximately one order of magnitude less on the atmospheric side of 3-10 mm float glasses. Concentration of Sn decreases exponentially into the bulk upon Ar^+ and/or 2%HF etching. The chemical state of Sn can not be determined using XPS only. Auger parameter, derived from combined XPS and Auger measurements, is a more sensitive probe for identification of chemical state. The Sn-Auger parameter on these glasses is also found to vary with the Sn/Si ratio.

I. INTRODUCTION

Sn is incorporated on to both surfaces of the glasses produced by the float-technique. This incorporation of Sn on to the surface in contact with the liquid tin-bath is unavoidable and sometimes desirable for it provides a uniform protective layer towards atmospheric corrosion. However, incorporation of Sn on to the atmospheric side is not uniform nor desirable since it involves precipitation of the volatile fragments. Various investigations attempting to characterize the composition of the surface and penetration depth of Sn have been reported using Auger Electron Spectroscopy (AES) [1,2], X-ray Photoelectron Spectroscopy (XPS) [3-8], Rutherford backscattering [6], Mössbauer spectroscopy [9], Cathodoluminesence [10], X-ray Absorption, Reflection and Fluorescence techniques [11]. In this work we report a combined XPS-XAES (X-ray induced AES) and UV-Reflectance study of Sn on these glass surfaces.

II. EXPERIMENTAL

Electron spectroscopic measurements were performed with Kratos ES 300 spectrometer using AlK_α/MgK_α excitations (hv=1486.3 / 1253.6 eV). The pressure in the analyzer chamber was maintained below $5x10^{-9}$ torr during analyses. C1s line (B.E. 285.0 eV) from the residual hydrocarbons was used as a reference. The accuracy in binding energies and Auger parameters are better than 0.1 eV. Float glasses with thicknesses of 3, 4, 5, 6 and 10 mm are provided by the Türkiye ÞiÞe-Cam A.Þ. Depth profiling was

carried out using either (i) in-situ Ar^+ etching with 1 keV ions or (ii) before introduction to the spectrometer with 2% HF solution. UV-Reflectance measurements were carried out using a specular reflectance attachment to a Cary 5E spectrophotometer.

III. RESULTS AND DISCUSSION

A simple UV reflectance measurement is a qualitative method to identify the Sn-bath surface of the float-glass. Ordinary soda-glass absorbs UV radiation near 300 nm very strongly. There is, however, a difference between the reflectance of the two surfaces (Sn-bath surface reflects more than the atmospheric one) approaching this absorption band as depicted in Figure 1. The reflection is considerably reduced after 1 min. etching with 2% HF solution. Quantification, however, is not possible using reflectance only.

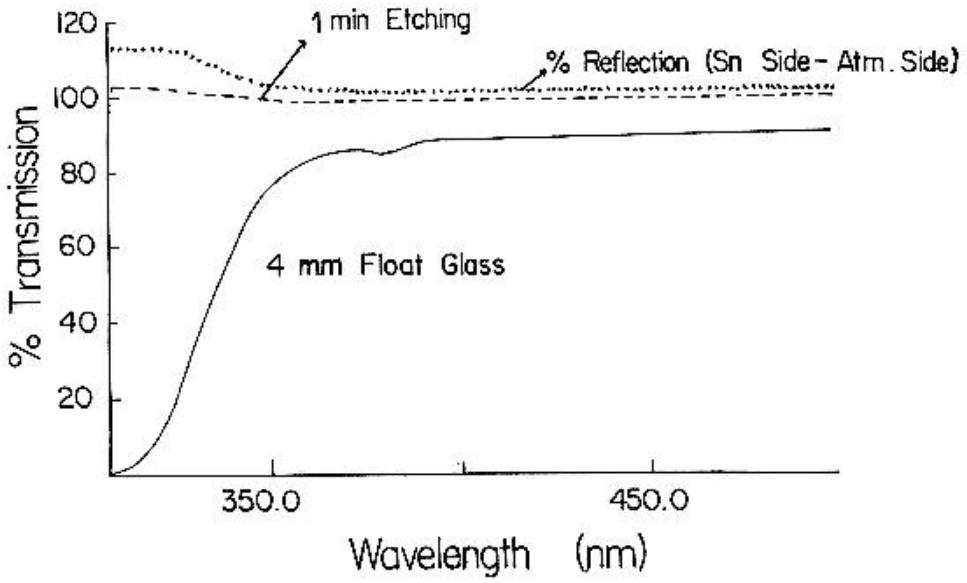

Figure 1. Transmittance of 4 mm float glass in Vis-UV region (lower part). Also shown in the figure is the difference in reflectance of the Sn-bath surface and the atmospheric surface of the same glass before and after etching with 2%HF solution.

Electron spectroscopic measurements are ideally suited for chemical identifcation and quantification of surfaces. Figure 2 depicts the electron spectrum of the Sn-bath surface of a 3mm float-glass induced by MgKα x-rays. In addition to Si, Mg, Ca, O photo and Na, Mg, O Auger lines, photo and Auger lines of Sn are observable with considerable intensity.

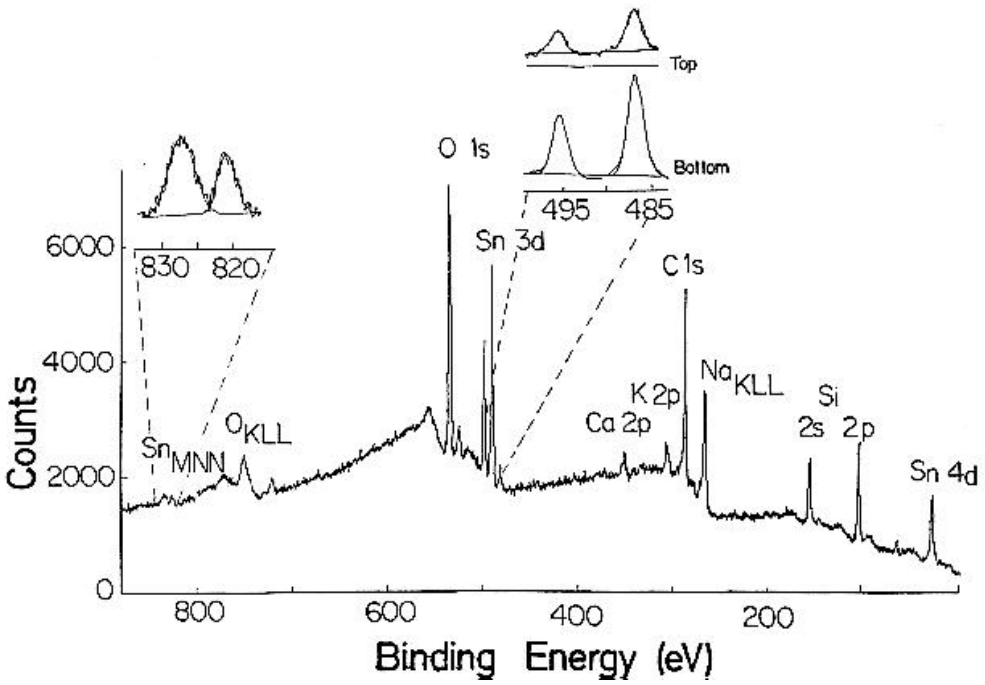

Figure 2. MgKa x-ray induced electron spectrum of the Sn-bath surface of a 3mm float-glass. Sn_{MNN} Auger of the Sn-bath side and Sn $3d_{5/2-3/2}$ photo peaks of both Sn-bath (bottom) and the atmospheric sides (top) are included.

Although any element (except H and He) can be detected by electron spectroscopic measurements, these methods can only give relative quantities. Therefore, we assume the Si to be constant and determine the relative atomic concentration of other elements with respect to Si. Table I gives the results for various glasses together with SnO and SnO_2. Of particular interest is the data on Sn. We have recently reported that the binding energy shifts of SnO and SnO_2 are very close to each other and one can differentiate between the two oxides only after calculating the Auger parameters [14,15]. The Auger parameter, α, is defined as the sum of the binding energy (E_b) and the kinetic energy (E_k) of the Auger electron involving the same electronic level and is known to be more sensitive to chemical environment [13]. Hence, in Table I we give both the binding energies and the Auger parameters. Etching with Ar^+ and/or HF reduces the Sn/Si ratio and causes a shift in Auger parameters as given in the lower part of Table I for a 5mm float-glass as also shown in Figure 3 and 4.

The chemical state of Sn on float-glasses has been the matter of an ongoing debate. Using a combination of analysis techniques Colombin et.al. argued that Sn existed as a definite compound of sodium, tin and silicon and formed in the first monolayer [6]. Using XPS analysis of only the Sn 3d binding energy in combination with argon ion etching, Jie Luo and Xu Chao determined that Sn was present in +4, +2 and O oxidation states [8], while Principi et.al., using Mössbauer Spectroscopy, reported that +2 oxidation state predominated at the surfaces [9]. We pointed out, on the basis of XPS binding energies alone, assignment of the oxidation state of Sn in oxides could not be done and Auger

parameter [13] needed to be determined to unambiguously distinguish between SnO and SnO_2 [14,15].

Table I. XPS/XAES Data of float glasses and some reference compounds.

Sample	**Sn $3d_{5/2}$**	**Sn_{MNN}**	**a_{Sn}**	**Atomic ratios**			
	B.E., eV	**K.E.,eV**	**(eV)**	**Sn/Si**	**O/Si**	**Na/Si**	**Ca/Si**
3 mm	487.8	431.1	918.9	0.24	2.9	0.23	0.18
3 mm (top)	487.7	430.6	918.3	0.02	2.6	0.04	0.09
4 mm	487.8	430.9	918.7	0.20	3.2	-	-
5 mm	487.8	431.1	918.9	0.26	3.6	0.16	0.16
6 mm	487.6	430.7	918.3	0.14	3.2	0.15	0.25
10 mm	487.5	431.1	918.6	0.19	2.7	0.18	0.09
SnO	487.1	433.0	920.0	-	-	-	-
SnO_2	487.5	431.6	919.1	-	-	-	-
5 mm	487.8	431.1	918.9	0.26	3.6	0.16	0.16
3 min etch.	487.6	431.3	918.9	0.18	2.8	0.08	0.16
10 min etch.	487.4	431.4	918.8	0.17	3.0	0.11	0.23
40 min etch.	487.3	431.3	918.7	0.11	2.9	0.16	0.22
90 min etch.	487.4	431.2	918.7	0.11	2.7	0.22	0.26

From Table 1 we can see that the $3d_{5/2}$ binding energies of SnO and SnO_2 are 487.1 and 487.5 eV while those for the glasses vary between 487.5 and 487.8 eV. The assigned Sn Auger parameters for SnO and SnO_2 are 920.0 and 919.1 eV respectively while those for glasses vary between 919.0 and 917.9 eV. The lower value for the Auger parameter in SnO_2 as compared with SnO was rationalized by the reduced Sn-Sn interaction and the higher ionic character of Sn in SnO_2 [14]. The Sn Auger parameters for the glasses have even lower values than SnO_2. Furthermore, an inverse correlation exist between the Sn Auger parameter and Sn/Si atomic ratio as shown in Figure 4. The Auger parameter for SnO and SnO_2 are also given in the figure for comparison. Remembering the fact that going from metal to the isolated atoms in the gas phase, the Auger parameter can decrease by as much as 9 eV [12,13], we can accordingly attribute the decrease in the Sn Auger parameter with Sn/Si atomic ratio in these glasses to the decreasing Sn-Sn interaction.

As for the oxidation state of Sn we can definitely rule out the previous assignment of a mixture of 0, +2 and +4 done on the basis of 3d binding energy shifts only [8]. On the basis of our derived Auger parameters which are lower than for SnO_2 we assign +4 for the oxidation state of Sn in these glasses, contradicting the Mössbauer results [9] which are usually known to be more exact. However, we must keep in mind that Sn in the glass matrix is in a much stronger ionic environment and the exact relationship between the dependence of the Auger parameter on the degree of ionic character of the matrix is not known. Calculations along these lines can help clarifying these points.

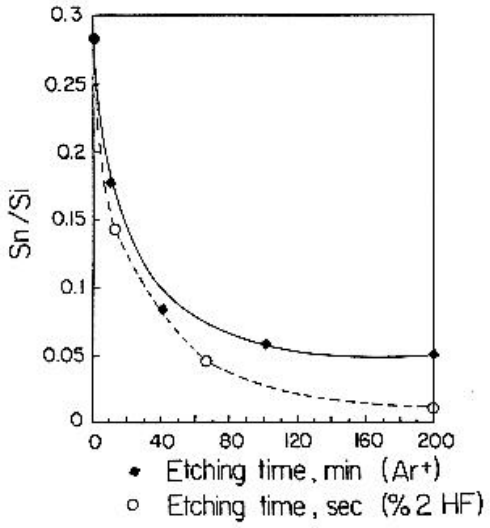

Figure 3. Variation of Sn/Si ratio with etching.

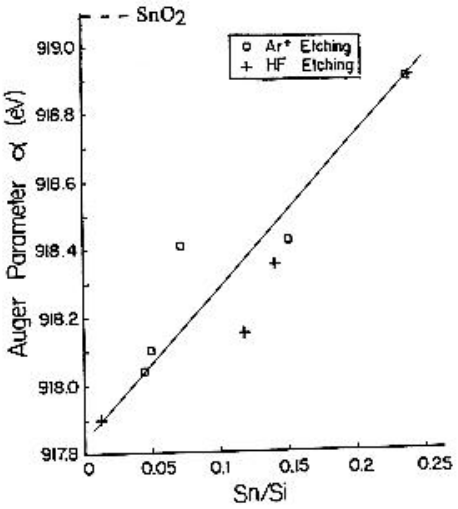

Figure 4. Variation of the Sn Auger Parameter with Sn/Si ratio.

REFERENCES

1. R.A. Chappell and C.T.H. Stoddart, Phys. Chem. Glasses 15 (1974) 130 and J. Material Science 12(1977) 2001.
2. D.A. Stephenson and N.J. Binkowski, J. Non-Cryst. Solids 19 (1975) 87.
3. L. Colombin, A. Jelli, J. Riga, J.J. Pireaux and J. Verbist, J. Non-Cryst. Solids 24(1977) 253.
4. N.J. Binkowski, R.F. Heitzenrater and D.A. Stephenson, J. Am. Cer. Soc. 59(1976) 153.
5. J.S. Jen and M.R. Kalinowski, J. Non-Cryst. Solids 38(1980) 21.
6. L. Colombin, H. Charlier, A. Jelli, G. Debras and J. Verbist, J. Non-Cryst. Solids 38 (1980) 551.
7. C.G. Pantano,"Materials Characterization for Systems Performance and Reliability" Ed. J.W. McCauley and V. Weiss, Plenum (1986) 127.
8. Luo Jie and Xu Chao, J. Non-Cryst. Solids 119(1990) 37.
9. G. Principi, A. Maddalena, A. Gupta, F. Geotti-Bianchini, S. Hreglich and M. Verita, Nuc.Inst. Met. Phys. Res. B76(1993) 215.
10. B. Yang, P.D. Townsend and S.A. Holgate, J. Phys. D.27(1994)1757.
11. M. Hüppauff and B. Lengeler, J. Appl. Phys.75(1994) 785.
12. J. Chastain,"Handbook of X ray Photoelectron Spectroscopy", Perkin-Elmer Co.(1992).
13. C.D. Wagner, L.H. Gale and R.H. Raymond, Anal. Chem.51(1979) 466.
14. S. Süzer, T. Voscoboinikov, K.R. Hallam and G.C. Allen, Fres. J. Anal.Chem. (accepted for publication).
15. S. Süzer, T. Voscoboinikov, A.Özcan and E. Aydýn, Proc. ECASIA'95 (to be published in Surf . Interf. Anal.)

INFLUENCE OF VARIOUS SURFACE TREATMENTS ON THE GLASS STRENGTH

Liu Zhongwei and **Ma Juanrong**
China Building Materials Academy, P.R. China

Abstract

Influence of various surface treatments on the glass strength was studied in this paper. The best way to increase the glass was obtained.

I. INTRODUCTION

The theoretical strength of the glass is very high, which is about 9800 MPa. But the practical strength only is 50- 100 MPa. The reason that causes the difference between the theoretical strength of the glass and the practical strength of the glass is that there are many micro-cracks on the surface of the glass. At the tips of micro-cracks, the stress is centralized, which causes great tensile stress and, under the tensile stress, the micro-cracks expand quickly. In the end, the glass is broken before its strength does not approach the theoretical strength very much, that is, the practical strength is very lower than the theoretical strength. Now that the micro-cracks on the surface of the glass have influence on the strength of the glass, various surface treatments to the glass will influence the strength of the glass. Thus there are many ways to increase the strength of the glass. This paper studied the influence of various surface treatments on the glass strength, and the best way to increase the glass strength was obtained.

II. EXPERIMENT

1. Specimen

The glass for the specimens is fresh. The dimension for tensile strength of glass is 120 mm x 20mm x 5mm and the number of specimens is 15. The dimension for impact strength of glass is 300mm x 300mm x 5mm and the number of specimens is 6. The edges of glass specimen are polished very well.

2. The tensile strength of glass

The method of three points tensile strength is used, and loading velocity is 0.5 mm/s.

3. Impact strength of glass

One steel ball which weighs 227g falls freely from certain height and impacts the glass. When one among six specimens is broken, the height is taken as the impact strength of glass.

III. RESULTS AND DISCUSSIONS

1. Results

The tensile strengths and impact strengths of specimens which respectively were treated with physical temper, ion exchange strengthening, acid etching method, acid etching method + ion exchange strengthening, physical temper+acid etching method and common specimens are listed in Table 1.

Table 1 Tensile strengths and impact strengths of glass

treatment methods	**tensile strength MPa**	**increment times**	**impact strength m**	**increment times**
common specimens	77.7	1.00	1.5	1.00
physical temper	238.3	3.07	3	2.00
ion exchange strengthening	126.2	1.62	3	2.00
acid etching	98.6	1.28	2	1.33
acid etching+ion exchange strengthening	181.6	2.33	4	2.66
physical temper+acid etching	368.7	4.79	>12	>8.00

2. Discussions

The results show that only to use single way can not increase the glass strength very much, but to use two ways or more ways can increase the glass strength very much. The tensile strength of glass which is treated with physical temper is as two or three times as common specimen. But it will be as five times as common specimen if the glass is treated with acid etching method after the glass has been treated with physical temper.

The impact strength of glass which is treated physical temper is only three meters. But it will approach twelve meters if the glass is treated with acid etching method after the glass has been treated with physical temper. It is important that the glass is not broken even at twelve meters and it is still not broken at twelve meters one month later.

IV. CONCLUSIONS

The best way to increase the glass strength is acid etching method after physical temper.

REFERENCES

l. R. C. Bradt et al., eds., Fracture Mechanics, Vol.4 Plenum Press, (1978)
2. A. Kelly, Strong Solid, Clarendon Press, (1973)
3. F. V. Tooley, The Handbok of Glass Manufacture, (1974)

MIXED MODE FRACTURE IN GLASS

Mehmet A. Tasdemir[1] , Reha Akçakaya[2], Canan Tasdemir[1] and **Saim Akyüz[1]**
[1]Istanbul Technical University, Turkey
[2]SISECAM Research Center, Turkey

Abstract

Mixed-mode fracture in glass is studied using the Brazilian test specimens with center notched. Under the Mode I loading condition, the test method is applied to determine the critical value of stress intensity factor, K_{IC}, for glass. The same disk specimen is used under combined Mode I and Mode II loading conditions. By changing the notch orientation angle with respect to the loading direction, the mode of fracture is varied from pure Mode I (opening) to mixed-mode (tension-shear or compression-shear). Theoretical criteria are used to describe the stability of crack growth. Based on the mixed-mode fracture envelope, it is shown that the disk specimen provides a wide range of K_{II}/K_I ratios. In pure Mode I loading case, if K_{IC} is known it is possible to obtain normalized critical load versus normalized crack length.

1. INTRODUCTION

Although a number of investigations were carried out on the failure of brittle materials under Mode I (opening) loading, in application, structure are generally subjected to mixed-type of loading. For a cracked specimen under mixed mode loading, the following three fracture criteria are available: i) The maximum hoop stress criterion [1], ii) The minimum strain energy density criterion [2], and iii) The maximum energy release rate criterion [3]. These theoretical criteria were used to predict the direction of crack initiation and the stability of crack growth. Some applications and comparisons of these criteria can be found in references [4] and [5]. Little information is available, however, on the fracture of glass under combined tensile and shear stresses. The main objective of the work presented here to develop a linear elastic fracture mechanics (LEFM) based model for glass, using analytical, numerical and experimental methods.

2. BACKGROUND

A disk of radius R with an internal diametral crack of length 2a, has many advantages as an experimental sample which has been solved analytically in Russian literature [6-8].

The experimental test program is based primarily on the compression test of disk specimens with an internal slant crack, as shown in Fig.1.

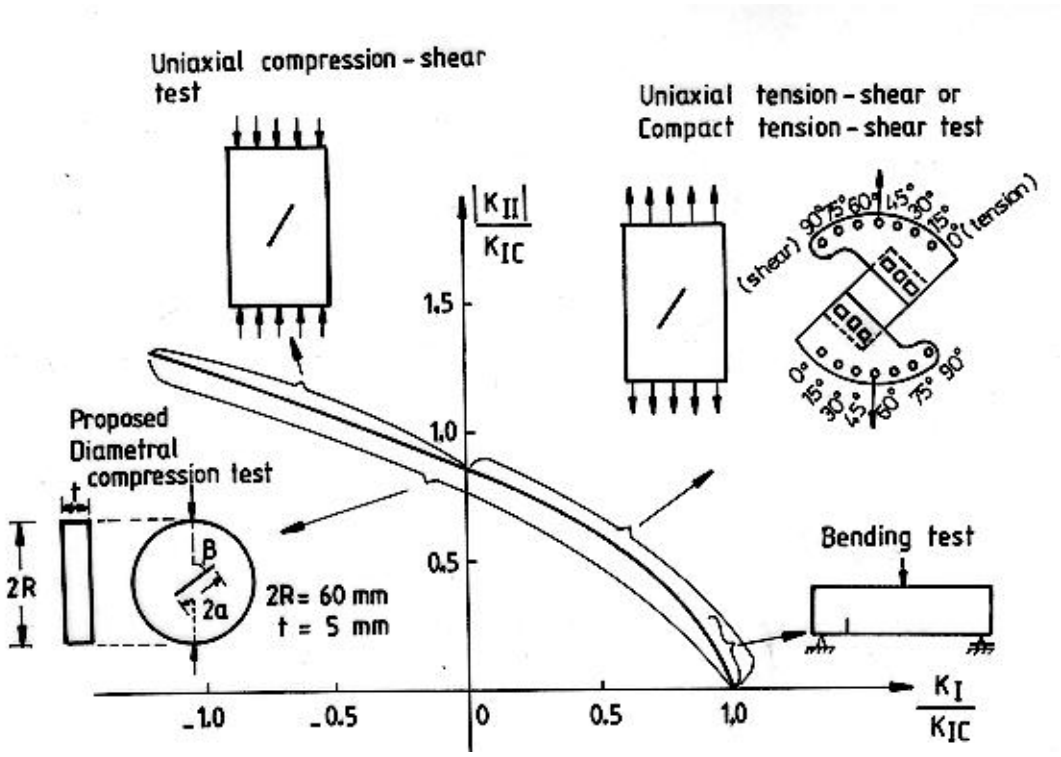

Fig.1. K_{II}/K_{IC} versus K_I/K_{IC} schematic envelope curve in the mixed-mode fracture for different loading configurations.

For the mixed-mode I (opening) and Mode II (shear) fracture of glass, there are the following advantages in using a disk shaped specimen with inclined crack subjected to diametral compression test: i)By changing the inclination of the notch with respect to the loading direction, it is possible to change the fracture of glass from Mode I to Mode II and to obtain combined loading conditions with a wide range of K_I versus K_{II}, where K_I and K_{II} are the Mode I and Mode II SIFs (stress intensity factors) at the notch tip, respectively, ii) It is not difficult to obtain higher K_{II}/K_I ratios using this type of loading configuration. One can also obtain both positive and negative values of the K_{II}/K_I ratio, and iii) The same specimen can be used to obtain test results in pure Mode I and mixed mode cases. Figure 2 shows how it is possible to change the mode of fracture from opening mode (mode I for $\beta=0^o$) to mixed mode (tension-shear for $\beta<30^o$ and compression-shear for $\beta>30^o$) by rotating the notch inclination angle β with respect to the loading direction [9, 10].

The SIF is of fundamental importance in the prediction of brittle failure in glass. It is a function of both the cracked geometry and the associated loadings. SIFs for the inclined crack in the diametral compression test specimens were calculated by Yarema et al. [6]. Mode I and Mode II SIFs are given by the relations

$$K_I = s\sqrt{pa}\, f_I(b, \frac{a}{R}) \quad \text{and} \quad K_{II} = s\sqrt{pa}\, f_{II}(b, \frac{a}{R}) \qquad (1)$$

where σ=P/pRt, in which P is the load applied in compression, a is the half crack length, and R and t are the radius and thickness of the disk, respectively. $f_I(\beta, a/R)$ and $f_{II}(\beta, a/R)$ are dimensional coefficients that ere functions of the relative crack size, a/R, and b the crack inclination angle (β) with respect to the loading direction.

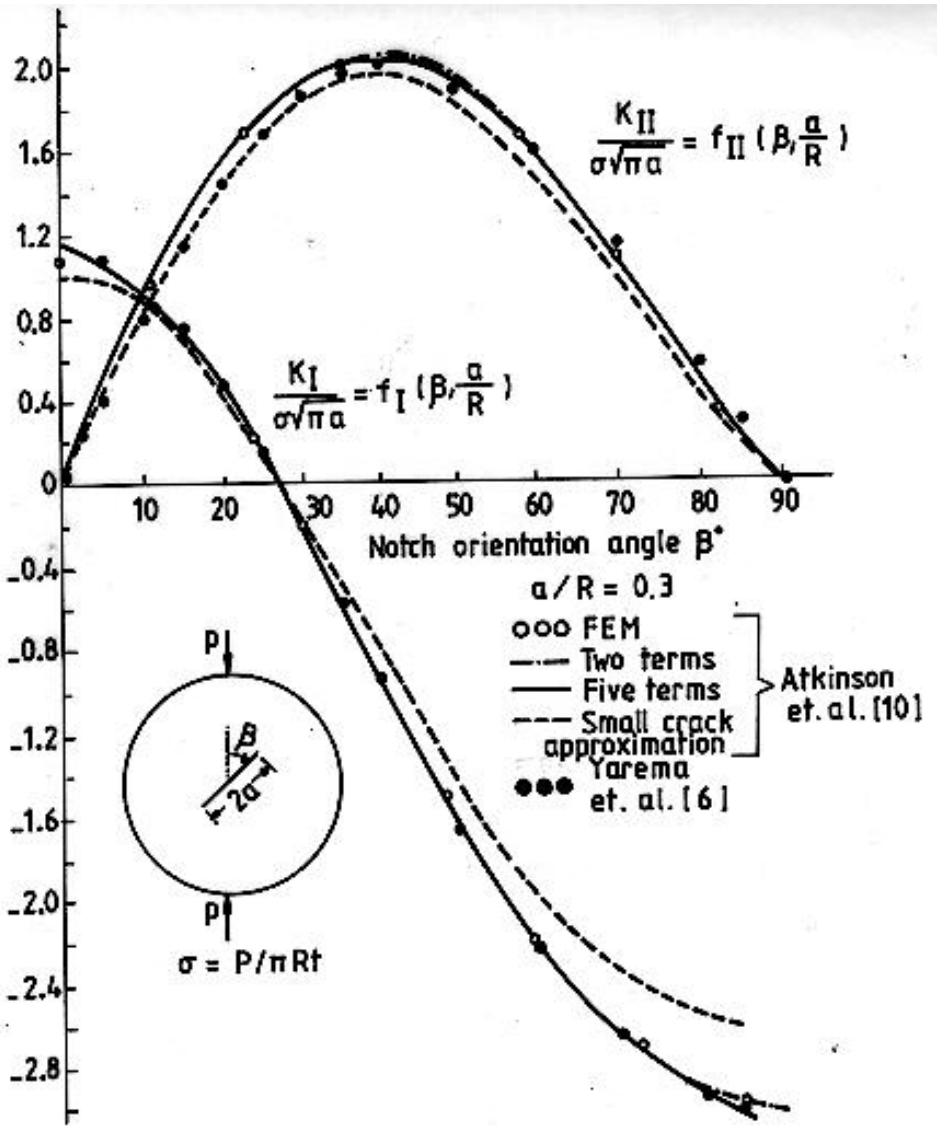

Fig. 2. Nondimensional SIFs under mixed-mode loading.

A comparison of the various calculation methods shows that with an increase in the crack inclination angle β, the factor K_I drops and passes through zero, and takes negative values. The factor K_{II}, however, increases and with angles β close to 10^o becomes equal to the factor K_I. K_{II} reaches its maximum value around 40^o.

3. DETERMINATION OF SIFs

Center notched disk (CND) specimens used in the present study were loaded in the Brazilian test configuration. For the preparation of samples, molten glass of typical float glass composition was cast into a cylindrical mold, so that 60 mm diameter, 8 mm thick samples with a diametral notch of 2 mm wide could be produced. The specimens were carefully annealed and were observed not to contain significant residual stresses. The annealed specimens were then ground to a homogeneous thickness of approximately 5 mm. Preliminary test with specimens cut from float sheets with center notch machined out using a diamond saw gave similar results with the cast specimens. Cast specimens were preferred due to their ease of production. Notch tips of 1 mm radius were lightly abraded for obtaining consistent fracture load values. To avoid the localized compressive stresses under the load, a narrow cardboard strip of 5 mm wide, 3 mm thick was inserted between the loading plate and the specimen, the load was distributed over this strip. The geometry of the center notched disk specimens used in the presented work is shown in Figure 1. For pure Mode I loading condition, four different notch rations (a/R=0.2, 0.3, 0.45. and 0.6) were chosen. For mixed mode loading, specimens were tested with four inclination angles (β=0^o, 5^o, 15^o, 25^o and 35^o). The test specimen is then loaded to failure (Pcr). Mixed-mode fractures were obtained by rotating the notch orientation angle with respect to the loading direction. Based on the finding of Russian researchers, the initial crack sizes were used to calculate K_I and K_{II}. In the pure Mode I loading case, the solution given for the normalized load at fracture as a function of the normalized crack length is represented by the relation

$$\left\{1+\frac{3}{2}\left(\frac{a}{R}\right)^2+\frac{3}{4}\left(\frac{a}{R}\right)^6+\frac{3}{64}\left(\frac{a}{R}\right)^8\right\}\sqrt{\frac{a}{R}}=K_I\frac{t\sqrt{p\ R}}{Pcr} \qquad (2)$$

Equation 2 can be re-arranged to the linear form of $Y=K_IX$ in which $Y=f(a/R)$ and $X = t\sqrt{pR}\ /\ Pcr$ **Error! Switch argument not specified.**. As shown in the inset of Figure 2, a linear regression analysis was used to determine the critical value of the SIF K_{IC}, from the slope of the line with correlation coefficient of 0.98. Here, K_{IC} can be taken as a material property. The results obtained are very close to those reported in the literature [7, 11].

In Figure 3, the critical load Pcr was normalized by using the critical value of SIF,K_{IC}, from disk specimens for different initial notch lengths. As shown in the figure, the experimental results follow the analytical results with an excellent correlation. The experimental results obtained for glass show that the method of determining K_{IC} described here can be used for application purposes.

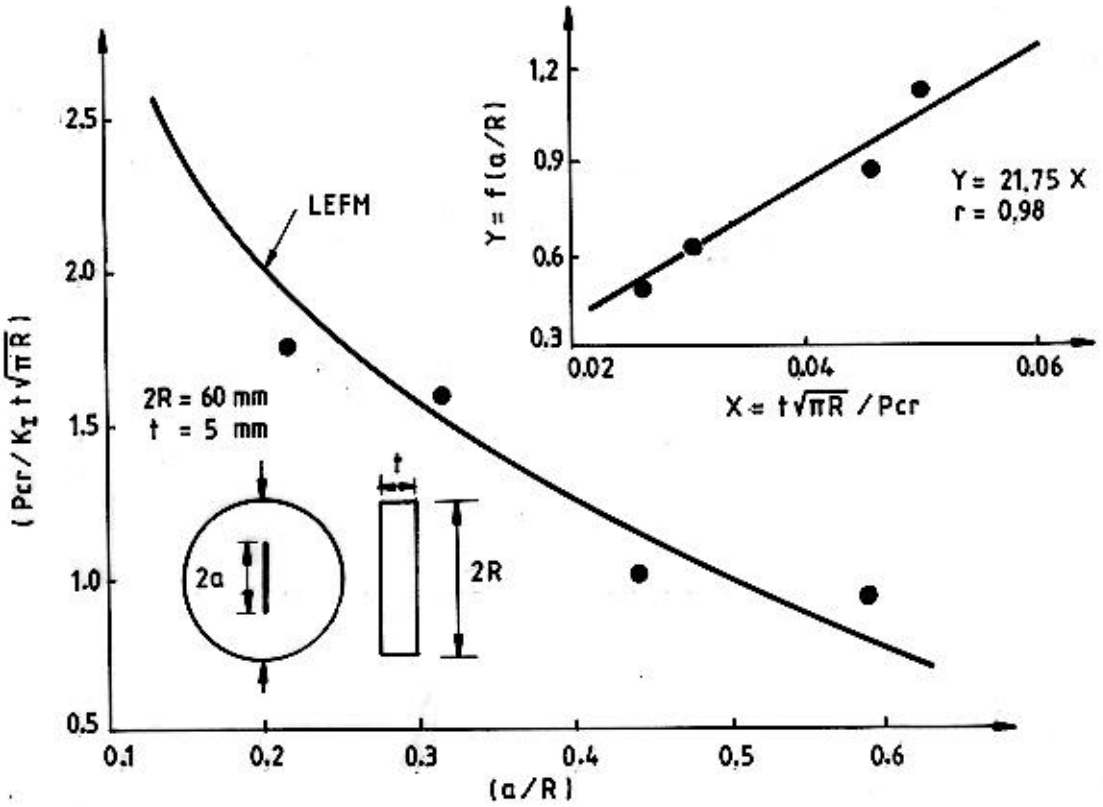

Figure 3. Normalized crack load Pcr / $K_{IC} t\sqrt{pR}$ ***Error! Switch argument not specified.*** *versus normalized crack length (a/R).*

4. MIXED-MODE FRACTURE ENVELOPE

There theoretical criteria were used to predict the direction of crack propagation and the stability of crack growth. For center notched disk (CND) specimens, a comparison of these criteria, the experimental results obtained in the present work, as well as sintered carbide and graphite test results published by other researchers [6, 12] is shown in Figure 4. Since CND specimens provide a wide range of K_{II}/K_I ratios, they are very useful in comparing design based predictive equations for mixed-mode fractures. In practice $K_{IC} \neq K_{IIC}$, and it is suggested that the fracture condition is more likely to be of the form

$$(K_I / K_{IC})^u + (K_{II} / K_{IIC})^u = 1 \qquad (3)$$

where u is a constant between 1.5 and 2. Figure 4 compares the normalized Mode I and Mode II SIFs for mixed-mode fracture in CND specimens. It can be concluded that the mixed-mode fracture criteria formulated do not satisfactorily account for the CND test specimens. The experimental results obtained in this work show that K_{IIC}/K_{IC}=1.22. On this basis, by taking u=1.9 it is possible to combine the equation K_{IIC}=1.22 K_{IC} and Equation 3 to propose the following fracture envelope

$$K_I^{1.9} + 0.67 \;\; K_{II}^{1.9} = K_{IC}^{1.9} \qquad (4)$$

The curve given by Equation 4 is also plotted in Figure 4. It is seen that in tension-shear, there is good fit between Equation 4 and the experimental results for both glass and other brittle materials.

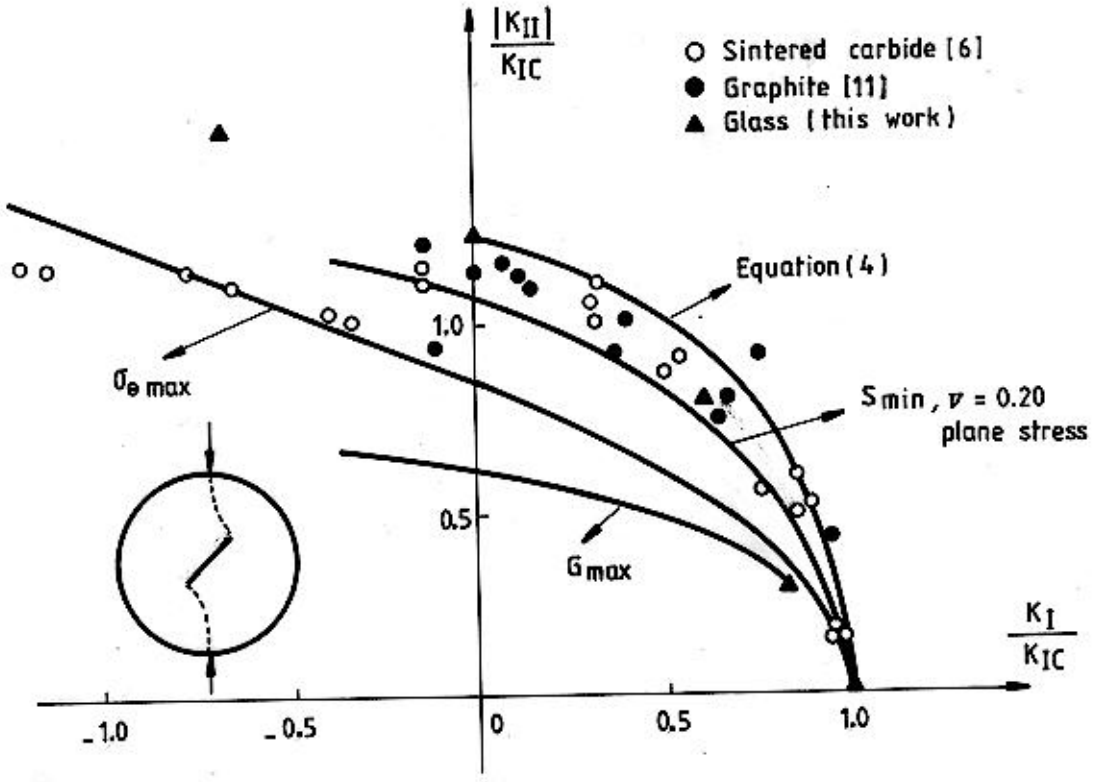

Figure 4. Mixed-mode fracture envelope

5. CONCLUSIONS

The results obtained in this work can be summarized as follows:

1. K_{IC} can be easily determined under pure Mode I loading condition using different pre-existing crack lengths in the same specimen. This critical value can be considered as a material property. By using the same center notched disk specimens, the experimental determination of the critical SIF under pure Mode II condition, K_{IIC}, is also possible.

2. The same disk specimen can be used under mixed-mode loading conditions. By changing the notch orientation angle with respect to the loading direction, the mode of fracture can be varied from pure Mode I (opening) to mixed mode (tension-shear or compression-shear). The mixed-mode fracture envelope can be obtained in a wide range of K_{II}/K_I ratios. There is good agreement between the experimental results and the proposed failure envelope in tension-shear case.

3. In pure mode loading conditions, with a knowledge of K_{IC} and the disk geometry, it is possible to obtain normalized critical load versus normalized crack length values.

ACKNOWLEDGMENT

This study was partially supported under TÜBÝTAK (Scientific and Technical Research Council of Turkey) grant INTAG 524. The authors wish to thank TÜBÝTAK for the financial support, and ÞÝÞECAM Research Center for the preparation of the samples. The authors also thank Mr. Hakan Atahan for his help during the mechanical tests.

REFERENCES

1. Erdoðan, F., and Sih , G.C. , On the Crack Extension in Plates under Plane Loading and Transverse Shear, ASME, *Journal of Basic Engineering*, Vol. 85, No:4, Dec. 1963, pp.519-527.

2. Sih, G.C., Strain - Energy - Density Factor Applied to Mixed -Mode Crack Problems, *International Journal of Fracture*, Vol.10, No.3, Sept., 1974, pp. 305-321.

3. Hussain, M.A., Pu, S.L., and Underwood, J., Strain Energy Release Rate for a Crack Under Combined Mode I and Mode II, *ASTM, STP 560*, 1974, pp. 2-28.

4. Taþdemir, M.A., Maji, A.K., and Shah, S.P., Crack Propagation in Concrete Under Compression, *Journal of Engineering Mechanics, ASCE*, Vol. 116, No.5, 1990, pp.1058-1076.

5. Maji, A.K., Taþdemir, M.A., and Shah, S.P., Mixed Mode Crack Propagation in Quasi -Brittle Materials, *Engineering Fracture Mechanics*, Vol. 38, No. 2/3,1991, pp. 129-145.

6. Yarema, S. Ya., Ivanitskaya, G.S., Maistrenko, A.L., and Zboromirskii, A.I., Crack Development in a Sintered Carbide in Combined Deformation of Types I and II, Translated from *Problemy Prochnosti*, No. 8, 1984, pp. 51-56.

7. Libatskii, L.L. and Kovchik, S.E., Fracture of Discs Containing Cracks, *Fiziko-Khimicheskaya-Mekhanika Materialov*, Vol. 3, No. 4, 1967, pp. 458-464.

8. Yarema, S. Ya, and Krestin, G.S., Determination of the Modulus of Cohesion of Brittle Materials by Compressive Tests on Disc Specimens Containing Cracks, *Fiziko-Khimicheskaya Mekhanika Materialov*, Vol. 2, No. 1, 1966, pp. 10-14.

9 Taþdemir, M.A., Maji, A.K. and Shah, S.P., Crack Growth in Concrete Under Combined Mode I and Mode II, *Bull. Tech. Univ., Istanbul*, Vol. 45, No. 1/3, 1992, pp. 133-164.

10 Atkinson, C., Smelser, R.E., and Sanchez, J., Combined Mode Fracture via the Cracked Brazilian Disk Test, *International Journal of Fracture*, Vol. 18, No. 4, April 1982, pp. 279-291.

11. Freiman, S.W., Gonzalez, A.C., and Mecholsky, J.J., Mixed-Mode Fracture in Soda-Lime Glass, *Journal of The American Ceramic Society*, Vol. 62, No. 3-4, 1979, pp. 206-208.

12. Awaji, H., and Sato, S., Combined Mode Fracture Toughness Measurement by the Disk Test, *Journal of Engineering Materials and Technology*, Vol.100, April 1978, pp. 175-182.

MODELLING MULTIAXIAL FRACTURE OF FLOAT GLASS*

L.J.M.G. Dortmans and **J. Gerretsen**
TNO Institute of Applied Physics, The Netherlands

Abstract

For strength modelling of brittle inorganic materials like glasses and ceramics, weakest-link fracture models can be applied, which are essentially based on Weibull statistics in combination with Linear Elastic Fracture Mechanics. Earlier work on a range of advanced technical ceramics has shown that these models can be applied successfully for strength prediction in both uniaxial and biaxial stress fields. In order to verify the applicability of these models for float glass, experimental strength data were gathered at room temperature and in inert environmental conditions using uniaxial 3- and 4-point bend tests and biaxial ball-on-ring and ring-on-ring tests. These tests were carried out on as-received and annealed specimens in order to analyse the effect of existing residual stresses for strength modelling. Also the effect of loading the tin-coated side in tension or compression was investigated.

---

* Full manuscript not available at the time of printing

NEW DATA ON AGING BEHAVIOR OF SILICATE GLASSES

Suresh T. Gulati
Corning Incorporated, USA

Abstract

In his pioneering work Mould studied the effect of aging on the strength of soda-lime glass and demonstrated a gradual increase of nearly 40% in its bend strength over 24 hours of aging in 100% RH (1). Stockdale et al. extended the aging studies to lead and borosilicate glasses and found similar strength increases (7). Doremus and his coworkers examined the crack tip morphology as function of aging time and concluded that crack tip blunting was caused by dissolution of glass which helped reduce stress concentration and increase the strength (5). The present study focuses on other silicate glasses of commercial interest, namely alkali strontium silicate glass used for CRT panels and potash soda-lime fluoride glass used as core glass for lightweight laminated dinnerware (10-12). These glasses also demonstrate the beneficial effect of aging over periods of up to 150 days. Both the threshold and inert strengths show appreciable increase implying the presence of crack tip blunting in certain compositions.

This paper examines the impact of crack tip blunting on threshold strength, product design and product reliability. Does aging alter fatigue behavior? If so, does it do so reliably? These questions are reviewed for the above glasses. The critical factors that control aging kinetics are also identified.

I. INTRODUCTION

The present paper is concerned with three aspects of aging behavior of silicate glasses. First, it provides a brief review of previous work on aging (1-7). Second, it presents new data on aging behavior of alkali strontium silica glass (Corning Code 9061) used for cathode ray tube panels and potash soda-lime fluoride opal glass (Corning Code 1001) used for laminated dinnerware (8-12). And third, it examines the impact of aging on both the threshold stress intensity and stress corrosion behavior of silicate glasses (13-15). The motivation for this work stems from the need for improved understanding of brittle failure which, in turn, helps optimize product design without compromising mechanical reliability [16-18]. Specifically, we focus on the following areas:

1. Efficient product design requires not only an accurate knowledge of service conditions, but also of the failure process. To promote long term reliability and serviceability, the product is generally designed to operate in the fatigue-free state, i.e. the design strength of an annealed glass article is taken as its threshold stress. The improvement in this stress, brought about by aging, may be insignificant when compared with the pristine strength of glass, but it is an appreciable fraction of its abraded strength–one that matters in product design. In those applications where the

product is not susceptible to impact or other type of handling damage leading to fresh flaws, the aging of initial flaws can result in 40% higher design strength.

2. The role of aging in measuring fracture parameters, such as the stress corrosion constant n, or in conducting fatigue studies has not been understood properly. For example, why are the *n* values obtained from static and dynamic tests different?

3. While slow crack growth (SCG) theory helps estimate the growth of initial flaw due to fatigue (13) , it does not shed any light on the crack blunting process. In fact, it assumes the crack tip radius to remain constant throughout the SCG process. The inability of SCG theory to predict the degree of crack blunting is understandable since it assumes the crack to be stressed above the threshold value, while aging takes place below this value or in the absence of stress. Thus, to assess the degree of crack blunting relative to the initial tip radius, we must appeal to the Inglis-Griffith flaw theory which takes proper account of the tip radius (19,20). By quantifying both the crack growth and crack blunting (or sharpening), our understanding of brittle failure will have improved.

Finally, if we assume that the theoretical strength and critical stress intensity are intrinsic material properties, the aging data can shed some light on the following questions critical to efficient product design:

1. How much rounding of the unaged flaw tip take place during aging?
2. Can aging render the flaw immune to SCG? If not, how much does the aged flaw grow relative to unaged flaw?
3. Can we quantify the increase in threshold stress brought about by aging?
4. What are the conditions for coexistence of aging and SCG?
5. Do aged flaws stress-corrode differently than unaged flaws? If so, in what way?
6. Can aging have a significant impact on product design?

II. REVIEW OF PREVIOUS WORK

The most comprehensive study of aging reported in the literature, was carried out by Mould (1). He studied this phenomenon for soda-lime glass using two different abrasions and various aging media, namely:

i) hand abrasion with 320 grit emery cloth which produces linear flaws, i.e. shallow but sharp flaws; and

ii) silicon carbide grit blast which produces point flaws, i.e. deep and seemingly blunt flaws.

The aging media he used included water, humid air, acidic and basic solutions.

Mould also studied the static fatigue behavior of both types of abrasions using aged specimens. He then compared the strength and fatigue data of specimens abraded and aged in various ways with those of similarly abraded samples which, instead of being water-aged, had been vacuum-baked at 470^{o}C.

For a true evaluation of the effect of aging, i.e. to circumvent SCG during strength measurement, he resorted to tests in inert environment of liquid N_2. He argued that this was an

effective way of "freezing in" the state of the specimen at any given time and measuring its true strength at the instant of immersion. His major findings are:

i) aging promotes rounding of the crack tips–a process which takes time depending on the nature of initial abrasion;
ii) emery cloth abrasion is almost completely aged after 24 hours in water, where as grit-blast abrasion requires 100 days; the enhanced aging of emery cloth abrasion is due to the stronger capillary action of these tight flaws;
iii) aging efficiency depends on the relative humidity of aging medium; distilled water was most effective with acidic and basic solutions coming close to water; lower the RH of air, slower the aging process; no aging was observed in dry air or in vacuum at room temperature;
iv) emery cloth abrasions, after being fully aged for 1 day in water, gave a 50% increase in inert strength; grit-blast abrasions after 1 day's aging in water, gave a 30% increase.
v) inert strength of unaged abrasions–whether emery cloth or grit-blast–was identical; thus the shallow linear flaws were also sharper at their tip such that the stress concentration factor remained constant for the two types of abrasions;
vi) linear flaws fatigued 50 times faster than point flaws despite the same SCF or same inert strength of the two types of flaws; thus either the threshold stress intensity K_{Io} or stress corrosion susceptibility constant *n* must be lower for the sharp linear flaw than for the blunt point flaw;
vii) for the short-duration strength tests (impact type) the strength increased linearly with log storage time up to 24 hours of aging in H_20; the rate of increase was 10 times higher in 70% RH than in 1% RH.
viii) although the threshold stress intensity for aged samples was appreciably higher, the static fatigue behavior of both aged and unaged specimens was identical (implying that once SCG begins. we are back to the sharp crack tip);
ix) aging effect in high temperature vacuum-baked abraded samples was identical to that of water-aged samples; in addition, high temperature vacuum baking rendered the glass surface (including flaw tip region) non-wettable, so that static fatigue rate was reduced by a factor of 25 compared with fresh or water-soaked abrasions.

The question "does the observed strength increase due to aging reflect higher threshold strength?" was answered by conducting static fatigue tests on unaged vs. aged specimens. The results showed that strength of aged samples was consistently higher than that of unaged ones at all load durations, indicating that there was a definite contribution to threshold strength of aged samples. To firm this up further and to discern the influence of aging on fatigue from that on threshold strength, Mould plotted the static fatigue curve (σ/σ_{ln} vs. t) for aged and unaged specimens, using proper values of σ_{ln} for each set, and found them to be identical! Thus he established clearly that strength increase due to aging in water is completely attributable to an increase in threshold strength.

Baker and Preston (2) believed that the strength and fatigue behavior of a freshly formed flaw might be markedly different from that of a flaw which had been exposed to atmosphere for some time. Because of the important role played by chemical attack in connection with the fatigue of glass, they concluded that the history of exposure of the glass surface will influence the results of strength tests.

Charles' original theory (21) assumed the crack tip radius to remain constant. Later, Charles and Hillig admitted the variation of tip radius whether during aging or fatigue (3). They believed that crack tip rounding reduces stress concentration factor and ensures that SCG is delayed. They found that as long as the stress concentration factor remains constant over time, the applied stress can be supported indefinitely and they called this stress the fatigue limit.

Doremus (5) reported that changes in crack tip radii can influence fracture and fatigue of glass. Crack tips are blunted by reaction with water thereby increasing the strength without changing the crack depth. He used Charles and Hillig theory to illustrate that the rate of tip sharpening is greater than the rate of crack extension when the crack is stressed in humid environment. Denoting fracture stress by σ_f, flaw depth by a, tip radius by ρ, rate of crack extension by $\dot{a}$, rate of crack tip sharpening by $\dot{\rho}$, and stress intensity by K_I, Doremus claimed that at $\sigma = 0.7\ \sigma_f$, $\dot{a} \sim 10^{-6}$ m/sec. and $a \sim$ 5-20 Nm making $\dot{a}/a = 0.1\ sec^{-1}$. However, he goes on to say, $\rho/\rho \sim -10\ \dot{a}/a$ at fracture indicating that the predominant factor for static fatigue at σ/σ_o is crack tip sharpening rather than crack extension! Below threshold, $\dot{a} \sim 10^{-11}$ m/sec and $\dot{a}/a \sim 10^{-6}\ sec^{-1}$ With such low velocities, crack extension is immeasurable and crack tip can only get rounder with time i.e. $\dot{\rho}/\rho > o$, making $dK_I/dt < 0$ and bringing about aging.

Doremus concludes that energy criteria for fracture are inadequate for understanding the relative rates of crack extension vs. crack tip sharpening.

Dozier (6) worked with soda-lime glass and examined crack-tip profile in dry and humid environments. Treating the crack as a thin air wedge they measured interference fringes under monochromatic light and inferred crack displacement or crack-tip sharpening/healing from these fringes. They concluded, contrary to Wiederhorn's observations (14), that both crack blunting and healing can occur in this glass. They also stated that for SCG to occur the stress concentration factor $\sqrt{a/\rho}$ must reach a certain value, and that either a or ρ or both begin to vary with time, i.e. as long as $\sqrt{a/\rho}$ does not change with time, SCG cannot take place and crack remains dormant. They went on to reinforce Doremus' contention that during the corrosion process a small increase in flaw depth is accompanied by a large reduction in flaw tip radius, and it is the latter that leads to failure.

Justice et al. (4) measured the tensile strength of aged optical fibers with borosilicate glass cladding. They found that the minimum strength (corresponding to deep and sharp flaws) increased 50%, mean strength increased 25% and the maximum strength (corresponding to shallow and blunt flaws) increased only 15%. These data suggest that the initially deep and sharp flaws, by virtue of their more efficient capillary action, are relatively more amenable to rounding by water.

The above review of previous work not only answers some of the questions posed earlier, it demonstrates consistency in the aging behavior of silicate glasses. In the next section, we present more recent aging data for two of the commercial glasses which help promote their field durability.

III. AGING DATA FOR COMMERCIAL GLASSES

In this section, we present the aging data for two new glasses of commercial importance. The first of these is a phase-separated potash soda-lime fluoride glass, Corning Code 1001, used as the core glass for lightweight laminated dinnerware (10,11). The lower expansion cladding glass, Corning Code 1000, induces a substantial amount of surface compression upon cooling from hot-

lamination temperature to room temperature rendering the dinnerware strong (12). The day-to-day serviceability of laminated dinnerware is enhanced further by thermal tempering which increases the depth of compression layer well beyond the cladding thickness. In this manner, the surface flaws induced by day-to-day handling are contained within the effective compressive layer which extends into the core. The motivation for studying the aging behavior of core glass arose from understanding the SCG behavior of surface flaws due to residual tensile stresses in core glass with poor chemical durability[1].

The aging data were obtained in bending using two different specimens, namely 1" x 4" x 0.25" modulus of rupture (MOR) bars of core glass and 10.25" diameter x0.105" thick laminated plates. The former were sandblasted, using ASTM Standard C-158, and tested in 4-point bending after soaking in water for different times. The strength data are summarized in Table 1. It is clear that in view of its poor chemical durability the phase-separated opal glass exhibits significant aging over the 50-day period approaching 30% improvement in its initial MOR value.

The surface flaw at the center of laminated plates was induced by a water cooled, low speed, precision diamond saw; the flaw depth was kept constant at 0.005". The plates were tested in biaxial bending using the 3-ball support on 4.5" diameter circle and 1" diameter loading piston at the center. The strength data are summarized as function of aging time in Table 2. The biaxial strength of laminated plates is considerably higher than the MOR values of core glass specimens due to the contributions of surface compressive stress in low expansion cladding glass and residual compression from thermal tempering. And yet, these data are consistent with MOR data in that they exhibit continuous aging over the 216 hours of exposure to water. Figure 1 shows the Weibull plot of biaxial strength data for 10.25" plates. The parallel shift of Weibull distribution is indicative of good control of "saw-cut" flaw. The largest shift occurs after one hour indicating that aging benefit is the greatest during the first hour of soaking; thereafter its impact on strength enhancement is asymptotically lower.

Table 1

Strength vs. aging time for sandblasted MOR bars of potash soda-lime fluoride opal glass (code 1001 glass)

Aging Time in Water	MOR (psi)	
	Mean Value	Std. Deviation
1 min	6525	± 420
1 hr	7390	± 720
24 hrs	6980	± 1500
100 hrs	8000	± 520
50 days	8480	± 1830

[1]It should be pointed out that both the chemical durability and weathering resistance of laminated dinnerware are primarily controlled by the cladding glass which is very durable (10).

Figure 2 shows the semilog plot of strength data from Tables 1 and 2. The best fit line through these data provides the empirical relationship between strength and aging time, namely

$$\frac{\sigma_t}{\sigma_o} = \left(\frac{t}{t_o}\right)^{1/\alpha} \tag{1}$$

In eqn.1, σ_t and σ_o denote strength values after aging times t and t_o respectively and α is the aging constant representing the kinetics of glass/water reaction whose value will depend on glass composition, flaw morphology, residual stress at flaw tip and water temperature. The higher the α value is, the lower the aging kinetics will be. It is interesting to note that the form of eqn. 1 resembles the dynamic fatigue equation relating strength σ to rate of testing σ through the fatigue constant *n*:

$$\frac{\sigma_1}{\sigma_2} = \left(\frac{\dot{\sigma}_1}{\dot{\sigma}_2}\right)^{\frac{1}{n+1}} \tag{2}$$

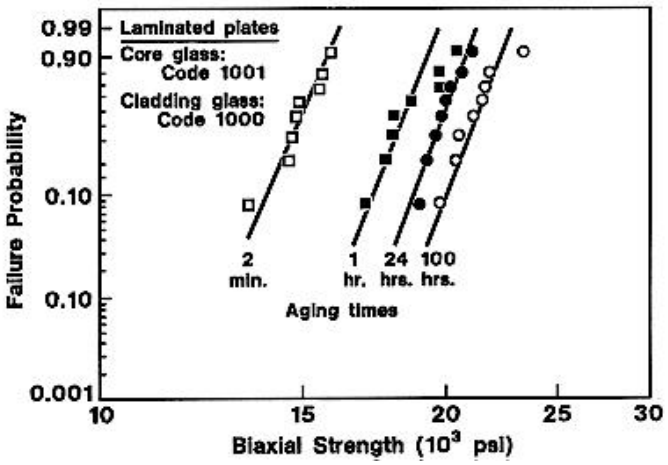

Figure 1. Weibull Plot of Biaxial Strength vs. Failure Probability for Laminated Plates with 0. 005" Deep "Saw Cut" Flaw at Center

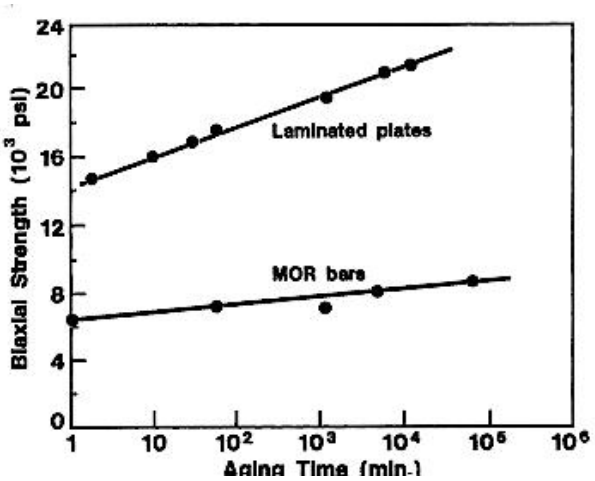

Figure 2. Strength vs. Aging Time for MOR Bars (with Sandblast Abrasion) and Laminated Plates (with Saw-Cut Flaw at Center) of Potash Soda-Lime Fluoride Opal Glass

Table 2		
Strength vs. aging time for 10.25" laminated plates with 0.005" deep saw-cut flaw at center (code 1001 glass)		
Aging Time in Water	Biaxial strength (psi)	
	Mean Value	Std. Deviation
2 min	14820	±740
10 min	16140	±1030
30 min	17140	±1300
1 hr	18530	±1170
24 hrs	19730	±640
100 hours	21080	±1100
216 hrs	21450	±1990

A regression analysis of the best fit lines in Figure 2 yields $\alpha = 25$ for laminated plates and $\alpha = 43$ for MOR bars. These values are similar to *n* value for the opal glass which ranges from 25 to 50 depending on flaw morphology and the state of aging. The lower α value for laminated plates could be interpreted as better aging kinetics for the "saw-cut" flaw due to its capillary action compared with the sandblast flaw in MOR bars. It is conjectured at this point that crack tip blunting during aging not only improves fracture strength, but also the threshold strength (i.e. it delays the onset of slow crack growth) thereby permitting a higher design stress.

The second glass of commercial importance whose aging behavior is of interest is the alkali strontium silicate glass, Corning Code 9061, used for manufacturing the front panel of cathode ray tubes (8,9,). Since the typical panel constitutes 67% of CRT weight and since the processing time for CRT is proportional to its weight, it is most desirable to minimize the panel weight through efficient design without impairing its mechanical reliability. One way to design the panel more efficiently is to improve its fatigue behavior due to vacuum loading in humid environment.

However, as noted above, the fatigue behavior is altered by aging of the surface flaws. Hence both aging and fatigue studies were carried out for the panel glass using 6" diameter plates with 150-J abrasion. The choice of 150-J abrasion was dictated by the fact that it represented field-induced flaws as verified by strength measurements.

The aging data for Code 9061 glass plates with 150-J abrasion are shown in Table 3 and plotted in Figure 3. The initial strength of 3620 psi increased to 4280 psi after 44 days of aging in water.

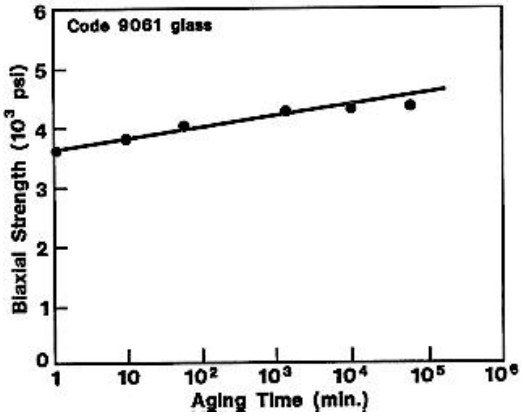

Figure 3. Biaxial Strength vs. Aging Time for alkali Strontium Silicate Glass Plates with 150-J Abrasion

This is a marginal increase of 18%. The aging constant estimated from Figure 3 is $\alpha = 52$ which is consistent with the marginal strength increase. However, the fatigue behavior of this glass reflected significant improvement with aging time in that the *n* value increased from 13.5 for unaged flaws to 27.0 for aged flaws (8,22). This translates to an increase of nearly 70% in threshold stress (13). This means that the design stress can be increased and the panel weight reduced provided the aging benefit is reliable throughout the product's lifetime.

Table 3
Strength vs. aging time for 6" plates of alkali strontium silicate glass with 150-J Abrasion at center(code 9061 glass)

Surface condition	Test Environment	Strength (psi)
Blanchard ground surface	10 min. soak in water	7035
150-J abrasion	Dry	3910
"	1 min. soak in water	3620
"	10 min. soak in water	3775
"	1 hr. soak in water	4015
"	24 hr. soak in water	4240
"	7 days in water	4260
"	44 days in water	4280

IV. ANALYSIS OF AGING DATA

In this section, we will apply the Inglis-Griffith flaw theory (19,20) to aged and unaged specimens and obtain an estimate of crack blunting (or sharpening) by assuming that the

theoretical strength of glass is an intrinsic material property. The basic equation which relates the theoretical strength, σ_{th}, to stress at failure, σ_f, is

$$\sigma_{th} = \sigma_f\left(1 + 2\sqrt{a_f/\rho_f}\right) = const \qquad (3)$$

where a_f and ρ_f denote flaw depth and crack tip radius at failure. The simplified form of this equation which will suffice for our purposes is obtained by neglecting unity in comparison with $2\sqrt{a_f/\rho_f}$:

$$\sigma_f \sqrt{a_f/\rho_f} = const \qquad (4)$$

Table 4 and Figure 4 summarize the terminology which will be used for applying eqn. 4 to aged and unaged specimens. In each case the flaw dimensions at the onset of

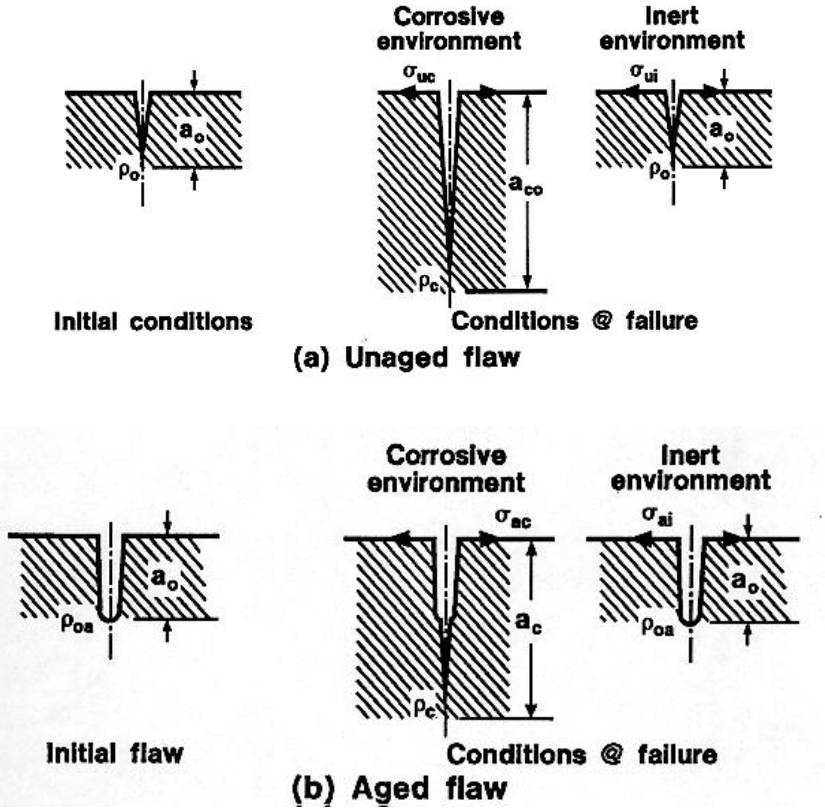

Figure 4. Schematic Representation of Flaw Parameters for (a) Unaged and (b) Aged Flaws

Table 4	
Flaw Parameters and Failure Stress for	
Aged and Unaged Specimens Tested in Corrosive vs. Inert Environment	
Flaw Tip Treatment	Test Environment

	Corrosive	Inert
Unaged	a_o, r_o (initial cond.)	a_o, r_o (initial cond.)
	a_{co}, r_c, s_{uc} (@ failure)	a_{co}, r_o, s_{ui} (@ failure)
Aged	a_o, r_{oa} (initial cond.)	ao, r_{oa} (initial cond.)
	a_c, r_c, s_{ac} (@ failure)	ac, r_{oa}, s_{ai} (@ failure)

slow crack growth (initial or threshold conditions) and at failure are indicated. Note that once the flaw begins to grow, its tip radius at failure is ρ_c whether it was aged initially or not. For illustration purposes we will use Mould's data for the strength of aged vs. unaged soda-lime specimens; see Table 5 (1). The general findings will also apply to other glasses though the numerical values may vary. It is clear from Table 5 that $\sigma_{ac}/\sigma_{uc} \sim \sigma_{ai}/\sigma_{ui} \sim 1.4$ and $\sigma_{ui}/\sigma_{uc} \sim \sigma_{ai}/\sigma_{ac} \sim 1.9$.

Thus, Mould's data point out two basic features, namely:

(i) aging improves the strength of soda-lime glass by about 40% whether the samples are tested in corrosive environment or inert environment; and
(ii) the inert strength of both aged and unaged soda-lime specimens is about twice the corresponding strength in corrosive environment.

Next, we apply eqn. 4 to aged and unaged data obtained in different environments:

A. Unaged Flaw Tested in Corrosive vs. Inert Environment

$$s_{uc}\,(a_{co}/r_c)^{1/2} = s_{ui}\,(a_o/r_o)^{1/2}$$

or

$$(r_o/r_c)\,(a_{co}/a_o) = (s_{ui}/s_{uc})^2 \qquad (5)$$

but

$s_{ui}/s_{uc} \approx 1.9$ (see Table 5)

and from SCG theory (13), for soda-lime glass,

$a_{co}/a_o \approx 4$

Hence

$$r_o \gg r_c \qquad (6)$$

Table 5
Mould's Data for Strength of Soda-Lime Glass Slides with Gritblast Abrasion [1] (psi)

Test Medium and Duration	Unaged Specimens	Aged Specimens (100 h in $H_2 0$)
Water (15 sec.)	5100 (s_{uc})	7100 (s_{ac})
Liq. N_2(30 sec.)	9500 (s_{ui})	13800 (s_{ai})

Thus, the radius of unaged flaw tip does not change appreciably during SCG. This is reasonable since there is little time for aging during the quasidynamic strength measurement process.

B. Unaged vs. Aged Flaw Tested in Inert Environment

$$s_{ui} (a_o / r_o)^{1/2} = s_{ai} (a_o / r_{oa})^{1/2}$$

or

$$r_{oa} / r_o = (s_{ai} / s_{ui})^2 \qquad (7)$$

but

$$s_{ai} / s_{ui} \approx 1.4$$

Hence

$$r_{oa} \approx 2\, r_o \qquad (8)$$

i.e. aging of soda-lime glass increases the initial flaw tip radius by a factor of 2.

C. Aged flaw Tested in Corrosive vs. Inert Environment

$$s_{ac} (a_c / r_c)^{1/2} = s_{ai} (a_o / r_{oa})^{1/2}$$

or

$$(r_{oa} / r_c)\,(a_c / a_o) = (s_{ai} / s_{ac})^2 \qquad (9)$$

but

$$r_{oa} / r_c = r_{oa} / r_o \approx 2$$

and

$$s_{ai} / s_{ac} \approx 1.9$$

Hence

$$a_c / a_o \approx 1.8 \qquad (10)$$

The aged flaw grows to nearly twice its initial size during SCG.

D. Unaged vs. Aged Flaw Tested in Corrosive Environment

$$s_{uc}\,(a_{co}/r_o)1/2 = s_{ac}\,(a_c/r_c)^{1/2}$$

or

$$(a_{co}/a_c) = (s_{ac}/s_{uc})^2 \qquad (11)$$

but

$$s_{ac}/s_{uc} \approx 1.4$$

Hence

$$a_{co}/a_c \approx 2 \qquad (12)$$

The unaged flaw in a soda-lime glass grows twice as much as the aged flaw during SCG. Also,

$$a_{co}/a_o = (a_{co}/a_c)(a_c/a_o) = 3.6 \qquad (13)$$

This is in good agreement with SCG theory (13).

Thus, the application of Inglis-Griffth equation to strength data provides useful information not only about the effect of aging on crack tip radius, but also about the relative growth of aged vs. unaged flaws during SCG. The lesser growth of aged flaw is physically consistent with its delayed threshold stage, similar to corrosion-resistant glasses with high value of n.

The foregoing equations point out another interesting feature about stress concentration factor at failure vs. threshold condition. For the aged flaw we find, by dividing eqn.10 by eqn. 8

$$\frac{a_c/\rho_c}{a_o/\rho_{oa}} = 3.6 \qquad (14)$$

or

$$\frac{\sqrt{a_c/\rho_c}}{\sqrt{a_o/\rho_{oa}}} = 1.9 \qquad (15)$$

Similarly, dividing eqn.13 by eqn. 6 for the unaged flaw leads to

$$\frac{a_{co}/\rho_c}{a_o/\rho_o} = 3.6 \tag{16}$$

or

$$\frac{\sqrt{a_{co}/\rho_c}}{\sqrt{a_o/\rho_o}} = 1.9 \tag{17}$$

Thus, the stress concentration factor at failure is nearly twice that at threshold whether the flaw is aged or not. Finally, it should be pointed out that glasses that are less corrosive than soda-lime glass will show correspondingly milder aging effect. As the fatigue constant *n* increases, both the inert strength as well as strength increase due to aging decrease.

V. EFFECT OF AGING ON FATIGUE BEHAVIOR

Mould (1) clearly showed that the physical effect of aging is to delay the onset of slow crack growth, i.e. to increase the threshold stress intensity factor, K_{Io}. This is in keeping with the Inglis-Griffith flaw theory that the reduced stress concentration factor at the blunted crack tip requires a higher stress to initiate slow crack growth. The larger the flaw tip radius is, the higher the threshold stress intensity will be; this is indicated schematically in the K-V diagram in Figure 5. If we treat the critical stress intensity factor, K_{IC}, as an intrinsic material property, then it follows from Figure 5 that the corrosion constant *n* must increase with aging time *t*, particularly if we postulate the existence of Region II defined by crack velocity V_{II}. The equivalence between aging and increasing *n* is also borne out by the high *n* glasses, i.e. less corrosive glasses, which are known to exhibit delayed threshold.

Fatigue measurements for glasses, which exhibit pronounced aging, are not easy to carry out. The current fatigue theories, unfortunately, do not account for the simultaneous presence of aging. We will report two studies-both related to fatigue measurements-whose results have not been understood well. The first study (23) dealt with static fatigue measurements for 10-1/4" diameter laminated plates. The author measured fatigue constant *n* of the highly corrosive core glass (Code 1001) and obtained a rather high value of ~35 (instead of ~15). When the specimens with aged flaws were stressed to as much as 75% of their short-term strength, they exhibited no fatigue for up to 100 hours after which the test was abandoned.

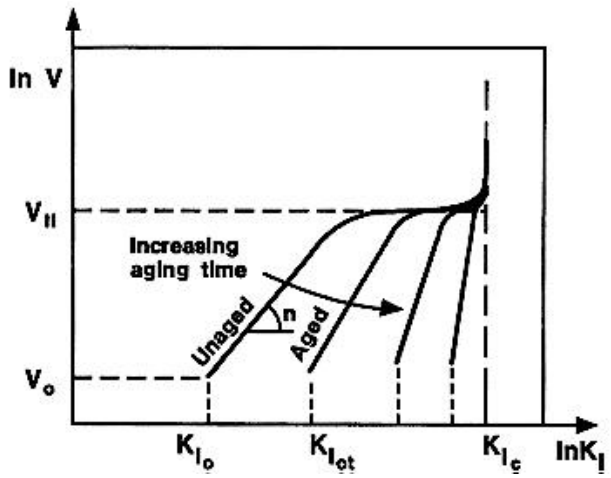

Figure 5. Schematic of K-V Diagram Showing the Effect of Aging on K_{Io} and n

Thus the threshold appeared to have increased from about 0.3 σ_f for glasses with n =15 to 0.75 σ_f. This indicates a significant contribution of aging! The scanning electron microscope studies of aged flaws indeed verified the presence of crack tip blunting. The author also tested the laminated plates at stresses near the short-term strength and measured failure times of 1-100 sec., too short to produce aging. Indeed, the failure was almost instantaneous indicative of high stress concentration due to unaged flaws.

In the second study (24), Helfinstine and Quan carried out static and dynamic fatigue tests on 10 m long optical fibers with borosilicate cladding. The static fatigue tests were conducted at three stress levels: 0.59 σ_f, 0.64 σ_f and 0.67 σ_f. The failure times spanned over months. Interestingly, the plot of percent failure vs. failure time turned out to be bimodal with initial slope being lower. They obtained an n value of 43 using initial slopes and 37 using the final slopes. One interpretation of these data would be that aging is more
effective at σ = 0.59 σ_f than at 0.64 σ_f, since the aging time is an order of magnitude greater at lower stress. In the later stages of this test, the failure rate is faster and aging benefit is minimal; hence a relatively low value of n is to be expected. In the dynamic fatigue test the failure times ranged from 70 sec. to 13 hours. Again, the failure rate vs. failure time plots were bimodal, and n values fell between 15 and 20 markedly lower than those obtained from static fatigue data. This discrepancy could be attributed to insufficient time for aging during dynamic fatigue tests. Only in the case of the lowest stress rate, where a stress of 0.4 σ_f or less was present for about 8 hours, could the aging effect have occurred.

If the service conditions for these fibers or any other glass article call for static load, then it appears logical that the n value based on static fatigue tests is more realistic than that based on dynamic fatigue tests for design purposes.

VI. SUMMARY

With the help of Inglis-Griffith theory and the available aging data, we have shown that:

i) aging delays the threshold stress and permits higher design strength values; the flaw tip radius is increased by nearly a factor of 2;
ii) percentage increase in threshold stress may be estimated by measuring the improvement in inert strength of aged flaws over unaged flaws;
iii) the effect of aging is equivalent to increasing the fatigue constant *n* which in turn permits a higher fraction of short-term strength for design strength;
iv) unaged flaws grow nearly fourfold while aged flaws grow half as much prior to becoming critical;
v) stress concentration factor at failure is twice that at threshold for both the aged and unaged flaws;
vi) once the SCG begins, the aging benefit is lost and the fatigue of aged and unaged flaws is identical.

ACKNOWLEDGMENT

The author is grateful to Virginia Doud and Nancy Foster of Science and Technology Division for their able assistance in the completion of this paper.

REFERENCES

1. R. E. Mould, J. Amer. Ceram. Soc.; 43 (3) 160-170 (1960).
2. Baker, T.C. and Preston, F.W.; J. App. Phys.;17, 3 (1946).
3. Charles, R.J. and Hillig, W.B.; High Strength Materials, John Wiley, New York (1965).
4. Justice, B. et al.; Am. Ceram. Soc. Bull.; 58,11 (1979).
5. Doremus, R.H.; Proc. XII Int'l Cong. Glass; Albuquerque (1980).
6. Dozier, S.A. et al.; Symp. Corrosion Fatigue: Chemistry, Mechanics and Microstructure; Univ. Conn.; Storres (1971).
7. Stockdale, G.F. et al.; J. Am. Ceram. Soc.; 34,.4 (1951).
8. Gulati, S.T and Ghosh, A.; Proc. XVII Int'l Cong. Glass; Beijing (1995).
9. Ghosh, A. and Gulati, S.T; Proc. '95 SID Conf., Orlando (1995).
10. Dumbaugh W.H. et al., U.S. Patent 3,737,294; June 5,1973.
11. Dumbaugh, W H.; "Laminated Glass," ASM Eng. Mat. Handbook, 4 (1991).
12. Gulati, S.T; Proc. XV Int'I Cong. Glass, Leningrad (1989).
13. Gulati, S.T; Proc. XII Int'I Cong. Glass, Albuquerque, NM (1980).
14. Wederhorn, S.M.; J. Am. Ceram. Soc.; 50 (1967).
15. Wiederhorn, S.M.; Frac. Mech. Ceramics; Plenum Press, New York (1974).
16. Gulati, S.T; Otto Schott Colloquium, Jena, Germany (1994).
17. Gulati, S.T and Powell, W.R.; '95 SPIE, San Diego (1995).
18. Gulati, S.T; EUROPTO'96; Glasgow (1996).
19. Inglis, C.E.; Trans. Inst. Nav. Archit., London, 55 (1913).
20. Griffth, A.A.; Phil. Trans. Roy. Soc., London, A221 (1920).
21. Charles R.J., J. App. Phys. 29 (1958).

22. Gulati, S.T; Proc. SID'93; Seattle (1993).
23. Janssen, C.M. and Gulati, S.T, Unpublished data, Corning Inc. Internal Report, December (1979).
24. Helfinstine, J.D. and Quan, F.; Optics & Laser Tech.; 14, 3 (1982).

RECORDING MICROINDENTATION AND CRACK INITIATION STUDIES ON SO_2-TREATED FLOAT GLASS

Ufuk Senturk and **James R. Varner**
NSF Industry/University Center for Glass Research
New York State College of Ceramics at Alfred University, U.S.A.

Abstract

The surface behavior of float glass that was exposed to SO_2 gas at temperatures in the glass transition region was studied using recording microindentation. Recording microhardness values were determined from the loading curves, and crack initiation was detected during loading and unloading by monitoring acoustic emission. Both microhardness and crack initiation characteristics were affected by the exposure of the glass to SO_2 .

The observed changes were affected by the treatment conditions. Microhardness values changed by various amounts depending on the specifics of the SO_2 treatments as well as the technique that was used in calculating the microhardness values. The crack-initiation behavior of the treated glasses differed from that of the as-received glasses, but was very similar to that exhibited by specimens of vitreous silica. Crack morphologies, obtained by examining cross-sections of the indentations, revealed that there is a consistent difference between the crack-formation characteristics of the untreated and treated surfaces.

I. INTRODUCTION

Heat treating alkali-containing glasses in atmospheres containing SO_2 gas causes partial or total removal of alkali from the surface. The extent of this alkali removal can be controlled by the treatment temperature, time, and the presence and concentration of water in the treatment atmosphere [1,2]. As a result of the selective removal of alkali, a surface layer which is rich in silica [3] is produced. This, according to Hench and Clark [4], corresponds to a Type II surface, which is a type of glass surface that is known to have improved chemical durability [5]. The strength of the glass has also been reported [2] to increase with SO_2 treatments. The surface mechanical properties of SO_2 -treated glasses, on the other hand, have not been extensively studied. The objective of this study was to determine the microhardness and crack-initiation behavior of SO_2 -treated float glass using recording microindentation.

II. EXPERIMENTAL PROCEDURES

A commercial float glass was used in the treatments performed in this study. SO_2 treatments were done in a silica tube furnace at three temperatures in the glass transformation temperature range (500, 550, and 600 ^oC) for treatment durations of 5, 30 and 60 minutes. For the treatments, SO_2 gas was mixed (~4-6 vol% of the air flow) either with dry air or with air containing water, the latter being produced by bubbling the dry air through distilled water at ~60 C to give ~20 vol.% water in air. The flow rate of SO_2 gas was maintained at 40cc/min throughout the treatment. After the process, samples were cooled in air, and the chemical residue (referred to as the bloom) formed on the surface was washed off using hot distilled water. The samples were stored in a dessicator until further tests were done.

Indentations for surface hardness measurements and for crack-initiation studies were done using a self constructed recording microindenter [6]. Measurements were performed at 0.5N maximum load for hardness determinations, and 10N maximum load for crack-initiation studies. Loading rates of 0.1 mlsec were used for 0.5N tests and 0.2µm/sec for the 10N tests, with no holding time at the maximum load. Approximately 12 measurements for hardness evaluations and 5 measurements for crack-initiation studies were taken at different locations on every specimen. The hardness average of 10 of these was calculated, after neglecting the maximum and minimum values obtained.

Three different methods were used for the calculations of recording microindentation hardness, namely the LVH, L_2VH [7], and LVH_2 [8] values. Briefly, LVH corresponds to the Vickers hardness which is determined at the maximum applied load. The L_2VH and LVH_2, which are "load independant" hardness evaluations, are based on the loading part of the graph of indentation load vs penetration, which is produced by recording the load and the corresponding depth of penetration of the indenter during loading and unloading of the indenter.

Crack-initiation studies were done using an acoustic emission device (Physical Acoustics Corp., LOCAN-AT), by monitoring the acoustic activities during the loading and unloading cycles by having a transducer in contact with the sample. Acoustic events (caused by crack formation) were recorded as a function of load. 10N and 20N loads with 10 seconds of holding time at the maximum load were applied for the crack-morphology investigation. This was done using a commercial microindenter (Shimadzu, HMV-2000). Cross-sectional views of indentations made for the as-received and SO_2-treated surfaces were investigated using an optical microscope. The cross-sections of the indentations were obtained by liningup a series of indentations in front of a previously made scratch and then bending the samples along the line containing the scratch and the indentations until fracture occurred.

III. RESULTS AND DISCUSSION

i. Recording Microhardness: Figures 1 (a) to (c) show the effects of treatment condition (SO_2 gas mixed with dry air or wet air (~20% water) on the microhardness values (LVH, L_2VH, and LVH_2) for float glass. The average error for the measurements, not given in the curves, is in the 5-7% range.

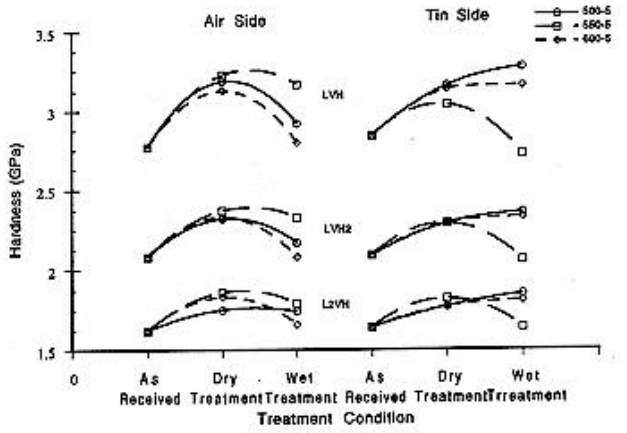

(a)

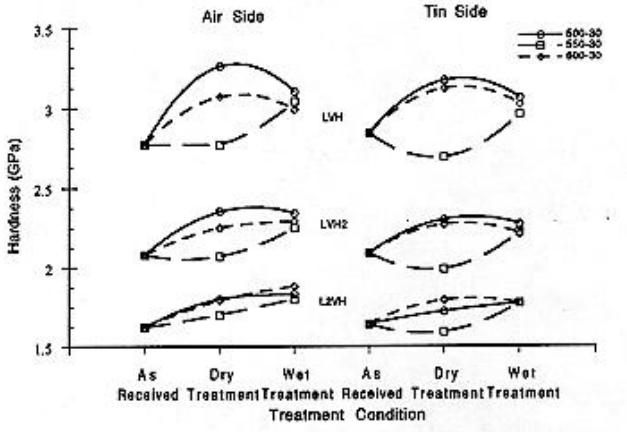

(b)

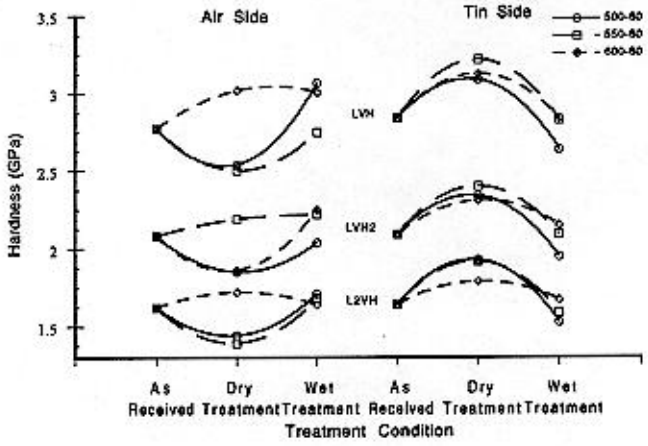

(c)

Figure 1. LVH, L_2VH, LVH_2 hardness of the air and tin sides of float glass with respect to the treatment conditions and temperature for (a) 5 minutes (b) 30 minutes and (c) 60 minutes treatment times.

According to the two figures, the curves show various trends in hardness with treatment. Statistical analysis (Analysis of Variables Test) indicates that there is an increase in the hardness with treatment. When the different hardness calculations are considered, the significant factors having an influence on the data are found to be changing. Specifically, the LVH values indicate time, temperature, treatment atmosphere, and glass side as the significant factors influencing the variations in the data. However, with LVH_2, atmosphere effects are found to be insignificant, and with L_2VH temperature effects are insignificant. Overall, the 60-minute treatment duration and the two sides of the float glass do not give any significant differences in hardness. The dry treatments are influential on improving the hardness, whereas the treatments at 550^oC cause no significant changes, even though these factors are significant at other temperatures. Statistical evaluations have also indicated the hardness data calculated using the LVH2 method to be the least biased from errors.

The above results suggest that the samples subjected to SO_2 treatment at elevated temperatures have increased hardness, regardless of which calculation method is applied. Considering that the LVH_2 method uses the entire loading curve for calculating the load-independent hardness [8], and that the errors are low, as indicated from the statistical evaluations, two treatment parameters were found to be the most important factors affecting the hardness, namely time and temperature. Note that long treatment times and temperatures in the glass transition range do not improve the hardness. Treatments must be performed at temperatures above and below the glass transition range and for short periods of time in order to improve the hardness.

ii. Crack Initiation: Figure 2 shows the cumulative number of cracking events during the loading cycle of the recording microindentation for the as-received and SO_2 -treated float glasses, as well as for a silica glass. From the acoustic emission studies performed on specimens that were treated at the same conditions used in studying hardness, it is recognized that the same number of cracking events was recorded for all the surfaces. Thus, the data shown in the figure represent average values for all SO_2 -treated glasses.

According to this figure, the soda-lime-silica glass (the untreated float glass) shows no cracking during loading, whereas silica glass has an average of 18 total cracking events. The cracking results for SO_2 -treated glass lie between those for silica and soda-lime-silica glass. It should also be noted that the initiation load of the cracks for vitreous silica and SO_2 -treated glass is below 2.5N (which is less than 25% of the maximum load). Hence, in terms of the crack-initiation characteristics and the number of cracking events during Vickers indentation loading, the SO_2 treatment can be said to cause the surface to act more like a silica glass. This, in fact, supports results presented earlier, based on measurements made using infrared spectroscopy [3], that show the surface to be high in bridging-oxygen concentration.

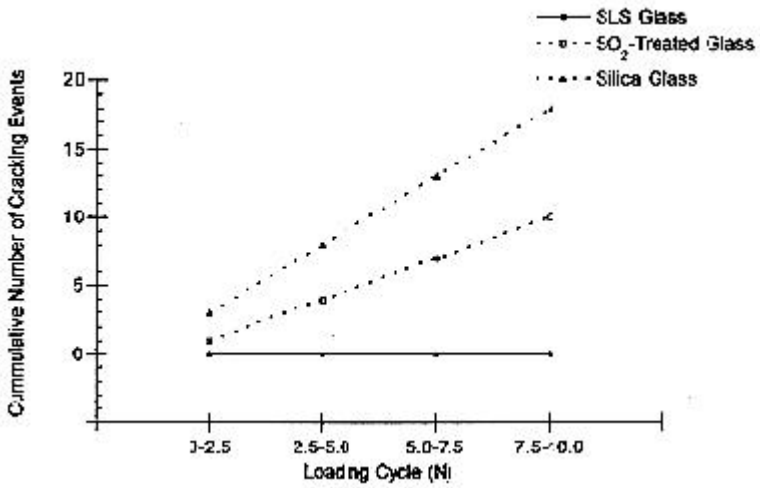

Figure 2. Cumulative number of cracking events during indentation loading for vitreous silica, untreated soda-lime-silica (float), and SO_2 -treated float glass.

iii. Fractography: Figures 3 and 4 show the cross-sectional views of the indentations done at maximum loads of 10 and 20N (with 10 seconds of holding time at the maximum load) for a non-SO_2 -treated and an SO_2 -treated glass, respectively. The crack-pattern studies for the glasses treated under the different conditions (with different temperature, time, glass side and atmosphere water) show a similar fracture pattern, which will be discussed below. This similarity agrees with the results of the crack-initiation studies, in which no significant differences among the treatment conditions were recognized.

The two figures illustrate the differences in the type of crack development that occur during indentation; the untreated glass (Figure 3) exhibits a penny crack for both the 10 and 20N indentations which grows into a half penny geometry. Lateral cracks are also seen to extend from the bottom of the indentation. It is not, however, clear from this picture, at what time or at what load during the indentation cycle the different types of cracks developed. It has been shown for a float glass [9] that a critical load is reached between 10N and 15N, which causes penny cracks to generate. It is most likely that this formation happens during the loading cycle, since there are high tensile stresses directly under the indenter, as well as compressive stresses. The penny crack grows into the half-penny geometry during the unloading stage, driven by residual stresses resulting from inelastic deformation in a zone immediately surrounding the indentation.

With the treated glass surfaces, the acoustic emission studies indicate that there are a number of cracking events during loading. Figure 4 illustrates cross-sections of indentations from a treated surface, at 10 and 20N loads, where a half-penny crack is seen for both cases, but with no penny crack. Lateral and median cracks are also recognized in the figure. It has been suggested [9] that the surface condition of the glass plays an important role in cracking produced by sharp indenters. With the dealkalized surface having a silica-like structure, the initial tensile forces created during the early stages of the indentation loading are at a high enough to level to cause cracks to nucleate and grow from the surface and to immediately
form the half-penny crack geometry without penny crack formation. As a matter of fact, crack initiation for both vitreous silica and treated glass was shown to be at loads below 2.5N,

reinforcing the idea that the silica-like surface has caused the cracks to start from the surface. Thus, even with the increased loads, the treated glass does not form the penny cracks.

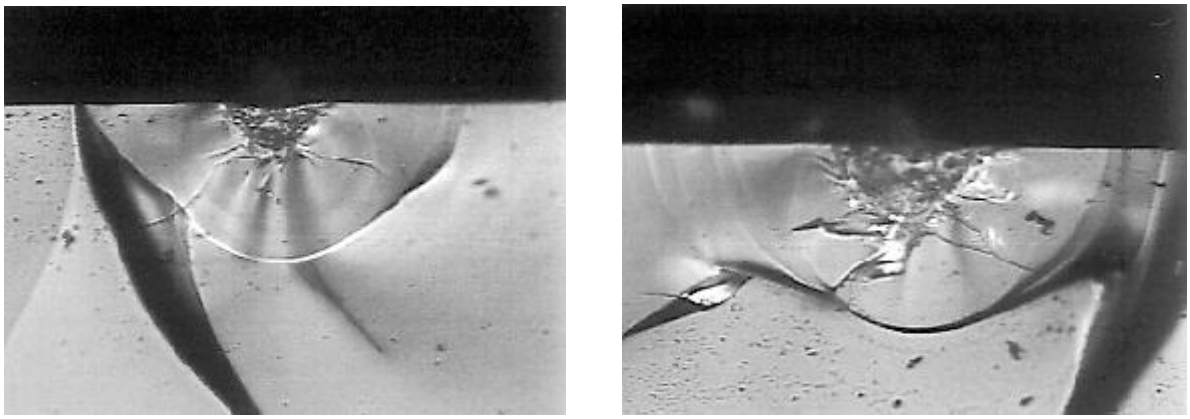

a b

Figure 3. Cross-section indentations on a non-SO_2 -treated glass, for (a) 10N and (b) 20N loading, using reflected light, bright field conditions (horizontal length of the image is 0.32mm)

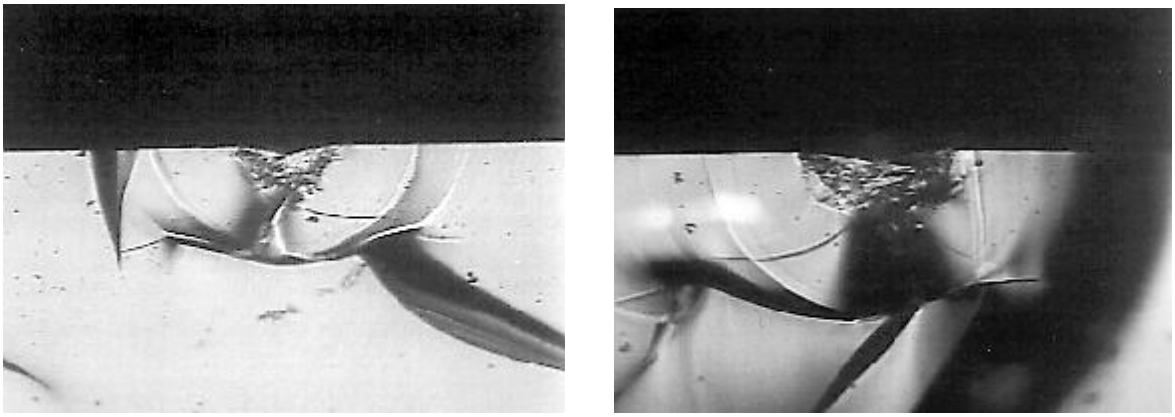

a b

Figure 4. Cross-section indentations on an SO_2 -treated glass, for (a) 10N and (b)20N loading, using reflected light, bright field conditions (horizontal length of the image is 0.32mm)

IV. CONCLUSIONS

SO_2 -treatment was recognized to improve the microhardness of float glass. Time and temperature are the two important parameters affecting the changes in hardness. Crack initiation characteristics during recording microindentation was also influenced by the treatment; cracks were observed to initiate during the loading of the indenter, these cracks had half-penny morphology.

Acknowledgment

The financial support of the NSF Industry/University Center for Glass Research at the NYS College of Ceramics at Alfred University is gratefully acknowledged.

REFERENCES

1. R.W. Douglas and J.O. Isard, "The Action of Water and of Sulfur Dioxide on Glass Surfaces," J. Soc. Glass. Tech., 33 (1949) 289.
2. J.N. Coward and W.E.S. Turner, "The Clouding of Soda-Lime-Silica Glass in Atmospheres Containing Sulfur Dioxide," J. Soc. Glass. Technol. 22 (1938) 309.
3. U. Senturk, D.H. Lee, R.A. Condrate, and J.R. Varner, ATR-FTIR Spectral Investigation of SO_2 -Treated Float Glass," (in press) in M.R.S. Symposium Proceedings, Vol. 407, edited by H.Z. Cummins, D.J. Durian, D.L. Johnson, and H.E. Stevens,1996.
4. L.L. Hench and D.E. Clark, "Physical Chemistry of Glass Surfaces," J. Non-Cryst. Solids 28(1978) 83.
5. H.R. Persson," Improvement of the Chemical Durability of Soda-Lime-Silica Glass Bottles by Treating With Various Agents," Glass Technol., 3(1962) 17.
6. T.M. Cleary and J.R. Varner, "Effects of Surface Treatments on Crack Initiation in Glasses," Glasstech. Ber. G/ass Sci. Technol.,68 C1(1995) 295.
7. F. Frolich, P. Grau, and W. Grellman,"Performance and Analysis of Recording Microhardness Tests," Phys. Status Solidi. A,42 [79] (1977) 79.
8. H.J. Weiss,"On Deriving Vickers Hardness from Penetration Depth," Phys. Stafus Solidi. A,99 [2] (1987) 491.
9. T. Haranoh, H. Ishikawa, N. Shinkai, and M. Mizuhashi, Crack Evolution in Vickers Indentation for Soda-Lime-Silica Glass," J. Mater. Sci.,17(1982) 1493.

EVALUATION OF DISCRETE ORDINATES AND DISCRETE TRANSFER METHODS FOR RADIATIVE TRANSFER IN RECTANGULAR FURNACES

Nevin Selçuk and Nuray Kayakol
Middle East Technical University, TURKEY

Abstract

Two of the most popular radiation models suitable for incorporation into CFD codes, namely Discrete Transfer Method (DTM) and Discrete Ordinates Method (DOM) were applied to the predictions of the radiative heat flux density and source term of a box-shaped enclosure problem based on data reported previously on a large-scale experimental furnace with steep temperature gradients typically encountered in industrial furnaces. The rectangular enclosure under consideration has interior black walls and an absorbing-emitting medium of constant properties. Radiation codes were developed for DTM and DOM. The effects of order of approximation (S_2 and S_4), angular quadrature (S_n and $S_{n\text{э}}$) and spatial differencing schemes (diamond, variable-weight and exponential), on the predictive accuracy of the DOM were investigated. Both methods were evaluated from the viewpoints of both predictive accuracy and computational economy by comparing their predictions with exact solutions available for the same enclosure problem. Comparative testing shows that the S_4 approximation produces better accuracy in radiative energy source term than in flux density in 3 orders of magnitude less CPU time than that required by the DTM, therefore proves to be an accurate and computationally more efficient method for use in conjunction with CFD codes. Order of approximation plays a more significant role than angular quadrature and spatial differencing schemes in the predictive accuracy of the DOM.

Nomenclature

A, B, C	control volume face areas in x, y, z direction, m^2	Subscripts	
d	slope of the axial temperature curve	burner	burner wall
E	emissive power, W m^{-2}	bw	black wall
I	radiant intensity, W $m^{-2}sr^{-1}$	e	end-face
k_a	gas absorption coefficient, m^{-1}	end	end wall
L	half of the side lengths of the rectangular enclosure, m	g	gas
		n	control volume or gridcell; order of approximation
l	direction cosines		
q	radiative heat flux, W m^{-2}	i	inlet
q_{net}	net radiative heat flux, W m^{-2}	m	discrete direction
r	position vector	max	maximum
S	radiative energy source term, W m^{-3}	o	reference value; emerging

T	temperature, K
v_p	volume of pth control volume, m^3
w_m	weight function in a direction m, m^2
x y, z	co-ordinate axes in Cartesian geometry
z'	dimensionless axial distance

Greek symbols

α	finite-difference weighting factor
θ	polar angle
μ, η, ξ	direction cosines in x, y, z directions
σ	Stefan-Boltzmann constant
τ	optical thickness
ϕ	azimuthal angle
Ω	direction vector of radiant intensity

Superscripts

+	leaving
-	arriving
~	dimensionless

p	control volume centre
r	reference-face; impinging
side	side wall
w	wall

Abbreviations

CFD	computational fluid dynamics
DOM	discrete ordinates method
DTM	discrete transfer method
DT16	DTM using 16 ray per wall node
DT64	DTM using 64 ray per wall node
DT144	DTM using 144 ray per wall node
DDS	dimond difference scheme
EXPS	exponential scheme
RTE	radiative transfer equation
VWDS	variable-weight difference scheme
RTE	radiative transfer equation
VWDS	variable-weight difference scheme

1. Introduction

Ever-increasing consumption rate of limited energy sources on one hand and environmental concern over the reduction of combustion-generated pollutant emission on the other, necessitates improvement of thermal and emission performances of combustion systems burning natural gas oil and coal. This can be achieved by developing mathematical models which could eventually be used for the design of environmentally acceptable combustion systems with improved energy efficiency. Thermal radiation is the predominant mode of heat transfer at high temperatures encountered in most industrial combustion chambers. Therefore, an adequate treatment of thermal radiation is essential to develop a mathematical model of combustion systems.

The exact (analytical or numerical) solution of integro-differential radiative transfer equation (RTE) is generally a formidable task. Although there have been a few attempts to formulate RTE for non-isothermal rectangular enclosures [1, 2], explicit solutions are only available for simplified situations such as black walls and constant properties etc. [3,

4]. Nevertheless exact solution even for these simplest systems are needed, as they can serve es benchmarks against which the accuracy of approximate solutions are tested.

There is growing interest in approximate multidimensional radiative heat transfer models mainly in response to the need for accurate, flexible and computationally economic models which couple easily with the differential equations governing the transport of mass, momentum, species and energy in comprehensive numerical models for turbulent, reacting and radiating flows.

Available approximate solution methods can be classified into four groups: Hottel's zone method, Monte Carlo methods, f1ux-type methods and the DTM which combines virtues of the first three.

The Hottel's zone method and the Monte Carlo technique have long been accepted as the most accurate methods for calculating radiative transfer. These traditional methods, however, have not found application in comprehensive combustion modeling due to their large computational time and storage capacity. At the same time, neither of these models requiring the solution of simultanenus algebraic equations are compatible with the solutions of the differential equations governing the transport of mass, momentum, species and energy in comprehensive numerical models.

The so-called flux methods which provide an alternative but less accurate method of solution converts the integro-differential equation into differential equations by discretization of angular variation of radiative intensity [5, 6, 7]. Being differential in form these equations are ideally suited to numerical solution simultaneously with the flow equations. Therefore, flux methods offer a very high degree of computational economy and for this reason they have been widely employed in combustion models. All conventional flux methods suffer from the difficulty in application to complex geometries whereas some of them suffer from inadaquate number of directional fluxes and a lack of coupling between these fluxes. The DOM which conceptually is an extension of flux methods, corrects these defects. The DOM achieves a solution by solving the exact RTE for a set of discrete directions spanning the angle range of 4π. Apart from the obvious ease with which the method can be incorporated into Computational Fluid Dynamics (CFD) calculations, it is relatively easy to code and requires single formulations to invoke higher order approximation. This method was first suggested by Chandrasekhar [8] for one-dimensional astrophysics problems. More recently, Carlson end Lathrop [9] developed the DOM to solve multi-dimensional neutron transport problems. Over the past decade, the method has been applied to one [10,11] and multi-dimensional [12-21] rediative heat transfer problems.

In response to the need for an accurate, flexible and computationally economic models, Discrete Transfer Method (DTM) has been developed as an hybrid method which combines certain features of Hottel's zone, Monte Carlo and flux-type methods. DTM is based on the solution of RTE for representative rays that will travel through the considered domain in selected directions. To this extend, it is related to Monte Carlo

methods but the directions of rays are specified by choosing the values of polar and azimuthal angles instead of being chosen at random and they are solved for only along the paths between the two boundary walls rather than being partially reflected at walls and tracked to extinction. The key to DTM is the discretizetion of solid angle into a number of elements within which the intensity is presumed constant. This feature is shared by flux-type methods. DTM is distinguished from the flux methods which solve a coordinate-system-based partial differential equation by being founded on a direct solution of RTE itself. In DTM as in case of Hottel's zone method, the enclosure is subdivided into many cells. Performing of radiation balances on cells for the calculation of energy source term relates DTM to zone method, but lengthy prior calculations of zone exchange factors are evoided in DTM method because this information is implicit in the known intensity in specified directions. DTM also offers other advantages such as simplicity of concept, ease of application to complex geometries [22]. It has been extensively used as a part of combustion models predicting the performance of various industrial chambers [23-27].

Previously published multi-dimensional evaluations of the accuracy of the DOM and DTM have taken three forms:

1) They have been employed as part of a complete prediction procedure : The predicted temperature distributions have been compared with experimentally determined data [12,27]. Discrepancies between predicted and measured values may be partly due to the errors in the experimentally determined data; even if the experimentally determined data are correct, it is impossible to decide whether discrepancies in the predicted temperature and radiative heat flux distributions are attributable directly to the radiation model employed or to inaccuracies in the models used for the prediction of flow, reaction, etc.

2) The accuracy of the radiation models have been tested in isolation from the modeling of other physical processes. Testing has taken two forms: i) The models have been employed by using prescribed radiative energy source term distributions (zero [14, 15, 22] or uniform [14, 16, 17, 29]) and comparing the predicted temperature and radiative heat flux distributions with the Hottel's zone method, Monte Carlo or exact solutions. This procedure for the evaluation of the accuracy of the models suffer from two major disadvantages, (a) even if acceptably accurate predictions are obtained for the uniform source term distributions, there is no certainty that similarly accurate predictions will be produced for the highly non-uniform distributions encountered in operating furnaces and combustors (b) considering the iterative sequence of solution in complete prediction procedure, input data provided should be temperature distributions, and the predicted and tested quantities should be radiative heat flux and radiative energy source term distributions. ii) The model hes been tested by using prescribed temperature distributions (uniform [18,16,15, 28] or non-uniform [16,17, 19, 22, 30]) and comparing the predicted heat flux distributions with those predicted by the Hottel's zone method. This procedure has two drawbacks: (a) Although uniform temperature distributions are computationally convenient they do not even approximately represent the extremely non-uniform distributions encountered in operating furnaces and combustors, (b) The use of the Hottel's zone method for testing the radiative heat flux distributions of an enclosure problem with steep temperature gradients requires finer zoning, which can be computationally inefficient due to extensive machine storage capacity and time.

What is required at the present time is testing the accuracy and computational economy of the two radiation models, namely the DOM and the DTM4, extensively used as part of complete prediction procedures in the past decade, in isolation from the models of flow and reaction on problems with highly non-uniform gas temperature distribution typical of operating fumaces. Assessment of the predictive accuracy of the DOM and the DTM have been reported in detail in an earlier papers [21, 31,32].

In this paper, these radiation models are applied to the predictions of the radiative heat flux density and source term of a box-shaped enclosure prublem. The problem is based on data reported previously on a large-scale experimental furnace with steep temperature gradients. The radiation models are tested from the points of view of both predictive accuracy and computational economy by comparing their predictions with exact values reported previously [3].

2. The Radiation Models

The physical situation to be considered is that of an enclosure containing an absorbing-emitting, non-scattering radiatively gray medium whose absorption coefflicient is the same at all points, and of known magnitude. Values of black-body emissive power are assumed to be available at all points within the enclosed medium and at all points on the interior bounding surfaces of the enclosure which are assumed to be black.

The radiative heat transfer equation for a ray of intensity $I(r, \Omega)$ in a gray absorbing-emitting medium is given by

$$dt/ds=-k_aI+k_aI_b \qquad (1)$$

where I is the radiant intensity in the direction of s, s is the distance traversed by the ray, k_a is the absorption coefficient and I_b is thc black body intensity of the gas at temperature T_g (Fig. 1). This equation simply states that the change in intensity I over the path length ds expressed by the left hand side of the equation is due to the loss by absorption, the first term of the right hand side, and the gain by emission of the medium, the second term on the right hand side.

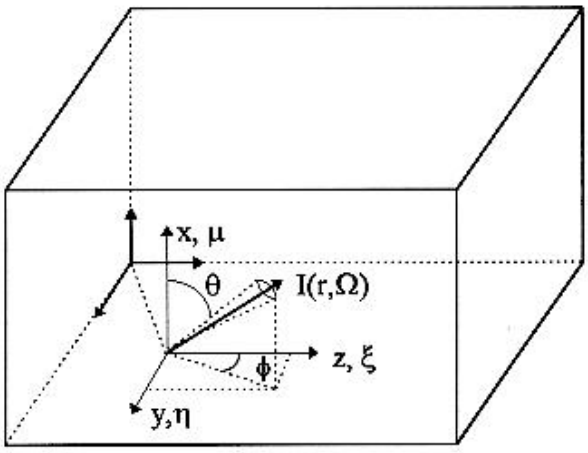

Fig. 1. Coordinate system

2.1. Discrete Transfer Method (DTM)

The DTM is based on solving Equation (1) for representative rays that will travel through the considered domain. The directions of rays are specified in advance (the values of the polar and azimuthal angle, θ end ϕ, are established, Fig. 2) and they are traced along the paths between two boundary walls (Fig.3a) The enclosure is subdivided into control volumes or cells. The intensities along each of chosen directions are solved for, and the values of intensities entering and leaving each cell are calculated (Fig. 3b).

Integration of Equation (1) analytically along the ray yields recurrence relation

$$I_{n+1}= I_n \exp(-k_a s)+ I_b (1-\exp(-k_a s)) \quad (2)$$

where I_n and I_{n+1} are respectively the intensities entering and leaving any control volume, or grid cell n.

Initial intensity I leaving a wall point initiate the use of recurrence relation (Equation 2). Consider the special case of black enclosure walls at prescribed temperature T_w. The intensity leaving a wall is simply

$$I_o =\sigma T_w^4 /\pi \quad (3)$$

The net radiation heat flux on a wall is given by

$$q_{net}= q^+ - q^- \quad (4)$$

where q^+ and q^- are leaving and arriving wall heat fluxes respectively. From known wall temperature q^+ can be found as follows

$$q^+ = \pi I_o \qquad (5)$$

Incident flux q^- is calculated from the integration of incoming intensities over the hemisphere.

$$q^- = \int_{2\pi} I \cos\theta \, d\Omega \qquad (6)$$

where Ω is the solid angle, $d\Omega$ is the discretised portion and θ is the angle between incident intensity and the surface normal. In enclosures with black surfaces, since q^+ is independent of q^- the net heat flux can be obtained in one step by calculating incident flux q^- . For the evaluation of q^- the integration (Equation 6) is discretised into a number of small solid angles. The ray is fired knowing its the position and direction. By simple geometrical consideration, the distance the ray travels in all control volumes in its path is calculated. Then, intensity I in each discretised portion, is obtained by applying the recurrence relation repeatedly along its path between the walls of the enclosure under consideration.

The radiative source term can be obtained by accumulating the energy left behind pencils of rays as they cross the control volumes. The energy accumulation in a control volume n after a pencil of rays passed through can be written as

$$S=(I_{n+l} - I_n) \, dA \cos\theta \, d\Omega \qquad (7)$$

It is considered that the pencil of rays emitted from the surface elemcnt dA in the solid angle $d\Omega$ crosses the control volumes as if all the energy were concentrated in the center of pencil of rays.

2.2. Discrete Ordinates Method (DOM)

The discrete ordinates representation of RTE for an absorbing-emitting gray medium in a rectangular coordinate system can be written (Fig.1)

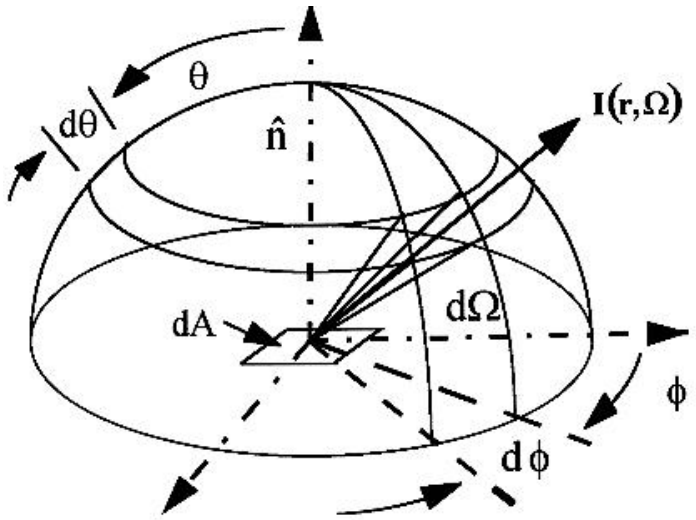

Fig.2 Typical ray travelling from a wall hemisphere

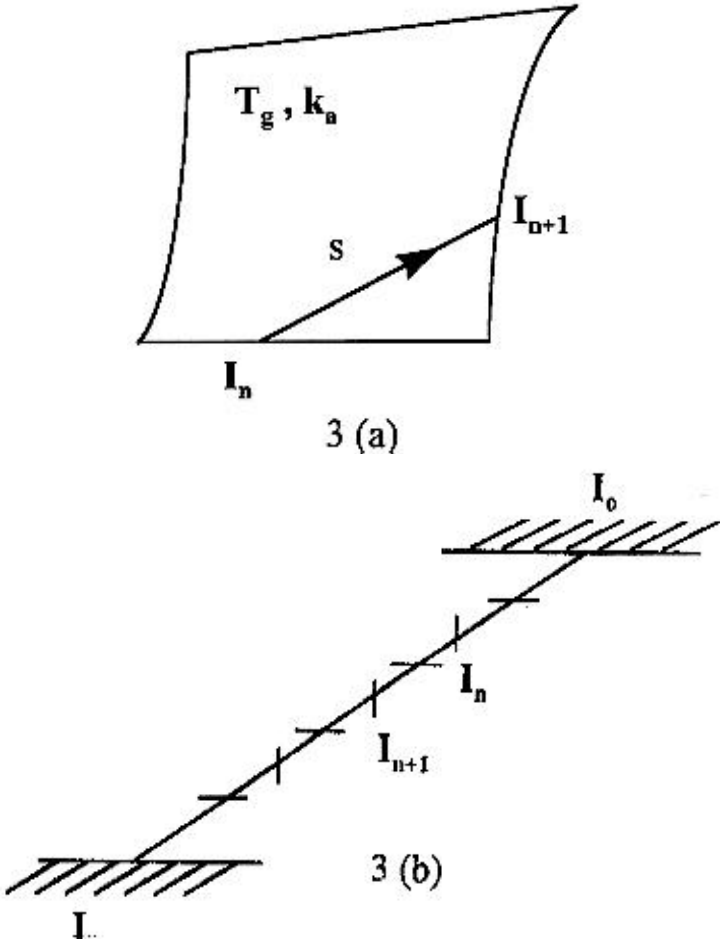

Fig. 3 Representative direction traversing a) a grid cell; b) the grid walls

$$\mu_m (\partial I^m / \partial_x) + \eta_m (\partial I^m / \partial_y) + \xi_m (\partial I^m / \partial_z) = -k_a I^m + k_a I_b \quad (8)$$

where $I^m[\equiv I(x, y, z ; \mu_m, \eta_m \ \xi_m)]$ is the total radiation intensity at position (x,y,z) in the discrete direction Ω_m ($\mu_m = \cos\theta$, $\eta_m = \sin\theta \sin\phi$, $\xi_m = \sin\theta \cos\phi$), k_a absorption coefficient of medium, I_b the total blackbody radiation intensity at the temperature of the medium. If the surface bounding the medium is assumed to be black, the" the radiative boundary condition for equation (8) is given by

$$I^m = I_{bw} = \sigma T^4_w / \pi \quad (9)$$

where I_{bw} is the blackbody radiation intensity at the temperature of the surface, T_w. Equation (8) and (9) represent m coupled partial differential equations for the m intensities, I^m.

The finite-difference form of equation (8) can be obtained by multiplying equation (8) by dx·dy·dz and integrating over the control volume as follows

$$\mu_m A\left(I^m_{xe} - I^m_{xr}\right) + \eta_m B\left(I^m_{ye} - I^m_{yr}\right) + \xi_m C\left(I^m_{ze} - I^m_{zr}\right) = -k_a v_p I^m_p + k_a v_p I_b \quad (10)$$

where I^m_p is cell-center intensity and $I^m_{xr}, I^m_{xc}, I^m_{yr}, I^m_{ye}, I^m_{zr}, I^m_{ze}$ are the intensities at each face of control volume. If the face intensities I^m_{xr}, I^m_{yr} and I^m_{zr} are assumed to be known from boundary conditions for a control volume adjacent to a boundary of the enclosure, following relationships [14] can be used to eliminate the unknown face intensities I^m_{xc}, I^m_{ye} and I^m_{ze} in equation (10).

$$I^m_p = \alpha I^m_{xc} + (1-\alpha) I^m_{xr} \quad (11)$$

$$I^m_p = \alpha I^m_{yc} + (1-\alpha) I^m_{yr} \quad (12)$$

$$I^m_p = \alpha I^m_{ze} + (1-\alpha) I^m_{zr} \quad (13)$$

Diamond and Variable-Weight Spatial Differencing Schemes

Finite-difference weighting factor, α assumes values in the range $0.55 \le \alpha \le 1$. Diamond Difference Scheme,(DDS), $\alpha = 0.5$, is based on the assumption of linear variation of the radiation intensity within each control volume. As is reported in the literature [33], it is spatial and gives oscillatory (positive negative) solutions that propagate throughout the spatial domain. The size of control volume should be made small enough to avoid negative and oscillatory radiation intensity. However, even with a small control volume,

this problem may occur if there is a significant difference between the radiation intensity values on the adjacent faces of control volume as in the case of an enclosure with one hot and three cold black walls. Therefore, it is necessary to employ negative intensity fix-up procedure (switch-to-step scheme (α=1.0), [14]) for DDS when negative intensity is encountered.

Variable-Weight Difference Scheme (VWDS) on the other hand, assigns a uniform finite-difference weighting factor α for all directions by increasing α from 0.5 up to 1.0 until no negative intensity is encountered in any direction.

With DDS and VWDS, solving Eq. (10) for cell-center intensity, I_p^m may be evaluated as

$$I_p^m = \frac{\mu_m A I_{xr}^m + \eta_m B I_{yr}^m + \xi_m C I_{zr}^m + \alpha k_a v_p I_b}{\mu_m A + \eta_m B + \xi_m C + \alpha k_a v_p} \qquad (14)$$

where

$$A=\Delta y\,\Delta z,\ B=\Delta x\,\Delta z,\ C=\Delta x\,\Delta y \qquad (15)$$

Exponential Spatial Differencing Scheme

Finite-difference weighting factor, α for exponential scheme (EXPS) is

$$\alpha_m=[1-\exp(-\tau_m)]^{-1}\,[\tau_m]^{-1} \qquad (16)$$

where τ_m ($k_a\,\Delta x/\mu_m$, $k_a\,\Delta y/\eta_m$, $k_a\,\Delta z/\xi_m$ for x,y,z coordinates, respectively) is the cell optical thickness along each direction m. Therefore, with EXPS, solving Eq. (10) for cell-center intensity, I_p^m may be evaluated as

$$I_p^m = \frac{\mu_m A I_{xr}^m + \eta_m B I_{yr}^m + \xi_m C I_{zr}^m + k_a v_p I_b}{\mu_m A/\alpha_m + \eta_m B/\alpha_m + \xi_m C/\alpha_m + k_a v_p} \qquad (17)$$

For all spatial differencing schemes every I^m value on every cell-center and faces of control volume can be computed by stepping from control volume to control volume. The direction of recursive evaluation is in accord with the direction of physical propagation of radiation beam as defined by ($\mu_m\eta_m\xi_m$).

Once the intensity distribution is determined, quantities of interest such as radiative flux and energy source term distributions can be readily evaluated. The net radiation heat flux on a wall is calculated as

$$q_{net} = \sigma T_w^4 - \sum_m w_m \ell]^m \tag{18}$$

The radiative energy source term distribution for problems where prescribed temperature distribution is available can be expressed as

$$S = k_a (4\pi I_b - \int_{4\pi} I d\Omega) = k_a (4\pi I_b - \sum_m w_m]_p^m) \tag{19}$$

3. TEST PROBLEM

The accuracy of DTM and DOM for three-dimensional radiative heat transfer has been assessed by applying this radiation model to the prediction of distributions of radiative flux density and radiative energy source term of a rectangular enclosure problem and by comparing its predictions with exact solutions produced previously [3]. The rectangular enclosure under consideration has interior black walls and an absorbing-emitting medium of constant properties. The problem is based on data reported by Strömberg [34] on a large-scale experimental furnace with steep temperature gradients typically encountered in industrial furnaces.

The experimental furnace under consideration is horizontal, of tunnel type with a square cross-section. It is fired horizontally from the center of left end wall, which is the burner wall, with the mixture of oil and gas with no swirl, and operates at atmospheric pressure. The four side wells are water cooled, and the burner and back end walls are refractory. Table 1. shows the complete dimensionless data obtained from the experimental furnace and used as input data for both the exact solution and DTM and DOM computer programs.

The temperature of the gases at any point within the enclosure were calculated by using Eqs. (11) and (20), together with either of Eqs. (26) and (29) of reference [3] depending on the z' value of the point under consideration. A detailed description of data obtained from experimental furnace and used as input data for the exact solution and the S_n method can be found elsewhere Strömberg [34].

Table l. Dimensionless data fed to the exact solution and DTM and DOM program

Dimensions of the furnace	$\tilde{L}_x = 1, \tilde{L}_y = 1, \tilde{L}_z = 6$
Optical thickness	$\tau_o = 1/6$
Wall black body intensities	$(\tilde{I}_{bw})_{side} = 0.0020$ $(\tilde{I}_{bw})_{burner} = 0.0574$ $(\tilde{I}_{bw})_{end} = 0.0167$
Gas temperatures	$\tilde{T}_i = 0.1775$ $\tilde{T}_e = 0.6222$ $\tilde{T}_{max} = 1$
Position of the peak	$z'_{max} = 0.8$
Slope of gas temperature distribution at furnace exit	$d_e = -0.220$

Reference values used to make the experimental data dimensionless;
L_o=0.48 mT_o=1673 K, E_o=4.4419x10^5 Wm^{-2}, I_o=1.4139 x 10^5 Wm^{-2} sr^{-1}

3.1. Numerical Solution Procedure

The test enclosure has been subdivided into 4x4x24 control volumes in x, y, z directions, respectively. This was the number of control volumes for which exact solutions were almost grid-independent [3].

DTM predictions were obtained for 16, 64 and 144 rays per wall node. The numerical solution procedure for DOM has been based on the method of Carlson and Lathrop [9]. Radiation codes were developed based on S_2 and S_4 discrete ordinates approximations which involve solving the radiation transport equation in 8 and 24 directions, respectively. S_2 and S_4 predictions using DDS, VWDS and EXPS and two angular quadrature schemes (S_n and $S_{n э}$ [9]) were evaluated against exact solutions. The quadrature ordinates and weights for S_n approximations are listed in Table 2.

Table 2. S_n arld $S_{n'}$ angular quadrature schema [9] for the first octant

Designation	Ordinates			Weight
	μ_m	η_m	ξ_m	w_m
S_2	0.7071070	0.5000000	0.5000000	1.5707963
S_4	0.9082483	0.2958759	0.2958759	0.5235987
	0.2958759	0.9082483	0.2958759	0.5235987
	0.2958759	0.2958759	0.9082483	0.5235987
$S_{2'}$	0.5773503	0.5773503	0.5773503	1.5707963
$S_{4'}$	0.8819171	0.3333333	0.3333333	0.5235987
	0.3333333	0.8819171	0.3333333	0.5235987
	0.3333333	0.3333333	0.8819171	0.5235987

4. EVALUATION OF THE RADIATION MODELS

In the discussion that follows, all physical quantities are expressed in dimensionless forms which are obtained by dividing them by the shortest dimension of the enclosure or by the maximum emissive power of the gas, depending on the quantity.

4.1. Flux Density Distributions

Fig.4 illustrates the comparison between the colour countours for dimensionless radiative flux density to the side wall in the positive x-direction predicted by DTM for 16 and 64 rays per wall node (DTl6 and DT64), DOM for S_2 and S_4 and DDS and exact solution. As can be seen from the figure, DT64 produces slightly better accuracy than S_4.

The effects of order and spatial differencing scheme on the colour contours for dimensionless radiative flux density predicted by DOM are illustrated together with exact contours in Fig 5. As can be seen from the figure, better agreement is obtained with S_4 with VWDS.

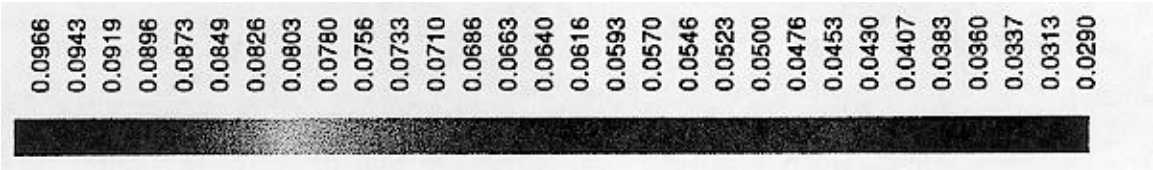

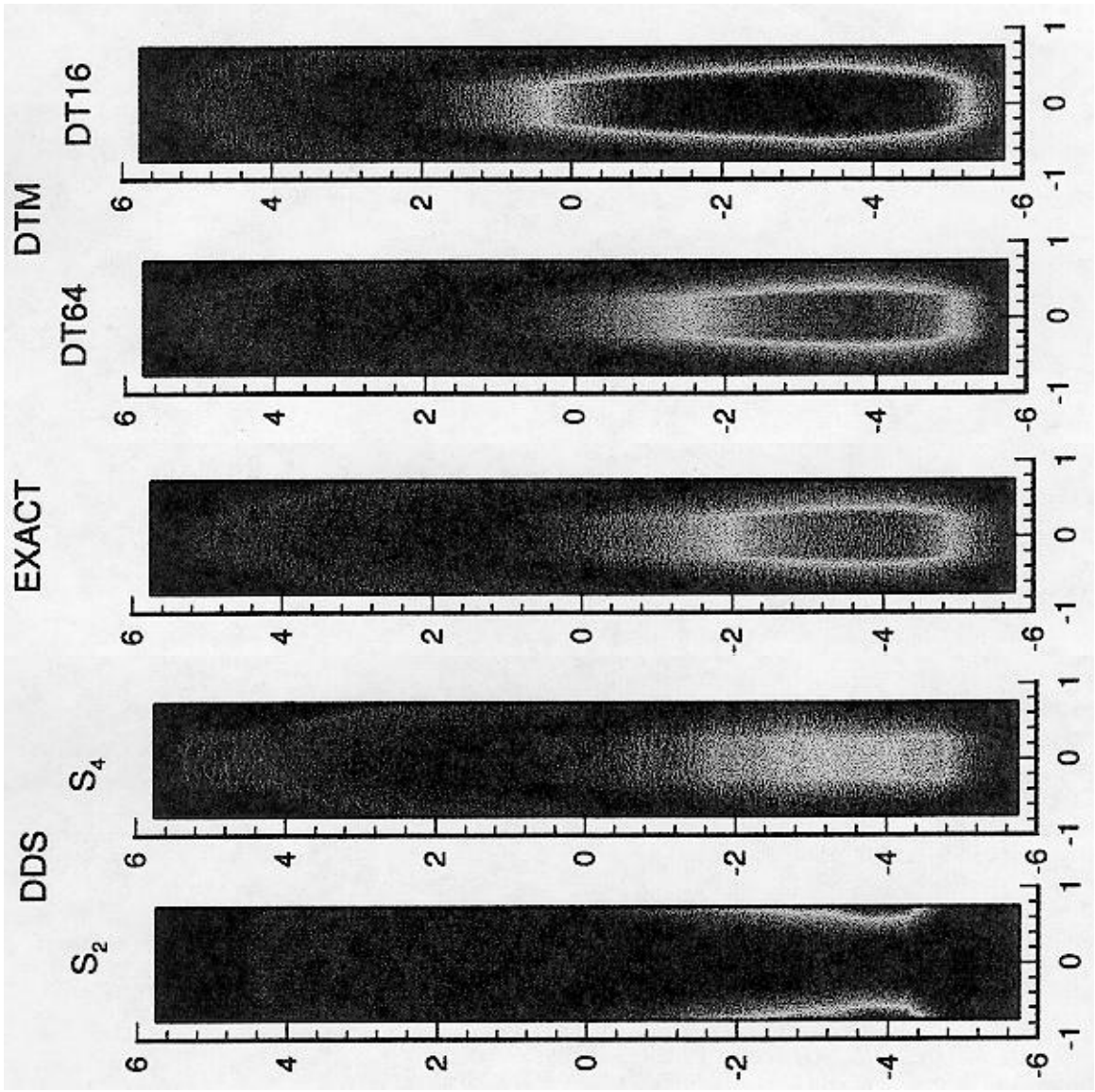

Fig. 4 Comparison between colour contours for dimensionless radiative flux density to the side wall predicted by DOM, DTM and exact solution.

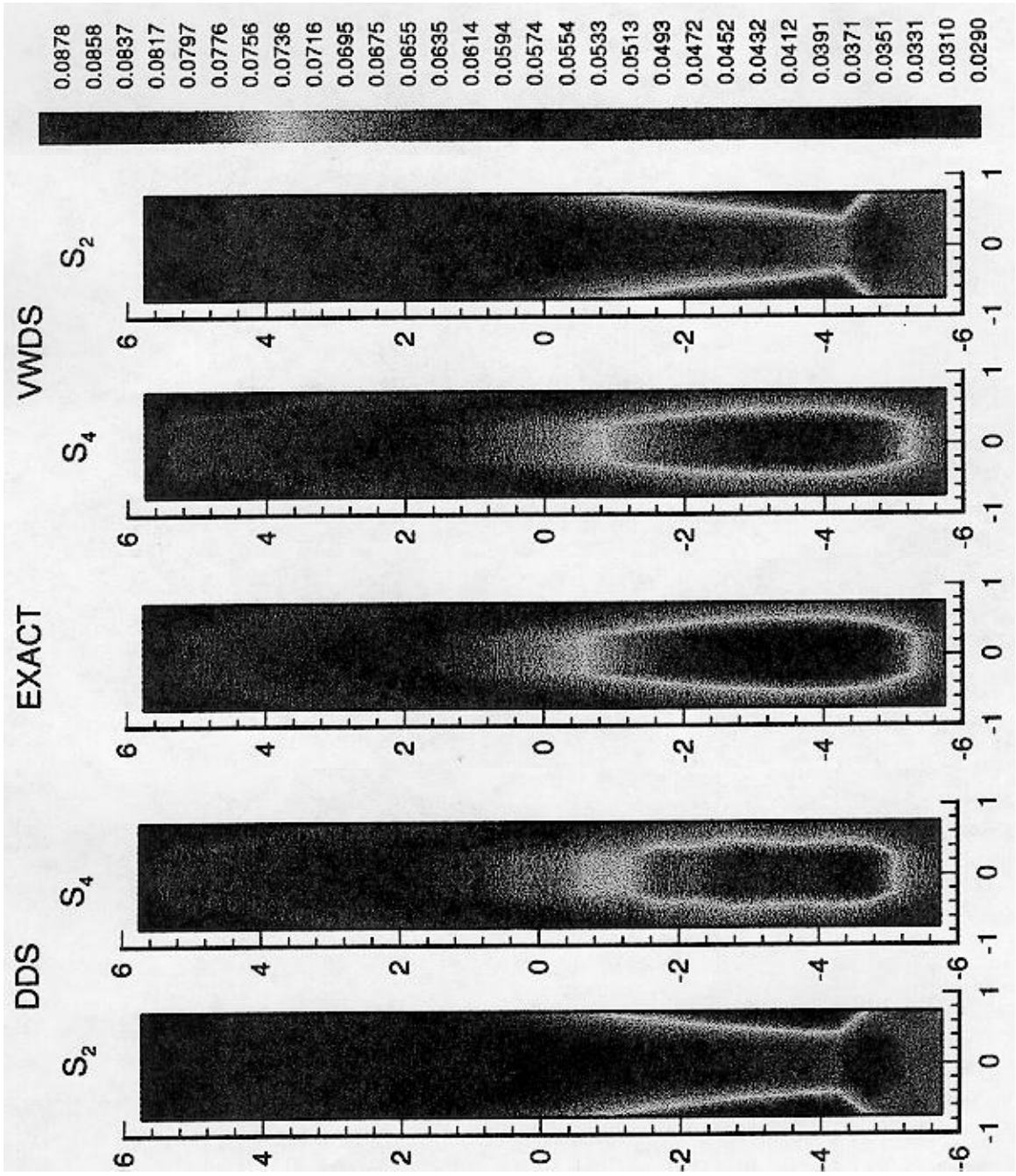

Fig. 5 Comparison between colour contours for dimensionless radiative flux density predicted by DOM and exact solution.

A condensed comparison between DTM and DOM predictions of flux densities using all spatial differencing and angular quadrature schemes taken into consideration is contained in Table 3. It can be noted that the accuracy in flux densities predicted by DTM increases with number of rays. As can be seen from Table 3, contrary to the conclusive remark of Jamaluddin and Smith [16] the S_2 approximation is too inaccurate to use irrespective of all spatial differencing and angular quadrature schemes. However, the S_2 and S_4 produce better accuracy than the $S_{2э}$ and $S_{4э}$ due to the failure of thc $S_{2э}$ and $S_{4э}$ to satisfy half range flux condition [15]. The agreement improves with the order of approximation, e.g. S_4 provides flux densities to the side wall with an average absolute error of 3 %. Only slight improvements in the accuracy of predicted radiative flux densities are obtained when VWDS is employed. For all spatial differencing schemes under consideration negative intensities are encountered when there is considerable difference between the intensity values on the adjacent faces of the control volumes, situated at the intersection of burner wall and water-cooled side walls. In case negative intensity is encountered in a control volume the value of α is changed from 0.5 to 1.0 for DDS with negative intensity fix-up procedure, from (0.5-0.52) to 1.0 for EXPS, but from 0.5 to 0.689 for all control volumes in VWDS which satisfies Fiveland's positive intensity criteria for S_4 approximation.

Table 3. Comparison between the exact values and the predictions of dimensionless flux densities for surface grid points using DTM and DOM with all combinations of spatial differencing and angular quadrature schemes

Designation		Avarage absolute error	Maximum percent error
DT16		7.70	17.90
DT64		1.52	10.21
DT144		0.51	4.04
S_2	DDS	19.50	41.30
	VWDS	18.65	37.67
	EXPS	18.24	38.10
S_4	DDS	3.13	9.43
	VWDS	2.45	8.60
	EXPS	2.65	8.18
$S_{2э}$	DDS	20.84	49.73
	VWDS	17.44	37.66
	EXPS	19.68	46.13
$S_{4э}$	DDS	4.90	11.56
	VWDS	3.38	8.84
	EXPS	4.34	10.24

Effects of order of approximation and spatial differencing scheme on the flux density distributions predicted by discrete ordinates method are illustrated in Fig. 6. With the S_2, large oscillations are encountered in all spatial differencing schemes. Oscillations are produced near the burner and exit wall where large temperature discontinuities exist. When the S_4 is used, the oscillations get smaller for all schemes, smoothness increasing with the value of α. In the light of the above discussion it can be concluded that spatial differencing scheme does not play a significant role in the predictive accuracy of discrete ordinates method for the test problem under consideration.

4.2. Source Term Distributions

Fig. 7 shows the comparison between the colour countours for dimensionless radiative energy source terms predicted by DT16, DT64 end exact solutions. As can be seen from the figure, DT64 predictions are in good agreement with exact values for all control volumes.

Effect of order of approximation on the colour countours for dimensionless radiative energy source terms predicted by DOM are illustrated together with exact solutions in Fig. 8. As can be seen from the figure, both S_2 and S_4 with VWDS produce good agreement with exact values for all control volumes. A condensed comparison between DTM and DOM predictions of source terms using all spatial differencing and angular quadrature schemes taken into consideration is given in Table 4. As can be seen from Table 4, DOM produces better accuracy in source terms than DTM, and both S_2 and S_4 approximations provide radiative energy source terms in close agreement with the benchmark solutions.

Table 4. Comparison between the exact values and the predictions of dimensionless source term distribution for medium grid points using DTM and DOM with all combinations of spatial differencing and angular quadrature schemes

Designation		Avarage absolute error	Maximum percent error
DT16		9.70	24.52
DT64		4.32	11.64
DT144		3.33	9.78
S_2	DDS	1.63	9.48
	VWDS	1.62	10.38
	EXPS	1.54	9.23
S_4	DDS	1.00	3.66
	VWDS	0.98	3.48
	EXPS	1.04	4.02
$S_{2ə}$	DDS	3.32	6.46
	VWDS	3.43	6.46
	EXPS	3.36	6.48

S_{43}	DDS	1.50	4.48
	VWDS	1.40	4.25
	EXPS	1.55	4.49

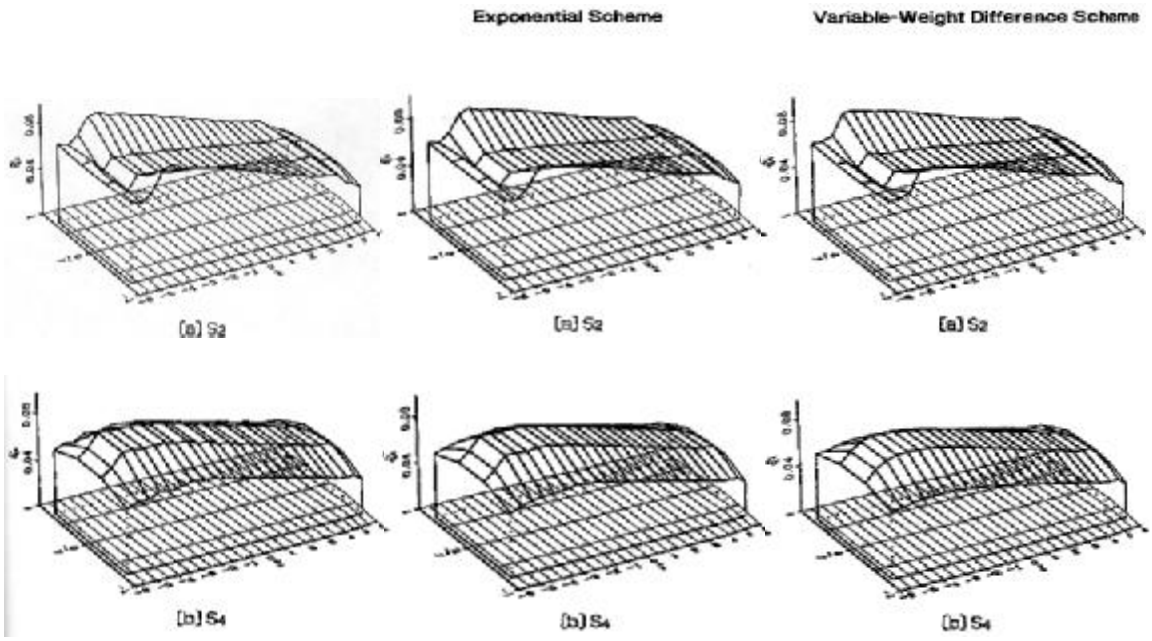

Fig 6. Effects of order of approximation and spatial differencing scheme on the flux density distribution.

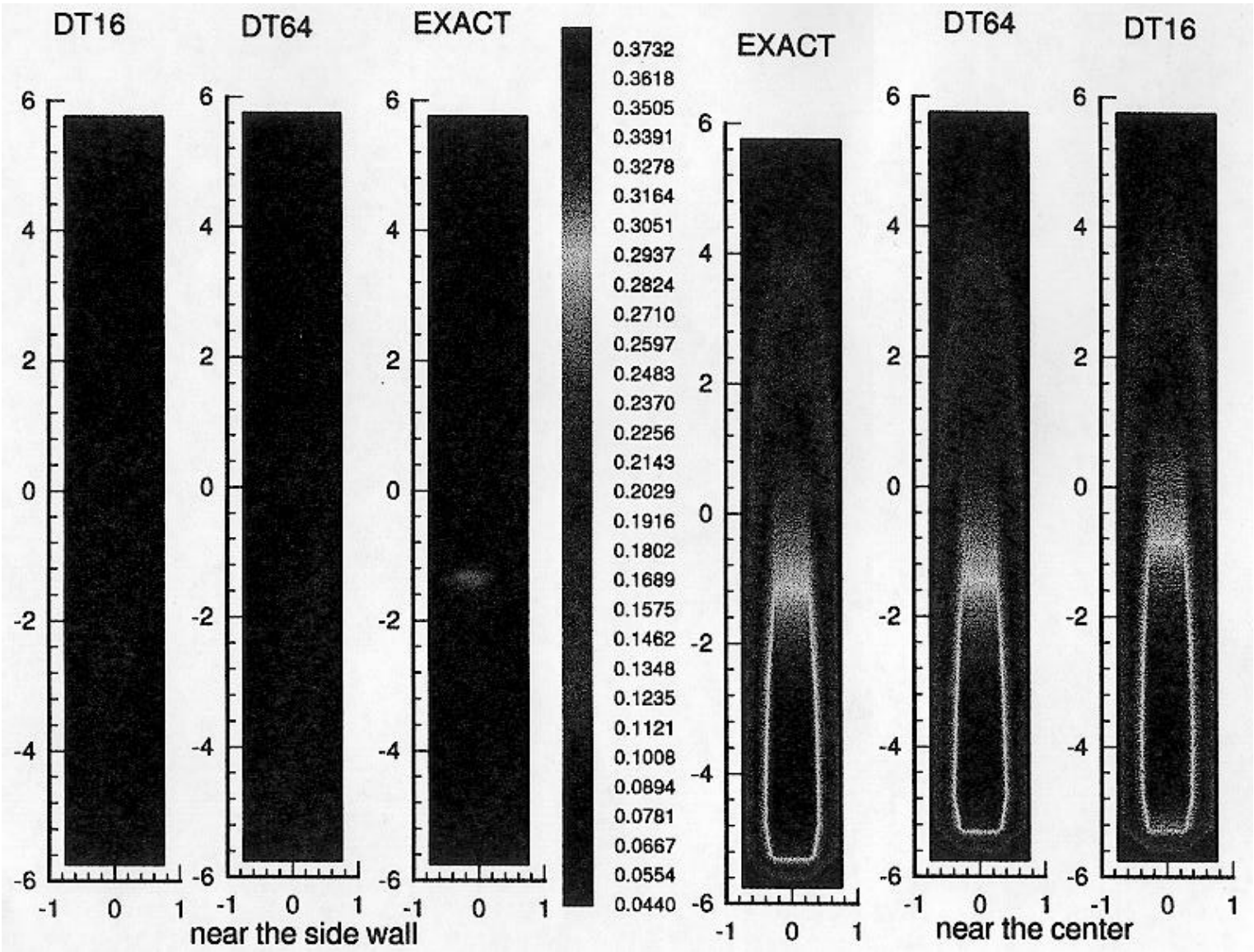
DT16
DT64
EXACT
0.3732
0.3618
0.3505
0.3391
0.3278
0.3164
0.3051
0.2937
0.2824
0.2710
0.2597
0.2483
0.2370
0.2256
0.2143
0.2029
0.1916
0.1802
0.1689
0.1575
0.1462
0.1348
0.1235
0.1121
0.1008
0.0894
0.0781
0.0667
0.0554
0.0440
EXACT
DT64
DT16
near the side wall
near the center

Fig. 7 Comparison between colour contours for dimensionless source terms predicted by DTM and exact solution.

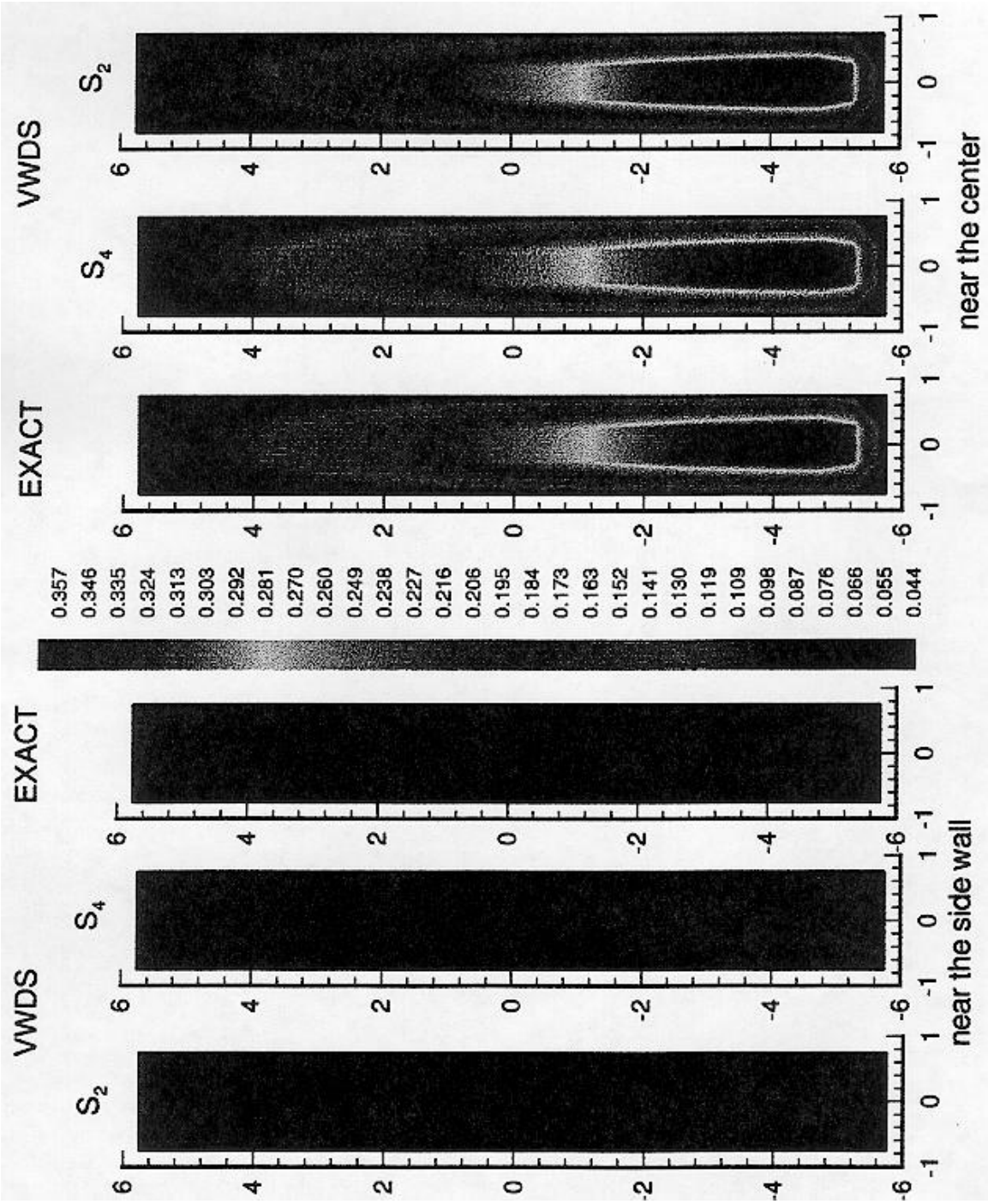

Fig. 8 Comparison between colour contours for dimensionless source terms predicted by DOM and exact solution.

Table 5. CPU time requirements for DTM and DOM

Designation		CPU time, s
DT 16		404
DT 64		1308
DT 144		3076
S_2	DDS	0.7
	VWDS	0.7
	EXPS	0.7
S_4	DDS	2.1
	VWDS	2.1
	EXPS	2.2

The CPU times for DTM and DOM using IBM Risc/6000 Model 590 are given in Table 5. It can be noted that DTM requires 3 orders of magnitude more CPU time than DOM.

Table 6. Comparison between the exact values and the predictions of the percentage errors in generated and removed radiative energy using DTM and DOM with all combinations of spatial differencing and angular quadrature schemes.

Designation		Percentage error in generation	Percentage error in removal
DT 16		-7.06	-6.75
DT 64		-2.34	-2.12
DT 144		-1.28	-1.39
S_2	DDS	0.22	-1.94
	VWDS	0.17	-1.97
	EXPS	0.18	-1.98
S_4	DDS	0.29	0.29
	VWDS	0.46	0.46
	EXPS	0.26	0.25
$S_{2'}$	DDS	-2.72	-4.05
	VWDS	-2.76	-4.09
	EXPS	-2.74	-4.08
$S_{4'}$	DDS	-0.54	-0.82
	VWDS	-0.40	-0.68
	EXPS	-0.56	-0.85

To provide a global check on the accuracy of DOM and DTM, the total rate of removal of radiative energy through the walls and the total rate of generation of radiative energy within the enclosed medium have been evaluated and compared with the exact values [3]. Table 6 shows the errors in generated and removed radiative energy produced by DTM and DOM using all spatial differencing and angular quadrature schemes. It can be seen that percentage errors produced by DTM decrease with increasing number of rays per wall node. As can be seen from Table 6, the percentage errors in generated and removed radiative energy are equal for the S_4 predictions.

5. CONCLUSIONS

Predictions of DTM and DOM for the distributions of components of radiative flux density and radiative energy source term in terms of wall and medium temperature distributions of a box-shaped enclosure problem containing and absorbing-emitting medium of constant properties bounded by black walls have been compared with the exact solutions reported earlier. The problem was based on data taken from a large-scale experimental furnace with steep temperature gradients typical of operating furnaces. The effects of number of rays on the predicted accuracy of DTM and the order of approximation, spatial differencing and angular quadrature schemes on the predictive accuracy of DOM have been investigated. Both methods were evaluated from the viewpoints of both accuracy and computational economy by comparing their predictions with exact solutions available.

Following is a summary of conclusions drawn from this study for the test problem under consideration:

. Comparative testing of S_4 approximation and DT64 indicate that their predictions are in good agreement with the exact solutions and that S_4 approximation requires CPU times 3 orders of magnitude less than that required by DT64. DOM can therefore be recommended to be used in conjunction with CFD codes.

· The order of approximation plays a more significant role than angular quadrature and spatial differencing schemes in the accuracy of predicted radiative flux densities and radiative energy source terms.

· S_n produces better accuracy than $S_{n'}$, the agreement improving with the order of approximation.

· The negativity cannot be avoided by using finer control volume when large temperature discontinuities are present. Some form of negative intensity fix-up procedure is needed.

· Only slight improvements in the accuracy of radiative flux and source term distributions are obtained when VWDS is employed irrespective of order of approximation and angular quadrature scheme.

REFERENCES

1.P. Cheng, Exact Solutions And Differential Approximation for Multi-Dimensional Radiative Transfer in Cartesian Coordinate Configuration, Prog. in Astronautics and Aeronautics 31, 269-308, (1972).

2. A. L. Crosbie and L.C Lee, Relation Between Multi-Dimensional Radiative Transfer in Cylindrical and Rectangular Coordinates with Anisotropic Scattering, J. Quant. Spectrosc. Radiant.Transfer 38, 231-241, (1987).

3. N. Selçuk, Exact Solutions for Radiative Heat Transfer in Box-Shaped Furnaces, J. Heat Transfer 107, 648-655, (1985).

4. N. Selçuk and Z. Tahiroðlu, Exact Numerical Solution for Radiative Heat Transfer in Cylindrical Furnaces, Int. J. Numer. Meth. Engng. 26, 1201-1212, (1988).

5. N. Selçuk, Evaluation of Flux Models For Radiative Transfer in Rectangular Furnaces, Int. J. Heat Mass Transfer 31, 1477-1482 (1988)

6. N. Selçuk, Evaluation of Flux Models For Radiative Transfer in Cylindrical Furnaces, Int J. Heat Mass Transfer 32, 620-624 (1989)

7. N. Selçuk Evaluation of Spherical Harmonics Approximation for Radiative Transfer in Cylindrical Furnaces, Int. J. Heat Mass Transfer 33, 579-581 (1990)

8. S. Chandrasekhar, Radiative Transfer, Dover, New York (1960).

9. B. G. Carlson and K.D. Lathrop, Transport Theory-The Method of Discrete Ordinates in Computing Methods in Reactor Physics (Edited by H. Greenspan, C. N. Kelber and D. Okrent) pp.165-266. Gordon & Breach, New York (1968).

10. W.A. Fiveland, Discrete Ordinate Methods for Radiative Heat Transfer in Isotropically and Anisotropically Scattering Media, J. Heat Transfer 109, 809- 812 (1987).

11. J. S. Truelove, An Evaluation of The Discrete Ordinates Approximation for Radiative Transfer in an Absorbing, Emitting, and Scattering Planar Medium, HTFS Report No.R8478 (1976).

12. E.E Khalil and J.S. Truelove, Calculation of Heat Transfer in a Large Gas Fired Furnace, HTFS Report No. R8747 (1977).

13. A. S. Jamaluddin and P.J. Smith, Predicting Radiative Transfer in Axisymmetric Cylindrical Enclosures using Discrete Ordinates Method, Combust. Sci. Technol.62,173-186 (1988).

14. W. A. Fiveland Three-Dimensional Radiative Heat Transfer Solutions by Discrete Ordinates Method, J. Thermophys 2(4), 309-316 (1988).

15. J. S. Truelove, Discrete Ordinates Solutions of Radiation Transport Equation, J. Heat Transfer 109,1048-1051(1987).

16. A. S. Jamaluddin and P.J. Smith, Predicting Radiative Transfer in Rectangular Enclosures using Discrete Ordinates Method, Combust. Sci. Technol.59,321-340 (1988).
17. D. J. Hyde and J. S. Truelove, The Discrete Ordinate Approximation for Multi-Dimensional Radiant Heat Transfer in Furnaces, HTFS Report No. R8502 (1977).
18. W. A. Fiveland, Discrete Ordinates Solutions of Transport Equations for Rectangular Enclosures, J. Heat Transfer 106, 699-706 (1984).
19. A. S. Jamaluddin and P.J. Smith, Discrete-ordinates solutions of radiative transfer in nonaxisymmetric cylindrical enclosures Combust. Sci. Technol.62, 173-186 (1988).
20. W. A. Fiveland, A Discrete Ordinates Method for Predicting Radiative Transfer in Axisymmetric Enclosures, ASME paper 82-HT-20 (1982).
21. N. Selçuk and N. Kayakol, Evaluation of Discrete Transfer Model for Radiative Transfer in Combustors, Proceeding of International Symposium on Radiative Heat Transfer, ICHMT, Kuþadasý, Türkiye, (1995).(in press).
22. N.G. Shah, New Method of Computation of Radiant Heat Transfer in Combustion Chambers, Ph.D. Thesis, University of London, London (1979).
23. M.G. Carvalho, D.F.G. Durao, and J.C F. Pereira, Prediction of the Flow, Reaction and Heat Transfer in an Oxy-fuel Glass Furnace, Int. J. Eng. Comp. 4(1), 23-34 (1987).
24. M.G. Carvalho, and P. J. Coelho, Heat Transfer in Gas Turbine Combustors, J. Thermophys.3(2), 123-131 (1989).
25. A. S. Abbas, F.C.Lockwood, aud A.P. Salooja, The Prediction of the Combustion and Heat Transfer Performance of a Refinery Heater, Combust. Flame 58, 91- 101 (1984).
26. J.P. Gore, S.M. Skinner, D.W. Stroup, D. Madrzykowski, and D.D. Evans, Structure and Radiation Properties of Large Two Phase Flames in Heat Transfer in Combustion Systems, Winter Annual Meeting ASME, San Francisco,77-86 (1989).
27. W.A. Fiveland, and C.E. Latham, Use of Numerical Modelling in the Design of a Low-NO_x Burner for Utility Boilers, Combust. Sci. and Technol. 93, 53-72 (1993).
28. A. Charette, A. Haidekker, and Y.S. Kocaefe, 3-D Comperative behaviour of Discrete Transfer with Imaginary Planes Method for Furnace Modelling, Can. J. Ch. En.70, 198-207 (1992).
29. M.G Carvalho, T. Farias, and M. Nogueira, Radiative Heat Transfer Method and Its Application to a Glass Furnace, Proceedings of Euroterm 21 Heat Transfer in Semitransparent Media, France,194-207 (1992).
30. M.G. Carvalho, T. Farias, and P. Fontes, Predicting Radiative Heat Transfer in Absorbing, Emitting and Scattering Media Using the Discrete Transfer Method, HTD.Vol 160, Fundamentals of Radiation Heat Transfer, ASME,17-26 (1991).
31. N. Selçuk end N. Kayakol, Evaluation of Discrete Ordinates Method for Radiative Transfer in Rectangular Furnaces, Int. J. Heat Mass Transfer (1996) (in press).
32. N. Selçuk and N. Kayakol, Evaluation of Angular Quadrature and Spatial Differencing Schemes for Discrete Ordinates Method in Rectangular Furnaces, Proccedings of 31st National Heat Transfer Conference, A.I.Ch.E.,Houston, Texas (1996) (in press).
33. K D. Lathrop, Spatial Differencing the Transport Equation:

Positivity vs. Accuracy, J.Comput. Phys 4, 475-498 (1969).
34. L. Strömberg, Calculation of Heat Flux Distribution in Furnaces, Ph. D. Thesis, Chalmers University of Technology, Göteborg, Sweden,(1977).

CORROSION FROM MELTED FRITS ON DIFFERENT REFRACTORIES USED FOR TANK FURNACES

Cristina Leonelli, Tiziano Manfredini, Cristina Siligardi,
Gian Carlo Pellacani and **Mariano Paganelli**
University of Modena, Italy

Abstract

It has been valuted the qualitative degree of chemical durability of two kinds of refractory used for industrial tank furnaces when they are in contact with four different molten glass compositions. The lining materials belong to the mullitic and on ZrO_2 refractory families. The glassy compositions are lead-frit, leadless-frit, glossy monoporosa-frit and $ZrSiO_4$-frit: all of which are commonly used in the tile ceramic industry. After heat treatment at 1400^0C for 4 hours, the refractory samples were investigated by SEM and EDS techniques. Accordingly to this study it is possible to design the proper refractory lining for tank furnaces depending on the chemical and physical properties of the glass compositions being melted.

1. INTRODUCTION

The refractories used in glass melting tanks are subjected to a permanent corrosive attack. Therefore, one of the most important requirement is a high corrosion resistance of refractories. Especially the corrosion and blistering tests are those which besides the determination of chemical and physical properties give decisive information on the behaviour of refractories in pratical use. Most of the methods for the determination of the corrosion behaviour of refractory materials in contact with melts are designed in such a way that they are relatively simple and they approach the conditions of practice as close as possible. For determining and comparing the corrosion behaviour of the refractory materials in contact with glass melts of modified chemical composition and for drawing conclusions on the tank campaign a relatively good reproducibility of the corrosion tests is needed.

The development of new fast firing technologies required more and more alkaline glaze compositions; to make them insoluble in water a melting process previous to application is necessary, so fritting the raw material is a common procedure especially for glaze application. Frits are glasses prepared by melting suitable raw materials in a gas fired or oil-fired furnace or in electric melting unit [1].

Frit-melting furnaces are either of the box or rotary type. The rotary melter is used when a number of frits are required in a lots of about 450 kg. In the rotary process, a charge of material is placed in the preheated melter, brought up to temperature, and held for the time necessary to achieve reasonably complete solution of the bach. The furnace is

slowly rotated during melting to enhance mixing and heat distribution. After melting the burners are shut off and subsequently the molten frit is discharge and quenched.

In the continuous frit melter, raw material is continuously added to a pile at one end of the preheated box melter by a screw feeder. Burners directed at the raw material pile melt the frit, and the molten materials flows by gravity to the other end of the melter where it is continuously discharge and quenched. The quenching and break-up of the frit may be carried out by pouring the molten frit into the water.

The refractory lining of a tank furnace is constantly subjected to chemical corrosion by the molten glass. Most lining materials, particularly in the beginning phase, chemically react with some components of the glass and either seep through the refractory matrix or form new crystalline phases. The parameters which control these reactions are: the contact surface glass/refractory, the refractory microstructure, the molten glass composition and its viscosity. The influence of the chemical composition of the glass melt on the corrosion of refractories has been studied in a number of projects [2-5], but the mechanism of this process has not been thoroughly investigated. Thus, in [2] it is shown that silicate glasses with high alkali-oxide content upon reaction with alumina refractories should be classifed as low corrosive materials, and those with high content of alkaline earth oxides as corrosive. Experimental studies carried out by the authors showed that replacing alkaline earths in the silicate glasses compositions by alkaline components reduces the corrosive action on the corundum and baddeleyite-corundum refractories. However, the reaction process underlying this was not explained by authors.

The aim of this work is to valute the qualitative degree of chemical durability of three kinds of refractory used for industrial tank furnaces when they are in contact with four different molten glass compositions. The lining materials belong to the mullitic and on ZrO_2 refractory families. The glassy compositions are lead-frit, glossy monoporosa-frit, leadless-frit, and $ZrSiO_4$-frit: all of which are commonly used in the tile ceramic industry. The attack on the refractory surface was evaluated by X-ray fluorescence emission of the different cations.

2. EXPERIMENTAL

The refractory materials (Table 1) were cut to obtain 10x1x1 cm bars; they were put in alumina crucibles and partially covered with the frits (Table 2).

Table 1

MULLITE REFRACTORY wt%

$AL_2O_3 + TiO_2$	SiO_2	Fe_2O_3
71	28,4	0,6

ZrO_2 REFRACTORY (wt%)

Al_2O_3	ZrO_2	SiO_2	Fe_2O_3	TiO_2	Na_2O	CaO
45, 5	41	12,2	0,1	0,1	1	0,1

All crucibles were inserted in a muffle kiln heated at 1400^0C for 4 hours. At this temperature all frits were molten; the quenching was made in air. Afterwards, it was carried out the cut on the section containing glass/refractory interface.

Table 2
FRITS COMPOSITION (wt%)

	SiO_2	B_2O_3	AL_2O_3	PbO	CaO	BaO	MgO	ZnO	K_2O	Na_2O	TiO_2	ZrO_2
I	33,5	5,0	3,2	43,9	-	3,8	-	1,7	3,2	1,5	3,8	-
II	55,3	6,2	9,6	-	11,9	-	1,0	10,9	4,6	0,2	-	-
III	50,1	9,2	13,0	-	1,1	-	0,6	-	4,9	13,3	-	7,5
IV	62,3	10,7	7,7	-	2,7	0,9	0,2	1,1	1,5	5,6	-	7,1

I = lead-frit, II=glossy monoporosa-frit, III=leadless-frit, IV=$ZrSiO_4$-frit.

The so-obtained disks were absorbed in an epoxidic resin and polished with SiC abrasive card and alumina paste down to 0.3μm in grain size. Microstructural observation were performed by SEM microscope (Philips XL4O) and energy dispersion spectrometer, EDS on surface polished specimens. The method of X-ray area scanning or dot mapping provided scanning images containing element-specificdistribution [6,7].

3. RESULTS

The main crystalline phases in the ZrO_2-refractory are: corundum Al_2O_3, baddeleyite ZrO_2, an amorphous phase and a cooprecipitate phase with a pseudo-eutectic structure (needlelike baddeleyite crystals in corundum phase). The structure of this material is that of an extremely dense refractory. The main crystalline phase of the mullitic material are: mullite $3Al_2O_32SiO_2$, corundum and an amorphous phase. The microstructure presents high porosity (open) and low compactation.

Investigations of the refractories after reaction with the melt during laboratory tests showed that:

a) The lead-frit attack all the lining materials tested, especially mullite refractories due to the presence of a high porosity [8] and weak microstructure. Both amorphous and corundum phases present feeble opposition to chemical agent: the lead-frit seep through into the material especially in the amorphous zones. The figure 1 show the difference between glass/refractory interface and bulk refractory microstructure.

Figure 1. EDS profiles of mullite/lead-frit sample (80x)

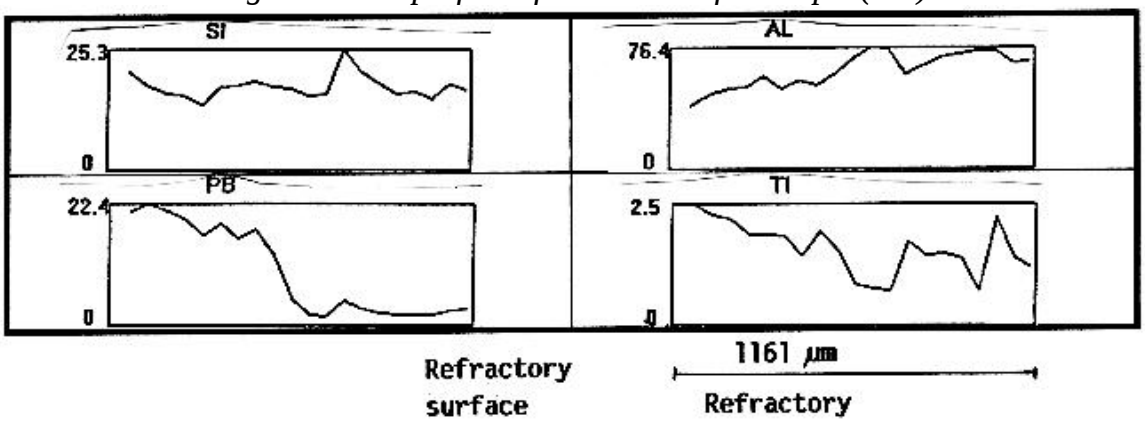

The second family of refractories, corundum-ZrO_2, shows higher corrosion resistance than the mullite refractory. The corrosion is more evident where the corundum and amorphous phase is present.

b) The glossy monoporosa frit has an interesting behaviour on both refractories; initially it reacts with mullitic-sample forming a new crystalline phase, anorthite, which protects the surface from further corrosion by glass. In figure 2 are evident the microstructures of glass/refractory interface and anorthite layer.

The high amount of Ca0 in such frit curtails the solubility of cooprecipitate phase in ZrO_2-refractory, increasing the material corrosion.

In figure 3 show respectively the bulk refractory microstructure and the interface with glass.

c) The remaining glassy compositions, on the contrary, show feeble corrosive properties on both refractory materials being their chemical inactivity very high even in the molten state and their viscosities high enough to prevent seeping.

According to this study it is possible to design the proper refractory lining for tank furnaces depending on the chemical and physical properties of the glass compositions being melted.

4. CONCLUSIONS

The ZrO_2-refractory materials, having low porosity, high density and compactness, must be used in presence of high aggressive frits such as lead-frits. However, in some conditions, for example in presence of glossy monoporosa frit, mullite has a better behaviour because the formation of anorthite crystals on the glass/refractory interface decrease further corrosion by glass.

Figure 2: SEM micrograph of mullite/monoporosa frit sample (300x).

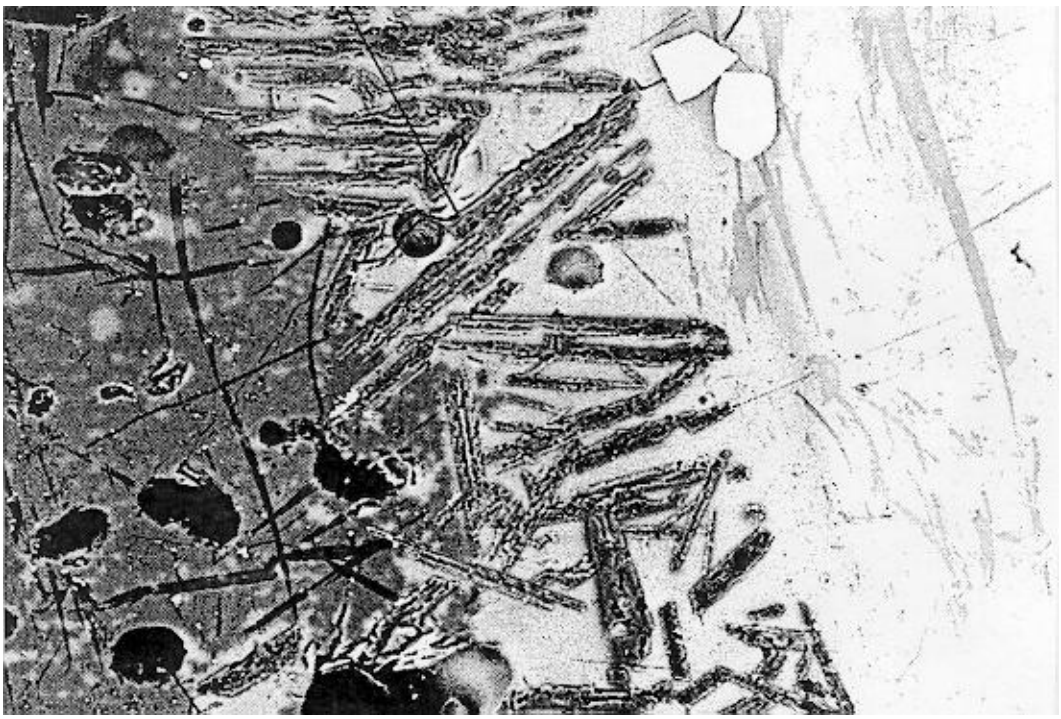

.

Figure 3: dot map of ZrO_2-refractory/monoporosa frit sample (40x).

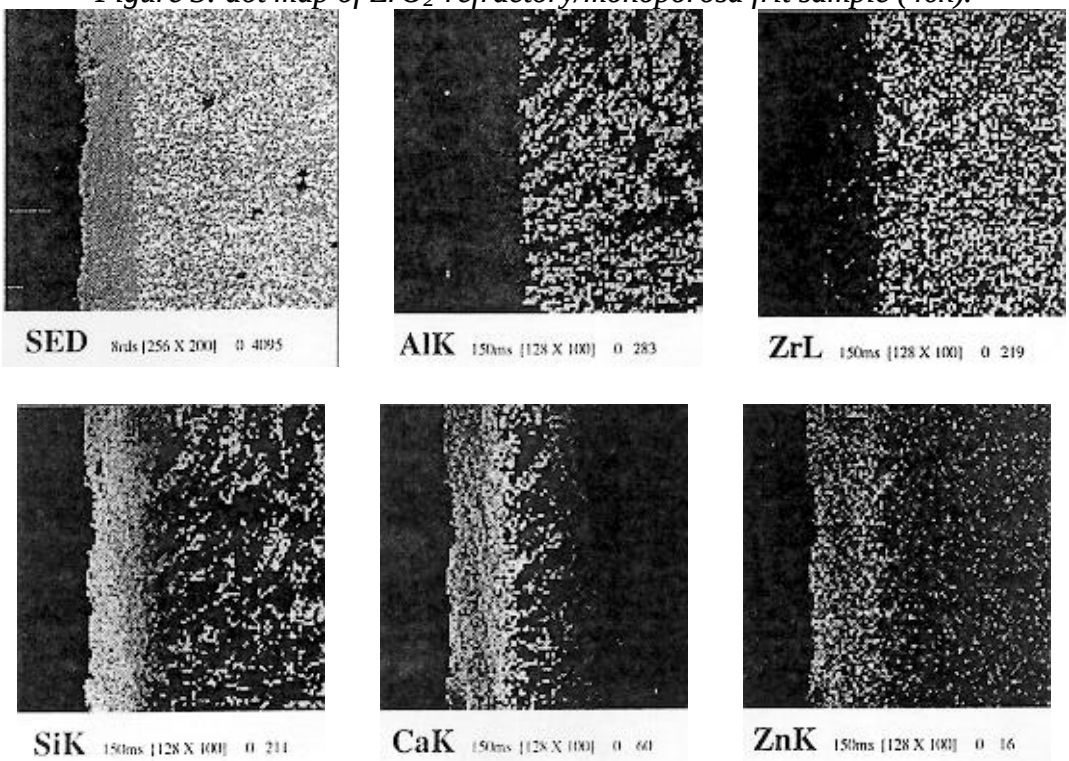

REFERENCES

[1] L. D. Gill and R. A. Eppler Chapt. 7, Lead Frits, J. S. Nordyke, Ed. Lead in the world of Ceramics, American Ceramic Society, Inc., OH, 1984, 99-105.
[5] O. N. Popov, P. T. Rybalkin, et al., Production and Use of Fusion-cast refractories (Russ), Metallurgizdat, Moscow,1985.
[6] D. E. Newbury, C. E. Fiori, R. B. Marinenko, R. L. Myklebust, C. R. Swyt and D.S. Bright, Anal. Chem. **62** 1159A (1990).
[7] D. E. Newbury, C. E. Fiori, R. B. Marinenko, R. L. Myklebust, C. R. Swyt and D.S. Bright, Anal. Chem. **62** 1245A (1990).
[8] K. J. Konsztowicz and J. Boutin, J. Am. Ceram. Soc. **76** 1169-76 (1993).

HOT EXTRACTION OF GASES DISSOLVED IN GLASS UNDER ULTRAHIGH VACUUM AND QUANTITATIVE ANALYSIS BY QUADRUPOLE MASS SPECTROMETRY

Hiroshi Imagawa, Nobukazu Saito and **Satoshi Uchiyama**
Toyo University, Japan

Abstract

In a recent paper titled "Redox behaviors of Ce and Sb in soda-lime glass studied by evolved gas and UV spectroscopic analysis" (Glastechnische Berichte, 68 C2(1995)217-224), we reported evolution of oxygen and other gases from glasses containing refining reagents with the scale of "ion currents" on a quadrupole mass spectrometer under ultrahigh vacuum.

In the present paper we would report gas evolution on absolute-amount scale using a calibration apparatus. Differences in concentrations of gases between glasses melted by an oxygen-enriched-burner-furnace and those by an air-burner-furnace would be discussed, especially for glasses containing sodium sulphate as refining reagents, or for alkali-free high-etch glasses.

---

* Full manuscript not available at the time of printing

INTERACTION OF GAS MIXTURES WITH GLASS MELT

Jaroslav Klouñek, LubomŘr N•mec, Ji Í i Ullrich*

Laboratory of Inorganic Materials of IIC ASCR and ICT, Czech Republic
*Glass Service, Ltd., Vsetin, Czech Republic

Abstract

The interaction of gas mixtures of SO_2 and O_2 with soda - lime - silica glass has been studied to reveal the appropriate reaction mechanism. The results show that the interaction at high partial pressures of SO_2 and O_2 and low temperatures is controlled by the chemical reaction of sulphate phase formation at the interface and by the appropriate decomposition reaction with increasing temperature. The same phenomenon most probably affects the bubble behavior in glass melt containing sulphate.

1. INTRODUCTION

The interaction between gas mixtures and glass melts determines some glassmelting processes as refining and glass foaming. The mathematical modeling of glassmelting tries to describe these processes quantitatively, however, experimental examinations are necessary to establish actual reaction mechanisms, to put experimental data into models and verify the proposed models. Recently, a method has been developed consisting in visual observation of gas or gas mixture absorption in a glassmelt from the closed silica glass vessel immersed in the melt [1,2]. The method has been formerly used for the measurement of diffusion coefficients of gases in glass. In this study, the reaction of gas mixtures of SO_2 and O_2 with the soda - lime - silica glass has been investigated. The aim of the work was to reveal the appropriate reaction mechanism and to explain behavior of bubbles in glasses containing sulphates.

2. EXPERIMENTAL METHOD AND CONDITIONS

The method is schematically illustrated by Fig. 1. The shifting of glass level brought about by gas absorption or desorption was videorecorded and evaluated by image analyzer. This procedure was completed by the analysis of gas content of the silica glass vessel. After finishing video recording the vessel - partially filled by a glass melt - was quickly drawn out of the glass melt and put into the closed silica glass tube being flushed by helium. The gases released by disintegration of the measuring silica glass cell were subsequently analyzed using gas chromatography.

In the presented experiments, the interaction of $SO_2 + O_2$ mixture was followed at 1200^oC, the oxygen content of the mixture being 0, 25, 50, 75 and 100 vol.%

respectively. The glass had composition 74% SiO_2, 16% Na_2O and 10% CaO (wt.), the maximum content of Fe_2O_3 was 0.005%, the average content of SO_3 was 0.22 %.
In another set of experiments, the stoichiometric mixture of SO_2 and O_2 (2:1) was quickly heated to 1460^oC after absorption period and subsequently analyzed. The following experiments studied the behavior of gas mixtures containing 50 and 25 vol.% of oxygen respectively, when slowly cooling the glass melt from 1460 ^oC to 1200 ^oC. The last observation involved the treating of the CO_2 gas at 1460 ^oC and analysis of the final mixture.

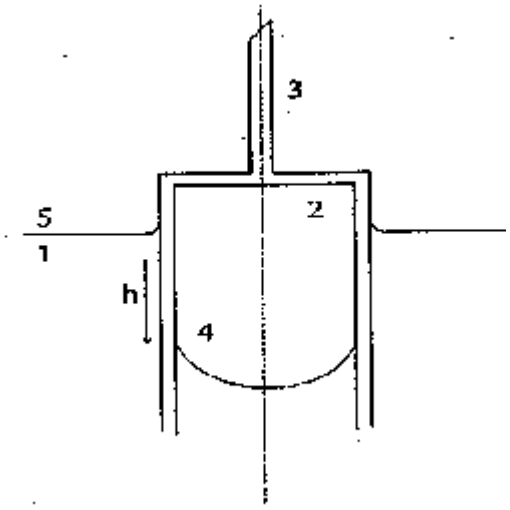

Fig.1: The scheme of exp. arrangement. 1 special silica pot with measured glass, 2 cylindrical silica vessel with gas, 3 holder of the cylindrical vessel,4 moving phase boundary gas- glass melt, 5 glass level inside the silica glass pot

3. RESULTS OF EXPERIMENTS

The examples of the absorption of SO_2 + O_2 mixtures containing 25, 50 and 75% of O_2, respectively, are plotted in Fig. 2. Obviously there is a rapid initial absorption period followed by a slow one. This observation is in accordance with older Greene and Platts [3] observations including artificial SO_2+O_2 bubbles. The final gas compositions of reaction vessels are presented in Table II. These results indicate the roughly stoichiometric absorption (SO_2:O_2 = 2) of the mixture in the glassmelt at all initial compositions. The interaction of pure SO_2 and O_2, respectively, is on the contrary very slow as is apparent from Fig. 3. The counter diffusion of gases dissolved in glass brings about the growth of gas phase volume in the case of SO_2. The transport of both single gases is apparently controlled by diffusion.

Table 1: The Results of Analyses of the Reaction Vessel Initially Containing Stoichiometric Mixture of SO_2 and O_2 after Reheating to Decomposition Temperatures.

Experiment	Gas Content in Volume%		
	CO_2	SO_2	O_2
2hs at 1200 ^oC	3	97	-
16hs at 1200 ^oC	4	96	-

The glass boundary shifting when heating the glass after absorption period of the stoichiometric gas mixture to 1460 ^0C is presented in Fig. 4. Similarly as in the previous experiments, two interaction mechanisms, characterized by the different rate of phase boundary shifting, can be noticed. The final gas compositions of the reaction vessel are in Table I.

The example of glass boundary shifting when cooling the glass with $SO_2 + O_2$ mixture from 1460 ^oC to 1300 ^oC is given in Fig. 5. The initial CO_2 volume increase with time at 1460 ^oC is obvious from Fig. 6. The corresponding results of gas analyses are in Tables III and IV.

DISCUSSION

The results in Fig. 2 - 3 and Table II raise the question about mechanism of reaction between $SO_2 + O_2$ mixture and glass melt. The correct knowledge of mechanisms is especially important for the identification of bubble origin in glasses and mathematical modeling of refining. The usual idea of independent diffusion of both gases into the glass is probably restricted only to low values of p_{so_2} and p_{o_2} in bubbles and corresponds to the second part of the dependence in Fig. 2. At high concentrations of SO_2 and O_2 in gas phase, the precipitation of sulphate phase in form of Na_2SO_4 droplets or surface layer may be expected [4]. The probable mechanism is following:

Surface absorption of both gases:

$$SO_2\ (g) \rightarrow SO_2\ (l)$$
$$O_2\ (g) \rightarrow O_2\ (l) \qquad (1)$$

Reaction with glass:

$$SO_2\ (l) + ½\ O_2\ (l) + Na_2O\ (l) \leftrightarrow Na_2SO_4\ (\text{layer, droplets}) \qquad (2)$$

To prove the formation of sulphate phase, the stoichiometric mixture of SO_2 and O_2 was introduced above glass level at 1200 ^oC for 30 min and the glassmelt was subsequently heated. The formation of flow cells typical for the surface force driven convection and caused by the decomposition of the sulphate layer was observed. The rate of sulphate precipitation is most probably determined by reaction (2); the rate of reaction itself or transport of Na_2O from glass to the surface may control this process.

Table II: The results of Analyses of the Reaction Vessel Initially Containing O_2, SO_2 or their Mixtures.

	Gas Content in Volume %				
Original Gas Composition	**CO_2**	**SO_2**	**O_2**	**Theoretical amount of SO_2 or O_2 in Vol. Units after Stoichiometric Absorption**	**Analyzed amount of SO_2 or O_2 in Vol Units after Stoichiometric Absorption**
100 % of O_2	2	0.2	97.8	-	-
100% of SO_2	0.5	99.5	not analyzed	-	-
$SO_2/O_2 = 3$	0	100	not analyzed	SO_2: 25	SO_2: 26.2
$SO_2/O_2 = 1/3$	0	0	100	O_2: 62.5	O_2: 62.0
$SO_2/O_2 = 1$	0	0.6	99.4	O_2: 25.0	O_2: 27.0

The temperature dependence of the rate of surface boundary shifting shows the steep decrease with temperature [2]. Assuming the sulphate precipitation is controlled by reaction (2), following equation may be derived for $dh/d\tau$

$$d_h/d\tau = k/\rho'_r \, (p_{SO_2r} \, p^{1/2}{}_{O_2r} - p_{SO_2s} \, p^{1/2}{}_{O_2s}) \qquad (3)$$

Where k is the rate constant of reaction (2), ρ'_r; is density of stoichiometric mixture SO_2 and O_2 and pso_2 and po_2 are the appropriate partial pressures of both gases. Here subscript r designates the pure stoichiometric mixture ($pso_2 + po_2 = 1$ bar) and subscript s designates the partial pressures being in equilibrium with precipitated sulphate phase or with saturation concentration of sulphate in glass.

Substituting the supposed temperature dependence of k and $p_{SO_2s} \, p^{1/2}{}_{O_2s}$, we get:

$$\frac{dh}{d\tau} = \frac{c_o \exp\left(-\frac{c_1}{T}\right) RT}{p_a M_r} \left[p_{so_2} \, p^{1/2}_{o_2} - A_o \, B_o \exp\frac{A_1 + B_1}{T} \right] \qquad (4)$$

Where p_a is atmospheric pressure, M_r corresponds to molecular weight of SO_3 and constants A, B and C relate to the temperature dependence of equilibrium constant of reaction (2), the sulphate solubility and the reaction rate constant k, respectively. As $A_1 + B_1 < 0$, $dh/d\tau$ goes to zero with increasing temperature. This fact is in agreement with results of experiments in [2]. The sulphate precipitation controlled by the transport of Na_2O into the layer should, on the contrary, show an increase of $dh/d\tau$ with temperature in relative broad interval of temperatures. The results therefore indicate the control of sulphate phase precipitation by the reaction (2), the rate constant k having the order of

magnitude 10^{-8} $kg.m^{-2}.s^{-1}.bar^{-3/2}$ between 1250 - 1350 ^{o}C (the values of the sulphate equilibrium constant and sulphate solubility were taken from [5] and [6], respectively).

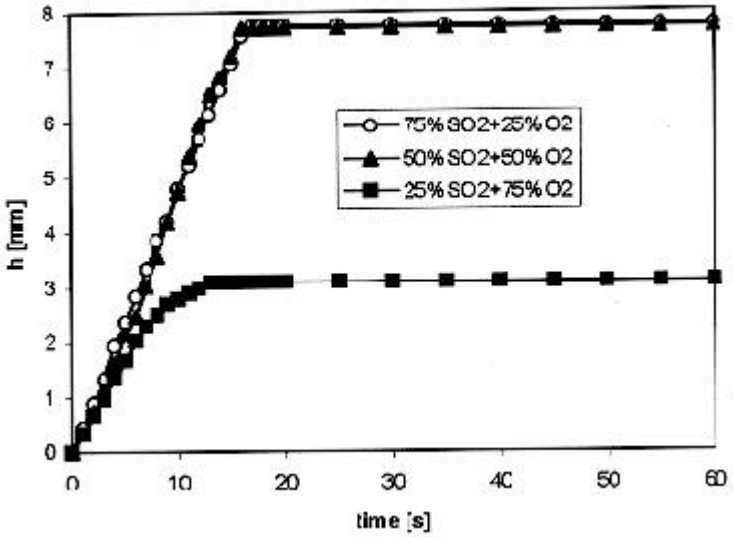

Fig. 2: The shifting of glass level in the reaction vessel during absorption of mixtures of SO_2 and O in the glassmelt at 1200 ^{o}C (h increase - gas absorption).

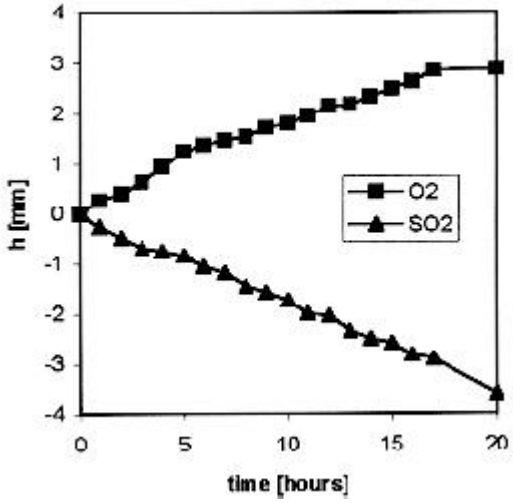

Fig. 3: The shifting of glass level in the reaction vessel during interaction between pure oxygen or sulphur dioxide and the glass melt at 1200 ^{o}C (h decrease - gas desorption)

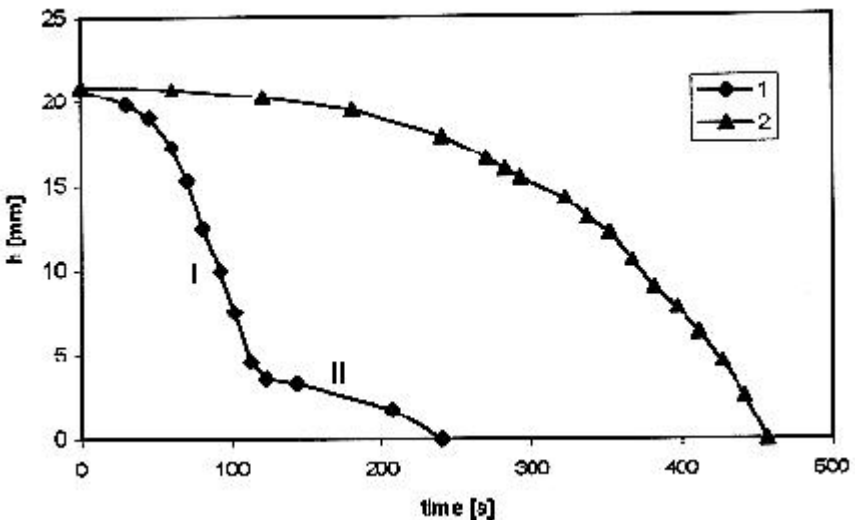

Fig. 4: The shifting of glass level when heating the glass melt with precipitated sulphate phase from 1200 ^{o}C to 1460 ^{o}C. 1 - heating just after phase formation 2 - 2 hours treating the glass with sulphate phase at 1200 ^{o}C (h decrease - gas volume increase)

To prove the dissolution of sulphate phase in glass melt, experiments with absorption of the stoichiometric mixture of SO_2 and O_2 at 1200 ^{o}C were performed, followed by rapid heating of observation cell with reaction vessel to 1460 ^{o}C. When reheating started just after finishing the absorption, rapid decomposition of sulphate layer started at about 1420 ^{o}C (after 40 s, see Fig. 4, curve 1); the layer was almost completely decomposed in about 110 s. The treating the sulphate layer for 2 hours at 1200 ^{o}C led to the considerable slowing down the gas volume growing (see curve 2 in Fig. 4). Apparently a part of sulphate phase dissolved in glass during two hours at 1200 ^{o}C.

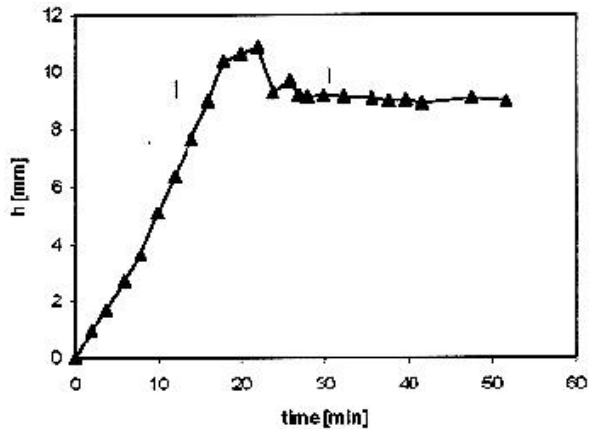

Fig. 5: The behavior of mixture of SO_2 + O_2 (3:1) when cooling it at the rate 2 ^{o}C/min from 1460 ^{o}C to about 1300 ^{o}C and reheating to 1460 ^{o}C. I - cooling, II - reheating

Table III: The Results Analyses of the Reaction Vessel Initially Containing Mixture of SO_2 and O_2 after Slow Cooling from Melting Temperature to about 1300 ^oC and Reheating to Decomposition Temperatures.

Original Gas Composition	**Gas Content in Volume%**		
	CO_2	**SO_2**	**O_2**
SO_2/O_2=1	6.0	-	94.0
SO_2/O_2= 3	5.0	95.0	-

The question arises about sulphate phase precipitation on bubble surfaces when slowly cooling bubbles from high to middle temperatures. The slow cooling of SO_2+O_2 mixture (3:1) from 1460 ^{o}C is presented in Fig. 5. The relative fast gas absorption following the temperature decrease obvious from the first part of the curve gives evidence of reaction (2), however, no sulphate phase decomposition was observed after reheating glass (see the second part of curve in Fig. 5). The final compositions of gas mixtures after experiments in Table III support the mechanism of reaction (2) too. The question of sulphate phase precipitation or dissolution at low rates of glass cooling should be however solved by further experiments.

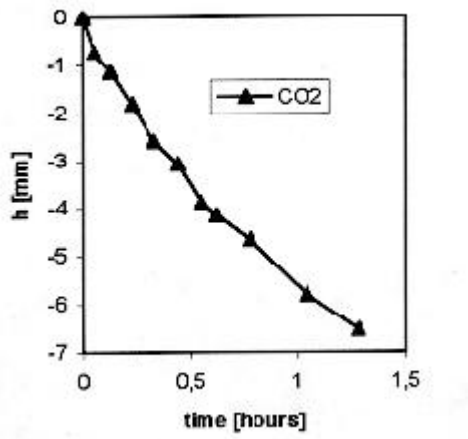

Fig. 6: The growing of the initial CO_2 volume by the diffusion of gases from the glass melt at 1470 ^{o}C.

The behaviour of CO_2 bubbles at high temperatures has been simulated in the last series of experiments (see Fig.6). The results of reaction vessel analyses presented as well in Table IV show concentrations SO_2 higher than the stoichiometric ones. This fact could explain the final low pressures and condensates in bubbles from glasses refined by sulphates (see Table IV). Further experimental work is needed to confirm and explain this behaviour.

Table IV: The Results of Analyses of the Reaction Vessel Initially Containing CO_2 Treated at 1470 ^oC and Results of Analyses of Quickly Cooled Melting Bubbles in Float Glass.

Time of Treating at 1470 ^oC	Gas Content in Volume%				
	CO_2	COS	SO_2	O_2	N_2
90 min	50.5	≈ 1.0	48.5	-	-
90 min	70.8	≈ 1.0	28.2	-	-
Bubble in float lass	46.8	TR.	48.0	0.7	4.2
	54.0	-	40.4	0.8	4.8
	8.1	TR.	90.0	0.9	0.9

CONCLUSION

The examination of behaviour of $SO_2 + O_2$ mixtures in glassmelt using the method of controlled volume absorption and gas phase analysis simulates the behaviour of melting bubbles in glass melts refined by sulphates. The results show that the bubble behaviour at high partial pressures of $SO_2 + O_2$ and low temperatures are controlled by the chemical reaction of sulphate phase formation and by the appropriate decomposition reaction when heating bubbles with sulphate phase. The same reaction is most probably taking place when slowly cooling melting bubbles to middle temperatures. The high concentrations of SO_2 in initially CO_2 bubbles at high temperatures and at very low concentrations of iron need further experiments. The results have significance for the mathematical modelling of refining process.

LITERATURE

1. Nemec L., Klouzek J.: Ceramics - Silikàty 39,1 (1995).
2. Klouzek J., Nemec L.: Glastechn. Ber. - Glass Sci. Technol 68C,128 (1995).
3. Greene C. H., Platts D. R.: J. Am. Ceram. Soc. 52,106 (1969).
4. Holmquist S.: J. Am. Ceram. Soc. 49, 467 (1966).
5. Klouzek J., Cerná M.: Proceedings of III. International Seminar on Mathematical Simulation in the Glass Melting, p.108, Vsetin, May 1995.
6. Zluticky J., Trnka P., Nemec L.: Sklár a keram. 29, 263,
7. (1979).

NITROGEN BUBBLES FROM AZS REFRACTORIES

Fritz W. Krämer
Schott Glaswerke Mainz, Germany

Abstract

At the production of many technical glasses in melting tanks there is a certain basic level of bubbles which is between 0 and 10%. The gas content of these bubbles is mainly nitrogen. It is supposed that these bubbles are formed by the corrosion of fused cast AZS refractories which are used as tank blocks. At fusion casting of these blocks properly air is entrapped as the closed pores of the refractory material contains mainly nitrogen besides oxygen and argon. The ratio of nitrogen-argon is near that of normal air. At first heating of the AZS blocks (start up period) but also during the normal furnace campaign bubbles with high nitrogen content (89% to 100% N_2, with minor percentages of oxygen, argon and carbon dioxide) are formed in the glass melt if these closed pores are opened by the normal corrosion process of the AZS material by the glass melt. This process takes place additionally to the oxygen bubble formation where due to a redox process of multivalent ingredients of the refractory material when temperature is increased, oxygen is released.

1. INTRODUCTION

Gaseous inclusions belong to the most common defects affecting the quality of glass. Therefore, the elimination of these gas bubbles from glass melts is a topic of great interest to the glass industry. Gas bubble analysis is the most important tool of bubble-fault diagnosis. By analyzing the gas content of the bubbles and with the knowledge of the interaction of the gases dissolved in the glass melt with these bubbles as well as the knowledge of how bubbles will change their content with temperature and time, the trouble shooter can suggest to the production personnel the source and cause of bubble defects.

One of these bubble sources is the refractory material of the melting tanks, e.g. the fused cast AZS blocks which form bubbles, stones and knots at the refractory-melt interface during the start-up period as well as during the normal furnace campaign.

2. PROBLEMS WITH BUBBLES

At the production of many technical glasses in melting tanks which are built with AZS material there is a certain basic level of bubbles which give rise to production losses of about 10 %. The gas content of these bubbles is mainly nitrogen with minor components of carbon dioxide and argon. Table 1 shows typical bubble contents

whereas the bubbles with low carbon dioxide contents are represented by 50 to 80 %.

Table 1

O_2/%	N_2/%	CO_2/%	Ar/%	diameter/mm
0	98.7	0	1.3	0.32
0	98.6	0	1.4	0.52
0	98.1	0.5	1.4	0.44
0	98.3	0.9	0.8	0.38
0	97.9	1.2	0.9	0.44
0	76.2	23.2	0.6	0.52
0	78.1	21.3	0.6	0.56

With the knowledge in gas bubble cause and effect relationship these bubbles can principally attributed either to an air entrapping by stirrers, plungers or by cracks, or to the corrosion of ceramic refractories, for instance to fused cast AZS refractories which form the walls of the melting tanks. There are several hints that the above mentioned bubbles are formed at the refractory-melt interface.

3. BUBBLES FROM FUSED CAST AZS MATERIAL

An earlier paper [1] shows that pristine fused cast AZS material but also AZS material which was heated in laboratory furnaces up to 1550^{o}C for several days has closed voids or pores. As content of these gas-filled pores mainly nitrogen, oxygen and carbon dioxide was found. With a now more sensitive analyzing technique additionally to nitrogen and carbon dioxide, also hydrogen and argon as minor gas components could be detected in these closed pores.

Recently the reaction between fused cast AZS-32 material and a television glass melt was studied in a laboratory scale [2]. To this crucibles made of ER 1681 were heated together with television glass cullets up to 1350^{o}C, 1425^{o}C and 1500^{o}C for 100 to 600 hours. A lot of bubbles were observed and analyzed showing oxygen, nitrogen, carbon dioxide and argon as content. Some of these results are given in Table 2.

Table 2

O_2/%	N_2/%	CO_2/%	Ar/%	diameter/mm
88.1	9.8	2.0	0.1	0.22
56.5	42.3	0.8	0.4	0.14
50.1	47.4	2.1	0.5	0.17
71.6	28.1	0	0.3	0.23
31.2	60.9	7.5	0.5	0.18
59.4	39.1	0.9	0.4	0.16
40.2	53.8	5.5	0.6	0.15
75.4	17.2	7.2	0.2	0.22
58.8	36.6	4.2	0.4	0.19

When plotting the oxygen content of the analyzed bubbles versus bubble diameter, Fig.1 shows a decrease of the oxygen content with smaller bubbles indicating that oxygen as the main component is diffusing out of the bubbles with time.[3]

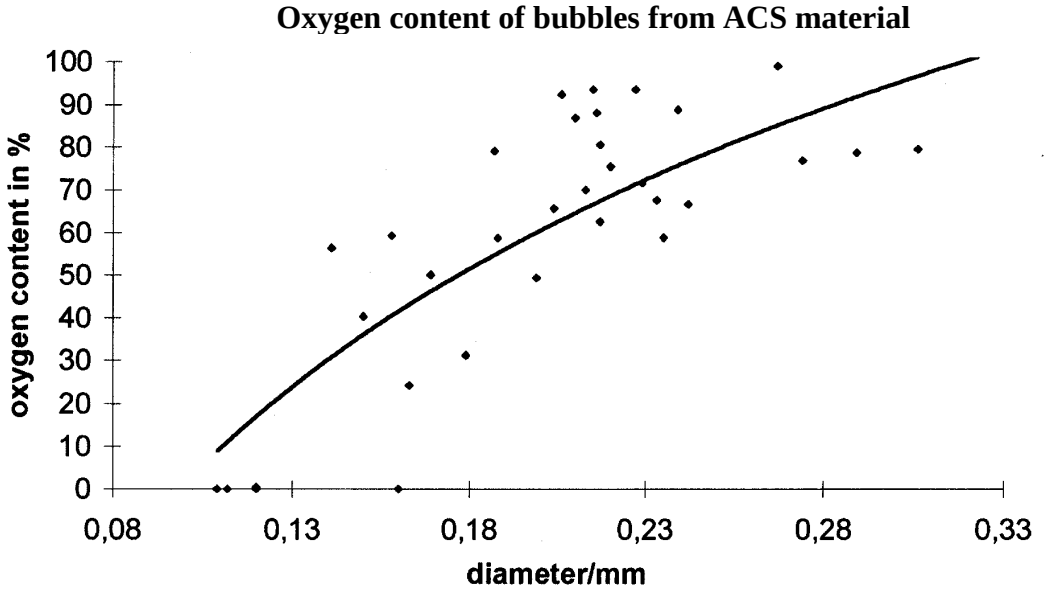

Fig.1 Oxygen content versus bubble diameter [2]

Due to the resorption of oxygen by the melt at conditioning all bubbles formed in the melting tank have no oxygen in the end product. Therefore the analyses of table 2 were calculated without oxygen - indicating now the bubble content and bubble diameter (diameter^{o}) when having cooled the melt - and are given in table 3

Table 3

N_2/%	CO_2/%	Ar/%	diameter^{o}/mm
82.4	16.8	0.8	0.11
97.2	1.8	0.9	0.11
94.8	4.2	1	0.13
98.9	0	1.1	0.15
88.4	10.9	0.7	0.16
96.8	2.2	1	0.12
89.8	9.2	1	0.13
69.9	29.3	0.8	0.14
88.8	10.2	1	0.14

Fig 2 shows the argon content versus bubble diameter indicating that argon neither diffuses into nor diffuses out of the bubbles but that argon was in the bubble from the very forming.

The absolute argon values of about 0.9 vol% and Fig.3 which shows the ratio of argon to nitrogen which is near the ratio in normal air indicate that nitrogen and argon originate from air.

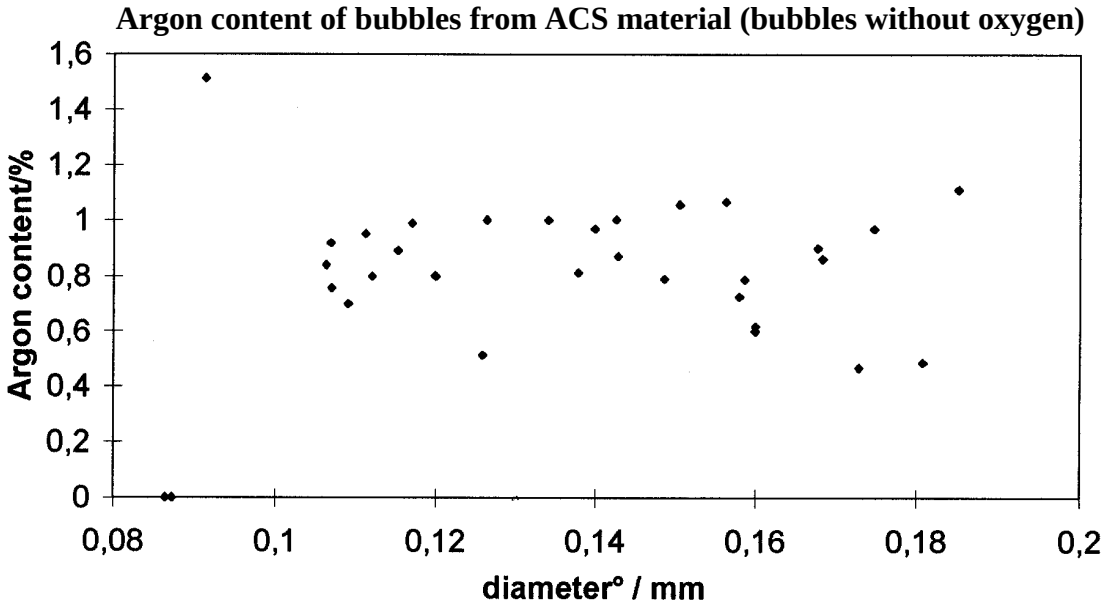

Fig.2 Argon content in bubbles (without oxygen) versus bubble diameter°.

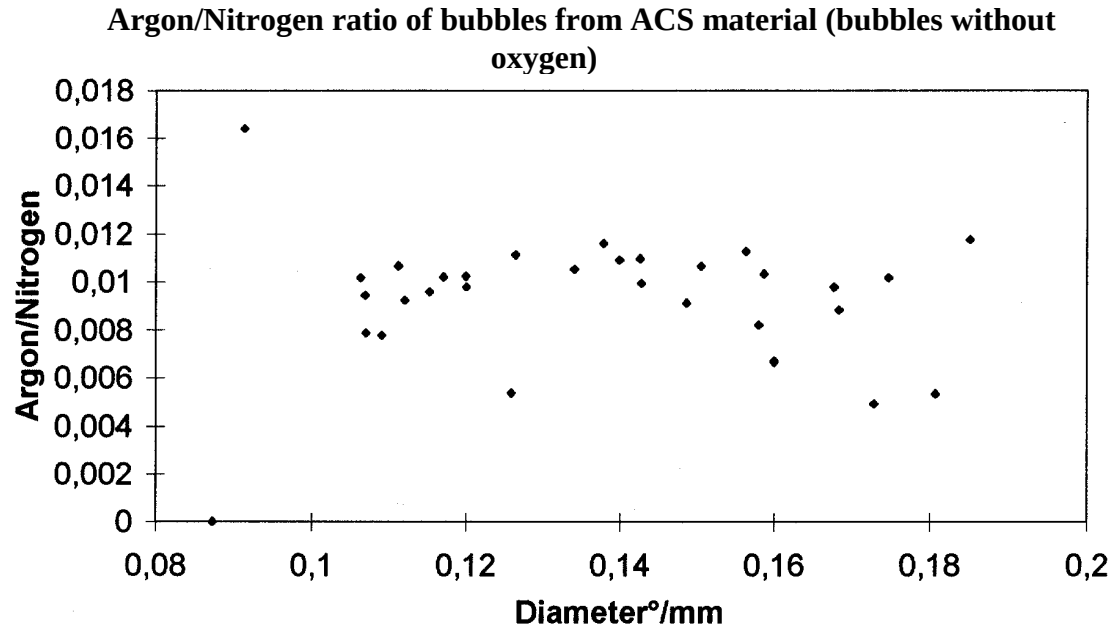

Fig.3 Argon-nitrogen ratio of bubbles versus bubble diameter°.

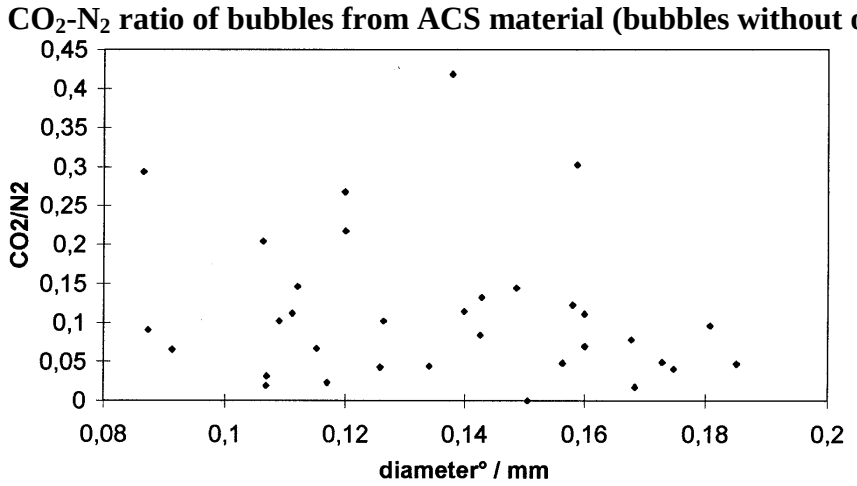

Fig.4 Carbon dioxide-nitrogen ratio of bubbles from AZS versus bubble diameter°.

As the carbon dioxide-nitrogen ratio (Fig.4) is also nearly independent on bubble diameter one can assume that most of the carbon dioxide amount was also in the bubbles from the very bubble forming process.

4. CONCLUSION

At the corrosion of AZS blocks in glass melting tanks the closed pores of this refractory material are opened and the gaseous content of the pores are released to the melt in form of bubbles. This corrosion is enhanced by the formation of oxygen bubbles inside the glassy phase of the refractory material due to redox processes when these oxygen bubbles penetrate the reaction layer at the melt-refractory interface and push the gaseous content of the refractory pores and also material of the reaction layer in form of knots and stones into the melt [2].

As the content of the AZS pores is mainly nitrogen with minor components of oxygen, hydrogen, carbon dioxide and argon and with a ratio of argon/nitrogen which is near the normal air ratio of 0.11, it is supposed that nitrogen of the pores arises from nitrogen of normal air rather than from oxidized chemically dissolved nitrogen (nitrides). It is furthermore supposed that the AZS pores are formed when casting the AZS-melt in normal air when producing the AZS blocks.

REFERENCES

[1] Krämer, F.W. "Analysis of gases evolved by AZS refractories and by refractory/glass melt reactions. Techniques and results. Contribution to the bubble-forming mechanism of AZS material." Glastech.Ber.65 (1992), 93-98

[2] Van Dijk, F.A.G. "Glass defects originating from glass melt/fused cast AZS refractory interaction". Thesis (1994), Eindhoven,NL

[3] Krämer, F.W. "Bubble defect diagnosis by means of a mathematical model" XIV Intl.Congr.on Glass (1986), New Delhi, Vol.II ,288-295

ORIGIN OF $K_2ZrSi_3O_9$ STONE IN GLASS

Kohzo Sakai
New Glass R & D Center, Asahi Glass Co., Ltd., Japan

Abstract

$K_2ZrSi_3O_9$ stone was found in Ba-Sr-Alkali Silicate glass for color TV panel. The Morphology of stones are two types. One is hexagonal cross section and lath like shape and the other is indefinite shape. $K_2ZrSi_3O_9$ is found in the neighborhood of ZrO_2 containing refractory after the reaction test between refractory and glass.

The difference of morphology is owing to environment of crystal growth. Hexagonal shape is derived from ZrO_2-rich and Al_2O_3-poor glass phase and the other is derived from ZrO_2-poor and Al_2O_3-rich composition.

1. Introduction

Bulb glass for Color Television Panel (CP) is one of the great glass market in the world. So, it is needed that production loss become minimize as possible as we can. Melting defects of CP glass are blisters, glass knots and stones. Normally, stones are small portion of defects. But sometimes acute stones have occurred. It is necessary to identify stones and to make an identification chart to minimize a time for some furnace actions to eliminate stones.

$K_2ZrSi_3O_9$ crystal is relatively rare stone in CP glass. But occasionally this crystal appears as acute stones. This crystal is belongs to hexagonal crystal system. Crystal data are shown in Table 1 [1]. A study about stones in glass was already reported for Pb-silicate glass[2][3]. But no reports are existed so far about CP glass. In this study, the occurrence of $K_2ZrSi_3O_9$ stones and the growth environment of this crystal are also discussed about CP glass.

Table 1 Crystal data of $K_2ZrSi_3O_9$

Crystal system : Hexagonal	Space group : $P6_{3/m}$ Z=2
Lattice constants : a=6.89Å	C=10.17Å
Refractive index : n_E=1.637	n_o=1.624

3. Results

3.1 Characterization of Stones

$K_2ZrSi_3O_9$ phase is crystallized in Ba-Sr-Alkali Silicate glass. Chemical compositions of glass are shown in Table 2. This glass is normally used for color television panel. Relative high content of BaO, SrO and K_2O is remarkable characteristic.

There are two types of $K_2ZrSi_3O_9$ stones. Fig.2 shows photographs of this stones. One is hexagonal cross section and lath like shape(Fig.2a) and the other is indefinite shape(Fig.2b). Sizes are about between 3.0 and 0.5mm. Normally, clear hexagonal shape is larger than indefinite shape.

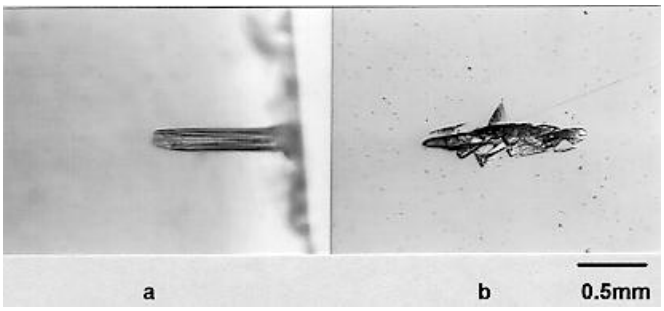

Fig.2 Optical micrograph of $K_2ZrSi_3O_9$ stones

Fig.3 shows back scattered electron image of stones obtained by EPMA. The surroundings of the crystal are different from each other. Relatively gray color is observed around the crystal in Fig.3b but no different color is observed in Fig.3a. This phenomena indicate the different chemical composition of glass between these two.

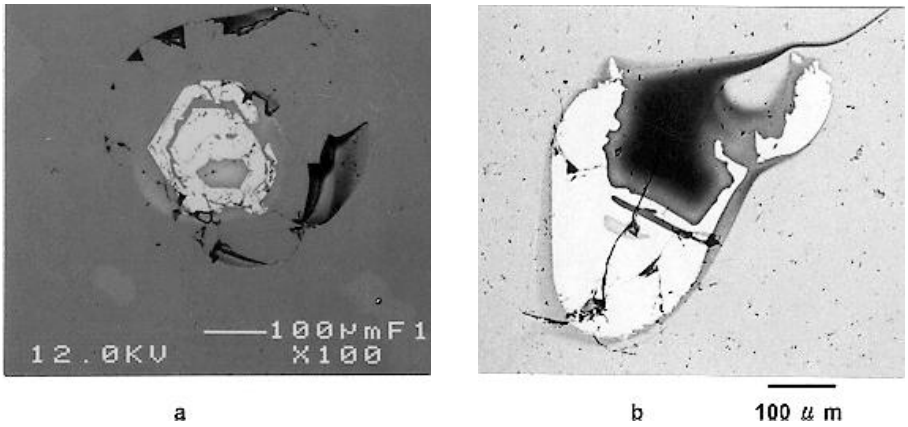

Fig.3 Back scattered electron image of $K_2ZrSi_aO_s$ stones

2. Experiments

Stones in glass are usually first observed optical microscope. Morphological characters are described. Then stones are cut and ground until stones appear on the surface of glass. After that stones are polished by diamond media and cleaned by ultrasonic bath. Back scattered electron image and chemical composition are obtained by electron probe micro analyzer(EPMA : JEOL JXA8900). Samples after reaction test between refractory and glass are observed and measured by same method as mentioned above.

Fig.1 shows the reaction test between glass and refractory. High alumina crucible (Al_2O_3:95.4%) was used for this test. Size of refractory was 10x10x10mm and CP glass cullet was used for this test. After heating at 1300^{o}C for 24h in electric furnace, furnace was cooled down to 1050^{o}C and kept for 24h. Table 2 shows the chemical composition of used glass. Chemical composition of used refractories are shown in Table 3. AZS means Al_2O_3-ZrO_2-SiO_2 fusion cast refractory and ZFC means high ZrO_2 fusion cast refractory.

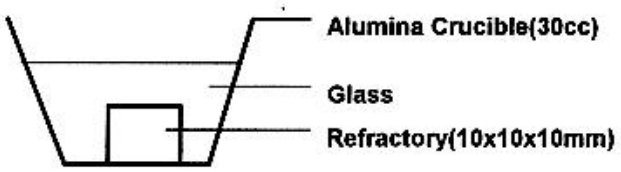

Fig.1 A schematic of reaction test between Refractory and Glass

Table 2 Chemical compositions of glass(wt.%)

Element	wt %
SiO_2	61.0
Al_2O_3	2.0
CaO	1.0
Na_2O	7.5
K_2O	7.5
SrO	8.7
BaO	8.9
ZrO_2	2.5

Table 3 Chemical compositions of refractories (wt%)

	AZS	ZFC
Al_2O_3	50.0	0.8
SiO_2	16.0	4.5
ZrO_2	33.0	94.0
Na_2O	1.0	0.4

Chemical compositions of crystal are shown in Table 4.

Table 4 Chemical compositions of $K_2ZrSi_3O_9$ crystal (wt.%)

	Hexagonal lath like shape (Fig.2a)			Indefinite shape (Fig.2b)			Theoretical value
	1	2	3	4	5	6	$K_2ZrSi_3O_9$
SiO_2	45.4	44.6	44.2	46.9	46.9	45.3	45.3
ZrO_2	27.9	30.6	31.4	29.1	29.4	29.6	31.0
K_2O	18.5	20.2	21.9	20.1	21.7	19.9	23.7
BaO	3.45	1.37	0.59	1.78	1.07	1.80	0.0
Na_2O	1.43	1.20	0.23	1.60	0.45	1.83	0.0

All crystals in Table 4 are almost the same including minor elements and also almost equal to theoretical value of $K_2ZrSi_3O_9$ crystal. But, K_2O content is slightly smaller than theoretical value of $K_2ZrSi_3O_9$. It is considered that Na and Ba element substitute to K element.

Table 5 shows the chemical composition of glass around $K_2ZrSi_3O_9$ crystals.

Table 5: Chemical compositions of glass around $K_2ZrSi_3O_9$ crystal (wt%)

	Hexagonal Lath like shape (Fig.2a)			Indefinite shape (Fig.2b)		
	1	2	3	4	5	6
SiO_2	55.8	53.8	54.5	61.6	60.8	59.9

Al_2O_3	3.53	2.49	2.37	9.29	5.91	4.76
Na_2O	10.2	9.90	9.32	6.69	7.99	7.62
K_2O	5.15	6.32	6.65	9.23	7.21	7.82
ZrO_2	7.55	12.9	9.08	3.36	6.52	7.11
SrO	7.47	6.75	8.40	3.96	5.10	5.91
BaO	8.47	6.25	7.37	5.13	5.47	6.03

It is clear that the chemical composition of glasses are different between the two type of crystals. One is rich in ZrO_2(hexagonal lath like) and the other is rich in Al_2O_3 (indefinite shape).

3.2 Reaction test between refractory and glass

After testing described in Fig.1, interface between glass and refractory was observed and analyzed by EPMA. Fig.4 shows the interface between glass and ZFC refractory. Some crystals are existed at the interface between glass and refractory. Chemical composition of crystal and glass are shown in Table 6. It is clear that this crystal is $K_2ZrSi_3O_9$ phase. But in the case of AZS refractory, $K_2ZrSi_3O_9$ crystal was not observed.

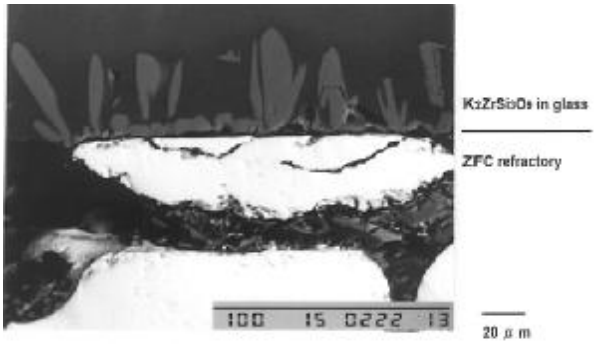

Fig.4 Back scattered electron image of ZFC and glass interface

Table 6 Crystal and glass after testing between glass and refractories(wt%)

	ZFC		**AZS**
	No.1	**No.2**	**No.3**
	Crystal	**Glass**	**Glass**
SiO_2	45.3	59.2	57.8
Al_2O_3	0.0	3.0	13.0
Na_2O	0.2	9.9	7.7
K_2O	21.7	5.6	9.4
ZrO_2	31.4	7.8	4.1
SrO	0.3	6.3	3.9
BaO	0.2	7.4	2.9

4. Discussions

$K_2ZrSi_3O_9$ stones are almost the same composition but morphology is two types(Fig.2). The difference of morphology is owing to growth environment. The difference of environment is ZrO_2, Al_2O_3, alkaline and alkali-earth content. It is considered that the high temperature viscosity of these two type of glasses are different from each other. For example, calculated value of same

viscosity(log η=3) temperature is about 1200-1240°C for No.1 to 3 and 1300-1380°C for No.4 to 6 in Table 5. It is clear that compositions from 1 to 3 are lower viscosity than 4 to 6 compositions. As above mentioned, hexagonal lath like $K_2ZrSi_3O_9$ crystals grow up in lower viscosity glass than indefinite shape. This observation suggests that hexagonal lath like crystals grow up in euhedral shape because of unrestricted growth condition. The ralative low viscosity gives the unrestricted growth of crystals.

On the contrary indefinite shape crystals are in the relative high viscosity glass because of Al_2O_3-rich composition. This suggests that crystal growth condition is relatively restricted compare to hexagonal lath like shape.

The chemical composition of glass after glass-refractory testing(Table 6, No.2) is similar to that of No.1 to 3 in Table 5. This findings leads to a conclusion that the growth environment of hexagonal lath like crystal is the interface of ZFC refractory and glass.

In the case of AZS refractory, no $K_2ZrSi_3O_9$ crystals were observed. But the chemical composition of glass after AZS refractory testing(Table 6) is similar to that of No.4 in Table 5. This suggests that indefinite shape of $K_2ZrSi_3O_9$ crystals grow up in the interface of AZS refractory and glass.

5. Conclusions

Above mentioned characterization of stones and results of reaction test exhibit following conclusions.

a. $K_2ZrSi_3O_9$ stones are divided two type morphology. One is hexagonal lath like and the other is indefinite shape.

b. This crystal grows up at the interface between ZrO_2 contained fusion cast refractory and CP glass.

c. Hexagonal lath like shape is derived from high ZrO_2 fusion cast refractory(ZFC)

d. Indefinite shape is derived from Al_2O_3-ZrO_2-SiO_2 fusion cast refractory(AZS)

References

[1] Bragg, L. et al., Crystal Structures of Minerals 213, G. Bell and Sons LTD., London(1965)
[2] Derabert, M., Trans. J. brit. Ceram. Soc., 75(3) 53 (1976)
[3] Takeuchi, Y., Taikabutsu, 39 428 (1987) in Japanese

SILICEOUS DEFECTS IN FLOAT GLASS PRODUCTION

Akif Özcan, Bülent Arman and **Esref Aydin**
SISECAM Research Center, Turkey

Abstract

As in other glass furnaces, silica defects form a good proportion of the overall defects in float glass furnaces. A good deal of experience has been gained through the years by applying a systematic approach of defect investigation in float glass production. The experience has been fortified by follow-up post-mortems of crown silica refractories during cold repairs, the effect of change of raw materials, and change from fuel oil firing to natural gas. Based on this experience, an attempt will be made to classify silica defects.

Silica defects encapsulated in alumina-zirconia glassy-phase (knot) are assumed to be the fingerprints of carryover occurring around the doghouse. This phenomenon accelerates the corrosion of superstructure refractories.

In furnaces fired with natural gas, the formation of some species of silica defects are frequently encountered on the crown and bridge wall silica refractories in the flame free area. The waist crown and entrance of conditioning zone are also prone to this type of defect formation. The surface of refractories appear to be dry and the nature of material seems to be loose and friable.

Conglomeratic plate-like tridymite crystals with a minor amount of glassy phases have been observed. The loose and friable silica defects popularly known as "frost" are highly sensitive to furnace operational parameters and silica brick quality. Very often, they fall on the glass and have no chance of dissolution thus ending up as defects in the glass.

1. Introduction

Silica defects, are in the form of quartz, tridymite and cristobalite, which arise from so many different factors during glass melting. By employing the concept of systematic defect analyses over 15 years, thousands of defects have been examined. Experience shows that the siliceous defects make up about 10 percent of the total defects. However at any time, they may became the most predominant defects, since the main ingredient of the batch is sand and very large areas of the superstructure are constructed with silica materials. In these cases rapid and correct determination of the origin of such defects will reduce the losses.

Identification of silica stones are carried out by microscopic techniques and analytical instruments such as electron microprobe (EMP) and x-ray diffraction (XRD). In order to determine the origin of stones, it is necessary to know some information such as the

general distribution of the defects, furnace parameters, any other defects showing parallel increase with silica defects and to check the furnace operations. Although numerous silica defects have the same composition as silicon dioxide, more than 90% of these defects can easily be identified by a simple binocular microscope after a certain period of experience. The form of defect and it's components, crystal type and its dimensions, the character of the borders with base glass, distribution and density on the ribbon gives several clues about the origin of defects. In addition to this, some chemical analyses by electron microprobe, especially some trace elements within the glassy phase of the defects helps for determination.

Besides the systematic defect analyses, observation of used materials during the cold repair of furnaces is an important source of knowledge. Corrosion points and extent, crystal types and forms of different zones, absorption of volatile elements, condensation regions and localities of flows give important information about the causes of corrosion.

2. Descriptions of Used Silica Refractories

As it is known, large areas of superstructure and all of the crown are covered by silica refractories and mortars. When the old melting furnaces are observed during cold repair, some parts of the superstructure and crown are observed to be intensively corroded. The areas which are critical for corrosion occur in the right and left sides of the crown around hot point, expansion joints 1/2, 3/4, back wall over the doghouse, front wall at the melting end. High temperature and carryover, alkali penetration and condensations are the main parameters that act directly on corrosion of silica materials. The superstructure of the refining area seems to be of darker colours towards the colder parts. Oxides of vanadium and nickel in fuel-oil, are absorbed in the glassy phases of superstructure materials and increase at lower temperature zones. The appearance of refractories in refining areas of the furnaces heated by natural gas seem to be dry, irregular and flake.

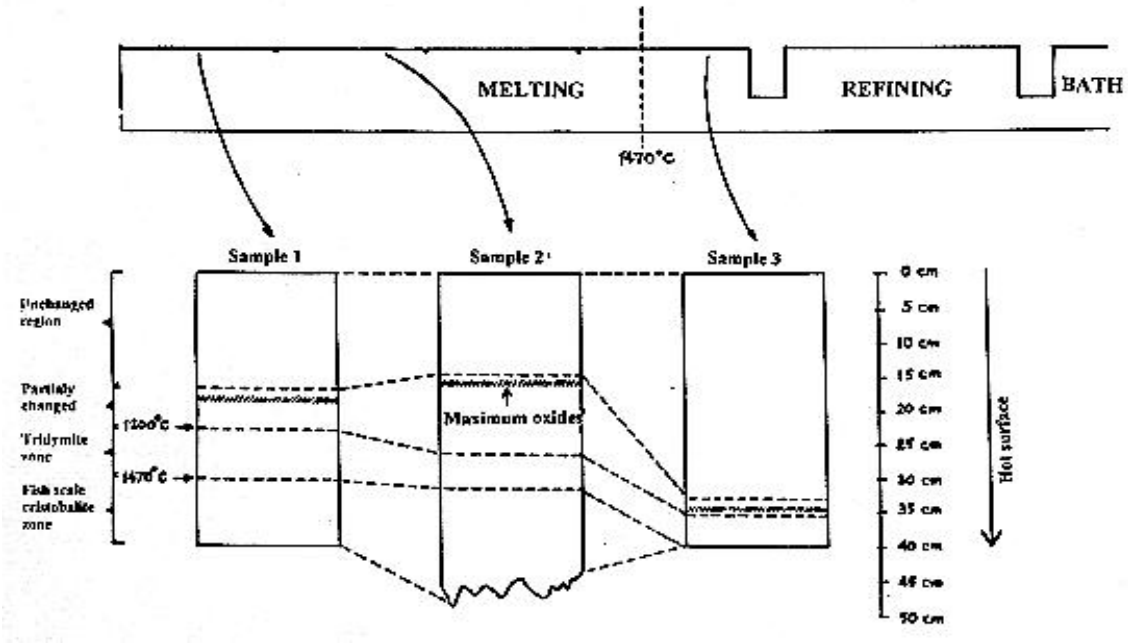

Figure 1 Petrographic structures of three samples

Detail studies were accomplished [1] on used silica refractories taken from some parts of the melting tank during cold repair (Fig. 1). 10 mm slices were cut from hot surface to the cold end for each sample and analysed by XRF, to obtain the element distribution profiles of each sample along the depth.

The following conclusions are summarized.

- Two kinds of mechanisms are affected on the element distribution along the depth. One is the diffusion of Na_2O and MgO from furnace atmosphere through the surface of the silica bricks. The second factor is the movement, towards the cold end, of CaO and other oxides such as Al_2O_3, Fe_2O_3, K_2O and TiO_2 which are homogeneously distributed in the original bricks. The oxides move towards the colder depth of the bricks by temperature gradient, diffusion and vapor pressure of the furnace atmosphere.
- From hot surface to the temperature gradient of 1470^oC, the bricks are composed of fish-scale crystobalite and some glassy phases.
-The amount of glassy phases increases towards the colder parts.
- The second zone is composed of plate or lath-like tridymites oriented vertically, because of compression and gravity.
- Na_2O and MgO contents of glassy phase decrease in depth but CaO and other oxides increase.
- Below the temperature point of 1200^oC, pseudowollastonite crystals appear.
- In the zone, which has abundant pseudowallastonite crystals, the other elements oxides are at maximum concentration.
- Some part of CaO and all the other oxides like Al_2O_3, Fe_2O_3, K_2O and TiO_2 are placed in the residual glassy phase after pseudowollastonite crystallization. This zone is between the temperatures of 1200 - 900 ^oC.
- After the last zone, the refractory structure does not show any change.

An example of chemical composition of pseudowollastonite and the adjacent glassy phase is given in the following table:

Oxides	Pseudowollastonite	Glassy-phase
SiO_2	49.99	70.30
CaO	50.53	7.20
Na_2O		4.50
MgO		0.99
K_2O		1.31
FeO		10.75
Al_2O_3		4.66
TiO_2		0.31

3. General Classification of Silica Stone Defects

The silica stones can be classified with respect to their origin:

Batch Stone
. inefficient melting Cristobalite
. segregation of batch
. corrosion of superstructure and crown
. carryover

Tridymite
. corrosion
. devitrification

Quartz
. coarse grained sand and clay contamination
. fragments from cold parts of the furnace

The schematic representations of silica transformations and probable sources of defects is shown in the following figure.

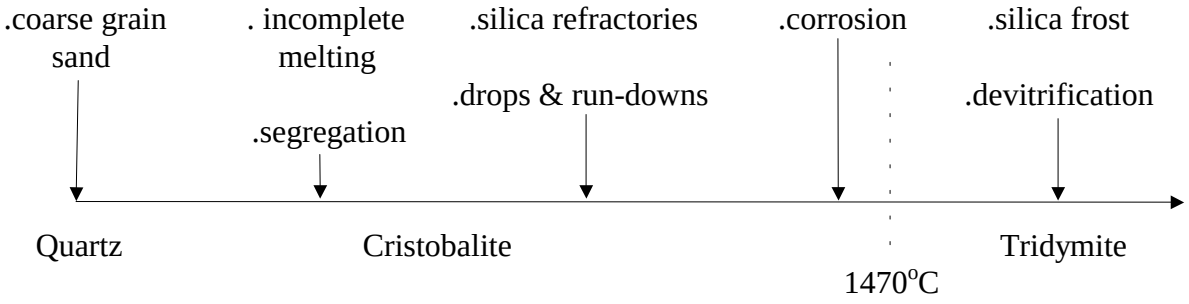

4.Silica Stones Arising from Corrosion of Furnace Refractories

Silica defects can be categorized into two main groups. The first group can be named as "drop-like" defects, arising mainly from increasing temperature, affected by fluxing agents and carryover, condensation of volatiles; the second group is "fragmental defects" originating from superstructure and crown by mechanical actions, slidings, sudden pressure differences , and repair activities.

4.1. Drop-like Defects

Crown drips: Drips are typically composed of secondary crystobalite /tridymite dentrites randomly distributed in a glassy phase having high silica content. Their forms are commonly apparent from the very smooth taper and the irregular shape of the larger end of the defect where they had broken away the parent drippage.

Drippage from expansion joints and silica mortars: They have the same form and crystalline characteristics as in crown drips, except the glassy-phase contains more iron, vanadium and nickel content, because of temperature drop within expansion joints and porous structure of mortar. Sometimes primary silica fragments can be seen besides secondary dentrites.

Superstructure run-down: Stones are largely secondary dentritic cristobalite in a certain orientation surrounded by glassy phase drived from fused AZS blocks. The defect have sometimes dentritic zirconia besides cristobalites. The principal source of stone is the crown or superstructure and they run-down over AZS fused cast breast walls, which pick up some zirconia dentrites or glassy phases including AZS components.

Breast wall run-down, arising from carryover: If the grain size of any batch component like sand, feldspar, dolomite and soda become finer, and the batch moisture content is low, improper firing and charging conditions can cause carryover. Dusty materials can be accumulated on the wet breast wall around doghouse and dissolve in time and run down to the melt. The petrographic features are the same as superstructure run-down, arising from crown. The only difference is rather fine and radial orientation of cristobalite dentrites starting from point sources.

4.2. Fragmental Defects

Silica fragments & spallings: Probable origin of such stones are the colder parts of the melter and refiner. Their common features show angular form, recent primary structure, mostly plate or lath-like tridymite crystals with no solution sac.

Siliceous scales (frost): Siliceous scale, known as "frost" which is formed on the surface of the silica bricks of the crown and side wall around melting end in the flame free zone of the float furnace heated by natural gas. When these siliceous scales drop on the surface of the melt in cooler part of the melter, being drawn up before it is completely dissolved into molten glass, causing serious production losses. Frost is composed of conglomeratic plate-like tridymite crystals with a minor amount of glassy phase. Experiences show that the atmospheric conditions of the melter and the quality of the silica bricks are the effective parameters on the mechanism of frost formation. This problem can be solved by permitting excess oxygen into the refining area.

During a frost problem, two different kinds of silica bricks of super-duty quality manufactured by different suppliers were placed together in the peep hole at the critical region at refining zone for 6 months. Later the bricks were removed and detail petrographic identifications and EMP analyses were carried out. The first brick was used in furnace having frost problem which had a CaO content of 2.9% and a flux factor of 0.32. The second brick had a CaO contents of 2.6% and a flux factor (Al_2O_3+ K_2O) of 0.39.

From the detail studies, the following points are summarized.

-Grain size distribution of two original bricks were different before testing.

-After 6 months of testing, the hot surfaces of both silica bricks were covered with tabular tridymite crystals with small amount of glassy phase.

-Thickness of tridymite zone of first brick was 35 mm and the second brick was 27 mm. Tridymite formation of the first brick was loose, friable with finger nail and oriented in a

certain direction; but the tridymite formation of the second brick was interlocking to each other and was not friable in spite of a knife. The results of the surface differences of the two bricks under testing in the same place and atmospheric condition were rather interesting.

-Pseudowollastonite crystals were formed in a depth of 27 mm for the first brick, and 20 mm for the second brick. That is to say the first brick was more permeable in such atmospheric conditions.

-Both original silica bricks were submerged into the Na_2SO_4 melt in 1100^oC and later they were kept for 5 hours at a temperature of 1450^oC. After the testing, the first brick was completely disintegrated.

It is believed that, the silica brick quality is important but not the single factor for frost formation. As a matter of fact, the problem was solved in spite of those bricks.

5. Silica Stones Arising from Batch Materials

These kind of defects may, from time to time, become the most predominant defect group. Their distribution is homogeneous along the ribbon and usually the defect density is suddenly increased. They originated from two principal factors. The first one is the batch feeding problems and contamination of batch materials (including coarse grain sand), the second one is the furnace operating conditions.

The following examples are given for such kinds of defects originated from batch materials.

Batch stone drifting along the flux-line: When the stones are drifted along the corroded side blocks at flux-line, because of shadow effect they are not dissolved but partly transformed to cristobalite within a glassy-phase belonging to AZS refractories or some primary or secondary zirconia with them. They are identified from breast wall run downs arising from carryover by their partial transformation.

Batch stone originated from incomplete melting: Small bubbles resulting from insufficient refining conditions are increased with such silica stones of batch origin. These kinds of defects show radial cristobalites started from a source points with a small amount of solution suc. Some small bubbles are commonly present within this kind of defect. Complete or partial cristobalite transformation is characteristic.

Scum is originated from alkali volatilization from surface of the molten glass at high temperatures and it is characteristic for tabular cristobalite crystals showing New-York pattern.

Silica segregation may arise from segregation of batch materials during storage, mixing or transportation. Nonconformity of grain size distribution of soda and sand may cause such silica defect also. This kind of defect is exactly the same with batch stones. The only difference is its lower density and no bubble defects beside it. It may not cause any severe production losses.

Conglomerated sand is the result of clay contamination of sand where clay materials envelope the sand grains to prevent dissolving.

Silica stones within aluminous matrix or silica with nepheline or mullite crystals are also the result of clay contamination of sand.

Silica defects arising from coarse sand grains identified by their massive structure, partial transformations and the absence of pore (no bubbles) within them.

6. Devitrification

The main sources of devitrification of the glass into tridymite are the water boxes and mixers in the furnace. The order of devitrification of components on such coolers is; devitrite, tridymite, diopside/wollastonite from cold to hot end. Therefore these devitrification components may be released from time to time by glass currents, temperature differences or mechanical actions. Such tridymite crystals are single or as crystal piles in glass with no solution sac. Rarely some broken refractories under the flux line or bottom can cause such devitrification problems.

7. Conclusion

Siliceous defects make up about 10 % of defects seen in glass production. They may originate from different sources like batch, corrosion of refractories and devitrification. These defects are all structural modifications of SiO_2 occurring as quartz, trydimite and cristobalite. A certain uncertainty still remains during identification, but by a built up of experience the origin of defects, interrelated with operational parameters, can be delineated.

The quality of refractories used play an important role for some of the silica defects. Frost is of this types. However, the application of suitable operational parameters may take care of the problem.

It is deemed to be important during the identification process to notice all details of textural differences of the minerals so that a sound correlation can be made.

[1]Arman, B., Özgen, S. and Aydýn, E., Mater. Sci. Monogr., 1991, 66 (A) 455-63

THE ADVANCED GLASS MELTER

G.Turton
KTG Systems, Inc., USA

1.0 INTRODUCTION

The Advanced Glass Melter (AGM) is a project initiated and sponsored by the Gas Research Institute (GRI) of Chicago, Illinois, USA. The basic idea was to directly inject the batch ingredients into a gas flame initiating rapid heating and melting of the fluxes and decomposition of the other carbonates. The heated material is then collected in a glass reservoir to continue homogenization and refining processes. In an initial project, a pilot facility sized to produce 7 US tons (6.4 tones) per day was constructed and operated by Textron Defense Systems (TDS) at their research facility in Everett, Massachusetts. This unit operated with enough success that GRI decided to sponsor a field unit, to include in a production line to produce a commercial quality glass. KTG Systems was the successful bidder- on this project, proposing a join effort with Knauf Fiber Glass and TDS to design, construct and operate a 13.8 US tons (12.5 tones) per day unit to produce commercial blown fiberglass wool. The unit was built at the Knauf plant in Shelbyvile, Indiana. Klug Systems of Rochester, New York were subcontracted to design the batch feed system. This paper describes the design, construction initial testing and present situation of this utility. The main objectives of this program were:

- Transfer AGM Technology from the laboratory to a field installation.
- Use the AGM to manufacture fiber glass.
- Develop a fully integrated melt system with all necessary ancillary components.
- Operate the AGM in a complete fiberglass run to life test to determine the long term economics of the AGM.

2.0 FIELD UNIT DESCRIPTION

The plan view overhead shows the main components of the system comprising:

- The batch supply cans containing Kanuf's normal pre-mixed batch.
- The melting unit.
- The prot, exhaust stack, and duct.
- The throat and riser.
- The forehearth and bushing.

The cross section overhead shows:

- The batch holing bins (2 off) and the screw feeder locations (4 off).
- The vitiation burner (combustion air pre-heater) to simulate pre-heated
- The batch feed section (4 injectors).
- The combustion mounted on the meter roof.
- The exhaust stack.
- The melter superstructure.

- The heat up burner.
- The batch material flow path.
- The glass holding bath.

The longitudinal section overhead shows:

- Further screw feeder detail and batch feed lines (rubber hose) to the sectors.
- Further detail of the stack sized and location.
- Detail of the throat, riser and forehearth connections.

The longitudinal section does not show the throat electrode locations. Five (5) 1'/ " diameter molybdenum electrodes were located in the throat (2) and riser (3) to assist glow flow during heat-up. The main concerns were the green glass color with poor heat conduction and the small throat opening of 6" x 10".

3.0 COMPONENT DETAILS

The forehearth was a conventional fiberglass type unit, gas fired.

The melter was 3'-6" (1.067 in) square and 41" of glass. The overhead shows these dimensions and also the electrode locations. A variety of materials were used for the glass contact areas and throat to monitor the performance and provide information for future units. The refractories used were from the bonded chrome alumina class (30% chrome upwards), the fused cast chrome class (30 % chrome upwards), and the 34 % and 41 % fused case AZS materials. The superstructure and stack was bonded AZS, and the roof was cast high alumina. All materials were typical glass furnace refractories with a glass wool compatibility bias.

The experimental and unique part of this system is the combustor. The important sections of the combustor, as shown on the overhead are:

- The vitiation burner system comprising the burner assembly, and adaptor, the burner block and housing and the de-coupling sections (flame development section).
- The vitiation burner is intended to simulate pre-heated air. Gas and air is burnt and air and oxygen are added to the combustion products through the oxygen and air rings. The oxygen is added to bring the level up to that of air (approximately 21 %). The air is added to cool the temperature to approximately 1400^{o} F -1450^{o} F to simulate that of an efficient recuperator.
- An air and water cooled refractory lined spool section to align the gas flow.
- An air and water cooled, refractory lined batch injector section with four (4) symmetrically positioned 3/4 " diameter batch injector tubes. The batch injector tubes are connected by rubber hose to the discharge hoppers from the four screw feeders shown on previous overheads.
- Immadiately below the batch injection section is the gas injector ring.
- Below the gas injector ring are three air and water cooled, refractory lined combustor sections in which the particle heating occurs.
- The diameter and length of these sections are significant in affecting the heat furnace.
- The final section is the nozzle section. This is refractory lined and air

cooled. The pre-heated batch components are directed vertically downwards by this nozzle onto the glass pool.

The unit had a significant instrumentation's package, supplied by ACSI of Toledo, Ohio, comprising:

- Batch flow control variable through four (4) screw feeders. Each feeder can be set at 0 - 100 % of total flow. Total batch flow is controlled from a laser glass level sensor located at the exit from the throat via a glass level control loop in the P.L.C.
- Significant temperature monitoring of the internal temperatures of the vitiation burner, spool and combustor sections and temperature gradients through the walls.
- Vitiation burner temperature, gas and air flows; dilution air flow and spool temperature; batch carrier air flow; combustor temperature, gas and oxygen flow and % of O_2, in the gas stream prior to introduction of the gas.
- Melter superstructure and glass temperatures, exhaust temperatures, throat and riser temperatures, throat boost volts and amps, forehearth temperatures, melter pressure and

The unit described above was put into operation in February 1994.

4.0 OPERATIONS

4.1 Heat-up and Fill

The unit was pre-heated with its own burner. The heat-up burner is a nozzle mix gas-air unit with flame supervision and spark ignition. The heat-up is typical for chrome and AZS refractories at 10 ^{o}F (5.6 ^{o}C) per hour up to 500 ^{o}F(260 ^{o}C), then 20 ^{o}F (11.1 ^{o}C) per hour up to 2200^{o} F (1204 ^{o}C), the 25 ^{o}F (13.9 ^{o}C). The vitiation burner was lit off at 840 ^{o}F (449 ^{o}C), the main burner at 1800 ^{o}F (982 ^{o}C). Batch feed began at 2100^{o} F (1149^{o} C). The total heat-up and fill time was less than 7 days (164 hours).

4.2 Testing

The main objectives of the test run were:

- A 30 day continuous production run.
- Produce commercial quality fiberglass.
- Evaluate Combustor and melter wear rates.
- Evaluate combustor operational performance.
- Evaluate batch injection velocity/method.
- Evaluate AGM effect to glass chemistry.
- Evaluate AGM for melting other materials.

The system was fine tuned, and batch adjustments made for the first 7 days of operation. Glass chemistry was adjusted to meet spinner requirements. The spinners were tested on day six, and at 7: a.m. on day seven a 24 hour fiber production run was started. The practical pull rate was about 850 lbs/hour 10.2 US tons/day; 9.3 tonnes/day). The melter superstructure temperature was 250 ^{o}F (1371 ^{o}C). A burner malfunction, caused by an electrical problem, shut down the fiberglass production after approximately 16 hours. During the run commercial fiberglass insulation wool was produced, mixed with Knauf's existing production from other furnaces and

sold. The unit was operated for a further seven days testing batch injection and overall performance. Significant emissions testing was carried out during this period. During this period the burner developed a significant "howling" and a burst sprinkler unit shut down the throat heating, which could not be saved, so after a total of 14 days operation the unit was shut.

Modifications have been made to the burner and burner related systems to solve the howl problem, some minor repairs have been carried out, and the unit is now ready to be restarted.

The main objectives and benefits of this unit for fiberglass wool production are seen to be:

- Reduced capital costs and rebuild costs as compared to conventional systems.
- Reduced operations and maintenance costs due to the compact size of the AGM.
- Improved melting Thermal efficiency.
- Reduced pollution emissions.

CONCLUSIONS

l. A commercial size AGM unit was built and operated.
2. Commercial quality fiberglass wool was produced.
3. Data was collected to provide solutions to problems encountered, and provide information for scale up to a larger unit.
4. Further testing of the existing field unit is still required before commercialization of the unit can be considered.

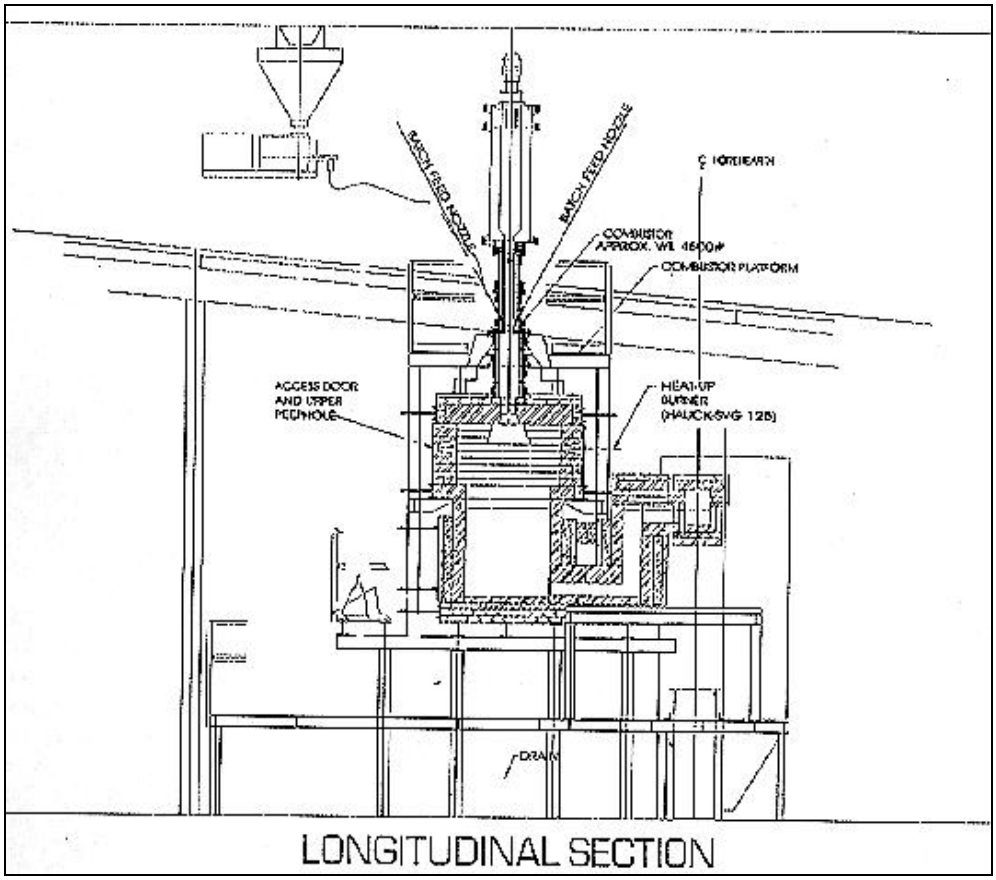
BATCH FEED NOZZLE
BATCH FEED NOZZLE
COMBUSTOR
APPROX. WT. 4600#
COMBUSTOR PLATFORM
ACCESS DOOR
AND UPPER
PEEPHOLE
HEAT-UP
BURNER
(HAUCK-SVG 125)
DRAIN
LONGITUDINAL SECTION

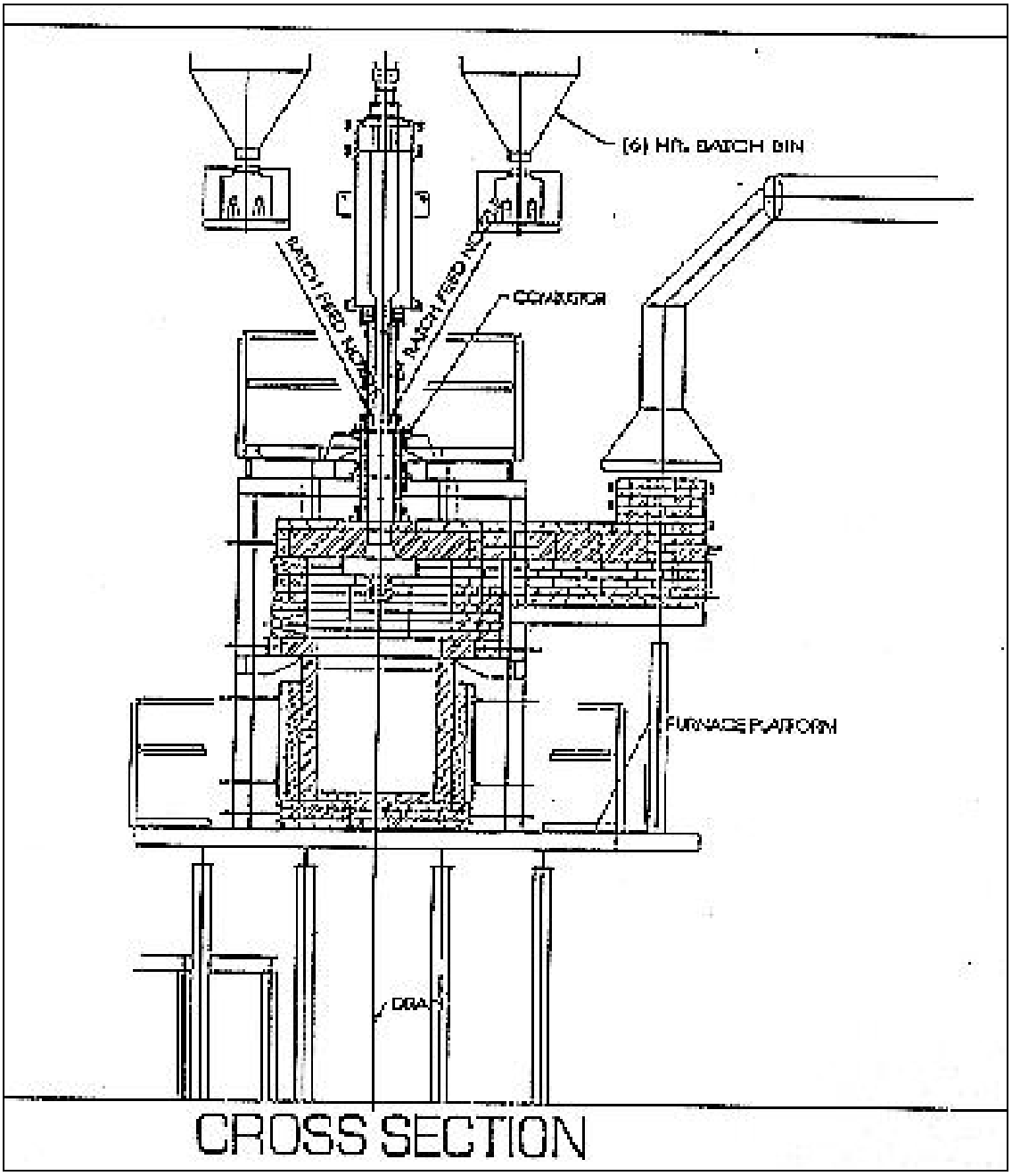
(6) HM. BATCH BIN
BATCH FED NO.
BATCH FED NO.
COMBUSTOR
FURNACE PLATFORM
DRA
CROSS SECTION

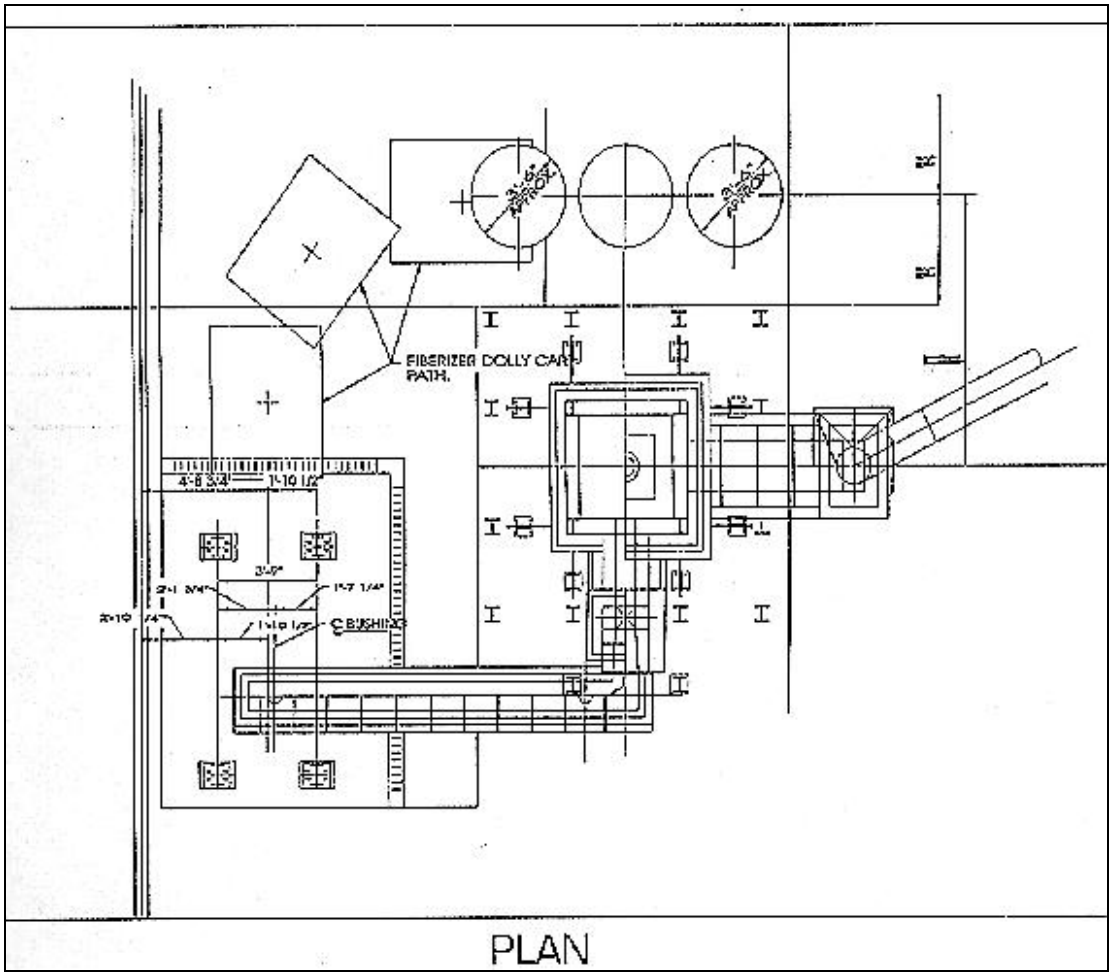
FIBERIZER DOLLY CAR PATH.
BUSHING
PLAN

ALKALI CORROSION OF SUPERSTRUCTURE REFRACTORY BRICKS IN OXY-FUEL FIRED GLASS FURNACES

John Brown[1], K.T. Wu[2] and **H. Kobayashi[2]**
1 Corning Inc., USA
2 Praxair Inc., USA

Abstract

Significant improvements to furnace operations and emissions have been documented for oxy-fuel fired furnaces. However, accelerated corrosion of silica crown has been experienced in some of these glass furnaces. The corrosion problem is believed to be caused by the higher concentration of volatile alkali species in oxy-fuel fired glass furnaces. Progress in furnace design and burner selection/placement/operation has resulted in reduction of these corrosion rates. This paper discusses corrosion problems experienced in commercial glass furnaces, techniques to measure alkali concentrations and deposition rates, and the application of a computer model to predict alkali volatilization and crown corrosion rates.

1. INTRODUCTION

Oxy-fuel firing can offer many advantages to the glass manufacturer. Cited[1] advantages range from lower NO_X emissions, capital reduction, energy savings, to production increase and improved glass quality. Typically, glass companies adopts the oxy-fuel firing technology based on the combined benefits of two or three from these advantages. Potential increase of oxy-fuel use by the year 2000 in each segment of the US glass industry has been reported[2]. We believe the adoption of oxy-fuel firing may be further amplified by the continued decrease in oxygen production costs.

Engineers have become more experienced in oxy-fuel design specifications due to the continuing progress of the conversion. Nevertheless, the requirement to understand more underlying physical and chemical processes about oxy-fuel combustion is recognized. One of these concerns is the long term performance of the silica crowns.

In a well constructed air-fired furnace, experience suggests that little loss of silica crown bricks should be expected for the entire furnace campaign. For oxy-fired glass furnaces, evidence gained from more than 60 furnace start-ups indicates a much lower severity of silica crown corrosion than had been anticipated. However, accelerated corrosion of silica crowns has been reported in some of the oxy-fired furnaces under certain operating conditions. To circumvent the corrosion problem, some glass manufacturers are substituting the silica crowns with the more expensive fused-cast crowns. This substitution may not be viewed as soly due to the application of the oxy-firing, since larger furnaces of over 50 m^2 in melting surface area have been investing in fused cast materials for breastwalls and sometimes crowns, long before the acceptance of the oxy-fuel firing.

The use of the fused-cast crowns can seriously off-set the capital savings gained from the elimination of the regenerators, primarily due to a cost increase of 20 to one. For example, in the 50 m^2 furnace this can increase the cost of the crown from $ 50,000 to a practically unaffordable cost of one million dollars. Clearly, the economic incentive to continue the use of the silica crown is immense. It Is this incentive that motivates our current interest in studying the corrosion phenomena of silica bricks under the oxy-fired environment.

2. OBJECTIVE AND APPROACH

The overall objective of this paper is to discuss the methodologies that are being developed to minimize the corrosion of silica crowns. The approach to address the corrosion issue involves: (a) A brief literature review on previous understanding of the silica-crown corrosion phenomena; (b) Discussion of alkali-vapor measurement techniques; and (c) The development and application of a three-dimensional computer model to predict alkali volatilization and crown corrosion rates. The following section discusses these topics and presents examples of the modeling results.

2. DISCUSSION AND RESULTS

Silica Crown Corrosion

Structural changes and corrosion behaviors of silica bricks in air-fired glass furnaces have been reported in several studies. Morsanyi[3] analyzed samples of slagged silica-brick taken from the superstructures of six glass tanks (float and TV). This study proposed a strong correlation between the total alkali contents (Na and K) in the slag and the brick temperature. Slag samples taken from the high-temperature zones contained low alkali concentrations, but those from the lower-temperature zones had higher alkalis. Loss of silica bricks was slightly higher for the samples with lower alkali contents, i.e., from the higher temperature regions. The author suggested that the rate of silica loss would depend on the mass transfer rate of alkali to the silicate slag layer.

In another investigation[4] a comparison was made on the behavior of silica bricks in the crowns of two soda-lime glass tanks. The bricks were supplied by various vendors and had different physical properties. It was found that all silica brick showed similar wear rates but the rate was higher at regions where crown temperatures were lower. The higher corrosion rate was explained by the formation of liquid alkali-silicates at the lower temperature locations, due to the condensation of alkali components from the combustion atmosphere.

As can be seen, there are conflicting data and opinions regarding the effects of temperature on the rate of silica loss. Most high-temperature corrosion accelerates rapidly with increasing temperature, but literature data and field experience suggest that silica crown corrosion has a relatively weak temperature-dependence.

The formation of a liquidus layer of alkali-silicates on the silica brick surface, followed by dripping or running down to the side walls, appears to be the physical mechanism causing the loss of silica bricks. Available data[3] suggests that the slagging can reach steady state after an "incipient" period. Under this picture, the alkali concentration in the slag builds up to a limiting level and makes the slag viscosity low enough for the slag to flow or drip. Morsanyi[3] proposed

that under this situation the alkali contents in the sample bricks are no measure of the corrosion rates, and the corrosion rates should be assessed in unit of loss in brick-length per unit time.

In oxy-fuel fired furnaces accelerated corrosion of silica crowns were observed often in lower temperature zones and around brick joints. In some furnaces silica crown exhibited a "wet" appearance covered with a liquid slag layer. The cause of the corrosion is believed to be the higher concentrations of alkali vapor species in the furnace atmosphere. Although the mechanism and the rate controlling steps of the corrosion are not well understood at present, it is expected that the velocity of the furnace gas near the crown will be an important parameter influencing the rate of alkali transfer and crown corrosion.

Improved Engineering Design

Alkali-rich silica rundown can cause glass quality problems if it erodes AZS breastwalls. The alkali-rich silica will pick up the more refractory-like alumina-silica glass and zirconia stones. Silica crowns can cause little damage to glass if they drip in the rear of the furnace and they do not carry other more refractory-like alumina-zirconia oxides. We have demonstrated that improved superstructure construction can greatly reduce the adverse impact associated with the silica rundown. This improvement includes additional care in brick sizing to minimize joints and in specifying chemical purity of the silica, as well as paying more attention to the quality of the superstructure construction.

Corning has engineered many improvements for the construction of the silica crown. Figure 1 shows an example where some design changes are applied to furnace superstructure construction in order to prevent defects from the AZS breastwalls. As shown in Figure 1, the use of the AZS in fused cast or bonded form for skews can strengthen a potentially weak area. Adding a neutral course next to the AZS skew prevents attack of the first silica course from the alumina contained in the skew block. The neutral course alone may not provide satisfactory protection to the first silica course.

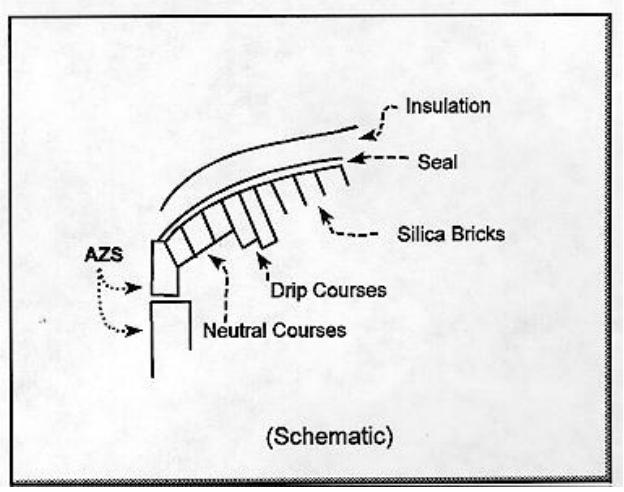

Figure 1. Improved Silica Crown Construction

Building a positive drip course starting several courses out from the first neutral course prevents drip from coming in contact with any AZS wall materials. Furthermore, the positive drip course are re-enforced by adding several more courses with each course extends more than the last one.

It is important to keep minimum joints between silica crown bricks. A seal course on top of the silica performs as a second barrier, to prevent transportation of furnace alkali vapors through the crown. In addition to the seal course, appropriate insulation of the crown with multiple layers of insulation brick will save energy and prevent alkali vapor condensation. The location and number of the exhaust ports should be selected with a goal to minimize radiation heat loss and the concentration of the alkalis in the combustion products.

Mathematical Modeling

Alkali volatilization is believed to be a major route contributing to particulate emissions and refractory corrosion in glass furnaces. Oxy-fuel conversion results in higher concentrations of water vapor in the flue gas stream and lower flue gas velocity in furnaces. Both of these factors have immediate impact on alkali volatilization rate, since higher water vapor concentration increases the volatilization rate while lower flue gas velocity reduces it. A 3D combustion space model has been developed and applied to evaluate the impact of burner elevation on the rates of alkali volatilization and crown corrosion.[6-7] Our ultimate goal of developing the computer model is to minimize particulate emissions and refractory corrosion through furnace design modeling.

The current alkali volatilization model assumes that the most important mechanism for NaOH volatilization from the soda-lime glass furnaces is caused by water vapor reacting with Na_2O in the melt, expressed as $Na_2O_{(l)} + H_2O_{(g)} \rightarrow 2\ NaOH_{(g)}$. The model also considers another NaOH volatilization route described as $Na_2C0_{3\ (batch)} + H_2O_{(g)} \rightarrow 2\ NaOH_{\ (g)} + C_{O2}$. The alkali volatilization model at its current format does not include other forms of NaOH sources such as Na_2SO_4 volatilization directly from the glass surfaces. Field experience has indicated that for other type of glasses batch chemistry might alter the partition of the particulate sources. Current model development efforts are directed at understanding the extent of batch contribution to volatilization and conducting field measurement to validate the model's predictions.

At present, the refractory corrosion modeling is limited to silica crown only. The corrosion model assumes NaOH vapor in the furnace atmosphere reacts with silica to form a liquid layer of sodium silicates, which runs down the crown and sidewalls. Although a detailed description of refractory corrosion mechanisms is not yet available, the transport of NaOH vapor to the refractory surface by gas phase diffusion through the bulk boundary layer near the crown may be the rate-controlling step. With these assumptions in place, the rate of refractory corrosion can be expressed as a function of local gas velocity, flue gas temperature, crown surface temperature, and NaOH concentrations. It should be noted that this model provides the upper limits of the corrosion rate, since other potential rate-limiting steps such as pore diffusion and solid phase diffusion of sodium species are assumed to be faster than the gas phase diffusion.

The 3D combustion space model was used to assist a 330 TPD furnace design project. Several furnace geometries were examined and the burner elevation was a design variable. The design goal was to minimize the alkali volatilization and the crown corrosion rates, while maintaining a desired level of furnace thermal efficiency and a preferred range of crown temperatures.

Figures 3 and 4 compare the predicted alkali volatilization and crown corrosion rates for two furnace arrangements, named as the "conventional" and the "low emission" designs. The ∇ symbols indicate the burner axial locations. The numerical numbers shown in Figure 2 represent the rate of NaOH volatilization in mass per unit time per unit melting area, and those in Figure 3 show the predicted silica corrosion rates in length per unit time. The modeling results show that

the low emission furnace has much lower alkali volatilization and crown corrosion rates. The low emission design reduces the peak volatilization rates from about 3.5 to 1.0, and decreases the peak crown-corrosion rates substantially from 2.0 to 1.0. In addition, the volatilization results imply a reduction of 43% in Na_2SO_4 particulate emissions downstream of the flue exit. Although not shown here, the model results also indicate the low emission furnace maintains the desirable thermal efficiency level and applicable crown temperatures.

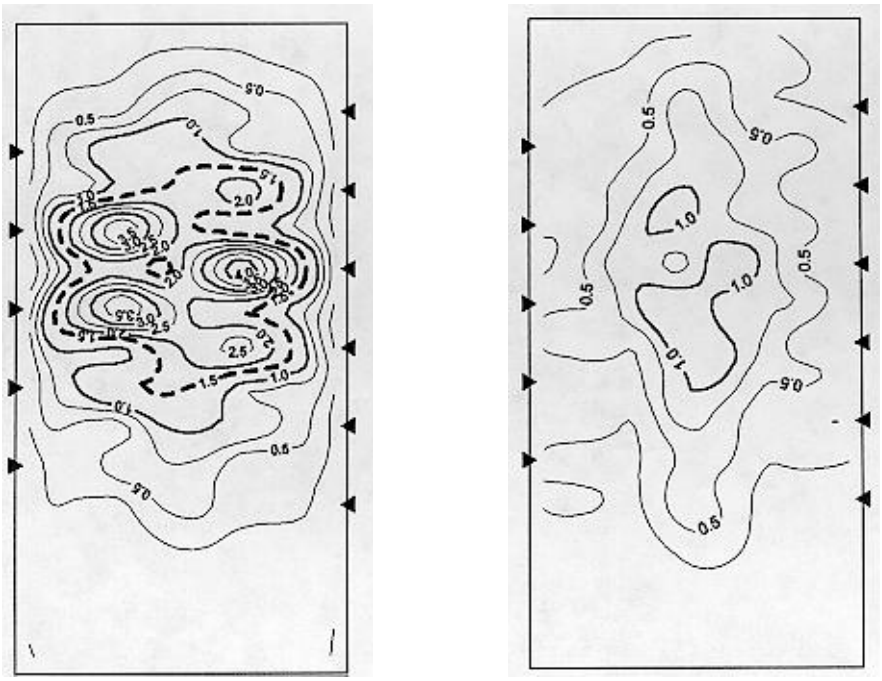

Charge End — Charge End

(a) Conventional Design (b) Low Emission Design

Figure 2. NaOH Volatilization Rate vs. Furnace Design (Prediction)

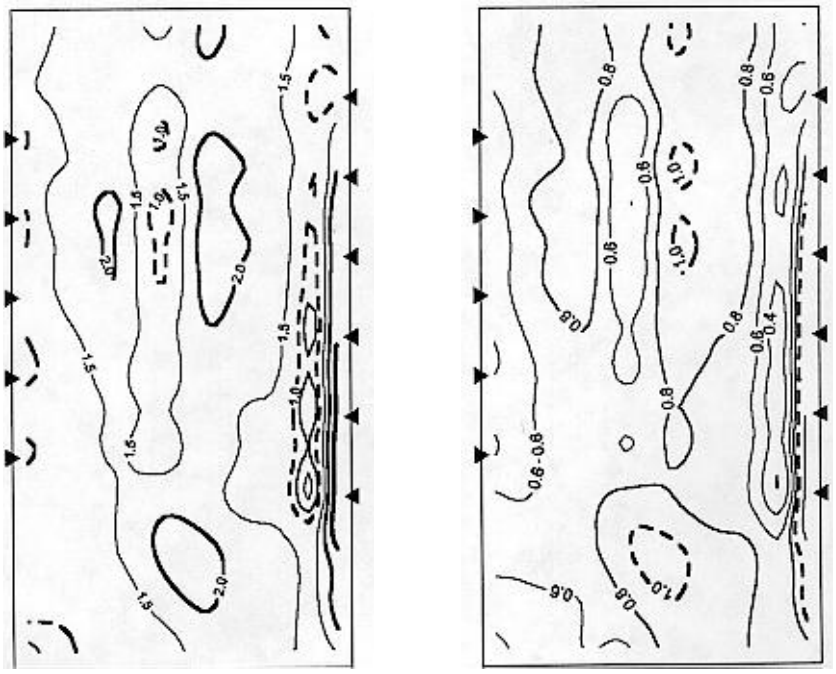

Charge End
(a) Conventional Design

Charge End
(b) Low Emission Design

Figure 3. Corrosion Rate of Silica Crown vs. Furnace Design (Prediction)

Development of Measurement Techniques

To understand the corrosion phenomena of silica crown better, it is desirable to measure the concentration of alkali species, crown temperature, gas temperature, and gas velocities near the crown. The measurement of alkali vapor concentration by gas sampling were carried out in several furnaces through peep holes. The procedure is tedious and time consuming because the volatile alkali-species can react with other gases in the sampling system during cooling and form various salts. For example, NaOH is the most dominant vapor species containing sodium in sulfate-fined soda-lime glass furnaces. As the sample gas is cooled down Na_2SO_4 formation occurs, which condenses on the sampling lines and also dissolves in the condensed water. Therefore, the entire sampling system must be washed with a pre-determined amount of water to dissolve all sodium-containing species. The water collected from the sampling system is analyzed for sodium content later. In theory, the same method can be applied to collect gas samples from near the crown but is very limited by available openings. In most cases the only available openings are thermocouple holes on the crown.

The measurement of gas velocity near the crown surface is extremely difficult. Model results indicate typical gas velocities near the crown surface are in the order of 0.5 to 5 m/sec, which provide only 0.0026 to 0.26 mm of water column in differential pressure and are difficult to measure accurately. Likewise, the access to the crown area is severely limited. By comparison the measurement of crown temperature is relatively easy. Extrapolation of crown thermocouple readings, if available, can provide good temperature data for use. Gas temperatures near the

crown may be estimated from the crown temperatures with the help of the modeling results, or measured by using conventional methods such as a suction pyrometer.

An alternative approach of alkali measurement is to use a deposition probe and measure the amount of alkali species deposited on the probe. The amount of alkali transferred to the probe surface depends on the probe geometry and materials used, gas temperature and velocity, local alkali concentration, and various gas transport properties.

Water-cooled probes are often used in glass furnaces to measure particulate carryover and volatiles deposition. To estimate the rate of alkali transfer to silica brick surface from the deposition probe measurement, the mass transfer rates of the alkali species must be correlated well with the deposition parameters mentioned above. Unfortunately, the cold surface of the water-cooled probe influences the mass transfer rate significantly. This is due to the formation of a cold boundary layer near the probe surface, and its subsequent interference with many chemical reactions of alkali species near the boundary layer[5]. It is better to use a "hot" deposition probe made of the same material as the silica brick, and maintain the deposition surface "hot". In this case, the amount of alkali deposition is closely related to the transport of alkali to a fresh silica-brick surface, if the geometry factor of the mass transfer coefficient is compensated for. Detailed furnace measurements are currently underway using these techniques.

3. CONCLUSION

This paper reviews the previous understanding of silica crown corrosion and discusses the methodologies that are being developed to minimize alkali corrosion of superstructure bricks. The paper shows an improved silica-crown construction method which has been applied to the full-scale oxy-fired furnaces. A 3D combustion space model was applied to examine the furnace and burner design options of a 330 TPD soda-lime glass furnace. The model predictions show that significant reduction of particulate emissions and crown corrosion rates should be achievable if the furnace geometry and burner selection/placement are optimized. The paper also discusses measurement techniques for alkali vapor and identifies important measurement parameters. In-furnace measurement of alkali vapor species are currently underway and the results will be presented elsewhere in the near future.

REFERENCES

1. Schroeder, R. and Zak, A.,"*Oxy-fuel Economics Update Based on Case Histories*" Paper presented at the 56th Annual Conference on Glass Problems, University of Illinois, Urbana-Champaign, October 23-25,1995.

2. Benedek, K., Morgan, M., Wilson, R., Hobbs-Moore, V., and Donaldson, L., "Industry Drivers and Economics of Oxy-Gas Use in the US Glass Industry," Paper presented at the AFRC Spring Meeting, May 6-7, Orlando, Florida, USA

3. Morsanyi, A. V.,"*Silica Brick in the Superstructure of Glass-Melting Furnace,*"Glass Technology, Vol.7, No.6, pp.193-196(Part I) and 196-202(Part II),1966.

4. Konopicky,K., Patzak, I., and Routschka, G.,*"Verhalten von Silikasteinen in Glaswannenofen fur Natronkalkglas*," Glastechnische Berichte Vol.34, No.1, pp.1- 141961.
5. Beerkens, R.G.C. and Waal, H. de., "*Experimental and Thermodynamic Characterisation of Deposition and Condensation Products from Exhaust Gases of Glass Furnaces*," Glass Technology, Vol.28, pp.246-251,1987.
6. Wu, K.T. and Kobayashi, H.,"*Three-Dimensional Modeling of Alkali Volatilization/ Crown Corrosion in Oxy-Fired Glass Furnaces*," Paper presented at the 98th Annual Meeting of the American Ceramic Society, April 14-27, Indianapolis, Indiana, USA
7. Wu, K.T. and Misra, M.K.,"Design Modeling of Glass Furnace Oxy-Fuel Conversion Using Three Dimensional Models," Paper presented at the 56th Annual Conference on Glass Problems, University of Illinois, Urbana-Champaign, October 23-25,1995.

ASYMMETRIC ALKALI PENETRATION IN TIN BATH BLOCKS IN FLOAT GLASS LINES

Esref AYDIN
SISECAM Research Center, Turkey

Abstract

The increasing demand on higher quality of float glass by the customers, as the field of applications vary, exerts an everlasting pressure on the float glass producers. The quality of float glass is affected by several problems that are inherent to this production. "Peeling" or "flaking" of tin bath blocks is one of the most serious problems which the glass producers encounter. In extreme cases, flaking becomes so frequent during the production, there is not much that can be done to maintain the quality other than complete shot down.

Flaking occurs as the result of Na diffusion from molten tin to bath blocks. Na itself is diffused to molten tin from the glass substance during production. In this study, it is put forward that the diffusion of Na to the bath blocks is not uniform both along the width and length of the bath. It is shown that this phenomenon is clearly asymmetric in character in the float bath. A detailed mapping of the potential flaking depth, during a cold repair, has shown that the maximum depth of penetration (diffusion depth of Na) is reached at about 1/3 of the width of the wide section of the bath in Bay 2. The depth measured at this points is about 30 mm, whereas values of 11 mm and 15 mm are recorded at the right and left sides of the bath respectively.

Flaking may be potential up to Bay 10; towards the cold end in the narrow section it becomes negligible. The Na_2O content of the top layer of the blocks sampled as marker level in different Bays, varies from 2-10 %. However free flakes obtained during production show a higher Na_2O content (7-14 %).

There is an intense formation of nepheline in this zone. The diffusion of Na into the glassy phase of the fireclay refractory has culminated in a clear rim of nepheline formation around the coarse grains of the tin bath blocks. The formation of nepheline leads to a considerable volume increase.

The diffusion of Na attains its maximum at the left hand side of the bath at Bay 2, where operational intervention is exercised. It is also believed that frequent thickness changes of the substance, inherently resulting in temperature changes, may accelerate the possibility of flaking.

INTRODUCTION

The quality of float glass, as it stands, will not be surpassed for a long time still to come. However, the increasing demand on higher quality of float glass by the customers, as, the field of applications vary, exerts an everlasting pressure on float glass producers. It is a challenge that goes on. The quality of float glass is affected by several problems

that are inherent to this production. "Peeling" or "flaking" of tin bath blocks is one of the most serious problems which the glass producers encounter. In extreme cases, flaking becomes so frequent during the production, that there is not much that can be done to maintain the quality other than a complete shot down.

Flaking essentially occurs as a result of Na diffusion from molten tin to bath blocks in contact with tin. The distribution of flaking is largely restricted to the wide section of the bath, nevertheless it can also occur down the cold end.

The depth of penetration of sodium into the bath blocks at the cold end, the narrow section, is much lesser than the depth observed at the hot end side.

THE PROBLEM OF FLAKING

The problem of "flaking" or as sometimes is called "peeling", starts to appear after 2 or 3 years from the start-up. The flakers are dull-grey in colour and a few millimeters in thickness depending on which bay it originated. As a rule of thumb, it is safe to say that the thicker the flake the hotter the region the flakes originate from. The chemical composition of the flake has very little relationship with that of the original block. The flake is characterised by a considerable enrichment in Na_2O. Sodium oxide is originally absent in the bath blocks. The concentration of Na_2O in free flakes may change between 7-14%. Typical examples are given in Table 1.

Table 1: *XRF analyses of free flakes*

(Wt %)							
SiO_2	**Al_2O_3**	**Fe_2O_3**	**TiO_2**	**CaO**	**MgO**	**Na_2O**	**K_2O**
45.25	38.20	1.34	1.90	0.36	-	6.79	1.23
46.42	36.10	1.19	1.72	0.51	-	8.23	1.67
46.24	36.61	1.31	1.69	0.46	-	7.49	1.51
46.36	36.88	1.14	1.54	0.39	-	7.65	1.30
43.33	31.18	1.02	1.42	0.30	0.28	14.50	0.97

The microscopic, x-ray diffraction and electron microanalytical investigation of flakes reveal that there is an intensive nepheline formation around the coarse grains in the form of a well defined rim. Grains of smaller size grogs indicate more or less a total transformation to nepheline. The glassy phase is also enriched by Na_2O. The formation of nepheline in the top few millimeters of the bath blocks results in a considerable volume increase (20%). The shearing forces set up in the top layers due to this increase in volume culminates in flaking. The shearing strength parallel to flaking is about 36% less than that of the perpendicular equivalent.

A CASE STUDY DURING A COLD REPAIR

A further study was carried out during a cold repair of a float bath to find out the extent of Na_2O penetration on the blocks. Starting from the hot bays down to the cold end a careful mapping was carried out across the bath. The traverse lines were selected along the edges of the blocks. It was clearly noticed that the depth which has been affected by Na_2O penetration displayed a distinctly grey colour. Figure 1, shows some of the traverses that were mapped along the bays by this approach.

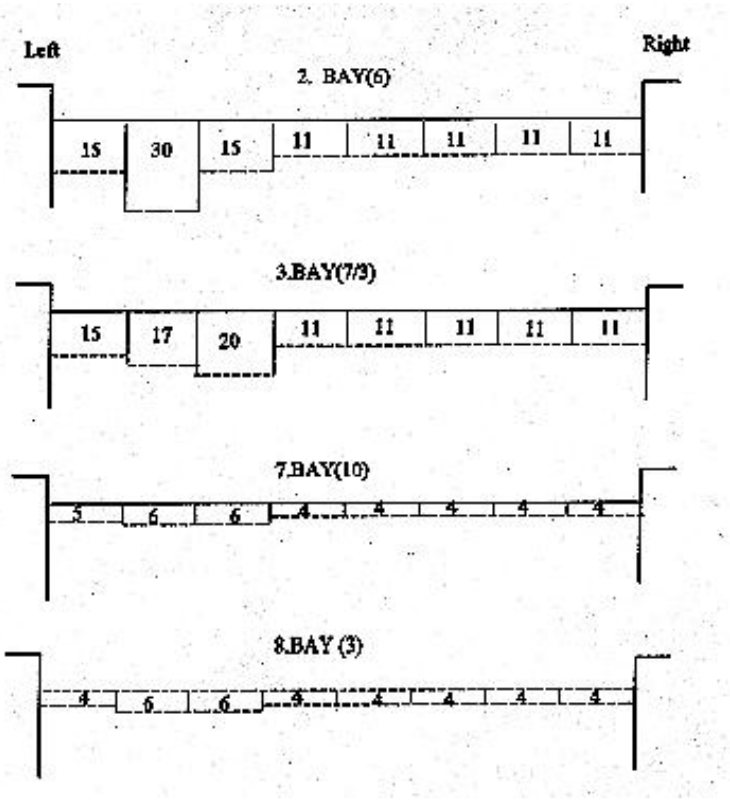

Figure 1: *Potential flaking levelat different bays*

It can clearly be seen from the traverses that the penetration (diffusion) of Na_2O is more prominant on the left hand side of the bath. Another important feature is that Na_2O diffusion gets less pronounced down the cold end. These lines clearly delineate the probable levels of flaking along the bath. The most interesting finding of this study is that the Na_2O diffusion into the blocks exhibits an asymmetrical nature. In other words, Na_2O attains its maximum diffusion depth across 1/3 of the width of the wide section of the bath on the left hand side. This is the side where operational intervention is largely exercised.

Sectional XRF analyses of the bath block indicates that the compositional changes occur predominantly in the first centimetre; quickly reaching the normal refractory composition after 2 cm (Figure 2).

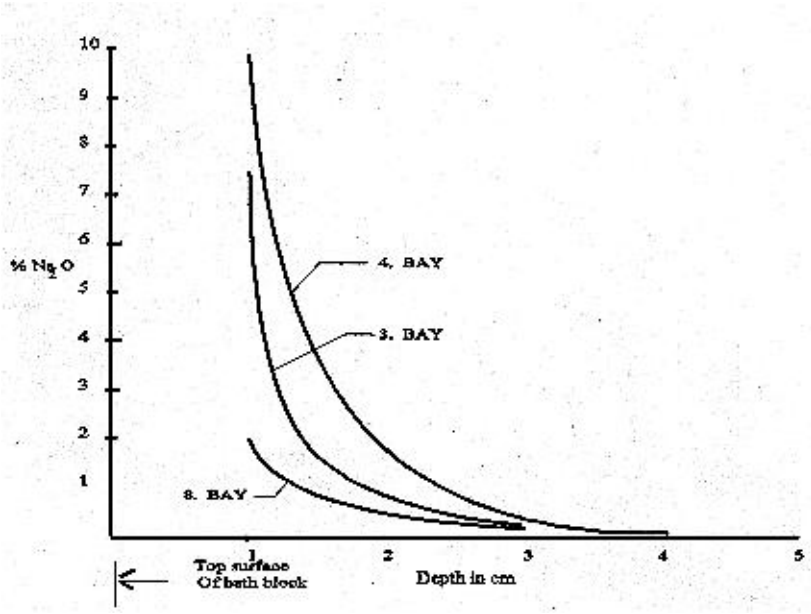

Figure 2: *XRF analysis of Sectional samples*

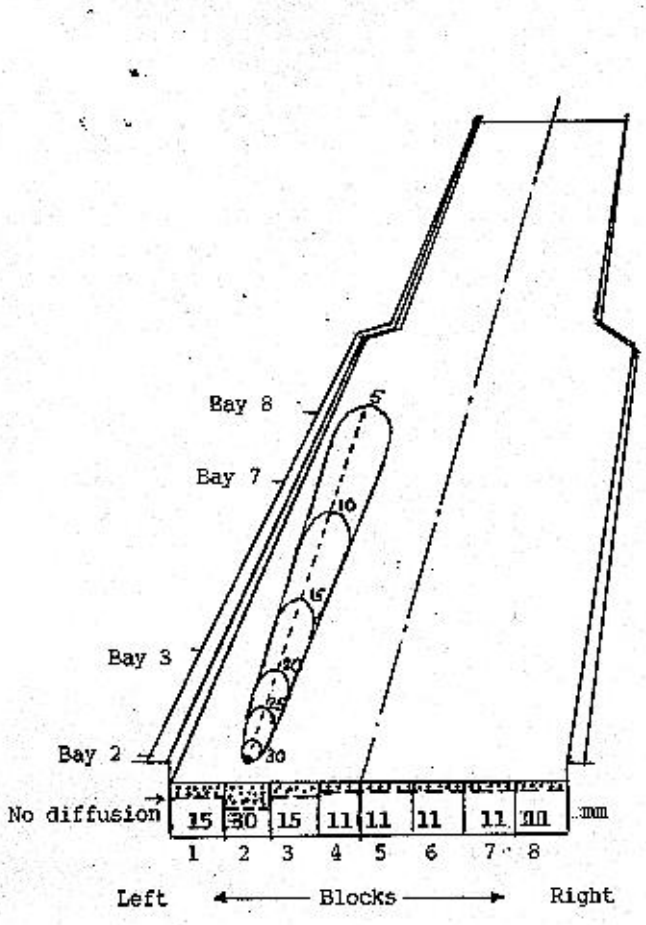

Figure 3: *Figurative display of flaking both across and along the length of tin bath*

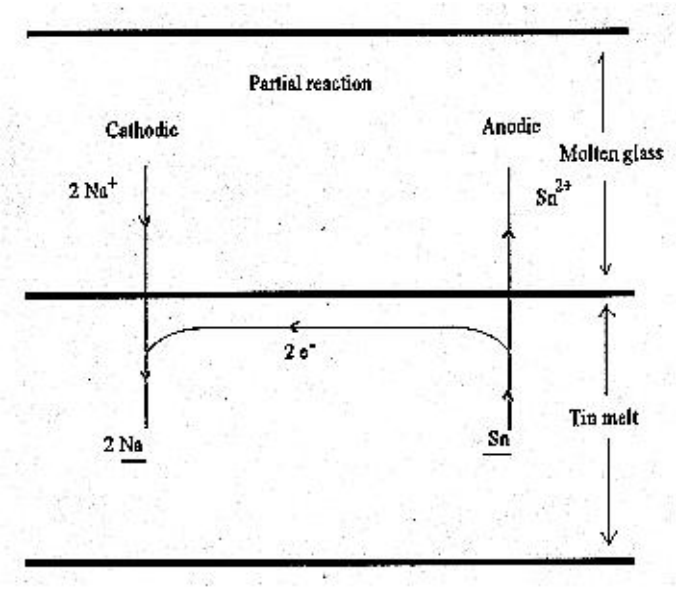

Figure 4: *Anodic and cathodic reactions of tin and sodium*

A figurative display of the flaking phenomena in the form of lines of equal depth is shown in Figure 3. Note that the focus of the lines converges around bay 2. Another point of interest is that the long axis of the figure is inclined towards the side of the bath rather than being parallel.

The same type of Na diffusion is seen in the side blocks of the bath where tin is in contact with the refractory.

DISCUSSION OF RESULTS

In the float glass process sodium is transferred from the molten glass via the tin bath to the refractory lining. The overall character of the reaction consists of the reaction of Na^+ ion to sodium which is dissolved in the tin bath[1,2]. The anodic part of the reaction is the oxidation of tin to Sn^{2+} ion (Figure 4).

The glass melt, in the float glass process, is continuously supplied to the float bath, and the glass melt floating on the molten tin is continuously renewed, while the tin is left in the float glass bath unit over longer periods of time. Experience shows that under this circumstances there is no noticeable increase in the Na_2O content of the molten tin. Na_2O is transferred from molten tin to the bath blocks during the campaign of the plant.

Changes of temperature in the bath as a results of thickness changes increases the flaking potential. Flaking develops mostly at the edge of the glass ribbon, more seldom in the centre of the tin bath[3]. The statement made by the above authors has been shown to be correct by the present study.

The refractory makers tend to act according to the needs of the glass maker. Therefore a good deal of research is carried out on bath blocks for improving the quality of refractory material, fired clay, so that flaking does not occur.

It is a fact that not all the refractories of this type act in the same manner. Currently, there are very few refractory suppliers which can meet the needs of glass makers.

Pilkington has set up several tests for bath refractories[4]. These are the basic guidelines for the glass maker and refractory suppliers.

Extreme dimensional tolerances, the absence of cracks and laminations, chemical and physical homogeneity of the blocks are the main parameters that are strictly controlled.

REFERENCES

1. Franz Müller and Sung-Ki Lim; Physico-chemical Investigation of the behaviour of Sodium in the float glass process.
Part 1. Distribution of Sodium and tin between the glass melt and the bath of molten tin Glastech. Ber. 62.(1989) Nr. 11, p. 369-379.

2. Franz Müller and Sung-Ki Lim; Physico-chemical Investigation of the behaviour of Sodium in the float glass process.
Part 2. Reactions of sodium and oxygen dissolved in the bath of molten tin. Glastech. Ber. 62 (1989) Nr. 12, p. 417-421.

3. Hans Petschauer, Helmut Ebigt, and Guenter Froehlich. Steps Toward the Solution of the Tin Bath Block Peeling Problem in Float Glass Lines. Ceramic Eng. Science Proceedings. 55th Conference on Glass Problems, 1995, March-April, p. 59-67.

4. Pilkington Standard Proof Test RDTM/47; Pilkington Standard H_2 Diffusivity Test RDTM/13.

FUSED-CAST REFRACTORIES SOLUTIONS FOR SUPERSTRUCTURE AND CROWN APPLICATIONS IN OXY-FUEL GLASS FURNACES*

Gérard Duvierre, Yves Boussant-Roux, and **Alain Zanoli**
SEPR, France

Abstract

Today's experience of traditional silica refractories in the superstructure of oxy-fuel glass furnaces tends to show that the corrosion may significantly be accelerated when compared to conventional furnaces. Corrosion and degradation mechanisms of superstructure materials in conventional glass furnaces are well known as well through field experience as lab tests. This knowledge sets the base for the understanding of the case of oxy-fuel furnaces. The new firing system has specific features which are today globally perceived and acknowledged even though not known in too many details. Using available informations regarding chemistry and temperature of vapors as well of solid particulate, it has been possible by simple lab tests to propose several clues to explain what is occurring in the field at the level of the corrosion of silica refractories. It is also possible based on these tests to look for the trends in the area of optimised fused-cast refractories for the superstructure of oxy-fuel furnaces.

The aim of this paper is to explain how we have gone through this process of understanding, testing and selecting the more adapted materials.

The paper also refers to practical issues which have been demonstrated to be of prime importance in the behaviour of glass furnaces superstructures because of the involvement of condensation mechanisms in the attack as minimising joints opening or using high insulation which creates the need for low creep refractories.

Finally, we comment industrial results of oxy-fuel furnaces equipped with fuse cast refractories which have been selected according to this global approach.

---

* Full manuscript not available at the time of printing

IMPROVEMENT OF FUSED CAST AZS THROUGH MOLYBDENUM REINFORCEMENT FOR SOME CRITICAL AREAS OF THE GLASS TANK

G. DINELLI[1], A. FANTINEL[1], M. DUNKL[2], R. TOGNON[1]
1. Refel, S.Vito al Tagliamento, Italy
2. Didier-Werke AG, Germany

Abstract

The corrosion resistance of fused cast AZS refractories used in critical areas of the glass tank is a key factor for the duration of the tank campaign. To prolong the service life of structural AZS blocks like the throat cover block, an insert of Molybdenum has been incorporated in the body of a block based on 41 % ZrO_2 material. The insert is completely immersed in the refractory matrix, to which it is strongly bonded, and its shape matches that of the external surface of the block which is exposed to contact with the glass.[1] Once in use, the purpose of the molybdenum reinforcement is to avoid the contact between the AZS material and the molten glass, thus acting as a separating barrier which prevents corrosion of the lying-behind AZS. The combination of the monolithic AZS material with a molybdenum reinforcement forms a new composite system with enhanced corrosion resistance properties when compared to the conventional AZS.

Introduction

Modern glass-making process requirements have put a greater demand on the performance of the materials for glass furnace construction. Today process temperatures are higher, the melting rate capacities are increasing, glass quality requirements are greater and a longer service life of the furnaces are expected. Higher temperature and increased melting rate implies a greater convection flow which strongly affects the wear of tank refractories.

The wear of a glass tank is not homogeneous in the glass contact areas: it is necessary to reinforce the critical zones subjected to heavy glass corrosion such as the throat, the bubbling area; etc.

Therefore identifying new materials, that allow for the elimination of weak points in the construction of the furnace to prevent unexpected campaign interruptions, has become more important.

Over the last few years, composite materials have received close attention and more widespread use in refractory applications. In the case of shaped refractories the most frequently-adopted solution is to combine two or more monolithic elements of diverse nature to obtain a single structural system which offers performance that is superior to that of the individual constituents.

[1] Refel Patent

These are referred to as "composed structures"; the component which is present in the greatest quantity and with continuity is considered the matrix of the composite, while the other materials are called reinforcements. The use of composed material has now been made more effective by the current development of the new metal and ceramic matrix composites.

A typical example of a composed structure consists of a refractory body which is the structural support for reinforcing materials which provide excellent corrosion resistance to the attack of aggressive agents.

The reinforcements are located in the critical areas of the entire body and strongly bonded to it (e.g. zirconia-reinforced submerged nozzles for continuous steel casting process). The reinforcing elements give the significant advantage of an increased service life of the whole structure when compared with the monolithic refractory matrix.

REFEL's aim is to improve the characteristics of critical elements of the glass furnace, such as the throat cover blocks, by producing a composed structure, based on a fused AZS block which incorporates a Molybdenum reinforcing agent that is extremely corrosion resistant to molten glass.

Experimental

As far as corrosion attack by the molten glass is concerned, the throat is one of the most critical parts of the tank. During its service life the region around the cover blocks and the cover block itself are subjected to severe corrosion.

The corrosion resistance of the fused-cast materials selected to build the throat is a decisive factor in the duration of the furnace campaign.

Taking as an example the refractory attack on a throat cover block of a container glass tank by the flowing molten glass, a typical corrosion profile at different times t_1, t_2 and t_3 where $t_3 > t_2 > t_1$, is shown schematically in fig.1a.

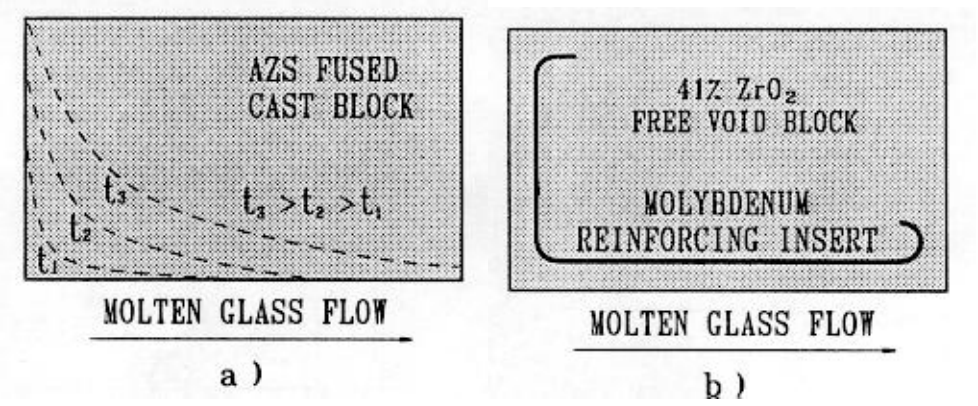

Fig.1. a) - Schematic progress of the corrosion profile of the throat cover block of a container glass tank. b) - Typical configuration of the composed structure REFEL 1240 FVMO, a Free-Void Block with a Molybdenum reinforcing insert. Section 500x300 mm.

The wear of the refractory tends to round the exposed edge of the block, thus progressively reducing its integrity.

In practice, the basic idea is to manufacture by casting a Free Void cover Block (e.g. 1200 x 500 x 300 mm) in Refel 1240 material which contains a glass corrosion-resistant body whose function is to prevent contact between glass and refractory. A view of the configuration of the resulting structure is indicated in fig.1 b; the Molybdenum insert is embedded into the AZS matrix which completely surrounds it while maintaining a strong bond with it. Every part of the insert is covered by fused-cast material thus avoiding Molybdenum from any contact with external agents.

In service after the initial removal, by the glass attack, of the outer layer of AZS material, the insert element will protect the remaining part of the block from corrosion.

In the design of the composed structure, the material selected as the reinforcing agent must meet different technological requirements and selection criteria, in order to obtain a composed structure with the desired properties. The most important characteristics of the reinforcing material are: corrosion resistance to molten glass, absence of harmful effects to the glass, adequate mechanical strength at the service temperature, no reactivity with the matrix, good thermal conductivity, thermal expansion behaviour similar to that of the matrix; finally, the presence of the reinforcing element must not require modification of the manufacturing process of the monolithic matrix.

Molybdenum, a refractory metal of high strength at high temperature, perfectly meets these requirements. Its excellent corrosion resistance to the molten glass and the characteristic of not altering the various properties of the glass, especially its colour, makes it the most commonly used electrode material in the glass furnace industry [1,2,3].

Besides being used for electrodes, it is also used for metering valves, flow dividers, stirrers, liners for conduits etc.

At temperatures higher than those normally reached during service in glass furnaces, it does not react with alumina and zirconia, the main components of the AZS matrix. This chemical behaviour allows the reinforcing material to maintain its integrity and performance in working conditions.

In the composed structure, the two components must be bonded in such a way that the overall system retains its structural integrity while performing the intended function. In the temperature range of zirconia polymorfic transition the Molybdenum thermal expansion curve remains within that of zirconia. During the manufacturing cycle, after the initial densification of the matrix, since the thermal expansion behaviour of the AZS (fig.2) is slightly higher than that of molybdenum, the insert is compressed by the surrounding matrix, making it possible to obtain a continuous strong bond between the matrix and the insert.

In order to satisfy the block design requirements, the usual procedure for the production of AZS fused cast material has been substantially adopted for the manufacture of the composed structure. A molybdenum foil, whose profile is shown schematically in fig.1 b, is appropriately positioned inside the mould before casting. The clean foil must be cautiously handled to avoid any contamination.

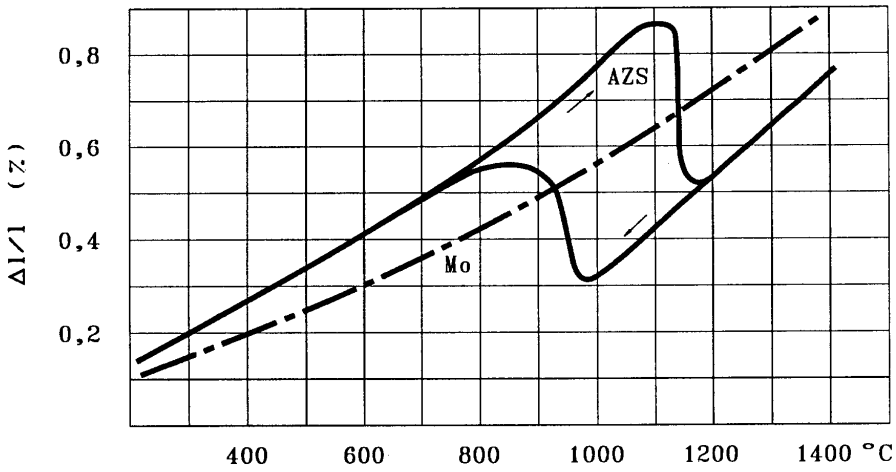

Fig. 2. - Thermal expansion behaviour versus temperature for molybdenum and fused cast AZS refractory with 41 % of ZrO_2 content.

During the casting of the melt, care must be taken to reduce the possibility of molybdenum oxidation by air and to improve the effectiveness of the wetting action of the matrix on the reinforcing element. After casting, the composed structure is subjected to a specific annealing cycle with a controlled cooling rate to allow a correct solidification process of the matrix around the reinforcing element. The cold composed structure is processed according the usual manufacturing cycle and machined as a normal fused-cast block.

Several problems frequently arise when using the casting technique to manufacture the composed structure. The most serious of these concern the possibility of chemical reactions in the interfacial zone between insert and matrix, due to the thermal environment necessary for the process to succeed, and the risk of obtaining an interfacial area without a strong bond. REFEL has overcome this problem: figure 3 shows in detail the insert/matrix interfacial morphology.

Fig. 3. Molybdenum insert / AZS matrix interfacial region. Backscattered electron micrograph.

An interfacial reaction layer is not apparent. The absence of a separation layer means that a strong bond between the two components is achieved by the manufacturing process. This characteristic will guarantee that, in the composed structure, molybdenum and AZS matrix maintain their continuous connection during service.

The configuration of a reinforced block similar to that shown in fig. 1 b makes it suitable for use in the throat assembly as a cover block or a sidewall block and offers the significant advantage of an increased service life. Thanks to the availability of the molybdenum foils in numerous complex shapes and the technological possibility of inserting them in any suitable position inside the body of the block, the reinforced AZS structures can be applied to several types of critical corrosion-stressed elements of the glass tank, including the submerged weir blocks and the facing throat blocks (fig.4.)

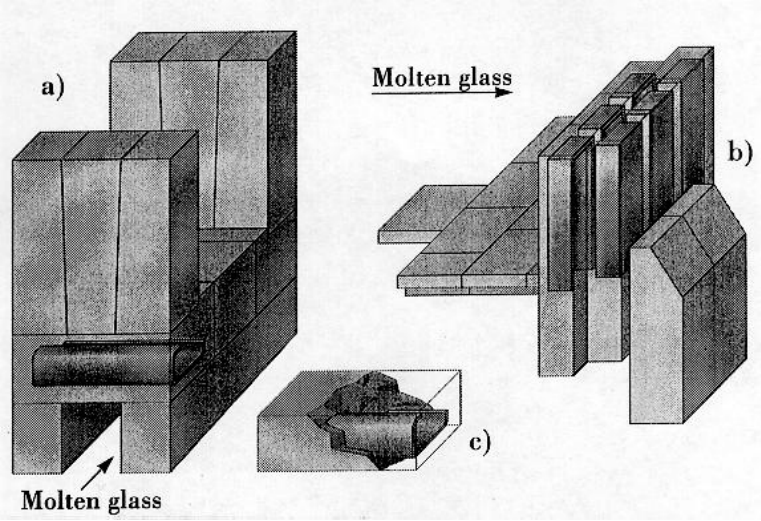

Fig.4. - Designs for a throat (a) and a submerged weir (b) with molybdenum reinforced blocks REFEL 1240 FVMO (c).

In many glass furnaces, critical corrosion-resistant elements are supplied in fusion-cast chromia containing refractories. These refractories are extremely glass-corrosion resistant but present a number of disadvantages, causing defects such as glass pigmentation, interaction in the delicate redox systems of many modern glasses or the dispersion of dangerous pollutants from the furnace emissions. Furthermore, concern about the potential long-term health hazards raised by waste disposal in land fill sites, has resulted in many countries restricting the dumping of chrome-based refractory after use. The new environmental regulations are encouraging glass manufacturers to replace chrome refractory with other equally effective products.

The fused-cast AZS molybdenum reinforced "composed structure" meets the requirements both of high performance and an environmentally friendly material.

Conclusions

A "composed structure" formed by an AZS refractory matrix containing a Molybdenum insert as reinforcing agent has been produced by using the fusion casting technique. The aim of this composed system is to provide a product whose corrosion resistance to the molten glass is better than that of the AZS matrix.

REFEL's 41 % Zirconia Free Void Block / Molybdenum "composed structure" offers numerous advantages such as:

- prolonged service life, compared with conventional AZS materials, with the benefits of reduced costs and less disturbance in glass production process
- enhanced quality of glass, with no colouring effect or negative influences, compared to chromia-based refractories and
- environmentally friendly material, designed to meet the strict regulations on pollution.

The product appears especially suitable for the construction of those crucial elements of the glass tank, submerged by the molten glass, such as throat and submerged weir, for which the resistance to molten glass attack as well as structural reliability is essential for a guarantee of long service life.

References

[1] W. Kahl, A. Petzold, "Zum Verhalten von Molybdan gegenüber Glasschmelzen", Silikattechnik, **29** (3) 1978, 76-78.

[2] G.A Pecoraro, et al. "Corrosion of Refractory Metals by Molten Oxides", Glass lnd., **51** (10) 1970, 454-58.

[3] Molybdenum Technical Information from Mettalwerk Plansee GmbH, Reutte, Austria.

STATUS REPORT ON MAGNESIA ZIRCON BRICKS FOR USE IN GLASS FURNACE REGENERATORS

K. Wieland, Dr. M. Dunkl, B. Schmalenbach
Didier-Werke AG, Germany

1. Introduction

Magnesia-zircon bricks mineralogically are forsteritic magnesia bricks containing cubically stablized zirconium oxide. The original idea was to solve the problem of magnesium-sulphate formation in the condensation area of regenerators in particular with oil-fired furnaces and to subsitute for magnesia-chrome bricks. In fact under the influence of alkali vapors contained in the exhaust gas watersoluable toxic hexachromates are forming and there is a continous discussion about the disposal of contaminated used magnesia-chrome materials. In 1987 just 7 regenerators were equipped with the new material. Meanwhile there are approx. 60.

Initially it was intended to use magnesia-zircon bricks in the condensation area only because of a limited temperature of application. Their advantage in the upper part of regenerators, however, was obvious. Forsterite bursting due to sand carry-over which destroys magnesia bricks is drastically reduced if not eliminated because magnesia-zircon bricks contain forsterite already. Meanwhile a high temperature version of magnesia-zircon bricks is available. This low lime material is also resistant to the attack of vanadium-pentoxide and the formation of low melting calcium-vanadates.

2. Chemical and mineralogical reactions

The common refractories for glass furnace regenerators are listed in table 1.

Table 1

Common Refractories for Glass Furnace Regenerators

Magnesia Bricks
Forsterite Bricks and Forsteritic Magnesia Bricks
Chrome-Magnesia and Magnesia-Chrome Bricks
Alumina Containing Refractories (high alumina bricks, fusion cast AZS materials)
Silica Bricks

The major reactions with components of the brick material and foreign matter, e.g. sand carry-over and aggressive vapors in the exhaust are shown in table 2.

Table 2

Chemical Reactions in Regenerators						
	Brick component	Foreign matter	Melting Temperature	Reaction product	Structure Changes	Area
1	2 M	S	1890 °C	M_2S Forsterite	Cracking Spalling	upper regenerator
2	3 C_2S + M	S	1575 °C	2 C_3MS_2 Merwinite	Reduction of Hot Strength	upper regenerator
3	C_2S + 2 M	S	1495 °C	2 CMS Monticellite	Reduction of Hot Strength	upper regenerator
4	M	SO_3		$MgSO_4$	Densification	condensation area
5	A + 2 S	N	1526 °C	NAS_2 Nepheline	Cracking Spalling	above 800°C
6	S	N	< ~ 1450 °C	Sodium-Silicates	Melting	in general below 1450°C
M = MgO, C = CaO, S = SiO_2, A = Al_2O_3, N = Na_2O						

Magnesium oxide and calcium-silicates which are present in almost all magnesia bricks react with silica as carry-over material. The reactions take place at high temperature. They are resulting in bursting because of forsterite formation or a reduction of the hot strength because of the formation of merwinite or monticellite. Details are shown in table 2 equations 1 to 3. Equation 4 shows the reaction of magnesite with sulphuric acid taking place in the condensation area of the regenerator, i.e. within a temperature range between 800^{o}C and 1100^{o}C. The bricks are destroyed due to infiltration and bursting.

Equation 5 shows possible reactions between alumina-silicates and alkalies occuring above 800^{o}C, i.e. from the upper regenerator downwards into the condensation area. As a result the brick material is spalling, cracking or the surface is peeling off.

The reactions between silica and sodium are shown in equation 6. Above 1450^{o}C the alkali resistant SiO_2 modification cristoballite is stable. Cristoballite melts at 1725^{o}C. Below 1450^{o}C under the presence of alkalies, cristoballite is transformed into tridymite. Depending on the alkali concentration partial or complete melting of the silica material occurs. Silica is not recommended below 1450^{o}C.

3. Influence of environmental regulations

Recycling of external cullet and internal filter dusts lead to an increase of a carry-over of fine particals and an increase of alkali-sulphate vapors.

Restrictions in NO_x emissions resulted in primary NO_x reductions measures. Table 3 shows the disadvantages:

Table 3

Reduction of NO_x Emission		
	Measure	Disadvantage
1	Low temperature combustion - low air factor	Melt formation with silica - REDOX conditions
2	NO_x reduction with methan	REDOX conditions
3	Oxy-fuel firing	High alkali sulphate and alkali hydroxides

Cullet and filter dust recycling cannot be seen as independent factors. Together with reduced air factors and low combustion temperatures redox conditions have to be considered. Besides of higher dust rates generated, under reducing conditions the melting temperature and viscosity of the dust particals is reduced with an increased danger of clogging in the regenerator. Free silica as contained in fusion cast AZS-material and certainly in silica bricks can be reduced, evaporate and the respective material is destroyed. Silicon vapors can sublimate, reoxidize and react with magnesia to forsterite with subsequent forsterite bursting. The NO_x reduction with methane (R3 technology) adds to the negative effect of reducing conditions. Oxy-fuel firing leads to a much higher concentration of vapors in the exhaust. In addition there is a higher proportion of alkali hydroxides which have a much higher impact in particular on silica refractories. Concerning regenerators this applies certainly only to oxy-fuel firing support. High batch moisture and recycling of hydroxides would have the same effect.

4. The advantage of magnesia-zircon bricks

Fosterite (2 Mg0 x SiO_2) has been identified to be resistant against the 2 most common reactions in regenerators, i.e. formation of magnesium-silicates and formation of magnesium-sulphates. Its disadvantage however is the pronounced cleavage property of its grains if coarse genuine forsterite raw materials are used. In magnesia-zircon bricks forsterite is formed as a secondary mineral during firing as fol lows

$ZrSiO_4 + 2\ Mg0 = Mg_2Si0_4 + Zr0_2$
zircon + periclase = forsterite + zirconia

The above reaction takes place between the fine magnesia grain, the zircon powder and on the surface of the coarser magnesia grain used as brick raw materials. The fines are transformed into forsterite and zirconia and the surface of the coarse magnesia grain reacts to form a protective forsterite coating as shown in the micrograph picture 1. Since the basic structure of the material is the coarse magnesia grain, cleavage of forsterite is not observed.

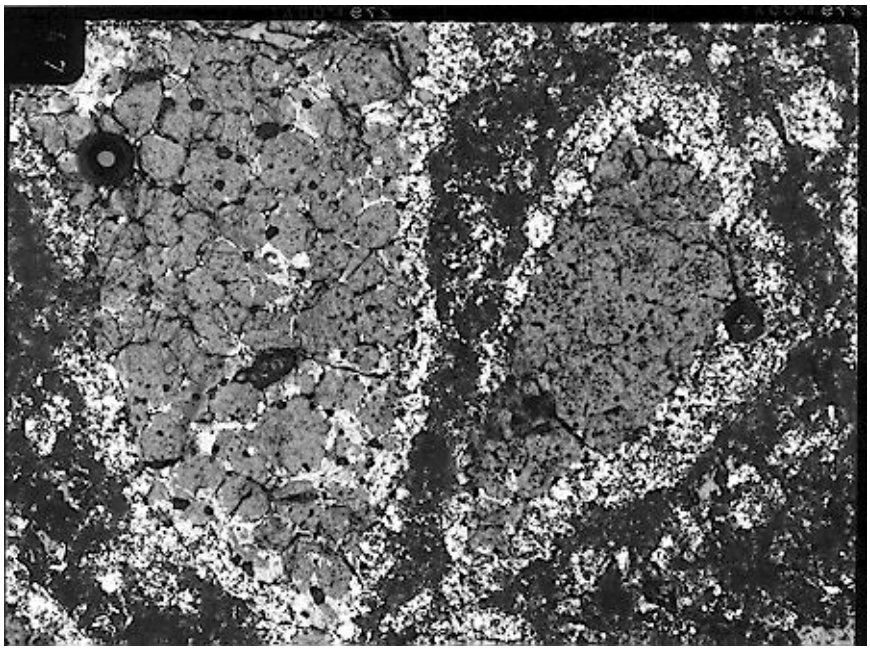

Figure 1: Microstructure of Magnesia-Zircon Bricks

5. Application of magnesia-zircon bricks in the condensation area

The furnaces in which magnesia-zircon bricks are installed in the middle section of their regenerators are shown in table 5.

Table 5

Application of Magnesia-Zircon Bricks in the middle part of Glass Furnace Regenerators since 1987

Totally 60 furnaces

- 10 Float Furnaces
- 43 Furnaces for Container Glass and Table Ware
- 5 Sodium-Silicate Furnaces
- 2 Lighting Glass Furnaces

17 Furnaces are equal or bigger 100 m² Melting Surface
20 Furnaces are smaller than 100 m²
but bigger than 50 m² Melting Surface
approx. 1/3 of all Furnaces are crossfired

Many of the listed furnaces in previous campaigns showed clogging in their regenerator flues. It was interesting to note that in many cases clogging disappeared totally or was drastically reduced. The checker system with magnesia-zircon bricks included all standard types as well as box blockes even with 30 mm wall thickness. In all cases the expected life time was achieved. Most of the furnaces are still inservice without any sign of premature wear.

The magnesia-zircon brick for medium temperatures with the trade name RUBINAL EZ became standard. Alternative materials are manufactured by the supplier only on special request. 6.Application of magnesia-zircon bricks at high temperature in the upper regenerator and regenerator grown

The limited temperature of application of RUBINAL EZ is due to a calcium oxide content of approx.1.5 % resulting in an excessive formation of monticellite (CMS) with a melting point of 1495 ^{o}C. The high temperature creep resistance was not acceptable for an appliction in the upper regenerator. In the early 90's a new recipe had been developed therefore whereby the calcium oxide content was reduced to 0.5 %. The new material which is on the market under the trade name RUBINAL VZ has lower creep values allowing the application in the upper regenerator side walls, the crown and the upper checker setting. Comparative data for different regenerator refractories are given in table 6.

Table 6

Comparative Data on Regenerator Refractories			
	RUBINAL EZ	RUBINAL VZ	Magnesia-Chrome
Chemical composition (%)			
MgO	73	77.5	49
ZrO_2	13	13	-
SiO_2	11	8	1.6
CaO	1.0	0.5	0.6
Fe_2O_3	1.0	0.5	13
Cr_2O_3	-	-	24
Physical properties			
Density (kg/dm³)	3.10	3.2	3.12
app. porosity (%)	15	11	18
CCS (N/mm²)	100	130	45
Rul To_5 (°C)	1570	1670	1700
Creep deformation % load 0.2 N/mm², 20 - 50 h at temperature: 1200°C	0.02	0.02	0.02
1400°C	0.46	0.16	0.09
1550°C	1.59	0.68	0.92

The first installations of the high temperature version of magnesia-zircon bricks are rather recent, i.e. starting from 1994. The respective furnaces are listed in table 7.

Table 7

Application of Magnesia-Zircon Bricks in the high temperature area of Glass Furnace Regenerators since 1994

Totally 25 furnaces
- 5 Float Furnaces
- 13 Furnaces for Container Glass and Table Ware
- 7 Furnaces for Borosilicate Glass and Sodium-silicate

1 Application as Entire Checker Setting
Use partly in Condensation Areas, Waste Gas Channels and Port Necks
approx. 1/3 of all Furnaces are crossfired

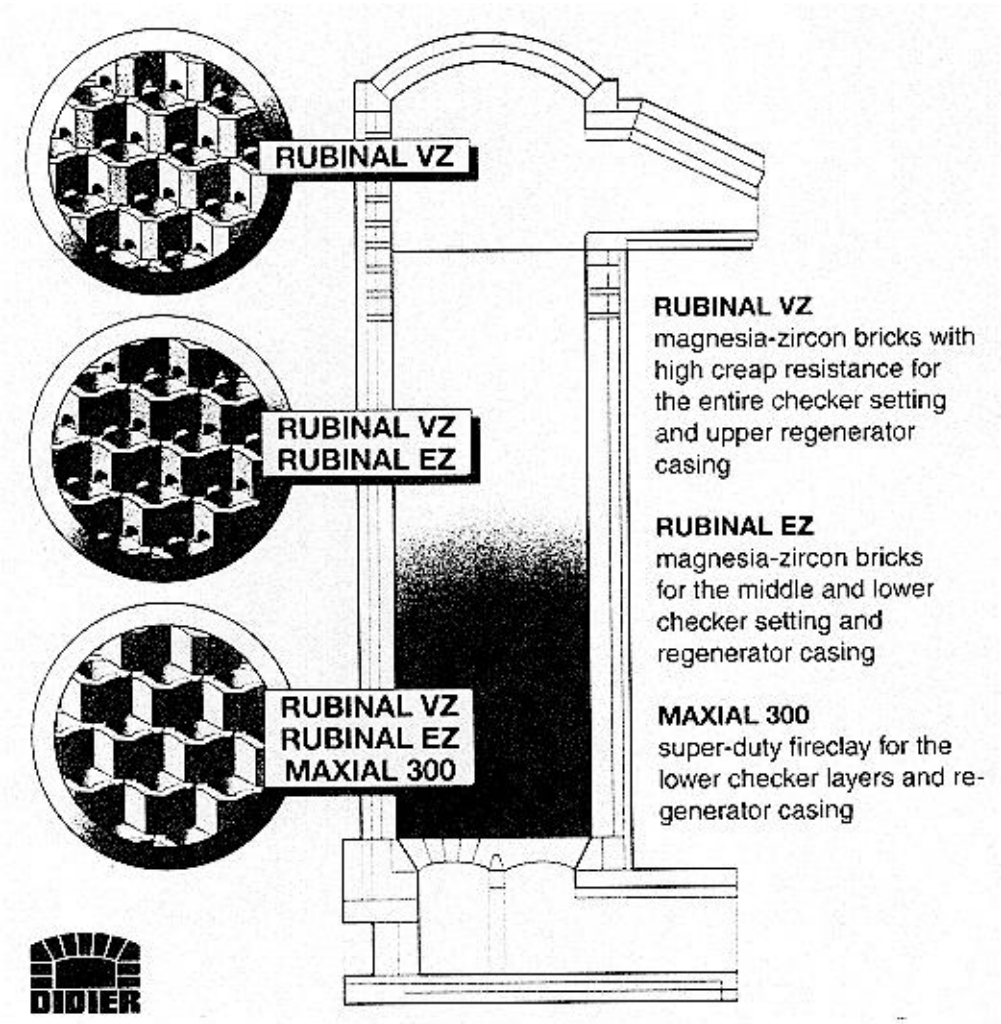

Figure 2: Regenerator Lining Concept

Some of the material was installed in a crown of a sodium-silicate tank. In one case almost the entire checker pack from top to bottom consisted of the high temperature magnesia-zircon material. This decision was made to be on the safe side in case of thermal cleaning of regenerator

channels should be necessary. Suitable would be the medium temperature version of magnesia-zircon material for this purpose too as a substitute of fireclay materials in the lower part of regenerators.

7. Lining concept

The lining concept is shown in figure 2. Standard is to use the RUBINAL EZ type starting from the rider arch/spanner tiles up to a temperature of approx.1300^{o}C followed by the RUBINAL VZ type up to the top. RUBINAL VZ is also used for the upper casing and crown. The checker setting consists preferably out of heat efficient box blocks.

NUMERICAL SIMULATION OF GLASS MELTING FURNACES, A REVIEW

A. Ungan
Purdue University School of Engineering and Technology at Indianapolis, USA

Abstract

Although glass is one of the oldest material for man, the interaction between physico-chemical processes taking place in inside the furnace is yet to be understood. However, with the introduction of 3-D numerical system modeling, quantification of interactive processes became a reality in the mid 1980's. Since then, numerical models developed for combustion space, batch melting, melt circulation, air-bubblers, electric boosting, refractory corrosion and regenerators can now be used not only to elucidate the coherent picture of the complex phenomena, but also as practical design tools to optimize the operational process and to reduce the pollutant emissions. The objective of this paper is to review the literature on glass melting process emphasizing the numerical studies published in the last decade. The recent developments in the general CFD trends along with some of the important experimental studies on glass are also discussed.

1. INTRODUCTION

It is not too much speculation to state that the basic rules of conventional furnace design were probably established mostly by trial-and-error procedures conducted with actual melters. Later, however, dimensional analysis established for fluid dynamics and heat transfer in 1910's and 1920's gave birth to the scaled physical models to be used for furnace development processes. These physical models not only illustrated glass currents in actual melters but also they offered a cost effective alternative way to test the design ideas before they are applied to the real furnaces.

By the early 1960's, the manufacture of computers for scientific and commercial use was in full swing. In the absence of the exact solution to the governing equations for fluid dynamics, the quest for solving these equations approximately on computers with iterative numerical procedures started giving the first successful results in the same years. Like other traditional industries, glass producers started seeing the opportunities in the predictive abilities of computer simulations.

In general, all prediction tools may basically be assessed on six requirements. They are accuracy (agreement with experience), speed (including learning time, set-up time, execution time, interpretation and design concept development), economy (with consideration of all costs), accessibility, and flexibility. Considering the complexity of the entire process among the predictive procedures employed by the glass industry, the tests, with simplified scale models, may be regarded as wishful approximations for the complete simulation of the melting operation; therefore, they suffer basically in the first and the last requirements. By late 1970's and early 1980's, taking advantage of the developments in software and hardware, numerical or computer-

based simulations (Figure 2) were transpired as the most promising predictive procedure for the glass industry with regard to the six requirements summarized above. But, economic cost was still high because numerical simulations necessitated the use of the main frame computers, and the algorithms specific to glass melting process were at their infancy. Since the 1980's the platform for the numerical simulations moved from main frame computers to workstations and PC's. While their price was decreasing, their computational power was increasing steadily. With the introduction of the 32 bit computer chips, speed in execution time has seen the most improvement. At present what used to be done on main frame computers a decade ago can be done much faster on PC's and work stations. These improvements on computer hardware also have reflected on the accuracy. The memory restrictions on the main frame computers was one of the stumbling blocks in the improvement on accuracy of the numerical predictions. Declining cost of memory chips allowed them to be used extensively on PC's, thus creating finer domain descritization for the numerical simulations. The new compilers and languages (such as FORTRAN 90, C++), and the advent of parallel processing along with the developments in software engineering designed specifically for PC's and workstations provided indispensable flexibility for the numerical models. User interfaces working on new or upgraded user friendly operational systems such as Windows 95 and Windows NT substantially increased the accessibility to the numerical models. Hence, for the prediction processes on all grounds of the criteria summarized above, the prospects of numerical simulation of glass melting furnaces in the mid 1990's has become brighter than ever.

In the light of a brief summary given above, the primary purpose of this paper is to present a review of the literature on the numerical simulation of glass melting process. Considering the inherent dependency of the numerical methodologies on experimental studies, emphasis will also be given to some of the key experimental studies on glass. In addition, relevant papers published in the general scientific literature will also be mentioned. The scope of the review in this paper is primarily limited with the studies published in the last decade, but earlier studies can be found in two previous review papers [1,2] on the topic.

2. A BRIEF SUMMARY OF NUMERICAL FORMULATIONS

As shown in Figure 1, in all domains of the glass furnace (i.e. batch, molten glass, combustion space, regenerators, forehearths etc.) the skeleton of the mathematical description is based on the differential conservation equation of mass, momentum, chemical-species, electrical charge (with electrical boost) and energy. Here conservation refers to the fact that one needs to balance all of the factors effecting changes. These laws are entirely reliable, more so than the transport laws which need to be implemented into the conservation laws to describe the flux of the conserved quantity.

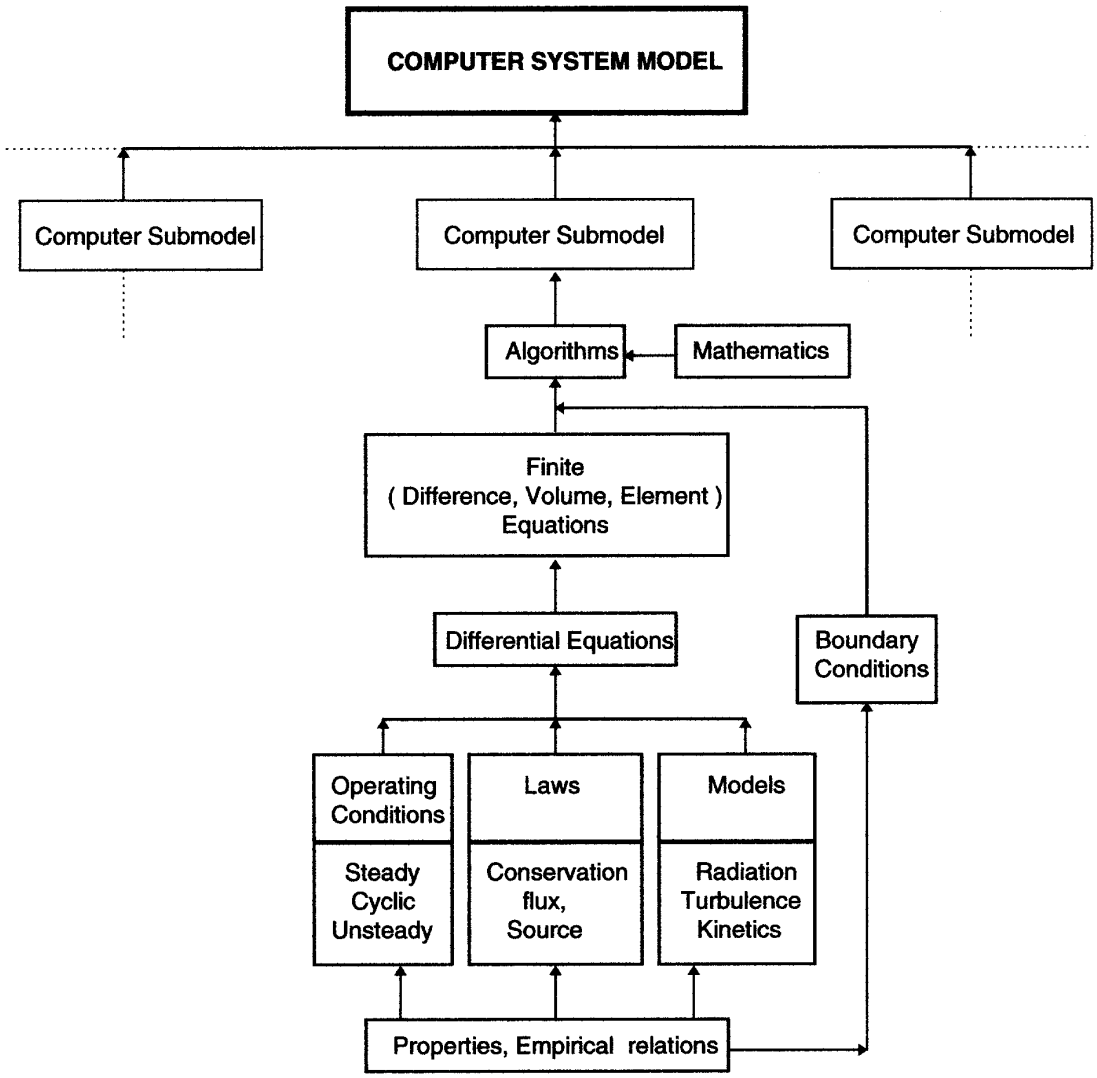

Figure 1 Schematical representation of a typical computer submodel used for glass melting process simulation.

2.1 General Conservation Equation

Although the complete mathematical formulation of the relevant conservation equations are not given here, it is sufficient to say here that the conservation laws in all physical domains of a typical glass melter can be casted into the following general differential equation:

$$\frac{\partial}{\partial t}(\rho\phi) + \nabla.(\rho\vec{u}\phi + \vec{J}_{\phi}) = S_{\phi}$$

In this equation, the first term on the right hand side represents the time rate of change of the conserved quantity, $\varnothing$, the second term is for the combined advective ($\rho u\varnothing$) and diffusive ($J_{\varnothing}$) flux. The term on the right-hand side represents the source term which sometimes provides means

for the coupling of one conservation equation with another. The diffusive flux is sometimes referred to as the transfer law. It exhibits a similar form in the conservation equations mentioned earlier, and thus can be cast into the following formulation:

$$\vec{J}_\phi = (\Gamma_m + \Gamma_t + \Gamma_r)\vec{\nabla}\phi = \Gamma_{eff}\vec{\nabla}\phi$$

Here, Γ_m ,Γ_t ,Γ_r represent molecular, turbulent and radiative diffusivities of the conserved quantity, $\varnothing$, respectively. In the glass bath, the flow is assumed to be laminar, and thus, the turbulent diffusivities are taken to be zero. The turbulent diffusivity, however, becomes important (roughly 2.5 times higher than the corresponding molecular diffusivity) in the combustion space only, and it may be calculated by the use of closure equation(s) such as k-ε method [3]. As employed by the researchers, Γ_r , shows up only in the energy equation of the glass melt in the absence of rigorous treatment for radiative heat transfer. In all other equations and domains, its value should be set to zero.

2.2 Discretization of the Governing Differential Equation

After defining the governing equations, the next step is to convert these (differential) equations into algebraic equations for finite regions of the calculation domains. In the general CFD literature, three major ways have been suggested for this step. They are: finite difference, finite volume and finite element methods, and a brief discussion about them can be found in [4].

In each technique, care must be exercised for the numerical formulation of the combined advective-diffusive flux. It is well known that the effect of molecular diffusion needs to be suppressed in the combined flux formulation in the presence of strong advection [5]. Also, special attention must be given to numerical diffusion (error introduction when the direction of the flow is not parallel with the presumed coordinate system), which can be reduced by the higher order formulations [6] in the expense of computational speed.

It is worth remarking here that no attempt was found in the (general and glass) literature, which accounts for the radiative diffusion in the combined (i.e. advective, diffusive and radiative) numerical flux formulation of the energy equation for the molten glass. To rectify the situation, work to this end is currently underway and will be reported elsewhere.

2.3 Algorithms

In the computational fluid dynamics (CFD) literature, the sequence of steps that solves the discretized governing equations (algorithms) shows a wide range of schemes [4]. The main reason for these variations is not the result of how the discritization is carried out, but rather, arises from the fact that the continuity of mass is linked to the momentum equations through pressure gradients, yet pressure does not explicitly appear in the continuity equation. In other words, pressure has a dual role as both the enforcer of the continuity and as a force in the conservation of momentum.

Exact enforcement of continuity typically involves eliminating the pressure by recasting the problem in terms of a derived state variable, the vorticity. Conservation of mass can then be satisfied automatically by coupling the resulting vorticity transport equation to a stream function (in 2-D) or potential functions (3-D).

Formulations designed to produce inexact or approximate enforcement of continuity of mass require modification of the continuity equation to find the (imperfect) pressure field. Developed

by the Imperial College CFD group in the early 1970s, the semi-implicit method for pressure-linked equations (SIMPLE) and the subsequent revision suggested by Patankar [5] (SIMPLER) found clear acceptance in simulations specifically designed for glass melting furnaces. Another formulation, the SIMPLEC method of Raithby and his coworkers [7] was originated from the same root. Although no systematic publication can be found in literature comparing these algorithms, comparative assessment of SIMPLER and SIMPLEC was reported for four different situation in the general CFD literature [8]. Accordingly, it was found difficult to ascertain clear superiority of SIMPLER over SIMPLEC or vice versa. In general, the steady-state formulations of these methods were found to be more robust than the unsteady formulations [8].

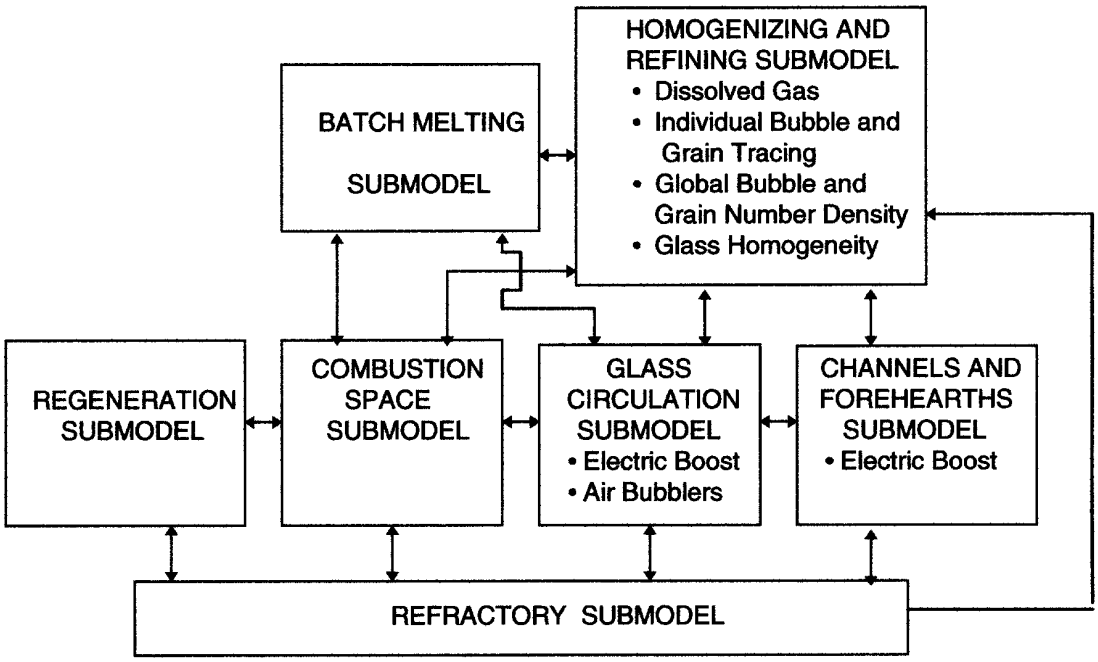

Figure 2. Typical computer system model for the numerical simulation of glass conventional glass furnaces.

3. TYPICAL DOMAIN SUBDIVISION FOR GLASS MELTING PROCESS

Following the physical subdivision in a typical conventional glass furnaces, the overall process simulation model is usually divided into parts as shown in Figure 2. The following sections summarize the recent developments in each submodel.

3.1 Glass Circulation Model

The first 3-D numerical studies designed for numerical simulations of glass melting furnaces preferred the finite difference discretization and the exact enforcement of continuity [9] by using streamline and vorticity as the dependent variables. However, in this approach, the difficulties in assigning boundary conditions especially for vorticity presented convergence problems. The first 3-D finite volume approach in glass furnace simulation was used by Moult [10]. In his work, inexact enforcement of continuity with the SIMPLE algorithm and the primitive variables

(velocities and pressure) as the dependent variables were used. Although this algorithm is still being used by some of the researchers, the majority of the subsequent studies [11] on glass melting tanks opted the use of the SIMPLER algorithm

In the literature, there are a few studies [12] in which finite element Discretization technique was used for the glass circulation model. The finite volume approach seems to be the most favored scheme used in the glass furnace simulations. Although some studies aimed to increase the convergence rate by using multi grid technique [13], most of the effort in glass melt circulation models were devoted to the coupling of the melt circulation model with the other submodels or to the inclusion of enhancement schemes such as air bubblers and electric boosting as discussed below.

Air Bubblers: Air bubblers are one of the enhancement schemes used in glass melters to improve glass uniformity and fining [14]. The effect of air bubblers on glass circulation patterns has been demonstrated by the numerical simulations [15-18]. It has been shown that the empirical correlations in the two-phase flow literature [19] can be used to estimate the friction force between an ascending train of bubbles released from the bubbler tubes [15]. The estimated force in turn can be implemented into the vertical momentum equation as a source term. In the other studies, the numerical predictions were compared with the experiments conducted in crucibles [17] and actual tank practice [18], and the agreement between them was found to be satisfactory [17].

Electric Boosting: The mathematical formulation of the other popular enhancement scheme, electric boosting, may find its roots in the magneto hydrodynamics literature. In addition, an extensive treatment of the subject as applied to glass melters can be found in the classical book of Stanek [20]. The first formulation of glass electric boosting process using Argand diagram and AC electric source was reported by Hoffman and Hilbig [21]. In the last decade, the problems with electric boosting were summarized [22]. With numerical simulations, the effect of electrodes on the melt circulation patterns were depicted in conventional [23], cold-top electric [24,25] and nuclear waste melters [26].

An important development on the topic in the past decade was the publication of the corrective remark on the inclusion of the Lorentz force [27] into the vertical momentum equation. This effect was ignored by the earlier studies. After comparing the results of temperature and flow field calculations, it was found that only the models which do not neglect this force were able to describe the true picture of electric heating.

3.2 Combustion Space Model

For conventional fossil-fuel fired glass melters, the performance of combustion space is measured by its ability to transfer maximum heat to the batch, to create favorable glass currents by controlled heat flux distribution on the glass bath, to create minimum amount of heat waste, NO_x and soot and particulate formation, and to achieve all of this while extending the life of refractories in the superstructure. In the last decade glass producing companies were faced with an immediate problem of complying with clean air legislation especially in the US and Europe; therefore, the major effort of glass producers was directed to the last objective [28] and the use of various degrees of oxygen has become popular [29,30]

The need for numerical simulation of combustion phenomenon is not specific to glass melting furnaces. Performance of the internal combustion engines, copper smelters, boilers etc. all depend on efficient use of combustion. They include turbulent flows and all share one common aim

which is minimizing the emission of the pollutants. Therefore, numerical models developed for one field may see direct or indirect application in the other. One major difference, however, is that in the engines the ultimate aim is to convert the released energy to work, in the furnaces and boilers, however, the aim is to transfer the released energy to the load. Because of this difference, the radiant energy is tried to suppressed in engines, while, it is encouraged in the furnaces and boilers.

In the past, several numerical studies devoted to the combustion space of glass furnaces have been published [31-42], and the importance of the combustion model on the overall furnace simulation has been stressed [41,42]. Three-dimensional flow patterns in the combustion space of a glass furnace were visualized [31,32]. The importance of radiation (95%) over convection heat transfer (5%) to the batch and glass has been established [33], oxy-fuel fired furnace characteristics have been documented [34,35] and compared with air-fuel fired furnace [36]. The effect of the crown emissivity was investigated [37], and found that increasing crown emissivity can improve the overall furnace efficiency [38]. Attention was also given to the comparative studies of oil and natural gas furnaces [39] It was found that in the oil fired furnace the total radiative heat flux was 5% higher and more localized in the vicinity of the burners [39]. In addition, the efforts were also directed to NO_x formation [40], and comparisons between predicted results and experimental measurements have been conducted [40].

Since the radiation is the dominant mode of heat transfer in combustion space, one may consider to focus on the radiation models used in the simulation. Because of its high accuracy, the Hottel's Zonal Method [43] was the clear choice in early system simulations in the absence of combustion gas flow or cross fired two-dimensional investigations [44]. Although highly accurate, the solution procedure for this method is quite different than the one usually used in the flow models discussed earlier. In order to increase the computational efficiency and to overcome the hardware limitations, in all kinds of industrial furnace or boiler simulations, researchers had to resort to use of approximate but fast radiation heat transfer methodologies [45].

At present, the quest for a flow field compatible radiation model is yet far from complete, but considerable strides have been made in the past decade [45-49]. Among the reported models which are compatible with the flow equations and which can be written on a spectral (per unit wavelength basis) are Lockwood and coworker's flux model [45], P_N method [46], S_N method [47]. They all eliminate the integral term in the radiation transfer equation by approximation, yield the same order of accuracy and simplify considerably in the absence of scattering [33].

Recently, new angular and spatial discretization practices called "Finite Volume Method" for predicting radiant heat have been suggested [48] in the general numerical heat transfer literature. In this approach, radiant energy is conserved within a control angle, control volume, and globally for any number of control angles and control volumes arranged in any manner. The test results indicated that the accuracy and convergence behavior is in the same order as the models mentioned above [49].

In glass melter system simulations, among the approximate models, only flux model [45] has been used by Carvalho and her coworkers [32, 34, 35, 39, 40], and utility of the other models have not been fully explored yet. One of the possibilities with these models include the extension of the radiation heat transfer into the glass bath, rather than using the effective thermal diffusivity in the glass melt as currently being done. To rectify the situation, efforts are presently underway and the results will be published elsewhere.

3.3 Batch Melting Model

In the conventional glass melting process, raw materials are fed into a furnace in the form of a blanket, pile, log, pellet, or briquettes. The physical and the mathematical description of each form differs due to its geometry and charging scheme. Typical cross sectional views on the top and the bottom of a blanket batch are shown in Figure 3.

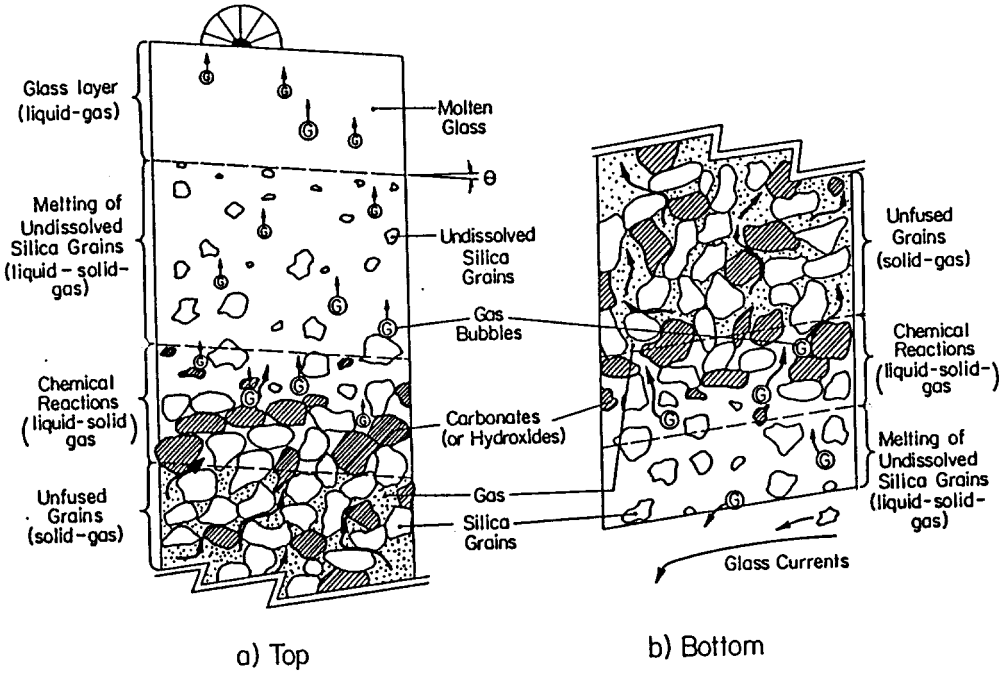

Figure 3. Phase transformation layers on the top and the bottom of a batch blanket [50]

Despite the incomplete rheological and thermophysical data, some detailed models have been published [50-54] in the past on the subject. Through these models, it has been revealed that the temperatures at the gas/batch and glass/batch interfaces basically remain constant [50]. Due to the poor conductivity of the raw materials, the interior regions maintain the original temperature, and the effect of vertical gas percolation within the blanket on the heat transport is not significant [50]. Therefore, it has been recommended that the best strategies to hasten the melting of batch, on practical terms, are to increase the heat transfer from glass rather than combustion space [53], decrease the thickness of the batch, increase the feed-speed [52], and to increase the batch preheating using a fluidized bed and flue gas [53]. Somewhat less practical nevertheless invaluable recommendations are on the sequence of the batch reactions and granular size/ heating rate [51]. In addition, the importance of batch melting on the overall energy saving strategies has been stressed and batch preheaters are rated as the most important systems to improve for the near future [53].

Some of the assumptions made for the numerical modeling were reviewed and assessed by the experimental study of Coradt et al. [54]. It was found that the primary melt did not form along any specific isotherm. Thus, the concept of a uniform melting temperature, valid for the entire batch heap as used in several theoretical models, was not confirmed [54].

These detailed numerical and experimental studies have quantified the batch melting phenomenon, revealed a coherent picture as well as the relative importance of various transport mechanisms, and paved the way for the construction of less detailed but fast batch melting models. From the overall furnace simulation point of view the most important single parameter is the extent of the batch layer on the glass melt, given the raw material feed rate, the charging temperature and the feeder type. This basically requires (correct) an energy balance or a heat flux distribution on the batch, and in turn necessitates estimation of temperature distribution on the batch.

A detailed batch model can predict both of these requirements along with the melt velocity under the batch. However, an educated guess for the interface temperature and the melt velocity profile, based on detailed batch models and/or practical furnace operation on the batch, may also serve the purpose while accelerating the prediction of the final results in the combined system simulations.

3.4 Homogenizing and Refining Models

Since one of the primary goals behind the numerical simulations of glass process is to improve the final glass quality, the mathematical formulation of homogenization and defects resulting from the bubbles and infused (silica) grains should be given special importance. In the past decade, important strides have been taken in this field also.

Quantification of the homogenizing process is one of the most difficult concepts in glass melting process. Although (the variation in) viscosity is the best parameter to assess the homogeneity, the numerical models having much coarser grid size typically ignore this small scale variation, and therefore, they are incapable of assessing homogeneity unless peripheral mathematical modeling is employed. To this end, three major theoretical papers appeared [55-57] in the literature on the topic. Another important experimental and numerical research on homogeneity was conducted by Hogerl and Frischat [58] in the presence of air bubbling.

Defects (bubbles and grains) were given more attention than the homogeneity. Tracing individual bubbles while they grow or dissolve in the glassmelt as a result of multi-gas diffusion has been investigated by several researchers [59-63] mostly by using the invaluable research conducted by Nemec and his coworkers in the 1970-90s. Since homogenous nucleation is strongly unlikely in glassmelts, the majority of the bubble tracing studies were devoted to bubbles originating in the batch by chemical reactions. However another possible site for bubble nucleation/generation is the refractories and dissolving sand grains, and three research papers [65-67] appeared to put this phenomenon into perspective. Several studies [70-72] numerically investigated the foam formation on the melt surface as a result of bubble disengagement from the glass melt, while giving special attention to the laboratory investigations [70], and the silica grains [72].

Dissolved gas concentration mechanisms [70] and fields [64] within the glass melts were investigated by combined system models giving attention to the gaseous composition of the combustion space and the batch to be used in bubble studies. They found that the concentration field within the melt is fairly uniform [64]. In addition, the effect of air bubblers and electric boosting on dissolved gas concentrations were investigated and quantified for the given operational conditions [64].

Since there may be numerous bubbles of different size and composition present in the glass melt at a given time, two approximate mathematical/numerical formulations were suggested to

investigate all the bubbles at once [68,69] Although these models are approximate, they may be used to assess the bubble disengagement ability of a given furnace for given operational conditions [68].

Having less complicated dissolution behavior, silica grains in glass melts are easier to describe mathematically than bubbles. The behavior of silica grains were also investigated in the last decade [73-75] from the individual [73,74] and the global point of view [75]. Mutual relations between refining and sand dissolution was discussed and ideal conditions were defined [74] Melting behavior of silica grains in the presence of air bubblers and electric boosting were demonstrated [75].

3.5 Channels and Forehearth Models

Among the studies devoted to numerical simulation of glass furnace channels and forehearths, Choudry [76] investigated variable cross sections. In this three-dimensional model specific attention was given to the radiative heat transfer. They found that the presence of natural convection significantly affected the flow paths lines. The distribution of the surface and bottom glass streams entering a channel into different forehearths was also investigated [76]. In the more recent study [77], it was found that, due to the shallowness of the forehearths, the effective conductivity approach for modeling heat transfer was not appropriate. This was valid especially for colorless glasses for which below 2.8 micrometer they are not optically thick. The exit temperatures were found to differ with and without radiation heat transfer modeling [77].

3.6 Regenerator Models

Regenerators used to increase the efficiency are one of the most important and old components of conventional glass melting processes. In the last decade, their performance was numerically evaluated [78-80]. One of them [78] was specifically designed to predict the decrease in the thermal performance due to fouling by flue gas condensates. The model included volatilization of sulfur, chloride and sodium components from the melt. The other [79] was devoted to the simulation of the dynamic behavior with the objective of assisting the design of control systems. Comparisons of numerical results and measurements in a clear glass furnace was presented [79]. In addition the effects of various geometric parameters which characterize the checkerpieces were investigated [80].

3.7 Refractory Models

Minimizing the refractory corrosion [81-83] is one of the prime aims in glass furnaces, and prediction of refractory corrosion can be implemented into the glass furnace simulation process. To this end, a mathematical formulation was developed in the last decade to calculate the rate of corrosion in the presence of free convection in the melt [81]. The formulation involved the convection of the melt, conduction in the refractory, and the cooling outside [81]. Recently, an assay appeared in the literature [82] on the topic to elucidate the recent developments.

4. CONCLUSION

Taking advantage of developments in the computer hardware, important strides were made in the numerical simulation of glass melting process in the past decade. As summarized by the review, the numerical researchers around the globe investigated the most pressing needs of the

glass industry via computer modeling. Also as indicated from the review, it was found that the experimental and numerical investigations started to complement each other, which can only speed up the quest for accurate, quick and economical predictability of glass formation.

In order to increase the usefulness of the numerical simulations, however, the following areas seem to be needing the most attention in the near future.

1) Homogenizing process: Although initial ground work has been laid down by some initial studies, rigorous modeling of the subject which measures the sub-grid viscosity variation at the outlet appears to be incomplete.
2) Radiation heat transfer: Although radiation heat transfer is the dominant mode of heat transfer in the combustion space, its interaction with the glass bath has not been fully investigated. The studies to this end are only limited to the forehearths and channels. They clearly showed some of the limitations of the effective conductivity concept in heat transfer in the glass melts.
3) Cyclic-firing with regenerative furnaces: Except a few studies, most of the studies published to date assume steady-state operational conditions even for the furnaces equipped with regenerators. However, important insight on batch stability, glass homogeneity, and furnace efficiency may be obtained from the simulations specifically designed for the simulation of cyclic-firing operations.

Finally, it is worth remarking here that the success of numerical simulations largely depends on the thermophysical and empirical data used in the numerical simulations. Thus, aside from numerical simulations, the supportive data generated by experimental investigations will gain more value in the future as they find an important role in the quest for the full comprehension of the complex nature of the glass melting process.

REFERENCES

1. Nolet, D.A. and Murnane, R.A. (1988) “Development of Modeling Techniques for Glass Furnaces,” Proc.1st Int. Conf. Adv. In Glass, p.13.1
2. Viskanta, R.(1994) “Review of Three-Dimensional Mathematical Modeling of Glass Melting,” J. Non-Cryst. Sol., Vol.177, p.347.
3. Patel, V.C. Rodi, W. And Scheuerer (1985) “Turbulence Models for Near-Wall and Low Reynolds Number Flows, A Review,” AIAA J., Vol.23, p.1308.
4. Williams, P.T. and Baker, A.(1996) "Incompressible Computational Fluid Dynamics and the Continuity Constraint Method for the Three-Dimensional Navier-Stokes Equations," Numer. Heat Transf., Part B, Vol.29, p.137.
5. Patankar, S.V.(1980) “Numerical Heat Transfer and Fluid Flow,” McGraw-Hill, New York.
6. Choi, S.K. et.al.(1995) “Evaluation of A Higher-Order Bounded Convection Scheme: Three-Dimensional Numerical Experiments, Numer. Heat Transf.,” Part B, Vol.28 p.23.
7. Van Doormaal, J.P and Raithby, G.D.(1984) "Enhancement of the SIMPLE Method for Predicting Incompressible Fluid Flows," Numer. Heat Transfer, Vol.7, p.147.
8. Jang, D.S., Jetli, R. And Acharya, S.(1986) "Comparison of the PISO, SIMPLER,

and SIMPLEC Algorithms for the Treatment of the Pressure-Velocity Coupling in Steady Flow Problems," Numer. Heat Transf., Vol.10, p.209.
9. Chen, T.G. and Goodsoon, R.E (1973) "Computation of Three Dimensional Temperature and Convective Flow profiles for an Electric Glass Furnace," Glass Technol., Vol.13, p.161.
10. Moult, A.(1982) ,Two and Three Dimensional Mathematical Models of Glass Tank Furnaces, Glass Technol., Vol.23, p.106.
11. Ungan A. and Viskanta, R.(1986) "Three Dimensional Numerical Modeling of Circulation and Heat Transfer in a Glass Melting Tank. Part 1. Mathematical Formulation," Glastech. Ber., Vol.60, p.71
12. Vanandruel, N. and Deville, M.(1993) “Unsteady Numerical Simulation of Circulation and Heat Transfer in a Glass Melting Tank”, Proc.2nd ESG Conf. on Glass, p.85.
13. Schill, P.(1990) "Calculation of 3D Glassmelt Flow in Large Furnaces via Two Grid Method," Glastech. Ber., Vol.63K, p.39.
14. Argent, R.D.(1992) “Bubbler Systems can Abet Melting Operations” , Glass Ind., Vol.73, p.27.
15. Ungan, A. and Viskanta, R. (1986) "Effect of Air Bubbling on Circulation and Heat Transfer in a Glass Melting Tank," J. Am. Ceram. Soc., Vol. 69, p. 382.
16. Franek, A. (1992) “Bubbling in the Three Dimensional Flow Temperature Model,” Proc. l6th Int. Congr. On Glass, Vol. 6, p. 9.

17. Hogrel, K. And Frischat, G.H. (1992) "Homogenizing of Glass Melts by Bubbling," Proc. l6th Int. Congr. On Glass, Vol. 6, p.179
18. Gelder, A.M. (1991) "Bubbling in Glass Furnaces," Proc.1st ESG Conf. on Glass, p.191.
19. Clift, R., Grace, J.R. and Weber, M.E. (1979) "Bubbles, Drops and Particles," Academic Press, New York
20. Stanek, J. (1977) “Electric Melting of Glass,” Elsevier, Amsterdam.
21. Hoffmann, D.R. and Hilbig, G. (1981) “Zur Berechnung bei der Elektroglasschmelze Direct Freigesetzten Joulescen Warme,”Glastech. Ber., Vol. 54, p. 36.
22. Stanek, J. (1989) "Problems in Electric Melting of Glass," Proc. l5th Int. Cogress on Glass, p.469.
23. Ungan A. and Viskanta, R. (1986) “Three-Dimensional Numerical Simulation of Circulation and Heat Transfer in an Electrically Boosted Glass Melting Tank,” IEEE Trans.On Ind. Appl., Vol. IA-22, p.922.
24. Schill, P. (1992) “Mathematical Modeling of Complex Shapes of Glass Tanks ,” Proc. l6th Int. Congr. On Glass, p.31.
25. Skvor, Z., et. aJ. (1992) "A New Method for the Calculation of a Power Field in the Melting Tank of an All Electric Glass Melting Furnace," Proc. l6th Int. Congr. On Glass, Vol. 6, p. 287.
26. Igaraski, H. and Takahaski, T. (1991) "A Three-Dimensional Mathematical Model for an Electric Glass Melter Used to Vitrify Nuclear High Level Liquid Waste," Glass Technol., Vol. 32, p.206
27. Phillips, G. and Hofmann, O.R. (1993) “Modeling of Electrically Heated Glass Melting Furnaces Needs Inclusion of Lorentz Force,” Proc. 2nd ESG Conf. On

Fundamentals of Glass Science and Technology, p.235.
28. Barton, J.L. (1992) “Innovation in Glass Melting,” Proc. 16th Int. Congr. On Glass, Vol.1, p. 65.
29. Joshi, M.L. et. al. (1995) "Cost Effective NOx Reduction Using Oxygen enriched Air Staging On Regenerative Glass Furnaces," Ceram. Eng. Sci. Proc., Vol.16, p.156.
30. Brown, J.T., McMahon, A. and Yum, D.Y. (1994) “The Development and Successful Application of 100% oxygen-Oil Combustion for Glass Melters,” J. Non-Cryst. Sol., Vol.177, p.324.
31. Gosman, A.D., Lockwood, F.C., Megahed, I.E.A. and Shah, N.G.(1982) “Prediction of Flow, Reaction and Heat Transfer in a Glass Furnace,” J. Energy, Vol.6, p.353.
32. Carvalho, M.G. and Lockwood, F.C. (1985) “Mathematical Simulation of an End Port Regenerative Glass Fumace,” Proc. Inst. Mech. Engrs., Vol.199, p.113.
33. Song, T.H. (1986) “Simulation of Flow, Combustion and Heat Transfer in a Two-Dimensional Natural Gas-Fired Industrial Furnace,” Ph.D Thesis, Purdue University, West Lafayette.
34. Carvalho, M.G., Durao, D.F.G and Pereira, J.C.F.. (1987) "The Prediction of Flow Reaction and Heat Transfer in an Oxy-Fuel Glass Furnace," Int. J. Eng. Comput., Vol. 4, p. 23.
35. Koayashi, H. and Richter, W. (1992) "Design Considerations and Modeling of the Glass Melter Combustion Space for Oxy-Fuel Firing," Proc. of the l6th Int. Congr. on Glass, Vol.6, p. 65.
36. Carvalho, M.G. and Nogueira, M. (1993) "Comparison of Heat Transfer Characteristics of Oxy-Fuel and Air Fuel Melting Furnaces," Proc. 2nd ESG Conf. On Fundamentals of Glass Science and Technology, p.85.
37. Viskanta, R., Chapman, K.S. and Ramadhyani, S. (1993) "Mathematical Modeling of Heat Transfer in High Temperature Industrial Furnace," Phase Change and Combustion Simulation, p.118.
38. Hoogendoom, C.J., Post, L. and Wieringa (1990) “Modeling of Combustion and Heat Transfer in Glass Furnaces,” Glastech. Ber., Vol. 63, p. 7.
39. Carvalho, M.G. and Lockwood, F.C. (1990) "Thermal Comparison of Glass Furnace Operation with Oil and Natural Gas," Glastech. Ber., Vol. 63, p.233.
40. Carvalho, M.G. and Nogueira, M. (1993) "Modeling of the Glass Melting Process Through 3-D Physically Based Procedures," Proc. 2nd ESG Conf. On Glass., p.623.
41. Muysenberg, H.P.H., Simonois, F. and Van Der Heijen, T.C. (1992) "The Use Numerical Flow Models in Glass Melting Process," Proc. of the l6th Int. Congr. On Glass, Vol.6, p. 3.
42. Hoker, B.C. and Gertýtein, V.Y. (1995) "Coupling Combustion Space and Glass Melt Models Improves Predictions," Bulletin of Am. Ceram. Soc., p. 75
43. Hottel, H.C. and Sarofim, A.F. (1967) “Radiative Heat Transfer,” McGraw-Hill, New York.
44. Mase, H. and Oda, K. (1980) "Mathematical Model of Glass Tank Furnace with Batch Melting," J. Non-Cryst. Sol. Vol 38, p.807.
45. Lockwood, F.C. and Shah, N.G. (1980) “A New Radiation Solution Method For Incorporation in General Combustion Prediction Procedures,” Proc. of l8th Int.

Symp. On Combustion.
46.Menguc, P.M. (1985) “Modeling of Radiative Heat Transfer in Multidimensional Enclosures Using Spherical Harmonics Approximation,” Ph.D Thesis, Purdue University, West Lafayette.
47.Truelove, J.S. (1988) “Discrete Ordinates Solutions of the Radiative Transfer” , J.Heat Transfer, Vol.109, p.1048.
48. Raithby, G.D. and Chui, E.H., (1990) "A Finite-Volume Method for Predicting A Radiant Heat Transfer in Enclosures with Participating Media," J. Heat Transf., Vol. 112, p.415.
49.Chai, J.C., H.S. Lee and Patankar, S.V. (1994) "Finite Volume Method for Radiation Heat Transfer," J. Thermophysics and Heat Tranf., Vol. 8, p. 419.
50.Ungan, A. and Viskanta, R. (1986) “Melting Behavior of Continuously Charged Loose Batch Blankets in Glass Melting Fumaces,” Glastech. Ber., Vol. 59, p. 279.
51. Kim, D.S. and Hrma, P. (1990) “Volume Changes During Batch to Glass Conversion,” Am. Ceram. Soc. Bull., vol. 69, p.1039.
52.Wu, X. and Li, L. (1992) "Melting Behavior of Batch Blanket in Glass Melting Tanks" Proc. l6th Int. Congr. On Glass, Vol. 6, p. 471
53.Faber, A.J. Bererkens R. and de Waal, H. (1992) "Thermal Behavior of Glass Batch on Batch Heating," Glastech. Ber., Vol. 65, p.177.

54.Conradt, R., Suwannathada, P. and Pimkhaokham, P. (1994) "Local Temperature Distribution and Primary Melt formation in a Melting Batch Heap," Glastech Ber., Vol. 67, p.103.
55. Cable, M. (1990), “The Principles of Homogenizing of Glass Melts,” Glastech. Ber., Vol. 63K, p.308.
56.Phillipp, G. (1991) "3D Modeling of Homogenizing in Glass Melts,” Proc.1 st ESG Conf. On Glass, p.184.
57.Berkeens, R.G.C., van der Heijen, T. and Muijsenberg, E. (1993) "Possibilities of Glass Tank Modeling for the Prediction of the Quality Melting Process," Ceram. Eng. Sci: Proc. Vol.14, p.139.
58.Hogerl, K. and Frischat, G. H. (1994) “Homogenization of Glass Melts by Bubbling on a Laboratory Scale,” Glastech. Ber., Vol. 67, p.145.
59.Balkanli, B. and Ungan, A. (1996) "Numerical Simulation of Bubble Behavior in Glass Melting Tanks. Part 3. Bubble Trajectories," Glass Technol., Vol. 37.
60.Chemelar, J., Franek, A. And Schill, P. (1992) “Computer Aided Tracing of Bubbles Glass Quality Control,” Proc. l6th Int. Congr. On Glass, Vol. 6, p. 45.
61.Beerkens, R., van Der Heijden, T. And Muysenberg, H. (1992) “A Model Study on Degassing of Sulphate Refined Glass Melts,” Proc. l6th Int. Congr. On Glass,” Vol. 6, p.15.
62.Hrma, P. (1989) "Bubble Removal from Molten Glass," Proc. l5th Int. Congress on Glass Vol. 3b, p.78. .
63.Hrma, P. (1989) "Bubble Removal from Glass Melts: Power Law Model," Glastech. Ber.,Vol 62, p.301.
64.Balkanli, B. and Ungan, A. (1996) "Numerical Simulation of Bubble Behavior in Glass Melting Tanks. Part 4 Dissolved Gas Concentration," Glass Technol., Vol. 37.

65.Smarts, E.L. (1992) “Bubble generation at glass/Refractory Interfaces: A Review of Fundamental Mechanisms and Practical Considerations,” Glastech. Ber., Vol. 65, p.87.
66.Kramer, F.W. (1992) "Analysis of Gases evolved by AZS Refractories and by Refractory/Glass Melt Reactions," Glastech. Ber., Vol. 65, p. 93.
67.Roi, T., Seidel, O, Nolle, G. and Hohne, D. (1995) “Formation and Behavior of Bubble Curtains in Glass Melts,” Glastech. Ber., Vol 68, p. 222.
68.Balkanli, B. and Ungan, A. (1996) “Numerical Simulation of Bubble Behavior in Glass Melting Tanks. Part. 4. Polydipersed Bubbles,” Glass Technol., Vol.37.
69.Nolle and Hohne, D. (1994) “Modeling of the Bubble Population in Glass Melts” Glastech. Ber., Vol. 67, p.263.
70.Beerkens, R.G.C. (1995) “The Role of Gases in Glass Melting Processes”, Glastech. Ber., Vol. 68, p. 369.
71.Hrma, P. and Kim, D. (1994) “Sulphate Mass Balance and Foaming Threshold in Soda-Lime Glass, Glass Technol.,”Vol. 35, p.
72.Hrma, P.(1990) "Model for a Steady State Foam Blanket," J. Colloid Interface Sci., Vol.134, p.161.
73.Beerkens, R.G.C., Muijsenberg, H.P.H. and van der Heijen, T. (1994) "Modeling of Sand Grain dissolution in Industrial Glass Melting Tanks," Glastech Ber. Vol. 67 p.179.
74.Nemec, L. (1992) "Refining and Sand Dissolution in the Glass Melting Process ", Tijds. Klei Glas. Keram., Vol.13, p.1 fi2.
75.Ungan, A., Payli, R.U. and Balkanli, B. (1994) “Numerical Model of Polydispersed Silica Grain Dissolution in Glass Meltin Furnaces,”, J. Am. Ceram. Soc., Vol. 77, p.1921.
76.Choudry, M.K. (1991) "Mathematical Modeling of Flow and Heat Transfer Phenomena in Glass Furnace Channels and Forehearths," vol 74, p.3091.
77.Roychowdhury, A.P. and Srinivasan J. (1994) “The Modeling of Radiation Heat Transfer in Forehearths Units in Glass Melting," Warme Stoffubetag.,” Vol. 30, p. 71.
78.Beerkens, R., Muysenberg, H. and Barklage-Hilgefort, H. (1992) "Effects of Deposition and Fouling on Thermal Behavior of Glass Furnace Regenerators," Tijd. Klei Glas. Keram., Vol.13, p.156.
79.Carvalho, M.G, Nogueira, M. and Silva, P. (1993) "Regenerative Cycle Optimization via Physically Based Dynamic Modeling," Proc. 2nd ESG Conf. On Glass., p.619
80.Boussant-Roux, Y, Zanoli, A. and Naturel, C. (1993) "Enhancement of Heat Transfer in Regenerators," Proc. 2nd ESG Conf. On Glass., p.63.
81.Choudhary (1989) “Analysis of Heat Transfer in the Corroding Sidewall of a Furnace,” J. Am Ceram. Soc., Vol. 72, p. 2325.
82.Roesky, R., Burdick, V. and Mortel H. (1994) “An Assay to Predict Corrosion of AZS Refractories,” Spechsaal, vol.127, p. 354.
83.Pavlovski, V.K. and Sobolev, Y.S (1992) “Corrosion of Refractory materials in Molten Lead Silicate Glasses,” Glass Ceram., Vol. 49, p. 367.

A LABORATORY TECHNIQUE TO MEASURE THE GROWTH RATE OF BUBBLES AT HIGH TEMPERATURE

B. Parker and **I. H. Smith**
Pilkington Group Research, United Kingdom

Abstract

Mathematical models of refining demand accurate bubble growth and decay data.

The paper describes an experimental technique developed to measure the growth rate of bubbles in sulphate refined float glass. Gases of known composition are introduced into a melt contained in a silica crucible through a platinum capillary. The bubbles are monitored by time lapse photography and their growth rates determined as they rise to the surface.

Measurements on the growth of carbon dioxide and nitrogen bubbles in the size range 0.2 mm - 6.0 mm diameter at a temperature of 1150^{o}C, show that the growth rate is proportional to bubble diameter.

1. INTRODUCTION

A computer flow model programme has been developed to improve the design, operation and understanding of Pilkington float glass furnaces. This computer programme relies upon a bubble growth or shrinkage model to predict the behaviour of these bubbles in the complex flows of a furnace. This model can only be generated from accurate scientific data describing the behaviour of these bubbles under specific conditions.

A number of workers have developed methods to observe bubbles in molten glass, however few appeared to meet the requirements of allowing a bubble of known composition to rise freely in a glass melt at high temperature. A method which allowed these criteria to be met was thus developed building on existing Pilkington methods. The apparatus designed to do this is shown in Figure 1.

2. EXPERIMENTAL PROCEDURE

The apparatus consists briefly of a Pentax LX camera, bellows, extension tubes and a 300mm lens mounted on an optical bench. The bubble to be studied is introduced into a vitreous silica cell using a platinum capillary after carefully purging the line to ensure that the gas to be studied is of known composition. The cell has been specially designed with a flat window at the front to enable direct observation of the bubbles without distortion and is maintained at the desired temperature using a furnace heated by silicon carbide elements.

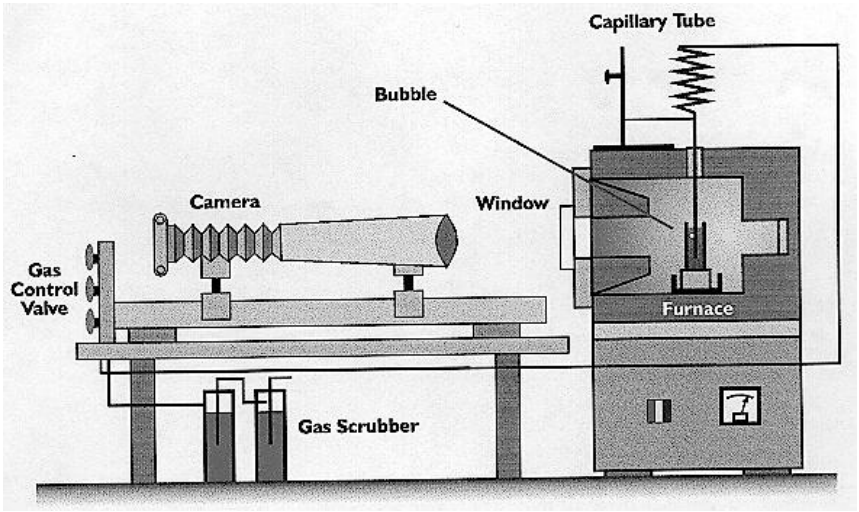

Bubbles are photographed using a time lapse photographic system for time intervals between 10 and 240 seconds. From the photographic negative bubble diameters can be measured and a growth or shrinkage rate determined.

A new vitreous cell is used every day and refilled with standard UK float glass. The cell is held at 1150^{o}C overnight to remove unwanted bubble before introducing the bubble of known composition.

3. RESULTS

Nitrogen

Plots of diameter vs. time for individual nitrogen bubbles were drawn from the time lapse photographs and a least squares linear regression plotted for each line.

FIG 2 LINEAR REGRESSION FOR NITROGEN BUBBLE

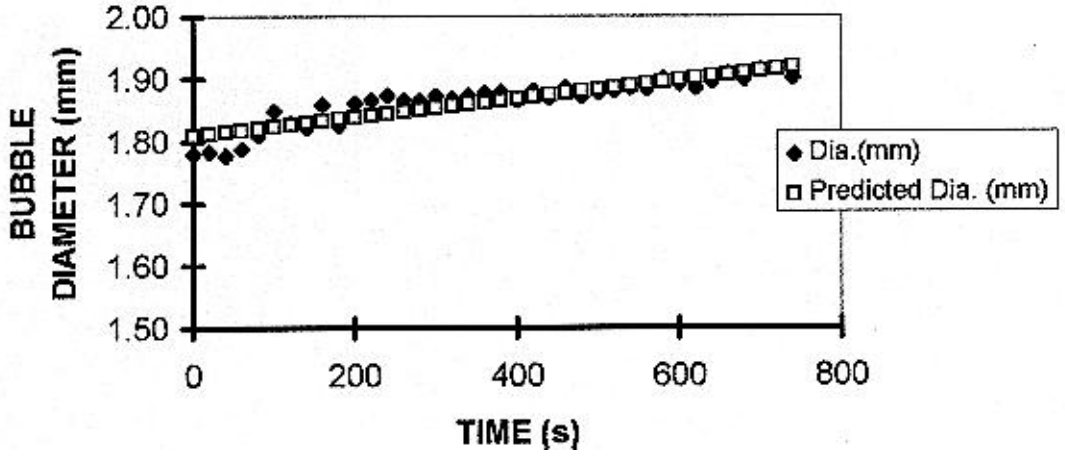

This linear regression enabled a bubble growth rate to be calculated from the slope of the line and a subsequent plot made of bubble growth rates vs. bubble diameter to be made.

FIG 3 GROWTH RATES FOR NITROGEN BUBBLES 1150°C FLOAT GLASS

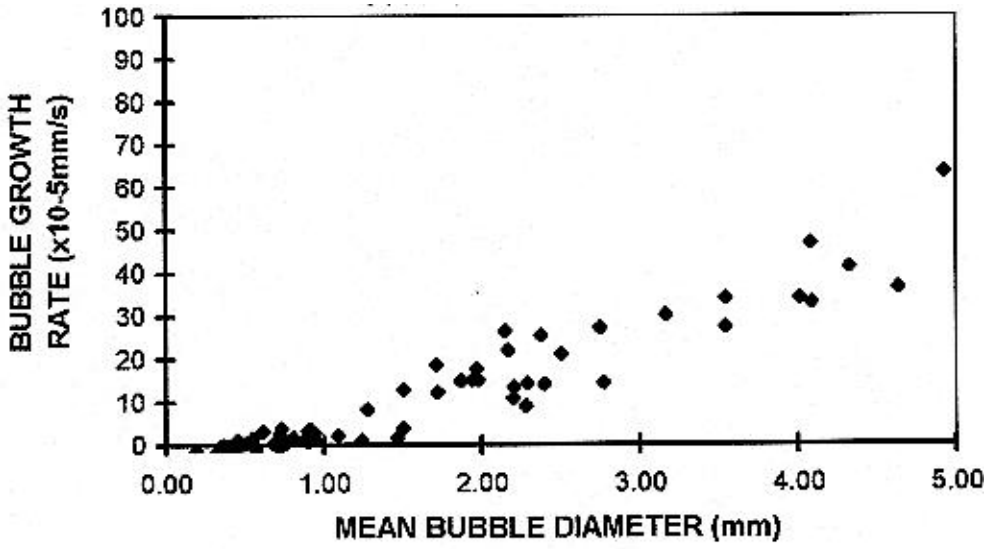

The graphs show that the bubbles grow at a constant rate and that the bubble growth rate is dependant on bubble diameter.

Carbon dioxide

Plots of diameter vs. time for individual carbon dioxide bubbles were also drawn using the same procedure employed for nitrogen bubbles and a growth rate calculated.

FIG 4 LINEAR REGRESSION FOR CARBON DIOXIDE BUBBLE

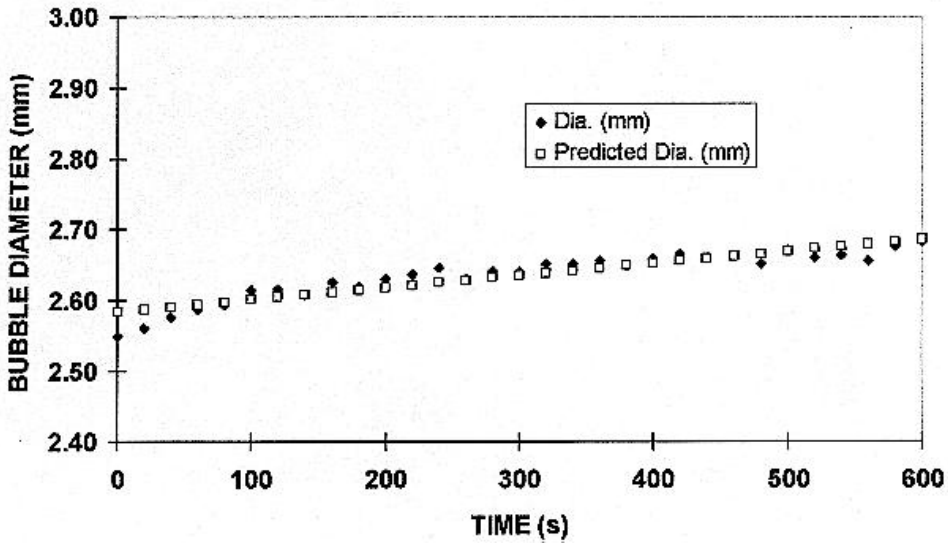

Again the bubbles grow at a constant rate and the bubble growth rate is dependant on bubble diameter.

FIG 5 GROWTH RATES FOR CARBON DIOXIDE BUBBLES 1150°C FLOAT GLASS

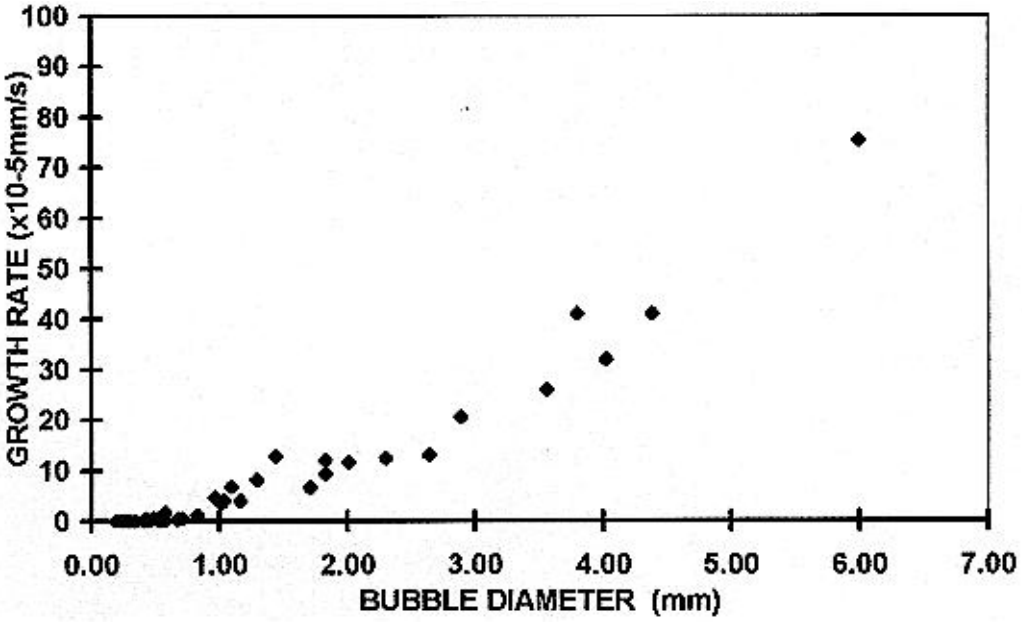

4. DISCUSSION

It has been shown in these experiments that the growth or shrinkage rates for each of the gases studied, is diameter dependant. The growth rate for a diameter change of less than 5 % is virtually the same as that for the full change in diameter. This shows that there are no species rapidly diffusing into the bubbles at an early stage, for example water vapour.

The equation which assumes the contraction of a bubble is diffusion controlled and uses the value of the concentration gradient valid for a stationary boundary was derived by Epstein & Plesset [(1)] :

$$\frac{da}{dt} = \frac{-D(c_i - c_o)}{\rho}\left[\frac{1}{a} + \frac{1}{\sqrt{(\Pi D t)}}\right] \qquad (1)$$

where
a is the radius of the bubble
t is time
D is the diffusivity of gas in liquid
c_i is the concentration of gas in the liquid
c_0 is the initial concentration of gas dissolved in the liquid around the bubble
ρ is the density of gas inside the bubble

This equation has been used in its original and modified forms by many other workers[(2-4)] to describe the diffusion of gas into a bubble.

Applying statistical analysis to the growth rate vs. diameter curves from this work gives the following equations for nitrogen and carbon dioxide:-

Nitrogen

$$\left[\frac{da}{dt}\right]^{1/2} = -2.446 + 5.678d - 1.649d^2 + 0.183d^3 \quad (2)$$

Carbon Dioxide

$$\left[\frac{da}{dt}\right]^{1/2} = -0.721 + 3.213d - 0.696d^2 + 0.070d^3 \quad (3)$$

These equations have been successfully incorporated into the 3D computer model and accurate predictions made.

REFERENCES

l. Epstein P.S. + Plesset M.S. (1950) J. Chem. Phys.18,1505
2. Cable M. (1961) Glass Technol. 2 (2) 60
3. Scholze H. (1962) Ber. Dt. Keram Ges. 39162
4. Frischat + Oel (1965) Glastech Ber. 38156

This paper is published with the permission of the Directors of Pilkington plc and of Dr. A. Ledwith, Director of Group Research.

COMPARISON OF THE SINGLE AND THREE-PHASE ELECTRIC HEATING SYSTEMS OF A GLASS MELTING FURNACE

Antonřn Lisý
Institute of Chemical Technology, Czech Republic

Abstract

The evolution of electric glass melting furnaces brought changes in the geometry of their melting tank, in the location of the throat, in the configuration of electrodes and in their connections with the feeding transformers. New furnaces for melting of crystal glass have tanks with square ground plan, which has higher heat efficiency and the glass melt entering the throat is good stabilized. The feeding of these furnaces is either single-phase or three-phase. When a single-phase feeding is used the released energy in the tank is better distributed which from technological point of view is very important. On the other side when using three-phase feeding system then only the electrical network is more uniformly loaded. The further following study tries to use the advantages of both feeding systems. There have been used two different physical models - one made from electroconducting sheets, the second was a three-dimensional one with model-liquid. By means of these models was the situation in the melting furnace simulated. There were obtained data especially from the liquid model, that by proper distribution of the feeding electrodes and their correct connections with the three-phase source (transformer) is possible to obtain conformable technological conditions in the furnaces as when using the single-phase feeding system.

I. INTRODUCTION

Electric melting furnaces have been used in the glass melt production for many years. Their evolution during those years brought changes in the geometry of their melting tank, in the location of the throat, and in the configuration of electrodes. Melting, homogenizing and conditioning of the glass melt are performed in the tank of an electric furnace. The space in which melting and conditioning zones are located depends on the geometry of a melting tank and on the way in which electric energy is released - the distribution of electrodes and their connections with the feeding transformers.

The experiences with the glass melting electric furnaces' run and the results of model investigations show that it is of advantage to use the melting tank with approximately square ground plan. In this square-shaped tank, heat losses through walls and the bottom are minimalized and the flow of the glass melt into the throat is uniform. The feeding of this furnaces is either single-phase, or three-phase. It is known that a single-phase feeding enables the more uniform distribution of electric energy in a melting tank, and the current load of electrodes can be modified by changing their number. Symmetrical current and power loads of the electrical network represent the main advantage of the three-phase feeding. The following study tries to

find the solution which would connect the advantages of the uniform distribution of released energy with those of symmetrical power load of a three-phase electrical network.

2. EXPERIMENTS

To get the data necessary for the choice of an optimal design of a melting furnace, the methods of measuring on electroconducting sheets and on physical liquid model were used. When choosing optimal arrangements of electric heating system in a melting tank, we took into account present technological possibilities of the electric melting furnace design, the experiences with this furnaces' run, and also the professional and patent literature. The uniformity of the distribution of released electric power and the current load of electrodes were evaluated. The measuring were carried out by means of three runs of a single-phase feeding system, and three runs of a three-phase feeding system, Fig.1.

For these runs 1 to 6 were measured potentials fields on electroconducting sheets models in horizontal crossection of the melting tank in the level of electrodes and power fields were calculated from those potential fields according to the relation:

$$P_{ij} = \frac{\kappa}{4h^2}\left[\left(\varphi_{i+1,j} - \varphi_{i-1,j}\right)^2 + \left(\varphi_{i,j+1} - \varphi_{i,j-1}\right)^2\right]$$

P_{ij} - electric power in the point with i, j co-ordinates
κ - conductivity of a medium
h - the distance of the nodes of measured potentials
φ - electric potential

The computer provided by the Surfer program was used for the graphic evaluation of power fields. The results of the individual arrangements of the electric heating systems are in following pictures.

The runs 1 to 3 were feeded from single-phase feeding system and distribution of the released electric power is in Fig. 2a, 2b and 2c. In the run 1 (Fig.2a) the electric circuit is closed between two trios of opposite horizontal electrodes. The highest values of released electric power are near the electrode tips, low values of power can be noticed near the walls with electrodes and there is a central zone of uniformly released power between the electrodes in the tank. In the run 2 (Fig.2b) were increased number of electrodes to 10 pieces. Trios of electrodes were substituted by pentades in walls of the tank. The measuring were carried out with the constant value of the electric power in the model. The zone of uniformly released power between electrodes were enlarged and values power released on electrodes by this run 2 were decreased because it was divided on 10 electrodes. In the run 3 (Fig.2c) were connected neighbour pairs of electrodes in the corners of the melting tank with the transformer in such a way that an electric current can flow along the walls. The highest values of power being on the electrodes and the lowest ones in the center area and in the corners of the tank.

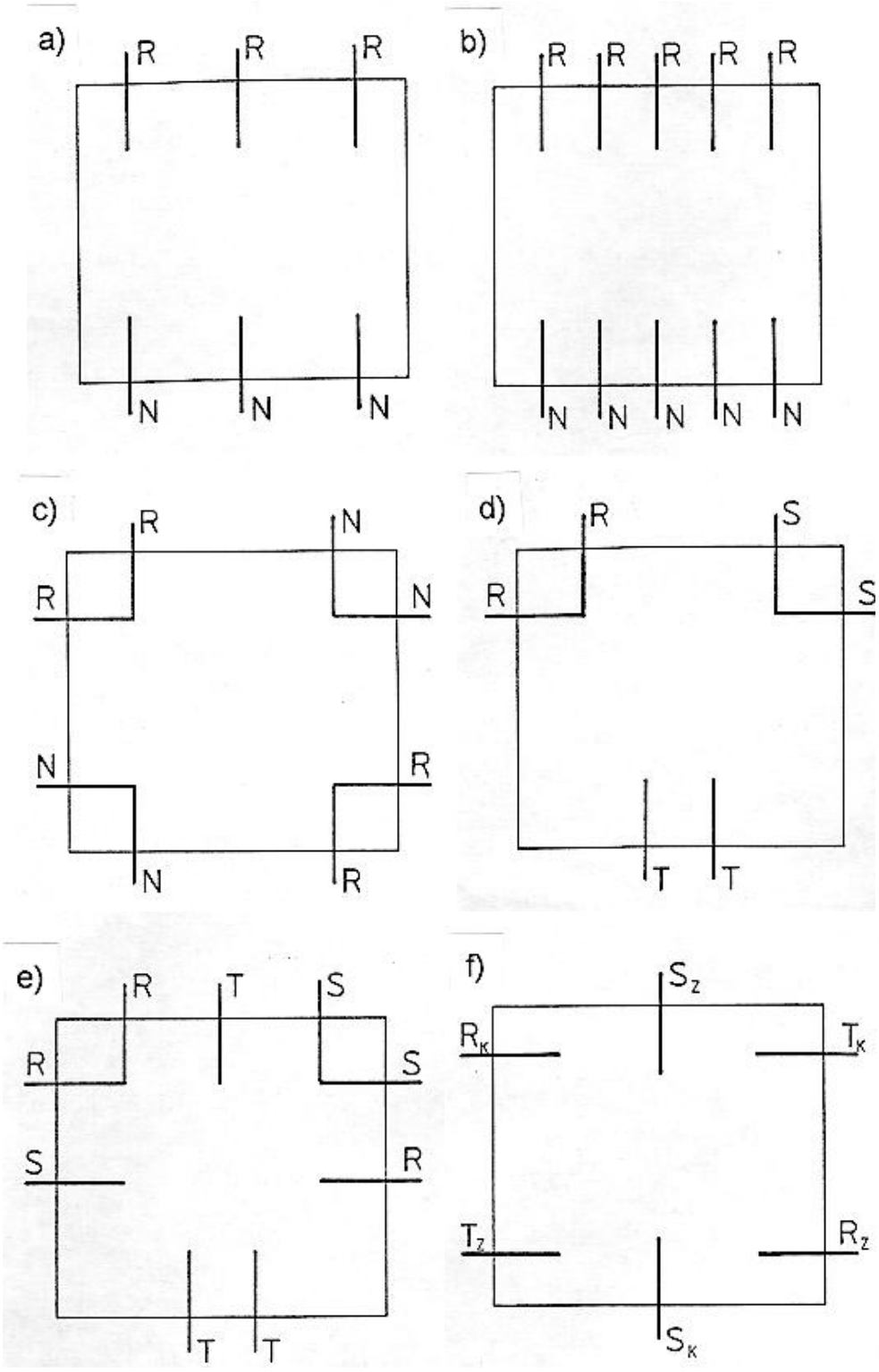

Fig. 1. The survey of the runs of the electrode arrangements in the melting tank of a furnace and their connections with the feeding transformers, a) run 1, b) run 2, c) run 3, d) run4, e) run 5, f) run 6

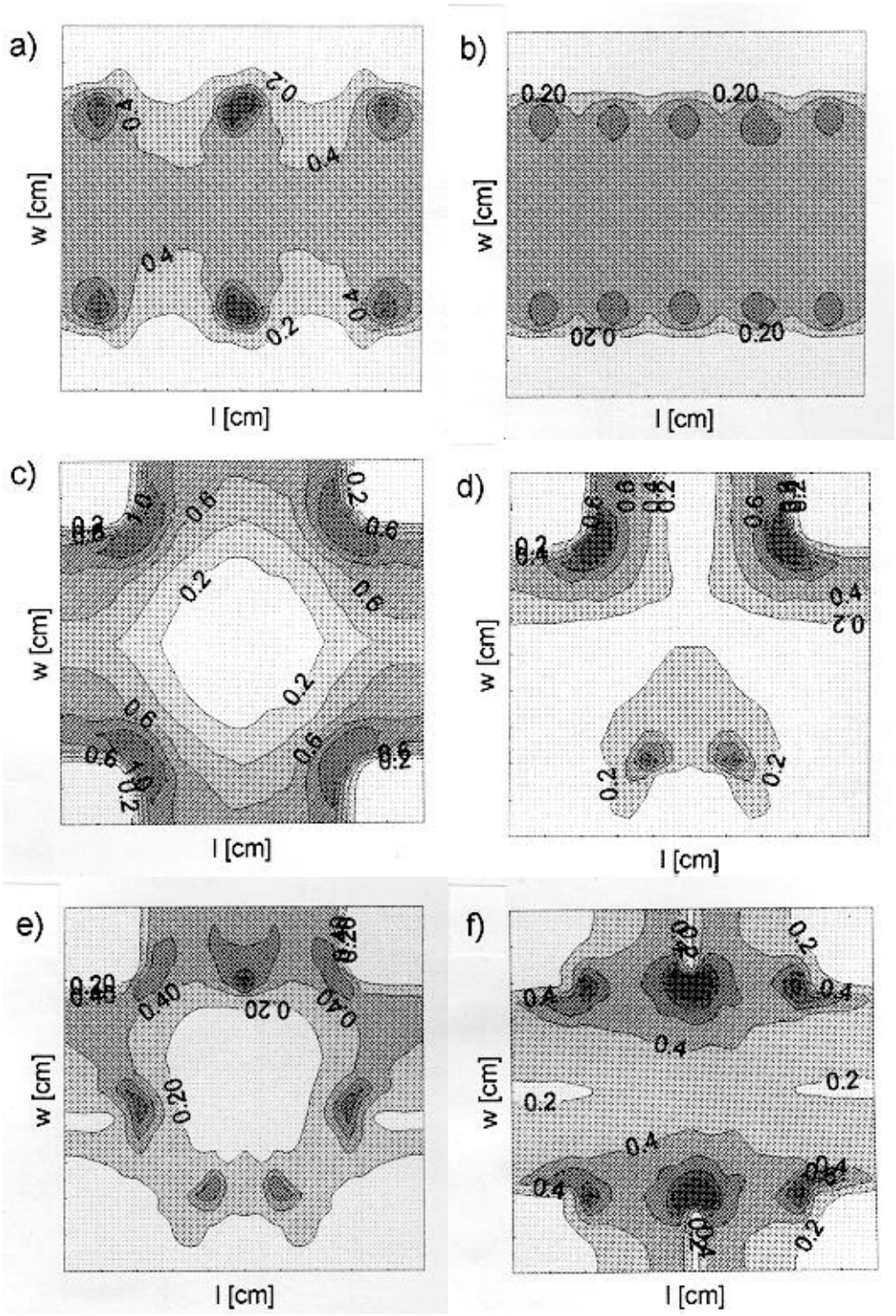

Fig. 2 The power fields in the melting tank of a furnace for the runs 1 to 6: a) run 1, b) run 2, c) run 3, d) run4, e) run 5, f) run 6

The runs 4 to 6 were feeded from three-phase feeding system and distribution of the released electric power is in Fig. 2d, 2e and 2f. In the run 4 three pairs of electrodes were connected with the second windings of the transformer with the delta connection. The power field in picture (Fig.2d) shows that electric power is not released uniformly. Larger part of the power is concentrated in one half of the melting tank and the highest electric power values are on electrodes. In the run 5 the number of electrodes has been increased to nine and their location on the walls of a melting tank and the way of the connection with the feeding transformer is in the Fig.1 e. The distribution of power field in a melting tank is in Fig.2e and shows that the electrical power is released decisive by the periphery walls. There are zones of a lower concentration of electric power. One is in the center of the tank, the next are around the tank wall with a pair of electrodes located in its center and finally in the corners of the tank. In the run 6 were located six electrodes on the walls of the tank and were connected to three-phase feeding transformer. Its second windings have the open delta connection. The resulting distribution of electric power in the melting
tank is on Fig.2f. The highest electric power values have been released near the electrode tips and zone of uniformly released power is between electrodes in the central part of the tank. The distribution of electric power is similar as in runs 1 and 2. Lower values power on electrodes in the corners of the tank in the both trios, can be compared with the geometry of the tank and the location of electrodes.

The technology of glass melting requires not to exceed the current load value 1 A/cm^2 on electrodes. Using all six runs with various distribution of electric heating system given before, the data for the calculation of electric resistance of a real furnace were measured on a physical liquid model, and the current load of electrodes for the electric power output 500 kW, which corresponds to the pull of the furnace, was determined on a base of this calculation. Table I gives a survey of calculated values of currents and voltages for the feeding transformer and the current load of electrodes.

Table I. Parameters of the feeding transformer, electrode currents and current load of electrodes

transformer			**electrodes**		
run	**voltage U [V]**	**current I [A]**	**number for phase**	**I_e [A]**	**I_e [A/cm^2]**
1	144,4	3460,4	3	1153,4	1,37
2	130,8	3819,2	5	763,8	0,91
3	121,7	4106,5	4	1026,6	1,22
4	126,8	2275,6	2	1137,8	1,35
5	84,9	3395,8	3	1131,9	1,35
6A	130,3	1278,9	1	1278,9	1,53
6B	113,3	1471,2	2	735,6	0,88

As can be seen from the survey given above, the current load of electrodes smaller than 1 A/cm^2 can be found only in the run 2 and the run 6B with doubled electrodes. The other runs were eliminated because of a higher current load of electrodes or due to the way of electric power releasing. The run 2 represents a single-phase feeding system and 6B a three-phase one.

Comparing measuring of power fields carried out on electroconducting sheets models, we can notice a similar distribution of released electric power in both types of feeding, there are run 2 with single-phase feeding system and 6B with a three-phase feeding system. We can assume, thus, that the distribution of temperatures and the characteristics of the flow in the melting tank of the designed furnace will be similar for both compared runs -2 and 6B.

The results of physical modelling of temperature and velocity fields of the designed furnace by means of a three-dimensional liquid model confirmed that the same characteristics of the released electric power distribution in the melting tank causes very similar distribution of temperatures and flows.

3. CONCLUSION

We can conclude that the important thing for the technology of a melting process is the distribution of released electric power, and, consequently, it does not matter if this power is released by means of a single-phase feeding system or by means of a three-phase one. But there can exist some other reasons to use either the single-phase feeding system, e.g. melting of a lead crystal by means of alternate, low-frequency current, or the three-phase feeding system, if huge electric power values are needed.

It is possible to reach the uniform distribution of released electric power in the melting tank of a furnace fed by a single-phase system. The results of the study above showed that by means of the optimal electrodes configuration and connection nearly equal technological conditions could be obtained, even when a three-phase feeding system is applied.

REFERENCES

1.Lisϖ, A., Kasa, S.,: Physical Modelling of the All-electric Melting Furnace for Ba-crystal Glass Melt. Research report, ICT Prague 1995

2.Durd<kov<, E.,: Physical Modelling of the Melting Furnace for the Melting of Ba-crystal. Diploma thesis, ICT Prague 1995

3. Stan k, J.,: Electric Melting of Glass. SNTL Prague,1976

COUPLED COMBUSTION MODELLING AND GLASS TANK MODELLING IN OXY- AND AIR-FIRED GLASS-MELTING FURNACES

A.M. Lankhorst[1], H.P.H. Muysenberg[2] and **M.P.J. Sanders[2]**
[1] TNO Institute of Applied Physics, Delft, The Netherlands
[2] TNO Institute of Applied Physics, Eindhoven, The Netherlands

Abstract

For the Oberland Glas AG end-fired furnace, subject to a German AIF funded study, results of coupled 3D simulations for both combustion chamber and glass tank will be discussed. For the *glass tank* the finite-volume based model TNO-GTM is used. A batch blanket model for calculating the raw materials melting process is incorporated in the model as well as electrical boosting. By aid of sub-models it is possible to study the effects of changes on glass quality. For the *combustion space* the finite-volume based model TNO-WISH3D is used. In this model radiative heat transfer between superstructure sidewalls, crown and glass surface as well as radiative absorption and emission by the flame and the flue gases is calculated. For combustion a diffusion flame model is used. In case of oxy-fired combustion the heat effects of formation and recombination of intermediate radicals is accounted for. Both numerical models can be used separately or coupled. In the coupled case, in an iteration loop, the most recent temperature distribution on the glass surface as calculated by the glass tank model is used as boundary condition for the combustion model whereas the most recent heat flux distribution on the interface as calculated by the combustion model is used as boundary condition for the glass tank model. The two models can have different numerical mesh-sizes. In this numerical study the effects of firing rate, air preheat temperature, air excess, etc. on flame length and shape, temperature and heat flux distribution on the glass surface, thermal efficiency, residence time distribution and glass quality in the melter will be discussed. The effects of oxy-firing as opposed to air-firing will be shown.

1. INTRODUCTION

Furnace design is a critical key for the glass industry. For every type of glass product, only one optimal glass tank exists. In order to reduce risks, until now for a new tank design existing tanks are only slightly modified. Especially because modern tanks last 5-14 years a wrong decision or too high investment is a long burden. Currently, typical modifications to existing furnaces are stretching the furnace slightly in length, width and depth making new furnace design more like an evolution process. Recently, the glass industry changed from an evolution to a revolution by applying oxy-fuel combustion to heat the glass melt. This option is so drastically different from air-firing, that it is astonishing to see that many furnaces have adapted this 'new' technology already. It is estimated that presently about 2% of all worldwide produced glass is melted by using 'pure' oxygen.

It is clear to the glass industry that for constructing the optimal glass tank, mathematical simulation models are a valuable tool. Especially when applying a new technology as oxy-fuel combustion, simulation models are indispensable for exploring all possibilities at a low risk.

All oxygen suppliers try to assist the glass industry by offering mathematical simulation of the combustion space and sometimes the glass bath. However TNO Glass Technology as an independent Research Institute can offer a complete glass furnace simulation, glass bath and combustion space, and predict the effects on melting performance and glass quality. Starting with extensive laboratory studies, melting experiments and industrial support, TNO-TPD has developed a Glass Tank Model and combustion model with great potentials (see Fig. 1).

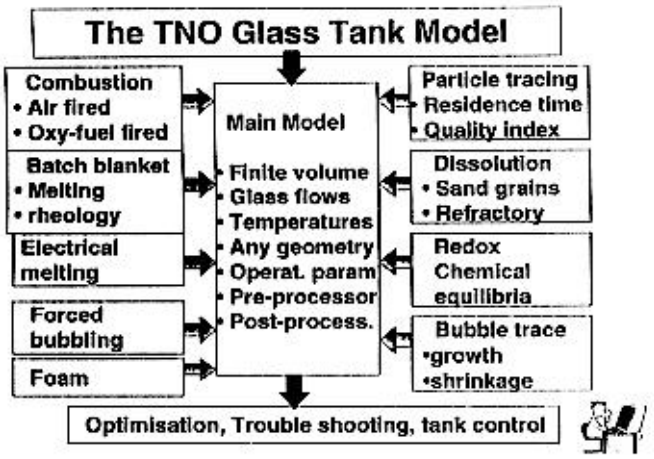

Fig.1 The TNO Glass Tank Model

One of our present studies is funded by the German AIF. In close cooperation with the HVG Frankfurt, we want to show the German glass industry the capabilities of advanced simulation models for medium and small glass producers. A furnace of Oberland Glas AG is subject to this study. The results in this paper were studied as an example and outside the scope of the AIF funding. To keep some information confidential for Oberland Glas adapted glass properties and process conditions were used.

With this paper we want to show how Glass Tank Modelling can help to optimise new furnace design. However, the majority of the results will be shown during the presentation.

2. THEORY

2.1 Glass Tank Model

For the *glass tank* the finite-volume based model TNO-GTM is used. In this model the mass continuity equation, Navier-Stokes equations and energy equation are solved in three dimensions according to the numerical method as described by Patankar (1980). A batch blanket model for calculating the raw materials melting process is incorporated in the model. Conduction in the furnace walls has been taken into account and the physical properties of the glass are temperature dependent. By aid of sub-models it is possible to study the effects of changes on glass quality.

2.2 Combustion Space Model

For the *combustion space* the finite-volume Patankar-based model TNO-WISH3D is

used. In this model the mass continuity equation, Navier-Stokes equations, energy equation, species concentration equation and k-ε turbulence equations are solved in three dimensions. Radiative heat transfer between superstructure sidewalls, crown and glass surface as well as radiative absorption and emission by the flame and the flue gases is calculated by means of the Discrete Transfer Model. For combustion a diffusion flame model is used. In case of oxy-fired combustion the heat effects of formation and recombination of intermediate radicals is taken into account by correcting the heat capacity of the gas mixture. Conduction in the furnace walls has been taken into account (conjugate heat transfer). Physical properties of the gas mixture are both composition and temperature dependent.

The most commonly used turbulence model for engineering applications, the two- equation k-ε model (Launder et al., 1972), has been used. For both variables k and ε a convection-diffusion differential equation is solved. The k-ε model with its set of empirical constants applies only to fully developed turbulent flow. In near-wall regions viscous effects play an important role. Therefore, for k and ε wall-functions have to be used instead of boundary conditions. The standard wall-function method is extensively described in literature (Gosman et al.,1969 and Launder & Spalding, 1972).

Radiative surface-to-surface heat transfer and radiation absorption and emission by non-transparent gas components in the combustion atmosphere (H_2O and CO_2) is modelled with the Discrete Transfer Model (Lockwood & Shah,1981). The DTF method is based on a direct solution of the radiation transfer equation. For each wall point the solid angle is discretized in a number of beams. The incident heat flux on a wall point coming from opposing wall points after crossing the non-transparent gas mixture is determined by summation of the contributions for each beam. The gas mixture extinction coefficient is calculated from the emissivities of H_2O and CO_2. The emissivities depend on temperature, partial pressure and on a characteristic length scale: the internal furnace dimension. Emissivities are taken from charts presented by Hottel and Egbert (1973).

In the flame sheet model the combustion process in a flame is approximated by a one-step irreversible infinitely fast global reaction (Burke & Schumann,1928). The reaction occurs on a very thin flame front. Outside this flame sheet no reactions take place, and hot combustion products are mixed with the oxidant or fuel stream. On the flame front itself only combustion products (and diluents) are present and outside the flame front either fuel and products (and diluents) or oxidants and products (and diluents) are present. Fuel and oxidants can not coexist at the same time and on the same place. It can be shown that with these assumptions all species mass fractions are piecewise linear functions of one conserved scalar variable: the mixture fraction. For this single variable a convection-diffusion differential equation has to be solved coupled with the Navier-Stokes, turbulence and energy equations. From the mixture fraction mass fractions of the individual species (CO_2, H_2O, O_2 etc.) are determined. More complex combustion models are incorporated in WISH3D, such as the turbulent mixing model with presumed probability density function (PDF). For the problem under consideration where the heat flux to the glass surface has to be predicted accurately, the global heat released by combustion is the most important parameter. This parameter is not very sensitive to the type of combustion model used. Therefore, the cpu-efficient and numerically more stable f-model is used in the present simulations. For predictions of NO_X -levels the actual maximum flame temperature should be predicted accurately and more complex combustion models, such as the turbulent mixing model, should be used.

A drawback of the flame sheet model is the absence of radical species. The existence of intermediate radical species (eg. OH, O, H) in the reaction zone gives lower flame temperatures. This can be modeled by an empirical correction function (Post,1988; Kee et al.,1991) for the mixture specific heat, thus reducing the temperature. The correction function becomes effective for temperatures above 2200 ^{o}C. In oxy-fuelled combustion, the standard dissociation correction has to be modified. The dissociation correction function has been tuned for a 1D oxy-fuelled flame by comparing flame temperatures with a constrained-equilibrium model as developed by Peeters (1995). This detailed model takes over 150 chemical reactions into account, including the formation and recombination of many intermediate radicals.

2.3 Complete Furnace Model

Both numerical models (WISH3D and GTM) can be used separately with assumed or measured boundary conditions on the glass surface. The models can also be coupled with shared boundary conditions on the glass surface. In the coupled case, the distribution of the total heat flux (the sum of convective and radiative) on the interface between the models (the glass surface) is calculated by WISH3D and is transferred to GTM where it is used as a new boundary condition. GTM calculates new temperature and velocity fields and transfers the temperatures on the interface to WISH3D where it is used as a new boundary condition. This procedure is repeated until convergence is obtained. The general procedure is to initially run both models separately. The coupled simulation is started when the solution for both the glass tank and the combustion space are sufficiently converged.

As usually both models have different meshes, determined by the specific geometrical requirements of the combustion space and the glass tank, temperatures and heat fluxes on the glass surface have to be interpolated from one mesh to the other and backwards. Care has been taken that the (linear) interpolation procedure is conservative.

3. RESULTS

3.1 Glass Tank

A schematic of the glass tank is given in Fig. 2. The glass surface area is 10.75x6.60 m. Green sodalime glass is melted and an additional 800 kW electrical boosting is applied. The pull rate is 220 metric tons/day or 3.1 metric tons/day per m^2 furnace area. Two different combustion chambers are considered with the same glass tank: an end-port air-fired regenerative U-flame combustion system and a cross-fired oxy-fuel combustion system. Both furnaces are fired with natural gas (Dutch natural gas, approximate composition: 81 vol% CH_4, 4 vol% higher hydrocarbons and 15 vol% N_2). For the glass tank a non-linear mesh of 93x45x82 gridpoints is used amounting to a total number of 343.000. Effects of alternated firing is taken into account by mirroring the heat flux around the furnace centre line.

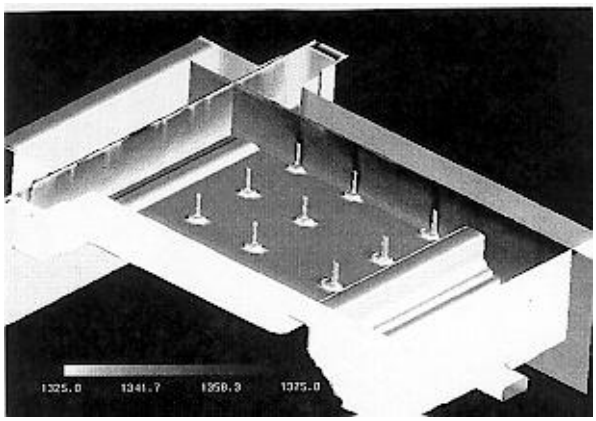

Fig. 2 Geometry and temperature distributions for the Glass Tank

3.2 End-port Air-fired Furnace

An end-port fired regenerative U-flame furnace is considered (see Fig. 3). Two burner ports are located below the air port (underport firing). Preheated air enters the combustion space at a downward angle with the normal to the furnace front wall of 20^o. The upward directed injection angle for fuel is 15^o. Both fuel and air are slightly directed towards the furnace midplane (2^o). The furnace is operated at an air factor of 1.075. In the regenerator air is preheated to 1300 ^{o}C. The total firing rate is 8.45 MW, equally distributed over the two burners. The sensible heat carried by the preheated air corresponds with 4.55 MW leading to a total heat input of 13.0 MW. The curved crown of the furnace is approximated by a number of steps. The thermal conductivity of the refractory material, determining the combustion chamber heat losses, is set to 3 W/mK. On the exterior surfaces of the furnace, a heat transfer coefficient of 15 W/m^{2}K to an ambient temperature of 30^oC is prescribed. Glass surface emissivity is assumed to be 0.75 and refractory emissivities have been set to 0.60. For the combustion space a highly non-linear mesh of 68x43x75 gridpoints is used amounting to a total number of 220.000. Gridpoints are concentrated near the fuel inlets. The number of radiation beams is 16.

The results of the coupled simulations show an average heat flux from combustion space towards the glass of 54 kW/m^2 leading to a total heat flow of 3.8 MW integrated over the glass surface. The maximum flame temperature in the large U-flame is 2360 ^{o}C. The radiative contribution to the surface heat flux is 3.7 MW or 97%, which means that heat transfer is totally radiation dominated. The thermal efficiency, defined as the ratio of heat flow towards the glass surface and the total firing rate, is 45%. The average gas composition in the outlet and in a large part of the furnace is:17 vol% H_2O, 8.5 vol% CO_2, 72.5 vol% N_2 and 2 vol% O_2. Superstructure wall heat losses are typically of the order of 3 to 5 kW/m^2 amounting to a total wall heat loss of l.l MW. The flue gases in the exhaust carry 7.2 MW with an average temperature of 1623 ^{o}C (this implies that regenerator efficiency is 63%). Due to the large size of the regenerator ports and its relatively low temperature, radiative heat losses through these ports are not negligible: 410 kW is lost through the air inlet and 140 kW through the flue gas outlet, in total 550 MW (4% of total heat input).

3.3 Cross-fired Oxy-fuel Furnace

A cross-fired oxy-fuel glass furnace is considered as an alternative for the above discussed end-port air-fired furnace. Operating conditions and geometry of the glass tank have been kept the

same as for the end-port air-fired furnace. The oxy-fuel furnace is an eight-burner non-staggered system (see Fig. 4). The oxy-burners are pipe-in-pipe burners. The oxidizer has a 99 vol% O_2 content and all burners are operated with 4.5% O_2-excess. Each burner has a firing rate of 900 kW (total firing rate 7.20 MW). The firing rate has been tuned to give the same heat input to the glass as for the U-flame furnace. Refractory material properties and ambient heat losses are the same as for the end-port furnace. For the combustion space a non-linear mesh of 80x53x49 (208.000) gridpoints is used. Gridpoints are concentrated near the burners. The number of radiation beams is 16.

The results of the coupled simulations show an average heat flux from combustion space towards the glass of 55 kW/m^2 leading to a total heat flow of 3.9 MW integrated over the glass surface. The maximum flame temperature in the oxy-flames is 2710 ^oC which is considerably higher than maximum flame temperature in the air-fired furnace. Due to oxygen combustion instead of air, the average gas composition in the oxy-fired furnace is very different: 60.5 vol% H_2O, 31 vol% CO_2, 6 vol% N_2 and 2.5 vol% O_2. Due to the much higher concentrations of H_2O and CO_2 the combustion products are more effective in radiating heat to the glass surface and therefore the thermal efficiency is much higher: 54%.

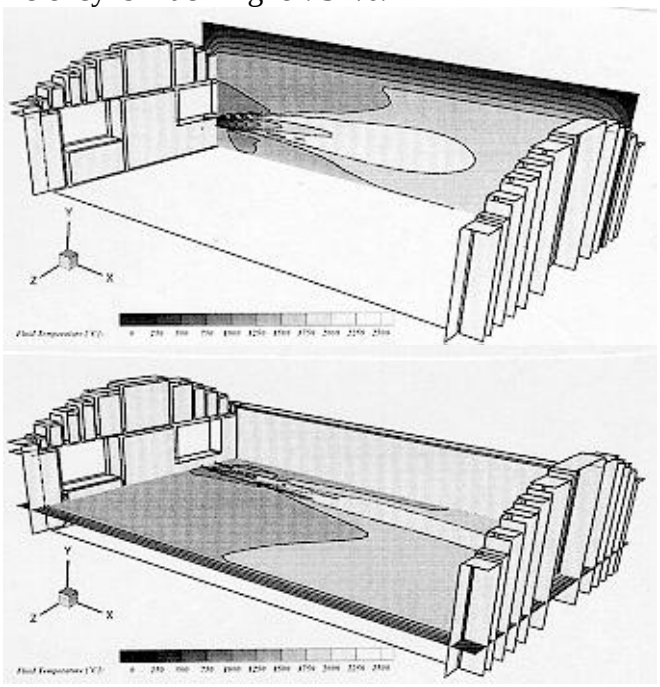

Fig. 3 Temperature distributions in End-port Air fired Furnace

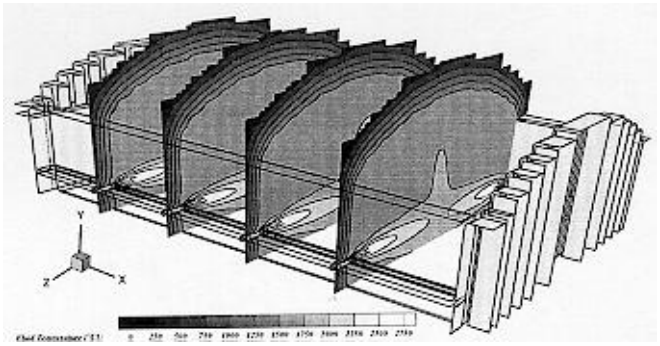

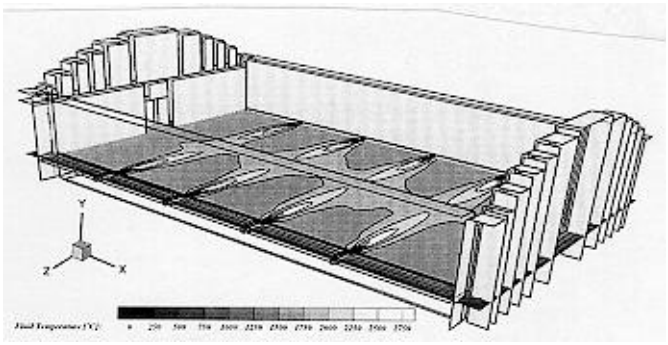

Fig. 4 Temperature distributions in Cross-fired Oxy-fuel Furnace

The radiative contribution to the total heat flux is 95%. Superstructure wall heat losses again are l.l MW. The flue gases in the exhaust carry 2.2 MW which obviously is much lower than those for the air-fired furnace. The average flue gas temperature is 1613 ^{o}C which is more or less the same for both cases.

4. CONCLUSIONS

The results presented in this paper and on the symposium show the capabilities of the TNO-TPD complete glass furnace simulation model. With this model it is possible to predict the effects of primary process variables as pull rate, firing rate, oxidizer preheat temperature and excess values, furnace and burner geometry on process performance parameters as thermal efficiency, residence time distribution and ultimately glass quality. It was shown that for the design of a new furnace, especially when switching from air-firing to oxy-firing, a simulation model for the complete furnace is a valuable and essential tool.

ACKNOWLEDGMENTS

We would like to thank Mr. Bauer from the Hüttentechnische Vereinigung der Deutschen Glasindustrie and Mr. Roger from Oberland Glas for preparing all the data. Further we thank the German' AIF Forschungsvorhaben' for funding parts of this study and we thank Oberland Glas to allow us to present some of the results.

REFERENCES

Beerkens R.G.C., T. van der Heijden, E. Muijsenberg, "*Possibilities of Glass Tank Modelling for the Prediction of the Quality of Melting Processes*", Ceram. Eng. Sci. Proc.14 [3-4], pp.139-160,1993.

Burke, S.P. and T.E.W. Schumann, "*Diffusion Flames*", Industrial Engineering Chemistry, Vol. 20, pp. 998-1004, 1928.

Gosman, A.D., W.M. Pun, A.K. Runchal, D.B. Spalding, M. Wolfshtein, *"Heat and Mass Transfer*" in Recirculating Flows, Academic Press, London and New York,1969.

Hottel and Egbert, "*Handbook of Heat Transfer*", ed. W.M. Rohsenow, J.P. Hartnett, McGraw-Hill Book Company, pp.15-76 to 15-78,1973.

Kee, R.J., F.M. Rupley, J.A. Miller, "*The Chemkin Thermodynamic Data Base*", Sandia National Laboratories Report SAND87-8215B, 1991.

Launder, B.E., D.B. Spalding, "*Mathematical Modelling of Turbulence*", Academic Press, London, 1972.

Lockwood, F.C., N.G. Shah, "*A New Radiation Solution for Incorporation in General Combustion Prediction Procedures*", l8th Int. Symp. on Combustion, Waterloo (Canada), Pittsburgh, PA: The Combustion Institute, pp.1405-1414,1981.

Patankar, S.V., "*Numerical Heat Transfer and Fluid Flow*", Hemisphere Publishing Corporation, Washington,1980.

Peeters, T.W.J., "*Numerical Modeling of Turbulent Natural-Gas Diffusion Flames*", Phd Thesis, Delft University of Technology, The Netherlands,1995.

Post, L., "*Modelling of Flow and Combustion in a Glass Melting Furnace* ", Phd Thesis, Delft University of Technology, The Netherlands, 1988.

ELECTRIC MELTING OF CRYSTAL GLASS

Stanislav Kasa
Institute of Chemical Technology, Czech Republic

Abstract

The contribution is divided into four parts. The first part contains the advantages of electric melting of crystal glass. The electric melting of glass is discussed from the point of view of ecology, energy, and material consumption and mainly from the quality of products. The types of electric furnaces used for melting of crystal glass is described in the second part of the contribution. The third part of the contribution contains the results of the modelling of all-electric melting furnaces. The physical modelling was used in order to find the optimum conditions for the operation of the furnaces. The investigated conditions cover up the influence of the shape and position of electrodes in melting end of the furnace on the surface current density, the temperature of glass in vicinity of electrodes, the distribution of power density and the position of thermal barrier in the furnaces. The final part of the contribution contains the evaluation of the measured variants on the physical models by means of six criteria important for the optimal operation of the furnaces.

I. INTRODUCTION

The usage of electric energy for melting of glass by Joule heat generated directly in a glass melt has a long tradition in the world. In the Czech Republic, electric melting of glass has been applied for more than 30 years. During that time significant experiences with both the electric melting furnaces design, and the technology of electric melting of glass have been obtained, as well as good knowledge of the questions of refractories and heating electrodes corrosion. We can say, thus, that there is sufficient knowledge to prepare the design of electric melting furnaces processing all types of industrial produced glass melts. Besides container glass, technical glass and jewelry glass, there are also crystal glass involved.

II. THE ADVANTAGES OF ELECTRIC MELTING OF CRYSTAL GLASS

It has been showed in practical application that for the most of glass melts, except for container glass, the all-electric melting furnaces with the pull below 50t/d are preferred to gas-fired ones [1]. There is also the special reason why to use electric melting furnaces instead of the gas-fired ones - it is the fact that there are places on the Earth with limited supplies of natural gas but with high supplies of electric energy (e.g. from water power stations).

Crystal glass melts are always melted in furnaces with the pull lower than 50t/d, which supports the application of electric melting instead of gas heating. Other reason why to use electric melting of crystal glass are connected with ecological, energetic, material and qualitative aspects.

Ecology

Electric melting contributes particularly to decreasing of the air pollution in smelting halls and near glass works. This effect is also connected with the cut of raw materials, first of all the expensive ones, e.g. boron oxide or lead oxide. Tables 1 and 2 show decreasing of the air pollution and the cut of raw materials if electric melting is used.

Table 1

Furnace	**NO_x**	**SO_2**	**Cl-**	**F-**	**Dust**
regenerative	1823	257	15,7	4,3	85,8
recuperative	799	140	10,1	25	35
all-electric	258	5	4,5	0,5	2

Table 2

Furnace	**PbO losses**
gas-fired pot	2,5
gas-fired continuous	2,0
gas-fired BM type	1,2
all-electric	0,1

The values are in kg of Pb0 per 100 kg of the glass melt.

Energy

During electric melting Joule heat is generated directly in the glass melt, and therefore the efficiency of electric heating is three times higher than that of gas heating [2]. In electric melting, the layer of a glass batch on the surface which has very good insulating ability contributes significantly to the cut of energy. Higher value of the rate between the volume and the surface of a melting tank represents the next aspect which determines energetic profitableness of electric melting. Figure 1 demonstrates the data given above. The utility of electric melting is shown also in Figure 2 which demonstrates the dependence of a specific energy consumption on a pull for various types of furnaces and glass melts.

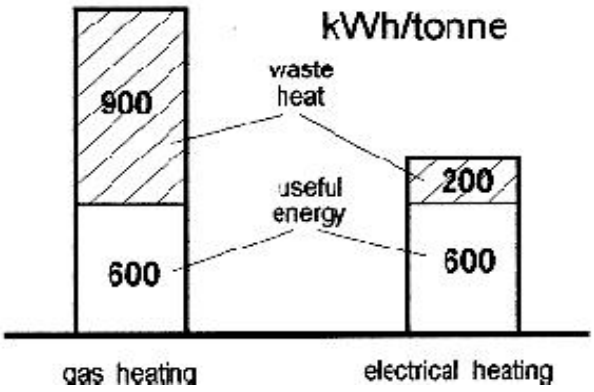

Fig.1 Energy requirements for gas and electric furnace

Material

From the point of view of materials, the consumption of refractories and heating electrodes is considered. The consumption of AZS refractories is always lower in electric furnaces when compared with gas ones, also due to higher specific pulls and the simple design of electric furnaces. It was proved in practical application that it is of advantage (from the AZS refractories consumption aspect) to use electric heating for furnaces with the pull lower than 30t/d. The utility of electric heating is accented also by increasing durability of melting furnaces which reaches more than 5 years. It is caused by the application of AZS refractories of a high quality, as can be seen from the corrosion indexes for various glass melts and AZS refractories given in Table 3.

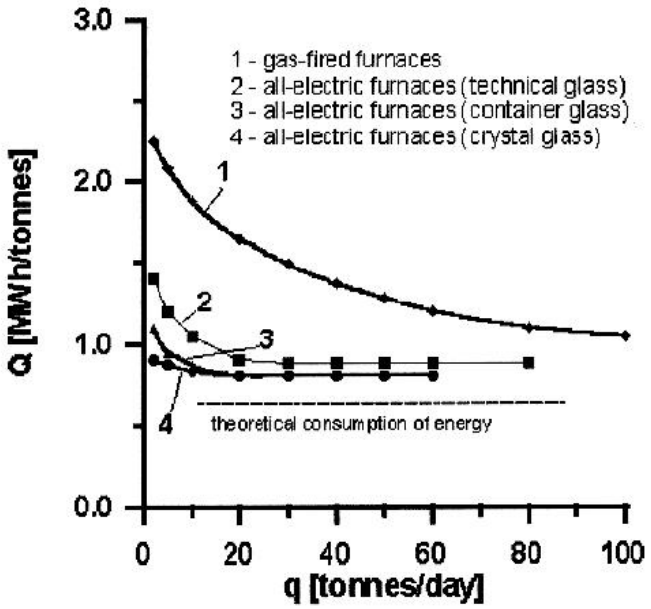

Fig. 2 Energy requirements for various glasses, compared to gas-fired furnaces

Table 3 Corrosion indexes of AZS refractories

Refractory	container	fiber glass	technical glass	lead crystal glass
E R 1681	100	100	100	100
ER 1711	130	130	130	130
ER 2161	340	380	-	-
ER 1195	150	-	520	170

When melting leaf crystal glass, either molybdenum electrodes, or tin oxide electrodes are used for heating. As tin oxide electrodes significantly restrict the durability of melting furnaces, the producers of lead crystal glass prefer molybdenum electrodes which, however, must be protected from a corrosion. One of the methods protecting molybdenum electrodes during melting of lead crystal glass is the low-frequency current melting. On the basis of ten-year practical experiences [3], [4], we can take this method for managed. 4,5 times lower consumption of molybdenum electrodes and more than 3 times lower content of molybdenum dissolved in the glass melt is reached.

The glass quality

According to the competition on the world markets, the lead crystal glass products must show the high quality. To provide this quality constantly, it is necessary:

· to use electric melting furnaces of an appropriate design
· to use the AZS refractories of the highest quality for the melting furnace construction
· to protect molybdenum electrodes from a corrosion by means of low-frequency current melting
· to provide efficient technological measures during the melting furnace run
· to control all technological nodes by means of computer

III. ELECTRIC FURNACES FOR MELTING OF CRYSTAL GLASS

Modem (from the point of view of their design) electric melting furnaces work on the CTVM (Cold Top Vertical Melting) principle, i.e. vertical melting with a cold surface. They are always double-space furnaces in which the glass melt from the melting tank pass through a cranked throat followed directly with the feeder channel. The size of the melting tank is derived from the furnace pull. The melting tank is, from the technological point of view, divided into two parts, a melting zone in which melting, refining and chemical homogenization are carried out, and a conditioning zone in which thermal and chemical homogenization of glass melt is provided. Only a thermal barrier separates these two zones.

These are the parameters in which electric furnaces for melting of crystal glass differ:

· the shape of a melting tank - the most frequent ones are melting tanks with the shape of a square, rectangular or hexagon · the position of electrodes - furnaces with horizontal electrodes prevail, furnaces with top-electrodes are starting to appear nowadays
· the shape of the melting tank bottom - when melting lead crystal glass, the shape of the bottom must be adapted to be able to drain liberated lead from the melting tank

The second group of electric furnaces for melting of crystal glass is represented by the furnaces with tin oxide electrodes whose design and refractories are nearly identical to

those of furnaces with molybdenum electrodes. The only difference is in the way of bedding the electrodes - tin oxide electrodes are usually put on two opposite shelves.

IV. MODELING OF ELECTRIC FURNACES

Designing of new melting furnaces or the reconstruction of older ones are based on modeling. Three methods of modeling given below are used in our institute:

· the method of physical modeling
· the method of modeling on electroconducting sheets
· the method of mathematical modeling

The task of modeling:

a) the design optimization of a melting furnace

It includes the optimization of the shapes of melting tanks, throats and feeder channels. The optimum shapes and parameters of these parts of melting furnaces are investigated in the relation to technological conditions in a furnace which are represented by:

· the distribution and magnitude of temperatures and flows in examined parts of a furnace
· the position of a thermal barrier
· the volume of melting and conditioning zones
· the pull of a furnace
· the kind of melted glass

b) the electrode optimization

The task of electrode optimization is to find an optimum position, connection and shape of electrodes in a relation to the technological conditions in a furnace given above, and to the corrosion of electrodes. The extent of the corrosion can be concluded from:

· the magnitude of surface current density on electrodes
· the distribution of surface current density along individual electrodes
· the temperatures of electrodes, or the distribution of the temperature along individual electrodes

To be able to realize the design and electrode optimization, it was necessary to define the optimization conditions as a optimum criteria which could be enumerated. In such a way, a lot of optimum criteria have been defined. Given below there are the criteria most often used for the optimization of electric furnaces for melting of crystal glass:

1. The electric input magnitude criterion

$$P_i = U_i \,.\, I_i \,.\, \cos\Delta\varphi_i \qquad \text{[V.A]}$$

2. The electrode current load criterion

$$i = \frac{1}{n} \cdot \sum_{1}^{n} \frac{I_j}{A} \qquad \text{[A/cm}^2\text{]}$$

3. The electrode load uniformity criterion

$$N = \frac{n \cdot |\Delta I_{max}|}{\sum_{n}^{n} I_i} \cdot 100 \qquad [\%]$$

4. The electrode positioning criterion

$$PE = \frac{V_{xp}}{V_{xp}} \qquad [1]$$

5. The ohmic resistances criterion

$$R_i = \frac{U_i \cdot \cos\Delta\varphi_i}{I_i} \qquad [W]$$

6. The distribution of the temperature along the electrode criterion

$$KT = \frac{1}{n} \cdot \sum_{i}^{n} \frac{\Delta T_i}{l} \qquad [\,^{o}C/m\,]$$

V. THE EVALUATION OF VARIANTS MEASURED ON A PHYSICAL MODEL

The optimum position of horizontal molybdenum electrodes has been examined on the physical model of all-electric melting furnace for melting of lead crystal glass. The position of electrodes was defined by the mutual distance between electrodes (X1 - X5) and by the distance of electrodes from the bottom of a furnace (H1 - H3) - see Tables 4 and 5 and Figure 3.

Table 4 The position of electrodes in the tank of a furnace
(The distance from the bottom)

Variant	H1[mm]	H2[mm]	H3[mm]
1	840	684	372
2	720	564	312
3	600	564	312

Table 5 The position of electrodes in the tank of a furnace
(The distance between electrodes)

Variant	X1[mm]	X2[mm]	X3[mm]	X4[mm]	X5[mm]
1	984	192	1200	204	1044
2	984	204	1260	192	984
3	984	204	1236	210	984

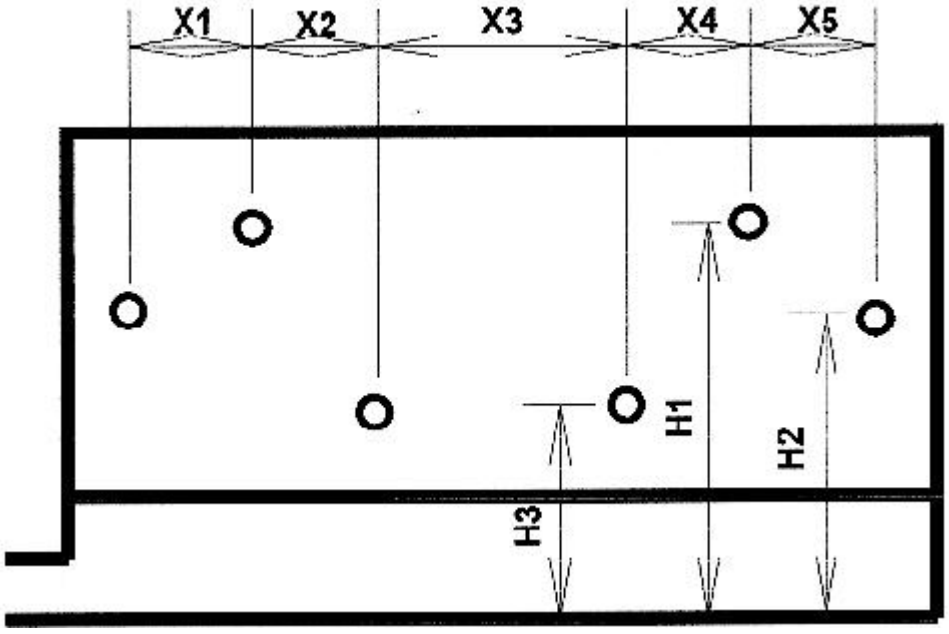

Fig. 3 The position of electrodes in the tank wall

The enumerated optimum criteria are presented in Table 6.

Table 6 The values of optimum criteria

Variant	P_i [kVA]	I [A.cm^{-2}]	N[%]	PE	R_i [W]	KT_i[^{o}C.m^{-1}]
1	504	0.66	7.2	1.36	0.024	18.3
2	525	0.72	10.6	1.72	0.021	35.0
3	507	0.68	7.0	2.87	0.023	22.6

After the evaluation of optimum criteria the following sequence of variants was obtained and the variant to be used in real furnaces run was found:

1. Variant 1 2. Variant 3 3. Variant 2

VI. CONCLUSION

The significance of all-electric melting of crystal glass from ecological, energetic, material and also qualitative aspects has resulted from the data given in this study. The modeling methods which enable us to find design and technological data for the melting furnaces construction are applied on a significant scale for designing of electric furnaces and their optimization.

References

1. Reynolds M.C.: The electric melting of glass, Proceedings of the 1st conference of the ESG, Sheffield 1991, p.211
2. Stanek J.: Electric melting of glass, Elsevier-Amsterdam, Oxford, New York,1977
3. Matej J.: Sklàr a keramik, 44, 4 (1994), in Czech
4. Novotny J.et al.:Sklàr a keramik, 44 ,17 (1994), in Czech

EVALUATION OF COMBUSTION CHAMBER IN FURNACES BY NUMERICAL SIMULATION

Hiroshi Takamuku and **Yoshiichi Ozeki**
Asahi Glass Co. Ltd. Research Center, Japan
Eiichi Kudo
Asahi Glass Co. Ltd. Head Office, Japan
Tsutae Miyamoto
Asahi Glass Co. Ltd. Takasago Factory, Japan

Abstract

A coupled model that consists of a three-dimensional (3D) combustion model, a heat transfer model including thermal radiation exchange in a combustion chamber and a two-dimensional (2D) molten glass flow model, has been developed. A numerical simulation is performed, and the calculated results are in close agreement with the measured results in a test furnace. Moreover, evaluation of oxy-oil conversion in an actual ceramic furnace will be reported.

1. INTRODUCTION

In recent years, full or partial oxy-fuel conversion has been widely adopted in many segments of glass manufacturing to save energy, to increase production, to reduce environmental emissions, and decreasing maintenance. Since oxy-fuel firing has different physical phenomena from air-fuel firing, the prediction of furnace performance is required. A mathematical model is useful for studying the physical phenomena in a glass furnace.This provides information about furnace performance, new furnace design, furnace construction, furnace operation, and control.

This paper presents a coupled model that includes a three-dimensional (3D) combustion model, a heat transfer model including radiation exchange in a combustion chamber, and a two-dimensional (2D) molten glass flow model [1]. Comparison will be made with measurements from a test furnace. The paper also discusses the application of actual oxy-fuel conversion in a ceramic furnace.

2. MODELING

2.1 Flow and Combustion Model

First we modeled the following items in a combustion chamber by using a commercially available code, STAR-CD ver.2.30 [2]. Here, 3-D steady-state conservation and chemical transport equations are solved. Two equation (k-ε) turbulence model, which gives us reliable prediction results on the whole, is considered in the temperature and flow field in a combustion chamber. The combustion model is based on the ideal of a

single step and the Eddy Breakup Concept. In this model the following six species are considered: fuel, O_2, N_2, H_2O, CO_2, and Soot. The absorption coefficient distribution, which is necessary for thermal radiation exchange in a combustion chamber, is obtained by the radiative species.

2.2 Heat Transfer Model with thermal radiation exchange

It takes much calculation time to analyze the combustion chamber by a fully coupled model of combustion and molten glass flow, which is not for practical use. In this paper we adopt a coupled model of heat transfer including thermal radiation exchange in the combustion chamber and the molten glass flow, which accelerates computation. To evaluate heat transfer in the combustion chamber, the conditions of fixed velocity, absorption coefficient, and heat generation distribution obtained by the flow and combustion model are assumed. Hottel's Zonal method [3] is adopted to evaluate thermal radiation exchange between gas to gas, gas to surface, and surface to surface in the enclosure. The absorption coefficient distribution as total emittive data is obtained by mixed-gray-gas formulation [4]. Multiple diffuse reflection is assumed at the surface. The heat energy equations are formulated in Table 1. Direct exchange areas are computed by numerical integrations, without recourse to tabulated values with fine mesh [5] in the complicated furnaces.

Table 1. Basic equation of heat transfer model

energy balance equation for i-th surface

$$h(T_{Gi} - T_i) + J_i - G_i + K'(T_{ref} - T_i) = 0$$

$$G_i = E_i + (1 - \varepsilon_i) J_i$$

$$A_i J_i = \sum_j \overline{s_j s_i} G_j + \sum_j \overline{g_j s_i} E_{Gj}$$

energy balance equation for i-th volume

$$\sum_j h(T_j - T_{Gi}) A_j + \sum_j \overline{s_j g_i} G_j + \sum_j \overline{g_j g_i} E_{Gj} + Q_i - 4K_i V_i E_{Gi} = 0$$

$$E_i = \sigma \varepsilon_i T_i^4, \quad E_{Gi} = \sigma T_{Gi}^4$$

(Nomenclature)

G_i: radiosity, J_i: irradiation of boundary element, ε_i: emissivity, T_i: surface temperature, A_i: area, h: heat transfer coefficient between gas and surface, K': overall heat transfer coefficient without contribution from inner total heat transfer, T_{ref}: reference temperature , T_{Gi} : gas temperature, s: Stefan- Boltzmann constant, Q_i: heat source or sink, $\overline{ss}$: direct interchange area for surface-surface, $\overline{sg}$: direct interchange area for surface-gas, $\overline{gg}$: direct interchange area for gas-gas.

2.3 Molten Glass Flow Model

For the numerical calculation of molten glass flow and temperature fields, the noncommercial code "GSMAC3D" in laminar flow with a high Prandtle number is applied. Details can be found, for instance, in [1].

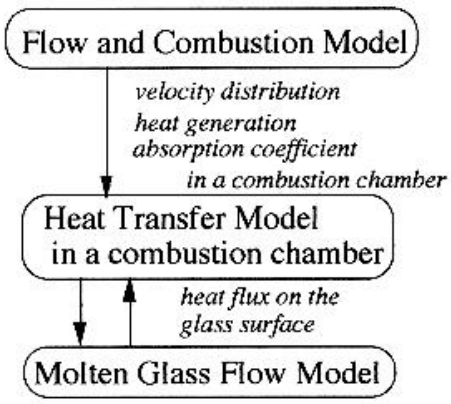

Fig. 1. Linkage among the flow and combustion model,the heat transfer model, and the molten glass flow model.

2.4 Coupled Model

This coupled model consists of three models: a flow and combustion model, a heat transfer model including thermal radiation exchange, and a molten glass flow model [1]. Linkage among these three models is shown in Fig. 1. First, calculation of the flow and combustion model is performed under a given glass surface temperature distribution. Then we can get (a) the velocity distribution, (b) the absorption coefficient distribution obtained by the concentration of each species, and (c) the heat generation distribution resulting from chemical reaction. Second, calculation of the heat transfer model including thermal radiation exchange is performed based on previous results. The heat flux distribution on the top surface of the molten glass flow, which is calculated in the molten glass flow model, is also incorporated as a boundary condition. Third, calculation of the molten glass flow model is performed. The heat flux distribution on the top surface of the molten glass flow, which is calculated in the heat transfer model, is also used as a boundary condition. The above procedures are iterated until the error in the temperature distribution becomes less than the predetermined value (Fig.1).

3. APPLICATION TO ACTUAL FURNACES AND DISCUSSION

3.1 Test Furnace

To verify the validity of this model, experiments were conducted in an enclosed test furnace. The measured results were compared with calculated results. An outline of the test furnace is shown in Fig. 2. The temperature of the refractory is measured by setting five thermocouples in a roof refractory. The water cooling box is located at the bottom of the furnace along its length, which is separated into five zones. The water-flow rate, and the inlet and outlet temperatures are monitored in each zone to evaluate the heat flux from the combustion chamber.

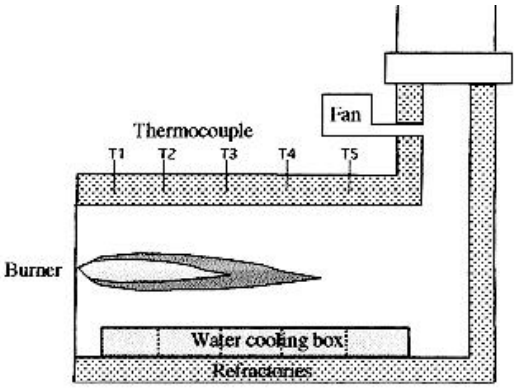

Fig. 2. Sketch of a test furnace on the vertical plane along the centerline of the furnace.

Three cases (Oxy-LNG, Oxy-Oil Firing), which are briefly characterized in Fig. 6, were chosen for the simulation. The comparison between the experimental and calculated roof temperatures in every experimental case are shown in Fig. 3 and 4. The comparison between experimental and calculated heat loss by the water-cooling box is also shown in Fig. 5. The heat balance is shown in Fig. 6. In this Figure, an arrow indicates the direction of heat transfer and the number indicates the magnitude of the heat energy, which is normalized by the total input energy and is expressed by percentage. The maximum temperatures of the refractory in Cases 1 and 2 are measured at the position of T2 and T5, respectively, which is caused by the flame length difference attributable to the input energy difference. The tendency for heat loss via the cooling-water box is also seen as well as the maximum refractory temperature. The heat loss of the water-cooling box No.4 and 5 covered with refractory is much less than any others. The heat loss via cooling water is uniform in Case 3 because of the different cooling box, which is not covered with refractory. In this test furnace, about 70%-80% of the total input energy is lost to the water-cooling box. Close agreement is obtained between the measured and calculated results. The longitudinal trend for the temperature of the refractory and the heat loss attributable to the water cooling box can also predicted. It appears, however, that the calculated roof temperature tends to be underestimated. The calculated temperature gradient in the longitudinal direction is slightly smaller than in the experiments. We think room for improvement still remains. Further investigation will follow.

	Fuel Type	**Fuel Input**	**(a)**	**(b)**	**(c)**	**(d)**
case 1	LNG	37.1 (Nm^3/h)	100	80.6	8.5	19.9
case 2	LNG	77.6 (Nm^3/h)	100	68.6	4.6	26.9
case 3	HFO	260 (L/h)	100	71.4	3.7	24.8

(a) Total Input energy
(b) Heat loss via Water Cooling Box
(c) Heat loss via Refractories
(d) Heat loss via Exhaust gases

Fig. 6. Heat balance in the test furnace. A number indicates the magnitude of the heat energy, which is normalised, and is expressed by percentage.

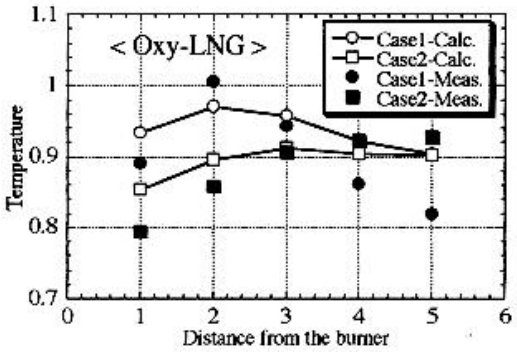

Fig. 3. Longitudinal roof temperature distribution of the test furnace (Case 1, Case2) in Oxy-LNG combustion. The temperature and longitudinal distance are normalized.

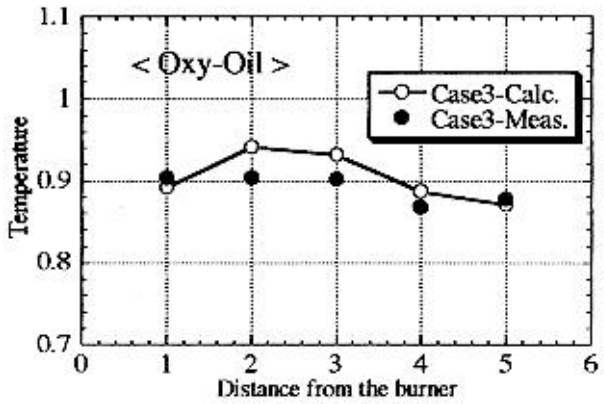

Fig. 4. Longitudinal roof temperature distribution of the test furnace (Case3) in Oxy-Oil combustion. The temperature and longitudinal distance are normalized.

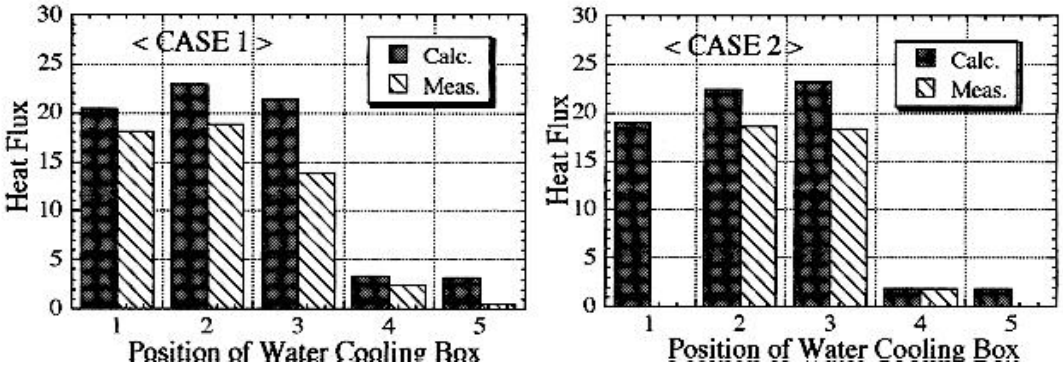

Fig. 5. Heat loss via Cooling Water Box(Casel, Case 2). No.4, No.5 Box are covered with refractories. The magnitude of heat loss is normalized.

3.2 Ceramic Furnace

A sketch of a ceramic furnace is shown in Fig. 7, which is an air-oil fired ceramic-frit furnace. The process is essentially continuous with batch material loaded through the charge door. The burners are directed at the charge material that is set at the opposite end of the furnace. The furnace's combustion gases are forced to induct through the incoming charge enable maximum heat transfer. Exhaust gases are ducted through a recuperator by using an induced draft fan. The furnace is operated to maintain positive pressure.To evaluate oxy-oil conversion testing, the presented model was applied to the ceramic furnace. The calculated roof temperature distribution is compared with the measurements in Fig. 8.

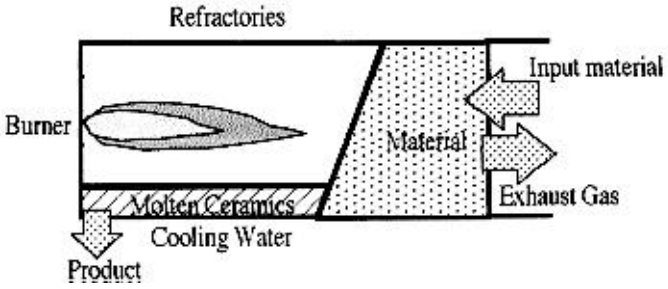

Fig. 7. Sketch of a ceramics furnace on the vertical plane along the centerline of the furnace.

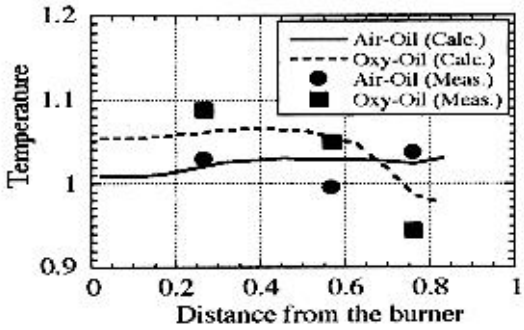

Fig. 8. Longitudinal crown temperature distribution of the ceramics furnace. The temperature and longitudinal distance are normalized.

The roof temperature was measured by thermocouple. The measured results are modified to inside-surface temperature by assuming one-dimensional thermal conduction. In the Figure the temperature is normalized by maximum temperature in the furnace. The calculated results are in good agreement with the measurement. These results indicate that (a) the flame length of oxy-oil firing is slightly shorter than in air-oil firing, and (b) the crown temperature (distance from burner: 0 to 0.4) in oxy-oil firing is about 10 % higher than in air-oil firing (Fig. 8). The heat balance is shown in Fig. 9. In this Figure, an arrow indicates the direction of heat transfer and number indicates the magnitude of the heat energy. The magnitude is normalized by the combustion heat of air-oil firing and is expressed by percentage. In oxy-oil firing, the amount of oil is about 75% of that used in air-oil firing. It is assumed that the pull rate and heat required to melt material are equal

for the air-oil and oxy-oil cases in this simulation. The sensible energy from the exhaust gases is largely reduced in oxy-fuel firing by a considerable reduction in the volume of fuel gases. This is the result of the practical elimination of nitrogen in the combustion process. Sufficient heat for the pile and molten ceramics exists in oxy-oil firing with convective and radiant heat transfer in comparison with air-oil firing. This result has made it clear that ceramic-furnace conversion to oxy-oil firing is possible. Based on the simulation, the oxy-oil firing trials were conducted in an actual ceramic furnace in February 1996, confirming that the usual pull rate can be continuously obtained.

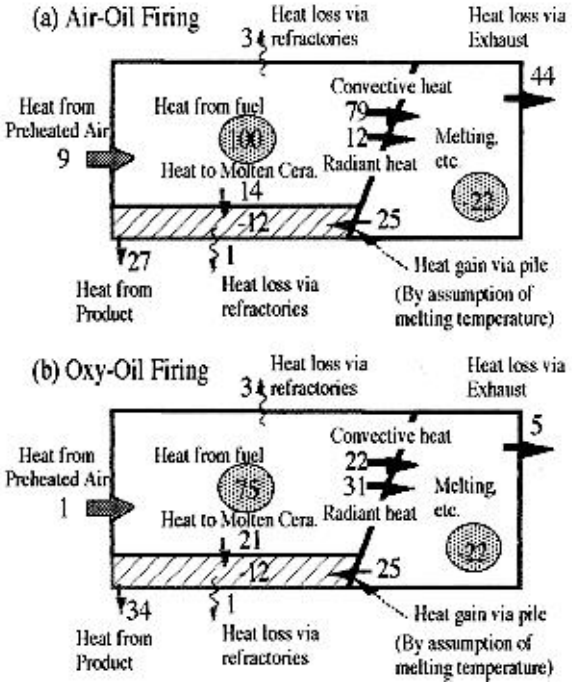

Fig. 9. Heat transfer in the ceramics furnace. An arrow indicates the direction of heat transfer. A number indicates the magnitude of the heat energy. The magnitude of the heat energy is normalized by heat generation of Air-Oil Firing case, and is expressed in percentage.

4. CONCLUSIONS

A coupled model that consists of a 3D combustion model, a heat transfer model including thermal radiation exchange, and a 2D molten glass flow model, has been developed for practical use. A numerical simulation was performed with calculated results that are in good agreement with the test-furnace measurement. Moreover, evaluation of oxy-oil conversion in an actual ceramic furnace is reported. We think that the of ceramic-furnace conversion to oxy-oil firing is possible. This coupled model can be utilized to study the mechanism in the furnace, and moreover to optimize operating conditions and to design furnaces.

ACKNOWLEDGMENTS

The authors gratefully thank to B.O.C and O.S.K group assisted with experimental data for this study.

REFERENCES

[1] H. Mase et al, THE GLASS, No.38,1995, WINTER, p24-31.
[2] STAR-CD ver.2.30 MANUALS, Computational Dynamics Limited.
[3] P. B. Taylor and P. J. Foster, J. Heat Mass Transfer, Vol.l7,1974, p1591-1605.
[4] Y.Ozeki, International Symposium of Room Air Convection and Ventilation Effectiveness, Proceedings of ISRACVE., ASHRAE,1993, p479-489.
[5] Hottel, H. C. and Sarofim, A. F., Radiative Transfer, Mc Graw-Hill, New York,1967.

INVESTIGATION INTO OXY-FUEL GLASS FURNACE BY MEANS OF COMPREHENSIVE MATHEMATICAL MODEL*

M.G.Carvalho, M.Nogueira and **Wang Jian**
Technical University of Lisbon, Portugal

Abstract

A comprehensive mathematical model for the prediction of the performance of a glass furnace has been developed by IST research group. The model is based on the solution of conservation for mass, momentum, energy and combustion related chemical species, and comprises three main coupled sub-models: the combustion chamber, the batch melting, and the glass tank.

The simulation of the whole glass furnace was performed through an integrated method. The three main sub-models were coupled by a cyclical iterative way, matched by the relation between the heat flux from the flame to the molten glass and the top surface of the batch blanket, and the heat flux from molten glass to the bottom surface of the batch blanket. The whole procedure is calculated until "convergence" of the coupled process is achieved. Interface temperatures between the flame and the batch, the flame and the molten glass, the molten glass and the batch were calculated by a cyclical iterative way.

The above referred comprehensive model was applied to an oxy-fuel glass furnace. The simulation results are comprised by the temperature field, the flow field of the glass tank and the combustion chamber, the chemical species concentration distribution, the radiative fluxes, the batch blanket area floating on the surface of the molten glass, and the batch melting process. Numerical results show that the glass furnace with oxy-fuel has higher thermal efficiency, yielding an energy save and a decrease in air pollution. Very useful information about whole oxy-fuel glass furnace may be supplied by the model. Analysis of the furnace performance is therefore possible. The presented comprehensive model constitutes a very powerful tool for understanding the thermal physical phenomena occurring in a oxy-fuel glass furnace, improving glass furnace design furnace control, and furnace operation.

---

* Full manuscript not available at the time of printing

SIMULATION OF LARGE FURNACES USING MATHEMATICAL MODEL

Petr Schill, J. Chmelař, A.Fran•k
Glass Service, Ltd., Czech Republic

Abstract

Original mathematical model is being successfully used for three-dimensional simulation of industrial glass-furnaces since 1991. This mathematical model-package (well-known as Glass Model and as Combustion model) was developed in company Glass Service as a special CFD program accommodated for application in glass industry. The presented mathematical model has reached the state of technological evaluation of important features of melting process. The results of mathematical simulation enable for characterization of the melting aggregate as a complex system.

Some experiences of simulations of large industrial glass furnaces with respect of technological function of melting process are presented. The character of flow- and temperature-pattern and of batch melting influenced by heat conditions in glass level and in combustion space are shown using three-dimensional graphic.

I. INTRODUCTION

The stage of mathematical simulation of glass furnaces has made a big step in the last five years. The need of mathematical models covers practically whole glass technology. The glass quality represents one of the main tasks which may be solved by means of mathematical modeling. Such a computer simulation opens a new view into melting process. The simulation results, glass-flow and temperature-distribution within glass and walls, show some trends which enable to predict the furnace behaviour by various conditions and by changing furnace design. The location of possible corrosion or the refining capability or function of throat dimensions may serve as examples.

The main controlling phenomena for furnace design and glass quality can be summarized as follows:

I. Sand dissolution

The process of sand dissolution is bounded with flow- and temperature distribution of glass. These distributions (called physical fields) represent direct results of furnace simulation.

II. Removal of bubbles

The refining process again depends on glass flow and on glass temperature. The time needed for bubble removal from glass not only rapidly rises with decreasing temperature but it is also influenced by glass circulations.

III. Generation of the defects due to high temperature

A high temperature increases the time needed for melting but it also increases the danger of material corrosion and consequently the generation of defects. These phenomena can be predicted by study of flow-and temperature-profiles within glass furnace. The furnace geometry is very important.

IV. Generation of the defects due to booster, bubbler, homogenisation and glass conditioning.

This situation is similar to that described in points II. and III. but it is more complicated. The analysis of all simulated fields (flow, temperature, electrical potential and Joule heat generation) has to be made.

The company Glass Service Ltd. has developed two original codes called *Glass Model* and *Combustion model.* This computer flow -, temperature- and combustion-simulation software has been created for special use in glass industry. This program package represents a complex software system including solvers, preprocessors and postprocessors. A set of special postprocessors is available for 2D and 3D displaying the physical-fields and for tracing sand- and bubbles-behaviour in glass melt. During the last three years about 100 industrial furnaces had been simulated by this software. Practically all kinds of glass furnaces (melters, regenerative and recuperative furnaces, all-electrical furnaces, electrical pot-furnaces and big float tanks) had been modeled up to this time. The influence of throats, distributors, barriers, forced bubbling, booster and of burners distribution had been analyzed by model case-studies.

Glass Model and Combustion Model are based on numerical solution of transport equations in three dimensions and they enable to simulate flow-, temperature- and electrical-fields within a glass furnace. Moreover, the Combustion Model enables to simulate turbulence, combustion chemistry and radiation within combustion space of glass furnace. A11 glass- and gas- thermophysical properties are represented by temperature functions. The thermal- and electrical-conductivity of building materials (refractory, insulations) are also specified as temperature functions. All property functions may be modified by user. Both models involve full scale that means the realistic furnace design is taken into account, including wall composition. The full set of actual boundary conditions (pull and thermal situation on glass level and on outer surfaces of all walls) is specified by user. The time needed for complete simulation depends on furnace dimension, on complexity of furnace geometry and on type of computer (Pentium-or workstation-base) which is being used. That is why the requested calculation-time lays between one half and seven days.

Examples of case studies of various types of furnaces are presented on slides. The high-standard 3D graphic is being used which had been created on SGI computer Indigo2.

A part of one of the case studies made in Glass Service is present in the next section of this paper. All pictures, numbers and furnace geometry were modified due to confirmation.

II. FLOAT TANK BEHAVIOUR

Several case studies of float tanks had been provided in Glass Service in the last two years. There are several types of float-furnaces working in glass industry.
These types are defined by following main features: .

* total dimensions and pull
* heating system
* length of melting part, of refiner and of working part
* batch charging system
* using the bubbling system
* presence of various types of skimming pockets
* waist type: geometrical shape and dimensions
* various assembly of mechanical stirrers located in waist
* type, number and design of barriers (coolers) located in waist
* step- or flat-bottom
* insulation and cooling of side-walls
* way of bottom insulation

The general flow pattern is schematically drawn on Fig.1. In common sense there are two main circulation flows in melting part (including refiner) and one circulation in working end. The position and intensity of these circulation-flows define the behaviour of whole furnace and consequently the quality of glass.

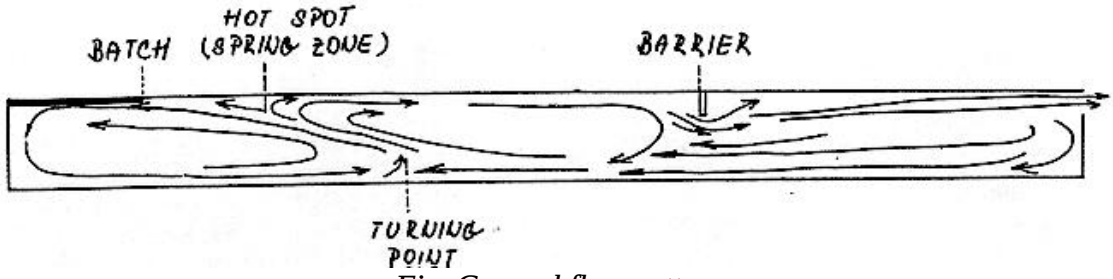

Fig. General flow pattern

The batch is melted in melting part where first circulation occurs which supports dissolving remaining sand particles in glass-melt. Between hot spring and waist there is area of second circulation which is responsible for refining. Location of this circulation is determined by position of hot spring (which depends on position of temperature maximum) and by position of turning point near bottom. The position of turning point is of great importance and it depends on several factors : temperature maximum on glass level (position and intensity), total pull, position and immersion of barrier, intensity of barrier cooling, shape of bottom (flat or step-wise). In case of step bottom the depth difference between melting part and working end is important. The turning point is a meeting point of forward and backward flows near bottom. The forward flow coming from melting area is stopped by backward flow coming from working end. Remaining sand particles, non-refined bubbles and possible defects from melting- or working-end are

brought up into hot spring. The glass temperature in hot spring is high and the conditions for dissolving are much more better then they are near bottom.

The disadvantage of such a system is very high energy consumption because the glass which had been cooled down in working end must be heated up again. But, the benefit is very good quality of sheet glass.

III. FLOAT TANK CASE-STUDY

The presented case study was realized by Glass Model which was run on Pentium 133 MHz computer. All pictures were created on SGI workstation Indigo2 by original graphical postprocessor based on Iris Explorer. The study deals with two phenomena:

A. immersion of cooled barrier in waist
B. variation of glass depth due to special design of step-bottom

The simulated float furnace is 60 m long and 11 m wide. Batch is charged into a doghouse located at back wall. There are no skimming pockets. In the waist there are stirrers and one cooled barrier. The pull varies between 530 and 610 t/day. The temperature maximum on glass level is around 1600 ^{o}C.

The general view of whole furnace is displayed on Fig.2. Temperature field on glass surface and on vertical central cut are displayed in left part of the tank. The process of batch melting is well visible due to variation of temperature (changing colours from dark to light ones). Temperature profile of "V"-shape is visible on the vertical cut. Glass flow in horizontal cut close to surface is displayed in the right part of the tank. The intensity of flow corresponds to the length of arrows and their colour (grey intensity) denotes temperature. Because of huge tank-dimensions zoomed displaying is necessary to detail analyzes.

Two partial parts (A and B) of case study are presented here as an example of using mathematical simulation:

Part A - change of barrier immersion

A step-bottom, slanting type of barrier and constant pull were used. Two cases of different immersion of barrier were simulated:

Case A1: normal slanting barrier
Case A2: deep slanting barrier : the immersion is 6.5 cm deeper than in case A1

Melting part, refiner ,waist and part of working end of the case A2 are displayed on partially zoomed Fig.3. Five longitudinal vertical cuts are displayed in various positions: four cuts of velocity fields and one cut of temperature field. The positions of hot spring and of bottom turning point are well visible on this graph. Estimation of the exact position of turning point was made in a similar way as it is done in the next part B.

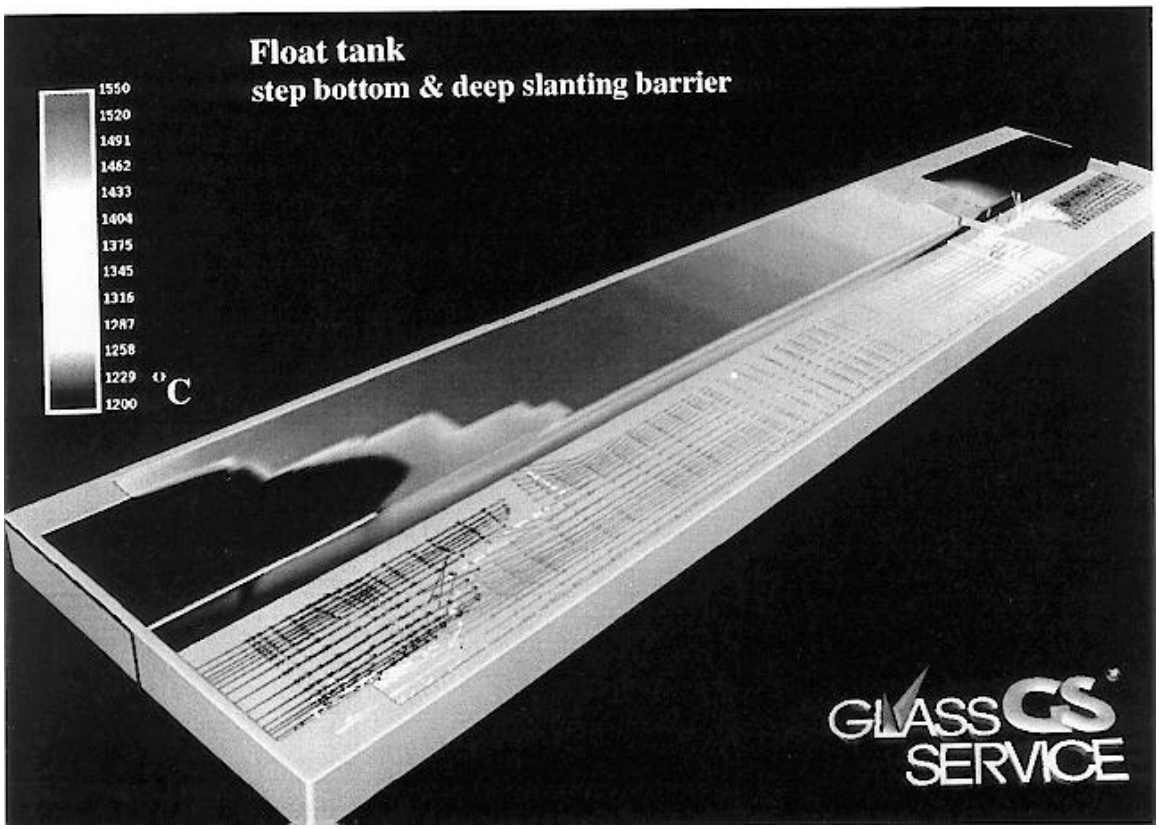

Fig.2 Float Tank : General view

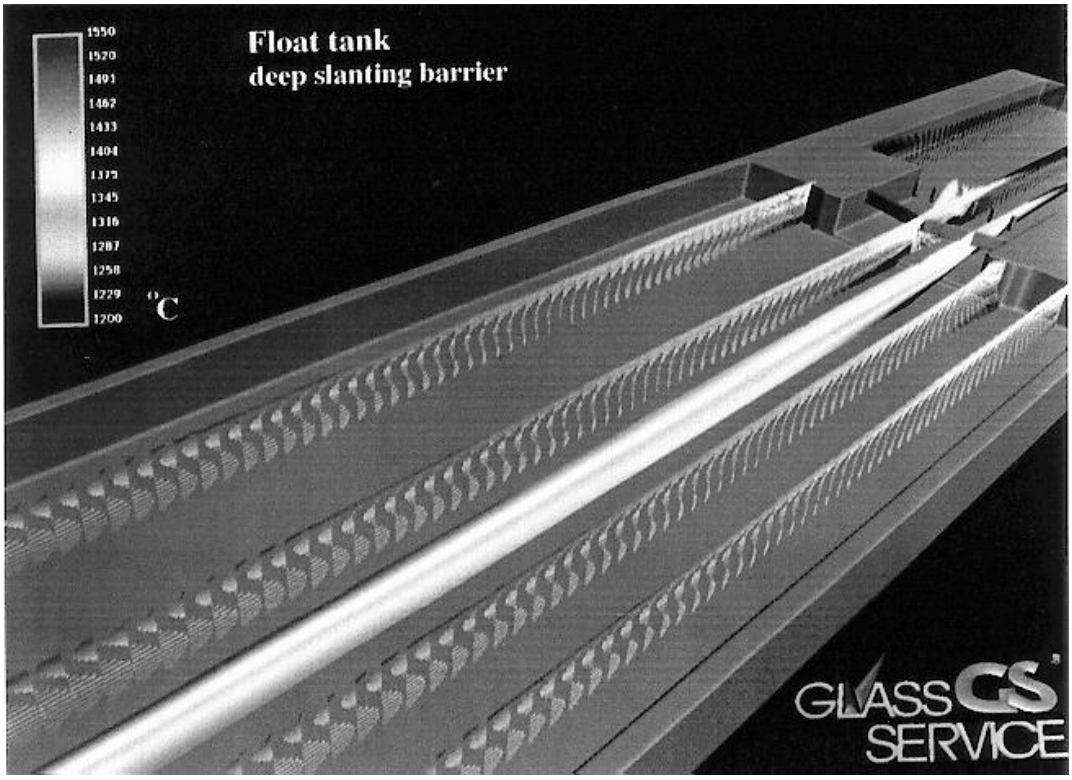

Fig. 3. Float Tank: deep slanting barrier, longitudinal cuts

After simulation analysis had been provided it was estimated that the position of turning point was shifted by 370 mm closer to waist in case A2. It means the forward flow is stronger in case of deeper barrier but it is still within reasonable range. The second circulation flow is more intensive and the refining ability is becoming more stable. In complete study of this phenomena it is necessary to make more case-calculations including critical stages. The result is a criterion function of value of immersion versus stability of main circulation. This function is being used by changing furnace design and by technological control.

PartB - change of bottom steps

A straight type of barrier (perpendicular to the waist side-walls) and constant pull (same as in part A) were used. Three cases were simulated having different glass depths in working end. The resulting flows in two longitudinal vertical cuts are displayed on three zoomed-graphs:

Case B1: Fig.4., flat bottom: normal stage, straight flat bottom through whole tank
Case B2: Fig.5., low step bottom : glass depth in working end is lower of 8 according to the case B 1
Case B3: Fig.6., high step bottom: glass depth in working end is lower of 8 cm according to the case B2

On this pictures the different positions of turning point, the bottom flatness and different bottom-steps are well visible.

Two dimensional graphics was used to estimate the different positions of turning point. These 2D-graphs of three cases B1, B2 and B3 are displayed on Fig.7. There are marked the distances x_o, x_o-δx_1 and x_o- δx_2 of turning point from waist entrace.

The simulation analysis shows that the position of turning point is being shifted closer to waist as the bottom step increases. This function is not linear, see TAB.1.

type of bottom	turning point-shift
flat (reference)	$\delta x_o = 0$ (reference)
low step = flat - 8 cm	$\delta x_1 = 1.3$ m
high step = flat -15 cm	$\delta x_2 = 1.7$ m

Tab.1. Shift of the turning point versus magnitude of bottom step

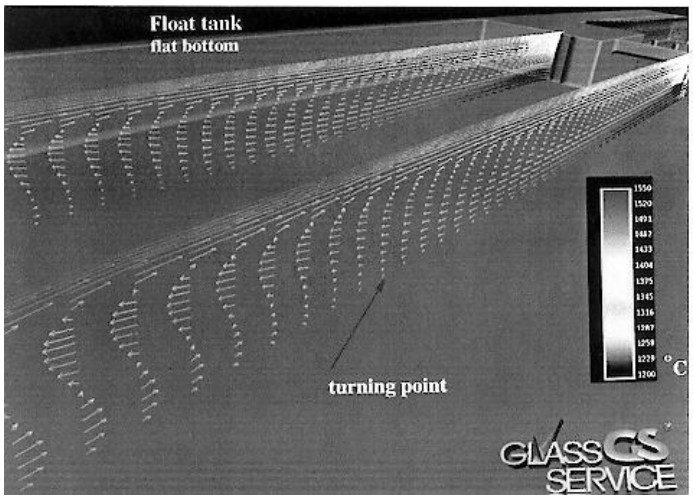

Fig.4. Float tank : flat bottom, detail of turning point-position in longitudinal cut

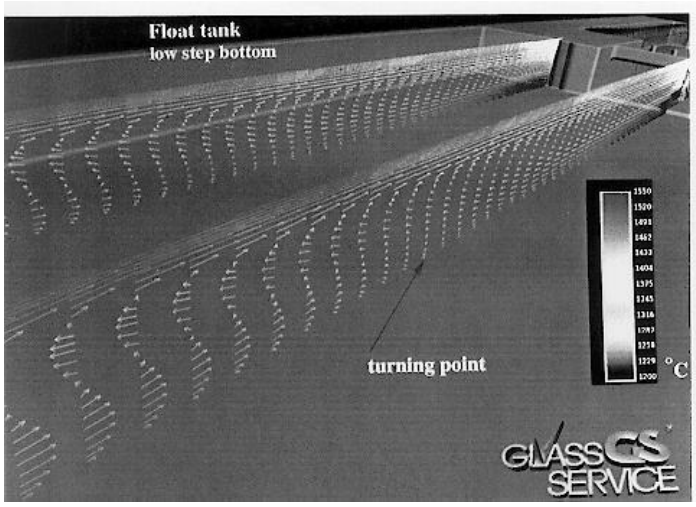

Fig.5. Float tank : low step-bottom, detail of turning point-position in longitudinal cut

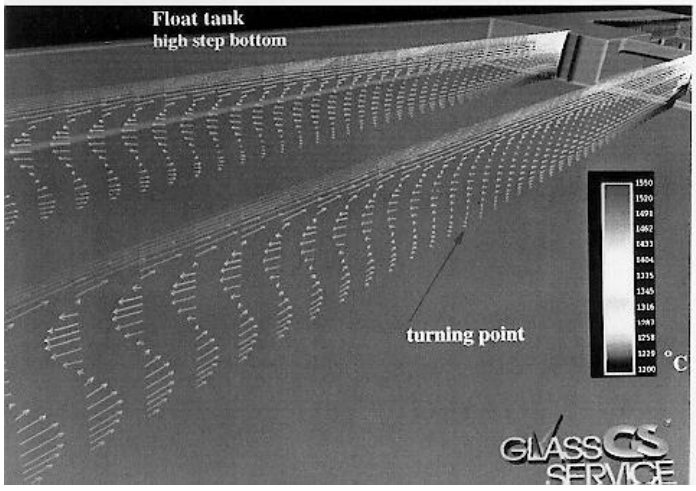

Fig.6. Float tank : high step-bottom, detail of turning point-position in longitudinal cut

FLAT BOTTOM

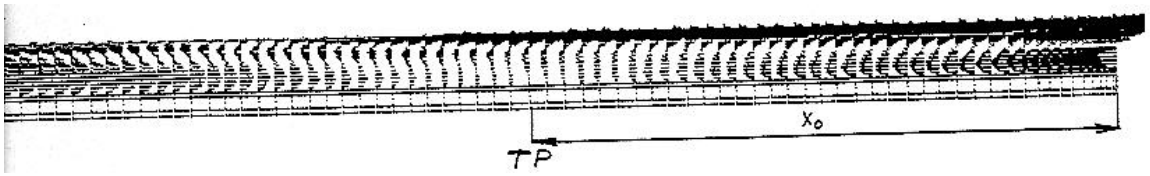

LOW STEP BOTTOM

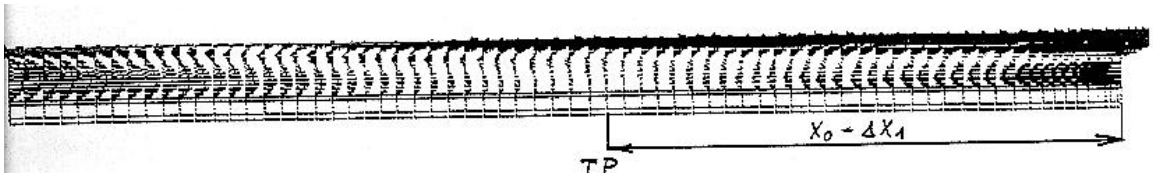

HIGH STEP BOTTOM

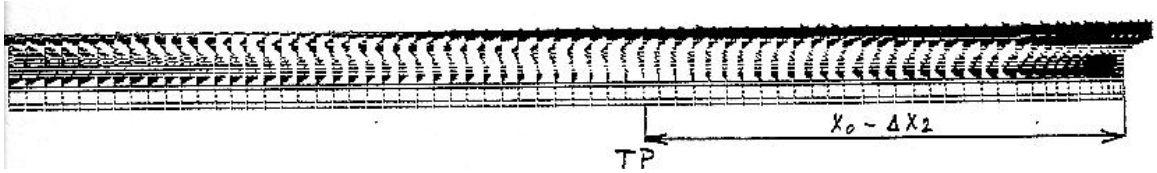

Fig.7 Estimation of positions of turning points (TP) using 2D graphics

It means the forward flow is stronger in case of higher bottom step. If the bottom step is greater and the backward flow still exists (it must not vanish) the second circulation flow will be more intensive and the refining- and defect dissolving-ability will become more stable. The result is a criterion function of value of bottom step versus stability of main circulation. This function has to be used for prediction of furnace operation before furnace design will be modified.

IV. CONCLUSIONS

Mathematical modeling of glass furnaces represents an important tool for furnace designers and technology engineers. The application of a specialized software package Glass Model has been demonstrated by a particular case study of float tank. Making complete study the results of mathematical simulations are being processed and various criterion function are created. These function are used before proper modifying the furnace design will be made. The process of creating two types of criterion functions was demonstrated: changing bottom type and variation of immersion of barrier. Using of this type of analysis is necessary to keep good glass quality and to maintain stability of glass furnace operation.

STUDIES ON FLOW STRUCTURE IN GLASS MELTING TANK BY MATHEMATICAL MODEL

H. Itoh, S. Yamamura, H. Todoriki and **M. Iga**
Asahi Glass Co. Ltd. Research Center, Japan

Abstract

Flow structure of molten glass in a glass melting tank was investigated by a three-dimensional FEM mathematical model.

It is well known that flow structure in a glass tank furnace makes significant effect on quality of glass products. The structure consists not only of global flow by longitudinal temperature distribution but also of local current by batch shape, side wall, electric booster, bubbler and so on. These local current sometimes gives rise to change in flow structure and glass quality.

A three-dimensional mathematical model of molten glass flow was presented, and some effects on local current by cooling of side wall were shown. Finite element method was used for space discretization because of its ability of analyzing complex shape and evaluating local flow structures.

We investigated effects of cooling rate of side wall on flow structure by mathematical model in typical glass melting tank for container glass. It was found, in case of throat tank, that the path of glass melt changes greatly by the condition of side wall.

1. INTRODUCTION

The flow of molten glass in a tank is largely related to the quality of glass products. While raw materials experience thermal history in the tank, physical and chemical phenomena such as melting of sand grain, homogenizing, chemical reactions of refining agents, and removal of bubbles take place. If there are some paths on which glass materials cannot experience good history, these glasses are supposed to be causes of defects. In fact, a variety of glass defects are observed which is thought to come through some kind of "short paths", such as relatively large sized bubbles, inhomogeneity and zircon-rich stones. To evaluate performances of tank designs and operations, it is necessary to know not only global flow of tank furnace but local paths such as currents near wall, under batch, near electric booster and so on.

Recently, with improvement of computer hardware, mathematical model of glass tank furnace has become a powerful tool for analyzing flow structure inside glass melts [1]-[4]. There still remains, however, a considerable gap between numerical results and quality of glass products in real process. As one of the ways to bridge the gap, we paid

attention to the role of local currents and studied some effects of the local currents on global flow structure and glass quality.

This paper presents a mathematical model to analyze three-dimensional unsteady molten glass flow and temperature in a tank. Finite element method was used for space discretization because of its ability of special interpolation, analyzing complex shape and evaluating local flow structures.

By numerical simulations of this model, we investigated effects of cooling rate of side wall on flow structure in typical glass melting tank for container glass.

2. MATHEMATICAL MODEL

We assumed the model to be as follows ;

Glass melt is incompressible
Governed by the Boussinesq approximation as the buoyant force
Effective thermal diffusivity is used for energy equation.

The three-dimensional molten glass flow in a glass tank furnace is described by the continuity equation, Navier-Stokes equations with the Boussinesq approximation, the energy equation, and mass transfer of glass inhomogeneity (variable *di*) equations.
The governed equations are as follows;

$$\frac{\partial u}{\partial x}+\frac{\partial v}{\partial y}+\frac{\partial w}{\partial z}=0 \tag{1}$$

$$\rho\left(\frac{\partial u}{\partial t}+u\frac{\partial u}{\partial x}+v\frac{\partial u}{\partial y}+w\frac{\partial u}{\partial z}\right)=-\frac{\partial p}{\partial x}+\frac{\partial}{\partial x}\left[2\mu\frac{\partial u}{\partial x}\right]+\frac{\partial}{\partial y}\left[\mu\left(\frac{\partial u}{\partial y}+\frac{\partial v}{\partial x}\right)\right]+\frac{\partial}{\partial z}\left[\mu\left(\frac{\partial u}{\partial z}+\frac{\partial w}{\partial x}\right)\right] \tag{2}$$

$$\rho\left(\frac{\partial v}{\partial t}+u\frac{\partial v}{\partial x}+v\frac{\partial v}{\partial y}+w\frac{\partial v}{\partial z}\right)=-\frac{\partial p}{\partial y}+\frac{\partial}{\partial x}\left[\mu\left(\frac{\partial u}{\partial y}+\frac{\partial v}{\partial x}\right)\right]+\frac{\partial}{\partial y}\left[2\mu\frac{\partial v}{\partial y}\right]+\frac{\partial}{\partial z}\left[\mu\left(\frac{\partial v}{\partial z}+\frac{\partial w}{\partial y}\right)\right] \tag{3}$$

$$\rho\left(\frac{\partial w}{\partial t}+u\frac{\partial w}{\partial x}+v\frac{\partial w}{\partial y}+w\frac{\partial w}{\partial z}\right)=-\frac{\partial p}{\partial z}+\frac{\partial}{\partial x}\left[\mu\left(\frac{\partial u}{\partial z}+\frac{\partial w}{\partial x}\right)\right]+\frac{\partial}{\partial y}\left[\mu\left(\frac{\partial w}{\partial y}+\frac{\partial v}{\partial z}\right)\right]+\frac{\partial}{\partial z}\left[2\mu\frac{\partial w}{\partial z}\right]$$

$$+g\rho\beta(T-T_0)-\sum_i g d_i(\rho_i-\rho) \tag{4}$$

$$\rho c\left(\frac{\partial T}{\partial t}+u\frac{\partial T}{\partial x}+v\frac{\partial T}{\partial y}+w\frac{\partial T}{\partial z}\right)=\frac{\partial}{\partial x}\left[\lambda\frac{\partial T}{\partial x}\right]+\frac{\partial}{\partial y}\left[\lambda\frac{\partial T}{\partial y}\right]+\frac{\partial}{\partial z}\left[\lambda\frac{\partial T}{\partial z}\right]+q \tag{5}$$

$$\frac{\partial d_i}{\partial t}+u\frac{\partial d_i}{\partial x}+v\frac{\partial d_i}{\partial y}+w\frac{\partial d_i}{\partial z}=\xi_i \quad (i=1...n) \tag{6}$$

where viscosity and thermal diffusivity are supposed to be functions of temperature and inhomogeneity in the following forms;

$$\mu = \mu(T, d_1, ..., d_n) \quad (7)$$

$$\lambda = \lambda(T, d_1, ..., d_n) \quad (8)$$

The inhomogeneity equation (6) represents concentration of minor contents in glass, such as new glass at glass change, refractory dissolution, volatilization, bubble density and so on. The buoyant force of Navier-Stokes equation (4) is made not only by temperature distribution but by density distribution caused by inhomogeneity which is governed by the inhomogeneity equation.

These equations are specially discretized by 3-dimensional Galerkin finite element method respectively, and integrated in time by the fully implicit scheme. Finite element method is applied because of;

1) Its applicability for analyzing arbitrary shaped domain, which enables not only any shapes of melting tank, but many kind of delivery process such as forehearth or working zone to be analyzed easily.

2) Its convenience for treating boundary condition, such as non-slip condition at wall or natural boundary condition for energy equation, which is important to consider local phenomena as flow by wall with accuracy and simplicity.

Fully-implicit method is applied to solve these equations because of analysis of slow transition of flow, temperature and inhomogeneity patterns with high viscosity in glass melt.

Each discretized equations are solved by using Conjugate Gradient and Conjugate Gradient-like methods, which enables faster solution of large-scaled discretized equation.

The validity of the model was assured by calculation of experimental model of tank furnace [5]. Both measured and calculated results agreed very well, including local flow structure near wall and Rayleigh-Benard cell under batch covering [6].

3. STUDY ON FLOW STRUCTURE BY SIDE COOLING

As a study of flow structure in melting tank, we investigated effects of side wall cooling on the flow by using the numerical model. A typical tank furnace for container glass is assumed for consideration. Schematic of the furnace is shown in Fig. 1, including definition of three-dimensional axes of coordinates.

Properties of glass melts, temperature distribution of glass surface, batch pattern and temperature are given beforehand. Thermal boundary conditions of wall are also defined initially. To investigate effects of cooling rate of side wall, heat transfer coefficient of side wall is changed as follows;

Case (A) : 1.0 [$W/m^2/K$]

Case (B) : 5.0 [W/m^2/K]
Case (C) : 15.0 [W/m^2/K]
Case (D) : 30.0 [W/m^2/K]

The reference temperature outside the wall is supposed to be same as room temperature. Several other conditions for calculation are shown in Table 1.

The inhomogeneity of glass melt is neglected because of simplicity of discussion. To evaluate steady state results, unsteady calculations are done for sufficiently long time to converge.

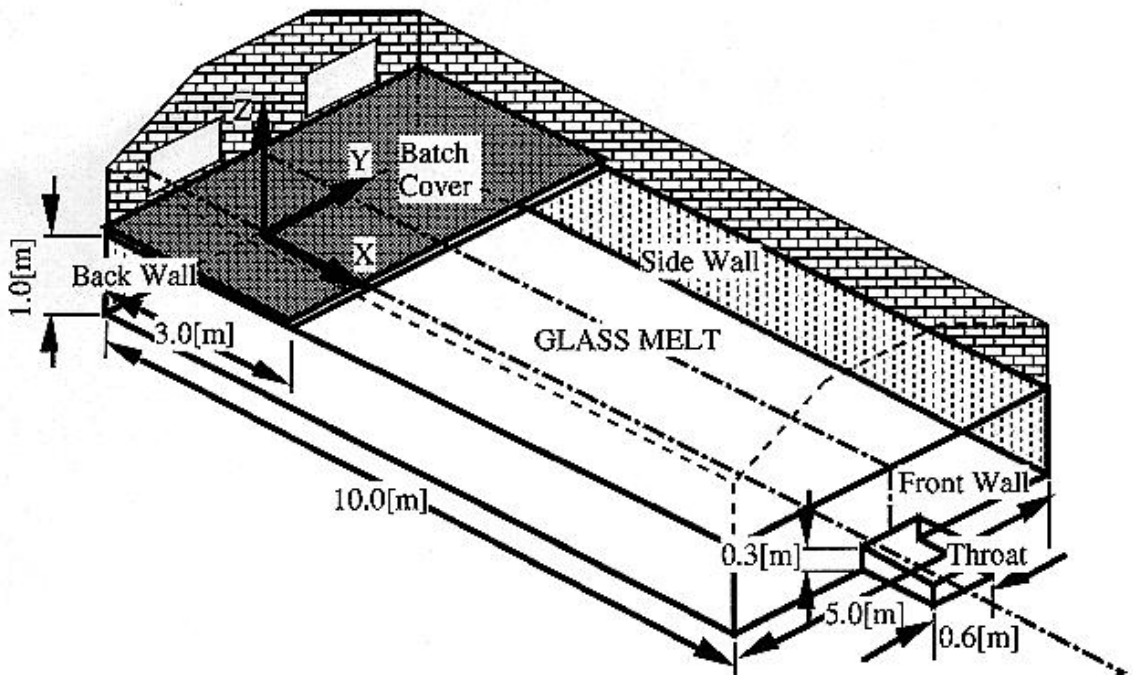

Fig. 1 Schematic view of the Glass furnace to be investigated

Table 1 Several conditions for calculation

Glass Feed Rate [kg/s]	0.5787
Temperature at Batch cover [K]	1523.0
Maximum temperature at glass surface[K]	1823.0
Heat transfer coefficient on bottom[W/m^2/K]	4.0
Heat transfer coefficient on back wall[W/m^2/K]	10.0
Heat transfer coefficient on front wall and throat W/m^2/K]	10.0

4. RESULTS AND DISCUSSIONS

Numerical results of each cases are shown below. Fig. 2-5 show stream lines on X-Z cross section at center of the tank (Y=0). These results show typical macroscopic flow pattern of container glass tank. From these patterns, little differences are observed for consideration.

Fig. 6-7 show stream lines on Y-Z cross section at X=5[m]. As cooling rate of side wall getting stronger, local downward currents near side wall are observed. Fig. 8 shows Z-directional velocity distributions of each cases on Y-direction at X=5[m], Z=0.5[m]. In case (A) and case (B), local currents near side wall are not found or relatively small from main flow. In case (C) and case (D), however, there exists relatively large local current by side wall. The thickness of local current is around 0.2[m] at these calculation, which requires fine special discretization for analysis.

To evaluate quality of glass by the flow structure, we investigated loci of glass which exits through throat by back-tracing method. This evaluation was done by positioning many particles at throat initially and tracing the movements of particles upstream by integrating velocity on time inversely. Fig. 9-12 show loci of glass melt which exists through throat in each cases. In case (A) and case (B), glass melt which exits through throat mainly comes from batch melting zone through bottom of the tank. These paths are easily conjectured from global flow pattern of the tank as shown in Fig. 2-5. On the other hand, in case (C) and case (D), most of glass melt which exits through throat comes from side of the tank. There, we can see loci of glass melt which comes from batch melting zone near side wall. These trajectories form some kind of "twisted tunnel" in the flow structure, which is different from global flow structure and can be hardly conjectured from the global flow pattern of the tank as shown in Fig.2-5.

It can be seen from these results that some kind of phase transition is raised and the flow structure in glass melting tank, which is thought to have great influences on the quality of glass product, is changed greatly by the local current.

5. CONCLUSION

A three-dimensional FEM mathematical model of molten glass flow was presented and effects of cooling rate of side wall on flow structure by mathematical model in typical glass melting tank for container glass were examined. It is found, in case of throat tank, that the path of glass melt changes greatly by the condition of side wall.

These studies were held with only very simple model, but in practice, there are many factors which affects the flow structure, such as dimension of tank, auxiliary equipments like bubbler or electric booster, shape of batch cover, and other physical and chemical phenomena like unsteadiness or glass inhomogeneity. To evaluate glass quality with mathematical model, sufficient analysis of flow structure including local current is needed about each factors mentioned above.

References

[1] H. Mase and K. Oda, J. Non-crst.Solids, 38-39(1980), 807-812.
[2] H. Mase, et al., Yogyo-Kyokai-Shi, 94(1986), 258-294.
[3] A. Ungan and R. Viskanta, Glastech. Ber., 60(1987), 71-78,115-124.
[4] H. Itoh, et al., Collected papers, XVII IntI. Congr.on Glass(1995),vol6., 81-86.
[5] N.W.E. Curlet et al., AlChE J., 30, No.2(1984), 249-257.
[6] H. Itoh, Proc. of Glass Processing Forum (1995).

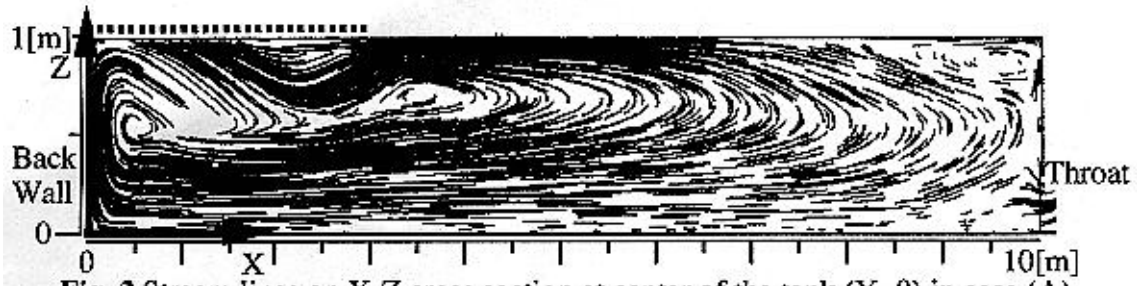

Fig. 2 Stream lines on X-Z cross section at center of the tank (Y=0) in case (A).

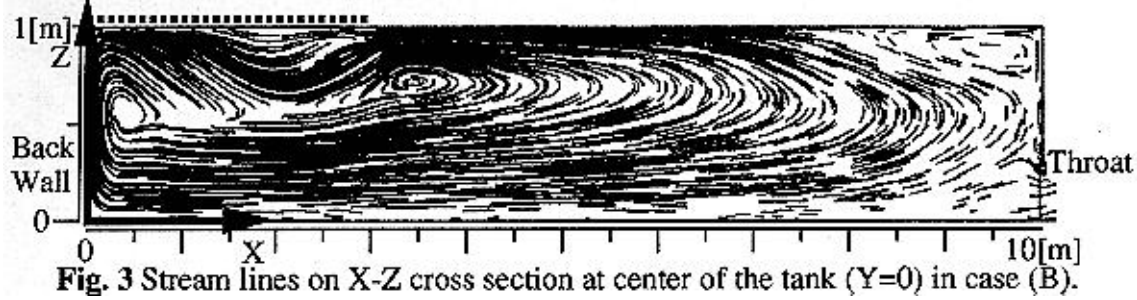

Fig. 3 Stream lines on X-Z cross section at center of the tank (Y=0) in case (B).

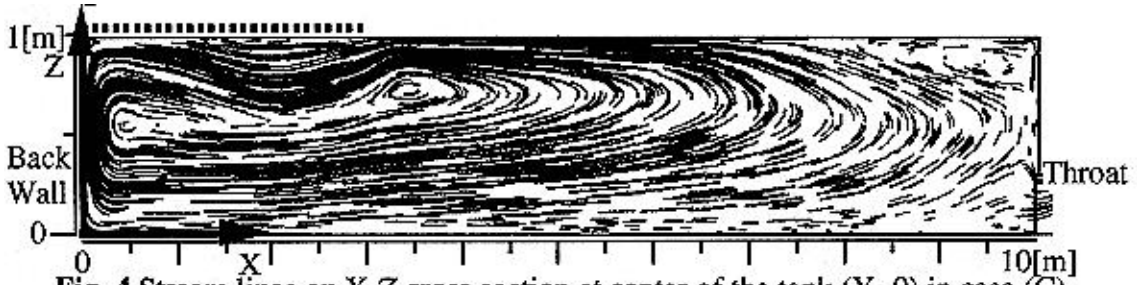

Fig. 4 Stream lines on X-Z cross section at center of the tank (Y=0) in case (C).

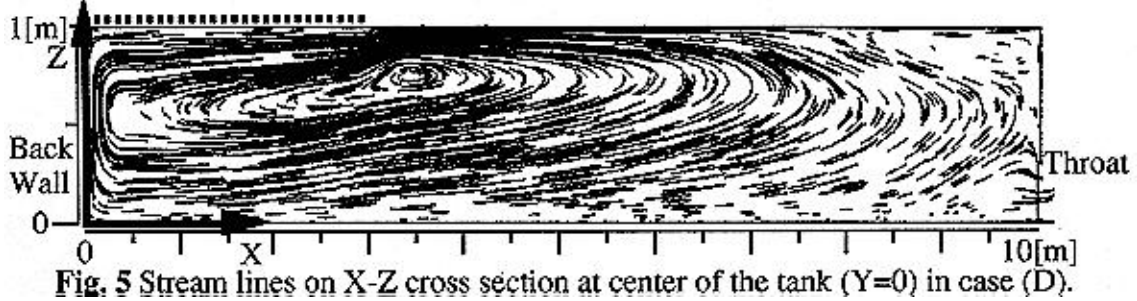

Fig. 5 Stream lines on X-Z cross section at center of the tank (Y=0) in case (D).

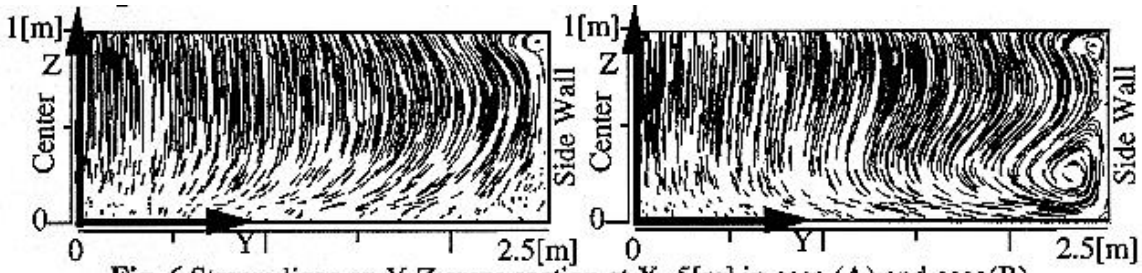

Fig. 6 Stream lines on Y-Z cross section at X=5[m] in case (A) and case(B).

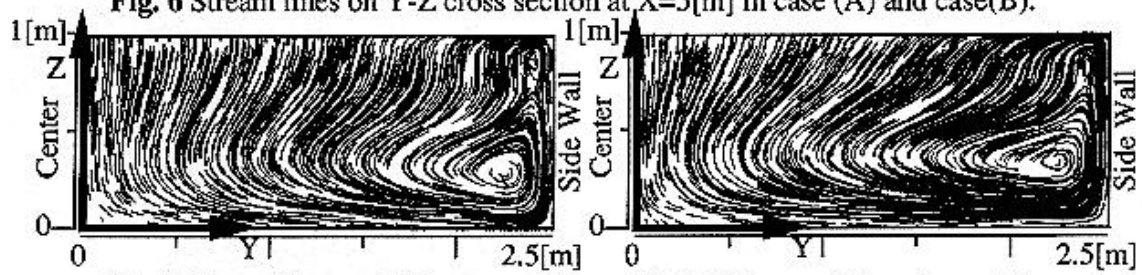

Fig. 7 Stream lines on Y-Z cross section at X=5[m] in case (C) and case(D).

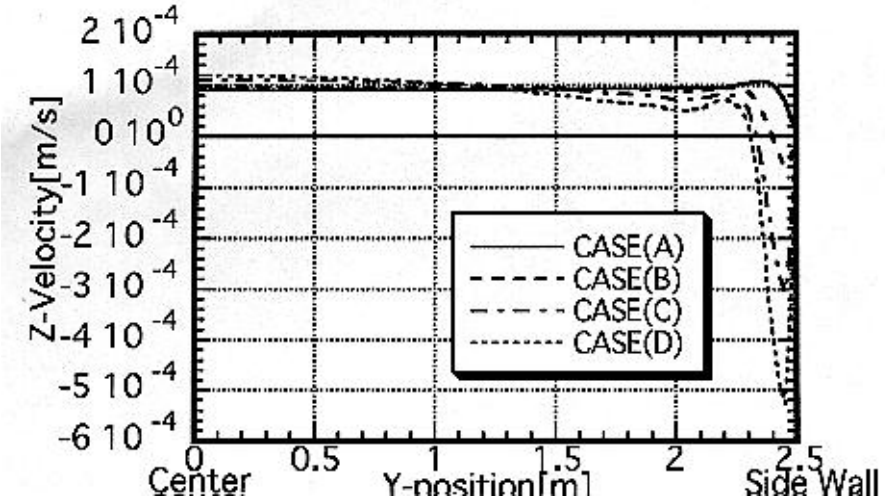

Fig. 8 Z-directional velocity distributions of each cases on Y-direction at X=5[m], Z=0.5[m]

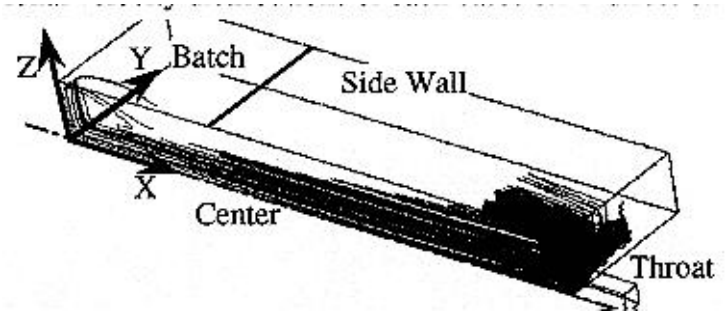

Fig. 9 loci of glass melt which exists through throat in case(A)

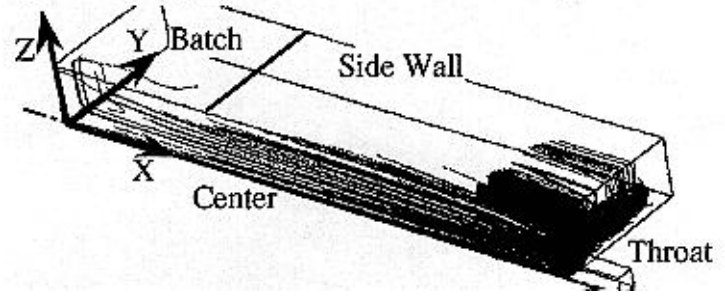

Fig. 10 loci of glass melt which exists through throat in case(B)

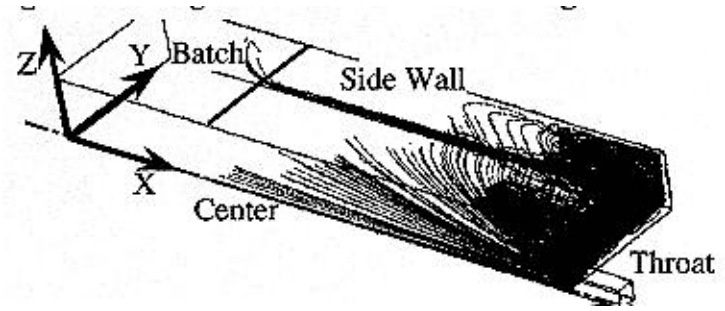

Fig. 11 loci of glass melt which exists through throat in case(C)

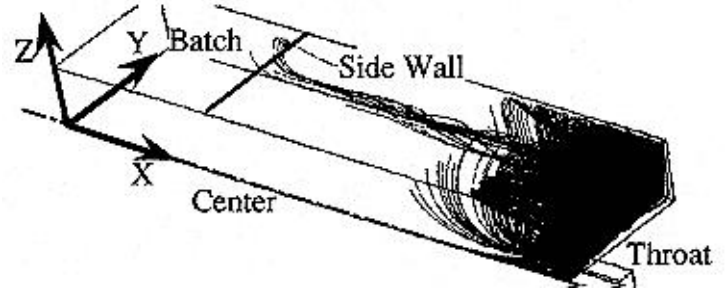

Fig. 12 loci of glass melt which exists through throat in case(D)

THE USE OF PHYSICAL MODELLING FOR THE VERIFICATION OF THE MATHEMATICAL MODEL OF A GLASS FURNACE

Lale Önsel and **Zeynep Eltutar**
SISECAM Research Center, Turkey

Abstract

In this study, the glass currents in an end-fired 200 t/day container furnace are investigated with a physical model. The data of the furnace and the data from the physical model are used to attain a reliable mathematical model of the furnace.

Since the physical models enable an easy access to convection currents within glass and since their results are verified by experience from the furnaces; the data from these models are used in the evaluation of the mathematical modelling results.

A commercial software is used to simulate the convection currents in the furnace. The data required for the boundary conditions are taken from the furnace and the physical model. Many data related to velocity and temperature within the glass are measured in the physical model, so that a pointwise comparison of the models could be achieved for the verification of the mathematical model.

The investigations are carried out at two different pull rates for both of the models. The effects of increasing the pull from 200 t/d to 250 t/d are discussed.

1. INTRODUCTION

With physical and mathematical modelling of glass furnaces; It is possible

- to improve production for better glass quality, higher pull rates and less energy consumption
- to develop the existing furnace designs and
- to make research studies for the realization of new glass melting technologies.

In Þiþecam, the physical modelling studies have started back in 1981 with the establishment of the necessary theory and the experimental set up. After the evaluation and testing of the results with furnace data wherever possible, the physical modelling has become an important tool for the research studies.

In order to be able to work on parameters which could not be handled with physical models, mathematical modelling has also been started along with physical modelling. Before the mathematical models could be used in the research studies, they have to be verified for a close simulation of the actual furnace processes.

In this respect, the experience in glass, glass furnaces and physical modelling have all been incorporated to realize a plausible mathematical model which could also be used as a reliable tool in the research studies.

In this study, first of all the glass currents in an end-fired 200 ton/day container furnace are investigated with a physical model. The velocity and temperature data have been collected at many points through various cross-sections.

Then the mathematical model of the furnace is formulated with a commercial software. The data required for the boundary conditions are taken from the physical model and the actual furnace.

The results of each model are compared at all measurement points for temperature and velocity. Also the general pattern of glass currents are investigated for the degree of similarity.

These studies are carried out at two different pull rates for both of the models. The effects of increasing the pull from 200 t/d to 250 t/d are discussed.

2. FURNACE AND THE PHYSICAL MODEL

The furnace physical model is set-up according to the similarity criteria. In the picture below, the main characteristics of the furnace could be seen.

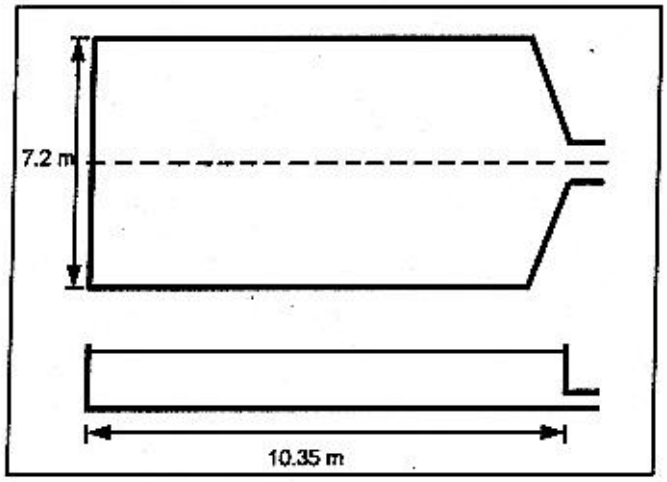

Figure 1: The main dimensions of the furnace.

2.1. The Observations and the Measurements with the Physical Model

The general pattern of the glass currents are observed and the velocity and temperature values are measured at three x-y and three y-z cross sections at 1 m gradients by length and width and at four x-z cross sections at 0.2 m gradients by height.

These measurements are carried out for two pull rates; 200 t/d and 250 t/d.

2.1.1. The Temperature and Velocity Measurements

The temperature profiles obtained from the model and the actual furnace for 200 t/day and 250 t/day are given in Figure 2.

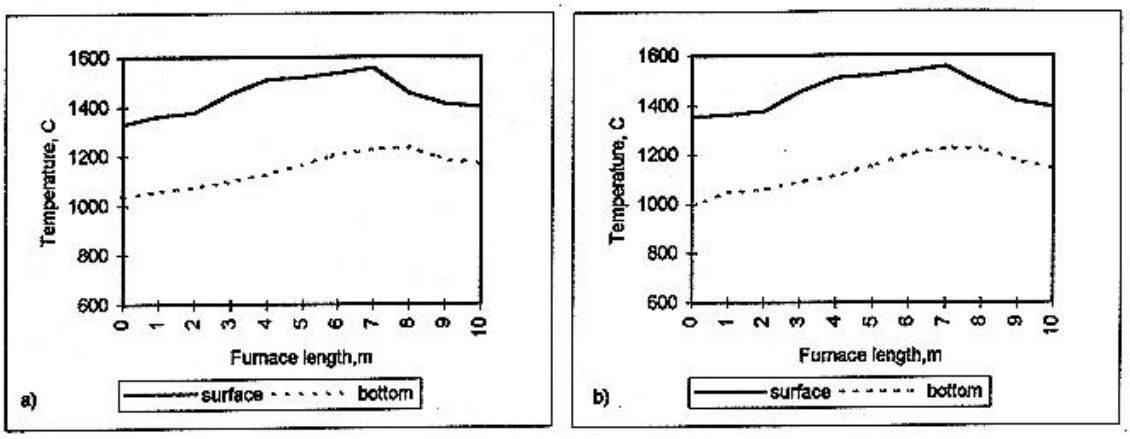

Figure 2: The surface and bottom temperature profiles along the centerline of the furnace, for a) 200 t/day and b) 250 t/day

The values of the measurements for velocity in the physical model are summarized in figures given below.

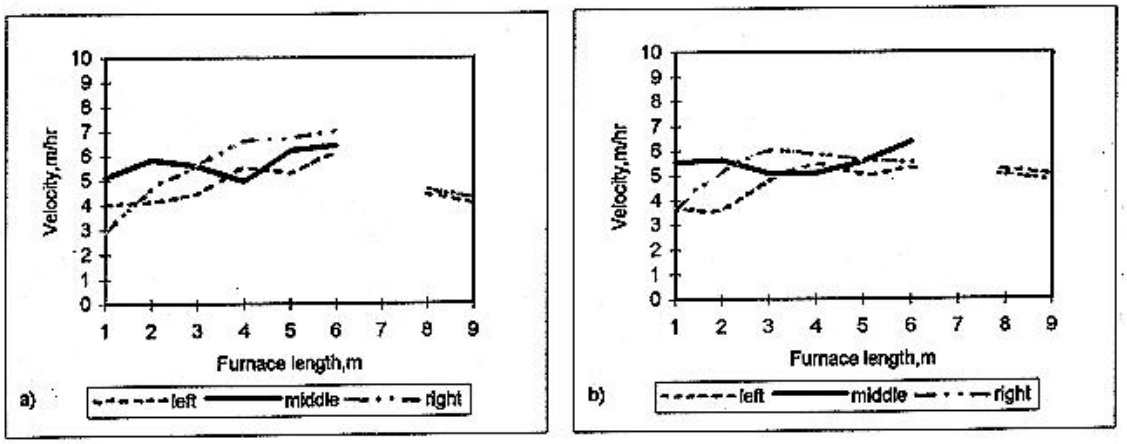

Figure 3: The surface velocities along the length of the furnace for a) 200 t/day, b) 250 t/day

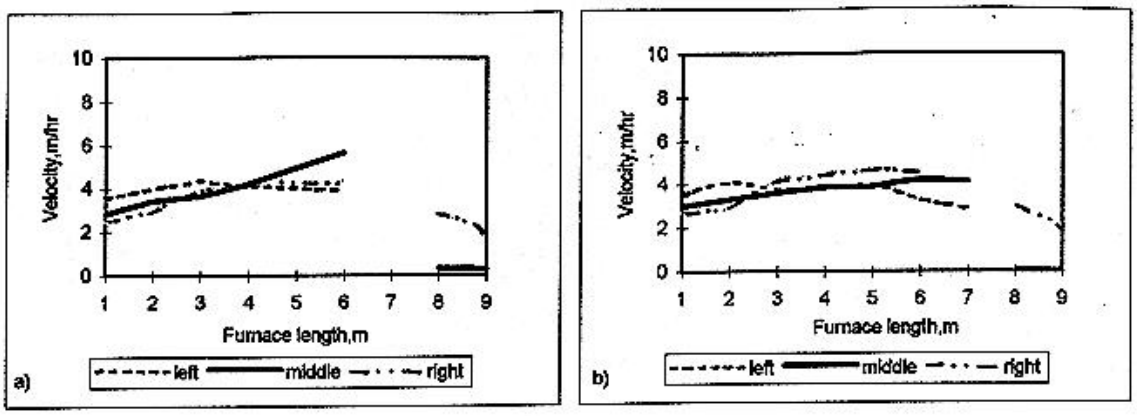

Figure 4: The bottom velocities along the length of the furnace for a) 200 t/day and b) 250 t/day

2.1.2. Glass Currents for 200 t/day and 250 t/day Pull Rates.

Glass currents as shown in Figure 5, form the two main circulations, one at the back until the hot spot and the other in the front before the front wall. The main glass current which rises at the hot-spot is mainly pulled towards the throat from a height of 0.4-0.5 m, and the remaining part rises to the surface at the hot- spot and completes the forward circulation at the front wall. The hot spot is formed at 67% of the furnace length.

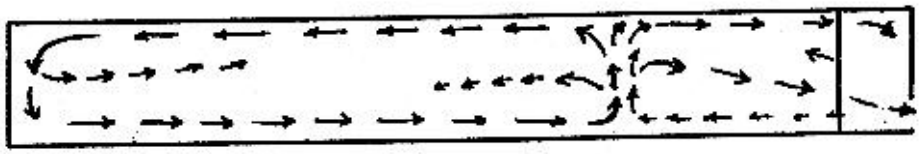

Figure 5: Glass currents for the 200 t/d pull; along the center line at the x-y plane

At the surface, the currents spread towards the back wall and the side walls. After the hot-spot there are low velocity bottom currents which move back from the throat side to the hot-spot.

Similar investigations are carried out for 250 t/day as well.

The two observations are compared to see the effect of increasing the pull by 50 t/day in this specific furnace.

The glass currents have changed as shown in Figure 6 for the centerline.

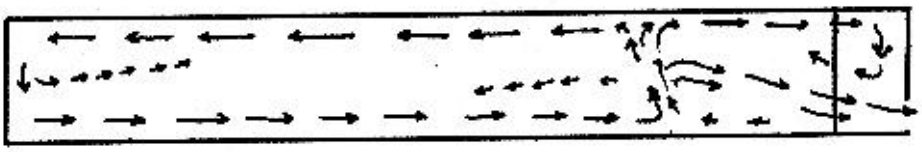

Figure 6: Glass currents for 250 t/day; along the center line at the x-y plane

The effect of increasing the pull from 200 t/day to 250 t/day has been as follows;

- The hot-point has moved from the 7 th meter to the 8 th meter. Increasing the pull by 50 t/day has changed the place of the hotspot from 67% to 77% of the total length of the furnace.
- The velocity of the main glass current has increased.
- The backward currents at the bottom from the throat towards the hot-point have completely disappeared.
- Also the velocity of the inner circulations backward from the hot-point and forward at the front corner have decreased.

3. MATHEMATICAL MODEL OF THE FURNACE

The furnace under consideration is modelled by a commercial software for fluid flow where the momentum, energy and mass transfer equations are solved by the finite difference method. The SIMPLE algorithm is used for the solution and the continuity equation is used to check the velocity values at each iteration.

3.1. The formation of the model

The furnace is investigated at 22 grids in length, 28 grids in width and 8 grids in height with a total of 4928 nodes. The symmetry function is employed in order to increase the number of nodes. The grid formulation is shown in Figure 7.

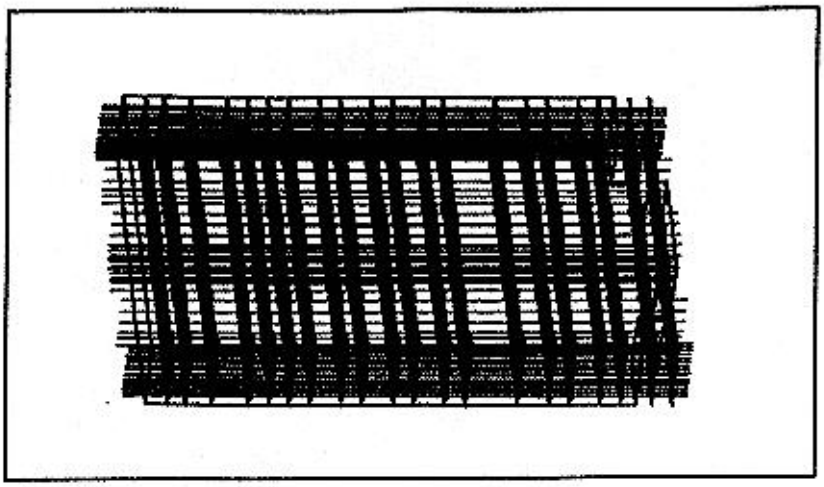

Figure 7: Grid formulation used in the mathematical model.

The boundary conditions for glass surface and furnace walls are taken from furnace and physical model data. The necessary temperature profiles and velocity values are set-up lengthwise along different sections through the width of the furnace.

The values related to glass like density, viscosity, specific heat and thermal conductivity are expressed either as constants or as functions of temperature.

The model has been developed with the use of symmetry, by varying the functional effects related to boundary conditions and by the use of different solution techniques involved in the software.

The final form of the model is run for the two different pull rates under consideration, 200 t/day and 250 t/day.

3.2. The Results Obtained by the Mathematical Model

3.2.1. The Results with 200 t/day

The solution of the model for 200 t/day resulted in the following pattern of glass currents along the centerline (Figure 8).

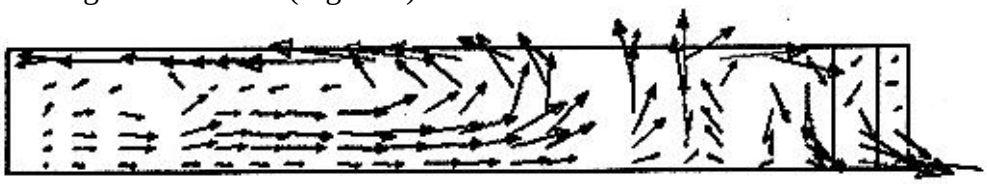

Figure 8: Glass currents for 200 t/d along the centerline.

The general pattern of glass currents have been formulated similarly with the mathematical model as in the physical model; with the bottom current rising at the hot-

spot to a certain height and with the main current being pulled to the throat. The hot-spot has been formed at the 67% of the furnace length. The inner circulations at the back of the hot-spot and at the front upper corner have again been similarly formed as can be seen from the Figure 8 above.

The velocity distribution for the surface and bottom currents along the centerline of the furnace are given in Figure 9 for 200 t/day mathematical model solution.

These velocity distributions when compared with the former physical model results for 200 t/day, show very parallel behavior, Figure 9.

The velocity values at the surface are in the range of 5-6 m/hr in the physical model, whereas they are in the region of 4-6 m/hr in the mathematical model. The similarity can also be seen at the trend of the profiles along the length of the furnace. The bottom current velocities are in the range of 2.5-5 m/hr in the physical model and 2-4 m/hr in the mathematical model. The values are very close as can be seen from the figure.

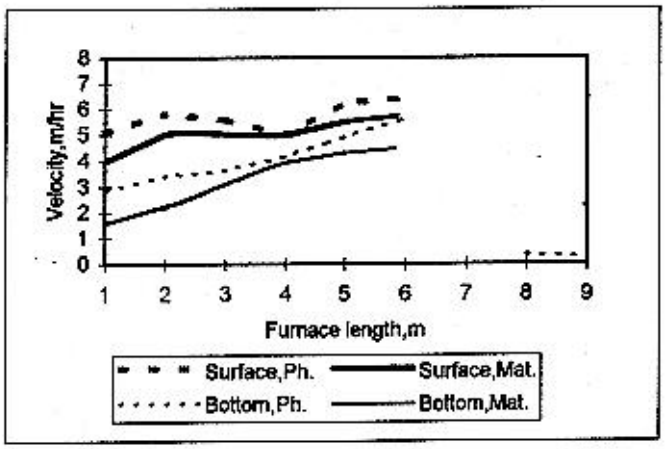

Figure 9: The velocity distribution for the surface and bottom currents both in the physical model and in the mathematical model studies for 200 t/day.

These values from the physical and the mathematical model show that a close simulation has been achieved for both models. In comparing temperature profiles, it has been seen that similar values are obtained from both of the models.

3.2.2. The Results with 250 t/day and the Comparison of the two Pullrates with the Mathematical Model.

The results from the investigation for the 250 t/day pull case also show the same parallelism with the physical model results for velocity and temperature.

The flow pattern obtained from the mathematical model can be seen in Figure 10.

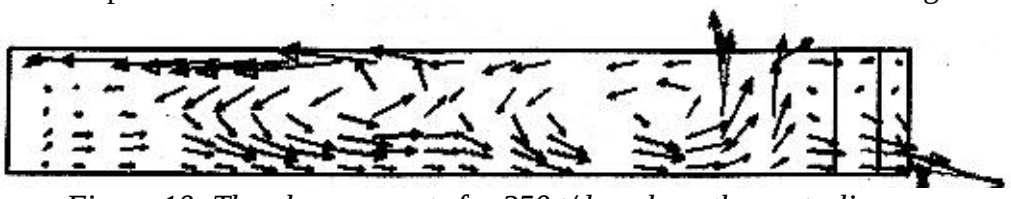

Figure 10: The glass currents for 250 t/day along the centerline.

The increase in pull has lead into changes which were predicted from the physical model.

These could be summarized as;

- The hot-spot has moved from 67% to 77% of the furnace length.
- The velocity of the main glass current in the refining zone has increased.
- The back currents in the refining zone at the bottom, have disappeared completely.
- The velocity of the inner circulations have decreased.

The velocity profiles along the length of the furnace at the centerline could be seen in the figure below for both 200 t/day and 250 t/day, as obtained, from the mathematical model.

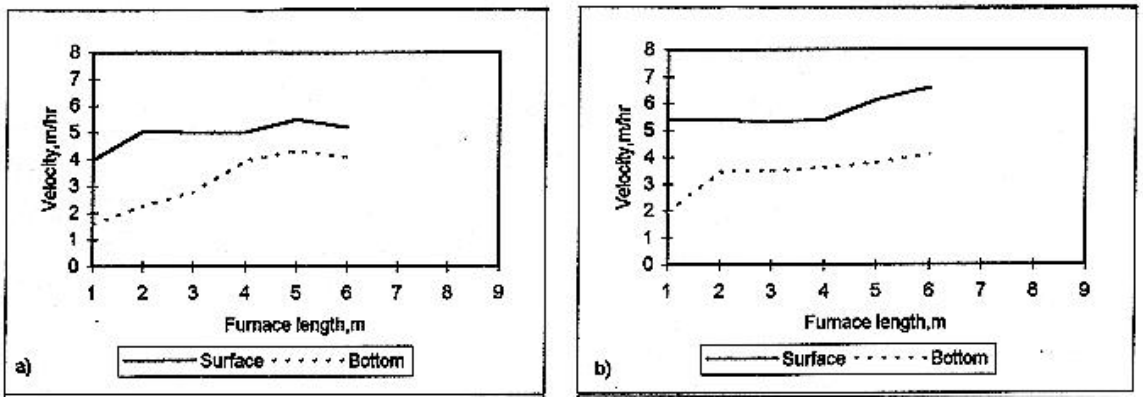

Figure 11: The velocity vectors along the furnace a) for 200 t/day b) for 250 t/day

3.2.3. Interpretation of Model Results for Furnace Operation

There has also been made an investigation for 220 t/day with both the physical and the mathematical model to enable a more realistic evaluation of the effect of the furnace pullrate on glass quality. The results for three different pull rates have been compared as in the figure below, for 200, 220, 250 t/day.

From the results of these investigations, it has been concluded that it is not possible to pull 220 t/day and higher from the furnace under consideration. As the pull is increased, the length for refining has decreased and the velocities of the main glass current have increased. Thus, the time for refining of the glass will be insufficient for the required glass quality.

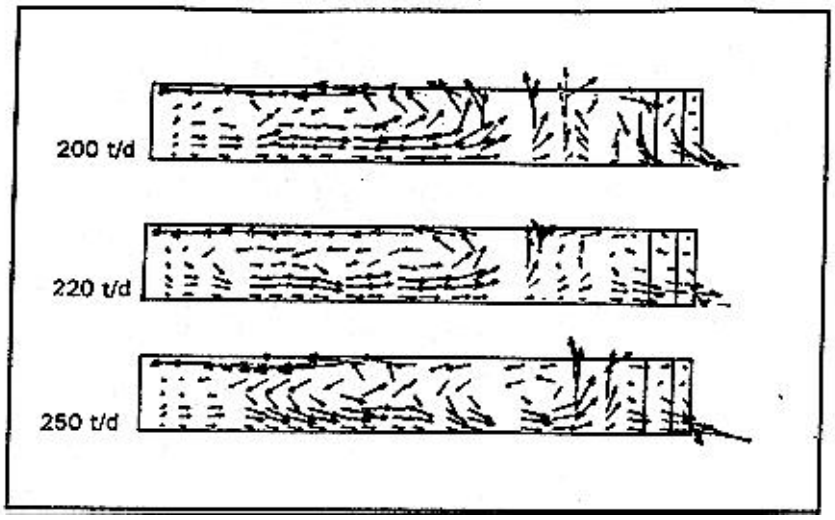

Figure 12: The glass currents for the three different pull rates

4. CONCLUSION

Detailed investigations are carried out in the physical model of an end-fired regenerative 200 t/day container furnace for different pullrates. The same investigations are repeated with a mathematical model. The glass currents, velocity and temperature distributions obtained from both of the models show good similarity. After the verification of the mathematical model, it is used to evaluate the effect of different pullrates on glass quality.

Physical modelling is used as an important tool in examining the behavior of glass in the furnace and in predicting the nature of the changes applied. Before using the mathematical model, it has also been verified with extensive data basis from the physical model and the furnace. Both of the modelling techniques are now utilized for design, operation and research purposes.

REFERENCES

1. Ungan, A. and Viskanta, R. "Identification of the structure of the three dimensional thermal flow in an idling container glass melter", Glass Technology, Vol. 28 No.6, Dec. 1987.
2. Ungan, A and Viskanta, R. "Melting of Glass Batch Blankets in Furnaces" AIChE Symposium Series, Vol. 80 No.236.
3. Carvalho, M. G. et.al. "Modelling and Optimization of an Industrial Glass Furnace" Dynamics of Reactive Systems, Part II.
4. Carling, J.C., "A reappraisal of the mathematical modelling of flow and heat transfer in glass tank forehearths", Glass Technology, Vol. 23, No.5, Oct.1982.
5. Leyens, G. "Contribution to the calculation of two dimensional convection currents in continuous lass tank furnaces, Glastechnishe Berichte, 47., No:11, Nov. 1974; No:12, Dec. 1974.

6. Mase, H. and Oda, K., Mathematical Model of Glass Tank Furnace with Batch Melting Process", Reports Res. Lab. Asahi Glass Co. Ltd. 30 (2), 1980.
7. Nolet, P. A. and Murnane, R. A. "Development of Modeling Techniques for Glass Furnaces" Advances in the Fusion of Glass.
8. Rawson, H., "Mathematical Modelling", Journal of Non-Crystalline Solids, 73,1985.
9. Hammonds, J. and Sutton, J. "The Practical Application of Mathematical Modelling to Glass Melting", Glass, Feb. 1987.
10. Curlet, N.W.E., et.al. "Experimental and Mathematical Modelling of 3-Dimensional Natural Convection in an Enclosure", AIChE (Vol. 30, No.2) March, 1984.
11. Ungan, A. and Viskanta, R. "3-Dimensional Numerical Modeling of Circulation and Heat Transfer in a Glass Melting Tank", Glastech. Ber. 60 (No.3), 1987.
12. Ungan, A. and Viskanta, R. "Effect of Air Bubbling on Circulation and Heat Transfer in a Glass Melting Tank", AIChE Symposium Series, Vol. 81. No. 245,1985.
13. Stanek, J. "Electric Melting of Glass" Elsevier Scientific Pub. Co. 1977.
14. Ungan, A. et.al. "Numerical Polydispersed Silica Grain Dissolution in Glass Melting Furnaces", J. Am. Ceram. Soc. 77 (7), 1921-27 (1994).
15. Ungan, A. and Balkanli, B. "Numerical Simulation of Bubble Behaviour in Glass Melting Tanks. Part 1. Under ideal conditions", Glass Technology Vol. 37, No. 1 Feb. 1996.

ANALYSIS OF THE ROUGHNESS OF GLASS SURFACES: FROM THE NANOSCOPIC TO THE MACROSCOPIC SCALE

Daniel Abriou, Yves Levillain, Herv J Arribart and **François Creuzet**
Laboratoire CNRS/Saint-Gobain "Surface du Verre et Interfaces," France

Abstract

A procedure for the characterization of the surface roughness of glass is presented. It is based on a Fourier analysis of the height profile recorded along linear traces. Measurements are performed with Atomic Force Microscopy (AFM) at the nanoscopic and microscopic scales, and with Mechanical Profilometry (MP) at the microscopic and macroscopic scales. The roughness spectral density can thus be obtained over seven decades in wavenumbers. From this knowledge, it is possible to derive the roughness value in any spectral window. Roughness values of different glass samples for the [10 nm ;100 : m] window are compared. It is found that the surface of float glass is remarkably smooth and presents a self-affine geometry.

I. INTRODUCTION

The characterization of the roughness of glass surfaces has became an important issue in the last past years, mostly because of the development of more and more sophisticated products. For instance, low roughness substrates are needed to improve the physical performance of thin optical coatings, and very flat and smooth surfaces are necessary to use glass as a material for computer hard disks.

Various experimental techniques are traditionally used to measure the roughness of glass: optical interferometry, X ray reflectometry, optical profilometry, mechanical profilometry (MP) [1]. X ray reflectometry and optical interferometry need an assumption about the distribution, often chosen Gaussian, of the height histogram. Mechanical and optical profilometries are limited by a lateral resolution not better than about one micrometer. The recent development of Atomic Force Microscopy (AFM) extends the scale of measurement of height profiles down to one nanometer. In the present paper, we show that it is possible to get a complete roughness analysis from the nanoscopic to the macroscopic scale, by jointly performing AFM and MP measurements.

II. BACKGROUND

Both AFM and MP measurements are based on the recording of the surface height profile h(x) along a trace of given length L. The number N of independent data points is limited either by the digitalization rate of the recording or by the shape function of the diamond stylus, in the case of MP, or the tip, in the case of AFM. In other words, for a given trace, the roughness analysis is valid for a spatial window limited by the two cut-off

values L and L/N. For example, the root-mean-square (rms) value of the roughness can be written as:

$$\sigma_{rms} = \sqrt{\frac{1}{N}\sum_{i=1}^{N} h_i^2} \qquad (1)$$

where the distance between nearest neighbour data points i and i+1 is L/N.

An important consequence of equation (1) is that the roughness value depends on the two spatial cut-off values. This is illustrated in figure 1 where the rms roughness measured by AFM for two glass samples are plotted as a function of L, keeping N constant and equal to 256. Clearly, a single number is not sufficient to characterize the roughness of a sample. One have to think of roughness in terms of a spectral parameter, and therefore, the suitable mathematical tool is Fourier analysis [1].

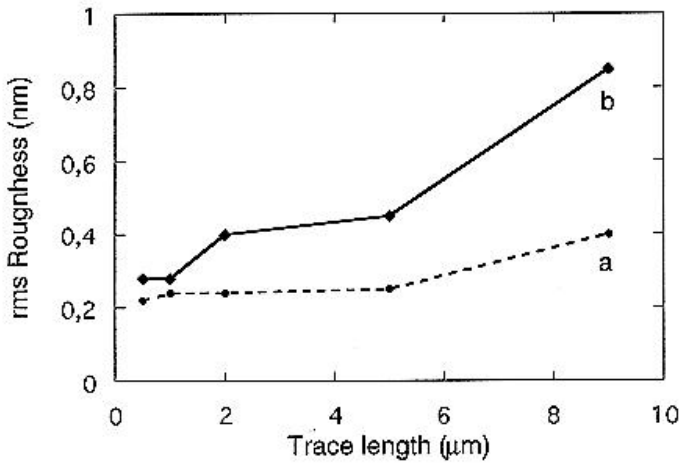

Figure 1. Variation of the rms roughness measured on AFM height profiles using relation (1) as a function of the profile length for two glass samples. a: clean float glass, air side, b: sample a after etching in a dilute solution of NaOH.

If we assume that h(x) is a random variable, as, for example, noise vs. time is in electronics, we can describe the roughness by its spectral density g(q):

$$g(q) = 1/q\ |H(q)|^2 \qquad (2)$$

where H(q) is the Fourier transform of h(x), and q is the wavenumber in the Fourier space.

As already stated, whatever the experimental method used, h(x) is measured in a limited spatial interval [L/N ; L]. Consequently, only a well defined domain of the spectral density g(q) can be inferred from each experimental profile. This domain is limited by, roughly, the two cut-off wavenumbers (or spatial frequencies) L^{-1} and $(L/N)^{-1}$.

In order to get g(q) over a large wavenumbers range, we make the superposition of different g(q) sections obtained from profile measurements in different spatial intervals. AFM is used to record short traces, below 100 : m, and MP is used for long traces, up to 5 mm.

In return, from the knowledge of g(q) for a given sample, it is possible to predict the rms roughness value σ_{rms} that would be measured on this sample by using any experimental technique, provided that the two cut-off wavenumbers q_{min} and q_{max}, that characterize the technique, are known. This value is given by:

$$\sigma_{rms} = \sqrt{\int_{q_{min}}^{q_{max}} g(q)\, dq} \qquad (3)$$

For example, in an optical interferometry measurement, q_{min} would be the inverse of the dimension of the light beam and q_{max} would be the inverse of the optical wavelength.

III. EXPERIMENTAL SECTION

Squared samples, 1 x 1 cm^2, were cut from a plate of glass. When float glass is used, only the air side of the sample has been examined.

It is important to choose a well-defined cleaning procedure, if a reliable comparison between various kinds of glass is desired. In this work, the following treatment was used:

. washing in clean water + Liquinox detergent, for 30 minutes, at 30°C, in an ultrasonic bath.

. rinsing in deionized water

. drying in a pure nitrogen gas flow

. UV irradiation under an 0_2 gas flow for one hour.

This last step is very efficient for the elimination of carboneous contaminants [2]. However, it leaves the surface with small inorganic contaminations, possibly sodium carbonate crystallites, as it can be seen on the AFM image given in figure 2.

After cleaning, the sample is mounted on the AFM head. We used a Park Scientific Instruments AFM, which is used both for standard imaging and for recording linear height profiles. In this latter case, a trace is chosen on the surface in such a way that it does not cross any of the crystallites described above. In fact, three different AFM heads are used successively, in order to record three traces of different length: 2.5 : m, 10 : m and 100 : m. As the software of the AFM does not allow for traces with more than 512 data points, a special subroutine has been written and the data has been aquired using an analog-to-digital conversion unit, model 2505 from Tektronix. It is thus possible to record 10,000 data points for each trace.

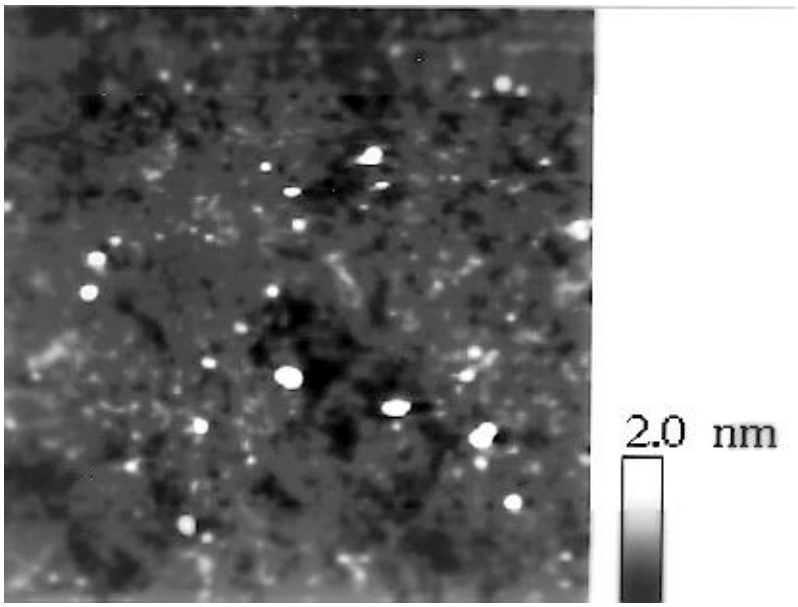

Figure 2. AFM image of a 2 x 2 : m^2 region of a float glass sample cleaned as described in text. The height grey scale, from 0 to 2 nm is given on the right. Small inorganic contaminants appear in white.

A Dektak model 1600 mechanical profilometer is used to record a height profile over a trace 5 mm long.

Therefore, for each sample, four height profiles are recorded, the mathematical treatment described in part II is used to compute the four different sections of the spectral roughness density.

IV. RESULTS AND DISCUSSION

On figure 3 are given in logarithmic scales the results of the roughness analysis performed on the air side of float glass. It can be seen that the overlap between the four different sections of the spectral density is quite satisfactory. Although a few points are dispersed, due to electronical noise during the profile recordings, most of them can be fitted, over more than six decades, using a power law $g(q) \propto q^{-a}$, with a =1.73. It is worth noting that this behavior extends the result obtained by Dumas et al. on a smaller spatial range [3], although that, strickly speaking, the materials are different and should not necessary have the same roughness exponent. The power-law dependence is also compatible with the theoretical variation that is expected for a self-affine surface of roughness exponent ζ[4]:

$$g(q) \propto q^{-(1+2\zeta)} \qquad (4)$$

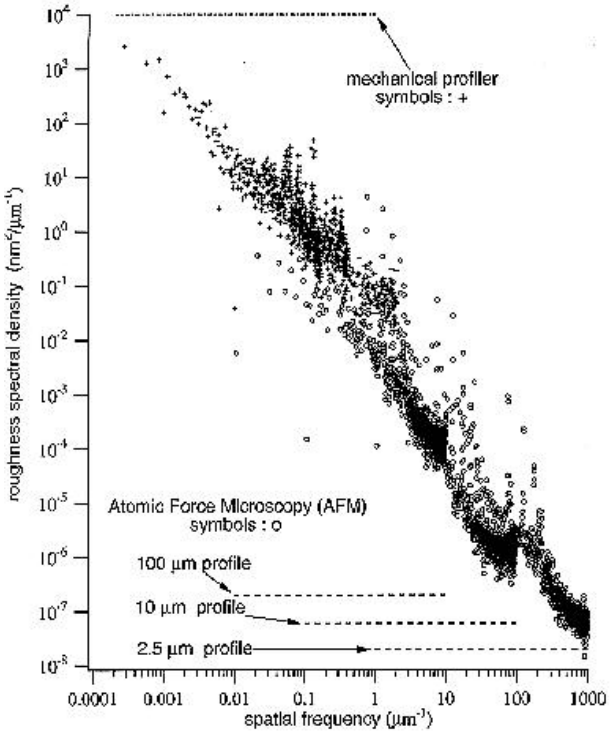

Figure 3. Roughness spectral density of the air side of a clean float glass sample. As explained in text, it is obtained from the roughness analysis in four different wavenumber domains, using experimental height profiles of different length measured by AFM for the three shorter ones and by mechanical profilometry for the longer one.

We recall that a self-affine surface is kept invariant by the transformation $(x,y,z) \rightarrow (\mathbf{8}.x, \mathbf{8}.y, \mathbf{8}.z \cdot)$, where $\mathbf{8}$, is a scaling factor and z is the direction perpendicular to the surface. Therefore, we conclude that the surface of float-glass is self-affine, with a roughness exponent equal to 0.36. We want to emphasize that the self-affine geometry is a very powerful approach of surface topography, as it can be shown by the analysis of fractured glass surfaces [5], for which two roughness exponents are relevant.

In order to compare quantitavely the roughnesses of different glass surfaces, including superpolished surfaces of two optical vitroceramics [6], we have chosen the spatial spectral range [10 nm ; 100 **:** m]. By integrating expression (3) between these two cut-off values, we have obtained the rms roughness values given in table 1.

sample	rms roughness (nm)
as produced float glass (air side)	0.45
optically polished float glass	0.82
superpolished amorphous silica	0.45
superpolished Borkron®	0.25
superpolished Zerodur®	0.43

Table 1

Float glass is found remarkably smooth up to the tenth of millimeter scale, at least. No polishing procedure able to lower this value has been found. It is only by using special substrates, such as optical vitroceramics, and superpolishing techniques that a significantly smaller roughness has been measured.

V. CONCLUSION

In this paper, we have shown that the analysis of surface topography should be carried out in two steps. First, localized defects (e.g. contaminants) must be identified since they are likely to obey a peculiar statistics in terms of size and spatial distribution. Second, wherever this is possible, the height vs. position may be treated as a random variable which is well described by the roughness spectral density. This approach permits to reconcile the results obtained by different experimental techniques. In the case of glass, the power law behavior which is observed over almost seven decades supports the relevance of self-affine geometry to model the surface.

REFERENCES

[1] J.M. Bennett and L. Mattson. Introduction to Surface Roughness and Scattering (Optical Society of America, Whashington, D.C.,1989)

[2] P. Na**N**l, H. Arribart and J. Jupille, Proceedings of the Fourth Conference of the European Society of Glass Science and Technology, V@xj ` , Sweden (1997)

[3] P. Dumas, B. Bouffakhreddine and C. Amra, Europhysics Letters 22 (1993) 717

[4] B. Mandelbrot, D. Passaja and A. Paullay, Nature 308 (1984) 721

[5] B. Nghiem, E. Bouchaud and F. Creuzet, to be published

[6] These two samples were studied in the framework of the EEC Research Program n°3425/1/0/185/91/4-BCR-D(30) " Characterization and development of surfaces with roughness in the 0.1 nm range "
For a report, see:
G. Ringel, F. Kratz, D.R. Schmitt, J. Mangelsdorf, F. Creuzet and J. Garratt, SPIE vol. 2536 (1995) 317

AUTOMOTIVE GLASS-A NUMERICAL METHOD OF MODELING FORMING PROCESSES AND OPTIMIZING OPTICAL DISTORTION*

Alejandro G. Bueno
Glasstech Inc., USA

Abstract

The complexity of surface design for automotive windshields and back-windows has presented new challenges to the suppliers in the glass industry . The refractive and reflective optical distortions, through and from a glass surface, become highly objectionable with increasing curvature and angle of incidence. Such is frequently the case with recent automotive styling trends. Additional distortions are introduced by the forming process which induces strains in the glass sheet; these are primarily compressive strains along or near the edges which cause localized wrinkles.

A method has been developed for the evaluation of optical in quality in formed automotive glass which takes into account the material behavior of glass, the forming process and the required design geometry. The method uses mathematical modeling techniques. A forming process can be modeled by describing all the operational parameters which influence directly on the deformation of the glass sheet. The resultant surfaces can be further manipulated by the model to minimize the distortions by following a prescribed criterion, such as the rate of change in curvature and localized optical distortions.

This method provides the automotive body engineer with a tool optimize the surface definition of the windshield or back-window for minimum optical distortion.

---

* Full manuscript not available at the time of printing

FORCED CONVECTION - THE SOLUTION TO TEMPERING LOW EMISSIVITY GLASS

Jorma Vitkala
Tamglass Engineering Oy, Finland

Abstract

It is problematic to heat up Low-E glass in a traditional radiation type furnace, because the glass will bend during the heating cycle which leads to different problems such as viscoelastic changes, coating distortion, surface defects, uneven bending etc.

If we add forced convection to radiation furnaces it becomes possible to temper Low-E glass with the current manufacturing methods on the market. However, the emissivity requirements will be lowered in the future and for this reason we need new manufacturing solutions. One such solution is the use of a high convection furnace.

This paper will give you an idea about the latest developments and test results in this field.

INTRODUCTION

I shall use the case of tempering Low-E glass for the purpose of describing the application of convection in a demanding process for a product growing in popularity.

Before the 90s, furnaces were mostly designed for the tempering of clear glass. For this reason, the main focus at the time was on even application of radiation heating in the furnace.

This was quite understandable, because clear glass has high emissivity and it absorbs heat very well. When the new low-emissivity glass products hit the market at the end of the 80s and early 90s, great difficulties in tempering of this kind of glass were initially experienced.

Most of the problems resulted from the unsymmetrical emissivity of the coated glass. See Figure 1.

The bottom of the glass displayed high emissivity and absorbed heat effectively, the coated side with low emissivity reflected heat radiation. This unsymmetrical behavior led to the bending of the glass in the furnace, as the uncoated bottom of the glass heated up more quickly.

The situation could have been helped by placing the coated side against the rollers, which would have resulted in less curving. This method has not, however, been used in Europe, because it causes defects to the coating.

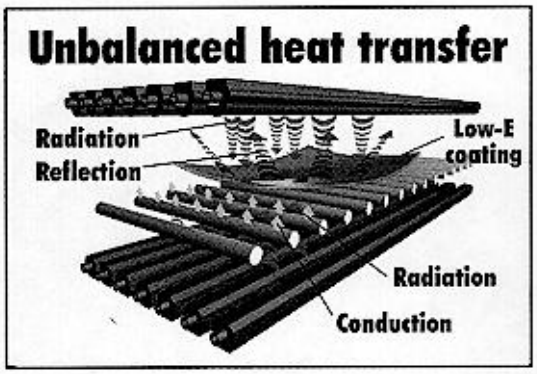

Fig. 1 UNBALANCED HEAT TRANSFER- A REASON FOR PROBLEMS

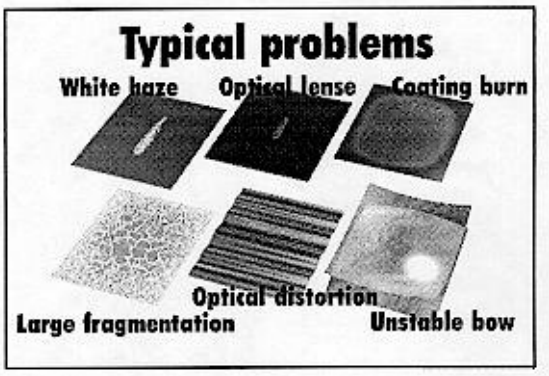

Fig.2 TYPICAL PROBLEMS

When the coating is on the top of the glass, the curving causes the following typical problems as displayed in Figure 2.

1. White haze
2. Optical lens
3. Coating burn
4. Large fragmentation
5. Optical distortion
6. Unstable bow

Low-emissivity glass has been available on the market since the 80s. Its emissivity was, however, rather high by today's standards. It was not until the late 80s and early 90s that toughenable Low-E glass with an emissivity of 0.1- 0.23 became available.

The demand for Low-E glass is expected to grow very quickly in the future. A typical indication of the preference put on this product is found in German legislation, where the requirements to save energy are so tough that Low-E glass is practically always required in window structures. The same trends are also visible in other European countries.

HEAT TRANSFER

The design of the heating section in a tempering furnace requires that the heat transfer process between the glass plate and the furnace environment is understood. This is also necessary when the furnace behavior is adjusted for different types of glass. In order to understand the importance of different heat transfer processes, the conduction in glass, radiation, convection and conduction from the rollers must all be considered.

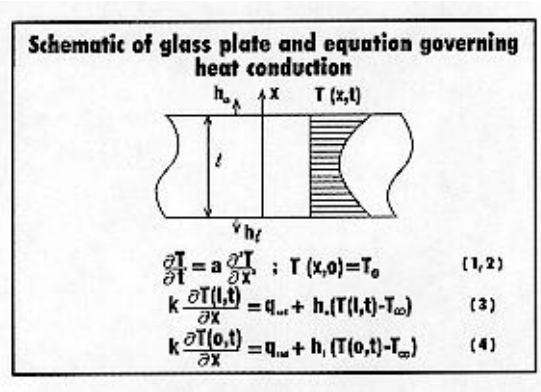

Fig.3

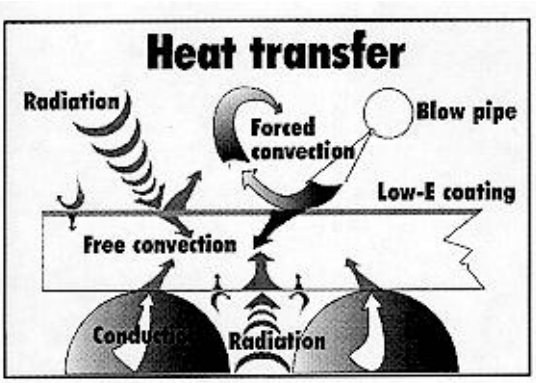

Fig.4

The temperature distribution of a glass plate as in Figure 3, is governed by the well- known heat conduction equation:

$$\frac{\partial T}{\partial T} = \alpha \frac{\partial^2 T}{\partial x^2}$$

where T is the temperature of the glass, t and x stand for time and space and a is the thermal diffusivity.

In order to solve equation (1), initial and boundary conditions have to be fixed. Using the notations of Fig. 3 they are:

$$T(x,0) = T_o$$

$$k \frac{\partial T(l,t)}{\partial x} = q_{rad} + h_u(T(l,t)-T_\infty)$$

$$k \frac{\partial T(0,t)}{\partial x} = q_{rad} + h_l(T(0,t)-T_\infty)$$

In the equations above q_{rad} is radiation heat exchange between the furnace and the glass, h_u and h_l are convective heat transfer coefficients of the upper and lower surfaces respectively. h_l also includes conduction heat transfer from the rollers. k is the thermal contactivity of the glass. T_o is the glass temperature before it goes into a hot furnace.

The solution to equation (1) is straight-forward with a numerical method if the boundary conditions (3) and (4) are known. According to equations (3) and (4), heat transfer from the top and bottom surfaces should be the same and uniform. For instance, if the emissivity of the glass to be heated is changed, it affects the radiation heat transfer q_{rad} . In order to keep the heat exchange from the top direction constant, convective heat transfer should be changed by the application of forced convection.

In order to control the heat transfer process of tempered glass, theoretically, the spectral radiation properties of the glass should be known. The understanding of convective heat transfer is most difficult. It has been approached with numerical simulation as well as experimental measurements. Heat transfer from the rotating rollers on the bottom side of the glass is also all but understood.

FORCED CONVECTION HEATING METHODS - THE SOLUTION TO TEMPERING LOW-E GLASS

In this context, convection is defined as heat transfer by a flow of air.

Glass can be heated or cooled by applying convection. When it is heating glass, the heat is moved to the surfaces of the glass with the aid of air flow. The heat then penetrates the glass through conduction.

The coefficient which denotes the speed of heat transfer is called alpha. It expresses the rate of speed at which heat can be applied to the surface of an object and conducted into it.

When heat is transferred by convection, the efficiency of the process depends mainly on the speed of the air flow and the difference in temperature between the glass to be heated and the surrounding air (Figure 4).

We are dealing with a complicated process and I shall not go into too much detail about that in this presentation.

A cold glass sheet to be heated in a furnace is affected by different types of heat transfer phenomena which are shown schematically in Figure 4 (Heat transfer).

Traditionally, radiation heating from hot, electrically heated resistance elements in the ceiling of the furnace is used.

When dealing with coated glass, however, this technique is not suitable because coated glass does not absorb radiation as effectively or as symmetrically as clear glass. In addition to radiation, we always have the presence of natural convection from the top and bottom surfaces of a glass plate. The heat transfer is not uniform, but rather results in a large temperature variation.

In order to avoid temperature non-uniformities in a radiation-type furnace, forced convection heating has been applied. Tamglass's first patent in this area is actually from 1980. Forced convection is applied by arranging small jets, from which air is injected in order to create a forced flow. The design of a jet configuration which leads to a uniform heat transfer coefficient is a complex problem.

Another heat transfer mechanism, in addition to those mentioned above, is the heat conduction from the rotating support rollers. That in turn, depends on the material properties of the rollers and on their geometry.

CONVECTION HEATING METHODS IN THE GLASS INDUSTRY

Convection has certainly been applied in a number of different ways in different types of processes. Convection has always been used in autoclaving. Convection is applied for the first stage in which the glass sheets need to be heated up to 130 degrees C and cooled down again before any pressure can be released.

Or take the case of windscreen production. In the pre-pressing stage of that production hot air is circulated around the glass pair while maintaining vacuum between them. In this way the glass panes and the PVB couple together before autoclaving.

Convection applies to bending in windscreen processes as well. That has actually been the case since 1985. Convection is used in the front end of the furnace to cool down glass which has already been bent. The energy released is transferred to the pre-heating stage of the glass.

Convection is not used just to transfer heat energy from the glass to be cooled to the glass to be heated. This process also ensures that the low- emissivity stainless steel mold heats up

simultaneously with the pair of glasses. It is a well known fact that emissivity is of no consequence in the convection heating method. The new solutions apply to the use of forced convection.

Flat laminating lines also utilise convection. The PVB is first heated up by short-wave radiation before the first pressing. The short-wave radiation penetrates the glass and is absorbed into the PVB. After the pre-pressing stage, forced convection is applied. Achieving a uniform temperature is vital when laminating Low-E or multiple-layer glass applications.

FORCED CONVECTION IN TEMPERING TECHNOLOGY

Flat tempering furnaces have used forced convection since 1980. That coincides with Tamglass's first patent in the area. The method was later modified to meet today's needs.

Forced convection, so called "Heating Balance", is used to compensate the heat transfer flow and to make the top and bottom surfaces of the glass heat up at the same speed. As a result, the glass remains flat during the heating process (Refer to Figure 4 - heat transfer). This is of particular importance in the case of Low-E glass.

It is well known that keeping glass, particularly Low-E glass, flat during the first half of the heating cycle is most difficult. To avoid the problems in this area there are four different possibilities:

1. the use of a one-stage radiation furnace and forced convection

2. the use of a two-stage radiation furnace with forced convection

The principles of one- and two-stage furnaces were explained earlier.

3. the use of a one-stage high-convection furnace (see Figure 5), or

4. the use of a two-stage convection system (see Figure 6).

HIGH CONVECTION SINGLE CHAMBER FURNACE

The Cattin high convection furnace is a very compact roller hearth furnace. The furnace design is modular and the top and bottom furnace shells are symmetrical.

The inside nozzle system generates a high convection heat transfer to both surfaces of the glass panels with reduced pressure loss of the circulating hot air and a high air exchange rate. The uniformity factor of the temperature distribution inside the furnace is very high due to the special nozzle tube system.

The glass charge is heated up to the tempering or bending and tempering temperature in such a way that non-uniformities of heat transfer for top and bottom of the glass sheets (i.e. reflective layer of Low-E glass and thermal conduction between ceramic rollers and the lower glass surface) are compensated for by the control of the top and bottom furnace ventilators. The thermal shock, especially for thicker glass (10 mm and more) is also eliminated by reduced heat transfer during a certain time at the beginning of the heating cycle. The optimal operating point of the top and bottom hot air ventilators can be easily reached by the continuous and accurate control system.

For this reason, the larger sized glass panels of more than 4 square metres can be kept very flat in the furnace during the whole heating process. The mechanical distortions of the lower surface are minimised for each glass thickness and thus for the weight of the glass sheet.

The phenomenon of anisotropy can be positively influenced by reduced furnace temparatures without any significant reduction of productivity.

Independent of the kind and type of glass (coated, tinted, structural or clear), the heating time will be shorter because the asymptotic heat-up curve has a steeper gradient at all times in comparison with the heat-up curve of glass heated in a radiation furnace.

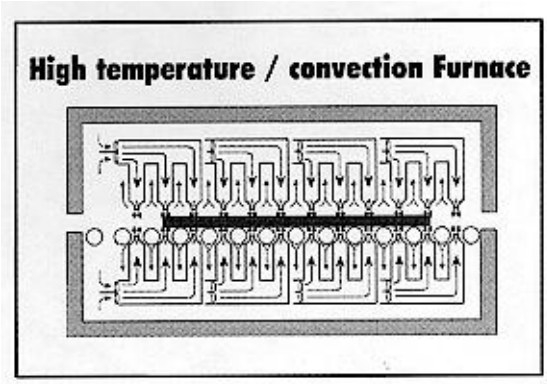

Fig.5

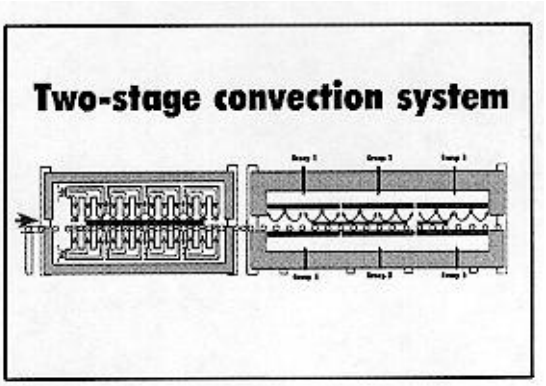

Fig.6

TWO STAGE CONVECTION FURNACES

In a two-stage high-convection furnace, the first furnace would be heated up to around 400 degrees C and the heating method would be high convection produced by blowers. See Figure 6.

In a low-temperature convection furnace, the glass is pre-heated in what is known to be the most difficult part of the process. It is natural that the control of temperature and heat flow are easier at lower temperatures.

Once the glass sheet has been heated up in the first chamber it is moved into the second furnace. In this chamber heating is applied by convection and radiation. The key point in this part of the process is that we can focus heat by radiation and a sophisticated heating system on the middle of the glass sheet which is necessary in order to heat up a large glass surface evenly.

An important point is that this works well for both thin and thick glass, such as 3 -19 millimeters can be processed without difficulty in this kind of process.

This way we can also be sure that the glass does not break inside the furnace and we can send this evenly pre-heated glass to the second furnace where convection and radiation are used.

Whatever the application of convection, the soul of the process always remains the furnace itself. Even if we use high-convection in the furnace, radiation is a factor which must be considered. The structure of the cooling section is also very important because it influences the tempering glass quality.

I should mention here that our experiences of how to temper Low-E glass are based on the products listed in Figure 7 (Toughenable Low-E glass).

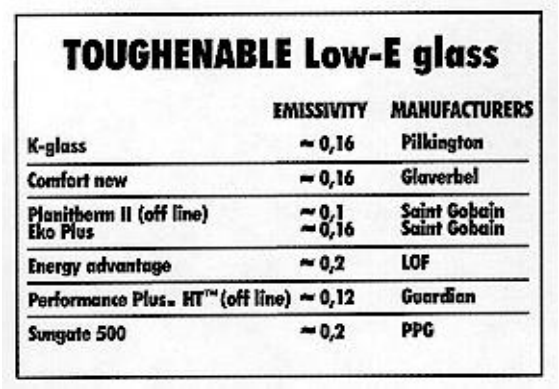

TOUGHENABLE Low-E glass

	EMISSIVITY	MANUFACTURERS
K-glass	~ 0,16	Pilkington
Comfort new	~ 0,16	Glaverbel
Planitherm II (off line)	~ 0,1	Saint Gobain
Eko Plus	~ 0,16	Saint Gobain
Energy advantage	~ 0,2	LOF
Performance Plus™ HT™ (off line)	~ 0,12	Guardian
Sungate 500	~ 0,2	PPG

Fig.7

When new coating materials are introduced, we usually carry out the first test runs at our factory in cooperation with the manufacturers. From time to time, we also get involved directly in the setting of process parameters with our customers.

CONCLUSIONS - 4 MM LOW-E

	Radiation furnace	High-convection	Two-stage convection system
Heating time/batch	200 sec ± 5%	125 sec ±5%	100 sec ±5%
Top temperature	675 - 695 °C	680 °C	350/695 °C
Tempering pressure	+10...25%	+10%	10...25%

In summary, our findings are that successful tempering of Low-E glass requires even and proper control of the heat transfer during the heating cycles where convection plays a very important role.

This presentation is a modification of an address given by Mr. Jorma Vitkala during the Glass Processing Days at Tampere in 1995 prepared jointly with professor Reijo Karvonen of the Tampere University of Technology and Dr.-Eng. Volker Thiessen of Cattin Machines S.A.

INCREASING PRODUCTION IN A SHEET GLASS FURNACE

Hande Sengel
SISECAM Research Center, Turkey

Selçuk Demirkiran
Çayirova Cam San. A.S., SISECAM, Turkey

Abstract

With an attempt to meet the increased demand for sheet glass from the market, a multidisciplinary program has been applied to a sheet furnace at the eighth year of its campaign to upgrade the glass quality, improve production performance, and decrease cost.

The goals of the study were set as; increasing net furnace pull by 5%, net production by 8% and the machine life by 10%.

Each of the above mentioned goals were assigned to a team as a project. The furnace pull was increased by securing the sagging refractory blocks in the furnace, minimizing the regenerator problems resulting from the furnace age, optimizing the batch chemistry, and temperature profile in the furnace.

The melt production and machine life was increased by taking the necessary precautions as a result of analyzing the reasons for reduced productivity due to aging in the furnace and short machine life.

1. INTRODUCTION

At the eighth year of its campaign, a flat glass furnace, producing sheet glass with Pittsbourgh technology, was facing certain production problems. These problems have mainly originated from the lack of energy fed to the furnace because some refractory blocks in the regenerator packing were damaged, and the sagging blocks, especially at the port arches carried the risk of falling. As a result, the glass defects have increased and the pull decreased.

In 1995, with an attempt to meet the increased demand for sheet glass from the market , an upgrading program has been applied out to eliminate the existing problems and increase production, improve glass quality and decrease cost.

This presentation reports the work done to reach this aim and results obtained.

2. PLANNING AND CONTROL OF THE UPGRADING PROGRAM

The goals of the upgrading program were set as;

1. increasing furnace pull by 5%,
2. increasing net production by 8%,
3. extending the machine life by 10%.

For realization of these goals, a multidisciplinary action was planned and applied as a team work. Three different teams were set, and to each of them, one of the goals mentioned above, was assigned as its project. Project teams defined their sub-targets as an integral part of the main target and made and applied their project plans.

3. EXECUTION OF WORK

3.1. Project No-1: Increasing the Pull Rate

3.1.1. This project was handled as three sub-project. Regenerator Problems and Solutions

The furnace was side-fired and had box-type vertical regenerators. Especially for the first 3 regenerator chambers, the following problems, which affect melting and therefore the pull rates negatively, were considered:

1. Breakage and corrosion of cruciform blocks which were used at the upper course of the regenerator packing,
2. Damage and sagging of blocks in lower courses, and
3. Intensive clogging at the cold regions.

These problems prevented the transfer of sufficient air, and thus energy, to the melting area, decreasing the melting capacity of the furnace. Existing air cross section was about 20% of the necessary amount.

Since it was ascertained that breakage and sagging at the upper courses blocked the air gates from the bottom level, the upper cleaning doors of the regenerators were released and the bricks in this region were removed.

As expected the source of blockage in the cold section was sulphate condensation. Longer inversion periods (45 minutes instead of 30, increased in a stepwise manner) were applied for 3 days, to melt down the condensed sulphate. In order to eliminate this problem completely, the flow-down process was carried out periodically by heating the regenerators from the bottom by gas burners.

3.1.2. Problems Due to Furnace Refractory Structure and Their Solutions

To increase the pull rate of the furnace, it was planned to reset the temperature profile of the melting chamber. This change in temperature profile would result in new expansions and shrinkages of the furnace refractory structure and cause the existing broken blocks to partly fall down to the bottom of the ports, especially at the port arches.

The sagging blocks in the port arches were supported by pipe coolers inserted into the ports through holes drilled at the bottom of the ports. The top of these risky port arches were covered with Zircon mortar.

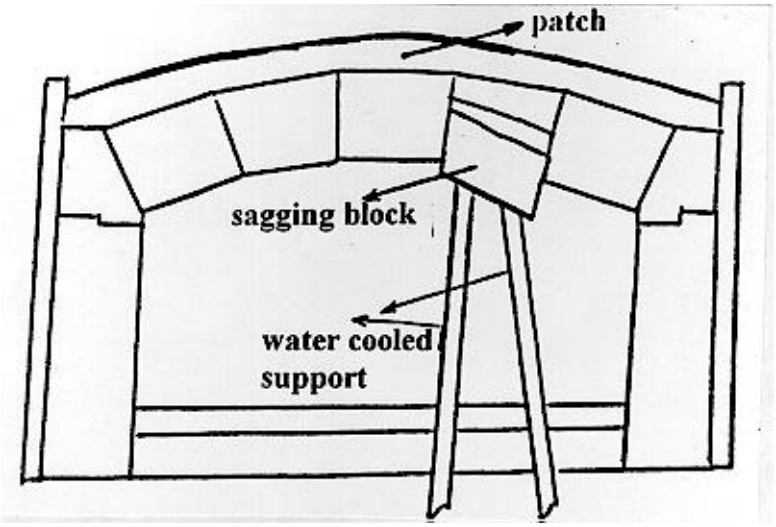

Figure 1: *Securing the sagging block*

3.1.3. Development of batch and glass composition

In addition the work carried out on the furnace itself, measure to modify the working properties of glass, was also undertaken to increase the pull rate of the furnace. The chemical composition of the glass was modified to make the glass "shorter" and easier to melt. Another dimension in this compositional modification was to decrease both the liquidus temperature and the crystal growth rate of the glass. Thus, the negative effect of devitrification on the machine life would also be minimized.

In conventional soda-lime-silica glasses, the mechanisms which affect both the viscosity properties and the crystallization character of the glass are:

1. The very strong Al-O bonds. Al_2O_3 increases the viscosity and reduces the tendency for devitrification by decreasing the liquidus temperature, when present up to 4% in a soda-lime glass compositions and by suppressing crystal growth.

2. The single electron on last orbital of sodium ion. This can make non bridging Na-O ionic bonds, which reduce the overall bond strength of glass and thus, decrease viscosity. However, the reduction in high temperature viscosity causes the crystal growth rate to increase in lower temperatures.

3. The bond strength of bivalent Ca^{++}. It is double that of monovalent Na^{+} and results in a distinct strengthening of the structure when substituted for Na_2O. It makes glass "shorter" while increasing both the liquidus temperature and crystal growth rate.

With the use of this information, in the present work, the Al_2O_3 content of the glass was increased by 0.15% and total alkali earth oxides was increased by 0.15% but reducing the CaO/MgO to dolomitic ratio. After this variation in the chemical composition of the glass, the new composition displayed the following properties (Table1).

Table 1: *Physical Properties of the glass before and after the modification.*

	Before modification	After modification
Melting temp., C (log = 2)	1458	1458
Gob temp. C (log = 3)	1201	1202
Working temp. C (log = 4)	1033	1034
Softening pt. C (log = 7.65)	722	725
Annealing pt (log = 13)	544	547
Working Range (Gobtemp.-Soft.pt)	479	477
Liquidus temperature	941	929

As can be seen from Table 1, low temperature viscosity values increased by 3 C, while keeping the high temperature viscosity almost constant. As a result, the glass became shorter, resulting in an increase in the pull rate at the machines. Another important property observed during this compositional change was the crystallization character of the glass. The liquidus temperature was decreased by 10 C and the crystal growth rate reduced (Figure 2).

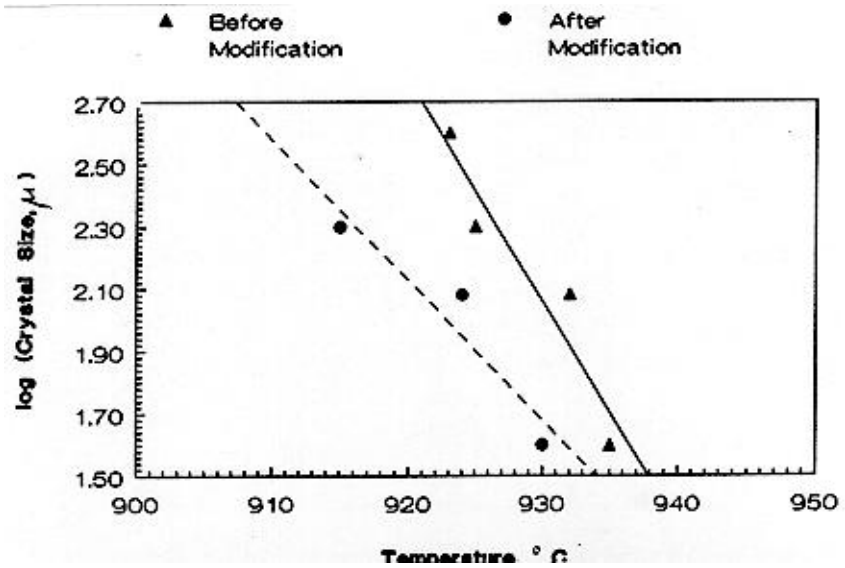

Figure 2: *The results of the crystal growth study*

3.1.4. Sub-project-4: Improvement of the Furnace Temperature Profile

The maximum crown temperature at the six-port furnace was originally located at the third port axis. Because of the problems of the first 3 ports, sufficient energy could not be supplied to the region between the doghouse and the hot-spot. The batch sometimes forced and passed the hot spot, resulting in seedy glass with many stones.

Increasing the furnace pull with the present temperature profile was decided to be impossible, and the hot spot was moved from the 3rd to the 4th port axis. With this operation, the fuel load on the problematic first three ports was decreased, and the melting area between the doghouse and the hot spot was increased.

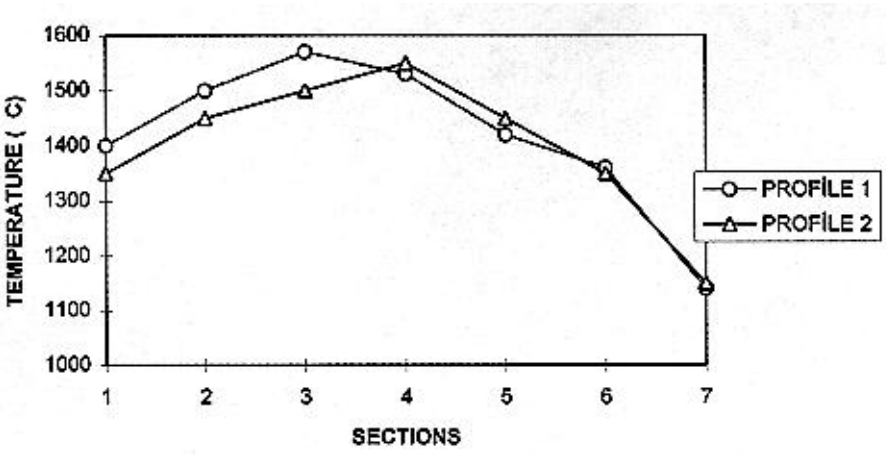

Figure 3: *Temperature profiles of the melting area*

3.2. Project No: 2: Work to Increase the Net Production

3.2.1. The Determination of the Factors which Cause Production Loss

To analyze the reasons for production loss and determine their share in the total loss, a database covering 30 day observation period has been developed.

By the evaluation of the data; the following defect levels were determined.

1. Stones, knots and other inclusions : 70%
2. Annealing faults : 20%
3. Edge quality faults : 7%
4. Others (mechanical and electrical failure, personnel, etc.) : 3%

From the microanalytical observation of the stone defects it was determined that they have originated mostly from the wash down of the superstructure in the melting zone and glass contact corrosion giving rise to primary and secondary AZS.

Annealing faults were due to the variations in air flow and environmental temperature, resulting from natural cooling in the annealing lehr.

3.2.2. Work to Eliminate Glass Defects

Existing literature and the result of the physical model studies for similar furnaces were reviewed.

The behaviour of the stones in the glass flow was speculated. As a result, the water coolers were submerged more deeply into the glass to enhance back currents.

These measures, together with the improved temperature distribution in the crown, resulted in the decrease of stone defects to a minimum. With the application of homogeneous forced cooling on the glass surface during annealing, glass temperature fluctuations were diminished, and thus, gave rise to a reduction in annealing losses.

3.3. Project No: 3 : Work to Extend Machine Life and Shortening Down Time

The development in glass composition in the direction of decreasing the crystallization temperature extended the machine life.

The work done during the renewal of machinery were examined by applying CPM, and the overall process time was shortened.

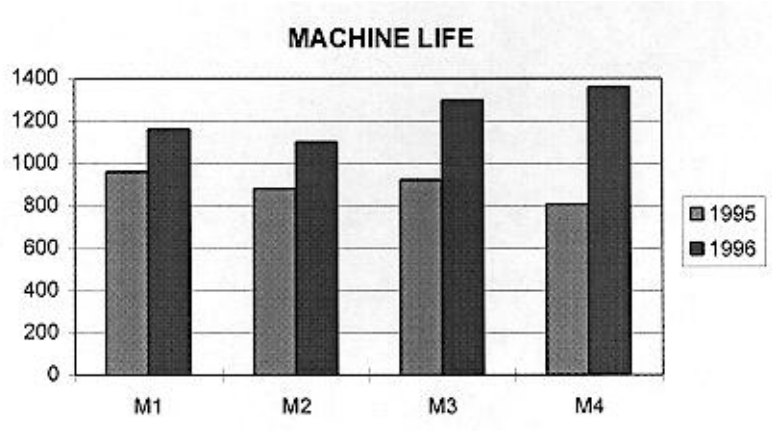

Figure 4: *Machine lives*

4. RESULTS

Furnace pull and fuel consumptions before and after the studies to increase the pull rate were carried out are given below.

As can be seen from the figure 5, with the work described above, it was possible to increase the pull by 4.3% and reduce specific fuel consumption by 1%.

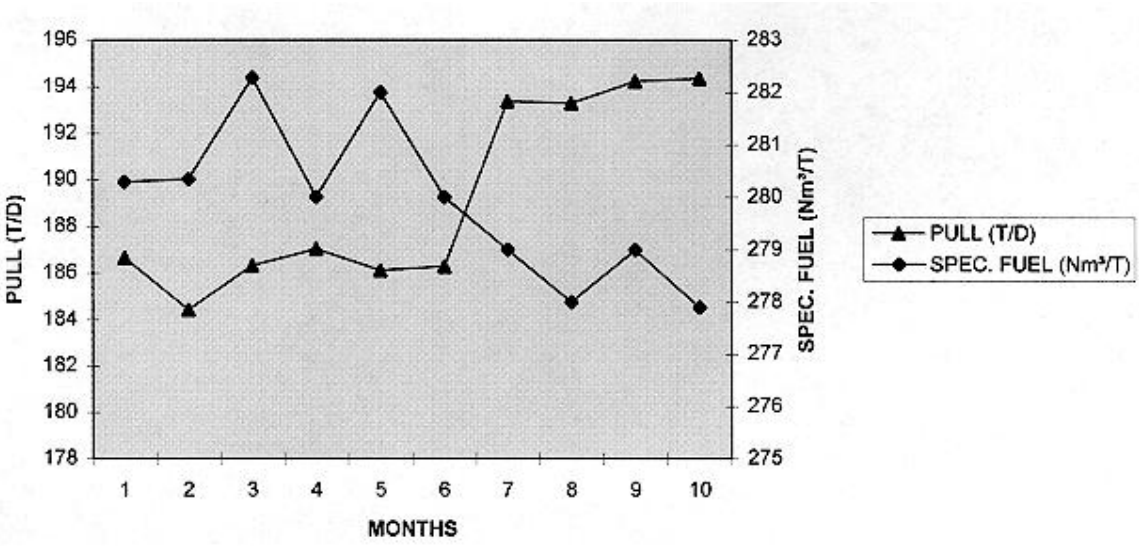

Figure 5: *The variation of pull rate and fuel consumption in 1995*

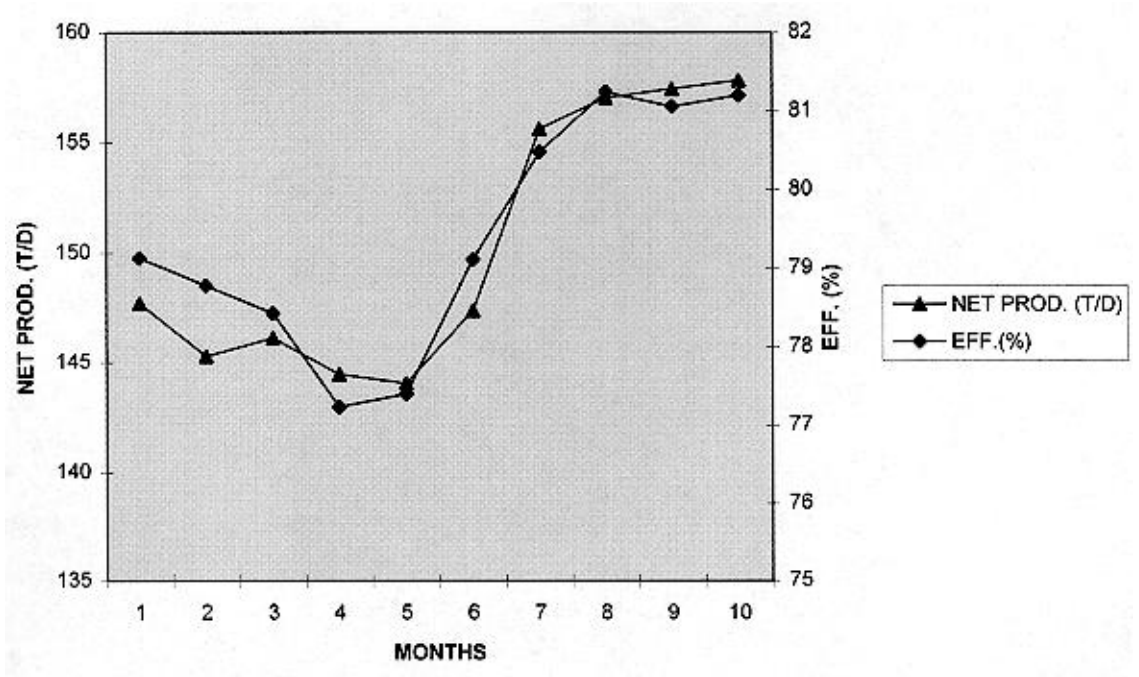

Figure 6: *The variation of net production and yield in 1995*

Net production and pull values before and after the studies were to increase the net production rate carried out are given in Fig. 6 The figure shows that by taking the measures described above, the net production and machine life increased by 6.8% and 36%, respectively.

5. CONCLUSIONS

With an attempt to meet the increased demand for sheet glass from the market, a multidisciplinary upgrading program has been applied to a sheet glass furnace at the eighth year its campaign. The main aspects of the upgrading program were to solve the problems resulting from furnace age, and thus to increase production performance and to improve glass quality.

The fundamental approach of this upgrading program was based on a multidisciplinary team work. Each team was assigned a certain project, which were the goals of the program. Creation of sub-teams, when necessary, increased the number of people involved in the program. Close follow-up and coordination of the work of different teams were the key factors in meeting the goals.

At the end of the upgrading program, the following goals were met:

1. The pull was increased by 6%.
2. Net production was increased by 8%.
3. Machine life was extended by 10% and the glass quality improved.

In addition to the accomplishments listed above, the program improved knowledge, experience, and above all, the motivation of the participating personnel and their dedication to team work.

PRODUCTION OF TEMPERED HOLLOW WARE*

Gérard Coudamy
CERIC, France

Abstract

Tempering of tableware is a process which has been in for many years. It imparts improved resistance to resistance to mechanical damage and thermal shock as well as reducing the risks of personnel injury when breakage does occur.

Tempering of hollow ware is very different from tempering of flat glass. For the latter the only stresses are those related to the speed of cooling. For the former, superimposed on these "tempering" stresses there are stresses resulting from the shape and differing glasswall sections of the articles.

The physical laws which control the formation of these two types of stresses are not the same. A separate study of each of the stress producing mechanisms has enabled a new technology to be developed for tempering hollow ware. This technology offers a significant improvement in article quality compared with traditional methods, and also makes it possible to widen the range of glassware which can be tempered to include thin walled and deep articles.

---

* Full manuscript not available at the time of printing

OPTICAL AND CHEMICAL MODIFICATION OF FLOAT GLASS SURFACES

Bülent E. Yoldas
Carnegie Mellon University, USA

Abstract

Float glass surfaces can be modified to induce optical, chemical and mechanical behaviors to create entirely new lines of products. Some of these modifications can be done on-line processes which adds very little to the overall cost. Among these are: formation of stain and corrosion resistant surface, formation of antireflecting and IR-reflecting surfaces, creation of a permanently hydrophobic glass surface, and strengthening float glass by a solid-state ion exchange process. In this presentation, a number of concepts by which float glass surfaces can be modified, particularly creation of antireflective and stain resistant surfaces with sol-gel processes, are discussed. Performance tests associated with these modified surfaces indicate that these concepts have considerable commercial potential.

1. INTRODUCTION

Composition of float glass is primarily dictated by properties that allow its production on float lines; a process which necessitates production of only large quantities. Any modifications to produce specialty products therefore, are severely confined. A method of circumventing this confinement is to modify float glass surfaces either on line processes or coatings. Vacuum coating and sputtering have been widely used for this purpose. Another method available is on-line spray deposition of films from solutions. Suitable precursor solutions can be sprayed on hot glass, depositing inorganic films ranging in thickness from several nanometers to several microns. These films interact with the surface creating optical and chemical effects with significant value-added attributes to[1]. Some of these effects are produced by changing the chemical composition of the surface, e.g., chemical durability, hydrophobicity, etc. Sol-gel deposited films produce optical effects which cannot be produced by any other way, e.g., non-scattering microporosity for antireflectivity, etc. In this presentation, several applications of these concepts are briefly discussed to point out the vast potential for producing specialty float glass products by surface modifications.

2. FORMATION OF WIDE SPECTRUM ANTIREFLECTIVE COATING

Float glass reflects 8% - 8.5% of the incident light from its surfaces (Figure 1). Under certain lighting conditions, this reflection can overwhelm the transmitted light, seriously impairing vision. Fraunhofer and Rayleigh observed almost a century ago that the reflection can be reduced by chemical treatment of the glass surface[2,3]. In these

methods, the reduction of the reflection does not lead to an increase in the transmission as is the case in the optical antireflective coatings.

A transparent material whose index of refraction is equal to the square root of that of the glass, when deposited as a quarter wavelength thick film on that glass, provides an interference minimum in the reflectivity. There is no inorganic material that would satisfy this low index requirement of a single-layer antireflective coating for a commercial soda-lime glass. MgF_2, with an index of 1.38 (vs. ~1.23 needed), is the lowest index coating material available and widely used in the glass industry.

The index of refraction is a function of density and thus may be further lowered by the introduction of nonscattering porosity, e.g., less than 10 nm in size. When broad band antireflectivity is needed, e.g., antireflectivity in blue as well as red, no single layer coating, regardless of its index, is sufficient. For that purpose, the index of refraction must be graded along the thickness of the coating; therefore, multilayer films are normally utilized. Sol-gel technology has the potential of both lowering the index of refraction by introduction of nanoscale porosity and providing the means of grading such a porosity.

Recently, it was shown that an excellent wide spectrum antireflectivity may be created on float glass with a sol-gel derived single $Si0_2$ layer [4]. These coatings are applied from a family of solutions derived from hydrolytic polycondensation of $Si(OC_2H_5)_4$ and $Si(OCH_3)_4$. The formation of precursor solutions are critical and are affected by a number of parameters.

The main properties which will determine the viability of commercialization of the coating on float glass can be classifed in three categories. These are: 1) Spectral transmission, 2) Mechanical hardness and, 3) Environmental stability. The single layer porous SiO_2 coating applied from sol-gel readily meets the optical requirements. However, an ideal pore morphology for optics is in fundamental conflict with hardness requirements. The pore morphologies that eliminate the entire reflection tend to be relatively soft due to the high level of porosity. We have now established the morphological conditions which will produce antireflective surfaces within the requirements of hardness. These silica modified surfaces cut the reflection from 8% down to 2-3% corresponding to a 60-75% reduction in reflection (Figure 2). This, coupled with a 5-6% increase in transmission, makes these coatings extremely pleasant to the eye. We have also formulated chemical and thermal conditions which will produce the desired pore morphology in these systems.

Thus, it was found that sufficient mechanical strengthening of porous $Si0_2$ coating with heat treatments up to 450^oC for 30 minutes (shorter time at higher temperatures) occurs without significantly compromising the optical properties. In Taber testing, such antireflective coatings, showed only 0.6% reduction in transmission after 100 cycles. After 500 cycles the reduction in transmission was 1.0-1.2%; this means after 500 cycles the transmission of the abraded glass was still 2.5% better than the untreated glass. In comparison, a commercial antireflective glass coating with $Ti0_2$-$Si0_2$, layers lost 4.5% transmission after only 50 cycles; and antireflectivity was entirely destroyed after 100 cycles of Taber testing. Thus, the feasibility of producing an abrasion resistant, sol-gel based single layer antireflective coating on float glass has been demonstrated.

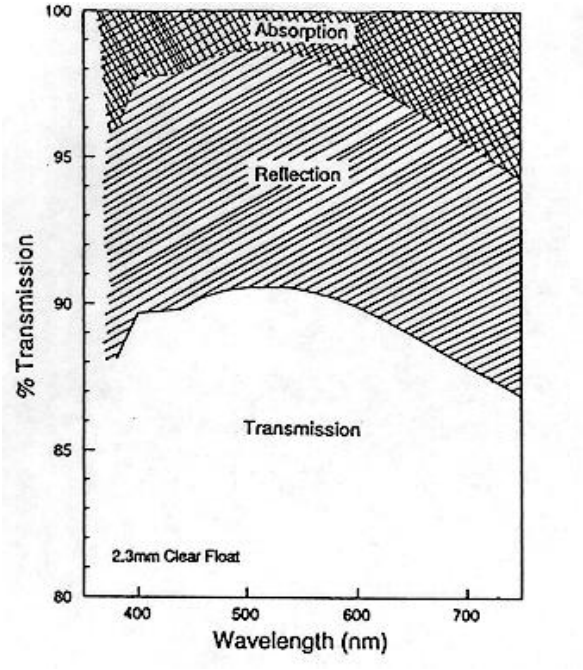

Fig.1. Absorption, Reflection, and Transmission components of a typical 2.3mm thick float glass (Reflection part can be converted to Transmission by an optical coating).

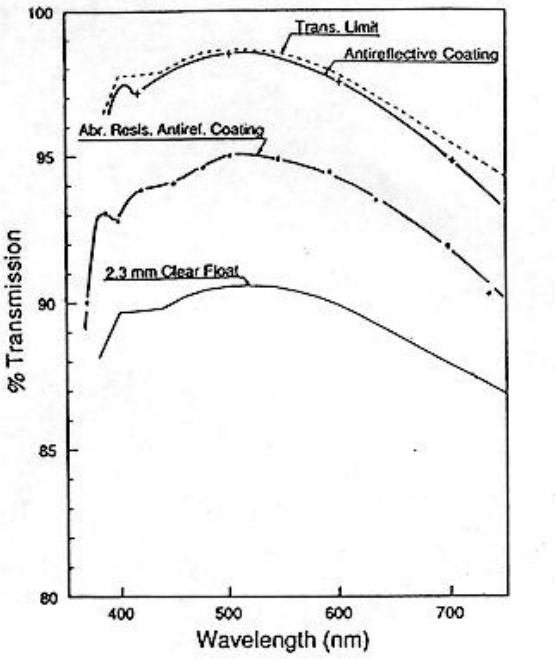

Fig. 2. Comparison of uncoated 2.3mm thick float glass to those coated with graded porous silica film before and after the film made abrasion resistant by sintering.

3. FORMATION OF STAIN AND CORROSION RESISTANT GLASS

It is found that boron diffusion into the surface of primary float glass creates a uniquely stain resistant surface [5]. Boron can be diffused into a soda-lime-silica glass at relatively moderate temperatures, e.g. 400-500^{o}C. When the boron diffusion is maintained within a relatively shallow surface layer rather than scattered throughout the glass, it produces an effective alkali-diffusion barrier (Figure 3). Application of a continuous thin film of boron on the glass surface is the first necessary step in producing uniform molecular diffusion. This in turn requires preparation of a clear precursor solution which can be sprayed, and uniformly diffused into the glass by a heat treatment.

Various tests indicate that the boron application can be performed by an on-line spray of the solution on a float glass ribbon at 1050-1150^{o}F on existing float lines. Particularly suitable boron precursors include: trimethylborate, $B(OCH_3)_3$, boric anhydride, B_20_3, boric acid, H_3B0_3. These compounds and all of their high temperature derivatives are water soluble at all temperatures, presenting no problem in spray units. Adaptation of the process to the float lines also require a well engineered integration of the time-temperature conditions in the lehr. Line speed of the ribbon has three main processing effects:

· The amount of boron delivered per unit area under a given spray condition
· The amount of time the glass spends in various temperature zones in the lehr
· Glass thickness

The first effect of line speed, the boron delivery rate per unit area, may be compensated with an adjustment in the spray rates to keep the boron concentration per unit area constant. Spraying cools the immediate surface of the glass significantly (almost 200^{o}F in laboratory experiments). This cooling is not merely due to solvent evaporation. A major portion of the cooling may be due to convective air currents caused by the spray and ambient air flow from the hood. Thus the surface cooling is strongly affected by the spray system design, i.e., nature of the solution itemization, velocity of the spray, and location of the spray heads, etc. The most important effect of line speed is the time that the glass spends in the lehr, which facilitates boron diffusion. With a line speed of 200 inches per minute in lehr, the glass spends over 6 minutes at temperatures above 450^{o}C, which is sufficient to create effective stain resistance. When line speeds are too fast to allow sufficient time for effective boron diffusion to occur, it may be necessary to modify lehr profiles. This may be done by either increasing the lehr temperature or keeping the glass at the diffusion temperature longer by adding 20-30ft more to the high temperature zone.

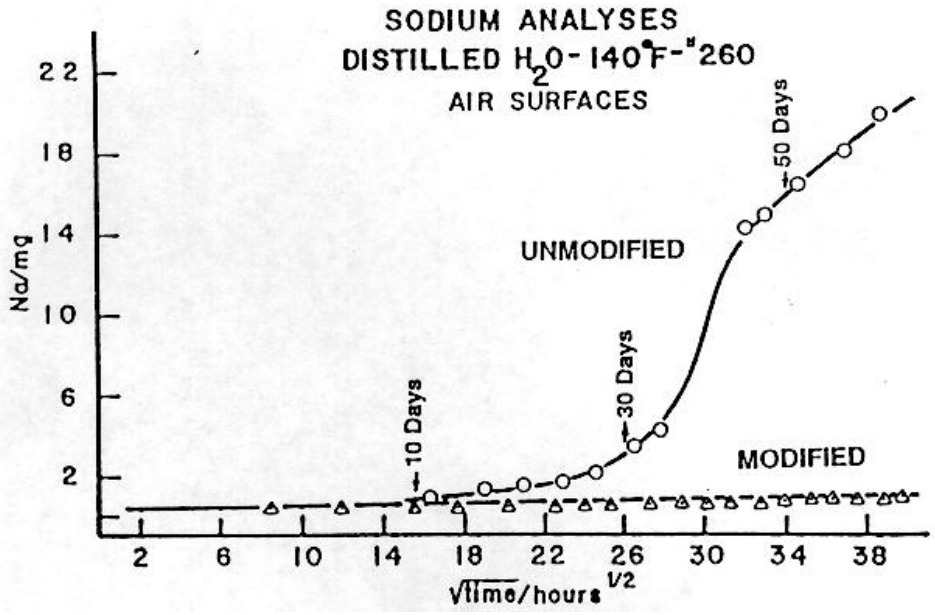

Fig. 3 Accumulated sodium leach from 4.5" x 4.5" clear float glass samples immersed in 250cc H_20 at 140^{o}F. Note that essentially no sodium leaches from the modified surface.

The temperature, T, has a greater effect because of a very large temperature dependence of the diffusion coefficient, D. This dependence is represented by the expression:

$$D=D_o e^{-Q/RT} \qquad (1)$$

where Q is the activation energy required for the diffusion to occur. The effect of line speed also relates to the glass thickness; the higher speeds yield thinner glass. Thinner glass cools more rapidly upon application of the solution. Glass cooling experiments in

the lab show a 50-60^{o}F decrease in temperatures for 0.15" thick glass and 30-40^{o}F for 0.25" thick glass when sprayed with the aqueous solution under the same conditions at ~1000^{o}F. The surface temperature rapidly recovers from this surface cooling. But it is of importance to recognize this cooling.

Boron diffusion into the float glass surface 10-50 ηm deep is found to produce an exceptional diffusion barrier layer for alkali ions as shown in Figure 3. Mechanism of this alkali barrier is discussed elsewhere.[5]. Accelerated corrosion tests indicate that boron modified glass surface remains pristine clear after being subjected to weeks of accelerated corrosion tests whereas untreated float glass surfaces severely stains and corrodes.

4. SOLID-STATE ION-EXCHANGE AND DIFFUSION STRENGTHENING OF GLASS

In the existing ion-exchange processes, the ion-exchange occurs between the glass and a molten bath. We investigated a process where ion-exchange occurs between the glass and a washable coating applied onto that glass. The coating contains the ions to be exchanged e.g. Na^{+} , K^{+} , and is washed off after the ion-exchange. Feasibility of the solid-state ion-exchange process between float glass substrate and a suitable coating applied on that glass has been demonstrated on float glass samples. Furthermore, a 35-40% increase in the glass strength related to this ion-exchange also took place in both glasses. These figures, however, are highly exploratory. Numerous parameters must be systematically investigated and optimized before an accurate judgment on the merits of the process can be made.

In the ion-exchange strengthening of glass, the smaller ions in the glass are exchanged with larger ions outside of it by a two-way diffusion process. The idea of one-way diffusion into the glass that may put the glass surface under sufficient compression was also explored. A suitable candidate is boron. Boron will diffuse into the glass readily at temperatures between 400^{o}C and the annealing temperature. Boron is applied as a coating on glass from soluble compounds. After the heat- treatment, the residual coating is washed away. Initial experiments showed a ~40% increase in glass strength.

5. HYDROPHOBIC AND PHOTOCROMIC SURFACES

These are numerous organic compounds which would import hydrophocity on glass when applied. These films however temporary and maintenance of hydrophocity requires frequent application. Relatively permanent, inorganic, hydrophobic surface condition can be created on glass by application of flouro and alkylalkoxy metal compounds. These compounds can be applied on hot glass from solutions by an on-line spray method which results in chemically bonded fluorine and alkali reach glass surfaces, which are hydrophobic. Wetting angles in excess of 100^{o} can readily be obtained. Durability tests with repeated scrubbing shows that commercial organic coatings, such as Rain-X, severely degrades after a few thousand cycles where as the inorganicly hydrophosized surfaces remains strongly hydrophobic after 10's of thousands of cycles.

It has been demonstrated that silver hallide-based photochromic films can be deposited on glass surfaces from sol-gel solutions. In these films, the optical density normally

attained in bulk materials must be produced in few micron thicknesses. This means that large quantities of optically active compounds, e.g., AgCl, must be incorporated in the film structure without affecting its clarity in the bleached state. Alumina sols described earlier provide a matrix for silver hallides where visible light transmission can be reduced to 20-30% level in darkened state with complete clarity in bleached state in 10-50ηm film thickness. In these systems, photochromicity strongly affected by solution chemistry as well as the microstructure of the film and heat treatment conditions. One outstanding problem encountered in these films is the loss of chlorine through the microporosity that eventually leads to loss of reversibility. The commercial viability requires solving this problem, as well as hardening the coating for abrasion resistance.

6. SUMMARY

With the application of suitable sol-gel based solutions, the surface of float glass can be fundamentally modified. These modifications affect the optical, chemical and physical properties of glass, creating the potential of entirely new lines of value added products. A number of novel concepts which can be created by surface modification of float glass surfaces have been demonstrated and briefly discussed here.

REFERENCES

[1] Schroeder H., Physics of Thin Films, Vol. 5, Academic Press, New York, (1969).
[2] Von Fraunhoefer J., Gesammelte Schriften, E. Lommel, Ed. Verlay der K. Akadimie, Minic, (1888), 35.
[3] Lord Royleigh, Proc. R. Soc., London 41, (1886), 275.
[4] Yoldas B.E. and Partlor, D.P., Thin Solid Films,129 (19856),1.
[5]Yoldas B.E., Hanson M.E., Duffer P.F., Proceedings of XVII International Congress on Glass, Beijing, Vol. 4 (1995), 73.

ATOMIC FORCE MICROSCOPY STUDY ON THE CRYSTALLIZATION AND CORROSION OF $Ti0_2$ COATINGS ON GLASS BY NaOH SOLUTIONS

Du Yongjuan, Edda Rädlein, G. H. Frischat
Institut für Nichtmetallische Werkstoffe, Technische Universitat Clausthal, Germany

Abstract

$Ti0_2$ coatings were prepared on microscope slide glasses by dipcoating using an alkoxide-based sol-gel method. Atomic force microscopy (AFM) was applied to study the nanoscale topography of the coatings obtained after anneling at different temperatures and after corrosion in 1 M NaOH solutions at 60 ^oC for 1 to 12 hours. The topography of the coatings appeared to be crystalline and amorphous, respectively, depending on annealing time and temperature. The corrosion process of the films depended on the status of the surface. Crystalline $Ti0_2$ (anatase) films were etched, however, a part of the surface kept its more regular nanoscale morphology. The corrosion of glassy $Ti0_2$ films proceeded differently. Probably due to a redeposition process regular-shaped crystal-like features were formed at the surface.

I. INTRODUCTION

$Ti0_2$ and $Ti0_2$-containing thin films prepared from alkoxide solutions display many actual and potential applications. These films are widely used on rear view mirrors, solar reflecting glasses, and as anti-reflective coatings [1]. The performance of $Ti0_2$-containing films has also been studied as protection against strongly alkaline solutions, and the changes in surface morphology have been monitored by X-ray fluorescence and scanning electron microscopy [2, 3]. Such methods allow overall and microscopic conclusions only. Atomic force microscopy (AFM), on the other hand, is an ideal tool to study the nanoscale performance of non-conductive surfaces [4, 5]. It has been shown already that this method is highly capable to investigate glass fracture surfaces as well as coated glass surfaces, e. g. alkoxide-made films of $Si0_2$-$Ti0_2$-$Zr0_2$ or $Si0_2$-$Ti0_2$-Al_20_3 compositions [6-10]. In this work $Ti0_2$ films were prepared from alkoxide solutions and their nanoscale morphologies were studied after annealing of the films and after corrosion in 1 M NaOH solutions at 60 ^oC.

II. EXPERIMENTAL

Appropriate amounts of titanium butoxide (Merck, Darmstadt, Germany) were mixed with ethanol under a 1 h vigorous stirring. The clear solution was diluted with ethanol to a concentration of 0.5 M. A few drops of HCI were added for stabilization. A part of the solution was aged for several hours, then $Ti0_2$ films were deposited on cleaned

microscope slide glasses by dipcoating with a withdrawal speed between 3 to 9 cm.min^{-1}. The naturally dried coatings were heated at 1 K.min^{-1} to 500 ^{o}C or 550 ^{o}C for annealing times between 40 min and 3 h. The thicknesses of the coatings were measured with a profilometer (Long Scan Profiler P-1, Tencor, München, Germany), accuracy about ± 10 %.

The uncoated and coated microscope slide glasses were immersed into 1 M NaOH solutions at 60 ^{o}C for 1, 3, 6, and 12 h, washed then in warm and in distilled water at least 4 times each, washed for 1 min ultrasonically in acetone, and stored in a desiccator at 20 ^{o}C until the further investigations.

The topographies of the surfaces of the slide glass and of the coatings were investigated by AFM (Nanoscope II with A-head, Digital Instruments, Inc., Santa Barbara, CA, USA) with a maximum scanning range of 1 μm^2. Si_3N_4 tips were used. The temperature was kept at 20 ^{o}C, the relative humidity at 40 %.

III. RESULTS AND DISCUSSION

III.1 Surface roughness

Table 1 shows the rms roughnesses (rms = root mean square) of the uncoated and coated and differently annealed and corroded slide glasses. The rms values were calculated from at least 10 measurements and are given in nm.

Table 1: Average rms roughnesses of glass substrate and $Ti0_2$ coatings

Corrosion time (h)	Uncoated slide glass	Annealed 500 ^{o}C, 3 h	Annealed 500 ^{o}C, 1 h	Annealed 550 ^{o}C, 40 min
0	1.1 ±0.1	0.70 ± 0.17	0.93 ± 0.26	3.9 ± 0.6
1	2.0 ± 0.5		3.0 ± 2.3	4.9 ± 0.8
3	2.0 ± 0.7		13.8 ± 2.1	3.3 ± 0.5
6	2.0 ± 1.4		7.1 ± 2.8	8.2 ± 1.1
12	5.6 ± 3.5		16.6 ± 2.2	9.5 ± 1.9

III.2 Anatase crystallization during heat treatment

Fig.1 displays some representative AFM height mode images of surfaces of ≈ 60 nm thick $Ti0_2$ coatings on the glass substrates. The film heated at 500 ^{o}C for 1 h is typical for a glass surface showing the so-called "glass pattern", similar to the untreated surface of the slide glass and similar to what has been found for other glass surfaces and for surfaces of glassy films [6, 10]. No significant features are to be seen, except the randomly distributed ripples of ≈ 15 nm in diameter and heights between valleys and peaks of 0.5-1 nm (Fig.1a). Fig.1b shows the AFM image of a $Ti0_2$ surface after a 3 h annealing at 500^{o}C. Although the rms roughness did not change, the topology appears differently. Some more or less tetragonal-looking features can be seen with lateral sizes between 60-150 nm and height variations of 0.5- 6 nm. Fig.1c shows a representative topology of a coating, where the samples had been heat treated for 40 min at 550 ^{o}C. Many typical

tetragonal crystals can be recognized, whose lateral sizes are between 50 -190 nm with height values between 1.5 -18 nm.The rms roughness has changed, too (see Table 1).$Ti0_2$ xerogels heated for 3 h at 550 ^oC display crystalline anatase by X-ray diffraction. The higher annealing temperature of 550 ^oC favors the crystallization more than the longer treatment at the lower temperature of 500 ^oC.

III.3 Corrosion of crystalline $Ti0_2$ films

Fig. 2 displays some AFM height mode images of mostly crystalline $Ti0_2$ coatings (40 min treatment at 550 ^oC) after corrosion at 60 ^oC in 1 M NaOH solutions for 1, 3, 6, and 12 h. It is noticeable that already after a 1 h corrosion the tetragonal crystallites became more evident (Fig. 2a). However, their lateral sizes between 60 -180 nm and their heights between 2 - 18 nm have not much been changed compared to the non-corroded surface. Only the rms roughness increased a little from 3.9 ± 0.6 nm to 4.9 ± 0.8 nm. Corrosion at this stage mainly proceeds by etching the glass residues from the grain-boundaries. Fig. 2b (note the change in xy-scale compared to Fig. 2a) shows the $Ti0_2$ surface after a 3 h corrosion. Although the tetragonal geometry of the crystals still can be seen, the image lost contrast. It looks "smeared out", which is also evidenced by the linear traces through tip scanning parallel to the x-axis. Although the lateral sizes between 100 - 180 nm are practically the same as before, their heights between 3 -10 nm are lower than those of the crystals in Fig. 2a, and the reduction of the rms value to 3.3 ± 0.5 nm is in line with this effect. At this stage of NaOH corrosion the crystals were etched away and their surfaces became softer. With the further corrosion the surfaces of the coatings were etched more strongly, but the etching became inhomogeneous. Fig. 2c and 2d are representative for the surface topographies after a 6 h corrosion. In one case the surface crystals nearly remain their tetragonal shapes (Fig. 2c), in the other case the habits of the crystals are mostly destroyed (Fig. 2d). The lateral sizes of the crystals are between 80 - 180 nm. The valleys shown on the image of Fig. 2d are 60 -130 nm in extent and 3.6 -16 nm deep. The rms roughness has increased to 8.2 ± 1.1 nm. With proceeding corrosion, see Fig. 2e and 2f, the morphologies of the $Ti0_2$ surfaces remain to some extent similar to those shown in Fig. 2c and 2d, although a further distortion can be noticed. There are still parts where some crystal-like remainders are visible (lateral sizes 100 - 240 nm, heights 5 - 45 nm), however, most parts of the surface display the corrosion valleys of Fig. 2f (lateral extent of the valleys 80 - 220 nm, 3 - 27 nm deep). In this stage the corrosion process has damaged the $Ti0_2$ coating considerably, however, a part of the film still protects the substrate.

III.4 Corrosion of originally glassy $Ti0_2$ films

Uncorroded $Ti0_2$ films, heat treated for 1 h at 500 ^oC, display a typical "glass pattern" surface topography, see Fig. 1a. Indeed, such films are glassy, but not necessarily fully dense. However, NaOH corrosion changes this topography strongly, see Fig 3 where stages after 1, 3, 6, and 12 h corrosion treatment at 60 ^oC are shown. AFM images in Fig. 3a and 3b display more or less regular granular surface features, whose rms roughness is 3.0 ± 2.3 nm. The sizes of the grains range from 70 - 210 nm with heights between 1 - 22

nm. It is difficult to decide whether they are already crystalline. However, the situation in Fig. 3c and 3d seems to be clearer. A majority of images display features with remarkably regular morphology, while the others show tetragonal grains with tip scanning traces parallel to the x-axis. Some of these traces became deeper during scanning, which means that the surfaces became softer through the corrosion process. The lateral extent of these features is 60 - 200 nm with heights between 7 - 40 nm. The depths of the tip traces range from 3 - 8 nm and the rms roughness was found to be 13.8 ± 2.1 nm. During the corrosion process regular crystals with tetragonal shapes are formed on the originally amorphous $Ti0_2$ coatings. Possibly these crystals are formed by a redeposition process. The glassy $Ti0_2$ material is dissolved. With ongoing NaOH corrosion the solution at the very surface is supersaturated with $Ti0_2$, owing to the stationary nature of the dissolution process. Crystals, whose composition is unknown thus far, are deposited at the surface. Possibly their formation is supported due to the presence of some (crystalline?) $Ti0_2$ nuclei. Of course, these solution-formed crystals are not as dense as crystals formed at higher temperature. Therefore, they are easily to be damaged by the scanning tip. Fig. 3e and 3f display the topographies after corrosion for 6 and 12 h, respectively. The lateral dimensions of the surface features are 80 - 190 nm with heights between 2 - 35 nm (Fig. 3c). Many of them have tip scanning traces (not shown here). The rms roughness is 7.1 ± 2.8 nm. After 12 h corrosion the rms value increases to 16.6 ± 2.2 nm and the $Ti0_2$ surface is strongly distorted.

By the way, the AFM images of the substrate glass do not display this regular tetragonal topography neither before nor after corrosion.

IV. CONCLUSIONS

Alkoxide-made $Ti0_2$ films (thickness ≈ 60 nm) were deposited on glass substrates by dipcoating. AFM images displayed that these coatings are glassy after a 2 h annealing at 500 ^{o}C. The nanoscale topography shows the typical "glass pattern". Annealing at 550 ^{o}C favors the formation of tetragonally looking crystalline anatase. The corrosion process of the films in 1 M NaOH at 60 ^{o}C depends on the crystalline/amorphous status of the surface. Crystalline $Ti0_2$ films are etched successively, however, a part of the surface keeps its more regular nanoscale morphology. The corrosion of glassy $Ti0_2$ films proceeds differently. With ongoing corrosion more regular-shaped crystal-like features are formed, perhaps due to a redeposition process from the solution.

REFERENCES

1. H. Dislich, in L. C. Klein (ed.) Sol-Gel Technology for Thin Films, Fibers Preforms, Electronics and Specialty Shapes. Noyes Publications, Park Ridge, NJ, USA,.1988, p. 50 - 76.
2. W. Beier, G. H. Frischat, Mat. Res. Soc. Symp. Proc.121 (1988), 817 - 822.
3. Q. Chen, G. H. Frischat, J. Cheng, J. Sol-Gel Sci. Technol. 2 (1994), 535 - 538.
4. F. Creuzet et al., Bol. Soc. Esp. Ceram. Vid. 31-C (1992), 7,105 -110.
5. E. Meyer et al., Glastechn. Ber. 66 (1993), 31- 37.

6. C. Wünsche, E. Radlein, G. H. Frischat, Glastechn. Ber. Glass Sci. Technol 68C1 (1995), 275 - 282.
7. R. Ambos, E. Radlein, G. H. Frischat, Glastechn. Ber. Glass Sci. Technol. 68C1 (1995), 351- 359.
8. E. Rädlein, R. Ambos,G. H. Frischat, Fresenius J. Anal. Chem. 353 (1995), 413 -418.
9. E. Rädlein, C. Wünsche, G. H. Frischat, Proc. XVII Intern. Congr. on Glass, Beijing 1995, Vol. 4, 3 -8.
10. Y. Du, G. H. Frischat, Proc. XVII Intern. Congr. on Glass, Beijing,1995, Vol. 4, 187-192

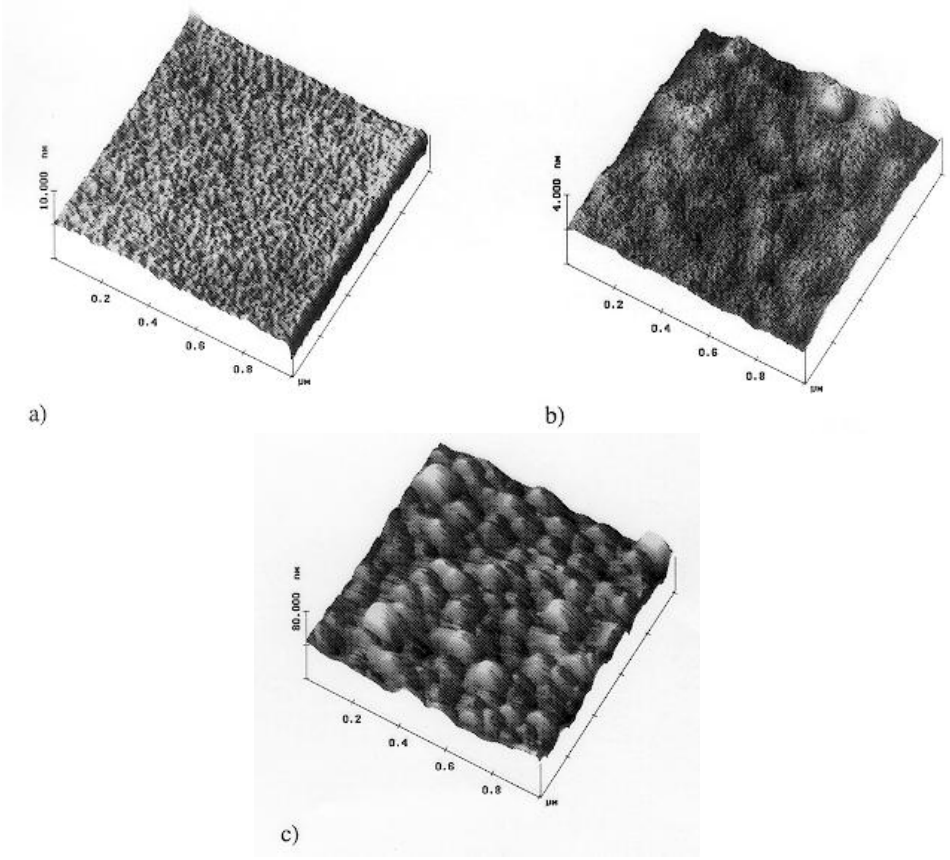

Fig.l: AFM height mode images of $Ti0_2$ coatings annealed under different conditions. a)treated at 5OO°C for 1 h, displaying the glass pattern, b)treated at 5OO°C for 3h, with almost tetragonal features, c)treated at 55O°C for 40 min, with clearly visible tetragonal crystals.

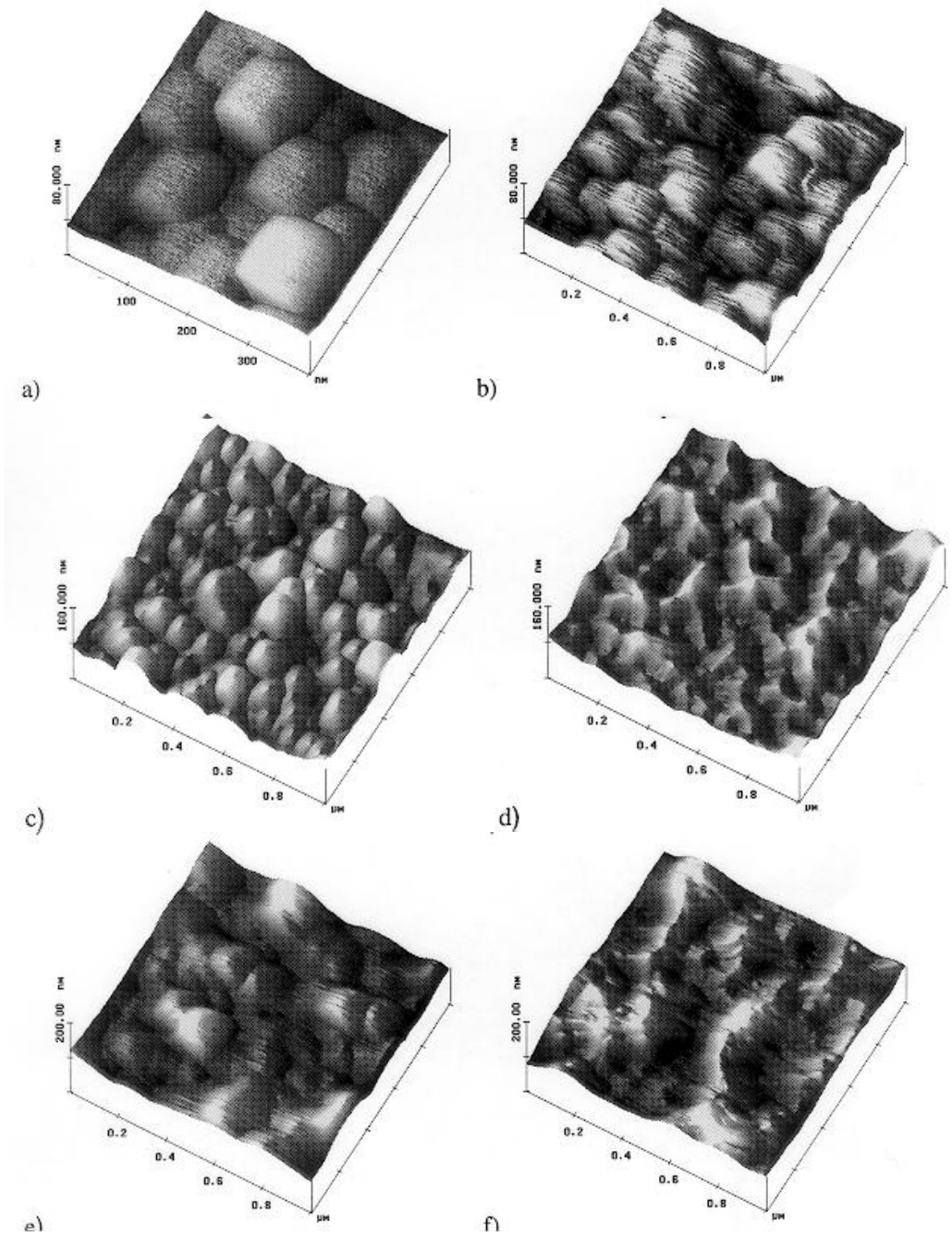

Fig.2: AFM height mode image of crystalline $Ti0_2$ coating anealed at 55O^{o}C for 40 min and corroded by 60^{o}C 1M NaOH solution. a) for lh, b)for 3h, c) and d) for 6h, e) and f) for 12h. The tetragonal crystals, which are clearly developed initially (see 2 a), become softer and are destroyed after longer corroding times. The corrosion renders rougher surfaces (note the smaller xy scale in 2a and the increasing z scale from 2a to 2e).

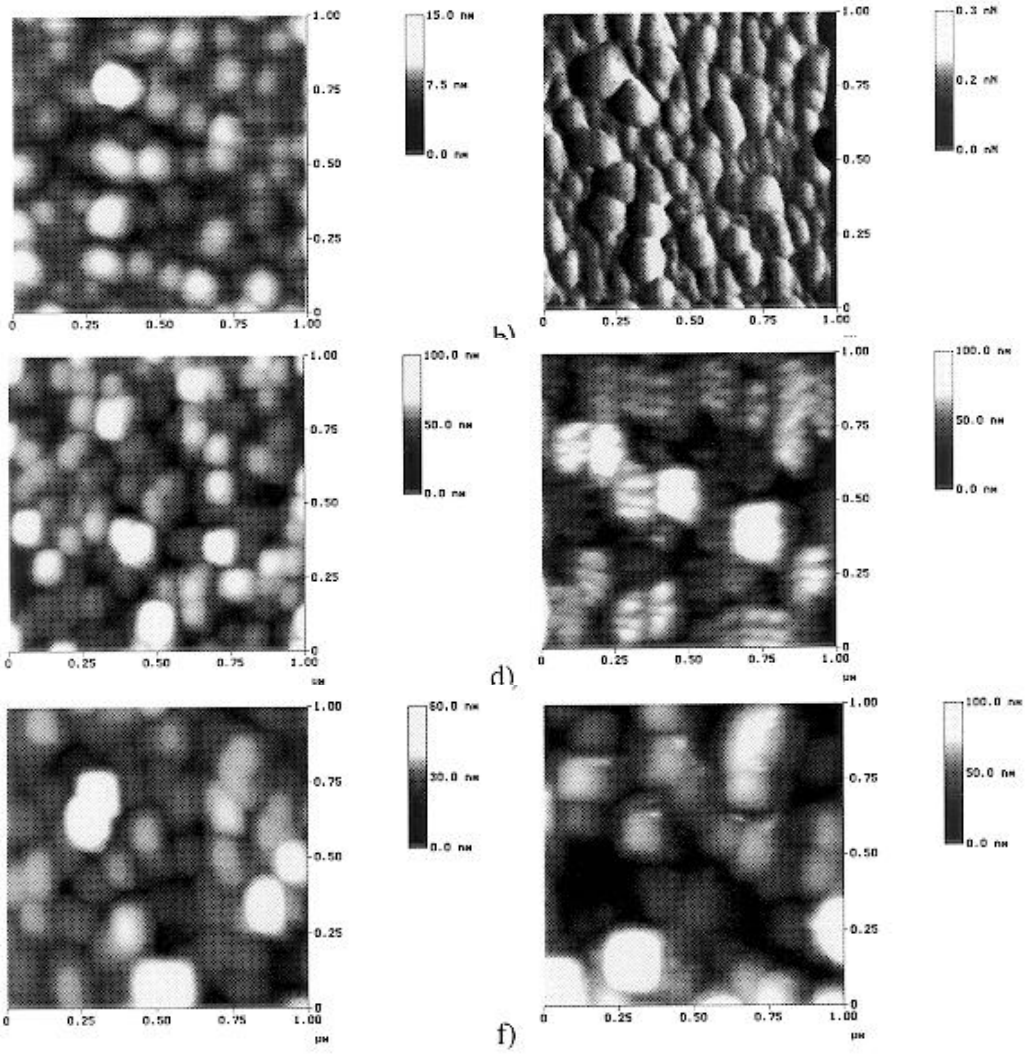

Fig.3: AFM images of originally glassy $Ti0_2$ coating annealed at 5OO°C for 1 h and corroded in 60°C 1M NaOH. a) and b) for lh, c) and d) for 3h, e) for 6h, f) for 12h. The plotting mode has been changed to topview to display the granular morphology better. Heights are expressed in terms of gray scales. 3b is a force mode image, the gray scale represents the forces acting on the tip. This mode is best suited to show the contours of the granular features.3d shows one example for the eroding of the soft crystals by the motion of the scanning tip.

CeF_3 AS A NEW ANTIREFLECTIVE COATING MATERIAL

Hülya Demiryont, Kubilay Kutlu and **Süha Akçiz**
*SISECAM Research Center, Turkey
Yildiz Technical University, Turkey

Abstract

Process parameters and resulting film properties of e-beam deposited CeF_3 were evalulated for various type of glass substrates. Visible region refractive indices of CeF_3 films were found in the range of 1.35-1.42. So CeF_3 suggested as a new single layer anti-reflective coating material. Deposition parameters of high quality CeF_3 coatings were studied.

II. INTRODUCTION

Low refractive index materials have been focused a strong attention for their wide industrial applications. Low refractive index material can be used in the single layer form or in the multi-layer systems. The multi-purpose usage make these types of materials very attractive for researchers. On the other hand, there are only few known low refractive index materials qualify for single layer industrial applications. MgF_2 is the most common one, even it forms rather poor films in terms of mechanical and environmental properties. Other exemples for AR coating systems are the various combinations of the semiconductors and oxides [1-3] e.g., layered structures or graded-index, GRIN, films of Si-SiO_2 . Some metal fluorides in thin film form have found widespread use in optical coating applications [4,5] as well as a buffer layer applications in between two crystalline media [6,7]. Refractive index of CeF_3 fýlms deposited by e-beam technique are given by various papers and patents being around 1.6 [8-11] . Ýn this paper we studied the optical proporties of CeF_3 films deposited by e-beam and thermal evaporation techniques. We showed thar CeF_3 is a low refractive index material exhibiting approximately 100% optical transmittance at the designed wavelength. Films deposited on 250^{o}C heated substrates formed durable and hard coatings. Adhesion of the films were improved by SiO_2 buffer layers on glass were used.

II. THEORETICAL BACKGROUND

Optical parameters of a weakly absorbing or non-absorbing film can be calculated by a spectrophotometric method [12]. Figure 1 shows spectrometric transmittance of a hypothetical sample. T_0, T^+, and T^-plots in this figure correspond to the transmittance of the bare substrate and maximun and minimum envelopes passing through the transmittance extrema, respectively. The separation between the $T^+(\lambda)$ and $T^-(\lambda)$ and the $T^0(\lambda)$ and $T^+(\lambda)$ couples are a measure of the refractive index and the absorption of the film, respectively. The Refractive index and the extinction coefficient are calculated [13,14] by using eqs.1.8.

$$C_{(\lambda)} = \pm \frac{T^{+}_{(\lambda)} - T^{-}_{(\lambda)}}{2T^{+}_{(\lambda)} T^{-}_{(\lambda)}} \qquad (1)$$

$$U_{(\lambda)} = \frac{T^{+}_{(\lambda)} + T^{-}_{(\lambda)}}{2T^{+}_{(\lambda)} T^{-}_{(\lambda)}} \qquad (2)$$

+ and - singns in front of the eq. 1 correspond to $n_f > n_s$ or $n_f < n_s$ respectively.Where n_f and n_s are the refractive indices of the film and substrate respectively.On order to decide if $n_f > n_s$ or $n_f < n_s$ one must examine spectrophotometric transmittance curve whether $T < T_0$ or $T > T_0$. Where T and T_0 are the transmittance of the film and the bare substrate respectively. Refractive indices of the film and the substrate can be deduced from eqs.3 and 4 respectively which are given by:

$$n_f(\lambda) = \frac{1}{2}\left\{\left[8n_s C_{(\lambda)} + (n_s+1)^2\right]^{1/2} + \left[8n_s C_{(\lambda)} + (n_s-1)^2\right]^{1/2}\right\} \qquad (3)$$

$$n_{s(\lambda)} = \frac{1+\left[1-T_0^2(\lambda)\right]^{1/2}}{T_0(\lambda)} \qquad (4)$$

For an absorbing film, extinction coefficient, k(λ) is calculated by using eq. 1 given by:

$$k(\lambda) = \frac{\lambda}{4\pi d} \mathrm{Ln}\left[\frac{U_{(\lambda)} + \left[U^2_{(\lambda)} - C^2_{(\lambda)} + \delta_{(\lambda)}\right]^{1/2}}{2a_{(\lambda)}}\right] \qquad (5)$$

Where $\delta_{(\lambda)}$ and $a_{(\lambda)}$ are given by the following eqs.:

$$\delta_{(\lambda)} = \left(\frac{n_s^2 - 1}{8n_s}\right)^2 \left[n_f(\lambda) - \frac{1}{n_f(\lambda)}\right]^2 \qquad (6)$$

$$a_{(\lambda)} = \frac{\left[n_f(\lambda)+1\right]^3 \left[n_f(\lambda) + n_s^2\right]}{16 n_s n_f^2(\lambda)} \qquad (7)$$

The film thickness, d, can be obtained from successive extreme, λ_i and λ_{i+1}, according to the following equation:

$$d = \left\{ 2\left[\frac{n_f(\lambda_i)}{\lambda_i} - \frac{n_f(\lambda_{i+1})}{\lambda_{i+1}} \right] \right\}^{-1} \qquad (8)$$

Values of the thickness can also be determined by a graphical method [12]..

III. EXPERIMENTAL PROCEDURES:

High purity white powder of CeF_3 was pressed into tablet form approximately 1 cm in diameter. Films were depesited mainly by two techniques namely; thermal evaporation and electron-beam evaporation. Corning 7059 glass and ordinary soda lime glasses were used as substrates in order to evaluate the substrate effects on the film properties. In the both deposition techniques sample properties were controlled by; 1)type of substrate, 2) deposition rate, 3)substrate temperature, 4)vacuum level, and 5)film thickness.The most important deposition parameters effecting on the film properties were experimentally found in order 1) substrate temperature, 2) type of substrate, and 3) deposition rate. The substrate temperatures during deposition were kept constant in the range between 50^{o}C and 350^{o}C. The film deposition rate, film thickness/deposition time, was changed from 25 nm/min to 100nm/min. Vacuum level was 10^{-5}-10^{-4} Torr range. Film thickness was kept nearly constant at around 0.5 µm to determine corresponding n and k spectra of CeF3 films. Spectrophotometric measurements of the substrates and film/substrate systems were evaluated by Perkin Elmer Lambda 2S unit with integrating sphere attachment.

IV. RESULTS AND DISCUSSIONS

Spectrophotometric results obtained on a typical CeF_3 film on Corning 7059 glass deposited under 10^{-5} Torr of vacuum level, at 220^{o}C of the constant substrate temperature during deposition, with the deposition rate of 35 nm/min are shown in Figure 2. Figure 3 illustrates T vs. λ plot of an inhomogenous film of CeF_3. T vs. λ spectrum of an homogenous film (fig.2) shows smooth waving between interference extrema whereas inhomogenous film exhibits irregular interferance pattern (see Fig.3).Inhomogenous film CeF_3 films were obtained under the following conditions:
1) At high substrate temperature during deposition, 2) High deposition rates, 3) Films deposited on soda lime substrates. Inhomogenities observed on the CeF_3 films could be possible mainly due to two raisons.These are:1)Fluorine lost from CeF_3 film due to the Na in diffusion from substrate into the film and 2) Fluorine lost from CeF_3 deposition source due to the excess source heating. In the former case the films deposited on the Corning glass exhibit inhomogenities depending on the source temperature, but not on the substrate temperature. In the latter case, independent of the substrate material, inhomogenities was found to be only source temperature dependent.

Sample thickness were chosen so that we could obtain a sufficient number of interference maxima and minima to determine the n and k spectra of the samples. The results obtained on the homogenous CeF_3 coatings are given in Figures 4 and 5. Because of the $T > T_0$ conditions were obtained in our CeF3 coatings, the films provide $n_f < n_s$ conditions. Hence minus sign in eq. 1 was used to calculate n vs. λ and k vs. λ values. From Figs. 2,4,and 5 we concluded that: 1) Typical CeF_3 films

exhibit very low level of absorption at $\lambda < 750$ nm region, but they are non absorbing at the longer wavelengths. This property makes the material attractive for IR optics, 2) CeF_3 films exhibit dispersion on both refractive index and the extinction coefficient, 3) CeF_3 is a wide band gap materal like glass. 4) Visible average of the refractive index of CeF_3 films was found to be 1.38. Thus CeF3 is a low refractive index material with the refractive index value in between 1.35 and 1.42 in the visible spectral region. Literature values [9-11] of the CeF_3 films depesited with the same e-beam technique and conditions indicates that material has n values inbetween 1.58 through 1.62. A comparative plot of our results calculated by using positive sign in eq. 1 together with the literature values are given in the inset of Figure 4. Very well fit observed in our results and the literature values, together with our T vs. λ measurements providing $T > T_0$ condition indicates that CeF_3 can be considered as a new low refractive index material, but not a medium refractive index material which is given in literature [9-11] . A new AR material, a CeF_3 film , was coated at the both sides of a glass substrate. Fig.5 illustrates the transmittance spectuum or this two-side coated glass. The total absorption of this both side coated glass is rather high due to the ~ 2μm total thickness of the CeF_3 films. If the film thickness, d, reduced to d_{AR} which is given by

$$\mathbf{d_{AR} = l_0 / 4n_f} \qquad (9)$$

where λ_0 is the wavelenght corresponding to AR condition and,

$$\mathbf{n_f @ q\ n_s\ n_o} \qquad (10)$$

and corresponding minimun reflection

$$R_{min} = \left(\frac{n_f^2 - n_s}{n_f^2 + n_s} \right)^2$$

In this study we worked on thick films in order to define n and k spectra of the CeF_3 films. If one deposits " 110 nm thick CeF_3 film at the R_{min} condition transmission of this both side coated glass at λ_0 will be much closer to 100 % then that of the thick film case which is given in Fig.5. R % and T % spectra of 110 nm thick CeF_3 AR film deposited on a both side of a float glass are shown in Fig. 6.. These values are calculated from eqs. 9.10 by using experimental data given in Fig. 4..As shown from this figure the visible average reflection is around 1% and transmission is around 99%. A sodium barrier e.g., SiO_x film approximately 110nm thick and $1.6 < x < 2$ would be necessary for deposition of CeF_3 film. The new thickness of the CeF_3 film.Deposited on SiOx / soda lime glass substrate must be defined depending on x and optical thickness of SiO_x film. So float glass coated with Na barrier and an adhesion improuved film of SiO_x can be coated with CeF_3 film, "110 nm thick, at 220^{o}C of deposition temperature as a new and high quality AR coating.

V. CONCLUSION

Optical properties of CeF_3 were studied in this paper. The folloving results were concluded: 1) CeF_3 is a high quality low refractive index material with the optical properties similar to MgF_3., 2) CeF_3 deposited on 220^oC heated substrate forms a hard and stable film., 3) Inhomogenous CeF_x films, x< 3 are obtained at elevated substrate temperatures and decomposed source material conditions., 4)CeF_3 film is a very good candidate for AR coating material.

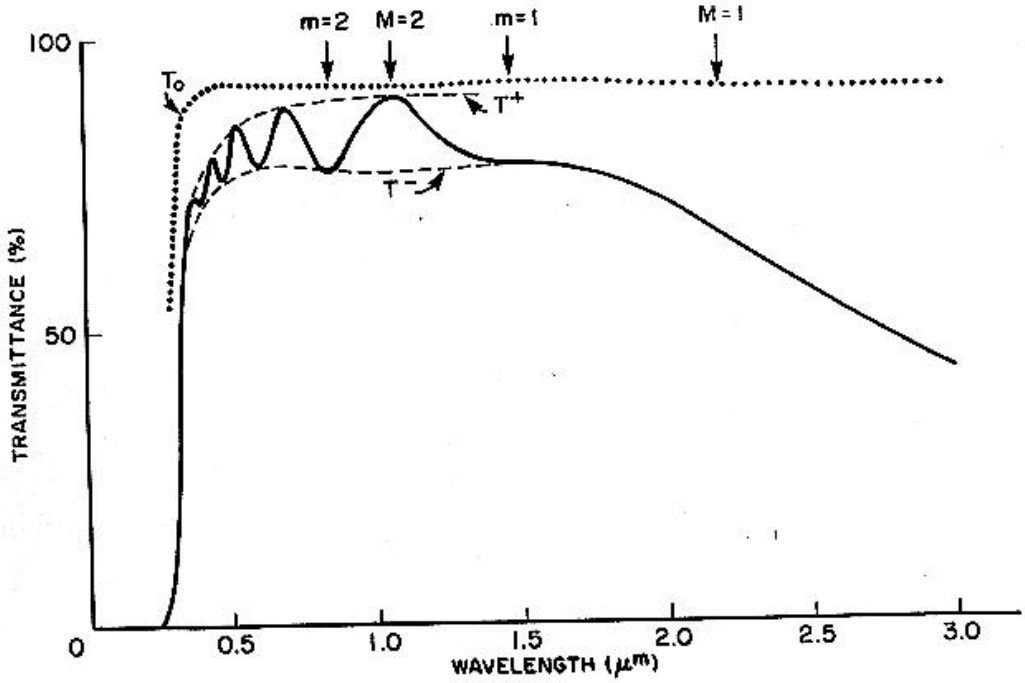

Figure 1. Spectrophotometric transmittance curve of a hipotetical film-substrate system Non-absorbing and absorbing region as of the film spectum are indicated in the figure $n_f > n_s$ codition is provided by film-substrate system.

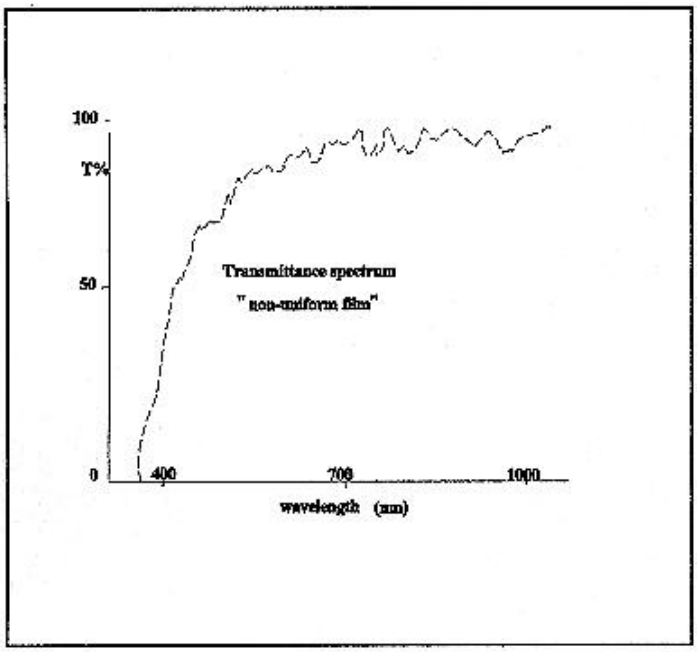

Figure 2. T vs l plot of a typical CeF_3 film deposited on corning 7059 class. Film thickness is around 750 nm.

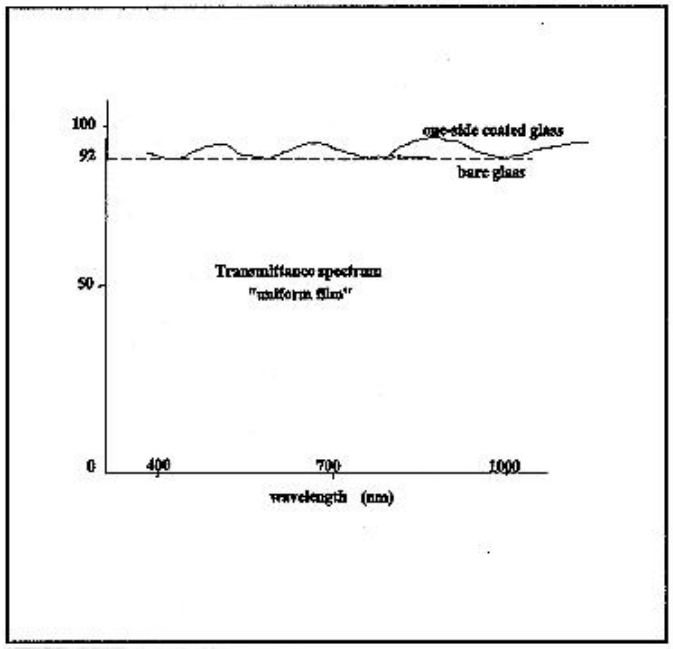

Figure 3. T vs. l plot of a typical CeF_3 from deposited at high temperature and deposition rate on sodas-lime glass.

Interference disorders indicate the inhomogenity of the film.

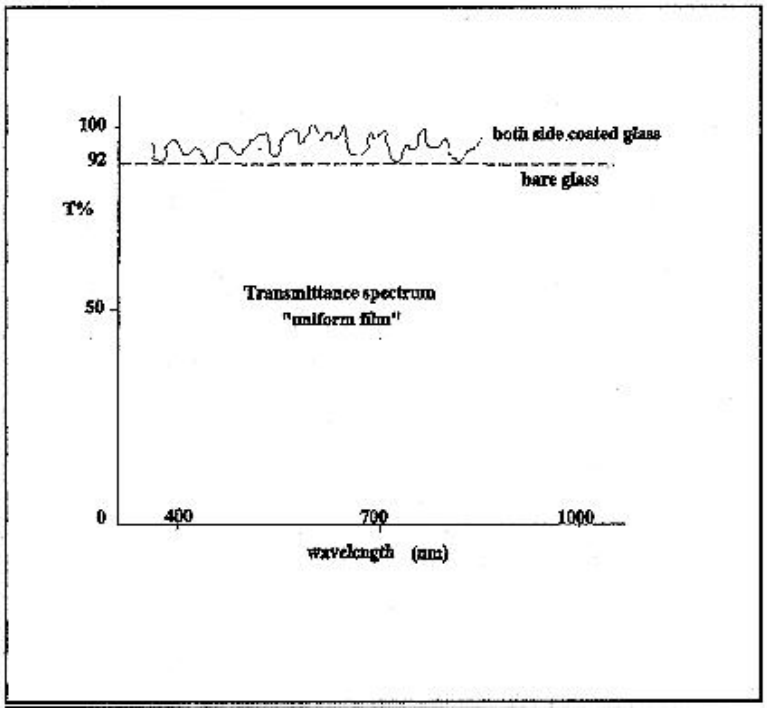

Figure 5. Spectrophotometric transmittance plot of a both side CeF_3 coated glass. Maching film tickness is around 1 m

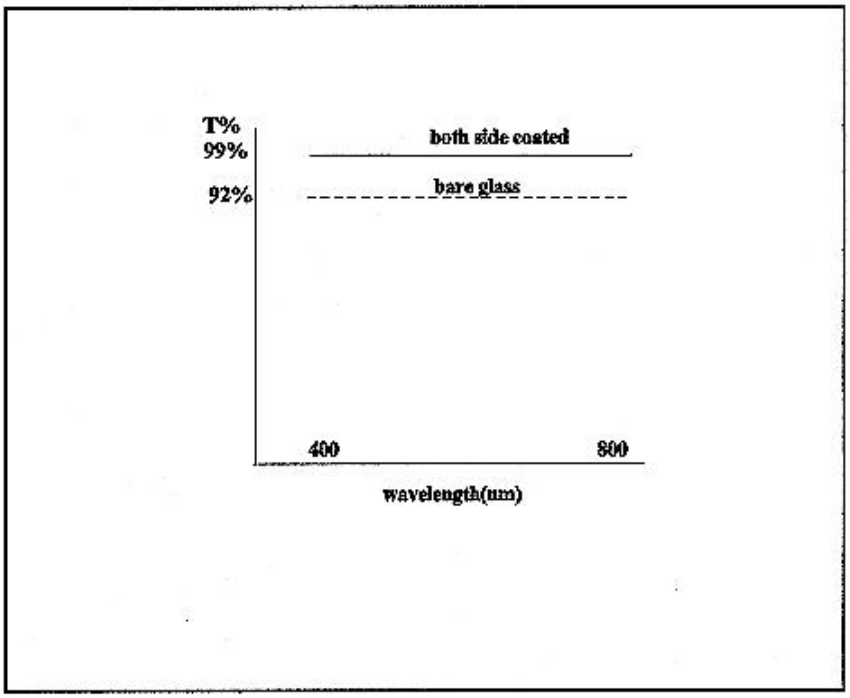

6-a

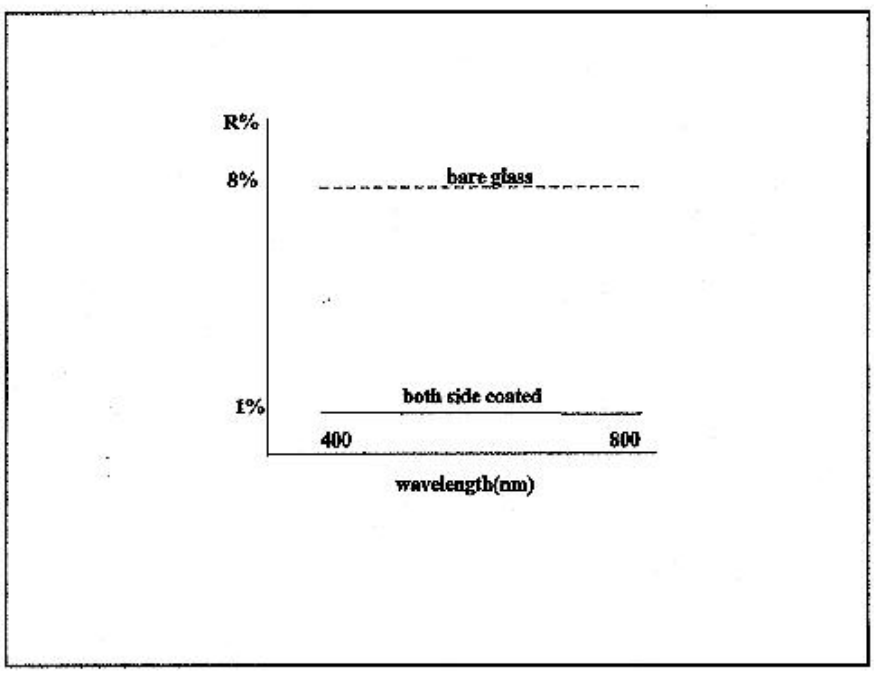

6-b

Figure 6.a-b T% and R% spectrum of 110 nm thick CeF_3 AR film deposited on a both side coated float glass, respectively.

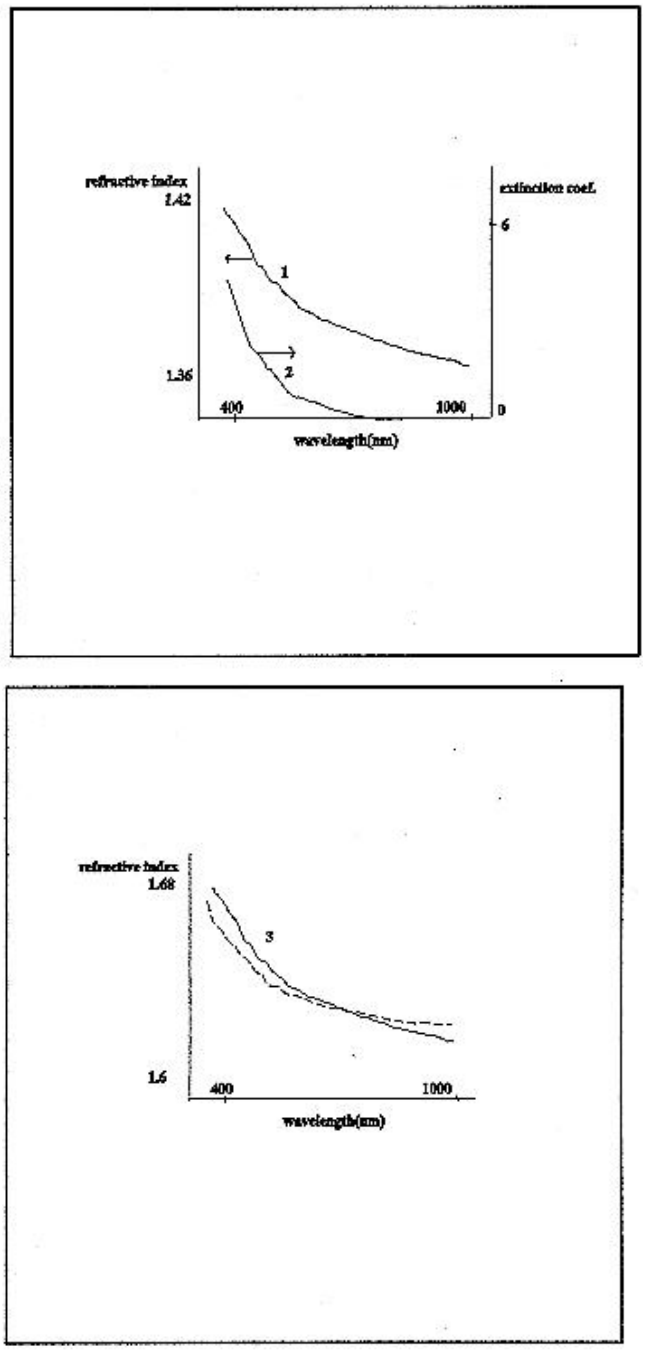

Figure 4. Wavelength dependence of reftavtive index and the extinction coefficient of CeF_3 film. (1) Refractive index spectrum exhibits a dispersion (2) Wavelength dependence of the extinction coefficient of the CeF_3 film Absorption threshold is around 750 nm. (3) Comparative results on refractive index spectrum of CeF_3 film: ---- present work; - - - literature values [9,10,11]

References:

[1] Hülya Demiryont, U.S. Patent # 5,245,468

[2] Hülya Demiryont, U.S. Patent # 5,171,414

[3] Hülya Demiryont, U.S. Patent # 5,106,671

[4] J.A. Savage, Infrared Optical Materials and Their Antireflection Coatings,p.43, Adam Hilger Ltd., Bristol (1985)

[5] H.A. Macleod, Thin-Film Optical Filters. 2nd., Adam Hilger Ltd., Bristol (1986)

[6] A.N. Tiwari, A.Freundlich, B. Beaumont, H.Zogg, S. Teodoropol, and C Verie, J.Cryst. Growthy,124,565-571 (1992)

[7] J.C. Alwarez, K. Hirano, A. Y. Kazimiroz, M.V. Kobvalchuk
A. Y. Kreines, N. S. Sokolov, and N.L. Yakovlev, Semicond. Sci. Technol., 7, 1431- 1438 (1992)

[8] Tyurmikova et. al., Russia Patent # 793956; Japan patent #, 51 150 508 and 51 150 509; US patent # 3 781 090.

[9] P. Chimdaudom and K. Vedan, Appl. Opt., 33, 2664-2669 (1994)

[10] D. Smith and Ph. Baumeister, Appl. Opt., 18, 111-115 (1979)

[11] A. Piegari and G. Emiliani, Thin Solid Films, 171, 243-250 (1989)
University, 1983)

[12] R. Swanepoel, Phys. E : Sci. Instrumi 16, 1214-1221 (1983)

[13] H. Demiryont, J. R. Site, and K. M. Geib, Appl. P.Opt., 24, 490-495 (1985)

[14] E. Aktulga " Optical parameters of a weakly absorbing film by spectrophotometric transmittance measurements ", PhD. dissertation (Istanbul)

CHEMICAL, ELECTRICAL AND OPTICAL PROPERTIES OF GLASSES COVERED WITH GEL-DERIVED SILICATE-PHOSPHATE LAYERS

M. ° • czka, M.Cieci½ska and **K.Cholewa**
University of Mining and Metallurgy,
Faculty of Materials Science and Ceramics, Poland

Abstract

Gel layers in SiO_2-P_2O_5, SiO_2-P_2O_5-Al_2O_3, SiO_2-P_2O_5-Na_2O and SiO_2-P_2O_5-CaO systems were obtained from alcohol solutions on melted quartz and sodium-calcium-silicate glass. The optical, chemical and electrical properties of glasses covered with the layers of SiO_2-P_2O_5, SiO_2-P_2O_5-Al_2O_3 and SiO_2-P_2O_5-Na_2O systems were measured. It has been found that the layers show anti-reflexive properties as well as that the chemical resistance of covered glasses is higher than the basic, sodium-calcium-silicate glass. Moreover, the silicate-phosphate layer modify the surface electrical conduction of the basic glasses. The layers of systems SiO_2-P_2O_5 and SiO_2-P_2O_5-Al_2O_3, show the electrical conduction considerable higher than the basic glass. The layers containing sodium, depending on its concentration, behave similarly to the basic glass or show the lower electrical conduction. The layers of SiO_2-P_2O_5-CaO system show bioactive properties.

INTRODUCTION

The silicate-phosphate glasses are characterized by interesting structure on account of the presence of two glass forming components and the formation of the mixed bonds -Si-O-P-. They exhibit also a number of interesting properties including the optical and electrical ones, and when having a certain chemical composition they may become bioactive [1,2]. The deposition of layers of silicate-phosphate systems onto the glass, ceramic and other basic materials makes it possible to modify their surface properties, thus considerably extending the area of application of these materials [3, 4]. A particularly useful method for this purpose is the chemical method consisting in the preparation of amorphous materials from solutions, called the sol-gel method [5, 6]. It allows to carry out the entire process of the layers deposition at a temperatures not exceeding 500^{o}C. Sol-gel techniques have been applied to silicate-phosphate systems and possibility of obtaining glassy solids were demonstrated [7-10]. However, there is no information available about the process of obtaining of gel layers of silicate-phosphate systems and about the properties of these layers.

The aim of the present study was to obtain on a glassy base the thin, amorphous gel layers of the systems: SiO_2-P_2O_5, SiO_2-P_2O_5-Al_2O_3, SiO_2-P_2O_5-Na_2O and SiO_2-P_2O_5-CaO and to determine:

- optical, chemical and electrical properties in the case of the layers of SiO_2-P_2O_5, SiO_2 P_2O_5-Al_2O_3 and SiO_2-P_2O_5-Na_2O Systems;

- the ability of surface crystallization of hydroxyapatite indicating on bioactivity of the material in the case of layers of SiO_2-P_2O_5-CaO system.

EXPERIMENTAL

The synthesis of gels was conducted for five defined oxide compositions (mol.%):

1. 80.77 SiO_2, 19.23 P_2O_5;
2. 79.80 SiO_2, 10.20 P_2O_5 10.00 Al_2O_3;
3. 80.50 SiO_2, 9.60 P_2O_5 9.90 Na_2O;
4. 70.00 SiO_2, 10.00 P_2O_5 20.00 Na_2O;
5. 60.00 SiO_2, 4.00 P_2O_5 36.00 CaO.

As the starting materials introducing the particular oxides there were used:

- $Si(OC_2H_5)_4$ (TEOS),
- H_3PO_4,
- $C_{12}H_{27}AlO_3$,
- $NaNO_3$,
- $Ca(NO_3)_2 \cdot 2H_2O$

The method of preparing the solutions was as follows (Table 1).

Table 1. Chemical composition of the parent solutions.

Chemical composition (mol%)	Amount of used components							
	TEOS (ml)	C_2H_5OH (ml)	H_3PO_4 (ml)	$C_{12}H_{27}AlO_3$ (ml)	$NaNO_3$ (ml)	$Ca(NO_3)_2 \cdot 2H_2O$ (g)	H_2O (ml)	HC1 (ml)
80.77S-19.23P	30	37	7.1	-	-	-	14.5	3
79.8S-102P-l0A	30	37	4.0	4.4	-	-	8.0	5
50.5S-9.6P-9.9N	30	37	3.7	-	2.8	-	30.0	4
70S-l0P-20N	30	37	4.4	-	6.5	-	45.0	4
60S-4P-36C	30	34	$C_6H_{15}PO_4$ 3.04	-	-	19.0	18.0	2

S - SiO_2, P - P_2O_5, A - Al_2O_3, N- Na_2O, C - CaO

The material to be covered were plates 2 x 2 x 0.5 cm, made from two kinds of glass: sodium calcium-silicate glass (containing about 15wt % of Na_2O) and melted quartz. The basic glass plates were washed several times in water with an addition of detergents, rinsed using distilled water and ethanol. The gel layers were deposited by immersing the plates in the solution and pulling them out at a rate of 1 mm/s. This operation was performed 1 to 3 times.

The covered glass plates were placed in a desiccator for a period of two weeks, and next heated to the temperature 450^0C. The glasses covered with the layers of chemical compositions No 1-4 were next the object of:

- microscopic SEM observations,
-light transmittance measurements,
- test of chemical resistance,
- investigations of surface electrical conduction.

The SEM examinations were conducted by means of scanning microscope ISM5200.

The light transmittance was tested on spectrophotometer UV-VIS Zeiss-Jena.

The chemical resistance was tested as follows: the basic glass plates covered with gel layers were boiled in a water bath for 3h and next the amount of leached Na_2O in the solution was determined by titration of 0.01 n HCl and directly - by the ASA method. The investigations were conducted on sodium-calcium-silicate glass covered with the layers. The results are shown in Table 2.

Table 2. Results of examinations of chemical resistance for sodium calcium-silicate glasses covered with the layer (amount of Na_2O in solution was determined by titration of 0.01 n HCl).

No	Kind of the layer (compositions in mol%)	Amount of Na_2O in solution mg /100 cm3
1	Basic glass	0.400±0.005
2	80.77S-19.23P	not existed
3	79.8S-10.2P-10A	0.047±0.006
4	80.5S-9.6P-9.9N	0.018±0.004
5	70S-10P-20N	0.0620±005

S - SiO_2, P - P_2O_5, A - Al_2O_3, N - Na_2O

The measurements of surface electrical conduction were conducted on samples in which the basic glass was the sodium-calcium-silicate glass as well as on samples made from melted quartz. Gold electrodes were sprayed on the surface of the examined samples, creating in this way an active surface in the form of a ring with the outer diameter d_2 = 12 mm and the inner diameter d_1 =10 mm. For the measurements of electrical conduction there was applied a standard measuring system comprising a high voltage feeder cable, electrometer and a digital voltmeter. The surface resistance was determined directly from the measurements on the basis of the relation:

$$\rho = (R/2\pi)\ln(d_1 / d_2)$$

where d_2 and d_1 are the outer and the inner diameter of the active ring, respectively.

The measurement results are listed as electrical conduction expressed in om^{-1} units to be interpreted as the inverse of the surface resistance for the supply voltage 1000V (Table3).

The glasses covered with the layers of chemical composition $60SiO_2$-$4P_2O_5$-36CaO were put into simulated body fluid with chemical composition close to human plasma (SBF). After soaking for various periods of time, the samples were removed from the solution and dried in air. Afterwards the surface of materials was subjected to FTIR examinations and scanning microscopy observations.

Table 3. Results of examinations of surface electrical conduction for melted quartz and sodium-calcium silicate glasses covered with the layers.

Kind of examined material	Electrical conduction (om^{-1})
melted Quartz	$1.75 \cdot 10^{-15}$
Q + layer 79.8S-10.2P-10A	$1.69 \cdot 10^{-8}$

Q + layer 80.5S-9.6P-9.9N	$6.89 \cdot 10^{-15}$
Q + layer 80.77S-10.23P	$1.10 \cdot 10^{-8}$
sodium-calcium silicate glass (G)	$3.3 \cdot 10^{-11}$
G + layer 79.8S-10.2P-10A	$1.78 \cdot 10^{-8}$
G + layer 80.5S-9.6P-9.9N	$1.83 \cdot 10^{-15}$
G + layer 70S-10P-20N	$3.62 \cdot 10^{-11}$
G + layer 80.77S-19.23P	$4.55 \cdot 10^{-8}$

S - SiO_2, P - P_2O_5, A - Al_2O_3, N - Na_2O

RESULTS AND DISCUSSION

The SEM observations have shown that the layers deposited on sodium-calcium-silicate glass as well as those on melted quartz are in general characterized by good quality and adhesion to the base. Defects such as cracks, pop-offs, "knobs" occurred sporadically.

The sodium-calcium-silicate glasses covered with the silicate-phosphate layers show higher light transmittance in the visible region than the basic glass (Fig.1). It points out the anti-reflexive properties of these layers.

From the investigations of the chemical resistance it follows that all glass samples covered with silicate-phosphate gel layers show a higher chemical resistance than the basic sodium-calcium-silicate glass. The sodium leached during boiling might in this case derive from the base, insufficiently shielded by the layer (systems: SiO_2-P_2O_5-Al_2O_3, SiO_2-P_2O_5) as well as from the layers itself (system SiO_2-P_2O_5-Na_2O). The obtained results, however, show that even in case when the amount of Na_2O present in the layer is comparable with that in the basic glass (sample No 5, Tab. 2), the amount of Na_2O deriving from the layer is more than 10 times smaller than that in the basic glass. This is an indication that sodium in the silicate-phosphate gel glass is stronger bounded with the glass structure than in silicate glass, which may be due to its direct neighbourhood with the tetrahedral [PO_4], containing doubly bonded oxygen ions.

Investigations of the surface electrical conduction of glasses with deposited gel layers yielded unexcepted results. Both in the case of melted quartz as a base as well as in the sodium calcium silicate glass the lowest surface conduction, close to that of melted quartz was exhibited by layers with the composition (mol%): 80 SiO_2, 10 P_2O_5,10 Na_2O (table 3). Considering that in this type of glass the conduction is, as a rule, of ionic character, and the current carriers are mainly the alkalies ions, this observation is an indication that in the presence of phosphorus, sodium becomes more strongly bounded with the silicate-phosphate matrix and in effect becomes a weak carrier of current. These results are consistent with the results of the investigations of chemical resistance, indicating little leaching of sodium from layers of composition: 80 SiO_2, 10 P_2O_5, 10 Na_2O (Table 2). From our investigations it follows that layers of the above composition may by used as coatings imparting the property of electric insulation to glass surface and at the same time increasing its chemical resistance. It is also worthy of note that these layers are stable, i.e. their conduction does not change when they remain charged with electricity for a longer time.

In the case of layer containing 20 mol% of Na_2O the conduction increases approaching that of the basic glass. With this amount of sodium its properties as a current carrier are thus similar to those of a melted silicate glass.

The gel layers in the remaining oxide systems (SiO_2-P_2O_5, SiO_2-P_2O_5-Al_2O_3), although not including alkalies in their composition, exhibit high surface conduction, exceeding considerably the conduction of the basic glass. It is very unlikely that any of the cations present in these gel layers (P^{+5}, Si^{+4}, Al^{+3}) might be an effective current carrier. Assuming that the electron conduction does not occur here in any significant degree (which in case of chemical compositions of this type is little probable), the only logical explanation for the observations made during the experiments is attribute the current conduction to the protons H^+, the presence of which in the silicate-phosphate glasses is justified [11]. However, the investigations show that such a situation exists in alkali-free silicate-phosphate glasses, and does not occur in the presence of alkalies. This observation may initiate a new approach to the structure and properties of the silicate-phosphate glasses, inspiring for further experimental studies in this field.

From the investigations carried out so far it follows that the surface conduction of conventional sodium-calcium-silicate glasses can be distinctly increased by coating them with gel layers of the alkali-free systems SiO_2-P_2O_5, and SiO_2-P_2O_5-Al_2O_3.

As distinct from the earlier described layers from the systems SiO_2-P_2O_5, SiO_2-P_2O_5-Al_2O_3 and SiO_2-P_2O_5-Na_2O, the applicability of layers from the system SiO_2-P_2O_5-CaO is connected with the possibility of their application for biological activation of biologically inert materials [1,2]. When materials used as bone implants are covered with layers from the system SiO_2-P_2O_5-CaO, on the surface of the implant hydroxyapatite crystallizes as a result of contact with the plasma; through the layer of hydroxyapatite formed on the surface the implant accretes with the bone in a living organism. Hence the ability of hydroxyapatite crystallization on the material surface can be regarded as the basic parameter, determining its bioactive properties. In the present study there have been investigated the changes of the surface occurring on the $60SiO_2$-$4P_2O_5$-36CaO layer, after its contact with simulated body fluid. It has been found that after 10 day-long contact with SBF there occur changes on the surface which give evidence of crystallization of calcium phosphates. This can be interpreted as a positive sign indicating the possibility of the application of layers of this type for biological activation of materials.

Acknowledgment

The authors wish to thank the Scientific Research Committee (KBN) for the financial support (Project No 7 S201 006 06).

REFERENCES

[1] HENCH L.L., SPILINTER R.J., ALLEN W.C., GREENLEE T.K. Jr.: J. Biomed. Mater.Res., Bonding Mechanism at the Interface of Ceramic Prosthesis Materials,2,1972,117-141.

[2] KOKUBO T.: Novel Bioactive Materials Derived from Glasses, Bol. Soc. Esp. Cer. Vidr., Proc. XVI Intem. Congr.on Glass, Madrid 1992, vol. I,119-137.

[3] KOOI E.: Formation and Composition of Surface Layers and Solubility Limits of Phosphorus during Diffusion in Silicon, J. Electrochem. Soc., III,12,1964,1383-1387.

[4] MIDDELHOEK J., HOLLEMAN J.: Low Phosphorus Concentrations in Si by Diffusion from Doped Oxide Layers, Sol.-State Scie. and Techn.,121,1,1974,132-137.
[5] MACKENZIE J.D.: Unusual Non-Crystalline Solids from Gels in 2004, J. Non-Cryst. Sol.,73,1985,631-637.
[6] SAKKA S., KAMIYA K., MAKITA K., YAMAMOTO Y.: Formation of Sheets and Coating Films from Alkoxide Solutions, J. Non-Cryst. Sol.,63,1984,223-235.
[7] SHENG L., ZARZYCKI J.: Evolution of the Structure of Gels of the System SiO_2 Al_2O_3-P_2O_5 Submitted to Thermal Treatment,112,1989,428-431.
[8] HAYRI E.A., GREENBLATT M., PRUNA P., GERHARDT R.: Na_2O-P_2O_5-SiO_2 Gels: Preparation and Characterization,111,1989, I67-172.
[9] LACZKA M., CIECINSKA M., BIALOTA J.: Synthesis, Structure and Properties of Sol- Gel GIasses of Sysems: SiO_2-P_2O_5,SiO_2-P_2O_5-Al_2O_3,SiO_2-P_2O_5-Na_2O. Bol.Soc.Espan. Cer. Vidr., Proc. XVI Intern. Congress on Glass, Madrid 1992, vol.7,233-238.
[10] LACZKA M., CIECINSKA M.: Synthesis and Structure of Gel Glasses of Mixed Network, Papers of the Commission on Ceramic Science, Ceramics 41, Pol. Ceram. Bull.79-85.
[11] WASYLAK J.: Structure and Properties of Non-Alkaline Phosphate Glasses, Scientific Bulletins of Academy of Minning and Metallurgy No.824, Ceramics 44,1985.

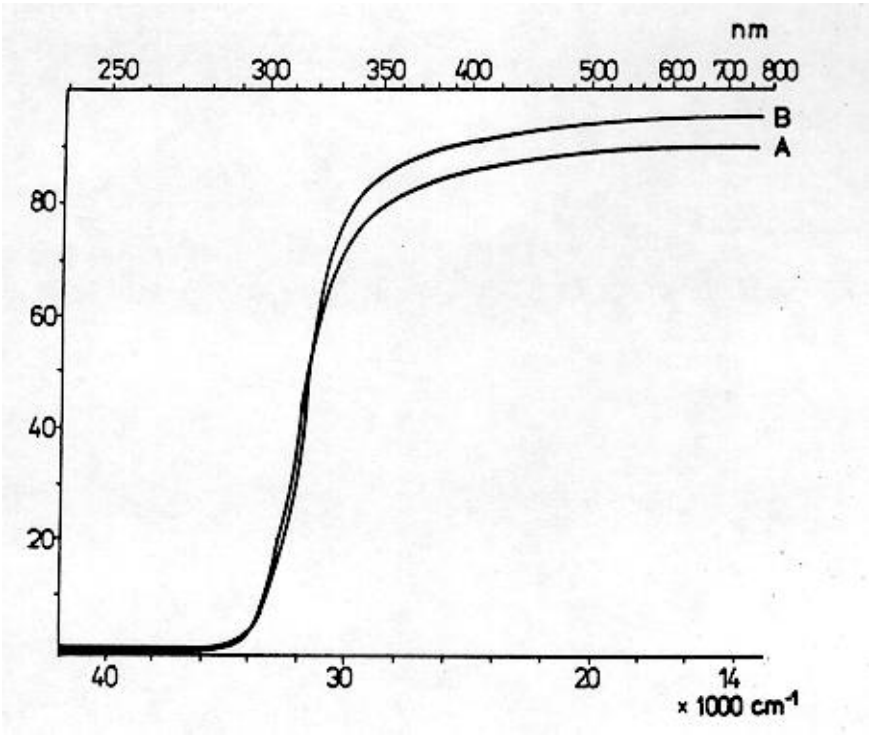

Fig.1. Light transmittance of sodium-calcium silicate glass covered with the $80SiO_2 \cdot 10P_2O_5 \cdot 10Al_2O_3$ layer.

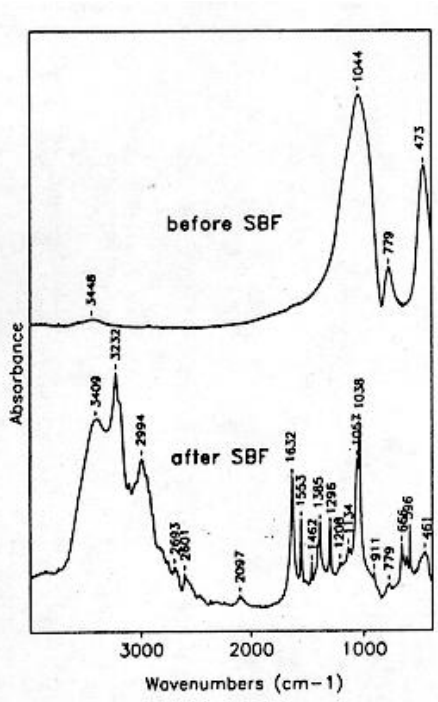

Fig.2. FTIR transmission spectra of the surface of $60SiO_2$-$4P_2O_5$-36CaO layer before and after contact with simulated body fluid.

GROWTH AND PROPERTIES OF BOROPHOSPHOSILICATE GLASS COATINGS DEPOSITED BY PLASMA CVD*

Wagar Ahmed
University of Northumbria, United Kingdom

Abstract

Borophosphosilicate glass coatings have become important in recent years for the fabrication plasma chemical vapour deposition (PCVD) has been used to grow glass coatings with approximately 4% boron and 4% phosphorus at low temperatures. The effects of the oxygen to silane flow ratio and deposition temperature have been examined and explained in terms relative transport and kinetic rates. It has been shown that the additions of phosphorus and boron are beneficial for the manufacture of microelectronics devices because the temperature required to reflow the coatings to give smooth profiles over sharp corners of complex structures normally employed can be reduced considerably. Various combinations of temperature, ambient and time have been employed to anneal and reflow borophosphosilicate glass films. The reflow characteristics have been studied using an SEM and the results obtained are presented.

---

* Full manuscript not available at the time of printing

HIGH GAS PRESSURE METHOD FOR THE PREPARATION OF SELENITE GLASSES

Luben Lakov, Stnncho Jordanov and **Krasimira Toncheva**
Bulgarian Academy of Sciences, Bulgaria

Yanko Dimitriev
University of Chemical Technology and Metallurgy, Bulgaria

Abstract

The main difficulty in the synthesis of selenite glasses is the sublimation of SeO_2 above 588^oK. An autoclave equipment is developed for melting at high gas pressure (P max=35 MPa) in order to prevent the volatilization from selenite liquids and the synthesis of glasses at maximum temperature 823^oK. The melting is done in platinum or quartz glass crucibles with 200 - 300 cm^3 volume. The conditions of cooling are gradually changing at rate 2^oK/min. The influence of different melting conditions are investigated and new stable multicomponent selenite glasses are obtained in the systems SeO_2-MoO_3-Sc_2O_3, SeO_2-MoO_3-Pr_2O_3, SeO_2-Bi_2O_3-Sc_2O_3 and SeO_2-Bi_2O_3-Pr_2O_3.

1. INTRODUCTION

The preparation of selenite glasses was first described by Rawson and Stanforth, who successfully synthesised glasses in the K_2O-SeO_2 and the TeO_2-PbO-SeO_2 systems [1,2]. As they pointed out, the main difficulty in the synthesis of glasses of this type is the rapid volatilisation of selenite melts and the sublimation of SeO_2 at atmospheric pressure and temperatures above 588^oK.

Until now, selenite glasses are exotic material, which have not been extensivity studied. There a few papers [3-10] consider the synthesis and properties of these materials. According to our earlier investigations, it is possible to obtain glasses from certain binary and multicomponent selenite systems [10-17].This paper is a continuation of our research programme in the preparation of new glasses with the participation of SeO_2 at high pressures.

2. EXPERIMENT

Experiments carried out to investigate the processes of melting and glass-formation in systems, containing sublimation and dissociation components, are quite few.. The reason for this lies in the technical difficulties that are present while combining simultaneously high-pressure and high-temperature under volatile substance environment [18-20]. Two methods of synthesis find application in work with such substances: in

vacuum proof crucibles and high pressure equipment. Most appropriate for the case at high scale experiments is used of the different type of autoclave equipment, where gas pressure and oxidation - reducing conditions in the system may be controlled within wide range.

An original optimum construction of autoclave equipment (Fig. 1) was designed, developed and tested. Major components of the autoclave are the reaction cell, framework, heaters, heat-insulation, thermo-couples and -measurement appliances.

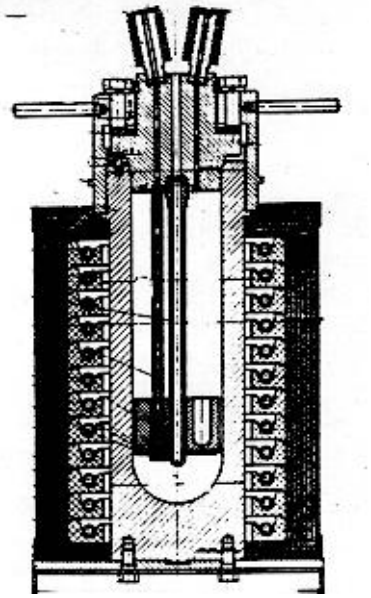

Fig. 1 Autoclave for synthesis of glasses under pressure at Pmax. = 35Mpa and T= 823^{o}K

The main component of the autoclave is the reaction cell. It is a cylindrical crucible shut with a metal cork from the upper side. Junction bonds for gas inlet and outlet, and a thermocouple input are mounted on the cork. All junction bonds along the inlet and outlet tracks are sealed in "metal-into-metal" form. The pressure in the autoclave is measured by means of a manometer up to 100 MPa. A resistant heating furnace reaching up to 973^{o}K was built-in on the external side of the cylindrical crucible. Inside the cell, there is a cavity fire-proof test-tube (platinum or quarts) frame, with test-tube volume reaching up to 500cm^{3}, during synthesis of smaller quantities of selenite glasses. Oxygen was used as gas environment for pressure transmission on the raw materials containing SeO_2, in order to maintain oxygen environment.

The components were introduced into the batches as analytical grade oxides. The samples were melted in quartz glass crucibles situated in autoclave device. The maximum oxygen pressure during the experiments was 35MPa and the maximum temperature was 823^{o}K, which was attained in 2h and maintained for 20 min. After melting they were quenched in water and the samples were characterized visually by optical microscopy, X-ray diffraction and IR spectroscopy.

3. RESULT

The vitrification regions for the new ternary systems SeO_2-MoO_3-Sc_2O_3 , SeO_2-MoO_3-Pr_2O_3, SeO_2-Bi_2O_3-Sc_2O_3 and SeO_2-Bi_2O_3-Pr_2O_3 are presented in Fig. 2 and 3.

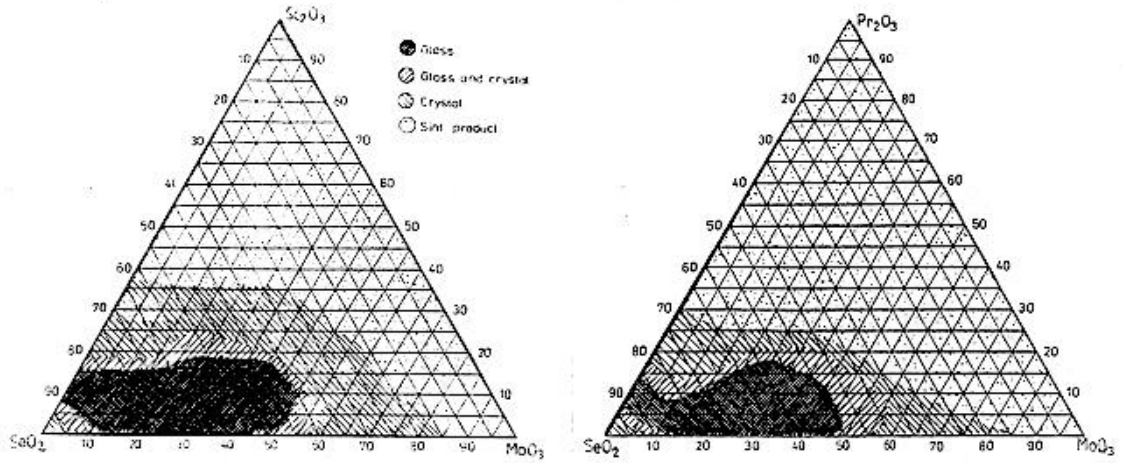

Fig.2. Glass formation regions in three component systems: SeO_2-MoO_3-Sc_2O_3 and SeO_2-MoO_3-Pr_2O_3 .

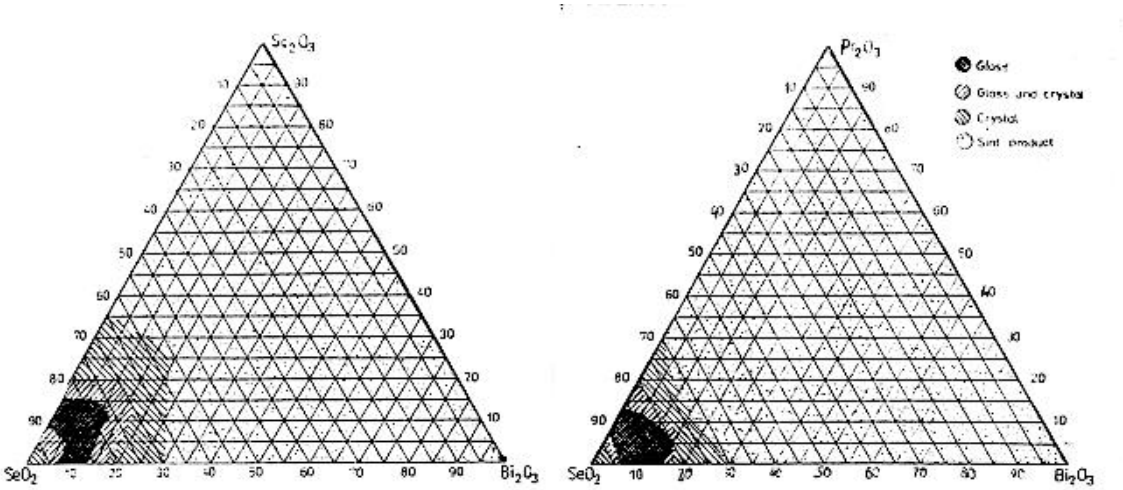

Fig.3. Glass formation regions in three component systems: SeO_2-Bi_2O_3-Sc_2O_3 and SeO_2-Bi_2O_3-Pr_2O_3

The stable glasses are situated near the SeO_2 corner. The widest region was obtained in the SeO_2-MoO_3-Sc_2O_3 /Pr2O_3/ systems. This obtained data are valid only at indicated conditions to experiment: low rate of cooling and maximal temperature of melting up to 823^oK

4. CONCLUSION

It has been proved that the autoclave is suitable for the synthesis of selenite glasses: SeO_2-MoO_3-Sc_2O_3, SeO_2-MoO_3- Pr_2O_3, SeO_2-Bi_2O_3-Sc_2O_3 and SeO_2-Bi_2O_3-Pr_2O_3. The obtained regions of glass formation are comparable with the data concerning other tree-component selenite systems [10-17]. It has been confirmed experimentally that SeO_2 may from MoO_3 an stable glassy network. The glasses synthesized with the participation of Sc_2O_3 are characterized by a better chemical stability with respect to the other trivalent oxides participating in the investigated systems.

REFERENCES

l. H.Rawson, Phys. Chem. Glasses 1 (1960) 170

2. I.E.Stanforth, J. Soc Glass Technol. 36 (1952) 217

3. C.S. Sunandana and A.K.Bhatnagar, J. Phys. C 17 (1984) 467

4. C.A.Angell, Solid State Ionics 18,19 (1986) 72

5. T.Minami, J. Non-Crist. Solids 56 (1983) 15

6. G.Govindaraj, N.Baskaran, K.Shahi, P.Monoravi, "Preparation, conductivity, complex permittivity and electric modulus in AgI - Ag_2O - SeO_3 - MoO_3 glasses", Solid State Ionics, 75(1995)

7. G.Govindaraj, N.Baskaran, "A.c. conductivity and electric modulus behavior of the vitreous system AgI - Ag_2O -[$XSeO_3$ - $(1-X)V_2O_5$]", Materials Science and Engineering,B25 (1994)135-140

8. G.Govindaraj, N.Satyanarayana, A.Karthikeayan, "Preparation and electrical conductivity studies of silver based molybdoarsenate glassy compound system", J.Mat.Sci.Lett. 9(1990)1123-112

9. A.Karthikeayan, G.Govindaraj, N.Satyanarayana, "Stady of dopant salt concentration in a silver molybdoarsenate glassy system", Materials Science and Engineering, Bl3 (1992) 295-298

10. N.satyanarayana, G.Govindaraj, A.Karthikeayan, "Effects of differing ratios of network (Ag_2O) to network formers (MoO_3 + V_2O_5) and dopant salt (AgI) concentration in silver-based superionic glassy compounds", J.Non-Cristalline Solids, 136(1991)219-226

11. L.lakov, Y.Dimitriev, Phys. Chem. Glasses 22 (1981) 69

12. L.lakov, Y.Dimitriev, Phys. Chem. Glasses 23 (1982) 76

13. Y.Dimitriev, V.Dimitrov, L.lakov and I.Kovachev, Proc. l3th Int. Congr. Glass, Hamburg, 1983;Bd.2, p.880

14. Y.Dimitriev, Y.Ivanova, V.Dimitrov and L.lakov, J. Mat. Sci. Lett. 21 (1986) 142

15. Y.Dimitriev, Y.Ivanova, V.Dimitrov, L.lakov and St.Yordanov, J. Mat. Sci. Lett. 9 (1990) 793

16. St.Yordanov, L.Lakov, K.Toncheva and Y.Dimitriev, Proc. Seventh Int. School. on Cond. Matter Phys., Varna, ed. J.Marshall, N.Kirov and A.Vavrec (World Sci.Singapore, 1992) p415

17. Y.Dimitriev, St.Yordanov, L.Lakov, J. NonCryst Solids 192&193 (1995) 179-182

IMMOBILIZATION OF SOLID WASTE BY VITRIFICATION PROCESSES

Manfred Krauß
Fraunhofer-Institut fur Silicatforschung, Germany

Abstract

Whilst household and industrial waste volumes have been constantly increasing, dumping capacities have been decreasing in the last few years. Therefore, incineration has become more important with time. The resulting solid waste residuals from waste incinerator flue gas cleaning systems and the fly ashes contain various alkalihalogenide salts, toxic heavy metal compounds and traces of organic pollutants, such as dioxine and furane. The vitrification is the most discussed and developed process for the safe and economic immobilization of these waste materials. The principal problems of all vitrification processes are the wide-spread composition variation of the waste materials and the lack of knowledge of the melting behaviour and the chemical and physical properties of the resulting waste glasses. The glass has to be of high chemical durability to prevent significant leaching of the hazardous components.

In this work, the correlation between waste composition, melting behaviour and long-term chemical stability of the resulting glasses will be investigated. The first results are reported.

I. INTRODUCTION

The increasing amount of waste materials causes a serious decrease of disposal capacity. Therefore, incineration is of increasing interest. For example, 9.000.000 tons of municipal waste were burnt in Germany in 1990. 40 to 70 kg of fly ashes and filter dusts from waste gas treatment were produced per ton of waste [1]. About 300.000 tons per year of incineration filter dusts and ashes accumulated in Germany. The flue ashes and filter dusts contain hazardous waste like dioxines, furanes, and large amounts of water-soluble toxic heavy metal compounds, e. g. lead, copper, and zinc (Table 1).

Prior to safe disposal or recycling, an effective immobilization of those hazardous components is strongly requested. Various routes of immobilization by vitrification have been recently summarized [2 - 4]. Some concepts are based on established technologies of the glass industry, e. g. the re-use of filter dust from glass melting plants [5] or of glass cullet [6]. Other investigations concentrate on new techniques of detoxification and vitrification of filter dusts [7]. Furtheron, first attempts to produce technical glass, e. g. glass ceramics, by melting municipal waste incinerator ash has been performed [8]. Up to now, a lot of unsolved problems remains and prevents vitrification of residual materials from a large-scaled application. The wide-spread compositional variation of the waste leads to an unexpected effect during the melting process. Segregation and crystallization occur and the prediction of an uncritical chemical and physical behaviour of the glasses is strongly restricted. Thus, the investigations reported concentrate on an

increased basic understanding of the melting behaviour of incineration filter dusts and the characterization of the long-term chemical durability of the resulting glasses.

Table 1. Average composition of filter dust from German incineration plants

component	content (wt.%)	component	content (mg/kg)
SiO_2	31.4	Cd	134
Al_2O_3	16.3	Cr	447
Fe_2O_3	2.7	Cu	667
TiO_2	1.9	Ni	35
CaO	19.3	V	131
MgO	2.7	Pb	3213
Na_2O	3.4	Zn	10386
K_2O	4.6	Ag	14
ZrO_2	< 0.05	Sb	227
P_2O_5	1.6	Se	7
BaO	0.3	Sn	1102
SrO	0.04	Hg	17
Mn_3O_4	0.16	Co	23
SO_3	2.9		
CI	4.4		
F	0.15		
C_{total}	7.6		
C_{free}	6.5		

2. EXPERIMENTAL

A model glass system SiO_2-Al_2O_3-CaO/MgO-Na_2O/K_2O has been defined in order to cover the compositional variations of the basic components of real incineration filter dusts. The partial substitution of CaO by heavy metal oxides or chlorides (Zn, Cu, Pb, Fe), P_2O_5, carbon and/or sulphate allows the systematic investigation of the influence of those components. The investigated variation of the model system and the substitutes are given in Table 2.

Table 2. Variations of the waste model glass composition

model system (wt.%)	CaO substitutes
20- 40 SiO_2	0- 5 Fe_2O_3
5-10 Na_2O/K_2O	0-1 CuO
5-15 Al_2O_3	0-1 PbO
15- 30 CaO/MgO	0- 3 ZnO
	0-10 P_2O_5
	0-7 SO_3
	0- 4 chloride
	0-1 fluoride
	0- 5 carbon

Pure oxides, carbonates or chlorides and carbon (graphite) were used as raw materials. The glasses were melted for 4 hrs at 1400 to 1500 ^{o}C in Pt/Rh or Al_20_3 crucibles in a resistant-heated electric furnace with normal air atmosphere. The glasses obtained were subsequently annealed in an electric furance at 600 to 620 ^{o}C.The glasses have been characterized in terms of the melting behaviour, devitrification, separation of metals, and chemical durability. The first three properties were determined by visual observation or light microscopy at first. For the transmission measurements polished glass sheets were used. For the "DEV S4" test the glasses were grained.

One of the most important properties is the resistance of the glasses against chemical attack by aqueous solutions. Due to the lack of a suitable realistic standard corrosion test, the durability was investigated in accordance to the German legally required "DEV S4" test [9]. This is a stationary test, where a glass grain fraction between 0.315 and 0.5 mm is exposed to distilled water with a constant ratio of the mass of the grain to the volume of water. Subsequently, the leached glass components were chemically analyzed by ICP-OES, and the electrical conductivity of the eluate was determined.

3. RESULTS

The high silica and calcium oxide content made it possible to synthesize glasses in a wide composition range (Table 2). The melting behaviour was different. Foaming was generally observed, but the quenched glasses were free of crystalline products in most cases.

Because of the presence of iron or copper oxide in some model compositions the resulting glasses were coloured. The darkness of the glass colour increases with the carbon content and varied from amber to black at a carbon content of more than 5 wt.% (results of transmission spectra).

Spherical metallic particles were sometimes found in glasses which contain copper as well as sulphur. Surprisingly, this is not the case with glasses containing other metals, e. g. zinc. The simultaneous excess of carbon and sulphur leads to a significant gall formation which consists of about 40 wt.% K, 39 wt.% S,13 wt.% O, 5 wt.% Na, 2 wt.% Ca and 0,6 wt.% Si (analyzed by X-ray fluorescence analysis).

The first results of the DEV S4 test are given in Table 3. The model basic glass (40 wt.% SiO_2, 15 wt.% Al_2O_3, 30 wt.% CaO, 5 wt.% MgO, 10 wt.% Na_2O) is compared to those glasses with systematic substitutions of CaO by CuO, PbO, and ZnO in terms of the glass colour, the leached amount of Cu, Pb, and Zn and the electrical conductivity. The leaching of the heavy metal increases with the metal content of the glasses. At the same time the electrical conductivity of the eluate is decreased. It is assumed that with increasing number of components in the glass the chemical resistance will be reinforced.

For comparison, the required limits for disposal, which are regulated by the German "TA Siedlungsabfall" [10], are also shown in Table 3. These limits are fulfilled for the conductivity, but not for all heavy metal contents of the glasses.

Table 3. Comparison of the glass composition, results of the test "DEV S4" and the limits of the German "TA Siedlungsabfall"

glass no.	**waste glass composition**	**glass colour**	**Content of the eluate**			
			Zn	**Cu (mg/l)**	**Pb**	**electrical conduct. (FS/cm)**
1	model glass	colourless	0.19	0.05	0.15	65
2	m + K_2O, Na_2SO_4, Fe_2O_3	green	0.06	0.09	0.01	< 1000
3	m + K_2O, Na_2SO_4, CuO, ZnO, PbO	blue	0.16	0.65	0.18	< 1000
4	m + K_2O, Na_2SO_4, Fe_2O_3, CuO, ZnO, PbO	brown	0.21	0.96	0.28	960
5	m + K_2O, Na_2SO_4, Fe_2O_3, P_2O_5, ZnO, CuO, PbO, 0.5C	green/brown	0.71	2.34	0.27	24
6	m + K_2O, Na_2SO_4, Fe_2O_3, P_2O_5, $ZnCl_2$, $CuCl_2$, $PbCl_2$, 0.5C	green	0.62	3.01	0.34	30
limit of the German TA "Siedlungsabfall" (disposal site class I)			< 2	< 1	< 0.2	< 6000

REFERENCES

[1] Reimann, D. O.: Reststoffe aus thermischen Abfallverwertungsanlagen. Müll Abfall (1991), Beih. 29: Reststoffe aus der Rauchgasreinigung, 12-16

[2] Pieper, H.: Das SOLUR-Verfahren zur Inertisierung von schwermetallhaltigen Stoffen. Das Sorg-Glasschmelzverfahren. Sprechsaal 124 (1991) 490 - 491

[3] Kipka, A., Luckscheiter, B. and Lutze, W.: Melting of fly ashes and product properties. Glastech. Ber. Glass Sci. Technol. 66 (1993) 214 - 220

[4] Rabiger, W., Keldenich, K. and Scheffler, J.: Experience in operation of a pilot plant melting residual substances. Glastech. Ber. Glass Sci. Technol. 68 (1995) 84 - 90

[5] Krauß, M. et al.: Characterization of filter dust in the glass container industry and definition on its influence on green glass melts. Glastech. Ber. Glass Sci. Technol. 68 (1995) 279 - 284
[6] Enneking, C.Q.M.: Bewertung von Altglasscherben und Konsequenzen fur den Glasschmelz-prozeß. Glastech. Ber. Glass Sci. Technol. 67 (1994) N55
[7] Faulstich, M.: Inertisierung fester Rückstande aus der Abfallverbrennung. Abfallwirtschafts-Journal 1 (1989) 20
[8] Karamanov, A. et al.: Synthesis of wall-covering glass-ceramics from waste materials. Glastechn. Ber. Glass Sci. Technol. 67C (1994) 227 - 230
[9] Deutsche Einheitsverfahren zur Wasser-, Abwasser- und Schlamm-untersuchung. Schlamm und Sedimente (Gruppe S), Bestimmung der Eluierbarkeit mit Wasser (S 4). DIN 38414, part 4,1984
[10] Dritte Allgemeine Verwaltungsvorschrift zum Abfallgesetz (TA Siedlungsabfall). Technische Anleitung zur Verwertung, Behandlung und sonstigen Entsorgung von Siedlungsabfallen. Vom 14. Mai 1993 (Bundesanzeiger Nr. 999)

LIGHT FILTER BASED ON SILICA GEL-FILMS DOPED WITH ORGANIC DYE

G.E.Malashkevich[1], E.N.Poddenezhny[2] ,I.M.Melnichenko[2] and **V.B.Prokopenko[2]**
1. Academy of Sciences of Belarus, Belarus
2. Gomel State University, Belarus

Abstract

Silica gel-films doped with some organic dyes, which are provided the optical density in a main functional band from 0.3 up to > 3 at thickness 0.2 μm, have been synthesised. The dependence of the water stability, obliteration and spectroscopic properties on the concentration of the dye and the temperature of heat treatment has been investigated. It was discovered that the essential decrease of doped silica gel-films specific absorption takes place with the increase of the dye concentration. It was found that the photo stability of these films is increased after the codoping with cerium chloride.

1. INTRODUCTION

The possibility of significant decrease of formation temperature of the inorganic matrix by using of the sol-gel technology permits to hope for obtaining of various composite materials doped with organic dyes on the stage of the sol-colloid system. In particular, recently was informed [1] on creation of colour covers for television tubes, representing of silica gel-films with incorporated molecules of some Xanthene dyes. The aim of the present paper was elucidation the possibility of the silica gel-films creation doped with organic dyes with high optical density, mechanical strength and water stability, as well investigation of molecular peculiarities of dye incorporating in formed glass-organic gel-film. In parallel, we have also tried to determine the possibility of increase of photo stability of these light filters by additional doping with cerium, which is widely used for increase of glass radiationly-optical stability.

2. EXPERIMENT

The process of film preparation included the tetraethylortosilicate hydrolysis in water solution of hydrochloric acid to obtain a sol. The exposure of this sole during a week and subsequent dissolution in it the organic dye. Drawing by means of spinning of the dye-containing sol on a substrate (quartz or silicon) and heat treatment obtained films at different temperatures, T_f, in during of 5 minutes.

The control of thickness of films, h, was performed using by profilograph-profilometer with the error of ±5 %. The water stability was controlled on decrease of the optical density, D, of the films after their exposure in flowing water during 4 hours. The test for mechanical strength was carried out on number cycles sliding by a rubber tip through

cambric lining at the presence of a spirit under a load of 0.3 kg, which are necessary for complete obliteration of the film.

The spectra of absorption in visible and UV regions were detected on a spectrophotometer (Beckman-UV5270). For measuring of IR spectra was used a spectrophotometer (UR-2). In all cases in a channel of comparison were placed the corresponding clean substrates.

The luminescence intensity of these films was controlled by means of spectrofluorimeter (SDL-2).

3. RESULTS

Test on obliteration of the obtained films has shown that with the increase of the dye concentration, C_{dye}, in the sol nonlinear easing of their mechanical strength takes place. In particular, for films with rhodamin 6 G at the C_{dye} increase in the range 1-5 mass % the number of cycles sliding up to complete obliteration of the film decreases with 5000 up to 1200. At further increase of the C_{dye} up to 12.5 mass % the quantity of these cycles decreases up to 300 and smaller. Influence of T_f on the films obliteration is more weak. The washing of the dye from the film with the C_{dye} = 3 mass % makes about 10 % at T_f = 300^{o}C and 25 % at T_f = 22^{o}C. For the film with the C_{dye} =12.5 mass % the washing exceeds 90 % at all T_f. However at additional covering of the dye-containing film with nondoped silica gel-film it is practically not washed.

Fig. 1 shows the visible and UV light attenuation spectra of the films with h = 0.2 μm doped with some the most soluble in the sol dyes. The structural formulas of these dyes are also indicated. It is seen that the greatest significance of D in the band $S_1 \leftarrow S_o$ is provided for films with rhodamin 6 G (curves 1-3) at C_{dye} =12.5 mass %. For the films with diamond green (curves 4 and 5) and cumarin 1 (curves 6 and 7) characterized by maxima values of the C_{dye} = 4.5 and 11.5 mass %, respectively, the values of D is essentially less. The increase of C_{dye} is accompanied by decrease of specific integrative intensity of the band $S_1 \leftarrow S_o$ and significant deformation of its contour. For the cumarin 1 at maximum C_{dye} is observed significant increase of light scattering.

Fig. 2 shows the absorption spectra in the region of $S \leftarrow S_o$ band of the films with rhodamin 6 G (C_{dye} = 3 mass %) obtained at various T_f. It is seen that the film with T_f = 22^{o}C is characterized by the two-humped $S_1 \leftarrow$So band with maxima at 505 and 530 nm (curve 1). The intensification of long-wavelength component of this band at the expense of weakening of its short-wavelength component (curve 2) takes place with the increase of T_f up to 300^{o}C. The value of D decreases approximately in three times at T_f = 350^{o}C (curve 3). The thickness of these films with increase of the T_f in the range 22-350^{o}C within the limits of measurement error does not change.

Fig. 3 shows the IR absorption spectra of nondoped and doped films with rhodamin 6 G at various C_{dye} (T_f = 250^{o}C). It is seen that in spectrum of nondoped film (curve 1) are observed the comparatively wide and lowly-intensive band at 3400 cm^{-1}, the two-humped intensity band with a maximum at 1075 cm^{-1} and lowly- intensive band at 945 cm^{-1}. The introduction of rhodamin 6 G with C_{dye} = 3 mass % is accompanied by intensification of the band at 3400 cm^{-1} as well the bathochromic shift approximately on 100 cm^{-1} of its maximum and expansion on the side of low frequencies. Moreover, there is observed the

bathochromic shift approximately on 7cm^{-1} of a maximum of the most intensive band and it expansion on the side of low frequencies, the intensification of band at 945 cm^{-1} and its shift on 15 cm^{-1} to highly-frequency side (curve 2), also the appearance of a number of lowly-intensive narrow bands in the region 1100-1750 cm^{-1}.

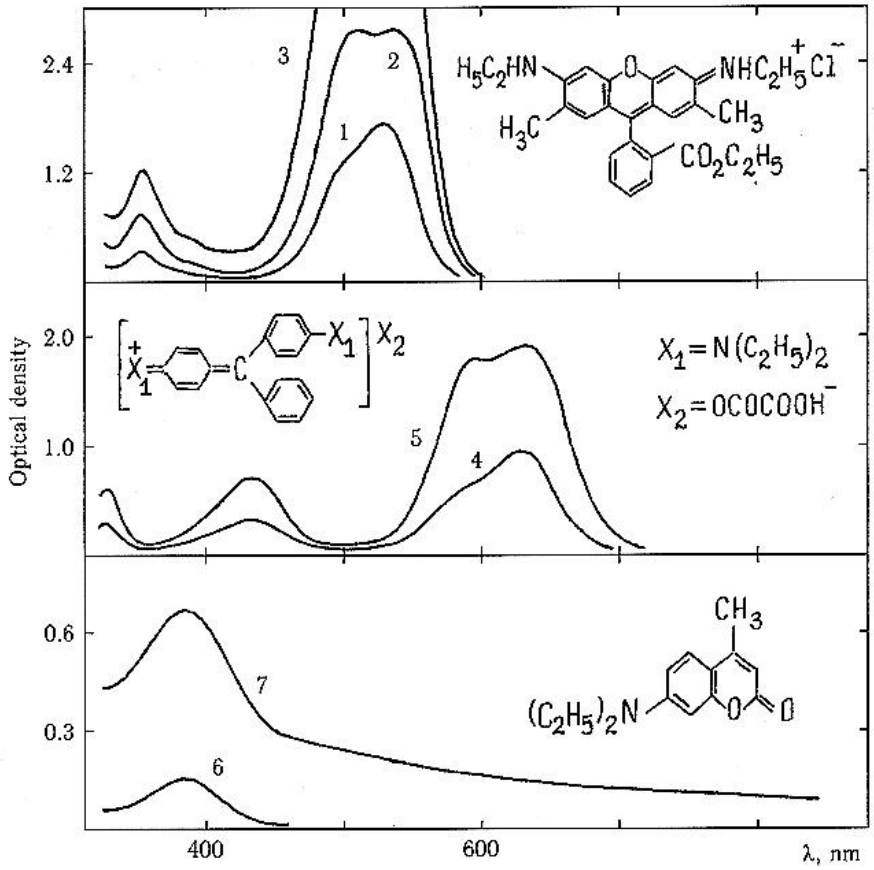

Fig.1. Light attenuation spectra of silica gel-films doped with dyes. 1-3 - rhodamin 6G; 4, 5 - diamond green; 6, 7 - cumarin 1. C_{dye}, mass %: 1 (6), 2(1, 4), 4.5 (5), 6 (2), 11.5 (7),12.5 (3). T_f = 250^{o}C. h = 0.2 mm.

As the C_{dye} is increased up to 12.5 mass % the intensification, shift and redistribution of bands intensity in the region 1000-1750 cm^{-1} also increase of intensity and shift of bands at 3300 and 960 cm^{-1} takes place (curve 3). Besides, for these films are observed very low-intensive bands in the region 5150-5800 cm^{-1} (in Fig. 3 they are not shown) and more intensive bands in the region 3570-3940 cm^{-1}, which are intensified with increase of C_{dye} and decrease of T_f as well as with increase of the exposure duration in damp atmosphere. Note that the position and correlation of narrow bands intensity in the region 1000-1750 cm^{-1} for rhodamin 6 G in KBr essentially differs from indicated in Fig. 3.

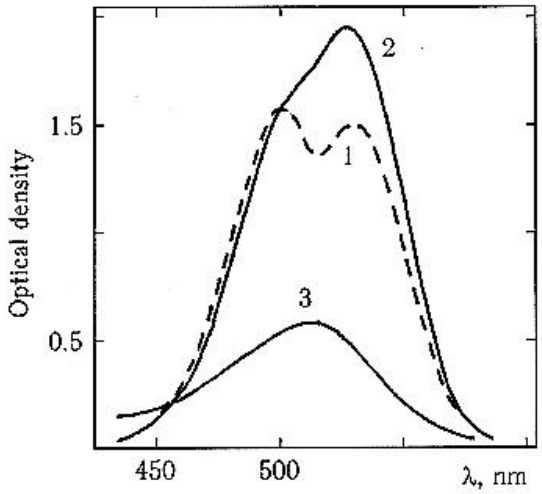

Fig. 2. Absorption spectra of doped with rhodamin 6 G silica gel-films at various T_f. T_f, ^oC: 22 (1), 300 (2), 350 (3). C_{dye} = 3 mass %. h = 0.2μm.

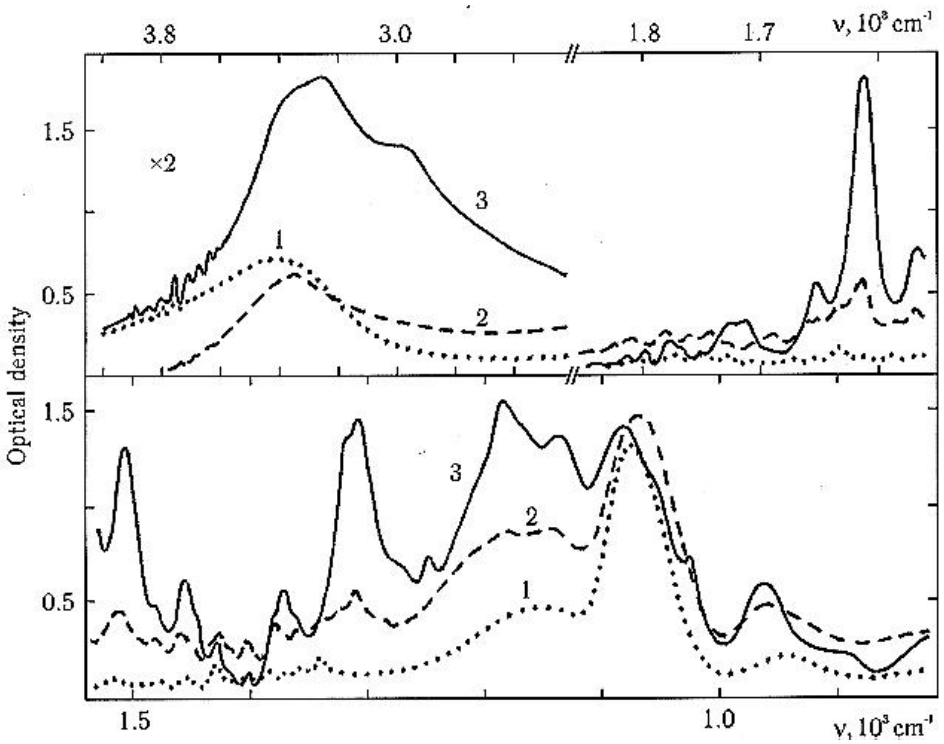

Fig. 3. IR absorption spectra of nondoped (1) and doped with rhodamin 6 G (2, 3) silica gel-films. C_{dye}, mass %: 3 (2),12.5 (3). T_f = 250^{o}C. h = 0.2 mm.

Fig. 4 shows the absorption spectra of doped with rhodamin C and $CeCl_3$ as well as the films codoped with these compounds before and after of irradiation during of 45 minutes by unfiltered radiation of a xenon lamp (C_{dye} = 3 mass %, C_{salt} = 2 mass %, T_f = 250^{o}C, h = 0.2 μm). The absorption spectrum of film with rhodamin C which was irradiated in

identical conditions through quartz substrate with $CeCl_3$-containing silica gel-films, is shown in the Fig. The irradiation power was about 200 W/cm^2 in all cases. It is seen that the unradiated film with rhodamin C is characterized intensive $S_1 \leftarrow S_o$ band with a maximum at 555 nm and 'shoulder' at 525 nm as well a number of less intensive bands in UV region (curve 1). The spectrum of codoped film differs by higher value of D in the region of shorter than 350 nm, expansion of $S_1 \leftarrow S_o$ band, small decrease of its intensity and weak increase of light scattering (curve 2).

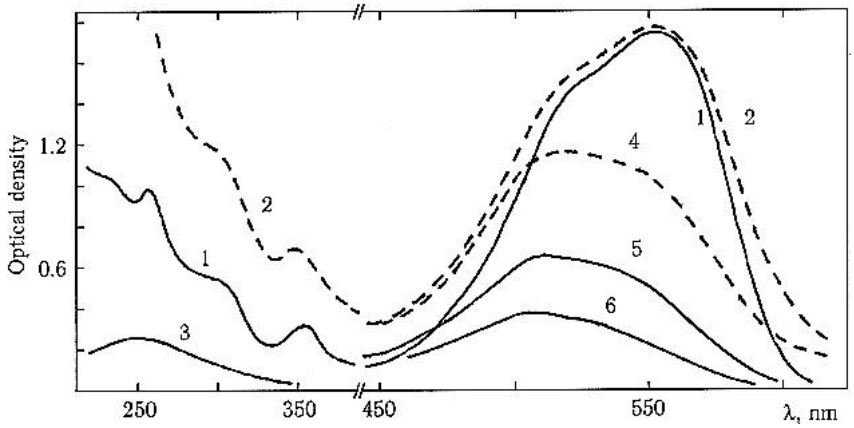

Fig. 4. Absorption spectra of nondoped (3), Doped with rhodamin C (1, 5, 6) and codoped with $CeCl_3$ (2, 4) silica gel-films before (1-3) and after (4-6) of irradiation by unfiltered radiation of a xenon lamp with power ~ 200 W/cm^2. 5 - film irradiated through the quartz substrate with $CeCl_3$-containing silica gel-film. C_{dye} = 3 mass % (1,2,4-6), C_{salt} = 2 mass % (2-4). T_f = 250^{o}C, h = 0.2 mm.

The film with $CeCl_3$ is characterized by wide lowly-intensive band with a maximum at 250 nm (curve 3). The irradiation of the codoped film leads to decrease of integral intensity of $S_1 \leftarrow S_o$ band approximately on 30 % (curve 4). For the film with rhodamin C, which is irradiated through quartz substrate with the $CeCl_3$-containing film, the decrease of D makes up ~ 60 % (curve 5), and at direct irradiation it makes up ~ 80 % (curve 6). The weakening of long-wavelength part of $S_1 \leftarrow S_o$ band more than the short-wavelength in all cases.

It is necessary the indicated results to supplement with the message that at transformation of sol-films doped with Xanthene dyes to the gel-films the intensity of luminescence decreases approximately on two order.

4. DISCUSSION

The analysis of spectra, which are indicated in Fig.1, testifies that the obtained silica gel-films doped with rhodamin 6 G and diamond green on the value of optical density in the main functional band ($S_1 \leftarrow S_o$) and steepness of it outline satisfy to the necessary for optical filters requirements. The absence of light scattering of these films at the maximum C_{dye} can be connected with presence of the polar functional groups $NHC_2H_5Cl^-$ and $OCOCOOH^-$ which increase the solubility of mentioned dyes in sol and, obviously, promote their incorporation to the matrix. The decrease of intensity of the short-

wavelength component of rhodamin 6 G $S_1 \leftarrow S_o$ band as the T_f increases (Fig. 2) testifies to reduction of association degree of the dye [2] that can explain by smaller polarity of OH^-group, remaining in matrix, in comparison with molecules of water. The significant decrease of integral intensity of the band at T_f = 350 ^oC is connected with its thermal destruction.

The bands at 3400, 1075 and 940 cm^{-1}, which are observed in IR spectrum of the nondoped film (Fig. 3, curve 1), are related by fundamental valence oscillations of OH-groups, antisymmetric oscillations of Si-O-bond and oscillations of $Si-O^-$-bond, respectively [3]. The bathochromic shift and weakening of the band at 3400 cm^{-1} for the film small C_{dye} (curve 2) testifies to increase of hydrogen bonds share [4]. For this film the similar shift of the band at 1075 cm^{-1}, accompanied by weakening of its relative intensity, and increase of the band at 940 cm^{-1} can be connected with lengthening and break of Si-O-bonds. At further increase of C_{dye} the loosening of matrix, judging from significant increase of wearability and decrease of moisture resistant, makes progress. This conclusion is confirmed by the changes in vibration spectrum of the film the maximum C_{dye} (curve 3), which are expressed in essential intensification of band connected with the centers of nonbridging oxygen and obvious manifestation in the spectrum of band at 880-920 cm^{-1} corresponding to the triple-coordinated oxygen [3]. To it testifies the repeated intensification of the band stipulated by OH^-groups since at break of the Si-O-bonds are formed free radical interacting with an atmospheric moisture. In such case the further low-frequency shift and weakening of band corresponding to the oscillation of Si-O-bonds should be observed. It is likely that this band is displayed on curve 3 as a 'shoulder' at 1055 cm^{-1}. The band screening of this latter as well as a series of bands in the region 1100-1750 cm^{-1} are related by rhodamin 6 G molecules.

Taking into account the extremely low luminescence intensity of doped gel-films at small association degree of dyes can to assume that the significant share of them molecules is in a solid phase. Obviously, the described loosening of the matrix will be accompanied by accumulation in it the adsorbed water molecules, presence of which can be specified by bands in the region 5150-5800 cm^{-1}. It will cause not only to improvement of conditions for association of dye molecules, but also to change of their distribution between the phases that in a final result is expressed in observable dependence of the specific intensity of absorption on C_{dye}.

The more weak photobleaching of short-wavelength part of $S_1 \leftarrow S_o$ band of rhodamin C at irradiated of the film by radiation of a xenon lamp (Fig. 4) can be related by transfer of energy from dimers to monomers. The weakening of photodestruction of dye-containing film at codoping its with $CeCl_3$, apparently, is explained by the several reasons. To those it is possible to attribute the absorption of part of UV radiation in the change transfer band of Ce(IV) oxygen complexes, which falls at the region shorter than 350 nm [5], inhibition of the photochemical reaction of dye due to the ability of cerium to intercept formed at irradiation the charge carriers of both marks as well as the quenching of excited states of dye by means of charge transfer or by nonradiative transfer of excitations to absorbing in visible region the cerium associations [5]. Judging by comparatively small photodestruction of film with rhodamin C irradiated through the quartz substrate covered with the $CeCl_3$- containing film, the main role in discovered effect play the noted processes of inhibition and quenching. In favour of such conclusion

testifies the above described change of absorption spectrum of dye for codoped film indicating on formation of the metal-organic complex.

5. CONCLUSIONS

At creation of the glass-organic light filters on the base of the doped on the sol stage the silica gel-films the preference should give up the dyes with polar functional group. The increase of T_f of this films leads to growth of moisture stability with simultaneous decrease of their wearebility and degree of dimerisation. The dye molecules incorporation into silica gel-matrix is accompanied by lengthening of Si-O- bonds with subsequent their break. In further these bonds may be to saturate by absorbed moisture. In so doing, increase of the dye molecules association degree and, perhaps, change of correlation of their concentrations in solid and liquid phases occurs that expresses in essential dependence of specific absorption intensity on C_{dye}. The codoping of dye-containing films with cerium leads to increase of their photostability. The photoprotective properties of cerium amplify at formation by them the complexes with dye.

LITERATURE

[1] I.J.M.Snijkers-Hendriks and J. van de Ven. Proc. XVI Int. Congr. Glass, Beijing (China) 4 (1995) 9.
[2] D.Avnir, D.Levy and R.Reisfeld, J. Phys. Chem. 88 (1984) 5956.
[3] A.R.Silin and A.N.Trukhin, Pointed defects and elementary excitations in crystalline and vitreous $Si0_2$ (Zinatne, Riga,1985) (in Russian).
[4] V.L.Mamoshin, V.G.Arkhipov, P.I.Buler et al., Fiz. Khim. Stekla 13 (1987) 510.
[5] G.E.Malashkevich, E.N.Poddenezhny, I.M.Melnichenko et al. J. Non-Cryst. Solids 188 (1995) 107.

PHOTO CONTROLLED PLANAR WAVEGUIDES BASED ON GLASS (OPTICAL PROPERTIES CHARACTERIZATION AND COMPUTER SIMULATION)

A. Dotsenko
Vavilov State Optical Institute, Russia

Abstract

Photosensitive (photochromic including) glasses are the promising materials to create by ion exchange technique the planar waveguides as an photo controlled elements of integral optical systems. A comparative analysis of photoinduced anisotropy of color centers absorption in glass bulk and waveguides based on it has been carried out. It has been found. In a waveguide, as it has been established, the dichroism has the sign opposite to that in bulk photochromic glass. The modes selection phenomenon has been investigated. The theoretical approach developed allows also to optimize the properties of photo controlled elements with periodic structures.

I. INTRODUCTION

In the recent years, a new direction has been developed in optoelectronics-integral optics. The essence of this direction implies that an optical design is created not from a set of bulk optical elements but with the use of bound-up planar waveguides, i. e. thin layers with increased refractive index at the surface of a material which provide light propagation in a layer at full internal reflection. For the creation of such waveguides some technological means are used depending on material type and the requirements made on the waveguide. For the case of glasses, most widely practiced is the manufacturing of planar waveguides on their basis by the method of ion exchange. The work presented is devoted to development of the theoretical approaches for optical properties of planar ion-exchange photocontrolled waveguides investigation.

2. ANISOTROPY OF PHOTOCHROMISM IN WAVEGUIDES

It is wellknown, one of essential properties of waveguides is optical anisotropy caused by diffusion-generated stresses in glass surface layer [1]. We have carried out a comparative analysis of photoinduced anisotropy of color centres absorption in glass bulk and waveguides based on it. That glass has its high darkening degree preserved for a long time at room temperature (so called "low-fading"). This is suitable for the investigation, though the obtained deductions should be but carefully applied to all the other types of heterogeneous photochromic glasses. It has been found that the maximal change of the induced absorption at photochromic glass darkening and bleaching is observed when the polarization actinic and probing radiation are identical. The magnitude of the dichroism depends on irradiation dose and on the wavelength of probing light.

In a waveguide, as it has been established, the dichroism has the sign opposite to that in bulk photochromic glass.

It has been also shown that in a waveguide, the influence of red light brings about additional formation of colour centres whereas in bulk material the influence of such longwave radiation causes the destruction of colour centres. The latter phenomenon was under special examination at the variation of actinic radiation intensity in a wide range (0.1 to 100 mW/cm^2 in bulk glass and 20 to 10^4 mW/cm^2 in waveguide [2]). The dichroism of photoinduced absorption in planar waveguides made on the basis of photochromic glass can be employed in the development of various photo-controlled elements of integral optics (polarization selectors, switches, etc.).

3. MODES SELECTION IN PHOTOCHROMIC WAVEGUIDES

It is clear that the rates of darkening and relaxation in photochromic waveguides are insufficient to fulfill high-speed operations like modulation or switching. However, there are operations that do not need high rates. Among them is, first of all, the selection of waveguide modes. Such a selection requires the providing of essentially different losses for different modes. As a rule, that is fulfilled by arranging absorbing layers at the surface or in the depth of a waveguide. Naturally, the preparation of such layers requires exceptionally high precision of technological procedure and does not permit readjustment. One of possible ways to solve this problem is the creation of selectors with the use of photosensitive glasses [3].

Let us consider a diffusion waveguide based on photochromic glass in which several modes of the same polarization can propagate. If a mode in such a waveguide is excited by actinic radiation, the waveguide will get coloured. The spatial profile of induced absorption will be defined by the intensity of the excited mode and by the kinetics of darkening depending on intensity. So, a sort of extended mask will be formed in the waveguide whose absorption profile is similar to that of intensity distribution of photoactinic radiation in the waveguide. Therefore, the losses for the excited mode will be growing as the waveguide gets colour. The subsiding of other modes will be defined by the overlap of their fields with the absorbing mask, i.e. with the field of the mode by the excitation of which the absorption was induced. In view of the fact that field distributions of the modes with different numbers in planar waveguides essentially differ from each other, one might expect that the losses for other modes would grow insignificantly. In this case, after the coloured segment has been passed, the intensity of the radiation propagating in a before-excited mode must be lower than in other modes. In other words, such a coloration shall lead to the selection of waveguide modes.

We have developed mathematical models allowing the description of the process of radiation propagation in a planar waveguide made on the basis of photochromic glass. Computer simulation of those models enables one to evaluate the effectiveness of the selection and to optimize the structure of waveguide components.

Let us dwell on phenomenological description of the process taking place in a photochromic waveguide under the influence of actinic radiation. When the radiation is propagating, electric field $E(r,t)$ forces the dielectric permeability $e(r,t)$ of waveguide material to change. Optical properties of such a waveguide in general are described by the equation

$$\frac{d\varepsilon(r,t)}{dt} = F\left[\varepsilon(r,t), E(r,t)\right] \qquad (1)$$

The form of function F in the right-hand side of the equation depends on the type of photosensitive material and the accepted model for its description. If the simplest model is applied (glass matrix containing spherical metal particles - colour centres), for the calculation of complex dielectric permeability averaged over the microvolume of composite material, Maxwell-Garnett's approach can be used. Considering the smallness of the specific volume of colour centres in photochromic glass, it is legitimate to put down:

$$\varepsilon(r,t) = \varepsilon_m(x) + \varepsilon_{ph}(r,t) \qquad \varepsilon_{ph}(r,t) = 3\varepsilon_m(x)Vc(r,t)\frac{\varepsilon - \varepsilon_m}{\varepsilon + 2\varepsilon_m} \tag{2}$$

where $e_m(x)$ is the diffusion profile of glass matrix dielectric permeability (regarded as real), $e_{ph}(r,t)$ is a complex item describing photoinduced changes in material structure, $c(r,t)$ is colour centres concentration, V is the volume of a single colour centre, and e is the complex dielectric permeability of the metal (silver or copper), depending on photosensitive dope used in photochromic glass.

The change of colour centres concentration under the influence of monochromatic radiation can be described by an equation of the following form:

$$\frac{dc(r,t)}{dt} = k_a |E(r,t)|^2 \left[c^* - c(r,t)\right] - k_f c(r,t) \tag{3}$$

where c* is the concentration of photosensitive microcrystals and k_a and k_f characterize respectively the probabilities of photoinduced formation of colour centres and their spontaneous decay.

The main objective of the calculation is the matrix $D_{ij} = lg(I_i/I_{ij})$ of photoinduced optical density, where I_{ij} is the power of i^{th} mode's radiation at waveguide output which is coloured by the influence of j^{th} mode up to its saturated state and I_i is the same power without coloration.

The propagation of TE-radiation mode $E = E_y(x,z,t)\, e_y$ in a waveguide is described by the equation

$$-\Delta E_y + \frac{1}{v_l^2}\frac{d^2}{dt^2}\varepsilon E_y = 0 \tag{4}$$

We worked out the set of formulae allows one to calculate the value of photoinduced optical density for different modes of a planar waveguide coloured to saturation under the influence of photoactinic radiation of one of the waveguide's modes. In order to interpret the above described experiment, a calculation was carried out for model "exponential profile",

$$\varepsilon_m(x) = \varepsilon_1\left\{1 - \Delta\left[1 - \exp(-x/a)\right]\right\}. \tag{5}$$

The calculation of the elements of D matrix was done numerically.

A good agreement between experimental data and the calculation is in favour of the correctness of physical assumptions taken at the construction of the theoretical model for real photochromic glasses and chosen conditions of irradiation. The performed computer experiments have shown, for instance, that in order to increase the effectiveness of the selection of high-order modes, it is helpful to create a gradient of photosensitive properties of photochromic glass, i.e. $k_a(x)$ in equation (4), along waveguide depth. However, the creation of a gradient of photosensitive microcrystals concentration, i.e. $c^*(x)$ in equation (4), leads to an improvement of low-order modes selection.

4. LIGHT PROPAGATION IN A SYSTEM OF PHOTOCHROMIC WAVEGUIDES

As was already mentioned, the main application of photochromic material is the modulation of light flows. However, for the case of identical plates used to attenuate radiation, the capacities of such a filter are too shortened. The thing is that actinic radiation is effectively absorbed in surface layers of such a filter, thus restricting its working thickness. Therefore, of interest are the development of the methods describing light propagation in a "sandwich" system of thin plates of photochromic glass separated from each other by clear gaps. Such a system of bound-up waveguides, when placed into a conic reflector is free from the above mentioned drawback and can effectively attenuate light flow.

Let us consider a system of planar waveguides shaped as a pile of interchanging layers in the following way: layers of photochromic glass with a refractive index n_1 alternate with layers of clear glass with a refractive index $n_2 < n_1$. A homogeneous light flow is incident on to the side surface of the pile at an angle q to the normal to the plane limiting the pile. When regarding the refraction at the input into the waveguide system, we deal with beam approximation (the methods of wave problem solution see in [4]). The general non-linear problem of flow transition to a steady state was solved by iterational method. The results of numerical calculation demonstrate that, by varying the extent of flling such a "sandwich" construction with photochromic material (designate it G), one can, other things equal, to intensify photoinduced optical density **)** D. In other words, the efficiency of the usage of photochromic glasses is improved by force of well-designed construction of a relevant component. Estimations have shown that, at the optimal value of G=0.85, **)** D value grows by more than 20 %.

REFERENCES:

1. Glebov L.B., Nikonorov N.V., Petrovsky G.T., On stresses arrising in glass during low-temparature ion-exchange, Fiz. Khim. Stekla (Sov. J. Phys. and Chem. Glass),14, 904,1988.
2. Dotsenko A.V., Nikonorov N.V., Kharchenko M.V., Photoinduced processes in bulk samples and waveguides based on FKhS-2 photochromic glass, Fiz. Khim. Stekla (Sov. J. Phys. and Chem. Glass),18, 393,1992.
3. Glebov L.B., Dotsenko A.V., Niconorov N.V., Tsypljaev S.A., Mode selection in planar photosensitive wavequides, Opt. i Spektr.(Sov.J. Opt.and Spectr.), 62, 905,1987.

4. Dotsenko A.V., Flegontov Ju.A., Petrova I.R., Poletaeva A.I., Cylinder and planar waveguides on the base of photosensitive glass, In Proc.11 Int. Conf. Coher. and Nonlinear Opt., S.-Pb., ussia,1991,191.

PRECIPITATION OF THE HARD DISSOLUBLE PRODUCTS AND THEIR CRYSTALLIZATION INSIDE THE POROUS LAYER DURING THE LEACHING OF THE PHASE-SEPARATED ALKALI BOROSILICATE GLASSES

Antropova T.V. and **Drozdova I.A.**
Institute of Silicate Chemistry of Russian Academy of Sciences, Russia

Abstract

The results of the investigation of the glass component extraction kinetics from phase-separated alkali borosilicate glasses into acid and acid-and-salt solutions and also the data of porous glass study by electron microdiffraction method are presented here. It is found to the precipitation of the boron and silica containing formations inside the glass leached layer and their partly microcrystallization within the roentgenoamorphous porous glasses.

INTRODUCTION

According to the model of the leaching of the phase-separated alkali borosilicate (ABS) glasses [1] the interaction of the chemical unstable boron-rich phase (hereafter referred to as unstable phase) of the glass with the acid solution is the process of the chemical dissolution of its components by forming of the hard dissoluble products as an intermediate stage of the process. Possibility of their precipitation and crystallization inside the leached layer of the two-phase ABS glasses was indirectly confirmed thermodynamically and roentgenographically at investigation of the acid stability of the one-phase ABS glasses being identical to the composition of the unstable phase of the two-phase ABS glasses (see Refs. in [2]). Formation of the crystal precipitates inside the porous layer generates the stress development probably [3]. It may be supposed that the stresses in the porous glasses (PGs) can be a causes on the one hand of the crack of the massive glass samples during of their leaching and on the other hand of the anomalous visible light scattering of the PGs (about last phenomena see for example [4]). Therefore evidence for possible microcrystallization of the products of the acid dissolution of components of the glass unstable phase inside the porous layer is of great significance. However the PGs under consideration are roentgenoamorphous [5].

In our study the electron microdiffraction (EMD) technique was used for determination of the PG microphase structure [5, 6]. Compared to X-ray diffraction analysis this technique is more suitable because the short wave length and strong interaction between electrons and the substances make it possible to produce well-defined reflections when the crystals are of smaller sizes and the substance is in smaller amounts. The EMD data were discussed together with the results of the investigation of the unstable phase component extraction from glass into acid solution. At the discussion of present problem the such principles of the glass leaching model were taken into consideration as hypothesis about pH value of the solution within leached layer [1]. According the glass leaching model the features of

the process are on the one hand the exceeding of the pH value of the solution near the reaction (between the acid and unstable phase components) zone in comparison with the external dilute acid solution pH value owing to the sodium-and-boron buffer effect (as much as ~7.5) or nearly keeping of the low pH value (< 0) in the case of concentrated acid solution.

II. EXPERIMENTAL

The objects of the present study were samples of 8/70 ABS glass (with initial analyzed composition of 6.8 Na_20, 20.9 B_20_3, 0.3 Al_20_3, 72.0 $Si0_2$ in mol. %) isothermally held at 550 ^oC for 144 h for phase separation. The two-phase glass (in the form of polish disks 2-4 mm thick and 20 mm in diameter) was treated with 0.9 or 3 M HCI solutions at 100 ^oC. The relation between glass sample surface area and the acid solution volume was ~0.045 cm^{-1} In the case of concentrated acid solution the kinetics of the interaction of the phase-separated glass samples and acid was investigated with/without 1.4 M KCl addition into acid solution. The leached layer thickness (h) values and the amounts of boron (Q) extracted from glass into acid solutions were determined by optical microscope or by titrating the mannitoboric complex with NaOH solution accordingly. The determinations were made accurate to within ± (10-15) %. The experimental values Q_e of the boron amount in the solution were compared to the boron amount values Q_c calculated using the following relation:

$$Q_c=V_lC_v$$

where V_l - the volume of the leached glass sample (cm^3), C_v - the volume concentration of the boron in the glass (mol/cm^3).

The glass samples were washed in distilled water at 20^oC for 5 days to remove the chlorine ions and then dried at 120^oC for 0.5 h after their completely acid leaching.

The electron diffraction patterns were taken from various parts of porous glass samples, and then a drop of alcoholic suspension of the glass powders was coated onto supporting collodion films (substrates) reinforced by carbon. The EMD morphological investigations were performed on an EM-125 electron microscope at an accelerating voltage of 75 kV. The EMD data were processed according to the procedure described in [5, 6].

III. RESULTS AND DISCUSSION

Fig.1 indicates that KCl addition into HCI solution does not increase the rate of the rise of the thickness of the glass leached layer in comparison with the thickness of the layer leached in HCI solution in KCl absentia. At the same time the amounts of boron extracted from the glass increase in the case of the KCl addition into acid solution. The data presented in the Table show that boron removal into HCI solution lags behind the boron removal into (HCI+KCl) solution. At last conditions Q_e and Q_c values are equal. It known that the solubility of the such boron containing formations as for example H_3B0_3 increases at the KCI presence in the solution. That is why the results mentioned above evidence for the precipitation of boron containing products of interaction of unstable phase and acid inside the leached layer during the leaching of phase-separated glasses on our opinion. It should be noted that the central part of porous glass samples under consideration is enriched with acid-treated products of

two-phase glass according to the results of the transmission electron microscopy study [6].Crystallization of these products was predicted by thermodynamical calculations (see Refs in [2]). Can such precipitates to crystallize in reality? Let us consider the results obtained by EMD technique.

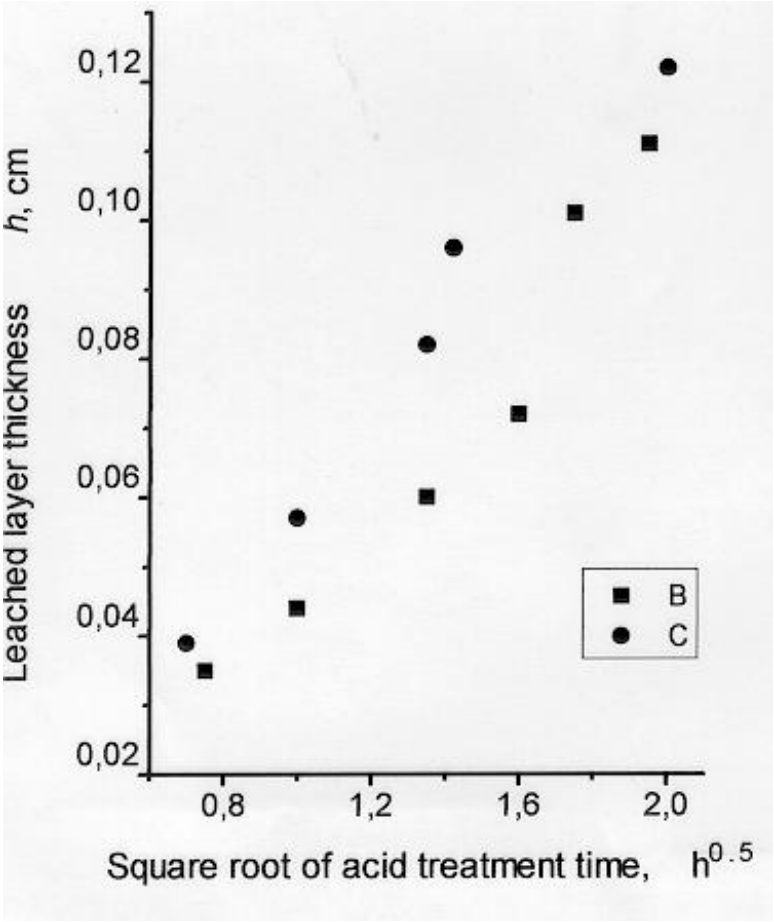

Fig. 1. The thickness h values of the layer leached in the samples of phase-separated glass 8/70 at their treatment by 3 M HCI solution with (B)/without (C) 1.4 Kcl addition vs. square root of treatment time t at 100 ^{o}C.

Table. Comparison of the boron amounts Q_e extracted from phase-separated glass 8/70 disks with the boron amounts Q_c were included by the sample layer leached in the acid solution at 100^{o}C during 1 h.

Solution	**Boron amount Q, mol 10^4**	
	Qe	*Qc*
3 M HCl	2.8	7.9
3 M HCl + 1.4 M KCl	7.7	7.6

Fig. 2 and Fig. 3 show the electron micrographs and electron diffraction patterns taken from the powder particles of porous glasses produced from two- phase ABS

glass under study in the 3 M HCl solution (Fig. 2) or in the 0.1 M HCI solution (Fig. 3) (without KCl). In addition to an amorphous phase that is identified by the presence of the diffuse halo in a photoplate, microcrystalline particles are also observed. Their diffraction patterns are characterized by electron diffraction spots calculating of which makes it possible to identify the such microcrystalline phases as the sassolite or boric acid H_3B0_3 (ASTM-23-1034) (Fig. 2, b), the ezcurrite (ASTM-20-1083) $Na_4B_{10}O_{17}7H_20$ or $2Na_20\ 5B_20_3\ 7H_20$ (Fig. 3, d) and the traces of α-quartz (ASTM-5-0490, [011]) (Fig. 2, c; Fig. 3,b).

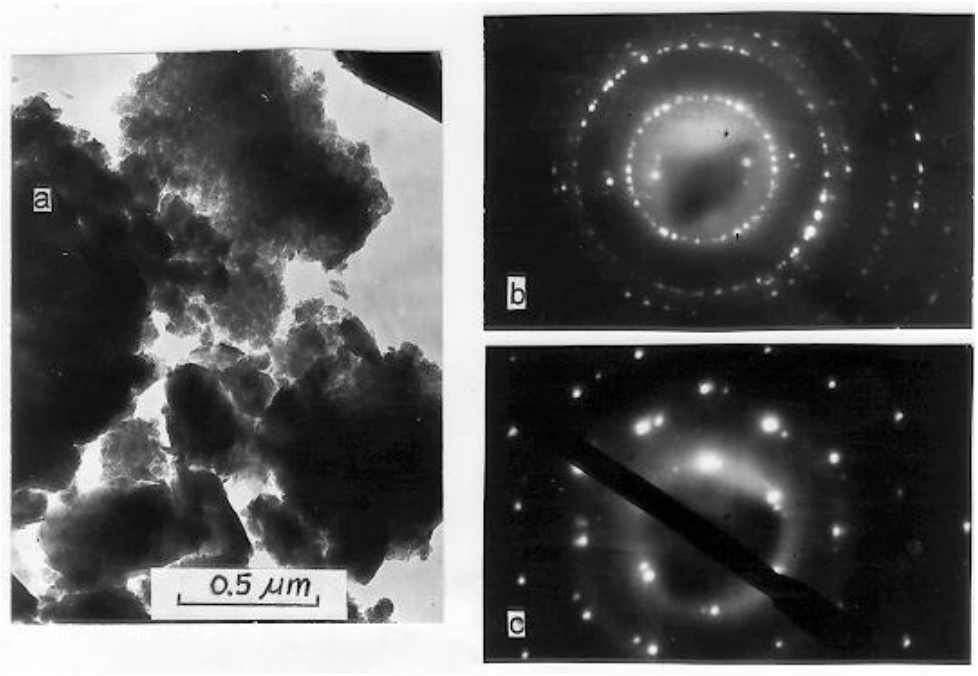

Fig. 2. Electron micrograph (a) and electron diffraction patterns (b, c) of the powder particles of the porous glass (initial thickness of disk, 2 mm) prepared from phase-separated glass 8/70 in 3 M HCl solution at 100 °C.

The results obtained on our opinion agree with the statement of the glass leaching model about the pH value in the pore space. For instance in the case of concentrated acid solution (3 M HCl) pH value inside pores is sufficiently low for the H_3B0_3 as more durable solid phase can be precipitate (as intermediate stage of glass leaching). The significant increasing of the pH value in the pore space (in the case of dilute acid solution) will in turn favor the precipitation of the alkali borates including crystalline hydrates which are most durable under prevailing conditions [6]. The probability of the silica microcrystallization at the presence of the alkali ions within solution is valid also (see Refs in [5]).

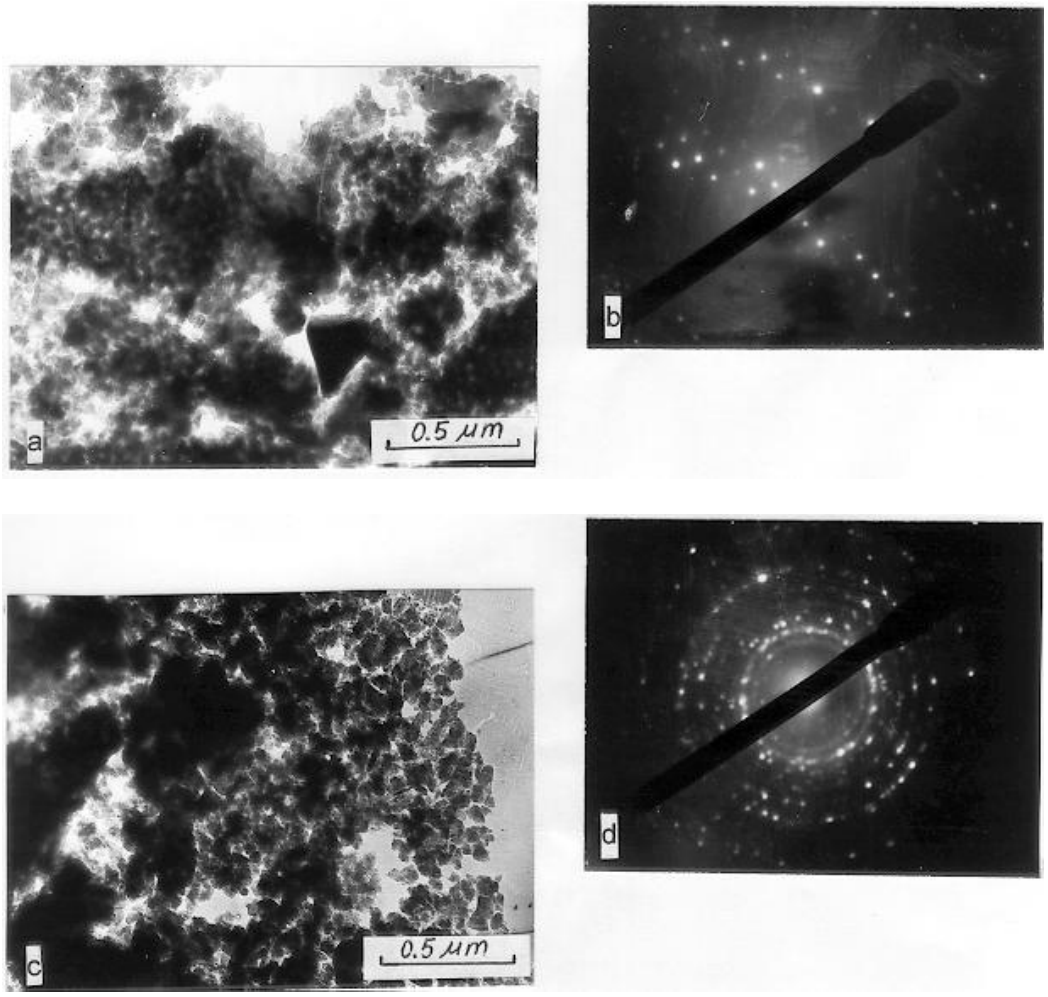

Fig. 3. Electron micrographs (a, c) and electron diffraction patterns (b, d) of the powder particles from periphery (a, b) and central (c, d) parts of the porous glass (initial thickness of disk, 4 mm) prepared from phase-separated glass 8/70 in 0.1 M HCI solution at 100 ^{o}C.

IV. SUMMARY

The data of the investigations of the chemical stability of the phase-separated alkali borosilicate glass samples and of the microphase structure of the porous glasses confirm the such hypotheses of the glass leaching model as (a) the precipitation of the hard dissoluble products inside the pore space (as intermediate stage of the process), (b) their partly microcrystallization, (c) the influence of the pH value of the solution within pore space on the composition of these precipitates.

V. REFERENCES

1.Antropova T.V. *A model of the porous glass producing process./* Bol. Soc. Esp. Ceram. Vid. 31-C. 1992. (Proc. XVI. Intern. Congr. On Glass, Madrid, Spain, 1992). Vol. 5. P.195-199.
2.Antropova T.V. *Study of the chemical stage of the phase-separated sodium borosilicate glass leaching process and the porous glass structure*./ Optica Applicata.1994. Vol. 24. P.131-140.
3.Antropova T.V., Drozdova I.A. *Physical and chemical features of the porous glass and their influence on its optical properties*. / Russ. J. of Appl. Chem. 1996. Vol. 69. No. 3 (in print).
4.Antropova T.V.,Roskova G.P. *Producing of the porous glasses with abnormal visible light scattering*./ Glastech. Ber. Glass Sci. Technol. 1995. (Fundamentals of Glass Science & Technol. - 3rd ESG Conf., Wurzburg, Germany, 1995). Vol. 68 C1. P. 490-494.
5.Drozdova I.A., Antropova T.V. *Electron microscopy and microdiffraction study of porous glasses*. /Russ. J. of Appl. Chem. 1993. Vol. 66. No 10. Part 1. P. 1678-1684.
6.Antropova T.V., Drozdova I.A. *The influence of synthesis conditions of porous glasses on their structure*./ Glass Phys. and Chem. 1995. Vol. 21. No 2. P. 131-140.

SOL-GEL DEPOSITED ELECTROCHROMIC FILMS FOR ELECTROCHROMIC SMART WINDOW GLASS

Nilgün Özer (1), Carl M. Lampert (2) and **Michael Rubin (3)**
1. lstanbul University, Faculty of Science, Turkey, 2.Star Science, USA,
3. University of California, E.O. Lawrence Berkeley National Laboratory , USA

Abstract

Electrochromic windows offer the ability to dynamically change the transmittance of a glazing. With the appropriate sensor and controls, this smart window can be used for energy regulation and glare control for a variety of glazing applications. The most promising are building and automotive applications. This work covers the use of sol-gel deposition processes to make active films for these windows. The sol-gel process offers a low-capital investment for the deposition of these active films. Sol-gel serves as an alternative to more expensive vacuum deposition processes. The sol-gel process utilizes solution coating followed by a hydrolysis and condensation. In this investigation we report on tungsten oxide and nickel oxide films made by the sol-gel process for electrochromic windows. The properties of the sol-gel films compare favorably to those of films made by other techniques. A typical laminated electrochromic window consists of two glass sheets coated with transparent conductors, which are coated with the active films. The two sheets are laminated together with an ionically conductive polymer. The range of visible transmission modulation of the tungsten oxide was 60% and for the nickel oxide was 20%. We used the device configuration of glass/ $Sn0_2$:F/ $W0_3$/polymer/$Li_zNiO_xH_y$/SnO_2:F glass to test the films. The nickel oxide layer had a low level of lithiation and possibly contained a small amount of water. Lithiated oxymethylene-linked poly(ethylene oxide) was used as the laminating polymer. Commercially available $Sn0_2$:F / glass (LOF-Tec glass) was used as the transparent conducting glass. We found reasonable device switching characteristics which could be used for devices.

1. INTRODUCTION

Electrochromism (EC) can be broadly defined as a persistent and reversible color change as a function of injected/extracted charge and their coloration can be controlled via the number of coulombs passed during electrochromic reaction. Electrochromic materials are attractive candidates for smart window applications (1). Electrochromic devices consist of thin films that provide optical modulation, ion conduction and transparent electrical conduction.

Electrochromic smart windows can be constructed in several different ways (2). One design these windows consist of oxide layers that are deposited on two conductive glass substrates. These coated glass substrates are then laminated together with the appropriate ion conductor(3). The electrochromic layer and ion storage layers conducts both ions and electrons. When a small current is applied across the multilayer film, ions will be inserted into or extracted from the

electrochromic oxide layer. As a result, the film changes its optical properties due to absorption and electron density changes, giving the switching effect. Such a window can change in transmittance continuously over a wide range (such as 80-15 %) in a time period of seconds to less then one minute depending on window size. The window will retains its optical properties once the power is turned off, and is fully reversible after many cycles.

Smart windows can be used in buildings to control day lighting to create efficient work conditions. Controlled modulation of solar radiation through smart windows has a large potential in buildings for energy savings(4). Properly designed and managed smart windows have the technical potential to save 50-70 % of the lighting energy used in exterior offices (2). Recently a number of tandem smart window systems have been investigated, and most have used $W0_3$ as the working electrochromic layer (5-9). Typically these windows consist of vacuum deposited layers. It is desirable for costs to be below $ 150/m2 for large area applications. Sol-gel processing requires less capital to deposit coatings over large areas than conventional vacuum methods, and hence offers a possible solution for lowering the deposition cost of these windows. Sol-gel processing also offers advantages in controlling the microstructure or depositing films containing multiple cations. These parameters can influence kinetics, durability, coloring efficiency and charge storage in the windows (10-11).

In this study, we present the characteristics of a sol-gel deposited smart window, using a Li+ conducting polymer layer. A $W0_3$ / polymer electrolyte / $Li_zNiO_xH_y$ electrochromic window is fabricated. Potentiostatic cycling coupled with transmittance measurement was performed at room temperature on the complete window in order to evaluate the performance of the window.

2. EXPERIMENTAL

Electrochromic $W0_3$ and NiO_xH_y layers were deposited by sol-gel spin coating technique onto transparent conductive F : $Sn0_2$ coated glass substrates (LOF-Tec type). W03 is used as the working electrode and electrochemically lithiated NiO_xH_y is used as the counter electrode. $W0_3$ coatings have been deposited from colloidal solutions of tungsten oxachloride in isopropyl alcohol. NiO_xH_y coatings have been deposited from solutions of nickel methoxyethoxide in methoxyethanol (12). These films were amorphous to X-ray diffraction. Their thickness, measured by a profilometer with an accuracy of ±10 nm was l20 nm for NiO_xH_y and 250 nm for $W0_3$. The films were electrochemically characterized after heat -treatment at 300°C. Lithiation of $Ni0_xH_y$ film was carried out by electrochemical insertion of lithium into the film from solution.

The polymer electrolyte was amorphous oxymethylenelinked poly (oxyethylene), [α-PEO), synthesized by the method given in ref. 13 .The ion conducting polymer prepared by dissolving 2 g of α-PEO and 0.48 g of $LiClO_4$ in acetonitrile, with a O:Li atomic ratio of 10:1, giving rise to the highest conductivity of 10^{-4} Scm^{-1}, This viscous polymer was dried in vacuum oven and residual solvent was allowed to evaporate slowly at a 40°C.

The electrochromic system was made by joining the pre-lithiated $LiNiO_xH_y$ / α-PEO / $F:Sn0_2$ coated glass with the $W0_3$ /$F:Sn0_2$ coated glass. The polymeric solid electrolyte was laminated between the two electrodes. The windows were hot- pressed at 80°C the dry box and sealed with a low vapor pressure adhesive (Varian Torr-seal). The optical performance of the windows was measured with a Perkin and Elmer Lambda 2 UV / VIS spectrophotometer.

3. RESULTS AND DISCUSSION

We have successfully fabricated prototype small area (2 cm x 3 cm) five layer smart window devices. Figure 1 shows the schematic of the laminated smart window. This is a five-layer device that has been deposited on a transparent conducting substrate. $W0_3$ is used as cathodicaly coloring electrode and lithiated NiO_xH_y is used as anodically coloring electrode.

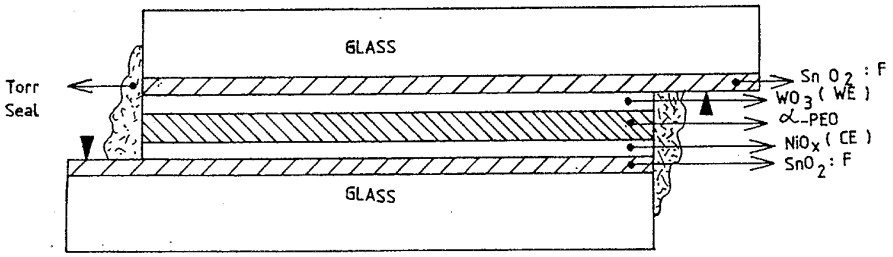

Fig. 1. Schematic diagram of a sol-gel deposited, laminated smart window.

The following reaction takes place as a lithium is transported from the NiO_xH_y layer to $W0_3$ via ion conductor.

$Li_zNiO_xH_y \leftrightarrow NiO_xH_y + 2\ Li^+ + 2\ e^-$

$W0_3 + z\ Li^+ + 2\ e^- \leftrightarrow Li_xWO_3$

(Bleached) (colored)

$W0_3$ goes through a large optical modulation from transparent to a deep blue tungsten bronze color when lithianated (14). NiO_xH_y changes from colorless state to a brown colored state with lithium extraction. This device exhibits good spectrally selective transmissivity in the visible range. Such a device has been switched between ± 1.4 V for more than 1200 cycles.

The cyclic voltammetry of the $W0_3$ /α-PEO-$LiClO_4$ / $LizNiO_xH_y$ window is shown in Figure 2. The window shows a reproducible electrochromic behavior for many cycles. During the cathodic scan the window becomes dark while during the anodic scan the window becomes transparent. Both coloration and bleaching took place in within 15 seconds as judged from visual observation.

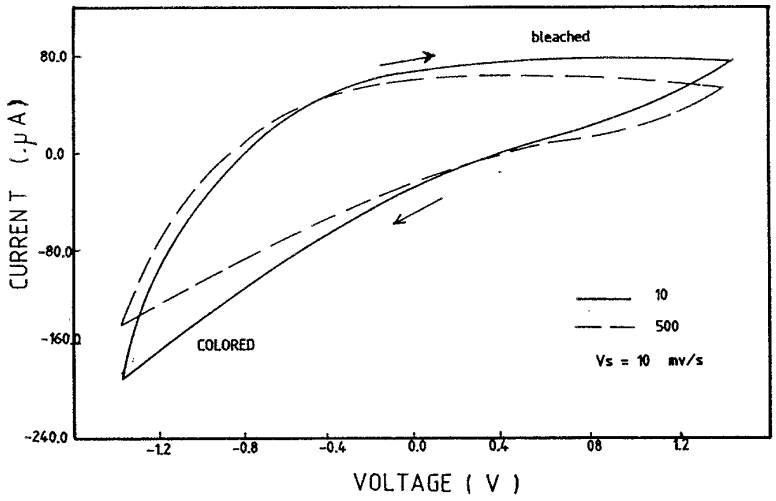

Fig. 2. Cyclic voltammagram of the prototype (F: $Sn0_2$ / $W0_3$ / a-PEO-$LiClO_4$ / $Li_zNiO_xH_y$ / F: $Sn0_2$), laminated window at room temperature.

The electrochromic response of $W0_3$ / α-PEO-$LiClO_4$ / $Li_zNiO_xH_y$ window is further demonstrated by Figure 3 and Figure 4 which show changes in current and transmittance with time under a constant potential of ± 1.4 V. Figure 4 reveals a good charge reversibility, with a total transmittance variation at 556 mm of ΔT=30 % and an acceptable switching time of the order of 50 sec .The solar optical transmittance spectra of the $W0_3$ / α-PEO-$LiClO_4$ / $Li_zNiO_xH_y$ window is shown in Figure 5. The window becomes dark blue by the cathodic scan and becomes transparent by anodic scan. The window was observed for more than 1200 cycles and little detectable change in their optical and electrochemical properties could be observed.

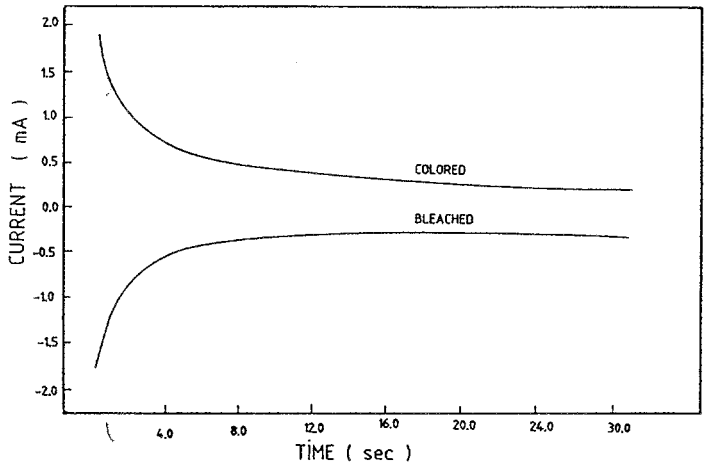

Fig 3. Transmittance change of the glass- F:$Sn0_2$ - $Li_zNiO_xH_y$ / a PEO - $LiClO_4$ / $W0_3$ - F: $Sn0_2$ - glass window, upon application of a voltage of ±1.4 V.

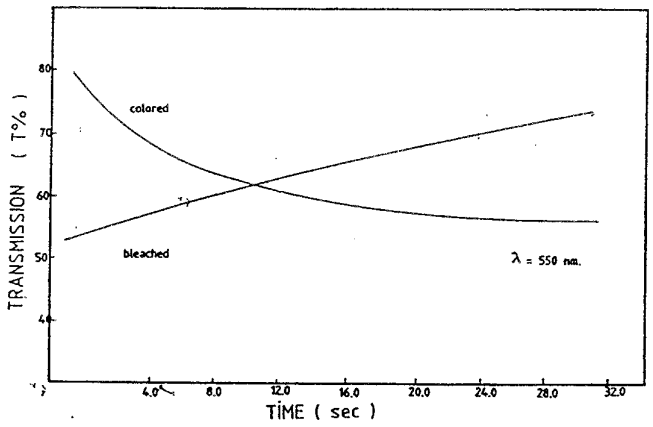

Fig. 4. Charge reversibly exchanged during the coloring - bleaching process of the window.

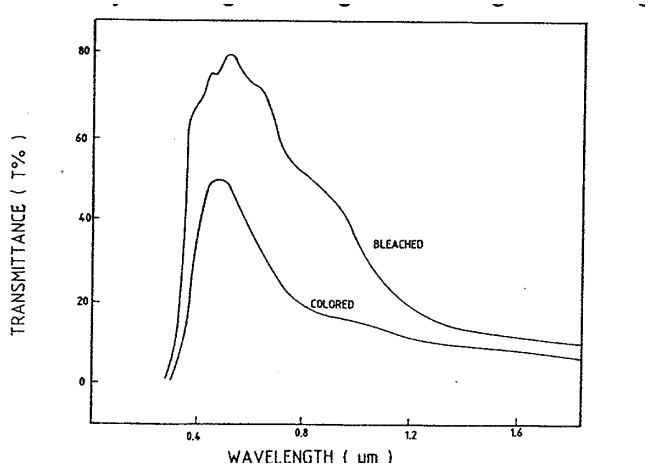

Fig. 5. Optical transmittance of sol-gel deposited smart window having the configuration: glass - F: $Sn0_2$ - $LiNiO_xH_y$ / a PEO - $LiClO_4$ / $W0_3$ -F: $Sn0_2$ - glass.

4. CONCLUSION

Sol-gel deposited electrochromic layers can be used for the fabrication of electrochromic smart windows. A prototype of smart window glass employing sol-gel deposited layers has been successfully fabricated. In the prototype device, a $W0_3$ film was used as a working electrochromic layer, and a $Li_zNiO_xH_y$ film as the counter electrode, and amorphous oxymethylene linked poly (oxyethylene) - $LiClO_4$ as an ion conducting layer .The polymeric ion conducting layer was transparent and showed a high ionic conductivity of the order of 10^{-5} Scm^{-1} at room temperature. Potentiostatic cycling (± 1.4 V) was performed on the elecrochromic window and reversible transmittance variance from 50 % to 80 % was observed at 550 nm. The device cycled unchanged for 1200 cycles.

ACKNOWLEDGMENT

Part of this work was supported by the Assistant Secretary for Energy Efficiency and Renewable Energy, Office of Building Technologies, Building Systems and Materials Division of the U.S. Department of Energy under Contract No : D E- 765 F00098

REFERENCES

1. C. G Granqvist, Solid State lonics, 53-56 (1992) 479.
2. S. Selkowitz and C. Lampert, Proc .SPIE V IS4 (1990) 22.
3. A.M. Anderson, A .Talledo, C.G. Grangvist and J.R. Stevens, Proc. Electrochem. Soc. 90-2 (1980) 261.
4. C.M. Lampert, Large-Area Chromogenics, LBL-27720 Internal Report, Aug1991
5. S. H. Lee, K. H. Hwang and S. K. Joo, Proc. Elecrochem. Soc. 94-2 (1994) 290.
6. J .P. Ziegler and B. M .Howard, ibid 94-2 (1994) 303.
7. P. Baudry and M. Aegerter, J. Electrochem. Soc .138-2 (1991) 460.
8. N .R. Lynam and A. Agrawal, Proc. SPIE V IS4 (1990) 46.
9. F. H. Moser and N. R. Lynam, US Patent, 4,855,161, Aug. 8, (1989).
10. K. Machida and M. Enyo, J. Electrochem. Soc .131 (1990)1169.
11. S. Passerini, B. Scrosati, V. Hermann, C.A. Holmblad and T. Bartlett, J. Electrochem. Soc .141-4 (1994) 1025.
12. N. Özer and C. M. Lampert, Technical Digest V.17 (1995) 344.
13. C. V. Nicholas, D. J. Wilson, C .Booth and J.R.M. Giles, British Polymer Journal, V. 20 N .3 (1988) 289.
14. C. G. Granqvist, Handbook of Inorganic Electrochromic Materials, Elsevier, Amsterdam (1995).

STUDIES ON THE ARC-PVD COATING APPLICATIONS IN GLASS MOULDS

Serkan Kuruoglu*, Erdal Yollu* and **Sadi Karagöz****
*) Ferro Döküm San. ve Tic. A.S., SISECAM, Turkey
**) Kocaeli University, Turkey

Abstract

Moulds used in the production of glass containers consist of several components and have a complicated structure in respect to material selection and construction due to the different properties which determine the performance. The plunger, used in bottle production with a WC-Ni/Co type cemented carbide coating, is chosen for an arc-PVD application. The AlTiN/TiN multilayer is introduced as the new coating. The wear process of the conventional coating as well as of the AlTiN/TiN multilayer coating is studied. The wear behavior of both coatings is documented by electrometallographical methods at various life times.

The conventional cemented carbide coating cracks by thermal fatigue. Superimposed on this process is a continuous adhesive wear as up to total sticking. In the AlTiN/TiN multilayer coating no visible coarse fatigue cracks are found; but they are also damaged by adhesion of glass melt. Attritive wear of the coating results and the increase in wear during formation also leads to total sticking.

1. INTRODUCTION

The glass container industry today enjoys increasing use of the NNPB (narrow-neck-press-and-blow forming) Process [1-2]. With the introduction of this process in bottle making and the manufacture of lightweight containers, material selection has gained much importance, However, material development seems to be very slowly. [1-3]. Although the requirements for material properties have increased, very little development with alternative materials has been made.

Plungers, the topic of this study, used in the NNPB Process operate at high temperatures in excess of 500-550^{o}C. The thermal and mechanical loading of the forming operation demand plunger materials which should exhibit hot hardness, resistance to thermal shock and resistance to oxidation. The life time of these materials are determined by the wear resulting from insufficient material properties, which allow different wear mechanisms. In the glass forming process, wear is introduced by the contact conditions existing between glass melt and the plunger material [1]. Interface reactions during viscous glass flow on the plunger surface result in sticking and adhesion of glass depending on the contact time, temperature and pressure [4].

In the related literature adhesion is discussed extensively [4-8]. The adherence temperature for mould materials is determined. The effect of surface roughness is studied

to understand the influence of the contact morphology. For an increase in the adherence temperature, mould material microstructures are modified by heat treatment. Surface coatings are introduced. Also lubricants are used to obtain an advanced contact geometry, although defects can arise easily. [9]. Build-up of their residues causes black specks. They flake off the mould surface and are embedded in the hot glass surface. Then they act as stress concentrators, which cause bottle strength to be greatly reduced [3]

Today's plungers for lightweight technology should fulfill all the requirements mentioned above. For this reason they are coated with cemented carbide, a metal-ceramic composite material, which does not seem to be the best solution [1]. The aim of this study is to understand the wear behavior of cemented carbide coating in glass forming and introduce new coating materials instead. The PVD (physical vapour deposition) Process lends itself to producing thin ceramic coatings with excellent wear and corrosion properties [10-14] and is used for the production of AlTiN/TiN multilayer coatings in this investigation. The wear behavior of the PVD-coating will also be studied to obtain a useful coating material for plungers.

The first results of the wear study of the conventional coating and the PVD coating on plunger materials are presented. The first run of experiments is a part of the R&D program on the development of mould materials, which is carried out by the Ferro Döküm Research Group of Þiþecam and the Department. of Metallurgy, Kocaeli University.

2. EXPERIMENTS

The wear development on plunger materials was investigated under production conditions. This type of testing new materials is actually very costly, but almost free of various influences given in a simulation test. The tests were performed during forming of a standard bottle glass with an average composition of 71.5 % SiO_2, 1.8 % TiO_2+Al_2O_3, 0.1 % Fe_2O_3, 10.1 % CaO, 2.9 % MgO, 13.2 % Na_2O, 0.2 % K_2O and 0.2 % SO_3. The mould entrance temperature of the glass melt was 1186^0C, the contact time between glass melt and the plunger was 3/4 sec. and the time between two bottle forming operation was 4 1/3 sec. This procedure resulted in thermal cycling with plunger temperatures up to 550^oC [2]. The plungers were cut after different life times as up to total wear, which was caused almost by sticking. The wear was documented by metallographic, electron-metallographic and microanalytical methods.

The conventional plunger material, used in the test is a low alloyed steel (DIN13CrMo 44). It is customary practice to coat the substrate material with tungsten carbide-nickel alloy mixture by plasma spraying. The WC-Ni/Co layer on the steel substrate is 0.5 mm thick. Its hardness (HV 0.1) is 1125 kg/mm^2, as measured by a Fisherscope H100 instrument.

The new coating material is selected to obtain a good combination of the desired properties mentioned above. In this study a multilayer of AlTiN/TiN is used as the coating material. The first layer on the substrate is a 0.28 μm thick TiN (HV0.1=2760 kg/mm^2), on which a 1.12 μm thick AlTiN (HV0.1= 3025 kg/mm^2) layer is deposited. This type of coating is repeated 4 times to produce a 5.6 μm thick multilayer. At this thickness, no additional roughness is caused by the deposit. The production of the coating

is done by cathodic arc evaporation due to excellent adherence of the coating on the substrate material obtained with this method [14].

3. RESULTS

3a. Wear of Cemented Carbide Coating

In Fig 1 a typical-coating microstructure as revealed by transversal fracture is shown. Different inclusions with sizes 2-25 μm can be seen in a relatively homogeneous matrix. Some particles have flaked off due to their weak bonding causing micropores.

Fig. 2 represents the conventional plunger surface on the top after total sticking (lifetime appr.120 hours). In the figure a broad crack is visible. The coarse crack on the surface is opened up to some hundred μm. EDX analysis reveals particles of glass stuck in the crack. Such cracks are formed due to thermal cycling and cyclic contact with the glass melt. During service, cracks propagate to form a network indicating thermal fatigue of the plunger material. Fig. 3 shows a small section of Fig. 2 at a higher magnification. The surface exhibits a rough surface topography due to the adhering glass layer. In the glass-free areas, craters mainly caused by the adhesive wear of the coating, are visible. A detailed study of the fatigue-crack surface shows many small cracks existing just below the surface (Fig. 4). At this stage the whole surface appears to be destroyed.

The study of the worn surface shows that two main mechanisms are acting: thermal fatigue and adhesive wear. Thermal fatigue causes cracks which propagate during service and the crack length on the surface increases. Adhesive wear causes small cemented carbide fragments which flake off the surface increasing its roughness. The surface density of the small craters increase during shaping of glass. Continuous contribution of both mechanisms ends in total sticking of the glass melt on the surface.

3b. Wear of the AlTiN/TiN Multilayer Coating

Fig. 5 shows the typical microstructure of the coating, also revealed by transversal fracture. Occasionally deposited small droplets are recognizable in the columnar structure of the coating. The TiAlN layer is the actual resistant layer for high temperature oxidation [13]. Thin TiN layers deposited in between TiAlN's oxidize at lower temperatures indeed, but they can cause branching off of a propagated crack into the TiAlN/TiN interface as indicated by the crack steps on the left of the figure.

After approximately. 30 hours lifetime the new coating indicates remarkable wear as shown in Fig. 6. Adhering glass particles of sizes up to 10 μm are visible on the image. Small craters exist, where some of which are full of adhering glass. In open craters the depth is estimated to be about 1 1 /2 μm showing that the fragmentation occurred at the first TiN/AlTiN layer. Fig. 7a gives a better survey of the situation in this stage of wear. Many rounded glass particles adhere to the surface. Also visible craters of the cracked and attrited layer particles is documenting the development of adhesive wear. Polishing scratches indicate the direction of glass flow,

Total sticking occurs after approximately. 90 hours lifetime, (Fig. 7b). The diameter and the depth of the crater left by pregmanted coating particles has been increased along with the density of the sticking areas. The light contrast of adhering coarse glass particles is due to topographical contrast in the scanning electron microscope, indicating the

fracture between the glass particle sitting in the crater and the flowing glass melt. Such strong interlocking contributes to the sticking behaviour of the glass melt. A noticeable feature on the surface is the areas of darker contrast. Such a change in the chemical contrast of a smooth surface indicates the formation of absorption layers with elements of smaller atomic numbers.

The study of the worn surface showed only one main mechanism acting: adhesive wear. It causes small coating segments to flake off the surface. These are then plucked off by adhesion to the glass melt. These fragments leave behind shallow craters with a broad size distribution. The surface density of the craters as well as their size, increases during formation. Continuous wear ceases, in this case, a total sticking of the glass melt on the surface.

The first results with the PVD-coatings are encouraging. Although no thermal cracks are detected, the substrate material should be fitted to the coating under the aspect of thermal fatigue. Interface studies are needed to enlighten the actual situation between the glass melt and the coating. Also the roles of chemical and mechanical bonds for adhesive wear should be identified for further development of coating compositions.

ACKNOWLEDGMENT

We are indebted to Dr. Metin Basaran, Operations Director of Metal Working of ÞÝÞECAM for his motivation, support and discussions on this project. The authors would like to thank Mr. Kemal Tokmanoglu, TinKap Ltd. for his valuable assistance in PVD coating.

LITERATURE

[1] VICKERS T.A.Y., The Development of the UK Glass Mould Making industry in the 20th. Century, Glass Technol., 35 (1994), p.146 -153.
[2] ENSOR T.F., Mould Materials, Glass Technol., 31 (1990), p. 85 - 88.
[3] WASYLYK J.S., AGRAPSlP Targets Container Performance-Limiting Factors, Glass Industry, April 1991, p.10 -15.
[4] COSTA P., Untersuchung der thermischen und geometrischen Kontaktverhaltnisse zwischen Glas und Metall bei der Formgebung heissen, zühflüssigen Glases, Glastechn. Ber., 45 (1972), p. 277-287.
[5] OEL H. J., GOTTSCHALK A., Die Klebetemperatur zwischen Glas und Metallen, Glastechn. Ber. 39 (1966), p. 319 - 323.
[6] PASK J. A., FULRATH R. M., Fundamentals of Glass-to-Metal Bonding : Part Vlll, Nature of Wetting and Adherence, J. Am. Ceram. Soc. 45 (1962), p. 592 - 596,
[7] DARTNELL R. C., FAIRBANKS H.V., KOEHLER A., Investigation of The adherence of Glass to Metals and Alloys, J. Am. Ceram. Soc., 34 (1951), p. 357 - 360.
[8] KAPNYCKY J. A., FAIRBANKS H. V., KOEHLER W. A., study of Adherence of Molten Glass to Heated Metals, J. Am. Ceram. Soc., 32 (1949), p. 305-308.
[9] DOWLING C., FAIRBANKS H. V. KOEHLER W. A., A Study of the Effect of Lubricants on the Adherence of Molten Glass to Heated Metals, J. Am. Ceram. Soc., 33 (1950), p. 269 - 273

[10] MANS P., DÖLL W., KLEER G:, Glass in Contact With Mould Materials for Container Production, Glastech Ber. Glass Sci. Technol. 68 (1955), p. 389 - 399.
[11] KLOSS K. H., BROSZEIT E., GABRIEL M., SCHRÖDER H. J., Thin TiN Coatings Deposited onto Nodular Cast Iron by Ion and Plasma-assisted Coating Techniques, Thin Solid Films, 96 (1982), p. 67 - 77.
[12] MATTHES. B., BROSZEIT. E., KLOOS H. K., Wear Behaviour of R. F.- Sputtered TiN, TiB_2 and Ti (B, N) Coatings on Metal Forming Tools in a Model Wear Test, Surf. Coat. Technol. 43/44 (1990), p. 721- 731
[13] MUNZ W.-D., Titanium Aluminum Nitride Films: A new Alternative to TiN Coatings, J. Vac. Sci. Technol. A 4 (6) (1986), p. 2717 - 2725.
[14] KARAGÖZ S. FISCHMEISTER H., Metallographic Observations on the Wear Process of TiN-Coated Cutting Tools, Surf. Sci. Technol, (1996),

FIGURE CAPTIONS

Fig.1 The cemented carbide macrostructure; fracture surface.
Fig. 2 The cemented carbide coating surface after total wear.
Fig. 3 The cemented carbide coating surface after total wear; note the adhering layer initiated by the reaction between glass melt and coating material.
Fig. 4 Thermal-fatigue crack surface showing the multiple cracking and fragmentation on the working surface.
Fig. 5 The structure of the AlTiN/TiN multilayer coating; fracture surface.
Fig. 6 The AlTiN/TiN coating surface after a lifetime of 30 hours; note the adhering rounded glass particles.
Fig. 7a The AlTiN/TiN coating surface after a lifetime of 30 hours; note that the adhering coarse glass particles are fractured.
Fig 7b The AlTiN/TiN coating surface after total wear.

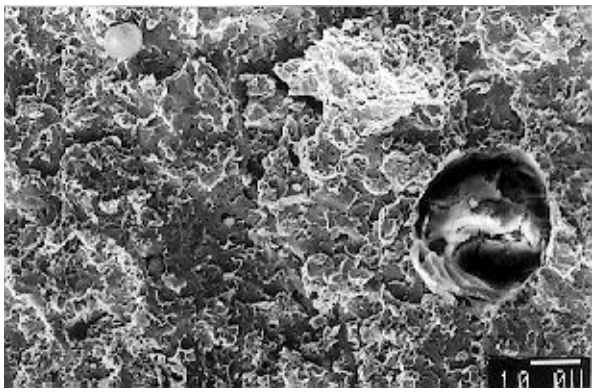

Fig. 1

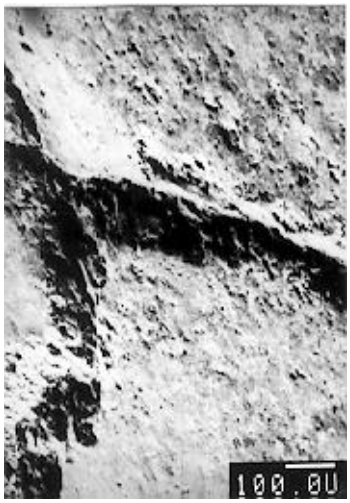

Fig. 2

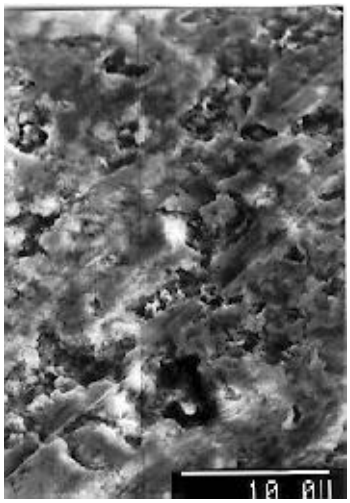

Fig. 3

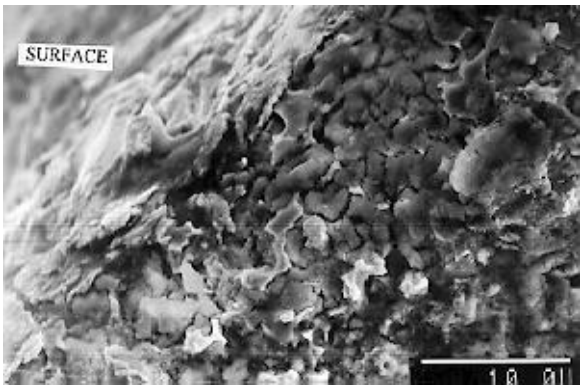

Fig. 4

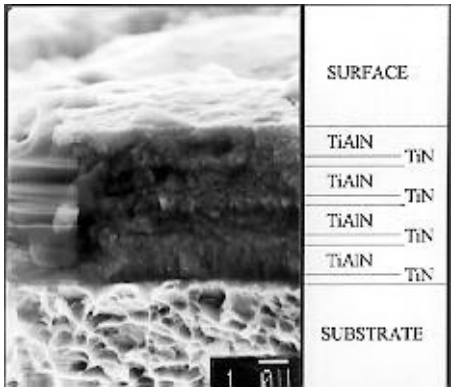

Fig. 5

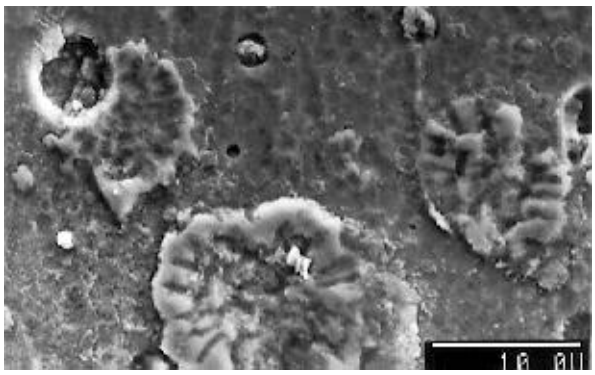

Fig. 6

Fig. 7 a

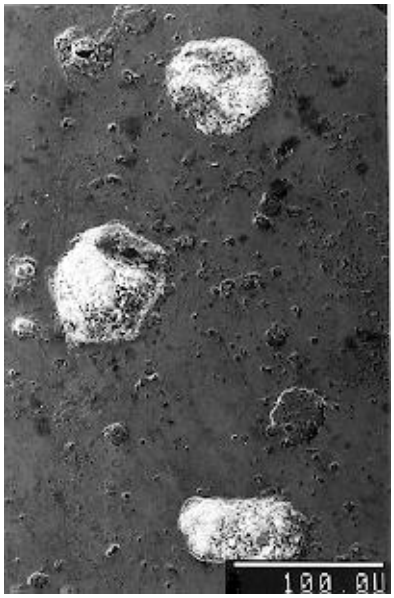

Fig. 7 b

THALLIUM-CONTAINING GALLATE GLASSES WITH HIGH OPTICAL NONLINEARITY

Bruce G. Aitken and **Nicholas F. Borrelli**
Corning Inc., USA

Abstract

Glass formation is extensive in the TlBi gallate system. Tl-rich glasses are characterized by lower T_g and an absorption edge at lower energy. Partial replacement of Bi by Tl leads to an increase in linear refractive index and to a sharp rise in both $\chi^{(3)}$ and the Kerr constant, making Tl-containing gallates the most nonlinear of all oxide glasses. Tl-rich glasses also display large diamagnetic magnetooptic effects, with V as high as 0.30 min/Oe-cm at 633nm.

1. INTRODUCTION

Oxide glasses containing high concentrations of the heavy metal ions Pb^{++} and Bi^{3+} are characterized by high third order optical susceptibility $\chi^{(3),}$ and as such are promising materials for a variety of nonlinear optical devices [1]. Previous studies have shown that, among the heavy metal oxide glasses, PbBi gallate glasses display some of the largest measured values of $\chi^{(3)}$ [1,2], as well as the electrooptic Kerr constant (B) [3]. Subsequently, the partial replacement of Pb or Bi by Tl was found to result in an enhancement of the optical nonlinearity of these glasses [4]. Femtosecond time scale measurements of $\chi^{(3)}$ at four different wavelengths between 600 and 1250 nm have indicated that the increased nonlinearity of Tl-containing gallate glasses may be due to resonant enhancement arising from a progressive redshift of the absorption edge of these materials with rising Tl content [5].

This paper describes the effect of using Tl as an additional heavy metal modifier in gallate systems; amplifying on the nonlinear optical results previously reported. In particular, the consequence of partially replacing Bi by Tl on glass formation, crystallization behavior, and physical properties is discussed.

2. EXPERIMENTAL

Tl-containing gallate glasses were prepared by melting appropriate 40-100 gm mixtures of Tl_2CO_3, Bi_2O_3 and Ga_2O_3 in Au crucibles for 15-30 mins at 850-1025^oC. The melts were quenched by pouring into brass or graphite molds on a steel plate, and the glasses were subsequently annealed near T_g (200-300^oC).

Density was measured in kerosene using the Archimedes method. T_g and T_x (temperature at the onset of crystallization) were determined by DSC at a heating rate of l0^oC/min. Refractive index was measured at 589 nm using the apparent depth technique with 2mm thick samples. Electrooptic and magnetooptic constants were measured

according to the methods described elsewhere [3,6], and are accurate to $\pm 0.2 \times 10^{-6}$ cm/kV^2 and ±0.02 min/Oe-cm, respectively. Heat treated glasses were characterized by XRD and SEM.

3. RESULTS

TlBi gallate glasses were prepared over the following range: 20-50% Tl_2O, 25-65% Bi_2O_3, and 15-30% Ga_2O_3, where compositions are reported in mol %. The glasses are orange to red in color, with the redder glasses corresponding to Tl-rich and/or Ga-poor compositions. For example, for glasses containing 20% Ga, the visible absorption edge shifts from 535 to 620 nm as the Tl concentration increases from 20 to 45%. The infrared absorption edge, here defined as the wavelength where the transmission is 50% of that at 2.5 μm, lies at about 7.5 μm. T_g ranges from 220 to 300°C, increasing with rising Ga for a constant Tl/Bi ratio. At constant Ga, T_g decreases monotonically with rising Tl concentration, whereas T_x-T_g attains a maximum value at an intermediate Tl/Bi ratio due to an inflection in T_x, as shown in Fig.1 and the following table.

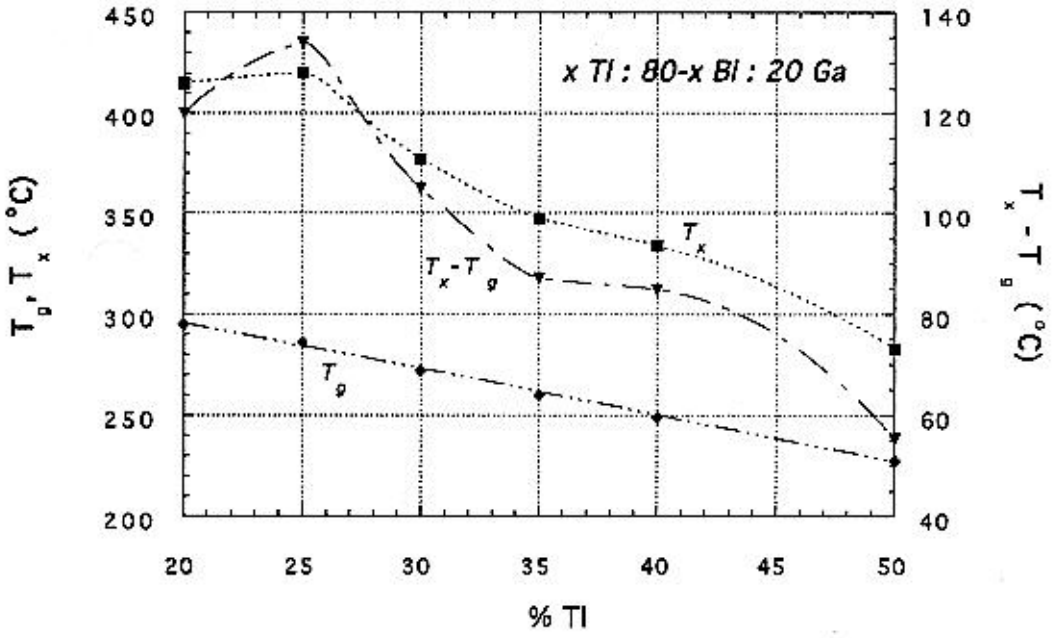

Fig. 1 Tg, T_x, and T_x-T_g of TlBi gallate glasses containing 20% Ga as a function of Tl concentration.

These glasses have steep viscosity curves such that, for a 30Tl : 50Bi : 20Ga glass, the viscosity decreases from 10^9 to 10^7 poise over a temperature interval of only 22°C. Glass density ranges from 7.9 to 8.5 gm/cc, increasing sharply with falling Ga content. At a fixed Ga concentration, density decreases with rising Tl.

Tl	Bi	(g/cc)	T_g (^{o}C)	T_x (^{o}C)	T_x-T_g (^{o}C)
50	30		227.6	283.0	55.4
40	40	8.350	249.1	334.0	84.9
35	45	8.360	260.3	347.5	87.2
30	50	8.365	272.4	377.4	105.0
25	55	8.364	286.3	420.3	134.0
20	60	8.378	295.1	369.8	74.7

The linear refractive index of these glasses is high, ranging from 2.40 to at least 2.47 at the Na D line, decreasing with rising Ga content at a constant Tl/Bi ratio. For glasses

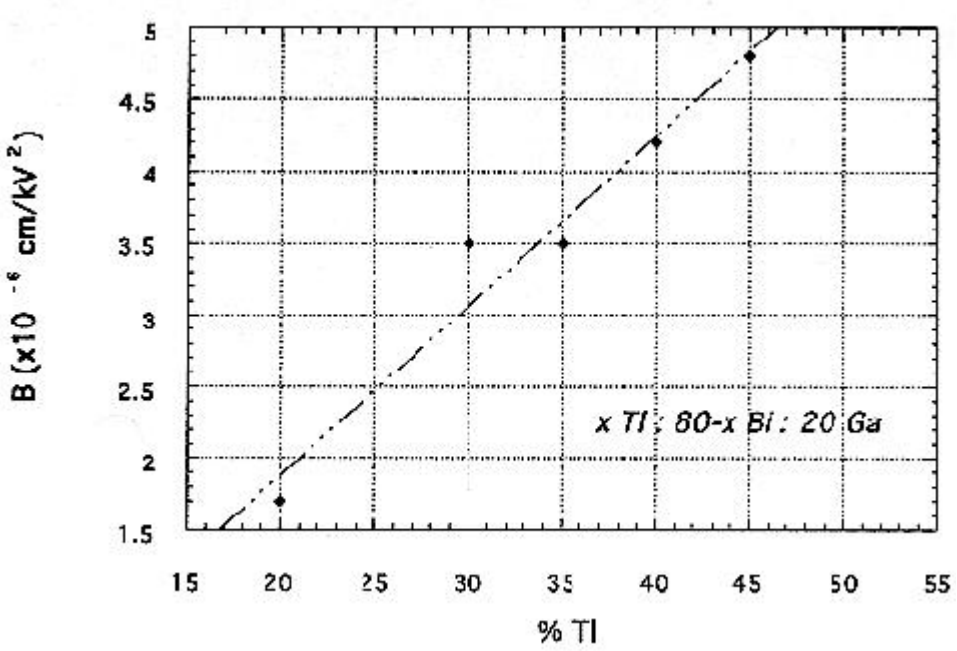

Fig. 2 Kerr constant of TlBi gallate glasses containing 20% Ga as a function of Tl concentration.

containing 20% Ga, refractive index increases from 2.45 to 2.47 as the Tl content rises from 20 to 40%. As reported elsewhere, $\chi^{(3)}$ shows a parallel increase from 44 to 79x10^{-14} esu at 1060 nm as the Tl concentration increases from 20 to 45% [4]. The Kerr constant, B (where $\Delta n = B \lambda E^2$), is found to increase from 1.7 to 4.8 x 10^{-6} cm/kV^2 over the same range, as illustrated in Fig. 2. The latter value is the largest B reported for an oxide glass.

These glasses are also characterized by a large positive, hence diamagnetic, Verdet constant, V, which increases with rising Tl content, as shown in Fig. 3 and the following table, where the subscripts to V refer to the measurement wavelength. There is manifest dispersion in the magnetooptic data, with V decreasing, for example, from 0.28 to 0.039

min/Oe-cm for a glass containing 40% Tl as the measurement wavelength increases from 633 to 1525 nm. Tl-rich glasses are more dispersive in this spectral range, i.e. the dispersion of V increases as the absorption edge of the glass shifts to longer wavelength.

Tl	**Bi**	$c^{(3)}$	**B**	$\mathbf{V_{633}}$	$\mathbf{V_{1150}}$	$\mathbf{V_{1525}}$
50	30				0.071	
45	35	79	4.8	0.29	0.067	0.043
40	40	74	4.2	0.28	0.067	0.039
35	45	59	3.5	0.26	0.060	0.039
30	50	56	3.5	0.245	0.059	0.038
25	55	55				
20	60	44	1.7	0.22	0.054	0.037

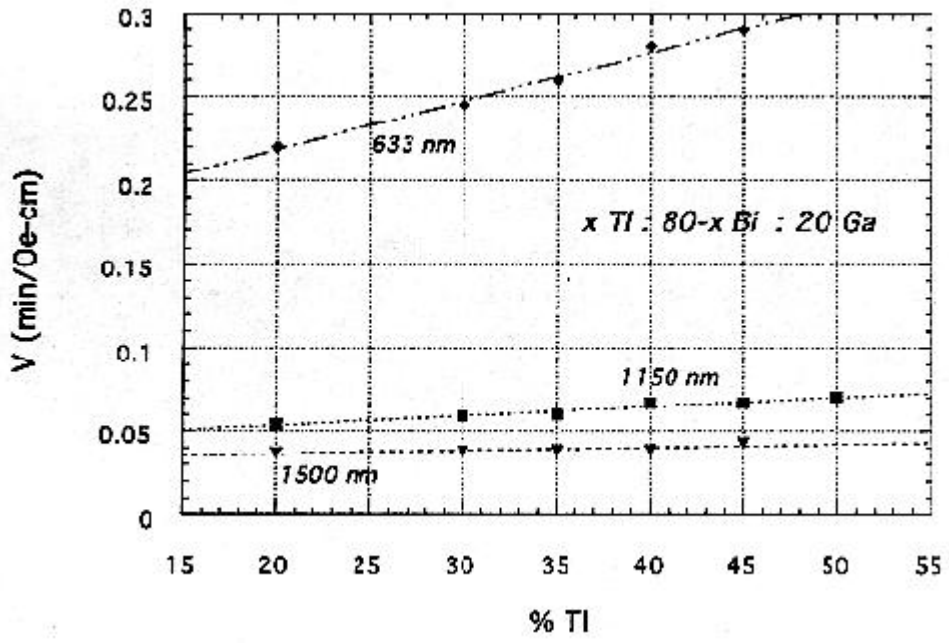

Fig. 3 Verdet constant at 633, 1150, and 1500 nm of TlBi gallate glasses containing 20% Ga as a function of Tl concentration.

The devitrification tendency of Tl-containing gallate glasses was evaluated by heating 5-10 gm samples of these materials for 150 mins at 430-440^{o}C. In all samples, the mode of devitrification is one of surface crystallization. The resultant crystalline assemblage is typically found to consist of three phases: γ-Bi_2O_3 ($Bi_{24}Ga_2O_{39}$), an unknown phase with a pyrochlore-like diffraction pattern, and an unknown phase with a diffraction maximum at a d-spacing of 3.27Å. The bulk compositional dependence of the relative intensity of the diffraction maxima of these phases in the heat-treated glasses is shown below in Fig. 4. The illustrated variation in relative abundance suggests that the pyrochlore-like phase is close in composition to Tl_2O, whereas the 3.27Å phase is probably a TlBi gallate with a Tl/Bi ratio slightly greater than unity. These chemical assignments are consistent with semiquantitative analysis carried out during SEM study. In Tl-rich glasses, SEM showed the pyrochlore-like "Tl_2O" to occur as relatively coarse, elongate, rectangular crystals that appear to have crystallized before the finer equigranular (cubic) γ-Bi_2O_3. This crystallization sequence is reversed in Bi-rich glasses, corresponding to the inflection in T_x illustrated in Fig.1.

4. DISCUSSION

The compositions of most of the studied ternary TlBi gallate glasses lie within the limits of the approximate glass forming region delineated by Fujino et al. [7]. Our data indicate, however, that the limits shown by the latter authors should be extended to higher Ga and Tl concentrations. The compositional dependence of T_x- T_g of these materials, coupled with the identity of the phases that develop upon heat treatment, suggests that the greater thermal stability of glasses with intermediate Tl/Bi ratios may be due to a depression of the liquidus associated with a γ-Bi_2O_3-"Tl_2O" cotectic. Such glasses are sufficiently stable that samples weighing several hundred gm can be cast without devitrification.

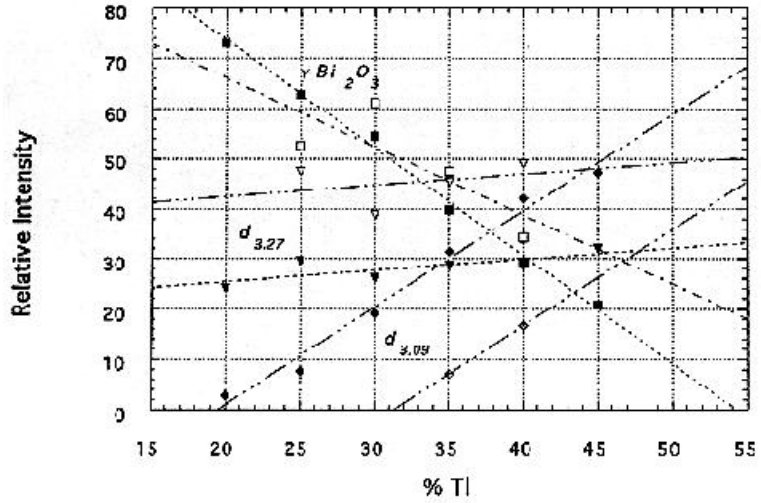

Fig. 4 Relative intensity of diffraction maxima of phases crystallized at 430- 440^{o}C from TlBi gallate glasses containing 20

(filled symbols) and 30% Ga (open symbols): g-Bi_2O_3(squares), "Tl_2O" (diamonds), and TlBi gallate (triangles).

As the Ga content of TlBi gallate glass decreases from 30 to 15%, the molar volume increases from 23 to 24 cc/mol, corresponding to a 4% reduction in the oxygen concentration ([O]) and indicating a less efficiently packed glass structure. For glasses containing 20% Ga, molar volume decreases from 24 to 23.5 cc/mol as Tl replaces Bi. However, as the O/metal ratio is lowered by this substitution, this small molar volume decrease actually corresponds to a near 18% reduction in [O], indicating that the structure of Tl-rich glasses is even less compact.

The pronounced T_g lowering effect of Tl in these glasses is consistent with the large size and low charge, hence low field strength, of the Tl^+ ion, which is clearly more effective than either Pb^{++} or Bi^{3+} in weakening the structure of these materials. Although the structural role of Tl in these glasses is unknown, it is possible that it may function as more of a traditional network modifier in contrast to the behavior of Pb and/or Bi. From Raman spectroscopy, the latter are thought to form asymmetric PbO_{3-4} and BiO_6 polyhedra, respectively, which, along with GaO_4 tetrahedra, comprise the structural network of PbBi gallate glasses [8].

Increasing the Tl content of heavy metal gallate glass also results in a shift of the absorption edge to longer wavelength, which is responsible for the resonant enhancement of $\chi^{(3)}$ and B. The absorption edge of these glasses is controlled by the energy of the $^1S_0 > {}^1P_1$, $^3P_1$ electronic transitions arising from the lone $6s^2$ electron pair on the heavy metal ions Tl^+or Bi^{3+}. The redshift of the absorption edge in Tl-rich glasses is a reflection of the fact that, for Tl^+, these transitions lie at lower energy than for either Bi^{3+} or Pb^{++} when incorporated in a heavy metal gallate host.

Both the linear and nonlinear optical properties of oxide glasses are known to be strongly influenced by the presence of the heavy metals Tl, Pb, and Bi. The magnitude of both $\chi^{(3)}$ and B has been shown to be positively correlated with heavy metal concentration in a wide range of glass types, including silicates, borates, as well as gallates [2,3,5]. However, the relative effect, if any, of Tl, Pb, or Bi on these optical properties is not well understood, although the higher $\chi^{(3)}$ of TlBi gallate glasses was ascribed to the presence of Tl [4]. In this study, the observed increase in both linear refractive index and B with rising Tl can be attributed to the large polarizability (α) of the Tl^+ ion. Due to the combination of its lone $6s^2$ electron pair and lower (relative to Pb and Bi) nuclear charge, Tl^+ is the most polarizable of all cations, with α=5.2Å^3, whereas that of the Pb^{++} ion is calculated to be 4.9 Å^3 [9]. However, high index, high $\chi^{(3)}$ Tl-rich glasses also have an absorption edge at lower energy, as discussed above. Therefore, the measured increase in linear index, $\chi^{(3)}$ and B of these glasses with rising Tl content is partly due to resonance enhancement. Nevertheless, the large α, and by extension hyperpolarizability, of the Tl^+ ion suggests that some fraction of the increased linear and nonlinear susceptibility of Tl-rich gallate glass is intrinsic and not accountable solely by resonance enhancement. The latter is consistent with the observation that, at a wavelength far from resonance (1125 nm), $\chi^{(3)}$ of a Tl-containing gallate glass ($\chi^{(3)}$= 3.7 x 10^{-13} esu) is about 50% greater than that of its Tl-free analogue ($\chi^{(3)}$= 2.4 x 10^{-13} esu) [5].

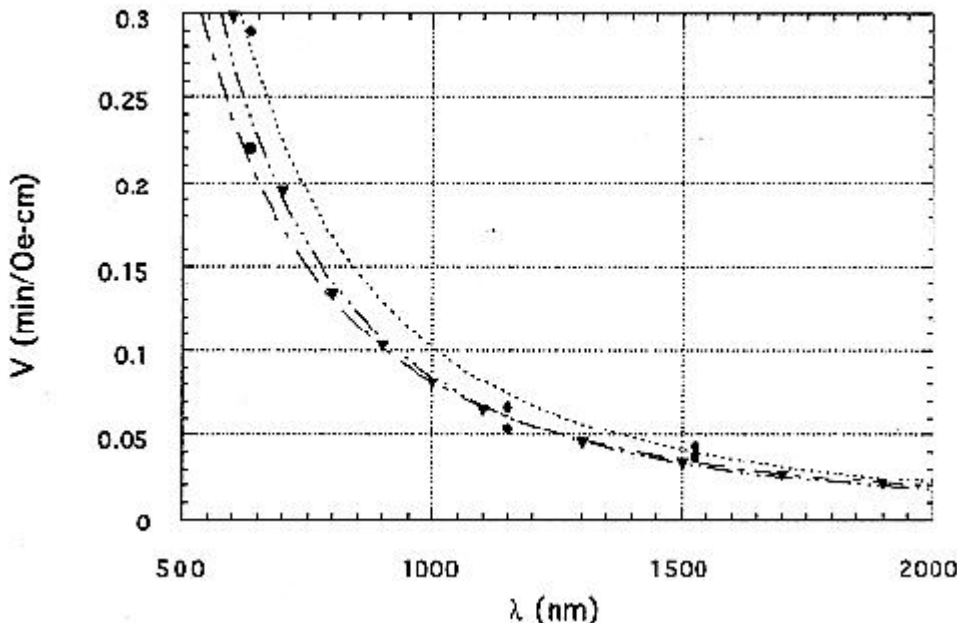

Fig. 5 Dispersion of V of TlBi gallate (20% Ga) glasses containing 20 (circles) and 45% Tl (diamonds) and vitreous As_2S_3 (triangles, data from [10]).

The large diamagnetic Verdet constant of TlBi gallate glasses is in agreement with previous findings that V rises with increasing heavy metal concentration [6]. The value of 0.29 min/Oe-cm at 633 nm for the 45% Tl glass is, to the best of our knowledge, the highest measured V for an oxide glass. In accordance with the Becquerel formula, where $V = (e/2mc^2)\lambda\, dn/d\lambda$, the data lie on a dispersion curve that rises steeply as the absorption edge is approached. In view of the dependence of the latter on the Tl concentration, it is therefore expected that V is higher for Tl- rich glasses due to resonance enhancement. This is illustrated in Fig. 5, where the points for 20 and 45% Tl glasses containing 20% Ga are seen to bracket earlier data for the sulphide glass As_2S_3 [10], which has its absorption edge at a wavelength similar to that of the gallate glasses.

5. CONCLUSIONS

The formation of stable glasses in the system Tl_2O-Bi_2O_3-Ga_2O_3 has been demonstrated. These materials share a number of the physical properties that are characteristic of the similar PbBi gallate glasses, including high density, steep viscosity curves, high linear and nonlinear refractive index, as well as extended IR transparency. Increasing the Tl content of TlBi gallate glass results in a progressive decrease in T_g, as well as a redshift of the absorption edge. As with $\chi^{(3)}$, the Kerr constant of TlBi gallate glass increases with rising Tl. This increase arises partly from resonance enhancement due to the shift of the absorption edge, but also from the greater polarizability of Tl^+ relative to Bi^{3+}. Finally,

these glasses display the highest diamagnetic Verdet constants ever measured for an oxide glass, with V as high as 0.3 min/Oe-cm and rivalling that of vitreous As_2S_3.

REFERENCES

[1] N.F. Borrelli, B.G. Aitken and M.A. Newhouse, J. Non-Cryst. Solids l85 (1995)109
[2] D.W. Hall, M.A. Newhouse, N.F. Borrelli, W.H. Dumbaugh and D.L Weidman, Appl. Phys. Lett. 54 (1989) 1293
[3] N.F. Borrelli, B.G. Aitken, M.A. Newhouse and D.W. Hall, J. Appl. Phys. 70 (1991) 2774
[4] J. Yumoto, S.G. Lee, B. Kippelen, N. Peyghambarian, B.G. Aitken and N.F. Borrelli, Appl. Phys. Lett. 63 (1993) 2630
[5] I. Kang, T.D. Krauss, F.W. Wise, B.G. Aitken and N.F. Borrelli, J. Opt. Soc. Am. B12 (1995) 2053
[6] N.F. Borrelli, J. Chem. Phys. 41 (1964) 3289
[7] S. Fujino, H. Takebe and K. Morinaga, J. Ceram. Soc. Japan 103 (1995) 340
[8] F. Miyaji and S. Sakka, J. Non-Cryst. Solids 134 (1991) 77
[9] J.R. Tessman, A.H. Kahn and W. Shockley, Phys. Rev. 92 (1953) 890
[10] C.C. Robinson, Appl. Optics 3 (1964) 1163

THE DEVELOPMENT OF GLASS FIBRE REINFORCED WASTE PLASTER

M. H. Ozkul[1], B. Kuban[2] and **B. Eren[3]**
[(1)]Istanbul Technical University, Turkey
[(2)]SISECAM Research Center, Turkey
[(3)]Cam Elyaf San. A.S., SISECAM, Turkey

Abstract

The mechanical properties of glass fibre reinforced gypsum composites were investigated. Each of three types of E-glass fibres introduced into the three different gypsum matrices, such as natural, sitro-, and desulpho-. The latter two gypsums are waste materials of citric acid and power plants, respectively. In general it is found that there is an optimum fibre content to improve the flexural strength of composites. The effects of fibre content on compressive strength and modulus of elasticity of composites are slight comparing with those on flexural strength.

1. INTRODUCTION

Gypsum has been used in building construction because of its lightweight, low thermal conductivity and high fire endurance as well as its water absorption properties in the interior volumes. Being a brittle material, gypsum needs to improve both flexural and impact resistance, and glass fiber reinforcement is a way of increasing these mechanical properties.

E-glass fibres, although being comparingly cheap materials, because of their low alkali resistance, can not find application in the production of Portland cement composites [1]. On the other hand, gypsum creates a weakly acidic medium (pH≈6-7) and for this reason makes no harmful effect on the durability of E-glass fibres embedded in it. It appears that gypsum is an alternative matrix to the polymer in the utilization of E-glass fibres in the production of composites.

Gypsum can be obtained from the nature by mining and has a composition of $CaSO_4.2H_2O$ as gypsum stone, and $3/2H_2O$ should be removed by partial dehydration process over a temperature of 170°C to form construction gypsum. On the other hand, many industries such as phosphoric acid, hydrofluoric acid, boric acid, citric acid and titanium oxide have by-products which have the same composition as gypsum stone. Besides, desulphurization process in power plants converts flue gases into a material similar to gypsum stone [2]. These by-products cause storage and environmental problems and utilization of them gains importance.

In this study, one commercial natural gypsum and two by-product, such as citro-and desulphogypsum as matrix material, and three types of E-glass fibres have been used in the production of glass fibre reinforced composites, and their mechanical properties were investigated.

2. EXPERIMENTAL

2.1. Materials

Gypsum

One natural gypsum commercially available (Entegre Plaster Company) and two waste gypsum of citro-and desulpho-obtained from Fursan Citric acid Company and

Cayýrhan Power Plant, respectively, were used and their chemical compositions and physical and grading properties were given in Table 1. The latters were heated in oven at 190°C for 48 hours to convert into hemihydrate.

Table 1. Properties of Gypsums.

Grading :	**Passing (%)**			
	400 μm	200 μm	100 μm	40 μm
natural	100	85	73	55
sitro-	100	82	15	5
desulpho-	100	73	16	3

Setting time :

natural : 5 min
sitro- : 8 min
desulpho- : 4 min

Composition :

	hemihydrate (wt. %)
natural :	%92
sitro- :	%95
desulpho :	%93

Fibres

Chopped E-type glass fibres were obtained from Cam Elyaf San. A.Þ., ÞÝÞECAM, and physical properties of them are given in Table 2.

Table 2. Physical Properties of Fibres.

	DE-07	**KCR-02**	**BMC-01**
Fibre diameter (μm) :	12-14	10-12	12-14
Fibre length (mm) :	13.5	13.5	4.8
Moisture (%) :	max. 2.5	max. 0.1	max. 0.1
Tex number (9/1000 m) :	265	85-115	265
Split :	Single	3	Single
Loss on ignition (%) :	0.15-0.35	0.85-1.25	1.20-1.60

2.2. Mix Proportions and Testing Procedure

Water-gypsum ratio was kept constant at 0.70 for all mixes. A melamine based superplasticizer was added into the mixture at a dosage of 2% by weight of gypsum content to improve the workability. After dry mixing of fibres with gypsum for 3 min., the water added into the pan mixer with a capacity of 5 dm^3, and then fibre-gypsum mixture is poured into the water gradually while the mixer was running. 4x4x16 cm prismatic moulds were used for mechanical tests. The samples were dried in oven at 40°C for 7 days. First dynamic modulus of elasticity of specimens were determined by measuring resonant frequencies, then three point-bending tests were applied on the same specimens. The broken parts of specimens after bending test were used for compression testing by using an Instron Universal Testing Machine at crosshead rate of 0.5 mm/min. The mean of three measurements for resonant frequencies and bending testing, and 6 measurements for compression testing were obtained, respectively.

3. RESULTS AND DISCUSSION

The DE-07 type fibres have an amount of loss on ignition less than those of other two fibres, as can be seen in Table 1, indicating that the coupling agent used for coating is smaller than those of others. For this reason, fibres in DE-07 strands separated from each other in the composite, leading decrease in workability of mixture. The other two fibres stayed in the mixture as strands, giving possibility of using in large contents. The length of fibres was also effective on the workability, i.e., the longer the fibre length, the lower the workability. For BMC-01 fibres, even at 9% by wt. fibre content, workable mixes were obtained. The superplasticizer, originally improved for Portland cement concretes, increased the workability of gypsum, giving possibility of using lower water/gypsum ratios. Higher fibre contents, as much as 13%, were reported [3] but their preparation techniques are different, i.e. spray-up or hand-lay up.

Flexural strengths of natural gypsum composites are given in Fig.1. This figure shows that there is an optimum fibre content for each fibre, such that 2% for DE-07 and 3% for both KCR-02 and BMC-01, respectively. The highest increase in flexural strength with respect to plain is obtained for DE-07 fibres as much as 63%, probably due to better separation of fibres. BMC-01 fibres gave the least increase, indicating that their fibre length is not sufficient.

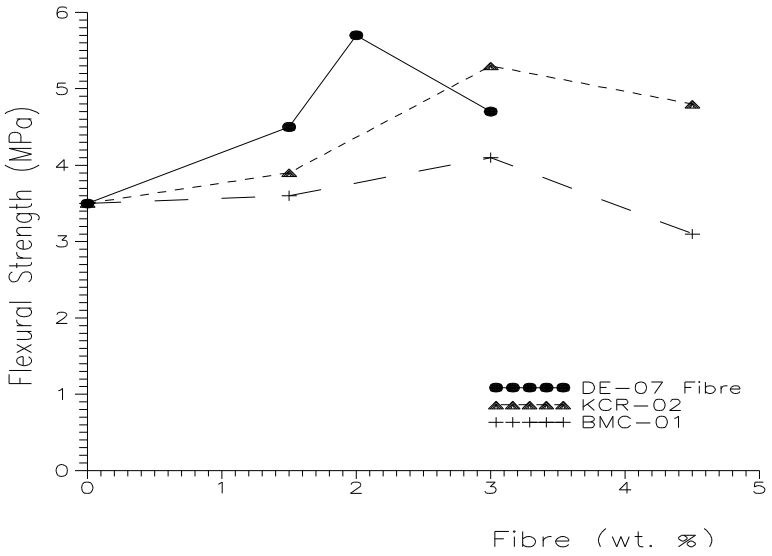

FIG.1. Effect of glass fibre content on flexural strength of natural gypsum composites.

Flexural strengths of three different gypsums are compared in Fig.2. The flexural strength of plain desulphogypsum is higher than those of natural and sitro-ones. While natural and sitrogypsums are showing an optimum at 3% fibre content, desulfo-one has an increasing trend at even 4.5%. It seems that there is an optimum for the latter composite greater than 4.5%.

The max. length of fibres used in this study is 13.5 mm. It is reported that better results were obtained with longer fibres, such as 34 mm [4,5] and 50 mm [6].

A commercially available plaster plate, reinforced with special cardbord on two faces, was also tested for comparison and as average 4.2 MPa flexural strength was obtained. The composites prepared with fibres in this study give better results than this plaster plate. The flexural strength of a special gypsum-fibrous slab, prepared by "Knauff" technology was given as 7 Mpa [7], which is comparable with the result of desulfogypsum-KCR-02 fibre composite at 4.5% fibre content, as presented in Fig.2.

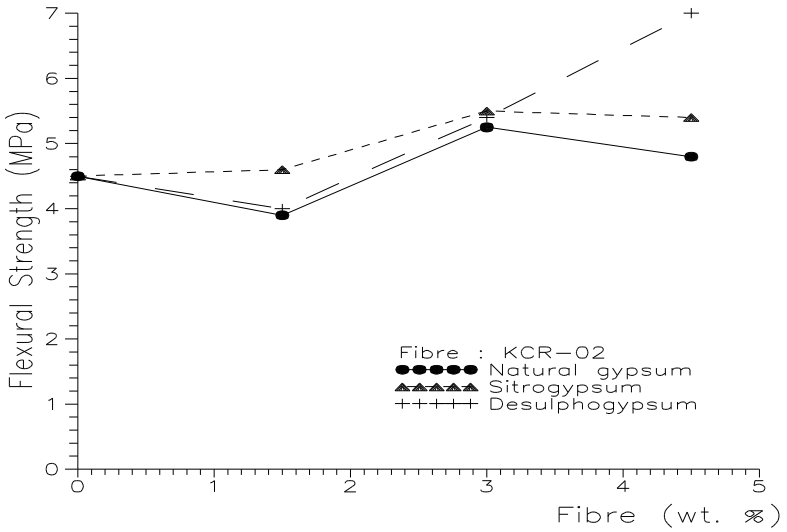

FIG.2. Effect of gypsum type on flexural strength of composites.

Variation of compressive strength for the composites are given in Figures 3 and 4. The increase in compressive strength is smaller than that in flexural strength indicating that the main increase in fibre reinforced gypsum is experienced in flexural strength as well as in tensile and impact strengths [4]. Even no increase was reported for the Portland cement composites in compressive strength [4] due to the poor bonding between fibre and matrix.

Dynamic moduli of elasticity for natural gypsum composites are shown in Fig.5. Slight changes were obtained for different fibres tested except DE-07 fibre at 3%; for the latter composite 27% increase is obtained. Similar results were reported [4] for the composites tested in compression.

Fig.6 shows the variation of density with glass content. It seems that the density remains fairly constant with an increase in the glass content.

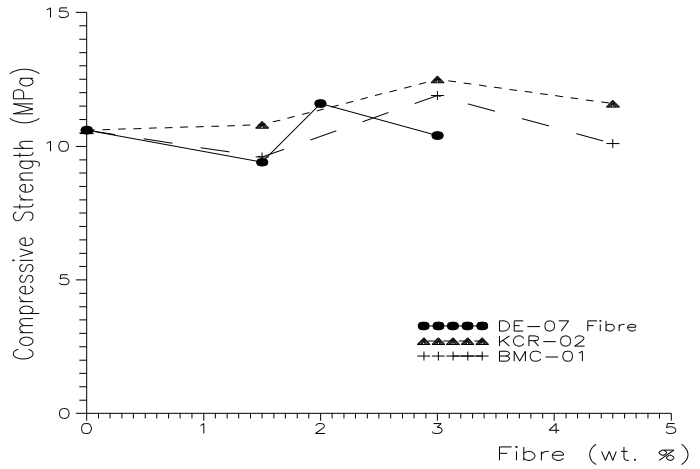

FIG.3. Effect of fibre content on compressive strength of natural gypsum composites.

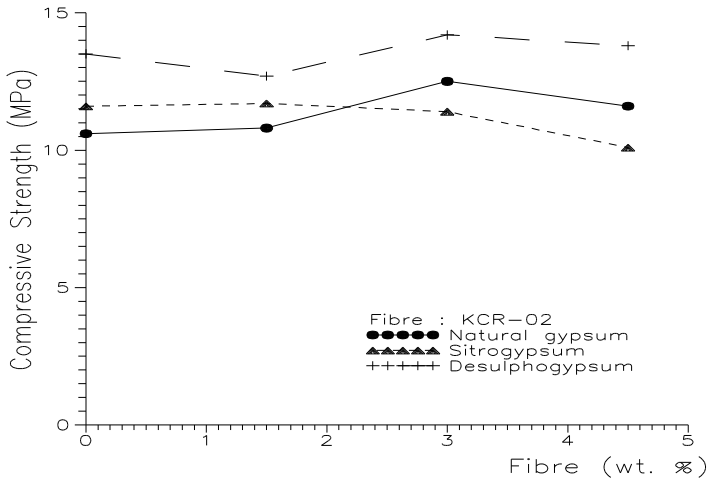

FIG.4. Effect of gypsum type on compressive strength of composites.

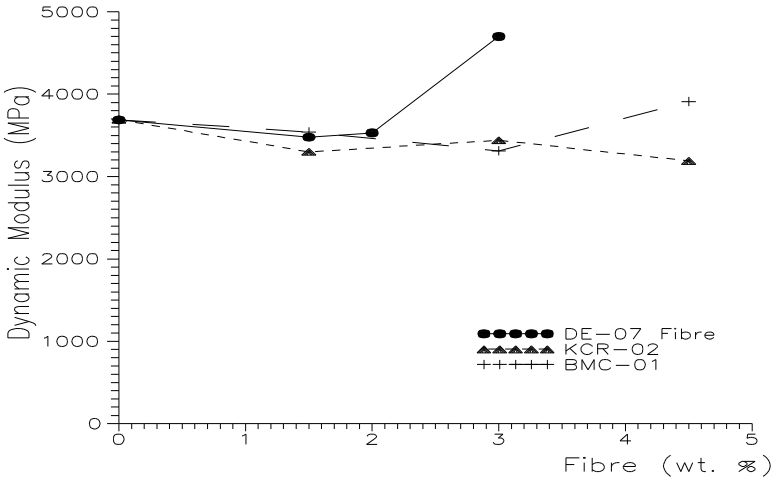

FIG.5. Effect of fibre content on dynamic modulus of elasticity of natural gypsum composites.

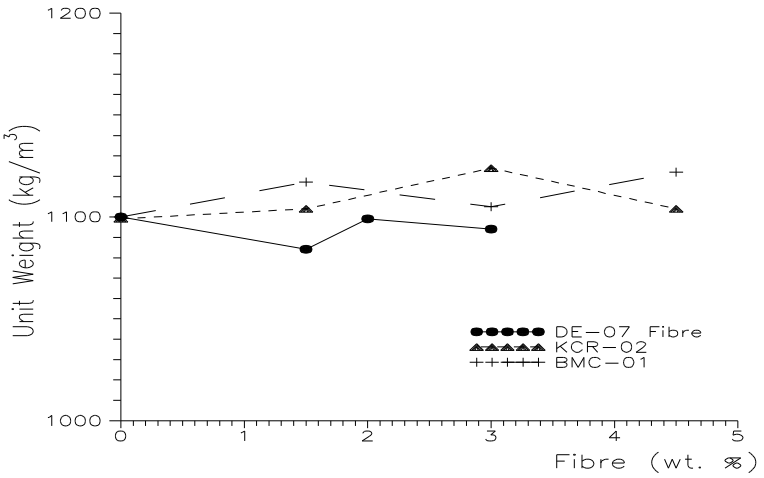

FIG.6. Effect of fibre content on unit weight of natural gypsum composites.

4. CONCLUSIONS

There is an optimum fibre content with respect to flexural strengths for the fibres and gypsums tested. Desulphogypsum gave higher flexural strengths for both plain and fibre reinforced materials. The effect of fibre on compressive strength and dynamic modulus of elasticity of composites is less than those on flexural strength.

ACKNOWLEDGMENT

This study was supported by a grant (No.INTAG 615) from the Scientific and Technical Council of Turkey (TUBITAK).

REFERENCES

1. Kuban, B., Ozkul, H. and Tasdemir, M.A., "Application of Composite Materials in Civil Engineering Technology", Sci. and Tech. Res. Council of Turkey (TUBITAK) Project Nr. INTAG-TOKI 621 (1995).
2. Ozkul, H. and Koral, S., "Waste Gypsums and Utilization in Civil Engineering", Symposium on Waste Industrial Materials, Chamb. of Turkish Civil Eng. (in Turkish) 267-277 (1993).
3. Bijen, I. and Van Der Plas, C., "Polymer-Modified Glass Fibre Reinforced Gypsum", Mat. and Struc., 25, 107-114 (1992).
4. Atan, Y. and Uyan, M., "The Behaviour of Gypsum and Portland Cement Domposites Reinforced with Glass Fibres", Technical Report Nr.35, Istanbul Technical University (in Turkish) (1979).
5. Yasa, H.Y., "Gypsum-Pumice-Glass Fibre Composites", PhD thesis, Istanbul Technical University (in Turkish) (1985).
6. Singh, M. and Mridul, G., "Glass Fibre Reinforced Water-Resistant Gypsum-Based Composites", Cem. and Conc. Composites, 14, 23-32 (1992).
7. Mitrofanov, A.A., Sushkevic, V.G. and Lashkevic, V.G., "Durable Fibrous Materials Based on Gypsum and Phosphogypsum", 3rd Int. Conf. Durability of Building Mat. Components, 235-239, ESPOO (1984).

VERY LOW MELTING GLASSES SUITABLE FOR MIXING WITH ORGANIC SUBSTANCES*

Petru Balta and **Camelia Ungureanu**
University "Politechnica" of Bucharest, Rumania

Abstract

In the last years more attention is paid to the very low melting glasses. Usually that means homogeneous glass melts that can be obtained at temperatures between 400 and 800 C, sometimes having T_g values smaller as 100^{o}C.

Besides low melting temperature these glasses must have a sufficient chemical stability. Such glasses may have many applications but a new unusual one is to host organic substances that resist to respective low melting temperatures.

Were synthesized and studied glasses mainly in the system Pb-Sn-P-O-F but also in oxychloride and containing other inorganic salts systems. In some cases the glass synthesis presents serious difficulties related to redox processes involving the components. Many compositions fulfill the above mentioned condition concerning the melt temperature but only a few have an acceptable chemical stability.

To measure the hygroscopicity a method was tested, based on continuous weighting of glass samples exposed to a humidified atmosphere. Interesting correlation between hygroscopicity and composition was evidenced.

The properties required to mix inorganic glasses with organic substances are reviewed and determined for some of the synthesized glasses. Mixed glasses were prepared and examined. The properties corresponding to some applications were evaluated.

---

* Full manuscript not available at the time of printing

ENERGY FEASIBILITIES OF THE GLASSMELTING

L. N • mec
Laboratory of Inorganic Materials of IIC ASCR and ICT, Czech Republic

Abstract

Energy consumption plays a significant role when appreciating the effectiveness of glass melting and when searching for new ways of glass melting. The introduction of melting kinetics into relation for energy consumption shows that the controlled forced convection for the dissolution processes and reduced pressure for the refining process, seem to be very hopeful in future arrangement of glass melting. These theoretical presumptions can be proved by laboratory measurements. The realization of new factors in full scale glassmelting is task for the mathematical modelling of processes.

1. AIM OF THE WORK

The mathematical modelling simulates the most important processes of glassmelting, however, it is not easy to find general features of the process from its systematic simulation under real conditions. That is why analysis of the process has been undertaken, to derive simple relations expressing the influence of single factors as is temperature, pressure, glass composition, glass batch granulometry and glass flow arrangement on the glass melting. The theoretical results have been verified by laboratory experimental data and projected into the energy consumption of the process.

2. GENERAL FEATURES OF THE GLASS MELTING PROCESS AND GOVERNING EQUATIONS

Two important groups of phenomena enhance the entire process:
- dissolution phenomena (particle dissolution, homogenization)
- separation phenomena (bubble and foam removing)

At high temperatures, the subsequence of the phenomena plays its role:

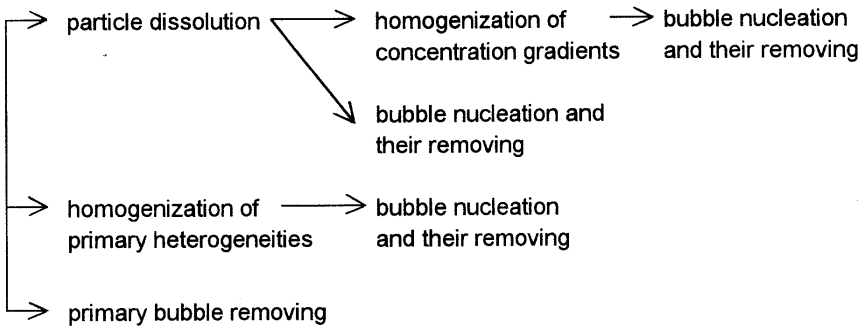

As the removing of nucleated bubbles is usually relatively fast, only particle dissolution, homogenization and primary bubble removing is considered. In this work, the glassmelting control by sand dissolution or by primary bubble removing is taken into account.

The dissolution time of polydisperse particles of SiO_2 in glass melt is in a simplified form given by /1,2/:

$$\tau_D = -\frac{1}{\kappa} \ln \frac{\alpha_{ch}}{\alpha_f} - \frac{\psi}{\alpha_f} \tag{1}$$

Where κ, α_{ch} and α_f are coefficients of mass transfer and ψ is value of integral depending on the glass composition and size distribution of SiO_2 particles.

The time necessary to remove a growing bubble by rising to the level is approximately given by /3/:

$$\tau_R = \left(\frac{27\, h\, \eta}{2\, g\, \rho} \right)^{1/3} \frac{1}{(da/d\tau)^{2/3}} \tag{2}$$

Where h is the bubble depth under the glass level, η and ρ are glass melt viscosity and density, respectively, and $da/d\tau$ is the bubble growth rate by diffusion as the most important factor of the refining process.

The influence of the most important and promising factors as is temperature, glass stirring and pressure on melting and refining times will be presented and compared in this work, the influence of remaining parameters see in /3/.

The specific energy consumption of the glassmelting process in simplified form is expressed by /3/:

$$H_M^o = H_G^M + C^G \left(T - T^e \right) + \frac{K_1 \left(T - T^{ex} \right) \tau_{Me}}{V^a} \tag{3}$$

where H^M_G involves the reaction, modification and evaporation heats as well as energy to heat the glass from ambient temperature to exit temperature, T^e, second therm represents energy to heat the glass from T^e to melting temperature, T, and the third term are heat losses through boundaries. Here, K_1, involves thermal conductivity of boundaries, $T - T^{ex}$ is temperture difference of inner and outer walls· of a melting space, respectively, τ_{Me} is technologically necassary melting time and V^a is the fraction of active volume of the glassmelting space related to given phenomenon.

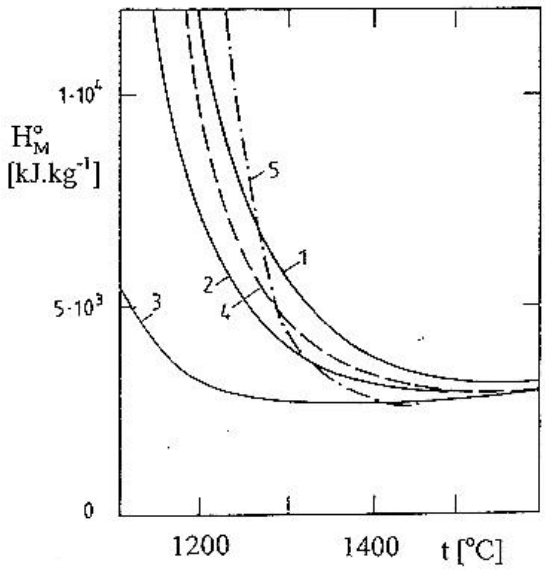

Fig. 1: Dependence of the specific energy consumption, H^o_M, for the model soda - lime- silica glass on the tempreture, $t_{Me} = t_D$, curve 1: $V^a = 0.1$, curve 2: $V^a = 0.2$, curve 3: $V^a = 1$, curve 4: $\P V^a/\P T = 1.8x10^{-3}\ K^{-1}$, $V^a = 0.1$ at 1100 °C, curve 5: same dependence for float glass, $t_{Me} = t_R$, melting is controlled by bubble removing, $V^a = 0.1$, $a_o = 0.5$mm, glass layer thickness l mm.

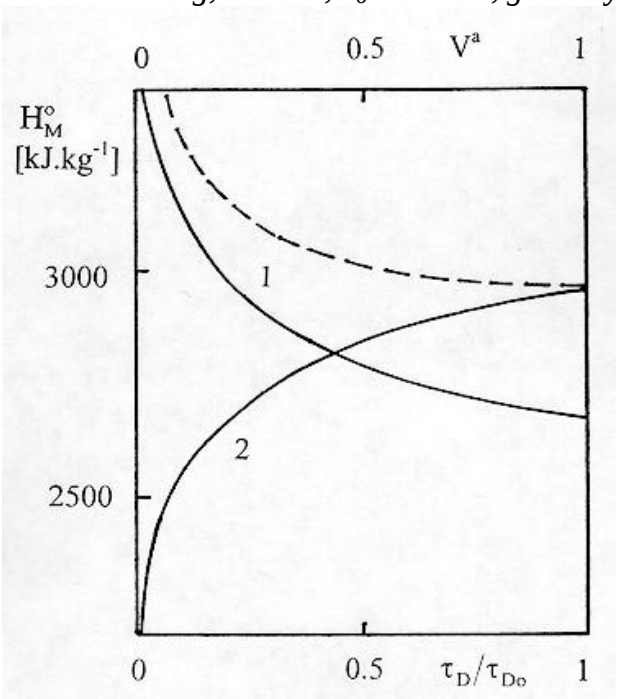

Fig. 2: H^o_M dependence of the sand dissolution process at the optimum melting temperature on the utilisation of the glassmelting space, V^a, and on the relative shortening of the dissolution process by melting factors difFerent from temperature, t_D/t_{Do}. 1. Dependence on V^a, $t_D/t_{Do} = 1$; 2: Dependence on t_D/t_{Do}, $V^a = 0.2$. - - - H^o_M dependence corresponding to t_D/t_{Do} attained only by temperature increase, $V^a = 0.2$, $T_o = 1300$ °C.

3. DISSOLUTION PHENOMENA

Influence of temperature

The influence of temperature on τ_D in eq. (1) can be approximated by the equation:

$$\tau_D = K^T_{D1} \exp\left(K^T_{D2}/T\right) \qquad (4)$$

Where K^T_{D1} and K^T_{D2} are constants independent from temperature. (Here the upper index designates the melting factor - temperature, and lower index the phenomenon- dissolution).

From the character of eq. (3) and consequently from the graphical representation of H^o_M, (T) in Fig. 1. results that there exists optimum melting temperature where , H^o_M has a minimum value. The lower is this optimum temperature, the lower is the specific energy consumption (see eq. 3). The position of the optimum melting temperature is influenced by the utilisation of the glassmelting space, V^a, and by other melting parameters determining the melting kinetics. In Fig. 2, there is presented the influence of both mentioned factors on the specific energy consumption when the whole melting process in soda - lime - silica glass is controlled by sand dissolution. The favourable influence of other potential accelerating parameters, different from temperature, is especially obvious from this figure. It is therefore worth dealing with significance of these factors on glass melting.

Influence of glass convection

The dissolution process may be accelerated by forced convection. Its effect consists in weekening the diffusion layer on the particle boundary. The proposed governing equation derived from (1) has the form:

$$\tau_D = \frac{K^c_{D1}}{1 + K^c_{D2}\,\mathrm{grad}\,v} - K^c_{D3} \qquad (5)$$

Where K^c_{D1} - K^c_{D3} are constants and grad v is the absolute value of velocity gradient in the particle vicinity.

The proposed dependence H^o_M (grad v) is obvious from Fig. 3. The deep favourable influence of the intensity of glass convection on the dissolution process is seen from this figure, being comparable with the influence of temperature.

The comparison of temperature influence and glass stirring on the specific energy consumption of sand dissolution process is brought in Fig. 4. As was expected the specific energy consumption of stirred glass shows lower values even in the right part of dependences owing to needed lower melting temperature of stirred glass (1300 ^oC).

The problem of glass flow arrangement arises when applying forced convection in a continual glass melting space. Two requirements should be fulfilled: high value of the portion of active volume (V^a Õ 1) and high rate of homogenization (τ_D = 0). The glass flow arrangement in the glassmelting space fulfilling these requirements could be represented by s.c. quasi piston flow /4/. In this arrangement, the glass melt is intensively stirred in the planes perpendicular to the through flow of glass. The realization of mentioned glass stirring using different means as is temperature distribution, mechanical stirring etc. is the challenge for the mathematical modelling of glass flow in glass melting spaces.

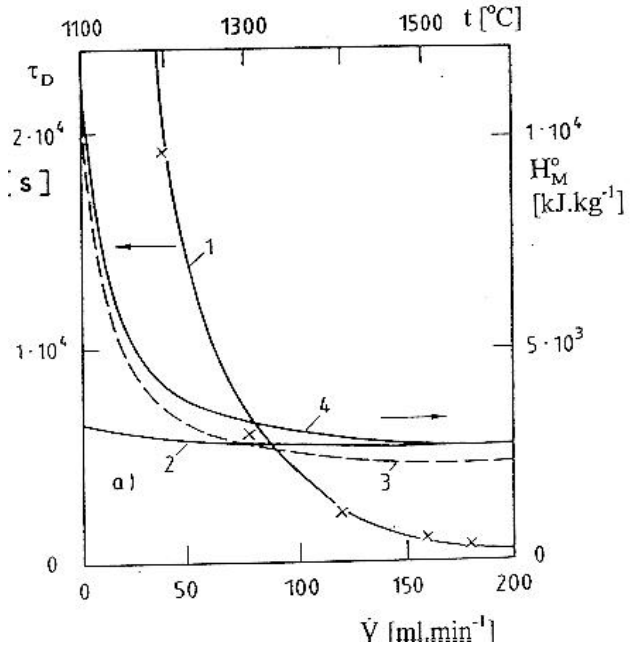

Fig. 3: lnfluence of the intensity of glass convection and glass flow distribution on the specific energy consumption in the model glass (composition in wt%: 74 SiO_2,16 Na_2O,10 CaO), 0,7 wt.% Na_2O as Na_2SO_4, $r_{max\ o}$ = 2.5 x 10^{-4} m, $t_{Me} = t_D$· Curve 1: Relation between the sand dissolution time and temperature for the model glass being bubbled bv 30ml O_2 min^{-1}; x - experimental values. Curves 2 - 4: Dependence of H^o_M on the glass convection intensity (V): curve 2: 1500 °C, V^a = 0.1; curve 3: 1200 °C, ¶V^a/¶V=4.5x10^{-3}; $min.ml^{-1}$, V^a = 0.1 at V = 0: curve 4: 1200 °C, V^a = 0.1

4. BUBBLE REMOVING

Influence of temperature

Among factors influencing the bubble rising velocity to the glass level, the bubble growth rate is the most important one (see eq. (2)). The simplified equation governing the growth of a single bubble has the following form:

$$\frac{da}{d\tau} = K^T_{R1} T \exp\left(-\frac{2a+b}{3T}\right)\left[K^T_{R2}\exp\left(-\frac{c_1}{T}\right) - K^T_{R3}\exp\left(\frac{c_2}{T}\right)\right] \qquad (6)$$

Where K^T_{R1} - K^T_{R3} are constants in the given temperature interval, a involves the activation energy of gas diffusion, b - activation energy of viscosity, c_1, and c_2 activation energy of solution enthalpy and reaction enthalpy of gas reaction with glass, respectively. As a result, bubble grow progressively with increasing temperature. The typical corresponding decrease of H^o_M, with temperature is obvious from Fig.1, curve 5.

The similar shifting optimum temperature to lower values as in Fig. 2 can be expected for the bubble removing process when increasing V^a and decreasing τ_R by factors different from temperature. The chemical effect of refining agents is currently exploited, however, the resulting

impact is usually restricted to high temperatures. Among other potential factors, reduced pressure seems to be most promising.

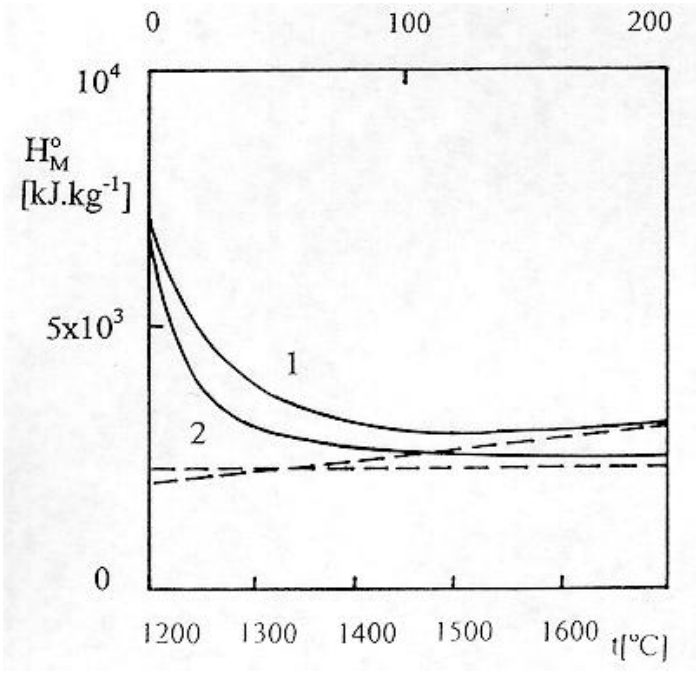

Fig. 4: The comparison of temperature and glass stirring effect on the specific energy consumption of the soda - lime - silica glass meltina in the model melting space. 1: temperature dependence, V^a=0.2; no stirring of glass 2: dependence on stirring intensity represented by amount of gas bubbled into the laboratory crucible (V), t =1200 ^oC, V^a = 0.2 - - - the courses of theoretical energy consumption

Influence of pressure

Taking into account only the influence of pressure on gas diffusion between bubbles and glass melt, the simplified bubble growth or dissolution equation has the form:

$$\frac{da}{d\tau} = \frac{K^p_{R1}}{p_{ex}} - K^p_{R2} \qquad (7)$$

Where K^p_{R1}, and K^p_{R2} are constants and p_{ex} is external pressure.

The experimentally verified dependence H^o_M (p_{ex}) in Fig. 5 confirms the importance of reduced pressures for the decrease in specific energy consumption of glass melting. The comparison of temperature and reduced pressure effect on the specific energy consumption of TV glass is presented in Fig. 6. The dependence between H^o_M and bubble growth rate, $\Delta a/\Delta\tau$, as the most important refining factor has been elected, however, temperatures and pressures are plotted as auxiliary scales too. The feasibility of replacing high temperature by reduced pressure (at 1300 ^oC, g.e.) is obvious from this figure.

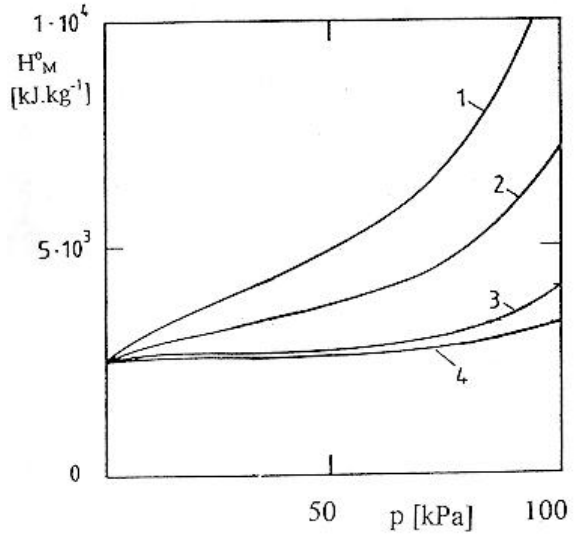

Fig. 5: Influence of external pressure on the specific energy consumption for the TV glass at 1400 ^{o}C, h_o = 0.25 m, a_o =1 x 10^{-4}, t_{Me} = t_R. Dependence of H^{o}_{M} on extemal pressure: curve 1: V^{a}= 0.1, without refining agents curve 2: V^{a} = 0.2, without refining agents curve 3: V^{a} = 0.1, with refining agents curve 4: V^{a} = 0.2, with refining agents

5. CONCLUSION

The analysis of glassmelting process, taking into account the influence of internal factors on melting kinetics, presents as the promising principles the controlled forced convection of glass in the stage of glass melting and reduced pressure in the refining stage. Their application could lead not only to the energy savings but also to the increase in output of glassmelting spaces or to their decrease in size. Both effects have economical and ecological consequences. However, the simultaneous application of both principles requires the local separation of dissolution and bubble removing processes and new technical solutions as is convenient stirring means as well as their arrangement and simple constructions of subatmospheric refining chambers. The mathematical modelling combined with laboratory experiments is obviously capable to solve the essential part of this task and its present activity is starting to realize it.

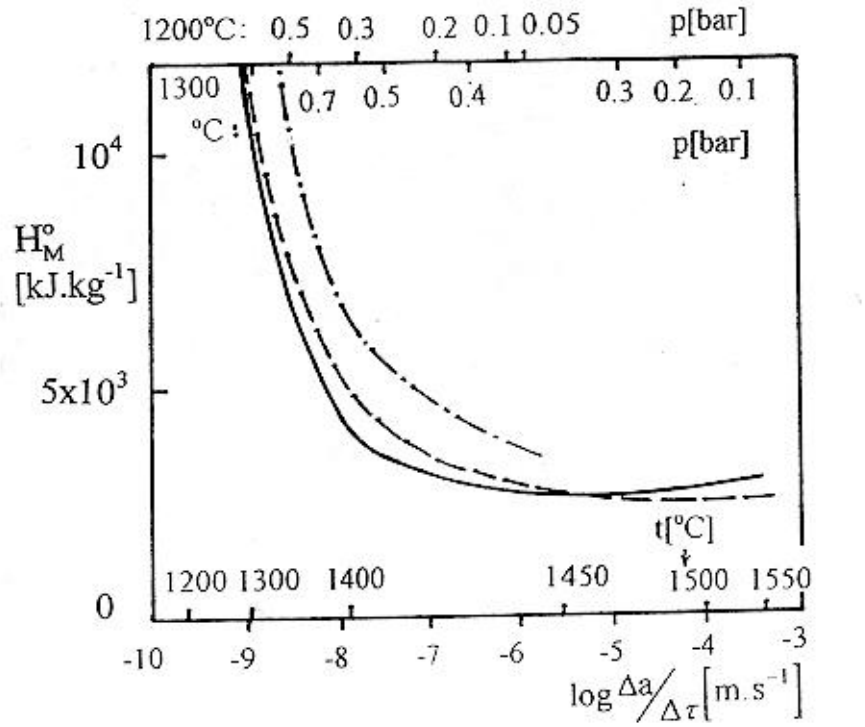

Fig. 6: The comparison of temperature and reduced pressure effect on the specific energy consumption of TV glass melting in the model melting space, mathematical modelling, glass layer thicness 0.25 m, $c_{o\ CO2}$, = 95 vol%, $c_{o\ N2}$= 5 vol.%, a_o = 0.1 mm - - temperature dependence, V^a = 0.2, p_{ex} = 100 kPa -x -x pressure dependence, V^a = 0.2, t =1200 °C - - pressure dependence; V^a = 0 2, t =1300 °C

REFERENCES:

1. Hrma P.: Ceramics - Silikaty 24 (1980), p. 7.
2. Mühlbauer M., N mec L.: Glastechn. Ber. 56K (1983), p. 82
3. N mec L.: Glass Sci. Technol. (Glastechn. Ber.) 68 (1995), p.1
4. N mec L., Luxov< I.: Ceramics - Silikaty 37 (1993), p. 29

MULTIRESOLUTION ANALYSIS AND CONTROL FOR CROWN TEMPERATURE AND BOTTOM TEMPERATURE OF A GLASS MELTING FURNACE

Toichiro Nakagawa and **Tsuyosi Kominami**
System Sougou Kaihatsu Co., LTD., Tokyo, Japan

Tokio Kimura
Asahi Glass Co., LTD., Tokyo, Japan

Abstract

A multiresolution analysis by the wavelet representation for actual running data of a glass melting furnace is described. The subject is mainly toward it's application to autonomous distributed control by the multiresolution analysis. The simulation is executed with the same condition through the real running data.

1. Introduction

The use of the wavelet decomposition and reconstruction is thought to be an efficient and instructive approach for identification and control in such environment as a glass melting furnace, in which the process characteristics are combined with different high and low frequency ranges and various long time lags. Therefore, system identification and control is very difficult to do. In this case, the decomposition of process behavior into several frequency bands by the wavelet analysis can improve the accuracy of identification and control. These decomposed subspaces are orthonormal each other by the orthonormal wavelet expansion. (1,2)

2. Wavelet transformation and auto regressive model building (3)

A process model of the furnace is hierarchically decomposed on three stages by the wavelet analysis. The sampling period of the original process model is every 40 minutes in this case, and that of three models D2, D3 and W3 which are decomposed by each time scale, are every 80 minutes, 160 minutes and 320 minutes respectively. That is, the original process is decomposed successively onto detail frequency zones V_1, V_2, and V_3. If the time scale j of the original process which has the minimum sampling period 40 minutes corresponds to the time scale 0, the time scale j of V_1, V_2, and V_3 becomes 1, 2, 3 respectively: To decompose the real running data by the wavelet transformation is equivalent to the projection of the process model onto each frequency zone V_j. Hence; if the process model is represented by $y(n)=P(Z-1)u(n)$, the projection of $y(n)$ onto V_j, namely, $T_j y(n)=y^{(j)}(n)$ is represented by $y^{(j)}(n)=T_j P T_j(u) = P_j u(n)$, provided that T_j is the projection operator onto V_j and $u^{(j)}$ is equal to $T_j u(n)$. The process model P in this case of

j=0 is given by Po=ToPTo. The original process model Po can be expanded. in the telescoping series as follows. (6}

Putting $S_j=P_{j-1}-P_j$, then $Po=\Sigma (S_jPS_j+S_jPT_j+T_jPS_j)+T_jPT_j$.

This constitutes a hierarchical decomposition of the process model, and this equation shows that the original process data is hierarchically decomposed on J=3 stages by the time scale j at this case. Control based on the above equation results in solving a series of optimization problem which has each own performance index like autonomous fashion. At this simulation, signals of six variables such as a crown temp., a bottom temp., an ambient temp., batch area, fuel and a lehr speed, selected by the contribution calculation (3,5,7), are decomposed by the on-line wavelet.

Signals decomposed by the on-line wavelet successively, are used for the modeling and controlled by the corresponding sampler with a hold function and then put into use for each control model D2, D3 and W3 respectively, and the sampler works every 80 minutes, 160 minutes and 320 minutes for each controller. Fig 1 shows the procedure of process identification and control with the wavelet analysis. Fig 2 shows the wavelet decomposition and reconstruction.

3. Simulation

The simulation, was tried for paralleled use of each control model identified by decomposed running data. The on-line real time wavelet decomposition analyzers are connected in series with the process model. Random noises are impressed for the driving force of the simulator on signals generated from the process model. These signals are decomposed successively into each frequency band. Values of manipulated variables are made by optimum control gain, calculated by the dynamic programming. Each value of manipulated variables is added linearly and the synthetic value is made as the summation at the individual sampling time. The mutual interactions are neglected became the orthonormal wavelet expansion is used. In this simulation, the D, model with the high frequency band at every 40 minutes sampling is discarded, because this model has less contribution among each variables. Fig 3 shows the skeleton diagram of general control system with the multiresolution analysis. Table 1 shows model parameter of the actual process. Table 2 shows DZ model parameter as an example.

4. Result of simulation

Variance of the original data is compared with variance of the simulated data in Case 1, 2, 3, and 4. Constitutions of each case are as follows.

Case 1 is the distributed control and weighted values of the performance index are standard (3), thereby the standard Q and R values are adopted.

Case 2 is the autonomous distributed control. In this case the crown temperature is more weighted than the normal Q and R values in the D2 model. And the bottom temperature is more weighted than the normal Q and R values in the D3 model and the lehr speed is kept constant.

Case 3 is the distributed control and the values of Q and R are standard for all variables. The lehr speed is kept constant.

Case 4 is the autonomous distributed control. The crown temperature is more weighted than normal Q and R value in D3. And the lehr speed in the model D2 and D3 is kept constant. The lehr speed in the model W3 is controlled under the normal Q and R values. Table 3 shows the result of comparison with the variance of normal original data and Case 1, 2, 3 and 4 respectively. (% of variance)

Roughly speaking based .on the limited number of simulation, it seems to be estimated that the trade off relation between the crown temperature and the bottom temperature is likely to exist. But the bottom temperature is strongly related with the batch area, and variance of the bottom temperature is exceedingly decreased. The reliable value of the batch area can be available with improvement of S/N by the wavelet. For instance, Fig 4 shows charts as the comparison among four variables. These charts are .reconstructed from the decomposed signal, W5+V5+V4+V3. 5 is meant by 1280 minutes of sampling interval, 4 is by 640 minutes and 3 is by 320 minutes, respectively. Therefore we can see the process in the large point of view. Fig 5 shows the simulated chart at Case 4 previously described, the lehr speed control is designed to work only the low frequency zone in the model W3 for practical use. The lehr speed is thought to have two roles in a real plant. One is as a change of production planning, the other is as a manipulated variable for control.

5. Conclusion

So far, resulting subjects are concluded as follows.

1. Improvement of S/N by the selective wavelet.
2. The multirate sampling control can be applied.
3. The possibility of realization for the autonomous distributed control by the cascade decomposition with the individual performance index for each resolution is, expected.
4. The batch area information is very useful and effective for the controlling of the bottom temperature. (8)

This report is focused on simulation of the distributed control through paralleled use of the model by the on-line wavelet representation.

References

1. S, G. Mallat, "A Theory for Multiresolution Signal Decomposition", IEEE transaction on PAMI, Vol.11, No. 7, July 1989

2. S. Takei, "Multiresolution Analysis of Data in Process Operation and Control", MSC Degree, MIT, May 1991

3. H. Akaike, T. Nakagawa, "Statistical Analysis and Control of Dynamics System", Kluwer Academic Publishers, 1968

4. J. F. Simon, V. Wertz, "Adaptive Predictive Bottom Temperature Control for a Glass Melting Furnace", ESG 2nd International Conference, June 1993, Venice, Italy

5. T. Nakagawa, T. Kimura, "Multivariable Control Through Fusion of Quantitative and Qualitative Complementarity for the Fuzzy Dynamical Process", ESG 2nd International Conference, Jurie 1993, Venice, Italy
6. A. E. Juarez, J. C. Kantor; "On the Application of wavelets to Model Predictive Control", 1992, ACC/TAS
7. T. Nakagawa, T. Kimura, " Multiresolution Analysis of Running Data in Operation and Control for a Glass Melting Furnace", I.C.G., Oct., :1995, Beijing
8. T. Kimura, T. Ito, K. Inagaki, T. Nakagawa, "Bottom Temperature Control by Image Processing with Wavelet Method", ISATA, June 1996, Italy

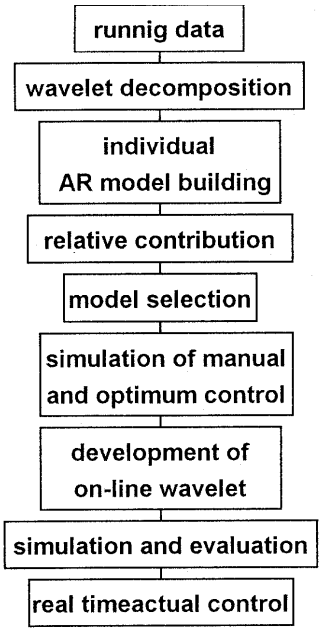

Fig 1 Procedure of process identification and control with wavelet

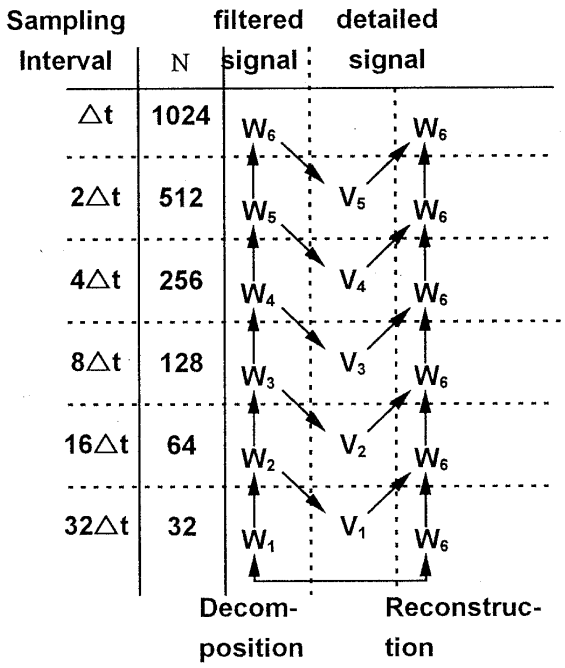

Fig 2 Wavelet Decomposition and Reconstruction

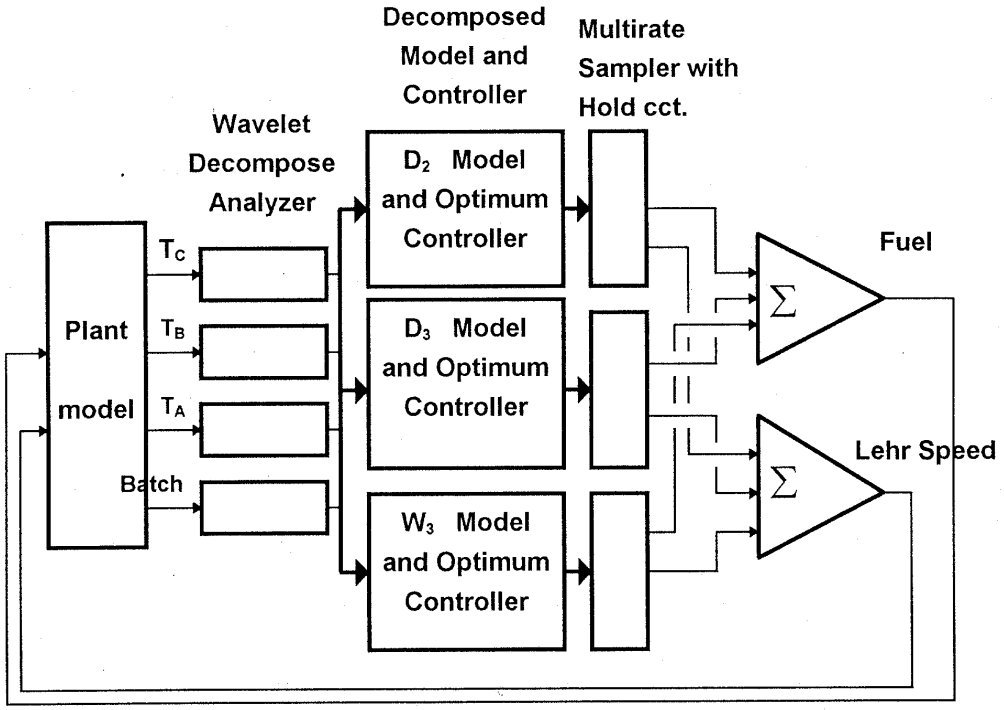

Fig 3 Skelton diagram of general Control system with multiresolution

A(I),B(I)

LAG=1

Variable	AXT206	AXT219	AXT233	AXCGT33	AXF016	AXCS600
AXT206	7.32E-01	5.63E-03	-2.95E-03	1.34E+00	7.38E-03	-2.04E-03
AXT219	1.98E-02	1.21E+00	-4.71E-02	4.46E-01	-1.40E-03	7.25E-04
AXT233	1.78E-02	-9.41E-03	9.90E-01	-3.91E-01	6.50E-04	7.88E-04
AXCGT33	-3.98E-03	-6.43E-04	-1.35E-03	2.82E-01	7.50E-05	4.39E-02
AXF016	-1.74E+00	-4.25E-01	5.74E-01	3.41E+00	7.50E-01	-2.10E-02
AXCS600	-5.99E-02	3.37E-01	4.48E-02	-2.06E+00	-9.80E-03	1.05E+00

LAG=2

Variable	AXT206	AXT219	AXT233	AXCGT33	AXF016	AXCS600
AXT206	1.75E-01	-6.68E-02	3.96E-02	9.23E-01	-4.22E-03	1.91E-03
AXT219	-1.36E-02	-9.49E-02	2.49E-02	2.15E-02	8.15E-04	-2.77E-04
AXT233	-1.12E-02	-5.43E-03	5.54E-02	-3.48E-01	4.09E-04	-9.98E-04
AXCGT33	1.49E-03	2.84E-03	-2.22E-03	2.01E-01	3.90E-02	-1.35E-05
AXF016	-5.37E-01	-9.42E-01	-3.28E-01	3.90E+00	6.83E-02	1.39E-02
AXCS600	4.53E-01	-4.94E-01	2.58E-01	-4.72E-01	-3.53E-02	-6.18E-02

LAG=3

Variable	AXT206	AXT219	AXT233	AXCGT33	AXF016	AXCS600
AXT206	-2.22E-02	9.39E-02	-3.13E-02	-1.24E+00	1.76E-03	2.02E-03
AXT219	8.86E-03	-4.25E-03	9.22E-03	-1.57E-01	-1.20E-03	2.32E-04
AXT233	-1.02E-02	5.29E-04	3.21E-03	-1.69E-01	-2.09E-03	3.57E-04
AXCGT33	-7.38E-04	-2.04E-03	2.10E-03	1.55E-01	-6.19E-05	-2.15E-04
AXF016	9.74E-01	1.27E+00	-2.48E-01	-2.31E+00	3.71E-01	9.37E-03
AXCS600	-3.90E-01	2.27E-01	-3.63E-01	-3.55E+00	5.27E-02	7.16E-02

LAG=4

Variable	AXT206	AXT219	AXT233	AXCGT33	AXF016	AXCS600
AXT206	-6.04E-03	-3.96E-02	1.87E-02	-3.75E-01	-5.11E-03	-1.62E-03
AXT219	-2.22E-02	-1.32E-01	1.86E-02	-1.59E-01	1.59E-03	-7.32E-04
AXT233	-1.19E-03	1.65E-02	-5.39E-02	-2.52E-01	1.99E-03	2.93E-04
AXCGT33	7.38E-04	-3.32E-04	9.74E-04	3.83E-02	4.72E-05	1.37E-04
AXF016	6.43E-01	-9.28E-03	7.73E-02	1.12E+00	-2.28E-01	-9.76E-03
AXCS600	-1.65E-01	-1.51E-01	8.22E-02	-2.26E+00	-1.65E-02	-7.04E-02

Table 1 Model parameter of actual process

LAG=1

	AXT206	AXT219	AXT233	AXCGT33
AXT206	1.20E+00	-7.88E-03	3.98E-02	-3.44E-01
AXT219	6.27E-04	1.25E+00	-9.57E-03	4.75E-02
AXT233	1.21E-02	-4.11E-03	1.27E+00	1.13E-01
AXCGT33	1.79E-03	1.29E-03	5.43E-03	1.24E+00

LAG=2

	AXT206	AXT219	AXT233	AXCGT33
AXT206	-1.69E+00	1.61E-02	1.32E-01	-1.28E+00
AXT219	-3.09E-03	-1.69E+00	5.54E-02	-4.72E-02
AXT233	-4.24E-03	2.27E-02	-1.64E+00	-1.14E-01
AXCGT33	3.00E-03	-4.60E-02	-7.25E-03	-1.61E+00

LAG=3

	AXT206	AXT219	AXT233	AXCGT33
AXT206	1.38E+00	-4.29E-02	-1.33E-01	7.66E-01
AXT219	2.38E-02	1.40E+00	-1.15E-01	5.85E-01
AXT233	1.47E-02	-1.40E-02	1.39E+00	4.85E-02
AXCGT33	-1.70E-03	4.55E-03	1.14E-02	1.33E+00

LAG=4

	AXT206	AXT219	AXT233	AXCGT33
AXT206	-7.91E-01	1.44E-02	1.80E-01	-1.04E+00
AXT219	3.56E-04	-8.27E-01	1.99E-03	-4.34E-01
AXT233	-3.96E-04	1.87E-02	-8.27E-01	-1.35E-01
AXCGT33	3.16E-03	2.37E-04	-6.04E-03	-7.59E-01

LAG=5

	AXT206	AXT219	AXT233	AXCGT33
AXT206	3.62E-01	3.91E-03	-1.41E-01	4.65E-02
AXT219	1.53E-02	3.52E-01	3.99E-02	4.61E-01
AXT233	5.56E-03	-1.98E-02	3.83E-01	8.89E-02
AXCGT33	-1.68E-03	1.45E-03	-9.63E-04	3.23E-01

Driving Matrix (Bi's)

LAG=1

	AXT206	AXT219
AXT206	3.18E-03	4.10E-03
AXT219	1.25E-03	-7.03E-04
AXT233	2.03E-04	-1.11E-03
AXCGT33	-5.44E-04	-3.63E-05

LAG=2

	AXT206	AXT219
AXT206	-2.59E-03	2.75E-03
AXT219	-3.56E-03	2.55E-04
AXT233	-2.06E-03	2.35E-03
AXCGT33	3.91E-04	-1.38E-04

LAG=3

	AXT206	AXT219
AXT206	2.68E-02	7.94E-04
AXT219	1.52E-03	-1.80E-04
AXT233	2.61E-03	-3.77E-03
AXCGT33	-5.30E-04	8.44E-05

LAG=4

	AXT206	AXT219
AXT206	-2.35E-02	3.67E-03
AXT219	-3.67E-03	4.02E-04
AXT233	-2.34E-03	2.37E-03
AXCGT33	4.70E-04	-2.07E-04

LAG=5

	AXT206	AXT219
AXT206	9.93E-03	2.39E-04
AXT219	-6.45E-04	5.25E-05
AXT233	1.15E-03	-2.43E-03
AXCGT33	-2.91E-04	2.04E-04

Table 2 D_2 Model Parameter

	Bottom Temperature	Crown Temperature	Batch Area
Case1	4.85%	96.32%	88.03%
Case2	4.55%	149.51%	102.25%
Case3	3.70%	121.45%	75.80%
Case4	3.44%	115.24%	68.23%

Table3. Comparison of Variance

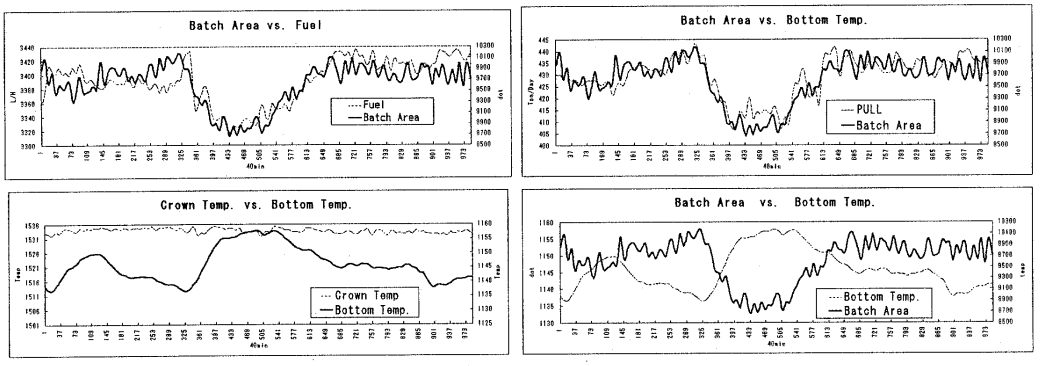

Fig4 Reconstruct Chart (W5+V5+V4+V3)

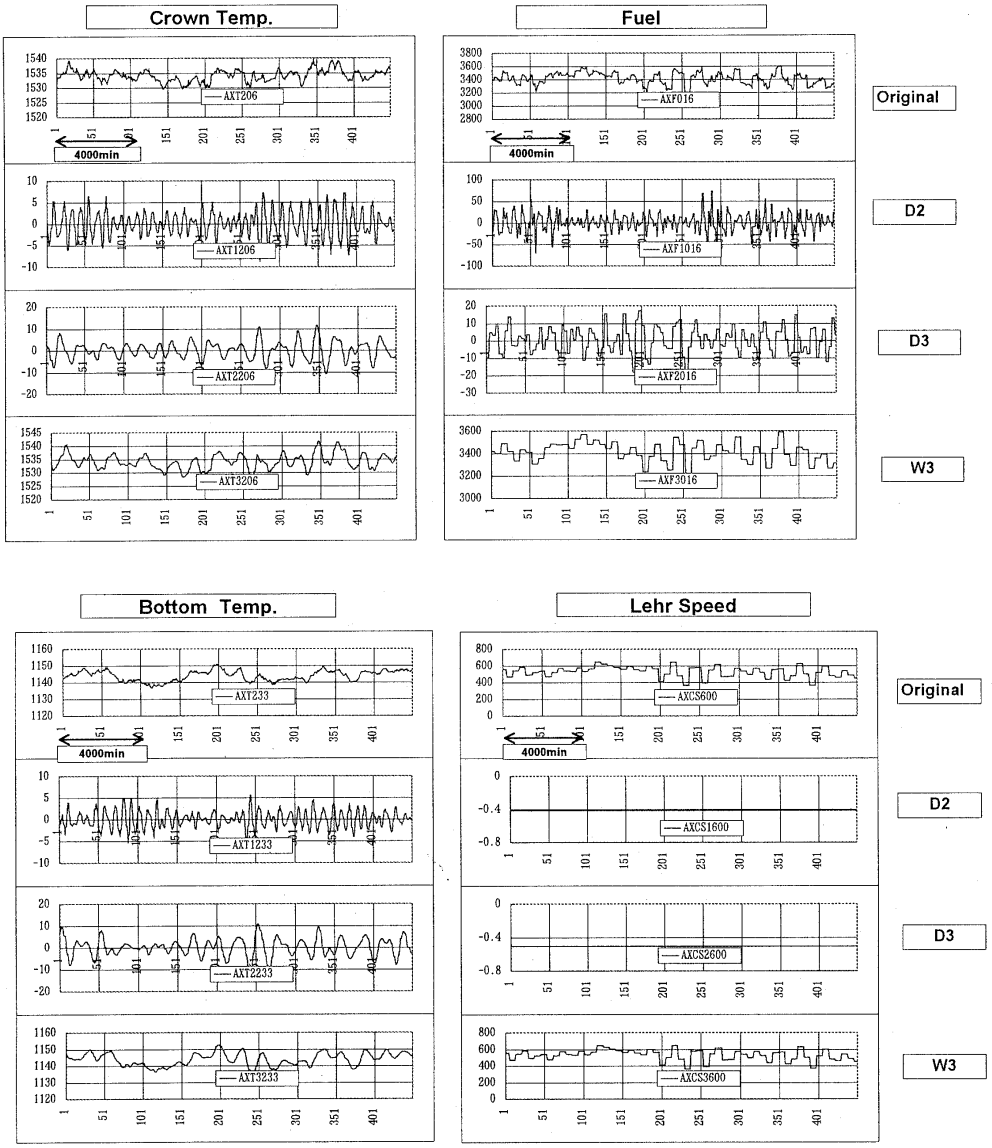

Fig5 Simulated Chart at Case 4

TECHNOLOGY MANAGEMENT; THE CASE FOR A MATURE INDUSTRY

Dr.Baha Kuban and **Reha Akçakaya**
Business Development Unit, SISECAM, Turkey

Abstract

The study of technical change in individual industries gives important clues on the industrial life cyle and innovation patterns in that particular production technology. Such historical modeling was attempted with this study for the cases of glass containers, sheet glass and furnace design. This knowledge was in turn used to draw the framework of a strategy formulation process in which the Technological Knowledge Levels approach was employed. The study raises the issue of empirical industrial research that needs to be carried out for filling the gaps in our understanding of technological change in glass manufacture.

"*The industry of artificers maketh some small improvement of things invented; and chance, sometimes in experimenting, maketh us to stumble upon somewhat is new*".

Sir Francis Bacon

1. Introduction

Technological developments are rapidly altering the nature of competition in the late twentieth century. Advances, particularly in generic technologies such as micro-electronics and new materials, are presenting managers and policy-makers with major discontinuities. Changes, that seem to be radically re-shaping the so called " hi-tech" sectors such as electronics, computers, telecommunications, machine tools, automobiles, aircraft etc. are rooted in several developments. These are;

- The emergence of new and improved manufacturing technologies (CAD-CAM, CIM, FMS) which have fundamentally altered the economies of manufacturing and removed the factory as a barrier to product variability and flexibility (1).
- The quickening pace of technological change and the associated shortening of product life cycles, bringing with them a proliferation of product variety (2).
- The shifting nature of consumer demand towards increased variety, more features and higher quality.

The wedding of micro-processor and computer technologies is allowing differentiation based on software. Software is replacing hardware in many applications and dramatically changing developmental vs. production costs. Many researchers have pointed out to the increased rate of technological diffusion. Mansfield (3) has noted that it takes on the average only 12-18 months before information on R&D and product decisions get known by competition. Again Mansfeld et al have found that 60% of patented inventions were imitated successfully in less than 4 years (4). Badarocco (5) has determined that in the electronics industry,

the time period between a new product being introduced in the US market and it being copied, manufactured and shipped back into the US from a second country is sometimes only several weeks.

These changes that appear to be impacting assembly sectors mentioned above are diffusing through to traditional continuous industries via developments in micro-electronics based process control and measurement technologies. New sensor and laser technologies are increasingly allowing continuous, flexible response and feed-back techniques to be employed. Faster and higher capacity micro-processors are making possible 3-D models that use dynamic simulation and artificial intelligence to be integrated into the control of the production process. Possibilities for smaller and more flexible economies of manufacture even in such large scale industries as chemicals and steel are worth mentioning.

Technological innovation and its dynamics thus turn out to be the fundamental source and driver of these developments. Without forgetting that technical change itself (and thus innovation) has its roots in society, i.e. technologies are social constructs per se and not some exogenous force available to everyone on demand, this paper will try to trace only briefly the history of technical change in glass manufacture (notably sheet glass, bottles and furnaces) fitting it into a model of technological innovation and finally, draw a feasible agenda for strategy formulation.

2. Technological Innovation and Industry Life cycles

Invention and innovation are two separate phenomena which can be defined as follows; invention refers to the creation of a new idea or concept and innovation refers to the act of developing the invention into a commercial product or technique. It has become clear, from studies of the correlation between innovation and firm growth that it is innovation and not invention that is essential for success and even survival. It was Schumpeter who first made this distinction that has generally been accepted in economic theory. The real difficulty, however, comes in the identification of innovation, as the true economic rents that accrue, are not always apparent in the initial event (6).

It is also well known that the production of any good or service involves a chain or network of industries (Figure 1) and technological innovation is one of the benefits wherein each part of the network is a potential source.

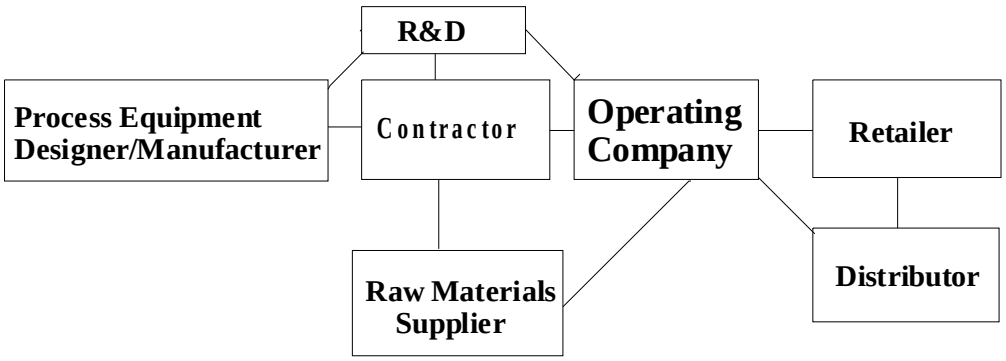

Figure 1. *Network of firms in the value chain of an industry.*

The two clear types of innovation identified by economic theory, i.e. product and process innovations, really depend on the vantage point within the network from where they are viewed. Innovations in the capital goods industry enhance the capabilities of the manufacturing process and not the manufactured item.

Utterback and Abernathy (7) have proposed a model that describes the evolution of technological innovation and interrelations between product and process developments throughout the creation, growth, maturity and decline of an industry with a view of product and process innovations. Figure 2 summarizes the profiles of product and process innovations with increasing industrial maturity.

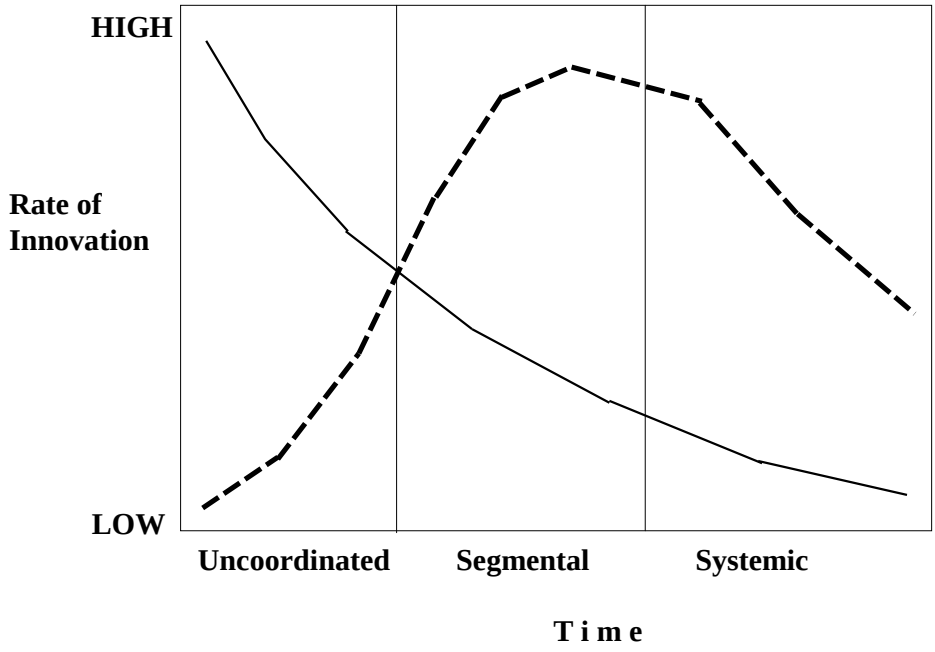

Figure 2. *Stages of Innovation and Industrial Life cycles.*

The pattern illustrated demonstrates an industry that passes from high product/low process through low product/high process to low product/medium process innovations phases. These three phases are termed by Utterback and Abernathy as the "uncoordinated", the "segmental", and the "systemic" phases. In this context, the research by von Hippel (8) can be used to identify the dominant sources of innovation within each phase. Von Hippel proposes to define a " locus of innovation" based on the functional relationship of the organization to the product. End-user, product supplier, product manufacturer are all functional relationship categories and von Hippel's basic premise is that the major source or "locus" of innovation can be predicted from an analysis of the "expectation of economic rents." Economic rents of course refer to the return on R&D investment and others inputs required in the creation and development of an innovation. Von Hippel's categorization can be seen in Table 1.

Table 1. *Types of innovation as seen from various vantage points in the network of manufacture.*

Innovation as seen by;	**Process Innovation Developed by;**			**Equipment Innovation Developed by**;		
	Operating Company	**Plant Contractor**	**Equipment Manufacturer**	**Operating Company**	**Plant Contractor**	**Equipment Manufacturer**
Operating Company	process innovation	process innovation	process innovation	process innovation	process innovation	process innovation
Plant Contractor		product innovation			product innovation	process innovation
Equipment Manufacturer			product innovation			product innovation

3. Mechanization in Glass Manufacture

Glass artifacts are known to have been produced circa 7000 BC, though some controversy exists as to whether the Phoenicians were the first accidental manufacturers. Archeologists tell us wealthy, privileged users utilized it as jewelry, exchange items and of course containers in various shapes and colours. The blow pipe seems to have been one important step change innovation introduced in Alexandria circa 200 AD. Records do not mention any fundamental change in manufacture nor are there, except for refinements in shape and composition no doubt by trial and error, any new products for almost 17 centuries. The winds of creative destruction and change that set in with the first stirrings of the Industrial Revolution in the second half of the 18th century also signaled the dramatic changes of the following century.

Bottlemaking

The universal move towards mechanization had its parallels in glass manufacture through the first attempts of Arbogast (1882) for semi-automatic press-blow machines and Ashley (1886) for blow-blow machines in bottle manufacture. Brooke innovated the feeding mechanisms with two patents in 1900; suction feeding and gravity feeding. The real impetus to the diffusion of automatic machinery however came with the Owens machine (1904) and its display in Trafford Park, Manchester. We learn from narrators that the European Cartel of users (Europaischer Verband der Flaschenfabriken) found it desirable to pay 600.000 British Pounds in patent rights. The next several decades saw a proliferation of bottle making equipment and feeding technologies that were sometimes used concurrently within the same plant. Most of these are known by their patent- holders name and are listed below (Owens not included) (9);

Country first installed	***Machine Type (Year)***	***Feeding Mechanism***
Great Britain	W.J.Miller (1917)	Gravity
Great Britain	Ed Miller (1919)	Gravity
Great Britain	O'Neill (1917)	Gravity
Great Britain	Lynch (1919)	Gravity
Great Britain	Monish (1929)	Suction

France- Belgium Roirant (1923) Suction

Although it might seem astonishing and obvious looking at it today, the individual section machine (IS) was nowhere near universal acceptance in the beginnings of its introduction in the year 1925 (10). It was invented by Henry Ingle, an engineer of the Hartford Empire Company. It's apparently obvious principle resided upon the age old advice; in the words of chroniclers of the time, "... to take Mohammed to the mountain instead of the mountain to Mohammed". In other words, the IS machine transported gobs of glass to stationary moulds instead of conveying the moulds on massive moving tables to positions for receiving the glass. Once again, the totally dominant position gained by the IS machine long after it was introduced was in no way certain at the time and competitors strived, often successfully to beat it back.

Sheet and Plate Glass Manufacture

Window glass was produced by manual techniques up until the end of the 19th Century. These hand processes were largely similar to those used in the manufacture of hollow-ware. This included the gathering on a pipe of molten glass and the blowing of it into a cylinder. The cylinder was then opened up flat and then cut. The earliest attempt at mechanization in sheet glass manufacture was undertaken by Lubbers who commercialized his invention in 1903. The real push towards machines in this area however, came with the Fourcault, 1913 (9 years after the patent) and the Colburn,1905-1916, processes (later Libbey-Owens). In 1918, Bicheroux developed an alternative method of casting the pot of molten glass between a pair of rolls, from which the plate moved forward on a table moving with the same velocity as the rolls. Other competing techniques were the Pilkington Brothers' continuous plate (1922) with both sides ground and polished and of course the Pittsburgh technology which was developed between 1921-1927 to overcome the difficulties of the Fourcault and Colburn processes.

The influence of mechanization on industrial structure can be seen clearly in the case of sheet glass manufacture. During the introduction of machines, the number of plants producing sheet glass in the US fell dramatically from close to 100 plants in 1919 to only 18 in 1930. A similar drop can be seen in Germany where the number of sheet glass producers fell from 70 in 1913 to just 9 in 1936. The impact of mechanization and rationalization hit the Belgium market within which a cartel of Fourcault plants was able to operate only 3 out of the 36 furnaces it owned in 1925. Demand had not expanded as fast as the new machines could deliver and enormous stocks created a crises of over-production.

Furnace Design

Among the most important components of the complex that is called glass manufacturing technologies is the furnace for melting the glass. Pot furnaces, with one time loading of the batch ingredients had been standard fare in glass production. Itself composed of a myriad of technologies such as batch charging, cooling, refractory materials, energy technologies etc., the furnace has been an area which was the focus of all manufacturing industries involving fusion processes. So it was not surprising that Robert Stirling (1916) and Joseph Crosfield of Warrington (1940) took out a patents for glass melting furnaces closely modeled after cast iron furnaces, which had undergone various improvements earlier on. It is speculated that Friedrich Siemens new of the earlier patents and developed his continuous-regenerative tank furnace

building on such knowledge in 1861. The first continuous tank furnace was 24.75x7.5 feet by 20" deep. It is chronicled that Windle Pilkington missed several board meetings to visit the Siemens regenerative furnace in Dresden. One of these were finally authorized to be built in St.Helens in 1872. It had allowed for a 60% saving in wages and between 25-50% saving in fuel economy. At the beginning though, due to the fact that impure glass easily passes to the working end, these tanks were only fit for bottle production until Lürman developed a design suitable for window glass (1882-86) (11). From the point of view of the general shape of the basin, design and location of burner ports, design and location of doghouses, little seems to have changed since F. Siemens innovated the continuous tank furnace. This of course conceals the dramatic improvements made in the auxiliary technologies such as refractory materials and furnace operation and control, non-stop developments which have allowed many-fold increases in furnace lifetimes and glass quality.

4. Innovation Patterns

The initial stages of the mechanization of glass manufacture, as mentioned above, changed the landscape of the industry within less than 30 years. Despite the drop in the number of manufacturers, employment continued to increase as the use of glass was "democratized" so to say, as glass artifacts became household items for the population as a whole. The machine either introduced glassware into new fields or maintained it against the competition of other materials. Packers of other commodities were able to mechanize handling, filling, capping, labelling, etc., operations as the glass containers were now produced to close tolerances with little error. Factory organization altered to become subservient to the machine, task definitions and skill requirements all transformed.

Allied innovations trailed the application of the machine. The physical properties of hand-made glass proved to be disastrous for machine operation. All early mechanization attempts were as a result frustrated due to inhibitingly low productivity. This was a case of science trailing technology, the rise of brand new phenomenological puzzles, a good example of which is the development of the Fourcault process. The prohibiting devitrification problems of hand-made compositions were prevented by the addition of soda which resulted in terrible weathering properties which in turn were solved by the development of magnesia and alumina containing batches. Other examples triggered by the introduction of machinery were the problems of annealing due to increased production rates and capacity. Methods of rapid inspection and handling were areas that experienced a series of innovations. Of course, completely new products and compositions were innovated as manufacturing technologies solved the initial bottlenecks. The general flow of industrial advance can be thus elaborated as follows:

Uncoordinated Stage of Innovation

In the case of bottle manufacture, this stage can be clearly seen to cover a period extending from 1870's to 1930's. The chief characteristic of the period is uncertainity with a plethora of machines and designs. The multifarious base of technological innovation is the machine itself and the market is the glass manufacturers. Changes in the final product characteristics is clearly determined by the problems originating from the introduction of machinery. Sheet glass manufacture seems to undergo a similar drive towards machinery at around the same time period. Fourcault, Libbey-Owens,

Pittsburgh, Bicheroux are all developed concurrently. The same innovative stage for furnace design would seem to have been realized half a century earlier with the beginnings of the tank furnace competing with the designs usually termed continuous pot. The Siemens continuous-regenerative tank furnace appears to be the culmination of earlier designs. The existence of the continuous glass furnace must have been a powerful impetus for the innovations towards mechanization and flow.

Segmental Stage of Innovation

This stage, sets in with the decrease of uncertainty and the gradual stabilization of machine and furnace design. Regenerative-continuous furnace design, IS machines, and Pittsburgh technique had pretty much become industry standards and refractory materials developments as well as better control of operational dynamics was resulting in dramatic rises in productivity. Demand structure signaled the dawn of mass markets and relatively stable, increasing demand, as in other commodities. The exception to the rule here is the development of the float process by Pilkington (1953), which went on to become the industry standard in flat glass manufacture.

Throughout this period which can be said to extend to the early 1980's, the fundamental scientific principles pertaining to the physical and chemical conversion processes were uncovered. Developments were pursued by glass manufacturers allied with equipment producers (glass machinery, forehearth systems, raw materials handling etc.) focusing on increased productivity, reduced input costs and specialization. The evolution between the segmental and systemic stages, the combination of equipment standardization and growing demand for this equipment, generates an economic environment encouraging manufacturers of the process equipment to participate in innovative activity. These firms will have developed the necessary specialized knowledge and skills to reduce the cost barrier to innovation and have the potential sales volume to generate high revenues, hence improved economic rents.

Systemic Stage of Innovation

The rapid changes in both technologies and markets heralded by the oil shocks of the mid-70's, have brought important developments in the glass industry. The new era of flexibility, market niches and differentiation have combined with the mature nature of the industry to produce a complex picture. With the limits of scale economies reached, the principal economic forces behind the industry has become energy consumption and the yields and quality of all outputs of the process. In a technologically mature process, knowledge is well diffused and differentiation from competition is difficult. It often cannot be achieved by equipment manufacturer and contractor innovations, as these become immediately available to the rest of the market. However, minor adjustments to optimize the process, driven by the specialist knowledge of the specific plant function held only by the glass plant operator, is a low cost, low risk and therefore attractive option.

5. Strategy Formulation

As can be seen from the account of the histories of some of its major components, which are generically called glass manufacturing technologies, the industry can be said to have reached a general state of maturity. One has to be careful though, not to underestimate the vigour of niche markets in glass artifacts nor the fast growing

secondary processes sectors such as, coatings on architectural and automotive glass. These, however, should be properly categorized as separate production technologies unless when the secondary process follows on-line right after annealing. There are no doubt important innovative rents accruing from product and process developments in this area.

In the systemic phase of the industrial innovation process, no major earthshaking turns are to be expected in production technologies. The various components will continue to be fine tuned, better control established by the utilization of advanced control techniques. Notwithstanding the fact that firm strategies vary greatly depending on size, position, geographic location, market environment, culture etc.., it is perhaps cautious enough to state that challenges exist for all producers in furthering the technological knowledge of the encompassing parts of glass manufacture and make better on the words of Professor Turner who stated back in 1926 that;

" ...the more able glass technologist can now make a furnace respond to their will as effectively and probably with less waywardness than a performing dog does for his master".

Measurement and control is still problematic within various points in the black box and mathematical understanding of the relationships between fusion processes and atmospheric reactions in the furnace, fairly rudimentary. As control of the output, which is glass, depends critically on the overall understanding and control of inputs, one way of looking at the process of glass manufacture is by the use of the "Technological Knowledge Tree" (12). The technique allows one to systematically study the various inputs, their importance and current level of technological knowledge. Bohn has carefully elaborated the inefficiencies pertaining to managing a technological process in which even a few key variables are at low stages of knowledge. The stages of technological knowledge are summarized below (from Bohn);

Stage 1: Complete ignorance: The existence of a phenomenon is not known
Stage 2: Awareness: The existence of a phenomenon and its relevance to the process is known
Stage 3: Measurement: Variables are measured but not controlled
Stage 4: Control of Mean: Variables are measured and controlled but only imprecisely
Stage 5: Process Capability: Variables are controlled with precision across a range of values, when all important variables reach stage 5, manufacturing using a recipe is possible
Stage 6: Process Characterization (know how): How the variable effects the process are known
Stage 7: Know Why: A scientific model of the process is developed. Non-linear and interaction effects of variables are also known.
Stage 8: Complete Knowledge: The complete functional form and parameter values that determine the result are known

Despite the fact that glass production is a mature industry it can be easily said that some of the important process variables are not known to a desirable degree. To be able to picture a process in terms of its important inputs and the level of their technological knowledge, has important implications for the management of that

technological process. Skill levels of the work force, managerial culture and control mechanisms, the level of automation feasible are all determined by this knowledge. This type of analysis should be carried out for all segments of the production chain. The sources of innovation at the systemic stage, their locus and probable impact are uncoverable only through such a systematic study. A cursory example of such an undertaking can be seen in Figure 3, elaborated for the glass making process.

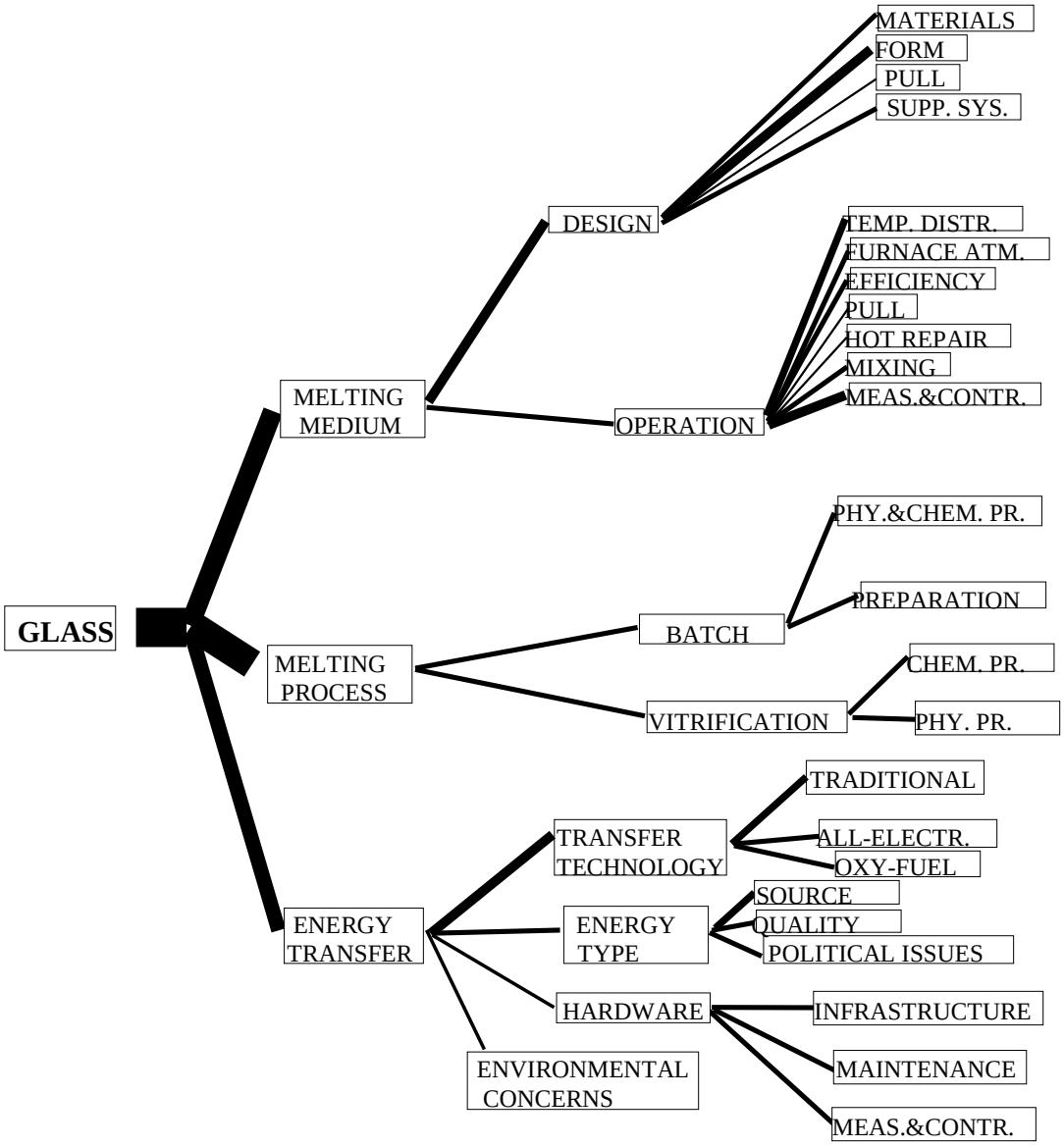

Figure 3. *The Technological Knowledge Tree approach to Innovation Management elaborated for glass manufacture. In this arbitrary exercise, the thickness of each branch of the tree represent its strategic importance for the manufacturer. The branches must also be shaded in different tones to represent how well the firm is performing at that branch.*

6. Recommendations for further work

The studies of technology and technological innovation clearly show that technology, as a multi-structured knowledge system, as well as being embodied in machines and physical assets, is also fundamentally anchored in people, organizational structures and cultural-behavioural patterns. Hence, the diffusion and generation of technical changes require to be discovered empirically. The techno-economic study of individual production technologies, their patterns of change, innovative dynamics, relationships with the markets and trade character, is of value not only for historians of the discipline but also for the practioners and managers of today. Shedding light on diffusion and generation patterns of yesteryear has important implications for the present and the future. This study presents a clear agenda for collaboration and joint research by the producers, technologists, scientists, managers of all the technological fields that come under the generic title; glass manufacturing technologies. Concrete research areas from both past and present can be identified, charting the market, technology, financial and economic maps of the industry in all its aspects. This endevour should try and shed light on the following;

- *What are the **underlying technologies** that make up glass manufacturing technology?*
- *What **stage of maturity** in the cycle of production technologies are each of these at?*
- *What are the **rates of innovation** and technical change related to them?*
- *What techniques of **forecasting** are best suitable for the underlying technologies?*
- *What are the possibilities of **international benchmarking** for these?*
- *What are the fundamental outlines of competitive **technological audits**?*
- *What are and have been the major trends in the **generation and diffusion of technology** in the glass industry? Paths of international flow, investment patterns, pros-cons?*
- *What will be the impact of generic technologies such as micro-electronics and new materials?*
- *What are the criteria, frame of reference for **investments in automation** and other tools of advanced control?*
- *What are the auxiliary or **non-direct technologies** and what is their influence on glass manufacture?*
- *How feasible is the setting-up of a **Business Environment Surveillance System**, BESS, what would be its operating principles, key functional areas (identification, monitoring and evaluation), how would this technological radar define and test the key technological descriptors?*
- *What type of an **organizational structure** could undertake all these?*

Bibliography

1. **Meredith, J**., "The Strategic Advantages of New Manufacturing Technologies for Small Firms", Strategic Management Journal, 8 (3), 1987, pp. 249-258.
2. **Sanchez, R.**, " Strategic Flexibility in Product Competition", Str. Man. J., Summer Special Issue, 16, 1995, pp. 135-159.
3. **Mansfield, E**., "How Rapidly does New Technology Leak Out", Industrial Economics, December 1985, pp. 217-223.
4. **Mansfield, E., Wagner, S**., Economic Journal, December 1981, pp. 907-918.
5. **Badarocco, J.L.**, "The Knowledge Link; How Firms Compete through Strategic Alliances", Harvard Business School Press, Boston MA, 1991.
6. **Rosenberg, N.**, "Inside the Black Box; Cambridge University Press, New York 1982.
7. **Utterback, J.M., Abernathy**, W.J., " A Dynamic Model of Product and Process Innovation", in "The Economics of Innovation" ed. C.Freeman, Elgar Publishing, London 1990.
8. **Von Hippel, E.**, " The Sources of Innovation", Oxford University Press, 1988.
9. " Glass and W.E.S. Turner, 1915-1951", Ed. **Gooding and Meigh**, The Society of Glass Technology 1951, Sheffield.
10. "The Story of the Glass Bottle", **Edward Meigh**, 1972, Stoke-on-Trent.
11. "The Collected Papers of W.M.Hampton", Vol.1, Published by Pilkington Bros., 1977.
12. **Bohn, R.E.**, "Measuring and Managing Technological Knowledge", Sloan Management Review, Fall 1994, pp.61-73.

THE EFFECT OF WASTE GASES ON GLASS FURNACE OPERATION

S. J. Slade and **I. H. Smith**
Pilkington Group Research, United Kingdom

Abstract

Many important facets of glass furnace operation are affected by the waste gases generated by the combustion of fuel and the batch melting process. The waste gas flow contains corrosive and pollutant compounds including gases and particulate matter. These gaseous and particulate compounds affect glass furnace operation in many ways. They may attack the refractory structure, block the flues, or be subject to legislative control.

Waste gas chemistry is dependent on various operating parameters. Glass composition, batch contamination, fuel type, and the method of combustion all affect the waste gas formed. One of the most important elements in the system, in relation to furnace operation, is sodium. This is involved in refractory corrosion and the formation of particulate matter.

The paper describes the factors affecting waste gas composition. Practical and theoretical methods for its study are discussed, and examples of the effect of waste gases on furnace operation are presented.

l. INTRODUCTION

The ‘hot end’ of a float glass production plant consists of a furnace melt chamber, a refiner, a thermal conditioner and then a tin bath where the glass is floated to make a uniform ribbon. The waste gases from a typical furnace, burning fuel in pre-heated air, pass out to the chimney through regenerative heat exchangers designed to recover as much energy as possible from the waste gases. Many different types of refractories are used in a glass furnace, each designed to survive different environments, from molten glass at 1550 ^{o}C (2822 ^{o}F), to corrosive gases at 1600 ^{o}C (2912 ^{o}F). The interaction of these refractories with the furnace atmosphere and waste gas is discussed in this paper.

Many important factors associated with the operation of the glass-making process are affected by the gaseous and particulate components of the furnace waste gas. Furnace life is affected because refractories may be attacked and regenerators blocked. Pollution control may be required, dependent on the composition of the furnace waste gas emitted to the atmosphere.

With a knowledge of the chemical reactions and processes occurring in the furnace, control or minimization of refractory problems and pollutant emissions may be achieved. Furnace atmosphere and waste gas composition is affected by the glass batch composition, the type of glass being made, the type of fuel burned, and the type of combustion system operated.

The factors affecting waste gas composition, and the important effects that this has on glass furnace operation are described in this paper.

2. WASTE GAS ANALYSIS

The glass furnace atmosphere and waste gas composition can be studied by many methods. Either extractive or *in situ* techniques can be used to take practical measurements on operating furnaces and many different types of equipment are manufactured. Pilkington uses many kinds of analytical equipment, including various techniques designed to analyse the waste gases, or the particulate matter.

The effect of waste gases on refractories or other important chemical reactions can also be studied by laboratory-scale experimental apparatus and physical models. Kinetic, fluid flow, and equilibrium prediction models are regularly used by Pilkington Group research in the study of waste gas composition and reaction. Particular examples are given in this paper of one equilibrium prediction technique used by Pilkington: MTDATA, a computational thermodynamic package developed by N.P.L. in London.

Pilkington uses all the above methods to study furnace waste gases. The furnace waste gases are studied in relation to production monitoring and improvement, fault assessment and remedy, and emission limit compliance. The important factors affecting furnace operation associated with the waste gas, are discussed below.

3. ENERGY SOURCE

Waste gas composition is greatly affected by the type of fuel used to provide the energy required to melt the glass. Fuels used by the Pilkington Group vary from simple natural gas to heavy oils and pitches. Electric melting of float glass is also now possible on a large scale. This is mentioned below. The relative amounts of the main gaseous components in the waste gas are related to the type of fuel burned. Combustion gases from oil fuel contain relatively more carbon dioxide, and less water vapour than those from gas fuel. One of the most important differences between the fuels normally used, in relation to waste gas composition and furnace operation, is the amount of sulphur (S) that they contain. This is important because it affects the amount of pollutant sulphur oxides (SO_x) in the waste gas. These are also involved in important reactions with other components of the gas and the refractory structure of the furnace.

4. SODIUM COMPOUNDS IN THE WASTE GAS

Analyses of the hot furnace waste gas, taken at the site where the gas leaves the furnace, indicate that there is more condensable material in the waste gas of gas-fired furnace. More sodium species volatilise from the melting glass batch when gas is used as the fuel. Sodium is arguably the most important element in the waste gases, in relation to furnace operation because it is involved in refractory attack. The concentration of sodium compounds in the waste gas leaving the furnace is also important in relation to regenerator blockage and compliance with dust emission limits, and this is discussed below.

One of the major factors affecting the amount of sodium compounds in the furnace atmosphere and waste gas is the concentration of sodium chloride (NaCl) in the glass batch. This is normally present as a contaminant, especially of manufactured soda ash, and is the main volatile sodium compound in the glass batch.

An MTDATA prediction of the equilibrium concentration of sodium compounds in a typical gas-fired furnace waste gas atmosphere is shown in Figure l.

Figure 1

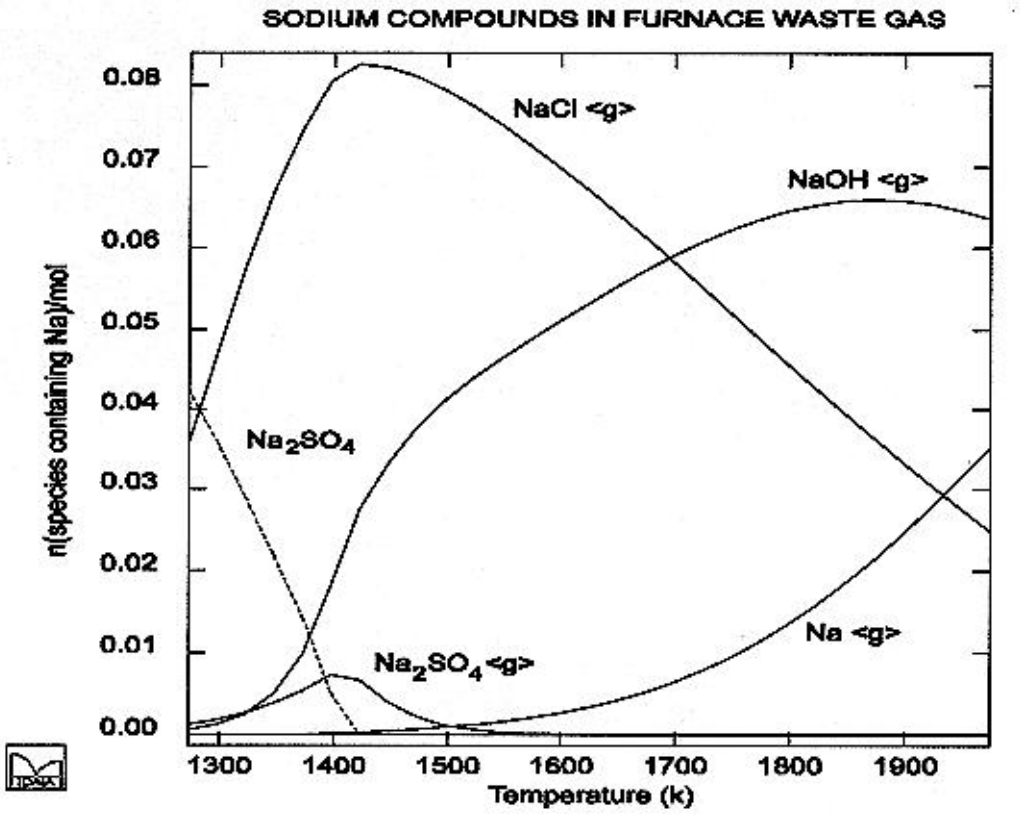

The main compound present over the lower part of the temperature range studied was NaCl gas. The NaOH gas concentration was higher at the higher temperatures, and at the highest temperatures assessed Na gas was predicted. No Na_2O gas was predicted. This agrees with practical measurements and is probably because the atmosphere contains an excess of water vapour which would form NaOH from the Na_2O. At high temperature, decomposition of Na_2O may also occur which would form Na gas. At the lower end of the temperature range, there was gaseous Na_2SO_4 present.

The only solid sodium compound predicted by MTDATA was Na_2SO_4, which formed at less than about 1100 ^oC (2012 ^oF). Thermodynamic predictions, in agreement with experimental sampling, have shown that, under all normal operating conditions, Na_2SO_4 is always the first compound to condense out of the waste gases.

Predictions indicate that other compounds condense only when insufficient sulphur is present in the waste gas, in relation to the amount of sodium compounds, for stoichiometric Na_2SO_4 to form. In practice, this is not a common situation; even when simple gaseous fuel is used there is sufficient sulphur in the glass batch to provide enough for Na_2SO_4 formation.

5. CORROSION OF FURNACE REFRACTORIES

One important factor affecting furnace operation and glass quality is refractory attack. Under some operating conditions the silica refractories in the furnace crown can be badly attacked. Silica, SiO_2, is the main component of the refractory bricks normally used in furnace crowns. Silica particles are bound in a matrix made of calcium silicate ($CaO.SiO_2$) and a high SiO_2 glass containing aluminium, calcium, titanium and iron. The main corrosive species in the gas is NaOH. In the furnace this reacts with the SiO_2 to form sodium silicates. These sodium species dissolve in and react with the glassy matrix, thus reducing its melting point. This weakens the structure. At the same time, the glassy matrix may migrate away from the front face of the brick, and, dependent on the actual conditions experienced by the brick, various faults may occur.

In practice, the refractory bricks in the furnace structure may appear to ‘run wet and drip’, or ‘produce frost or scale’ or become ‘glazed’. These descriptions relate to the appearance of the refractory bricks resulting from different types of attack. Fig. 2 Silica drip or scale falling from the furnace superstructure onto the molten glass is one of the important problems faced by glass makers.

Figure 2

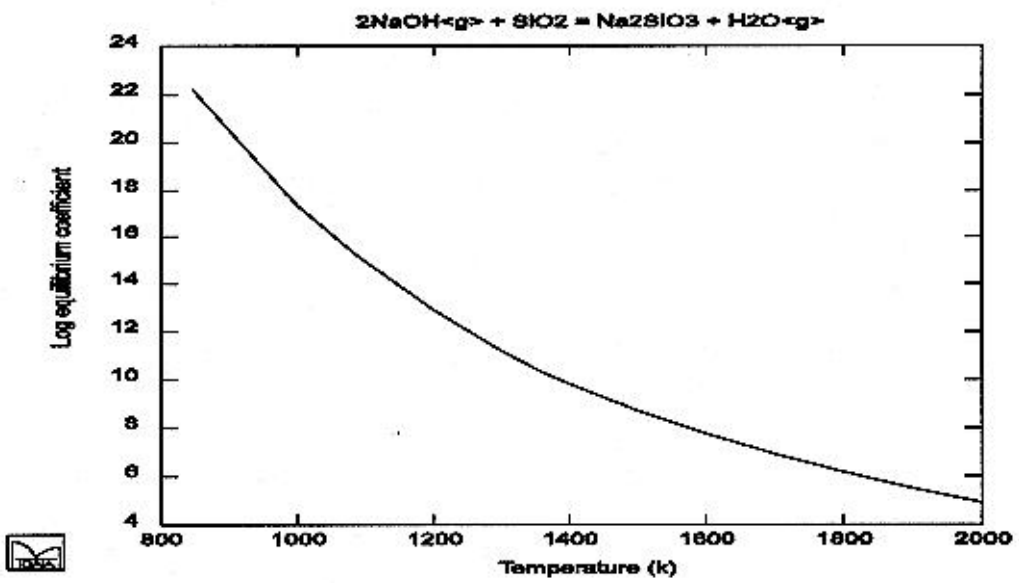

The refractories are often most severely attacked in a particular place in the furnace. The reason for this is complex and still under investigation. Understanding crown refractory attack is further complicated, because the nature and precise site of the attack often varies with time.

The pattern of the refractory attack clearly relates to the complex gas flows through the furnace system, but other factors are involved. MTDATA has helped understand one of these factors. The Thermotab module of the MTDATA program plots thermodynamic functions. This module has been used to show that the equilibria of the SiO_2 corrosion reactions moves away from the products of corrosion as the temperature increases.

The relationship between equilibrium coefficient and temperature is similar for all the refractory attack reactions between Na compounds and SiO_2. An example is shown in Fig. 3.

Figure 3

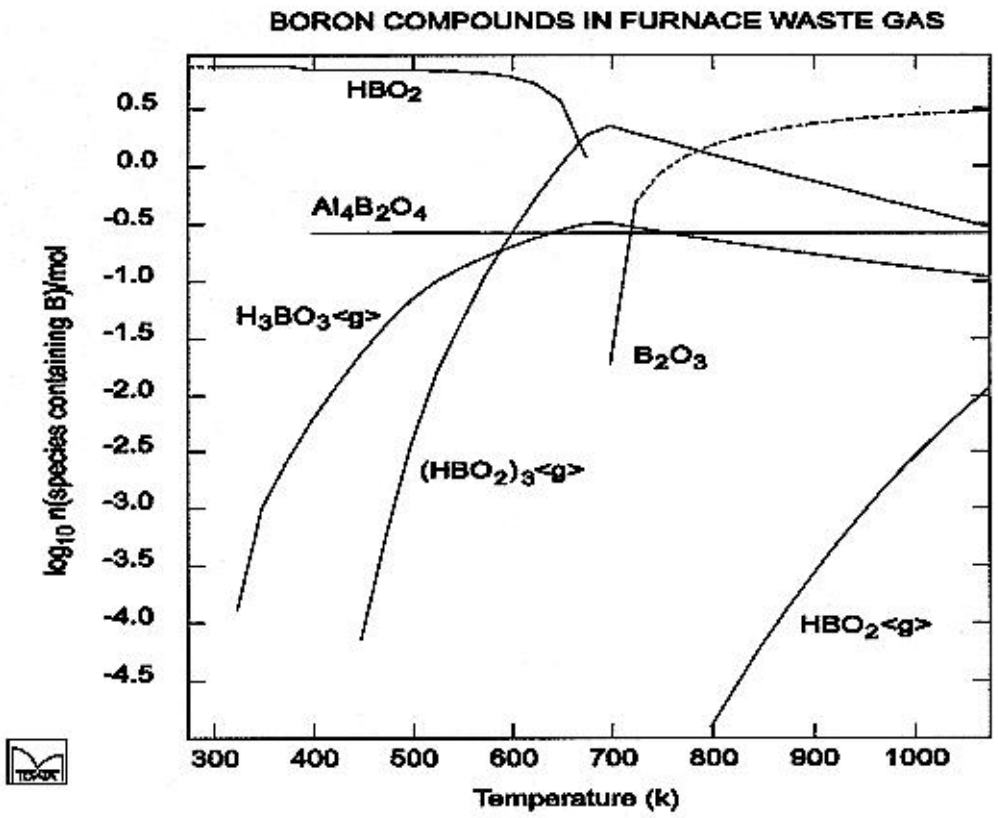

This indicates that although the amount of corrosive sodium species is higher in otter parts of the furnace, the equilibrium of the SiO_2 corrosion reaction favours attack at lower temperatures. Our understanding of the complex refractory attack processes is increasing, although there is much left yet to learn.

6. OXY-FUEL COMBUSTION

Initial investigations suggest that the furnace refractory attack processes are even more prevalent when the fuel is burned using oxygen instead of air. Oxygen is used to limit the formation of pollutant nitrogen oxide from the nitrogen in the combustion air. In such an oxy-fuel furnace atmosphere, the concentration of all the gases, including the corrosive sodium species, is increased by about three times compared to normal operating conditions. This is because there is much less nitrogen in the atmosphere. We have also used MTDATA to study these conditions. Thermodynamic predictions show that as well as major shifts in gas concentrations in an oxy-fuel atmosphere, compared to normal air combustion, other changes occur. The temperature at which compounds form or condense is also altered by using oxygen to burn the fuel.

7. BLOCKAGE OF REGENERATORS

The most important condensate in the waste gas flues of most glass furnaces is sodium sulphate, Na_2SO_4. Under normal furnace operating conditions most of the sodium precipitates out of the gas as sodium sulphate; only under unusual conditions when S is limited relative to Na

inhibiting stoichiometric Na_2SO_4 formation do other Na compounds form. Sodium carbonate and sodium chloride may then be found in the waste gas dust. During oil combustion, much S is derived from the oil, but S is also present in glass batch (as SO_4 refining agent) and even during gas combustion there is excess S for Na_2SO_4 formation. The gaseous S compounds in the waste gas are normally oxides, SO_x.

In the absence of NaCl volatilising from the melt, the Na_2SO_4 is formed in the waste gas by reactions between NaOH and sulphur trioxide (SO_3) gas. These reactions form sticky condensates at between 900 and 800 ^oC. However, normally some NaCl is present and this complicates the reaction scheme. Also, when NaCl condenses in association with Na_2SO_4, a sticky eutectic melt can form. This is liquid at a lower temperature than either of the two pure compounds, and this corrosive mixture accumulates in the regenerators and flues with the other condensing and solid particulates.

The dust carried by the waste gas from a flat glass furnace is normally about 95% condensed Na_2SO_4. Other condensates and material such as silica sand carried over from the glass batch can also be present. This material collects in parts of the regenerator and flue system, reducing their efficiency and eventually causing blockage. These problems still concern glassmakers, but are much less important than they used to be now that the cause of the problem is understood. The use of low chloride content soda ash in the batch raw materials has greatly extended furnace operating life.

8. OTHER COMPOUNDS IN THE WASTE GAS

There are many other important compounds present in the furnace atmosphere and waste gases. These may interact with the sodium compounds. For example, vanadium, V, is often present in fuel oil, and sodium vanadates may form in the waste gas. Alkali vanadates precipitate from the waste gas at a higher temperature than sulphates and mixed condensates occur. Although the chemistry of V compounds in cooling waste gases is very complex and poorly understood, it is known from work in the power generation industry that condensed vanadates are corrosive to many alloys and refractories. Also, vanadium compounds catalyse the formation of SO_3 from SO_2. This process is involved in the gas reactions that form sulphuric acid mist in the emitted waste gas.

Special glasses contain a much wider range of constituents than simple float glass. When special glasses are made, volatile compounds may enter the waste gas that are not normally present in a typical furnace system. For example, boron (B) would be present in a borosilicate glass furnace waste gas, and lead (Pb) may be present in the waste gases from a furnace making radiation shielding glass.

Figure 3 shows the MTDATA prediction of B compounds in the waste gas from a furnace making optical glass. This was part of a study assessing the gaseous compounds present at low temperatures in the waste gas from the optical glass tank. MTDATA predicted that boric acid compounds would be volatile at lower temperatures than that at which dust control equipment normally works. After the study, a method was devised to condense the volatile B compounds allowing them to be captured by a baghouse before the clean gases were emitted to the atmosphere.

9. POLLUTION FORMATION AND CONTROL

Legislative emission limits apply to many gaseous and solid compounds in the furnace waste gas. Development of furnace operating procedures to minimise their production may be based on a good knowledge of the processes that form these compounds.

Often it is necessary to control the emission of pollutants after they have been formed and there are many techniques available to do this. Acid gases (i.e. HCl, HF and SO_x) may be scrubbed from the flues using alkali-based reagents, and particulates may be removed by electrostatic precipitators or baghouses. The very small particle size and relative stickiness of the complex Na_2SO_4 condensates make them especially difficult to remove from the waste gas flue.

Until recently, NO_x, the other important pollutant in waste gases, could not be economically removed from many types of furnace systems. Pilkington plc have recently developed the 3R process for NO_x removal.

10. CONCLUSION

Many very important aspects of the furnace operation are affected by the components of the waste gases produced by the melting process. The type of fuel used, the method of combustion and the type of glass being made all affect the waste gas composition.

Furnace life is affected by waste gas corrosion of refractories or blocking regenerators and flues. The waste gases may contain compounds that are subject to emission limits and thus require the use of pollution control equipment.

This paper is published with the permission of the Directors of Pilkington plc and of Dr. A. Ledwith, Director of Group Research.

THERMAL INSULATION OF GLASS FURNACE CROWNS

Prof. S. Lutskanov
Lubisol Engineering Co., Bulgaria

Abstract

The positive experience described in the paper is based on observations on the performance of more than 50 glass furnace crowns with LUBISOL monolithic crown insulation implemented all around the world, including 6 float furnaces in the USA. It has been achieved a service life 10 years, and heat loss reduction of 90 %, when the crown and the insulation have been part of a joint design. Data are given about the elimination of the loose joints in the silica crown and the reduction of the alkaline corrosion to a negligible degree.

I. INTRODUCTION

Most glass producers all over the world use furnace insulation as a standard practice. The glass furnace crown covers a large area, and it can give significant savings of energy when insulated, reducing the heat losses from about 5000 W/sq.m. to 1750-2200 W/sq.m. (1).

The main obstacle for the implementation of an efficient thermal insulation of glass furnace silica crowns is the strong conservative tradition in the glass industry.

A false conception still prevails, that the more efficient insulation can bring a higher corrosion rate and "Rat holes" in the silica crown.

Starting our investigations back in 1970, we came quickly to the conclusion from a theoretical point of view, that silica crowns with an efficient insulation work at higher temperature, which reduces the risks from condensation of alkaline vapors, the main reason for alkaline corrosion.

One of the most important aim of our study was to collect correlation between the efficiency of the crown insulation and the rate of alkaline corrosion during the whole furnace campaign, and to use our positive experience in overcoming the doubts and fears towards the efficient crown insulation. The other aim was the elimination of the loose joints and the "Rat hole" formation in the silica crowns melting soda-lime glasses.

II. CRITICAL ANALYSIS

Our first investigations in the filed of furnace crown insulation indicated, that all existing materials and applications have some setbacks which are still valid in recent days.

* All existing materials are showing a rapid rise of thermal conductivity at higher temperatures, and a thicker insulation does not give the corresponding higher efficiency
(see fig. 1).

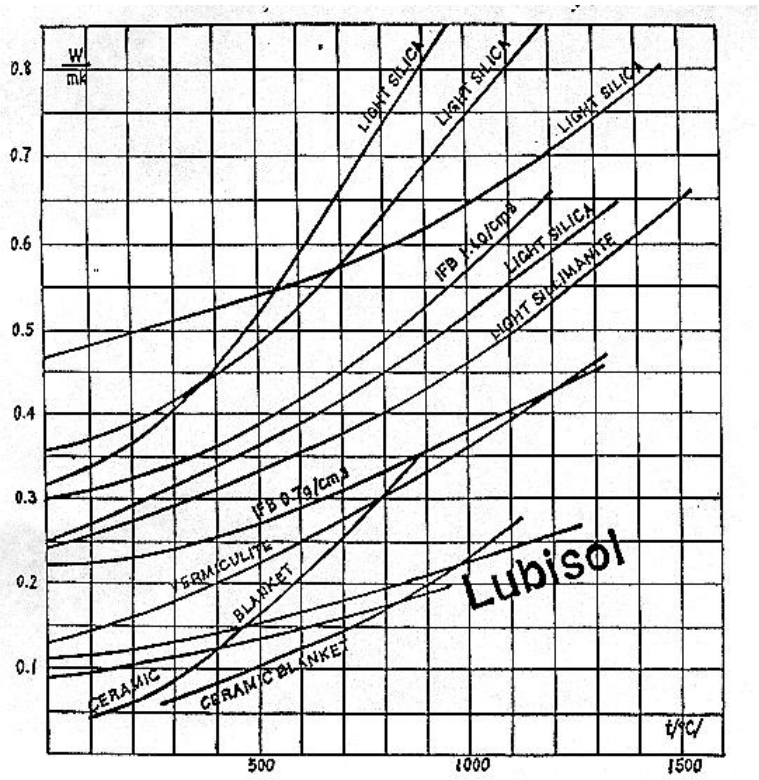

Fig. 1 THERMAL CONDUCTIVITY OF INSULATING MATERIALS

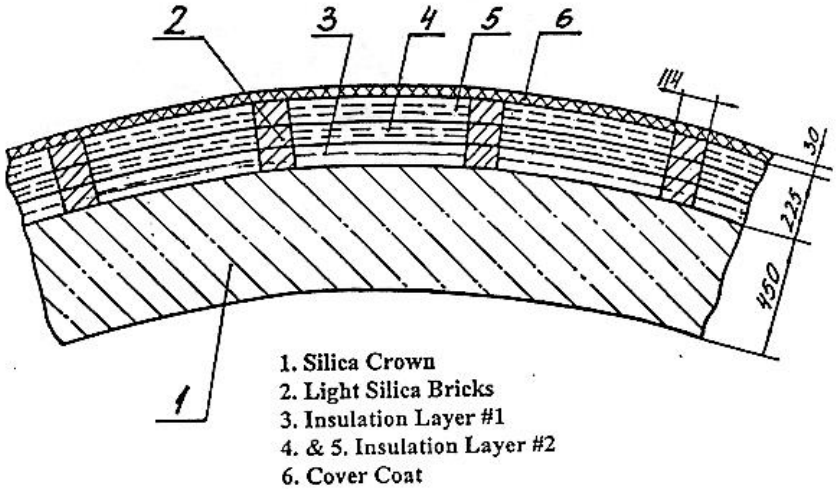

Fig. 2

* The light silica bricks have a rather high specific weight, limiting the thickness of the insulation on large span crowns.

* The light silica bricks have a very good corrosion resistance against alkali fumes leaking from the silica crown, but this proves to be no advantage. This high corrosion resistance does not prevent, but only delays the "Rat Hole" formation, making the damage of the crown bigger and the hot repair more difficult.

* Most of the top coating materials available on the market give cracks or peel of after 2-3 years of service life. They do not give a hermetic sealing of the insulation.

*The ceramic fibber insulations have a major disadvantage - they are not air tight. We have observed in many locations ceramic fiber crown insulation in very bad shape after a few years of service.

All these observations gave us incentives to develop our new LUBISOL technology, which made possible the elimination of most of the set-backs of the existing insulation.

III. THE "LUBISOL" TECHNOLOGY

A new type monolithic insulation material was developed, based on a new poreformation technology.

The LUBISOL insulation are a mixture of silicate materials, expanded fillers and burning particles, and this mixture is converted into a light porous body under the action of the heat of the furnace, the burning out taking place "in situ" on the furnace crown.

The LUBISOL insulation has a composite structure, being reinforced with light silica bricks and having a strong Cover coat with thermal-sensitive properties (See fig.2). This Cover coat becomes dark at higher temperatures and shows any local overheating prior to flame incoming.

It was found, that the monolithic insulation can be easily transported, packed in plastic bags, and compared with any type of bricks, no breakage takes place.

Thus it was possible to avoid several stages of the usual production process such as forming, drying and firing, which made possible to achieve a lower thermal conductivity, a low specific weight and a competitive low self cost.

Due to the rather low thermal conductivity (See Fig. 1) it was possible to obtain 90% heat loss reduction at a thickness of the LUBISOL crown insulation of 260 mm.

We came to the conclusion, that the thermal insulation of a glass furnace crown should be part of a complex design, including both crown and insulation.

We have accepted in our calculations, that the temperature in one- third of the thickness of the silica crown should not exceed 1450-1500^{o}C. At the same time, we carried out a lot of measurement of the temperature at the intermediate layer between the crown and the insulation.

We have found considerable differences between the calculated and the directly measured values, the calculated values being higher than the measured ones every time.

This results allowed us to develop our own system for calculation of the heat losses and the intermediate temperatures.

We came very soon to the important conclusion, that the complex design of the thermal insulation and the glass furnace crown should include all specific parameters, such as maximum temperature in the furnace, type of glass being melted, size of the furnace crown, etc.

IV. POSITIVE EXPERIENCE

Using our own system for calculations, we accepted as a safe upper limit of efficiency 90 % heat loss reduction (HLR) for furnaces melting soda-lime glass. We have achieved such high

figures of efficiency insulating crowns of furnaces working at 1580-1600 ^{o}C, and in order to be on the safe side, we always recommended a thickness of the silica crown of 450 mm for all crowns with spans between 3000 and 9000 mm. and 500 mm for larger spans.

We have achieved 90 % HLR when the thickness of the crown was 450 mm and the thickness of the LUBISOL insulation was 260 mm (see fig.2).

Reaching a rather high level of efficiency with our LUBISOL insulation we calculated a pay back of the insulation costs by the fuel savings within one year.

It is very important to note, that the high degree of thermal insulation on silica crowns melting soda-lime glasses does not have any negative effect on the furnace life when a high quality silica refractory is used, and when the loose joints in the crown are totally eliminated.

We have observed this on many glass furnaces melting soda-lime glass with LUBISOL crown insulation, and some of them had 10 years of service life without any serious "Rat hole" problems.

Taking into account the big importance of the tight brickwork, we have developed our own system for elimination of the loose joints, which we implement under the commercial name "ZERO-JOINT" Technology (2).

The ZERO-JOINT Technology incorporates checking for size tolerances of all silica bricks in the glass factory; elimination of both primary and secondary formed loose joints formed during the building and heating-up of the silica crown; special measures to avoid loose joints near the expansion joints, etc.

The ZERO-JOINT Technology is based on the company's practical experience and know-how gathered over a period of 30 years period, combined with a theoretical approach to the problem.

The ZERO-JOINT Technology becomes now days more important, due to the fact, that in silica crowns with oxy-fuel firing the problem of "Rat Hole" formation becomes a very one, due to the increased rate of corrosion.

The efficient thermal insulation of the glass furnace crowns gives considerable heat and fuel savings as a result.

The efficient crown insulation is very important for heavily loaded glass furnaces with constant pull with a melting temperature near to 1600 ^{o}C, and the percentage of saved fuel is higher at furnaces with higher fuel efficiency and low fuel consumption.

The positive effect of the efficient thermal insulation is not limited to fuel savings. There is a positive effect on the whole glass melting process.

The insulated crown accumulates about twice as much heat in comparison with the uninsulated one. The accumulated heat acts as a buffer reducing the temperature fluctuations in the furnace.

It is well known that maintaining constant temperature in the furnace is of prime importance to the glass melting process and hence to achieving homogenous glass.

The heat radiation from the crown towards the glass melt and the batch is the main source of energy for glass melting. The insulated crown keeps a constantly high temperature and speeds up the process of glass melting.

The well insulated crown creates preconditions for higher quality of the glass, and in flat and container glass furnaces - for higher quality and productivity due to better homogeneity of the glass.

REFERENCES

(1) Trier W., Glass Furnaces, Society of Glass Technology, UK,1987, pp 91.
(2) Lutskanov, S., Eliminating Rat Holes in Furnace Silica Crowns, Glass, January 1995, pp 26.

A MOLECULAR DYNAMICS SIMULATION OF MoF_5 GLASS STRUCTURE*

V. Goncharuk and **E. Merkulov**
Russian Academy of Science, Russia
V. Ignatijuk, I. Uschipovskaya and **R. Lednev**
Far Eastern State University, Russia

Abstract

The MoF_5 - glass structure was investigated by means of Monte-Carlo (MCM) and Molecular dynamics (MDM) methods of a numerical simulation. The algorithm of Molecular dynamics method are briefly described. Results of the calculations for MoF_5 - glass are discussed. The MCM simulated structure can be used for theoretical modeling of fundamental physical properties of the MoF_5 - glass.

---

* Full manuscript not available at the time of printing

A NEW ALUMOTHERMIC ROUTE FOR PREPARATION OF OXYNITRIDE GLASSES*

I. Penkov*, R. Pascova**
*Institute of Metal Science and Technology, Bulgaria
**Institute of Physical Chemistry, Bulgaria

A new alumothermic route for synthesis of oxynitride glasses was developed. In this method fine milled glasses of appropriate compositions were treated by powdered aluminium in reduction atmosphere at 730-760^{o}C. As a result of redox reactions occurred mixtures containing large amounts of fine dispersed elemental Si and Al_20_3 (with particle sizes of 1 to a few micrometers) were prepared. The nitridation of the mixtures thus obtained was carried out at 1350^{o}C under nitrogen atmosphere. The high surface to volume ratio of the elemental Si facilitated the synthesis of fine dispersed Si_3N_4 during the process of nitridation. Since oxides like P_2O_5 and B_20_3 favour both the nitrogen incorporation into the glass network and the dissolution of $A1_20_3$ obtained at the alumothermic treatment, compounds containing P_20_5 and B_20_3 were added to the mixtures after completing the nitridation. Through the alumothermic method described homogeneous oxynitride borophosphate silicate glasses with high nitrogen content (up to 20 at.%) were prepared. The glasses synthesized are characterized by very good corrosion resistance to molten Al and enhanced mechanical properties.

---

* Full manuscript not available at the time of printing

A NEW APPROACH TO LOWERING PRODUCTION COST OF MOLDS FOR GLASS CONTAINERS

Erdal Yollu,* Yusuf Coskun, Hüsnü Konuk***
*) Ferro Döküm San.Tic.A.S., SISECAM , TURKEY
**) Anadolu Cam San. A.S., SISECAM, TURKEY

Abstract

Properties of the mold considerably affect the cost, productivity and quality of glass containers and glassware. Due to high manufacturing costs, it is hoped that molds will be used for a longer period of time. Therefore, certain mold surfaces which have contact with glass are coated by either welding special powder alloys or placing solid inserts onto molds using special welding methods which require know-how. Although these are costly operations, the cost can be lowered if inserts are placed while casting the molds. The purpose of this study is to explore whether this technique can be applied.

In this study, the bond between insert and mold is achieved during casting of the mold. The mold-insert interface was examined by metallography and SEM. The casting parameters which affect the interface structure were optimized in order to get satisfactory bonding during pouring of the mold. The findings show that bonding has been achieved successfully. This technique brings significant amounts of savings in mold manufacturing cost.

I. INTRODUCTION

It is known that the properties of the molds for glass containers greatly affect the product quality and mold production productivity. The following list summarizes the, generally accepted mold properties.

- Good machinability
- Ability to produce a good surface finish
- Resistance to heat checking
- Low thermal expansion
- High thermal conductivity
- Resistance to growth
- Resistance to oxidation
- Resistance to wear
- Density or homogeneity
- High graphite particle distribution

Gray cast iron seems to be the most suitable material for the above mentioned requirements. Owing to the nature of gray iron, presence of graphite in the structure presents difficulties in achieving a good surface finish.

Another difficulty arising from gray iron material is its brittleness, where breakage and cracks often occur on the edges of molds. These disadvantages, however, may be eliminated by the application of the surface modification techniques, such as surface coating and welding. It is a common practice to use spray welding on the mold surface, blank neck and bottom, (4).

Powder welding is another technique in use to increase the life of cast iron components. It is generally applied to the plunger and the outer face of the neck ring, (1). In practice modern welding equipment is used. The mold surfaces are machined to the final shape following the application of welding. Because of application difficulties and economic reasons, however, the above mentioned techniques are always in need of improvement by either development of techniques or by establishment of new methods. In conjunction with this, using of insert materials and applying of PVD (Physical Vapor Deposition) techniques are being considered, (7), (8).

2. POURING TRIALS AND EXPERIMENTS.

The method of bonding of insert material with iron was investigated. The preformed insert which contacts the glass was placed into the mold cavity, and gray iron was poured onto it.

Inserts supplied by ACS (Anadolu Cam Sanayii) were chromium and nickel containing iron alloy. The effects of pouring temperature of the liquid iron and of the gating design were investigated. The neck-ring casting shown in Fig.1 was chosen in order to determinate pouring parameters for achieving the best bond between the insert and iron poured onto it.

Pouring trials, with the gating design shown in Fig.2 were carried out at 1350 ^{o}C. After cooling, coldshut defects were detected in some of the castings. This may indicate the bad bond between the insert and cast iron. In the second trial with the gating system shown in Fig. 3, iron was poured at 1370^{o}C. After cooling and cleaning, visual inspection has shown satisfactory results.

The bond between the insert and cast iron was examined under optical microscope. Photomicropraphs in Fig. 4 shows the section through A-A of Fig.1. Mechanical tests have also been carried out on the cross section shown in Fig.1,and a perfect bonding was observed between the insert and the iron.

SEM analysis of sections revealed bonding characteristics. Fig.5. shows the SEM photo of sections covering insert material, interface and cast material. When iron is poured on the insert, the liquid iron heats up and melts the surface of the insert and readily forms a weld by surface alloying and diffusion. This idea is supported by the results of EDX analysis of the carbides on the interface. The formed iron and chromium carbides are shown in Fig.6 and Fig.7.

After leveling of the surfaces of two pieces, casting-insert interphase was also tested by turning the castings on a turret lathe. During machining no loosening of the insert has been detected through passage of the cutter from insert to casting.

Strength of bond between insert and casting was also tested on the Universal Test Machine. Two samples were joined together as shown in Fig.8, and load was applied. When the maximum load which can be applied by the machine reached up to 19050 kgf without rupture, shear strength calculated as

S_{shear} = load / interface area = 8.89 kgf/mm^2

The test was repeated by decreasing the contact area between the interface and casting. Again, the maximum load was reached without rupture, where shear strength was calculated as 39.65 kgf/mm^2. This value is above the shear strength of most gray iron castings. Therefore no further tests have been done. This result has proved the perfect bonding of the insert to the cast material.

Neck ring samples poured with the technique described above have been machined to final dimensions and put into glass production. Results have shown longer production runs than glass produced from molds made by powder weld process.

3. CONCLUSIONS

According to the results of this study, neck-rings produced by castings with inserts can safely be used in glass production bringing considerable savings in neck-ring manufacturing costs.

It is possible to obtain insert containing molds with a suitable gating design and pouring temperature. Manufacturing costs of molds were more economical than other processes, where 10%-15% cost reductions in molds have been achieved.

4. ACKNOWLEDGEMENT

We are indebted to Dr. Metin Baþaran for his kind support and valuable contributions made by reading the manuscripts and making proposals through discussions.

REFERENCES

1. ENSOR, T. F. "Review of the Literature on Mould Materials Used in the Glass", Glass Tech., Vol.ll No.2, April 1970, P. 42~47

2. VANICK, J.S. "Metallurgical Analysis of Glass Mold Cast Irons" Chapter 65 P.322-30, Forming in the Glass Industry, Part II, Alexis Pincus,1983, Ashlay Publishing Co.

3. ANON, "Glass Molds", Chapter 69, P. 341-344, Forming in the Glass Industry Part II Alexis Pincus,1983, Ashlay Publishing Co.

4. VICKERS, T.A.Y., "The Development of the UK G/ass Mould Making Industry in the 20 Century", Glass Technology, Vol. 35 No.4, August 1994, P.146-153

5. WARDLEY, T., "Glass Forming Moulds: Material and Design", Journal of the Society of Glass Technology, P.50-G7

6. ANON " 20 Years of Progress in Glassware Molds", Chapter 66, P.331-332, Forming in the Glass Industry Part II, Alexis Pincus,1983, Ashlay Publishing Co.

7. MANNS, P., DÖLL, W., KLEER, G., Glass in contact with mould materials for container production'; Glastech. Ber. Glass Sci. Technol. 68 (1995) No.12, P. 389-398.

8. Kuruoglu, S., Yollu, E., Karagoz, S. "Studies on the Arc-PVD Coating Applications in Glass Moulds.'; Original Paper,1996.

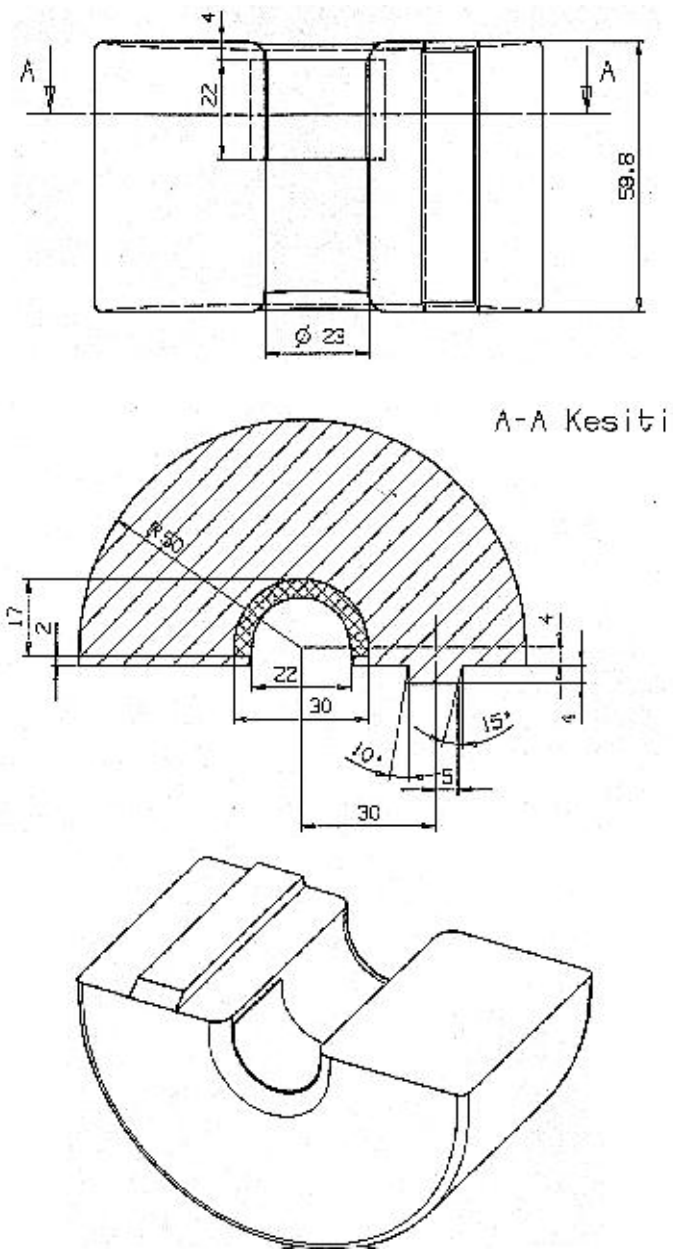

Figure - 1

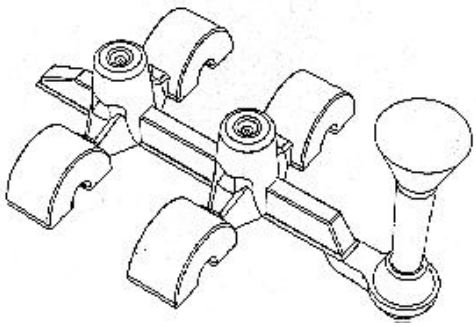

Figure - 2

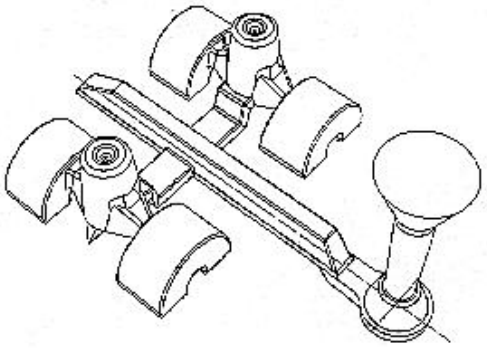

Figure - 3

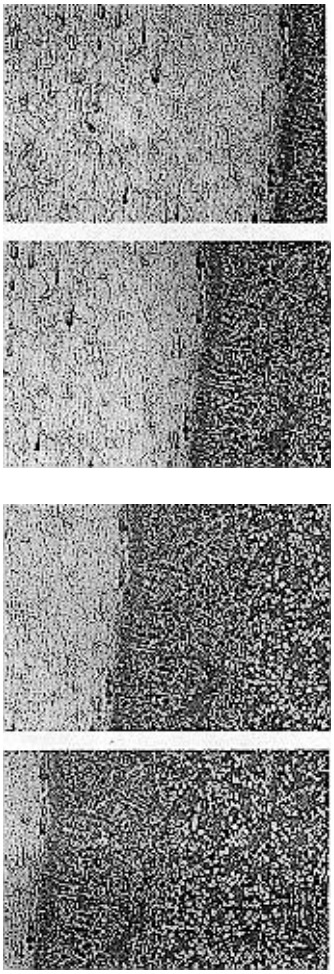

Figure - 4

Figure - 5

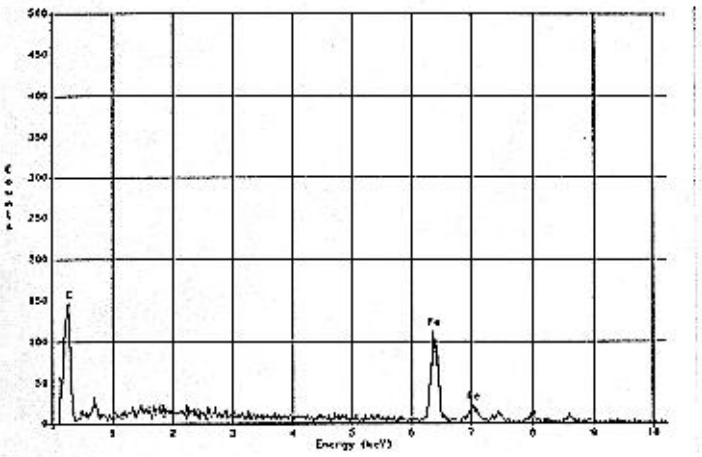

Figure - 6

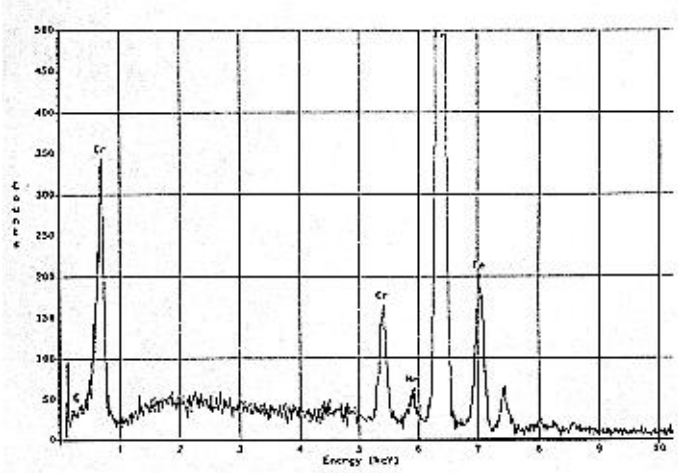

Figure - 7

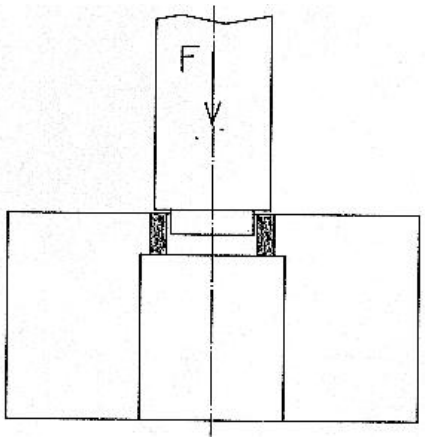

Figure - 8

ADMIXTURES STABILIZING $2CaO \cdot Al_2O_3$ GLASS

L. Stoch and M. Đroda
University of Mining and Metallurgy, Poland

Abstract

Influence of small additions of several substances on the stability of $2CaO \cdot Al_2O_3$ glass was investigated.

They were: 1. substances incorporating into the aluminate glass network as $[AlO_4]$ tetrahedra substitutions i.e. SiO_2 and B_2O_3, 2. substances forming chemical bonds with Ca^{2+}, but not isomorphous with AlO_4 tetrahedra. Admixtures of the first group appeared effective vitreous state stabilizers. Substances of the second group as enhanced the crystallization ability. Stabilising components form complexes composed of $[SiO_4]$, $[BO_4]$ tetrahedra. They hamper the ordering tendency of the amorphous structure, preventing devitrification.

I. INTRODUCTION

Calcium-aluminate glasses are characterized by their specific structure. Their framework is formed of AlO_4 tetrahedra, and the shortage of positive charge of a tetrahedron is compensated by the cations Ca^{2+} which are situated beside them. The glass-forming range in the system CaO-Al_2O_3 has been determined by Rawson [1] as very narrow section limited by the eutectics of the $12CaO \cdot 7Al_2O_3$ with $3CaO \cdot Al_2O_3$ and $CaO \cdot Al_2O_3$ compounds.

Application of solar furnace melting and split quench techniques allows to extend the glass-forming region to 25-70 mole % of Al_2O_3 or 25-50 mole % of Al_2O_3 depending on the cooling rate [2, 3].

Addition of about 5 wt % of SiO_2 or GeO_2 considerably increases the stability of CaO-Al_2O_3 glasses. A marked reduction of the ability for crystallization of these glasses can be obtained changing their composition through the introduction of additional components such as alkalies (about 10 mole %), BaO and MgO (about 5 mole % each). The best results were obtained when additionally 2 mole % of Fe_2O_3 2 mole % of La_2O_3 and 2 mole % of SiO_2 were introduced. Stable glasses transmitting IR radiation up to 5μm were obtained by introducing 3 wt % of BaO with 4.7 wt % of MgO or 6.1 wt % of SiO_2 with 4.1 wt % of MgO [4].

Such stable aluminate glasses are produced on commercial scale. They are characterized by infrared transmittance similar to that of sapphire and stability at high temperatures (T_g about 800^oC). Calcium aluminate glasses have been proposed as materials for infrared windows and as high strength optical fibres and photomemory materials.

It is believed that the structure of $CaO\text{-}Al_2O_3$ glasses corresponds to the structure of crystalline aluminates $CaO{\cdot}Al_2O_3$ and $12CaO{\cdot}7Al_2O_3$

The structure of monoclinic variety of $CaO{\cdot}Al_2O_3$ is equivalent to the structure of tridymite. It consists of six-membered rings built of AlO_4 tetrahedra with Ca^{2+} ions stuffing the sites within the framework structure [5]. In this structure the tetrahedra are linked their all four corners forming fully polymerized Q^4 units.

The structure of $12CaO{\cdot}7Al_2O_3$ has the character of three-dimensional network formed by a combination of rings built of 8 tetrahedra which join with each other through 4 or 3 bridging oxygens (Q^4 and Q^3 units) [6].

It is believed that the structure of glasses in the $CaO\text{-}Al_2O_3$ system is built of polymerized tetrahedra of AlO_4, and Ca^{2+} ions are located in the vacant sites of the framework [2, 7]. Recent investigations [8] have revealed, that when the ratio $CaO{:}Al_2O_3$ 1 the glass structure contains only Al of fourfold co-ordination to oxygen and AlO_4 tetrahedra are connected through four bridging oxygens (structure Q^4) When $CaO{:}Al_2O_3$ <1 aluminium appears in co-ordination V and VI to oxygen and tetrahedra are linked only through two oxygen bridges (Q^2 units).

It has been found that the rearrangement of Ca and Al in the next nearest neighboring co-ordination environment, around the central Al atom, changes with the cooling rate of the melt. The slower cooling causes the more ordered arrangement of Ca [8].

It is difficult to obtain pure $CaO\text{-}Al_2O_3$ glasses of such structure by cooling greater quantities of the batch at the cooling rate usually applied in practice. Hence investigations were undertaken by us on the effect of the addition of components which might be incorporated into the aluminate framework on the stability of the glassy state of calcium aluminates. So far the stability of aluminate glasses was improved by adding mainly the components-modifiers. Attempt was also made to determine the position of the stabilizing additions in the structure and to explain why they stabilize the disordered state of the structure specific for glass. Results obtained were described below.

II. EXPERIMENTAL

Glasses were melted in alumina or platinum crucibles from 100-200 g batches at 1550^oC. The molten glass was poured out on a steel plate as a layer 5 mm thick. Chemically pure components were melted to obtain the glasses. The basic chemical composition $2CaO{\cdot}Al_2O_3$ was corrected by introducing additions which played a different role in the glass structure. Infrared spectra of the glass were measured using MR-80 Zeiss Spectrophotometer. The derivatograph MOM Budapest and X-ray diffractometer DRON 3 were applied to study the glass crystallization. Perkin-Elmer TMA-7 apparatus was applied to determinate thermal expansion coefficient. Density of the glasses was measured using AccuPyc 1330 equipment. Specord UV-VIS and Specord M80 Carl Zeiss Jena was used to measure the light transmittance in the visible and infrared range of spectrum.

III. RESULTS

The glass formation oxides incorporating into the aluminate network as single co-ordination polyhedra or their groups were used as stabilizing additions. According to the flexible network model of the glass structure formulated earlier [9], these polyhedral with strong cation-anion chemical bonds can impede the rearrangement and ordering of the parent glass structure elements inhibiting the crystallization of glass. Substances of the following properties were used:

1. substances incorporating into the aluminate glass network as AlO_4 tetrahedra substitutions and simultaneously creating the chemical bonds of different strength with calcium i.e. SiO_2 and B_2O_3,
2. substances forming bonds with Ca^{2+} and Al^{3+} but not isomorphous with AlO_4 tetrahedra: PO_4^{3-} and SO_4^{2-},
3. F^- which can combine with Ca^{2+} and Al^{3+} but acts as a depolymerizing agent on the aluminate network.

Results of glass melting experiments (Tab. 1) indicated that two component glasses was successfully obtained when the melt contained about 50 wt % CaO and 50 wt % Al_2O_3 which corresponds to the stochiometric formula $2CaO \cdot Al_2O_3$ or $Ca_2Al_2O_5$. A little excess of CaO was acceptable or even help to obtain stable glass. On the other hand increase of the Al_2O_3 content has caused increase in the crystallization ability.

The addition of SiO_2 up to 6 wt % makes the glass formation easier, while 8-10 wt % or more SiO_2 causes volume crystallization of gehlenite ($2CaO \cdot Al_2O_3 \cdot SiO_2$). Up to 10 wt % of B_2O_3 addition increases significantly the ability of glass formation. Higher B_2O_3 content causes calcium borates crystallization. The stabilizing action of SiO_2 is enhanced by B_2O_3 addition. The glass can be obtained even when 1 wt % SiO_2 and 1 wt % B_2O_3 are added. The F^- , PO_4^{3+} or SO_4^{2-} admixture causes the destabilisation of the glassy structure and rapid crystallisation of the glass.

Their destabilising effect is diminished when besides P_2O_5 or CaF_2 few percent of B_2O_3 is added.

Glasses obtained are homogeneous and transparent. They are green or red colored. Color of calcium aluminate glass is the result of low transmission of the glass at the short wave part of spectrum [4].The transmission threshold moves from 420 nm (green glass) to 310 nm (red glass) as the content of stabilising oxides increases. The glass transmits infrared light up to 5 **:** m (80-90 % transmittance value). The refractive index of glass is about 1.667.

Glass density changes from 2.882 to 3.033 g/cm^3 depending on the admixtures content and the thermal history of the sample.

Thermal expansion coefficient of SiO_2 stabilised glasses changes from $74 \cdot 10^{-7}$ 1/^{o}C for 1.5 wt % SiO_2 to $84 \cdot 10^{-7}$ 1/^{o} C for 6 wt % SiO_2 content. It is constant in the temperature range 20-600 ^{o} C. Softening point of glasses is about 835^{o}C

Table 1

Allundum crucibles

Melt No	**Composition wt.%**							**Glass quality**
	Al_2O_3	CaO	SiO_2	CaF_2	P_2O_5	SO_4^{2-}	B_2O_3	
1	50	50						glass+cryst.$12CaO.7Al_2O_3$
2	52	48	-	-	-	-	-	glass+cryst.
3	47	43	10	-	-	-	-	glass+cryst. $2CaO.7Al_2O_3SiO_2$
4	48	52	-	-	-	-	-	glass+cryst.
5	51	44	-	5	-	-	-	cryst. material
6	48.5	46.5	5	-	-	-	-	phase separation
7	48	46	6	-	-	-	-	glass
8	46	44	-	-	10	-	-	cryst.material$12CaO.7Al_2O_3$, $CaO.3Al_2O_32P_2O_5$
9	46	44	5	-	5	-	-	some glass
10	46	44	-	-	5	5	-	cryst. material
11	46	44	-	-	-	10	-	cryst. material
12	46	44	-	-	-	-	10	glass, surface cryst. $3CaO.B_2O_3$, $CaO.Al_2O_3$
13	48.5	46.5	-	-	-	-	5	glass
14	50	48	-	-	-	-	2	glass
15	46	44	5	-	-	-	5	glass
16	48.5	46.5	2.5	-	-	-	2.5	glass
17	50	48	1	-	-	-	1	glass
18	48.5	46.5	-	-	2	-	3	glass, surface cryst.
19	49.5	45.5	-	2.5	-	-	2.5	glass with cryst. 11 $CaO.7Al_2O_3$ CaF_2, $12CaO7Al_2O_3$

Platinium crucibles

20	50.2	48.3	1.5	-	-	-	-	glass
21	49.5	47.5	3	-	-	-	-	glass
22	47.9	46.1	6	-	-	-	-	glass

Thermal analysis

DTA curves show that the transformation temperature (T_g) and crystallization temperature of glasses are under strong influence of the admixtures. SiO_2 containing glasses has T_g and T_c temperatures higher (T_g - 810-840^oC and T ~990^oC) than B_2O_3 stabilized glass (T_g ~ 720^oC and T_c - 840-870^oC). Shape of the crystallization peak changes with admixtures content. Diffuse peak indicates slow crystallization and optimum stabilising admixtures concentration. Excess of admixtures causes a rapid crystallization (sharp DTA peak).

X ray diffraction

X-ray diffraction patterns have revealed that the aluminate $12CaO{\cdot}7Al_2O_3$ is a product of the $2CaO{\cdot}Al_2O_3$ glass crystallization. The admixtures, although in small quantities, distinctly affect the kind of the crystallizing phases. The product of the crystallization process in the presence of 10 wt % SiO_2 admixture is gehlenite (Table 1).

The borate $3CaO{\cdot}B_2O_3$ and the aluminate $CaO{\cdot}Al_2O_3$ appears in the case of 10 wt % B_2O_3 addition. An addition of 10 wt % P_2O_5 causes the crystallization of calcium alumino phosphate and the remaining components form $12CaO{\cdot}7Al_2O_3$. The addition of sulphate anion causes the crystallization of $CaSO_4$ but the remaining glass components form $12CaO.7Al_2O_3$ and $2CaO{\cdot}Al_2O_3$ compounds.

On the infrared spectra of $2CaO.Al_2O_3$ glass one can observe the intensive band 840cm^{-1} connected with the stretching vibrations of Al^{IV}-O bonds. This band is typical for "condensed" AlO_4 tetrahedra. AlO_4 tetrahedra give band of 480cm^{-1} as well, which is assigned at least in part to the bending motion Al ^{ýv}-O [5].

On the spectrum of glass with SiO_2 admixture there occurs a double band about 1100 cm^{-1} related to Si-O-Si and Si-O-Al mixed vibrations [5]. The band is assigned to aluminosilicate elements in the glass network. Simultaneously, the $Al^{ýv}$-O band vibrations move to the region 800 cm^{-1} characteristic for the $3CaO{\cdot}Al_2O_3$ compound frequency. Furthermore, the $Al^{ýv}$-O band around 480 cm^{-1} appears. A similar band is given by $3CaO{\cdot}Al_2O_3$ compound with SiO_2 admixture. It could be explained as an effect of the solid solution with well-ordered distribution of Si^{4+} substitutions instead of Al^{3+}.

Glass with B_2O_3 addition give the bands of "condensed" AlO_4 tetrahedral structure, which are also similar to the $CaO{\cdot}Al_2O_3$ bands. Besides, two additional bands in the 1100-1200 cm^{-1} region corresponding to the $B^{ýv}$-O bonds, typical for borates are observed.

It should be noted that glasses containing 5 wt % SiO_2 and 5 wt % B_2O_3 have very weak Si-O-Al bands. Vibration bands of aluminosilicate groups appear at 1100cm^{-1}.

IV. Conclusions

In the system $CaO\text{-}Al_2O_3$ the area of best glass forming power is around 50 wt % CaO and 50 wt % Al_2O_3. Glasses from this area can be formed by pouring 100-200 g batches out on a steel plate at 1500^oC. The melts has the ability to form glasses when CaO and Al_2O_3 are in stochiometric ratio given by the $2CaO{\cdot}Al_2O_3$ i.e. $Ca_2Al_2O_3$ formula.

The obtained glasses have high tendency for crystallization and can not be produced on the larger scale. It may be concluded from the results presented above that this

tendency could be diminished by adding components incorporating into the aluminate glass network. SiO_2 and B_2O_3 can play this role in the quantities of 6 wt % and 7 wt %, respectively. Glassy state is stabilized more efficiently using these two oxides together. Homogeneous glass may be obtained already with both 1 wt % SiO_2 and 1 wt % B_2O_3 admixtures.

The introduction of PO_4^{3-}, SO_4^{2-} and F^- anions destroys the glass forming ability and make the crystallization rapid.

These results correspond well with the calcium-aluminate glasses structure concept [2, 7, 8].

The network of $2CaO \cdot Al_2O_3$ glass contains "condensed" AlO_4 tetrahedra and glass-forming ability of the calcium aluminate melt is the consequence of an structural analogy between Si_2O_4 and $CaAl_2O_4$ groups. The formula of this glass may be written as $Ca[Al_2O_4]CaO$. Thus, the structure of the glass will consist of AlO_4 tetrahedra joined together by oxygen bridges and by Ca^{2+} cations, which are connected with them and compensate a deficit of electrical charges of Al^{3+} tetrahedra. The excess of CaO courses the four-hold co-ordination of all Al^{3+} cations. Surplus Ca^{2+} cations should appear in this structure, outside the condensed tetrahedra groups, which are weekly connected with them. The spectra of the glass are similar to the spectrum of the $12CaO \cdot Al_2O_3$ compound. This indicates close structural similarity between both substances.

It is supposed, that the aluminosilicate clusters are formed inside the glass-network, when SiO_2 is introduced into the glass. These clusters are built of SiO_4 and AlO_4 tetrahedra, which are join by oxygen bridges. Then, the vibration Al-O-Si band occurs in the IR spectrum and the glass spectrum becomes the similar to the gehlenite (pyrosilicate $Ca_2Al[AlSiO_7]$) spectrum. During the crystallization process the gehlenite is formed as well. BO_4 tetrahedra build into the glass network, when B_2O_3 is introduced to the batch. Then the typical vibration bands of $B^{ýv}$ -O appear in the IR-spectrum. When B_2O_3 content is 10 wt % or higher, glass crystallizes intensively and $Ca_3B_2O_3$ is formed. When aluminate network is modified by SiO_2 plus B_2O_3 additions, the main band of Al^{IV}-O moves to $800cm^{-1}$. This indicates that the glass structure becomes more similar to the aluminate $CaAl_2O_4$.

Vitreous state stabilizing function of admixtures can be explained if we assume that the following conditions must be satisfied to obtain the glass of a considerable kinetics stability [9]:

1) The glass structure must posses enough elasticity to enable its elements to occupy varying positions with respect to each other and adjust to each other to a degree sufficient to maintain their random arrangement.

2) Agents must operate to stabilize the randomness of structure and counteract of their ordering.

In the normal glass the polymeric network with the flexible but strong chemical bonds acts as the vitreous state stabilizer.

In non-polymeric glasses or glasses with weak structural network vitreous state can be established by the proper admixtures incorporation. They are the substances distributed in the glass structure, forming strong chemical bonds with main glass components and thus preventing its ordering.

The structure of $2CaO \cdot Al_2O_3$ glass is formed of AlO_4 tetrahedra and Ca^{2+} associated with them ($Ca[AlO_{4/2}]_2$ groups) which are joined together by oxygen bridges. The oxygen bridges make it possible to change the angle between tetrahedra, making the network flexible. Thus, an amorphous structure of disordered geometry can be formed. SiO_4 tetrahedra introduced into the glass network join the neighboring AlO_4 tetrahedra and probably pairs of $[SiO_4]$-$[AlO_4]$ are formed as in the gehlenite structure.

These aluminosilicate clusters make it difficult to rearrange the aluminate network units. The rearrangement is necessary for the structure ordering and crystallization of glass. In this way the clusters stabilize the amorphous state. Likewise, $Ca_2Al_2O_5$ glass is stabilized by boron-oxygen tetrahedra or triangles when B_2O_3 is added. This provides an explanation how small amounts of additions stabilize structure of glass.

The stabilizing additions are effective in relatively narrow ranges of their concentrations. If the solubility limit of additions in the aluminate network is exceeded, the network will be destroyed and a rapid glass crystallization process will follow.

The ions PO_4^{3-}, SO_4^{2-}, F^- are bound stronger with Ca^{2+} than with Al^{3+}. The above mentioned anions take the part of Ca^{2+} cations from the network to form their own compounds. The Ca^{2+} cations are necessary to ensure the stability of the network, so when the calcium sulphate, phosphates or fluorides are being crystallized, the aluminate network is destroyed. A similar effect is observed when an amount of SiO_2 is above 8 wt % or when content B_2O_3 is 10 wt % or higher. At that time the aluminates $12CaO \cdot 7Al_2O_3$ or $CaO \cdot Al_2O_3$ are formed.

Too large differences in the affinity of the these anions to the Ca^{2+} and Al^{3+} seem to be the reason for the glass network destruction and its crystallization.

Acknowledgment

This work was supported by National Committee for Scientific Researches of Poland, grant 3P 407 03406.

References

[1] Rawson H, et al.: Inorganic Glass-Forming Systems, London Academic Press, 1967, 317.
[2] McMillan P., Piriou B.: J. Non-Cryst. Solids, 55,1983, 221.
[3] Weber J.K.R., Merkeley C.D., Anderson C.D., Nordine P.C.: J. Am.Ceram.Soc., 76,1993, 2139.
[4] Davy J.R.: Glass Tech.,19,1978, 32.
[5] H@rkner W., Müller-Buschbaum H.K.: J. Inorg. Nucl. Chem., 38,1976, 983.
[6] Bartl H., Schellar T.: N. Jahr. Mineral. Monatsh.,109,1968,192.
[7] Morikawa H., Marumo F., Koyama T., Yamane M., Oyobe A.: J. Non-Cryst.Solids, 56,1983, 355.
[8] McMillan P.F., Petusky W.T., Coté B., Massiot D., Landron C., Coutures J.P.: J. Non-Cryst. Solids,195,1996, 261.

[9] Stoch L.: High Temp. Materials and Processes,10,1992, 245.
[10] Tarte P.: Spectrochim. Acta, 23A,1976, 2127.

CALCULATION OF BREAKDOWN THRESHOLD PARAMETERS TAKING INTO ACCOUNT THE SELF-FOCUSING OF LASER IRRADIATION ON DYNAMIC SHOCK LENSES IN GLASSES

S. Gribin and **B. Spesivtsev.**
State Technological University of Plant Polymers, Russia.

V. Dotsenko
S.I.Vavilov State Optical Institute, Russia.

Abstract

Mathematical and physical models have been suggested of the phenomenon, explaining the lowering of the damage threshold of a transparent dielectric by self-focusing of light energy on the refraction index dynamic inhomogeneity (RIDI or shock lens), arising in the compression wave which appears in transparent media around absorbing inhomogeneities (AI) in the process of their absorbing a part of light impulse. On the basis of this model the dependence have been obtained connecting parameters of light impulse, physical and chemical properties of the glass and absorbing inhomogeneity characteristics with the level of local concentration of light energy.

Keywords: Mathematical and physical models, self-focusing of light energy on shock lenses, power impulse laser.

I. INTRODUCTION

The glass optical strength (OS), or the glass damage threshold depends on both laser pulse parameters and glass properties.

One can conventionally divide "intrinsic" and "impurity" OS. The intrinsic OS is defined by glass matrix free from absorbing inhomogeneities (AI) and is described by the multiphoton absorption (electron avalanche) model [1,2,3]. The impurity OS is defined by AI properties or by the totality of AI and glass properties. It is described by the thermal explosion model [4,5,6,7] and its modifications, by dynamic lenses [8,9].

Based on the latter model, the present work is devoted to the calculation of light power local concentration in the shock lens caustic and to the discussion of the limits of the model's application.

II. MODEL

The presented model includes the following fundamental statements:

1. The transparent dielectric can contain the light absorbing AI (0.01-10) micron in size, such as metal drops ,carbon dust, dye segregation zones [10].

2. Under conditions of laser impulse initial part absorption by the AI occurs its fast heating with forming the region of plasma. Fast expanding of plasma produces elastic compression in the surroundings. It leads to short time changing of refractive index (RI) around the AI. These short living regions with changed refractive index would be named the dynamic inhomogeneities of the refractive index (DIRI) or a shock lenses.

3. Focusing or defocusing of the rest of the laser impulse takes place depending on optical properties of medium.

4. Under conditions of forming focuses or caustics power of laser impulse can an essentially exceed initial value in front of lens Fig.1.

a. At the first stage (let's name it hydrodynamic) it's to solve the problem of light absorption by the Al and to define spatial and temporal distribution of the refractive index around the AI.

b. At the second stage (optical) it's to calculate change of the laser radiation field on defined refractive index distribution according to laws of optics of inhomogeneous media.

Formulation of the problem mentioned above has some uncertainties. So the shape, sizes, physic-chemical properties of the AI and its orientation are unknown beforehand. That makes the process of the transparent dielectric damage stochastic.

Assume that the AI is a sphere with radius Ro. Laser radiation is spatially homogeneous and the medium around the Al is isotropic. The absorbed energy is supposed to distribute within the AI uniformly. It's also assumed that interaction between the AI and surroundings is limited by the processes of pressure and mass velocity balance at the boundary of the fast heated AI. The energy of the Al radiation is supposed to absorb in a thin layer around the AI.

The physical model for the process under considerations the model of perfect elastic liquid, which contains a small sphere volume evenly heated by means of the light absorbing. The model describing the parameters of the shock waves is based on the assumption that the flow is isentropic. Mathematical model was presented in the paper [9].

III. RESULTS AND DISCUSSION.

Fig 2 show examples of calculation of parameters pressure waves outside plasma region for quarts. Fig 3 shows relative change of RI around plasma region (shocklens) at the moment ti/2. The refractive index for fused quartz n is adopted in the form:

$$n(q) = no(q) + dn/dp * P,$$

where: no(q) =1.458 ,dn/dp = 0.00083 /96.2 MPa (from tab.1 [9]), P - from Fig. 2.

Light deformation on the shocks lens is calculated on the base of the ray theory [11].

Fig. 4 shows ratio of energy density at the optical axis behind the lens W and energy density in front of the lens Wo depending the distance L from the lens center at the moment ti\2. Diffraction angle u for this lens estimated according to [11] u = 0.61 (h / r) is less than 0.0122 rad. where h - wavelength, r - radius of shock lens. It is seem that value W/Wo can increase in hundreds times.

IV. TYPE OF THE SHOCK LENS

Generally dependence of dielectric's refractive index in the region of absorption inhomogeneity on pressure can be described by the following equations [12]:

$$dn/dp = q^* dz/dp + r^* dz/dp$$

where the first term characterizes change of the refractive index when density q rises, the second term describes change of the refractive index due to reduction of polarization ability z and change of effective radius of molecules with pressure change.

Such complicated dependence of n(P) on properties of transparent media explains the fact that few success has been achieved in determining correlation between physic-chemical properties of matter and the value of the optical breakdown threshold.

Data on change of refractive index of polymers, glasses and liquids under conditions of shock growth of pressure in literature are small in numbers. Nevertheless value of n = f(P) can be made on the base of change of n on conditions of static growth of pressure [12.13,14] with temperature 298 K. (Tab.1 [9]).

In general case function n(P) can have minimum and maximum and the problem what kind of lens would be formed around AI must be solved for each separate type of material.

When lager impulse duration increases thermo - optical properties of the matter increase their influence on the change of RI. For each matter there is such a duration of the laser impulse that change of n around AI is determined by n(T) i.e. "thermal lenses " are forming around AI. According to our estimations transition from "shock lenses" to "thermal lenses" can take place when laser impulse duration is within (100 -1) micro sec. for different types of the matter.

It should be noted that change of lens type in same matters can cause transition from defocusing lenses to focusing ones (MgO, Diamond) and vice versa [12].

V. APPLICABILITY OF THE SHOCK LENS MODEL

Generally RI of the shock lens n and threshold damage power density J(*) = W(*)/ti in presented model depend on some parameters of the transparent matter and laser impulse: n = f{ P(a, B,k, Wo,ti),dn/dp, r }, r = f(a,ti, Ro), where a, B,k - velocity of sound and constants of shock adiabatic of the transparent medium, Wo and ti - energy density and impulse duration, dn/dp - piezo- optical coefficient of the matter, Ro - radius AI. J(*)=f(I,Z, Ro,h,n), where I - sample thickness, Z - breaking point of the sample, h - radiation wavelength.

Recommended sequence of the account of the parameters of medium and laser impulse is as follows:

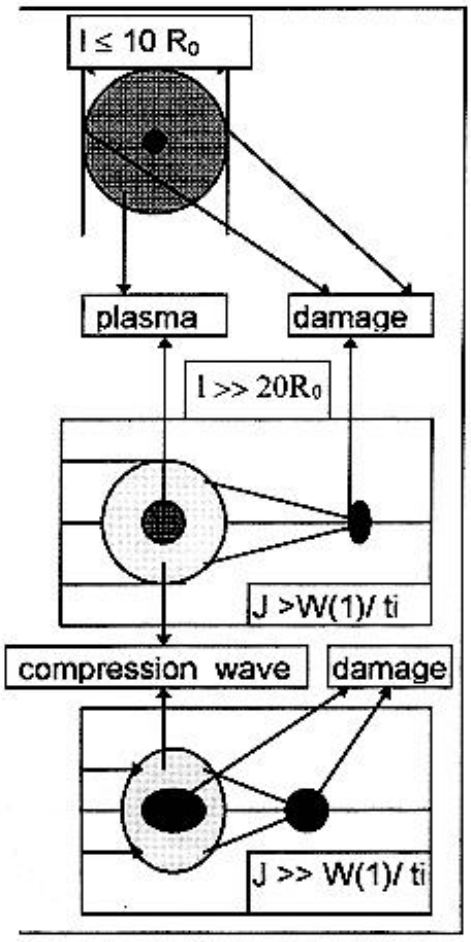

1. Mechanism N1:
If I<(10-20)Ro then damage is determined by AI or medium evaporation. J1(*)= f(Tg, K, C, S), where Tg - temperature of evaporation of AI or medium, K - temperature conductivity the matter, 2 - specific heat of AI,S-specific vaporization heat AI or medium.

2. Mechanism N2:
When I >> 20Ro and J > W(1)\ti, damage takes place in focus of the shock lens forming around plasma region. In this case J2(*)=f{n(P(a,B,k,),dn/dp,r}, r = f(a,ti, Ro). There W(1) is minimum damage energy for a single impulse.

3. Mechanism N3:
If I >> 20Ro and J >> W(1)\ti then besides mechanism N2 there can be damage of the matter due to wall damage around plasma region when plasma pressure P on the walls exceeds compression break point Z, P > Z. In this case J3(*) = f{ P(a, B,k,),Z}.

It is evident that use of mechanism N2 is limited in single laser impulse duration for "short " impulses as well as for "long" one. "Short" impulse limitation is cased by the fact that within impulse a rather big lens (compared to wavelength) must be formed. Otherwise diffraction

scattering would prevail. The same cause restricts thickness of the sample "Long" impulse limitation is caused by heat dissipation from plasma zone and forming " thermal " lens.

VI. CONCLUSIONS

1) Mathematical and physical models have been suggested of the phenomenon, explaining the lowering of the threshold of bulk damage of a transparent dielectric by self-focusing of light energy on the refraction index dynamic inhomogeneity (RIDI or shock lens),arising in the compression wave which appears in transparent media around absorbing inhomogeneities (AI) in the process of their absorbing a part of light impulse.

2) It is shown that characteristics of a shock lens and density of damage power are determined by a complicated influence of some parameters of transparent medium and laser impulse.

3) Sequence of recommended account of parameters of medium and laser impulse concerning the problem of damage is presented.

4) The statement concerning a role of heat lenses in "long" impulse medium damage is formulated.

5) On the base of the presented model it is formulated a statement that there are ways to rise a damage threshold of a transparent matter destruction:

a) to get the matter with no AI;

b) to make optical detail using matter with $dn/dp < 0$.

c) to make coating of components using matter with $dn/dp < 0$ and sound velocity exceeding sound velocity in the transparent medium.

REFERENCES

[1] Mednic P.M., Fain V.M.,Journ of Exper. and Theor. Phys. (Russia),1972,v.62,N 2,p.812.

[2] Epifanov A.C., Manenkov A.A., Prochorov A.M., Joum. of xper. and Theor. Phys.(Russia),1976,V.70.N2,p, 728.

[3] Rady J., Power Laser Radiation Effect, Moskow, Mir,1975.

[4] Butenin A.Ya., Kogan B.Ya., Kvant. Electr.(Sov) ,1971,v.5 p.143.

[5] Anisimov C.I., Makshantsev B.I., Journ. of Phys. Sol. State (Russia),1973,v.15, N 4, p.1090.

[6] Aleshin I.V., Anisimov S.I., Bonch-Bruevich A.M., Imas Ya.A., Komolov V.L., Journ. of Exper. and Theor. Phys.(Russia),1976,v.70,N 4,p.1214.

[7] Koldunov M.F.,Manenkov A.A.,Pokotilo I.L., Filimonov D.A.,Izv.Akad.Nauk. SSSR Ser. Fis. (Russ),1989,v.53, N3, p.439-464

[8] Gribin S.V., Spesivtsev B.I.,Proc.Vlll All Union Conf. on Interaction of Optical Radiation with Substance, Leningrad, 1990,v.1,p.156

[9] Gribin S.V., Spesivtsev B.I., Proc. 27 Annual Symposium on Optical Materials for High Power Lasers, Boulder, USA, 1995

[10] Dmitruk AV., KarapetyanG.O., MaksimovL.V. “Jurnal Prikladnoi Spektroskopii. (Sov),1975, v.22, N 1, p.153 -182.

[11] Born M.,Wolf E., Principles of optics, M,Nauka,1970,855 p.

[12] loffe B.V., Refraction measure methods in chemistry, Leningrad, Himiya,1983, p.352.

[13] Rosen J.S., J. of Chem.Phys; 1949, v.17, N12,p.1192.

[14] Kormer S.B., Jom. Sucsess of Phys.Sci. (Sov), 1968, v.94, N4,pp.641-687.

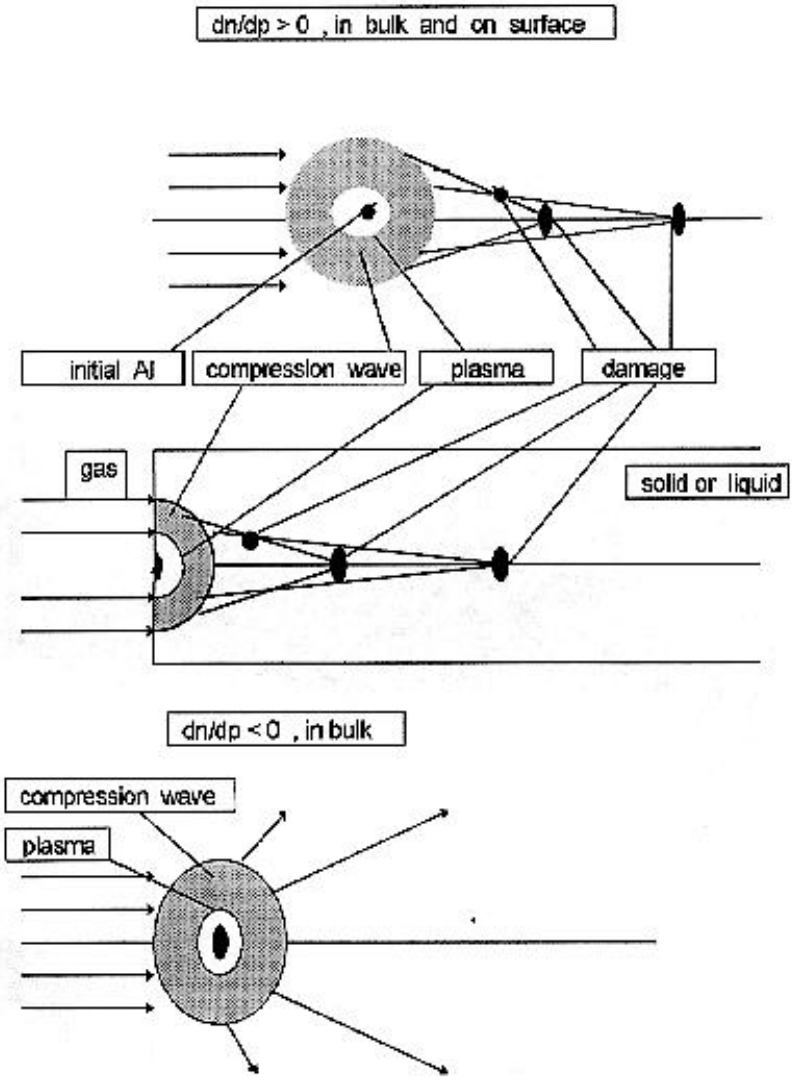

Fig.1. Model of the self-focusing of laser radiation by dynamic lenses.

Fig.2 The dependence of pressure P as function of distance r outside plasma region for moments ti/2. Where: B =1000 MPa, Ro - radius of AI -1 micron, Wo - energy density -15 J/sm^2, ti - impulse duration -10 nsec.

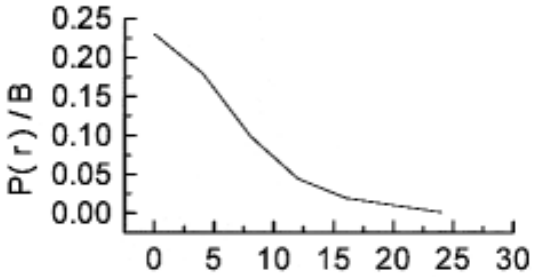

Fig.3 The ratio of (n -no) / no as function of distance inside compression wave region for the moment ti / 2. ti, Wo, B ,Ro are shown at Fig 2.

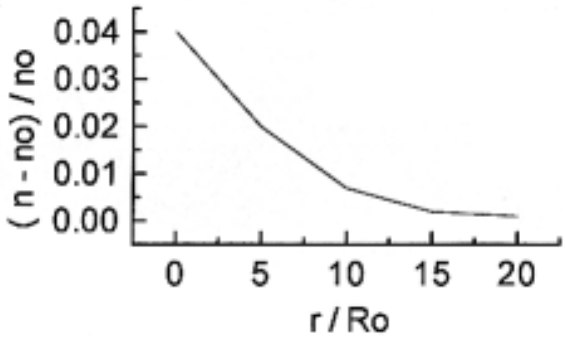

Fig.5 Ratio energy density at the optical axis after shock lens W and energy density behind lens Wo versus distance from the center of lens L, t=ti/2. Wo, B, ti, Ro are shown at Fig 2.

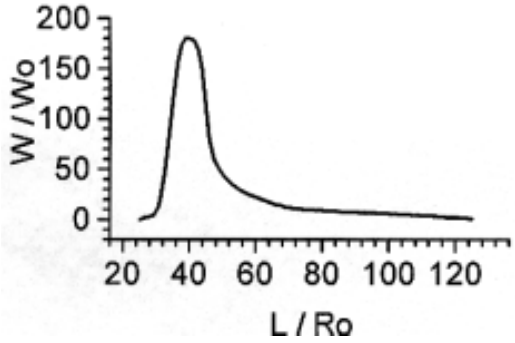

COMPOSITION AND STRUCTURE OF SLAG GLASSES FROM THE CaO-MgO-SiO_2 SYSTEM*

V. Vulkov, N. Delchev
University of Chemical Technology and Metallurgy, Bulgaria

Abstract

In general, the dependences established on the influence of the chemical composition of the glassy slags on their hydration ability do not show always good results. In fact, they do not determine but forecast the formation of definite structure of slag glasses, or based on an empirical way allow to predetermine their properties as well as to use the results obtained in the practice.

The report presented exhibits the results obtained from the study on the influence of the chemical composition upon the formation structure of slag glass. The glasses from the CaO-Al_2O_3-MgO-SiO_2 system in the limits of variation of CaO from 38% to 50%, Al_2O_3 from 6 to 23%, MgO from 4 up to 18%, SiO_2 from 28 to 38% have been investigated.

The molecular mass distribution, the average extent of polymerization and the mean alkalinity of silicon-oxygen anions in dependence on the cation-anion forming oxides have been determine on the basis of the method of molibdenum kinetic analysis. The results obtained have been compared to those produced for the hydration activity of the studied slag glasses.

It is established that the structure affects the hydrolysis and the hydration activity of slag glasses while the structure itself is determined by the initial chemical composition of the melt as well as by the fabrication conditions.

---

* Full manuscript not available at the time of printing

COMPUTER ESTIMATIONS FOR DARKENING OF GLASSES CONTAINING CuCl MICROCRYSTALS*

A. Efremov and **M. Vasiljev**
S.I. Vavilov State Optical Institute, Russia

Abstract

Photochromic glass with CuCl photosensitive microcrystals are well known and widely used for investigation in extion light absorption, kinetics of darkening and relaxation, and so on.

The aim of the work is to improve the model suggested by Ruppin previously for spectrum of darkening calculation for different CuCl structure at various temperature.

The consideration is concerning to the spectra dependence on size of CuCl microcrystals, size, shape and volume fraction of photo-induced copper sub particles in CuCl microcrystals. These and other input parameters are used to fit the experimental spectra with model calculations. The copper refractive index temperature dependence so as particles size correction are taken into account. The refractive index of CuCl crystals with copper inclusions are estimated in frame of effective refractive index theory. Mie and Aden-Kerker theories are in use for light absorption and scattering calculation.

The estimated data demonstrate the structural changes in CuCl microcrystals affect by UV irradiation at low ordinary temperature.

---

* Full manuscript not available at the time of printing

COMPUTER SIMULATION STUDY OF STRUCTURE OF HIGH-DENSITY AMORPHOUS ICE

S. Ozawa[1], A. Iijima[1], H. Tanaka[1], Y. Sasajima[1] and **Y. Hiki[2]**

1. Ibaraki University, Japan
2. Tokyo Institute of Technology, Japan

Abstract

In order to study how the pressure-induced amorphous structure is different from the usual amorphous structure formed by quenching, Monte Carlo computer simulations of high-density amorphous ice are carried out. The modelice crystal Ih is compressed 1-20% in linear dimension at 77 K. The structural change is studied by using pair distribution function (PDF). The results of the computer simulation are compared with those of the real high-pressure experiments. It is shown that the shape of PDF obtained from the 5% compression is similar to that of experimental PDF.

l. INTRODUCTION

Glass structure or amorphous structure of materials usually occurs when they are quenched from their high temperature states, i.e., liquids or gases. For the production of amorphous state, there is another interesting method in which material is compressed at high-pressure. This method has been used for materials which have sparsely packed microscopic structures, e.g., ice or silica [1]. Mishima et al. compressed ice crystal Ih at pressure 10 Kbar and at temperature 77K and obtained high density amorphous ice [2-5]. They studied structure of the amorphous ice by X-ray method and discussed the data in terms of pair distribution functions. In the present paper, we carry out Monte Carlo (MC) computer simulations to study the formation process of high-pressure amorphous ice. The relaxation process and the resulted structure of high-pressure amorphous ice are discussed on the basis of microscopic information obtained from the computer simulation.

The authors are also planning to carry out computer simulations of deposition of water molecules on a cold solid surface. By comparing the two lands of amorphous formation, quenching and compressing, we expect to answer, through the computational approach, to the old and popular but still challenging question "What is amorphous?" This report is the first step to the strategy and deals with the high pressure computer simulation of amorphous ice.

2. COMPUTATIONAL METHOD

In the present simulation, we use a canonical Monte Carlo method [6]. This method generates a Markov chain of states. Whatever state is adopted for the start of the Markov chain, we can reach a series of states which forms a collect canonical ensemble. It is ensured that we can have collect microscopic states at a given temperature by this method. The procedure of MC is sometimes

called as MC annealing. There are some versions for the canonical Monte Carlo method. Here, we use Metropolis Monte Carlo algorithm [7]:

1) Specify an initial configuration of the system.
2) Generate a new configuration with the aid of a random number generator.
3) Compute the energy change ΔH associated with the transition.
4) If $\Delta H < 0$, accept the new configuration and return to step 2.
5) Compute $\exp(-\Delta H / k_B T)$.
6) Generate a random number R.
7) If $R < \exp(-\Delta H / k_B T)$, accept the new configuration and return to step 2.
8) Otherwise, retain the old configuration as the new one and return to step 2.

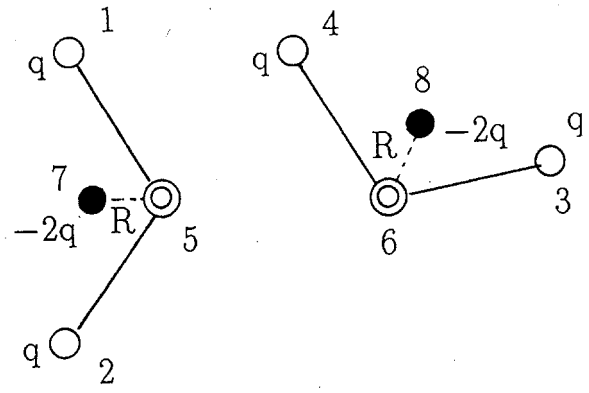

Fig. 1 Interaction of two water molecules; an open circle is a proton with charge (+q), a filled circle is a fictitious charge (-2q) and a double circle is an oxygen atom.

There are various types of expressions for intermolecular potentials of water. Here, we use a type reported by V.Carravetta and E.Clementi [8]. We call it CC-potential in this paper. It is a pairwise potential. It neglects the internal freedom of molecular motion. In other words, the molecule is treated as a rigid body. The butterfly motion, twisting motion and dissociation of the molecule are not taken into account. Within this framework, we,try to simulate structure of water system. The CC-potential Φ is expressed as follows:

$$\Phi = q^2(1/r_{13} + 1/r_{14}1/r_{23} + 1/r_{24}) + 4q^2/r_{78} - 2q^2(1/r_{18} + 1/r_{28} + 1/r_{37} + 1/r_{47})$$
$$+ a1 \exp(-b_1 r_{56}) + a2[\exp(-b_2 r_{13}) + \exp(-b_2 r_{14}) + \exp(-b_2 r_{23}) + \exp(-b_2 r_{24})]$$
$$+ a3[\exp(-b_3 r_{16}) + \exp(-b_3 r_{26}) + \exp(-b_3 r_{35}) + \exp(-b_3 r_{45})]$$
$$- a4[\exp(-b_4 r_{16}) + \exp(-b_4 r_{26}) + \exp(-b_4 r_{35}) + \exp(-b_4 r_{45})]$$

Here, r_{ij} is the distance between i and , j particles. The numbers are labeled to atoms and fictitious charges in water molecules (see Fig.l). The parameters are derived from the ab inatio study of water dimer [8]: $q^2 = 0.998565 \times 10^{-18}$ [J·A], R = 0.2499356[A], $a_1 = 3157.08 \times 10^{-18}$ [J], $a2 = 24.8732 \times 10^{-18}$ [J], $a3 = 14.6940 \times 10^{-18}$ [J], $a4 = 3.18140 \times 10^{-18}$ [J], $b_1 = 4.7555$ [A^{-1}], $b_2 = 3.8446$ [A^{-1}], $b_3 = 3.1763$ [A^{-1}], $b_4 = 2.4806$ [A^{-1}].

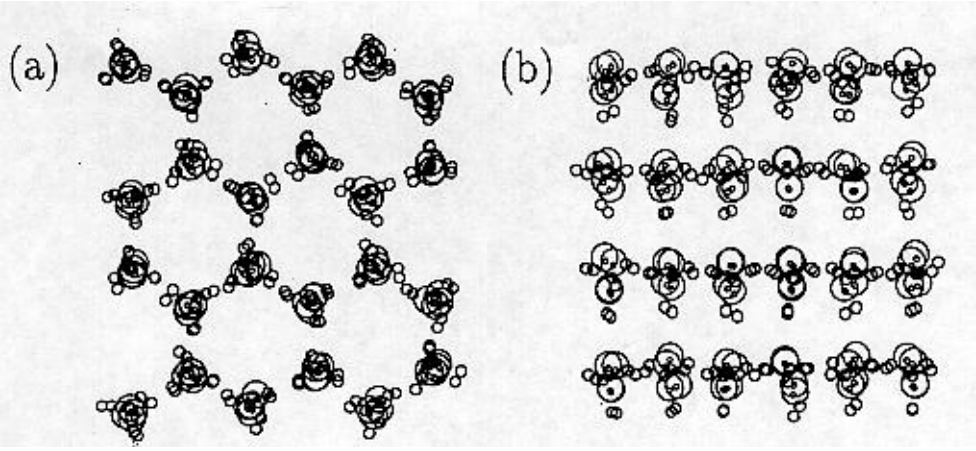

Fig. 2 A configuration of ice Ih at 77K viewed in c-direction (a) and a direction (b). The large circle represents oxygen atom, the medium size circle is proton and the small circle is the ficticious charge.

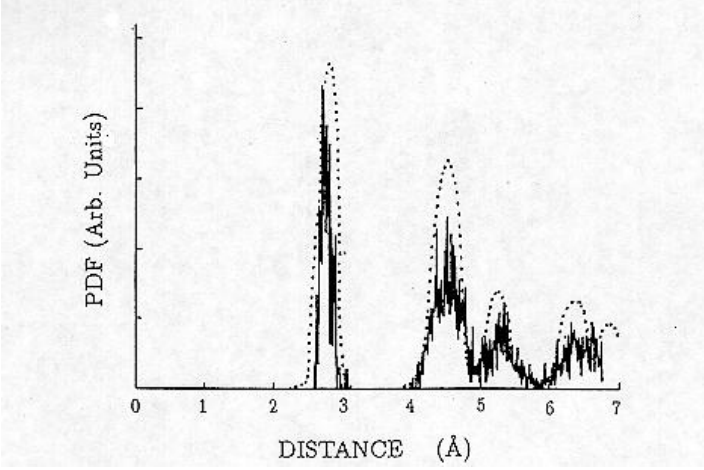

Fig. 3 PDF of the state Ih at 77K, the solid line shows the result of the computer simulation and the dotted line shows the X-ray result.

In the MC simulation, we calculate the total potential energy of the modeled water system. The calculations are done before and after a trial movement of a water molecule. The difference of the enegy values ΔH is used in the MC procedure. For this purpose, we sum up the values of the potential function over all the particle pairs in the system. We do not have much difficulty for the Born-type short range repulsive interaction, since the summation converges rapidly. However, for the Coulomb-type long-range interaction, the direct summation has no sense. We must use a rather tricky method named as the Ewald's method [9,10]. The method separates the sum into a real space shielded term and a reciprocal space term. The summation for each of the terms converges satisfactorily. The real space term is expressed by a complementary error function $\mathrm{erfc}(\alpha r)$, where α is a shielding parameter and r is the distance between constituent particles of

molecules. In the present simulation, we take a recommended value α = 0.431 [$Å^{-1}$]. For the convenience of efficient calculation of total potential energy of the system, the conventional minimum image method is used for the real space sum; the cut-off length is the half of the system size. The other supplemental technique used here is the book-keeping method which saves CPU time quite dramatically for large system [6].

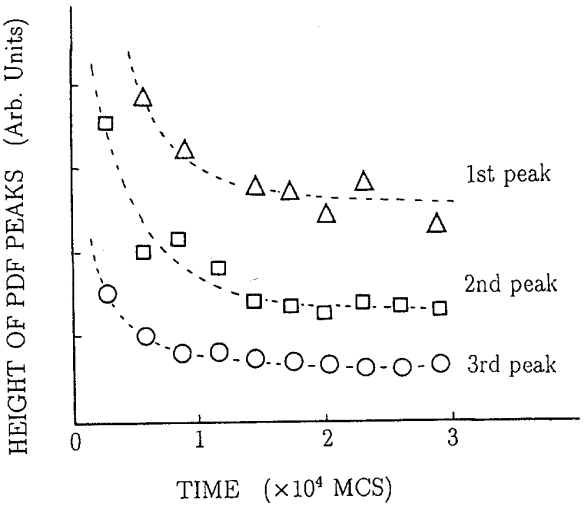

Fig. 4 Change of peak height of PDF in the process of MC annealing at 77K.

3. COMPRESSION EXPERIMENTS

We are trying to simulate high-pressure experiments which were carried out by Mishima et al. They pressed ice crystal Ih at 77K. The first step of our work is to obtain a microscopic configuration of ice Ih at 77K. This is done by the MC annealing described just before. We arranged water molecules precisely on the sites of proton ordered ice Ih and let them move according to the MC algorithm. The number of water molecules in our system was 96 or 768. Here, both translational and rotational movements of water molecule were allowed to occur. After a suitable length of MC calculation, in this case 3.13 x 10^4 Monte Carlo Steps (MCS), we got an aimed configuration. Figures 2(a) and (b) show the molecular configurations of ice Ih at 77K viewed in c-direction and in a-direction, respectively. Figure. 3 shows the results of PDF obtained from the configurational data. The solid curve represents the PDF obtained from the simulation and the dotted curve shows the PDF from X-ray study. We see fairly good agreement between the two curves. It is worthwhile to note that the computational PDF was determined from the position data of oxygen atoms alone. The proton data were not used there, because X-ray is not so sensitive to proton as compared with to oxygen. Before we proceed to compression computer experiments, we have to study relaxation time of the above MC annealing. For this purpose, we calculated PDF at various stages of the annealing process, and measured the height of peaks in the PDF curves. The results are shown in Fig.4. It is seen from this figure that the relaxation attains nearly at a time 1 x 10^4 [MCS]. The annealing time adopted in the present study is about three times longer than this value. The computational results obtained so far seem reasonable, which suggests that the used model nicely works in our system.

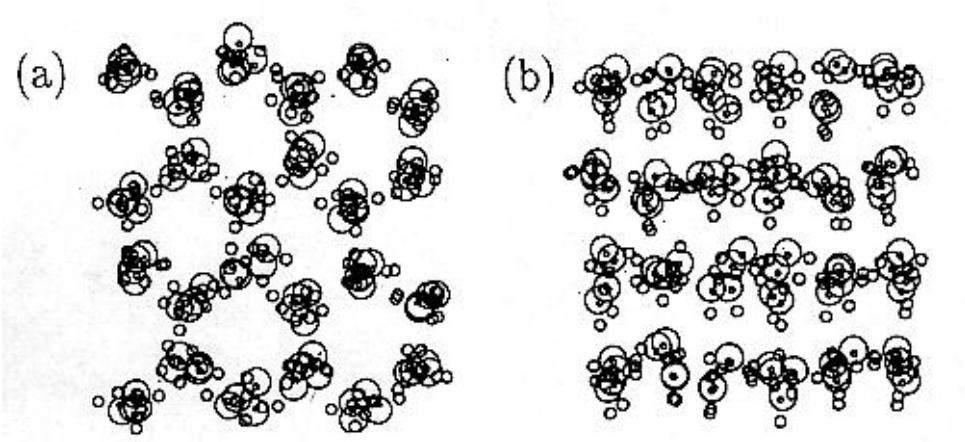

Fig. 5 A configuration of amorphous ice viewed in c-direction (a) and a-direction (b). The compression rate is 5% in linear dimension.

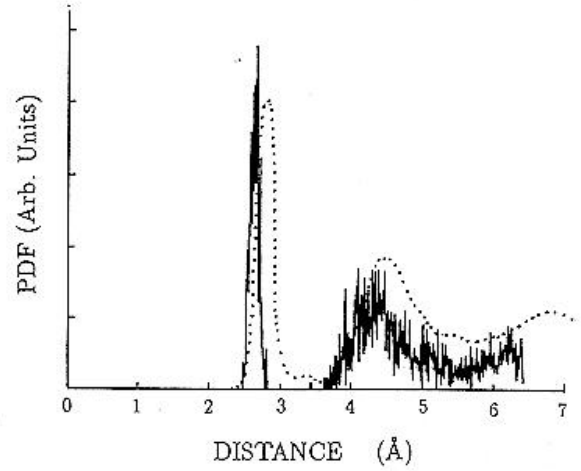

Fig. 6 PDF obtained from the configuration in Fig. 5.

Now, we describe the compression experiment of the model crystal Ih at 77K. The compression was done instantly and in isotropic manner, namely, a geometrically similar arrangement of molecules to that of the state obtained in the above MC annealing was adopted as the initial configuration of the MC experiment. All the distances between water molecules were reduced at a certain rate. As the result, the system size was also reduced at the same rate. By the same procedure as in the MC annealing, we can get an aimed microscopic state, this time, a configuration of the compressed ice. Note that direct controlling parameters in our simulation are the temperature and the volume (system size). The pressure of the system can be calculated secondary from configurational data with the aid of the Virial's formula [5]. Figure 5 shows the configuration obtained by the MC relaxation after the 5% compression in linear dimension. The time needed for the relaxation is almost same as that in the case shown in Fig. 4. The PDF

determined from the compressed state is shown in Fig. 6. The dotted line is the PDF curve obtained from the X-ray study of high-density amorphous ice. It is seen that the shape of the computational curve is similar to that of the experimental one. It should be noted that the third nearest neighbor peak is not seen here. The similar computer experiments were carried out at different compression rates ranging 1 - 20%. Much disturbed structures were seen at high compression rates. It was difficult to determine a critical compression rate for the occurence of amorphous ice. The structual change by pressure seems to occur continuously. Authors consider that there is no sharp phase transition from ice Ih to the amorphous phase.

4. DISCUSSION

What is amorphous ice? A possible answer given by the X-ray experiment is that we can produce high-pressure states which have diffused X-ray diffraction patterns. The PDF curve obtained from the X-ray data have a clear nearest neighbor peak, a diffused second nearest neighbor peak and no other clear higher ordered peaks, which shows that the high-pressure states have a short-range order but not a long-range order. Since we have observed the similar shape of PDF also in the computer simulations, we seem to have succeeded in obtaining high-pressure or high-density amorphous ice. It should be noted, however, that the obtained state was amorphous or not was judged only by the shape of PDF. Remember PDF was calculated from configurational data of oxygen atoms alone. This is related to the fact that X-ray is insensitive to protons and the experimental PDF also represents the oxygen configuration. In the present study, we try to compare the simulation data to the real experiment and we focused our attention to the analysis of the configurational data of oxygen alone. But the author consider that it is important to examine the configurational data of proton for the discussion of amorphous ice because the positions of proton are closely related to formation of hydrogen bonds, the bond breaking and the bond distortion. These elemental processes are needed for the occurrence of amorphous state. We must know what land of parameter is suitable for the description of proton configuration. And also we must look for experimental approach to detect proton state at high pressures. Another interesting work is to carry out computer experiment of deposition of water molecules on a cold substrate and obtain the PDF data to compare with the present results. So, we note that there remain many things to do experimentally or computationally for the full understanding of physics of high-pressure amorphous ice. The author are continuing this study and the related reports will appear elsewhere.

ACKNOWLEDGMENTS

The authors are indebted to the Information Processing Center of our university for using the facility of HITAC M-660L. The present study is partly supported by NTT Data Communications Systems Co.

REFERENCES

1. S.Tsuneyuki, Y.Matsui, H.Aoki, and M.Tsukada, Nature 339, 209 (1989).
2. O.Mishima, L.D.Calvert, and E.Whalley, Nature 310, 393 (1984).

3. O.Mishima, L.D.Calvert, and E.Whalley, Nature 314, 76 (1985).
4. Y.P.Handa, O. Mishima, and E.Whalley, J. Chem. Phys. 84, 2166 (1986).
5. E.Whalley, D.D.Klug, M.A.Floriano, E.C. Svensson, and V.F.Sears, J. Phys.[France] 48, Cl-429 (1987).
6. D.W.Heermann, Computer Simulation Method in Theoretical Physics (Springer-Verlag, Berlin,1990).
7. N.Metropolis, A.W.Metropolis, M.N. Rosenblath, A.H.Teller, and E.Teller, J. Chem. Phys. 21, 1087 (1953).
8. V.Carravetta and E.Clementi, J. Chem. Phys. 81, 2646 (1984).
9. M.D.Morse and S.A.Rice, J. Chem. Phys. 76, 650 (1982).
10. M.Born and K.Huang, Dynamical Theory of Crystal Lattices (Clarendon, Oxford, 1954).

CREEP AND RECOVERY OF A THERMALLY TEMPERED SODA-LIME SILICATE GLASS PLATE AT ROOM TEMPERATURE

Rene GY
SAINT-GOBAIN RECHERCHE, France

Abstract

Better knowledge of the long-term behaviour of glass is required to ensure safe use of permanently loaded glass beams for structural application in buildings. For this purpose, the creep-recovery behaviour of a large thermally tempered thick glass plate was investigated in a more than one year long experiment. From a viscoelastic analysis of this experiment, it is shown that the observed creep of glass at room temperature is not viscous in nature but is a delayed elastic effect. No true viscous deformation is measurable. A long-term extrapolation of this behaviour is attempted from which it is concluded that the deformation of a permanently loaded glass structural element should increase by less than 3% over 50 years. It is also concluded that the attenuation of the residual stress field intensity in the tempered glass should also be less than 3% over the same period.

I. INTRODUCTION

Better knowledge of the long-term behaviour of glass is required to confirm that permanently loaded glass beams can be used safely for structural applications in buildings. Ageing glass under permanent loadings may be detrimental because of static fatigue. It is known that this phenomenon can lead to delayed failure. Static fatigue is basically caused by the subcritical crack growth that can take place in glass, even in a weak tension field. The load below which glass would be free of fatigue is not well known and moreover, static fatigue which is very sensitive to the environment is accelerated in particular by temperature and atmospheric humidity. Since control of the environment over very long times is not practical, an upper limit to load for the safe use of permanently loaded glass structural elements is difficult to determine. A convenient way to overcome these difficulties could be the prescription of thermally tempered glass for such applications. Since in a properly thermally tempered glass plate, the critical flaws always originate at the surface or edges and since surface and edges are in a state of compression, an immunization against static fatigue is obtained, provided that the permanently applied tensile stress does not exceed the original residual compressive stress in tempered glass. In this case, the design of structural glass elements should be quite simple. A question that arises however is to know whether any significant creep in permanently loaded tempered glass will take place over a very long time and whether the quenched residual stress field will be maintained. The aim of the present paper is to investigate these questions in the case of thermally tempered silico soda-lime glass.

II- EXPERIMENTAL

II-1 Test-sample

The test-sample is a 4 m long, 19 mm thick glass plate that has been tempered in a conventional horizontal tempering installation. It is 621 mm wide. The residual surface compression is 120 MPa, measured with the Epibiascope [1]. Compression of the edge, averaged over the thickness is 80 MPa, measured with a Babinet compensator.

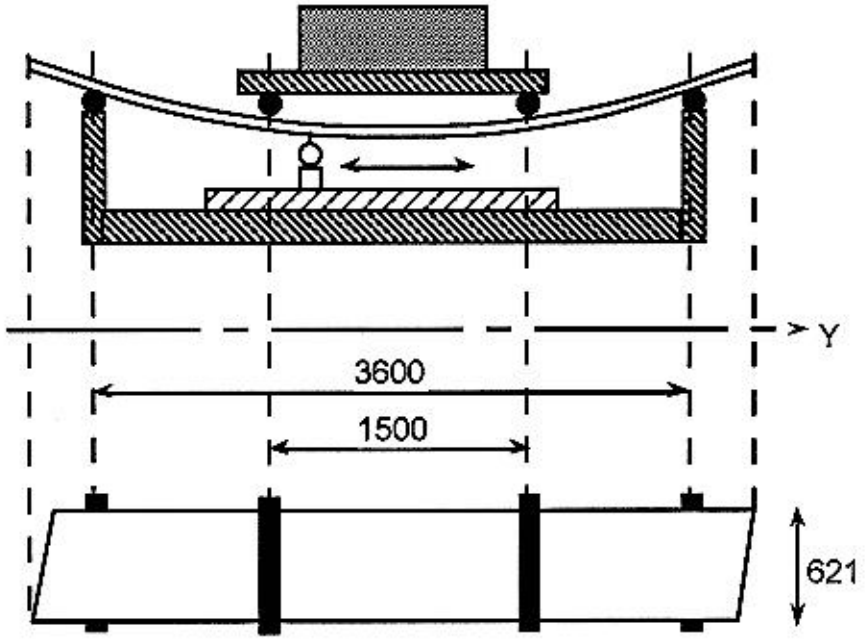

Figure 1.

II-2 Loading

A specific four point loading device has been built and a finite-element calculation of the maximal applied stress carried out. According to this calculation, the glass weight plus an external applied load of 4000 N, lead to a maximal tensile stress of 72 MPa. This is below the residual compressive level and hence it should prevent the beam from suffering from static fatigue during a long experiment. The supporting and loading cylinders are inserted into roller bearings in order to minimize the membrane effects and to be as close as possible to the pure bending state. The applied load was made with concrete bricks enveloped with a tight polyethylene film. This ensures a negligible variation in the loading during the long experiment. Figure 1 is a schematic view of the device.

II-3 Measurements.

A rectified heavy base-plate, 1.5 m long is layed below the loaded test-sample. A moving displacement sensor (LVDT) allows the deflection of the beam with respect to

the base to be recorded along the Y-axis, in the middle of the beam's width at 10 equidistant points. An adjustment of the recorded data with a second order polynomial allows the beam curvature to be derived. Such an identification of the curvature is possible since it can be considered as roughly constant along the inner span in the four-point bending apparatus. By considering the second derivative of deflection, and not directly the deflection itself, one expects to eliminate any artifact, i.e. any additional creep originating for instance from the supporting points where concentrated loads are applied. Recording one set of data along the inner span took about 1 minute. The first record took place about 2 minutes after the loading. Measurements were performed for 200 days at increasing time intervals. The beam was then unloaded as quickly as possible, and the first record after unloading took place two minutes later. Again, measurements were performed for 200 additional days, at again increasing time intervals. The temperature was not controlled. Its variation from one measurement to the other is in the range 15-25^{o}C. The corresponding relative variation of the curvature is 10^{-4} (thermoelastic effect).

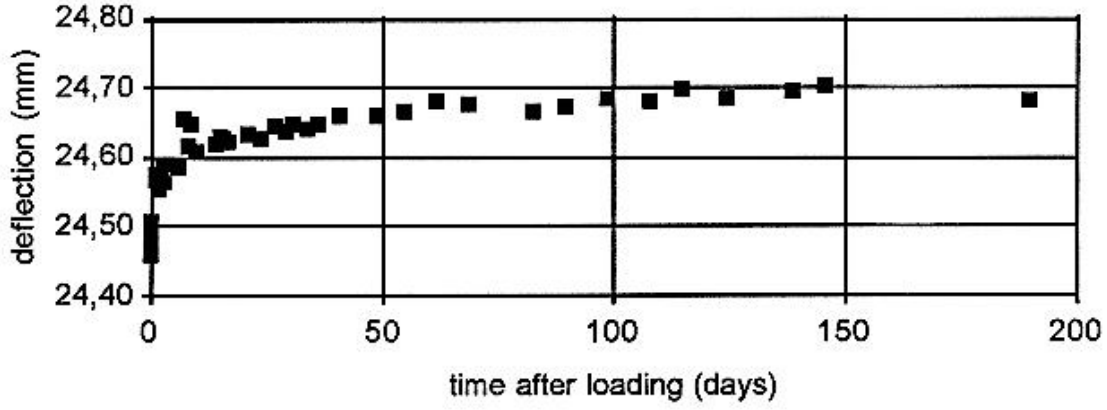

Figure 2.

II-4 Results

In Figure 2, the maximal deflection over the scanned length is plotted as a function of time. Figure 3 is the plot of the recovery of the deflection.

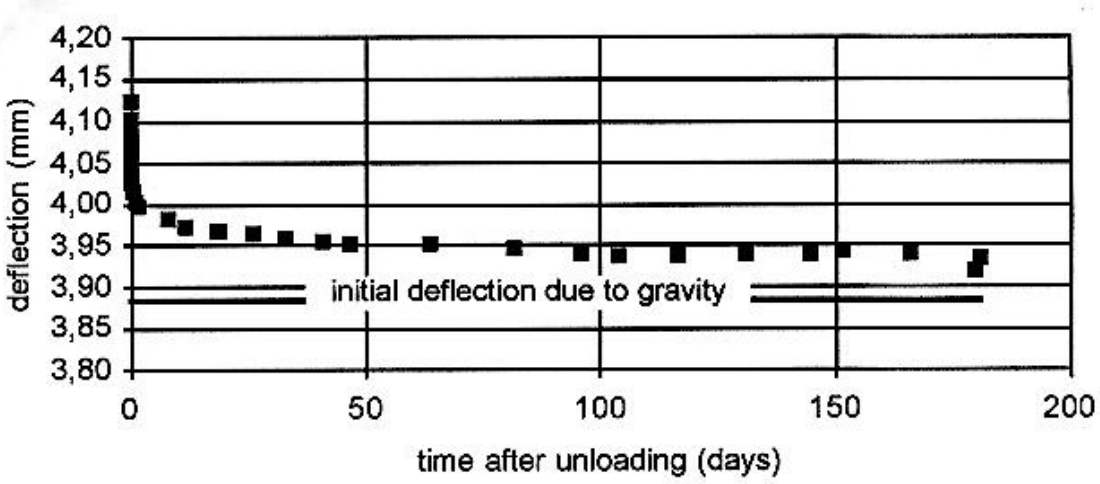

Figure 3.

III- DISCUSSION: VISCOELASTICITY ANALYSIS

III-1 Nature of the creep.

From the general expression of the viscoelastic compliance [2], the beam's curvature K during the creep phase can be termed:

$$K(t) = K_0 + (K_\infty - K_0)(1 - \Phi(t)) + K_0(t/<\tau>) \quad (1)$$

with $(K_\infty - K_0)/K_0 = <\tau^2>/<\tau>^2 - 1$ (2)

where t is time, K_0 is the instantaneous elastic curvature, K_∞ is the total elastic curvature, Φ the retardation function, $<\tau>$ the mean relaxation time, $<\tau^2>$ the mean squared relaxation time. During the loading phase, the applied loading as well as the gravity contribute to the beam curvature K(t):

$$K(t)=C(t)+G(t) \quad (3)$$

where G refers to the curvature due to gravity and C to that due to the applied load. According to the finite-element numerical simulation, G≈K/6 in the present experiment. A general expression for the beam curvature k(t), also valid during the recovery phase is

$$k(t) = K(t) - H(t - t_1)C(t - t_1) \quad (4)$$

where H is the step function, t_1 the duration of the loading phase. A widely used, approximate, but convenient representation of the retardation function is:

$$\Phi(t) = \exp(-(t/\theta)^b) \qquad (5)$$

At room temperature, t is very small compared to θ and $<\tau>$, b<1, hence $t/<\tau>$ is negligible when compared to $(t/\theta)^b$. From Eq.(1), an approximate expression for the relative change of curvature during loading is obtained:

$$\frac{K(t)-K_0}{K_0} \approx \frac{K_\infty - K_0}{K_0}(t/\theta)^b \qquad (6)$$

The best fit of the experimental data to Eq.(6) gives b=0.23. Moreover, since the order of magnitude of the ratio $(K_\infty-K_0)/K_0$ is not very different from 2 [2], an estimation of the magnitude of time θ can also be obtained: $\theta((K_\infty-K_0)/K_0)^{1/b} = 4.76\ 10^{15}$ s, hence θ is of the order of 10^{14} s. These numerical values for b and θ are very comparable to those of Pearson [3] for soda-lime rods at room temperature. Figure 4 is the relative variation in the beam curvature as a function of the time on a logarithmic time scale.

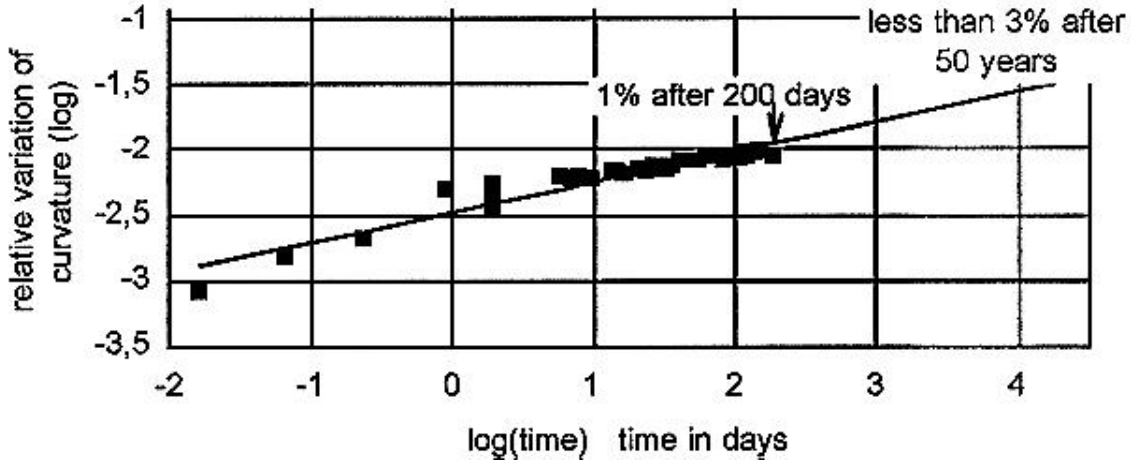

Figure 4.

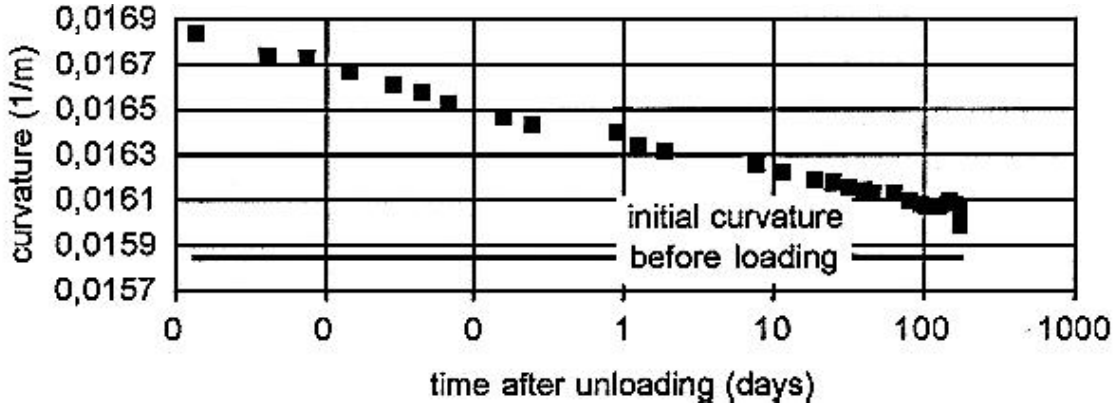

Figure 5.

An extrapolation up to 50 years, based on Eq.(6) is also shown. In Figure 5, the beam's curvature is plotted as function of the time on a logarithmic time scale, during the recovery. From Figure 3, it can be seen that 200 days after unloading, the beam has not recovered the initial deflection it had before loading; a difference of about 50 microns still remains. Since this is also true of the curvature, this difference cannot be considered to be an artifact of the apparatus. In the following, it is shown that it cannot be considered either as residual deformation due to viscous flow at room temperature: let us consider the curvature after the completion of the experiment (at time $2t_1$). It is given by Eq.(4):

$$k(2t_1) = K(2t_1) - C(t_1) \tag{7}$$

With the same approximations as above:

$$k(2t_1) \approx G_0 + G_0 \frac{t_1}{<\tau>} + (G_\infty - G_0)\left(\frac{t_1}{\theta}\right)^b + K_0 \frac{t_1}{<\tau>} + (K_\infty - K_0)\left[\left(\frac{2t_1}{\theta}\right)^b - \left(\frac{t_1}{\theta}\right)^b\right] \tag{8}$$

Finally, the following approximate expression for the change of curvature over the whole experiment (creep+recovery) is obtained:

$$\frac{k(2t_1) - G_0}{K_0} \approx \left(1 + \frac{G_0}{K_0}\right)\left(\frac{t_1}{<\tau>}\right) + \frac{K(t_1) - K_0}{K_0}\left[2^b - 1 + \frac{(G_\infty - G_0)}{(K_\infty - K_0)}\right] \tag{9}$$

On the right hand-side of this equation, the first term is the expected viscous effect. The second term, involving the magnitude of the increase in curvature during loading, can be estimated with: b=0.23, $(K(t_1)-K_0)/K_0 \approx 1\%$ and $(G_\infty-G_0)/(K_\infty-K_0)=G/K\approx$1l6 in the present experiment. This second term is found to have the same magnitude as the observed final variation in curvature (it may even be higher due to the possibility an overestimation of the instantaneous initial curvature G_0, since G_0 was not measured immediately after the beam has been set into the four point bending apparatus). The conclusion is that the first term on the right hand-side of Eq.(9) is negligible, and hence that no measurable true viscous deformation can take place in the present experiment.

III-2 Attenuation of tempering stress field at room temperature.

According to the above extrapolation, the apparent Young's modulus is less than 3% lower than the instantaneous one, after the glass has been maintained under constant load

over 50 years. On the other hand, according to the well-known Adams-Williamson formula, the intensity of the residual stress field is linearly related to the room temperature Young's modulus. However, since in a free tempered plate, glass does not undergo pure creep (constant loading), one cannot so readily conclude on the residual stress attenuation over 50 years. In terms of Laplace transformations the most general relationship between the retardation F and relaxation y functions is given by [2]:

$$1/\Psi(p) - 1/\langle\tau\rangle = p\left[\langle\tau^2\rangle/\langle\tau\rangle^2 - \left(\langle\tau^2\rangle/\langle\tau\rangle^2 - 1\right)p\Phi(p)\right] \quad (10)$$

It is again assumed that for the "short" duration that is considered, the relationship:

$$\Phi(t)\approx 1-(t/\theta)^b \quad (11)$$

is a valid approximation. By substituting the Laplace transformation of Eq.(11) into Eq.(10), then taking the inverse Laplace transformation, and taking Eq.(2) into account, an approximate expression for the relaxation function $\psi(t)$ is obtained:

$$\psi(t) \approx 1-((K_\infty-K_0)/K_0)(t/\theta)^b \quad (12)$$

From Eq.(12) it can be concluded that for short enough times, the magnitude of the stress relaxation rate is equal to the relative increase of the deformation due the delayed elastic effect over the same short time. In other words, after the glass has been maintained under constant strain over 50 years (which are considered as a "short enough" time at room temperature), the apparent Young's modulus is also less than 3% lower than the instantaneous one. However a free tempered glass does not experience a pure stress relaxation (constant strain) either. The attenuation of the residual stress field takes place under a complex combination of creep and relaxation. Since in both extreme cases, the Young's modulus is decreased by less than the same 3%, it is eventually concluded that a less than 3% attenuation of the tempering stress is expected over 50 years.

ACKNOWLEDGMENTS

S. Valladeau designed the experimental device and performed all the measurements. The author is grateful to C. Guillemet and J.Barton for their fruitful discussions and assistance with the manuscript.

REFERENCES

[1] C. Guillemet; Revue Française de Mecanique (1962) p.157-163.
[2] R. Gy, L. Duffrene, M. Labrot; J.of Non-Cryst Solids 175(1994) 103-117.
[3] R.W. Douglas; The Rheology of Glassy Materials - A General Survey; in Amorphous Materials, Papers presented to the Third Int. Conf. on the Phys. of Non-Cryst Solids, Sheffield, Sept.,1970.

CRYSTALLIZATION BEHAVIOURS OF THE GEL AND MELT-DERIVED GLASSES*

Volkan Günay
Istanbul Technical University, Turkey

Abstract

Since 1970's there has been a growing interest in the sol-gel processing of the glasses and glass-ceramics due to the some advantages of this process over the conventional melting of appropriate raw materials. Advantages of the sol-gel processing in glasses are especially apparent in coatings, fibres and composites.

In the present work, the crystallization behaviours of the gel and melt-derived glasses in MAS (MgO-SiO_2-Al_2O_3)and LAS (Li_2O-Al_2O_3-SiO_2) systems are given and compared. Gel-derived glass powders are produced by using alkoxides and salts as precursors to LiO_2,SiO_2,Al_2O_3, and MgO. The melt-derived glasses were produced by melting appropriate oxides and corbonates.

The results showed that the gel-derived glass powders crystallized faster than the melt-derived glasses, but the crystalline phases were identical. These behaviours could be attributed to the slight differences in chemical compositions, differences in the thermal histories between the gel and melt-derived glasses during preparation and to the different OH contents of the gel and melt-derived glasses.

---

* Full manuscript not available at the time of printing

SOME ASPECTS OF CRYSTALLIZATION IN THE GLASSES OF THE $ZnO-B_2O_3-SiO_2-PbO-Li_2O$ SYSTEM ASSIGNED AS VITRIFIED BONDS FOR TOOLS OF SUPERHARD MATERIALS

B. Stainewiez-Brudnik and **K. Majewska-Albin**
Institute of Metal Cutting, Poland
B. Procyk
University of Mining and Metallurgy, Poland

ABSTRACT

The paper presents the investigation results of some physical and chemical properties of the glasses in $ZnO-B_2O_3-SiO_2-PbO-Li_2O$ system, which are assigned as ceramic bonds mainly for CBN tools. The glasses of five sets, obtained by means of fritting were subjected to following investigations: DTA, density testing (by helium method). X-ray radiography, wettability testing (by sessile method) and TLEC in selected glasses the crystallization process was investigated as well as the effect of crystallization on some physical and chemical properties of obtained glass-crystalline materials.

1. INTRODUCTION

Glass is the material which has been known for centuries and applied in various branches of economy. The possibilities of controlling the properties of glasses contribute to the application of the same $ZnO-B_2O_3-SiO_2-PbO-Li_2O$ system both as vitreous solders to bind glasses with other materials (e.g. ceramic or alloys), as TV kinescope stoppers and also as components of ceramic bonds for tools made of cubic boron nitride.

The research project comprised:

- determining the basic physico-chemical properties of the obtained materials, i.e. density by means of the helium method, phase composition by means of the X-ray diffraction, thermogravimetric properties by means of the DTA method, wettability of backgrounds made of cubic boron nitride and some metals (nickel, cobalt, iron, chromium, aluminium);
- obtaining of devitrificates;
- effect of crystallization on certain physico-chemical properties (DTA, wettability of the CBN sinter by devitrificates, phase composition, TLEC) of the obtained glass-crystalline materials.

2. OBTAINING OF GLASSES

Five sets of glasses were used for investigations out of which the first one did not contain lithium oxide at all. The initial raw materials for the production of glasses were: (all analytically pure) zinc oxide ZnO, boric acid H_3BO_3 silicon dioxide SiO_2 lead oxide Pb_3O_4 and vanadium pentoxide V_2O_5 serving as the crystallization nucleator.

The material preparation consisted in initial screening, weighing, exact mixing and, next, firing up to 1250^oC in corundum crucibles (first version), platinum crucibles (second version) and to 15^o), for the iron background the wettability angle increased from 14^o for Set 1 to 40^o

for Set 5. Additionally, to evaluate the possibility of interdiffusion on the phase boundary of background-sample, the X-ray microanalysis of the surface fracture of the Set 1 sample and the kiborite background was performed. A slight diffusion of zinc and apparent of lead to the background was observed (Fig.1).

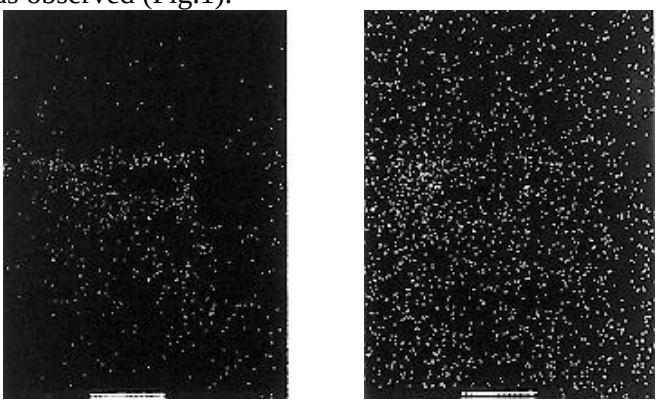

Fig.1. The distribution of zinc (a) and lead (b) on the glass surface of Set 1 and kiborite (XZn Ka, 1000x, XPb Ka, 1000x).

6. THE DATA MEASUREMENTS

The DTA measurements were executed with the Derivatigraph 1500 Q apparatus. Analysing the graphs it was observed that the transformation temperature increased with the lithium oxide content as opposed to the melting temperature which increased violently (from 695^{o}C for Set 1 to 885^{o}C for Set 5). In Sets 2,3 and 5 crystalline phases, hard to be identified, were precipitated, and melted subsequently.

7. MICROHARDNESS MEASUREMENTS

These measurements were performed on the samples heated in the gradient furnace manufactured by the ISM in Kyev by means of the PMT3 hardness tester with a diamond pyramid in the temperature range 750-920^{o}C. The highest microhardness was reached by glass no 4 in the range of 71 MPa at 890^{o}C. Other glasses oscillated within 19.4-45 MPa at 750-920^{o}C. According to the obtained results (mainly wettability and microhardness), Sets 1 and 4 were directed to further investigations which were subjected to additional heat treatment in the range crystallization temperatures, read from DTA by means of the unistage treatment.

8. DTA INVESTIGATIONS OF DEVITRIFICATES

The DTA investigations were used to record the exothermic effect, accompanying the process of crystallization in glass.

The area of the effect is proportional to the formed crystalline phase. This is proved by the investigations carried out by Gutzov, China and Sarked Birga. The crystallization rate a (%) was calculated from the formula:

$$\alpha = 100 \,.\, (S_{\alpha} - S_{x}) \,/100$$

where:

S_α - area of the exothermic effect on the thermogram of the initial glass;
S_x - area of the exothermic effect on the thermogram of the subjected to heat treatment

The effect area was calculated by weighing the effect cut off from the thermogram of the tested glass sample. The figure shows a clear decrease of the area of the exothermic effect with the growth of the crystalline phase content. It can be also observed that with the decrease of the fraction of the glassy phase, used for forming of the crystalline phase, the size of the exothermic effect, responsible for the precrystalline changes in glass, decreases. The results are listed in Table 1.

Table 1. Crystallization rate of glasses of set 4

	glass	400 ^oC -1h	420 ^oC -1h	480 ^oC -1h	510 ^oC -1h
PbLi4	0	60	78	80	85

9. THE LINEAR EXPANSION COEFFICIENT OF DEVITRIFICATES

The measurements of the linear expansion coefficient were performed on the research stand constructed in the Institute of Metal Cutting on sinter samples of 20 x 4 x 4 mm in air at the air heating velocity 100 C/minute. The values of the coefficient were calculated from the formula:

$$TLEC = TLEC_{quartz} + (1/l_o) \times (\Delta l / \Delta T)$$

where:

$TLEC_{quartz} = 0.55 \times 10^{-6}$ 1/deg

It is significant to make the TLEC of glasses and devitrificates during heating and cooling be close to the TLEC of CBN. According to Kingery, the mismatch of coefficients is the main reason of forming of stresses which can be strong enough to cause slight cracks. If the value of a_s a_{CBN} then around a "stretched" grain the tangent tensile stresses are developed which lead, at a strong mismatch, to forming of semicircular cracks around the grain. The"compression" of bonds causes the increase of the resistance of the abrasive mass. In the opposite case, when the value a of the bond is higher than a of the grain, radial compressive stresses and tangent tensile stresses should develop around the "compressed" grain and they make radial cracks appear. These cracks are more dangerous because they can join and form a network of cracks among the grains. Assuming, according to Cooley and Juchem, that the TLEC of CBN changes from 4.2 to 4.8 x 10^{-6} 1/deg in the temperature range 20-800 ^oC, it is important for the obtained glass-crystalline materials to have TLEC close to the above, especially on the stage of initial cooling The coefficient of the sample of the initial PbLi4 glass changed from (4.1-4.4) x 10^{-6} 1/deg in the range 100-600^o C at the maximum 5.8 x 10-6 1/deg at 560^{o}C. The value of a grew with the increase of crystallization and it decreased during cooling (-15 x 10^{-6} 1/deg at 400^{o}C). For the samples of Set 1 the value of a ranged within 3-5.5 x 10^{-6} 1/deg. The increase of crystallization did not cause any significant changes of the value of a as compared to the initial glass.

10. X-RAY RADIOGRAPHIC INVESTIGATIONS OF DEVITRIFICATES

These investigations of the samples of glass-crystalline materials of Set 1 and 4 were performed with the same equipment and in the same conditions in which the samples (not subjected to additional heat treatment at crystallization temperature) were tested. It is apparent that with the increase of the temperature of heat treatment, with the same time of tempering (1h), the reflexes were more intensive whereas the phase composition was not changed (for Set 4 it was larsenite $PbZnSiO_4$, small amounts of ZnO, PbV_2O_6 and Li_3BO_3 while for Set 1 willemite Zn_2SiO_4, V_3O_5 and $Pb_3(VO_4)_2$). The scanning photographs of initial materials show shell fractures and sharp edges of particles of medium sizes 30-45 mm and the smaller ones 10-15 mm which are characteristic for the glassy phase. The particle edges got rounded with the growth of heat treatment temperatures.

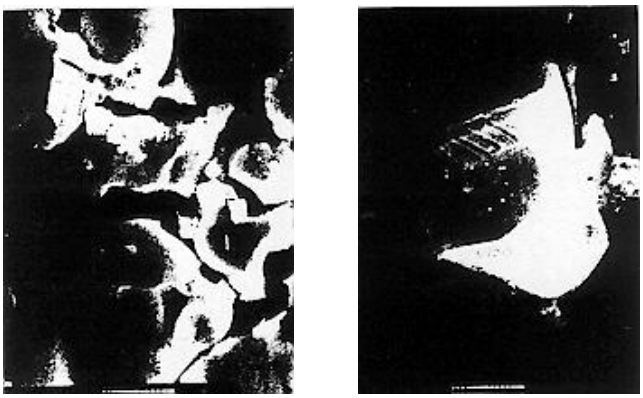

Fig. 2 Scanning photographs of glasses of Set 1 (a) initial glass, (b) after heat treatment at 510^o C - SEI 3000x.

11. WETTABILITY INVESTIGATIONS

The wettability tests were carried out with the same high-temperature microscope and on new plates, made in Poland. The value of the wettability angle between the initial materials and the obtained devitrificates was also visible. The more crystallized the devitrificate was, the higher was the value of O For Set 4 it ranged within 25-45^o and for Set 1 the range was 25- 35^o

12 CONCLUSIONS

The introduction of lithium oxide as a modifier into the zinc-boron-lead glasses showed that:

-- already its slight addition leads to the structure ordering (X-ray investigations)

-- wettability of kibrite by the glasses of all sets was good (Θ=18 and 25^o), similarly as for metallic backgrounds (e.g. wettability of titanium was 12-21^o for all sets) where as the lower was the content of the modifier, the better was the wettability of a metal;

-- the transformation temperature decreased with the growth of Li_2O content while the melting temperature increased (from 695^o C for Set 1 to 885^o C for Set 5).

Additional heat treatment in the range of crystallization temperatures, read from DTA (400-510^o C), resulted in obtaining devitrificated materials in 85% in Set 4 and in 70% in Set l.

Larsenite $PbZnSiO_4$ was identified in Set 4 as a dominating phase together with small amounts of ZnO, PbV_2O_6 and Li_3BO_3 while in Set 1 it was willemite Zn_2SiO_4 and small amounts of V_3O_5 and $Pb_3(VO_4)_2$.

The growth of the content of the crystalline phase caused changes of the WCRL content during heating and inert cooling (in Set 4 - 2-6.2 x 10^{-6} l/deg at 600^o C and -15.2 x 10^{-6} 1 /deg at 400^o C during cooling). These changes were not visible in Set 1.

The increase of the content of the crystalline phase deteriorated clearly the wettability of backgrounds of cubic boron nitride by devitrificates.

LITERATURE

[1] ENLU Z., ZHONGSHEN Z.: Crystallization behaviour of devitryfiable solder glass in the system PbO-ZnO-B_2O_3. Materialy konferencyjne XVII Kongresu Szk≈a, Beijing, 1995, vol. 2, s. 224-230.

[2] IMANAKA Y., AOKI S., KAMEHARA N.: Thermal expansion of glass- ceramic composites for multilayer ceramic board. Fujitsu Scientific and Technical Journal,1989, vol. 25, nr 1, s. 73-79

[3] KIELSKI A.,WODNICKA K.:Pomiar g stoVci metod helow Szk≈o i Ceramika,1994, nr3

[4] KUCIiARSKI J.: Kierowana krystalizacja piroksen∴w w szkle. Zeszyty PAN, Prace Komisji Nauk Ceramicznych, Ceramika 1988, nr 37

[5] PRACA ZBIOROWA: Fizykochimija formirowanija abrazivosoderzascich materialov instrurnietal'nogo naznacenija. Kiev,1988.

[6] STANIEWICZ-BRUDNIK B., MAJEWSKA-ALBIN K.: The glasses of PbO-ZnO-B_2O_3-SiO_2 system with addition of microporous glasses as the components of binders for CBN tools. Materialy konferencyjne z XVII Kongresu Szk≈a, Beijing,1995, vol. 5, s. 441-447

[7] WANG M.H.: Crystal growth and characterization of CaO - bearing Li_2O-$A1_2O_3$-SiO_2-TiO_2 glass - ceramics. Ceramic Int.,1993, nr 19, s. 223-230.

This work was supported by KBN, research project No 7 3201-005 07

CRYSTALLIZATION of $AlPO_4$ IN THE SYSTEM Li_2O-Al_2O_3-P_2O_5 WITH SiO_2 ADDITION

J•czmionek °., Kucharski J. and **Wasylak J.**
University of Mining and Metallurgy, Poland

Abstract

The main subject of the present work, is concentrated on investigating the crystallization behaviour of glasses in the system Li_2O-Al_2O_3-P_2O_5 to produce glass-ceramic materials with $AlPO_4$ as the prevailing phase, which would provide these materials with desirable thermo- and chemo-resistant properties. Glasses in the system Li_2O-Al_2O_3-P_2O_5 crystallize well with $AlPO_4$ as the main crystalline phase, together with unwanted other phase, e.g. lithium phosphates which decrease considerably, the chemical resistance. It is found that addition of SiO_2, even in minimal amounts, limits the formation of the unwanted phases, without affecting the formation of $AlPO_4$.SiO_2 addition does affect the crystallization of different polymorphic forms of $AlPO_4$. Addition of 0.05 mol % SiO_2 completely inhibits formation of tridymite form of $AlPO_4$.

I. INTRODUCTION

In the present study it has been observed that the glass-crystalline materials obtained from the system Li_2O-Al_2O_3-P_2O_5 are not stable enough since besides $AlPO_4$, the disadvantageous crystalline phases: lithium phosphates are likely to occur, which considerably reduce the chemical resistance of the material. Silica introduced as an addition into the glasses of this system reduces the appearance of the undesirable phases without disturbing the crystallization of $AlPO_4$. It may contribute, however, to the formation of various polymorphous varieties of aluminium ortophosphate [4].

II. EXPERIMENTAL

Investigations of crystallization were conducted in the system Li_2O-Al_2O_3-P_2O_5-SiO_2 on glasses in which the amount of silica was within 5-50 mole % and for glasses without any silica content or glasses in which silica represented only a small addition of 0,05 mole % (above 100 %). The glasses were melted in a furnace, at the temperature 1400 °C, in unglazed porcelain crucibles and in alundum crucibles and next destressed at the temperature 420-500 °C, depending on the glass composition. The particular oxides were introduced by means of the following raw materials: Li_2O-Li_2CO_3 pure, Al_2O_3-$Al(OH)_3$ p., P_2O_5-$(NH_4)_2HPO_4$ p. SiO_2 was introduced using chemically pure silica. The composition of the glasses can be found in the enclosed system (Fig.1). X-ray diffraction, infrared spectroscopy and thermal differential analysis were used to identify the phases obtained in the process of glass crystallization before and after thermal treatment in a gradient furnace.

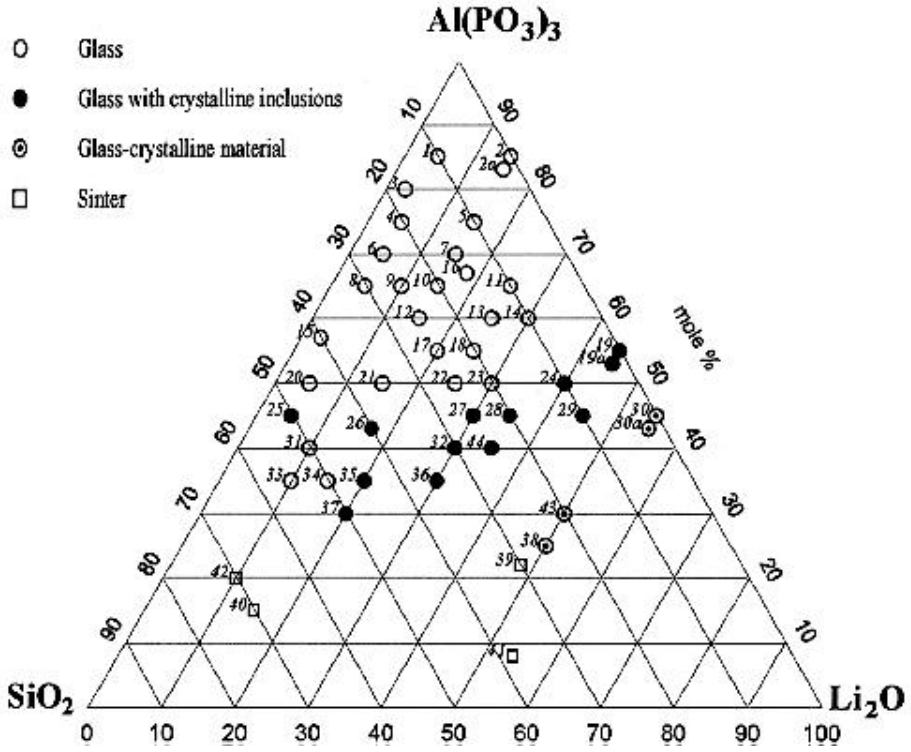

Fig.1. Areas of glasses in the system Li_2O-Al_2O_3-P_2O_5-SiO_2.

III. DISCUSSION OF THE INVESTIGATION RESULTS

The area of the glass formation in the examined system is shown in Fig.1. Colourless, transparent glasses are formed during melting batches containing in all more than 60 mole % phosphorus and aluminium oxides. According to the melting requirements [1] these oxides in each glass were introduced in the amount corresponding to the stoichiometric compound $Al(PO_3)_3$.

Glasses containing 5-20 mole % of silica, in which the presence of any crystalline phase after casting was not observed by XRD, were subjected to thermal treatment in a gradient furnace in the temperature range 600-1000 °C for 2 hours and next subjected again to X-ray diffraction. It has been found that in glasses containing 5-20 mole % of SiO_2 and 55-80 mole % of $Al(PO_3)_3$ in the temperature range 750-900 °C the crystobalite form of $AlPO_4$ undergoes crystallization. This is evidenced by the lines appearing on the X-ray pattern, characteristic for these phase [5,6,7]. The presence of this phase was also confirmed on basis infrared analysis. For the crystobalite form $AlPO_4$ the doublet 720 and 740 cm^{-1} in the infrared spectrum are characteristic [2, 3]. It derives from the Al-O bonds in $AlPO_4$ [1,2,8] (Fig.2a). Moreover, bonds deriving from the bonds P=O (470, 620 cm^{-1}) are also present. Bonds deriving from $AlPO_4$ were absent in glasses before their thermal treatment which is evidence that $AlPO_4$ did not crystallize during its cooling (Fig.2b).

Crystallization in glasses without silica or glasses with very small silica content (0.05 mole % above 100 %) takes a completely different course. Glasses without silica and their equivalents containing an admixture of SiO_2 and crystallizing during cooling (19, 30,19a, 30a) do not differ visually in any respect. They were melted in alundum crucibles since, as it has been observed earlier, when porcelain crucibles are used the silica from the crucible material passes into the glass. Glasses without silica and glasses containing very small amounts of SiO_2 (0.05 mole %) differ considerably what regards the course of their crystallization. X-ray diffraction has revealed that when casting glasses without silica there crystallize the phases: the tridymite and the cristobalite forms of $AlPO_4$ and lithium ortophosphate Li_3P0_4. In the course of casting glasses with 0.05 mole % admixture of SiO_2 only the cristobalite form of $AlPO_4$ becomes crystallized.

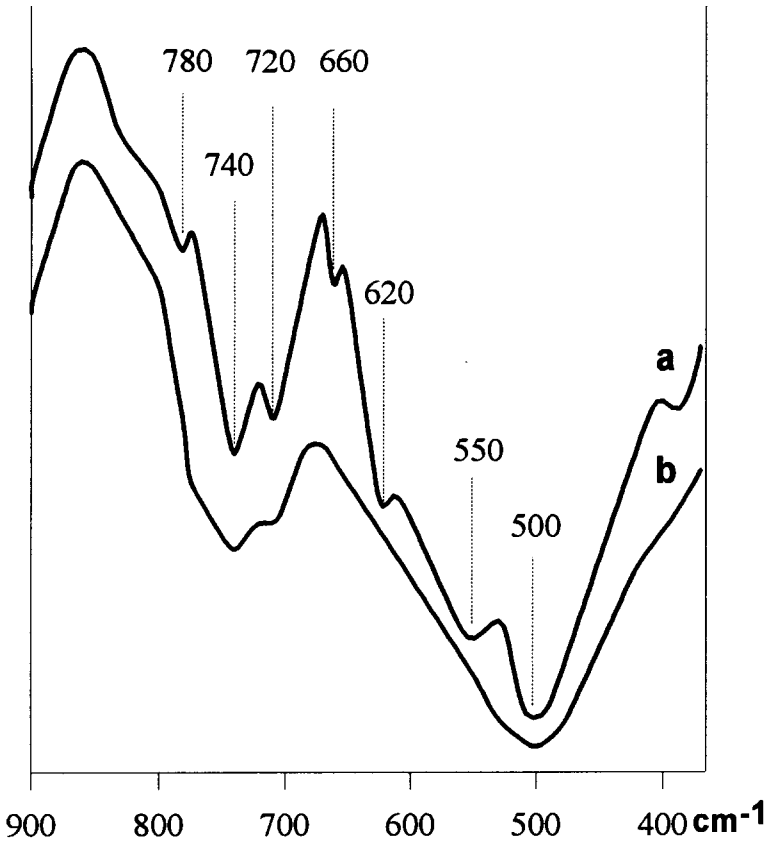

Fig.2. Spectra of glasses in the system Li_2O-Al_2O_3-P_2O_5-SiO_2
a) IR spectra of glass No 17 after thermal treatment
b) IR spectra of glass No 17 before thermal treatment

These glasses were next subjected to thermal differential analysis in order to determine the course of their crystallization and the characteristic temperatures of the formation of crystallize phases. Fig.3a shows the DTA curve for cooling glass without silica No 30 from 1300 °C to 20 °C . On the curve one can observe the crystallization of a few phases in the temperature interval 880-840 °C. X-ray diffraction of glass samples subjected to thermal treatment a temperatures from the range of crystallization effects obtained within 1 hour, has shown the following progress: at 880

°C there crystallizes the cristobalite form of $AlPO_4$, at 840 °C the tridymite form of $AlPO_4$ together with Li_3PO_4. Fig.3b shows the DTA curve for heating the same glass up to 1000 °C. It follows from the curve that in the interval 480-770 °C there occur the effects of crystallization and melting of the crystalline phases. X-ray diffraction of samples heated for 1 hour at the particular temperatures of the crystallization effects has revealed that lithium pyrophosphate $Li_4P_2O_7$ crystallizes at 480 °C, and lithium metaphosphate at 570 °C. An attempt to identify the phase crystallizing at 530 °C failed. It may be aluminium metaphosphate $Al(PO_3)_3$ or the tridymite form $AlPO_4$. This, however, is not very probable considering its earlier crystallization during cooling. The peaks at 610 and 770 °C illustrate the melting of lithium phosphates at these temperatures.

A different course of crystallization was observed in glass No 30a whose composition was the same as that of glass No 30, but with 0.05 mole % admixture of $Si0_2$ above 100 %. Fig.3c shows the DTA curve for cooling the alloy of this glass from 1300 °C only one crystallization effect is visible at 880 °C. On the basis of X-ray diffraction it has been identified as the cristobalite form of $AlPO_4$ which has been also confirmed by infrared spectroscopy examination. Fig.3d shows the DTA curve for heating this glass to 1000°C. Two crystallization effects illustrating the crystallization and one effect of melting are visible. Crystallization occurs in the interval 460-550 °C . Using the same method as in the case of glass No 30 it has been found that at 460 °C Li_3PO_4 is formed, and at 550 °C probably the aluminium metaphosphate $Al(PO_3)_3$. At 720 °C there probably takes place the melting of $Al(PO_3)_3$ phase. The similarities and differences in the crystallization progress of both glasses, differing only in 0.05 mole % admixture of silica, are listed in Table 1.

Table 1. Crystallization of glasses Nos. 30 and 30a.

	Glass No 30		Glass No 30a with 0.05 mole % of SiO_2	
	temp. [°C]	phase	temp. [°C]	phase
Crystallization effects during cooling	880 840	K-$AlPO_4$ T-$AlPO_4$, Li_3PO_4	880	K-$AlPO_4$
Crystallization effects during heating	480 530 570	$Li_4P_2O_7$ $Al(PO_3)_3$(?) $LiPO_3$	460 550	Li_3PO_4 $Al(PO_3)_3$(?)
Effects during heating associated with melting	610 770	$Li_4P_20_7$ also $LiPO_3$	720	$Al(PO_3)_3$(?)

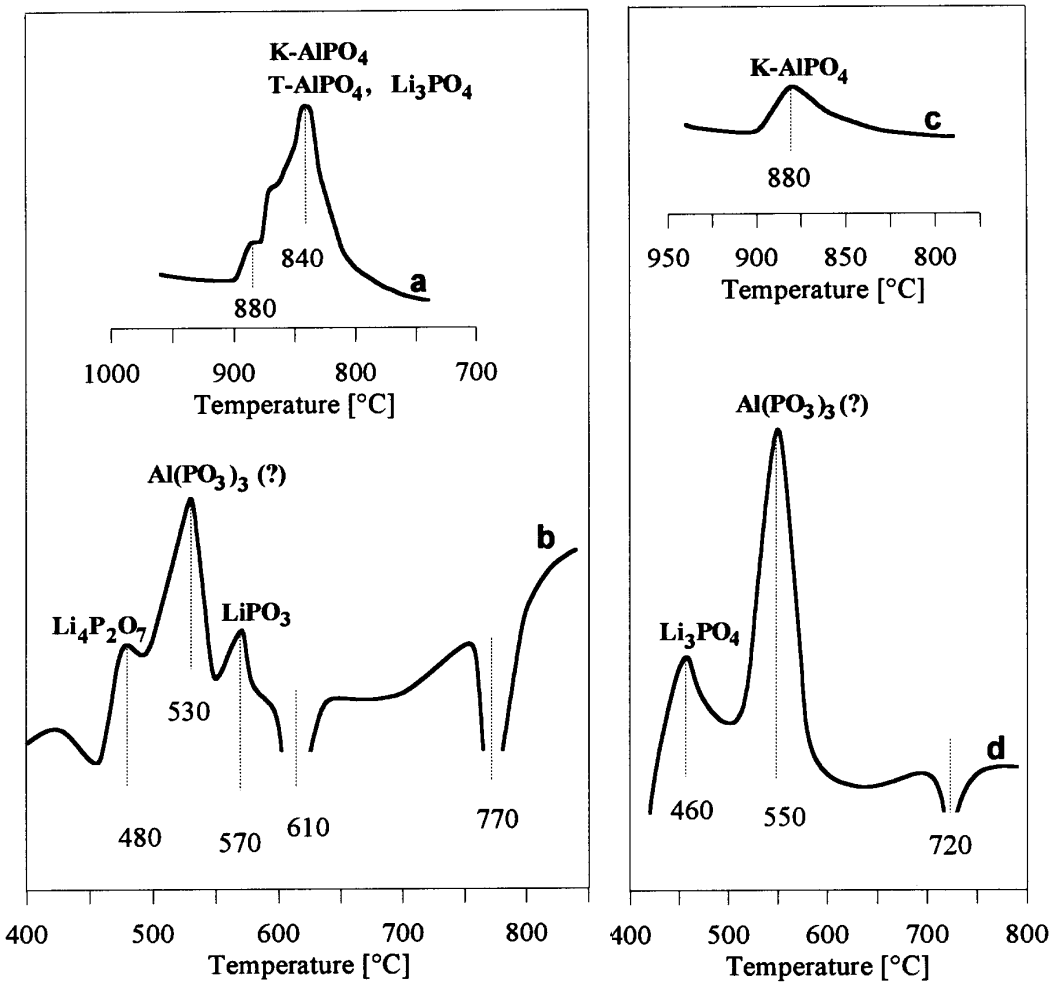

Fig.3. DTA curves of glasses Nos. 30 and 30a
***a** - Glass No 30 cooling curve, **b** - heating curve*
***c** - Glass No 30a cooling curve, **d** - heating curve*

IV. SUMMARY REMARKS AND CONCLUSIONS

An addition of SiO_2 in the amount of 0.05 mole % above 100 % to glasses in the system Li_2O-Al_2O_3-P_2O_5 has a significant effect on the crystallization course and the kind of the obtained phases in the process of their thermal treatment and during casting. Small amount of silica prevents the appearance of the tridymite form of $AlPO_4$ without disturbing crystallization of the cristobalite form at casting. During heating of these glasses the presence of SiO_2 prevents crystallization of lithium pyro- and metaphosphates, while inducing crystallization of lithium ortophosphate. Speaking in general, silica addition contributes to the reduction of the crystallizing phases both at casting and during thermal treatment.

The presence of silica in the amount of 5-20 mole % stabilizes glasses in the system Li_2O-Al_2O_3-P_2O_5-SiO_2 [1]. It inhibits the crystallization of adverse phases such as lithium phosphates

or aluminium metaphosphate. It does not disturb crystallization of the cristobalite form of $AlPO_4$ during thermal treatment of the glasses.

REFERENCES

1. ° .J czmionek, J.Kucharski, J.Wasylak - Zjawiska krystalizacji szkie≈ w uk≈adzie Li_2O-Al_2O_3-P_2O_5-SiO_2. Szk≈o i Ceramika 2(1995),12-14.
2. M. ° czka, M.Ciecinska - Berlinite $AlPO_4$-containing glass-crystalline materials produced by sol-gel method. Proc. of XVll Inter. Con. on Glass, Beijing 1995 v.4, 29-295.
3. J.Wasylak, J.Kucharski, ° .J czmionek - Berlinite glass-crystalline materials. Proc. of XVll Inter. Con. on Glass, Beijing 1995 v.5, 294-299.
4. O.W.Flörke, H.Lachenmayr - Ber. Dtsch. Keram. Ges.39H1(1962).
5. P.Robinson, R.McCartney - Subsolidus relations in the system SiO_2-Al_2O_3- P_2O_5. J.Amer. Ceram. Soc.47(1964) 587.
6. O.W.Flörke, H.Lachenmayr - DTA und Roentgenuntersuchungen an $AlPO_4$. Ber. Dtsch. Keram. Ges. 59(1962).
7. E.Z.Alridge, V.C.Farmer, B.D. and W.A.Mitchell - IR, X-ray and thermal analysis of some aluminum and ferric phosphates. J.Appl. Chem.,13 January, 1963.
8. G.Fuxi, I.Yasi, I.Fusong-Formation and structure of $Al(PO_3)_3$ - containing fluorophosphate glass. J. of Non-Cryst. Solids 52(1982) 263-273.

CRYSTALLIZATION OF GEL - GLASSES IN THE MgO - Al_2O_3 - SiO_2 SYSTEM

B. Samuneva, Y. Dimitriev, Y. Ivanova, P. Djambazki, V. Dimitrov,
C. Kashchieva and **A. Staneva**
University of Chemical Technology and Metallurgy, Bulgaria

Abstract

In the present work are presented the results from the investigation on the crystallization of gel - glasses with the stoichiometric cordierite composition ($2MgO.2AI_2O_3.5SiO_2$) prepared on the basis of different precursors SiO_2 - sol, TEOS, $AI(NO_3)_3.9H_2O$ and $Mg(NO_3)_2.6H_2O$.

The structural evolution in the gels has been studied during their heat treatment till 1500 °C. The phase formation in the powder samples of gel-glasses has been determined by means of X-ray diffraction analysis, IR-spectroscopy, TEM and TEMD.

It was established that the types of the precursors influence on the processes of gel - sol formation. The microstructure of the studied materials was observed and the sizes of the formed crystals were determined.

I. INTRODUCTION

Cordierite ideal formula ($2MgO.Al_2O_3.5SiO_2$) and cordierite based glass-ceramics are promising materials for different industrial applications such as automotive and gas-turbine heat exchangers, electronic packaging refractory materials, because of their high strength, corrosion resistance, low thermal expansion and low dielectric constants [1-3]. Cordierite materials with good physical and chemical properties are difficult to obtain using conventional methods (crystallization from glass or solid state reaction) because of the very narrow sintering range of the stoichiometric compound (3). That is why the sol-gel synthesis of cordierite glass- ceramics is of great interest as it permits to obtain this kind of materials at low temperatures by direct crystallization of gels and gel - glasses without melting process. A number of papers have been published in the last few years in the field of the sol - gel synthesis of different cordierite materials (powder, bulk, fiber) [2-8].

The purpose of the present study is to compare the process of gel, silicate and glass formation of stoichiometric composition $2MgO.Al_2O_3.5SiO_2$ by using different ways of preparation of the batches.

II. EXPERIMENTAL

Stable cordierite gels were prepared using different precursors :

- SiO_2 - sol, $Al_2O_3.9H_2O$ and $Mg(NO_3)_2.6H_2O$

- $Si(OC_2H_5)_4$ (TEOS), $AI(NO_3)_3.9H_2O$ and $Mg(NO_3)_2.6H_2O$.

The thermal treatment of the gels was performed in the 200 to 1500 °C temperature range using corundum crucibles. The glass ceramics materials were prepared directly from gels without melting and by a conventionally by crystallization of the melted glass. The IR - spectra were recorded by a double - beam spectrophotometer SPECORD-M80 (Karl Zeiss, Jena) in the 14000 - 400 cm^{-1} range. The samples for these measurements were prepared as suspensions in liquid paraffin. The wave number accuracy was ± 3 cm^{-1}. X ray diffraction analysis was made using DRON- 2TM diffractometer CuK_α , Ni - filter) and transmission electron microscopy was performed by means of a Philips-505 microscope.

III. RESULTS AND DISCUSSION

The IR spectra of the investigated cordierite gels during thermal treatment in the temperature range 25 -1500 °C are presented in Figs.1 and 2. Figure 1 shows the IR spectra of the cordierite composition obtained from TEOS while Fig. 2 presents the IR - spectra of the same composition obtained from SiO_2 sol . In the spectrum of an air - dry cordierite gel prepared on the basis of TEOS (Fig.1) the band at 1080 cm^{-1} is determinative. It is well known that this band is structurally sensitive in relation to the silicate structure formation. According to [9] this band is assigned to the anti-symmetrical stretching vibrations of the Si - O - Si bonds in the network. On the other hand, the absorption band at 950 cm^{-1} can be attributed to the Si-OH vibrations in the gel structure. With increasing of the temperature up to 200 °C. the main maximum shifts to 1050 cm^{-1} and the band at 950 cm^{-1} disappears. This is an indication for an early formation of networking of the cordierite gel - glass structure. It is evident (Fig.1), that this structure exists from 200 to 1000 °C. The observed IR - bands at 1040, 925 and 450 cm^{-1}, are in good agreement with IR - spectra of pure cordierite glass obtained by the conventional method. [10].

The shift of the main maximum to 1040 cm^{-1} is an indication of depolymerization of the silicate network on one hand resulting from the Mg -cations effect, and on the other hand it is due to the lattice -forming role of the AI - cations with the appearance of the Si - O -Al bonds.

The latter increase of the temperature leads to crystallization of the gel-glass at 800 °C with the formation of a metastable quartz -like phase μ- cordierite and α- cordierite. The second one is the main crystalline phase above 1000 °C. These crystalline products were established by means of X- ray diffraction analysis.

A homogeneous cordierite glass with absorption maxima at 1065, 940 and 450 cm^{-1} was produced at temperatures of the order of 1450 °C which is lower than the glass melting temperature of an oxide batch.

The IR - spectra of the gels prepared from a SiO_2 - sol show a delay in the formation of the cordierite structure (400 °C), but on the other hand the gel - glass crystallizes with an unique crystalline phase α - cordierite at about 800 °C(Fig. 2).

The development of the cordierite microstructure during the thermal treatment at 900 and 1200 °C. obtained by TEM is presented in Fig 3 a, b.

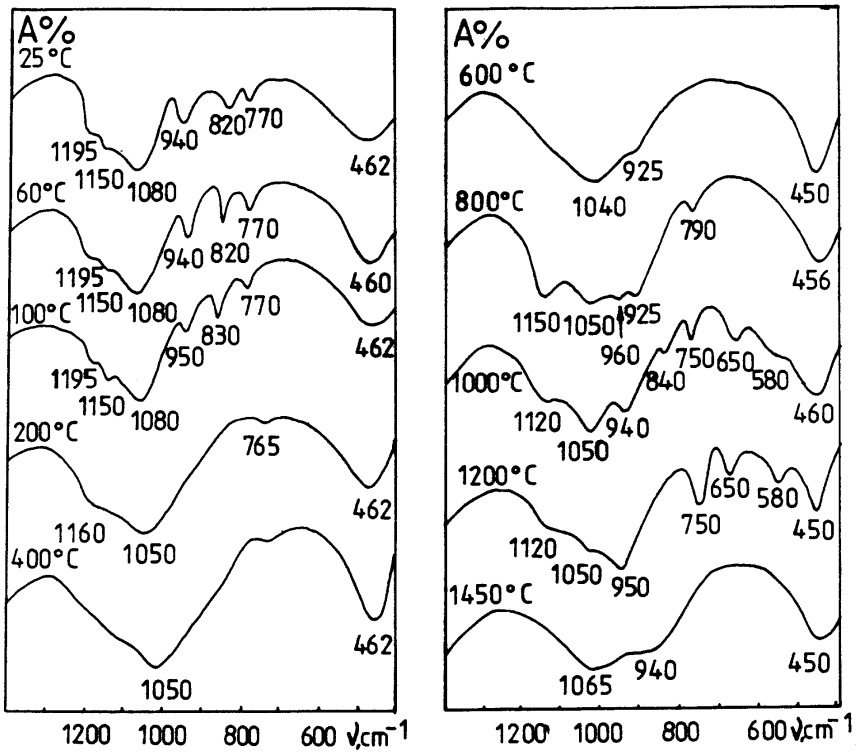

Fig.1 IR - spectra of cordierite gel obtained from TEOS.

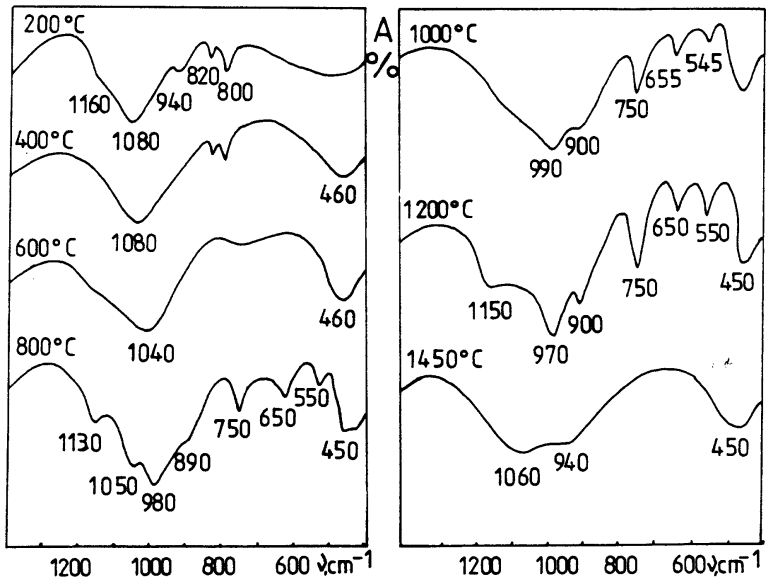

Fig. 2 IR - spectra of cordierite gel obtained from SiO_2 - sol.

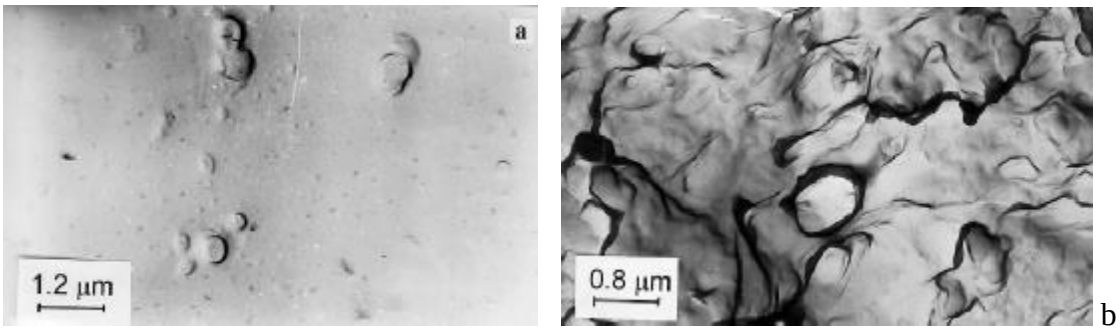

Fig. 3 Microstructure of cordierite glass - ceramics : a - 900 °C; b -1200 °C.

IV. CONCLUSIONS

As a result from the studies on processes of the gel - silicate, and glass- formation of the cordierite composition, it was established that the processes of the network formation take place at lower temperatures compared to similar oxide batches . On the other hand the formation of cordierite structure in the gel obtained from SiO_2- sol shows an delay in comparison to the gel obtained from TEOS. α - cordierite is the main crystalline phase at high temperatures in both cases.

Acknowledgment

The authors are grateful to the Bulgarian National Research Fund for the financial support of this work under grant No X - 437 / 1994.

REFERENCES

1. C. Ballesteros, R. Gonzalez and J. Llopis, J. Mat. Sci. , 21, 674, (1986).
2. P. Thomas, J. Mercurio and B. Frit, J. Mat. Sci. Lett. , 8, 52, (1989).
3. J. Boulton, K. Jones and H. Emblem, J. Mat. Sci. Lett. , 8 ,1087, (1989).
4. A. Douy, J. Non-Cryst. Solids ,147 & 148, 554, (1992).
5. R. Cirakovic, S. Milonijc and L. Kostic, Third Euro - Ceramics, Ed. P Duran and J. Fernandez, Faenza Editrice Iberica S.L.1, 273, (1993).
6. T. Heinrich, W. Tappert, W. Lenhardt and J. Fricke, J. Sol-Gel Sci. Techn. , 2, 921, (1994).
7. B. Samuneva, Y. Dimitriev, Y. Ivanova, V. Dimitrov, and P. Djambazky, Proc.10 Int. Baustoff und Silikat tagung, Weimar, p. 288 (1988).
8. B. Samuneva, Y. Dimitriev, Y. Ivanova V. Dimitrov, E. Kashchieva and P. Djambazky, Proc. XV Int. Congress on Glass, Ed. O. Mazurin , Leningrad, 2a, 26, (1989).
9. I. Plusnina, Infrakrasnie Spektri Mineralov (Infrared Spectra of Minerals), Moskva, 1972. (In Russian).
10. A. Gregory and T. Veasey, J. Mat. Sci. 8, 333, (1973).

CRYSTALLIZATION OF GLASS TO GLASS-CERAMICS IN THE SYSTEM SiO_2-CaO-Na_2O

Togan, D., Radicescu, S. and **Protopopescu, N.**

National Glass Institute, Romania

Abstract

The glass-ceramics in the soda-lime-silica system has been studied for their good thermal stability, mechanical properties, chemical resistance, low production costs, the capability of easy to form glasses and the existence of a large compositional zones exhibiting high volume phase nucleation. Investigated glasses belong to various subsystems of the multicomponent system Na_2O-K_2O-Ca0-Al_2O_3-SiO_2. The selected compositions with some of the 0^{2-} ions replaced by an equivalent number of F^- ions and containing catalytic additives were characterized by a melting temperature below 1500^oC; the annealed glasses were homogenous and present no separations. The crystallization behaviour of isothermally treated glasses was investigated by thermal analysis, X-ray diffraction, IR spectroscopy and scanning electron microscopy.

I. INTRODUCTION

Several systematic studies on glasses and glass-ceramics in Na_2O-CaO-SiO_2(P_2O_5) systems, composition dependent properties and structure had been reported [1-8]. By controlled crystallization, the crystal phase composition can be quite different, from colloid particles to complex solid solutions of silicates and silicophosphates [9]. Continuing these investigations, we studied the influence of composition on the properties and structure of glass-ceramics in the systems Na_2O(K_2O)-CaO(MgO)-Al_2O_3-SiO_2, which were prepared by adding single nucleating agents F, P_2O_5. Some peculiarities of the formed crystalline phases and the nucleation temperatures of different compositions are considered.

II. EXPERIMENTAL

The glasses were prepared from high purity raw materials: natural quartz, $CaCO_3$, Na_2CO_3, MgO, alumina, tribasic calcium phosphate and sodium silicofluoride. Mixed batches were melted in an electric furnace at 1450^oC for 4h, poured in slabs on steel plates and proper annealed. For physical properties measurements there were used the Pulfrich refractometer PR2, Linseis dilatometer and a Zeiss Jena UV-VIS spectral photometer SPECORD M 40. Selected samples from obtained transparent glasses were thermally treated at Tc. The crystalline phase formation and structure development was

investigated by means of X-ray diffraction analysis (Zeiss URD6-Cu-K_α), IR spectroscopy (Zeiss SPECORD M 80) and SEM (Tesla 350 BS).

III. RESULTS AND DISCUSSIONS

The compositions of studied glasses and their influence on the physical properties are given in table 1. The melted and annealed glasses are colourless and perfectly transparent, with a high spectral transmission in the visible range (fig.1).

Table 1 Compositions (% wt) and physical properties of glasses

Type of glass	OP 9	OP 17	OP 28
SiO_2	71.2	61.7	65.2
Al_2O_3	7.3	0.6	-
CaO	4.8	14.5	13.8
Na_2O	14.2	19.0	14.5
MgO	-	-	3.0
P_2O_5	-	4.2	3.5
F_2	4.2	-	-
Refractive index, n_e	1.489	1.533	1.531
Abbe value, ν_e	69.7	57.9	59.7
Wavelength (nm), corresponding to a transmission of:			
50%	310	315	300
80%	330	340	325
Coefficient of linear thermal expansion ($10^{-7o}C^{-1}$)	90	98	103
Transformation temperature, T_g (^oC)	450	535	538
Dilatometric softening point, M_g (^oC)	490	552	575
Crystallization temperature, T_c (^oC)	706	723	762
Density,(g/cm^3)	2.52	2.74	2.63

DTA was used to determine the temperature of nucleation and crystallization, all glasses have an exothermic peak [Tc, table 1] and OP 17 glass shows a second strong peak at 885^{o}C too. Powder X-ray diffraction patterns of thermally treated glasses were shown in fig.2. Data were collected over the range 14^o to 50^o (2θ) using a 0.02o step interval and a step time sufficient to give a good signal to noise ratio. On OP 9 samples [700^{o}C, 2h] regarding the planes with the indices of JCPDS file [11] the peaks of the XRD pattern correspond almost perfectly to anorthite, $CaO{\cdot}Al_2O_3{\cdot}2SiO_2$; the XRD peaks of OP 28 samples [760^{o}C,24h] shows the crystallization of beta-wollastonite, $CaO{\cdot}SiO_2$ and hydroxyapatite, $Ca_5(PO_4){\cdot}3OH$.

On OP 17 samples [720^{o}C, 17h] no peaks are observed in the diffraction patterns. The opaque appearance of thermally treated glass, with low transmission in the spectral range 300 to 700nm (less than 7%, fig.1) allowed the presumption of the spherolites formation,

with fibrelike structure. This assumption are comparable to those reported for other calciumsilicate glasses [5, 14] and was confirmed by the scanning electron microscope micrograph (fig.4a). As can be seen, the fibres are more compact near the center and diverge at a great angle in the periphery of crystal, the space between fibres being filled with a glass phase.

Further method employed to characterize both the glasses and glass-ceramics included FTIR spectroscopy, in the range 1600-400 cm^{-1} (fig.3). The samples were dispersed in KBr pellets.

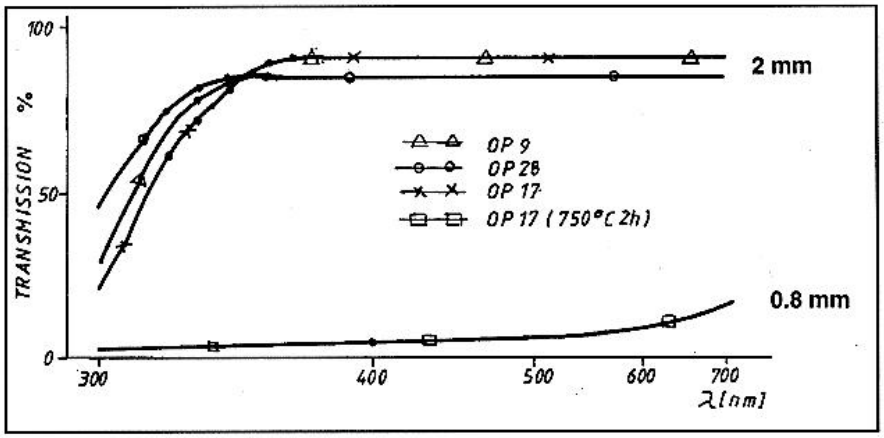

Fig.1 UV-VIS spectral transmission

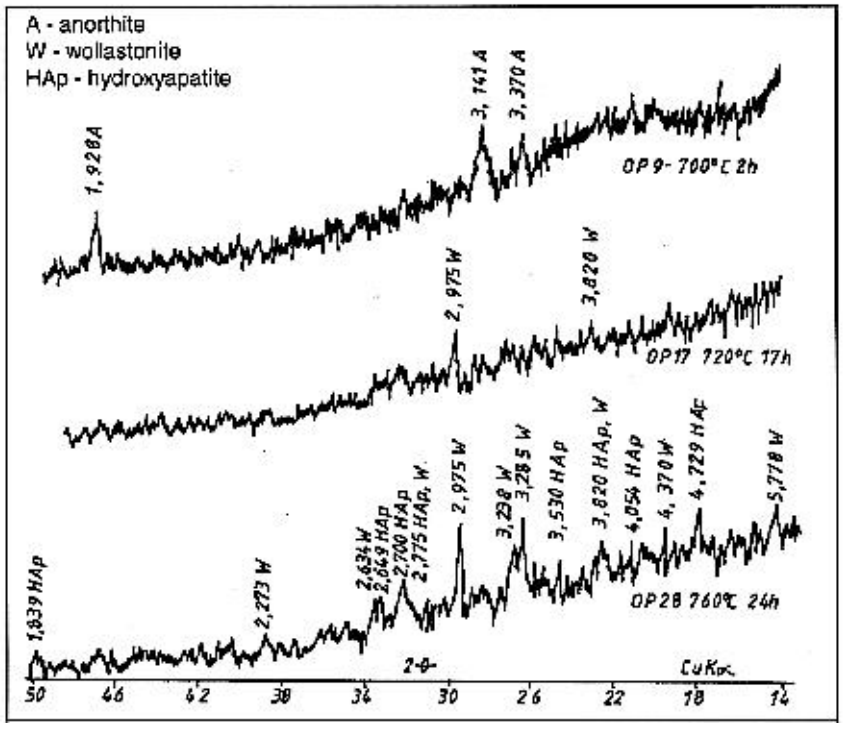

Fig. 2 X-ray diffraction patterns

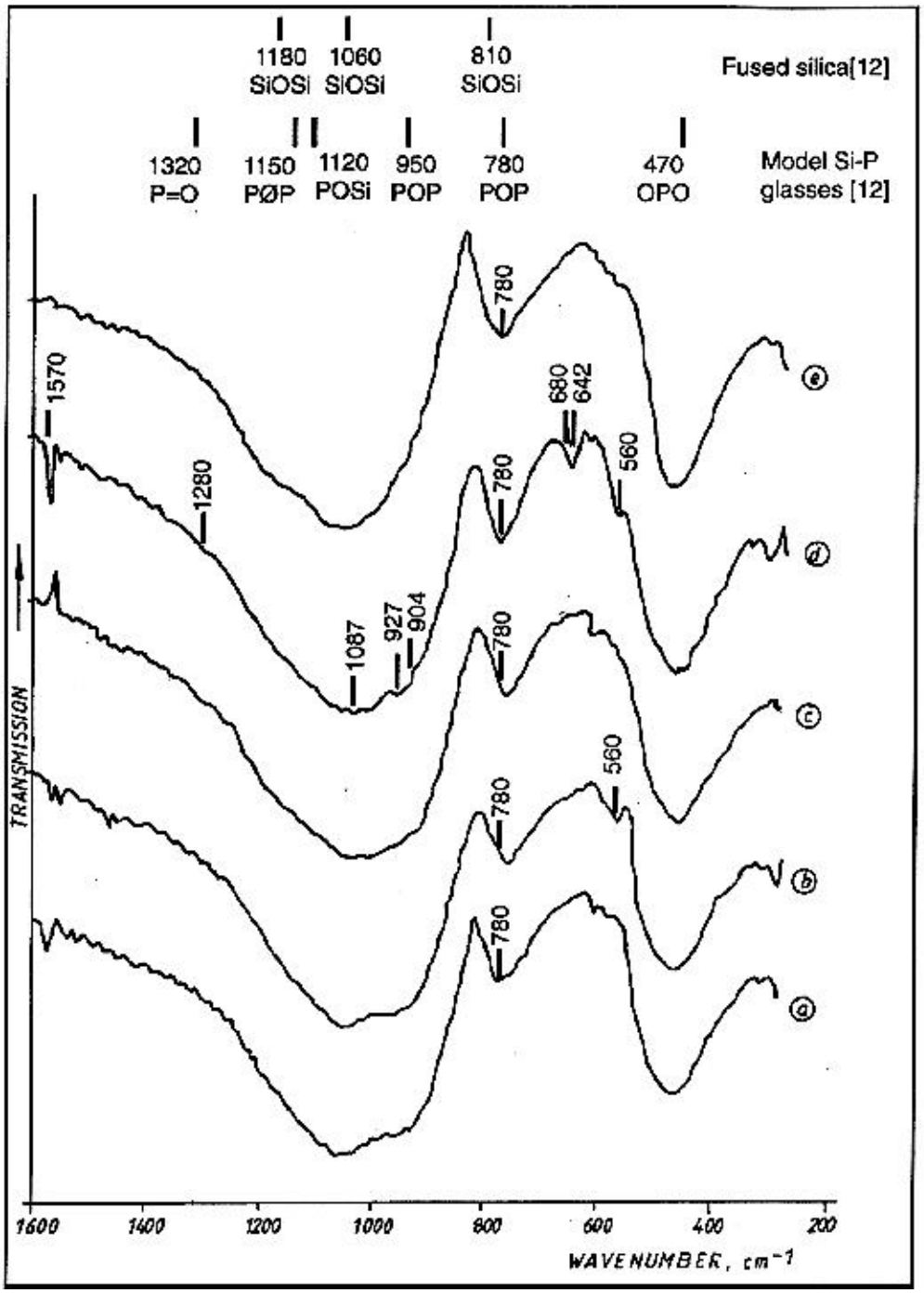

*Fig. 3 IR transmission on spectra: a) OP 17 glass; b) OP 17 (*720^{o}C*,17h); c)OP 28 glass; d)OP 28 (760^{o}C, 24h);e) OP 9 glass*

The analysis of infra-red transmission spectra structure allows to find a general regularity in forming vibration spectra of oxide glasses with silicate and phosphate bases, out of a relatively small number of constant spectral forms - comparted with the amount of samples that differ in composition - belonging to structure groupings with constant composition or chemical formations. For a helpful spectral assignments the characteristic

bands of fused silica and silico-phosphate model glass (10% P_20_5) according to reference [12) are also shown at the top of fig. 3. The 1620 cm^{-1} band in the model glass clearly assigned to P-OH bonds is shifted to 1570 cm^{-1} in our OP 17 and OP 28 glasses. No bands in this position appeared in OP 9 glass without P_20_5. The 1340 cm^{-1} band assigned to P=O bond stretching vibration (in calcium phosphate content glasses) is shifted to 1280 cm^{-1} in OP 17-OP 28 glasses and no bands appear in OP 9 glass. The specific shoulder at 1280 cm^{-1} is more pronounced in heat treated glasses according to [12]. The medium absorption at 1260 cm-1 indicates the intensity of P=O vibration of metaphosphate. The spectra of all glasses are also characterized by a strong absorption maximum at 1090-1070 cm^{-1} (mainly di- and metasilicate groups); a maximum of an average intensity present at 970-940 cm^{-1} can be referred to the bridge stretching vibration SiO, $\mathbf{q}$Si$\mathbf{q}$, and SiO_3 (meta). The characteristic 810 cm^{-1} band (Si$\mathbf{q}$Si, $\mathbf{q}$Si$\mathbf{q}$) is shifted, all samples showing a strong absorption at 780 cm^{-1} (specific for sodium silicate). The broad symmetric double peak at 950 cm^{-1} and 1050 cm^{-1} more accentuated in heat treated glasses, is attributed to Si-O-Ca/Si-O-Na and Si-O-Si bondings respectively (2,13].

The vibration of Ca-O bonds are included in the 460-470 band [12]. A striking feature of thermally treated glasses is the occurrence of specific shoulders 680, 642, 560 cm^{-1} on OP 28 and 560 cm^{-1} on OP 17 IRT spectra. The assignments are the probable structural groups or compounds, a "defect structure" in vitreous SiO_2 or double peaked distribution of bond angles / bond lengths less distorted SiO_6 units or a "higher density". XRD and SEM showed the apatite/wollastonite crystallization (OP28) or spherulites formation (OP 17).

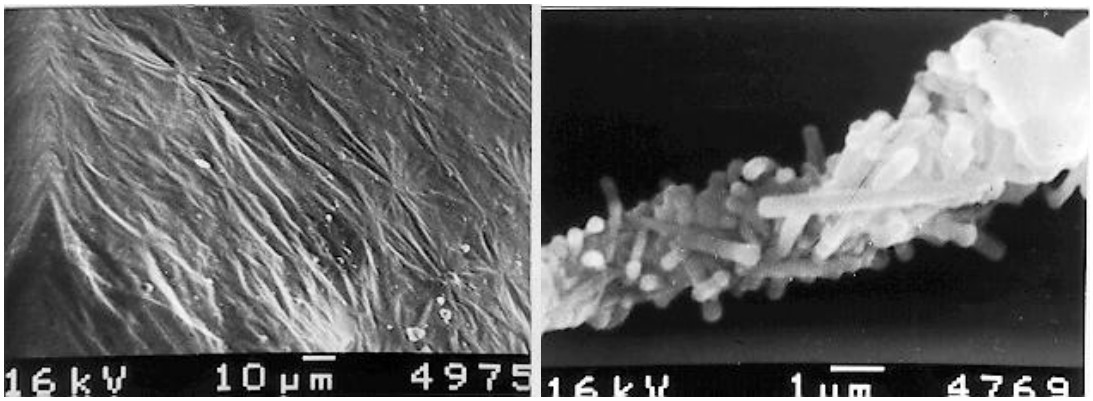

Fig. 4a, b SEM: a) cryptocrystallization of thermally treated OP 17 glass (720°C,17h); concentric wollastonite needles organized in spherules [5]; b) very thin cylindrical needles-shaped wollastonite, full growth on hair like crack.

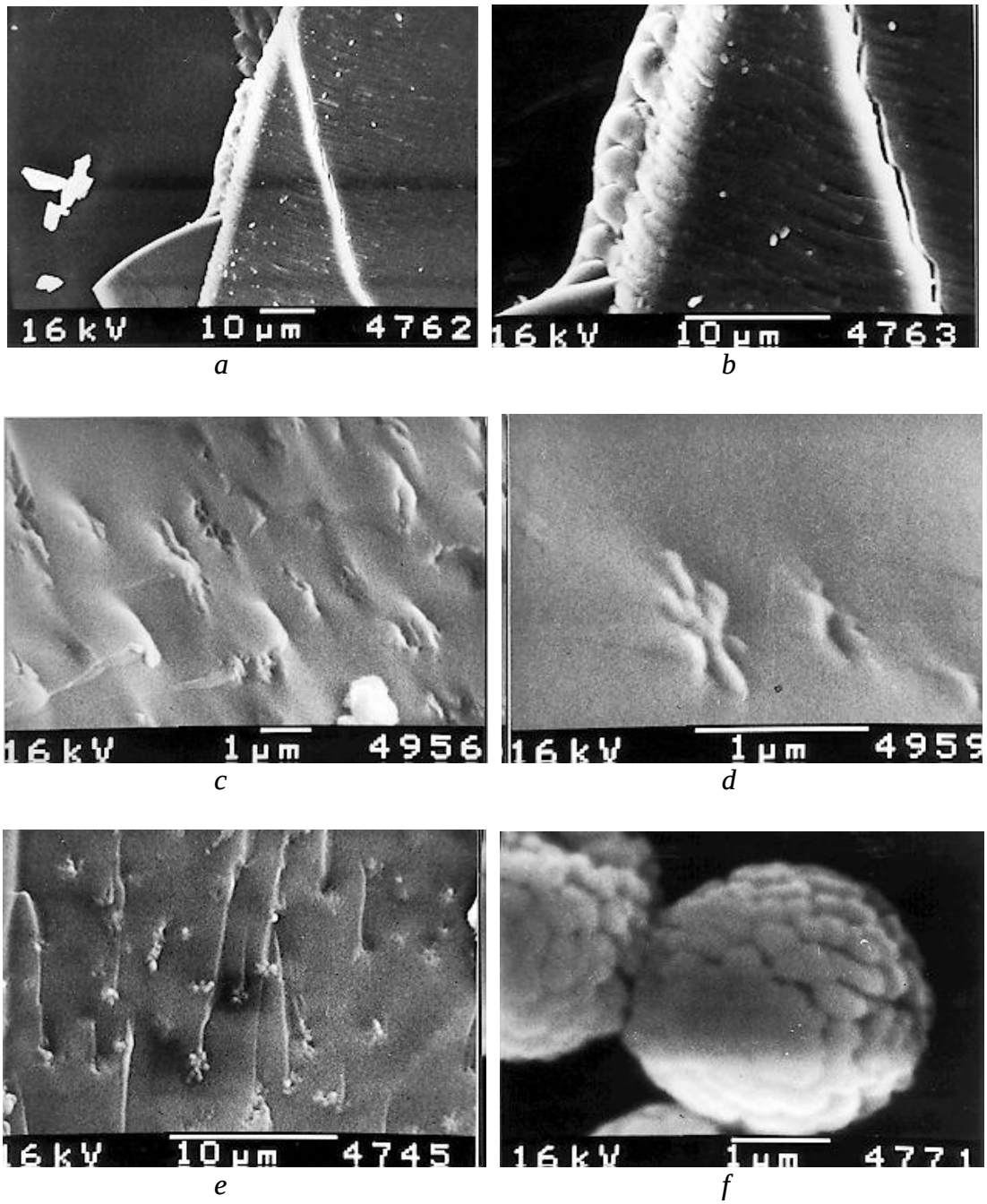

a *b*

c *d*

e *f*

Fig. 5a, b, c, d, e, f SEM a), b) Bulk crystallization of glass OP 17 (720^{o}C, 17h) "wollastonite precipitates only from the outher surface of a thick body" [10] causing a large crack in glassy volume; c) glassy microphase separation being the promotor for crystallization during transition from the glassy to glassy crystalline state, glass OP 17 with 4.2% P_2O_5; d) detail-hexagonal calcium ortophosphate-symmetrical segregation as primary crystalline phase [2]; e) apatite on siliceous striae [10]; f) apatite formed on the inner surface of bubble, glass OP 28 [760^{o}C, 24h]

REFERENCES

1. STRNAD, Z. and DOUGLAS, R. W. - Nucleation and crystallization in soda-lime-silica system, Phys. Chem. Glasses,14 (1973), 2, 33-36
2. VOGEL, W.- Glaschemie, Deutscher Verlag fur Grundstoffindustrie, Leipzig (1979)
3. GONZALES OLIVIER, C.J.R., JAMES, P.F., ROBBINS, C.R. and McMURDIE, H.F.- Rates of crystal nucleation and growth in $(100-x)Na_2O{\cdot}2CaO{\cdot}3SiO_2{\cdot}xNaF$ glasses, XVlth Intern. Congress on Glass, Madrid (1992), 5, 3-8
4. McMILLAN, P.W.-Glass-ceramics, Academic Press, London-N.Y.- San Francisco, 1979, 2nd Ed.
5. SARKISOV, P.D.-The modern state of technology and application of glass-ceramics, Survey papers of the XV-th International Congress on Glass, Leningrad (1989), 411-441
6. MAZURIN, O.V.- Porai-Koshits, E.A., Amsterdam, Elsevier,1983
7. GALLIANO, P.G., PORTO LOPEZ, J.M.- Magnesium content effects on the crystallization behaviour of bioactive glasses in the system $CaO-MgO-SiO_2-P_2O_5-CaF_2$, XVlth Int. Congress on Glass, Madrid (1992) 5, 75-80
8. WANGE, P., VOGEL, J., GOTZ, W., HOLAND, W. and VOGEL, W.- Phase formation and crystallization behaviour of phosphatic glass-ceramics, XVlth Int. Congress on Glass, Madrid (1992) 5, 69-73
9. VOGEL, W. - Struktur und Kristallisation der Glaser, Deutscher Verlag fur Grundstoffindustrie, Leipzig (1971)
10. KOKUBO, T. - Glass-Ceramic A-W : Structure, Properties and Biomedical Applications, 5th International Otto Schott Colloq., Jena (1994),105-110
11. J.C.P.D.S.1972 :19-249;19-249+19-249A; 24-33; 20-20A
12. SPURCACIU, C. - The IR spectra of silicophosphate glasses and their structure, Mat. Const. XVII (1),1987, 58-64
13. LAZAREV, A.M. - Vibration spectra and silicates structure, Leningrad,1968
14. KATZSCHMANN, A. WANGE, P.- Crystallization Behaviour of Aluminosilicate Glasses and Glass-Ceramics with Different Content of MgO, 5th Int. Otto Schott Colloq., Jena,1994, 412-415

CRYSTALLIZATION OF HIGH-ALUMINA SILICATE GLASSES

Ali A. Omar
National Research Centre, Egypt

Abstract

The crystallization behaviour of some high-alumina Na_2O-CaO MgO Al_2O_3-SiO_2 glasses was investigated. In the law-magnesia compositions nepheline, or nepheline solid solution, first develop and then transform at higher temperatures into plagioclase feldspars. In compositions containing considerable amounts of magnesia a preferential formation of pyroxene solid solutions takes place and nepheline only forms at high temperatures.

Titanium and chromium oxides are effective in catalyzing the crystallization process. The presence of fluorine facilitates the formation of the framework silicates-nepheline and feldspars.

The thermal expansion coefficients and microhardness of the resultant crystalline products are considerably higher than those of the original glasses. The obtained results reveal that attractive glass-ceramics may be produced from such compositions by controlling the heat treatment parameters.

The formation of the different solid solutions is discussed in the light of crystal chemistry of nepheline and pyroxene phases.

INTRODUCTION

Many glass-ceramics with good physical and chemical properties contain high amounts of aluminium oxide in the structure of their crystalline phases. The presence of alkali aluminosilicate crystal phases is most desirable in glass-ceramics. Nepheline- containing glass-ceramics have been investigated by many authors; they enjoy high strength and can be easily glazed (1-5).

On the other hand, during glass manufacture the part of soda-lime(magnesia) glass in contact with aluminosilicate refractories becomes increasingly enriched in alumina and aluminium-containing crystal phases, hybrid in composition between the refractory and the glass, develop in it.

The study of the role of aluminium during the crystallization of alkali and alkaline- earth aluminosilicate glasses is thus of great interest. In this context the crystallization behaviour of some low magnesia compositions (~1% MgO), expressed mainly by the system nepheline ($NaAlSiO_4$) - anorthite ($CaAl_2Si_2O_8$) - silica (SiO_2), and others containing considerable amounts of magnesium oxide (>5%), related to the pyroxene-nepheline compositional system, was investigated.

EXPERIMENTAL TECHNIQUE

The compositions of the investigated glasses fall within the following range in wt.% (without the nucleating agents): 48-55 SiO_2, 20-28 $A1_2O_3$, 0.6-0.9 Fe_2O_3, 5-11 CaO,1-7 MgO, 0-3 BaO or ZnO, 9-13 $Na_2O + K_2O$, 0-0.5 Li_2O.

Kaolinitic clays, quartz sand, dolomite, limestone and soda ash were the main batch ingredients used. Some Li_2CO_3, TiO_2, Cr_2O_3, ZnO, $BaCO_3$ were used to introduce the corresponding oxides into the glass composition. Some other ingredients including boric acid, arsenic trioxide and fluorine-containing compounds were sometimes used to facilitate batch melting and fining of the resultant melts. TiO_2 (up to 6%) and Cr_2O_3 (up to 0.5%) were added to play the role of nucleation and crystallization catalysts in the investigated glasses.

Melting of the batches was conducted at 1500°C for 2-4 hours in an electrically heated furnace. The resulting melts were cast as rods and buttons and were properly annealed at 550-600 °C. The annealed glasses were then subjected to differential thermal analysis and were heat-treated according to different one and double-stage schedules..

The developed crystalline phases were determined by powder X-ray diffraction. The coefficient of thermal expansion, density and the indentation microhardness were measured for the parent glasses and their crystalline products after heat-treatment.

RESULTS

CRYSTALLIZATION OF LOW MAGNESIA GLASSES

After double stage heat-treatment at 700 °C and 820 °C with a holding period of 45 minutes at each temperature the glass samples preserved their glassy appearance with a high degree of gloss without any sign of deformation, however, their colour darkened to nearly black imparting the samples a very attractive appearance. After heat-treatment at 900 °C the samples became opaque and acquired gray and chocolate brown colours.

Samples treated at 820 °C developed ultra fine-grained microstructure, those treated at 900 °C developed a uniform very fine-grained microstructure (with TiO_2), and a fine- grained microstructure composed of interlocking randomly oriented short needle-like crystals, with some six-sided crystals in the interstices (with Cr_2O_3).

XRD analysis of the glass-ceramics, obtained after the double stage heat-treatment (700 °C /45 min. + 820 °C /45 min.), revealed a considerable degree of crystallinity with the formation of a nepheline crystal phase as the predominant crystalline structure (e.g., Fig. la), sometimes with minor plagioclase crystals. After heat-treatment of similar glasses at 900 °C for two hours, a major plagioclase crystalline phase developed (e.g., Fig. lb).

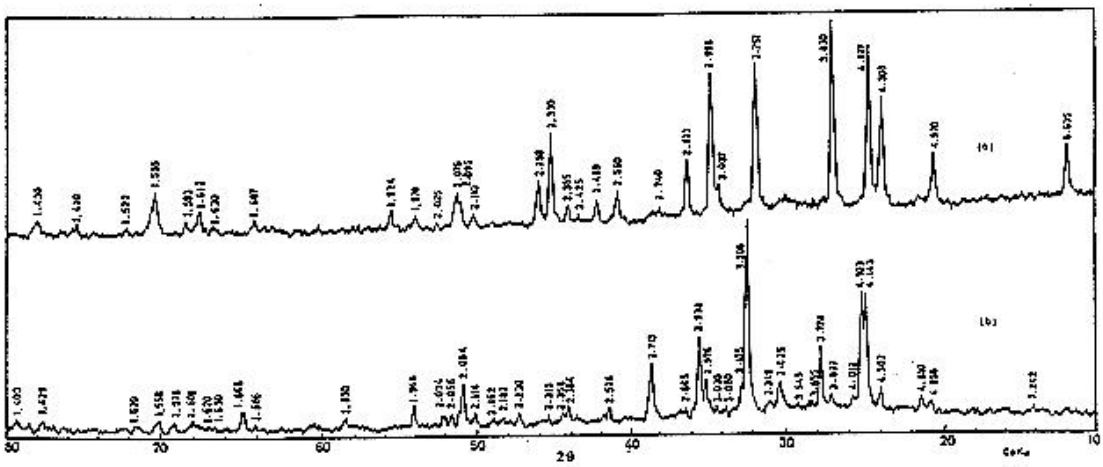

Fig.1 X-ray diffraction patterns of low-magnesia glass No.1 after heat-treatment

This investigation also revealed the effectiveness of Cr_2O_3 as a nucleating agent in promoting the process of crystallization and nepheline phase formations in such glass compositions. The use of Cr_2O_3 reduces batch cost by the unnecessity of addition of much TiO_2 to promote crystallization. The inherent titanium dioxide of the used clays (sometimes exceeds 1.8%) together with Cr_2O_3 (0.5%) can provide efficient nucleation during the ceramming of such compositions.

CRYSTALLIZATION OF GLASSES CONTAINING CONSIDERABLE MAGNESIA

The parent glasses were amber in color and changed through crystallization to opaque light brown, gray, bluish gray, grayish white and white. Many of the samples developed bands of different shades within the above mentioned color range exhibiting a beautiful marble-like effect.

The investigated glasses developed major pyroxene phases upon heat-treatment, up to l000 ^oC for durations up to 4 hours, sometimes with minor nepheline (e.g., Fig.2). The crystallization of nepheline was enhanced at the higher temperatures and in the presence of boric oxide and fluorine in the parent glass composition. Such additives obviously facilitated the crystallization of this structurally more complex framework silicate phase.

The formation of nepheline was also enhanced in samples containing Na_2O, as the sole alkali oxide, rather than in the presence of K_2O in the parent glass composition. The amount of nepheline developed in samples containing ZnO was slightly greater than in samples with BaO heat-treated under the same conditions. Some low - form carnegieite may also develop.

Titanium dioxide (6%) was found effective in catalyzing the crystallization process leading to the formation of fine- and very fine-grained microstructures.

PROPERTIES OF THE OBTAINED GLASS-CERAMICS

Table 1 summarizes some of the properties measured for the obtained glass-ceramics.

Table l Properties of some obtained glass-ceramics

Sample No.	Heat-treatment T°C	Time (h)	Visual examination	Microscopic examination	Crystal phase	Density	Thermal expansion α (20-300°C) x10^7	Vickers hardness No.
Low magnesia								
1	----	—	Amber glass	Amorphous	----------	2.517	69.2	751
	700	0.75	Black glassy	ultra fine-grained	Nepheline	2.575	87.9	888
	+820	0.75		microstructure				
2	-----	—	Amber glass	Amorphous	----------	2.512	66.9	702
	700	0.75	Black glassy	ultra fine-grained	Nepheline	2.569	90.8	830
	+820	0.75		microstructure				
With considerable magnesia								
3	—	---	Amber glass	Amorphous	----------		73.0	727
	1000	4	Opaque,light grey	Very fine-grained uniform microstructure	Diopsidic pyroxene			
	710	1	Opaque,white		,,	2.766	82.4	946
	+1000	2						
	800	1	Opaque		,,	2.729	82.2	877-892
	+1000	1	whitish grey					
4	----	—	Amber glass	Amorphous	----------		79.0	742
	690	1	Opaque,	Fine-grained micro-	Diopsidic	2.764	84.6	843-866
	+950	1	light grey	structure of acicular crystals	pyroxene, traces of nepheline			

DISCUSSION

During the crystallization of alkali and alkaline earth aluminosilicate glasses the aluminium ions combine with the alkalies (K and/or Na) to form either alkali aluminosilicates, or alkali aluminium silicate, molecules.

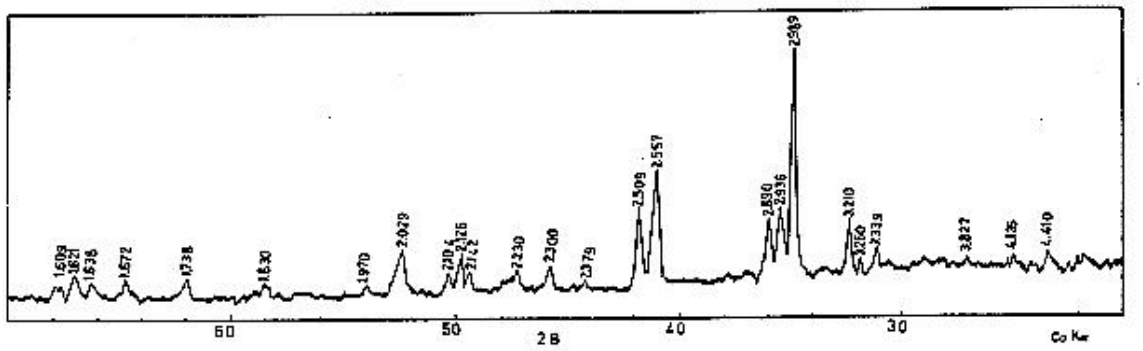

Fig.2 X-ray diffraction pattern of glass No.4 after heat-treatment

In low-magnesia compositions (~1% MgO), such as those of the present investigated glasses, the aluminium ions preferentially assume tetrahedral coordination, substituting for silicon in the Si-O tetrahedra, forming alkali aluminosilicate molecules which first separate out in the glass as nepheline ($NaAlSiO_4$) or nepheline solid solutions.

Calculations of such glass compositions (apart from the nucleating agents) to the possible crystalline phases reveal the following approximate composition:-

Nepheline $NaAlSiO_4$ 48 wt %
Anorthite $CaAl2Si_2O_8$ 25

Silica SiO_2 20
The rest being pyroxene and eucryptite.

Nepheline, however, is capable of accommodating considerable amounts of other molecules into its structure. Thus, up to 37 molecular percents of anorthite ($CaAl_2Si_2O_8$) can dissolve in $2NaAlSiO_4$ forming solid solutions. Silica itself can be accommodated in the nepheline structure up to about 25 mole percents (6). Nepheline is capable of mixing with $CaAl_2O_4$ up to 60% of the latter (7). $NaAlSiO_4$ and $KAlSiO_4$ mix together in all proportions at high temperatures; at low temperatures they form limited solid solution series. Similarly the present author believes that some $LiAlSiO_4$ molecules can also be incorporated in the nepheline structure with lithium substituting for the sodium ions.

Thus, in view of the crystal chemical characteristics of the nepheline phase, many of the elements present in such low-magnesia experimented glasses can be well tolerated within a crystalline nepheline solid solution structure. In this manner the appearance of nepheline as a major crystalline phase in samples treated at 820 ^oC can be substantiated.

The nepheline phase is incompatible with silica with which it reacts, under favourable conditions, to form the more saturated sodium aluminium silicate ($NaAlSi_3O_6$) or sodium aluminosilicate ($NaAlSi_3O_8$) phases. The formed nepheline crystal phase in these investigated glasses after heat-treatment at 820 ^oC should, thus, be considered thermodynamically metastable.

In such low-magnesia compositions containing excess silica, over the nepheline stoichiometry, the nepheline molecules react with the excess silica, at such higher temperatures, to form albite ($NaAlSi_3O_8$) molecules. These molecules rather develop solid solutions with the possible anorthite ($CaAl_2Si2O_8$) molecules forming a mixed plagioclase crystalline structure.

Calculation of the glass compositions (apart from the nucleating agents) to plagioclase molecules reveals the following approximate composition :-

Nepheline (or carnegeite) 24 wt%
Plagioclase 69
The rest being pyroxene and eucryptite.

Consequently, in spite of the considerable silica content of the system, the crystallization of such and similar glasses starts with the formation of nepheline, or nepheline solid solution, which then transforms to plagioclases at higher temperatures.

It is understood that varying amounts of glass, cementing the developed crystals, can still be present after any of the heat-treatment cycles applied. The composition of this residual glassy phase is likely to be more siliceous than the original parent glass before heat treatment. The presence of residual siliceous glassy phase in the present investigated glass ceramics is desirable. The high viscosity of such glass helps in reducing the deformation of the samples during heat-treatment. It also possesses a lower coefficient of thermal expansion (due to its high silica content) which may generate a system of favourable internal stresses in the material imparting high mechanical strength to the samples.

In compositions containing considerable amounts (>5%) of magnesia, a substantial part of the aluiminium ions assumes octahedral coordination, beside the tetrahedral coordination, especially under nonequilibrium conditions of crystallization and is hosted in a pyroxene structure. The sharing of aluminium in these coordination positions is favoured by the ratio of its ionic radius to

that of oxygen which approaches the geometrical limit of stability between the 4 and 6 coordinations. In such glasses, crystallization of diopsidic pyroxenes as a major phase takes place in spite of the fact that the calculated amounts of diopside in these compositions are relatively low.

The formation of such great percentages of diopsidic pyroxene phases is due to the wide range of isomorphous substitutions in the pyroxene formula. Thus, instead of the formation of a nepheline phase $(Na,K)AlSiO_4$, sodium aluminium silicate molecules $(Na,K)AlSi_2O_6$ (jadeite) are formed and stabilized as an isomorphous component in a host pyroxene structure of complex composition. The accommodation of aluminium containing components in diopside increases under nonequilibrium conditions of crystallization (8). Calculation of these investigated glass compositions reveal the possibility of formation of over 60% of pyroxene solid solutions in which the jadeite component constitutes about 40%. The ease with which the pyroxene phase is formed relative to nepheline can be correlated with the difference in structural complexity and activation energies for crystallization of these phases.

REFERENCES

(1)Duke, D.A. et al, J. Am. Ceram Soc., 50,2,67(1967).
(2)Russak, M.A. and Kivlighn Jr, H.D., ibid. 58,5-6,258(1975).
(3)MacDowell, J.F., Ceram. Bull., 63, 2, 282 (1984).
(4)Omar, A.A. and Ali, E.M., European Ceramic Society Third Conference, 2,1169, Madrid (1993).
(5)Omar, A.A., 5th International Otto Schott Colloquium, 428, Jena, Germany (1994).
(6)Winchell, A.N. and Winchell, H. The microscopical characters of artificial inorganic solid substances, Academic Press, New York and London(1964).
(7)Goldsmith, Am. Min., Vol. xxxiv, 471 (1949).
(8)Omar, A.A. The Desert Inst. Bull., Vol. xx, No.2, July (1970).

ACKNOWLEDGEMENTS

This work was done within the framework of a research project sponsored by the Egyptian Academy of Scientific Research and Technology.

DETERMINATION OF THE OPTICAL CONSTANTS OF GLASS IN THE INFRARED USING KRAMERS KRONIG ANALYSIS

Peter A. van Nijnatten
TNO Institute of Applied Physics, The Netherlands

Abstract

Kramers-Kronig analysis (KKA), is a technique for deriving the optical constants from a single reflectance spectrum, using the KRAMERS-Kronig relations (KKR's). Its application in the determination of optical material constants of glass in the infrared, for which glass is generally opaque, is investigated. KKA requires integration over an infinite frequency domain, for which the reflectance must be known which can only be measured in a finite frequency range, necessitating extrapolation methods. The paper presents a new extrapolation formula for the infrared reflectance of dielectrics. The performance of three ordinary KKR's and three modified (M)KKR's, among which two new MKKR's, is evaluated using synthetic spectra based on a Lorentz oscillator model for the permitivitty. A method is used in which the CPV (Cauchy Principal Value) integrals are partly integrated with respect to the frequency in one interval, and to the wavelength in the other, leading to finite integration domains. An 11-point integration rule for CPV integrals is derived improving the computation accuracy considerately. In experiments, the optical constants of BK7 are determined, yielding accurate values of the complex refractive index in the wavelength range from 5 μm to 50 μm.

1. INTRODUCTION

The interaction of electromagnetic radiation with matter is described by optical material constants such as the permitivity, the conductivity or the complex refractive index. The use of different types of glass in interference filters, optical fibres, optical instruments, coated glazing for windows and other devices, require an accurate knowledge about their optical constants over wide ranges of wavelengths. Spectral values of the refractive index n and extinction coefficient κ of glass in the UV/VIS/NIR wavelength range, can be accurately determined from the spectral reflectance and transmittance[1]. This method, however, cannot be used in the case when the transmittance tends to zero as for glass in the far infrared. In this case, an alternative lies in the application of Kramers -Kronig relations (KKR's)[2,3].

The procedure for determining the optical constants n(ω) and κ(ω) using the Kramers -Kronig relations, usually consists of the following four steps:

1. The spectral (near)normal reflectance R(ω) is measured with a spectrophotometer for a frequency range as wide as possible.
2. Measurement data is extended in the unobserved regions by extrapolation, e.g. with the aid of known physical relations describing the optical behavior in these regions.

3. Using the Kramers-Kronig relations, the argument $\phi(\omega)$ of the amplitude reflection coefficient is determined from the extended reflectance spectrum.
4. The optical constants $n(\omega)$ and $\kappa(\omega)$ are determined from $R(\omega)$ and $\phi(\omega)$

For normal incidence, the complex amplitude reflection coefficient $\subseteq = R^{1/2}\exp\{i\phi\}$ at the air interface of a semi-infinite medium is related to the optical constants n and κ through a Fresnel equation. Inverting this equation results in

$$n(\omega) - i\kappa(\omega) = n_a \frac{1 - R(\omega) + 2i\sqrt{R(\omega)}\sin(\phi(\omega))}{1 + R(\omega) - 2\sqrt{R(\omega)}\cos(\phi(\omega))} \qquad (1)$$

where n_a is the refractive index for air. From Eq.(1) the optical constants $n(\omega)$ and $\kappa(\omega)$ can be determined if both $R(\omega)$ and $\phi(\omega)$ are known. $R(\omega)$ can be measured directly with a spectrophotometer.

The research discussed in this paper is an extension of work published earlier [1], which involved the determination of optical constants of glass in the UV/VIS/NIR wavelength range. In the following sections, 6 equivalent KKR's are evaluated and their numerical integration investigated. As an example, the optical constants in the infrared of BK7 are determined.

2. KRAMERS -KRONIG RELATIONS

It can be shown [4] that Kramers-Kronig relations exist between the spectral argument $\phi(\omega)$ of the amplitude reflectance (also referred to as the phase spectrum) and $\ln(R(\omega))$. For the calculation of $\phi(\omega)$ from the measured power reflectance $R(\omega)$, each of the following equivalent KKR's can be used [5,6].

$$\phi(\omega_j) = -\frac{\omega_j}{\pi} P\int_0^\infty \frac{\ln(R(\omega))}{\omega^2 - \omega_j^2}\, d\omega \qquad (2a)$$

$$\phi(\omega_j) = -\frac{\omega_j}{\pi}\int_0^\infty \frac{\ln(R(\omega)) - \ln(R(\omega_j))}{\omega^2 - \omega_j^2}\, d\omega \qquad (2b)$$

$$\phi(\omega_j) = -\frac{1}{2\pi} P\int_0^\infty \frac{d\ln(R(\omega))}{d\omega} \ln\left|\frac{\omega + \omega_j}{\omega - \omega_j}\right| d\omega \quad . \qquad (2c)$$

If the argument $\phi(\omega)$ of the amplitude reflectance at one point can be determined , an expansion around that point will yield a modified integral whose value is less determined by the contribution of the interval where $\omega^2 >> \omega_j^2$. The following Modified Kramers -Kronig equations (MKKR's) have proved to be useful [7]:

$$\phi(\omega_j) = \frac{\omega_j}{\omega_h}\phi(\omega_h) + \frac{\omega_j(\omega_j^2 - \omega_h^2)}{\pi} P\int_0^\infty \frac{\ln(R(\omega))}{(\omega^2 - \omega_j^2)(\omega^2 - \omega_h^2)}\, d\omega \qquad (3a)$$

$$\phi(\omega_j) = \frac{\omega_j}{\omega_h}\phi(\omega_h) + \frac{\omega_j(\omega_j^2 - \omega_h^2)}{\pi} P\int_0^\infty \frac{\ln(R(\omega)) - \ln(R(\omega_j))}{(\omega^2 - \omega_j^2)(\omega^2 - \omega_h^2)}\, d\omega \quad , \qquad (3b)$$

$$\phi(\omega_j) = \frac{\omega_j}{\omega}\phi(\omega_h) + \frac{\omega_j(\omega_j^2 - \omega_h^2)}{\pi} P\int_0^\infty \frac{\ln(R(\omega)) - \ln(R(\omega_h))}{(\omega^2 - \omega_j^2)(\omega^2 - \omega_h^2)}\, d\omega \qquad (3c)$$

in which the function ϕ is known for $\omega=\omega_h$.The first equation has been derived by Ahrenkiel[8] The other two have been derived by replacing $\ln(R(\omega))$ in Eq.(1d) by $\ln(R(\omega)/R((\omega_m))$ with m=j or m=h. As a result, one of the two poles in Eq.(3a) is removed.

3. NUMERICAL INTEGRATION SCHEME

The aim of the present investigation is to determine optical constants in the frequency range $\omega <$ 2000 cm^{-1} (defined as $\omega = 1/\lambda$), for which glass is nontransparent. A frequency interval of 10 cm^{-1} gives sufficient resolution in order to describe the optical behavior of glass in this range. The output data files of the KKA computer codes contain 380 values of $\phi(\omega)$ in the frequency range 205 cm^{-1}-3995 cm^{-1} with 10 cm^{-1} intervals. The choice of the abscissa values (205, 215, 225,235, ...) proves to be convenient for the evaluation of the CPV part (Cauchy Principle Value) of the integrals.

Since measurement data for the (IR) frequency range 200 cm^{-1} - 4000 cm^{-1} is usually available in 1 cm^{-1} intervals, and for the (UV/VIS/NIR) data is presented as function of the wavelength in 1 nm intervals (range 200 nm - 2500 nm), it is convenient to adapt these intervals for the numerical integration. The input data files prepared for the KKA programs, therefore contain the entire reflectance spectrum, divided over 6502 reflectance values, of which 4001 values at frequencies ω in the range 0 cm^{-1} - 4000 cm^{-1} (1 cm^{-1} intervals), and 2501 values at wavelengths λ in the range 0 nm - 2500 nm (1 nm intervals). The reflectance at λ =2500 nm is given twice, once as R(2500nm) and once as R(4000cm^{-1}). By deviding the integration domain into two ranges, integrating the high frequency part with respect to the wavelength λ and the low frequency part with respect to the frequency, we obtain two finite integration domains. Taking into account the format of the input data and the 10 cm^{-1} interval of the output data $\phi(\omega)$, the following integration scheme has been chosen for the numerical evaluation of the KKR's

$$I(\omega) = \sum_{\lambda}^{19} F_{\lambda}(\lambda) + \sum^{249} F_{\lambda}(\lambda) + \sum^{p} F_{\omega}(\omega) + I_{CPV}(\omega) + \sum^{399} F_{\omega}(\omega) - \sum^{19} F_{\omega}(\omega) \qquad (4)$$

where p = (ω - 5)/10 with ω = 205, 215, 225,....., 3995 and

$$F_{\lambda}(\lambda) = \sum^{10} W_j \, f(\lambda'_{10m+j};\lambda) \quad , \quad F_{\omega}(\omega) = \sum^{10} W_j \, f(\omega'_{10m+j};\omega) \qquad (5)$$

with f the integrand in the KKR and Wj (j = 1, 2, 3,....., 10) a weighing factor depending on the choice of integration rule.

Table 1 Weighing factors of W_j of integration rules 1-4 for Eqs. (5)

j	W_j			
	rule1 trapezium rule	**rule 2 Simpson's rule**	**rule 3 Newton-Cotes**	**rule 4 11 points rule**
0,10	0.5	1/3	95/288	480/1512
1,9	1	4/3	375/288	2100/1512
2,8	1	2/3	250/288	900/1512
3,7	1	4/3	250/288	2100/1512
4,6	1	2/3	375/288	900/1512
5	1	4/3	190/288	2160/1512

In Table 1, values for Wj are listed for the Trapezium rule, Simpson's rule, a 6- points Newton-Cotes rule [9], and for an 11-points rule which has been derived using the Euler-Maclaurin summation formula [10].

The term I_{CPV} (ω) in Eq.(4) contains the point ω=ω′. The following three methods for the calculation of I_{CPV} have been compared:

Method A involves the use of one of the four integration rules listed in Table 1, and excluding the pole at $\omega=\omega_j$ from the integration.

Method B is similar to Method A, but the integrant in the pole is replaced by the average of the two neighboring values [11].

Method C is the following 11-points integration rule which has been derived

$$I_{CPV} = \int_{-\varepsilon}^{+\varepsilon} \frac{f(\delta)}{\delta} \, d\delta = 1.5964874\,(f_{j-1} - f_{j+1}) + 0.05752918\,(f_{j-2} - f_{j+2}) +$$

$$+ 0.1547147\,(f_{j-3} - f_{j+3}) + 0.3730299\,(f_{j-4} - f_{j+4}) + 0.0593331\,(f_{j-5} - f_{j+5}) \quad .$$

according to a method given by Davis and Rabinowitz [9]:

(6)

In the case of Eq.(2c), Method C has to be excluded since its integrand does not change sign when passing the point $\omega=\omega_j$ and therefore does not agree with the behavior of the type of integrand for which Eq.(6) has been derived.

For the evaluation of the integration rules, a synthetic spectrum of crystalline quartz has been used, simulated by a Lorentz oscillator band model (see Fig.1). This model fully complies with the KKR's and offers the possibility of calculating $\phi(\omega)$ for all ω and comparing the result with that obtained by KKA. The synthetic model spectra represent a worst case since for glass the peaks in the spectra are less sharp. Having 3 integration methods

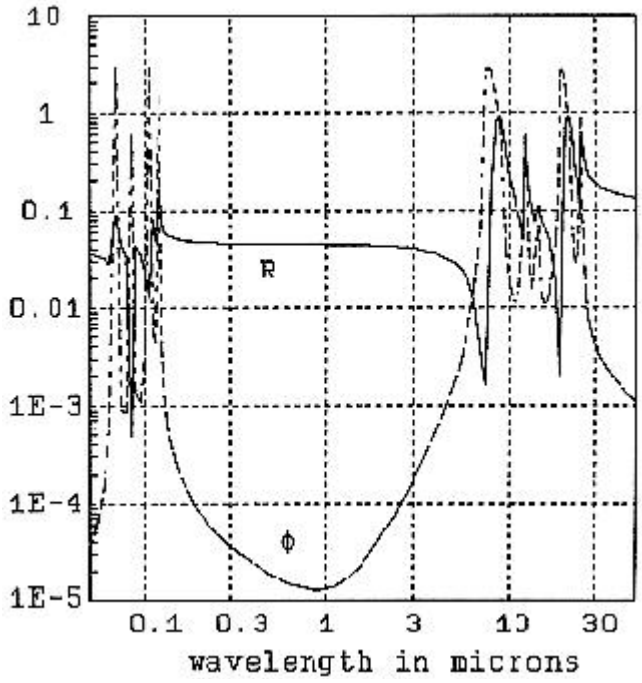

Figure 1. Model spectra of quartz.

for I_{CPV} (A, B and C) and 4 integration rules (1, 2, 3 and 4) for the rest of the spectrum, 12 different combinations can be evaluated. The result is summarized in Table 2. The best results are obtained with the new MKKR's Eq.(3b) and Ec.(3c) and integration method C1 in which I_{CPV} is computed by Eq.(6) and the trapezium rule is used for the evaluation of the remaining integrals.

Table 2 Average absolute error in the computation of $\phi(\lambda)$ the KKR's for various integration methods. In the case of Eq's.(3a-c), ω_h=2005 cm^{-1}.

	Eq(2a)	**Eq(2b)**	**Eq(2c)**	**Eq(3a)**	**Eq(3b)**	**Eq(3c)**
A1	9.0%	6.2%	63%	134%	7.1%	5.5%
A2	14%	8.1%	80%	179%	9.5%	7.4%
A3	6.3%	4.9%	73%	89%	4.8%	3.6%
A4	15%	9.0%	82%	192%	10%	7.9%

B1	2.6%	2.6%	11%	0.024%	0.24%	0.24%
B2	1.6%	1.6%	13%	0.11%	0.87%	0.087%
B3	2.9%	2.9%	82%	0.41%	0.29%	0.29%
B4	1.4%	1.4%	28%	0.070%	0.064%	0.064%
C1	2.6%	2.6%	-	0.016%	0.016%	0.016%
C2	1.6%	1.6%	-	0.062%	0.062%	0.062%
C3	2.9%	2.9%	-	0.29%	0.29%	0.29%
C4	1.3%	1.3%	-	0.036%	0.036%	0.036%

4. EXTRAPOLATION OF THE MEASURED REFLECTANCE SPECTRUM

An extensive literature search didn't reveal an extrapolation formula for dielectrics in the low-frequency range. The following formula, which proved to fit excellent on the Lorentz Model, has been obtained by expanding the Lorentz model equation for the permitivity in factors ω^2 and neglecting terms with a degree in ω higher than 4:

$$R(\omega) = R(0) + C_1\omega^2 + C_2\omega^4. \qquad (7)$$

R(0) is calculated from the static permitivity data from literature, C_1 and C_2 are calculated from R(ω) and his derivative at $\omega = 200$ cm^{-1}. In the present research Eq.(6) has been used for the range $0 < \omega < 200$ cm^{-1}. For extrapolation of the UV part ($0 < \lambda < 200$ nm), R(λ) is assumed to be constant and equal to R(200nm).

As a result of these extrapolations, a systematic error Δφ(ω) will occur. Zaitsev and Fedorov [13] have proposed a phase correction procedure which in the present case yields:

$$\Delta\phi(\omega) = a\,\omega + b\,\omega^{-1} \qquad (8)$$

The constants a and b are found by fitting Eq.(7) on $\Delta\phi(\omega) = \phi_{R,T}(\omega) - \phi_{KKA}(\omega)$ in the transparent range where φ(ω) can be determined using the R,T-method. Table 3 summarizes the results of the error analysis of the extrapolation with and without the phase correction. Applying the phase correction drastically improves the accuracy for all extrapolated spectra, except for Eq.(2b).

Table 3 Average absolute error as result of the extrapolations.

(M)KKR :	**Eq. (2a)**	**Eq. (2b)**	**Eq. (2c)**	**Eq. (3a)**	**Eq. (3B)**	**Eq. (3C)**
int. method :	C4	C4	B1	C1	C1	C1
error before correction :	662 %	291 %	324 %	327 %	326 %	326 %
error after correction :	2.9 %	282 %	17 %	4.6%	1.3 %	1.2 %

5. THE OPTICAL CONSTANTS OF BK7

For the reflectance measurements, test samples of size 30 mm x 30 mm x 20 mm have been used, the back surface approximately 10° tilted with respect to the front surface in order to prevent the second surface reflectance from being detected during measurement. The specular reflectance in the infrared range (200 cm^{-1}-4000 cm^{-1}) has been measured using a Perkin Elmer 983 Infrared spectrophotometer equipped with a specular reflectance accessory. The low frequency part of the spectrum has been extrapolated using E.(7) for which R(0) has been calculated from the static permitivity [7]. For the reflectance in the wavelength range from 250nm

- 2500 nm results from a previous investigation have been used [1] . The high frequency reflectance was assumed to be constant R(λ< 250 nm) = R(250 nm). The KKA results were obtained using Eq. (3c) (with integration method C1) , taking $\phi(\omega_h) = 0$ at $\omega_h = 1505\ cm^{-1}$. The phase spectra were corrected using Eq.(8) with b=0, since the second term led to large extrapolation errors (negative values for ϕ), especially in the range > 30μm. The results are shown in Fig.2. The results for wavelengths smaller than approximately 7 μm are not very accurate due to the large amount of noise obtained in this range. The error in ϕ is large for wavelengths > 25 pm, possibly due to the error in R(0).

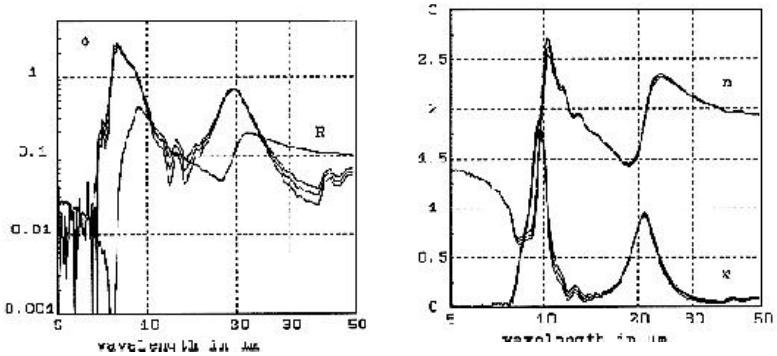

Figure 2 Averages and upper and lower limits (three curves per quantity), based on measurement uncertainty, of R(ω) and ϕ(ω) and of n(ω) and k(ω). ln case of the reflectance, the three curves seem to fall together due to its relatively high accuracy.

6. CONCLUSION

The application of KKA for the determination of optical material constants of glass in the infrared, for which glass is largely opaque, has been investigated. A method has been developed by which the Kramers -Kronig integrals, which essentially are Cauchy Principal Value (CPV) integrals, were partly integrated with respect to the frequency, and partly with respect to the wavelength, thereby obtaining two finite integration domains. An 11-point integration rule for the CPV part of the (M)KKR integrals has been derived which improved the accuracy of the integration. The performance of three ordinary KKR's and three modified (M)KKR's, from which two new MKKR's, have been compared using a synthetic model derived from the Lorentz dispersion model, with optical properties similar to those of glass. The new MKKR's gave the best performance in terms of accuracy. A newly derived extrapolation formula for the infrared reflectance of dielectrics (necessary for extending the finite measurement range) has been evaluated and proved to be successful. It was shown that when a constant reflectance extrapolation in the high-frequency region is used, the phase correction procedure proposed by Zaitsev and Fedorov drastically improves the result. Accurate values of optical constants of BK7 have been obtained with KKA in the wavelength range from
5μm to 50 μm.

REFERENCES

[1] Nijnatten, P.A. van, Determination of the optical constants of glass using the RT-method, Proc. of the Europ. Conf. of Glass Sc., Venice, Italy, June 1993.
[2] Rubin, M., Optical properties of soda lime silica glasses, Sol. En. Mat.,12 (1989), p.275-288.
[3] Hsieh, C.K. and Su, K.C., Thermal radiative properties of glass from 0.32 to 206µm, Solar Energy,22(1979), p.37-43.
[4] Smith, D.Y., Comments on the dispersion relations for the complex refractive index of circularly and elliptically polarized light, J. Opt.Soc.Am.,66(1976), p.454-460.
[5] Jahoda, F.C., Fundamental absorption of barium oxide from its reflectivity spectrum, Phys. Rev.,107(1957), p.1261-1265.
[6] Andermann, G., Caron, A. and Dows, D.A., Kramers -Kronig analysis of infrared reflection bands, J.0pt. Soc. Am.,55(1965), p.1210-1216.
[7] Nijnatten, P.A. van, Application of Kramers-Kronig relations in the frequency domain for the determination of optical constants of glass in the infrared. TN) report HAM-RPT-95-363, Eindhoven, March 1995.
[8] Ahrenkiel, R.K., Modified Kramers -Kronig Analysis of Optical Spectra, J.0pt.-Soc.Am.,61(1971), p.1651-1655.
[9] Davis, P.J. and Rabinowitz, P., Methods of numerical integration, Academic-Press,1984.
[10] Press, W.H. et. al., Numerical Recipies in Pascal, Cambridge University Press, Cambridge (UK),1989.
[11] Costaño Gonzàlez,0.D., de Dios Leyva, M. and Perez Alvarez, R., The Beta Parameter and Velicky's Approximation in the Calculation of the Optical Properties of GaAs, Phys. Stat. Sol.,71(1975), p111-116.
[12] Zaitsev, V.K. and Fedorov, M.I., Phase correction in Kramers-Kronig analysis, Opt. Spectrosc.,44(1978), p.691-693.

DOPING-INDUCED NANOCLUSTERS AND PECULIARITIES IN OPTICAL AND ELECTRICAL PROPERTIES OF CHALCOGENIDE SEMICONDUCTOR GLASS*

Emilia A. Smorgonskaya
Russian Academy of Sciences, Russia

Abstract

The concept of "ideal glass" implies random spatial distribution of interconnected constituent structural elements, so that the glass is homogeneous and isotropic on a macroscopic scale. Chalcogenide semiconductor glasses (CSG) are commonly considered as typical examples of such systems. Doping CSG with metal impurities, as a rule, results in a decrease of the optical and electrical gap, with no impurity conduction, and a nearly parallel red shift of the Urbach absorption edge suggesting the formation of homogeneous solid solutions.

In this paper, new evidence for strong deviations from this rule in metal-doped CSG are summarized. The deviations were first observed in thermally evaporated glassy $As_2Se_3Bi_x$ films (x=0.001-0.1) and then in In-and Ga-doped bulk As_2S_3 glass. The data on the non-Urbach absorption edge in these alloys as well as on electroabsorption, electrooptical effect and temperature dependence of conductivity in $As_2Se_3Bi_x$ films are presented to show a tendency for forming nanometric metaly-enriched clusters in a metal-depleted matrix.

The most surprising phenomenon related to nanoclusters in CSG is well-pronounced stable linear dichroism and briefringence discovered in glassy $As_2S_3In_{0.05.}$ As detailed X-ray diffraction data demonstrate, this optical anisotropy is closely connected with structural anisotropy due to predominant orientation of the In-enriched non- crystalline with nanoclusters 1-5nm in size. The impurity-induced "clusterization" is discussed as a way for producing novel "non-ideal" glasses offering properties of crystals.

---

* Full manuscript not available at the time of printing

EFFECT OF CERIUM AND IRON ON REGULARITIES OF RADIATION COLORING ISOTHERMAL RELAXATION IN SILICATE GLASSES*

Valerii I. Arbuzov
S.I.Vavilov State Optical Institute, Russia

Abstract

It is well known that the additions of the variable valence elements affect very strongly the efficiency of radiation color centers (CCs) formation in optical glasses. The reason of such an effect is the ability of the above elements to change their charge states when interacting with the electrons and holes which are generated in the glass matrix by the primary radiation. Thereby the cerium oxide additions make optical glass more transparent in the visible region of the spectrum as compared with the glass without cerium. In the case of Fe^{2+} ions the iron additions influence the CCs formation in the same way but in the case of Fe^{3+} ions they raise the accumulation efficiency of the hole CCs with absorption bands in the visible region.

The aim of the work was to estimate how cerium and iron-both separately and together - influenced the rates of radiation CCs regression in silicate glasses which form the basis of optical materials. It was shown that the additions of Ce^{3+} or Fe^{2+} ions made the isothermal relaxation of the visible coloring more fast. As for Fe^{3+} ions they capture electrons thus forming the impurity color centers (Fe^{3+})- of electron type. These CCs are very stable at room temperature in the glass with iron additions only and hence they restrict the rate of intrinsic hole CCs dissipation in the process of their recombination with electrons. At the same time the simultaneous availability of Ce^{3+} and Fe^{3+} ions in the glass matrix leads to the acceleration of the process of (Fe^{3+})-centers decomposition. The different schemes of recombination processes are discussed.

---

* Full manuscript not available at the time of printing

EFFECT OF HEAT TREATMENT ON THE ELECTROCHEMICAL CORROSION BEHAVIOUR OF GLASSY Fe - Ni - P - B ALLOYS

V. Zaprianova and **R. Raicheff**
University of Chemical Technology and Metallurgy, Bulgaria

Abstract

The effect of heat treatment (up to 550°C) on the electrochemical behaviour of glassy $Fe_{40}Ni_{40}P_{14}B_6$ alloy in a model acidic solution (1N H_2SO_4) has been studied using electrochemical potential sweep technique in conjunction with X-ray diffraction, electron microscopy and differential thermal analysis. It is established that the susceptibility of the metallic glass to passivation is enhanced after structural relaxation. Thermal treatment of the alloy above the temperature of crystallization however lowers its corrosion resistance - the rate of corrosion increases more than an order of magnitude.

I. INTRODUCTION

In the recent years the studies on various properties of metallic glassy alloys have received a growing scientific and technological interest. It has been shown [1-3] that the rapid quenching method gives wide possibilities for obtaining amorphous alloys with high corrosion resistance.

The studies on the electrochemical and corrosion behaviour of amorphous alloys are of great significance for defining the fields for application of these alloys as well as for introducing appropriate corrosion control. From a practical point of view it is important to determine the thermal stability of the amorphous alloys as well as the changes in their physical and chemical properties as a consequence of heat treatment. In most cases the good corrosion characteristics of the glassy alloys defined by both their composition and structure could be lost after thermal treatment over a given temperature: metastable phases could be formed and a transition in crystalline state may occur, as established for amorphous Fe-Ni-Cr-P-C [4], Fe-B [5] and Ni-P [6] alloys. The thermal treatment however, may also result in an improvement of the corrosion resistance of metallic glasses after structural relaxation as found out for Pd-Ni-Si [7] and Co-Fe-Si-B alloys [8].

The amorphous alloy $Fe_{40}Ni_{40}P_{14}B_6$ processes good magnetic properties and a high mechanical strength [9]. However there are limited data concerning its electrochemical and corrosion behaviour and the perspective for its application as a corrosion resistant material. Thus, it has been found, that the amorphous alloy undergoes an active to passive transition in sulfate solutions with different pH values [10-12] as well as in sodium chloride solutions [13], but the current densities in the active and passive regions are rather high.

The effect of thermal treatment at different temperatures on the electrochemical corrosion behaviour of this alloy is not studied. This determined the main purpose of the present work: a study on the effect of heat treatment on the dissolution and passivation .of the alloy. It is also an objective of the work to make an assessment of the corrosion resistance of the alloy in various acid solutions.

II. EXPERIMENTAL

The glassy alloy $Fe_{40}Ni_{40}P_{14}B_6$ was produced in the form of ribbons (thickness 30 μm) by a rapid quenching from a melt. Samples from the alloy were subjected to heat treatment in evacuated quartz tubings for 1 hour at different temperatures (up to 550°C). The structure of the alloy without and after heat treatment was characterized by X-ray diffraction (TUR-M 62 apparatus, CuK_α radiation), by transmission electron microscopy (Philips EM - 400) and by differential thermal analysis (Paulik apparatus).

Potentiodynamic polarization technique was applied in the electrochemical measurements. A conventional three-compartments electrochemical cell and a specially designed Teflon holder for the sample-electrode were used [14]. The polarization potential-current curves of the alloy in a model corrosive solution (1M H_2SO_4) were automatically recorded (potential sweep rate 1 $mV.s^{-1}$) in semilogarithmic scales and the main electrochemical and corrosion parameters of the alloy obtained.

The corrosion rates of the glassy $Fe_{40}Ni_{40}P_{14}B_6$ alloy and the pure metals nickel and iron in various corrosive solutions (1M H_2SO_4, HNO_3, H_3PO_4 and HCl) were also obtained from gravimetric measurements.

III. RESULTS AND DISCUSSION

The DTA curve of the as-quenched $Fe_{40}Ni_{40}P_{14}B_6$ alloy is shown on Fig.1. As seen the alloy undergoes a single stage crystallization and the exothermic maximum is at 380 °C. This result is in good agreement with the data reported by other authors [15].

X-ray diffraction patterns of the as-quenched alloy as well as of heat-treated at temperatures up to 300 °C samples show broad halo typical for an amorphous structure (Fig.2). At 400°C diffraction maxima were established and the alloy undergoes crystallization. The crystalline phases were identified as Fe-Ni and $(Fe,Ni)_3(P,B)$ compounds. The heat treatment at higher temperature (550°C) does not considerably alter the X-ray diffraction patterns.

The corrosion tests show that the glassy alloy has a lower corrosion rate in comparison with the pure metal nickel and especially iron in all acid solution studied, as those differences being much more pronounced in the oxidizing acid (cf. Fig.3). The higher corrosion resistance of the amorphous alloy is obviously related to the formation of protective layers containing the metalloids P and B. However in all cases the pure nickel exhibits a higher tendency to anodic passivation.

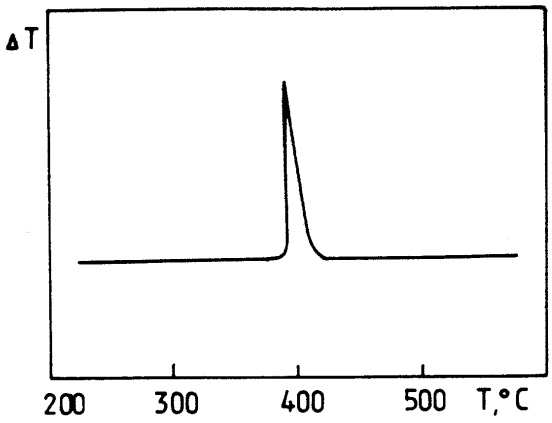

Fig.1 DTA-curve of amorphous $Fe_{40}Ni_{40}P_{14}B_6$ alloy.

Typical polarization curves illustrating the effect of thermal treatment on the active dissolution and anodic passivation of the alloy in 1 M H_2SO_4 are presented on Fig.4. The polarization curve for as-quenched alloy (curve 1) shows typical transition behaviour from active dissolution to anodic passivation, both regions being well defýned.

The thermal treatment at 300 °C (preserving the amorphous state of the alloy) leads to a considerable decrease of the active anodic dissolution region and to an enhanced susceptibility of the alloy to passivation (cf. curves 1 and 2). Similar results have been obtained [7, 8] for other glassy alloys and they may be related to the structural relaxation which leads to a denser amorphous structure with low residual stresses.

As one can expect, the appearance of crystalline phases upon heat treatment above the temperature of crystallization of the alloy (e.g. 400 °C; cf. curve 3) results in a signifýcant increase of the rate of anodic dissolution of metal as well to a lowering of the overpotential of hydrogen evolution (i.e. increase in the rate of cathodic reaction), the overall result being a substantial increase in rate of corrosion of the alloy.

The data both for the composition and the electrochemical properties of the crystalline phases (Fe, Ni $)_3$(P,B) however are largely missing in order to make a quantitative assertion of the mechanism for enhanced corrosion of the alloy upon crystallization.

The effect of thermal treatment on some basic corrosion parameters: corrosion potential, corrosion current and current in the region of passivity is illustrated also in Table 1.

Table 1: Effect of heat treatment on the corrosion parameters of $Fe_{40}Ni_{40}P_{14}B_6$ alloy in 1M H_2SO_4, at 2O °C : corrosion potential (E_{corr}), corrosion current (i_{corr}) and passive current (i_p)

Corrosion parameter	Untreated thermally	Temperature of heat treatment		
		300 °C	400 °C	550 °C
$E_{corr,}$ V (SCE)	0,02	0,03	- 0.15	- 0,17
i_{corr} , A/cm^2	5,0.10^{-5}	4,5.10^{-5}	2,2.10^{-4}	2,5.10^{-4}
i_{p} , A/cm^2	1,8.10^{-3}	1,0.10^{-3}	3,5.10^{-3}	3,5.10^{-3}

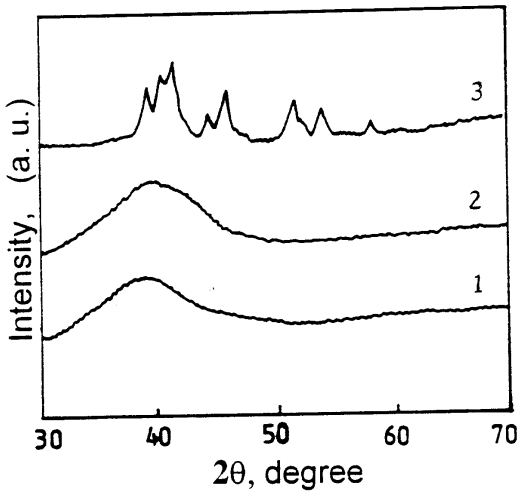

Fig.2 : X-ray diffraction patterns of $Fe_{40}Ni_{40}P_{14}B_6$ alloy:1-as quenched, 2 and 3 - after thermal treatment at 300 °C and 400 °C.

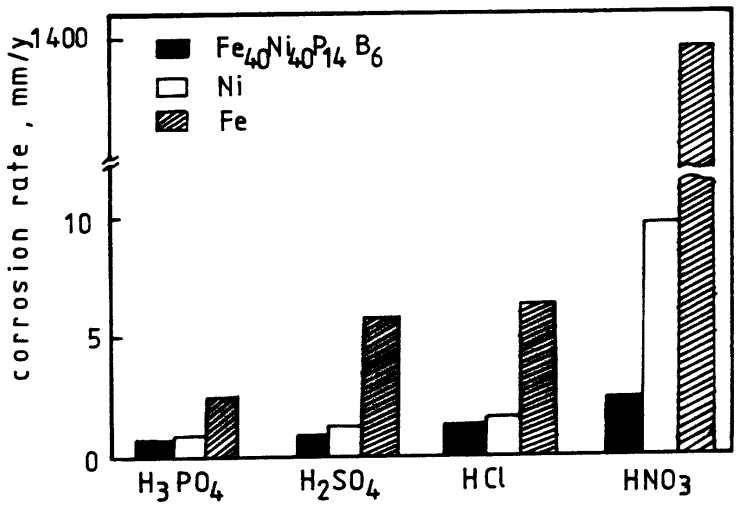

Fig .3 Corrosion rate of glassy $Fe_{40}Ni_{40}P_{14}B_6$ alloy and pure Ni and Fe metal in various 1 M acid solutions at 20°C.

It is seen that up to 300 °C the structural relaxation practically does not exert an effect on the corrosion current, while the crystallization (at 400°C) leads to a considerable increase (about an order of magnitude) in the corrosion rate of the alloy. The heat treatment at a higher temperature (e.g. 550°C) has no further effect on the corrosion parameters - they are practically the same as for the samples treated thermally at 400°C.

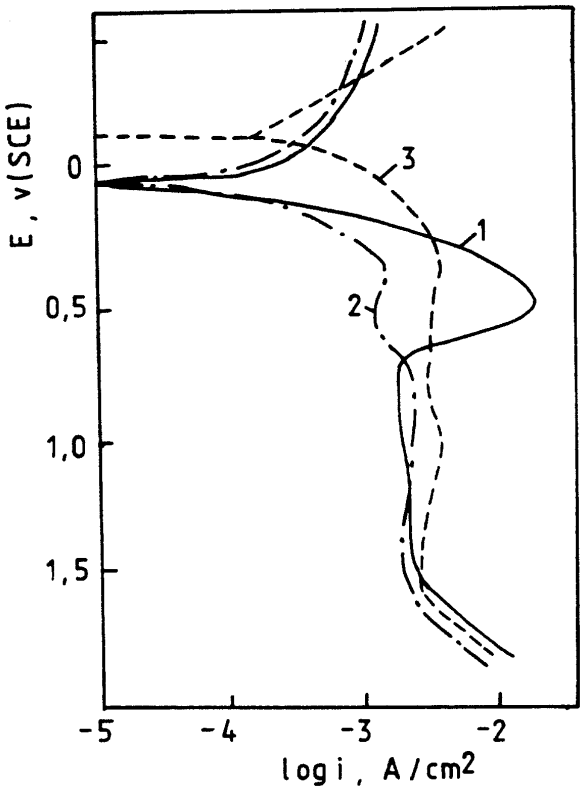

Fig.4 Potentiodynamic polarization curves of $Fe_{40}Ni_{40}P_{14}B_6$ alloy in 1 M H_2SO_4 at 2O °C: 1-as-quenched sample; 2- and 3-thermally treated samples at 300 °C and 400 °C.

IV. CONCLUSIONS

The results of the present study on the electrochemical corrosion behaviour of $Fe_{40}Ni_{40}P_{14}B_6$ alloy show that the alloy possesses a higher corrosion resistance in mineral acid solutions in comparison to pure metal nickel and especially iron. The susceptibility of the glassy alloy to passivation is enhanced after structural relaxation at heat treatment up to about 300°C. The crystallization of the amorphous alloy however leads to a considerable decrease of its corrosion resistance in acidic medium.

The electrochemical behaviour of the glassy Fe-Ni-P-B alloy in non-oxidizing acid solutions are sensitive to the structural changes upon heat treatment and they may be used for an additional evaluation of its thermal stability.

REFERENCES

1. M.Archer, C.Corke and B.Harj, Electrochim. Acta,32(1987) 13.
2. P. Searson, P. Nagarkar and R. Latanision, in : " Modern Aspects of Electrochemistry", R. White, J. Bockris and B. Conway etc. (Plenum Publishing Corporation, New York, 1990) 121.
3. K. Hashimoto, in: "Current Topics in Amorphous Materials: Physics and Technology", Y. Sakurai, Y. Hamakawa, T. Masumoto, K. Shirae and K. Suzuki eds.(Elsevier Science Publishers,1993) 167.
4. M.Naka, K.Hashimoto and T.Masumoto, Corrosion,36 (1980) 679.
5. P. Kovacs, J. Farkas, L. Takacs, M. Awad, A. Vertes ,L. Kiss and A. Lovas J.EIectrochem.Soc.,129(1982) 695.
6. V.Zaprianova, R.Raicheff, E.Kashchieva and L.Fachicov, Bulg.Chem.Commun.,27 (1994) 167.
7. Y. Masumoto, A. Jnove, A. Kawashima, K. Hashimoto, A. Tsai and T. Masumoto, J.Non-Cryst.Sol.86(1986) 121.
8. V. Zaprianova, R. Raicheff and V. Dimitrov, J.Mater. Sci. Lett.13(1994) 927.
9. I. Dismukes and G. Sellers, in: "Rapidly Quenched Metals II", B.Cantor ed. (The Metals Society, London,1978) 343.
10. N.Sorensen, F. Hunkeler and R. Latanision, Corrosion,40(1984) 619.
11. T. Moffat, W. Hanagan and B. Lichter, Corrosion,43(1987) 589.
12. I. Singh, R. Chandhary and T. Namboodhiri, Mat. Sci. Eng.,83(1986) 123.
13. I. Singh, T. Namboodhiri and R. Chandhary, J.Mater. Sci.,22(1987) 2723.
14. V. Zaprianova and R. Raicheff, in: "Proc. Eurocorr.'91", I. Karl and M. Bod eds.(GTE, Budapest ,1991), vol.1,419.
15. G. Cirerd and P.Guiraldeng, Wear,102 (1985) 233.

EFFECT OF P_2O_5 AND CaO PRECURSORS ON THE FORMATION OF GLASS-CRYSTALLINE MATERIALS OBTAINED BY THE SOL-GEL METHOD

K. Cholewa, M. ˚ •czka
Technical University of Mining and Metallurgy, Poland

Abstract

The present study refers to the synthesis of glass-crystalline materials of the CaO - P_2O_5 - SiO_2 system using the sol-gel method. Sol-gel processing offers an alternative to conventional melting method, several potential advantages such as: higher purity and homogeneity, lower processing temperatures. The influence of P_2O_5 and CaO precursors on the formation process of gels glass-crystalline materials has been examined using the following compounds

P_2O_5 -	triethylphosphate	$OP(OC_2H_5)_3$
	phosphoric acid	H_3PO_4
CaO -	calcium nitrate	$Ca(NO_3)_2 * 4 H_2O$
	calcium acetate	$Ca(CH_3COO)_2 * H_2O$

Gels dried at ambient temperatures were next heated with controlled rate up to the temperatures 700 ^oC (and hold in this temperature 20h) and 1000^oC.

It has been demonstrated by means of DTA method that the kind of the P_2O_5 and CaO precursors affects the formation process of gels materials and their ability to crystallization. The structural evolution of gels during and after thermal treatment has been investigated by FTIR and XRD method.

I. INTRODUCTION

The chemical method of synthesis, called the sol-gel method, is a low-temperature method of obtaining glasses, ceramic materials and composites. It utilizes the possibility of the formation of a continuous structure of a solid state as a result of the reaction of appropriate compounds, occurring in the solution. In this method polymerization in the liquid phase leads to colloidal dispersion and the formation first of sol and next of gel from which by appropriate thermal treatment a solid body is obtained. Since the substrates in this process may be various substances in a liquid state (alcoholates chelates, esters) or substances which can be liquefied (nitrates, chlorates, acetates) it is difficult to predict the course of the occurring chemical reactions which lead to the formation of gel [1-2].

Another problem is the determination of the effect of the kind of the precursors of the respective oxides on the process of wet gel transformation into a solid body and the description of the basic structural properties of the obtained gel materials.

The present study is an attempt to determine the effect of the compounds introducing CaO and P_2O_5 on the formation of glass-crystalline materials from the system CaO- P_2O_5 - SiO_2 during thermal treatment and to describe the occurring structural changes.

II. EXPERIMENTAL

The investigations comprised materials of present oxide compositions as follows (mole %) [3-4]:

S	16 CaO	80 SiO_2	4 P_2O_5
T	36 CaO	60 SiO_2	4 P_2O_5

The scheme of the preparation of solutions is given on Fig.1.

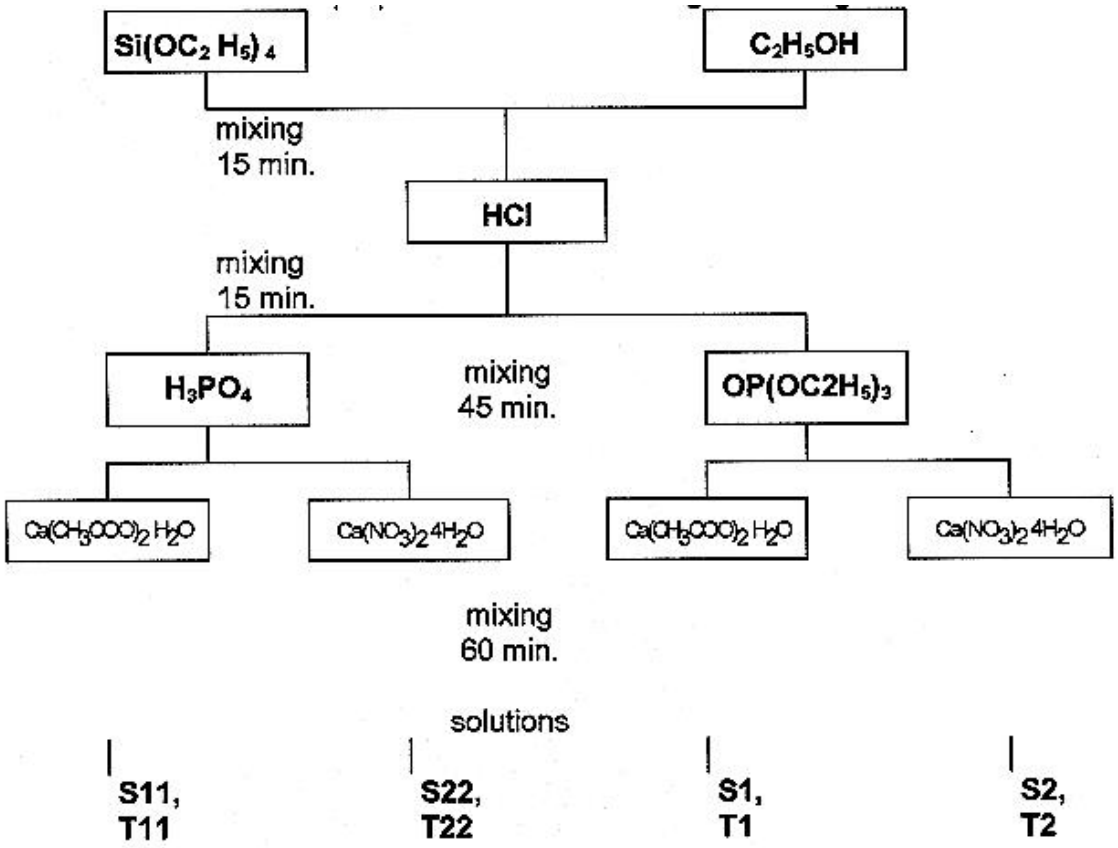

The gels obtained by the above method were dried at ambient temperature for 14 days, and next heated to 700 ^oC and 1000 ^oC and kept at these temperatures for 20 h and 1 h, respectively [4].

In order to determine the influence of CaO and P_2O_5 precursors on the process of obtaining gel-derived glasses and glass-crystalline materials were applied the following research methods: DTA, FTIR, XRD.

III. RESULTS

On the DTA curves (Figs 2, 3) there appeared the following endothermal effects:
- for all gels in the temperature range 125-170 ^{o}C, this effect is due to the evaporation of water and alcohol present in the gel and deriving from the starting solution as well as chemically bound with gel, formed as a result of the occurring processes of hydrolysis and polycondensation;
- in the case when phosphate ester (triethylphosphate) $OP(OC_2H_5)_3$ is used as precursor of P_2O_5 ,at about 260 ^{o}C - gels S1, T1; at about 330 ^{o}C - gels S2, T2, these effects may be associated with the decomposition of ester;
- in the case when the nitrate $Ca(NO_3)_2 \cdot 4\ H_2O$ is used as CaO precursor, at about 400 ^{o}C, 475^{o}C - T22; at about 530^{o}C - T2,
these effects are due to thermal dissociation of nitrate with the release of water and NO_2, (decomposition of calcium nitrate)[5];
- when ortophosphoric acid H_3PO_4 is used as a precursor of P_2O_5 and calcium acetate as precursor of CaO (gel T11) at about 760 ^{o}C, this effect is probably connected with the dehydroxylation of hydrated calcium silicate formed earlier.

Moreover, on the DTA curves there appear the exothermic effects:
- at about 270 ^{o}C, when nitrate is the precursor of CaO; at about 540 ^{o}C, when acetate is the precursor of CaO, and P_2O_5 is introduced through via phosphate ester, this effect is due to the oxidation of the organic matter present in the gel structure, the temperature being dependent on the applied precursor of CaO; for the material T1 there occurs a double effect at 420, 525 ^{o}C [6];
- when P_2O_5 is introduced through phosphate ester, in the temperature range 770-940 ^{o}C - gels S2, S1, T2, T22, T1- these effects are connected with the crystallization of new phases identified by XRD method.

Any distinct exothermic effects on the DTA curves were not observed for the remaining gels, where H_3PO_4 is the precursor of P_2O_5, although XRD and FTIR analyses indicated phase crystallization.

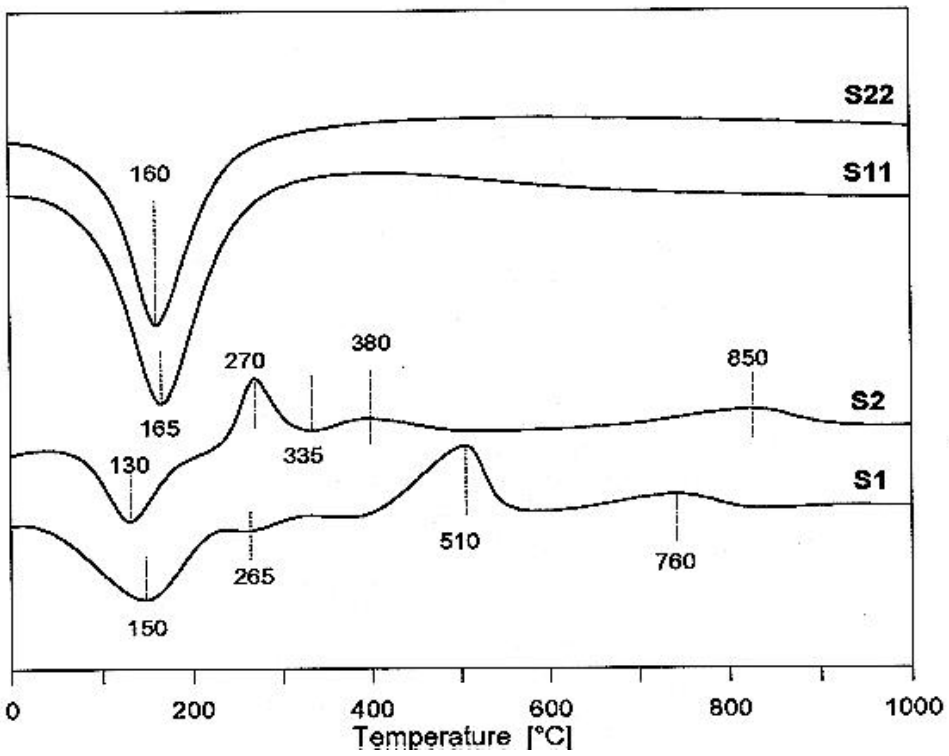

*Fig.2. DTA curves of gel materials series **S***

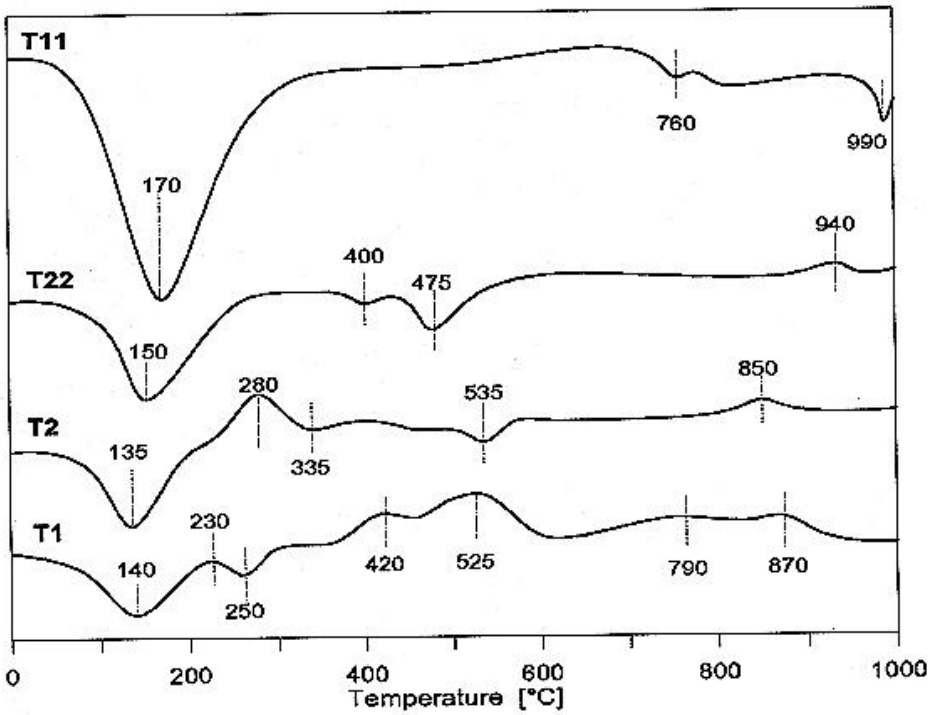

*Fig.3. DTA curves of gel materials series **T***

Results of X-ray analysis are present in table 1.

No of gels	Crystalline phases at temperature 700^{0}C	Crystalline phases at temperature 1000^{0}C
S1	amorphous	apatite cyclowollastonite
T1	$Ca_8Si_5O_{18}$ $CaCO_3$	apatite cyclowollastonite $Ca_4P_2O_9$
S11	beginning of crystallization	apatite
T11	apatite cyclowollastonite $CaOSiO_2H_2O$	apatite cyclowollastonite $Ca_4P_2O_9$
S2	amorphous	apatite
T2	beginning of crystallization	apatite wollastonite $Ca_4P_2O_9$ $Ca_3(PO_4)_2$
S22	amorphous	$Ca_3(PO_4)_2$
T22	apatite	apatite wollastonite CaP_2O_6 $Ca_4P_2O_9$

In FTIR spectra (Figs.4,5) of all gels dried at ambient temperatures there are present three main absorption bands situated at ≈ 460 cm^{-1}, ≈ 1080 cm^{-1} associated with the respective bending and stretching vibration of the bands in the [SiO_4] tetrahedra. Greater intensity of these bands for gels of the composition S is evidence of a higher degree of polymerization of these materials in comparisons with gels of the T series. Within the ranges of wave numbers corresponding to the above bands there occurs also the vibration of P-O-P and Si-O-P bonds. Combination of these vibrations is responsible for the asymmetry of the band with the maximum at ≈ 1080 cm^{-1}. Extension of the band up to about 1220 cm^{-1} may be evidence of the of the occurrence, in the structure of the gels, of P=O bonds in [PO_4] groups. The formation of such groups is also confirmed by the presence of a band at about 550 cm^{-1}, ascribed to the bending vibrations O-P-O [7]. The presence of water is evidenced by bands at ≈ 1630 cm^{-1} connected with the bending vibration of the O-H groups in water particles present in gel pores, and a band at 960 cm^{-1} which derives from the vibration of OH groups bound in the structure with Si or P (Si-OH, P-OH), with a rather small proportion of the stretching vibration of P-O-P. For gels, in which nitrate is the precursor of CaO, there appear bands in the spectra which are connected with the vibration of bonds in NO_3 groups (≈820, 1420 cm^{-1}). In the spectra of most gels there are also present bands deriving from the vibration of bonds in alcoxilate groups in the range 1380-1480 cm^{-1}.

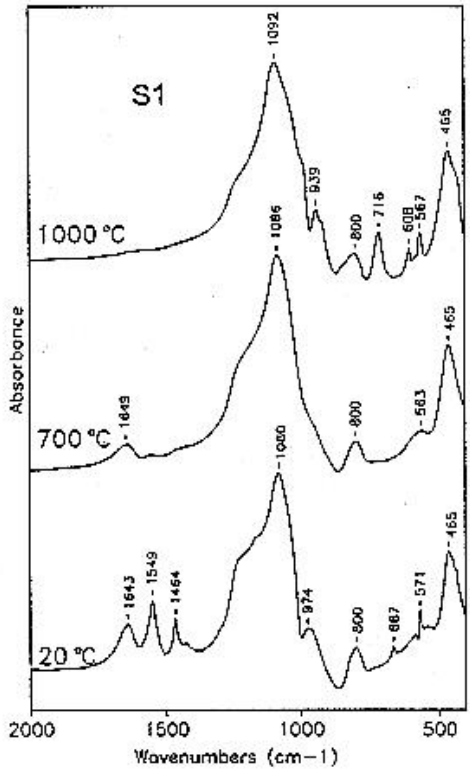
S1
1092
939
800
716
608
567
465
1000 °C
1086
649
800
583
465
700 °C
1050
1643
1549
1464
974
800
667
571
465
20 °C
Absorbance
2000
1500
1000
500
Wavenumbers (cm−1)

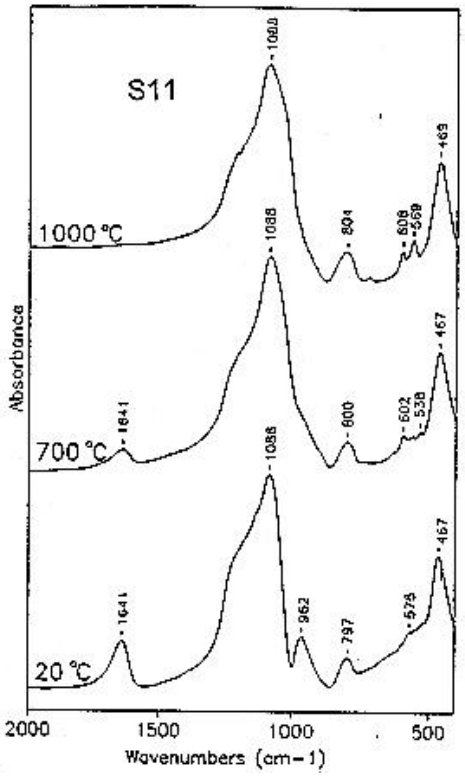
S11
1080
804
609
569
469
1000 °C
1088
800
602
538
467
700 °C
1641
1088
962
797
573
467
20 °C
Absorbance
2000
1500
1000
500
Wavenumbers (cm−1)

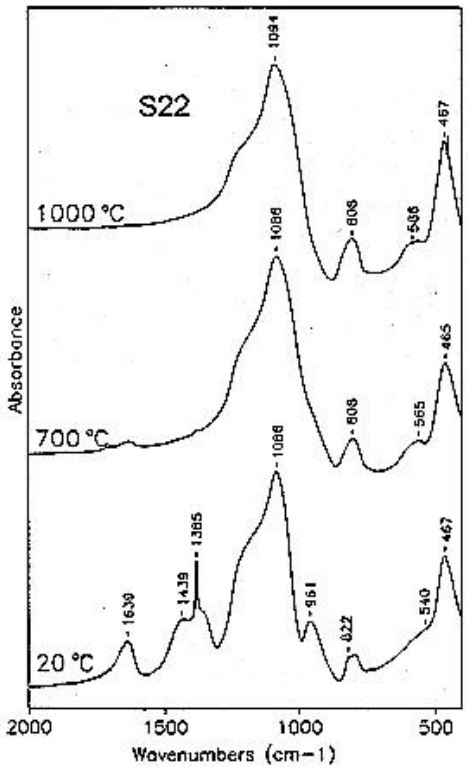
S22
1094
808
585
467
1000 °C
1088
808
565
465
700 °C
1088
1639
1439
1385
961
822
540
467
20 °C
Absorbance
2000
1500
1000
500
Wavenumbers (cm−1)

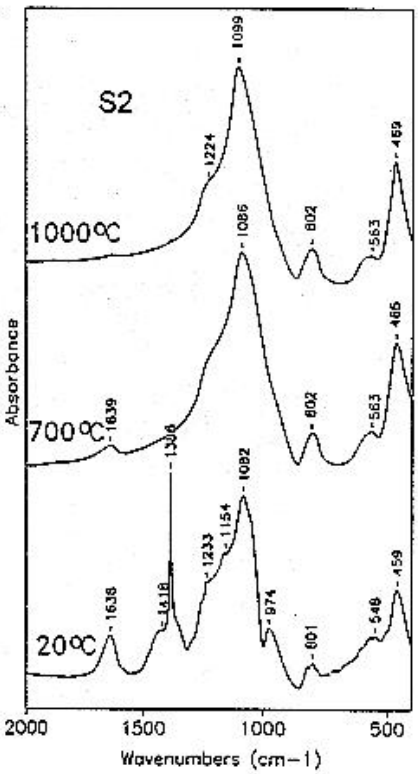
S2
1099
1224
802
563
459
1000°C
1086
1639
1308
802
563
465
700°C
1638
1418
1233
1154
1082
974
801
549
459
20°C
Absorbance
2000
1500
1000
500
Wavenumbers (cm−1)

Fig.4 FTIR spectra of wet gels and gel-derived materials series ***S***

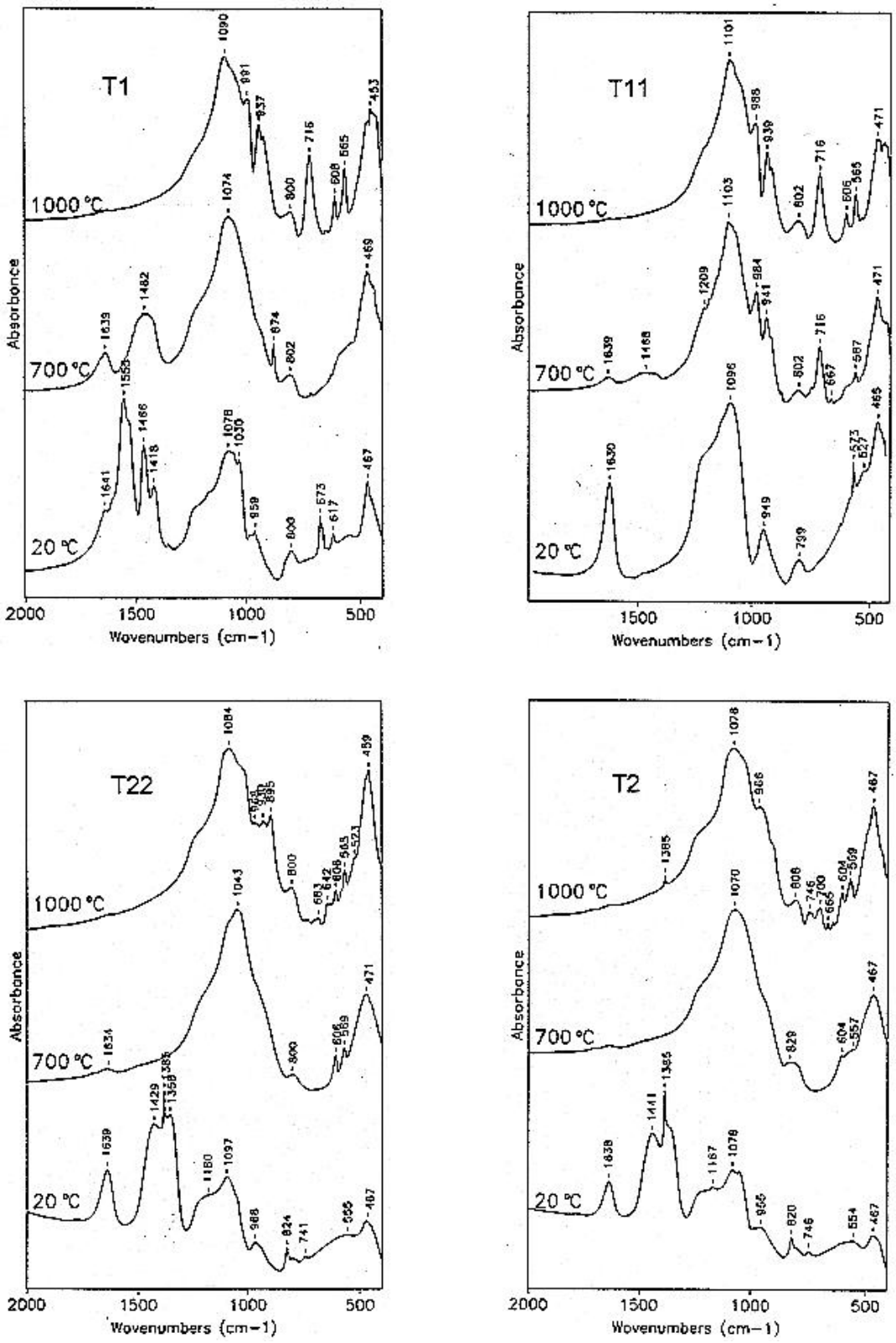

*Fig. 5 FTIR Spectra of wet gels and gel derived materials series **T***

In the spectra of gels heated to the temperature of 700 ^{o}C for 20h the decay of bands associated with the presence of organic matter can be observed. Increased intensity of bands characteristic for bonds in the [SiO_4] tetrahedra and the associated vibration of Si-O-P, P-O-P groups is evidence that a continuous framework has been formed, which in the case of materials of S composition is almost completely amorphous. An conception here is the gel S11- in which there appear bands at 540, 602 cm^{-1}, characteristic for apatite the initial crystallization of which has been confirmed by XRD analysis in spite of the absence of any effect on the DTA curve. Thermal treatment at 700 ^{o}C causes also considerable reduction of the intensity of the bands at 1630 cm^{-1} and 960 cm^{-1} caused by the loss of water as well as the OH groups from the gel structure.

In the spectra of gels of the composition T there appear bands at ≈ 570, 606 cm^{-1} characteristic for the crystallized phases identified by X-ray diffraction. These bands are connected with the bending vibration of P-O-P in [PO_4] groups occurring in apatite. For gels, in which acetate is the precursor of CaO, there appear bands at 1460 cm^{-1}, 870 cm^{-1}, derived from C-O bonds in CO_3 groups, the intensity of these bands being definitely greater when triethylphosphate is the substance introducing P_2O_5. In the case when acetate Ca and the acid H_3PO_4 are used as precursors of the respective oxides (T11) there appear bands at 984 cm^{-1} connected with the vibration of Si-O-; at 941 cm^{-1} deriving from the overlapping extending vibration of $Si\text{-}O^{-}$ and P-O-P, and a band at 716 cm^{-1} which is characteristic for vibration in the rings of the [SiO_4] tetrahedra of cyclowollastonite [8].

One-stage thermal treatment of gels up to 1000 ^{o}C brings about the decay of the bands: ≈ 1630 cm^{-1} connected with the presence of water and ≈ 1460 cm^{-1}, 870 cm^{-1}, derived from vibration in CO_3 groups. In the case of S1 gel, where acetate is the precursor of CaO and ester of P_2O_5, there appear bands at 570, 610 cm^{-1}, characteristic for vibration of [PO_4] groups in apatite, and bands corresponding to the vibration of bonds in recrystallized cyclowollastonite (716, 925, 939 cm^{-1}).

In the spectrum of S11 material (CaO-acetate, P_2O_5 - acid) one can observe increased intensity of bands connected with the vibration of bands in apatite (570,610 cm^{-1}). On the other hand, when nitrate is used to introduce CaO, the spectra of the materials do not show any greater changes after heating at 1000 ^{o}C, only the band at 1224 cm^{-1}, corresponding to the vibration of P=O groups when ester is the precursor of P_2O_5, becomes conspicuous.

In the spectra of all gels of the T series intensive bands at 570, 610 cm^{-1}, attributed to the vibration of the apatite groups [PO_4], are visible.

Thermal treatment of T1 and T11 gels in which CaO was introduced via acetate, caused the occurrence or increase in the intensity of the bands at 925, 937, 991 cm^{-1} connected with the extending vibration $Si\text{-}O^{-}$ in cyclowollastonite. The band described as deriving from the vibration of the rings of the SiO_4 tetrahedra above compound is very distinct.

On the other hand, in the spectra of materials, for the synthesis of which the nitrate Ca was used as precursor of CaO, independently of the applied precursor of P_2O_5, there appear several bands ascribed, respectively, to the extending vibration of the bands Si-O-Si (700, 930 cm^{-1}) and $Si\text{-}O^{-}$ (665, 683, 895, 968 cm^{-1}) in crystallizing wollastonite.

IV. CONCLUSIONS

While carrying out the synthesis of gels of the compositions S and T from the system CaO- SiO_2- P_2O_5 it has been observed that the mode of the formation of these materials depends on the precursors of the oxides CaO and P_2O_5. With the applied preparation method the final product obtained as a result of thermal treatment up to the temperature of 1000 ^oC is a glass-crystalline material of various degree of recrystallization.

The main crystalline phase is apatite and besides it, depending on the applied precursors, other phases undergo crystallization. In the case when acetate is used as precursor of CaO, cyclowollastonite is crystallized, and when CaO is introduced via nitrate - it is wollastonite. Independently of the precursors there appears crystalline calcium phosphate.

The greatest tendency for crystallization is manifested by gels in which acetate was used as precursor of CaO, and the smallest - when nitrate is the precursor of CaO and phosphate ester is used to introduce P_2O_5.

References

1.Hayashi T., Saito H., J. Mat. Sci. vol.15 (1980);
2. Pancrazi F., Phalippou J., Sorrentino F., Zarzycki J.,J. of Non-Crystal. Sol. vol.63 (1984)
3. Li R., Clark A.E., Hench L.L., J. Appl. Biomat. vol.2 (1991);
4. Pereira M.M., Clark A.E., Hench L.L., J. Biomed. Mat. Res. vol.28 (1994)
5. Pereira M.M., Clark A.E., Hench L.L., J. Mat. Synthesis and Proces., vol.2 (1994)
6. ≡ czka M., Ciecinska M., J. Sol-Gel Science and Technol.,(1994)
7. Wong J., J. Non-Crystal. Sol, vol.20 (1976)
8. Handke M., Ph. thesis (1985)

Acknowledgment

The authors wish to thank the Scientifc Research Committee (KBN)
for the financial support (Project No 7 S20100606).

ELASTIC AND INELASTIC BEHAVIOUR OF THE NEW NON-CRYSTALLINE SOLIDS: TELLURITE GLASSES*

Raouf El-Mallawany
Menofia University, Egypt

Abstract

Elastic properties at room temperature are very informative about the structure of solids and they are directly related to the interatomic potentials. The elastic properties have been calculated after measuring both longitudinal&shear ultrasonic velocities and density of the prepared amorphous solid "Tellurite Glasses". The rest of the other elastic moduli (Bulk, Young's, Poisson's and Debye temperature) have been deduced. Information about the structure of the glass can be deduced after calculating the number of network bonds per unit volume, value of the stretching force constant of each bond and the mean crosslink density.

The shape of the loss peaks of ultrasonic attenuation in the rang 100-300 K for the present tellurite glass (i.e., the relaxation spectra), the activation energy and the elastic moduli at room temperature were analysed and correlated with the bulk modulus and cation-anion stretching force constant.

---

* Full manuscript not available at the time of printing

ELECTRICAL PROPERTIES OF COPPER - CADMIUM PHOTOCHROMIC GLASSES

E.Rysiakiewicz-Pasek, B.Ziemba* and **E. ò elazowska***

Institute of Physics, Technical University of Wroc≈aw, Poland
*Institute of Glass and Ceramics in Warsaw, Cracow Branch, Poland

Abstract

The electrical properties of copper - cadmium photochromic glasses using thermally stimulated currents (thermally stimulated polarization TSPC and depolarization TSDC) technique were investigated. The measurements were performed for the glass after heat treatment because untreated glass has no photochromic properties. The photochromic properties (spectral curves of the optical density) after various heat treatments are also presented.

1. INTRODUCTION

Silver halide photochromic glasses, the largest group of photosensitive glasses, have so far been extensively used as spectacle glasses [1-3]. Such an application requires glass to be able to attain as short as possible darkening times (from over a dozen sec. to 30 sec.) when exposed to irradiation, and as short as possible relaxation times (0.5 - 5 min) after irradiation ceases.

Over the last years there have been more and more frequent mentions to another possible application of photochromic glasses as an information (image) carrier of multiple use [4,5]. There have been no data, however, evidencing that these glasses had already been employed for the above mentioned purposes. As opposed to spectacle glasses, they should have a relatively short darkening period and a very prolonged bleaching period (slow relaxation). It has been assumed that the bleaching period of such glasses should be longer than 30 min.

This new trend in the applications of photochromic glasses, suggested in the literature, has prompted us to undertake research work in this field at the Institute of Glass and Ceramics, Cracow Branch. The main purposes of our investigations performed within a research project included the synthesis of phototropic glasses which could be used as reversible information carriers of multiple use. This purpose determined the requirements to be met by base glasses, our starting point of experimental research work.

In this paper we investigate the electrical properties of copper-cadmium photochromic glasses using thermally stimulated current technique. This method was efficiently applied to determine of structure of silicate and germanate glasses [6.9].

2. EXPERIMENTAL

The SiO_2 -B_2O_3 -Al_2O_3 -Na_2O system was chosen as a point of departure for laboratory trials because it had so far been studied the most thoroughly [10-13]. Based on the data relative to the compositions largely adopted for photochromic glasses in this system it has been found that the average content of particular components oscillated about the following values (mol %, rounded numbers): 61 SiO_2, 19 B_2O_3, 6 Al_2O_3 , 14 Na_2O. On its basis a net of matrix glasses was established, and chemical compositions of over a dozen glasses were determined. for laboratory melting. The content of particular components in a matrix glass changed in the following range (mol %): SiO_2 from 57 to 64, B_2O_3 19 - 23, Al_2O_3 6 - 7, Na_2O 9 -14.

In agreement with the literature data, copper and cadmium compounds (corresponding to 0.5 - 0.75 mas % of Cu and 1.0 -1.5 mas % of CdO), chloride and fluorine were introduced as the main components of the photochromic phase. Tin oxide and a reducing agent were also used as additives. The content of active additives was introduced over 100 mass parts of a matrix glass. Glasses were melted in a laboratory silite PSK-7 furnace in unglazed porcelain crucibles, 250 cm^3 capacity each, at 1420 -1440 ^oC

According to expectations, none of copper-cadmium glasses melted in the laboratory trials showed photochromity or became coloured under UV irradiation directly after annealing. That is why all these glasses were subjected to the single - stage heat treatment by holding at a chosen temperature in the range 530 - 650^oC for a time of 15 min to 6 hours. It was only after such a treatment that some of the glasses reacted to radiation and took on smoky color (sometimes with a greenish tint). Glasses held at temperatures above 600^oC sometimes displayed distinct opalescence and even slight opacity.

The subject of investigation was glass with the basic composition (mol %): SiO_2 - 57, B_2O_3 - 23, Al_2O_3 - 7, Na_2O - 13 (glass A) to which was added copper and cadmium compounds (glass B). Glass B was submitted heat treatment at 600, 610 and 620^oC during 1h (glasses B1, B2 and B3 respectively).

The transmittance measurements were performed on the samples in an initial state and after 10 min. irradiation with a 200W mercury discharge lamp without filter as a light source

The thermally stimulated polarization TSPC and thermally stimulated depolarization TSDC measurement procedures have been described in detail [7,8]. In TSPC measurements, an unpolarized sample is cooled to a low temperature (~100 K). An electric field F is applied and the sample is heated with a constant rate. During heating TSPC-1 current is recorded. Then the sample is rapidly recooled with the field still applied. The sample is again heated and TSPC-2 current is measured. The dc conductivity σ was calculated from TSPC-2 curve from the equation:

$$\sigma = I / F . A \qquad (1)$$

where I is the current, and A is the electrode area, F is the field [V/m] .

The activation energy for dc conductivity E_{dc} was obtained from plots of $\log \sigma$ vs 1/T using the equation:.

$$\sigma = \sigma_o \exp(-E_{dc} / kT) \quad (2)$$

where σ_o is the preexponential factor, E_{dc} is the dc activation energy, k is the Boltzmann constant, T is the temperature.

For thermally stimulated depolarization TSDC measurement a sample is polarized by an applied electric field F_P at a temperature T_P for a time t_P. This polarization is frozen-in by cooling the sample to a low temperature. Then the electric field is switched off an the sample is heated, while depolarization current is measured. The activation energy of TSDC peak was determined by partial-discharge technique. In this technique the sample after being polarized is then depolarized by partial heatings.

The apparatus used for TSPC/TSDC measurements has been described previously [14]. Corresponding investigations were performed in the system consisting of a cell, vacuum system and an electrometer. All TSPC/TSDC measurements were carried out by means of computerized automatic measuring system. Before measurements the glass samples were preheated to 450K to remove the surface moisture. The thermally stimulated currents were measured in the temperature range 100-450K with a constant rate 5 K/min. The glass samples were of the following dimensions 10 . 10 . 0.5 mm^3, the surfaces were polished from both sides.

3. RESULTS AND DISCUSSION

The majority of the samples darkened after that irradiation. The optical density of these glasses has increased significantly over the whole spectral range. This is illustrated by diagrams shown in Fig.1. which relate to the glass B1

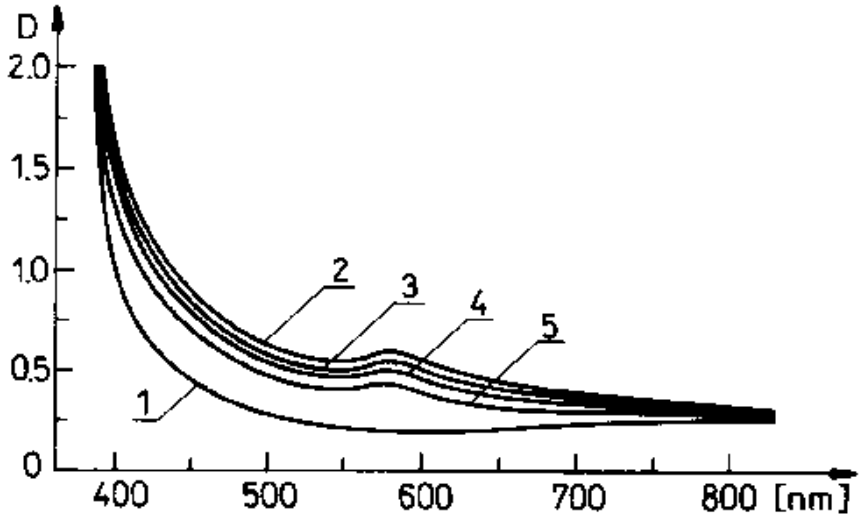

Fig.1. Spectral curves of the optical density, D, for the glass B1. Optical density of a sample - curve making: 1- before irradiation, 2 - directly after irradiation, 3 -15 min, 4 - 60 min, 5 -180 min after irradiation.

The diagrams in Fig.2 show the time dependence of glass bleaching process at room temperature after the end of irradiation. At first, the bleaching process (a decrease in

optical density, D) is fast, and then it starts to slow down, and the sample reaches the initial optical density after 24 or even after 48 hours. As a measure of bleaching progress, the time after which the added optical density of a given sample decreases to its half starting value can be adopted. This coefficient, designated by $\tau_{1/2\ \Delta D}$ is also dependent on the heat treatment temperature of a glass. In the example shown in Fig.2 $\tau_{1/2\ \Delta D}$ is equal about 45 min. for a sample held at 620 ^{o}C for 1 hour (glass B3) and about 250 min. for a sample held at 600 ^{o}C for 1 hour (glass B1).

The dc conductivity curves for glass A, B and B2 are presented in Fig.3. The activation energy, E_{dc} , values are equal: 47 kJ/mol for glass A and 48 kJ/mol for glass B before and after heat treatment (ΔE_{dc} = ±2 kJ/mol). The influence of photochromic elements on dc conductivity is not significant. The values of dc conductivity for glass A and B are almost similar. After heat treatment dc conductivity of glass B increases.

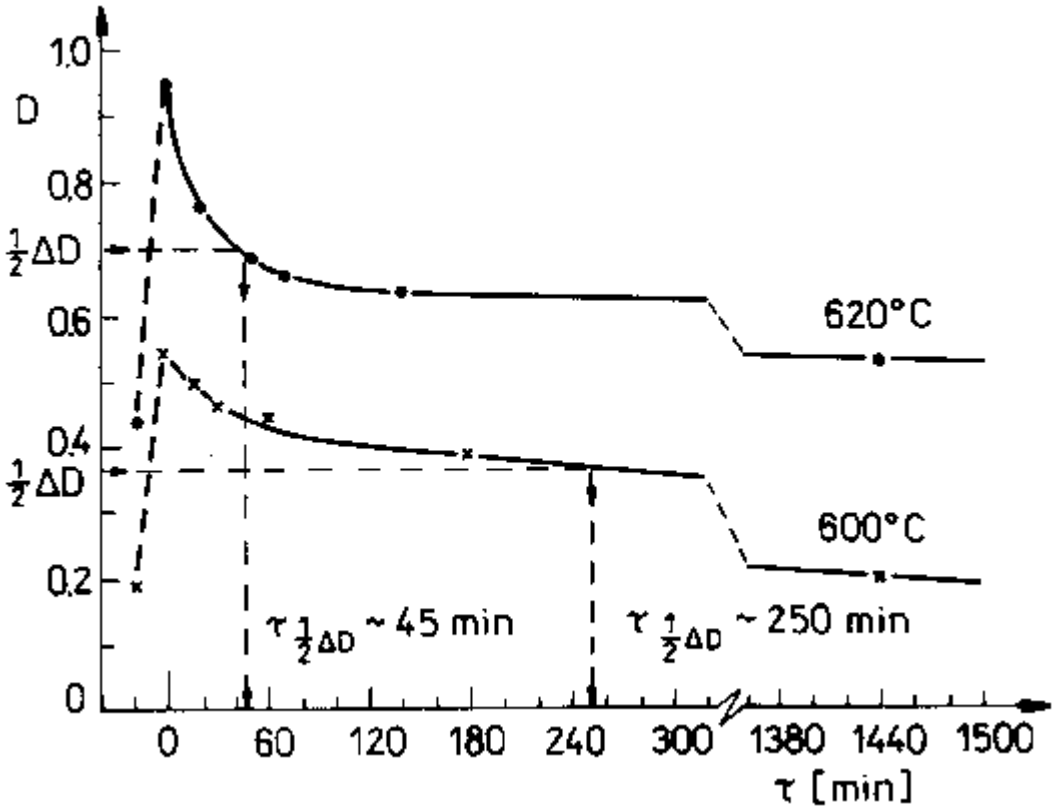

Fig.2. Optical density ,D, of the glass B1 and B3 as a function of bleaching time, t , at room temperature.

In Fig.4 and 5 the dependencies of TSDC current on polarization electric field and polarization temperature of glass B2 are presented. Three peaks Pl, P2 and P3 are observed in the glasses B and B2. The magnitude of the low temperature peaks (P1) is similar for unheated and heated glass B. The magnitude of the high temperature peak (P2 and P3) varied with the heat treatment. Glass B2 which was heated has smaller P2 and P3 peaks than homogeneous glass B [15]

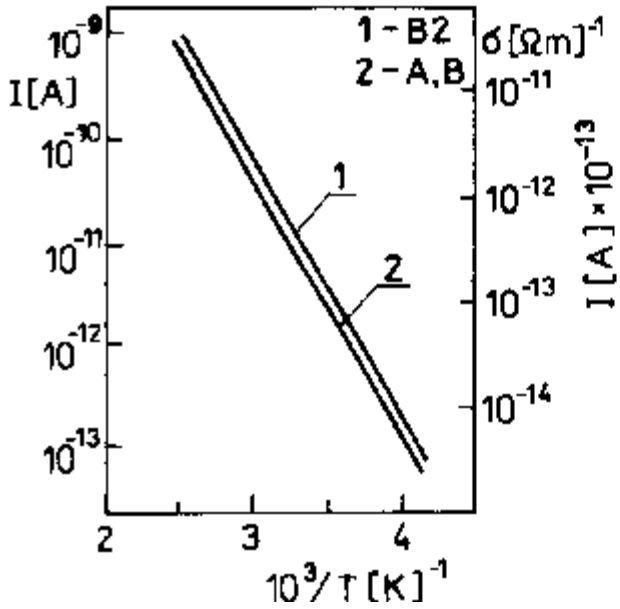

Fig.3. The dc conductivity for glass A and glass B before and after heat treatment.

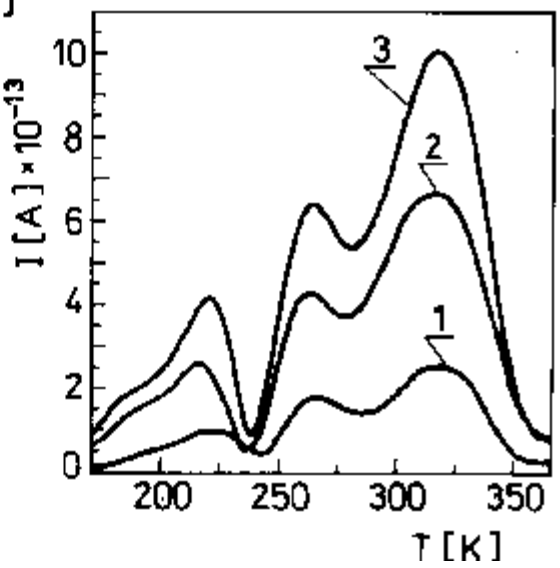

Fig.4. Dependence of TSDC peaks on polarizing field for glass B2 (T_p = 243 K, t_p =l5min) F_p = 1-3 10^5 V/m, 2 - 7 ·10^5 V/m, 3 - 9 10^5 V/m.

The values of activation energy, E_a ,obtained from partial discharge experiments are presented in Table 1

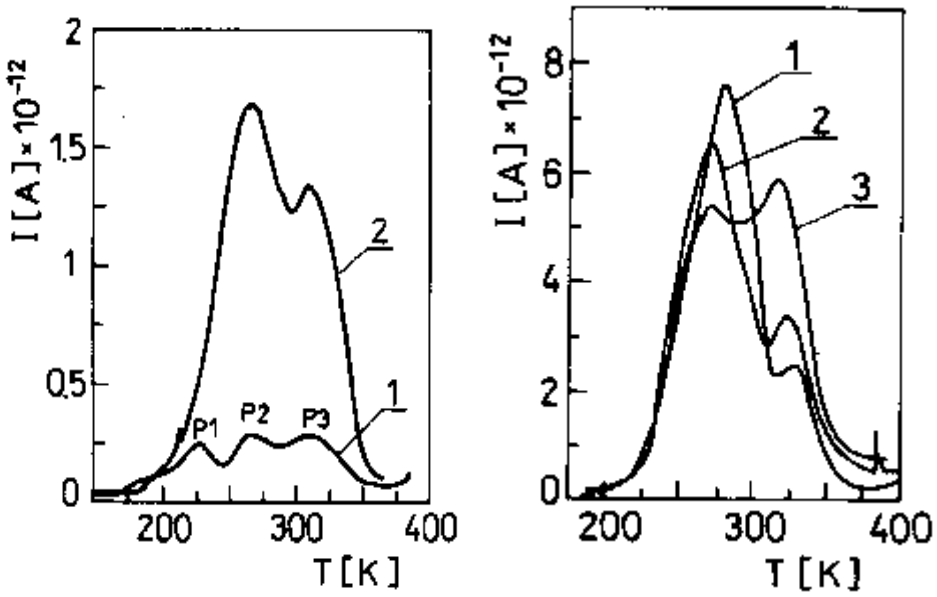

a b

Fig.5. Dependence of TSDC peaks on polarization temperature for glass B2 (F_p=5 10^5 V/m, t_p =10min) T_p = a) 1-243K, 2-273K, b)1-323K, 2-363K, 3 - 383K.

Table 1
The activation energy values, E_a ,of TSDC peaks for glass B2

Peak	**P1**	**P2**	**P3**
E_a [kJ/mol]	18	30	36

$\Delta E_{dc} = \pm 2$ kJ/mol

The increase in dc conductivity and the changes of magnitude of TSDC peaks after heat treatment are attributed to the structure of investigated glasses.

Generally it is known that the incorporation of aluminum oxide in the glass network results in the formation of tetrahedra (fourfold coordination) up to a ratio of $Al_2O_3/Na_2O=1$. At higher ratio the excess of aluminum ions is believed to form octahedra (sixfold coordination). In the investigated glasses the Al_2O_3 / Na_2O ratio equals 0.54. According to Milberg [16] and Bray [17] in the borosilicate glasses with $Na_2O/B_2O_3 <0.5$ all Na_2O is incorporated in the borate network and SiO_2 dilutes this network. Therefore it can be supposed that sodium ions in the investigated glass may be divided between the aluminate and borate units.

Glasses A and B are homogeneous. After heat treatment the transparent glass B became Milky. The insignificant increase in dc conductivity after heat treatment can be related to partially phase separation into silica and sodium-rich phases. It can be supposed that sodium-rich phase starts to be interconnected and dc conductivity is defined by this conducting phase.

The more detail information about structure of glass B can be determined from TSDC data. The obtained results indicate different activation energies for TSDC peaks and dc conductivity. The activation energy values for P1, P2 and P3 peaks are smaller than for dc conductivity. The temperature maximum of the low temperature P1 peak is independent on the polarization time and the polarization field. The magnitude of this peak is linearly dependent upon the polarizing field (up to $9 \cdot 10^5$ V/m) and the polarization time. These facts confirm the dipolar origin of P1 peak. The low temperature peak in both B and B2 glasses can be attributed to reorientation sodium ions around $[AlO_4]$- or and $[BO_4]$- groups. The high temperature TSDC peaks (P2 and P3) are obviously dependent upon the microstructure of glass. The observed changes of magnitude of these peaks in glass B and B2 can be explained by phase separation occurring in glass B after heat treatment. It can be supposed that a translational sodium ions motion in sodium-rich phases is responsible for high temperature TSDC peaks (Day's model [6]). Presently, more precise explanation of the origin of P2 and P3 peaks is difficult because of complicated structure of the examined glasses.

4. CONCLUSIONS

The darkening - bleaching process in the investigated glasses has a reversible character. The results obtained show that these glasses keep a generated image

sufficiently long in the state of darkening that allows to use them as reversible data recording media.

The increase in dc conductivity and change of the magnitude of thermally stimulated peaks for cooper - cadmium photochromic glasses are related to phase separation occurring in these glasses after heat treatment.

Acknowledgment

The work was financially supported by Polish Committee for Scientific Research as a part of the research project No 3 P407 026 06

REFERENCES

[1] D.Caurant, D.Geurier, M.Pressas, J.Appl,Phys., 71,3,1982,1981
[2] C.I.Marquardt, G.Gliemerath, J.Appl.Phys , 50,1979,4584.
[3] N.F. Borolli, J. B. Chodak, G. B. Hares, J. Appl. Phys., 50,1979, 5978.
[4] K. Kawazoe, R.Suzuki. S.Inoue, M .Yamane, J.Non.Cryst.Sol.,111,1989,16.
[5] K.Kumata, H.Namikawa, K. Yamamoto, J.Non.Cryst.Sol., 34,1979,437.
[6] H. D. Jannek, D. E. Day, J. Amer. Ceram. Soc., 64,4,1981,227.
[7] E.Rysiakiewicz-Pasek, K.Pater, Proc.XVII Int.Congress on Glass, Beijing, 2,1993, 333.
[8] A. Mogus-Milankovic, D. E. Day, J.Non. Cryst. Solids,162,1993, 205
[9] P. Pissis, J .Laudat, E. Daoukaki, A. Kyntis, J. Non.Cryst. Solids,171,1994,201.
[10] R.J.Araujo, US Patent No 3 325 299,1967.
[11] R.J.Araujo, P.A.Tick, Bull.Am.Ceram.Soc., 55,1974,355.
[12] P.A. Tick, D.A.Nolan, J.Non.Cryst.Solids 33,1979,383.
[13] D.M.Trotter, Jr J.W .H.Schreurs, P.A.Tick, J.App.Phys., 53,7,1982,4657.
[14] A.Gubanski, B.Macalik, Bull.Pol.Acad.Sci., 35, 1987,537.
[15] E.Rysiakiewicz-Pasek, B.Trojanowska, in press.
[16] M.E.Milberg, J.G.Keefe, R.A.Verhelst, H.O.Hooper, Phys.Chem.Glasses 13,1972, 79.
[17] Y.H.Yun, P.J.Bray, J.Non.Cryst.Solids, 27,1978,363.

ELECTROCHEMICAL DISSOLUTION OF GLASSES

Valery A. FUNTIKOV
Kaliningrad State University, Russia

Abstract

For the first time the electrochemical dissolution is investigated of vitreous alloys. We investigated anodi dissolution of telluride glasses of the binary and ternary systems. The electrochemical and chemical equivalents is investigated for glasses of the mentioned systems. The means of electrochemical and chemical equivalents are shown for valuation of features of a structure of glasses. The example is shown of a research of a electrochemical dissolution of glasses of a system T1-Ge-Te. Results specify inclusion in a glassy grid of a system Tl-Ge-Te of fragments of a metastable combination $GeTe_2$.

I. INTRODUCTION.

The researchers are engaged as a rule kinetics of a dissolution of glasses in various solvents. The information about a study of the electrochemical dissolution of glasses is completely away. For the first time the research is carried out with the purpose of the study of the electrochemical anodi dissolution of the chalcogenide glasses of systems A^{IV}-B^{VI}, A^{V}-B^{VI}, A^{IV}-B^{V}- C^{VI}, A^{I}-B^{IV}- C^{VI}, A^{III}-B^{IV}-C^{VI}, A^{I}-B^{V}- C^{VI}, A^{III}-B^{V}-C^{VI},The dependence of a rate of the anodi dissolution of glasses from density of the current is investigated for mentioned systems. The significances of the electrochemical equivalent were determined for the vitreous alloys investigated. The various gears of the electrochemical dissolution of glasses are offered.

II. EXPERIMENTAL RESULTS

In this report the example is shown of a research of a electrochemical dissolution of glasses of a system Tl-Ge-Te. For synthesis of glasses is used a standard method of synthesis from elementary substances of a semi-conductor cleanliness. The electrodes joined to example of glasses with the constant area of section. Another parties of example are coated by a dielectric. The telluride glasses are dissolved electrochemically easiest. The electrolyte for a electrochemical dissolution is selected individually for different glasses. For example, 1m solution of NaOH was used for glasses of a system T1-Ge-Te. The electrochemical equivalent (ECE) is calculated by stationary method under the formula (1):

$$ECE = \Delta m/Q = \Delta m/JQ\tau \qquad (1)$$

where Δm is a loss of a weight of a example;
Q is a quantity of the electricity;
J is current during time τ.
The molar weight of chemical equivalent (CE) is calculated under the formula (2):

$$CE = ECE \cdot F \quad (2)$$

where F is Faraday constant (F = 96500 $C \cdot mol^{-1}$).

The speed of electrochemical dissolution W is calculated by stationary method under the formula (3):

$$W = \Delta m/\Delta\tau \cdot S \cdot A \quad (3)$$

where S is the area of section of a sample, adjoined with the electrolyte; } is the average weight of a mole of atoms of a glass.

The speed of electrochemical solution W is calculated by stationary method under the formula (4):

$$W = (d\Delta m/d\tau)\ \ 1/S.\} \quad (4)$$

where $d\Delta m/d\tau$ is determined on a angular factor of a tangent to graph of dependence of a loss of a weight Δm from a density of a current J/S. The condition ($J/S=const \cdot \tau$) give manually or automatically. At the moment of weighing the current in a circuit was disconnected. The electrochemical equivalent and a molar weight of chemical equivalent are calculated under the formulas (4, 5) :

$$ECE = K \cdot A \quad (5)$$

$$CE = K \cdot \} \cdot F \quad (6)$$

where K is the angular factor of a linear graph of the dependence of the speed of electrochemical dissolution W from density of current J/S.

The results of investigation are submitted on a figure for glasses of a system T1-Ge-Te on section $GeTlTe_{x.}$.

III. DISCUSSION

The dependence of the speed of electrochemical dissolution of chalcogenide glasses from density of a current is linear in the case, if a electrolyte select correctly. The sizes of electrochemical and chemical equivalents do not depend on choice of stationary or unstationary methods of research. The exception was made by glasses of a system T1-Ge-Te with the shortage of a tellurium. The glasses of a system Tl-Ge-Te on a section GeTl-Te are dissolved electrochemically in 1m solution of NaOH. The graphs are submitted of the dependence of mole weight of a chemical equivalent of glasses of a given section, received unstationary (1) and stationary (2) methods by electrochemical dissolution in 1m

solution of NaOH and as well as calculated to next gears: (3) by a loss in a deposit of combination $GeTe_2$, (4) by a loss in a deposit of combination GeTe, (5) by a complete solution of glasses. The fragments of metastable combination $GeTe_2$ were found out by the by stationary method. It is followed from a figure. In this case the advantage was realized by stationary method consisting that in difference from a stationary method, its use require of the frequent weighing of examples each 3-5 mines. The sample was always cleared before weighing. In case of the stationary method a sample is cleared through 40-60 mines, therefore the deposit of metastable combination $GeTe_2$ dissolve electrochemically partly (4) or completely (5).

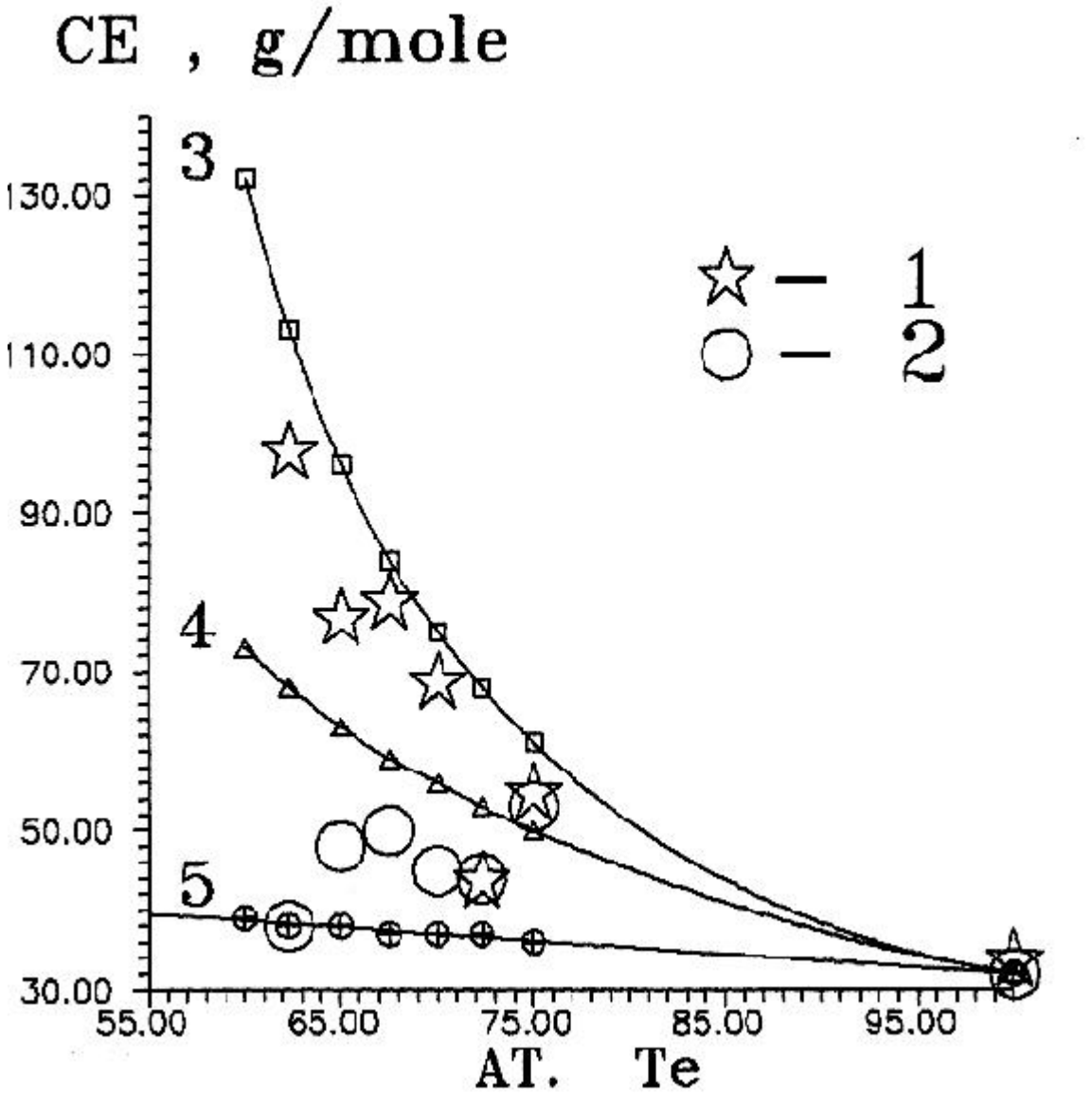

Figure. The dependence of the experimental and theoretical sizes of a molar weight of a chemical equivalent of glasses of a system Ge-Te-T1 on section $GeTlTe_x$ from a composition of glasses. The senses of symbols are in a text.

IV. RESUME

For the first time the electrochemical dissolution is investigated of glassy alloys. It is shown, that the electrochemical and chemical equivalents, received in relation to reaction of the anodi solution, is the structure-sensitive size. It is shown that the research of the electrochemical dissolution of the glasses gives the applied information and the information about a nature of the microheterogeneous structure of the glassy alloys with electronic conductivity. The fragments of metastable combination $GeTe_2$ were found out by the unstationary method of the electrochemical dissolution in glasses of a system Ge-Te-T1.

ELECTRONIC STRUCTURE AND PROPERTIES OF INTRINSIC DEFECTS AND LOCALIZED STATES IN BINARY PHOSPHATE GLASSES*

A. F. Zatsepin, J.V. Shchapova and **V.S. Kortov**
Urals State Technical University, Russia

Abstract

This work is addressed the investigation of electronic states in the gap of mobility and defects in the bulk and surface layers of glasses $MeO-P_2O_5$ (Me=Be, Zn, Ca, Sr, Ba). The methods applied are quantum-chemical cluster simulation, luminescence optical absorption. ESR and exelectronic spectroscopy of the surface. Electronic structure is governed by the cation-modifier type and the short range order in glass. In case of cations with weak ionic field (Me=Ca, Sr, Ba) band tails are formed by O2p orbitals of oxygen atoms on coordinations P=O=Me and P-O for valency band and by a complex molecular orbitals involving P, O and Me atomic orbitals for conduction band. In case of "strong" cations (Me=Be, Zn) valency and conduction band tails are maked up by O2p orbitals of oxygen atoms P-O-Me and by space and energetically isolated P 3s, 3p, 3d states, respectively. Radiation-induced optical and ESR centers are subdivided into two classes according to the type of short-range structural disturbances (1) discreet (defect) states of bond breaks (PO_4^{2-}, PO_3^{2-} centers); and (2) continual (localized) states of band tails, caused by dispersion of short-range order parameters (PO_4^{4-}, $(Me^{2+})^{2-}$ centers). The features of electron-hole processes depend on the cation type in glass as well. The exoelectron emission observed from the surface takes place due to Auger mechanism: the recombination of holes from PO_4^{-2} centers with electrons of PO_3^{2-} (weak cations) or $(Me^{2+})^{2-}$ centers (strong cations). Hole induced processes result from high hole mobility and short valency tail length in phosphate glasses.

---

* Full manuscript not available at the time of printing

ELECTRONICS IN PROCESS AUTOMATION OF IS MACHINES

Ing. Daniele Sasso
BOSCATO & DALLA FONTANA SPA, Italy

Abstract

By automating the I.S. machine by means of the Feeder, Parallel Cutting, Invert and Take-out servomechanisms and by means of a powerful and flexible control electronics that is configurable by the customers, BDF fulfills the requirements of the glass industry with some electric mechanisms which are the result of the state-of the-art automation technology and modern mechanics and which consist of a small number of components. Thanks to its new automation project, BDF manufactured some mechanisms that are driven by electric servomotors and that are able to optimize the movement of those mechanisms which were usually driven by mechanical cams. The need of an electric servocontrol of the Feeder, Invert and Take-out mechanisms is due to the fact that the mechanisms working "in contact with glass" should be more and more flexible and it is also the result of a thorough analysis of the manufacturing defects and of the scraps due to a malfunction of these mechanisms.

I. INTRODUCTION

Speedup, weight lightening and higher quality standard were the spur for the manufacturers of machines in the mid-eighties in Europe. At the beginning of the nineties, instead, the manufacturers of hollow glass were interested in high-productivity forming machines for ordinary articles (bottles for beer, mineral water, wine, etc.) and very flexible machines for special articles as a result of the greater demand for this type of articles and of the strong domestic competition.

The production mix is a strategic component for the management of a company where there is not one single product but where the range of products includes articles that are similar from a technological point of view but that differ in their appearance.

For a glass industry, manufacturing means also choosing the articles to be manufactured at the same time, so that the pull of the melting unit is constant. The more the pull of the melting unit is constant, the better it is; in this way, the costs of the melting energy are lower, the temperature of the melting glass is constant, the properties of glass are more stable, the melting unit is used under the best operating conditions and the gob weight varies very little during the manufacturing cycle.

In order to meet the above mentioned requirements, modernizing the present technologies is not enough. New solutions with up-to-date automation technologies are necessary.

II. ELECTRONIC CONTROL SYSTEM

The new control of the I.S. machines is the BDF-TDE128T integrated system with distributed intelligence architecture controlled by a supervision computer which is

series connected with the various control modules and which is managed by a view windows software for a guided dialogue and for an easier and quicker usage.

The control modules, one per each section, are independent units with their own CPU with double microprocessor which is able to control 48 inputs and 48 outputs for each section and to control the electronic pusher and the invert and take-out servomechanisms.

Each section module is independent and it may be controlled and programmed autonomously, so that it is possible to manufacture different articles with the same machine at the same time.

The integrated drive module, a flex-line type, is able to control and synchronize all the motors with the machine speed, the independent motors and the motors of the Invert and Take-out servomechanisms.

The system has brushless motors with a speed of 100 - 2000 rpm, characterized by small size, accurate positioning repeatability, reliability, constant torque during almost all the speed range. The motor is coupled with its drive by the machine computer so that the max. flexibility of the system is achieved.

BDF, of course, together with the new integrated control system, manufactured also a new line of servomechanisms which can fulfill the requirements of the latest electronic digital controls.

III. SERVO FEEDER

Recently BDF introduced the Feeder with electronic control in the flexible line. According to this new project, the two mechanisms, Shears and Plunger, are independent one of the other and each one is driven by a brushless servomotor, which is controlled by a microprocessor card. In this way, the mechanical cams are not used any more thanks to the management of an electronic cam file.

Thanks to the new shears mechanism with parallel cut the cut of the gob was improved: in fact, the time when the shears are in contact with glass, which should be as shorter as possible according to the gob dimensions, is controlled accurately and continuously.

Very short times of contact with glass, when the weight of the gobs is of few grams, implies a strong side push against the gob during the cutting operation, because the inertial mass of the gob is very small and therefore the gob might side-skid off the theoretical trajectory.

This is the reason why BDF designed 16 different types of cams, according to the type of gob to be cut: cams with quick cut and triangular profile for low speed and big gobs or cams with slow cut and harmonic profile for medium-high speed and light gobs.

For each selected cam, the time of contact with glass is always constant also when the cutting speed changes and this is the contrary of what happened before; in fact, a mechanical cam could be used in a rather wide range of speed and, therefore, the time of contact with glass were different and this resulted in a defective cut and in a defective fýnished product.

Moreover, BDF solved the problem of the shears vibration, which was due to the mechanical cam drive and, by doing so, also the defects and the problems of loading were solved, thanks to a rigid mechanical drive between the motor and the roller screw driving the alternating motion of the blade-holding trolleys.

Thanks to the plunger mechanism it is possible to select the desired cam by means of the computer and to change the starting point and the stroke according to the production requirements; all this improves the control of the gob formation, especially at low and high speed and the weight of the gobs is more constant.

Thanks to the above mentioned characteristics, the machine flexibility is increased, the operator does not have to operate the Feeder directly and there is a saving of raw materials and energy, resulting from an increase in productivity and in output.

IV. SERVO GOB DISTRIBUTOR

This mechanism, which is driven by a brushless motor, works with a number of sections and with a delivery order that is programmable by the machine terminal automatically.

The theoretical positioning angles and the delivery order may be checked and changed by means of the portable terminal or machine computer.

The servocontrolled gob distributor combines programming flexibility with a high productive capacity, up to a speed of 220 gobs per minute.

The positioning movements are governed by a law with sinusoidal acceleration so that the motion is continuous and free of vibrations.

The gearing, which is oil-bath lubricated and consists of helical gears and of a rack with inclined and ground teeth, offers top reliability and repetitive positioning in time.

The position is controlled by a double resolver, one on the motor and one on the pinion driving the rack, thus obtaining the max. safety.

V. ELECTROPNEUMATIC VALVE BLOCK

The control of the movement of the section mechanisms is performed by means of the new electropneumatic valve block 05-BVE with 21 lines, which is characterized by:

· pneumatic slide valves with shutter for high speed of response and low flow resistance;
· valve body made of light alloy with seals made of vulcanized polymer;
· 16 mm diameter air vents;
· operation with air up to 120^{o}C:
· the valves are positioned vertically for a balanced operation of the shutter;
· quick replacement of the single valves;
· possibility to feed all the lines independently;
· independent adjustments of all the 21 lines;
· enblock light alloy frame;
· interchangeability with the existing ones.

VI. MACHINE CONVEYOR AND HIGH SPEED TRANSFER WHEEL

The pushers with electronic cam by BDF are the result of an accurate design aiming to optimize the drive of the mechanism and the pusher cylinder.

A bipolar stepping motor with 10,000 pulses/revolution is really ideal for this type of mechanism, which is characterized by low speed of rotation, low inertia and, therefore, low torque. The BDF pusher with stepping motor is equipped with a

continuous cooling system throughout the conveyor tunnel, to prevent overheating problems due to the small fires which usually take place under the conveyor.

The timing belt drive, the light alloy support and cylinder and the cylinder with fixed stroke, which may be adjusted from the outside, guarantee the reliability of these mechanisms.

By means of the portable terminal or of the machine computer, it is possible to change all the regulating parameters of the Pusher mechanisms manually.

The conveyor drive includes a microprocessor-controlled brushless motor. In this way, it is possible to change the relation of minimum speed to maximum speed of the machine from 1:8 (in case of an inverter system) to 1:20 (in case of a brushless system).

This is possible thanks to a brushless motor exerting the rated torque also at low rotation speed, when the synchronous and induction motors suffer from power losses because of heat dissipation to a greater extent.

By means of the flexible drive of the BDF conveyor it is possible to program all the speeds of the conveyor belt in a range of number of machine sections from 4 to 12, in a range of section speeds from 2 to 20 cuts per minute and in a range of belt conveyor step from 5" 1 /4 to 31 "1 /2.

The new transfer wheel 20-TR1 is controlled by the machine drive electronically. The machine drive controls the tip speed of the transfer fingers automatically according to the machine speed, to the type of process (SG-DG-TG) and to the step between the transfer f ngers.

The drive of the transfer wheel was made independent by assembling a servocontrolled brushless motor.

Thanks to a system for the electronic timing of the transfer wheel by means of a proximity switch, it is possible to synchronize the wheel movement with the articles arriving on the conveyor, without the mechanical clutch unit which is usually assembled on this mechanism.

The cross-conveyor control is an useful additional unit in a flexible line with a step which may be programmed by the computer without the traditional mechanical speed variator.

Also for the cross-conveyor there is a fixed-ratio drive controlled by a brushless motor; this may work in the whole range of speed necessary to obtain a step of 1.2" to 30".

VII. SERVO INVERT AND SERVO TAKE-OUT

A great step forward in the technological development of I.S. machine by BDF was the control of the Invert and Take-Out mechanisms by electric servomotors.

The innovation consists in replacing the pneumatic cylinders with electric servomotors controlling the rotation of the invert and take-out arms by means of ball screws.

The high output speed of the I.S. machines with one single delivery (450-500 articles/minute) have shown the limits of the compressed-air mechanisms; in fact, this type of energy cannot guarantee a "perfect repeatability" of the movements in time and "the same setup" of all the mechanisms.

Presently the parison delivery time is about 0.55 seconds and the return of the invert arms into the blank mould is 0.4 seconds; it is easy to understand, therefore, that a pneumatic cylinder working at low pressure, even if it is servocontrolled, cannot

guarantee a constant motion and a continuous trend of acceleration and deceleration in time.

After some tests in a glass industry, it was found out that it is possible to reduce the manufacturing defects of the manufactured piece finish by using BDF mechanisms with electric control, thus increasing the output of about 2-2.5%.

In view of the cost of the finished product when it is scrapped because of defects in workmanship, the cost of compressed air, the noise, the pollutants and the cost of maintenance of the pneumatic mechanisms, it is clear that the application of a servomotor to the mechanisms working in contact with glass certainly benefits productivity, energy saving and work environment.

The control electronics and software are integrated with the section control of the forming machine and it is possible to program all the mechanisms by means of the machine computer without operating them manually.

A sensor at the end of stroke, assembled on the mechanisms, check that the arms have been positioned correctly in every cycle.

The servomotor resolver controls the position continuously. The motor control card includes an absolute meter which, by reading the resolver signal, checks the theoretical position (electronic cam) with the actual position of the motor in real time, so that it stops the whole section module if a mechanism is not positioned properly.

VIII. CONCLUSION

What above mentioned is what BDF designed for its own machines and control systems, but new projects are being worked out, particularly about:

· safety systems;
· reduction of noise level;
· processing of statistical data of the cold control line.

ESTIMATION OF STRUCTURAL AND ENERGY ORDER IN ALKALI-BORATE, SILICATE AND PHOSPHATE GLASSES BY DSC*

Ushakov V.M. and **Borissova N.V.,**
Institute of silicate chemistry, Russia

Abstract

The thermodynamic similitude method was applied for estimation of structural and energy order for glasses in the Na_2O-SiO_2, $Rb_2O(Cs_2O)$-B_2O_3, Na_2O-ZnO-P_2O_5 systems. Excess functions (enthalpy, entropy, Gibbs energy) of glasses with relative to the crystals of the same composition were calculated using the temperature dependencies of heat capacity obtained by DSC. Analysis of the results suggests the existence of two types of structural order (that of a crystal and of a metastable liquid) in alkali borate glasses as distinguished from the sodium silicate glasses (of a metastable liquid only). For alkali borate as well as alkali phosphate glasses the structural equilibrium increases with the alkali ion content.

---

* Full manuscript not available at the time of printing

EVALUATION OF THE GEOMETRIC EFFICIENCY FOR CURTAIN WALLS WITH RECTANGULAR GLASS PANES

Dr. Murat Aygün
Istanbul Technical University, Turkey

Abstract

Most contemporary buildings of high technology are enclosed with a metal framed curtain wall comprising double glazing units as infill panels. The proposed comparative method ascertains the geometric efficiency of alternative glazing modules for selecting the most rational among alternative façade modules for such external envelope systems. The basic attributes of planar geometry for rectangular glass panes are here considered. As both dimensions of the glass pane increase while the shape approaches a square, the total number of panes, the total length of joints and the number of panes on the façade decrease, therefore reducing the risk of water penetration through joints as well as the assembly time on site. The mechanical performance of such panes is also improved since they act as membranes under wind pressure and an interaction occurs between the outer and inner panes of the double glazing units.

1. INTRODUCTION

There are 2 parameters on rectangular glass panes for describing the planar geometry. These are the width (a) and the length (b). Different pane sizes for given increments of these are here tabulated as a matrix and also as a one-dimensional array below.

Table 1: Matrix and Array of Pane Sizes

b_1	1		
b_2	2	3	
b_3	4	5	6
	a_1	a_2	a_3

a_1,b_1	a_1,b_2	a_2,b_2	a_1,b_3	a_2,b_3	a_3,b_3
1	2	3	4	5	6

The area (A=a.b) and the aspect ratio (r=b/a) are then derived from the above quantities. Hence a and b can be expressed in terms of A and r.

$a=\sqrt{(A/r)}$ $b=\sqrt{(A.r)}$ (1a) (1b)

The joints along the perimeter of panes are considered as locations for potential air infiltration, water leakage or heat loss. The failures are attributed either to deficient joint design or errors in assembly on or off site. Consequently a reduction of the total length of joints on the façade is desirable for averting such failures.

In the case of curtain walls, for constant aspect ratio, a larger pane implies a smaller total length between the adjacent panes mounted on a metal carrier frame. The assembly time of the façade system is reduced as well owing to the smaller number of panes required on that façade [1]. This advantage is somewhat offset by the increased pane weight.

Similarly, for constant pane area, a smaller aspect ratio also yields a smaller total length on the façade. This parameter influences the mechanical behaviour of panes under wind pressure. The membrane effect becomes more significant as the pane shape becomes a square and this ratio approaches 1.0 allowing a smaller glass thickness to be achieved. The relevant design standards and failure models are reviewed in Reference [2]. The shape also affects the mechanical interaction which occurs between the outer and inner panes of a double glazing unit under wind pressure [3]. On a square unit the wind load is distributed more evenly between the two panes through the sealed air-gap. This effect is accentuated on higher wind pressures.

When windows are in consideration, the total length of joints increases with the window area, contrary to curtain walls. In that case the perimeter length becomes a direct criteria.

Thus 3 performance criteria emerge for evaluating the geometric efficiency of glass panes in curtain walls: 1. Large area, 2. Small aspect ratio, 3. Large division of area by aspect ratio expressing the combined effect of the first two criteria.

2. METHOD

The quantitative method employed here for comparing pane sizes is described below, followed by an implementation on a set of alternative sizes in the context of curtain walls.

The actual values of parameters for the alternatives are first tabulated to provide input for evaluation.

Since some parameters have different dimensions, these are required to be non-dimensional for the purpose of comparing parameter performances with each other. Therefore the actual values are converted to relative values by interpolation between the maximum and minimum actual values in the set of alternatives for each parameter. The interpolation may be applied as linear or curvilinear depending on the circumstances. In this case linear is deemed to be appropriate.

$$x_r = ((x_a - x_{a\,min})(x_{r\,max} - x_{r\,min})/(x_{a\,max} - x_{a\,min})) + x_{r\,min} \quad (2)$$

x_r : Relative parameter performance value
x_a : Actual parameter value
$x_{a\,min}$: Minimum actual value encountered in the set
$x_{a\,max}$: Maximum actual value encountered in the set
$x_{r\,min}$: Lower limit (e.g.1)
$x_{r\,max}$: Upper limit (e.g.10)

If the performance values are in an inversely proportional relationship with the actual values then the equation above is modified which indicates a rise in performance with a fall in actual values and vice versa.

In case that there are only 2 unidentical values among the alternatives for a given parameter, the maximum performance value will be assigned to the greater and the minimum to the smaller, since there are no intermediate values.

This comparative analysis enables to ascertain the performance of alternatives relative to each other rather than to establish their absolute adequacy.

The relative values are then multiplied by the appropriate weight factor of the relevant parameter, thereby reflecting the degree of significance which arises from the objectives stipulated by prevailing environmental or economic conditions and constraints.

$$x_s = (x_r - x_{r\ ave}) / S_{xr} \qquad (3)$$

x_s : Standard relative value
x_r : Relative value
$x_{r\ ave}$: Arithmetic mean of relative values
S_{xr} : Standard deviation of relative values

Subsequently the weighted relative values are converted to standardized values for taking the statistical characteristics of the set of alternatives into account.

Finally, the 3 statistical performance criteria of arithmetic mean (Ave), standard deviation (Dev) and coefficient of variation (Var) of the parameters for each alternative are calculated and converted to relative performance values as above. For any system to be regarded as satisfactory all 3 criteria must be above their respective average values. The alternatives that fulfill this condition are then ranked in order of their statistical performance. Hence the method enables pre-defined performances of alternatives as well as individual parameters to be compared analytically, providing an effective design tool.

The successive steps of the method are listed below. Computer- coding is done in Pascal 7.0 programming language [4].

1. Input of actual parameter values
2. Transformation to weighted relative performance values
3. Statistical Analysis
4. Transformation to standard performance values
5. Criteria test and Sorting of results

3. IMPLEMENTATION

10 alternative sizes of glass panes (G01, G02, ...) for a curtain wall are assumed to be available for the purpose of implementing the comparative method above. The minimum and maximum parameter values of alternatives and their sizes are given below. A constant dimensional increment of 30 cm. is used.

	Dimension (a,b)	Glass Area (A)	Aspect ratio (r)
Min:	60	0.36	1.0
Max:	150	2.25	2.5

Table 2: Matrix and Array of Sample Pane Sizes

b(cm)					
	60	G0l			
	90	G02	G03		
	120	G04	G05	G06	
	150	G07	G08	G09	G10
		60	90	120	150 a(cm)

60,60	60,90	90,90	60,120	90,120	120,120	60,150	90,150	120,150	150.150
G0l	G02	G03	G04	G05	G06	G07	G08	G09	G10

The effects of pane parameters on the performance criteria are tabulated below. The plus or minus sign denotes the rise or fall of performance for that criteria provided that all other parameter values remain constant. Zero signifies that there is no relationship in-between. While a affects all 3 criteria positively, b only has such an effect on A.

Table 3: Correlations between Parameters and Criteria

	A	r	A/r
a:	+	+	+
b:	+	-	0

The 3 consecutive tables below present the actual geometrical criteria values, the relative geometrical performance criteria values and finally the relative statistical performance criteria values for each of the 10 alternative panes in the set. The weight factors of the criteria are taken as equal. The minus sign in the performance tables denotes that the corresponding value is below average.

Table 4: Actual Geometrical Criteria Values for each Pane

G0l	G02	G03	G04	G05	G06	G07	G08	G09	G10

A:	0.4	0.5	0.8	0.7	l.1	1.4	0.9	1.4	1.8	2.3
n:	1.0	1.5	1.0	2.0	1..3	1.0	2.5	1.7	1.3	1.0
A/n:	0.4	0.4	0.8	0.4	0.8	1.4	0.4	0.8	1.4	2.3

Table 5: Relative Geometrical Performance Criteria Values (%) for each Pane.

	G0l	G02	G03	G04	G05	G06	G07	G08	G09	G10
A:	-	-	-	-	-	20.5	-	19.0	26.2	33.3
n:	33.3	-	33.3	-	26.7	33.3	-	-	28.3	33.3
A/n:	-	-	-	-	-	20.5	-	10.5	20.5	33.3

Table 6: Relative Statistical Performance Criteria Values (%) for each Pane.

	G0l	G02	G03	G04	G05	G06	G07	G08	G09	G10
Ave	-	-	16.5	-	-	23.9	-	-	24.1	33.3
Dev	-	-	-	24.6	-	20.5	24.8	24.2	26.3	33.3
Var	-	-	-	-	22.1	26.4	-	26.0	29.6	33.3

4. CONCLUSION

The panes satisfying the requirement that all 3 statistical criteria should be above average are G10, G09 and G06, as can be anticipated, with respective overall performance values of 100%, 80% and 70%. While G10 has equal, i.e. perfectly balanced, relative statistical criteria values, G09 and G06 appear to perform the highest in terms of the variation coefficient. The initial assumption that pane performance increases with both pane dimensions is thus confirmed. Any one of these 3 panes is deemed as geometrically efficient.

REFERENCES

1. CWCT, Standard Guide for Good Practice for Curtain Walling, Centre for Window and Cladding Technology (CWCT), University of Bath, Bath, pp.9-10, 1993.
2. FISCHER-CRIPPS, A. C., COLLINS, R. E., Architectural Glazings: Design Standards and Failure Models, Building and Environment, Elsevier Science Ltd., Vol.30, No.1, London, pp.29-40,1995.
3. VALLABHAN, C.V.G., CHOU, G.D., Interactive Non-linear Analysis of Insulating Glass Units, Journal of Structural Engineering, American Society of Civil Engineering, Vol.112, No.6, New York, p.1318,1986.
4. SEDGEWICK, R., Algorithms, Addison-Wesley Publishing Company, Reading, Massachusetts, pp. 93-95,1988.

FLUORESCENCE OF Eu^{3+} IONS AS A PROBE FOR MICROSTRUCTURAL CHANGES IN THE SILICA GEL TO GLASS CONVERSION

Qian Guodong, Wang Minquan, Wang Mang, Fan Xianping, and **Hong Zhanglian**
Zhejiang University, P. R. China
Lu Shaozhe
Chinese Academy of Sciences, Changchun,
P. R. China

Abstract

The fluorescence of Eu^{3+} ions is an environment-sensitive probe, which can be used as a new tool in the study of the microstructural changes in the gel to glass transformation. With increasing the heat-treated temperature, the total fluorescence intensity of Eu^{3+} ions doped in silica gel from the $^5D_0$ excited state and the relative intensity of the hypersensitive transition $^5D_0 \rightarrow {}^7F_2$ (defýned as asymmetry parameter R) increase, and the emission spectrum shift takes place. These results show that the following processes may cause upon heating of the gel. Being heated at 250^{o}C, the physical absorbed water and ethanol molecules in the gel have been desorbed, and one- and two-dimensional polymerizations form. Treated at the temperature range of 250^{o}C and 500^{o}C, the SiO_4 tetrahedral three dimensional network structure forms and strengthens gradually with removing the coordination water of Eu^{3+} ions and residual organic molecules. The glass network has basically formed upon heating to 500^{o}C, and then the volume relaxation and viscous sintering take place at elevated temperature (up to 800^{o}C). The high resolution emission spectrum of Eu^{3+} ions measured at 8.5 K indicates that the symmetry of Eu^{3+} ion sites in silica glass prepared by sol-gel process is Cs.

1. INTRODUCTION

As a new wet chemical technique, sol-gel process has been successfully applied to prepare the inorganic powder, fýlm, fýbre and monolithic glasses. By sol-gel process, the oxide-glass can be prepared at lower temperature with respect to conventional melt method, and homogeneous doping at a molecular level can be performed in solution at room temperature. This technique with the ability to trap photoactive substances in an inorganic glass is expected to lead to new applications in nonlinear optics, solid state tunable lasers, photochemical hole býýrning, etc. [1]. To obtain a crack-free and homogeneous glass from wet gel, two main steps may be distinguished: wet gel to xerogel conversion and xerogel to fully densifýed glass conversion. Iýý order to make clear the complicated gel to glass transition, a variety of techniques have been applied to study the changes in the porous gel as a result of heat-treatment, including dilatometry, gas adsorption, DTA, TGA, TEM, IR, Raman spectroscopy, resonance techniques and

SAXS, as reviewed by P. F. James [2]. A great deal of information has been obtained about the chemical and microstructural changes occurring in the gel to glass transition.

Most of the f - f* transitions in trivalent lanthanides are not much affected by the environment of the ion because of shielding from out shell electrons. Some, however, are very sensitive in a complex field. Such transitions are termed "hypersensitive" and obey the selection rules $|\Delta J| \leq 2$, $|\Delta L| \leq 2$, $\Delta S=0$ which are the selection rules on $\Gamma(2)$ [3]. Here J, L and S are total angular, orbital and spin quantum numbers, respectively, and $\Gamma(2)$ defines the crystalline fýeld. The transition $^5D_0 \rightarrow {}^7F_2$ of Eu^{3+} ion is identified as hypersensitive transition. In this work, the fluorescence of Eu^{3+} ions is used as an environment-sensitive probe to study the microstructural changes in the silica gel to glass conversion. This will help to further advance the scientific understanding of the gel to glass transition.

2. EXPERIMENTAL

2.1. Preparation of Eu^{3+} doped silica xerogels

The Eu^{3+}-doped silica gels were prepared by the acidic (HCl) hydrolysis of tetraethoxysilane (TEOS) in ethanol as has been reported previously [4]. Europium chloride was prepared from Eu_20_3, 99.99 % purity, by dissolution in hydrochloric acid. The molar ratio of TEOS : water : ethanol in starting solutions was 1 : 4 : 4. Appropriate amount of $EuCl_3$ solution was introduced in these solutions. The mixed solutions were adjusted to a pH of about 2 by the addition of HCl and stirred vigorously for 1 hour at room temperature, and then were placed in sealed plastic containers. The precursor solutions converted to wet gels after several days' gelation at 40^oC. The containers should be left a perforation on the top allowing further hydrolysis and condensation reactions to take place at ambient temperature. The wet gels were continuously dried to obtain xerogels at room temperature.

2. 2. Heat-treatment of Eu^{3+}-doped silica xerogels

The derived Eu^{3+}-doped silica xerogels were heat-treated as following: heated up to the required temperature and kept at that temperature for 24 hours in air, and then cooled in the furnace. In order to obtain crack-free monolithic gel glasses, the examples should be heated at the rate of 20^oC / hour below 300^oC and 60^oC / hour at elevated temperature to avoid cracking and bloating induced by the rapid vaporization of water and residual organic molecules.

2. 3. Measurement

The DTA and TGA curves were measured with a Lcp-1 differential thermal analyser and a PRT-1 thermogravimetric analyser, respectively. The fluorescence spectra were measured at room temperature with a Hitachi 850 spectrofluorometer. The high resolution emission spectrum of Eu^{3+} ions was performed at 8.5 K using the fourth harmonic of Nd : YAG laser at 266 nm, Spex-1403 monochrometer and boxcar.

3. RESULTS AND DISCUSSION

3.1. Temperature dependence of asymmetry parameter R

The electric-dipole transition $^5D_0 \rightarrow {}^7F_2$ of Eu^{3+} ion is identified as hypersensitive transition, its transition intensity varies remarkably with the change in the site symmetry of Eu^{3+} ion. But on the other hand, the $^5D_0 \rightarrow {}^7F_1$ transition intensity which is of the magnetic-dipole type is independent of the site symmetry. Therefore, it is generally suggested that the ratio of the emission intensities

$$R = \frac{^5D_0 \rightarrow {}^7F_2}{^5D_0 \rightarrow {}^7F_1}$$

is an asymmetry parameter for the Eu^{3+} ion site [5]. The variation of R reflects the variation of the surroundings of Eu^{3+} ions and the covalency degree of the Eu-O bond in gel glasses.

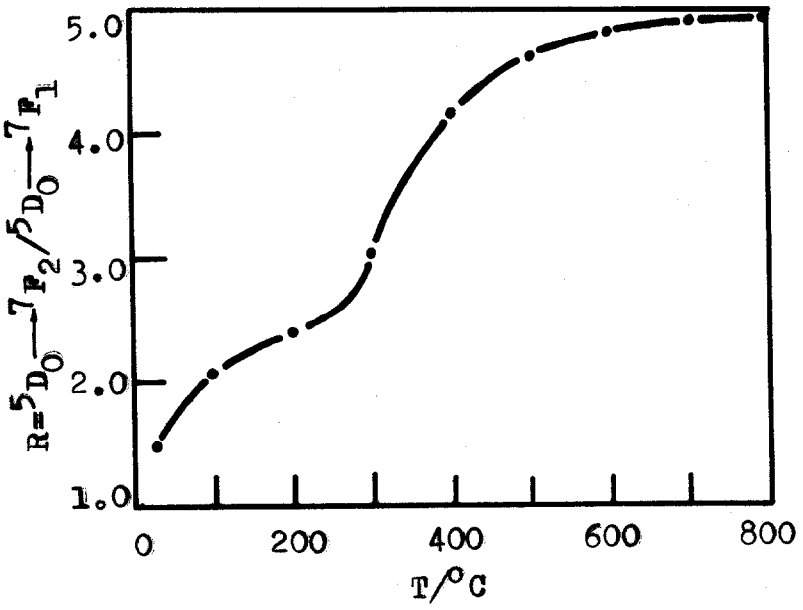

Fig.1 Asymmetry parameter R as a function of the heat-treatment temperature.

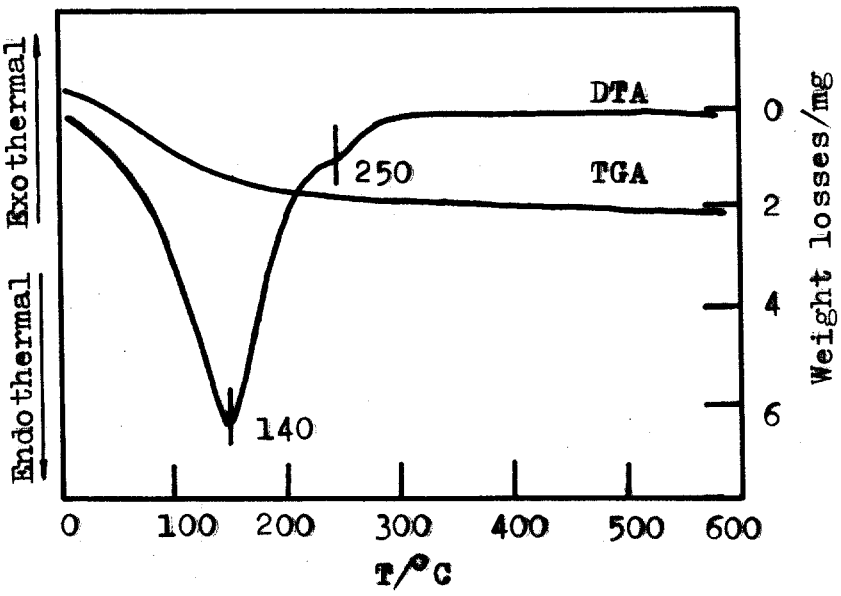

Fig. 2 DTA and TGA curves of silica xerogel doped with Eu^{3+} ions.

Fig. 1 shows the fluorescence intensity ratio R of the $^5D_0 \rightarrow {}^7F_2$ to the $^5D_0 \rightarrow {}^7F_1$ transitions versus the heat-treatment temperature. R increases remarkably when the Eu^{3+}-doped silica xerogel is heat-treated in the range 250°C to 500°C, and increases slowly both below 250°C and above 500°C. Fig. 2 shows the DTA and TGA curves of Eu^{3+}-doped silica xerogel. The DTA endothermic band peaking at 140°C is attributed to the vaporization of physically absorbed water and residual organic molecules. The TGA curve shows marked weight losses in the same temperature range corresponding to the endothermic DTA peak, as a result of the removal of water and organics. The TGA curve between 250°C and 500°C shows smaller weight losses corresponding to the endothermic should DTA peak at around 250°C, which may be attributed to the results of the slow removal of the chemical absorbed water, e. g. coordination water, and the water resulted from further condensation-polymerization reactions. The TGA curve shows few weight losses at higher temperature (up to 800°C).

When the Eu^{3+}-doped xerogel is heated between room temperature and 250°C, R increases slowly because that the linear and planar polymerizations remain in the sample and the nearest neighbour of Eu^{3+} ion has few changes compared to that in no heat-treatment xerogel. Being heated in the range 250°C to 500°C, Eu^{3+} ions are gradually coordinated by $Si0_4$ tetrahedral instead of H_20 as a result of the removal of the chemical absorbed water and the formation of three dimensional polymerization. Eu^{3+} ion is situated in a distorted cube with eight nonbridging oxygens belonging to the corners of four SiO_4 tetrahedra, each tetrahedron donating two oxygens [6]. This results in lowering the site symmetry of Eu^{3+} ions, and then increases greatly the asymmetry parameter R. The slow increase in R at elevated temperature (up to 800°C) shows that the nearest neighbour of Eu^{3+} ions exhibits few further changes and only volume relaxation and viscous sintering take place in this temperature range. The IR spectra indicate that silica glass can be obtained from xerogel after being heated at 800°C for 24 hours [7]. It implied

that the $Si0_4$ tetrahedral three dimensional network structure has formed upon heating to 500°C.

3. 2. Shift effects of $^5D_0$ ® $^7F_2$ emission bond of Eu^{3+} ions

During the gel to glass transition, the polarizability of the environment surrounding Eu^{3+} ions and the nearest neighbour of Eu^{3+} ions change with the removal of water and residual organics and the formation of three dimensional network structure, and then shift of Eu^{3+} ion emission spectrum will take place. Fig. 3(a) shows the heat-treatment temperature dependence of the peak site v_m, the wave number in cm^{-1}, of $^5D_0 \rightarrow {}^7F_2$ emission. The emission band shifts to blue part below 500°C, to red part at elevated temperature.

The loss of energy between absorption and emission of light, known as stokes' shift, is a result of the changes in the polarity of Eu^{3+} ions surrounding environment. If the silica xerogel can be regarded as a continuum, the relation of stokes' shift Δv and the polarity of the environment surrounding Eu^{3+} ions is described by the Lippert equation [8]:

$$\Delta \nu = \frac{2f(\mu^* - \mu)^2}{hca^3} + Const$$

where h is Planck's constant, c is the speed of light, a is the radius of the cavity in which Eu^{3+} ion resides; μ and μ^* are the ground and excited state dipole moments respectively, and f is the orientation polarizability of the entire set of surrounding environment rather than one or a few neighbouring molecules.

Being heated between room temperature and 300°C, the relatively polar solvents, water and ethanol, evaporate, and the orientation polarizability decreases remarkably. The decrease in Stokes' losses results in a blue-shifted emission spectrum with respect to the emission spectrum of no heat-treatment xerogel. Being consecutively heated at elevated temperature, the increasing in the covalency degree of Eu-O bond brings an additional interaction as a result of substituting $Si0_4$ tetrahedra for water to coordinate with Eu^{3+} ions, and then introduces another shift effect, known as Nephelauxetic effect. This causes shift of the emission spectrum to longer wavelength. Stokes' shift has disappeared after heating at 500°C, and Nexphelauxetic effect has become the dominant shift effect from that temperature.

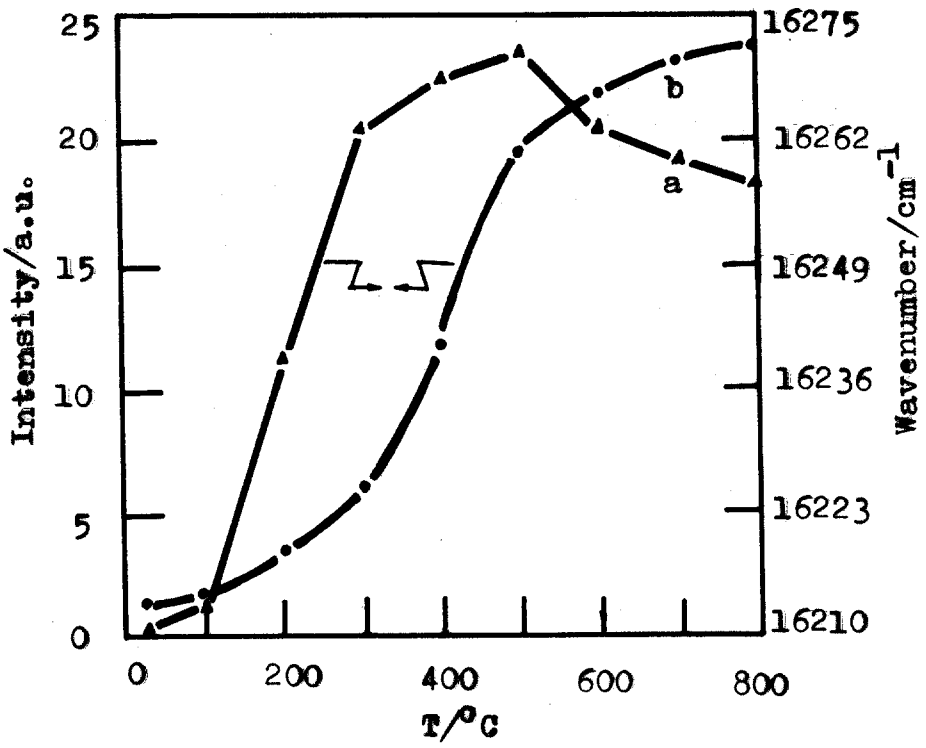

Fig. 3 Peak wavenumber ν_m (a) and fluorescence intensity (b) of $^5D_0$ ® $^7F_2$ transition emission of Eu^{3+} ions doped in silica gel as a function of heat-treatment temperature.

3. 3. Temperature dependence of the emission intensity arising from the $^5D_0$ ® $^7F_2$ transition of Eu^{3+} ions

Fig. 3(b) shows the $^5D_0 \rightarrow {}^7F_2$ transition emission of Eu^{3+} ions versus the heat-treatment teýnperature. The temperature dependence of the $^5D_0 \rightarrow {}^7F_2$ emission intensity is similar to that of asymmetry parameter. The result of the Eu^{3+}-doped xerogel linear shrinkage versus heat- treatment temperature shows that the shrinkage in the range room temperature to 500°C is much smaller than that at higher temperature (up to 800°C). This indicates that the great increase in fluorescence intensity in the range 300°C to 500°C isn't caused mainly by the increase in Eu^{3+} ion concentration as a result of the decrease in the sample's volume. From the DTA and TGA curves of the doped xerogels and the shift effects of Eu^{3+} ion emission spectrum, as shown in fýg. 2 and fýg. 3(a), we suggest that the change .in the fluorescence intensity is caused mainly by the change in the hydroxyl group (O-H) concentration in the gel to glass conversion.

The study of Stein and Wurzberg [9] has conformed that the radiative transitions of lanthanide ions in the aqueous solutions are quenched strongly by the high-frequency vibrations of O-H groups located at around 3500 cm^{-1}. Taking Eu^{3+} ions for example, the energy gap between the lowest fluorescent level $^5D_0$ and the highest nonfluorescent level $^7F_6$ is about 12150 cm^{-1}. This energy of the gap can be dissipated by 4 hydroxyl groups, and thus quenching by O-H vibration becomes an important mode of radiationless

transitions. The fluorescence intensity of Eu^{3+} ions, however, increases slowly between room temperature and 250°C although much water loses in the same temperature range (see Fig.2). We suggest that the O-H groups which quench strongly the radiation transitions of Eu^{3+} ions are from the coordination water rather than the physically absorbed water. As mentioned above, with increasing the heat-treatment temperature, the three dimensional network forms and strengthens gradually, and the coordination water molecules are substituted by SiOa tetrahedra in the range 250 to 500 °C. The frequency of Si-O stretching vibration is about 1100 cm^{-1} [6]. The energy gap of Eu^{3+} ion need about 12 vibrational quanta to match. It is obvious that there are lower probabilities of the non-radiative transitions induced by Si-O stretching vibration. So the fluorescence intensity increases greatly. After heating at 500°C, the coordination water molecules are almost removed with forming the $(Si\text{-}O)_nEu$ bonds. Increasing the fluorescence intensity is due to the increase in Eu^{3+} ion concentration as a result of the decrease in the sample's porosity and volume at higher temperature.

3. 4. Symmetry of Eu^{3+} ion sites in silica gel glass

J levels of Eu^{3+} ion split under the effect of crystal fýeld. The number of sublevels and bands is related to symmetry of Eu^{3+} ion sites. Transition features between Eu^{3+} ion sublevels depend obviously on the local symmetry of Eu^{3+} ion. By means of group theory and quantum mechanics, the $^5D_0 \rightarrow {}^7F_J$ transitions can be classified in accordance with 7 crystallographic systems and 32 point groups. Fig. 4 shows the high resolution emission spectrum of Eu^{3+} ions in silica gel glass measured at 8.5 K. There is one band at 17250 cm^{-1} arising from the $^5D_0 \rightarrow {}^7F_0$ transition, three bands at 16985 cm^{-1}, 16855 cm^{-1} and 16730 cm^{-1} from the $^5D_0 \rightarrow {}^7F_1$ transition and five bands at 16271 cm^{-1},16210 cm^{-1},16133 cm^{-1},16029 cm^{-1} and 15943 cm^{-1} from the $^5D_0 \rightarrow {}^7F_2$ transition. The splitting numbers of the $^5D_0 \rightarrow {}^7F_J$ (J=0, l, 2) transitions correspond to l, 3 and 5, respectively. Therefore, the local symmetry of Eu^{3+} ion sites is Cs [6,10].

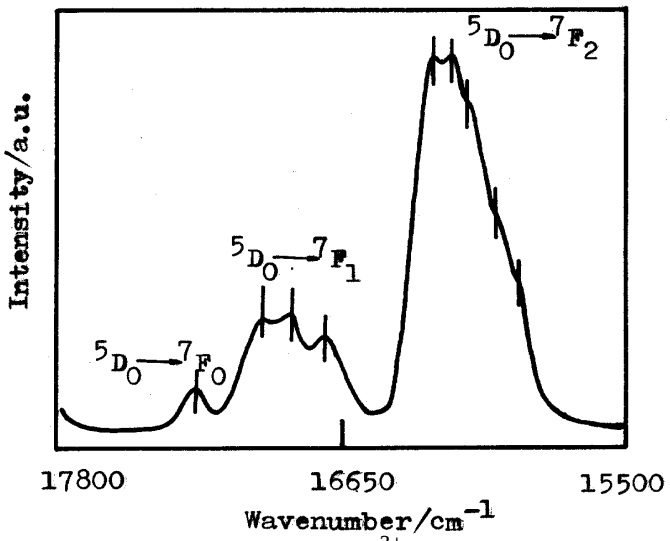

Fig. 4 High resolution emission spectrum of Eu^{3+} ions in the sample treated at 800°C for 24 hours measured at 8.5 K.

4. CONCLUSIONS

The fluorescence of Eu^{3+} ions can be used to probe the changes in the nearest neighbour of Eu^{3+} ions and the microstructure of the Eu^{3+}-doped silica gel in the gel to glass conversion. Three steps may be distinguished during the gel to glass transition. Being heated between room temperature and 250^{o}C, the linear and planar polymerizations form and remain. Treated in the range 250^{o}C to 500^{o}C, the $Si0_4$ tetrahedral three dimensional network forms and strengthens gradually. The volume relaxation and viscous sintering take place at elevated temperature, until silica glass is obtained after being heated at 800^{o}C. The symmetry of Eu^{3+} ion sites in this glass is Cs.

Acknowledgment

This work is supported by the grants from National Natural Science Foundation of China (No. 59572020) and Natural Science Foundation of Zhejiang Province (No. 594074).

REFERENCES

1. J. D. Mackenzie and D. R. Ulrich, In: Sol-Gel Optics I, Proc. SPIE 1328,1990, P. 2.
2. P. F. James, J Non-Cryst. Solids, l00 (1988) 93.
3. C. K. Jorgensen and B. R. Judd, Mol. Phys., 8 (1964) 281.
4. G. D. Qian, M. Q. Wang, M. Wang, X. P. Fan and Z. L. Hong, In: Proceeding of the l7th International Congress on Glass, Vol. 4, Beijing, October 1995, edited by F. T. Gong, P. 332.
5. P. K. Gallagher, C. R. Kurkjian and P. M. Bridenbaugh, Phys. Chem. Glasses, 6 (1965) 95.
6. R. Reisfeld, Journal of Research of National Bureau of Standards -A. Physics and Chemistry, 76A (6) (1972) 613.
7. X. P. Fan, M. Q. Wang and G. H. Xiong, Mater. Sci. Eng., B21 (1993) 55.
8. J. R. Lakowicz, Principles of Fluorescence Spectroscopy, New Youk: Plenum,1983, P. 187.
9. G. Stein and E. Wurzbery, J Chem. Phys., 62 (1) (1975) 208.
10. X.Y. Zhang, Chinese J. Lumin., 3 (1983) 18.

GLASS AND GLASS CERAMICS FROM THE INDUSTRIAL BY-PRODUCT BY-PASS CEMENT DUST*

Morsi M. Morsi
National Research Center, Egypt

Abstract

One of the local waste by-product that represents a serious problem is the by-pass cement dust accumulated during the manufacturing of cement by the dry technology method. The amount of cement dust which accumulate in one plant may reach 600 ton/day. These dust accumulations represent not only significant loss of money, energy and raw materials but also have a negative impact to the environment. The very fine nature of the cement dust causes air pollution which would negatively affect the health of man and living things.

The present work make use of the by-pass cement dust to be used as raw material for preparation of glass and glass-ceramics. Glass samples were prepared using batches containing about 50% of the by-pass cement dust, natural sedimentary materials and small percentage of chemical materials. Melting was carried out at 1450 ^{0}C and the obtained glasses were yellow to green in colour, and have micro hardness (Vickers) values ranging between 610-596. Their optical absorption in the visible region and DTA were studied. The glasses were heat-treated at the temperatures revealed by DTA curves. The obtained glass-ceramics were found to have micro hardness (Vickers) values ranging between 618-702. X-ray examinations of glass-ceramics samples that heat-treated at 910 ^{0}C indicated formation of gehlenite and wolastonite phases.

---

* Full manuscript not available at the time of printing

GLASS CERAMIC MATERIALS FOR COATINGS ON METAL BASED BODIES

Peter R. Djambazky
University of Chemical Technology and Metallurgy, Bulgaria

Abstract

This paper summarizes results from the studies on the synthesis of glass ceramic materials from the systems SiO_2 - CaO - Na_2O - B_2O - P_2O_5 - CaF_2 and CaO - Al_2O_3 - P_2O_5 / R_2O. The synthesis of the compositions was carried out by the conventional glass-making technology and by the sol-gel method. The phase-formation areas are established and the corresponding phase diagrams are presented. The crystal products are studied and identified by the application of IR -spectroscopy in the range 1300 - 300 cm^{-1} .By using X-ray phase analysis it was proved that the phases predominantly formed are $CaSiO_3$, $Ca_2P_2O_7$ and borates in accord with the preset chemical composition of the glasses. In parallel with the formed silicates and phosphates mixed phases are present too. The results from the analysis of the thermal, mechanical and chemical properties of the synthesized products are presented.

1. INTRODUCTION

The investigations carried out were aimed at the synthesis of glass ceramic materials for coatings on metal bodies , based on the systems SiO_2 - CaO - Na_2O -B_2O_3 - P_2O_5 - CaF_2 and CaO - Al_2O_3 - P_2O_5 / R_2O. The compositions were obtained by using the conventional glass-making technology and by the sol-gel method. The areas of phase formation were studied and the corresponding phase diagrams were plotted. On the ground of the synthesized glass ceramic materials detailed investigations of the crystallization processes were carried out. Some physicochemical properties such as the chemical resistance, the coefficient of linear thermal expansion, the softening temperature of the glassy materials and their mechanical behavior were determined as well . On the ground of the prepared compositions in the form of suspension and after thermal treatment coatings were formed on a Co-Cr alloy finding application as artificial dentures.

2. EXPERIMENTAL

As initial raw materials were used predominantly oxides and carbonates with a purity over 99 %. After good homogenization of the batch the melting was carried out in a super canthal furnace at a temperature up to 1300^{o}C. The time for achieving

chemical and thermal homogeneity of the melt was about 2 hours at maximum temperature . The glassy samples used for the study were cast in graphite moulds with consequent annealing at 540 ^{o} C for one hour. Part of the melt was cooled in cold water for easier grinding. The samples prepared were characterized visually, microscopically by X-ray analysis and by IR-spectroscopy. The initial raw materials for the synthesis of the composition of the glasses by the sol-gel method were: Na_2SiO_3, $NaNO_3$, $Ca(NO_3)_2 .4H_2O$, H_3BO_3, P_2O_5 and finely milled CaF_2. According to reference data from 10 % solution of Na_2SiO_3 and 10 % solution of HCI is obtained good quality sol which is stable at pH = 3-4. Then are added in stoichiometric quantities the solutions of the other substances, as CaF_2 was the only one added as a finely milled powder after the complete gel drying [1-5] at the end. The complete homogeneity of the colloidal solutions was achieved by using magnetic stirrer. The solutions of the initial raw materials were mixed by continuous stirring and the solution pH = 3-4 was achieved by adding 10 % solution of HCl. The mixing sequence was as follows : 10 % solution of Na_2SiO_3 + H_3BO_3 + $NaNO_3$ + P_2O_5 + $Ca(NO_3)_2.4H_2O$ + 10 % solution of HCl. Finally proceeded gel-formation, drying and melting of the synthetic batches. The prepared samples were studied in parallel with those obtained by the conventional method.

3. RESULTS AND DISCUSSION

The areas of glass formation of the compositions synthesized by the conventional technology and by the sol-gel method are shown on the phase diagrams (Fig.1 and Fig. 2). Accounting for the results from the sections the spatial image of the area of glass formation in the system SiO_2 - Na_2O - CaO - (B_2O_3 + P_5O_5 + CaF_2) was plotted -Fig.1. In both systems five glass compositions were prepared and investigated.

On Fig. 3 and 4 are shown the IR - spectra of some selected compositions prepared by the conventional technology and by the sol - gel method. Accounting for the results from the Differential Thermal Analysis (DTA) studies on the 5 compositions - glasses in the system SiO_2 - CaO - Na_2O - B_2O_3 - P_2O_5 - CaF_2, the samples were thermally treated for 2 hours at T = 800 ^{o} C. The IR - spectra were recorded in the range 1300 - 300 cm^{-1} by a double beam spectrophotometer Specord M-80. The IR - spectra on Figures 3 and 4 are of a similar type. They have the features typical for the glass ceramic material. It is obvious that the crystallization processes are considerably accelerated with the treated samples of compositions 1 - 5, prepared by the sol - gel method (Fig. 4). Clearly expressed bands were observed at 1035 - 960 cm^{-1} , 780 - 600 cm^{-1} , 470 - 450 cm^{-1}. The occurrence of more intensive crystallization processes in the samples obtained by the sol - gel technology was indicated by the greater number and the more expressed absorption maxima for the crystal phases formed (Fig. 4). In accord with the preset chemical compositions of the glasses the phases of $CaSiO_3$ and $Ca_2P_5O_7$, are formed predominantly. This was confirmed by the X-Ray phase Analysis (XRA) data. The complexity of the system made possible the formation of borates and mixed phases, but the absorption maxima of these phases were with close values which impeded their interpretation to a considerable extend.

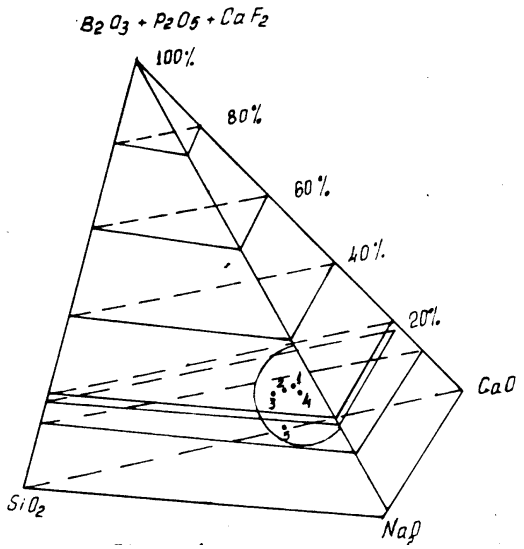

Figure 1

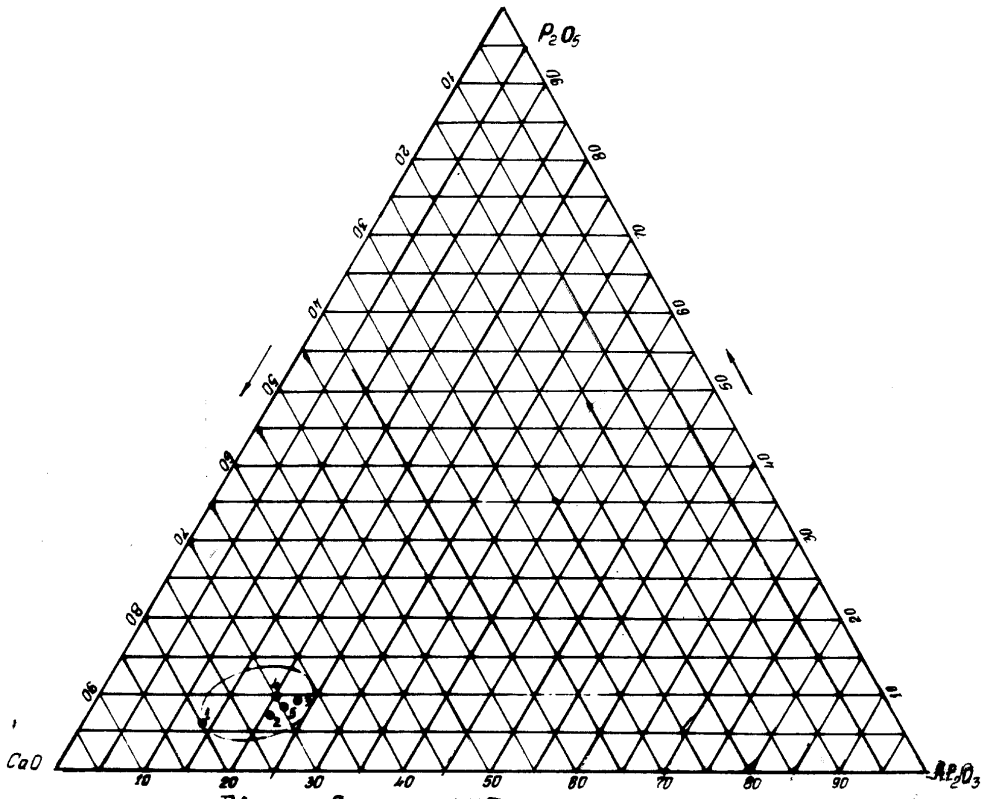

Figure 2

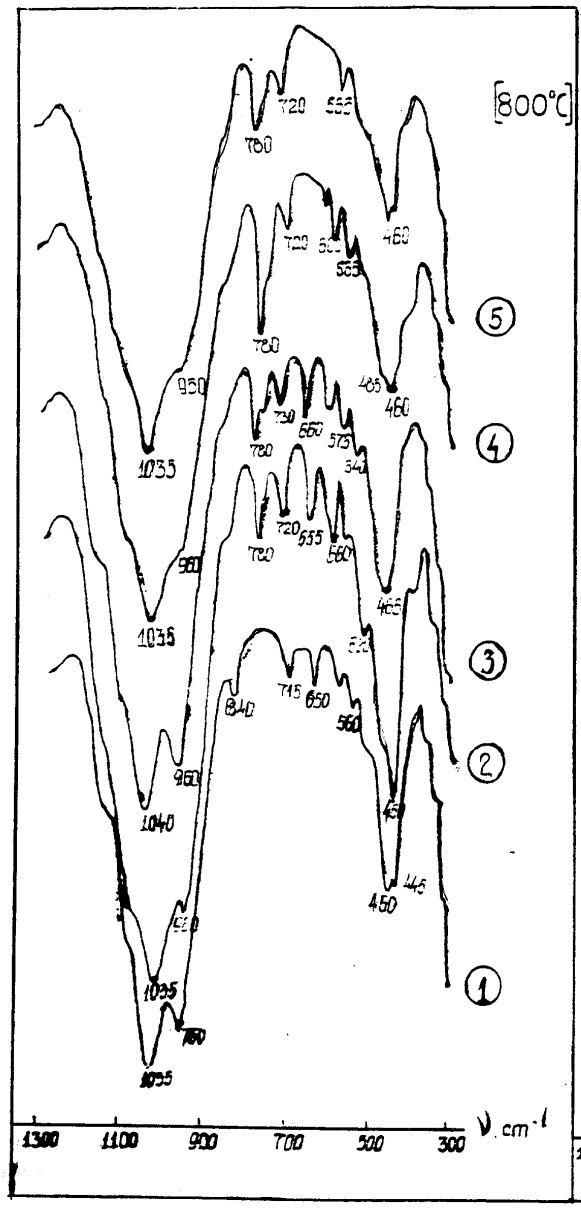

Figure 3.

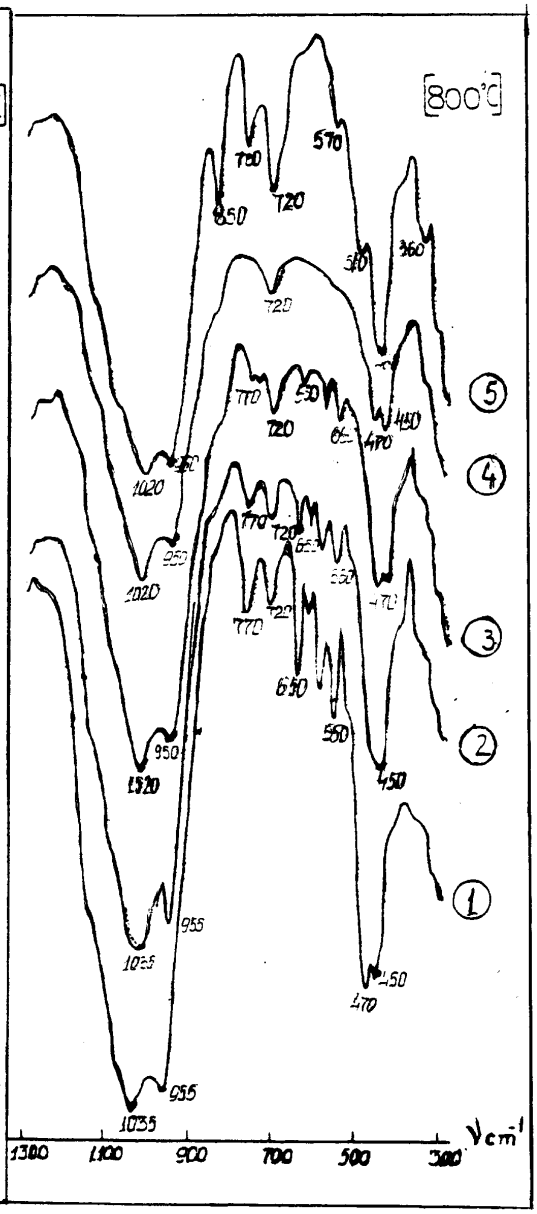

Figure 4.

From the recorded IR - spectra of the studied compositions, it is seen that with both synthetic methods occured actual consumption of SiO_2, evidenced by the absence of the maximum at 1100 cm^{-1}, featuring the presence of free SiO_2 in the spectra of all samples (1-5). It was established that the crystallization of the glassy materials occurred above 700°C.

To investigate the physicochemical properties of the obtained glasses specially moulded samples were applied. The samples were characterized in relation to their

softening temperature, their chemical resistance an their microhardness in glassy and in crystalline state.

The values of the Coefficient of Linear Thermal Expansion (CLTE) - α for both systems are presented in Table 1.

Table 1

Compositions	α	1	2	3	4	5
I system	$\alpha.10^{-7}\ K^{-1}$	144	145	147	148	142
II system	$\alpha.10^{-7}\ K^{-1}$	127	124	121	120	123

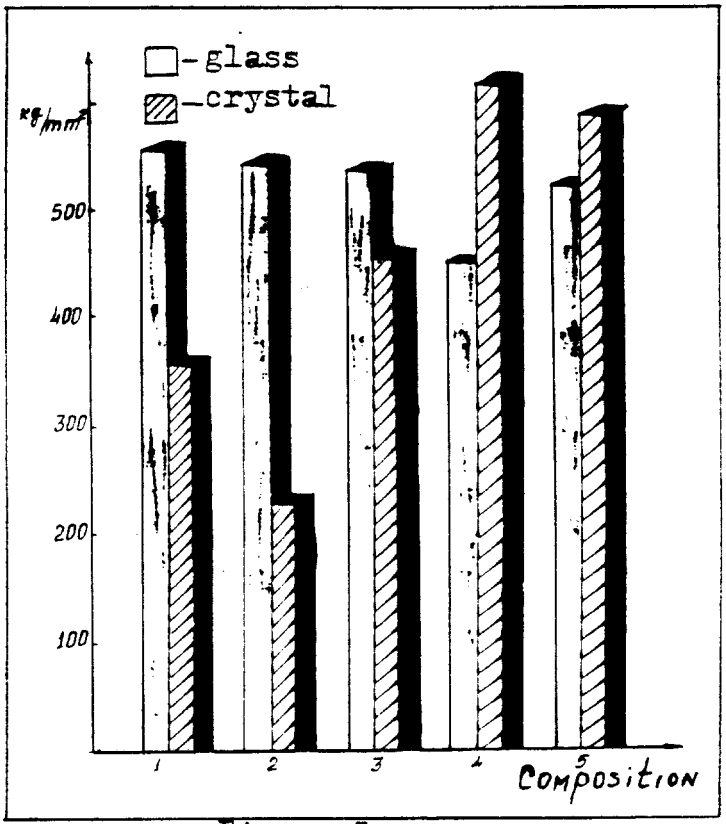

Figure 5.

It was established that the temperature of glass softening for the system SiO_2 - CaO - Na_2O - B_2O_3 - P_2O_5 - CaF_2 is in the temperature range 500 - 625 ^{o} C and for the second system in the range 535 - 600 ^{o} C.

The values of the microhardness were determined by the formula :

$$MHV = 1854{,}3\ P/d^2,\ kg/mm^2 \qquad (1)$$

where,

MHV is the value of the microhardness of the glass / glass-ceramics ;

P is the loading, kg ;

d is the diagonal of the square footprint / mm^2.

The samples were preliminary treated mechanically as to obtained polished surface. The microhardness of the corresponding glass samples of the first system before and after the crystallization is shown on Fig. 5. The preparation of a glass ceramic coating of some compositions on a chromo-cobalt alloy, used for artificial dentures was successfully experimented. It was established that as to prepare good quality coating it was obligatory to carry out the drying, melting and crystallization under vacuum.

4. CONCLUSIONS

a. Investigated and plotted were the spatial areas of glass - formation in the systems SiO_2 - CaO - Na_2O - B_2O_3- P_2O_5 - CaF_2 and CaO - Al_2O_3 -P_2O_5/ R_2O.

b. On the ground of the data from the XRA and the IR - spectra it was concluded that after crystallization are formed predominantly the phases $CaSiO_3$ and $Ca_2P_2O_7$.

c. With the help of DTA it was determined the temperature crystallization range (700-870^oC). The softening temperature is in the range 500 - 625 ^{o} C . For the various compositions, the CLTE (α) varies within the range 120 - 148 $.10^{-7}$ K^{-1}.

d. After the occurrence of the crystallization process, the chemical resistance of the glasses (IV hydrolytic class) was increased by approximately one hydrolytic class The microhardness is varying differently and reaches to values of 690 kg/mm^2.

REFERENCES

[1] The roles of precursors in the structure of the SiO_2 - Al_2O_3 sols and gels by the sol-gel process, Journal of Sol-Gel Science and Technology 1: 47-56, (1993).

[2] J.M. Thomas, J. Klinowski P.A. Wright and R. Roy, Angew. Chem. Int. Ed. Engl. , 22: 614, (1983).

[3] T. Heinrich and F. Raethma, " Structural characterization and phase development of sol - gel derived mullite and its precursors, Journal of Non-Crystalline Solids, 147 & 148:152-156, (1992) ,.

[4] Jeffrey C. Huling and Gary L. Messing, " Chemistry - crystallization relations in molecular mullite gels, Journal of Non - Crystalline Solids ,147 -148 : 213 - 221, (1992).

[5] Sahuran U. Voβ, and H. Schneider, J. Mat. Sci. , 29 : 3261 (1994).

GLASS FORMATION AND ^{19}F NMR-INVESTIGATION ON THE SnF_2-ZrF_4-NaF SYSTEM*

Evgeny B. Merkulov, Valery Ya Kavun and **Vladimir K. Goncharuk**
Russian Academy of Science, Russia

Abstract

The vitreous areas have been found in the ternary system SnF_2-ZrF_4-NaF. In a typical composition 60 SnF_2-35ZrF_4-5NaF (mol.%) T_g occurs at 370 K, and T_c at 443 K. The structural and dynamic characteristics of fluorine subnets of these glasses were studied within the temperature range of 200-400 K by NMR method. Analysis of NMR parameteres spectra of there glasses allowed to state the factors effecting the character of inner ion mobility in glass structure, to determine types of ion motions and estimate its activation energies.

---

* Full manuscript not available at the time of printing

GLASSES FOR IMMOBILIZATION OF RADIOACTIVE WASTES

B.Samuneva, P.Tzvetkova, P.Djambaski and **I.Gugov**

University of Chemical Technology & Metallurgy, Bulgaria

Abstract

Glasses and glass-ceramics for immobilization of High Level Waste (HLW) and Intermediate Level Waste (ILW) are developed. They are synthesized on the basis of some borosilicate and phosphate systems, basalt rock, zeolite and metallurgical slags. Different type of model HLW and ILW are added in the glass batches up to 50%. The sol-gel technology has been used for synthesis of borosilicate glasses and the processes of structure evolution have been investigated by means of X-ray diffraction analysis, IR-spectroscopy and TEM. Some physical and chemical properties of glasses and the influence of the chemical composition on them have been studied. The special attention has been paid on the investigations about the kinetics of hydrolytic solubility and the crystallization processes.

I. INTRODUCTION

The environmental protection is one of the most important problems for the modern society. The radioactive wastes are considered as especially hazardous pollutants produced from the nuclear power stations, scientific medical and other different laboratories using radioactive isotopes [1]. Glasses belong to the most suitable matrices for immobilization of intermediate and high-level radioactive wastes. They possess a high chemical, thermal stability and radiation stability. Glasses based mainly on borosilicates are used in the practice for immobilization of radioactive wastes [2-3]. The sol-gel method is considered to be a promising technology for radioactive waste storage [4 - 6]. The method allows the preparation of products with very good homogeneity in which the wastes are strongly fixed. In this method borosilicate matrix is prepared in advance using sol-gel technology, then the radioactive wastes are added to it. There is a definite interest [7, 8] in the synthesis of phosphate-based glasses to be used for immobilization of radioactive wastes. Glasses based on the natural raw materials as basalts, zeolites, clays and etc. allow to be regarded as reliable and suitable from economical point of view [9,10]. These raw materials are widely spread on the Earth's surface and contain all necessary glass forming components. They are able to accumulate large amounts of radioactive wastes.

The purpose of the present work is to synthesize and to examine glasses of different chemical composition for immobilization of the radioactive wastes. Generally, some special attention is paid on the vitrious materials on the PbO-Fe_2O_3-P_2O_5-BaO as well as on the natural products (basalts and zeolites), and to examine the processes of gel and

glass formation in the borosilicate system with the addition of model radioactive waste using sol-gel technology.

II. EXPERIMENTAL

The chemical compositions of the obtained phosphate glasses containing radioactive wastes are given in Table 1 (P-1, P-2). The batches for glass melting were prepared by mixing Pb_2O_3, BaO, Fe_2O_3, P_2O_5, and the oxides of simulated radioactive wastes in an amount of 20 wt%. The glasses were melted in corundum crucibles at 800-950^oC, the temperature being kept constant for 100 min. homogenized melt was cast into graphite forms pre-heated up to 500^oC. The glasses obtained were kept at 500^oC for 200 min and allowed to cool to room temperature.

Table 1 *Chemical composition (in wt%) of samples*

Component	P-1	P-2	B2	Z1	P
Pb0	18.34	18.34	-	-	-
Ba0	6.37	4.00	1.00	7.77	0.55
P_2O_5	50.52	52.00	0.25	-	0.30
Fe_2O_3	10.78	7.29	7.10	1.34	8.33
La_2O_3	-	2.57	-	-	-
MnO_2	3.19	-	1.55	-	0.95
MoO_3	0.67	2.51	1.00	-	2.00
Na_2O	3.19	-	2.28	8.77	13.42
NiO	1.51	-	-	-	-
SiO_2	0.29	0.53	39.70	47.76	41.00
ZrO_2	-	3.07	-	-	-
SrO	0.38	0.70	1.75	-	0.35
Al_2O_3	2.06	3.90	16.05	8.28	9.35
CaO	2.56	1.20	14.25	2.82	4.50
CeO_2	-	1.44	-	-	-
Cr_2O_3	0.14	1.70	-	-	-
Cs_2O	-	0.75	1.75	-	1.00
TiO_2	-	-	1.45	-	-
MgO	-	-	7.60	0.34	-
Nd_2O_3	-	-	2.50	-	4.00
K_2O	-	-	1.83	-	-
$S0_3$	-	-	-	0.83	-
B_2O_3	-	-	-	11.26	12.25
Li_2O	-	-	-	-	2.00

Glasses based on basalt (Table 1-B2) are prepared by melting 50:50 (wt%) mixtures of basalt and simulated nuclear waste. The zeolite has in advance absorbed 0.1 mg/eqv Cs (Table 1-Z1). The glasses were melted in corundum crucibles at 1350^oC for 100 min. The

homogenized melt was poured into graphite forms pre-heated up to 500^{o}C. The glasses obtained were treated at 500^{o}C for 200 min and allowed to cool to room temperature. The composition of the borosilicate glass constituted 20% of the simulated wastes (Table 1-T). All glass components and radioactive oxides were included as soluble nitrates and silica hydrosol. The solution obtained was homogenized for 30 h and gelled at room temperature after 24h. The gel was dried at 60-100^{o}C for 48h and melted at 1050^{o}C. lt was found that by using this technology the inclusion of the waste in the structure of glass could be achieved during the process of synthesized the gel [11].

The structure of the glasses synthesized was investigated by infrared spectroscopie, and X-ray diffraction (XRD).

The nuclear waste glasses were leached under the ISO (International Organization for Standardization) type test condition [12], according to which the leachant was periodically renewed. Experiments were conducted at 90+1^{o}C for 1,3,7,14 and 28 days. Solution analyses were carried out for the leachates of waste glasses using the Inductively Coupled Plasma Spectroscopy (ICP).

III. RESULTS AND DISCUSSION

It is established that the phosphate glasses are characterized by higher value of the density (3.44 - 3.51 g/cm^3). The relatively high percentage of radioactive wastes in glasses (20 mac.%) and the density cited above determines also the higher bulk concentration of the waste in them.The value of bulk concentration was in the 0.68-0.78 g/cm^3 range. Therefore, it could be suggested that barium-lead phosphate glasses are near to lead-phosphate glasses show better parameters to the borosilicate and basalt glasses. The relatively higher temperature of softening (T_s) of glasses (480-666^{o}C) makes them suitable for immobilization of holh active wastes separated in the process of the storage of large amounts of heat. It has been established that the thermal expansion coefficient of glasses (90 - 92.10^7 deg^{-1}) is near to the coefficient of some iron and steel materials used for containers. The basalt based glasses show a lower coefficient of linear thermal expansion (75.10^{-7}deg^{-1}) and higher T_s values in comparison to those based on zeolites (550 -666^{o}C). The last one contain a larger quantity SiO_2 and smaller Al_2O_3, CaO and MgO amounts which affect the values of the coefficients of linear thermal expansion and T_s. All glasses synthesized are distinguished by high acidic and alkaline durability in 98-99% range.

Fig.1 shows the IR- spectra of the phosphate glasses investigated. Absorption bands at 1260,1150,1090, 940 -920, 740 - 720 and 520 cm^{-1} are observed.

The high-frequency bands at 1260, 1150 and 1090 cm^{-1} may be associated with antisymmetric and symmetric vibrations of the PO_2 groups in the PO_4 polyhedra forming the polyphosphate chain. The bands at 940 - 920 cm^{-1} and 740-720 cm^{-1} can be attributed to antisymmetric and symmetric stretching modes of the P-O-P bonds in the chains. The low-frequency band at 520 cm^{-1} can be assigned to bending modes of the PO_4 groups (Fig.1 a).

In the spectrum of the P-1 composition there are two bands in the high-frequency region at 1150 and 1080 cm^{-1}. It should be pointed out that in the spectra of compositions P-2 (Fig.1 b) the number of the high-frequency bands increases. Since high frequency

vibration in the spectra is a treehold degenerated, the larger number of bands in the spectra of compositions P-2 can be regarded as a result of the decreasing symmetry of PO_4 groups. This means that the degree of deformation of the PO_4 tetrahedra is more pronounced than is the case of composition P-1.

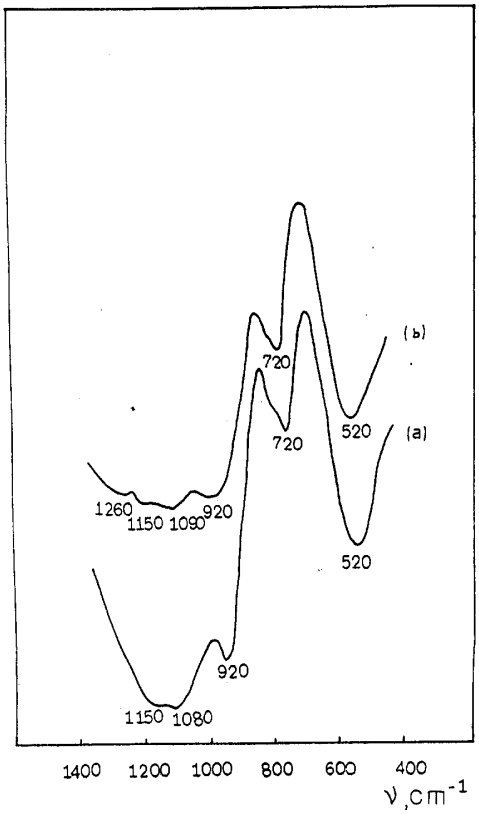

Fig.1 The IR spectra of phosphate waste glass :
(a) - sample P-1, (b) - sample P-2

The decreasing symmetry of the PO_4 tetrahedra is probably due to the presence of various polyvalent cations participating in the composition of the oxides in the radioactive wastes. With compositions P-2 the wastes contain some oxides such as La_2O_3, ZrO_2, CeO_2 and Cs_2O which are absent from composition P-1. The cations in these oxides have large electric charges and exercise a polarizing effect on the neighboring ions. When incorporated in the glassy network they cause, perhaps, a more pronounced distortion of the PO_4 polyhedra.

In order to follow the processes of gel and glass formation of the samples obtained by the sol-gel and conventional technologies the samples are thermally treated in 300-1000^oC range. The IR spectra presented in Fig.1. The main absorption bands recorded could be assigned to the following chemical bonds: bands at 1080 cm^{-1} and 820 cm^{-1} - to antisymmetric and symmetric stretching vibrations of the Si-O bonds. In the 550-450 cm^{-1} range were observed bending vibrations of B-O and Si-O bonds.

The band at 960-940 cm^{-1} is due to the stretching vibrations of the Si-OH bonds. A band at 1200 cm^{-1} is attributed to the vibrations of the B-O bond in the clusters with a triple-coordinated boron. The presence of BO_4 was not verified, but nevertheless it could

be expected the a combined presence of these polyhedra. At 750 cm^{-1} were observed vibrations of the B-O-Si bridge.

The bands at 1400, 820 and 640 cm^{-1} are explained by the vibrations of nitro groups incorporated in the gel structure through the corresponding nitrates. The bands at 3500 cm^{-1} and 1640 cm^{-1} were observed which are assigned to the stretching and bending vibrations of the constitution and water. These bands decrease its intensity with increasing the temperature of gel heat treatment.

Fig.2 shows that more significant changes were observed in the IR spectra of the samples thermally treated in the 500-600^{o}C temperature range. The bands at 1200 cm^{-1} and 640 cm^{-1} disappear and those at 900 cm^{-1} and 800 cm^{-1} pass into shoulder. In general, it could be suggested that at this temperature begins the process of networking of the gel structure.

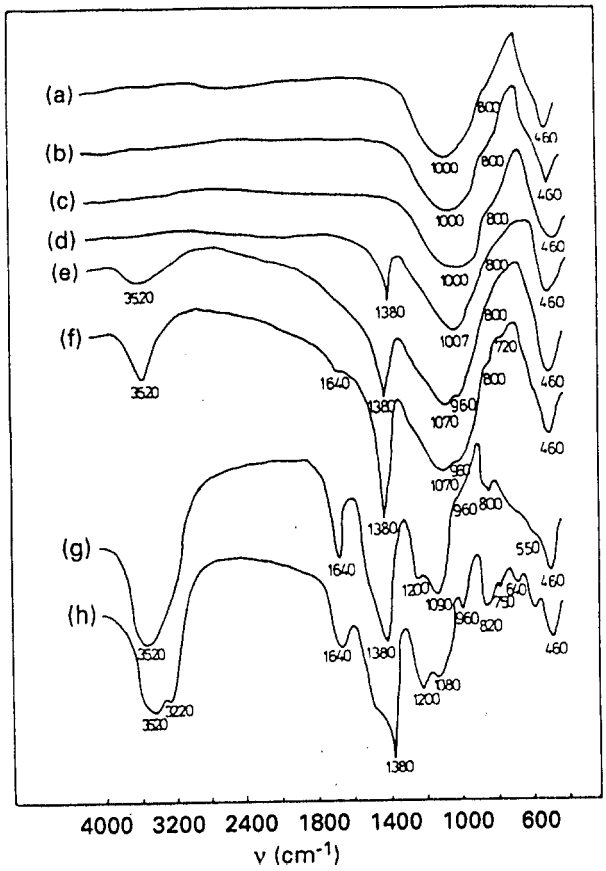

Fig.2 The IR of borosilicate waste glass obtained using sol-gel technology. (a) 1000,(b) 900, (c) 800, (d) 700, (e) 600, (f) 500,(g) 300, (h) 25^{o}C

At 700^{o}C the band at 960-940 cm^{-1} has already disappeared. Its disappearance in the process of thermal treatment of the gel is explained by the fact that the gel has converted into gel-glass [13]. But, at this temperature the nitro groups not separated entirely, which suggests that some of nitrates are not completely decomposed. At 800^{o}C these groups have disappeared and we could examine the waste gel glass. The IR spectra at 900 and 1000^{o}C are identical to those at 800^{o}C.

The IR spectra of the gel and gel products observed are confirmed from the X-ray investigations.

Furthermore, by comparison of the IR spectra of the samples examined and the data from the X-ray diffraction analysis, it was established that the processes of glass formation take place more intensively with the samples synthesized by the sol-gel technology where the networking of the structure begins at 600^{o}C with a shift of the main absorption maximum at 1080 cm^{-1} in direction to the lower frequencies. At 700-800^{o}C the gel has completely converted into gel glass.

Finally, the process of glass formation of samples obtained by the conventional technology ends just when the temperature of 1000^{o}C has been achieved.

The chemical durability (resistance to leaching) of glass samples was measured by the normalized leach rate NLR_i expressed in g/m^{2}d, and the normalized elemental mass loss NL_i in deionized water for each element according to the next formula:

$$NLR_{\acute{y}} = C_i V / S_A X_i t \qquad (1)$$

where C_i is the analytically determined concentration of the element "i" in solution (g/ml), V is the volume of solution (ml), X_i is the mass fraction of element "i" of the glass specimen, S_A is the surface area of the specimen (m^2) and t is the leaching time (days).

The date in Figs. 3 and 4 are plotted as normalized elemental mass loss (gm^{-2}) and are calculated by dividing the solution concentrations by the geometric surface area of the unleached specimen and the mass fraction of the particular element contained in the glass. It can be seen, that from the components of the phosphate glass matrix.

Of the matrix components, the lowest leach rates are exhibited by Pb and Fe followed by AI and Mo (from the nuclear waste). The leach rates of P and Sr from a P-1 specimen on the 28th day are (in gm^{-2} d^{-1}): $NLR_P = 1.2.10^{-1}$ and $NLR_{Sr} = 1.1.10^{-1}$.

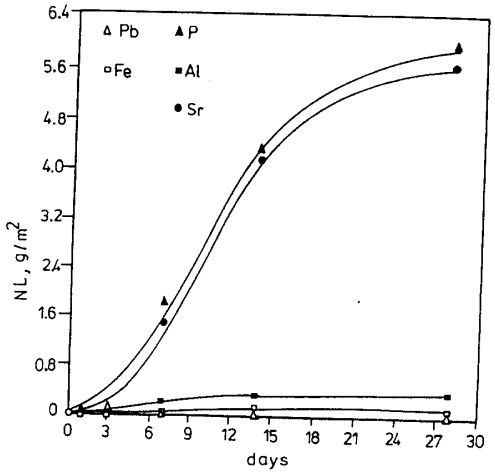

Fig.3 Relationship between normalized mass losses of different elements from specimen P-1 and leaching time in days

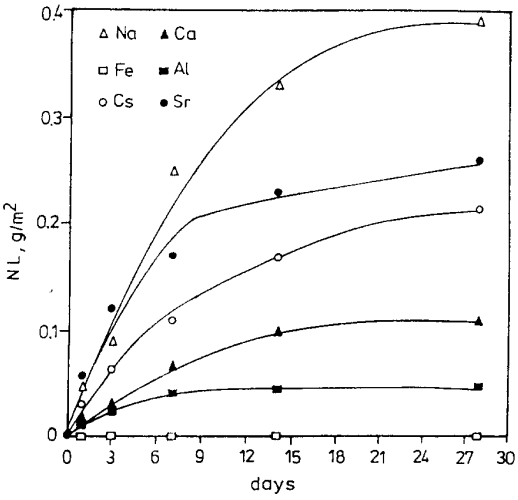

Fig.4 Relationship between normalized mass losses of different elements from specimen B-2 and leaching time in days

Under the same conditions the leach rates of Pb, Al and Fe are (in $gm^{-2}\ d^{-1}$): $1{,}5.10^{-3}$ for Pb, $2{,}81.10^{-3}$ for Al and $1{,}8.10^{-3}$ for Fe (Fig. 3).

The basalt glasses are characterized by a high of the order of $2.10^{-2}\ gm^{-2}\ d^{-1}$ on the 28^{th} day, leach rate of the alkaline element (Na and K). The lowest leach rate of the order of $2.10^{-5}\ gm^{-2}\ d^{-1}$ on the 28^{th} day, is shown by Fe and Mg, which proves that they are more strongly connected in the glass structure network (Fig.4).

As a result of the investigations, carried out and elsewhere is assumed the following mechanism of solubility of the nuclear waste glasses exposed to water:

The first stage includes the process of hydrolysis of the glass exposed to water, as a result of which in the reactionary zone the diffusion of H^+ from the water and the alkaline metals-ions from the glass (Na^+, K^+, Cs^+) takes part. As a result of this process on the glass surface is formed a hydrated silica-rich gel-layer, which is a silicic acid (H_4SiO_4).The process of hydrolysis is carried out in an alkali environment and the pH of the solution increases with increasing the solubility from 7.14 to 8.04. The obtained silicic acid is barrier for the solubility of silica network, but it is also unstable in an alkali environment. Some of the wastes components Fe,Sr,Zr,Al,Ca,Cd form hydroxides, hydrosilicates and hydrated oxides which are insoluble in alkali environment. These elements are not included in the solution, but are incorporated in the surface gel-layer and its stability increases considerably. The formation of this gel-layer influences on the dissolve kinetics of the glasses in two aspects: The first one consists in the diffusion barrier, which suppresses the formation of silicic acid on the glass surface. The second one consists in that the multicomponent layer restrains part of the hydrated Si. As a result of the investigations the primary rate of drawing out is higher but during, the time it decreases and it remaines approximately constant and the structure of the glass becomes more stable [14].

IV.CONCLUSIONS

A new family of barium-lead phosphate glasses for immobilization of radioactive wastes have been synthesized. The glasses allow the inclusion of radioactive wastes with different chemical composition. The existence of Ba and Pb in these glasses favors the absorption and scanning radiation of radionuclei and this way decreases the possibility of their penetration into the environment. The glasses providing economical effectiveness, good physicochemical properties are synthesized on the basis of basalt and zeolite. They show some advantages which include a much higher water resistance compared to that of borosilicate glasses.

By the sol - gel method has been preparated glass with very good homogeneity in which the wastes are strongly fixed. It was found that by using this technology the inclusion of the waste in the structure of glass could be achieved during the process of synthesized the gel.

REFERENCES

1. Magrabi C., Smith W.,Larkin M.,J Radioactive Manag.Nucl.Fuel Cycle,9 (1-30), 1987, 85-106
2. G.F.Piepel, G.B.Mellinger, A.N.Reimus, Waste Managem 9 (1989) 3
3. E.Vernaz, J.L.Dussoy, Appl.Geochem.Suppl.,1 (1992) 13
4. A.Bruno, FR Patent, 2 596 909,1987
5. E. Zimmer,Adv. Ceramics, voI.20: (Nuclear Waste Management II) (1986).
6. P. Gerontopoulos, Key Engineering Materials Vols. 56-57 (1991)
7. B.C.Sales, L.A.Boatner, J.Non-Cryst.Sol., 79 (1986) 83
8. L.A.Chik, D.Clark, W.White, in The Third International Symposium on Ceramics in Nuclear Waste Management, American Ceramic Society, 20 (1986) 149
9. Lebeau M.J.,Girod M.,Amer.Ceram.Bull.,66,11,1987,14-15
10. Lifanov F.A.,Stefanovskii, S.V.Steklo i keramika,3,1990,23-25
11. B. Samuneva, P. Tzvetkova, Y. Yvanova, V. Dimitrov, J.Mater. Sci. Lett.,13 (1994),1484.
12. Long-term leach testing of radioactive waste solidification products.ISO/DIS-6961 (1982)
13. B.Samuneva, P.Tzvetkova, I.Gugov, P.Djambazki, 11th Conference on glass and ceramics, Proceedings Varna,october 25-27,1993 Editors: B.Samuneva, I.Gutzow, Y.Dimitriev
14. P. Tzvetkova, B. Samuneva, I. Gugov, P. Djambaski, Bulletin of the Chemists and Thechnologists of Macedonia,1996 (in press).

GLASSES WITH SMALL THERMOOPTICAL CONSTANTS

Stalina S. Kasimova
2nd Tashkent State Medical Institute, Uzbekistan

Abstract

While searching for new composition glasses, the random combinations of the components are hardly effective. This problem advisably should be solved by the way of systematic investigation of the influence of different properties of oxides while using different bases. The system of K_2O-SrO-SiO_2 is selected because glasses with small thermooptical constants might be expected. As a result, the glasses with small thermooptical constants are obtained. These glasses may be used in the different laser systems with a minimum of optical distortion.

1. INTRODUCTION

The details of optical systems (the lenses, portholes, active elements of the laser, etc.) and the temperature gradients lead to the distortion of wave front of light beam and results in a change of optical detail, and the index of refraction changes with exploitation of temperature and with stress. These distortions considerably aggravate the characteristics of optical systems and the quality of lasers radiation.

The development of a quick technique demands the creation of optical and laser systems that do not lose tone in variable temperature conditions. The successful solution of this problem is impeded by the lack of sufficiently large set of glasses with small thermooptical constants of so named athermal glasses.

2. EXPERIMENTAL DESIGN

The optical distortions, arising in the bar at pumping of the active element of the laser, are described with help of three thermooptical constants W, P and Q:

$$W_{\lambda,t} = \beta_{\lambda,t} + \alpha_t (n_\lambda - 1), \tag{1}$$

$$P_{\lambda,t} = \beta_{\lambda,t} - \frac{\alpha_t E}{2(1-\mu)} (C_1 + 3C_2), \tag{2}$$

$$Q_{\lambda,t} = \frac{\alpha_t E}{2(1-\mu)} (C_1 - C_2), \tag{3}$$

where $W_{\lambda,t}$ the constant characterizing the distortion of wave front as a result of temperature change of the index of refraction and geometrical sizes of the glasses; $P_{\lambda,t}$ the constant characterizing the distortion of the wave front of the light, average for two orthogonal polarization planes; $Q_{\lambda,t}$ the constant characterizing the dual refraction; $\beta_{\lambda,t}$ =dn/dt - the temperature coefficient of absolute index of refraction n_λ;α_t - the coefficient of thermal expansion; μ the coefficient of Poisson; E Young's module; C_1 and C_2 - the photo elastic constants.

The measurements of α and β were carried out by heating of the samples from room temperature to 220^{o}C on the visual Interferometer IZK-13 [1]. On the base of the results of measurements, the values of the α and W glasses at 70^{o}C and 170^{o}C temperatures are defined, and also the temperature coefficients of the expansion $\varphi=\Delta\alpha/\Delta t$ and thermooptical constant $\Theta = \Delta W / \Delta t$ are defined.

The distortions in flat bar are defined by the values of sums of the P + Q for polarization plane in the direction of x axis and by the difference of P - Q - for the polarization plane in the direction of y axis. For round bars the distortion is defined correspondingly by the sums of P + Q/2 and by the difference of P-Q/2. Thermooptical constants W, P and Q or P±Q and P ± Q/2 of the glasses used as active elements of the laser should be close to the zero. Since the thermooptical constants of the glasses depend on temperature and length of the wave, it is necessary that the condition of athermality should be executed at the working temperatures of the active element and at the length of wave generation. For the different kind of bars and for the different polarization, the glasses may be athermal simultaneously at different temperatures. It is necessary to take into account the choice of the athermal glass for specific laser.

3. RESULTS AND DISCUSSION

For the creation of the completely undistorted systems, it is necessary to have sufficiently large set of glasses with small thermooptical and different optical constants which respond to different areas of Abbe's diagram and also have the glasses for laser with decreased thermooptical constant. So, the systematic qualitative research of optical, thermal and thermooptical properties of strontium containing silicate and phosphate glasses was undertaken by us.

For obtaining glasses with a small value of P, in first approximation may be obtained glasses with small value of W, because the W is the relative simple measured parameter and correlates with thermooptical constants of the P and Q [2]. It allowed us to carry out the widescale investigation of the thermooptical constant's W which depended on the glasses composition, the laboratory investigation of simple three-component system, and the complicated silicate and phosphate systems. The glasses with small value of the W were selected as the base for the development of the industrial glasses.

The coefficient off the thermal expansion and the temperature coefficients of the index of refraction ß are defined for the glasses of the K_2O-SrO-SiO_2 system. The range and common tendencies of the change of the studied parameters of the glasses are visually seen on the triangle of the compositions, the part of which in rectangular coordinates is shown in Fig.1.

The coefficient of expansion of glasses range from 63.10^{-7} to 142.10^{-7} degree^{-1} (Fig.2), and the thermooptical constant from 15.10^{-7} to 68.10^{-7} degree^{-1} at 70^{o}C (Fig.3).

In general, it is known that the values of the α have the tendency to decrease and the values the W - to increase when the silica concentration is increased and when the K_2O content is decreased. The temperature coefficients of the expansion and the thermooptical constant also appreciably depend on the composition. The common tendency of their change with the glasses' composition are the same as for the values of the α and W.

In the studied system, the glasses of IV-th section containing (mol.%): 24-26 K_2O, 8-17 SrO and 59-65 SiO_2 possess the least value of W. At 70^{o}C, and at a wave length of 480 nm the least value of the W glasses are equal to (15-21) 10^{-7} degree $^{-1}$. At room temperature, in the red part of the spectrum, the values of the Θ were shown, and the dispersions of the thermooptical constant of the W glasses were approximately 10. 10^{-7} degree $^{-1}$.

For obtaining more common data, the investigation of the properties of SrO in the glasses was carried out by using the identical methods of the treatment of experimental data. The optical and thermooptical constants, the density and the coefficient of the thermal expansion of the strontium containing silicate and phosphate glasses (obtained by method of pseudobinary systems where the SrO was introduced into initial glasses in constantly increasing quality) were investigated. Using these methods, the 7 silicate and 6 phosphate pseudobinary systems, the glasses were synthesized.

By the help "adherence - property" diagram, the average adherence properties of the glasses can be calculated when we introduce 1% SrO, and we may judge the partial values of the SrO properties in the glass. It was found that for silicate glasses the partial value of the α_{SrO} close to 120-10^{-7} degree $^{-1}$ and in the phosphate close to 140-10^{-7} degree $^{-1}$. The thermooptical constants for the initial phosphate glasses is greater than 5.10^{-7} degree $^{-1}$ and for the initial silicate glasses more than 50.10^{-7} degree $^{-1}$. Thus, the introducing of the SrO decreases the thermooptical constant W.

Values, less than these of the SrO proves to increase the W. It follows that the partial value of the thermooptical constant of the SrO in the phosphate glasses are smaller than in the silicate ones. So, the athermal glasses with SrO are easier to obtain on the phosphate base than on the silicate one.

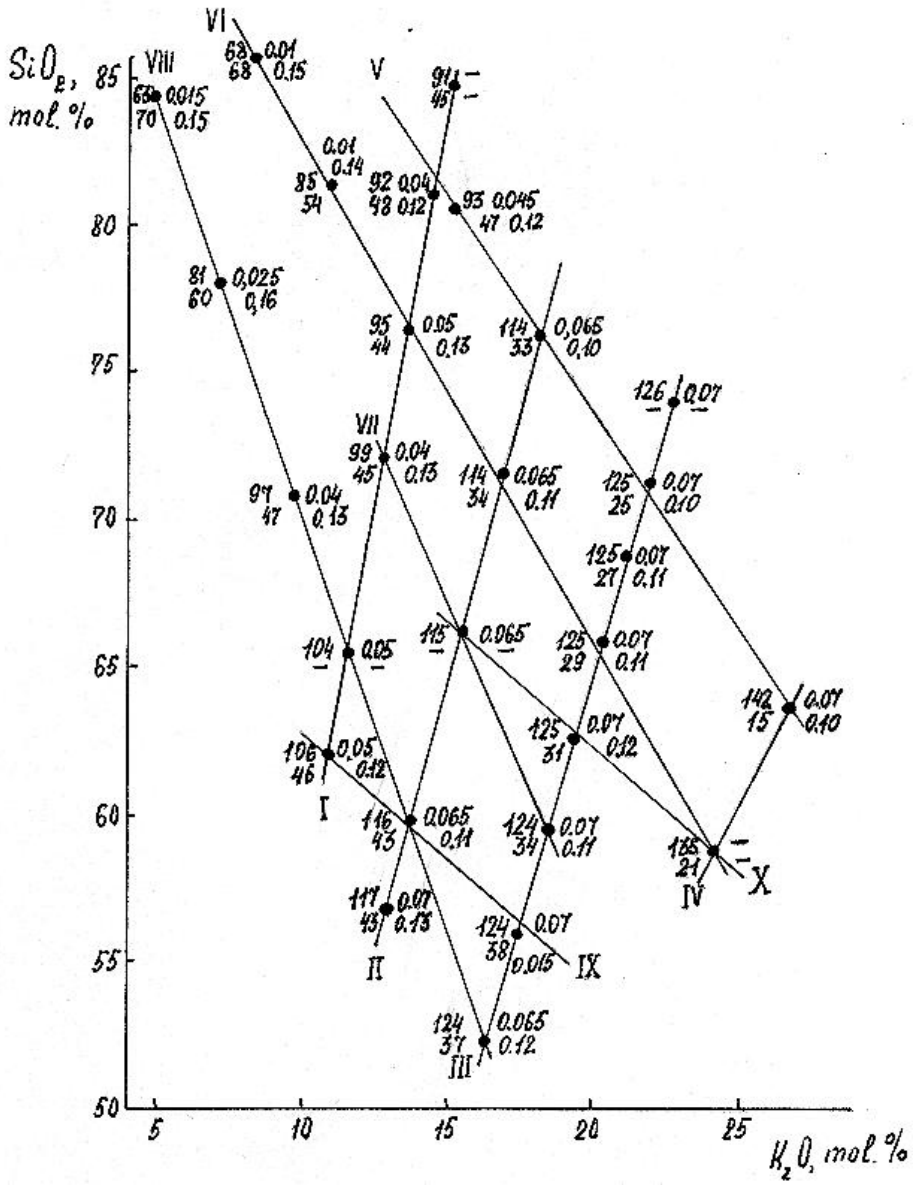

Fig.1: Position of the glasses of the K_2O-SrO-SiO_2 system on the right angled triangle of the compositions.

Near the points the values of the coefficients of the thermal expansion a and its temperature coefficient j , thermooptical constant W and its temperature coefficient Q.($t=70^oC$, $l=480$ nm) are indicated.

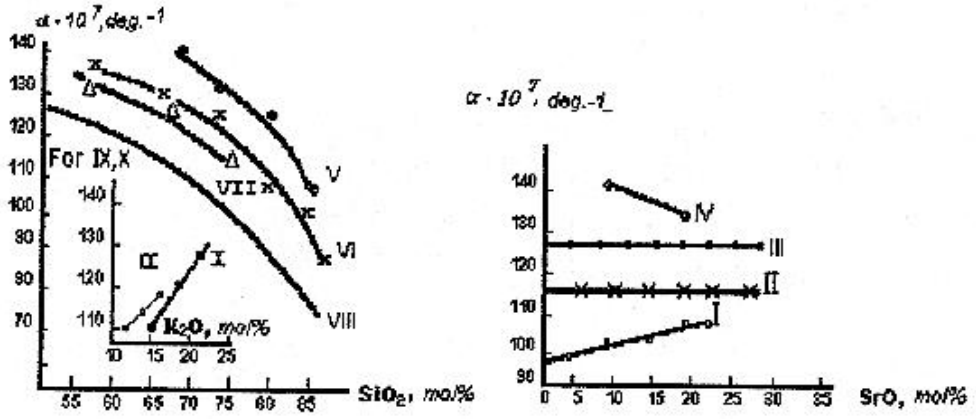

Fig.2: The dependence of the coefficient of expansion of the glasses of K_2O-SrO-SiO_2 system from the concentration of the introduced oxides (t=70°C, l = 480 nm)

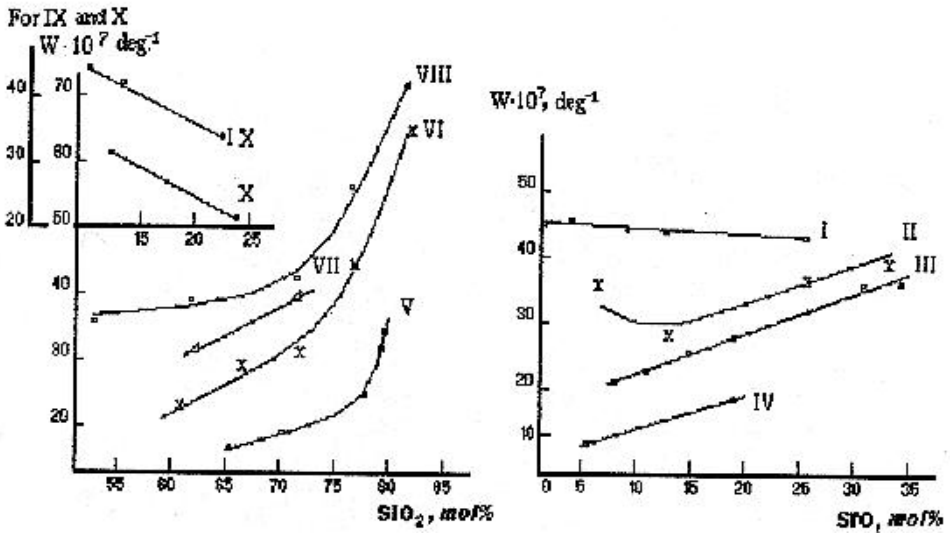

Fig.3: The dependence of the thermooptical constant of the glasses of K_2O-SrO-SiO_2 system from the concentration of the introduced oxides (t = 70°C, l = 480 nm)

Thus, the experimental material allowed us to estimate the partial values of the coefficient of the thermal expansion and of the thermooptical characteristics of the SrO and provided a well founded answer to the question of what composition to use for the industrial silicate and phosphate glasses.

As noted, for the creation of the optical systems with small thermowave aberrations, and for the removal of the resonator's distortions of the laser, it is necessary to use glasses of the active elements with small thermooptical constants. For obtaining laser glasses in the laboratory conditions, the whole series of the experimental strontium containing glasses is synthesized, the compositions of which were selected by calculation of additive formulas, so that the absolute value of W should be minimal. As a result, the glasses with values W of which ranged from (-6 to +23).10^{-7} degree $^{-1}$ at 30°C and λ= 644 nm were obtained. In industrial situations, the

vessel capacity goes up to 300 liters where the best samples of 4 silicate and of 3 phosphate glasses were found. From all the glasses, the active elements by size is ϕ10x130 mm and 8x20x105 mm and corresponds to the requirement of laser glasses by inactive absorption and homogeneity.

The values of the P ± Q and P ± Q/2 at 30^{o}C experimental and industrial laser glasses developed by us are compared. The glasses KGSS 6T and KGSS 8T with the thermooptical characteristics sufficiently surpassed existing athermal silicate industrial glasses and can be recommended for industrial use.

The advantage of the developed glasses is that the optimal temperatures of the active elements is close to room temperature; that's why special heating of active elements is not needed in the construction of the laser devices.

The generating properties of the developed glasses are not suitable for industrial uses; they have a large photochemical stability, and the luminescence duration and the spectrum of absorption and luminescence don't differ from those for industrial silicate and phosphate laser glasses.

4. CONCLUSION

The glasses may be used in the different laser systems for obtaining brightness of radiation because they provide a minimum of optical distortions in the active elements, provide an available temperatures gradient, and give the diminished angular difference, i.e. the abnormally high energy density on the target.

Thus, the developed glasses possess a profitable combination of the thermooptical, generating, photochemical and technological properties, and provide a series of advantages over well-known laser glasses and will allow a series of important problems in the field of laser technology to be solved.

REFERENCES

1. A.A.Mak, V.A.Mit'kin, L.N.Soms, A.I. Stepanov, O.S.Schavelev. Optical Mechanical Industry, N 9, 1971, p.42
2. O.S.Schavelev, V.A.Babkina. Optical-mechanical Industry, N 7, 1969, p.45.

GLASSY COVERINGS FOR CEMENT

Todorka S.Datzkova, Christina I.Bojadjieva, Martina G.Stefanova and **Dobrinka A.Stavrakeva**
University of Chemical Technology and Metallurgy, Bulgaria

Abstract

Glassy coverings for cement, fusible at low temperature, have been synthesized in the system RO_2 (SiO_2, TiO_2) - R_2O_3 (B_2O_3, Al_2O_3) - RO(PbO) - R_2O (Na_2O, K_2O, Li_2O). The planned frit properties are consistent with the cement pad features: the linear-expansion coefficient $(10\text{-}12).10^{-6}.K^{-1}$, a heat treatment response, and a requirement for nondurable heating at the lowest possible temperature.

The coverings are compounded of 10 % mill agent of kaolin and 90% frit, melted at 900-1000 ^oC. The molecular composition of frits is SiO_2 0.73-1.26; TiO_2 0-0.37; B_2O_3 0-0.33; Al_2O_3 0-0.14; PbO 0.26-0.58; Na_2O 0.28 - 0.74; K_2O 0-0.27; Li_2O 0-0.12. The frits are from III to V hydrolytic class and have linear-expansion coefficient from 20 to 350 ^oC $(10\text{-}14).10^{-6}$ K^{-}'. The phase composition, defined by an optical microscopy and X-ray phase analysis, shows over 90 % glassy isotropic mass. In them Si_2O, B_2O_3 and PbO have a glass formation role, and TiO_2 - a crystal formation role. At a temperature of 550 ^oC the melting frits form an area of under 5 mol percentage Al_2O_3 and $SiO_2/(R_2O+RO)$ under 1.1 mol parts. The coverings are laid on the cement pad by a pulverization of water slickers. The firing has been carried out in a specially designed shield furnace.

As a result of the researches there has been defined an area of melted at 550^oC and well bound to the cement pad glassy coverings: Al_2O_3 from 3 to 7 mol percentage and $SiO_2/(R_2O+RO)$ 0.8-1.2 mol parts.

I. INTRODUCTION

The laying of glassy coverings on cement stone or concrete modifies their properties. The micro-porous permeability is greatly diminished, the corrosion resistance is increased, the building design is improved.

The glassy coverings for cement defer from those for ceramics and metal because of the necessity for correlation with the pad, which has the following characteristics:

- a large thermal-expansion coefficient $\alpha = (10\text{ -}12).10^{-6}\ K^{-1}$
- temperature sensitivity because of dehydration processes, which change the phase composition and structure of the cement stone and decrease the strength.

The main requirement to the coverings is the lowest possible firing temperature for the shortest possible period of time.

Compounds with a firing temperature below 900°C [1] and about 800°C [2] have been advanced in the specialised literature. It has been claimed that the strength and stability of concrete works do not change in the process. Our previous experiments, carried out in even short-time thermal influences of 10-20 min in temperatures of 600-800°C, showed a considerable diminishing of strength characteristics.

The aim of this investigation is to synthesize coverings for concrete with a firing temperature below 600°C and high α. These conditions are satisfied by some enamels for steel [3-5] and by the greatest part of enamels for aluminium [6-10].

II. EXPERIMENTAL

On the basis of literature compounds of enamels for aluminium [6-11], some theoretical considerations, and our previous experiments there have been synthesized low-temperature glassy frits in the system RO_2 (SiO_2,TiO_2)- R_2O_3 (Al_2O_3,B_2O_3)-RO(PbO)-R_2O(Na_2O, K_2O, Li_2O).

In the first **5** compounds Al_2O_3 and PbO systematically change, the rest are similar to known compounds for steel and aluminium with a firing temperature of 500-530°C. In a part of the compounds TiO_2 has been put (table l). The frits are melted at a temperature of 900-1000°C.

Table 1. Chemical composition of the frits, mol %

N	K_2O	Na_2O	Li_2O	PbO	B_2O_3	Al_2O_3	SiO_2	TiO_2
1	-	28.0	-	10.0	10.0	2.0	40.0	10.0
2	-	28.0	-	10.0	12.0	4.0	40.0	6.0
3	-	24.0	-	20.0	12.0	4.0	40.0	-
4	-	22.0	-	20.0	12.0	6.0	40.0	-
5	-	26.0	-	10.0	12.0	6.0	40.0	6.0
6	11.8	12.3	-	19.7	-	-	41.4	14.0
7	7.7	21.5	6.0	14.2	14.6	-	36.0	-
8	-	17.6	-	29.7	-	-	52.7	-
9		16.0	-	22.0	-	-	48.0	14.0
10	5.1	16.2	-	22.2	14.1	-	42.4	-

The phase composition of frits is defined by an optical microscopy in passing light and in immersion and by an X-ray analysis. The thermal-expansion coefficient is defined by quartz dilatometre. The defining has been done up to 350°C, since the transformation temperature of investigated frits is about 350-400°C. The melting qualities of frits are defined visually after a 20-minute treatment in different temperatures. The water resistance is defined according to Griss method [12].

For obtaining of coverings there have been compounded finely ground water suspensions of 90% frit and 10% mill supplement-washed kaolin, which brings 3,3 mass % Al_2O_3 and 5,4 mass % SiO_2. The slickers have been laid by pulverization on cement

samples. The firing has been carried out in a specially designed electric shield furnace, in which after a certain temperature is reached the samples are brough in.

The phase composition of baked coverings is defined by an optical microscopy and X-ray surface investigations. The influence of the covering on strength characteristics of concrete is defined by comparison of compressive strength of samples without a covering and thermal treatment to the strength of glazed and baked samples.

III. RESULTS AND DISCUSSIONS

The definition of phase composition of frits shows that compounds **7,8** and **10** are fully isotropic. Compound **6** with a high content of TiO_2 has glassy-crystal structure. A distinguishing feature of systems TiO_2-SiO_2 and Na_2O-TiO_2-SiO_2 is the simultaneous course of crystallization and liquation of drops, which cause their fine-grained structure. The initial crystal phase is metastable titanate [13]. Capability for crystallization does not always happen and depends on the composition and stability of titanium complexes in a glassy and crystal condition. The presence of K_2O and PbO, increasing the number of components did not impede the crystallization of compounds **6** and **9**, which contain over 0,3 mole parts TiO_2 in their molecular formula (table 2). In compounds **1, 2** and **5**, where TiO_2 participates with 0,26 mole parts and less, and B_2O_3 is present, the crystallization of titanium compounds is not shown. By radiography Na_2TiSiO_5 and Na_2TiO_3 have been found in compound **6** (fig.1). The remaining compounds are mainly isotropic, glassy - with composition of glassy phase over 95%. In compound **9** there also is some quantity of crystal phase of Na -Ti - Si compositions.

Table 2. Seger formulas of the frits

Frit / mol	**1**	**2**	**3**	**4**	**5**	**6**	**7**	**8**	**9**	**10**
SiO_2	1.05	1.05	0.91	0.95	1.11	0.94	0.73	1.11	1.26	0. 98
Al_2O_3	0.05	0.11	_0.09	0.14	0.12	-	-	-	-	-
TiO_2	0.26	0.16	-	-	0.17	0.34	-	-	0.37	-
linear thermal expansion coefficient [10^{-6}, K^{-1} $_{20\text{-}350}$ ^oC]										
	13.2	12.1	13.3	12.2	10.0	14.3	11.8	14.0	11.7	10.6

In all investigated frits SiO_2, PbO and B_2O_3 have a glass formation role. The crystal formation role of TiO_2 is emphasized. From all the compounds, which are well-melted and do not contain Al_2O_3, **7, 8** and **10** are fully glassy, **6** and **9** have crystal phase. With the increasing of Al_2O_3 some raising of the melting temperature shows itself and in SiO_2 /(RO+R_2O) > 1 and Al_2O_3 > 4 the compounds can not be melted at a temperature of 550^{o}C.

The area of frits with good melting properties at 550 and 500^{o}C has been defined. They form a differentiated area according to the relation mol % Al_2O_3 and SiO_2/ (RO+R_2O) (fig.2). The coordinates of the graphic satisfy the classical Seger molecular formula of glazes.

The frits are III to V hydrolytic class and have linear-expansion coefficient (10-14).10^{-6} K^{-1}.

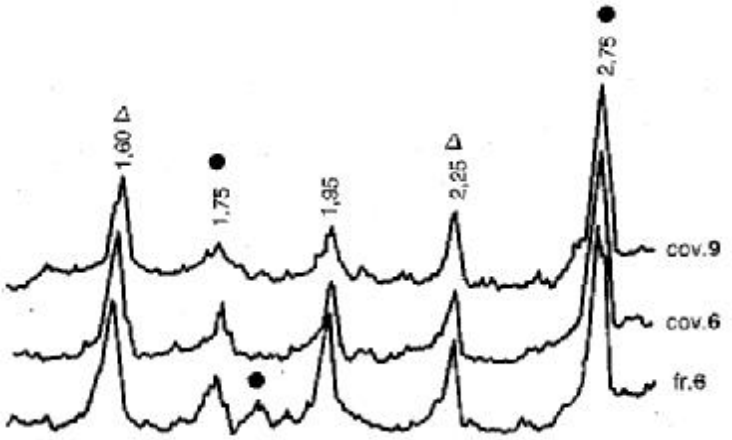

*Fig.1. XRD patterns of frit **6** and coverings **6** and **9**; ·Na_2TiSiO_5;D Na_2TiO_3*

During the firing of the coverings on concrete at 500°C processes of the main glassy phase, from which the frits are composed, take place. The kaolin supplement dehydrates. Since the thermal treatment is of short duration - 5-10 min, after a quick cooling of cement samples it is evident that the coverings are just slightly melted and do not have strong cohesion with the pad. As with clear frits, the particles are almost fully glassy, amorphous with the participation of crystal phases up to 5%. They also contain amorphous, uniformly distributed metakaolinite. Optically and by radiography there has been established that the compounds with TiO_2 are fine-crystal, and the crystal phases are difficult to be defined. Most probably in the compounds with less TiO_2, it's the phase $NaTiSi_2O_6$. In compounds **6** and **9** the main mass is optically isotropic, amorphous with microlitic crystallization, probably from Na_2TiSiO_5 and one more unidentified phase (Na_2TiO_3 ?).

In compound **8**, in which the frit is fully glassy, in a thermal treatment a new crystal phase (most probably α III form of $Na_2Si_2O_8$) is formed. At 550°C for 5 and 10 min the melting of glassy covering on cement stone is considerably fuller. The area of well-melted compounds is presented in fig.3. When compared to the melting of clear frits, it is evident that with the increasing of Al_2O_3 the area of good coverings is diminished. The best coverings are **1, 2, 3** and **10**. The crystal phase in them is considerably under 5% and, consequently, is under the sensitivity of the X-ray-phase analysis. Compound **6** has micro-crystal structure with the participation of Ti-containing phases. Diphractogram of the glaze surface (fig.1) show, that crystal phases are same as with frits - most probably Na_2TiSiO_5 and Na_2TiO_3. Some maximums are missing, probably because of structuring.. Compounds **7, 8** and **10** are almost fully isotropic, they consist of glass-phase and gas bubbles.

IV. CONCLUSIONS

As a result of the investigation there have been obtained glassy coverings for concrete, which conform well with the pad on thermal expansion and which are melted at 550°C.

The coverings form a differentiated area which for the firing temperature of 550°C is $SiO_2/(RO+R_2O)$ from 0,8 to 1,2 and Al_2O_3 from 3 to 7 mol %. The thermal treatment of 10 min. at 550°C decreases the strength of glazed cement samples with 15-25%.

In order to obtain practically applicable compounds it is also necessary to lover the firing temperature for coverings and to carry on with the investigation of synthesizing new coverings.

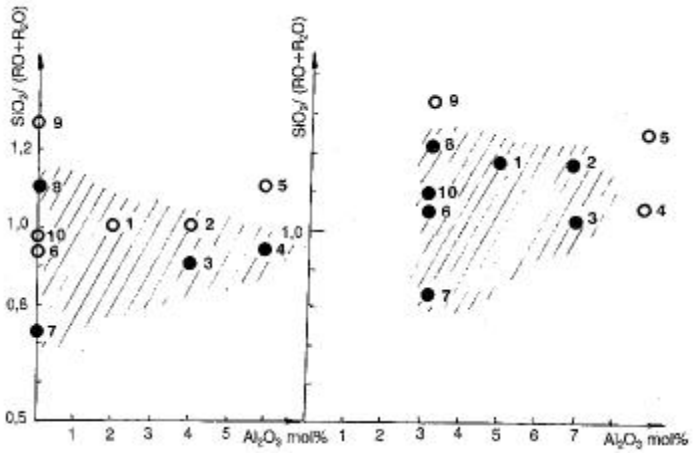

Fig.2. Low temperature frits *Fig.3. Low temperature glassy coverings*
I - melting by 500°C,10 min , /// - the area of melting by 550°C,10 min

Acknowledgements

The present investigation has been performed under the financial support of the Bulgarian National Research Fund Contract N^0 TH-357/1993.

REFERENCES

l.Pat.Japan 1215775
2.Pat.Japan 2124784
3.Popov E., Technologia na emailite I emailiraneto na metalni izdelia, MNP, Sofia,1982
4.Invertor's certificate URSS 1551668
5.Invertor's certificate URSS 1609752
6.Invertor's certificate URSS 1622305
7.Invertor's certificate URSS 11613440
8.Invertor's certificate URSS 1608145
9.Invertor's certificate URSS 1145347
l0.Invertor's certificate URSS 1520031
ll.Pavlushkin N.M., A.K.Juravlev, Legkoplavkie stekla, Energia, Moskva, l970

l2.Bachvarov S., B.Kostov, B.Samuneva, D.Stavrakeva, Rukowodstwo po technologia na silikatite, Tehnika, Sofia,1978
l3.Hodakovskaja R.A., Chimia titansoderjasthih stekol i sitallov, Chimia, Moskva, 1978

HIGH GRADE GLASS AND MINIMUM REMOVAL OF ITS SURFACE IRREGULARITIES USING ULTRA-PRECISION PLANAR PROCESSING TECHNIQUE

Toshiroh Karaki Doy, Haedo Jeong[1], Hitoshi Ohmori[2]
Takeo Nakagawa[3] and **Toshio Kasai[4]**

Faculty of Education, Saitama University, Japan, [1]Pusan National University, Korea,
[2]The Institute of Physical & Chemical Research (RIKEN), Japan,
[3]University of Tokyo, Japan, [4]Faculty of Engineering, Saitama University, Japan

Abstract

A new polishing method which pertorms surface removal within the minimum amount of the polishing margin was devised and led to the development of a new equipment, to which an uniform pressure application mechanism with a water-back system and another mechanism to provide uniform relative speed have been introduced. On this equipment a newly designed polisher made of high rigid, non-forming synthetic resin with a continuous groove was mounted. Basic processing characteristics have been grasped by using this new equipment with a sample prepared by depositing a high grade glass flm of 8000X on a Si wafer having 6000X micro-irregularities. Subsequently, substantially better improvement was obtained yielding 150~250X planarity and uniformity.

1. Introduction

With the multi-media age just ahead of us, high pitched development of components aiming toward the advanced electronic and optical fiber communications has been rapidly progressing. Si wafers and new glasses which are applied to the manufacturing process or the components as above, are typical examples and indispensable in today's industrial sector as an advanced material. For instance, Si wafer surface during the fabrication of LSI device is deposited with a high-grade glass film as an IDL, which, as the fabrication process advances, comes to exhibit micro-irregularitias over the surtace. In order to realize highly developed LSI devices, these irregularities have to be planed in a certain stage of the fabrication process. Ultra-precision polishing is thereby applied to such planarization process. This technique is called as "Planar Polishing/CMP" (Chemical & Mechanical Polishing) and has been drawing a good deal of attention as a key technology to develop highly integrated LSI.

However, since irregularities of over 0.5μm should be removed wherein the processing margin is limited only to 1 μm, and the entire wafer surface should be made uniformly planar, it is obvious that the achievement of the above goal is extremely diffcult if processed with the conventional polishing methods and conditions.

In this research, taking as an example the wafers in the device fabrication process for realization of next generation LSI, a study of ultra precision polishing technique has been undertaken, which is applied to the processing of CVD glass film to be used as an IDL. In order to establish polishing technique for the global planar polishing of micro-amount, proposing a kinetic mechanism of a new processing equipment with a polisher designed to remove a constant amount uniformly off the wafer surface. An investigation has been also carried out and reported here-under on the characteristics of planar processing using the model wafer, on which a glass film had been deposited.

2. A proposal of a new polishing equipment and experimental conditions

2.1 Basic concept of ultra-precision polishing

Polishing machine : In general, stock of removal(V) in polishing is expressed using the Preston's Law,

$$V=k\cdot p\cdot v\cdot t$$

(k: constant, p: processing pressure, v: relative speed, t: processing time)

which leads us to think that uniform polishing of device wafers can be obtained through the accurate control of processing pressure (p) and relative speed (v) within the wafer. As regard the evenness of processing pressure (p) within the wafer, variation of thickness and warp of the base (Si wafers), which are inherent in the wafers in device fabrication process, should be first taken into account. Even distribution of pressure is to be secured by forcing device wafer from its reverse side against the polisher by the Water/Air back system (see Fig.1) introduced based on the Pascal's Law, which at the same time straightens warp of the wafer.

Meanwhile, kinetic mechanism of the polishing plate is found more advantageous, as compared with the conventional method of simple rotation of the plate, which obtains uniform relative speed of one's choice through exercising same small locus circular motions at any point and place of the wafer. From the viewpoint of slurry, it is also advantageous, because slurry can be supplied and distributed uniformly onto the entire surface of the wafer. However, it is desirable to give a slight rotation to the wafer sample or polishing plate in order to promote recycle use of slurry and to avoid uneven wear of the polisher.

Figure 1 shows a diagram of the even distribution of uniform pressure and kinetic mechanism of small circular motions.

Polisher: Notwithstanding the pattern size or density, it is required, in the planar polishing of device wafers, to remove projecting features preferentially in order, without the polisher coming to contact the recessed region of the pattern. More importantly, if the end of process is intended to be controlled by the processing time, the polisher should be designed in such a way that it enables to obtain a constant processing rate without being influenced by the processing time.

In the following, designing conditions of polisher are sorted out for the global planar polishing : (a) surface of the polisher to have suitable rigidity, (b) recessed area to be created on the surface of the polisher allowing slurry supplied onto the entire surface of wafer (sample surface), (c) recessed area to be provided on the surface of the polisher to facilitate easy discharge of processing chips. Items (b) and (c) among above are to secure reproducible relative speed, and

very important to prevent loading from occurring. In order for the polisher to possess these two functions, forming a continuous groove on the surface of the polisher has been considered as one of the most effective measures. Meanwhile, those pocket-shape fine pores existing in the surface of the conventional polisher are thought to exert rather adverse effect due to its easy generation of loading. Consequently, non-forming bulk materials (item (a) mentioned above) having suitable rigidity are suggested when selecting materials.

2.2 Experimental equipment, samples and conditions

Experimental equipment: A processing machine (prototype) was designed and experimentally manufactured incorporating the kinetic mechanism and polisher devised as described in the preceding paragraph, the exterior view of which is shown in Fig. 2. This processing machine can process simultaneously 4 evenly placed samples of ϕ 4~6” wafer. The polishing plate was made such that it performs eccentric small circular motions (max. dia. 60mm, max. revolution 100rpm : relative speed in this case = 18m/min), and a slight revolution is given to the guide rings which are holding wafers. An even distribution unit of the uniformly applied pressure was designed incorporating the water back system which presses the device wafer from its reverse side with a thin elastic bag (silicon rubber of 0.1~0.3mm) filled with water. For the polisher, a "continuously grooved, high rigid, non-forming synthetic resinr" was used (continuous groove: "v" shape spiral groove of 0.5mm depth, 0.5mm width and 2mm pitch).

Samples used for the experiment : Certain patterns (0.6μm depth), composed of irregular dimension and density were formed on 4” Si wafers, which were then deposited (CVD) functional glass flm of 8000X (model wafer).

The patterns formed on the sample are shown in Fig. 3. The objective of the polishing is to obtain a complete planarity across the entire surtace before the Si surface comes out, by preferentially removing only the projecting features from the top surface of the glass flm.

3. Experimental results and discussions

3.1 Basic characteristics of the experimental equipment

In the prototype machine, the reference plane corresponds theoretically to the polishing surface due to the pressure applied by the water-back system from the reverse side of the wafer. In order to check the processing accuracy of the experimental equipment, the characteristics of a thick Si sample (ϕ3" x 5^{t}mm) without using pressure application jig by the water-back was first examined, and a surface planarity of ± 0.5μm over ϕ3" was obtained, which has proved the effectiveness and accuracy of the kinetic mechanism of the experimental equipment. On the other side, the effectiveness of the newly developed water-back processing method has been also confirmed through the experiment where a model wafer (ϕ 4" x 0.55^{t}mm warp ±50μm, TTV 6μm) with a 6000X glass film formed over the entire wafer surface was subjected to the polishing, using the water-back processing system, the glass film of which has been found uniformly removed. In the next, the characteristics of the ultra-precision planar polishing using the model wafer have been investigated.

3.2 Processing characteristics with the model wafer and its evaluation

Figure 4 shows an example of the processing done on the glass film removing approx. 0.5μm by using the new "continuously grooved, high rigid, non-forming synthetic resin polisher". For

comparison purpose, the processing results with the conventional polisher are also given. It reveals that the devised polisher left remaining gaps below 100X despite uneven dimension and density of its pattern (step height: 0.5μm, width: 300, 200 and 150μm, length: 1 mm). In other words, not to mention local planarity, global planarity over a chip size has been accomplished. In the case of the conventional polisher, the recessed area of the pattern was also processed, which, however, still leaves irregularities of ±0.3μm. From this comparison, it is obvious that the newly developed polisher has a great advantage over the conventional ones.

Moreover, when polished with the new polisher, the variation of step heights fell within 150X (Fig.5), which led us to confirm successful realization of the global planar processing for wafers to an almost complete level.

Linearity of the processing rate relevant to the ultra-precision planer polishing technique herein proposed was investigated. Figure 6 indicates relationship between polishing time and stock of removal of the glass film, using slurry, composed of cerium oxide whose processing rate against glass film is high. As seen from this figure, the processing characteristics of the model wafer display three phases against processing time. That is, in the first phase when projecting features of the glass film are removed, processing rate becomes relatively high. In the 2nd phase when only already planed glass film is removed, it becomes about half due to the decreased processing pressure per area as the processing area increased over that of the 2nd phase. In the third phase when the glass film in the bottom (recessed area) and silicon of the exposed base wafer are simultaneously removed, the processing rate increases slightly over the 2nd phase because of alkaline slurry of pH10, which works on silicon surface at higher rate than on the glass film. All phases present good linearity characteristics. In general, when planarization polishing/CMP is performed over device wafers, removal should be completed by the 2nd phase.

With reference to the processing advantage of the "continuously grooved, high rigid, non-forming synthetic resin polisher", discussion was held from the angle of the global uniformity observed on the processed surface of the glass film. Figure 7 shows dependency of the number of wafers processed by the devised polisher (A) and the conventional polisher (B) upon the uniformity of each processed surface. Polisher (A) has no loading thanks to the material of bag-shape pore-free, non-forming synthetic resin, because of which, uniformity degradation was not observed although processed continuously. Instead, the uniformity improved. On the other hand, in the case of polisher (B), the uniformity worsened as the number of processed wafers increased. This implies that the fine pores of the surface get clogged with processing chips (loading). Therefore, if the conventional polisher is used, dressing should be pertormed in order to secure processing reliability so that the processing chips are removed during the polishing process. Such intricacy coupled with the problem of reproducibility has been overcome thanks to the development of the polisher (A).

In consequence, it has been confirmed that with almost no dressing, excellent processing characteristics with good reproducibility can be obtained through the use of the polisher (A). In other words, the end-point detection of processing becomes possible by controlling the time.

4. Conclusion

For interlevel dielectric layers/glass films of VLSI device wafers with micro- irregularities, planarization polishing methods have been investigated, performing micro-removal within an extremely limited margin through the ultra-precision polishing technique. In order to develop

processing machine incorporating kinetic mechanism for ultra-precision planar polishing and to realize more reliable global planarity, a new polisher made of continuously grooved, high rigid, non-forming synthetic resin (high rigid plastic polisher with groove) was developed as herein proposed. This prototype machine with a new polisher was employed for the investigation to better understand processing characteristics of the model wafer prepared forming thin glass film with micro-irregularities over a Si wafer. The investigation has revealed excellent characteristics such as planarity and uniformity of less than 150X with good reproducibility, while the global planar processing is diffcult when using the conventional polishing machine and conditions. In addition to the device wafers in LSI process, the present research has a great deal of prospects to be applied also to the ultra-precision planarization polishing of SOI substrates and color filters for LCD.

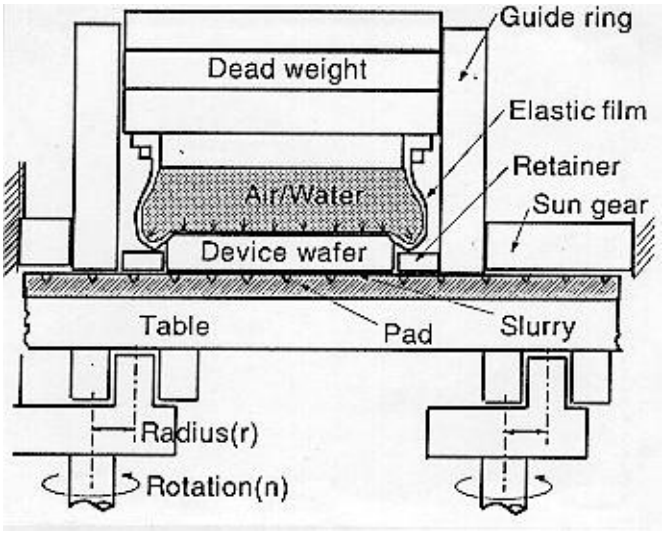

Fig. 1 Diagram of the even-distribution of uniform pressure and kinetic mechanism of small circular motions.

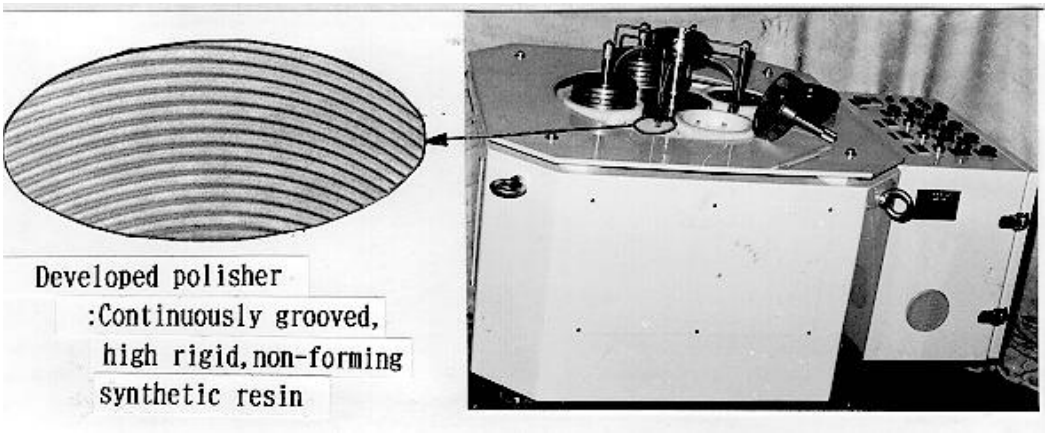

Fig. 2 Photograph of a processing machine (prototype) and a newly developed polisher

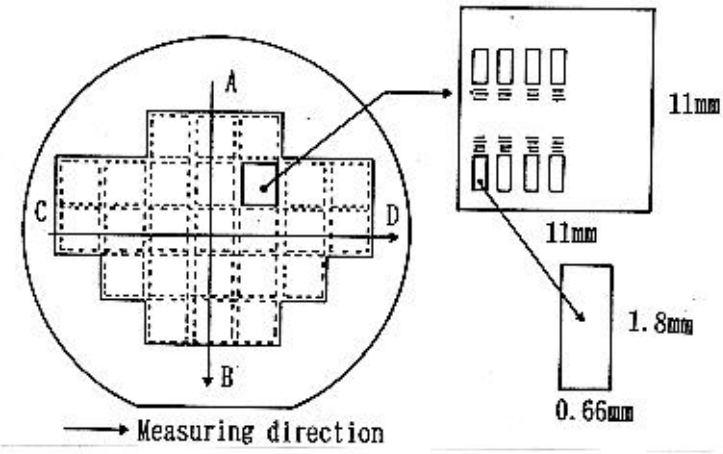

Fig. 3 Patterns on a sample wafer

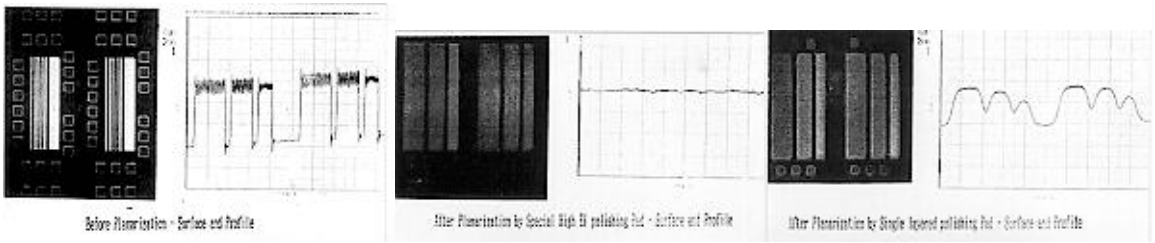

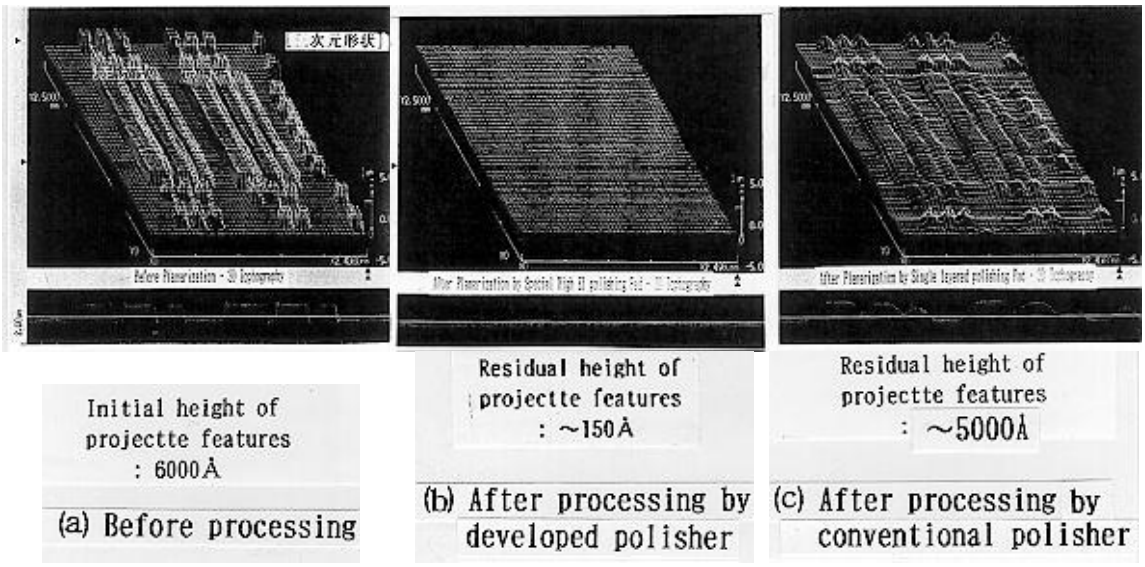

Fig. 4 Surfaces of chips before and after polishing with a new polisher and conventional one

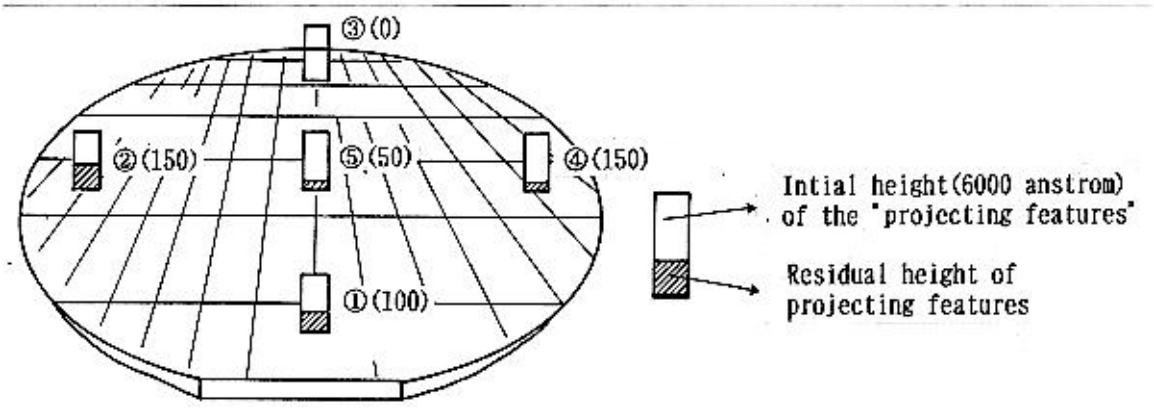

Fig. 5 An example of uniform global planarity using a newly developed polisher (distribution of the step heights within a wafer)

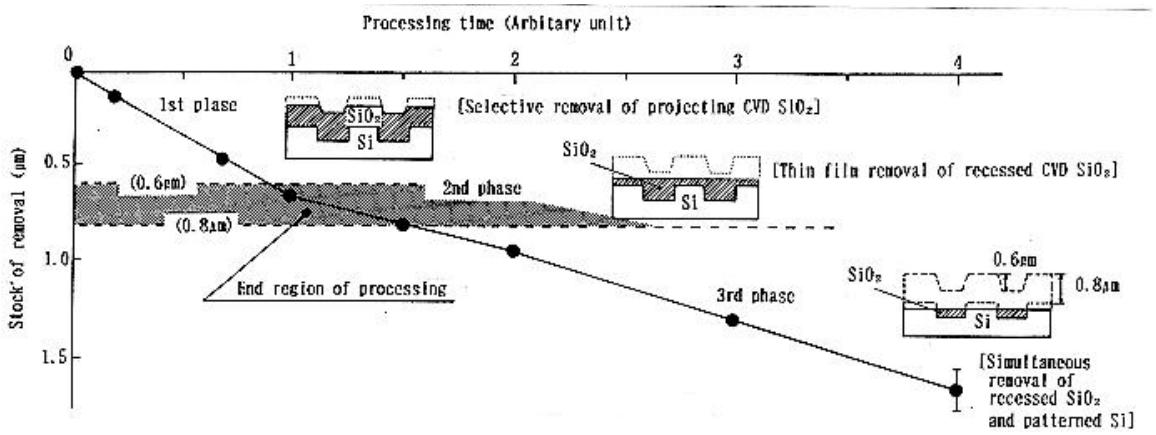

Fig. 6 Relation between processing time and stock of removal of a model wafer (using $Ce0_2$ slurry <980nm CeO_2, pH10> and a newly developed polisher)

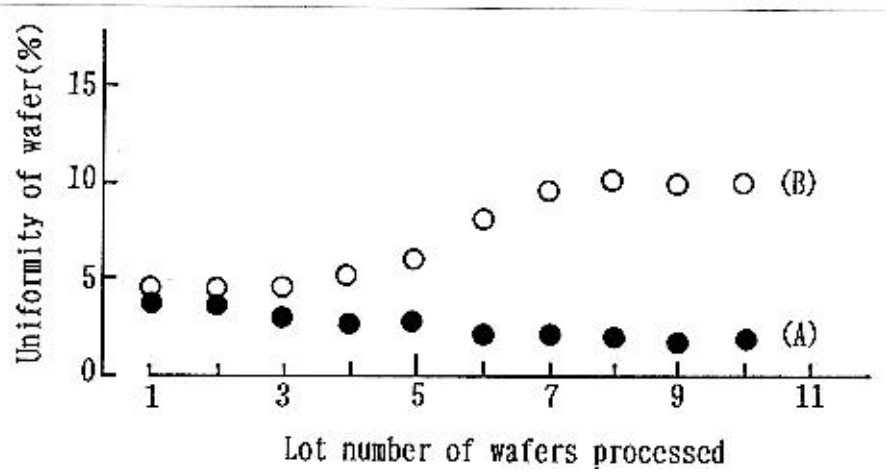

Fig. 7 Dependency of number of wafers processed by a newly developed polisher (A) and a conventional polisher (B) upon the uniformity of each processed surface

INFLUENCE OF GLASS COMPOSITION ON X-RAY TO VISIBLE LIGHT CONVERSION IN ACTIVATED GLASSES

Nikolai Timofeev, Alexander Dmitryuk and **Vladimir Savostyanov**
S.I.Vavilov State Optical Institute, Russia

Abstract

An efficiency of X-ray to visible light conversion is studied as a function of alkali oxide concentration in model silicate, germanate and phosphate glasses, activated by Tb^{3+}, Mn^{2+} and Cu^{+} ions. Conversion efficiency is shown to be high in those glasses where alkali content is low. Obtained results are discussed from the viewpoint of the influence of non-bridging oxygen atoms on X-ray to light conversion process.

1. INTRODUCTION

Scintillating glasses are widely used as detectors of different kinds of ionizing radiation (X-rays, synchrotron radiation, neutrons, etc.) [1,2]. The operation of this glasses is based on conversion of ionizing radiation energy absorbed in glass matrix into the luminescence light. The feasibility of scintillating glasses primarily depends on conversion efficiency Tc defined as relation of generated scintillating light energy to absorbed radiation energy [1]. The conversion mechanism in glasses is not yet clear enough to elaborate efficient glass scintillator basing on scientific method of attack.

Present work is aimed to study the influence of glass composition on X-ray to light conversion efficiency in phosphate, germanate and silicate glasses activated by Tb^{3+}, Mn^{2+} and Cu^{+}.

As it was shown in our previous work [3] and in ref. [2] X-ray excited luminescence of activated glasses is characterized by the emission spectra of activator centers and to a variable extent corresponds to the photoluminescent properties of these centers. In general the elementary scheme of X-ray to light conversion in solids is following [4]. The ionizing radiation absorbed in medium give rise to cascade ionization process as a result of which a low energy free electrons, holes and excitons are generated. As is considered in ref. [4] the main contribution to the total luminescence yield give electrons which after the generation stage migrate over the lattice being captured by different kinds of traps. In particular the thermolized electrons are captured by ionized activator ions. The following after this recombination is accompanied by activator emission.

Glasses being a disordered systems are characterized by a small compared to crystals free length of thermolized electrons. So the way of electron migration is not long and the last low energy free electrons in the cascade ionization process of electron multiplication do not migrate far away from the place of its origin being trapped. This fact is proved by the linear dependence of the luminescence intensity on X-ray exposure dose rate which we demonstrated earlier [3] for Tb^{3+} activated phosphate glasses. The analogous linear dose rate dependence was found also for germanate and silicate glasses activated by Mn2+, Cu+ and Ce^{3+} and seems to be the common property of glasses.

This linear law can be explained only from the view point of monomolecular recombination scheme according to which low energy knock-on electron, being not far from activator center which gave him birth through ionization, returns back and recombinates with this ionized center. In another case of migration scheme free electrons and holes get mixed up through migration. As the result the recombination process in this case should be characterized by bimolecular scheme described by quadratic dependence of luminescence intensity as a function of X-ray dose rate.

2. EXPERIMENTAL

The following model glass systems were studied: Na_2O-SiO_2 -Tb_2O_3; Na_2O-P_2O_5-La_2O_3-Tb_2O_3; ZnO-P_2O_5-MnO; R_2O-GeO_2-MnO; R_2O-SiO_2-CuO; CaO-P_2O_5- CuO; (R=Na,K). The concentration of such activators as Tb_2O_3 and MnO was varied in wide range from 0.1 mol% 6 to 25 mol %Tb_2O_3 and 50 mol% MnO. Concentration of CuO did not exceed 2 wt % because of difficulties to keep copper ions in one valence state Cu^+.

Glasses were melted from industrial raw materials in laboratory Globar-heated furnace at temperature range from 1100 to 1450^o C. We used fused silica and alumina crucibles of 100 g capacity. The melt was poured onto a steel plate and then the glasses were annealed during one hour. Polished samples of 4 mm thickness were irradiated by X-ray beam at accelerating voltages 40-50 keV. X-ray excited luminescence was detected at room temperature by photo multiplier at different wavelengths selected by light filters and grate monochromator.

3. RESULTS AND DISCUSSION

As it was noted in introduction the luminescent properties of activated glasses under X-ray irradiation as a first approximation correspond to luminescent properties of activator centers under photo excitation.

The luminescence spectrum of terbium activated glasses is a composition of narrow inhomogeneously broadened bands corresponding to intra configurational f-f electronic transitions. Approximately 70 % of emitted energy is concentrated inside the band 550 nm (transition $^5D_4$ $^7F_5$).We investigated phosphate, germanate and silicate glasses doped by Tb^{3+} The Tb^{3+} luminescent parameters are moderately dependent on glass matrix because of deep lying 4f shell shielded by the outer shell electrons.

As for the X-ray excited emission spectrum of Cu^+ studied in this work it depends on host matrix and consists of a broad vibronic band with a peak at 450 nm in phosphate glasses and 510 nm in silicate glasses. The spectral half width is 110 and 125 nm correspondingly for phosphate and silicate glasses.

Luminescent properties of Mn^{2+} under X-ray excitation were studied in phosphate and germanate matrices. The spectroscopy of Mn^{2+} is more complicated than the properties exhibited by previous ions. The spectral position of Mn^{2+} broad luminescence band depends not only on host matrix but also on Mn^{2+} concentration and varies for example in phosphate glasses from 600 to 730 nm as MnO concentration grows from 1 to 50 mol %.

The X-ray to visible light conversion efficiency Tc was studied as a function of glass composition from the point of view of the influence of alkali oxide concentration on the conversion process. These results obtained for silicate, phosphate and germanate glasses are

illustrated in Fig.1. As is seen the increase of alkali content leads to the decrease of conversion efficiency Tc in all studied glasses. For terbium silicate glasses this effect is most conspicuous.

We also studied the influence of activator concentration on conversion efficiency. All concentration dependences were nonlinear in character. Though in this case the initial stages of all curves were close to linear law reflecting the increase of conversion efficiency with the growth of activator concentration.

Terbium glasses had the saturation of the rising curve beginning approximately from 10 wt % Tb_2O_3 in silicate glasses and from 35 wt % Tb_20_3 in Phosphate glasses. As for the X-ray to light conversion efficiency of Cu^+ doped silicate glasses measured as a function of CuO concentration varying from 0.1 to 2 wt % it had a peak at 0.5 wt % CuO. The MnO concentration dependence of Mn^{2+}doped phosphate glass conversion efficiency had a maximum at 14 wt % MnO.

The low value of CuO concentration corresponding to the maximum conversion efficiency in silicate glasses is caused from our point of view by the presence of copper in a higher valence form Cu^{2+}. Beginning from 0.5 wt % CuO it was difficult to keep copper ions in one valence form Cu^+ in silicate glasses. The same reason, namely the impurity of Mn^{3+}, caused the decrease of conversion efficiency in Mn^{2+} doped phosphate glasses beginning from 14 wt % MnO.

As for Tb^{3+} doped phosphate glasses we did not observe the concentrational quenching up to the limit value of 46 wt % Tb_2O_3. This is because the terbium phosphate glasses can be simply prepared without noticeable Tb^{4+} impurity even at very high Tb_2O_3 concentration.

So an admixture of activators in the higher valence states presents an obstacle on the way of enhancement the conversion efficiency in glasses. Most likely it is caused by efficient trapping of electrons by these ions during an electron generation stage of X-ray to light conversion process.

As for the results illustrated in Fig.1 from our standpoint the decrease of conversion efficiency at high alkali content is caused also by the competitive electron-hole trapping process.

The introduction of alkali ions in silicate and germanate glasses leads to the formation of non-bridging oxygen atoms. In ref. [5] it was shown that non-bridging oxygen atoms are required for the hole trapping that in its turn is important for the glass photosensitivity. Vice versa, the elimination of non-bridging oxygen atoms supresses the photosensitivity. In general the glasses with low content of all kinds of impurities and defects show high radiation resistance. In particular, the vitreous silica with the network containing non-bridging oxygen atoms at the minima in comparison with silicate glass provide a good example of the glass with high radiation resistance [6].

That means that holes and electrons generated in silica glass by ionizing radiation recombinate to one another not being trapped by defects and impurities. As it was noted in introduction, an activator ionized through the cascade ionization process takes on the properties of the hole and recombinates with its own electron which migrates not far from ionized center.

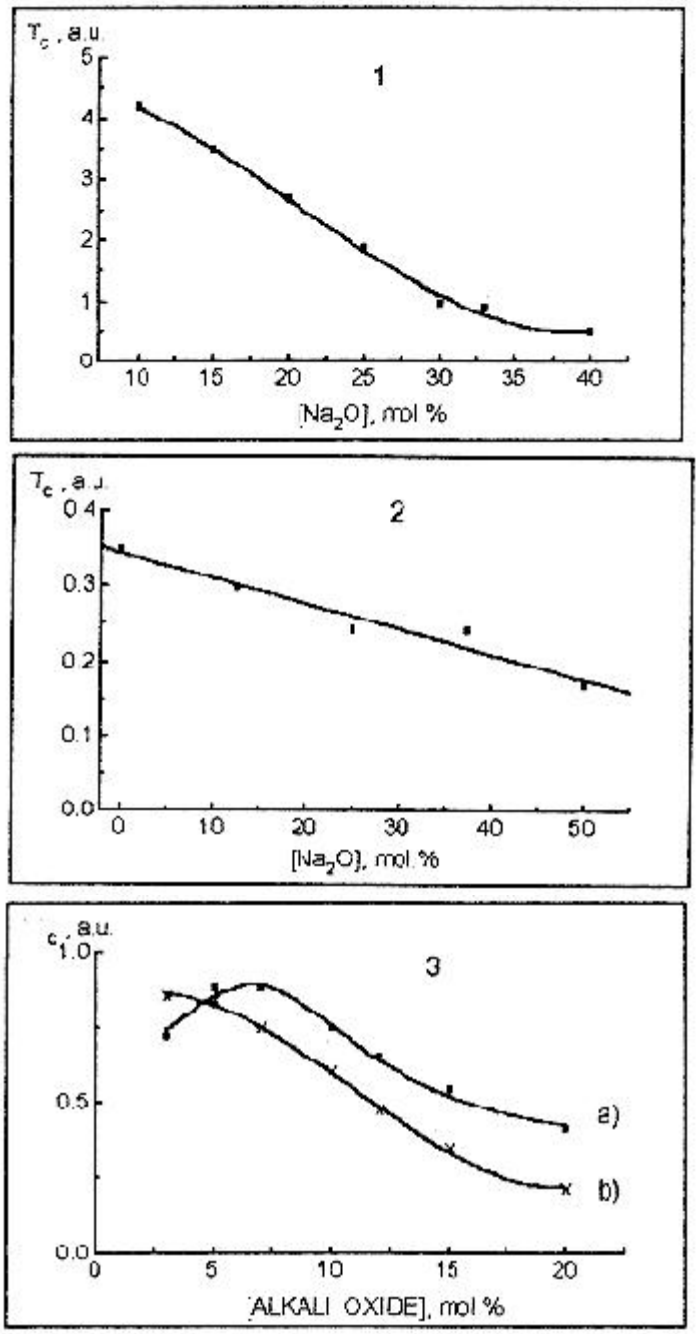

Fig.1. X-ray to visible light conversion efficiency as a function of alkali oxide concentration. Glass systems:

1. *Na_2O - SiO_2 - Tb_2O_3; b mol %Tb_2O_3*
2. *Na_2O - P_2O_5 - La_2O_3 -Tb_2O_3; 2 mol %Tb_2O_3*
3. *a) Na_2O- GeO_2 - MnO; 1 mol % MnO*
   b) K_2O -GeO_2- MnO; 1 mol % MnO

If the glass matrix contains hole traps such as non-bridging oxygen atoms then the radiation induced holes in the form of ionized luminescent centers may be trapped at 2p-orbital of non-bridging oxygens and electron-hole recombination accompanied by activator luminescence will not take place at this center.

So the increase of X-ray to light conversion efficiency with the reduction of alkali content in the glass we explain by elimination of hole traps in the form of non-bridging oxygen atoms. This effect is more pronounced in silicate and germanate glasses where the quantity of non-bridging oxygens depends on the content of alkali ions. As for the phosphate glasses and, in particular, for metaphosphate glasses studied in this work the network mainly consists of chains of phosphorus-oxygen tetrahedra and includes the non-bridging oxygen atoms as an integral part of network structure. The quantity of non-bridging oxygens does not depend on alkali content when rare-earth metaphosphates are replaced on alkali metaphosphates. This is illustrated in Fig.1(2) as a gentle slope of the curve in comparison with alkali concentration dependence for silicate and germanate glasses.

4. CONCLUSION

The X-ray to visible light conversion efficiency was found to be high in those model silicate, germanate and phosphate activated glasses where content of alkali oxide was low. Obtained results are discussed from the point of view of non-bridging oxygen atoms suppressing the X-ray to light conversion.

REFERENCES

[1] H. Shao, D.W. Miiler, C.R. Pearsall, IEEE Transactions on Nuclear Science 38 (1991) 846
[2] P. Polato, G. Zanella, R. Zannoni, M. Bettinelli, Glastech. Ber. Glass Sci. Technol. 68 C1 (1998} 571
[3] N.T. Timofeev, A.V. Dmitryuk, V.A. Savostyanov, Glastech. Ber. Glass Sci. Technol 68 G1 (1996) 566
[4] D. Aluker, D.Ju. Lusis, S.A. Chernov, Electronic Excitations and Radioluminescence in Alkali Halides, Riga (1979), 252 p.
[5] R.J. Araujo, N.F. Borrelli, SPIE 1590 Submolecular Glass Chemistry and Physics (1991)
[6] S.M. Brekhovskikh, V.A. Tyulnin, Rad tional Centers in Nonorganic Glasses, Moscow (1988),197 p.

INFLUENCE OF MELT OVERHEATING ON LOW TEMPERATURE MECHANICAL PROPERTIES OF METALLIC GLASSES RIBBONS PREPARED BY MELT QUENCHING

E.D.Tabachnikova [1], V.Z.Bengus [1], D. V.Egorov [2], V. S. Tsepelev [2], V. Ocelik[3]
[1] Ukraine National Acad. of Sciences, Ukraine
[2] Ural Poiytechnical Institute, Russia
[3] Institute of Experimental Physics, Slovakia.

Abstract

The mechanical properties of metallic glasses are greatly influenced by the thermal treatment of its melt before rapid quenching. The strength and the fracture toughness of some metallic glasses obtained after the melt heating above the melt critical temperature T_c are essentially higher than those obtained from the melts that were not heated above T_c. Such difference is considered as caused by changing of the melt atomic structure under heating above T_c

1. INTRODUCTION.

Mechanical properties of metallic glasses (MG) prepared by rapid quenching of the melt is greatly dependent on their atomic structure to a considerable extent inherited from the melt that they are obtained from. It is known [1] that under a solidification of a liquid there are two processes of the competitive formation of non-crystalline nuclei (clusters) and crystalline nuclei. Many investigators found experimental indications on a high density of non-crystalline clusters in glass forming metallic melts [2-6] that results in polyclusterous structure of metallic glasses [7].

Such a structure is formed by chaotic packing of ordered polyatomic clusters and embedded in them crystalline nuclei. Boundaries between clusters form a system of internal boundaries in metallic glasses. According to [7] the specific disorder at intercluster boundaries predetermines spreading of a plastic shear along these boundaries and afterwards spreading of the ductile shear failure. Crystalline nuclei in their turn are the sources of the brittle failure of the material.

Therefore the state of intercluster boundaries in MG (similarly to a state of grain boundaries in polycrystalline materials) controls proceeding of the plastic deformation and the mode of the failure of metallic glasses. The same role belongs also to a quantity and dimensions of crystalline nuclei. The structure of clusters, the state of intercluster boundaries, a quantity and dimensions of crystalline nuclei can be varied by the different thermal treatments of the melt before its rapid quenching. The main in these thermal treatment is their relation to the critical temperature T_c of the melt. The transition through this critical temperature under heating of the melt varies its physical properties [8-11] that is supposed to be caused by destroying of noncrystalline clusters [6,7] and of crystalline nuclei [12]. .

2. MATERIALS AND METHODS.

Experiments were performed on metallic glasses ribbons $Fe_{73.5}Nb_3Cu_1Si_{l3.5}B_9$ (1), $Fe_{7l}Cr_{l0}Si_7B_{l2}$ (2), $Fe_{8l}B_{l3}Si_4C_2$ (3), and $Co_{60}Fe_5Ni_{l0}Si_{10}B_{l5}$ (4) chemical compositions. They were produced by planar flow casting method in air and were 25-30 μn thick and 10 mm wide (for alloys 1 and 2) and 50 mm wide (for alloys 3 and 4). The amorphous state of the ribbons was checked by an X-ray diffraction technique. Measurements of the strength σ_f were carried out at 300 and 77 K with the extension rate 1.5 x10-4 s^{-1} using deformation machine with the stiffness of 25 kN/mm. Each experimental point of the strength was obtained by averaging the results of measurements on five samples. Spread in values of σ_f was 3-5 %. Samples for measurements of the anisotropy of σ_f were cut out from a " wide" ribbon at an angles Θ of 0^o, 22.5 ^{o}, 45 ^{o}, 67.5 ^{o} and 90 ^{o} to the ribbons length axis. Their width and gauge length were 5-6 mm and 15-20 mm respectively. Fracture toughness K_{lC} was measured under uniaxial tension of samples with a transversal crack made beforehand on the axis of the sample. The surfaces of the failure of the samples were studied by means of a JSM-T20 scanning electron microscope, surfaces of the samples were studied using an optical microscope. The kinematic viscosity of melts was measured by the method of damping of torsional vibrations of the crucible with the melt suspended on elastic fibre [13].

3. EXPERIMENTAL RESULTS

3.1. Determining of the critical temperature T_c of the $Fe_{73,5}Nb_3Cu_1Si_{13}B_9$ ("Finemet" type) from the temperature dependence of the kinematic viscosity.

The temperature dependence of the kinematic viscosity v of the $Fe_{73,5}Nb_3Cu_1Si_{13.5}B_9$ melt under heating and cooling is shown in Fig.l. It is seen that the lower curve 1 obtained under heating of the melt coincides with the upper curve 2 obtained under cooling only down to 1490^o C. Below this temperature the hysteresis of ν is observed i.e. curves 1 and 2 do not coincide. The temperature of branching is approximately 1490 ^{o} C and it is considered as T_c for the melt of the given composition.

3.2.. Dependence of the strength s_f, the mode of the failure and the surface relief of metallic glasses ribbons on the thermal treatments of the melt before quenching.

3.2.1. The $Fe_{73,5}Nb_3Cu_1Si_{13.5}B_9$ ("Finemet") metallic glasses.

Two different regimes of the thermal treatment of the melt before quenching were used:

Regime 1:a) heating of the melt up to $15OO^o$ C (higher than T_c and keeping at this temperature during 15 min.;

b) cooling to 1400^o C and keeping at this temperature during 5 min before quenching.

Regime 2 : heating to 1400^oC (lower than T_c) and keeping this temperature during 5 min before quenching.

Both these regimes were realized in an induction furnace. Values of the strength σ_f of the $Fe_{73,5}Nb_3Cu_1Si_{13.5}B_9$ metallic glasses ribbons at 300 and 77 K are indicated in the Table 1 for these two regimes of the melt thermal treatment before quenching.

It is seen from the table 1 that heating of the melt above T_c gives higher magnitudes of the strength of ribbons both at 300 and 77 K. Lower values of the strength at 77 K than at 300 K for both regimes is caused by the quasi-brittleness of this metallic glass under cooling down to 77 K.

Table 1.

Dependence of the strength of the $Fe_{73,5}Nb_3Cu_1Si_{13.5}B_9$ ribbons on the thermal treatments of the melt before quenching

Thermal Treatment	Strength, s_f, GPa	
	300 K	**77 K**
Regime 1	1,43	1,13
Regime 2	1,10	0.97

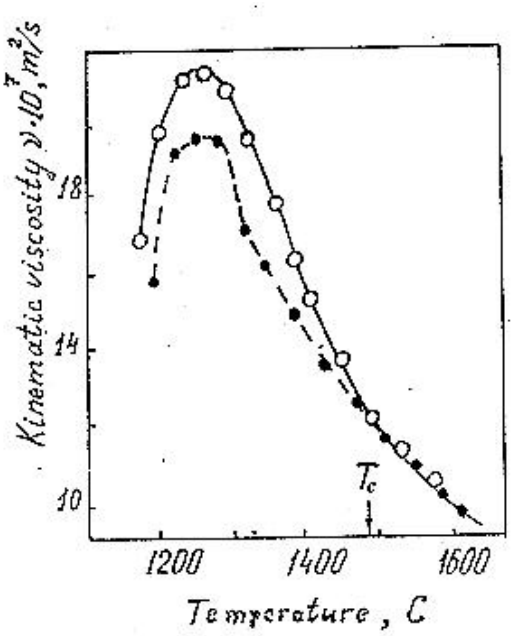

Fig.1 Temperature dependences of the $Fe_{73,5}Nb_3Cu_1Si_{13.5}B_9$ melt kinematic viscosity under heating (I) and cooling (i).

3.2.2. The $Fe_{71}Cr_{10}Si_7B_{12}$, $Fe_{81}B_{13}Si_4C_2$ and $Co_{60}Fe_5Ni_{10}Si_{10}B_{15}$ metallic glasses.

The regimes of the thermal treatments of the melts for these alloys were :

Regime 1: a) heating to 1560 ^oC (above T_c), keeping during 15 min at this temperature;

b) cooling down to 1480^oC and keeping at this temperature during 5 min before quenching.

Regime 2: heating to 1480^0 C (below T_c), keeping 5 min at this temperature before quenching.

Values of the strength σ_f for these alloys at 3000 K are indicated in the Table 2 for both regimes of the melt thermal treatment before quenching. It is seen that the same regularity is observed as it was in the Table 1: heating of the melt above T_c before quenching increases the strength of metallic glasses ribbons and makes them ductile. Fractography of the failure surfaces of the ribbons shows that in MG obtained after the melt heating above T_c the ductile shear failure is realized with the "vein' pattern formation [14]. The mixed quasi-brittle failure is observed in MG obtained from the melts which were not heated above T_c (see last column of the Table 2) with the "chevron " pattern formation.

3.3. Surface relief of metallic glasses ribbons prepared after different thermal treatments of the melt.

Characteristic relief typical of the "contact" surface of MG ribbons obtained by the planar flow casting usually contains "caverns" elongated along the ribbons length. Qualitative and quantitative characteristics of these "caverns" are different for the ribbons obtained after the melt different thermal treatments. In the case of the regime 1 "caverns" are more elongated and anisotropic than in the case of the regime 2. For example Fig.2 shows the statistical distribution density of the depth h of the "caverns" for both regimes.

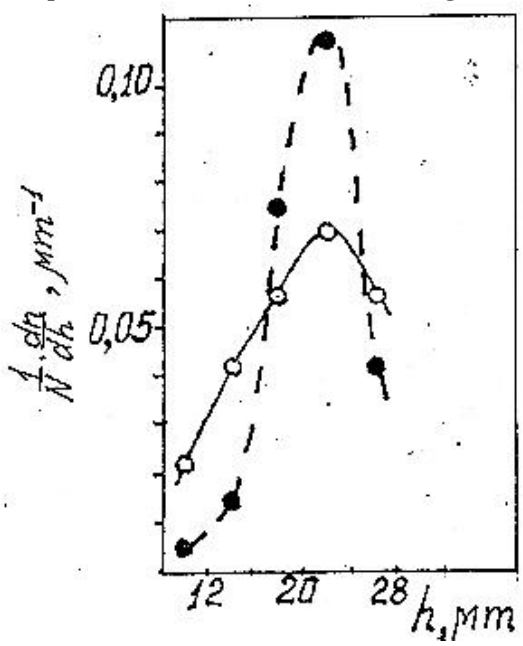

Fig.2. The statistical distribution density of the depth h for both regimes

3.4.Dependence of the anisotropy of the strength s_f and fracture toughness K_{IC} on the melt thermal treatments.

An anisotropy in the ribbons plane of the strength as and of the fracture toughness K_{IC} of metallic glasses ribbons is dependent on the melt thermal treatment [15]. Polar diagrams

Table 2. -
Dependence of the strength of metallic glasses on the thermal treatments of the melts before quenching

Thermal treatment	Strength , s_f, **GPa**			Mode of Failure
	$Fe_{81}Si_4B_{13}C_2$	$Fe_{71}Cr_{10}Si_7B_{12}$	$Co_{60}Fe_5Ni_{10}Si_{10}B_{15}$	
Regime 1	2,420	2,80	2,40	Ductiles shear failure “vein pattern”
Regime 2	1,115	1,70	1,80	Quasi-brittle failure, “chevron” pattern”

s_f (θ) for the $Fe_{81}Si_4B_{13}C_2$ and $Co_{60}Fe_5Ni_{10}Si_{10}B_{15}$ metallic glasses ribbons for regimes 1 and 2 of the melts treatment show that smaller s_f values are observed for each direction in the

ribbons plane for ribbons obtained from melts non-heated above T_c. A degree of the anisotropy is also different for MG ribbons obtained after different thermal treatments of the melts.

The fracture toughness K_{1C} of the $Fe_{81}Si_4B_{l3}C_2$ MG obtained after the melt treatment in the regime 1 is 69.3 MPa √m. After the regime 2 the K_{1C} is 22.2 MPa √m i.e. almost three times lower. The statistically significant anisotropy is observed also for the fracture toughness K_{1C} of the $Fe_{81}Si_4B_{l3}C_2$ MG after the melt heating above T_c (Fig.3).

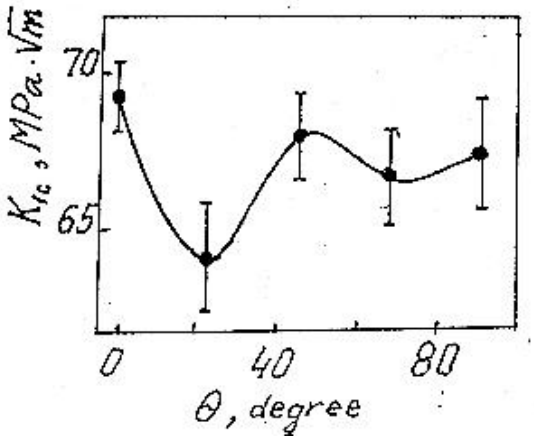

Fig.3. K_{1C} (q) for the $Fe_{81}Si_4B_{l3}C_2$ after the melt heating above T_c.

At the same time K_{IC} is isotropic for this glass obtained without the melt heating above T_c,

4. DISCUSSION OF RESULTS

The hereabove reported dependence of MG mechanical properties on the thermal treatment of the melt as an indirect evidence of the correlation between a microscopically heterogeneous atomic structure of the glass-forming melt and mechanical properties of the metall glass obtained from this melt. Heating of the melt above T_c before quenching have already long ago been used in technology of preparing of MG for obtaining the perfect amorphization [8]. It is supposed [10,12] that under such thermal treatment of the melt crystalline clusters existing in the melt are destroyed that promotes the perfect amorphization. The 15 min time necessary for the microhomogenisation above T_c had been found empirically.

An essential peculiarity of our experiments was that for the both regimes of the melt thermal treatments we have the same conditions of the rapid quenching (quenching temperature, cooling rate etc).Therefore it was possible to relate observed differences in the mechanical properties of MG (obtained after the different regimes of the melt treatment) strictly to different atomic clusterous structures inherited from the melt. Existence of non-crystalline clusters and their aggregates in liquids is now well known both from experiments and from molecular-dynamics simulations [11,15-17].

The basis of our study was the notion on destroying of the ordered aggregates in melts by additional heating of the melt exceeding the binding energy of these aggregates. Metallic glasses after thermal heating above T_c (regime 1) have the high strength and fracture toughness because of their good ductility and cohesion along intercluster boundaries. Glasses obtained without heating of the melt above T_c contained miccrocrystalline inclusions (observed by electron microscopy) and had bad cohesion along intercluster boundaries. This is considered as a reason of their low strength and fracture toughness.

5. CONCLUSIONS

1. Mechanical properties of the $Fe_{73,5}Nb_3Cu_1Si_{13.5}B_9$, $Fe_{81}Si_4$ $B_{l3}C_2$, $Fe_{71}Cr_{10}Si_7B_{12}Co_{60}$ and $Fe_5Ni_{10}Si_{10}B_{l5}$ metallic glasses ribbons obtained by the planar flow casting (from the melts subjected to the different thermal treatments relative to the critical temperature T_c of the melt before quenching) were measured experimentally.
2. The melt critical temperature T_c was determined experimentally for each alloy as the temperature of branching of the melt viscosity temperature dependences under heating and cooling of the melt.
3. The strength and the fracture toughness of metallic glasses, obtained from the melts heated above T_c are essentially higher than for the same glasses obtained from melts which were not heated above T_c. Such difference is explained by different clusterous structures inherited from the melts and by the different state of intercluster boundaries.

ACKNOWLEDGMENTS

The research described in this publication was made possible in part by Grant No. U22200 from the Joint Fund of the Government of Ukraine and International Science Foundation and in part by Grant No. U22000 from the International Science Foundation.

REFERENCES

[1] A.S.Bakai, Low Temper. Physics.,20,(1994) 373,379.
(2] A.R.Ubbellode, Melting and Crystal Structure, Clarendon Press,Oxford ,1965.
[3] N.Mattern,A.G.Ilinsku,H.Hermann and A.V.Romanova, Phys.Status Solidi,17(1983) 397.
[4] W. Weiss and H. Alexander, J. Phys. F ,17(1987),1983.
[5] L.E.Mikhailova, Chen Si Shen, A. V.Romanova, A.G. Ilinski, Metallofizika,13 (1991) 116(in Rusaian).
[6) P.Andonov, S.Kimura, T. Savada, J. Non-Cryst. Solids ,156158(1993) 783. [7) A.S.Bakai ,Glassy Metals III, H.Beck and H.- J.Gunterodt (eds.), Springer (1994) 209.
[8] E. V. Kolotuhin, B.A.Baum, G.V. Tiagunov, P.S.Popel, E.L. Arhangelski, Izvestia Vuzov, Chornaia metallurgia,6(1988) 68,(in Russian).
(9) E.V. Kolotuhin, P.S. Popel, V.S.Tsepelev, Rasplavi ,3(1988) 95,(in Rusaian)
[10] B.M. Kuleshov, V S. Tsepelev, ISSN 0038-920X "Stal'; No.7(1993) 69,(in Russian).
[11] T.Tomida, T. Egami, Phys.Review B,52, No 5(1995) 3290. [12) V.Manov, A. Rubshtein, A. Voronel, P. Popel, A. Vereshagin, Mater. Sci.Eng.,A 179/A 180,(1994)91.
[13] G.V. Tiagunov, V.S.Tsepelev, M.N. Kushnir, G.P. Jakovlev, V.B. Malzev, Zavodskaia Iabor.,46, No 10(1980) 919,(in Russian).
[14] E.D.Tabachnikova, Fizika Metal.&Metallaved.,64, No 6(1987) 1205,(in Russian).
[15] V.Z.Bengus, G.Vlasak, P. Duhaj, V.0celik, E.D. Tabachnikova, G.V. Biletchenko, E.B.Korollcova, L.D.Son, V,S. Tsepelev, S.V.0rlov & V.V.Smirnov, Key Engineering Materials,81-83 [1993) 501.
[16] E. Nold, P. Lamparter, H.Olbrich, G. Rainer Harbach S. Steeb, Z. Naturforsch, 36a (19811032.
[17] H. Jonsson, H.C. Andersen, Phys.Rev. Lett,32(1988) 2295.

INFLUENCE OF TEMPERATURE ON THE GROWTH RATE AND DISSOLUTION OF DISPERSED PHASE PARTICLES IN THE PHASE SEPARATED SODIUM BOROSILICATE GLASS*

E.V. Morozova
INSTITUTE OF SILICATE CHEMISTRY, RUSSIA

Abstract

In this work, using the method of quantitative electron microscopy, studies have been made of growth and dissolution kinetic of a polydispersed system of spherical particles appearing in the process isothermal phase separation in the glass. The 3.1 Na_2O, 25 B_2O_3, 70 $Si0_2$.1.2 CaO (mol %) glass was studied at temperatures of 700^0C and 800^0C within the time interval of 1 to 70 hrs.

...

An incresse of heat treatment from 700^0C to 800^0C causes three-fold incresse of the average radius of particles which influences the magnitude of the preexponential multiplier A, the valus of index & remanies unchanged.

Using the available valuse of distribution functions, the growth and dissolution rates of particles belonging to the definite size fractions have been calculated. It has been estabiiehed that at T=700^0C and 800^0C rate of the change par diales size is a non-monotonic (usdnilation) with time.

At 800^0C three-fold increase of dissolution rate of small particles is observed, the growth rate of large particles be ing practically unchanged.

The results obtained show that there is the correlation between the dissolution rate of particles and the magnitude of the average radius of the particle assembly.

---

* Full manuscript not available at the time of printing

INFLUENCE OF THE CORRELATION BETWEEN PbO AND Bi_2O_3 ON THE DECORATIVE PROPERTIES OF MULTICOMPONENT GLASSY COATINGS

Stoyan Djambazov, Yanko Dimitriev, Elena Kashchieva and **Albena Yoleva**
University of Chemical Technology and Metallurgy, Bulgaria

Abstract

New low- melting glassy coatings with original decorative effects are synthesized for application in the ceramic tiles productions. The multicomponent non-traditional compositions with participation of Bi_2O_3, PbO, and TeO_2 are studied. The influence of the ratio between PbO and Bi_2O_3 on the characteristics of the glassy coatings is investigated. A correlation is found between the decorative effects obtained and the microstructure and phases presented in the coatings.

I. INTRODUCTION

The synthesizing of new multicomponent compositions for special glassy materials and their application as new glazes is work line of research-workers in this moment in many countries. The reason is that the widespread use of glazed ceramic tiles requires to find new frits and glazes with more attractive decorative effects and good mechanical properties. Over last years is imposed the tendency for development of dry glaze application in form of powder, crushed frits or granules. [1-3]. This work is continuation of our previous investigations in which we were obtained new original compositions of low melting frits with nontraditional attractive decorative effects, containing Te, Mo, W, Bi_2O_3, PbO, B_2O_3, feldshpat, BaO, ZnO. In previous investigations our attention was directed mainly on influence of metals such as Te, Mo and W on the development of nontraditional special decorative effects. [4-6] The aim of this work is investigation of the influence of the ratio between PbO and Bi_2O_3 on the decorative properties of multicomponent glassy coatings.

II. EXPERIMENTAL PROCEDURE

The selection of the components was made according to published data for special compositions of frits and glazes. [7, 8] B_2O_3 and PbO participates in every composition as traditional fluxs. As a nontraditional component was introduced Bi_2O_3 which effect as a good flux, enlarges melting interval and may be use as a base of many low-melting glass. For frits and coatings this component is used very rarely. The main reason for the TeO_2 choice as a component is that the tellurium dioxide is low melting compound also and otherwise it is a glass former. The presence of Te in heavy metal oxides in the batches leads to the obtaining of tellurite phase after thermal treatment. [6] This enables additional opportunity for controlling oxidation-reduction processes during the thermal treatment of the frits and obtaining of different metastable phases. The studied compositions are shown in Table 1.

Table 1. Frit compositions [mol %]

Components	**Frit 1**	**Frit 2**	**Frit 3**	**Frit 4**	**Frit 5**
TeO_2	20	20	20	20	20
B_2O_3	20	20	20	20	20
Bi_2O_3	35	30	20	10	5
PbO	5	10	20	30	35
feldspat	10	10	10	10	10
BaO	5	5	5	5	5
ZnO	5	5	5	5	5

The content of PbO and Bi_2O_3 varied at permanent participation of the other components. The batches are prepared by mixing of elemental Te, H_3B0_3, Bi_2O_3, Pb_3O_4, feldspat, $BaCO_3$ and Zn0 in appropriate amount. The batches in quantity of 100 g were homogenized in a hating mill and melted in laboratory electric furnace in alumina crucibles at temperature 1000-1200 °C depending of the composition. The obtained glass like melts were cooled in water for obtaining of frits. After that frits are crushed to grains with size 1-1,5 mm and are applicated on white zirconium glazed tiles. The additional thermal treatment was performed in temperature range 500-700 °C.

The phase formation, processes of crystallization and microstructure of synthesized glassy coatings was studied with X-ray diffraction (aparat DRON-UN, Cu Ku, radiation), Infrared spectra (spectrophotometer "SPECORD"), DTA (aparat "Hench"), and TEM (electron microscope "Philips"). Vickers hardness of the glassy coatings are determinated with device for hardness toward microscope "Nu" (Carl Zeiss-lena), loadind 30 g, duration - 30 sec.

III. RESULTS AND DISCUSSION

All compositions after melting are amorphous. The colour of frits are changes depending of composition from yellowbrown to blackbrown. The frits are subject to thermal treatment at 550-600 °C in duration of 5 h for development of appropriate crystallization. X-ray diffraction data of frits (fig.1) shows that in considerable degree they remain the amorphous, especially compositions 4 and 5. In compositions 1, 2 and 3 is established fine crystallization of phase with orthorombic fluorits structure corresponding to solid solution $Bi_{1-x}Te_xO_{3+x/2}$ ($0{,}33 \leq x \leq 0{,}50$) which diffraction data are taken from [9]. As confirmation of the X - ray analysis are presented infrared spectra of the samples (fig. 2). The bands may be ascend to the characteristic frequencies of the building units of the compound Bi_2TeO_5: 425, 465, 540, 570, 610 cm^{-1} corresponding to the vibrations of Bi - 0 poliedra and 670 and 705 cm^{-1} and 380 cm^{-1} corresponding to Te - 0 poliedra. [10]. The band around 1020 -1040 cm^{-1} may be interpreted with formation of polimerizated SiO_2 tetraedra in the lattice.

Glassy coatings after thermal treatment in temperature range 500 - 700 °C give interesting decorative effects. In compositions 1 and 2 at 500 - 550 °C is observed phase separation of two phases - the one with metalsgrey colour and the other with darkbrown colour. At this temperature crushed frits are soft and forms glass - like granules. The same composition at high temperature 600 - 700 °C shows other decorative effects. The two phases change their colour and a transition observed into interconnected darkgreen and yellow - whitephases in the coating over the ceramic body. Composition 3 at 700 °C is transform in to milkwhite blue glassy coating. It is seen at the

cross section of the coatings the formation of two layers. The upper one is with high brilliance and big lustre and the other one which is in contact with the ceramic body is mainly crystallized. For composition 4 at 700 °C it is tipicle the formation of nontransparent coating with small transparent darkblue microformations. The composition 5 forms glass-like coating with liquid phase separation. The observations shown that the most of the interesting decorative effects are obtained in the composition in which PbO and Bi_2O_3 participate in equivalent content.

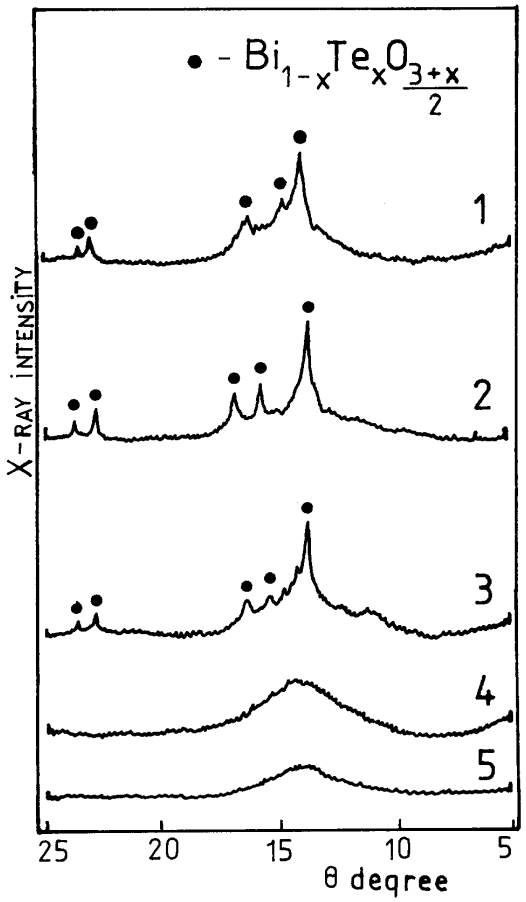

Fig.1. X - ray diffraction of the frits frits after thermal treatment at 600°C, 5h 5h

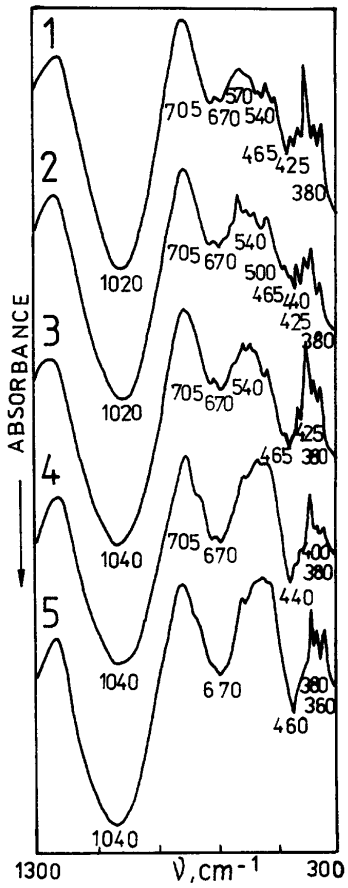

Fig. 2. Infra-red spectrum of the after thermal treatment at 600°C,

On the bases of the discussed visual observations of the samples after their thermal treatment and also taking in to account the DTA analyses it is possible to make a conclusion about crystallization and melting behaviour of the compositions. The coatings have glass transition temperature between 400 - 450 °C. The crystallization of the bismuth - tellurite phase developed above 500 °C. The crystalline tellurite phase is possible to be separate only in compositions containing low amount of lead oxide (compositions 1, 2 and 3). One typical crystalline structure of the coating is shown in fig. 3. The crystal sizes are between 5 - 10 μm. The melting temperature of the crystallized samples is about 620 - 650 °C depending of the composition. Above 700°C are developed mainly liquid phase separation processes in the amorphous matrix.

All coatings are characterize with very good adhesion to the ceramic body. The glassy coatings posses good Vickers hardness between 4,9 - 5,6 GPa (tabl. 2) and Moch hardness 5, which are similar to the results published for other glazes with lead content. [11]

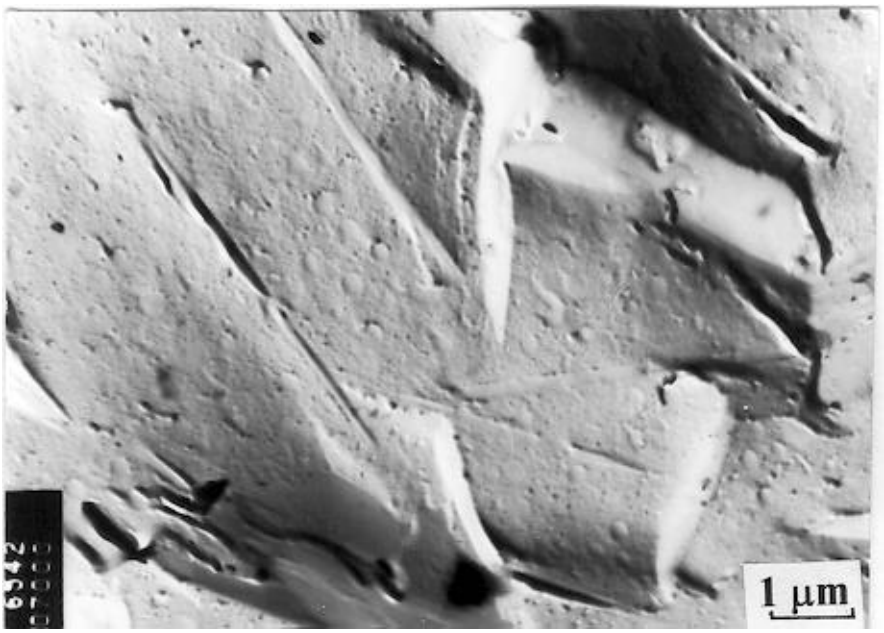

Fig. 3*. TEM micrograph of frit 3 after thermal treatment at 600 °C , 5 h.*

Table 2.Vickers hardness of the glassy coatings

Glassy Coatings	Vickers Hardness, GPa
1	5,1
2	5,2
3	5,6
4	5,0
5	4,9

IV. CONCLUSION

It is establish that multicomponent compositions containing together TeO_2, B_2O_3, Bi_2O_3, PbO, feldspat, BaO, ZnO may be vitrified in the temperature range 1000-1200 °C. They are appropriate for dry application as coating over ceramic body. Different decorative effects are obtained depending of the thermal treatment regime between 500 - 700 °C. They are connected with the crystallization of the $Bi_{1-x}Te_xO_{3+x/2}$ phase and liquid phase separation of two interconnected glasslike phases. The equivalent content of Bi_2O_3 and PbO are appropriate for creation of the original decorative effects.

The investigation are financially supported by Bulgarian National Foundation of Science under Contract N x - 308 / 1993.

REFERENCES

1. Amoros J., II WORLD CONGRESS ON CERAMIC TILE QUALITY, QUALICER '92,69-100,1992.
2. Amoros J., Bruni S., Industrial Ceramics,11(1),7-10,1991.
3. Leonelli C., Amoros J., Amer. Ceram. Soc.,74(5),983-987,1991.
4. Djambazov S., Nedelchev N., Dimitriev Y., Ivanova Y., Yoleva A.,2th INTERNATIONAL CERAMICS CONGRESS, 24- 28 Oct., Istanbul, TURKEY, 216- 220,1994.
5. Dimitriev Y., Kashchieva E., Djambazov S., The 4th EUROPEAN CONFERENCE ON ADVANCED MATERIALS AND PROCESSES,25-28 Sept., Padua/Venice, Italy,613-617,1995.
6. Djambazov S., Ivanova \Y., Yoleva A., Kashchieva E., Dimitriev Y.,Nedelchev N., IV WORLD CONGRESS ON CERAMIC TILE AND QUALITY, QUALICER 96, CASTELLON, ESPANOLLA,15-17 mart,1996.
7. Stefanov S., Batcschvarov S., Smalti Ceramici, Gruppo Editionale Faenza Editrice S. p. A.,1994.
8. Tozzi N., Smalti Ceramici Considerazioni Teoriche e Pratiche, Gruppo Editionale Faenza Editrice S. p. A.,1992.
9. Farissi M., Mercurio D., Frit B., Materials Chemistry and Physics,16,133- 144,1987.
10. Kucha V., Chomich V., Kravchenko V., Perov P., Neorganichni materiali, v.20, N2,314-317,1984.
11. Moreno A., Toledo J., Gazulla M., Garrote R., IV WORLD CONGRESS ON CERAMIC TILE AND QUALITY, QUALICER 96, CASTELLON, ESPANOLLA, 15-17 Mart,731-732,1996.

INFLUENCE OF THERMAL TREATMENT IN HYDROGEN OF Co-AND Cu-CONTAINING SILICA GEL-GLASSES ON STRUCTURE AND SPECTROSCOPIC PROPERTIES OF OPTICAL CENTERS*

Malashkevich G.E[1]., Poddenezhny E.N.[2], Melnichenko I.M.[2], Gaishun V.E.[2], Semchenko A.V.[2]

1. Academy of Sciences of Belarus,
Gomel state University, Belarus

Abstract

The mixtures of cobalt and copper are widely utilized as a doping component during production of glass optical filters. Due to polyvalency of these elements and the weak screening of their optical electrons, the spectroscopic characteristics of obtained filters are, to a considerable extent, stipulated by the composition and technological conditions of synthesis. We have shown that in the air-vitrified Co-containing glasses the activator exists in triply and doubly charged states. Moreover, in the latter case its coordination is mainly tetrahedral. Thermal treatment of these glasses in hydrogen permits to achieve the full transition of triply charged cobalt to doubly charged one and is accompanied by changes of its distortion degree. Especially, the changing of such parameter takes place for glasses obtained from xerogels, additionally impregnated with ortophosphorus acid. In air-vitrified Cu-containing silica gel-glasses the activator exists mainly the singly charged state. However, its spectroscopic behavior essentially dependents on the chemical composition and concentration of doping mixtures. Thermal treatment of these glasses in hydrogen is accompanied by appearance of intensive red color connected to the formation of colloids atomic copper. We would like to note the high stability cobalt and copper silica gel-glasses singly-doped to liquidification at the annealing in hydrogen and the high thermostability of reduced form of activators.

---

* Full manuscript not available at the time of printing

INVESTIGATION OF RELATIVE BASICITY (pO-INDEXES) OF THE SYSTEM Li_2O-K_2O-SiO_2*

Konakov V.G., Shultz M.M.
Russian Academy of Sciences, Russia

Abstract

The question on the basicity values of oxide systems in the quantity presentation is one of the most important problems in the chemistry of oxide melts. The problem of determination of "the measure basicity of melt" in numeral presentation has arisen time and again. Also the question was raised to what component of melt we should attribute to the parameters interpreted as the basicity. Two main ways were determined.

The first one accepts the activity of alkali component of oxide melts as the measure of basicity. The main advantage is thermodynamic definition of parameters obtained from experiment. However it is very difficult to compare basicities of dissimilar systems, such as Na2O-SiO2 and K2O-B2O3 or to interpret the acid-base characteristics of systems containing several alkali oxides or not containing them

In the second case the ion O^{2-} is considered to be the carrier of basic properties in oxide melts and its activity or the value $pO=-lga_o^{2-}$ is supposed to be the measure of basicity . According to the unique procedure based on the EMF-method two compositions of the systems Li_2O-K_2O-SiO_2(x_{Li2O}=0.6 and 0.66) were studied at the range from 1173 to 1273 ^{0} C. The dependencies gotten can be explain on the basis of the concept of the chemical constitution of melts. The model describing basicity changes of three-component melt was made. This model is based on the information about concentration dependencies of pO for the systems K_2O-SiO_2 and Li_2O-SiO_2.

---

* Full manuscript not available at the time of printing

INVESTIGATION OF SODA GLASSES THAT ARE EXPOSED Co-60

Nilgün DOGAN and **A. Beril TUGRUL**
Istanbul Technical University, Turkey

Abstract

Energetic gamma rays can be effected on glass and caused the colors of it in this study, Co-60 radioisotope have been used for experiments as a exposing source. After the exposure, the color of glasses turn to brown according to doses. For 10 mm glass thickness, transmission and reflection rates for visual and solar lights have been measured by using spectrophotometer. Some different measurements have been also done to determination of transmission for ultraviolet rays, X-rays and gamma rays. Results are evaluated according to each other and unexposed glasses comparatively.

I. INTRODUCTION

Today, there are different types of glasses about of them approximately 700 commercial use. But they can classified in five main groups; soda glasses, borosilicate glasses, lead glasses, wire glasses and special glasses. Most wide versatile glass is soda glasses that are used in different areas widespread. Sodium carbonate or soda ash, decomposes to sodium oxide as the batch of raw material melts.

In this study, investigation have been done on a common type soda glasses that consist of SiO_2, Al_2O_3, Fe_2O_3, TiO_2, CaO, MgO, Na_2O, K_2O and SO_3. Colorless glasses have been supplied by ÞÝÞECAM Research Center in 10 mm thickness, but in the same chemical compound and they are cutting as square shape in 5 x 5 cm^2 dimensions [1,2].

In the other hand, gamma rays are the same physical nature as visible light, radio waves, etc., but which have a wavelength which allows them to penetrate all materials with partial absorption during transmission. They travel in straight lines outwards from a source according to the "inverse square law" [3].

2. GLASS BEHAVIOUR

Investigations of glasses in the different ways, it is related to their physical properties. Therefore, physical properties and material interactions are important on their behaviour. In here, viscosity, thermal properties, density and homogeneity are effected on transmission, reflection, absorption of electromagnetic radiation in the glass [4].

Correlation between the reflection (R), absorption (τ) and transmission (I) can be given as [5,6] :

$$R + \tau + I = 1 \qquad (1)$$

For the reflection;

$$R = (\eta - 1)^2 + \tau^2 / (\eta + 1)^2 + \tau^2 \quad (2)$$

can be determined. In here, η represents refractive index. For a typical transparent glass, $\eta >> \tau$ and then;

$$R = (\eta - 1)^2 / (\eta + 1)^2 \quad (3)$$

can be written.

Light transmission of the glass (Tv) according to CEN (1992):

$$T_V = \frac{\sum_{\lambda=380}^{\lambda=780} D_\lambda \; T(\lambda) \; V(\lambda) \; \Delta\lambda}{\sum_{\lambda=380}^{\lambda=780} D_\lambda \; V(\lambda) \; \Delta\lambda} \quad (4)$$

In here:

$D\lambda$, : Spectral dispersion according to lighting of D65
D_{65} : Standard lighting according to CEN definition
$T(\lambda)$: Spectral transmission of glass
$V(\lambda)$: Efficiency of spectral luminescence for the photopeak in the photometry
$\Delta\lambda$: Wavelength interval

For the light reflection of the glass (Rv):

$$R_V = \frac{\sum_{\lambda=380}^{\lambda=780} D_\lambda \; R(\lambda) \; V(\lambda) \; \Delta\lambda}{\sum_{\lambda=380}^{\lambda=780} D_\lambda \; V(\lambda) \; \Delta\lambda} \quad (5)$$

can be written. $R(\lambda)$ denotes spectral reflection of the glass.

3. EXPERIMENTAL STUDIES

Energetic gamma rays can be effected on glass and caused changing the colors of it. In this study, Co-60 radioisotope which has 1.17 MeV and 1.33 MeV gamma energy peaks, have been used for experiments as a exposing source that had 14,8 Ci activity level. A soda glass has been placed against the source, and exposed at the different dose levels.

After the exposure, the color of the glasses turn to brown according to the dose levels. Their color information can be seen in the color map (Fig.1). For all the glasses, transmission and reflection rates for visual and solar light have been measured by using spectrophotometer between 185 nm-2500 nm. Fig. 2 and Fig.3 shows transmission and reflection rates for 4.568 KGray dose level exposed glass.

Some different measurements have been also done related to determination of transmission for ultraviolet rays, X-rays and gamma rays. In here, black light and sun lamp are used as two different ultraviolet sources in the experiments. For the ultraviolet measurements, a special device and sensors that have sensitive for the different ultraviolet wavelength ranges. Fig. 4 shows the results of Ultraviolet experiments. An X-ray tube is used as a source, and transmission is measured for 30 KeV energy range and then, absorption ratio is calculated for soda glasses. Results can be seen in Fig. 5.

Seven different gamma radioisotopes that are Co-57, Co-60, Cs-137, Ba-133, Na-22, Cd-109 and Mn-54 are used as a source, and experiments of transmission measurements have been done separately for each radioisotope. A scintillation detector with multichannel analyzer counting system is used for the measurements. Comparative graphs can be seen in Fig.6.

4. RESULTS

After high level gamma ray exposing which caused the change in the color of the glasses, are observed in the point of view of interaction with electromagnetic radiation. Differences according to each other are determined by measurements of transmission rate of electromagnetic radiation. When the dose level increase then the coloring rates goes up. This results determined and showed on color map.

Exposed glasses are more absorbent for the solar light comparatively unexposed glasses. Inversely, reflection rate and transmission rate of the exposed glasses are low then the colorless glasses for solar and ultraviolet lights. X-ray absorption rates for exposed glasses are high according to unexposed glasses, but no important differences between glasses that are exposed over 10 K gray (1000 KRad) dose levels.

ACKNOWLEDGMENT

We are grateful to research personnel of Research Center of ÞÝÞECAM, especially to Mrs. Gülçin ALBAYRAK, Health Physics Laboratory of Çekmece Nuclear Research and Training Center and research assistants of Nuclear Application Division of ITU Institute for Nuclear Energy.

REFERENCES

1. Doðan, N., (1996), "Behaviour of Soda Glasses Against The Electromagnetic Radiation", M.Sc. Thesis, Istanbul Technical University Institute For Nuclear Energy, Istanbul, (in Turkish).
2. Doðan, N., Tuðrul, A.B., (1995), "Investigation of Effectiveness of Energetic Electromagnetic Radiation on Soda Glasses", 15th National Physics Congress, Kaþ-Antalya (in Turkish).
3. Bilge, A.N., Tuðrul, B., (1990), "Principles of Industrial Radiography", Istanbul Technical University - Institute For Nuclear Energy, Publ. No: 20, Istanbul. (in Turkish).
4. Þiþecam (1992), "Temel Cam Bilimi", Istanbul (in Turkish).
5. CEN (1992), "Glass in Building Determination of Light Transmittance Solar Direct Transmittance and Ultraviolet Transmittance and Related Glazing Characteristics", CEN/TC 129/W69/N.4E Rew.7.
6. TSE (1993), "Glass in Building Determination of Light Transmittance, Solar Direct Transmittance and Ultraviolet Transmittance and Related Glazing Characteristics", UDK 628.925.021: 698.3 (in Turkish).

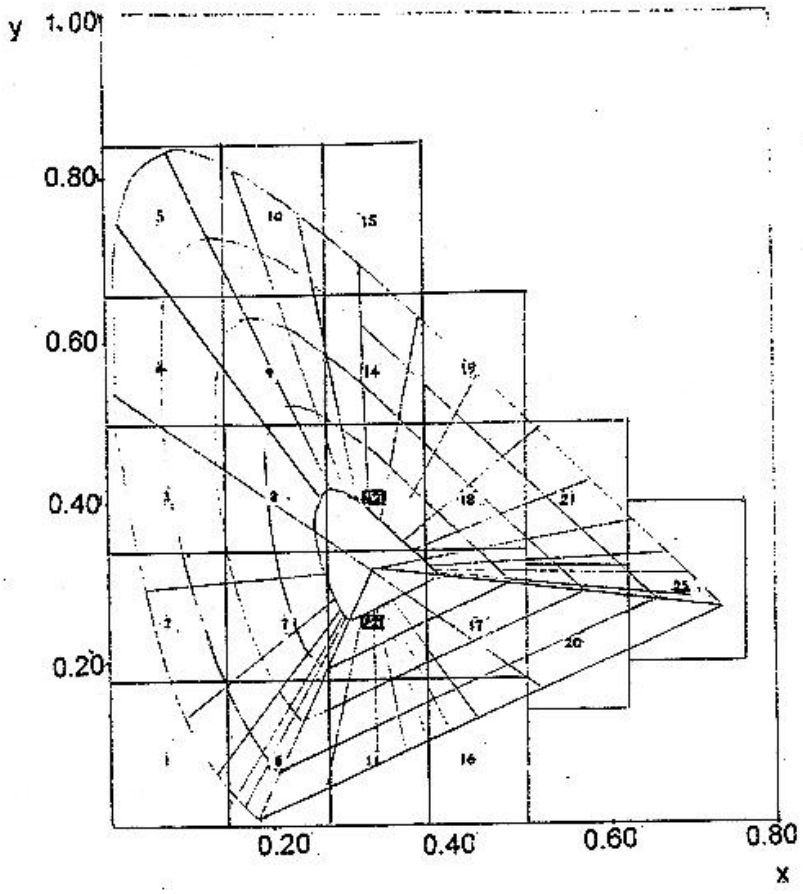

Fig:1. Places of Exposed Glasses in The Color Map

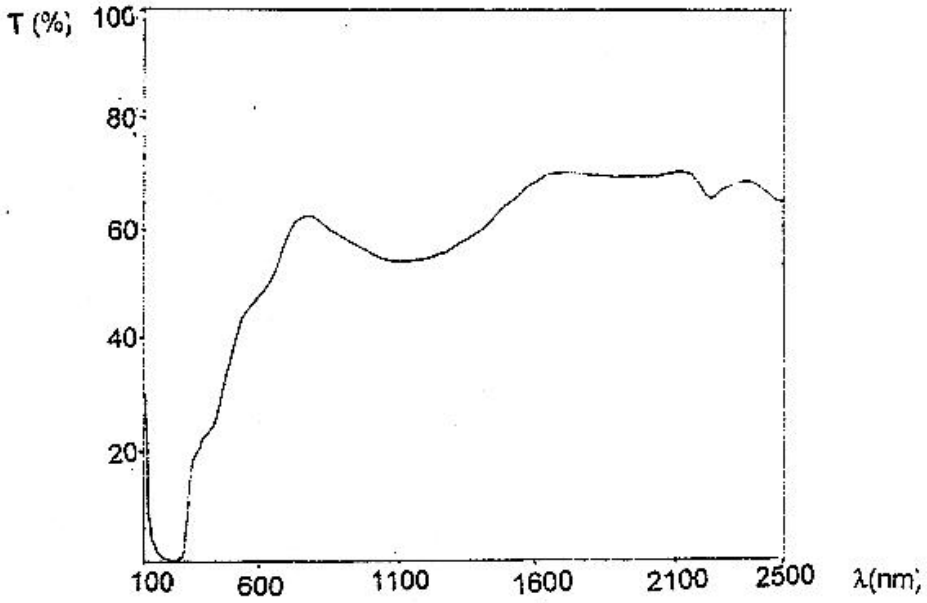

Fig. 2. Transmission Rate For 4.568 KGray Dose Level Exposed Glass

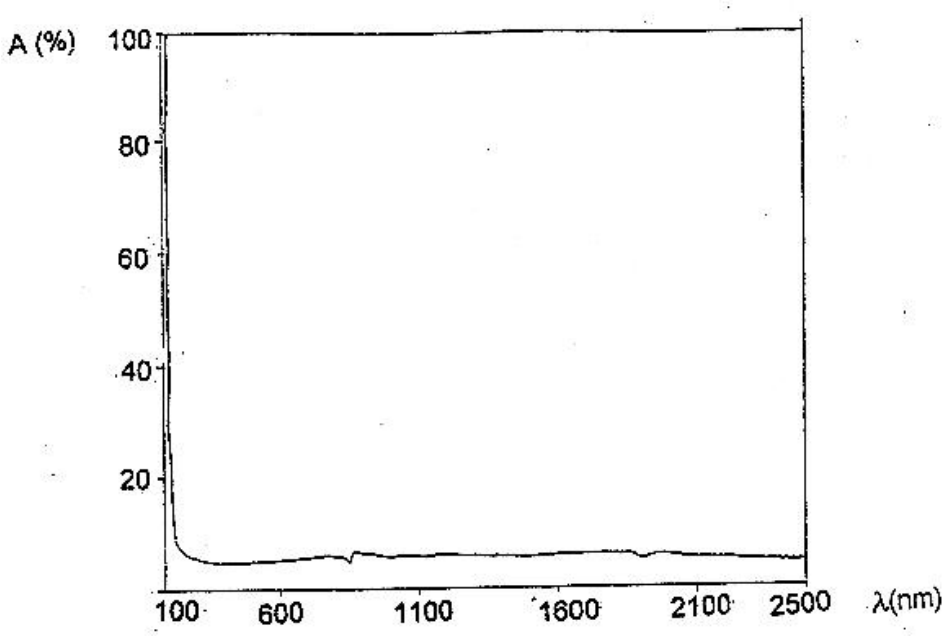

Fig.3 Reflection Rate For 4.568 KGray Dose Level Exposed Glass

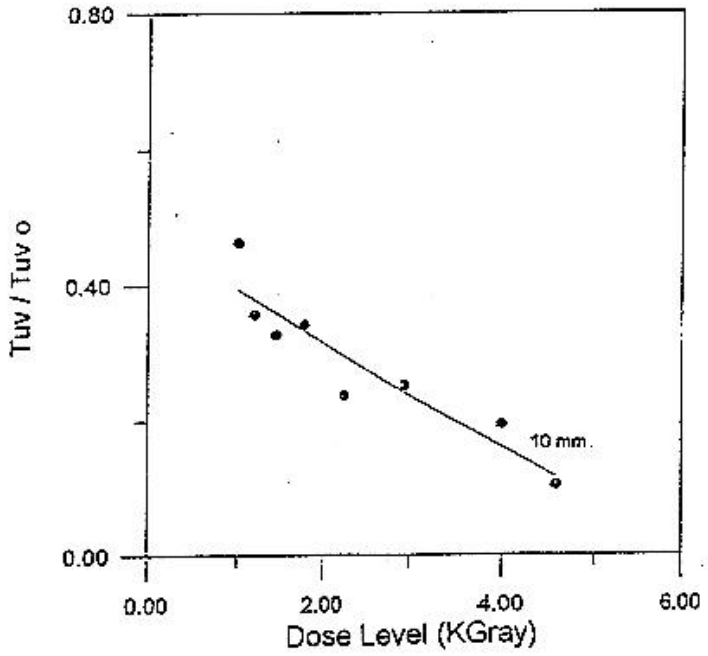

Fig.4 Transmission Rate For UV of Exposed Glasses

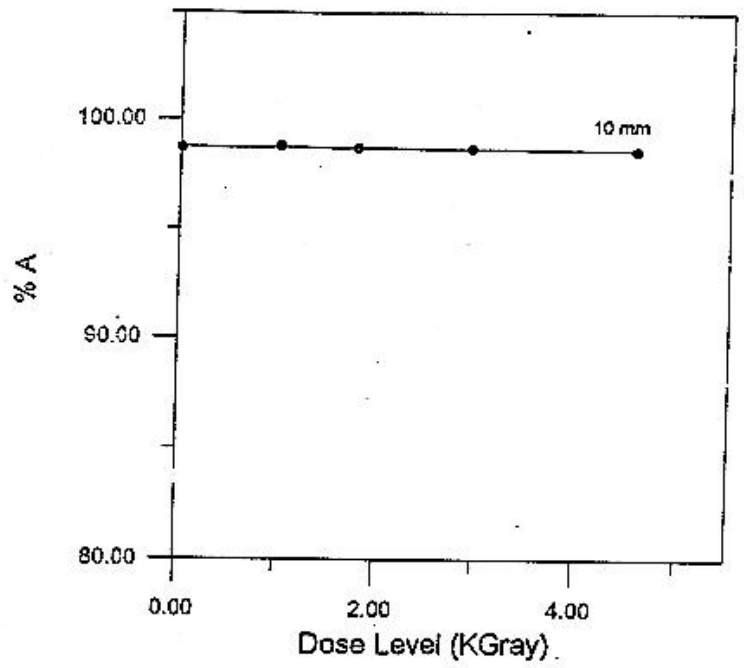

Fig.5 X-Ray Absorption Rate For Exposed Glasses

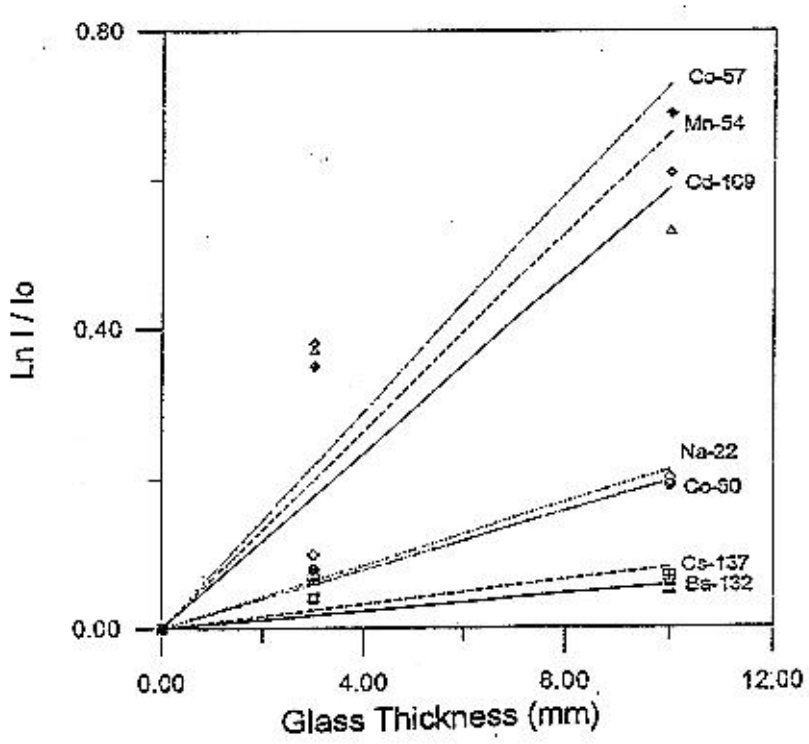

Fig.6 Gamma Ray Transmission For 4.558 KGray Dose Level Exposed Glass

INVESTIGATION OF THE PHASE SEPARATION PHENOMENON IN THE GLASSES

B.Procyk, B.Kuczek, M.Ðroda, M.Figura, A.Zawada
University of Mining and Metallurgy, Poland

Abstract

Borate phase separation has been occurred during thermal treatment of the glasses, belong to Na_2O-B_2O_3-SiO_2 system. The glass has become opaque, due to the opalescence of borates separated. The borates are in the form of small drops, joined to each other. The influence of the temperature and time on the phenomenon of phase separation in these glasses has been defined.

I. INTRODUCTION

The phenomenon of phase separation is a process of disintegration of a multicomponent, initially homogenous, melt into two or more immiscible phases.

The educing new phase (or phases) may occur in the form of isolated globules or continuous, immiscible, mutually penetrating layers. Depending on the volume of the educing new phase there occurs the phenomenon of macro- or microliquation.

Phase separation of a system into two other systems, differing in their chemical compositions and properties may take place only then when for random, physicochemical reasons the coming close together and the following increase in the concentration of its structural elements is energetically more advantageous than their separation.

From the thermodynamics point of view the spontaneous phase separation may occur when this process leads to the reduction of the thermodynamic potential of the system: $\Delta G_m = \Delta H_m - T\Delta S_m$. With increasing temperature the importance of the entropy member increases while the deflection on the curve becomes reduced. At a certain temperature, known as the critical temperature of the immiscibility T_c it disappears completely. Above this temperature the phase separation will not take place (Fig.1).

The system which the composition is found inside the spinodal curve (spinode) will decompose, if the mobility of the ions is sufficiently great. The formation of a new phase proceeds without nucleation. On the other hand, when the composition is found outside the spinode, in the binodal region, then phase separation does not take place spontaneously and requires the formation of nuclei.

In the process of phase separation three stages: nucleation, the decomposition stage in which the compositions of the newly forming phases approach the equilibrium compositions, and the last stage which resembles the process of evaporation and condensation are occurred. At this stage the thermodynamic potential of the system becomes reduced through the reduction of the surface area of phase separation. This process proceeds by way of diffusion from the regions of higher concentration of the

dispersed phase into regions of smaller drops reduce their dimensions and disappear while the big ones are growing. The final result is the stratification of the liquid.

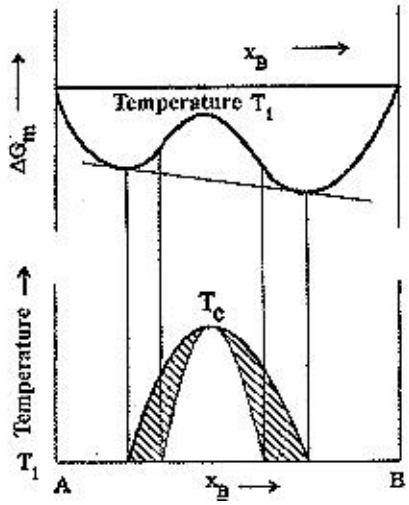

Fig.1

The nature of glass is that of an over-cooled liquid frozen without crystallization. Phase separation is a very frequent phenomenon in silicate melts. The best known phase separation systems are borosilicate and phosphate-silicate glasses.

The phenomenon of phase separation in glasses has its own special character. On account of great viscosity (small diffusion) the last stage of process is inhibited earlier. Thanks to it the glasses do not stratificate, but have a drop-like or sponge like nature. The macroscopic effect of this phenomenon is the opalescence or opacity. The phenomenon of phase separation undoubtedly affects several consisting of a matrix and a dispersed phase. The properties of decomposited glasses depend mainly on the chemical composition, their structure, mutual position and character of phases forming as a result of decomposition.

Most of the properties depend chiefly on this phase which forms the permanent skeleton and they change only slightly depending on the contents of the particular phases.

It is generally believed that phase decomposition is disadvantageous, however in certain cases it is a positive phenomenon. It could be is utilized in the production processes of silica glass, porous glass and glass-crystalline materials.

II. EXPERIMENTAL

Investigations of the phenomenon of phase separation in glasses were conducted using the basic system Na_2O-B_2O_3-SiO_2 and its modifications which consisted in the introduction of small amounts of aluminium, titanium and zirconium oxides.

T a b l e 1

Glass No	SiO_2	B_2O_3	Na_2O	Al_2O_3	TiO_2	ZrO_2
P1	70.0	23.0	7.0	-	-	-
P2	70.0	25.0	5.0	-	-	-
A1	58.0	31.7	10.0	0.3	-	-
A2	57.0	32.5	10.0	0.5	-	-
T1	57.0	32.5	10.0	-	0.5	-
T2	61.5	28.0	8.0	-	2.5	-
Z1	57.0	32.5	10.0	-	-	0.5
Z2	61.5	28.0	8.0	-	-	2.5

The chemical compositions of the examined glasses (in mole %) are given in Table 1.

The glasses were melted by the standard method at the temperature about 1400^{o}C and annealed at the temperature 520^{o}C. The glasses were undergoing thermal treatment at the temperature:575^{o}C, 625^{o}C and 700^{o}C for 4, 8 and 24 hours in order to induce the phenomenon of phase liquation and to examine the dependence of the advancement of the process on temperature and duration of treatment. After thermal treatment all glasses showed opalescence. Depending on the temperature and duration of treatment the opalescence varied from being visible with naked eye to so intense that the glasses became opaque assuming the colour of milk glass.

X-RAY DIFFRACTION

The occurrence of crystalline phases has not been observed in any of the examined glasses. Figure 2 shows illustrative diffractograms. There can be observed only two diffused bands in the angular range 2θ =15-35^o (with maximum at 20^o) and 2θ = 40-50^o (with maximum at 45^o). They are characteristic for the amorphous substances such as, in this case, the silica phase and borate phase.

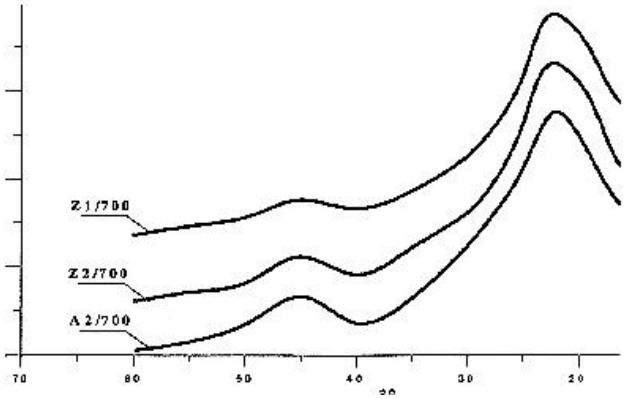

Fig.2. Diffractograms of selected glasses.

THERMAL DIFFERENTIAL ANALYSIS

DTA investigations have revealed the inability of the examined glasses to crystallize. Fig.3 shows, by way of example, DTA curves for glass A2 before and after thermal treatment. There appear on them two distinct endothermic effects connected with the transformation process: for borate phase at the temperature of about 445^{o}C and for silica phase at about 730^{o}C. Any greater differences between the curves for glasses subjected to various temperatures of treatment were not observed.

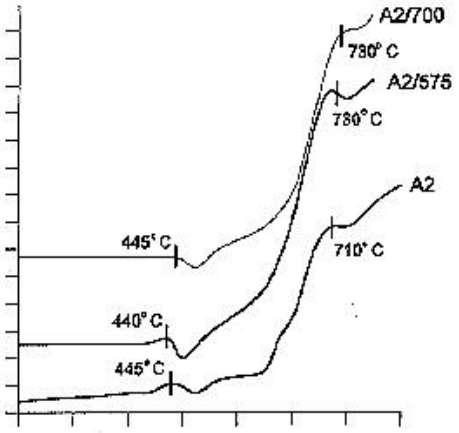

Fig.3. DTA curves for glass A2 before and after thermal treatment.

TRANSMITTANCE OF VISIBLE LIGHT

It has been found that with increasing temperature of thermal treatment of light transmittance diminishes until it vanishes completely. The absorption thresholds are also shifted towards longer waves. This is an indication of an advanced degree of liquation in this glasses with respect to the number and the size of the areas of heterogeneity. The obtained curves are consistent with the macroscopic observations of the glasses.

ELECTRON TRANSMISSION MICROSCOPY

The aim of investigations with the use of the electron microscope was the analysis of the relief of mapped surface by means of carbon replica. The character, shape, size and mutual position of the some heterogeneities in glass were the subject of analyzing.

Both types of disintegration, i.e. spinodal and binodal, have been observed in the examined glasses.

In Photo 1 there occur isolated, spherical particles of the dispersed phase. They reveal the tendency for a disordered state with respect to dimensions and positions in the matrix which is well visible. This glass shows the tendency for binodal phase decomposition. Non-spherical particles of the dispersed phase, with a high degree of interrelation and regular distribution what regards the size have been showed in the Photo 2. The boundary between the matrix and the regions of inhomogeneities is broadened and indistincted. This glass shows the tendency for spinodal phase decomposition.

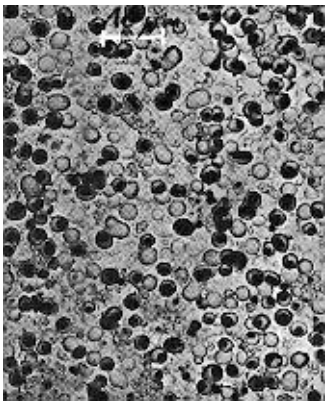

Photo.1. Glass T1/700/24, magn.1000x.

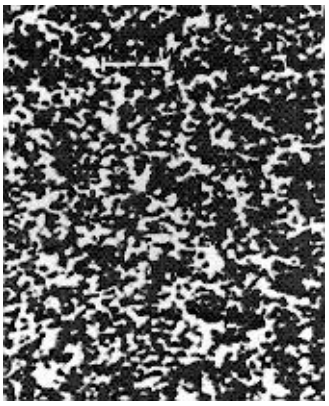

Photo. 2. Glass Z1/700/24, magn.1000x.

In glass A1/700/24 one can observe both types of decomposition (Photos 3 and 4). The spherical particles of the dispersed phase are clearly visible against the background of considerably matter, non-spherical regions of heterogeneities, connected with each other. In this glass the matrix is invisible.

In general, the heterogeneities occurring in the investigated glasses have a drop-like character. In some cases they show the tendency for coalescence (Photos 5, 6). The phenomenon of coalescence occurs in the cases of binodal and spinodal phase decomposition.

The extend of inhomogeneities varies from about 0,1 μm to 5 μm. Certain agglomerations, however, from areas of the order of 10 μm, and even larger, creating continuous chains (Photos 7, 8, 9).

The effect of temperature on the size of the regions of heterogeneity is visible in each of the examined glasses. It is shown by way of example on glass A1 (Photos10-16).

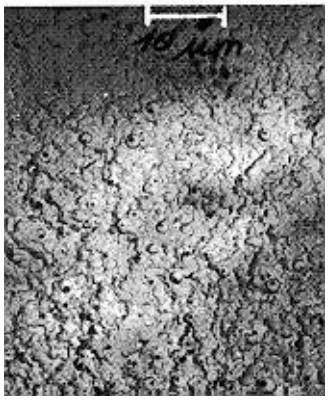

Photo. 3. Glass A1/700/24, magn.1000x.

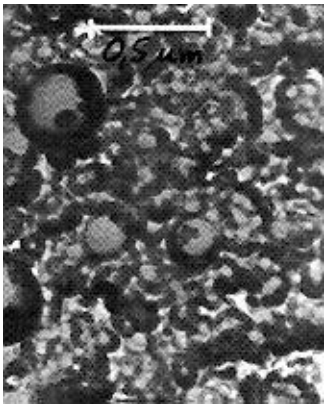

Photo. 4. Glass A1/700/24, magn. 30000x.

Photo. 5. Glass P1/700/24, magn.1000x.

Photo. 6. Glass A1/700/24, magn.1000x.

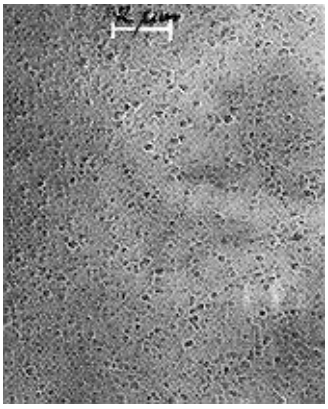

Photo. 7. Glass Z1, magn. 5000x.

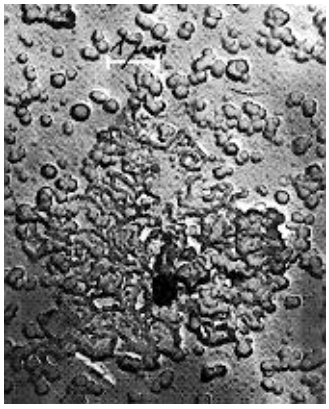

Photo. 8. Glass P1/700/24, magn. 9000x.

Photo. 9. Glass T1, magn. 9000x.

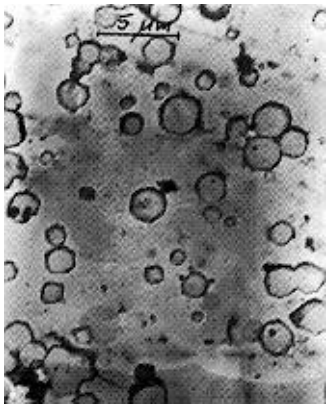

Photo.10. Glass A1/575/4, magn. 3000x.

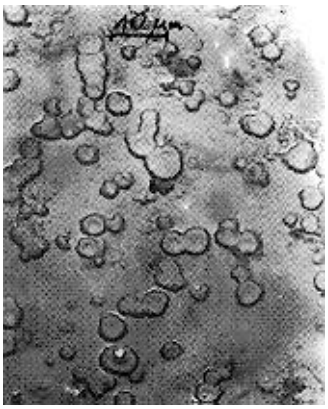

Photo.11. Glass A1/575/8, magn.1000x.

Photo.12. Glass A1/575/24, magn.12000x.

Photo.13. Glass A1/625/8, magn.16000x.

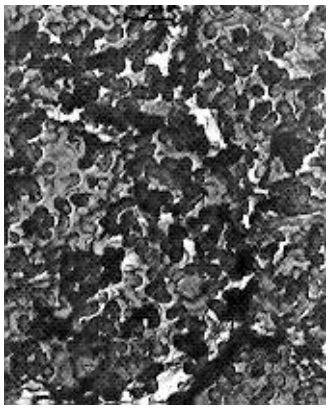

Photo.14. Glass A1/625/24, magn. 9000x.

Photo.15. Glass A1 /700/8, magn.1000x.

Photo.16. Glass A1/700/24, magn.12000x.

III. SUMMARIZING REMARKS

The process of phase decomposition in the examined glasses increases with the temperature and the duration of thermal treatment. It causes changes in the appearance of

glasses: from opalescence to complete opaqueness. This has been confirmed in the investigations of visible light transmittance (reduction of light transmittance till complete drop).

The glasses did not reveal the presence of crystalline phases (XRD and DTA investigations - Figs 2,3- and TEM investigations). Basing on investigations using the TEM method the occurrence of two types of phase decomposition: binodal (Photo 1) and spinodal (Photo 2) has been established, as well as a simultaneous occurrence of both types (Photos: 3 and 4).

Liquation inhomogeneities have a drop-like character, with greater density they show the tendency for coalescence. Their size depends on the chemical composition of the base glass and on the temperature of thermal treatment.

A smaller resistance of the silica phase to the action of hydrofluoric acid is observed. Particles of the borate phase show a positive relief.

Increased temperature of thermal treatment causes an increase of the phenomenon of phase decomposition and the increase of the possibility of simultaneous occurrence of both types of decomposition.

On the basis of the conducted investigations it can be said that temperature is the main factor affecting the phenomenon of phase decomposition in glasses, while the duration time of thermal treatment allows to observe the particular stages in the progress of this process.

References

[1] Balta P., Radu D., Spurcaciu C.: XVI International Congress on Glass, Madrid, vol.3,1992.
[2] Amal P.: Chemistry of Glasses, London-N. York,1982.
[3] Andriejew N.S., Mazurin O.W., Paraj-Koszic E.A.: Jawlenije likwacji w stieklach, Izd. ‘Nauka’ ,1974.
[4] Vogel W.: XI International Congress on Glass, Prage,1977.
[5] Zarzycki J.: Les verres et I'etat vitreux, Masson, Paris-N. York,1982.

LIQUID PHASE SEPARATION AND NUCLEATION IN GLASSES OF THE $MgO-ZnO-Al_2O_3-SiO_2-TiO_2$ SYSTEM STUDIED BY RAMAN SPECTROSCOPY AND SAXS METHODS*

Dong Soo Baik, O.S. Dymshits, V.V. Golubkov, M. Ya. Center, T.I. Chuvaeva**
S. I. Vavilov State Optical Institute, Russia
**Silicate Chemistry Institute, Russia

Abstract

It was found that the crystalline phases of (Zn, Mg) spinel and quartz solid solution could be selectively grown in glasses of the $MgO-ZnO-Al_2O_3-SiO_2-TiO_2$ system. This can be arranged by controlling the first stage of heat treatment, in which the liquid phase separation and the nucleation occur in glasses.

In order to understand the phenomenon, the processes of the liquid phase separation and the nucleation were studied by Raman spectroscopy and X-ray scattering at small angles (SAXS) methods. The glasses contained titania, zirconia and fluorine as nucleation agents and were heat treated in the temperature range from 680 to 800 C for 2-24 h. The regularities of phase separation and transformations in the phase separated regions were studied. On the basis of results of the study, the conclusion was drawn regarding the structural peculiarities and chemical compositions of those amorphous phases.

It was found that variation in heat treatment schedule bringing about the composition change of the phase separated regions led to variations in the character, the sizes and the amounts of the initial phases precipitated.

---

* Full manuscript not available at the time of printing

LOW - TEMPERATURE SPIN DYNAMICS OF Cu^{2+} IONS IN FLUORIDE AND OXIDE GLASSES

S. Sebastian[1], G. Scholz[1], R. Stöber[1], G. Jeschke[2], A. Schweiger[2], M. Nofz[3], T. Grande[4] and **S. Aasland[4]**

1. Humboldt University of Berlin, Germany
2. Swiss Federal Institute of Technology, Switzerland
3. Federal Institute of Materials Research and Testing, Germany
4. Norwegian University of Science and Technology, Norway

Abstract

Electron Spin Echo Envelope Modulation (ESEEM) spectroscopy has been applied for the first time to Cu^{2+} - doped fluoride and oxide glasses. Valuable information could be obtained about the spin dynamics and on the nature of the surrounding nuclei of Cu^{2+} ions using the findings of cw- and pulse EPR. The analysis of the ESEEM spectra of copper doped ZBLAN glasses yields for the neighbours of Cu^{2+} the nuclear transition frequencies of ^{19}F, ^{27}Al, ^{23}Na and ^{139}La. The low temperature spin dynamics is discussed in terms of contributions of local motions of structural subunits as well as spin-spin interactions of the paramagnetic species.

I. INTRODUCTION

In view of the outstanding optical and macroscopic properties on the one hand and the specific dynamics on the other hand, fluorozirconate glasses like ZBLAN (53% Zr_{F4}, 20% BaF_2, 4%LaF_3, 3% AlF_3, 20% NaF [mol%]) belong to the intensively investigated materials in industry and science. However, at present time no microscopic theory exists to describe the dynamic and static behaviour of these systems.

One way to get insight into the properties of glassy matrices is the investigation of the local structure of incorporated transition ions, e.g. Cu^{2+} ions, and their interactions with surrounding nuclei by cw-EPR spectroscopy [1]. As a rule, cw-EPR lines of disordered systems containing transition metal ions are usually inhomogeneously broadened. As a consequence, only a partial resolution of hyperfine and superhyperfine structures results. Methods to improve the spectral resolution of EPR spectroscopy are time-swept and field-swept electron spin-echo (ESE) experiments [2], e.g. electron spin echo envelope modulation (ESEEM), and electron nuclear double resonance (ENDOR) spectroscopy [3]. Especially ESEEM spectroscopy has become a promising method to identify the nuclei coupled to transition metal ions incorporated into phosphate [4], oxide [5] and borate [6] glasses. A further advantage of these methods comes from the fact, that they deal explicitely with the spin dynamics of the paramagnetic subsystems.

It is the intention of this contribution to figure out some characteristic differences in the glassy state between doped fluoride and oxide glasses using cw- and pulsed EPR methods. Typical low-temperature properties of glasses should be examined by time domain EPR measurements.

For the first time we could identify the neighbours of Cu^{2+} ions in fluoride glasses at different spatial areas in the neighbourhood of the paramagnetic species by the ESEEM spectroscopy in combination with field-swept ESE spectra at low temperature. Additionally, to estimate the contribution of nuclei to the spin-spin relaxation pathway, the phase memory time T_M has been determined as a function of copper concentrations.

The spin-spin relaxation time is known to be a sensitive parameter to detect slow motions in molecular systems. While the orientation dependence of the spin- spin relaxation has been determined in frozen solutions [7], there is no such report available concerning glassy states of inorganic materials. Therefore, this paper deals also with the investigation of the phase memory time T_M of Cu^{2+} ions in fluoride and oxide glasses measured at different magnetic field positions in the EPR spectrum.

II. EXPERIMENTAL

Materials - From a series of copper doped glasses two examples of fluoride (0.58mol% Cu2+, 0.06mol% Cu^{2+}) and of oxide glasses (0.66mol% $Cu^{2+,}$ 0.006mol% Cu^{2+}) have been investigated. The preparation of the fluorozirconate glasses ZBLAN (53ZrF_4, 20BaF_2, 4LaF_3, 3AlF_3, 20NaF [mol%]) and of oxide glasses (14.2K_20, 33.3CaO, 2.8 Al_2O_3, 49.7 $Si0_2$ (mol%)) has been described in [1] and [8].

cw-EPR spectroscopy - The equipment to measure cw-EPR spectra at low temperature T=4.2K and the procedure for complete simulations of the spectra of disordered systems has been described in [9].

Electron spin echo measurements - ESEEM and field-swept ESE measurements have been performed at temperatures between 3.5 and 30K using a home-built pulsed EPR spectrometer operating at ν~9.2 GHz [10). In the two-pulse sequence $\pi/2$-τ-π-τ echo, applied for both ESEEM and field-swept ESE, the pulse lengths have been optimized to reach maximum echo intensity. The time τ has been changed in increments of $\Delta\tau$=10-40ns. Instantaneous diffusion was excluded as a source of relaxation by varying the pulse lengths until the phase memory time T_M reached a constant value within an error of less than 10%. In order to get information regarding the orientation dependence of the signals ESEEM experiments were carried out at different external magnetic field positions of the echo-detected EPR powder pattern. Values of T_M were obtained by nonlinear least-squares fits of the decay data to the function $y=A\cdot\exp[-(\tau/T_M)^n]$ with n=1. Since ZBLAN glasses show strong echo envelope modulation the fit includes only the maxima of the modulation. To get the FT-ESEEM spectra, the Fourier transformation of the measured two-pulse ESEEM was performed after subtraction of the background relaxation decay from the experimental data. The theoretical basis for the interpretation of the echo modulations in glassy materials was developed by Mims et al [11].

III. RESULTS AND DISCUSSION

Fig.1 shows typical X-band cw-EPR and field-swept ESE spectra (ν≈9.1 GHz) for all glasses investigated. The g-values given in [9;14] correspond to axially elongated coordination polyhedra of the Cu^{2+} ions in both fluoride and oxide glasses ($g_{\perp}<g_{//}$)·

The spectra are characterized by remarkable differences in i) their overall shapes, and ii) their distribution of the static spin-hamiltonian parameters as determined by simulation [9;13;14]. Cw-EPR measurements on Cu^{2+} - doped fluoride and oxide glasses have shown that the tendency of Cu^{2+} ions to form aggregates depends on both the copper concentration and the properties of the glassy host material [9;14].

For all copper concentrations investigated at low temperature (T=4.2K) the intensity in the high-field region ($g_{\perp}$) of the field-swept ESE spectra is less than in the $g_{//}$ region (Fig.1b,e). This situation would be reversed by more effective relaxation at temperatures >10K (Fig.1 c,f). There is no increase in spectral resolution for Cu^{2+}- doped fluoride glasses as compared to the cw-EPR spectra.

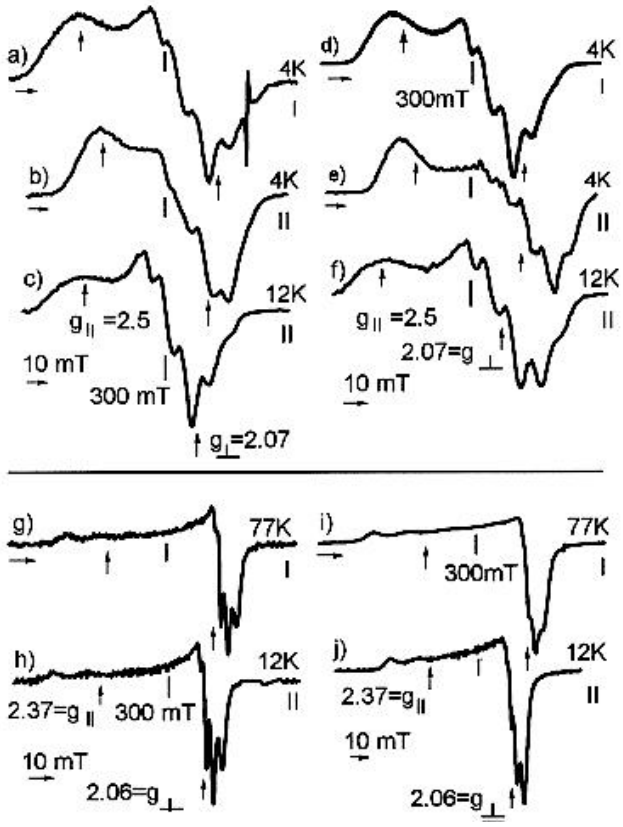

Fig.1 Comparison of experimental cw-EPR X-band spectra (I) and field-swept ESE spectra (II, obtained by numerical differentiation) at n~9.2GHz of Cu^{2+} - doped fluoride (a-c-0.06mol%, d-f -0.58mol%) and oxide glasses (g,h - 0.006 mol%, i,j - 0.66mol%). The arrows in the spectra indicate the field position of the g-values $g_{//}$ and $g_{\wedge}$ obtained by simulation in [9] and [14].

Also in oxide glasses, it can be stated that in view of the observed small modulation effects, the field-swept ESE spectra for the oxide glasses are very similar to the X-band cw-EPR spectra with one exception: There is a better spectral resolution of the hyperfine components in the $g_{\perp}$ region (Fig.1 g-j).

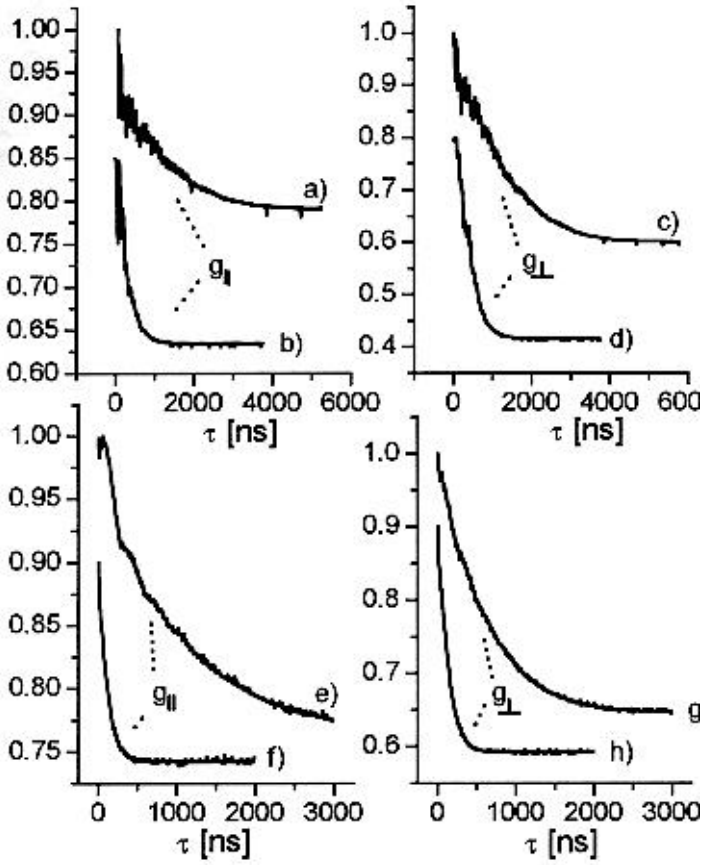

Fig.2 Experimental two-pulse ESEEM patterns of Cu^{2+} - doped fluoride (a,c - 0.06 mol%, b,d - 0.58 mol%) and of oxide glasses (e, g - 0.006mol%, f,h - 0.66mol%) at T=4K. The g-values ($g_{\wedge}$, $g_{/\!/}$) correspond to the observer position used in the ESEEM experiments.

Fig. 2 represents the two-pulse ESEEM patterns of Cu^{2+}-doped fluoride (a,c - 0.06 mol%, b,d - 0.58 mol%) and of oxide glasses/Cu^{2+} (e, g - 0.006mol%, f,h - 0.66mol%) taken at 4K. Since the whole echo decay can be fitted with one monoexponential function, the measured phase memory time TM can completely characterize the spin-spin relaxation. The echo modulation observed for fluoride glasses is mostly caused by the fluorine nuclei. The decrease of the modulation depth with copper concentration and the external magnetic field (going from $g_{/\!/}$ to $g_{\perp}$) can be explained as an effect of faster decay (Fig.2a,b;c,d). The substantial nuclear modulation (Fig.2a,c) is one reason for the observed differences between cw-EPR and field-swept ESE powder patterns (Fig.1 a-f) of

Cu^{2+} - doped fluoride glasses (2]. Caused by the short phase memory time TM for the investigated Cu^{2+} - doped oxide glasses only a small (s.Fig.2e-h) modulation effect was detected for the low copper concentration (0.006 mol%). In order to interpret the response of the three-pulse ESEEM experiments (not shown here), the observable oscillations were entatively assigned to the nuclear precession frequency ω_n of ^{27}Al.

Inspecting the FT-ESEEM magnitude spectra of Cu^{2+}- doped fluoride glasses, (Fig.3) the sum frequency (e) close to twice of the free Larmor frequency of fluorine are observed. This pattern is characteristic for disordered systems [15]. The free Larmor frequencies of ^{23}Na and ^{27}Al are hardly distinguishable ($\Delta\omega \approx 0.06$ MHz at B_o=3350G) and appear as an envelope peak (b). Finally, the peak (a) can be assigned to the free Larmor frequency of ^{139}La.

In principle, the strongly coupled fluorine nuclei detected with X-band cw-EPR [9] contribute to the ESEEM pattern. However, the large dipolar coupling between Cu^{2+} and ^{19}F in the first coordination
sphere causes a broadening which can not be detected in the time domain due to the spectrometer dead time. Additionally, from the absence of a peak above the sum frequency (e) it can be inferred that the ^{19}F nuclei detected by cw-EPR or field-swent ESE cover different spatial areas in the neighbourhood of the Cu^{2+} centres than the ^{19}F nuclei observed with ESEEM.

For the glasses studied in this work the phase memory time TM shows a temperature dependence, which is caused by fluctuations in the matrix (s. Fig.4). For all Cu^{2+} - doped samples studied in this work we bound that the relaxation time of the oxide glasses is shorter than for the fluoride glasses.

The increase of the phase memory rate $1/T_M$ with temperature and copper concentration (cf. Fig.4) indicates that spin-spin interactions are the dominating relaxation pathway. This can also be used to elucidate the observed decrease of the spectral resolution of the FT-ESEEM spectra (Fig.3) with increasing copper concentration.

The dependence of TM on the resonance field position B_o is given in Figs.5d,e and Figs.6d,e. One reason for the change of TM with the field position in the temperature region below T=18K originates from the anisotropy of the g tensors.

Using $dB_o/d\theta$ as a measure of the orientation dependence of the hyperfine (hf) couplings Figs.5c;6c, it follows from Figs.5c;6c and Figs.5d,e;6d,e that the observed field dependence of TM corresponds to the orientation dependence of the hf couplings. Regions of smaller $dB_o/d\theta$ (Fig. 5c; Fig.6c) belong to the longer relaxation times T_M, and vice versa. The anisotropy and distribution of the hyperfine couplings of all glassy materials studied cause an effective overlap of the individual transitions of the Cu nuclei. Therefore, the orientation dependence of T_M is indicated only in part for the m, = -3/2 and m, = 3/2 transitions. At higher copper concentrations the orientation dependence of T_M is obscured by more effective spin-spin interactions (Fig.6).

IV. CONCLUSIONS

FT-ESEEM magnitude spectra measured for the first time on fluoride glasses allowed the assignment of the transition frequencies of ^{19}F, ^{23}Na, ^{27}AI, ^{139}La. They are located in the neighbourhood but outside the first coordination sphere of the Cu^{2+} ions. The detection of the couplings with the fluorines in the first coordination sphere of Cu^{2+} was not possible by this non-stationary method because of the large dipolar couplings. Indication for the Cu-F interaction inside the coordination polyhedra was obtained by simulation of the cw-EPR spectra.

The phase memory relaxation times T_M showed a pronounced temperature ($T<35K$) and orientation dependence for both Cu^{2+} doped fluoride and oxide glasses. In both cases the observed field dependencies of T_M are in correspondence with the orientation dependencies of the hyperfine interactions.

As expected, the phase memory relaxation times are diminished with increasing copper concentration. Actually, they are lower for Cu^{2+} - doped oxide than for fluoride glasses even at very low Cu^{2+} concentrations (0.006 mol%). This is a dynamic expression of the macroscopically known differences of the two types of glasses.

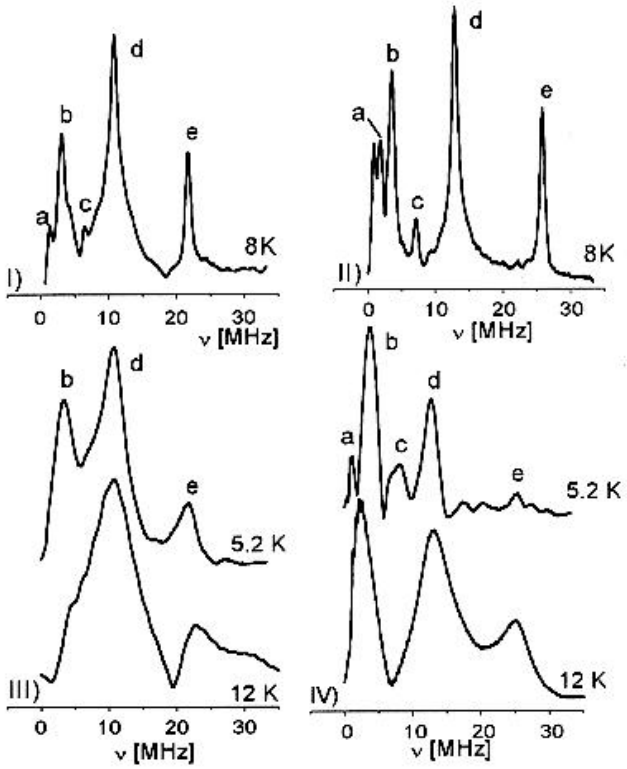

Fig.3 FT-ESEEM magnitude spectra of Cu2+ doped fluoride glasses with copper concentration of (I) 0.06 mol% at $g_{/\!/}$=2.5, (II) 0.06 mol% at $g_{\perp}$ =2.07, (III) 0.58 mol% at $g_{/\!/}$=2.5 and (IV) 0.58 mol% at $g_{\perp}$ =2.07. Peaks of nuclear frequencies are labelled by a : ν_{La}, b : $\nu_{Na/Al}$, C : $2\nu_{Na/Al}$, d : ν_F and e : $2\nu_F$.

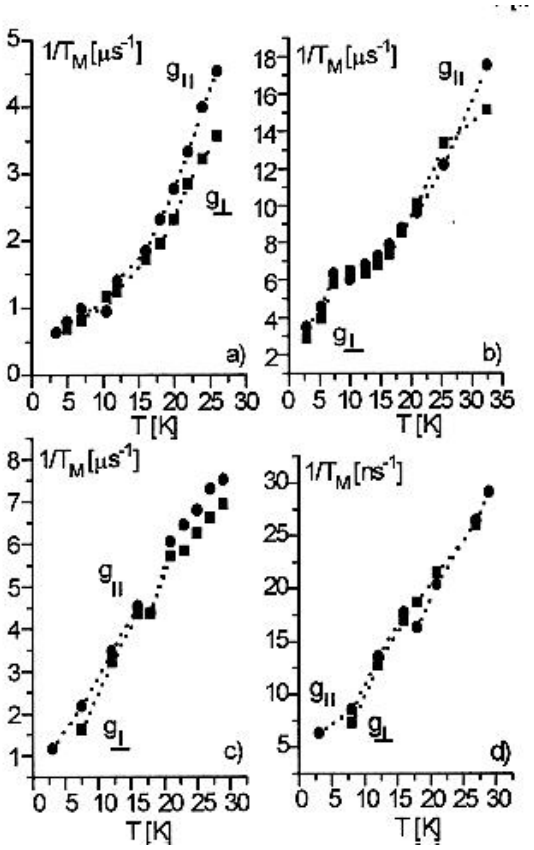

Fig.4 Temperature dependence of the phase-memory time TM of Cu^{2+} - ions in (a) fluoride glasses (0.06 mol%), (b) fluoride glasses (0.58 mol%), (c) oxide glass (0.006 mol%) and (d) oxide glass (0.66mol%) at different field positions

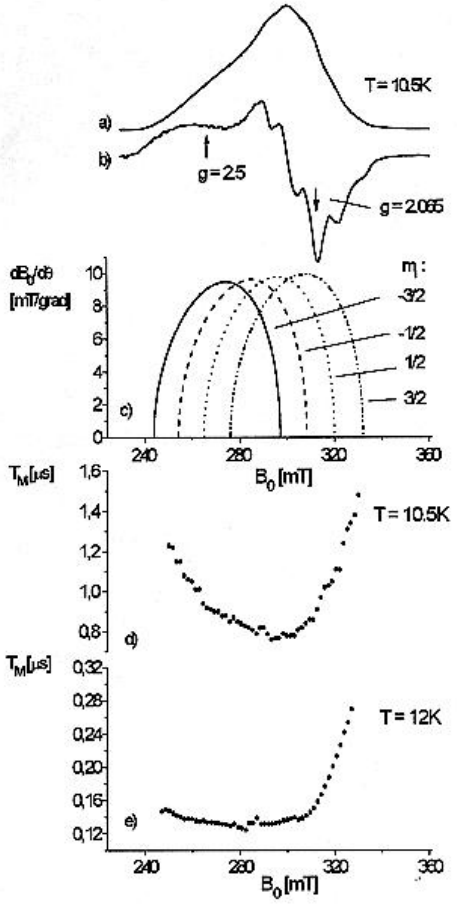

Fig.5 (a) Experimental field-swept ESE absorption spectrum of fluoride glass/Cu^{2+} (0.06 mol%) recorded at T=10.5K,(b) numerically differentiated spectrum of (a), (c) plots of dB_o/dq as a function of B_o for each of the individual transitions m, of the Cu nucleus. For computation of the resonance field (B_o) as a function of the angle (q) between the molecular z axis and the external magnetic field the simulation parameters were taken from the literature [9] ($A_{//}=A^F_{//}+A^{Cu}_{//}$; $A_{\wedge}=A^F_{\wedge}+A^{Cu}_{\wedge}$). (d) Field position dependence of T_M of Cu^{2+} - ions (0.06 mol%,(e) - 0.58 mol%) in fluoride glasses at T=10.5K (d) and T=12K (e), ν=9.1 GHz.

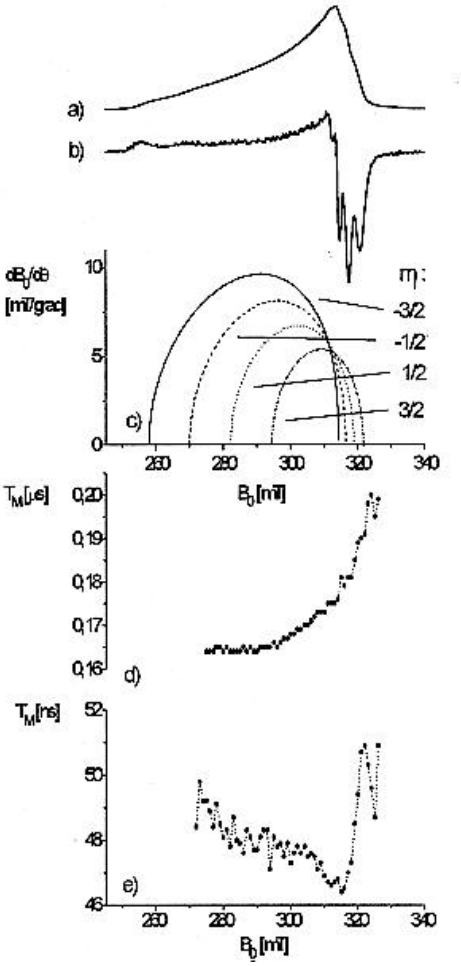

Fig.6 (a) Experimental field-swept ESE absorption spectra of oxide glasses/Cu^{2+} (0.006 mol%) recorded at T=10.5K, (b) numerically differentiated spectrum of (a),(c) plots of dB_o/dq as a function of Bo for each of the individual transitions m_1, of the Cu nucleus. For computation of the resonance field (Bo) as a function of the angle (q) between the molecular z axis and the Field external magnetic field the simulation parameters were taken from the literature [14]. (d) Field position dependence of T_M of Cu^{2+} - ions (0.006 mol% (e)- 0.66 mol%) in oxide glass at T=21 K and ν=9.1 GHz

REFERENCES

1. R. Stöβer, and M. Nofz, Glastech.Ber.GIass.Sci.Technol.67,156(1994)
2. D. Goldfarb, L. Kevan, J. Magn. Reson.76,276(1988)
3. A. Schweiger, AppI.Magn.Reson.5,229(1993)
4. I.A. Gromov, S.B.Orlinskii, R.M. Rakhmatullin, Yu. Rozentsvaig, Proceedings of XVII. Int. Congress on Glass Vol.2, Peking,527(1995)
5. K. Arai, S. Yamasaki, J. Isoya, H. Namikawa, VIII. Int. Conference on the Phys.0f Non-Cryst. Solids, Abstracts, Turku,52(1995)
6. W.B. Mims, G.E. Peterson, and C.R. Kurkjian, Physics and Chemistry of Glasses Vol.19(1),14(1978)
7. J.-L. Du, M.More, S.S. Eaton, G.R. Eaton, Israel Journal of Chemistry 32, 351(1992)
8. S. Aasland, T. Grande, and S. Julsrud, J. Non-Cryst. Solids 161,177(1993)
9. G. Scholz, R. Stoßer, S. Sebastian, T. Grande, S. Aasland, M. Nofz, Ber. Bunsengesellschaft (1996), in press
10. Th. Wacker, Ph.D.Thesis, ETH Zürich, No.9913(1992)
11. W.B. Mims, J. Peisach, J.L: Davis, J.0f. Chem. Phys.66(12),5636(1977)
12. A. Schweiger, J. Chem. Soc. Faraday Trans. 91(2),177(1995)
13. L.D. Bogomolova, V.A. Jachkin, N.A. Kasilnikova, V.L. Bogdanov, E.B. Federushkova and, V.D. Khalilev, J. Non-Cryst. Solids 125, 32(1990); E.A. Harris, Phys. Chem. Glasses 28(5),196(1987)
14. R. Stöβer, M. Nofz, G. Scholz, S. Sebastian, Molec. Phys. Rep.(1996) in press
15. W. Mohl, A. Schweiger, and H. Motschi, Inorg.Chem. 29,1536 (1990)

LOW TEMPERATURE ULTRASONIC ATTENUATION IN TELLURITE GLASSES

R. El-Mallawany, M. Sidky* and **H.Afifi***.
Menofia University, Egypt
*National Institute for Standards, Egypt

Abstract

The new semiconducting non-crystalline solid "tellurite glasses" of the form 0.7 TeO_2 -(0.3-x) V_2O_5 - xCeO_2 have been prepared in bulk form with different compositions. Longitudinal ultrasonic attenuation in these glasses has been measured at frequencies 2,4,6 and 8 MHz and in the temperature range 100-300° K. The results showed the presence of a very well defined peak which shifts to higher temperature with increasing frequency, suggesting a kind of relaxation process. The acoustic activation energy has been found to be strongly depend upon the value of the oxygen density in the glass. The ultrasonic loss is thought to arise from the thermally activated transitions of the bridging oxygen atoms from one minima in the two-well potentials. The number of cation-anion-cation units in unit volume has been calculated. So, the macroscopic activation energy could be correlated to the barrier height of the two-well potentials.

1- Introduction:

Considerable international progress has been made during 1990's both in the discovery of new tellurite glasses, and in knowledge of the optical & physical properties, structural & bonding nature of these glasses (1-25). The main justification for research in this field is the possibility of extending the infrared transparency domain towards long wavelengths and consequently achieving of mid IR ultratransparently. Tellurite glasses with high refractive indices are promising materials for photonic switches(4,5). TeO_2 -V_2O_5 - M glasses have the property of switching phenomena (3) where M= CeO_2, La_2O_3, Y_2O_3.

2- Experimental Work:

Mixtures of reagent grade TeO_2, V_2O_5, CeO_2 were placed in an alumina crucible. The glass was prepared by putting the batch in an electric furnace at temperature in the range of 700-800°C. To improve homogeneity the high viscosity melt was stirred a few times. The melt was then cast into a heated steel mold followed by annealing at 250°C for 1 h. The ultrasonic attenuation of each sample was measured for the longitudinal waves at the frequencies 2,4,6 and 8 MHz in the temperature range 120-300 K. A cryostat arrangement with liquid air was used to cool the sample. The sample with the bonded transducer was mounted on a sample holder and placed inside a chamber. The temperature was checked by a thermocouple placed in direct contact with the

sample. The pulse echo technique was the method used for the measurements as descried before(22).

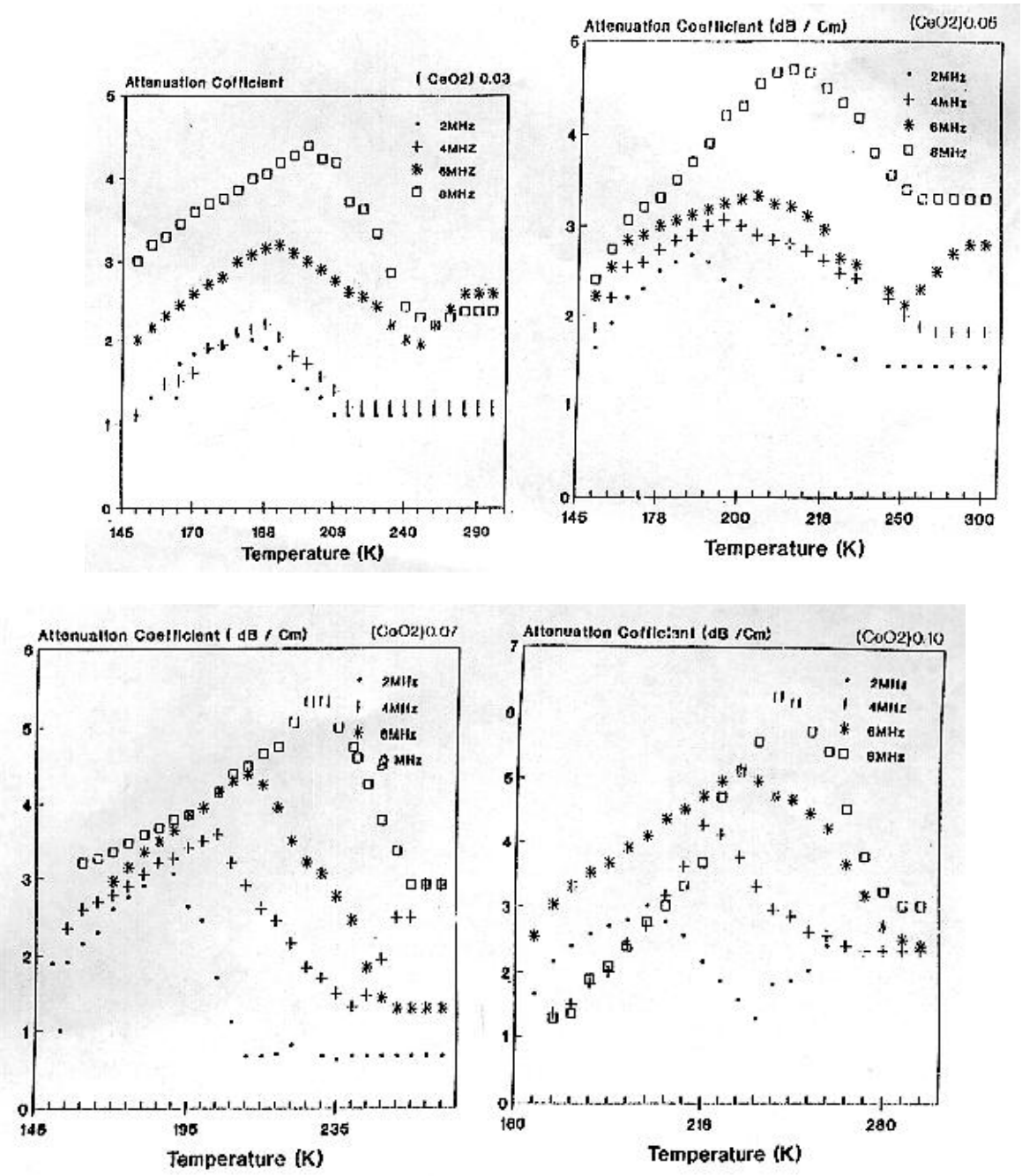

Fig. 1 : Absorption Coefficient a for TeO_2-V_2O_5-CeO_2 glasses in the temperature range 140 - 300 K.

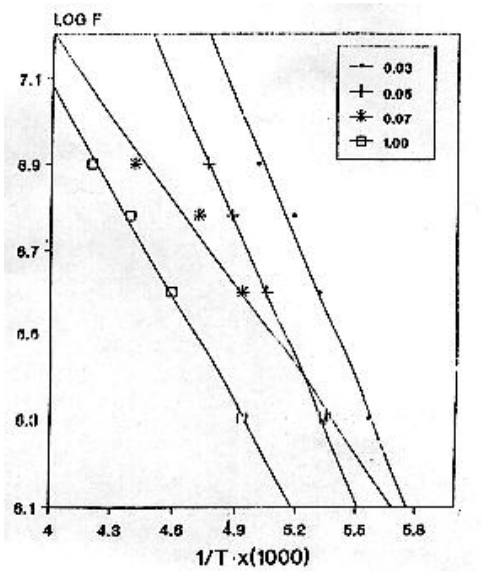

Fig. 2 : Variation of (1/Tp) against log f

3- Results and Discussion:

The attenuation coefficient of each sample is given by: α=(20 log h1/h2)/2x, where x is the length of sample and h1, h2 are the heights of the first and second echoes respectively. The ultrasonic absorption α vs. temperature for all samples are shown in Fig. 1. The peak occurs at temperature ranging 180-238 K depending upon the sample composition and frequency. For each sample the attenuation, especially at the peak temperature, increases with the frequency. The peak temperature shifts to higher values for higher frequencies. Table 1 summarizes the values of the attenuation at the peak temperature for all samples. Plots of log frequency (f) against inverse peak temperature ($1/T_p$) yield straight line as shown in Fig. 2. It is clear from fig. 2. that the present glass fit an equation of the form $\omega\tau_0 \exp(E/kT)=1$. From the slope and intersect of these lines the activation energy E and attempt frequency f_0 have been calculated in Table 1.

The present analysis of ultrasonic attenuation at low temperatures of these glasses is based on the fact that in all noncrystalline solids (Glass) there is a distribution of the thermally averaged cation-anion-cation spacings about the equilibrium values. It has been reported(26) that there would exist two-well systems with a distribution of barrier heights (activation energies) for both longitudinal and transverse vibrations of the anions (oxygen in the present glass) as shown in Fig. 3.

The relaxation process can be described to a particle moving in a double-well potential and the sound wave disturbs the equilibrium and produce a relative energy shift between the minimum if the two wells by an amount ΔE. According to the Debye relation (27,28), the absorption coefficient is given by

$$\alpha = n A \{\varpi^2 \tau(V) / (1 + \varpi^2\tau^2(V)\} \qquad (1)$$

Comp.	f (MHz)	α (dB/Cm)	A*10-6	Tp (K)	f_o (sec-1)	E (ev)	F N/m	n *10^{28} m^{-3}
0.03	2	2.06	3.7	180	2.66	0.095	234	6.21
	4	2.22	4.0	188				
	6	3.20	5.8	193				
	8	4.40	8.1	200				
0.05	2	2.68	3.76	188	1.05	0.092	229	6.12
	4	3.06	4.29	198				
	6	3.32	4.66	205				
	8	4.70	6.59	210				
0.07	2	3.20	3.88	187	0.66	0.056	224	6.4
	4	3.59	4.35	203				
	6	4.40	5.34	212				
	8	5.33	6.46	227				
0.10	2	3.00	2.05	203	0.20	0.049	216	6.41
	4	4.26	2.91	218				
	6	5.13	3.51	228				
	8	6.24	4.27	238				

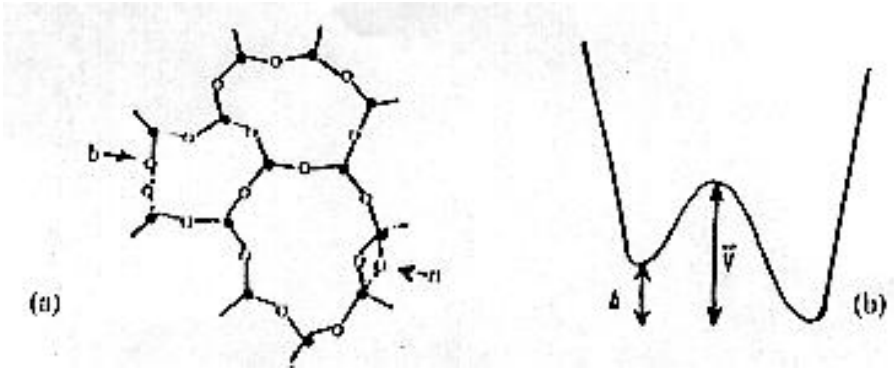

Fig. 3 : Schematic two-dimensional representation of longitudinal and transverse vibrations of the amorphous solids.

where n is the number of relaxing particles per unit volume which (calculated from the chemical formula for each glass) which increased from 6.21 to 6.41*10^{28} m^3 for the change of CeO_2 from 0.03 to 0.10 mol %, A is the relaxation strength is given by:

$A = 2\alpha_{max} V L / \pi f_0$, VL is the sound velocity (29). The relaxation strength has been increased due to increase in the frequency for each sample. While the attempt frequency has been decreased from 2.66 to 0.2 Sec.$^{-1}$ for higher CeO_2 in the glass. So, the higher number of vibrating anions is the present glass is responsible for the attenuation. The decrease in the experimental values of activation energies from 0.095 to 0.049 eV for higher CeO_2 could be attributed to the decrease in the value of the average force constant in the glass due to the presence of CeO_2 from 234 to 216 N/m.

4- Conclusions:

The maximum absorption of ultrasonic waves that propagated in a noncrystalline solid (tellurite glasses) at low temperatures has been analyzed quantitatively according to the increase

in the number of oxygens. The values of the acoustic activation energy (activation energy of anion atoms in the two-well system) depends upon the value of the cation-anion force.

References

1- S. Kim and T. Yoko, J. Am. Ceram. Soc., 78(4) 1061-65 (1995)
2- S. Kim, T. Yoko and S. Sakka, ibid, 76(10) 2486-90 (1993)
3- Y. Dimitriev, M.Marinov and E. Gatev, C.R. Acad, Bulg. Sci., 26,675 (1973)
4- R. El-Mallawany, J. Appl. Phys. 72(5), 1774 (1992)
5- H. Takebe, S. Fujino and K. Morinaga, J. Am. Ceram. Soc., 77(9) 2455-57 (1994)
6 -R. El-Mallawany, L.S. El Deen and M. Elkholy, accepted for pub. J. Mat. Sci. (1996)
7- R. El-Mallawany, J. of Mater. Sci.: Materials in Electronics, 6,1,6 (1995)
8- M. Elkholy and R. El-Mallawany, Mater. Chem. and Phys. 40,163 (1995)
9- R. El-Mallawany, A. El-Sayed and M. A. Gawad. ibid, 41,87 (1995)
10- M.Sidky, R. El-Mallawany, R. Nakhla and A.A. Moneim, 17. Inter. Congress on Glass, China, Vol. 3, 714 (1995)
11- Idem, accepted for publication J. Non Crystalline Solids (1996)
12- R. Singh and J. Chakravarthi, Physical Rev. B.51,22,16396 (1995)
13- S. Suehara, K. Yamamoto, S. Hishita, T. Aizawa, S. Inoue and A. Nukui, Physical Rev. B. 51,21,14919 (1995)
14- K. Tanaka, K. Kashima, K. Hirao, N. Soga, A. Mito and H. Nasu, J. Non-Crys. Solids 185,123, (1995)
15- T. Sekiya, N. Mochida and S. Ogawa, ibid, 185,135 (1995)
16- S. Tagg, R. Youngman and J. Zwanziger, J. Phys. Chem, 99, 5111 (1995)
17- I. Shaltout, Y.Tang, Y. Braunstein and A. Abu-Elazm, J. Phys. Chem. Solids, 56,141 (1995)
18- M. Elkholy, J. Mater. Sci. Lett. in Elec. 6,404 (1995)
19- H. Mori, J. Igarashi and H. Sakata, Glastech. Ber. Glass Sci. Tech. 68,10 (1995)
20- T.Sekiya, N. Mochida, A. Soejind, J. Non-Crys. Solids, 191,115 (1995)
21- A. Abel-Kader, R. El-Mallawany, M. Elkholy and H. Farag, Mater. Chem & Phys. 36,365 (1994)
22- R. El-Mallawany, M. Sidky, A. Khafagy and H. Afifi, ibid, 37,197 (1994)
23- Idem, ibid, 37,295 (1994)
24- R. El-Mallawany, ibid, 37,376 (1994)
25- Idem, ibid, 39,161 (1994)
26- B. Bridge and N. Patel, J.Mat. Sci., 21,3783 (1986)
27- S. Hunklinger and M. Schickfus in W.A Philips (ed.), Amorphous Solids Low temperature properties, Springer, Berlin,1981, p81
28- J.Jackel,L.Piche, W.Arnold and S. Hunklinger, J. Non-Crys. Solids, 20,365 (1976)
29- R. El-Mallawany, M.Sidky and H.Afifi, to be published.

MECHANISM OF SPHERULITIC CRYSTALLIZATION IN CaO-Al_2O_3-SiO_2-R_2O-F GLASSES CONTAINING CHROMIUM*

Teng Lidong, Zhang Xiaokai* and **Chen Xiaofeng**
Shandong Institute of Light Industry, China
*Shandong Normal University, China

Abstract

The effects of Cr_2O_3 on the nucleation and crystallization of CaO-Al_2O_3-SiO_2-R_2O-F system glasses have been investigated by means of ESR, STEM, EDAX, SADP, XRD, DTA and so on. The base glass composition was approximately 22.0 CaO, 7.0 Al_2O_3, 59.0 SiO_2, 6.0 R_2O, 2.0 F_2(wt.%). Cr_2O_3 has been incorporated in the glass with-in the range 0.5-2.5 wt.%. The experiments show that the parent glass containing more than 1.5 wt.% Cr_2O_3 can be nucleated internally and converted to spheroidal crystal glass materials. The spherulite diameter ranged from 2 to 4 mm, depending upon the heat treatment schedules. The spherulites were made up of fibrous wollastonite crystals radiating from a center. The residual glass phase filled in the interstices between the wollastonite fibres and between the spherulites. EDAX analysis proved that the centre composition was rich in Cr^{3+} and Ca^{+2}. In the base glass melted under oxidizing conditions chromium can simultaneously exist in the form of Cr^{6+}, Cr^{5+} and Cr^{3+}, but Cr^{6+} ions were predominant. During heat treatment process, the valence states of chromium changed from Cr^{6+} to Cr^{3+}, and the Cr-spinel solid solution [(Ca Ba Zn)Cr_2O_4] precipitated following this change. This result has been verified by ESR and EDAX spectra. AT the primary stage of crystallization, the Cr-spinel could act as a nucleating center on which the principle crystalline phase β-$CaSiO_3$ grew epitaxially. The close similarity of lattice parameters in some dimension of Cr-spinel and β-$CaSiO_3$ made it possible to nucleate heterogeneously. The microstructure of spherulite depends on the glass composition and heat treatment schedule. The large spheroidal crystals inlaid the glass matrix and formed beautiful patterns after the sample surface had polished. Because of the polycrystalline structure of this materials, their mechanical strength is higher than that of glass. This new kind of material by the name of Macrocrystal Glass can be used as building materials in place of marbles or granites.

---

* Full manuscript not available at the time of printing

MICRO-DEFECTS ON GLASS SURFACE TO BE DETECTED BY THE POLISHING

Toshio Kasai, Kenichiro Horio, Tsugio Yamazaki and Toshiro K.Doy [1)]

Faculty of Engineering, Saitama University, Japan
[1)]Faculty of Education, Saitama University, Japan

Abstract

Since there are a great number of imperfections such as inherent defects and heterogeneity on a multi-component optical glass that has a desired refractive index, it has been often found difficult to produce a flat planar surtace even under the mirror-finish processing conditions.

In this report the differences of machined qualities resulted from applying various polishing conditions have been compared and discussed. Using an oil-type polishing slurry of low removal efficiency, defect or heterogeneity on th e glass surfaces were clearly detected whereas these defects have become less defined when water-type slurry was used. There was, however, found to be a powerful water-type slurry to reveal the defect in a lot of slurrys.

1. INTRODUCTION

When a heterogeneous material is polished, the amount of material removed at weak point is larger than that around it and digs or pits may be left on the polished workpiece. For example, the surtace roughness of polished zirconia ceramic with a chromium oxide powder slurry and an acetate fiber polisher was found to become 0.2 ,u m Ry, having many digs or pits formed with rounded edges and centered on pores in spite of glossy surface.

There may be also a great many defects on a polished glass surtace, ranging in size from atom order to millimeter order, i.e., defects inherent in the material, defects due to polishing and defects from previous working. It is never easy to discern defects inherent in the material from others, especially micro defects as revealed in mirror polishing.

In this report, a polishing method for revealing micro-defects on optical glass surface will be described, and the material removing mechanism in polishing will be discussed.

2. EXPERIMENTAL PROCEDURE

Polishing conditions are shown in Table 1. Glass as work material was cut to six of 10 mm cubes which were waxed at regular intervals on the outside circumference of a flat stainless steel plate 60 mm diameter x 10 mm thick.

In order to obtain a mirrorlike or smooth surface on glass work, a conditioning ring type polishing machine, as shown in Figure 1, were used with a conventional cerium oxide slurry suspended in distilled water and pitch polisher. On the other hand, for revealing inherent defects

or heterogeneity on work a newly proposed polishing slurry and polyurethane fiber polisher were adopted. Polishing slurry and polyurethane fiber polisher were adopted.

In the evaluation of polished surfaces, a stylus-type three-dimensional surface roughness measuring instrument (Kosaka Laboratory Ltd.) and an optical-type instrument (Zygo Ltd.) were used.

3.RESULTS AND DISCUSSIONS

3. 1 Influence of Dust and Polisher for Surface Quality

Examples of surface roughness profiles of polished glass is shown in Figure 2 (a), (b) and (c). First pitch-polished surface with cerium oxide slurry is of course smooth as shown in Figure 2 (a). With such conventional optical glass polishing, a mirrorlike surface having a fairly high quality can be satisfactorily ensured.

In order to finish superior surface, every mechanical action including the useful material removing actions must be small. Figures 3 (a) and (b) show a basic model concerning mechanical actions. Presuming the existence of a remarkably large grain, as shown in Figure 3 (a), it will be forced into the work and polisher faces corresponding with the indentation hardness on each and will make rubbing tracks on the works. Surface roughness is formed by the crossing of such tracks and if will be in direct proportion to the grains diameter d, indentation hardness of the polisher material Hp and in inverse proportion to indentation hardness of the works Hw. This implies that a soft polisher will reduce the deterioration of surface smoothness, if an unfortunate large abrasive or dust particle is encountered.

On the other hand, considering the fine irregularity of a polisher surface and in spite of very fine abrasives, as shown in Figure 3(b), such irregularity of polisher surface will form surface roughness on the work. Small ups and downs on the polisher face will generate irregular polishing pressure Δp, when close-contacting the work surface under a suitable weight loading W. Since material removal is in proportion to polishing speed v, pressure p and time t in normal polishing, surtace roughness is formed by the crossing of the paths of finely irregular pressure, and in direct proportion to the height of the irregularity hp and in inverse proportion to the polisher elastic deformation constant ξ.

It is not easy to get a satisfactorily smooth face polisher for high level polishing. However, a pliable material which shapes itself to correspond with a workpiece during working can be useful as a polisher. For instance, the approach using pitch polisher seems to be satisfactory in the final stage of polishing.

3.2 New Polishing Condition to Detect Material Micro Heterogeneity

Although the optical glass as multi-component glass was heterogeneous materials, fairly smooth surface could be obtained by applying pitch polishing. Considering the mechanism of stock removal or formation of surface roughness in polishing, abrasive powders, solutions and polishers will be pointed out as important factors.

Figure 2 (b) and (c) show surface roughness profiles on polished glass with cerium oxide slurry suspended in silicone oil and polyurethane fiber polisher. With increasing polishing time, the smooth polished surface as shown in Figure 2(a) changed into the defective surtace. Digs or pits seem to grow with rounded edges around micro defects as polishing advances and to take on a new appearance. There are no scratches or indentations due to abrasives or dusts.

Cerium oxide powder slurry suspended in water has been superior ability to polish optical glass. Formation and removal of soft hydration film during polishing process seem to be carried on and to be profitable for ensuring smooth surface and large stock removal in such polishing condition. Although the use of fine abrasive powders and soft polishers has been effective for obtaining a high level mirrorlike surface, the influence of solution in slurry for surface quality cannot be ignored as shown in Figure 2 (a), (b)and (c).

This implied that the weak parts on a glass surfaces, namely micro defects, are attacked by the polishing slurry, and that similar results may be obtained by replacing a superior solution for material removal, namely water, by inferior silicone oil.

Figure 4 shows the result of surface roughness on polished BK7 glass under similar condition. Appearance of digs or pits was not remarkable though 4 hour elapsed for polishing. It seemed to be long and to be hard because silicone oil was used. For improvement of such polishing condition, water-type polishing slurrys was examined.

Since an effective slurry to reveal defects and heterogeneity on glass was inferior in material removal, 0.06μm γ-Al_2O_3 slurry suspended in pure water was adopted. Figure 5 and 6 show surface roughness on BK7 glass after only 5 minutes elapsed. New water-type slurry distinguishes oil-type slurry in the texture of polished surfaces. It seems to form hillocks or small projections at rather short time. There are different mechanisms in material removal between these polishing slurry conditions.

4.CONCLUSION

In polishing optical glass, a conventional polishing with cerium oxide slurry and pitch-polisher was adopted and discussed to ensure high quality mirror surfaces. In order to reveal inherent defects or heterogeneity on the glass, it was important to adopt an abrasive powder or suspending solution with an inferior ability for material removal. Newly proposed polishing slurry using silicone oil could attack the weak part as digs or pits appeared. On the other hand, polishing slurry of 0.06 μm γ-Al_2O_3 powder and water-type solution could form hillocks or small projections at rather short time. There seem to be different mechanisms in material removal between both polishing slurry conditions.

Table 1 Experimental conditions

Work	optical glass (CdFD3, BK7)
Abrasive powder	cerium oxide powder

	0.06μc m γ-Al_2O_3 powder
Polishing solution	silicon oil (300 cSt,3*10^{-4} m^2 /s)
	pure water
Polisher	pitch polisher
	polyurethane fiber polisher
Polishing machine	conditioning ring type polishing machine
Polishing speed	13-17 m/min
Polishing pressure	3-13 kPa
Surface roughness	stylus method (Kosaka)
measuring instrument	optical method (Zygo)

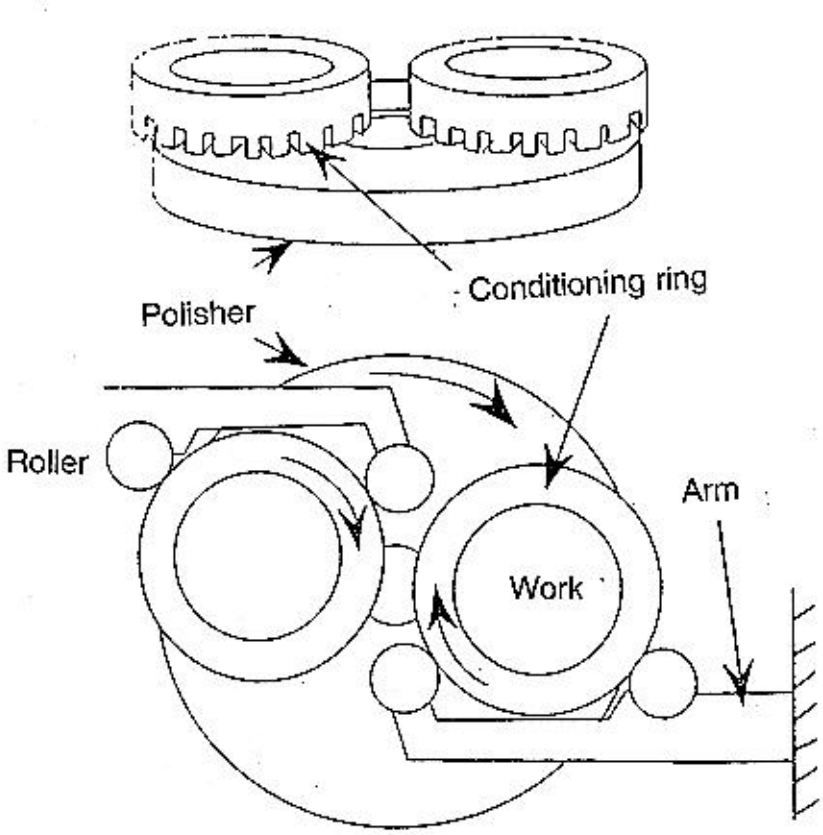

Figure 1 Conditioning ring type polishing machine

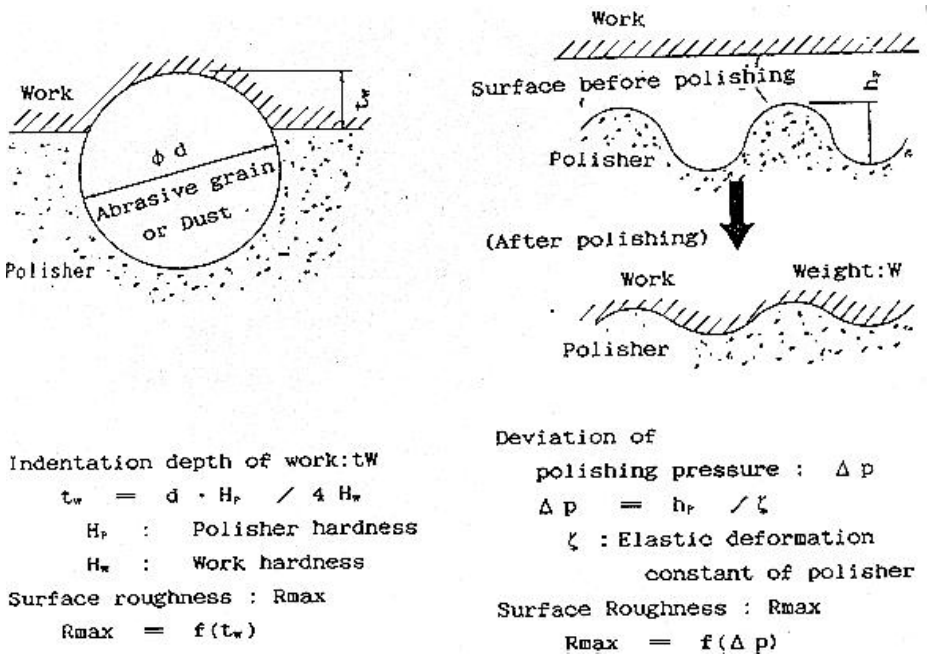

(a) (b)

Figure 2 State of polished optical glass surface (CdFD3) under specific polishing condition for revealing micro-defect: (a) after smooth polishing; (b) 1 h elapsed in detec trevealing polishing; (c) 4 h elapsed.

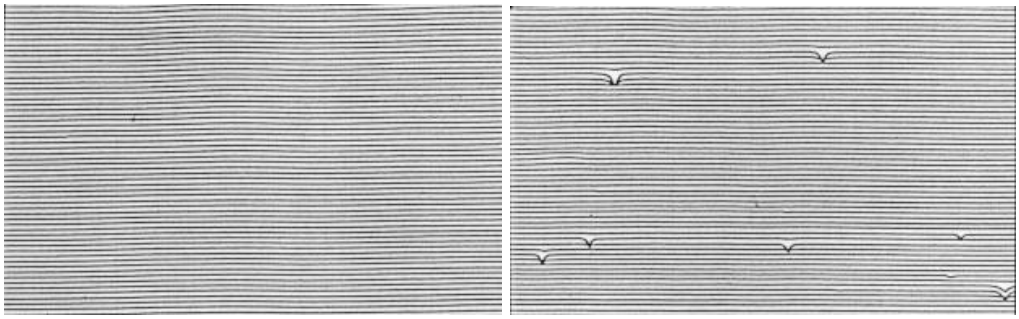

a) After smooth pol i shing (b) 1 hour elapsed in defect revealing polishing

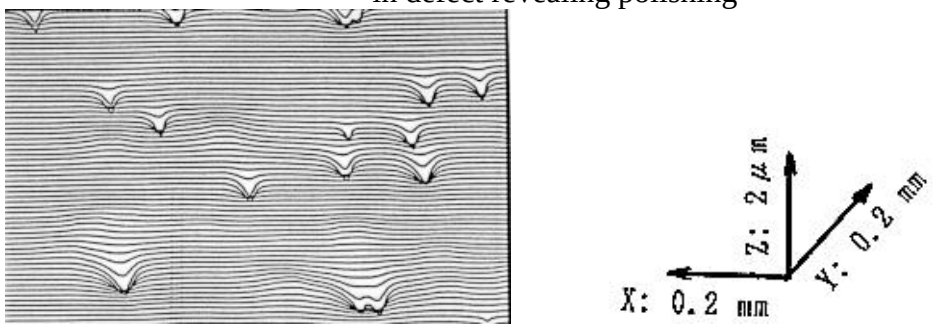

(e) 4 hours elapsed

Figure 3 Basic formation models of surface roughness: (a) relation between work, polisher and abrasive or dust; (b) relation between surface texture of polisher and irr egularity of polishing pressure.

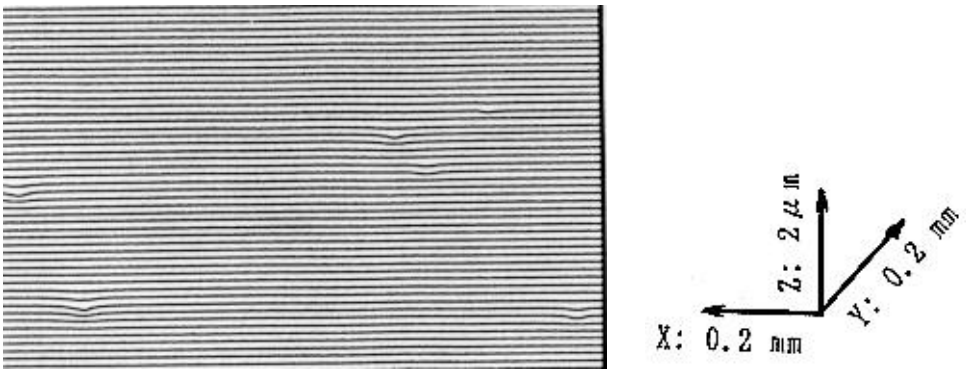

Figure 4 Surface roughness of polished optical glass (BK7) with oil-type slurry.

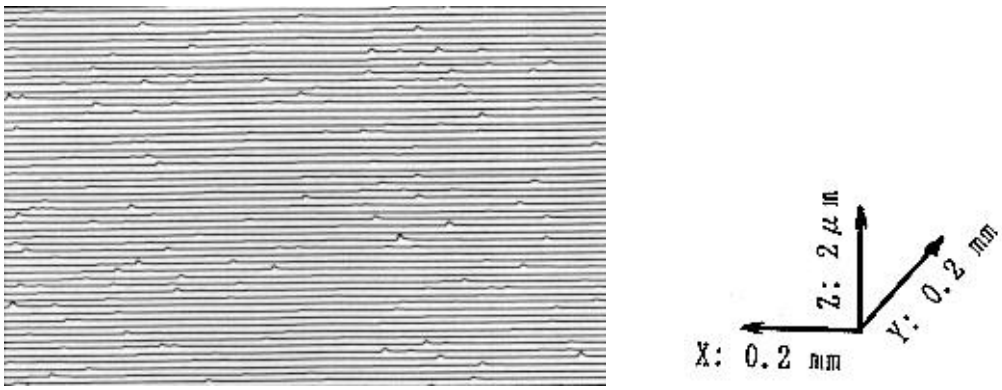

Figure 5 Surface roughness of polished optical glass (BK7) with water-type slurry.

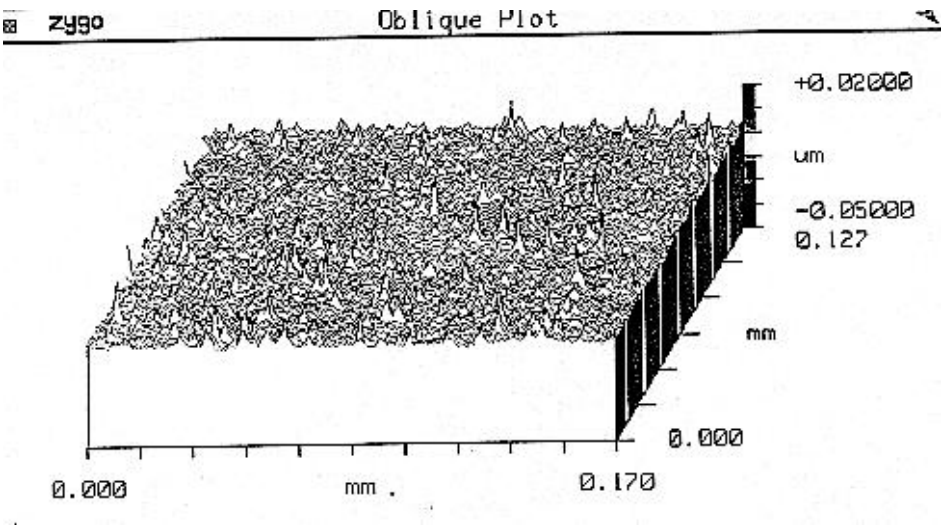

Figure 6 Tree-dimensional surface roughness of optical glass (BK7)

MIXED ALKALI EFFECT ON DENSITY, REFRACTIVE INDEX AND RELATED PROPERTIES OF ALKALI BORATE GLASSES*

N.A. SHARAF
Tanta University, Egypt

A.A.AHMED and **A.F.ABBAS**
National Research Center, Egypt

Abstract

The density and refractive index of single and mixed alkali boratic glass systems have been measured and used to calculate the molar volume, molar refractivity and molar refraction of oxygen ion in order to investigate the configurational changes that might be induced in the glass structure, as the constituent alkali ion is gradually replaced by another, keeping the total alkali content constant. Three alkali borate glass systems [$R(Na_2O\text{-}Li_2O)B_2O_3$; $R(K_2O\text{-}Li_2O)\ B_2O_3$ and $R(K_2O\text{-}Na_2O)B_2O_3$ in addition to the simple binary lithium, sodium and potassium borate glasses have been measured over the range of $O < R = 35$ mol% alkali oxide. The properties of single alkali borate glasses exhibited systematic variations with the glass composition. The mixed alkali borate glasses containing up to 15 mol% total alkali oxide did not exhibit any deviation in their property-composition relations. A slight positive deviation from linearity in the plots of density against composition was observed for glasses containing 20 mol% ($K_2O\text{-}Na_2O$). The deviation increased with increased with increasing alkali content reached a maximum value in the case of glass containing 30 mol% ($K_2O\text{-}Na_2O$). The results did not reveal a configurational change in the glass structure. The results are consistent with a view of the structure in which a constant boron-oxygen frame work is maintained independent of the alkali type. This view suggests that the observed deviation results from the intractions between dissimilar alkali ions rather than a structural rearrangement of the local glass network.

---

* Full manuscript not available at the time of printing

MIXED GLASSFORMERS & MULTIMODE VIBRONIC SPECTRA*

Alexander Chikovsky
S.I. Vavilov State Optical Institute, Russia

Abstract

This paper demonstrates unique opportunities of Vibronic Spectroscopy in the study of complex glassy systems. There are reported vibronic spectra of Rare Earth ions (Eu^{3+}) in oxide glasses based on mixed glassformers which were couples of both traditional glassforming oxides (B_2O_3, P_2O_5, SiO_2, GeO_2, TeO_2) and conditional ones (Nb_2, WO_3,BiO_3) mixed in different proportions. There were the following intriguing results:

. vibronic spectra of mixed glasses demonstrated multimode behaviour; for the first time vibronic sidebands of conditional glassformers (Nb_2O_5, WO_3, Bi_2O_3) were registered

. causes of such a behaviour differed from vibrational ones; this effect may be used for study of the Rare Earth's distribution all over matrices of complex glasses.

. for glassformers may be proposed some peculiar scale of capture ability realive to Rare Earths

. sometimes Rare Earth's distribution in such hosts differed from statistical one, i.e. RE ions demonstrated a strong tendency to be accepted in a certain surrounding

. It was shown that data obtained from vibronic spectra of one glass may be used for some predictions about the role of the studied component in other glasses; i.e. vibronic data possess a peculiar transferability

---

* Full manuscript not available at the time of printing

NEW ELEMENTS AND ARRAYS ON THE GLASS SURFACE PRODUCED BY ION-EXCHANGE AND LASER BEAM TECHNOLOGY*

Tat'yana V. Bocharova and **Garegin O. Karapetyan**
Saint Petersburg State Technical University, Russia

Abstract

Ion-exchange is common for fabrication of gradient-index rod lenses. But at present a new application of molar volume change in conjunction with laser radiation resulting in crystallization of exposed region and formation of spherically shaped protrusions and hollows on the surface has been developed. Thus mirolens arrays abd devices for optoelectronics are manufactured.

It should be emphasized that silver ion-exchange under low-temperature conditions in glass causes the development of photosensitive superficial layer. Elaborated thermal-temporal schedules result to creation of optical elements with given crystalline surface relief. Unexposed non-crystalline region of glass bulk can be used as a gradient-index medium.

Diffusion processes in activator-doped glasses open up a new filed of their application. The diffusion of copper in alkalisilicate glasses from a salt melt forms thin layer connected with $Cu^{(2+)}$ ions at the depth of 5 mm. The UV radiation is absorbed within superficial layer. The diffusion of Cu(+) ions leads to the appearance of luminescent layer at the depth of 100-180 mcm. This technique can be used for fabrication of luminescence screens with high spatial frequency.

Two-stage ion-exchange diffusion connected with penetration of Li (+) ions can be carried out in sodiumsilicate glasses. It yields microcracks on a glass surface and frosted glass. Glass sample is easily impregnated with d-elemens ions from a salt melt. As a result the surface of optical element obtains various colours.

---

* Full manuscript not available at the time of printing

NEW RAW MATERIAL BASIS FOR EARTHENWARE GLAZE

M. Stefanowa, T. Datzkowa and **Chr. lonchev**
University of Chemical Technology and Metallurgy, Bulgaria

Abstract

The present studies discuss the problem of synthesising the earthenware glaze containing minimum zircon frit at firing temperatures in the 960-1000^{o}C range .The aim is to realise partial substitution of the frit by more reactive raw materials as tuff and halcedonite. The tuff contains high amounts of glassy phase .The halcedonite was used as a mineral with a high active SiO_2 content .The investigations were performed on the basis of the designed experiment in a four component system : zircon frit -high marl clay (22.9 % CaO) - low marl clay (8.6 % CaO) - tuff : halcedonite = 1:1 ratio .

1. INTRODUCTION

The pure raw materials, minerals and technical products are important conventionally used sources for the fabrication of fine ceramic glazes. Recently, the search of substituents, especially of feldspars with more cheaper and more available rock materials appears to be a general trend. The nepheline-syenite, perlite, granite, rhiolite, obsidian characterised with low content of colouring oxides. For ceramics with a coloured body are used glazes with the participation of perlite, diatomite, andesite, basalt, trahyte, zeolites, tuff, etc. [1-8].

The participation of natural raw materials substituting the expensive technical products and especially frits is of interest mainly from of economic point of view. The use of some volcanic rocks as volcanic glass, pumice, zeolites allows to increase the efficiency by reducing the grinding time of glazes. The usage of ready glassy phase from volcanic glasses leads to diminishment of their reactivity and the melting temperature of the green glazes and frits.

2. EXPERIMENTAL

The aim of the present study is to prepare low melting semi - fritted glazes for faience with firing temperature in the 960-1000^{o}C with the participation of non-deficit natural raw materials and diminished content of the frit. The earlier studies for earthenware tiles performed in the Department of "Technology of the Silicates" at the University of Chemical Technology and Metallurgy-Sofia were used as a basis for the present work. The glazes contain 30 % clay with an increased CaO content and 70 % zirconium frit [9,10]. In order to diminish the zirconium frit content, part of it is replaced by a reactive natural raw materials - volcanic tuff and silicide.

The taffs are pyroclastic rocks formed from the accumulation of materials released from the volcanoes- ash, powder, sand particles and they are considered as an intermediate form between the volcanic and sedimentary rocks. They possess comparatively constant chemical content. The Bulgarian tuffs have softening temperature in the range from 1100- to 1130 ^{o} C.] the silicide is

typical chalcedonite and it is formed from many very fine crystalline particles. It is soft and possess very large specific surface which predetermines its high reactivity.[9 ,10].

The chemical composition of all raw materials used is presented in Table 1.

Table 1.

Raws	**SiO_2**	**Al_2O_3**	**Fe_2O_3**	**CaO**	**MgO**	**Na_2O**	**K_2O**	**3H**
Low	54.4	15.2	6.2	8.6	2.0	0.7	1.9	10.9
marl								
clay								
High	39.5	12.4	4.6	17.3	1.8	1.3	2.0	21.2
marl								
clay								
Tuff	62.2	11.0	1.9	8.7	0.9	3.8	0.5	11.0
Silicide	96.0	0.3	0.9	0.7	0.5	0.1	0.2	1.5
Frit	60.5	5.3	0.1	3.3	0.5	6.8	1.0	-

BaO=2.1, ZnO=11.1, ZrO_2=8.8, B_2O_3 =11.8

The investigation has been performed by a designed experiment in a four component system, high marl clay-silicide and tuff (1:1 ratio) - zirconium frit.

The target parameters and their limits of variation were determined in accordance with the exploration requirements of these products.

For earthenware tiles :

$6 < y_1 < 7.5$
$120 < y_2 < 200$
$1 < y_3 < 6$

where: y_1, is the coefficient of thermal expansion ,10^{6} $^{o}C^{-1}$
y_2 is the coefficient of thermal stability, °C
y_3 is the external appearance of the glaze, established by the method of expert assessment.

The factors (the time of variation) correspond to the components of the mixture :

$0.000 < x_1 < 0.600$
$0.000 < x_2 < 0.600$
$0.000 < x_3 < 0.300$
$0.300 < x_4, 0.700$, where
x_1 - low marl clay
x_2 -high marl clay
x_3- silicide and tuff in a 1:1 ratio
x_4 - zirconium frit.

Since the system investigated is a multicomponent, multiphase, it is suggested that the processes taking place in it should be described by a more complicated composition :properties relationships. It is expected to observe a non-linear dependence. A model of a third uncompleted order is expected to be observed.

$$Y = \Sigma b_i X_i + \Sigma b_{ij} X_i X_j + \Sigma b_{ijk} X_i X_j X_k + b_{1,2,3,4} X_1 X_2 X_3 X_4$$

Table 2

No	Experimental Design				Properties of the coatings		
	x_1	x_2	x_3	x_4	y_1	y_2	y_3
1	0, 000	0,600	0, 000	0,400	7,59	180	2
2	0, 000	0, 000	0,300	0,700	8,85	110	5
3	0,600	0, 000	0,100	0,300	8,43	190	2
4	0, 000	0,600	0,100	0,300	7,40	190	2
5	0,600	0,100	0, 000	0,300	7,82	180	1
6	0, 000	0,300	0, 000	0,700	8,32	140	4
7	0,100	0,600	0, 000	0,300	7,33	190	1
8	0,300	0, 000	0, 000	0,700	7,35	190	1
9	0, 000	0,380	0,140	0,480	7,66	190	1
10	0,380	0, 000	0,140	0,480	8,28	140	4
11	0,267	0,267	0, 000	0,466	7,32	190	2
12	0,284	0,283	0,133	0,300	7,73	190	1
13	0,133	0,133	0,300	0,433	5,00	170	3
14	0,100	0,300	0,100	0,700	7,47	180	1
15	0, 000	0,450	0, 000	0,550	7,52	140	2
16	0, 000	0,500	0,200	0,300	7,60	140	6
17	0, 000	0,200	0,300	0,500	8,56	180	1
18	0,000	0,150	0,150	0,700	7,10	180	4
19	0,450	0,000	0,000	0,550	7,13	190	1
20	0,500	0,000	0,200	0,300	7,91	190	1
21	0,200	0,000	0,300	0,500	8,69	180	1
22	0,150	0.000	0,150	0,700	7.72	110	6
23	0.350	0.350	0,000	0.300	8.23	180	1
24	0.150	0.150	0.000	0.700	6,38	130	3
25	0.050	0..600	0.000	0.350	7.60	180	2
26	0.200	0.200	0.300	0.300	10.30	180	2
27	0.236	0,236	0.100	0.428	7.41	180	2
28	0,400	0,000	0,000	0.600	7,34	180	6
29	0,500	0,000	0,000	0.500	7,71	180	6
30	0,300	0,000	0,200	0,500	7,33	180	6

On the basis of the above mentioned equation with the help of a systematic program was possible to built up the optimal plan of the experiment, presented in Table 1.

The glazes are prepared by using the conventional technology for earthenware glazes by joint wet grinding. The firing is performed at maximum temperature of 980 ^{o}C under laboratory conditions. The main properties thermal stability and the coefficient of thermal expansion are defined in accordance with the existing methods [11]. The results of the investigations are presented in Table 2.

3. RESULTS AND DISCUSSION

From the results obtained is seen that it was possible to prepare qualitative coatings by partial substitution of the frit by tuff and silicide in a 1:1 ratio. The best results were observed when this substitution is carried out with a high marl clay at the highest clay content up to 50 %. Here the additionally included quantity of SiO_2 compensates its lower content in the clay-composition - No 16. At the glazes based on low marl clays the substitution of frit could be realised only with compositions in which the clay content is up to 30 %, composition N 30. Since the quantity of SiO_2 in the low marl clays is high (about 60 %) ,their participation is limited as a result of the enrichment of glaze with SiO_2. In this case the partial replacing of the frit by tuff and silicide causes low quality of melting and the appearance of some hair cracking due to additional inclusion of large SiO_2 amounts.

After the treatment of the experimental data by a regression analysis computer program, the coefficients of the given model have been evaluated. The coefficient of the multiple correlation for y_1, y_2 and y_3 are as follows : $y_1 = 0.887$, $y_2 = 0.821$ and $y_3 = 0.758$.

The model could be determined as adequate since the coefficients for y_1, and y_2 are significant, i.e. above 0.800, Y_3 has been calculated too, and its value was below 0.800 as a result of the influence of the individual factor during the assessment of the external appearance.

The optimal compromise composition-property hatched area on Fig. 1 which correspond to the requirements has been determined by the overlapping of the optimal areas of the three properties from the given diagrams.

Generally, it could be taken by an expert assessment of the external appearance. The glazes with expert assessment above 4.0 are dependent mainly on the chemical composition. The coatings with assessment below 4.0 contain a higher quantity of crystalline phase which varies with the various compositions. In areas near to z_1 the crystalline phase is formed mainly from unmelted starting materials. The same behaviour was observed with the compositions containing extremely high CaO contents located in the vicinity of z_2. It was observed a range of compositions with an expert assessment of about 4.0, the crystalline phase of which is assigned to the soaking of the glaze melt in the body and the high extent of the surface crystallization.

Thus, as a result of the existence of some phase transitions the above mentioned properties pass through extremum which hinders their univocal interpretation. In spite of that there exists a range of compositions corresponding to the requirements for the faience tiles.

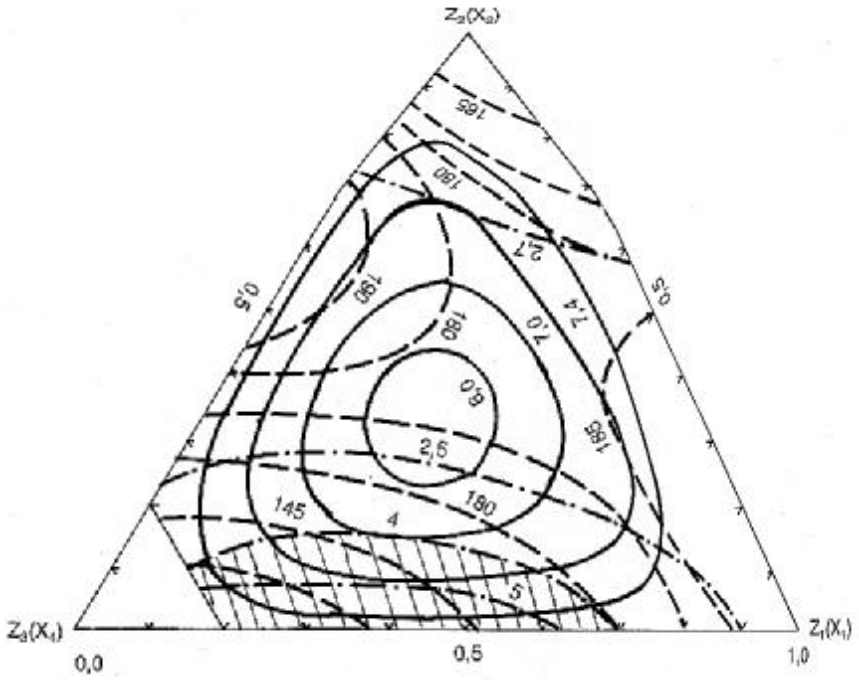

Figure 1. Optimal area of compositions-properties on the section x_3 =0.200.
The ratios of the components of the compromise -optimal ranges are as follows

x_3 = 0.200
x, = 0.100 - 0.350
x_2 = 0.000 - 0.160
x_4 = 0.450 - 0.700

The properties of the section in the limited area of compositions vary in the following ranges : y_1 = 6,6 - 7,4, y_2 =130 -170, y_3 = 4 - 5,7.

4. CONCLUSIONS

As a result of the investigation were synthesised glassy coatings for earthenware glazes in which participate reactive materials -tuff and silicide. The new materials diminish the amount of frit. The use of a designed experiment permitted to determine the range of compositions with preset properties. The prediction accuracy could be raised by inclusion of new structure depending properties.

Acknowledgments

The present investigation has been performed under the financial support of the Bulgarian National Research Fund Contract No TH -357/1993.

REFERENCES

1. Bachvarov S., S. Stefanov - Glazes for ceramic items, Tehnika, Sofia,1985
2. Moroz I.I., Technologia pharpharo-phaiansovih izdelii", Stroiizdat, Moskwa 1984
3.William M.Jackson, American Ceram. Soc. Bull.1989,1, 87-89
4.Inventor’s certificate USSR 1100259
5.Inventor’s certificate USSR 1104120
6.Andreeva V. ,G. Fekeldjiev ,Stroitelni materiali I silikatna promishlenost 1982, 7, 20-22.
7. Kersten W. Sprechsaal 1988,10,976-980
8.Lennhauser W., M. Sussieck, Keram. Z.1987, 8, 509-511,1987 ,12, 866-867,1988, 493-497
9. Paneva A et al., fina keramika, Tehnika,1986,12,.
10. Andreeva V., G. Fekeldjiev, Ceram. Intern. ,1986,12. 229-235
11.Bachvarov S. et al Rukovodstvo za uprajnenia po tehnologia na silikatite, Tehnika, Sofia, 1978.

NEW SINTERED GLASS-CERAMICS BASED ON ZIRCONIA and APATITE

M. Schweiger, M. Frank, V. Rheinberger, and **W. Höland**
IVOCLAR Company Limited, FL-9494 Schaan, Principality of Liechtenstein

Abstract

The aim of this paper was the development of glass-ceramics for dental restorations. It was possible to develop glass-ceramics in two systems. Glass-ceramics of the new SiO_2-Li_2O-ZrO_2-P_2O_5 system were heat pressed to produce dental restorations (temperature below 1200 ^oC and approx. 0.5-0.8 MPa). The glass-ceramics demonstrated a high basic strength of approx. 280 MPa with a fracture toughness of 2.0 $MPam^{0.5}$. The glass-ceramic was bonded to ZrO_2-ceramic (TZP) through heat pressing. The similar thermal expansion coefficient of ZrO_2-ceramic and the glass-ceramic made it possible to produce a composite having a strong interface.

In the SiO_2-Al_2O_3-K_2O system, the addition of small amounts of CaO, P_2O_5 and F permitted the formation of needle-like apatite in the glass-ceramic. The sintering of glass powder induced the precipitation of leucite crystals by surface crystallization and the precipitation of needle-like apatite by volume crystallization. The crystallization of needle-like apatite in glass-ceramics was new.

1. INTRODUCTION

Restorative biomaterials for dental applications have to fulfill a wide range of requirements. They should possess a high degree of translucency, good chemical resistance, biocompatibility and good mechanical strength in order to meet the standards of appearance of natural teeth. The processing parameters for fabricating dental restorations with the biomaterial should not be complicated or time consuming. This paper will focus on two glass-ceramic systems that meet these requirements.

Moreover, a multiphase glass-ceramic in the SiO_2-Li_2O-ZrO_2-P_2O_5 system was produced. It was possible to incorporate a remarkably high ZrO_2-content of up to 3O wt% into the glass. In this system two glass-ceramics were developed having different properties. The first type of glass-ceramic, containing 20 wt% ZrO_2, in this system showed good mechanical strength of approx. 28O MPa caused by the multiphase microstructure after heat pressing at 1000^oC [1]. In addition, the material demonstrated excellent processing properties. The second type of glass-ceramic, with 15 wt% ZrO_2 and lower P_2O_5 content, showed a high degree of translucency. Furthermore, the linear thermal expansion coefficient of this glass-ceramic was compatible with the high strength ZrO_2-ceramic (TZP). The glass-ceramic was bonded to a ZrO_2-ceramic in a heat-pressing procedure to produce dental composites. These materials fulfilled the requirements for a high degree of biocompatibility and good optical properties (translucency). Thus they have been used to produce dental posts [2].

In the SiO_2-AI_2O_3-K_2O-CaO-P_2O_5-F system the crystallization behaviour of leucite ($KAlSi_2O_6$) and calcium phosphate phases, especially needle-like apatite or fluor apatite and the

resulting properties of the glass-ceramic are discussed [3]. The crystallization of needle-like apatite in glass-ceramics was new. It had previously been reported in apatite formation by hydrothermal synthesis [4, 5].

2. EXPERIMENTAL

2.1 Sample preparation in the SiO_2-Li_2O-ZrO_2-P_2O_5 system

In order to obtain a material with high mechanical strength and good fracture toughness, the glass formation and crystallization behaviour were investigated in this system. Up to 30 wt% of zirconia were incorporated in the glass. The zirconia was fully dissolved in the melt. Glass was successfully formed within the composition range (in wt%) 42-59 SiO_2, 7-15 Li_2O,15-28 ZrO_2, 4-14 P_2O_5. Additions of $Me(I)_2O$, $Me(II)O$, $Me(III)_2O_3$, $Me(IV)O_2$ and F^- up to approximately 11 wt% favourably influenced glass processing using a heat pressing procedure.

The glass-ceramic formation was done by powder processing, sintering and heat pressing.

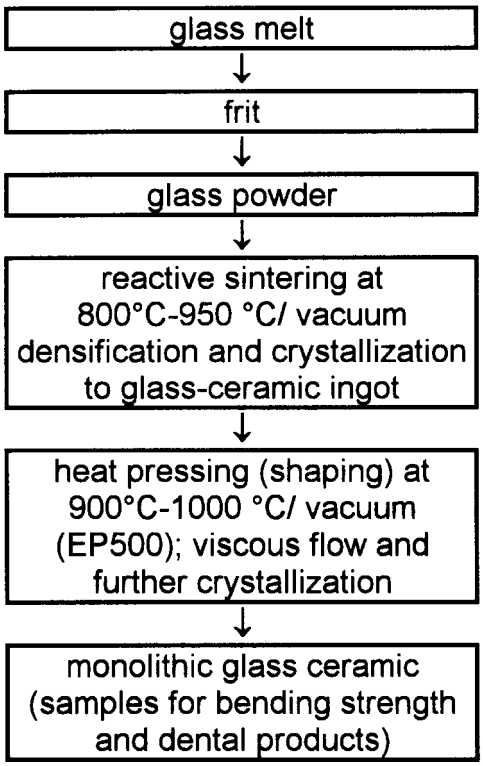

Fig.1 Glass-ceramic formation process by powder processing, sintering and heat pressing

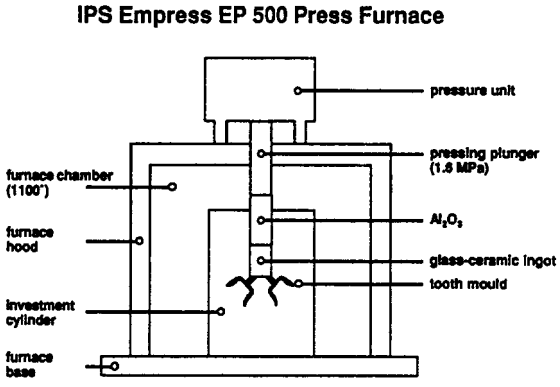

Fig. 2 Schematic diagram of an IPS Empress EP500 press furnace

Heat pressing was conducted in the IPS Empress EP500 (IVOCLAR AG) press furnace (Fig. 2). Since the material demonstrated viscous flow at 900°C-1000°C and 0.5 MPa pressure, it was possible to fabricate dental restorations with complex shapes as well as standardized test samples. The viscosity of a typical pressable glass-ceramic was in the range of 10^5-10^6 Pas. Test samples were pressed to investigate the microstructure, flexural strength, linear thermal

expansion and fracture toughness of the glass-ceramic. Microstructural analyses were conducted on fractured and etched (2.5% HF,10s) samples using SEM (Zeiss DSM 962).

The flexural strength was tested on samples measuring 20 x 4.7 x 1.5mm^3 using the three point bending method. The fracture toughness was investigated using the Vickers indentation method [6] and the single edge notched beam method (SENB) [7].

For the Vickers indentation method, the surfaces of the samples were polished with 1 μm diamond polishing medium. The samples used for conducting the flexural strength and SENB measurements were ground with SiC paper (1000 grit). The notches in the SENB samples measured 0.1 mm in width and 2.5mm in length.

The fracture toughness K_{lc} was calculated using the following equations:

Vickers indentation (Niihara [6]) $$K_{1c}= (0.035\ H\ \sqrt{a})/[\Phi\sqrt{(l/a)}(H/(E\Phi))^{0.4}] \quad (1)$$

where H is the Vickers hardness, a is half the diagonal length of the indentation, Φ is a constant of ≈3 and l is the crack length measured from the corner of the indentation to the crack tip

SENB [7] $$K_{1c} = [(Fs)/(BW^{1.5})]\ f(a/W) \quad (2)$$

where f(a/W) is a geometrical factor, F is the load, s is the span of the test apparatus (here 15mm), B is the breadth of the sample, W is the width of the sample and a is the notch length

The formula of Niihara was chosen because the measured samples showed crack behaviour described by Palmqvist ($0.25 \leq l/a \leq 2.5$).

2.2 Sample processing in the SiO_2-AI_2O_3-K_2O-CaO-P_2O_5-F system

Special additives in the SiO_2-AI_2O_3-K_2O base glass system were investigated to control the microstructure and the resulting thermal and mechanical properties of the glass-ceramic. The addition of CaO, P_2O_5 and F made it possible to crystallize needle-like apatite in addition to leucite [8]. Leucite was precipitated by surface crystallization, while needle-like apatite was precipitated in the bulk of the glassy powder particles. The composition of this type of glass-ceramic was in the range of (in wt%) 49-58 SiO_2,11-19 Al_2O_3, 9-23 K_2O, 2-12 CaO, O.5-6 P_2O_5, 0.2-2.5 F with additives of up to 9wt% $Me(I)_20$, Me(II)0, $Me(III)_20_3$ and $Me(IV)0_2$.

The formation process of the glass-ceramic is described below.

glass melt → frit → milling → tempering 950 ^{o}C-1100 ^{o}C/1 h → milling →
sintering a) on a metal substrate; e.g. 950 ^{o}C/1 min
b) to monolithic glass-ceramic ingots; e.g. 950 ^{o}C/30 min
ingots for heat pressing as illustrated in Fig. 2.

The test samples used to conduct flexural strength and thermal expansion measurements were sintered or heat pressed. The heat pressing parameters were in the range of 1000 ^{o}C-1150 ^{o}C with 0.5-0.8 MPa pressure.

3. RESULTS AND DISCUSSION

3.1 SiO_2-Li_2O-ZrO_2-P_2O_5 glass-ceramic

3.1.1 Microstructure

The glass-ceramic showing high strength consisted of 20wt% ZrO_2. The microstructure of a sintered ingot (950^{o}C) demonstrated liquid liquid phase separation and primary lithium phosphate phases (Fig. 3). At this stage, no zirconia crystals had been precipitated. After the heat-pressing procedure at 1000 ^{o}C the multiphase microstructure developed due to controlled crystallization. These phases were analyzed using X-ray diffraction. The glass-ceramic consisted of tetragonal ZrO_2, monoclinic ZrO_2 (baddeyelite), $ZrSiO_4$, rod-shaped lithium phosphate of the Li_3PO_4-type and a glass matrix. In Figure 4, the ZrO_2 and $ZrSiO_4$-crystals appear as white objects as a result of the analytical method used (SEM-compo). The lithium phosphate crystals have been partially dissolved by HF etching. The remaining holes indicate the original locations of these crystals.

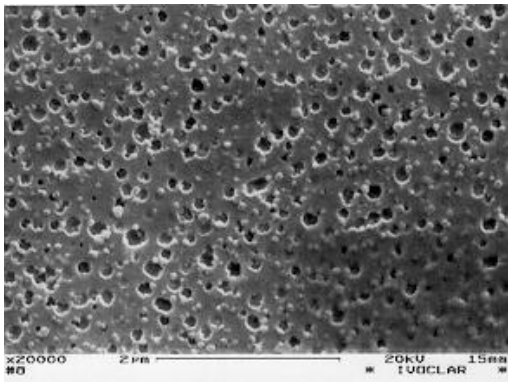

Figure 3 Microstructure of sintered (950 ^{o}C) glass-ceramic containing 20wt% ZrO_2 (SEM, 2.5%HF,10s)

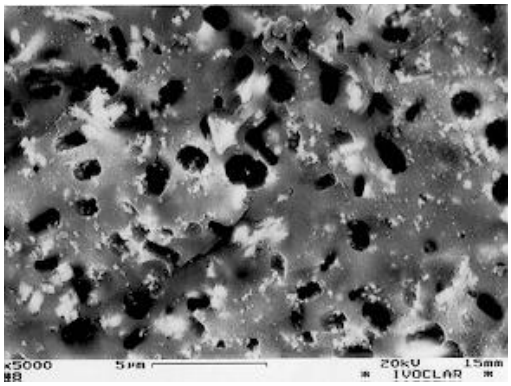

Figure 4 Microstructure of sintered and heat pressed (1000 ^{o}C) glass-ceramic containing 20wt% ZrO_2 (SEM-compo, 2.5%HF,10s)

3.1.2 Mechanical Properties

For the glass-ceramic containing 20 wt% ZrO_2, the three point bending strength of the heat pressed samples reached mean values of up to 280 MPa. The toughening mechanism closely depended on the complex microstructure of the glass-ceramic. The calculated results for fracture toughness are listed in Table 1.

Method	sintered ingot 950 ^{o}C K_{1c} (MPa$\sqrt{m}$)	heat pressed 1000 ^{o}C K_{1c} (MPa$\sqrt{m}$)

S E N B	1.4±0.25	2.0±0.1
Vickers indentation	1.3±0.2	1.9±0.1

Table 1:Fracture toughness K_{Ic} of a sintered glass-ceramic and a sintered and subsequently heat pressed glass-ceramic containing 20wt% ZrO_2

The fracture toughness of a sintered and heat pressed sample was 40 to 50% higher than that of a sample that had only been sintered. The heat pressing procedure induced further crystallization of all the crystal phases, which resulted in a remarkable increase in fracture toughness. The same toughness values were measured with different methods. The SENB method was used to investigate a macroscopic area of the samples (crack length approx 2-3mm), while the indentation method was used to investigate a microscopic area of the samples (crack length approx. 0.1 mm).

3.1.3 Thermal expansion coefficient

The glass-ceramic with 15wt% ZrO_2 demonstrated very good translucency after heat pressing at 900 ^{o}C. This esthetic advantage made the glass-ceramic suitable for dental restorations, e.g. dental posts. The glass-ceramic was bonded to prefabricated densely sintered ZrO_2 (TZP) pins in a heat pressing procedure. The linear thermal expansion coefficient (100^{o}C-500^{o}C) of the pressable glass-ceramic ($9.5\text{-}10.0\cdot10^{-6}$ K^{-1} m/m) was lower than that of the ZrO_2-ceramic (approx.$11.0\cdot10^{-6}$ K^{-1} m/m). The bonding of these two materials resulted in composites demonstrating low thermal residual stress. In addition, the glass-ceramic was reinforced by the ZrO_2-pin. In Figures 5 and 6 the bonding areas are free of defects, such as debonding or porosity, caused by thermal residual stress. The shear strength is in the range of 30 MPa measured by push-out tests.

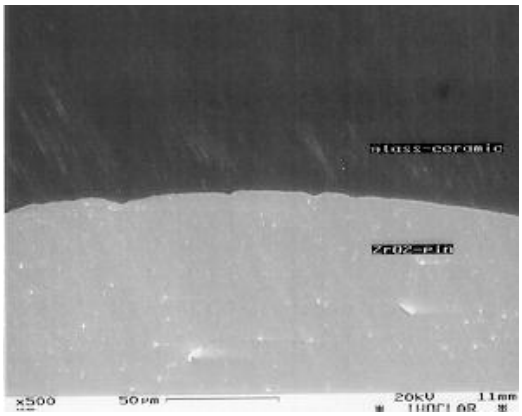

Figure 5

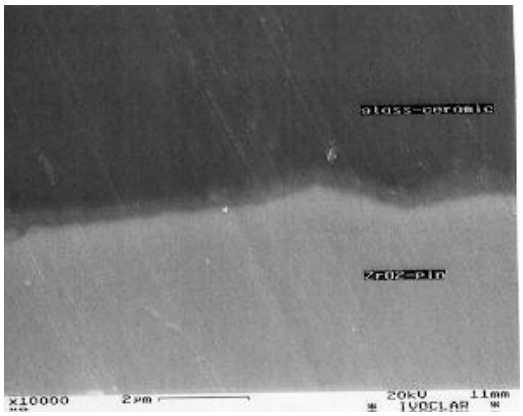

Figure 6

Figure 5/6 Interface of ZrO_2-ceramic and pressable glass-ceramic (SEM, surface polished 1 µm)

3.2 SiO_2-AI_2O_3-K_2O-CaO-P_2O_5-F glass-ceramic

In the base system SiO_2-AI_2O_3-K_2O, the mechanism of crystal development was the surface crystallization of leucite. This type of glass-ceramic has often been used in conventional dental materials. A new crystal phase was precipitated by adding CaO, P_2O_5 and F to the base system. At heat treatment in the range of 850 ^oC-1200 ^oC for 30 minutes to 4 hours, additional phosphate phases or preferred fluorine apatite was precipitated in the bulk of the glass grain. The habit of the apatite was found to be needle-like as shown in Figure 7. This modification of apatite in a glass-ceramic was new and had previously been determined only in apatite crystals produced by hydrothermal synthesis [5].

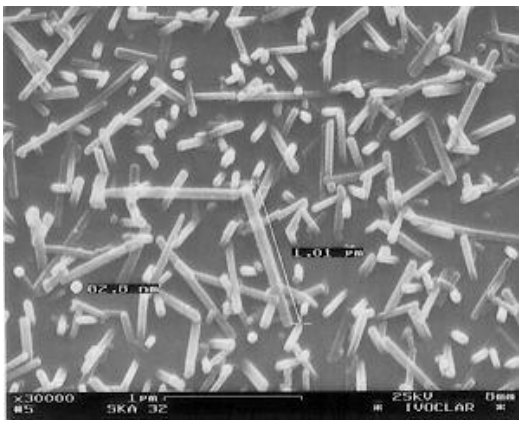

Figure 7 Needle-like apatite precipitated in the bulk of a glass grain at 1050^oC (SEM, 2.5% HF,10s)

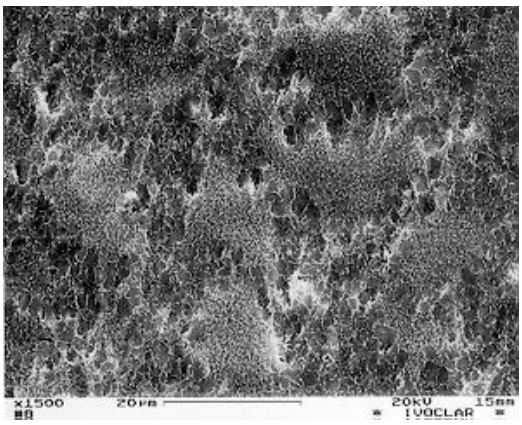

Figure 8 Surface crystallization of leucite and bulk crystallization of needle· like apatite in a sintered glass-ceramic (SEM, 2.5% HF,10s)

The controlled crystallization of leucite resulted in a homogenous distribution of small crystallites (<5µm) embedded in a glassy matrix (Fig. 8). The dispersion strengthening due to the thermal expansion mismatch of leucite and the glass matrix resulted in high flexural strengths of up to 190 MPa. The measurements were conducted on heat pressed samples (1000 ^oC-1200 ^oC). Flexural strengths of up to 300 MPa were achieved with self glazing, which was induced by additional heat treatments at 900^oC -1000^oC. The glass-ceramic containing leucite and apatite showed a high degree of translucency as a result of the small crystal size and the similar dispersion coefficient; of the crystals and the glass matrix. The degree of translucency was controlled by the crystallinity of the glass-ceramic. The linear thermal expansion coefficient was in the range of 12.0-19.0·10^{-6} K^{-1} m/m, depending on the amount of leucite crystals. Esthetic dental restorations were produced by sintering (850^oC-950^oC) the glass- ceramic powder on a metal substrate with a similar thermal expansion coefficient or by heat pressing (1000^oC-1200^oC).

4. CONCLUSIONS

In the SiO_2-Li_2O-ZrO_2-P_2O_5 system, it was possible to develop two glass-ceramics having different properties after heat pressing. The microstructure of the heat pressed glass-ceramic was mainly influenced by the variation of the ZrO_2 and P_2O_5 content and the resulting heat press parameters. It was possible to form individual dental restorations with complex shapes using a special heat-pressing technique in combination with viscous flow.

The first type of glass-ceramic containing 20 wt% ZrO_2 showed viscous flow at 1000°C. The resulting glass-ceramic, exhibiting a multiphase microstructure, had a high flexural strength of approximately 280 MPa. The fracture toughness was 2.0 MPa$\sqrt{m}$. The second type of glass-ceramic containing 15 wt% ZrO_2 was pressable at 900°C. Due to the low content of crystalline phases, the heat pressed samples showed high translucency. The similar thermal expansion coefficients of the glass-ceramic and the ZrO_2-ceramic (TZP) allowed these two materials to be bonded together in a heat-pressing procedure. The resulting composite showed biocompatibility, good shear strength and translucency.

In the SiO_2-Al_2O_3-K_2O-CaO-P_2O_5-F system, it was possible to precipitate leucite with surface crystallization and needle-like apatite with bulk crystallization. The resulting glass-ceramic demonstrated good biocompatibility and a high degree of translucency. The linear thermal expansion coefficient was in the range of 12.0 to $19.0 \cdot 10^{-6}$ K^{-1} m/m Flexural strengths of up to 190 MPa were measured. These properties made this glass ceramic suitable for producing functional and esthetic dental restorations.

REFERENCES

1. Höland, W., Frank, M., Schweiger, M., Wegner, S. and Rheinberger, V. Glastech. Ber. Glass Sci. Technol.1996, **69**, 25-33
2. Meyenberg, K.H., Lüthy, H., Schärer, P. J. Esthet. Dent.1995, **7**, 73-80
3. Höland, W., Frank, M., Schweiger, M. and Rheinberger, V. Glastech. Ber. Glass Sci. Technol.1994, **67C**, 117-122
4. Newesely, H. Mechanism and action of trace elements in the mineralisation of dental hard tissues, Zyma SA,1972
5. Walsh, D., Kingston, J. L., Heywood, B. R. and Mann, S. J. Cryst. Growth 1993, **133**,1-12
6. Niihara, K. J. Mat. Sci. Lett.1982, **1**, 13-16
7. Heckel, K. Einführung in die technische Anwendung der Bruchmechanik, Hanser Munich 1983, 66
8. Höland, W., Rheinberger,V., Frank, M. and Wegner, S. Bioceramics 9; in print

NOVEL INTERFERENCE TECHNIQUE OF GLASS INDEX MEASUREMENT*

D. K. Tagantsev and **G. O.Karapetyan**
S.I.Vavilov State Optical Institute, Russia

Abstract

We offer to apply the GRIN element index distribution like parabolic one as an index scale for novel interference technique to measure glass index. In case GRIN element is of a traditional shape one can use this scale with great difficulties. However, it is possible to exhibit this scale if the elements are shaped into a cone, or a pyramid, or a wedge. Cone-, pyramid-and wedge-shaped GRIN elements may be used as index reference standard (RS) if the index distribution parameters are known exactly. Here we represent a brief description of the technique of glass index measurement using these RS.

The optical cell with immersion oil, experimental specimen and RS are placed into the measurement unit of an interferometer, the parameters are known exactly. Here we represent a brief description of the technique of glass index measurement using these RS.

The optical cell with immersion oil, experimental specimen and RS are placed into the measurement unit of an interferometer, the experimental specimen being shaped arbitrarily, Fringe-shift picture is observed by a microscope. The subject plane of the microscope is located into RS plane. Then oil is being heated until the specimen becomes invisible because the oil index becomes equal to the glass index. At this moment a fringe shift picture of RS should be analyzed. The fringe crossing a singular points of wave surface was called the characteristic fringe.

One can calculate oil index using positions of characteristic fringes due to the analytical expression of the wave surface which has been found by the authors. The derivation and analysis of the wave surface expression, the definition of singular wave surface points, the correlation between a characteristic fringe positions and oil (or specimen) index for each RS are discussed.

---

* Full manuscript not available at the time of printing

OPTICAL NONLINEARITY OF CdSe DOPED PHOSPHATE GLASSES

A.G.Belyaev, V.I.Bogdanov, A.A.Onushchenko, G.T.Petrovsky,
E.L.Raaben and **A.G.Spiro**
S.I.Vavilov State Optical Institute, Russia

Abstract

Nonlinear response of phosphate glasses containing CdSe nanocrystals has been investigated by degenerate and nondegenerate four photon scattering. The resonent third order susceptibility due to CdSe crystallites has been measured in wide range of jumping intensities for different frequency detunings. A three level model is proposed to explain third order nonlinearity of the System The model takes into account trap states governing nonlinear response at low pumping power and for zero or small frequency detunings. Some evidence for the states has been obtained from spectral dependence of the susceptibility and differential absorption measurements.

1- INTRODUCTION

Starting from pioneer work [1] , glasses doped by crystallites of II-VI group have been investigating intensively in connection with their large and ultrafast nonlinear response. Different linear and nonlinear optical methods were used to get information on electron-hole-pair states and carrier dynamics in crystallites [2-7] . Values of the resonant third order susceptibility ranging from 10^{-7} to 10^{-9} esu were reported [8-11] . Even taking into account that the values were obtained with different samples and under different experimental conditions, it is difficult to agree the high efficiency of nonlinear wave mixing ultrafast carrier dynamics (free carrier time $T_1 \sim 10^{-12}$ s and dephasing time $T_2 \sim 10^{-14}$ s [12-15]) in the framework of a two level model though such approach was used to explain third order nonlinearity of the system [15]. More complex model was proposed in [4]. The model takes into account both volume and surface electronic states. However, authors [4] point out that one of two peaks observed in $|\chi^{(3)}|$ spectra in the vicinity of the lowest quantum confined resonance can be attributed to surface state only tentatively. According to [6], the structure of the resonance for CdSe crystallites (usually hidden in linear absorption spectra) is connected with transitions from different hole states $1S_{3/2}$ and $2S_{3/2}$.

In this paper we try to elucidate what mechanisms determine third order nonlinearity of CdSe doped glasses and consequently what states participate in nonlinear wave mixing process using nondegenerate and degenerate four photon scattering measurements in wide range of pumping intensities. Such investigation seems to be impossible with silicate glasses due to their photodarkening [8]. However, our preliminary experiments showed that phosphate glasses did not demonstrate appreciable change of optical properties after powerful laser illumination.

2.EXPERIMENTAL

Glasses of basic composition $55P_2O_5$-16BaO-$17K_2O$-$7Al_2O_3$-CaO-$3B_2O_3$ (mol%) were used as a matrix for CdSe crystallites. Colorless samples were prepared by comelting this matrix (T=1100-1200°C) with CdSe in excess (1-5 mol%) to compensate its volatilization during synthesis. Precipitation of the semiconductor phase was carried out by secondary heat treatment of the samples under isothermal conditions at different temperatures of 480-550°C range. Sizes of crystallites were determined by small angle X-ray scattering (SAXS) [16].

To control formation of CdSe crystallites we measured absorption spectra with spectrophotometer "Perkin-Elmer" model 555. Spectral position of the lowest confined resonance was taken into account when we chose samples for nonlinear measurements. Third order nonlinearity was investigated in detail for one sample containing crystallites with an average radius about 2.5 nm. The sample turned out to be the most suitable for tuning range of our experimental setup. We investigated frequancy nondegenerate and degenerate four photon scattering (three wave mixing version). Two nanosecond dye lasers pumped by the second harmonic Nd:YAG laser were used. Three wave mixing signal was detected at frequency $\nu_3=2\nu_1-\nu_2$, where ν_1 and ν_2 are the output frequencies of the pumping lasers. Frequency ν_1 was centred on the maximum of the quantum-confined resonance. In experiments the power $I_1(\nu_1)$ of the first pump beam was varied up to 10 MW/cm^2, while that of the second one was kept at low level (0.02 MW/cm^2). We used values of signal intensity $I_3(\nu_3)$ normalized to product of the incident intensities $I_1^2(\nu_1)$ $I_2(\nu_2)$ to determine absolute values of the resonant third order susceptibility. Information on experimental setup in more detail can be found in [17]. We also controlled photobleaching of the sample measuring transmission of a probe beam at frequency $\nu_p=\nu_1-\nu_d$, where ν_d is small detuning in order to exclude coherent contribution.

In addition, differential absorption measurements were performed with a standart pump-and-probe setup consisting of two dye lasers: narrow-band powerful laser for selective pumping within the inhomogeneously broadened resonanse and weak broad-band one to probe photobleaching spectra [5].

3.RESULTS

The data on radii of crystallites obtained by SAXS measurements for two phosphate glasses are given in Table 1.

Table 1. Heat treatment regimes and radii of crystallites

Glass N1 480 °C **t hours**	**R,nm**	**Glass N1 550** °C **t hours**	**R,nm**	**Glass N2 510** °C **t hours**	**R,nm**	**Glass N2 550** °C **t hours**	**R,nm**
24	2.3±0.1	2	10	2	1.6	2	3.3
43	2.7	4	12.3	8	1.6	24	4.1
72	2.9	8	16	19	1.95	48	5.4
		16	19	46	2.05		
		29	21	72	2.2		

The observed difference in sizes between two glasses can be connected with different preparation procedure (temperature and time of melting) which determines amount of semiconductor components in matrix. Time dependence

$R \sim t^{1/3}$ corresponding to the coalescence stage of the precipitation process [18] was found to hold only for glass N1 heat treated at 550ºC. This regime provides crstallites of large size only. As can be seen, crystallite radius changes weakly with increase of heat time for all other sets of samples. It means that that growth of small crystallites (1.5-3.0 nm)proceeds in early stages of the process where the narrowest size distribution functtion can be expected [19,20].

Fig. 1 shows adsorption spectra of representative series of samples (glass N2, T=510ºC). The samples contain crystallites with radii much less than exciton Bohr radius of CdSe (r_b=5.6 nm). The situation corresponds to the strong confinement regime [21]. A distinct quantum confined feature superimposed higher energy adsorption bands of CdSe crystallites is observed for all the samples. The total adsorption of the samples increases strongly within time interval 2-19 hours. It can be referred to an increase of the volume fraction of CdSe. This is an additional evidence allowing us to consider that the heat treatment regime provides an early stage of the precipitation process. The observed shift of the peak to higher higher energy with decrease of crystallite radius is due to quantum size effect [22]. As can be also seen, the shift is accompanied with a considerable broadening of the feature. There are no reasons to considerthat size dispersion increases strongly with the decrease of heat time and we believ that other mechanisms of broadening should be taken into account.

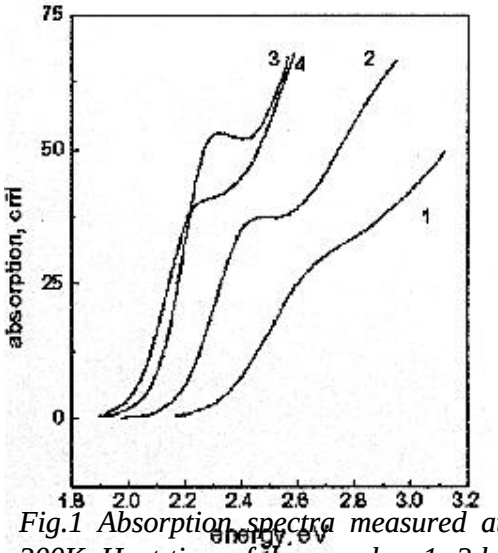

Fig.1 Absorption spectra measured at 300K. Heat time of the samples: 1 -2 h; 2-8 h; 3-19 h; 4-72 h.

To get additional information along this direction we used nonlinear optical technique. Dispersion curve of the resonant third order susceptibility was measured in the frequency detuning range 15-1000 cm^{-1} to estimate the width of the homogeneous spectral component in absorption band. Theory of the method was developed in [23]. The estimation yields $\Delta E \approx 0.12$ eV. The value is in accordance with that obtained pump-and-probe method from differential absorption spectra (DAS) for CdSe crystallites grown in a silicate matrix [20]. Different absorption measurements of some of our sammples showed the following. A broad hole having the width more than 0.15 eV is observed for crystallites with average radious R<2.0 nm. The spectral position of the hole is close to the maximum of the quantum confined peak and does not shift when we tune excitation energy along lower energy tail of the band. When excitation energy approaches the maximum, some structure can be resolved in DAS, namely, a weak pecularity arises at its higher energy side. The structure becomes more pronounced for crystallite of larger size (R>2.0 nm). Lorentzian fit of the DAS gives two bands, with lower energy one being broader and more intensive. The observed behaviour differes strongly on that for CdSe crystallites in silicate glasses where holes burnt follow the enrgy of the pumping laser [20].

To elucidate the matter whether we deal with optical transitions that determine third order nonlinearity or other mechanismd are important, we measured intensity dependencies of the resonant third order susceptibility for different frequency detunings. The data are presented in Fig.2a. Fig.2b shows data on photobleaching of the sample. As can be seen, values of $|x^{(3)}|$ differs strongly (10-10^3 times) for frequency degenerate and nondegenerate wave mixing. At the same time one can see that intensity dependence of the susceptibility correlates with that of optical density for large frequency detunings. On the contrary, frequency degenerate mixing (or the case of small detunings) demonstrates a strong saturation, while optical density of the sample is nearly constant. The results undoubtedly show that optical nonlinearity is due to several mechanisms. It should be noted here once again that we did not observe any appreciable change of optical properties after powerful laser illumination of the sample (10^3 shots, 10 MW/cm^2). Therefore, we can exclude from consideration a process of carrier trapping into deep levels. Then we conclude that a "slow" mechanism determines nonlinear susceptibility of the system in the region of small frequency detunings and low pumping power, but other "fast" mechanism determines the susceptibility at higher pumping power and for large detunings. So, a three level model including shallow longliving traps can be used to describe third order nonlinearity of the system.

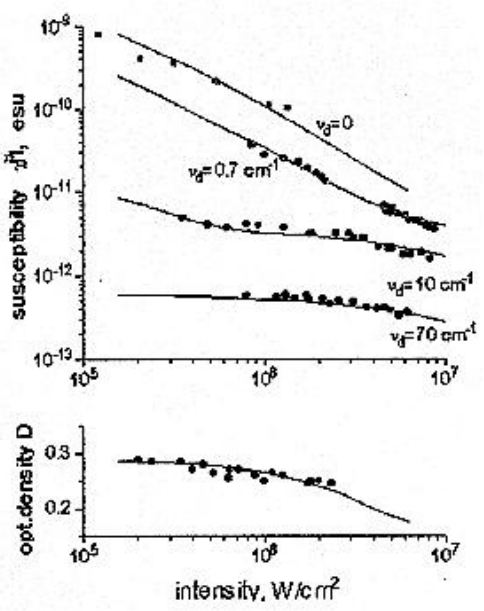

Fig. 2 Dependencies of $|c^{(3)}|$ (a) and optical density (b) on ýnput intensity, n_d - frequency detuning. Solid squares-

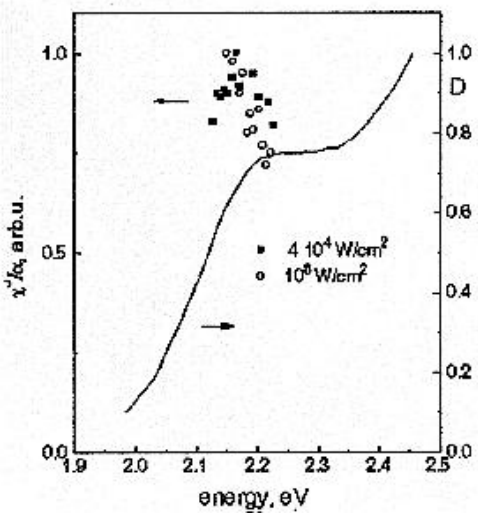

Fig.3 Absorption spectrum and spectral dependencies of the ratio $|c^{(3)}|.a$ for two different pumping power

An expression for the modulus of the resonant third order susceptibility was obtained in [24] in the framework of the model. The calculated dependencies of $|x^{(3)}|$ according to the expression are shown in Fig. 2 by solid lines. The best fit corresponds to the following values of the parameters: carrier trapping quantum yield $\gamma = 3\ 10^{-3}$, free carrier lifetime $T_1 = 10^{-12}$ s and absorption cross section $\sigma = 3\ 10^{-15}$ cm^2.

We also measured spectral dependence of the susceptibility for the case of frequency degenerate mixing. The data are given in Fig.3. A distinct peak is observed at low pumping power close to the maximum of absorption band. It saturates with increase of pumping power and one can see that ratio $|\chi^{(3)}|/\alpha$ increases monotonously to lower photon energies for l_1=10 MW/cm^2 We could not measure in this spectral range with our experimental setup and can only suppose that some peak, if any, exist there.

4. DISCUSSION

There is only space modulation of the population change in the case of degenerate wave mixing and a stationary grating is produced by interference of the intersected pumping beams. Capture of carriers to the longliving (in comparison with the pulse duration) traps provides the accumulation of the stationary grating during the nanosecond laser pulses that results in large value of susceptibility ($|\chi^{(3)}|\sim10^{-9}$ esu). The increase of pumping beam intensity causes a space uniform trap filling. It decreases the depth of the population grating and consequently the susceptibility which is due to this mechanism. The weak photobleaching observed shows that the trap concentration and/or quantum yield of carrier trapping are likely to be low.

The resonant nonlinear wave mixing is controlled by space-time modulation of the population change in nondegenerate case. The period of beating of the dynamic grating is $(c\nu_d) < 3*10^{-12}$ s at frequency detuning $\nu_d > 10$ cm^{-1}. In this case, the susceptibility is practically constant at low pumping power and can be considered as a true cubic nonlinearity governed by "pure" two level mechanism. Taking the obtained value of the free carrier life time T_1=1 ps, we estimate the maximum value of the "fast" unsaturated susceptibility $|\chi^{(3)}|=8.4*10^{-12}$ esu. This small value is due to fast radiationless decay of the excited state and small dephasing time determining large value ($\delta E> 0.1$ eV) of the homegeneous width in nanocrystals.

Our estimations of the absorption cross section of nanocrystals from the unsaturated regime at large frequency detunings and also made by shaping experimental and theoretical dependencies of the susceptibility on pumping power give different values by a factor of 5. However, we believe that this discrepancy can be excluded if higher excited states of nanocrystals [6] are taken into account. Actually, an overlapp of subbands should result in decrease of the ratio $|\chi^{(3)}|/\alpha$ as compared with the single band.

Considering the data of differential absorption measurements and spectral dependencies of the susceptibility, we can suppose that trap states lie close to electron-hole-pair states in the energy spectrum of nanocrystals. To our opinion, the resonance of states can be responsible for low efficiency of edge emission observed in our samples. Analogous situation was already discussed to interpret luminescent properties of CdSe quantum dots in [25].

5. CONCLUSION

We have demonstrated that third order nonlinearity of CdSe doped glasses can be better understood in the framework of a three level model, The model takes into account shallowtraps and describes well the contradictory behaviour of the resonant third order susceptibility for different frequency detunings. We have obtained some evidence for energy position of trap states, however, further investigation along this direction is required.

Acknowledgments

The authors are grateful to Dr. V.V Golubkov for SAXS measurements and also to F.Gindele for differential absorption measurements. The work was supported by RFBR under grant No 95-02-06140.

REFERENCES

1. R.K.Jain and R.C.Lind. J. Opt. Soc. Am. 73 (1983) 647
2. M.C.Nuss, W Zinth and W. Kaiser, Appl. Phys. Let. 49(1986) 1717
3. S.H.Park, R.A.Morgan, Y.Z.Hu, M. Lindberg, S.W. Koch and N.Peyghambarian, J. Opt. Soc. Am. B7, (1990) 2097
4. M.C. Schanne-Klein, F. Hache, D. Ricard and C. Flytzanis, J. Opt. Soc. Am. B9 (1992) 2234
5. U. Woggon, S. Gaponenko, W.Langbein, A. Uhrig and C.Klingshirn, Phys. Rev. B47 (1992) 3684
6. A.I.Ekimov, F. Hache, M.C. Schanne-Klein, D. Ricard, C.Flytzanis, I.A.Kurdryavtsev, T.V.Yaseva, A.V.Rodina and AI. L. Efros, J.Opt.Soc.Am. B7 (1990) 1198
7. J. Puls, V. Jungfickel, F. Henneberger and A. Schülzgen, J. Cryst. Growth 138 (1994) 1004
8. M. Tomita and M.Matsuoka, J.Opt.Soc.Am. B7 (1990) 1198
9. J.Yumoto, S. Fukushima and K.Kubodera, Opt. Lett. 12(1987) 83210.
10. J.T.Remillard, H.Wang, M.D. Webb and D.G.Steel, IEEE J.Quantum Electr. 25
11. S.M.Saltiel, B van Wonterghem and P.M.Rentzepis, Opt. Lett. 12(1987) 832
12. A.P.Alivisatos, A.L.Harris, N.J.Levinos, M.L.Steigerwald and L.E. Brus, J.Chem. Phys. 89 (1988) 4001
13. N.Peyghambarian, B.Fluegel, D.Hulin, A. Migus, M.Joffre, A.Antonetti, S.W.Koch and M.Lindberg, IEEE J. Quantum Electr. QE25 (1989) 2516
14. P.Roussignol, D.Ricard, C.Flytzanis and N.Neuroth, Phys. Rev. Lett. 62 (1989) 312
15. S.H.Park, M.P.Casey and J.Falk, Appl. Phys. 73 (1993) 8041.
16. V.V.Golubkov, A.I.Ekimov, A.A.Onuschchenko and V.A.Tsekhomsky, Sov.J.Glass Phys.&Chem. 7(1981) 265
17. B.S.Neporent, S.V.Kulya, A.G.Spiro and I.N.Myakisheva, Opt.Spectrosc. 68 (1990)755
18. I.M. Lifshits and V.V.Slyozov, Sov. Phys. JETP 8(1959) 331
19. M.P.Shepilov, J.Non-Crys. Solids 146(1992) 1
20. S.V.Gaponenko, U.Waggon, M.Saleh, W.Langbein, A.Uhrig, M.Müller and C.Klingshirn, J.Opt.Soc.Am. B10 (1993) 1947
21. AI.L.Efros and A.L.Efros, Sov. Phys. Semiconduct. 16(1982) 772
22. A.I.Ekimov, A.A.Onuschenko and AI.L.Efros, Solid St. Commun. 56(1985) 921
23. T.Yajima, H.Suoma and Y.Ichida, Phys.Rev. A17 (1978) 309
24. A.G.Belyaev, V.L.Bogdanov, B.S.Neporent, A.A.Onuschenko, G.T.Petrovsky, E.L.Raaaben and A.G.Spiro, J.Opt. Techn. 62(1995) 790

PHASE FORMATION DURING THE SOL-GEL SYNTESIS OF APATITE - MULLITE GLASS-CERAMICS

B. Samuneva, R.Hill*, V. Dimitrov and **S. Kalimanova**
University of Chemical Technology & Metallurgy, Bulgaria
*University of Limerick, Ireland

Abstract

The phase formation during the sol-gel synthesis of apatite-mulite glass-ceramics has been investigated by means of X- ray diffraction analysis, IR-spectroscopy, TEM and TEMD. As precursors have been used SiO_2-sol, TEOS, $Al(NO_3)_3.9H_2O$, $Ca(NO_3)_2.4H_2O$, $(NH_4)_3PO_4.3H_2O$ and CaF_2. The phase formation during the heat treatment of the gels from 950^oC to 1250^oC is quite different depending on the precursors type of SiO_2 - sol or TEOS. It has been established the apatite - mullite glass-ceramics can obtained when the gels, synthesized using SiO_2 - sol as precursor, are treated at 1050 -1150^oC independently of the addition way of CaF_2 (before or after gelling)

I. INTRODUCTION

The phase formation during sol-gel synthesis of glass-ceramics is of a considerable interest because this kind of materials have many advantages: high purity, high homogeneity, low melting temperature of the initial glasses and possibility of producing glass-ceramics of new compositions (1). Besides, the sol-gel glass-ceramics can be obtained at low temperature by direct crystallization of gel-glasses without melting process.

Mucherjee, Zarzycki and Traverse (2) have established that the rate of nucleation and crystallization of silicate glasses of different compositions made from gels are much higher than those made from mixture of oxides.

Uhlmann et al. (3) summarized the published results about crystallization of glasses prepared by sol-gel method and by melting. Many authors have investigated the preparation, phase formation and properties of sol-gel glass-ceramics of different chemical and phase compositions (4-10).

It is well known that the glass-ceramics for application in medicine and dentistry are very perspective biomateriais and they are connected with the names of Hench (11), Vogel and Holland (12-15), Kokubo (16-18) etc.

Bioglass-ceramics are successfully synthesized by sol-gel methods (19, 20,21). In the CaO - Al_2O_3 - P_2O_5 - ZnO the bioactive porous glass-ceramic materials have been obtained (22).

Hill and Wood on the basis of their investigations about ionomer glasses (23,24) have developed a new castable bioglass-ceramics with main crystalline phases-fluorapatite and

mullite (25, 26). M. Dimitrova - Lukacs has obtained apatite-mullite glass-ceramics based on hydroxyapatite and received high mechanical properties of these materials (27).

The main purpose of the present work is to investigate the processes of phase formation in the gels during the sol-gel synthesis of apatite-mullite glass-ceramics.

II. EXPERIMENTAL

The gels of the composition $1{,}5SiO_2.0{,}5P_2O_5.1Al_2O_3.1CaO.0{,}75CaF_2$ marked as glass B in (25), were synthesized using the following precursors in appropriate amounts: SiO_2 - sol (laboratory obtained according [28]), TEOS, $Al(NO_3)_3.\ 9H_2O$, $Ca(NO_3)_{2.}4H_2O$, $(NH_4)_3PO_4.3H_2O$ and CaF_2.

The manner of the component mixing, gel formation and thermal treatment are shown at scheme 1. The samples studied are characterized as follows:

sample 1 - glass B, SiO_2-sol, CaF_2 before gelling;

sample 2 - glass B, SiO_2-sol, CaF_2 after gelling;

sample 3 - glass B, TEOS, CaF_2 before gelling;

sample 4 - glass B, TEOS, CaF_2 after gelling;

The phase formation after thermal treatment in the 950 -1250^{o}C temperature range was followed by means of X - ray diffraction analysis (Diffractometer DRON-UM1, Cu K_α radiation), IR - spectroscopy (Spectrometer Specord M - 80), transmission electron microscopy (TEM) and transmission electron microdiffraction (TEMD) Electron Microscope EM - 400, Phillips).

III. RESULTS AND DISCUSSION

The gels of the composition $1{,}5SiO_2.0{,}5P_2O_5.1Al_2O_3.1CaO.0{,}75CaF_2$ were prepared and thermal treated according the scheme 1. The results of X - ray diffraction study on the phase formation in thermal treated gels (samples 1 and 2) are presented in figs. 1 and 3. It was established the crystallization begins at 950^{o}C when SiO_2 has been introduced as SiO_2 and the main crystalline phases are apatite and mullite. The samples 1 and 2 present different behavior during the thermal treatment. For the sample 1, when the CaF_2 was added before gelling, at 950^{o}C its peaks are absent. For the sample 2, when the CaF_2 was added after gelling, the peaks of CaF_2 are presented at 950^{o}C and 1050^o. At higher temperatures the intensity of the mullite and fluorapatite diffraction peaks decreases, which is more clearly expressed in X-ray data of the sample 1, where some diffraction maxima of gehlenite appear. In special experiment it has been established that at 1350^{o}C the sample is almost melted, the pores are absent and the specimens possesses good mechanical strength. The morphology of the samples was studied by TEM.

The phase formation is different when the SiO_2 has been introduced by TEOS. Anorthite, fluorapatite and mullite crystallize at 950^o C from the amorphous gels.The presence of free CaF_2 is also found.

The assignment of the IR-spectra of the investigated specimens is made on the bases of the spectra of the main crystalline phases: fluorapatite and mullite (29,30). IR-spectrum of pure fluorapatite is characterized by a strong triplet band at 1100, 1050 and 970 cm^{-1} and a well defined absorption doublet bands at 607 and 577 cm^{-1} (29). The

observed bands are assigned to the stretching and bending vibrations of the PO_4 - tetrahedra in the fluorite structure. IR-spectrum of pure mullite is determined by a strong broad absorption maximum at 1060 cm^{-1} and two others at 790 cm^{-1} and 460 cm^{-1}.

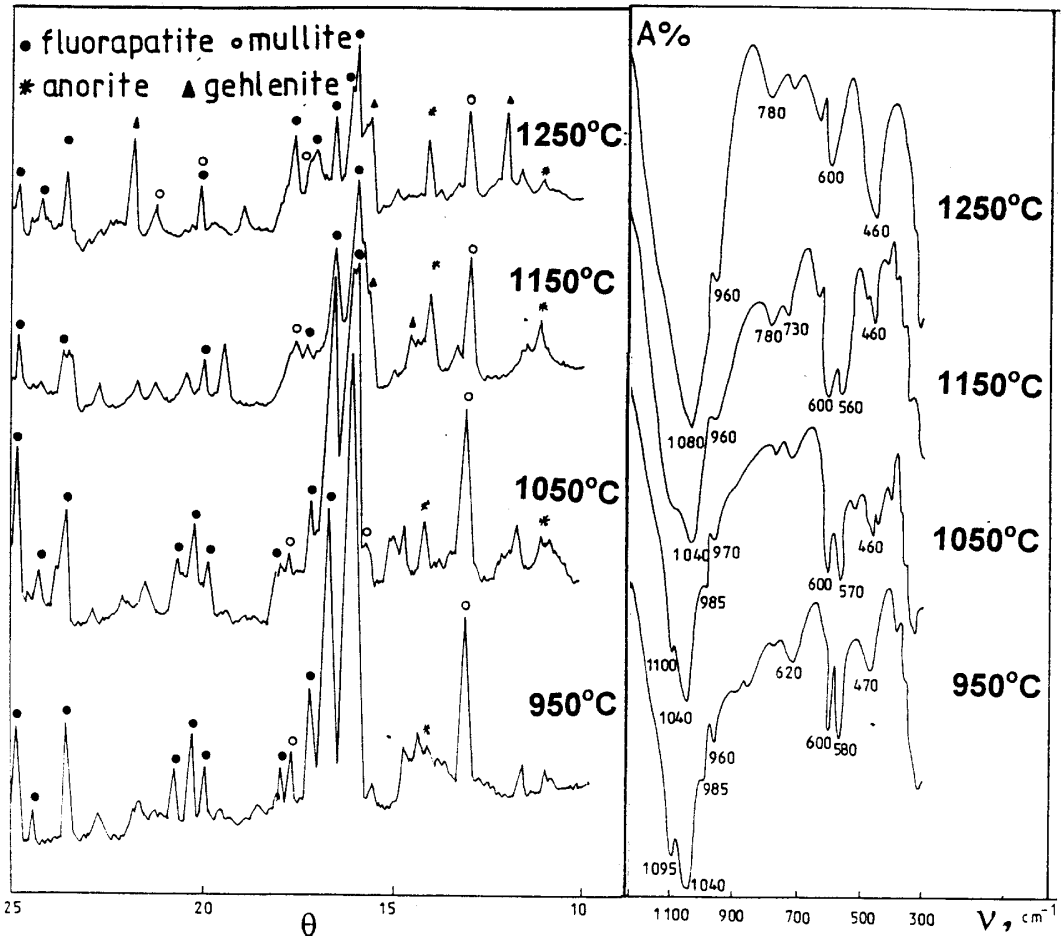

Fig.1. X-ray diffraction pattern of sample 1. Fig.2. IR-spectrum of sample 1.

These bands are assigned mainly to the stretching and bending vibrations of SiO_4 - tetrahedra. The IR-spectra of the multicomponent samples (compositions 1 and 2) are shown in Figures 2 and 4.

A good agreement exists between the spectra of samples 1 and 2 and the spectrum of pure fluorapatite. Therefore fluorapatite and mullite are the main crystalline phases in these samples which is in an agreement with the X-ray diffraction data.

The IR-spectra of the samples 3 and 4 show a difference in respect to the spectra discussed above. There is a broadening of the main absorption band around 1040 cm^{-1} and a new band of 940 cm^{-1} appears. This change could be related to the formation of the anorthite phase. The main absorption band is located at 940 cm^{-1}.

According to the purpose of the observations the samples for the TEM investigations were prepared as follows : 1) powdered gels deposed on electron microscopic grids ; 2) replicas from fresh fractured surfaces of the bulk samples.

In the frst case the initial stages of the formation of crystals were observed using bright and dark fýeld TEM mode in combination with TEMD. The replica technics was applied to study the morphology on the products obtained after heat treatment of the gels.

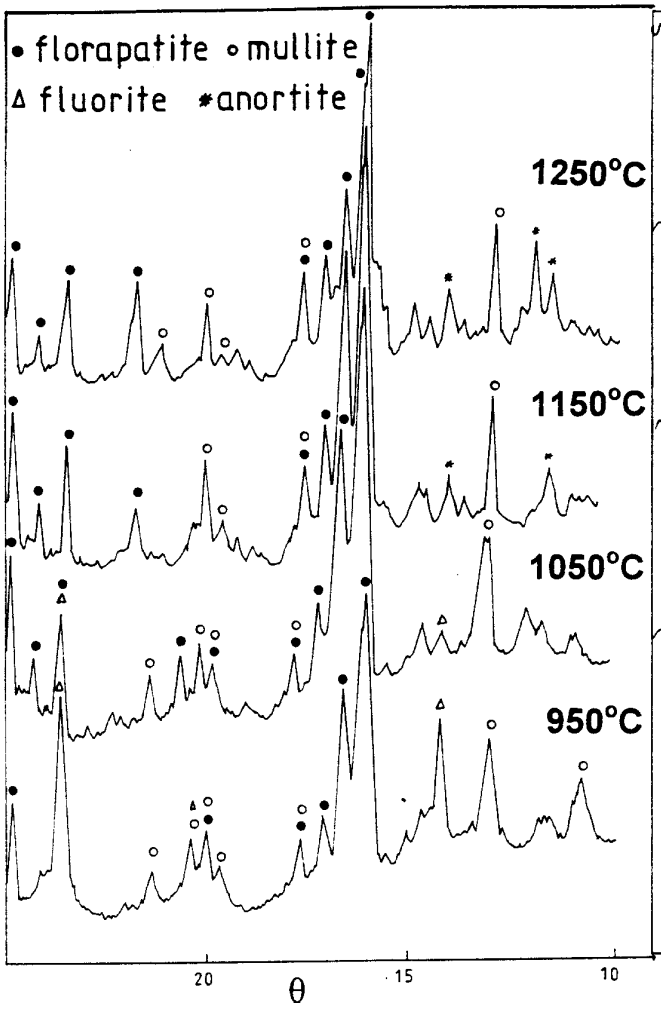

Fig.3. X-ray diffraction pattern of sample 2.

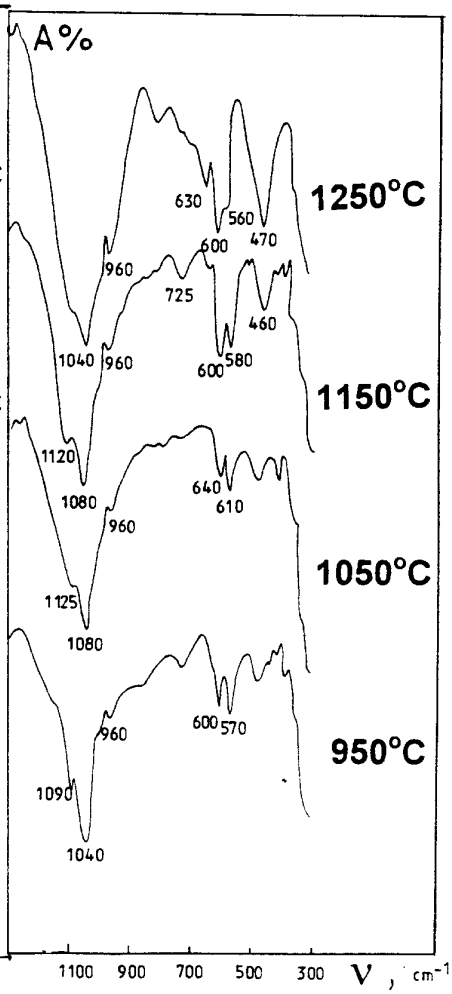

Fig.4. IR-spectroscopy of sample 2.

From the electron micrographs of the samples and their corresponding electron diffraction patterns the formation of crystals which are dispersed in an amorphous matrix, starts at 950^{o}C. The sizes of the crystals vary from 0,05 μm to 1 μm.

The morphology of the heat treated at 1350^{o}C sample 1 is found to be rather complicated (Fig.5). There exist different kinds of microstructure presented as: 1) crystallized gel grains (Fig. 5, a) ; 2) well - shaped crystals developed separately from the grains and probably they crystallize from the amorphous matrix (Fig. 5, b) ; 3) amorphous matrix connecting the crystals and grains (Fig. 5, c).

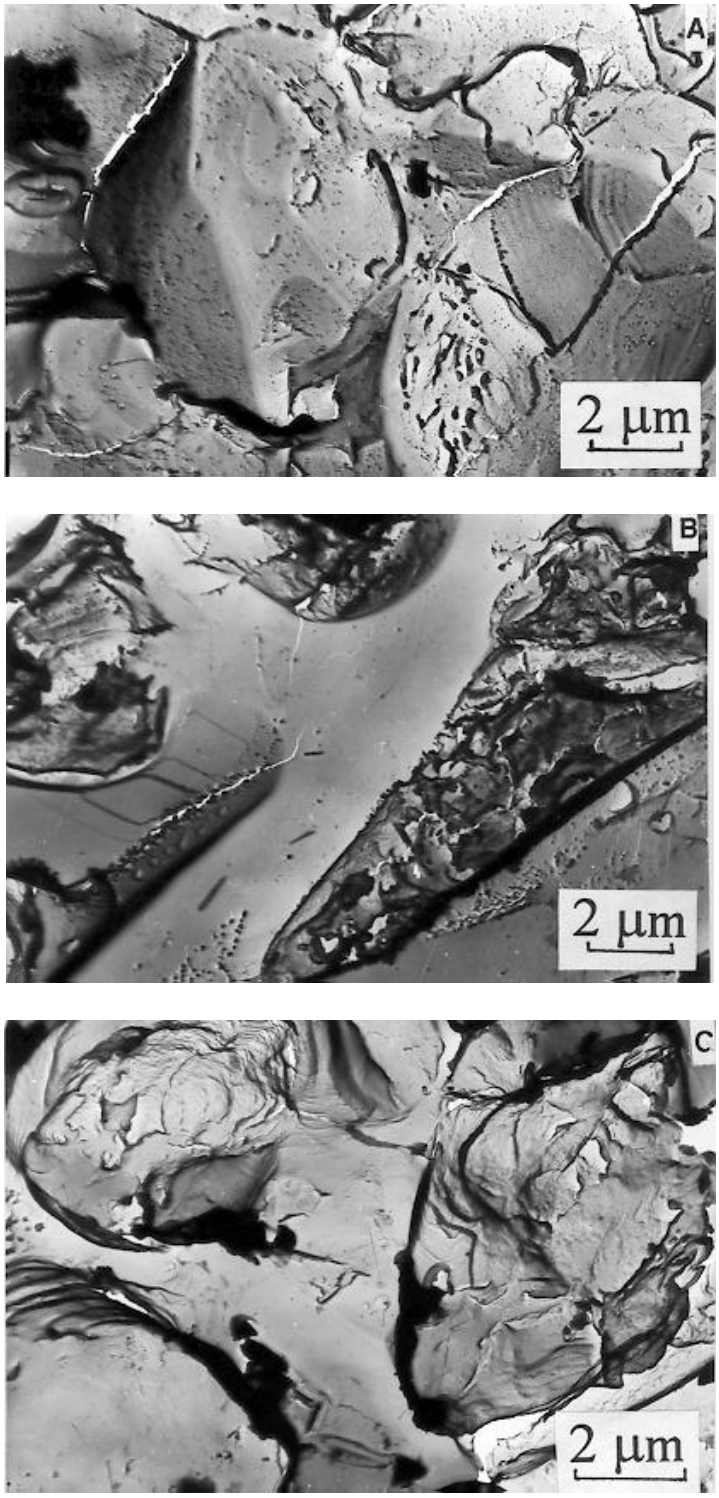

Fig.5. Morphology of sample 1 treated at 1350^{o}C.

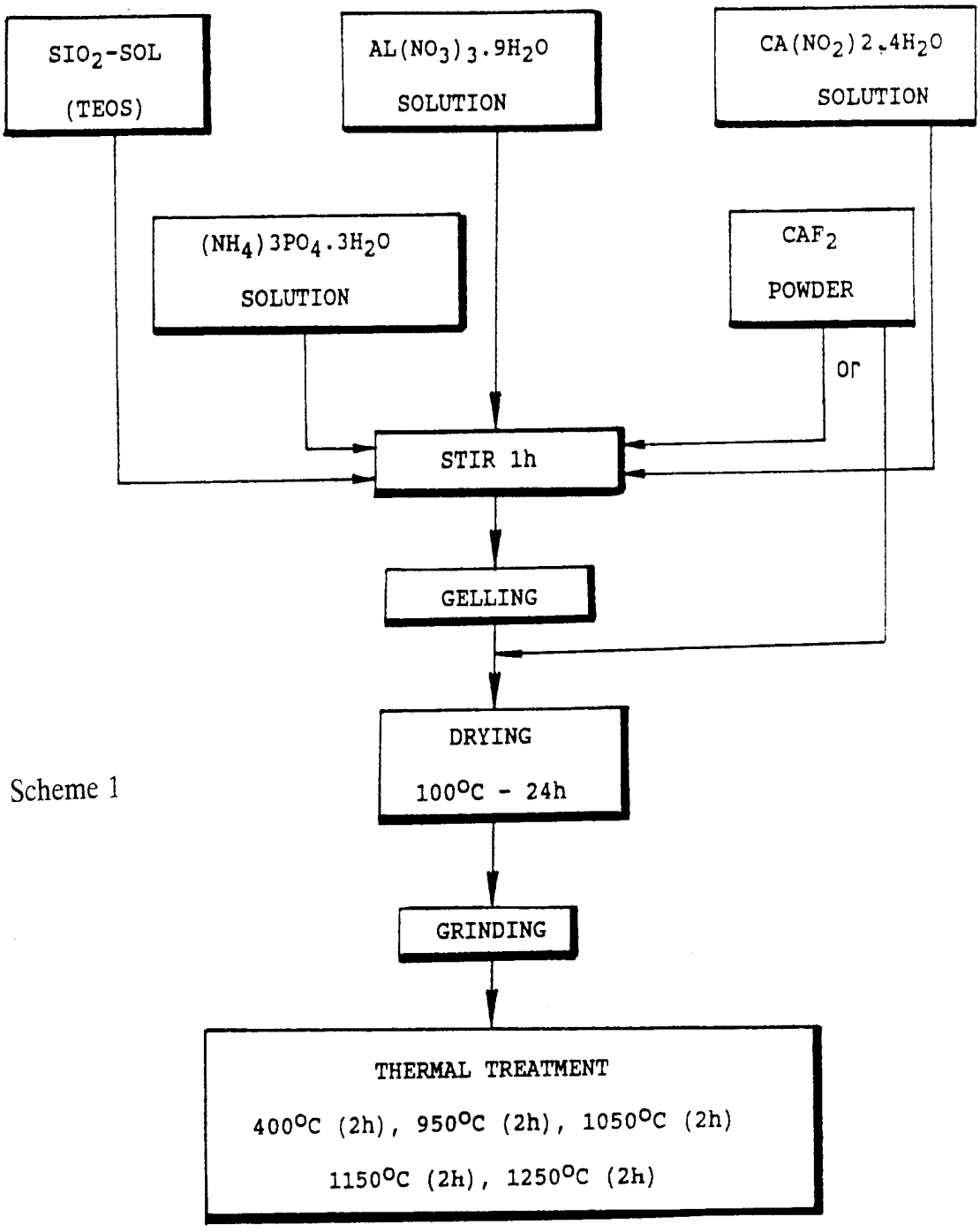
SIO2-SOL
(TEOS)
AL(NO3)3.9H2O
SOLUTION
CA(NO2)2.4H2O
SOLUTION
(NH4)3PO4.3H2O
SOLUTION
CAF2
POWDER
or
STIR 1h
GELLING
DRYING
100°C - 24h
GRINDING
THERMAL TREATMENT
400°C (2h), 950°C (2h), 1050°C (2h)
1150°C (2h), 1250°C (2h)

Scheme 1

IV. CONCLUSIONS

The phase formation during the synthesis of apatite - mullite glass-ceramics is studied at thermal treatment of gels in the 950-1250^{o}C temperature range, using X-ray diffraction analysis, IR - spectroscopy, TEM and TEMD.

It is established that the SiO_2 precursors influences strongly the process of phase formation. The SiO_2 - sol stimulates the fluorapatite and mullite formation and also the amorfisation of these materials at low temperatures, while the TEOS provokes the crystallization of fluorapatite, anorthite and mullite.

From the X-ray diffraction and IR - spectroscopy data in can conclude that the best way for synthesis of apatite - mullite glass-ceramics is by direct crystallization of the gels (1150 -1250^{o}C) prepared by SiO_2 - sol and the addition of CaF_2 powder after the gelling processes.

Acknowledgment :

We would like to acknowledge the fýnancial support from the EU under the COPERNICUS Project No ERB3512PL940583 Contract No CIPA - CT94-0145.

REFERENCES

[1] S. Sakka, Transactions of Indian Ceram. Soc., 46 (1987)1.
[2] S. Mukherjee, J. Zarzycki, J. Traverse, J. Mat. Sci.,11 (1976)341.
[3] D. Uhlmann, M. Weinberg, G. Teowee, J. Non-Cryst. Solids,100(1988)154.
[4] M. Nogami, J. Matt. Sci., 21 (1986)5313.
[5] M. Nogami, K. Nagasaka, K. Kadono, T. Ishimoto, J. Non-Cryst. Solids, 100 (1988) 298.
[6] M. Chen, W. Zee, P. James, J. Non-Cryst. Solids,147/148 (1992)532.
[7] M. Sales, J. Alarcon, Third Euro- Ceramics, v.2 1121, Edited by P. Duran and J. Fernandez, Faenze Editrice Iberica S. L.,1993, Spain.
[8] B. Unger, H. Jancke, R. Muller, B. Peplinski, M. Hahnert, Glasstech. Ber. Glass Sci. Technol., 67C (1994)448.
[9] B. Samuneva, Y. Dimitriev, V. Dimitrov, Y. Ivanova, E. Kashchieva, P. Djambaski, Proc, XI Inter. Congress on Glass, Leningrad, v. 2a(1989)26.
[10] B. Samuneva, V. Dimitrov, E. Kashchieva, V. Chernev, P. Hinkov, Glasstech. Ber. Glass Sci .Technol. 67C (1994)440.
[11] L. Hench, J. Non. Crist. Solids,19 (1975)27.
[12] W.Vogel, W. Holand, Z. Chem. 22 (1982)429.
[13] W.Vogel, W. Holand, K. Nauman, J. Non-Crist. Solids, 80 (1986)34.
[14] W. Holand, M.Frank, M. Schweiger, V.Rheinberger, Glass-tech. Ber. Glasses Sci. Technol., 67C (1994) 117.

[15] W. Holand, M.Frank, M. Schweiger, V.Rheinberger, Proc. XIII Congress on Glass, Beijing, 5 (1995)133.
[16] T. Kokubo, Third Euro-Ceramics, v. 3, 1, Ed. P. Duran, J. Fernandez, 1993, Spain.
[17] T. Kokubo, Glastech. Ber. Glass Sci. Technol., 67C (1994)105.
[18] T. Kokubo, Proc. XIII Int. Congr. Glass, Beijing,1995, v.1, 3.
[19] P. Li, K. de Groot, T. Kokuybo, Third Euro-Ceramics, v. 3,101,1993, Spain.
[20] P. Li, K. de Groot, J. Sol-Gel Sci. Technol., 2 (1994)797.
[21] P. Li, C. Ohtaski, T. Kokubo, J. Amer. Cer. Soc., 75(1992)2094.
[22] Y. Ivanova, E. Spasova, Y. Dimitriev, B. Samuneva, E. Kashchieva, J. Sol-Gel Sci. Technol., 2 (1994)819.
[23] D. Wood, R. Hill, Biomaterials,12(1991)164.
[24] D. Wood, R. Hill, Clinical Materials 7(1991)301.
[25] R. Hill, M. Patel, D. Wood in: "Bioceramics", v.4, Ed. W. Bonfýeld, G. Hastings and K. Tanner (Butterworth Heinemann, London,1991, p. 79.
[26] R. Hill, C. Goad, D. Wood, J. Amer. Ceram. Soc. 75 (1992) 778
[27] M. Dimitrova-Lukacs, L. Gillemot, Third Euro-Ceramic, v. 3,179,1993, Spain.
[28] V. Tihonov, E. Galabutskaya et al., Laboratornii Praktice on Silicon Chemistry and Physical-Chemistry on Silicates, Ed. N. Todorov, Publishing House of the University of Lvov,1965, p.135.
[29] S. Sakka, K. Kamiya, J. Non-Cryst. Sol., 42(1980)40.
[30] K. Okada, Y. Otsuka, J. Am. Ceram. Soc., 69(1986)652.

PHYSICAL AND CHEMICAL PROPERTIES OF SOME NATURAL GLASSES WITH REGARD TO THEIR APPLICATION IN BUILDING MATERIALS

R. Stodolski[1] ,Y. Gülebakan[1] , I. Sauer[1] , U.Hildebrandt[1] , K. Forkel[2] , C. Köcher[3] and **F.-G. Wihsmann[3]**

[1] Technical University of Berlin, [2] Advanced Technical College of Wildau, [3] Federal Institute for Materials Research and Testing (BAM), Germany

Abstract

Thermally treated natural glasses such as perlite and pumice can be used in the building industry for lightweight concrete and excellent thermal insulating materials without any environmental problems.The quality of these products is determined by the physical and chemical properties of the raw and the modifed materials. Therefore, investigations have been made for better understanding of the physical-chemical properties as well as the microstructure of a new pumice variety from the Turkish region Afyon.The elemental analysis was conducted by EDAX. The microstructure of the pumice specimens was observed using scanning electron micrographs (SEM). The bulk density of the pumice specimens was found to be about 1.15 g/cm^3.Thermal behaviour was studied by a simultaneous TGA/DTA apparatus. Crystalline phases in the materials were identified by powder XRD and glass phases were characterized by IR spectroscopy. Microstructural and mechanical properties are useful references and guidelines for industrial practice, especially for natural inexpensive brick-like products with good insulation characteristics as well as a support for metallic catalysts and biotechnological applications.

I. INTRODUCTION

Volcanic glasses such as obsidians, perlites, pitchstones and pumices with chemical compositions mainly of rhyolites and dacites, i.e. SiO_2 % ≥ 63 [1], represent a characteristic group of natural glasses. When the volcanic melt was quickly quenched it solidified to glass. On the other hand, slower cooling led to more or less complete devitrification with an assembly of crystalline inclusions (phenocrystals) such as soda-sanidine, a mixture of soda-potash feldspars, plagioclase, quartz and less frequently biotite and limonite. These inclusions were probably formed due to the preservation of composition fluctuations during quick heating and cooling of the volcanic melt.

Obsidians are formed by rapid quenching from acidic volcanic melt flows with 70 to 75% SiO_2, i.e. rhyolites. The content of water usually does not exceed 1 wt.% but that of volcanic gases HCI, SO_2, H_2S or CO_2 is rather high. Because of that, obsidians transform at about 1000^{o}C to pumice-like products with a frothy texture. Pitchstones with a similar

chemical composition like obsidians, are characterized, however, by much higher water concentrations from 5 to 9 wt.% but much lower contents of volcanic gases. The water is released at 200 to 300 ^{o}C. Pitchstones are probably formed by hydration of obsidians.

Perlites are metastable amorphous, i.e. glassy aluminum silicates formed from rhyolites similar to obsidians. A typical average chemical analysis would be: 71-75 wt.% SiO_2,12,5-18 wt.% Al_2O_3, 4-5 wt.% K_2O,1-4 wt.% sodium and calcium oxides, traces of other metal oxides and 2-5wt.% water[2]. Perlites can be formed by low-temperature postmagmatic hydration of obsidians with a characteristic concentric-spheric, mainly glassy, microstructure. The perlites are widely applied in the non-metallic industry due to their specific properties. Because of their low melting temperatures, perlites may be used as a raw material in the glass-making industry. When perlites are rapidly heated to a temperature in the range from 1000 to 1200^{o}C, thereby driving off the water, these are expanded to very lightweight pumice-like products with extreme pouring densities of up to approx. 0.03 g/cm^3. These products are used in the building industry especially for artificial lightweight aggregates with excellent heat insulating properties. There is considerable increase in the application of lightweight concretes using lightweight aggregates from volcanic glasses such as artificial expanded perlites [3]. The high acidic character of the perlites suggests, however, that pozzolanic reactions take place. The consequences for the properties of the concretes are not so clear. In some studies on the microstructure of such concretes it has been suggested that pozzolanic reaction between the aggregate and the paste matrix is a factor contributing to strength, whereas in others no such interactions were observed.

Pumices, froth-like volcanic rocks with a bulk density ranging from 300 to 1200 kg/m^3, can be formed from volcanic glasses such as obsidians and perlites by heating to between 1000 - 1200^{o}C. By rapid decompressions and degassing of magmatic melts with high contents of volcanic gasses during the extrusion period, high porous frothy materials with elongated macropores were formed. A typical pumice consists of approx. 55 wt.% SiO_2, 22 wt.% Al_2O_3,11 wt.% alkaline oxides and traces of other metal oxides. Pumice pebbles with grain sizes of about 7 up to 40 mm are used in the production of lightweight concrete, the so called pumice concrete. Those varieties of pumice which are not too weak structurally and free from fine volcanic dust and materials, not of volcanic origin such as clay, produce a satisfactory lightweight concrete with a dry density of concrete of between 700 and 1450 kg/m^3 and provides a better thermal insulation than other types of lightweight concrete do. Pumice is more widely employed than any of the other natural lightweight aggregates such as diatomite, scoria, volcanic cinders and tuff, except for diatomite, all of these also being of volcanic origin. Recently, pumice was used as a raw material for the production of mineral fibres which could be used in thermoinsulating material. Because of its frothy microstructure, pumice can be easily machined. Further using pumice are adsorbents such as that for phosphate removal from waste water [4] and as a support for catalysts [5].

The aim of the present study is to investigate the mineralogical composition, the physical-chemical properties, and the microstructure of a new natural pumice rock from the Turkish region Afyon with regard to its prospective applications, especially in the building industry, for natural inexpensive brick-like products with good insulation characteristics as well as a support for metallic catalysts and adsorbents.

II. EXPERIMENTAL

The microstructure of the pumice specimens was observed using scanning electron micrographs (SEM) obtained from a Philips XL 20. Energy dispersive X-ray analysis (EDAX) was carried out employing an EDAX MODELL XL 20 to determine the elemental contents of the different phases. The specimen surfaces were subjected to light microscopical examinations with an OLYMPUS BH 2 microscope using a cold light source KL 1500 electronic. Differential thermal analysis (DTA) and thermal gravimetric analysis (TGA) were carried out on a simultaneous thermal analyzer Netzsch STA 429. IR spectra was recorded by means of a Pye Unicam PU 9512 infrared spectrophotometer employing the KBr pellet technique.The crystalline phases were analyzed by X-ray analysis (XRD) with a .Philips diffractometer PW 17 (range of angles $2\theta = 5 - 75^{o}$ Cu Kα radiation). The phases were identified from peak positions and intensity by computer analysis using reference data from the JCPD- Handbook.The bulk density of the pumice was determined for specimens of 4x4x16 cm by weighting after drying at 105^{o}C. The BET measurements were pertormed by nitrogen adsorption at liquid nitrogen temperature with an ASAP 2000 Surface Area Analyzer (Micromeretics) to measure the specific surface area.

III. RESULTS AND DISCUSSION

From the EDAX results, an average composition of the pumice matrix was found, as shown in Tab.1, which can be approximately represented by the formula: $Na_{0,25}$ $K_{0.35}$ $Mg_{0.15}$ $Ca_{0.2}Ti_{0.1}$ Fe_x $Al_{0.9}Si_3O_{8.2+X}$ (0.22-x) Fe_2O_3. This is similar to soda orthoclase $Na_xK_yAlSi_3O_8$, a mixed crystal of orthoclase $K(AlSi_3O_8)$ and albite $Na(AlSi_3O_8)$.

Table 1. Average chemical composition of the pumice from the Afyon region

Oxide	Na_2O	K_2O	MgO	CaO	Fe_2O_3	TiO_2	Al_2O_3	SiO_2
Weight%	2.6	5.0	2.1	3.8	11.05	2.45	14.95	58.05

Typical EDAX spectra are shown in Fig.1. With a SiO_2 content of 58 wt. %, the Afyon pumice was found to be arranged in the transformation region between dacites and acidic andesites [1], whilst the pumice of Lipari with 70 wt.% SiO_2 is of rhyolitic origin.The Afyon pumice is especially characterized by its rather high iron content. Because of the promotional affects of iron related to some microorganisma, as well as those of the porous texture of the pumice, it could be a very promising candidate for biotechnological applications.The oxide concentration of calcium is characteristic for pumices of the Turkish region Anatolia which was determined by Onar et al. [4] as between 1.8 and 7.6 wt.% in contrast to that from the Marmara region, which was found to be extremely high, up to about 33 wt.%. Due to the low CaO content, it is expected that the Afyon pumice is not suitable as an adsorbent for phosphate removal from waste water [4]. Titanium is an inherent constituent of the volcanic glasses.

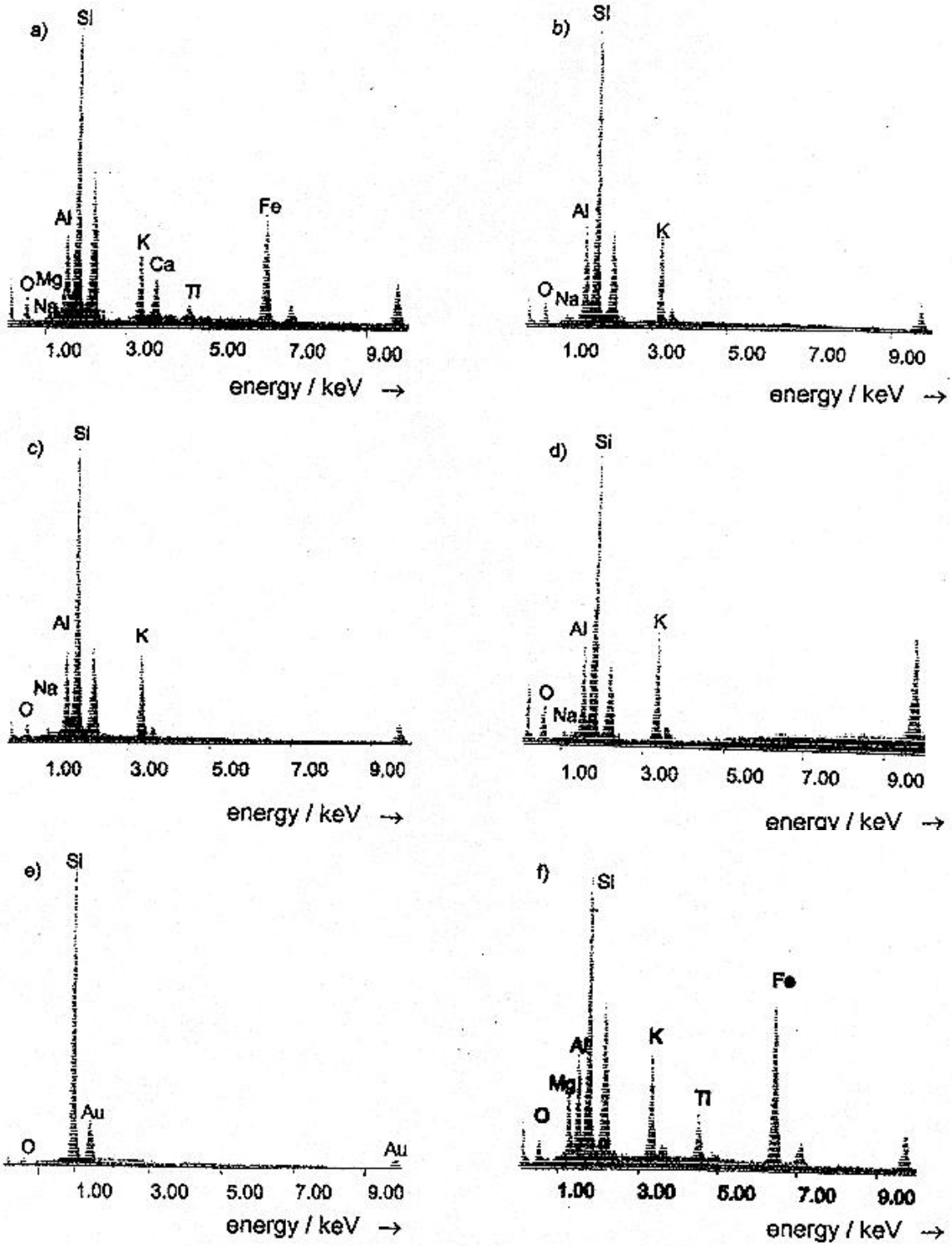

Fig.1 EDAX spectra of the a) pumice matrix and the inclusions b) yellow-white c) green d) red e) transparent green f) golden glittering

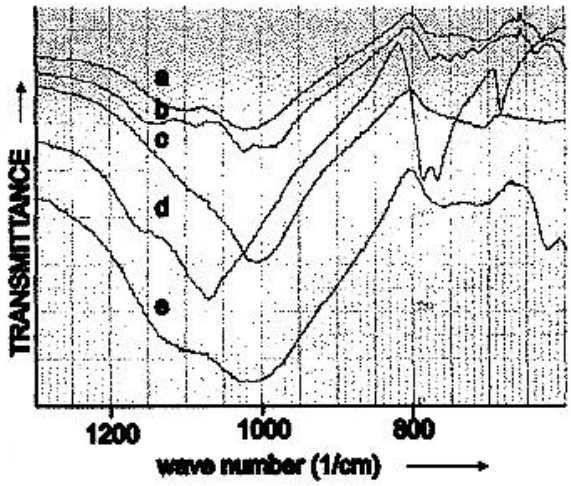

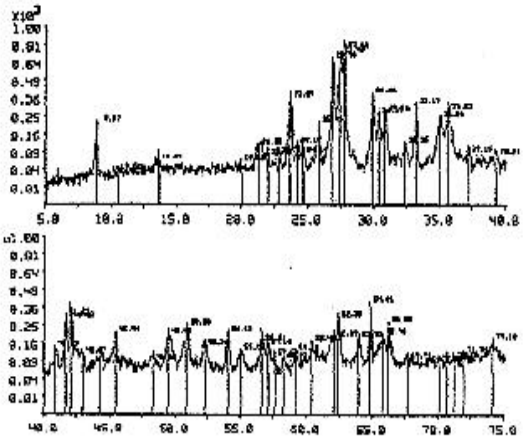

Fig. 2 IR spectra of the indusions a)yellow-white c)golden glittering d)transparent and e)pumice matrix b)albite

Fig. 3 XRD pattems of the Afyon pumice

The comparison of the IR spectra of the pumice matrix and albite in Fig.2e and 2b also reveals that the matrix of the Afyon pumice consists mainly of silicate anions with a feldspar like three-dimensional structure of which a quarter of the silicon atoms are substituted by aluminum atoms. Compared to the spectrum of quartz in Fig.2d the Si-O valence frequency is therefore shifted to lower wavenumbers and the SiOSi(Al) bridge vibration is broadened because of the statistical distribution of the aluminum atoms in the monocline sanidine as a result of rapid quenching.

Rittmann [6] has suggested the following empirical parameters to distinguish between orogenic and cratogenic volcanites by a λ'/σ'-diagram

$$\sigma = (Na_2O + K_2O)^2 / (SiO_2 - 43) \quad (1)$$

$$\lambda = (Al_2O_3 - Na_2O) / TiO_2 \quad (2)$$

$$\sigma' = \sigma/(10 + |\sigma|) \quad (3)$$

$$\lambda' = \lambda/(10 + |\lambda|) \quad (4)$$

whereby the oxide concentrations are also given in weights%. With such calculated values of $\sigma' = 0.28$ and $\lambda' = 0.34$, the Afyon pumice is positioned in Rittmanns so called basalt field (B) which is characteristic for cratogenic volcanites. Indeed, there is a volcanic crater nearby the deposit of the Afyon pumice that gives evidence for the cratogenic origin of it.

The X-ray diffractogram in Fig. 3 indicated that the major crystalline phases in the pumice were hematite Fe_2O_3 and sanidine, the monocline high temperature(>900^oC) modification of orthoclase or soda orthoclase, respectively. A biotite-like phase was also found.The feldspars and biotite were formed by partial devitrification of the glassy volcanic silicate melt which had a feldspar-like composition. Because of the rapid quenching of the melt, the instable mixed soda sanidine crystals were not transformed to perthites at lower temperatures. During further cooling, the biotite was found to become unstable and partially decomposed with liberating iron oxide, which was oxidized by oxygen to hematite.

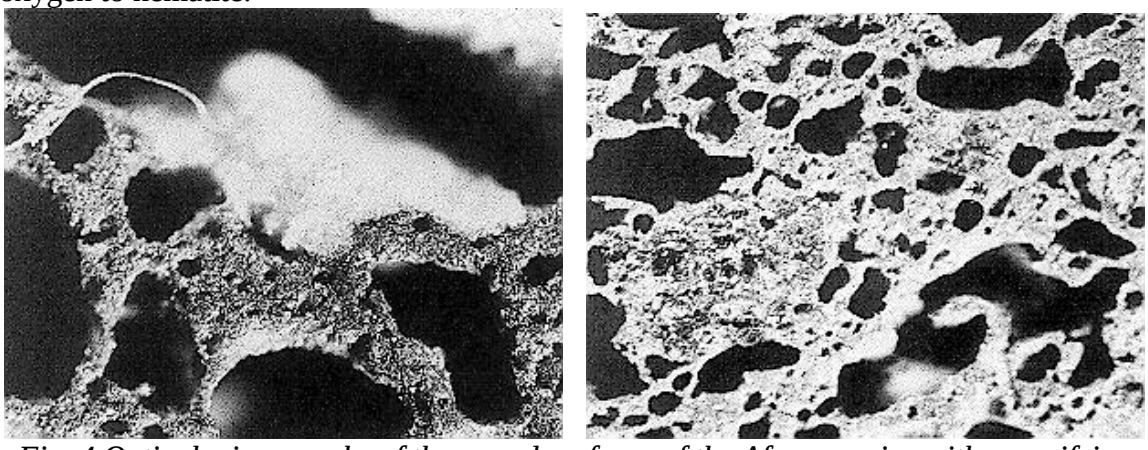

Fig. 4 Optical micrographs of the sawed surfaces of the Afyon pumice with magnifying power a) 50 b) 25

Different coloured crystalline inclusions, e.g. more opaque compact yellow-white and platelike golden glittering particles, as well as more transparent red or red-brown, green

and colourless particles were observed in the optical micrographs as can be seen in Fig. 4 a and b for yellow-white and green, respectively. The corresponding phases can be identified by the EDAX spectra in Fig.1 and the IR spectra in Fig. 2. The transparent colourless and sometimes blue-green glittering inclusions essentially consist of quartz. The inclusions with red or green colour are composed from soda sanidine $Na_xK_yAlSi_3O_8$ with x=0.3 or 0.45, respectively. The yellow-white crystalline inclusions, mainly observable, can be described by the formula $Na_{0.3}K_{0.6}Fe(3)_{(0.1)/3}AlSi_3O_8$, i.e. they have essentially the same composition as the green and red, but have additional traces of iron incorporated in them. These results were found to be in accordance with the structural criterias for the incorporation of cations in potash feldspar, whereby small cations such as Mg, Ca and Fe can not be, or only with very low contents, incorporated. The platelike golden glittering particles represent a biotite-like phase (magnesia mica) with the approximate formula $K_{0,55}(Mg_{0,7},Fe(2)_{0.75},Fe(3)_{0.15},\ Al_{(4/3)0.2+0.1})\ Ti_{0.2}Al_{1-(4/3)0.2}Si_3O_{10}$. z H_2O. This phase, so called cat gold, was apparently formed by the weathering of the biotite, whereby iron became oxidized by oxygen and together with potassium was partially leached [7], which may be described by the following schematic reaction:

$$KMg_{3-x}Fe(2)_xAlSi_3O_{10}(OH)_2 + 3/4\ O_2 \rightarrow K_{0.5}Mg_{3-x}Fe(2)_{x-y-1.5}\ Fe(3)_y\ AlSi_3O_{10}{+}0.5KOH + 1.5\ FeOOH$$

Based on that reaction, for the original biotite it can be suggested a chemical composition with a Fe/Mg ratio of about 3.2 being near that of the pumice matrix of about 2.7 from which the biotite was crystallized. Additionally, titanium was present which substitutes itself for aluminum or eventually magnesium and not silicon as suggested for Wodanite [8].

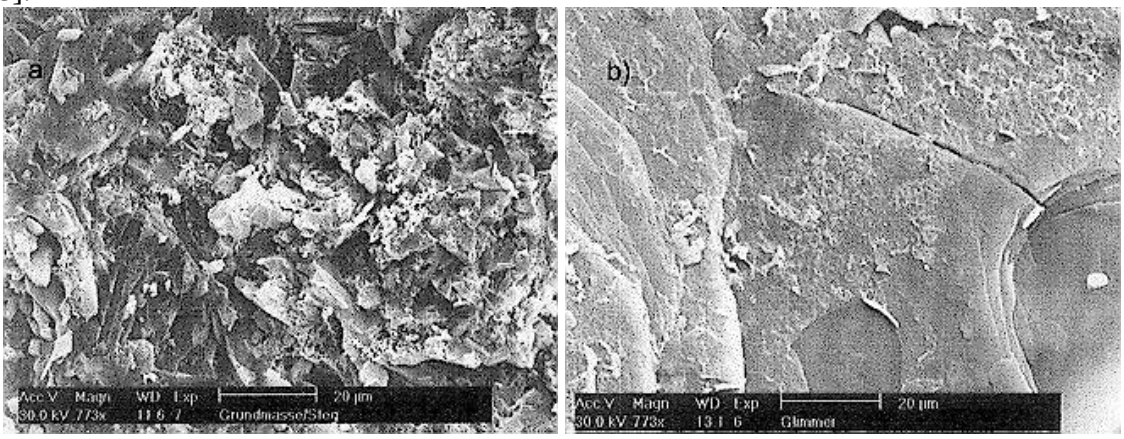

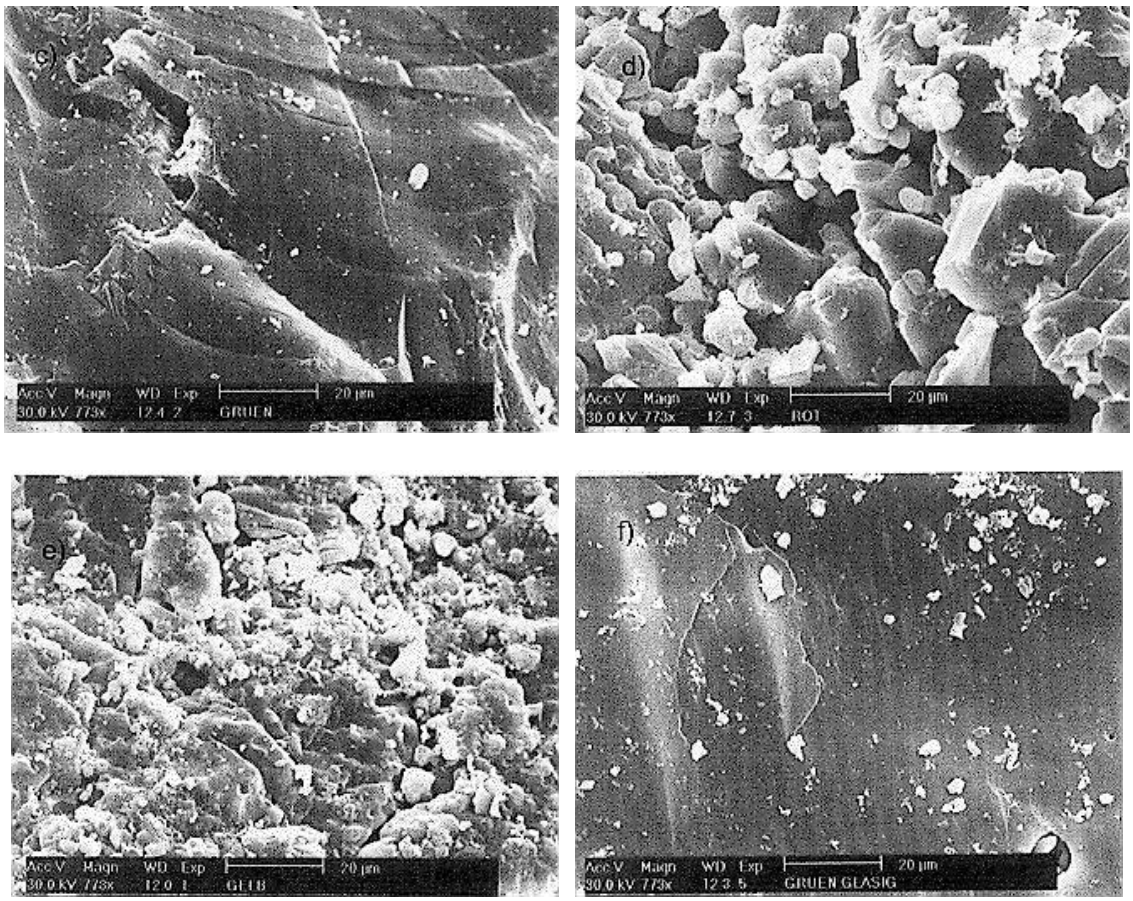

Fig. 5 Scanning micrographs of a) the pumice matrix and the inclusions b) golden glittering mica particles c) green d) red e) yellow-white f) blue-green

The morphology of the inclusions is illustrated in the SEM micro graphs in Fig. 5 b - f. Whilst the yellow-white inclusions exhibit more fused aggregates, the biotite-like phase as well as the quartz, the green and the red inclusions form large crystals. The optical micro graphs in Fig. 4a and b show the typical flow structure of the pumices, with near parallel elongated macropores, which are separated by walls forming an unordered deformed honeycomb-like texture. The walls are build up from assembles of glassy or crystalline particles, mainly 1-10 µm size, which are more or less fused, sintered or intergrown together with some of the pores between. This can be observed in the optical and SEM micro graphs shown in Fig. 4a and Fig. 5a, respectively. The characteristic flow texture of the pumice macropores is caused by the extreme behaviour of their volatile components, especially water as well as CO_2, SO_2, N2, HCl and Cl_2, which were originally bounded or soluted in the melt. The following processes can be suggested: The forming of the bubbles starts during the rise in the chimney caused by decompression, whereby the bubbles were larger but then elongated by the influence of the shear forces. The high content of gas bubbles in the magmatic melt increased the viscosity of that mainly by surface tension and the decrease of temperature due to the adiabatic expansion of the gas. Due to this, the walls between the bubbles were reinforced and the bubbles conserved.

The bulk density of the pumice specimens was found to be about 1.15 g/cm^3 and that of powdered pumice to be 2.45 g/cm^3. The true porosity determined from this is about 55 vol.%. The major part of this consists of macropores, the content of micropores, as evaluated from BET measurements, was very low. Because of the partial fusion and densification of its constituents, the pumice from Afyon is characterized by a very low specific surface area of about 1.3 m^2 / g. Most of the other varieties of pumice have much higher surface areas between 5 m^2/g for that of Lipari[9] and of about 24 m^2/g for pumices from other Turkish regions [4].The apparent porosity calculated from the water absorption at atmospheric pressure was found to be about 22 vol.%. These results revealed that only approximately half of the pores volume can be penetrated by water. The remained pores volume consisted of closed pores.

In the DTA curve, two broad thermal effects was observed with T_{max} at about 1135oC and 1180 ^{o}C, respectively, which correspond to the melting process of the pumice. The transformation temperature was determined from the point of inflection to about 1080^{o}C and the softening intervall reaches from about 1000 ^{o}C to 1135^{o}C. Potassium feldspar is incongruently melting at 1150^{o}C and forming leucite and melt, whilst sodium feldspar melts at 1118^{o}C [10]. The melting point of a sodium sanidine with about 40 wt.% albite, which corresponds to the composition of the pumice matrix, is to be expected at about 1140^{o}C near the T_{end}=1135^{o}C of the DTA curve. During the melting the red colour of the pumice, mainly caused by the hematite, changes to dark green due to the incorporation of the iron in the formed glass.

IV. CONCLUSIONS

Because of its properties which have been discussed above, we think that the pumice of Afyon promises to be most suitable for applications in the building industry for which are required natural inexpensive brick-like products with good insulating characteristics. It may also be useful in biotechnology due to its promotional affects related to microorganisma.

REFERENCES

[1] Taylor, S. R. (1969): Trace element chemistry of Andesites and associated calc-alcaline rocks. - In: McBirney, A. R. [ed.]: Proceedings of the AndesiteConference-Oregon Dept. Geol. Mineral. Ind. Bull., 65: 43-65; Portland/Oregon.

[2] Wallace, P. B. (1995): Annual Minerals reviews. Am. Ceram. Soc. Bull. 74(6): pp.143-144

[3] Han, S. (1994): Ground waste aerated concrete based wall materials. CN 1,083,798 (CI. C04B28/00);16 Mar 1994, Appl. 92,110138, 07 Sep 1992; 7pp.

[4]Onar, A.N. (1996): Phosphate removal by adsorption. Environm. Techn.17: 207 - 213

[5)Deganello,G., Duca, D., Liotta,L. F., Martorana, A., Venezia, A. M., Benedetti, A., structural characterization, and liquid-phase hydrogenation of 1,3cyclooctadiene.J. Catal.151 (1):125-34
[6]Rittmann, A. (1981): Vulkane und ihre Tatigkeit. Ferdinand Enke Verlag Stuttgart, p.156
[7]Ramdohr, P. and Strunz, H. (1967): Lehrbuch der Mineralogie. Ferdinand Enke Verlag Stuttgart, pp.569 - 570
[8] Betechtin, A., (1980): Lehrbuch der speziellen Mineralogie. VEB Deutscher Verlag fur Grundstoffindustrie: p. 708
[9JRossi, A., Venezia,A:M., Floriano, M.A. and Deganello, G. (1995): Natural pumice by XPS. Surf. Sc. Spec. 3(2), pp.112
[10] Hinz, W. (1970): Silikate Bd. 2, VEB Verlag fur Bauwesen, Berlin

PHYSICOCHEMICAL PROPERTIES AND STRUCTURE OF THE TELLURIUMPHOSPHATE GLASSES*

N. V. Ovcharenko
S.I. Vavilov State Optical Institute, Russia

Abstract

The telluriumphosphate glasses are of interest to use as the basis of the new type glasses, which combine high refractive index with increased transmittance in ultraviolet region. Unlike the optical glasses with refractive index n_e more than 1.8, for example lead silicate glasses having yellow coloration, what limits their application in optical system, the telluriumphosphate glasses are colorless.

Based on investigation of the previously studied system TeO_2-P_2O_5 the relationship between physico-chemical properties and composition of systems TeO_2-P_2O_5-BaO and TeO_2-P_2O_5-PbO had been explored. The studies of optical and physico-chemical properties were conducted in the following way: as the concentration of one component changed, the ratio of two another was held constant.

Thus we have discovered that the optical constants fall in the following ranges: n_e,1.91729-2.09417, $n_{F,}$-$n_{C,}$0.03613-0.05543, ν_e 25.4-17.2. The transmittance of the glass (samples thickness 10 mm) for λ=400 nm comes to 90-97%. For comparison we shall exemplify some data for mach used heavy flint glass HF10 with refraction index n_e-1.8137: the transmittance of this glass (sample thickness 10 mm) for λ=400 comprises 61%. The glass crystallization had been studied by the polythermal method. The correlation between glass crystallization and the glass composition position in the equilibrium diagram was revealed.

---

* Full manuscript not available at the time of printing

PRODUCTS OF CERAMIC FIBRES; CHARACTERISTICS AND INDUSTRIAL USES

Eng. Lidia Cerchez
PROCEMA S.A. - Research, Design and Experimental Production Institute for Construction and Construction Materials, ROMANIA.

Abstract

Manufacture of ceramic fibres has opened the way to designing and building of thermotechnically performant furnaces.

The increasing energy costs have also led to the solution of extensively applying ceramic fibres to designing, building and operation of furnaces in all hot industrial sectors that are big energy-consumers.

The paper describes the present manufacture stage of the Romanian ceramic fibre-made products, with special reference to their application in various furnaces.

1. INTRODUCTION

During the last decade Romania has laid a great emphasis on improvement of industrial productivity and on reduction in energy consumption especially in energy-consuming industries, such as: metallurgy, petrochemistry, ceramics and building materials.

The ceramic fibres are alumino - silicate fibres obtained by melting a mix of refractory oxides (AI_2O_3 ;SiO_2) in an electric - arc furnace and by fibering the melt with centrifugal action disks.

The paper describes the present manufacture stage of the Romanian ceramic fibre - made products, with special reference to their application in various furnaces.

The fibres and ceramic fibre products have been locally produced as a result of research works carried out by the Laboratory of Ceramic Fibres wihin PROCEMA S.A., Bucharest.

2. POSSIBLE MEASURES FOR ENERGY-SAVING

Replacing the heavy thermotechnical equipment of high heat losses with reduced overall size equipment that is more easily handled, operated and maintained has been based on appearance, within the range of light-weight insulation products, of ceramic fibre-made products: rigid boards, shaped elements, moulds, blocks, cardboard and paper, applicable within a temperature range of 1000-1450^{o}C, in application.

The major characteristics and application fields of these products are given in tables 1,2.

Table 1. Characteristics and practical applications of ceramic fibres, paper and cardboard

Characteristics	BULK FIBRE			PAPER/CARDBOARD			Field of application
	1250°C	1350°C	1450°C	1250°C	1350°C	1450°C	
1.Definition	Silico-aluminious fibres with content of:			Products based on silico-alluminous fibre:			* sealing joints * fillers * roller axis hinges at ceramic furnaces
	Al_2O_3 45-50%	Al_2O_3 45-50% Cr_2O_3 3%	Al_2O_3 45% ZrO_2 12-18%	Al_2O_3 45-50%	Al_2O_3 45-50% Cr_2O_3 3%	Al_2O_3 45% ZrO_2 12-18%	
2.Average diameter µm	2.5-3	2-3.5	2.5-3	-	-	-	
3.Average length,mm	80-150	80-150	80-150	-	-	-	* metal pipe insulation
4.Apperant density, kg/m^3	100-200	180-200	220-240	250/320	250/320	250/320	*insulating of shielding and thermal enclosures
5.Coefficient of themal conductivity, W/mK, at 600°C 800°C 1000 °C	 0.095 0.135 0.185	 0.119 0.160 0.210	 0.125 0.170 0.220	 0.110 0.200 0.290	 0.08 0.16 0.25	 0.10 0.19 0.28	* Belts and parts cut up for sealing *materials for filtering plants *buner joints *insulating of thermocouples and electrical devices
6.Linear contraction after 24 hours at 1250°C	-	-	-	2.3	2.0-2.6	2.0-2.5	* asbestos substitude
7.Manner of presentation	bagged wool			Dimensions, mm:			
				length width thickn.	1000±10 500±5 2;3;4±3 6;8;10±1		

Table 2. Characteristics and practical applications of rigid boards and shaped elements

Characteristics	**RIGID BOARDS**			**SHAPED ELEMENTS**			Field of application
	1250°C	1350°C	1450°C	1250°C	1350°C	1450°C	
1.Definition	Rigid board based on silico-aluminous fibre with:			Shaped elements made of silico- aluminous fibre with:			* as exterior coat of refractory linings
	Al_2O_3 45-50%	Al_2O_3 45-50% Cr_2O_3 3%	Al_2O_3 45% ZrO_2 12-18%	Al_2O_3 45-50%	Al_2O_3 45-50% Cr_2O_3 3%	Al_2O_3 45% ZrO_2 12-18%	*in the form of thermal shields for electric gas-fired furnaces
2.Apparent density, kg/m^3	350	350	350	350	350	350	* suspedded vaults
3.linear contraction after 24 hours at maximum application temperature%	3	3	3	3	3	3	* thermal industrial and household aggreate doors * for replacing of asbestos boards * forced convection furnaces
4.Average specific heat, KJ/kgK	1.21	0.75-0.95	0.85-0.98	0.77	0.75-0.91		* in metallurgy of aluminium *as exterior insulation of refractory pots for melted steel
5.Coefficient of thermal conductivity, W/mK, at: 600°C 800°C 1000°C	 0.097 0.120 0.180	 0.075 0.090 0.120	 0.075 0.087 0.110	 0.110 0.200 0.290	 0.120 0.160 0.250	 0.075 0.090 0.123	*linins inside the thermotechnological aggregates of various sizes or interior lining of regenerating chambers
6.Manner of presentation	Dimensions, mm: -legth 1000±10 -width 500±5 -thickness 10,20,30±3			Various vacuum-cast parts ranging from several mm to several cm			* insulating of pipes; * casting gutters in non-ferrous metall. (Zr,Al) * burners embrasures, supports, resistorrs

2.1. For energy-saving purpose the following current systems of furnace building can be distinguished:

- lining of close-grained refractory material provided that the refractory material meets the requirements for increased resistance to mechanical stresses and corrosion;
- "hot insulation", i.e. coating the interior furnace surfaces with lining of refractory materials that, in order to obtain long periods of service, should not be submitted to mechanical stresses or corrosion;
- easy building manner, almost exclusively of insulating lining materials.

2.2. The advantages of the easy building system using ceramic fibres are evident:

- low weight: the linings made of ceramic fibres are lighter in weight by up to 75% than the linings of refractory bricks with conventional refractory close-grained products or firebricks;
- lower accumulated heat: at the intermittent running furnaces losses due to accumulated heat can be reduced by up to 25 %;
- simpler and lighter metal structures;
- increased furnace capacity thanks to smaller thickness of walls;
- greater control capacity of furnace parameters;
- rapid heating.

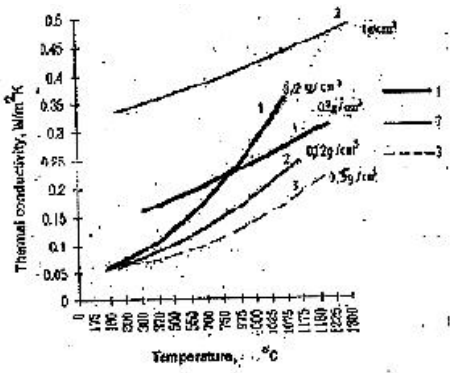

Fig.1- Thermal conductivity of fibre products compared to that of conventional refractory bricks
1- products of ceramic fibres
2 - light - weight refractory firebricks (1g/cm^3)
3 - light - weight refractory firebricks (0.5 g/cm3)

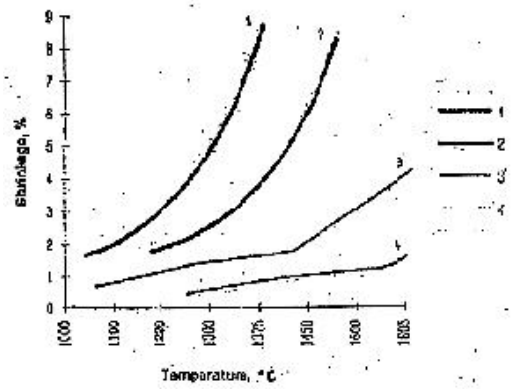

Fig.2 - Shrinking behaviour of ceramic fibre products
1- mattress of ceramic fibres 1250^{o}C, in application
2 - mattress of ceramic fibres 1350^{o}C, in application
3 - block of ceramic fibres 1250^{o}C, in application
4 - block of ceramic fibres 1450^{o}C, in application

3. CHARACTERISTIC PROPERTIES OF CERAMIC FIBRE PRODUCTS AND CRITICAL POINTS IN THEIR APPLICATION

The main characteristics of the ceramic fibre products, compared with other conventional refractory products, are given in Fig. 1 for conductivity and Fig. 2 for shrinkage.

4. FURNACE BUILDINGS, THERMOTECHNICAL ADVANTAGES

The ceramic fibres and products of ceramic fibres have been used, depending on the application temperatures of the furnace where they are applied, for integral or partial burner linings combined with conventional refractories, for door insulation or repair works (replacing of demaged refractory masonry).

Table 3 shows the types of furnaces and application field of the Romanian ceramic fibre-made products.

Table 3. Fields of application for some types of furnaces where products of

Serial No	Field of Application	Type of Equipment	Products Used
A. 1.	**Glass industry** Enterprise of flat glass “Gemamuri Mediaþ”	* protection screens at glass flowing * burners	* fibre, mattresses, shaped products:1250^{o}C
2.	Enterprise of flat glass “Geamuri Buzàu”	* protection screens * burners	* fibre, mattresses, shaped products:1250^{o}C
3.	Container and tableware enterprize”STIROM Bucharest”	*glass tanks(vault shoulders, working basin, manholes)	fibre, boards, blocks cardboard paper: 1250^{o}C, 1350^{o}C, 1450^{o}C
4.	Ceramics enterprice”CERO Cluj”	* porcelain burning kiln	* completely lined with ceramic fibre products 1250^{o}C, 1450^{o}C
B. 1.	**Building material industry** Ceramic material enterprise”Roman”	*tunnel furnace cars	* fibre :1250^{o}C, 1450^{o}C
2.	Sanitary ware and ceramictile factory “CESAROM Bucharest”	*tunnel furnace cars	* fibre :1250^{o}C, 1450^{o}C

Table 3. continued

Serial No	Field of Application	Type of Equipment	Products Used
C. 1.	**Chemical industry** Chemical combine Piatra Neamt	*cracking plant	* completely lined with ceramic fibre products, 1450^{o}C
2.	Fertilizer combine Turnu -Màgurele”	* insulation of piping at the ammonia synthesis plant	* fibre, mattresses, boards 1250^{o}C
D. 1.	**Metal-working industry** Metallurgical combine “Metalurgica Aiud”	* annealing and normalizing furnaces	* boards, mattresses, fibres: 1350^{o}C,
2.	Metallurgical combine “IAMCRS Galati”	* steel furnaces	* fibres, boards, shaped products ; 1250^{o}C
E 1.	**Machine-building industry** Enterprise of machine-building and rolling stock ”FAUR Bucharest”	* batch pre-heating plant for smelting arc furnace * heat-treatment and forging furnaces	* completely lined with ceramic fibre products * boards, mattresses;1250^{o}C, 1350^{o}C, 1450^{o}C
2.	Furnace enterprise “Independenta Sibiu”	* heat-treatment furnace	* fibre, mattresses, 1250^{o}C * boards 1450^{o}C
3.	Car enterprise “ARO Càmpulung”	* heat-treatment furnace	* fibre, mattresses, boards 1450^{o}C
4.	Hot sector enterprise “INTEC Bucharest”	* heat-treatment furnace * regenerative type burning modulus	* mattresses, boards, shaped products :1250^{o}C

By application of ceramic fibre products to lining of furnaces and other thermal outfits it is possible to obtain thermal energy savings of 25-50% by way of reductions in external heat losses and heating-cooling cycle duration as well as by improvement of product quality as a result of a better heat distribution. These advantages result from low thermal conductivity, reduced caloric capacity and good resistance to thermal shock. As regards the batch-type furnaces, when the application temperature is attained, the quantity of heat lost through the ceramic fibre lined wall is reduced by 27.5% compared to that lost by a furnace of conventional conception (Fig.3).

Besides, the quantity of heat stored by a furnace lined with ceramic fibre products is reduced by 21 o/a compared to a brick-made furnace.

The quantity of heat usually lost through the furnace walls amounts to 50-60% of the total quantity, which allows for the total obtained savings ranging from 30 to 50% to be estimated (Tables 4 and 5).

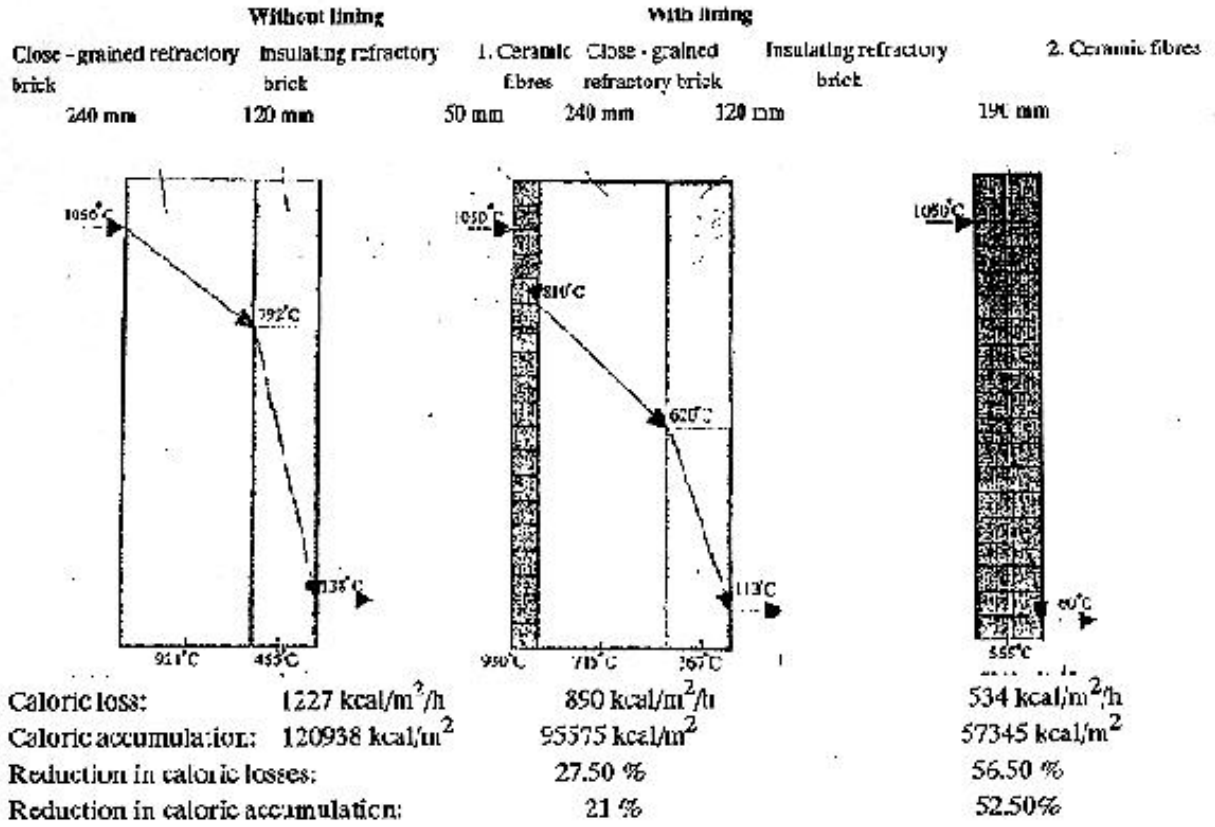

Fig.3 - Thermal profile of a wall with refractory brick lining as compared to the same wall showing an addition of ceramic fibre lining and a lining completely designed in ceramic fibres.

The ceramic fibre linings apllied over brick lining show additional advantages such as:

- reduction in heat transfer and brick temperature results in significantly reducedquantity of heat absorbed by furnace substructure and hence in important fuel savings;
- reduced temperature results in the brick masonry getting protection against thermal shocks, in diminishing of its degradation and implicitly of its maintenance costs;
- reduction in sound level by 15% is also recorded.

Applying a thin layer of fibrous product over the existent masonry of a furnace or making the lining of a new furnace completely designed in fibre products is practiced to enhance the furnace qualities, the application depending on the existent masonry condition (a good masonry condition allows for lining with ceramic products).

Table 4. Assessment of fuel-savings in furnaces lined with ceramic fibres of 1250°C and 1450°C

Serial no	Practical application	Temperature °C	Fuel-saving %	Remarks
1.	Heat-treatmentfurnace (metallurgy)	1300	50	gas firing
2.	Forge-equipped furnace	1350	20	application furnace vault only
3.	Porcelain biscuit burning furnace	1050	30	
4.	Enamelling furnace	1120	44	electric heating
5.	Glazing furnace	1250	35	life time of ceramic fibre product is greater than brick

*Table 5. Heat transfer into batch-type porcelain biscuit burning furnace walls; comparison between a ceramic fibre product lining and a light-weight refractory brick lining * increase in temperature: 8 hours; waiting time:1 hour; cooling: 8 hours (fibres),11 hours (brick)*

Serial no.	Characteristics	Lining	
		Refractory brick 230mm	Ceramic fibre products 190mm
1.	Heat transfer into lining(Kcal/m^2) * increase in temperature * waiting time *total cycle	19900 3500 23400	5200 1300 6500
2.	Fuel- saving (Kcal/cycle) *%of reduction in losses through walls		16950 72

5. CONCLUSIONS

- by application of ceramic fibre products to industrial furnace lining it is possible to obtain an energy or fuel saving of 25-50%, as compared to using of conventional refractory products;

- it is considered that at a continuous increase in prices of electrical energy and fuels along with increased production of ceramic fibres the price ratio of various refractories or insulating materials is expected to be more and more in favour of the ceramic fibre products;

- it can be proved that, by durability of ceramic fibre linings, the additional costs of investments for operation are redeemed in relatively short time as a result of energy or fuel savings.

BIBLIOGRAPHY

1. L. Cerchez, P. Voiculescu - III rd Conference for Ceramic Fibres and Refractory Concretes, Bratislava, R.P. of Czechoslovakia, 17 - 19 May 1983; - "BUILDING MATERIALS ” Journal, Romania, vol. XV, no. 3,1984 .133 -137 - Silico - aluminous ceramic fibres. Effect of heat treatment and manufacturing technology on their characteristics.

2. L. Cerchez - International Ceramics Congress, US West Coast, Los Angeles, 3-7 June 1992 - Achievments and prospects in research and production of modern refractory and heat insulating materials.

3. L. Cerchez - " BUILDING MATERIALS " Journal, Romania, vol. XXII, no. 3,1993, pg. 226 - 229 - Obtaining silico - aluminous ceramic fibres by wet synthesis.

4. L. Cerchez, L. Popescu - " BUILDING MATERIALS " Journal, Romania, vol. XXIII, no. 4,1994, pg. 295 - 298 - Ceramic fibre shaped products.

PROPERTIES AND APPLICATION OF THE FLUOROPHOSPHATE GLASSES*

L. N. Urusovskaja
S.I. Vavilov State Optical Institute, Russia

Abstract

In 1950's a new class of fluorophosphate glasses had been emerged. Fluorophosphate glasses attracted the investigators owing the their specific optical constants, namely considerably increased partial dispersions in the blue spectral range and a high Abbe numbers v. Relative partial dispersions of some fluorophosphate crowns in blue spectral range are close to those of crystalline fluorides. These specific optical properties make those glasses extremely useful for the correction of optical systems residual chromatism.

Glasses of fluorophosphate crown type are characterized by the negative sign of refractive index temperature coefficient, and thermooptical constant W. The usage of such glasses in an optical system allow one to produce instruments that are able to operate within broad temperature limits. Thus the usage of fluorophosphate glasses allows one to eliminate both residual chromatism and thermo-ware aberration. Fluorophosphate glasses are characterized also by small or close to zero optical tension coefficient values. Therefore they produce no birefringence effect at high mechanical stresses. High transmittance in the expands the application field of the glasses. Such properties of fluorophosphate glasses as low non-linearity refractive index coefficient and high acid resistance are also of importance.

Based on a study of the optical, physico-chemical and technological properties of fluorophosphate glasses the four type of fluorophsphate long crown with refractive index in the range from 1.44 to 1.60 and dispersion coefficient from 94 to 70, had been placed in commercial operation in Russia.

Some data for the commercial and novel devised, glasses used in UV microscopy are presented in this report.

---

* Full manuscript not available at the time of printing

QUALITY CONTROL OF GLASSWARE MADE FROM CASING GLASSES*

Sharagov V.A. and **Schegelskaya T.Yu.,**
Beltsy State University, Moldova

Abstract

The most important parameter in glass producing is the constancy of its chemical composition, the technological properties of liquid glass and operational characteristics of glassware being depended upon the parameter. Manufacturing the articles from casing glasses the stability of their physical properties is of prime importance. There are only a few literaturary data about the criteria of casing glassware production stability.

The results of casing glass articles quality control (mainly, scatters) are analysed and generalised at the paper presented.

The investigations were carried out during few years at Beltsy electrolighting Fittings Plant. The following physical parameters of glasses were monitored regularly: density, uniformity, the coefficient of linear thermal expansion (CLTE) and softening temperature. The colorless transparent glass, milk-glass and colored glass were used to produce the casing glassware.

The density of colorless transparent glass was found in analytical treatment of experimental data to be rather stabile, the deviation from the mean value being equal to 1-2 kg/m^3 (relative error didn't exceed +/- 0.5 kg/m^3). In the case when the glass density has been deviated from the stabile level (more than 3 kg/m^3) the quantity of manufacturing scraps has scraps occurred.

Glass density data are in agreement with glass non uniformity index values, which were measured by glass powder centrifuging in the mixture of organic solvents.

To supply the stability of casing glassware producing the difference between values of CLTE for milk-glass and transparent glass should make up about (5...10) * 10^{-7} $^oC^{-1}$ (relative error was equal to 1...2 ^oC). If the difference is about zero or negative value the mass scraps arise.

The closed connection between output of high quality articles and glass physical properties stability was established.

In order to improve the technique of glassware casing the practical recommendations are proposed.

* Full manuscript not available at the time of printing.

RADIOPHOTOLUMINESCENT GLASSES

Alexander Dmitryuk and **Nikolai Timofeev**
S.I.Vavilov State Optical Institute, Russia

1. INTRODUCTION

Radiophotoluminescent (RPL) glasses - glasses where room temperature stable RPL centers not present in nonirradiated glasses are formed under the influence of ionizing radiation. RPL centers are responsible for UV-excited visible luminescence.

RPL glasses doped by silver ions are of the most practical importance. They are widely used for individual dosimetry of ionizing radiation because they have high sensitivity and large dynamic range of detected doses from 10^{-4} to 10^{-3} Gy. RPL glasses accumulate an absorbed dose information and keep it during its reading. The long-term stability of RPL glasses is very high.

Inspite of intensive studies of RPL phenomena in silver doped glasses its theory was not evolved until recent time. We analyzed the model of RPL centers proposed in Ref. [1,2] and came to conclusion that these models are not supported by experimental results.

We have elaborated and experimentally proved new theory of radiophotoluminescence phenomena in silver doped glasses. This theory makes possible to explain the influence of glass composition on the main properties of RPL glasses such as sensitivity and "build-up" kinetics. i.e. an increase of RPL center concentration as a function of time after irradiation. By means of this theory we made a prediction and have found the influence of mixed alkali effect on the “build-up” kinetics of RPL centers.

2. RESULTS AND DISCUSSION

The sum total of experimental data on the properties of silver doped RPL glasses is a complicated pattern. The spectroscopic properties of RPL glasses depend on after irradiation time, concentration of silver ions, sample temperature, irradiation dose, thermal treatment of irradiated glasses. This is caused by the formation of not one but two RPL centers with different spectroscopic properties [3]. The ratio between concentrations of two types of RPL centers depends on activator concentration. One type of RPL centers is observed when Ag_2O content is less than 0.1 wt %. These centers are responsible for the luminescence band with the peak at 640 nm. The band contour is well described by Gaussian function $I(\nu) = I_o \exp[-4\ln 2\ (\nu-\nu o)^2/\Delta\nu^2]$, where I_o, ν_o - the intensity and frequency at the maximum of luminescence band, $\Delta\nu$ - band halfwidth. The spectral parameters: $\nu_o = 14842$ cm^{-1}, $\Delta\nu = 4356$ cm^{-1}. The luminescence excitation spectrum has a peak at 320 nm,

If there is only one type of RPL centers in the glass then the luminescence spectrum does not depend on such external parameters as irradiation dose, temperature, thermal treatment of irradiated glasses.

The main feature distinguishing RPL glasses from usual (luminescent glasses lies in the fact that concentration of RPL centers increases in time after irradiation (Fig.1). This phenomena is called radiophotoluminescence “build-up” [4]. The “build-up” time varies from 10^2 to 10^6 sec and

depends on activator concentration, temperature and glass composition. The RPL "build-up" time decreases with the growth of activator concentration, temperature and alkali oxide content.

Obviously the theory of radiophotoluminescence in silver doped glasses first of all must involve the kinetic model of RPL centers formation.

To justify experimentally this model we used ESR method of research. With the help of this method and on the basis of phosphate glasses doped by isotopes ^{107}Ag , ^{109}Ag and by the natural mixture of silver isotopes we have found that radiolysis leads to the recharging of activator cations - Ag^{+}. As the result such activator centers as Ag^{2+} , Ag^{0}, Ag^{2+} , Ag_3^{2+} are formed [2], [5,6].

On the basis of the mechanism and kinetics of these centers formation it was shown that these centers are formed in phosphate glasses as the result of the following postradiational reactions [7,8]:

$$PO_4^{2-} + Ag^{+} \rightarrow Ag^{2+} + PO_4^{3-} \quad (1)$$

$$Ag^{+} + e \rightarrow Ag^{o} \quad (2)$$

$$Ag^{o} + Ag^{+} \rightarrow Ag_2^{+} \quad (3)$$

$$Ag_2^{+} + Ag^{+} \rightarrow Ag_3^{2+} \quad (4)$$

Reactions (1) - (4) go as quasi-monomolecular reactions when the activator concentration is more than 0.01 wt % and exposure doses less than 10^4 Gy.

Reaction (1) describes the capture of the hole localized at the non-bridging oxygen by the silver ion. Two-charged silver formed as the result of this reaction is not RPL center. This was proved by means of Ce^{3+} introduced into the glass as the hole trap. Ce^{3+} suppresses the formation of centers Ag^{2+} but at the same time the intensity of radiophotoluminescence remains unchanged. On the basis of these experimental data we have shown that center Ag^{2+} has a more thermal stability than electronic activator center Ag_3^{2+}. As a consequence the thermal treatment of irradiated glasses at 300 ^{o} C leads to situation when with the help of ESR method we detect only Ag^{2+} ions. In this case the radiophotoluminescence is not present.

Reactions (2-4) describe the conversion of silver atoms leading to the formation of room temperature stable three-charged molecular ion Ag_3^{2+}. Intermediate products Ag^{0} and Ag^{2+} of successive reactions (2-4) are thermally nonstable and their concentration decreases in time after irradiation. Therefore these centers cannot be considered as RPL centers. Kinetics of Ag_3^{2+} centers formation coincides with the radiophotoluminescence "build-up" kinetics. Therefore we consider molecular ion Ag_3^{2+} to be the RPL center responsible for the luminescence band with the peak at 640 nm. This deduction is supported by incorporation of electron acceptor Pb^{2+} into the RPL glasses that suppresses the concentration of such electronic centers as Ag_2^{+} and Ag_3^{2+}. Simultaneously the decrease of radiophotoluminescence intensity was observed. As it was shown in Ref. [7,8] kinetics of the room temperature reactions (1-4) is controlled by the common process, namely, the diffusion of a single-charged silver cation Ag^{+} into the reaction sphere. So the postradiotional relaxation of silver doped glasses is to be explained by transport processes. In particular these processes are responsible for electrical conduction of glasses. The postradiational kinetics being not elementary is described by fractional exponent:

$$\Phi(t) = \exp[-(t/t_o)^{\beta}] \quad (5)$$

where $0 < \beta < 1$. Nonexponential kinetics in studied glasses is caused by the distribution of Ag^+ diffusion coefficients [7].

The proposed model of RPL center Ag_3^{2+} made possible to explain for the first time the composition dependence of RPL glass sensitivity [9]. This dependence may be very strong (Fig.2). Drastically decreased curve in the figure reflects very slow "build-up" kinetics of RPL centers which takes place in the glasses with low alkali concentration. Therefore the reactions (2-4) do not go to completion under the given conditions.

Rates of the reactions (2-4) may be controlled not only by variation of alkali oxide concentration in the glass but also may be decreased with the help of mixed alkali effect. This is due to the fact that the rates of room temperature reactions (2-4) depend on Ag^+ diffusion coefficient dose to that of Na^+ [10]. The mechanism of the influence of mixed alkali effect on the mobility of alkali cations is analyzed in Ref. [11]. We observed the variation of the (1-4) reaction rates passing through a minimum under the successive substitution of sodium for potassium in silver doped phosphate glasses. The similar effects should be observed under the substitution of sodium for other alkali metals.

3. CONCLUSION

The new model of RPL centers formation in silver doped oxide glasses is proposed. The model is based on the fact that the main RPL center is molecular ion Ag_3^{2+} formed as a result of the reactions (2-4). The rate of Ag_3^{2+} "build-up" is controlled by the diffusion of Ag^+. Varying the glass composition one can influence on Ag^+ diffusion coefficient and as a consequence on the rate of the reactions (2-4). The increase of reaction rates leads to the reduction of radiophotoluminescence "build-up" time and the decrease of reaction rates causes the room temperature thermal stability of Ag^0 centers in glasses.

REFERENCES

[1] J.H. Schulman, R.J. Ginther, C.C.Klick, R.S. Alger, R.A.Levy, J.Appl. Phys. 22 (1951) 1479

[2] R. Yokota, H. Imagawa, J. Phys. Soc. Japan 23 (1966) 1038

[3] N.B. Belyankina, A.V. Dmitryuk, S.E. Paramzina, N.T. Timofeev, Sov. J. Glass Physics and Chemistry 21 (1993) 415

[4] K. Becker, Atomic Energy Rev. 5 (1967) 43

[5] R.A. Zitnikkov, D.P. Peregud, Fiz. Tv. Tela 27 (1985) 1778

[6] V.M. Syutkin, A.V. Astashkin, A.V. Dmitryuk, Sov. J. Glass Phys. Chem.18 (1992) 75

[7] V.M. Syutkin, A.V.Dmitryuk, V.A. Tolkachev, Fiz. i Khim. Stekla 17 (1991) 273

[8] V.M. Syutkin, A.V. Dmitryuk, V.A. Tolkachev, Sov. J. Glass. Phys. Chem.18 (1992) 224

[9] A.V. Dmitryuk, S.E. Paramzina, A.S. Perminov, N.D. Solov'eva, N.T. Tmofeev, J. Non-Cryst. Solids (in press)

[10] V.M. Syutkin, A.V. Dmitryuk, V.A. Tolkachev, Sov. J. Glass Phys. Chem.18(1992) 440

[11] M.D. Ingram, Glastech. Ber. Glass Sci. Technol. 67 (1994) 151

[12] A.V. Dmitryuk, N.D. Solov'eva, N.T. Tmofeev, Glastech. Ber. Glass Sci. Technol. 67 C (1994) 265

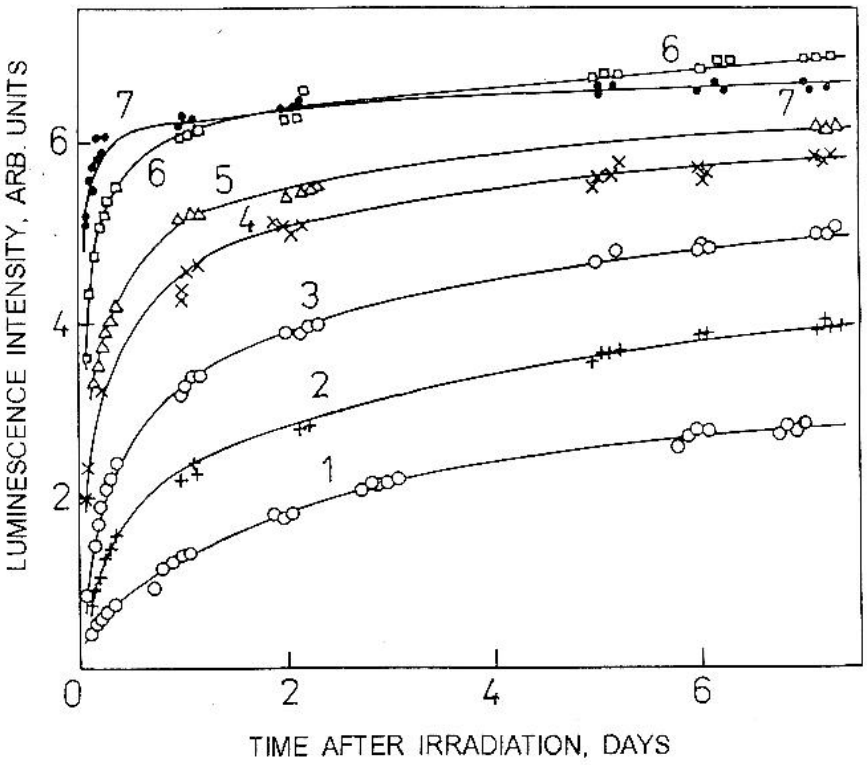

Fig.1 Time dependence of radiophotoluminescence intensity after irradiation. Lithium aluminophosphate glass with different silver concentrations, wt % Ag_2O: 1-0.2;2-0.3;3-0.4;4-0.6;5-0.7;6-1.0;7-1.5

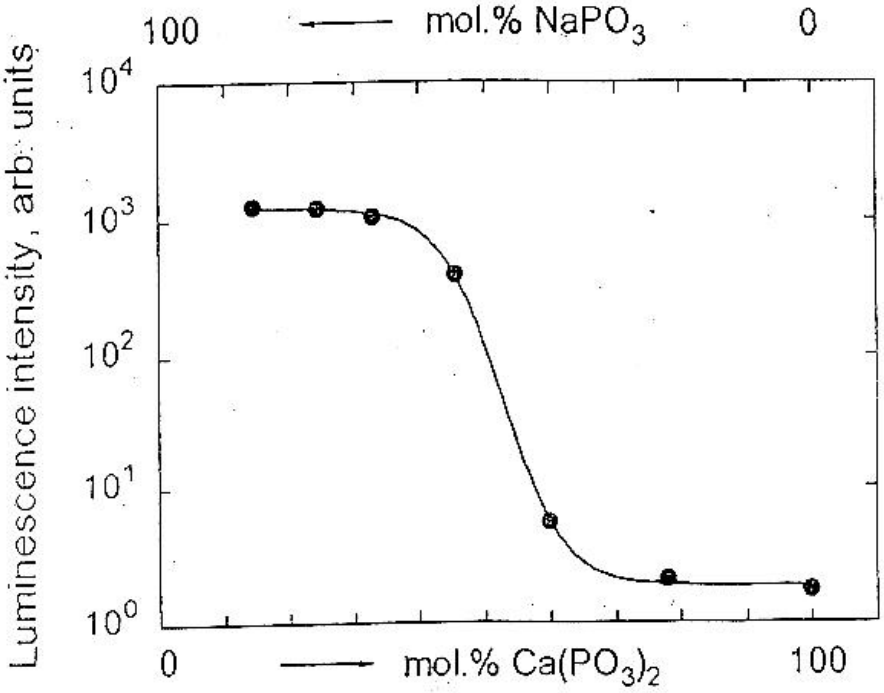

Fig.2 Gamma-radiation sensitivity as a function of $NaPO_3$ - $Ca(PO_3)_2$ glass composition. Ag_2O concentration - 0.1 wt %

REGULARITIES OF THE LIQUID PHASE SEPARATION PROCESS IN TITANIA CONTAINING GLASSES STUDIED BY RAMAN SPECTROSCOPY*

Ya.S. Bobovich, B.G. Varshal, O.S. Dymshits, A.A. Zhilin, M.Ya. Center, T.I. Chuvaeva, G.T. Petrovsky
S.I.Vavilov State Optical Institute, Russia

Abstract

Regularities of liquid phase separation in glasses of the Li_2O- Al_2O_2- SiO_2-TiO_2, MgO-Al_2O_3- SiO_2-TiO_2, ZnO-Al_2O_3-SiO_2-TiO_2 systems were studied by Raman spectroscopy. The initial glasses were heat treated in a wide temperature range in which the processes of liquid phase separation take place, and kinetics of phase transformations in the titania containing phase was studied. It was found that according to Raman Spectroscopy data, in all the systems the process of liquid phase separation develops in a similar sequence.

In initial glasses Ti^{4+} ions probably acquire tetrahedral coordination. Heat treated glasses are separated into two amorphous phases, an aluminotitanate one in which Al^{3+} and Ti^{4+} ions acquire octahedral coordination and which can contain also MgO and ZnO, depending on the glass composition, and a silicon enriched phase. An octahedral coordination of Ti^{4+} ions is confirmed by Raman spectra of heat treated glasses demonstrating a characteristic wide band at 800cm^{-1}.

The next step depends on the composition of the aluminotitanate phase and the TiO_2 content. At further heat treatment, titania containing amorphous phase either remains a stable phase in a wide temperature range or rapidly decomposes into a TiO_2 containing phase (pseudobrookite and/or anatase or magnesium titanate) and spinel type alumina containing crystalline phase.

The obtained results were proofed by an X-Ray analysis.

---

* Full manuscript not available at the time of printing

RELAXATION IN GLASS: THEORY AND APPLICATION*

I. Avramov
Bulgarian Academy of Sciences, Bulgaria

Abstract

Study of the relationship betwen equilibrium and non-equilibrium properties of physical systems is one of the fascinating problems of contemporary science. The vitreous state that is obtained when a melt is cooled through a glass transition region is a good example of a system falling out of equilibrium. Moreover, the kinetics of relaxation process is of prime importance for the properties of glasses.

Rheology and thermal history of samples is of prime importance for the determination of equilibrium and of frozen-in relaxation parameters of glasses. In present contribution a mathematical formalism is discussed connecting the cooling rate with structural temperature and with the thermodynamic properties of glasses. In order to achieve a better understanding we use computer simulation and description of the process within the framework of non equilibrium thermodynamics. A comparison of the predictions with experimental results is briefly discussed.

---

* Full manuscript not available at the time of printing

REVERSIBLE ELECTROCHROMIC EFFECT AND COLOR CENTERS IN ALKALINE Nb (W) - PHOSPHATE GLASSES IN CONTACT WITH SOLID PROTONIC ELECTROLYTE

S.L.Kraevsky and **V.F.Solinov**
Scientific-Research Institute of Technical Glass, Russia

Abstract

Electrochromic lithium niobium-phosphate glass in combination with a solid protonic ectrolyte displays the reversible electrochromic effect over 1000 cycles. One of the problems occurring in the work of the glass formation of a space charge in the electrocolored region when electrons of color centers can not be easily extracted during bleaching phase since they are trapped in the pairs Li^+- e^- of the color centres. Electrons are localized at Nb ions as polarons, giving rise to an intervalent absorption band 13000 cm^{-1}, or as bipolarons (two paired polarons at the nearest Nb atoms) with an intervalent band 17400 cm^{-1}. Observation of absorption spectra up to the temperature 350^oC reveals an isobestic point between these two bands witnessing the balance of the two kinds of centers. ln the induced electrochromic spectra the bipolaron band is absent. In electrochromic W-glasses the bipolaron is formed by two polarons at the same site (W^{4+}).

I. INTRODUCTION

Existing WO_3 film based electrochromic devices have been demonstrated to be able to operate for a long time in a continuous cycling mode. But their shelf-life is usually short, working sizes not large and characteristics are unstable. There is an alternative electrochromic material - oxide glass - which can be used for low-rate applications [1]. Besides, studies of electrochromic effect in oxide glasses are useful from the point of view of understanding the electrochromic process and; particularly, the nature of the color centers induced by electrons injection, their properties and the process of their creation and dissolution.

Because we had not a polymerising electrolyte with lithium conduction, we used a protonic electrolyte. In this case the behavior of glass under reversible voltage has much in common with the behavior of ion-exchanged glasses and the same problems.

Schematic view of an electrochromic glass device is given in Fig.1. The scheme is applicable also for an electrochromic film having small level of initial electron conductivity, so the coloration starts at the film/electrode interface. The only difference of the film and glass devices lies in the fact that for the latter ions of conductivity in the electrochromic material and electrolyte are not the same. In Fig.1 layer 1 is the region of field assisted ion exchange, layer II - is the region of electrons injection; space charges in both layers should be compensated to allow current flow at low voltage level. In Fig.1 is

shown the spurious current of H^+ ions through the left electrode during the half-cycle of bleaching. This current exists also in film devices with a proton-permeable electrode.

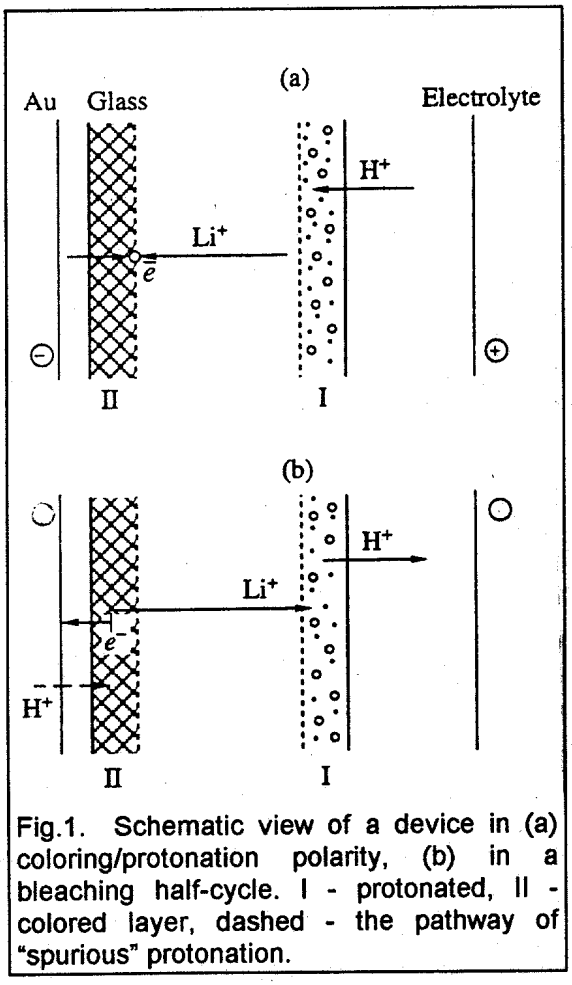

Fig.1. Schematic view of a device in (a) coloring/protonation polarity, (b) in a bleaching half-cycle. I - protonated, II - colored layer, dashed - the pathway of "spurious" protonation.

The processes in layers I and II of Fig.1 and at their interfaces govern the properties of the electrochromic device. For example, diffusion of protons in the electrode and its substrate (if such one exists) or diffusion of lithium ions from the glass into the proton electrolyte during shelf-life make the processes in the layers I and II during operation more complicated.

2. EXPERIMENTAL

The mol% composition of the electrochromic glass was $52Li_2O.18Nb_2O_5.30P_2O_5$, its electrical conductance - about 10^{-6} S/cm at room temperature (the electrical conductance of the electrolyte was three orders of magnitude higher). On the polished 0.5 mm thick samples of glass was deposited at one side a conducting coating, the other side was covered with a layer of polyacryl-based electrolyte and a metal grid counterelectrode above it. The effective area of the device was 2 to 5 cm^2.

3. RESULTS AND DISCUSSION

Dynamics of electrochromic process and local resistivity: The glass with electrodes and without electrolyte under constant current and periodical change of its polarity demonstrates increase of the sample resistance R in each cycle, the half-cycle maximum of R varied with time t approximately as $R \sim \sqrt{t}$ over 90 cycles [2]. Such dependence is typical for samples having layer where the host ion is exchanged for a guest ion with lower mobility. Since we observe resistance anisotropy for every change of polarity and since the sample is initially symmetrical,. such behavior of R is the sign of the fact, that bleaching (and so extracting of guest ions) is hindered and can not go to the end. This is confirmed by the fact that this simple device can not be bleached, color density increases with every cycle.

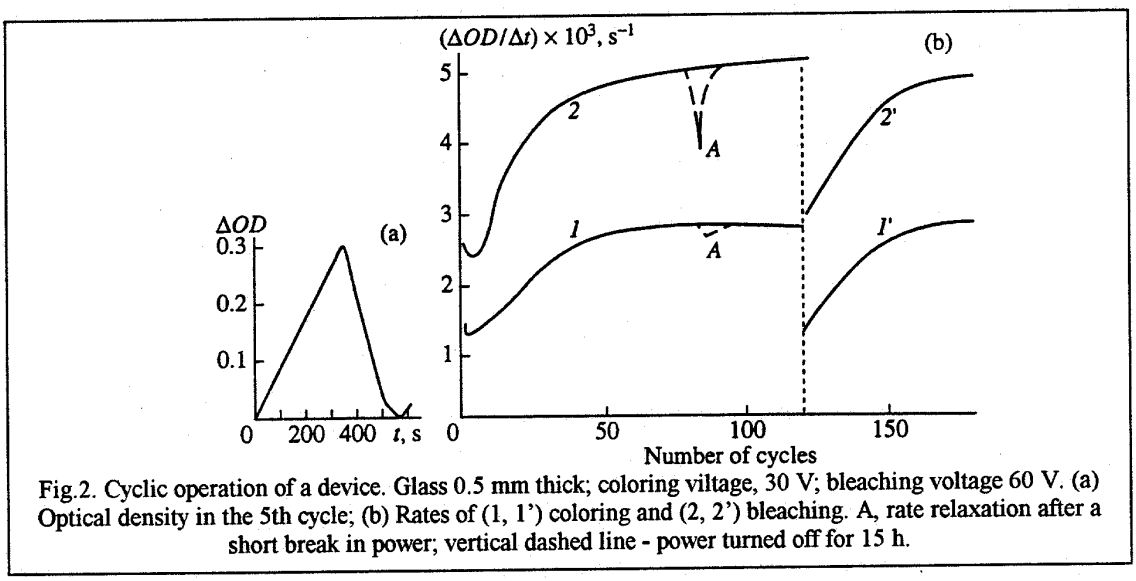

Fig.2. Cyclic operation of a device. Glass 0.5 mm thick; coloring viltage, 30 V; bleaching voltage 60 V. (a) Optical density in the 5th cycle; (b) Rates of (1, 1') coloring and (2, 2') bleaching. A, rate relaxation after a short break in power; vertical dashed line - power turned off for 15 h.

The device with electrolyte bleaches to initial value of optical density but the rate of coloration is cycle dependent and obeys some complicated law (Fig.2). Rates in the half-cycles of bleaching are always higher than in the half-cycles of coloring. In the case presented in Fig.2 the voltage was the same for all half-cycles of coloring and also constant but higher for all half-cycles of bleaching. But the same law of rate dependence on cycle number was observed for cycling in the mode of constant current. Since in the latter case the voltage in the bleaching half-cycles was higher and increasing with time within the half-cycle, the reason for higher rates of bleaching seems to be higher efficiency of bleaching due to higher voltage.

Very interesting and not fully understood is the stationary state of the device operation (nearly horizontal regions of Fig.2 curves). In the stationary state with constant current the device resistance is constant in the coloring half-cycle and increases with time in the bleaching half-cycle, the mean value of the latter being twice as that in the coloring half-cycle (that was the reason for choosing the ratio of voltages for the case of Fig.2).

The above can be interpreted in the following way. There are no evidence of device resistance increase with time within the half-cycles of coloring; more than that,. it slowly decreased. The role of colored layer II in this half-cycle can be neglected: its resistance is

lower than that of initial layer due to electron conductivity, but even zero resistance would not mean anything since the layer thickness is about 50 times less than the sample thickness. The layer I resistance in the above example with the sample having film electrodes on both sides increased due to proton injection through the thin film electrodes. Now we see that this is not the case we have with layer I: that means that we have not "pure" case of protons injection in every cycle. If we remember that the process of device preparation includes the phase of polyacryl electrolyte polymerization, we will recognize, that role of cations interdiffusion can be great and layer I before the first cycle of operation is already the ion-exchanged layer with mixed ion type of conduction.

Our explanation of layer II resistance behavior is based on the results of Baucke (3,4] who have shown that there is some boundary between lithium ions and protons in the glass under electrolysis and have found the concentration profile of lithium ions in this boundary. According to Baucke, the protonated-layer boundary separating the injected protons and Li^+ cations in the glass is very stable in the absence of the electric field that created it. From Fick's second law

$$\frac{\partial C}{\partial t} = \frac{\partial}{\partial x}\left(D\frac{\partial C}{\partial x}\right), \tag{1}$$

here C is the cation concentration, D is the diffusion coefficient, and x is the coordinate in a direction perpendicular to the layer boundary, it follows that the condition for the stability of the boundary after the applied voltage has been removed

$$\frac{\partial C}{\partial t} = 0$$

has two solutions. One is obtained if D is deemed independent of cation concentration and, as a consequence, of the x coordinate. This is a trivial solution, which is of no interest in the case at hand. If, however, D is a function of both x and C, then the condition for the stability of the boundary will take the form

$$D\frac{\partial C}{\partial x} = const \quad \text{or} \quad \frac{\partial C}{\partial x} \approx \rho\left(x\right), \tag{2}$$

where p is the resistivity of the glass.

Condition (2) signifies that for the boundary to be stable it is essential that the resistivity of the glass has a sharp maximum and that position of this maximum coincides with the middle of the boundary. Such kind of resistivity maximum could happen in the case of the mixed alkali effect. Apparently, there is certain reason to speak of a similar proton-alkali effect. The existence of such an effect follows from Molinelli et al. [5] and

Mazurin et al. [6, p.129) data. It can be shown that ∂c/∂x as a function of x from [3,4] is close in form to ρ(γ(x)) from [5, 6].

In all probability, the peak of ρ(x) thus defined at the boundary of the protonated layer is the same as the peak of ρ(x) in the "barrier layer" of the glass reported by Z.Bokshai and M.Varga in 1975.

Suppose we adopt the resistivity of the proton-alkali layer as interpreted above and asses p, using the data from [6, p.129]. Then we will be able to show that a noticeable contribution to the total resistance of the sample comes only from the resistance of the boundary between the protonated ariode layer and the glass bulk (in Baucke's definition). The behavior of the sample resistance will be then governed by changes in the slope ∂c/∂x of the protonated boundary rather than by the increase in the thickness of the protonated layer. The slope decreases as the boundary moves into the interior of the glass, the peak ρ broadens and the integrated resistance increases: When the current is reversed, the more mobile lithium ions appear behind the less mobile protons causing their mixing and increasing and broadening the peak ρ. The latter explains the anisotropy of the sample resistance and, in part, the increase of it in the bleaching half-cycle.

Fig.2 shows that the above movement of the peak can be stationary, performing with maximum efficiency. In this stationary mode only odd and even half-cycles differ from each other, the cycles as the whole are similar to each other. But even short time

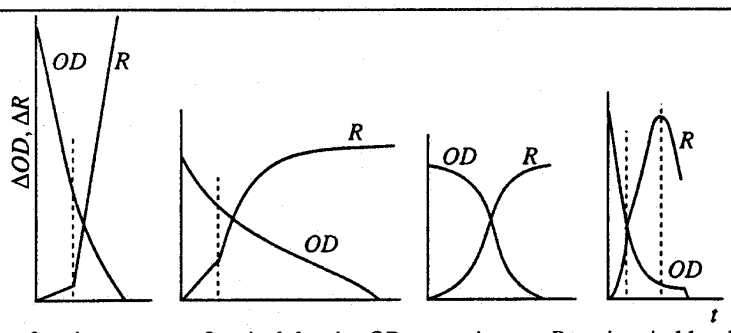

Fig.3. Comparison of various curves of optical density *OD* ans resistance *R* vs time in bleaching cycles for the same device in j=const mode. Scale: OD, 0.05/cm; time, 2 min/cm, *R*.arbitrary.

interrupter in cycling causes decrease of efficiency; mostly in bleaching half-cycles. When cycling is interrupted for several hours, the system relaxes to the original state and then the process of rate coming to the stationary state repeats. When the device operated for 1000 hours, we had five almost identical regions of "flare-up". We must note that this have nothing in common with color relaxation in the shut-off state, the rate of such relaxation is extremely small.

There has been found one more source of problems which marks out the half-cycle of bleaching: this is the color center itself. From the electrical point of view it is the pair Li^+-e^-. When creating this center, we produced very strong electric field at the front boundary of developing color wave which distorted the Li-O octahedron to make it capable to accommodate the injected electron and extra cation for charge compensation. To extract these electron and cation from the color center can be a complicated problem. Some reasons to such a conclusion give examples of combined figures of optical density and

device resistance for the bleaching half- cycles (Fig.3). Note, that departure from linear law of OD vs. t dependencies is always bleaching rate decrease accompanied by more fast growth of resistance R. Obvious correlation of these two tendencies allow to confirm, that the bleaching process at some phase of it meets complications which now begin to govern the behavior of the device resistance and so are the source of efficiency decrease and, it is possible, of the electrochromic process disturbing. We believe that the reason for this is the following: the destruction of the color center will be delayed in time
from the formation of the space charge associated with the migration of Li^+ ions toward the new cathode; to neutralize this charge; protons will be injected through the electrode into layer II, thus causing an increase in resistance and interfering with the color center rupture.

Nature of color centers in electrochromic glass: Electrochromic glasses are usually colorless in initial state. But varying the composition and conditions of synthesis we can obtain colored glasses. The spectra of initial color differ from the spectra of electrocolored (initially colorless) glasses. We studied the spectra of both types to understand their common nature(7)

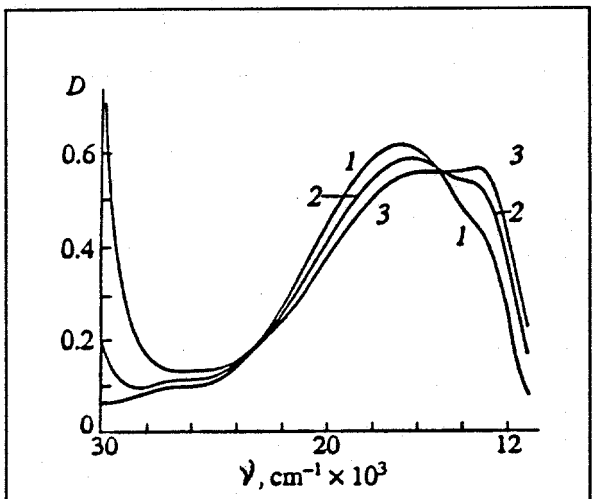

Fig.4. Absorption spectra of initial color at different temperatures, T: (1) 30, (2) 203, and (3) 342°C

At Fig.4 are given spectra of initial color for a glass sample of the composition (mol.%) $40Li_2O.15Nb_2O_5.45P_2O_5$ held during spectra measurements at constant elevated temperatures. It was found that spectra at temperatures below the temperature of plastic deformations threshold do not depend on time of observation and only on temperature level. So, two isobestic points (points, where optical density is independent on temperature) in spectra of Fig.4 tell us that there are at any rate two kinds of color centers and three optical bands; more detailed computer analysis shows that there are four bands within the interval 19000 - 28000 cm^{-1}. Similar set of spectra and one isobestic point were discovered for $LiNbO_3$ crystal [8]; it was guessed that the band with the peak near 13000 cm^{-1} belongs to electrons localized at Nb ions in the form of polarons and the band with peak near 20000 cm^{-1} belongs to bipolarons - two bonded polarons at nearest Nb

ions. The fact of bimolecular type of equilibrium between bipolarons b and polarons p was confirmed by the fact that Logarithm of intensity value p^2/b shows linear dependence on l/T. For all our glasses this dependence was also linear, its inclination and, therefore, energy of bipolaron dissociation, varied with glass composition in the interval 0.05 - 0.13 eV and was complex function of glass composition. Temperature dependence of absorption spectra for electrochromic color is somewhat different. There are no isobestic points and no signs of the bipolaron band, in fact we have in this case only the asymmetric polaron band 13000 cm^{-1} and weak band near 26000 cm^{-1}. Both bands with temperature increase show time and temperature dependent bleaching behavior caused by diffusion-controlled dissociation of color layer.

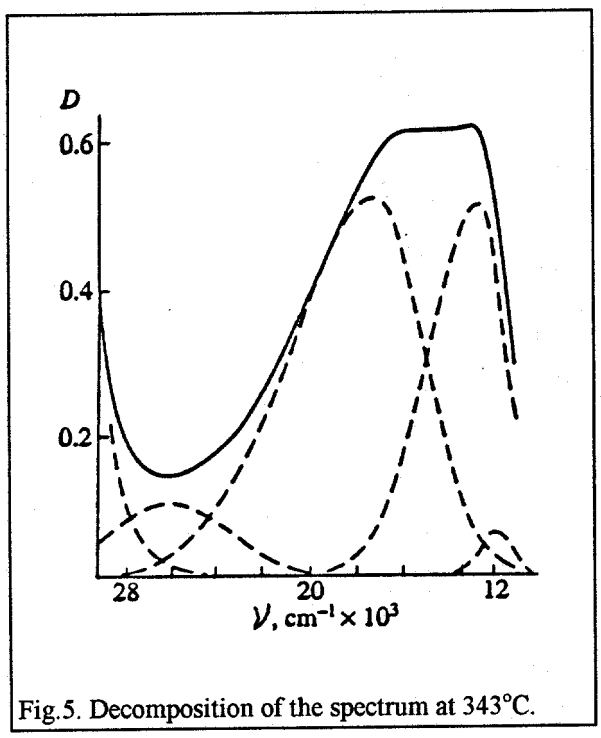

Fig.5. Decomposition of the spectrum at 343°C.

Believing, that the bands with peak near 13000 cm^{-1} in spectra of initial and electrochromic color, we apply the asymmetry parameters of the band to the computer analysis of spectral composition for spectra of initial color. Under such strong condition the isobestic point was obeyed in the spectral deconvolution. As the result of deconvolution of spectra deconvolution we obtain four bands. The less intensive of them, narrow band with peak at ~12000 cm^{-1}, we ascribe to d-d transition 0→1 of Nb^{4+}, $^2B_{2g} \rightarrow {}^2E_g$ (Fig.5). Existence of this band can be deduced from ESR measurements [the ESR spectrum with g-factors $g_\wedge$=1.88, g=1.91 gives for λ=750 using Abraham-Price formula

$$\delta = \frac{2k^2 \lambda}{2 - g_\perp}, \qquad (3)$$

δ =17000 -18000 cm^{-1} with k=1. Delocalization can be accounted for by the value of k found from the equation for energies of transitions

$$E_{0\to 3} \cong E_{0\to 1} + E_{0\to 2} \tag{4}$$

k is ~ 0.85 and δ ~ 13000 cm^{-1} (the real peak position is 12000 cm^{-1}). Then the transition 0 - 2 (band with the peak at 13000 cm^{-1} in the spectra) corresponds to the intervalent light absorption by small radius polarons ($^2B_{2g}(a_1)\to{}^2B_{2g}(a_2)$) and the transition 0→3 (band with the peak at 26000 cm^{-1}) corresponds to the intervalent absorption too, but to the higher level, ($^2B_{2g}(a_1)\to{}^2E_g(a_2)$). Both the latter bands form the spectrum of electrocolored glass, consisting of only these bands.

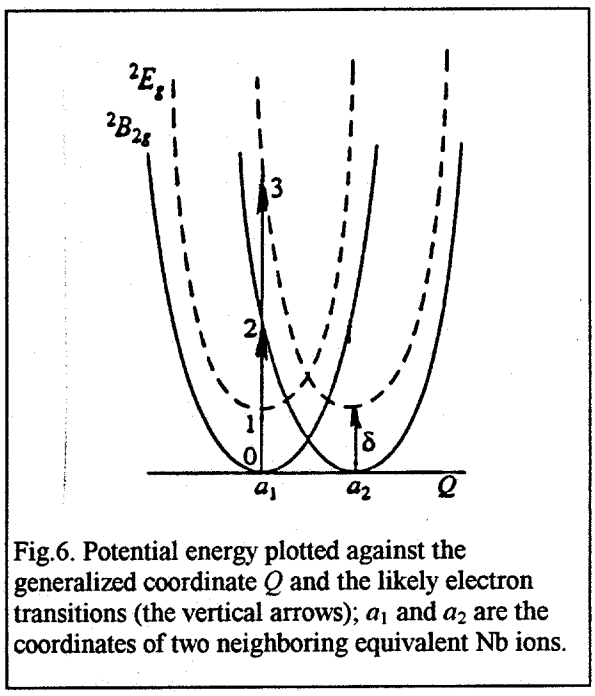

Fig.6. Potential energy plotted against the generalized coordinate Q and the likely electron transitions (the vertical arrows); a_1 and a_2 are the coordinates of two neighboring equivalent Nb ions.

A strong asymmetric band with the peak at 17400 cm^{-1} belongs to bipolarons intervalent absorption. The kind of asymmetry for this band and the band belonging to polarons was taken from the spectra of electrochromic color; only this type of asymmetry allowed us to reproduce the isobestic points in computer simulations. The bipolarons here are, as was said above - two polarons at nearest Nb ions belonging to the structural fragment Nb-O-Nb. For similar electrochromic glasses where $W0_3$ oxide takes place of the Nb_2O_5 oxide, bipolaron has another form: it is two polarons at the same W ion. This fact has been confirmed by ESCA data: in electrocolored layer of W-glass 1/4 of all W ions are W^{4+}.

The polaron ↔ bipolaron transmutation described above applies to a uniformly and strongly reuced material. If, however, the degree of reduction is low, the probability that two polarons will meet and form a bipolaron is apparently low, and we may hypothesize a

spectrum where the bipolaron band would be unnoticeable and which would retain solely the bands corresponding to the transitions presented in Fig.6. This seems to be the case with the glass samples that, instead of turning blue; acquire a faint yellowish-brown color in the course of melting [7].

The electrochromic color spectra turn irreversibly weaker as the temperature increases (at room temperature, the color memory is infinitely large). Apparently, this bleaching occurs because the electrochromic color is concentrated in a layer next to the cathode.

In initially colored glasses, one ought not to expect the same local cation concentration gradients and a similar temperature bleaching. But for the glass compositions low in Nb_20_5 this partial bleaching upon heating was observed.

REFERENCES

l. Evdokimova, T.F., Kraevskii, S.L., Prasolov, A.P., Solinov, V.F., and Shishmentseva, E.V., *Electrochromic Effect in Tungsten Phosphate Glasses,* Fiz.Khim.Stekla,1978, vol:4, no:l, pp.88-91.

2. Kraevskii S.L., Solinov V.F., *Electrochromic Effect in the Lithium Glass-Solid Protonic Electrolyte System,* Glass Phys. Chem.1994. vol 20. No.6, pp.484-491.

3. Baucke, F.G.K., *Cation Migration in Electrode Glasses, Mass Transport Phenomena in Ceramics*, Mater. Sci. Res.,1975, vol. 5, pp. 337-354.

4. Baucke, F.G.K. and Bach, H., *II Field-Driven Formation and Electrochemical Properties of Protonated Glasses Containing Various Proton Concentrations*, J. Am. Ceram. Soc.,1982, vol. 65., no. l, pp.534-539.

5. Molinelli, J., Tomozava, M., and Takata, M., *Sodium Transport in the Na_20-H_20-$Si0_2$ Glass System*, J.Am. Ceram. Soc.,1985, vol. 68, no.3, pp.165-168.

6. Mazurin, O.V., Strel'tsina, M.V., and Shvaiko-Shvaikovskaya, T.P.; Svoistva Stekol i Stekloobrazuyuschikh Rasplavov (A Handbook on Properties of Glasses and Glass-Forming Melts), Leningrad: Nauka,1987, vol.5.

7. Kraevskii, S.L. *Spectral Analogues between the Lithium Niobate Crystal and Lithium-Niobium Phosphate Glass*. Glass Phys. Chem. 1994: vol. 20. No.3. pp.199-205.

8. Schirmer O.F., Thiemann, O., Wöhlecke, M., *Defects in $LiNbO_3$. I. Experimental Aspects*, J. Phys. Chem. Solids, 1991, vol. 52, no.1, pp.185-200.

SCALING IN THE RELAXATION OF GLASS-FORMING LIQUIDS AND THE LOCAL CONFIGURATIONAL ENTROPY

A.I.Gusarov, A.O.Votchek and **A.V.Dotsenko**
S.I.Vavilov State Optical Institute, Russia

Abstract

Within the framework of the hierarchically constrained dynamic model for glassy relaxation we found a procedure that allows to reduce the relaxation rates spectra of a glass-forming system for different temperatures onto a single universal curve. This procedure is valid in a wide temperature region, where simple approximation of time-temperature scaling is violated.

1. INTRODUCTION

In the glass transition region the relaxation of many supercooled liquids is characterized by non-exponential behavior and in a wide time region is described satisfactory by means of empirical Kohlrausch - Williams - Watts function [1]:

$$\Phi(t) = \exp(-(t/\tau_k)^{\beta}). \qquad (1)$$

Another approach is the based on a model distribution φ(k) of relaxation rates k. The relaxation function Φ(t) is represented as the Laplace transformation

$$\Phi(t) = \int_0^{\infty} \varphi(k) \exp(-k \cdot t)\, dk. \qquad (2)$$

Experimental investigations [2] have shown, that non-Debye character of the relaxation is enhanced when temperature is decreased. It means that not only the characteristic relaxation time depends on the temperature but other parameters that define the shape of φ(k) as well. As a result, a simple approximation of time-temperature scaling is not valid in the wide temperature region. However, for different supercooled liquids it was shown that the dielectric susceptibility data taken over a wide range of temperature can be scaled by means of a rather non-trivial transformation as to lie on a single curve [2]. The availability of this scaling implies existence of universal physical reasons, which determine the relaxation behavior of the glass-forming materials.

Recently, it was shown [3], that the distribution of the relaxation rates have a physical correspondence to the local configuration entropy distribution over the cooperatively rearranging regions, with size of these regions being determined by the scale of intermediate order in glasses. If a model of relaxation processes near the glass-transition is based on the constructing of quasiequilibrium distribution of independent cooperatively rearranging subsystems then analysis

of the relaxation rate spectra gives opportunity to investigate a relationship between universal properties of the relaxation processes and the structure of glass-formers. In order to obtain this relationship we suggest scaling procedure for φ(k) of the modified version of hierarchically constrained dynamic model [4]. The transformation of φ(k) is constructed in such a way as to exclude dependence of φ(k) on temperature and on characteristics of material and to keep only universal properties of the atomic dynamic. This scaling holds only in the time region, where Kohlraush law is valid.

2. MODEL

A class of models of hierarchically constrained dynamic (HCD) far glassy relaxation was suggested in [5]. These models take into account correlative character of the atomic rearrangements in disordered strongly interacting systems. Modified version of HCD model [4] implies a set of subsystems, with atomic rearrangements obeying HCD in each of them. In this approach the relaxation function is defined by eq.(2) with

$$\varphi(k) = \int_0^\infty dn\, w(n)\, \delta(k - k(n)),$$
$$w(n) = \ln\lambda / \lambda^n, \quad 1 < \lambda < \infty,$$
$$k(n) = k_0 \exp(-\mu\zeta(n)). \qquad (3)$$

Here n is the number of hierarchy level, w(n) is a statistical distribution of subsystems over these levels. The parameter μ determines a cooperativity degree of atomic rearrangements, k is the relaxation rate determined by the time scale of atomic rearrangements, which are not connected with the correlation between the hierarchy levels. The function ς(n) is the Riemann function.

The model eq. (3) has three parameters, whereas the stretched exponent, eq.(1), has only two parameters. However, it was shown [6] that in the time interval, where eq.(1) is valid, φ(k) can be considered as continuous distribution with only two free parameters:

$$\varphi(x) = (\chi\mu)^{-1} \exp(-x) x^{\mu+1}, \qquad (4)$$

where

$$\chi = k_0 (\ln\lambda)^\mu,$$
$$x = n\ln\lambda$$

Thus, for Φ(t) we have:

$$\Phi(t) = \int_0^\infty dx\, \exp(-x - t\chi x^{-\mu}). \qquad (5)$$

3. SCALING FOR RELAXATION RATES SPECTRA

In this section a transformation of the model spectra eq.(4) to a single universal curve is considered. A transformation of the relaxation rates scale $\gamma = k/k_m$, where k_m is a peak position of $\varphi(k)$ [4,6],

$$k_m = \chi(\mu+1)^{-\mu}, \tag{6}$$

aligns all peaks to one maximum position. The division of $\varphi(k)$ by $\varphi(k_m)$ compensates a change of the peak magnitude. It is also convenient to introduce a new function

$$g(\gamma) \equiv \varphi(\gamma)/\varphi(\gamma = 1) \tag{7}$$

For $g(\gamma)$ we have:

$$g(\gamma) = \left[\exp(-\gamma^{-1/\mu} + 1)\gamma^{-1/\mu}\right]^{(\mu+1)}. \tag{8}$$

If $g(\gamma)$ is considered as function on $x = \gamma^{-1/\mu}$ a change of T will give rise only in a change of exponent $(\mu+1)$ [6]. By analogy with constructing of the scaling curve in multifractal analysis [7,8] we introduce the following function:

$$y(x) = (\mu+1)^{-1}\log[g(x)], \tag{9}$$

Now y(x) does not depend on μ and consequently on T. Thus, the spectra of $\varphi(k)$ for different values of parameters can be reduced onto a single universal curve (Fig.1) described by relations:

$$y(r) = (\mu+1)^{-1}\log[\varphi(k)/\varphi(k_m)],$$
$$r = -\mu^{-1}\log(k/k_m). \tag{10}$$

One should note that eq.(4) and eq.(6) are valid when maximum of the relaxation rates spectrum is located in the region $k_m << k_o$. This candition is violafed if $\mu << 1$ [4]. On the other hand ,u gaes down when T is increased [6]. It means that a temperature T_c exists and when $T > T_c$ the scaling above is not valid.

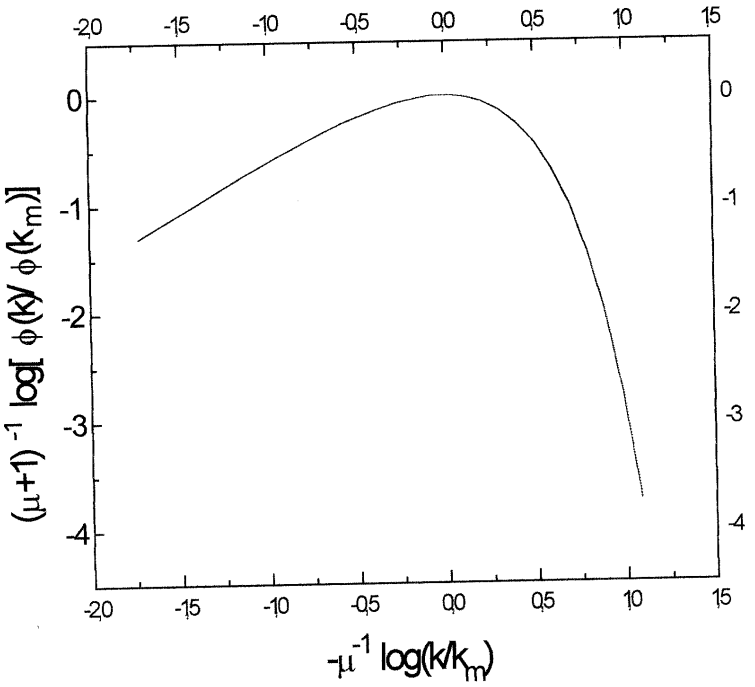

Fig.1 Scaling curve for relaxation rate spectra.

4. CONCLUSIONS

For relaxation rates spectra of modified HCD model [4] a scaling procedure was determined. This scaling is valid for temperatures $T<T_c$, where T_c is defined by cooperativity parameter of the model. Variable of the universal curve coincides with the natural variable of model, that is the number of hierarchy level. The relationship between relaxation rates and the local configurational entropy [3) means that the distribution of the latter for the HCD model [4] has scaling properties as well. This agrees with the suggestion about universal features of the liquid structure that are defined by intermediate order. These features offer evidence to the physical origin of the non-exponential character of structural relaxation kinetics.

One should note that the present "structural" scaling is not explicitly connected with the scaling procedure determined in [2]. The reason of it is that the latter establishes universal relations between different time regimes of the relaxation function behavior [9], whereas the scaling for the HCD model is applicable only for Kohlraush regime and implies the connection of this regime with a universal character of the intermediate order in glass-forming liquids.

REFERENCES

1. Klafter J., Shlesinger M.F. Proc.NatI.Acad.Sci. USA 83 (1986) 848
2. Dixon P.K., Lei Wu, Nagel S.R., Williams B.W. and Carini J.P. Phys. Rev.Lett. 65(1990) 1108
3. Moynihan C.T., Shroeder J. J.Non-Cryst. Solids 160(1994)52
4. Volchek A.O., Gusarov A.I. and Mashkov V.A. Sov.Phys.JETP 74 (1992)307
5. Palmer R.G., Stein D.L., Abrahams E., Anderson P.W. Phys.Rev.Lett. 53(1984)985
6. Gusarov A.I., Volchek A.O. J.Non-Cryst. Solids 195(1996)165
7. Halsey T.C., Jensen M.H., Kadanoff L.P., Procassia I., Shraiman B.I. Phys. Rev. A. 33(1986)1141
8. L. P. Kadanoff, S. R. Nagel, L. Wu, S.-m Zhou Phys. Rev. A. 39(1989)6524
9. Kim B., Mazenko G.F. Phys.Rev.A. 55(1992)2393

SILICA GEL-GLASS DOPED WITH FLUORINE FOR OPTICAL FIBRE FABRICATION*

Poddenezny E. N., Melnichenko I. M., Plusch B. V., Neroda I.U.
Gomel State University, Belarus

Abstract

The silica glass, doped with fluorine having low OH contents (3-5 ppm) was prepared by a sol-gel method. The process of synthesis incorporate tetraethylorthosilicate hydrolysis in water solution of the acid to obtain a sol, preparation of the sol-colloid system by adding fumed silica (aerosil T-30, Wacker-Chemie GmbH, Germany) into the sol, the neutralisation of the sol-colloid system up to pH ~ 6.5 by introducing an ammonia solution, sonoactivation, centrifugal separation, liquid slip casting, gel-formation, drying and vitrification in the atmosphere of helium. The gels were dried at 20-60^{o}C after 2 days ageing in the deionized water. The BET surface area, bulk density of xerogels were found to depend on the concentration of the aerosil and on the conditions of the drying. The dried gels exhibited bimodal pore size distribution. Scattering electron microscopic investigation, atomic force microscopic, DTA, TGA of the xerogels and monolythic glass were using for characterisation of the gel and glass parameters. Transparent silica glass in the form of the rods and tubes was obtained by sintering the gels at 1280-1300^{o}C in the mixed atmosphere of freon ($C_2Cl_3F_3$) and helium.

The result of the present work is the production of the gel-glass rods and tubes with length up to 150 mm, diameter up to 20 mm and with the fluorine contents up to 0.6 wt. %. The transmission loss of the sol-gel fibre was 10-15 dB/km at a wavelength of 0.85 mm.

---

* Full manuscript not available at the time of printing

SPECTRAL AND RADIATION PROPERTIES OF PHOSPHATE GLASSES WITH ADDITIONS OF VARIABLE VALENCE ELEMENTS*

Valerii I. Arbuzov, Nadezhda S. Kovaleva
S.I. Vavilov State Optical Institute, Russia

Abstract

Phosphate glasses play an important part in the field of laser engineering and optics. For this reason they undergo often the action of powerful ionizing or UV radiation which cause the appearance of elementary electronic excitations. These excitations can lead to the color centers (CCs) formation or to the changes in the spectral properties of activator ions especially in the case of activators of variable valence.

The aim of the work was to investigate the spectral and radiation properties of metaphosphate glasses with additions of iron, europium or cerium oxides. It was estimated that, under the action both ionizing radiation and UV light with the energy quanta in the limits of the absorption bands of activators, Fe^{2+} and Ce^{3+} ions change their charges undergoing to the $(Fe^{2+})^{+}$ and $(Ce^{3+})^{+}$ states respectively. Their radiation induced oxidation allowed us to estimate the quantitative characteristics of intrinsic hole CCs which were depressed because of Ce^{3+} and Fe^{2+} recharge. It was shown that the protector action of Ce^{3+} ions in phosphate glasses was as high as in silicate ones. As for Fe^{3+} and Eu^{3+} ions which are very effective electron acceptors in silicate glasses their behaviour in the radiation processes in phosphate glasses differs. So Eu^{3+} ions capture electrons very efficiently thus diminishing the number of intrinsic electron CCs. Unlike this Fe^{3+} ions doesn't participate in the radiation processes in the above glasses. The investigation of Eu^{3+} containing glasses allowed to identify the CCs absorption band with radiation properties of metahosphate glasses with additions of iron, europium or cerium oxides. It was estimated that, under the action both ionizing radiation and UV light with the energy quanta in the limits of the absorption bands of activators, Fe^{2+} and Ce^{3+} ions change their charges undergoing to the $(Fe^{2+})^{+}$ and $(Ce^{3+})^{+}$ states respectively. Their radiation induced oxidation allowed us to estimate the quantitative characteristics of intrinsic hole CCs which were depressed because of Ce^{3+} and Fe^{2+} recharge. It was shown that the protector action of Ce^{3+} ions in phosphate glasses was as high as in silicate ones. As for Fe^{3+} and Eu^{3+} ions which are very effective electron acceptors in silicate glasses their behaviour in the radiation processes in phosphate glasses differs. So Eu^{3+} ions capture electrons very efficiently thus diminishing the number of intrinsic electron CCs. Unlike this Fe^{3+} ions doesn't participate in the radiation processes in the above glasses. The investigation of Eu3+ containing glasses allowed to identify the CCs absorption band with the maximum at E>6 eV as one caused by the intrinsic electron color centers.

---

* Full manuscript not available at the time of printing

STORAGE OF CAESIUM AND STRONTIUM SALTS IN SINTERED BOROSILICATE GLASS

Mihai Cerchez and **Monica Mihai**
National Glass Institute, Rumania

I. INTRODUCTION

The specialized literature shows the possibilities of storage various radioactive atomic species, wastes resulted from the nuclear fuel fission, for their controlled keeping. For the environmental protection, the storage is made in natural rocks or rocks obtained through synthesis, various types of cements and concretes, metals, vitroceramics, or glass [1-5]. For medicine and other technical applications, there are also obtained sources with radioactive isotopes included in the same types of materials [1-5]. The inclusion of various radioactive isotopes in glass and vitroceramics is made through the process of vitrification of raw materials together with the radioactive components.[1-2].

The paper presents the possibilities of using a sintered borosilicate glass for the storage of caesium and strontium salts. The researches have been conducted with inactive caesium and strontium salts. Caesium and strontium chlorides have been used, in view of the fact that solubilisation by means of acids is used at the treatment of radioactive wastes.

The utilization of inclusion method by sintering could be very advantageous in comparison with the vitrification technique, which requires temperatures of 1400-1550^{o}C and special materials. As the sinterized glass for inclusion has no porosity, and it could be obtained at 725-750^{o}C results important advantages, including the diminishing by volatilization of the radioactive substances.

II. DOCUMENTARY DATA

Table 1 presents the limits of oxide composition of borosilicate glasses used for the storage of the radioactive wastes.

Table 1: Oxide composition of the borosilicate glasses used for wastes storage [2,3]

Oxides wt %										
SiO_2	B_2O_3	R_2O	RO	Fe_2O_3	Cr_2O_3	NiO	Al_2O_3	TiO_2	ZrO	CuO
42-83	15-34	13-32	0-10	1.5	-	3.3	0-17	0-5	0-37	0-5

Table 2 presents the general characteristics of the borosilicate glasses used for the storage, by melting, of radioactive wastes.

Table 2: Main characteristics of the borosilicate glasses used for the storage of radioactive wastes

Characteristic	Unit	Value
Thermal expansion (30-400°C)	$^oC^{-1}$	$7\text{-}12 \cdot 10^{-6}$
Viscosity	p	1000 at 900°C 100 at 1070°C
Transformation temperature (t_g)	°C	450-500
Density	$g.cm^{-3}$	2.7*
Dissolving speed	$g.cm^{-2}.day^{-1}$	10^{-3} - 10^{-5}

* only for MW glass - UK

III. EXPERIMENTAL PROCEDURE

The following substances have been used: $SrCl_2 \cdot 6H_2O$, of p.a. purity and CsCl prepared in laboratory from Cs_2C0_3 and HCI, checking up that at the chloride formation the reaction should be complete.

Tables 3 and 4 presents the limits of oxide compositions and respectively the characteristics of the used borosilicate glass made in the National Glass Institute (NGI).

Table 3: Oxide composition of NGI glass

Oxides wt%				
SiO_2	B_2O_3	R_2O	RO	Al_2O_3
55-65	6-12	10-15	2-7	6-10

Table 4: Characteristics of NGI glass

Characteristic	Unit	Value
Thermal expansion (20-300°C)	$^oC^{-1}$	$8.1\text{-}8.9 \cdot 10^{-6}$
Transformation temperature (t_g)	°C	525-540
Littleton temperature	°C	720-730
Working temperature	°C	1000-1027
Density	$g.cm^{-3}$	2.46-2.59
Hydrolitic stability	class	I-II

After having obtained the glass, it was ground to the grain size of 98%<0.063 mm and afterwards mixed with a solution containing polyethileneglicol and caesium or strontium salt, dissolved in the water.

The obtained suspension was dried at the room temperature, and the obtained solid samples were crushed and then sieved through the 0.315 mm sieve The grains obtained in this way have been pressed at 125 bars, resulting samples with sizes 75 x 75 x 7 mm, which have been further sintered at 725-750°C for 0.5 -1.0 hours.

The samples of sintered glass, with a content of 11.1 - 29.5 wt% caesium or strontium salt have been characterized physically and structurally, after sintering, through:

-water absorption by weighing the sample before and after boiling for 3 hours at 98^{o}C, in order to estimate porosity;

- hydrolytic stability, as per ISO 719,

- hydrolytic stability at the surface: determination temperature: 98^{o}C; ratio V/S of 0.05-0.063 m; determination duration:1 hour;

- X-ray diffraction with difractometer URD-6, Germany;

- spectrophotometry in infrared with spectrophotometer SPECORD M 80.

IV. RESULTS - DISCUSSIONS

IV.l. Main characteristics of the sintered with chloride glass.

Tables 5 and 6 presents the main data regarding the obtaining of sintered glasses with addition of caesium chloride and strontium chloride.

In glasses with included CsCl it may be noticed a weight loss at sintering of 10.06-10.74 wt% CsCl for the samples having 10 wt% Cs_2O included and respectively 20.21-25.64 wt% for the samples with 20 wt% Cs_2O included.

The glasses sintered with $SrCI_2.6H_20$ included lose only maximum 4.50 wt% $SrCl_2$ at a content of 15 wt% SrO, thus having, as anticipated, a smaller volatilization tendency when heated, as compared to the glasses with CsCl.

Even when such a volatilization exists, the glasses sintered with addition of chlorides lose, when heated, a much smaller quantity than the similarly glasses melted together with the same salts at temperatures of over 1400^{o}C.

Another important characteristic of the glasses sintered with included caesium and strontium chlorides, is that, as shown in tables 5 and 6, they may be also obtained with an absorption capacity of water of 0%.

By relating this low absorption capacity with determination of hydrolytic stability used for the laboratory of household glassware, it comes out that up to a concentration of 10 wt% Cs_2O or SrO in the sintered glass, the assembly glass-salt is included in the stability classes III-IV

Making similar dissolving determinations at the surface of the glasses sintered with stored caesium and strontium chlorides, after one hour, it resulted a loss of 10^{-5}-10^{-4} g/cm^2 for the glass sintered with 10-20% Cs_20 introduced as CsCl and for the one with 5-10 wt% SrO introduced as $SrCl_2.6H_2O$.

The values of solubilisation in water at 98^{o}C obtained through the two methods may be considered satisfactory, as compared to the solubilisation data obtained on the glasses vitrified with compounds of this type [1]. Mention should be made of the fact that besides the advantage of diminishing the volatilization at inclusion, the method of using the sintered glasses can be improved, for instance, by a slight increase of the temperature or by introduction of more B_2O_3 in the glass.

Table 5 : Parameters of obtaining and main characteristics of sintered glasses with included CsCl

Crt. No.	Characteristics	Sample specifications			
		C 10-1	**C 10-2**	**C 20-1**	**C 20-2**
1	Composition of unsintered mixture (wt%) -glass powder -CsCl -polyetileneglicol	83.42 11.08 5.50		72.76 21.74 5.50	
2	Sintering treatment	400^0C-1.5 h 725^0C-0.5 h	400^0C-1.5 h 750^0C-1 h	400^0C-1.5 h 725^0C-0.5 h	400^0C-1.5 h 750^0C-1 h
3	Theoretical weight loss at sintering (wt%)	5.50		5.50	
4	Theoretical content of CsCl in sintered glass wt%	11.73		23.01	
5	Theoretical content of Cs_2O in sintered glass wt%	10.00		20.00	
6	Weight loss at sintering wt%	6.74	6.79	6.79	8.53
7	CsCl content in sintered glass wt%	10.55	10.47	21.95	20.45
8	Cs_2O content corresponding to the CsCl quantity left in the sintered glass wt%	8.83	8.76	18.36	17.11
9	CsCl quantity lost by volatilization * wt%	10.06	10.74	20.21	25.64
10	Sample aspect after, sintering	smooth, fairly glossy	smooth, glossy	smooth, mat	smooth, mat
11	Volume contraction of the sintered sample as compared to the raw one (%)	28.50	33.48	14.93	20.15
12	Water absorption capacity (%)	0.00	0.00	0.00	0.00
13	Hydrolytic stability on grains (class, $MgNa_2O$ dissolved/g glass)	IV 0.6014	IV 0.3286	-	over class V 1.1780
14	Hydrolytic stability per area (g/cm^2) Volume/Surface ratio (cm)	$7.42x10^{-5}$ 6.06	$5.15x10^{-5}$ 5.02	$2.06x10^{-2}$ 5.75	$1.47x10^{-2}$ 5.72

* Considering that, besides binder, chloride is also volatilised

Table 6: Parameters of obtaining and main characteristics of sintered glasses with included $SrCI_2.6H_20$

Crt. No.	Characteristics	Sample specification		
		S5	**S10**	**S15**
1	Composition of unsintered mixture (wt%) -glass powder -$SrCl_2.6H_2O$ -polyetileneglicol	 83.23 11.27 5.50	 73.49 20.01 5.50	 64.99 29.51 5.50
2	Sintering treatment	400^0C-1.5h 750^0C-1 h	400^0C-1.5h 750^0C-1.0h	400^0C-1.5h 750^0C-1.0h
3	Theoretical weight loss at sintering (wt%)	5.50 PEG 4.75 H_2O 10.07	5.50 PEG 8.51 H_2O 14.01	5.50 PEG 11.95 H_2O 17.45
4	Theoretical content of anhydric $SrCl_2$ in sintered glass wt %	7.45	14.54	21.27
5	Theoretical content of SrO in sintered glass wt%	5.00	10.00	15.00
6	Weight loss at sintering wt%	10.45	16.41	21.95
7	Anhydric $SrCl_2$ content in sintered glass wt%	7.06	12.08	16.73
8	SrO content corresponding to the anhydric $SrCl_2$ quantity left in the sintered glass wt%	4.60	7.89	10.93
9	SrCl quantity lost by volatilisation* wt%	0.38	2.40	4.50
10	Sample aspect after sintering	glossy, smooth	relatively mat, smooth	smooth, mat
11	Volume contraction of the sintered sample as compared to the raw one %	35.63	33.24	33.24
12	Water absorption capacity %	0.00	0.00	0.00
13	Hydrolitic stability on grains class, mg Na_2O dissolved/g glass	III 0.0074	IV 0.3658	V 0.7130
14	Hydrolytic stability per area (g/cm^2) Volume/Surface ratio (cm)	$1.84x10^{-4}$ 5.61	$1.28x10^{-4}$ 6.29	$5.47x10^{-5}$ 5.34

* Considering that, besides binder, chloride is also volatilised.

IV.2. Structural characteristics

IV.2.l. X-ray determinations

By comparing the X-ray diffractograms of the glasses sintered with Cs and Sr chlorides with that of the basic glass and the two calcinated salts (figure 1), the following conclusions may be drawn:

- the glass sintered with caesium chloride has a high ß-quartz crystallisation tendency than the one with strontium chloride (figure 1 b and 1 c);
- the strontium chloride plays an adverse part, seeming to decrease the crystallisation tendency of ß-quartz, rendered evident through d=3.34Å (figure 1 c) as compared with the basic sintered glass (figure 1 a);
- caesium chloride remains in the sintered glass as such, which points out to the fact that the mixing of the sintered glass with this salt leads to a structure of oxidic-halogenuous, partially crystalised, glass type;
- in the glass sintered with included strontium chloride, a compound of strontium oxide or strontium chloride seems to be formed, rendered evident through d=2.81Å.

IV.2.2. Infrared spectrophotometry

The glasses with 10-20 wt% Cs_2O has the general appearance of the absorption spectra of the basic borosilicate glasses, (figure 2), with the mentioning:

According to the X-ray data, it is rendered evident the crystallisation of (3-quartz in the sintered glass with addition of caesium chloride, which is formed in bigger quantities in the samples with 20 wt% Cs_2O; the main absorption maxima registered are at 1040-1060 cm^{-1} and at 740-780 cm^{-1} , and are due to the extension of the link Si-O intetrahedrons [$Si0_4$]; the absorption maxima at 460-480 cm^{-1} , are due to the deformation of the link Si-O in tetrahedrons[SiO_4] [6,7].

By comparing the IR spectra of the basic glass and of calcinated CsCl with those obtained for the investigated samples, it is noticed that the crystallized caesium chloride is maintained in the sintered samples; the absorption maxima of the caesium chloride, which are higher for the samples with 20 wt% Cs_2O, are at 1720 cm^{-1} , and in the area of 1350-1550 cm^{-1} .

However, part of the caesium chloride seems to react structurally with the glass, leading probably to specific structural geometric units of caesium with the oxidic structure of the basic glass. This structural modification of the sintered glass with addition of CsCl is rendered evident by the occurrence of a shoulder in the spectrum, at the samples with 20 wt % Cs_2O, in the area of 860-920 cm^{-1} ,

The glasses with 5-15% SrO has the general appearance of the absorption spectra of the basic borosilicate glasses, (figure 3), with the remark that:

- according to the X-ray data, it is rendered evident the crystallization of (3-quartz is lower in the sintered glasses with $SrCl_2$ as compared with those with CsCl;
- in the areas of $Si0_2$ absorption centered at 460-480 cm^{-1} caused by the deformation of the links Si-O in tetrahedrons [SiO_4], it is noticed the structural influence of the $SrCl_2$ content in glasses; - this influence is related with the absorption variations in IR at approximately 400 cm^{-1} .

V. CONCLUSIONS

l. Using borosilicate glass powder homogenous mixed with an organic binder and caesium or strontium chlorides by sintering, predominant vitreous materials, were obtained.

2. The investigated glass samples with chlorides included, containing 10 wt% Cs_2O and respectively 5-15 wt% SrO, had zero water absorption.

3. Relating the water absorption obtained values with the durability tests of laboratory glass articles but also of some radioactive wastes, it results that the sintered with chloride salts glasses, have the hydrolytic stability in the range of values of the III-IV glass of hydrolytic stability for contents up to 10 wt% of added CsCl or $SrCl_2$

4. The structural investigations made on the assembly sintered glass with stored chloride show:

-the sintered with chlorides borosilicate glass has a structure type like mixture of an oxidic glass with ß-quartz and chloride crystals;

-the favourising of the crystallization of ß-quartz in the sintered glass with CsCl;

-the hampering of the crystallization of ß-quartz by sintering the same glass with $SrCl_2$;

- there appear also some structural interaction between the glass and the chloride salts especially in the case of CsCl.

REFERENCES

1. J.A.C Marples - Glass Technology, 29,1988, 6, p.230-247
2. P.J.Hayward - Glass Technology, 29,1988, 4, p.122-136
3. C.M.Jantzen - Extended Abstracts,1994, Fall Meeting of Glass and Optical Materials Columbus Ohio, p.13-15.
4. M.Fryda, G.Vetter and P.Boch - Proceedings of the Third Euro-Ceramics, 3, 1993, p.213-218.
5. S.V. Stefanovskii, I.A.Ivanov and A.N.Gulin - Glass Physics and Chemistry, 1994, p.103-109.
6.D.Becherescu, V.Cristea, Fr.Marx, I.Menessy, Fr.Winter - Physical Methods in the Chemistry of Silicates,1977,p.45-47.
7. L.L.Hench, R.G. Newton, S. Bernstein - Glass Technology, 20,1979, p.144

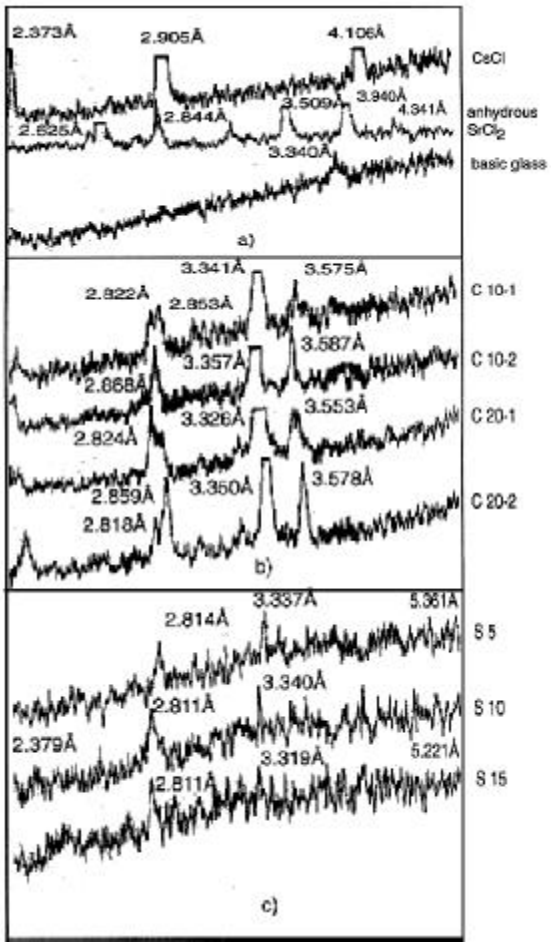

Fig.1 X-ray diffractograms of the investigated samples. a) chlorides and basic glass diffractograms, b) sintered glass with CsCl, c) sintered glass with $SrCl_2$.

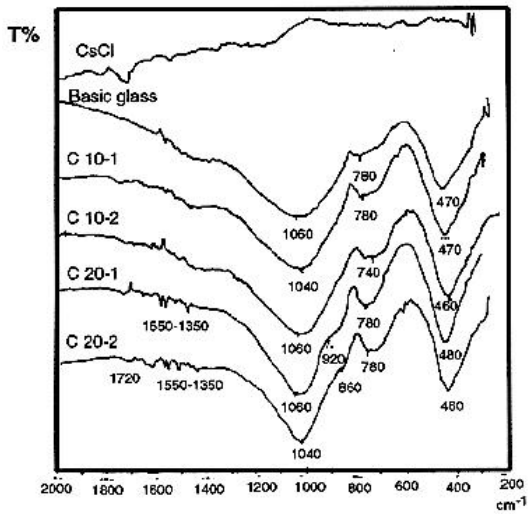

Fig. 2: IR spectra of CsCl, basic glass and the assembly sintered glass - CsCl

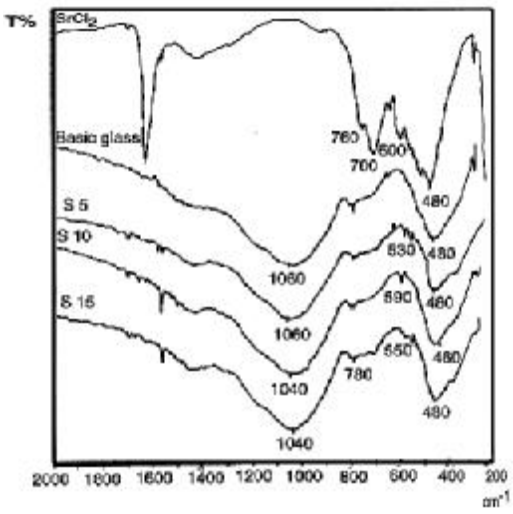

Fig. 3: IR spectra of SrO_2, basic glass and the assembly sintered glass - SrO_2

STRUCTURAL CHANGES IN MOLTEN OXIDE GLASSES

G. Herms, W. Gerike and **J. Sakowski**
Rostock University, Germany

Abstract

Examples of X-ray diffraction results are presented, which demonstrate the great diversity of oxide glass melts. Sometimes structural changes can already be observed about 150 K above T_g in contrast to Riebling's comment according to which changes can be expected beyond T_g + 300 K or T_g + 400 K. In some cases the radial distribution function (RDF) reveals a change of the short range order (SRO) in spite of the fact that the scattering curves of the melt and of the solid glass, apart from the first sharp diffraction peak (FSDP), seem to be fully identical.

I. Introduction

Previous high-temperature diffraction studies seemed to show that there are no worth mentioning differences between the structure of a glass and the structure of its melt. More or less, the essential result was the finding that the distributions of the atomic distances are broader in the melt than in the solid glass. This can clearly be seen in the radial distribution functions (RDFs) of B_2O_3 presented by Zarzycki [1] and Misawa [2], see Fig. 1 and 2. Also in the G(r) curve of a calcium silicate glass, studied by Waseda [3], the peaks become flatter in the melt (Fig. 3). In addition minor shifts of peaks beyond 5 X are detectable. However, it seems very doubtful whether the effect reflects a real process connected with the melting or not.

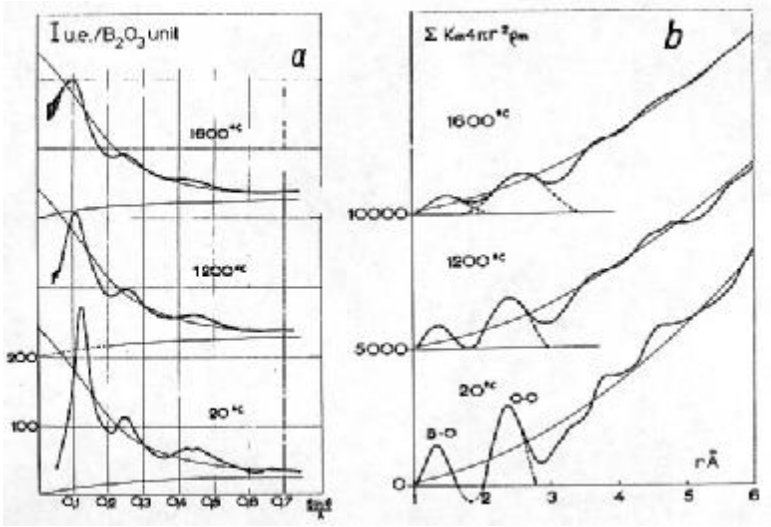

Fig.1: Scattering curves (a) and radial distribution functions (b) of vitreous and molten B_2O_3 at 20 °C, 1200 °C and 1600 °C (taken from [1]).

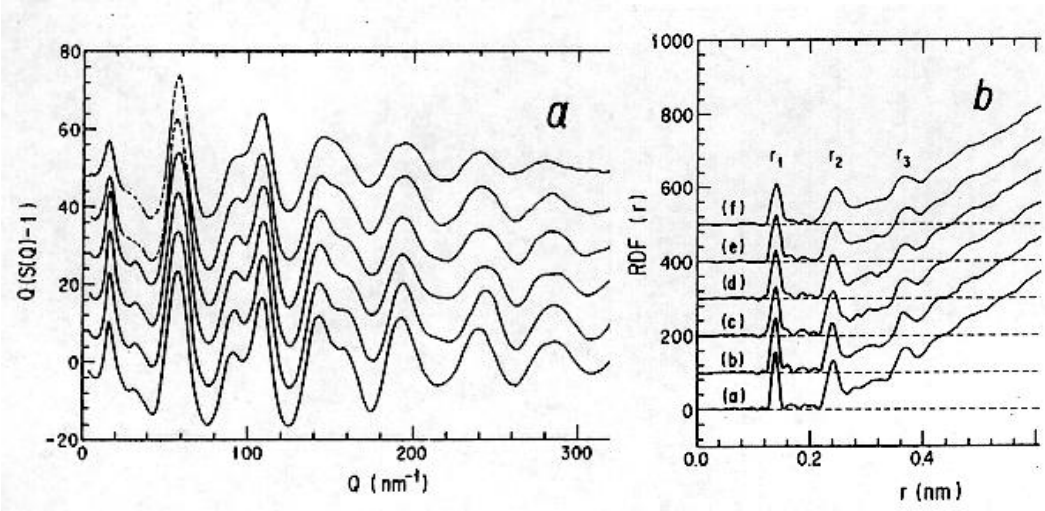

Fig.2: Reduced interference functions (a) and RDF (b) of vitreous and molten B_2O_3 at 121, 298, 523, 633, 733 and 1073 K (taken from [2])

In summary, it may be said that the previous high-temperature experiments seemed to confirm the opinion that "with respect to the nearest-neighbor correlations, information from glassy samples is applicable to the molten state, as a first approximation" [3]. Riebling [4] even spokes from " an exact structural correlation between an oxide melt and its corresponding glass" and concedes however, that ***sometimes*** the exact correlation can be "limited to temperatures below $T_g + \Delta T$ (where $\Delta T \approx 300^o$ to 400^o)".

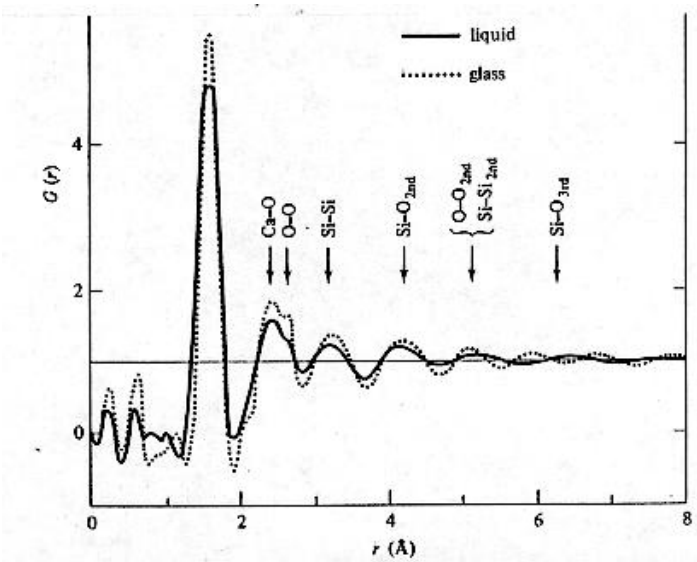

Fig. 3: Comparison between the structure of the glassy state and that of the liquid state in the case of 45 mol % CaO-SiO_2 (taken from [3]).

II. Results of recent high-temperature diffraction studies

Sometimes already the scattering curves reveal the replacing of a given amorphous structure by another amorphous structure in the course of melting. An example is shown in Fig. 4. It is an overall view of scattering curves, which are measured during heating up with a mean heating rate of 10 K/min. The curves change their character between 850 K and 900 K. As can be seen here the exact structural correlation is limited to about T_g + 150 K (T_g = 757 K). The temperature range of exact correlation finishes off with a much lower temperature as predicted by Riebling [4].

More often the glasses show the behaviour which is depicted in Figs. 5 and 6. Applying the same heating rate these glasses run through an crystalline intermediate state. In the case of calcium metaphosphate glass the structure is partly-crystalline between about 1000 K and 1200 K. Above 1200 K the material scatters in another way as can easily be seen from the structure factor (see Fig. 7). The changes beyond $s=3X^{-1}$ indicate a transition of the short range order (SRO). The decrease of the first sharp diffraction peak (FSDP) with increasing
temperature is abnormal compared with the most binary oxide glasses (e.g. sodium metaphosphate or sodium borate glasses). It is still vague what can be the reason for this conspicuous behaviour. (In case of Mg metaphosphate glass the FSDP slightly increases during melting.) The most important change of the SRO is the decrease in height of the peak at 3.5 A (Fig. 8). The same effect can be observed in the RDF of sodium metaphosphate glass [5].

In contrast to the glass, just described, another type of glass is to be presented here: lithium borate glass with 15 mol % Li_2O. The scattering curve of the melt does not differ from that of the solid glass (Fig. 9) with the exception of the FSDP, which is shifted to lower scattering angles and increased in the melt. In other words, the scattering seems to indicate the constancy of the SRO. Nevertheless, the difference distribution functions show distinct changes in the distance range from 3 to 5 X, in such way revealing that the topology of the network changes with rising temperature.

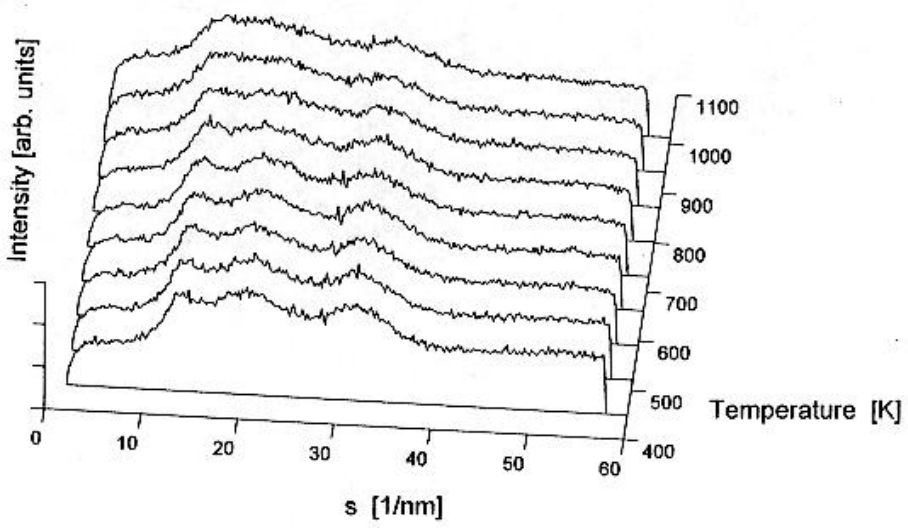

Fig. 4: Temperature dependence of the scattering curves of sodium borate glass with 28 mol % Na_2O (electronic position sensitive detector, heating rate 10 Klmin, T_g =760 K). Please note that the shape of the curves changes between 850 K and 900 K.

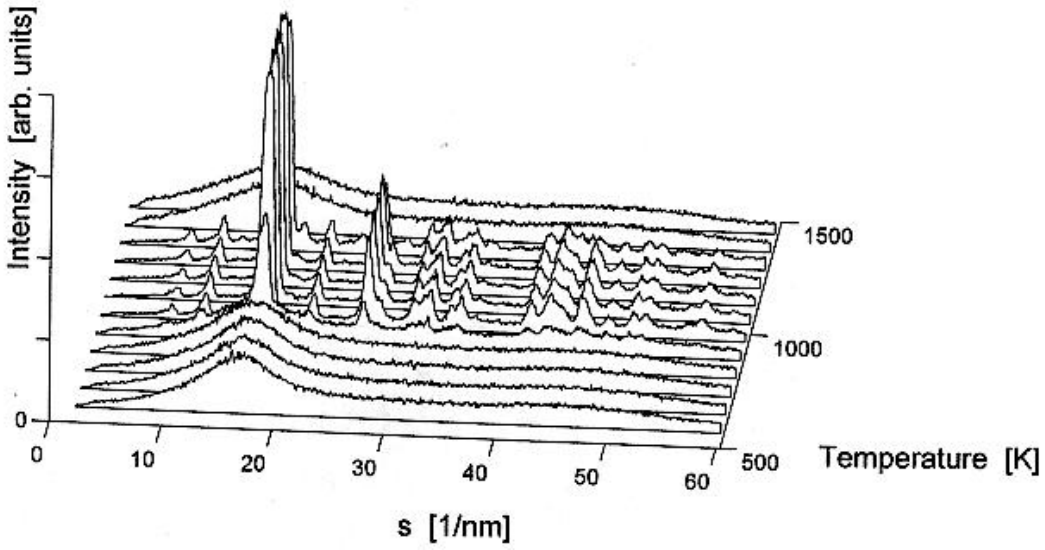

Fig. 5: Temperature dependence of the scattering curves of lithium disilicate glass (Tg»730 K). The crystalline phase is orthorhombic $Li_2Si_2O_5$ (C1c1)

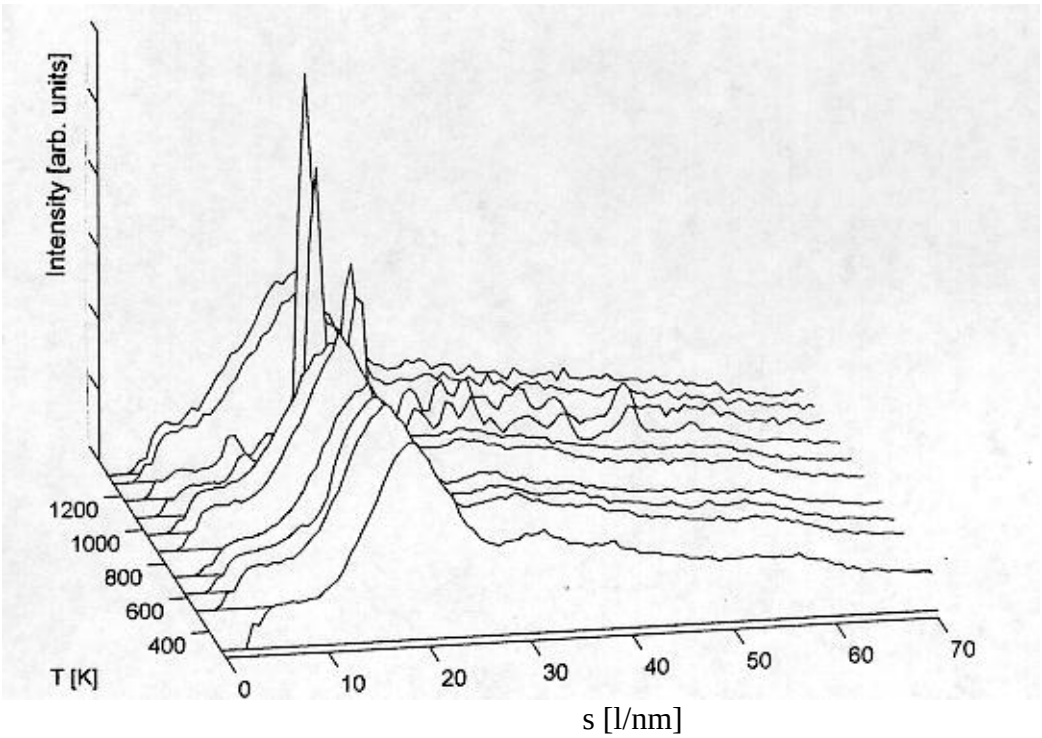

Fig. 6: Temperature dependence of calcium metaphosphate glass (T_g» 790 K)

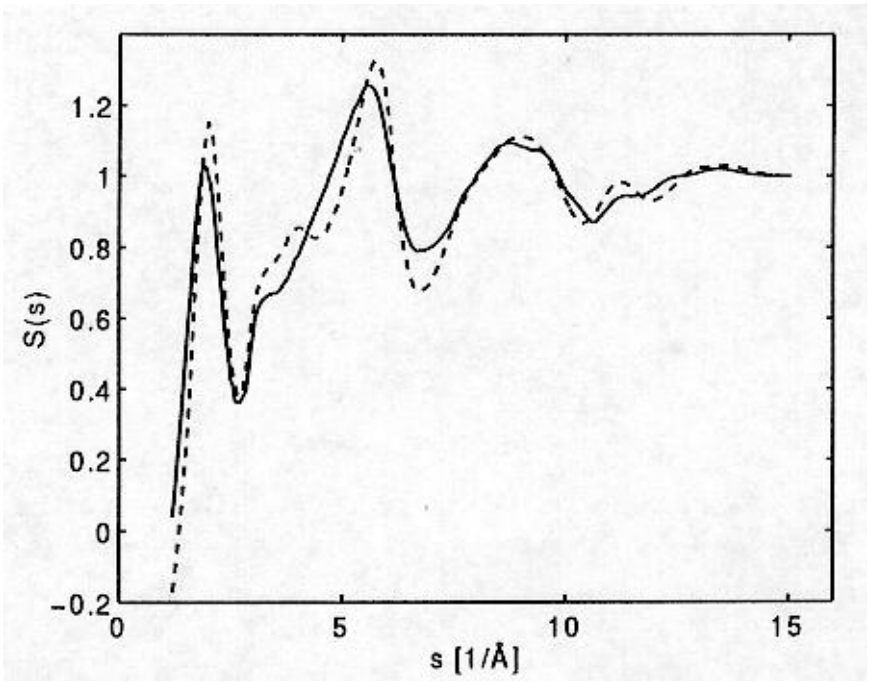

Fig. 7: Structure factor of calcium metaphosphate glass (solid line: 1420 K, dashed line: room temperature)

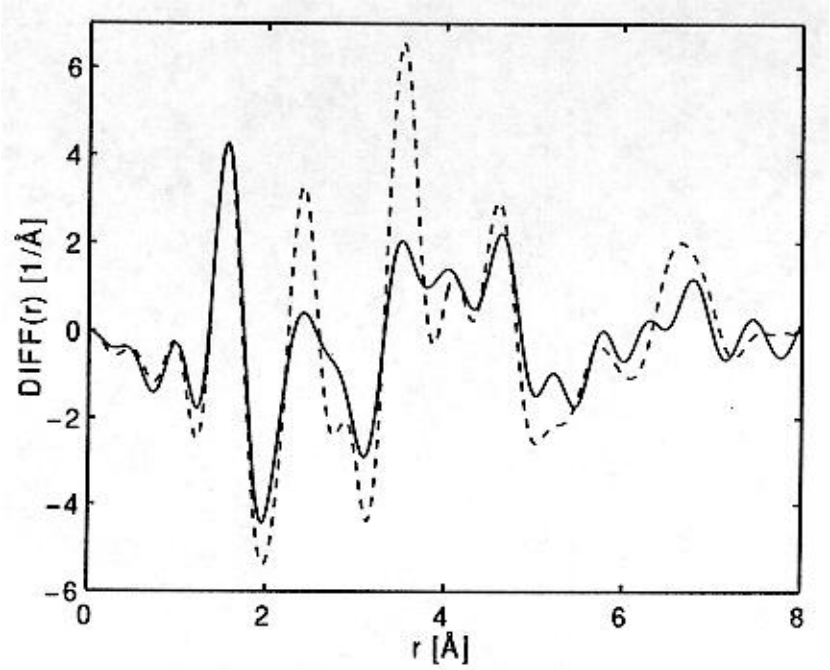

Fig. 8: Difference distribution functions corresponding to Fig. 7

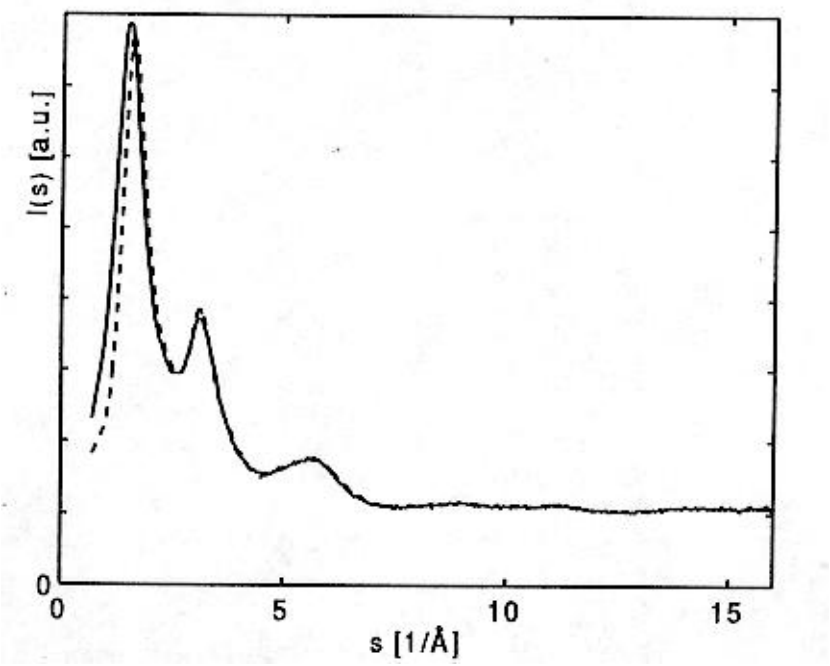

Fig. 9: Scattering curves of Li borate glass with 15 mol % Li_2O (solid line: 1160 K, dashed line: room temperature)

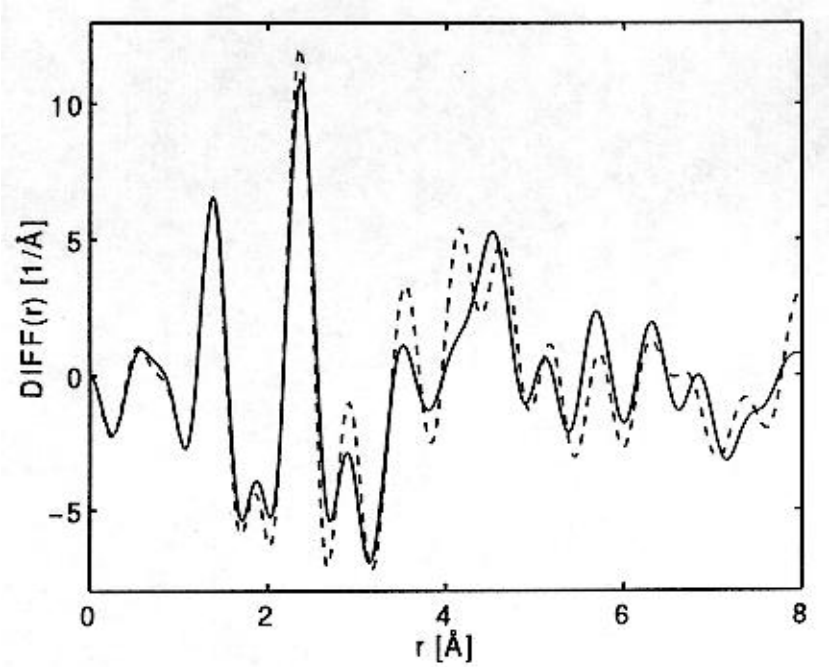

Fig. 10 Difference distribution functions corresponding to Fig.9

References

[1] J. Zarzycki in Borate Glasses, eds. L. D. Pye, V. D. Frechette a. N. J. Kreidl, Plenum New York 1978, p. 201
[2] M. Misawa, J. Non-Cryst. Solids 122 (1990) 33
[3] Y. Waseda, The Structure of Non-Crystalline Materials, New York 1980
[4] E. F. Riebling, J. Amer. Ceram. Soc. 51 (1968) 143
[5] G. Herms, W. Gerike a. J. Sakowski, Structural Classification of Oxide Glass Melts, paper at this conference

Acknowledgment

The authors are indebted to Mrs. Prof. D. Stachel, Otto-Schott-Institut Jena, for preparing the glasses and to BMBF for financial support

STRUCTURAL EVOLUTION IN GELS FOR SYNTHESIS OF APATITE-ANORTHITE GLASS-CERAMICS

B. Samuneva, M. Dimitrova-Lukacs*, Y. Ivanova, P. Djambaski, and **S. Stefanova**
University of Chemical Technology & Metallurgy, Bulgaria
*ALUTHERY - FKI., Hungary

Abstract

The sol-gel synthesis of apatite-anorthite glass-ceramics has been carried out by the crystallization of gel-glasses in the SiO_2-P_2O_5-AI_2O_3-CaO-F system, without melting process. The structural evolution in gels, during their heat treatment till 1250 °C was studied using X-ray diffraction analysis, IR-spectroscopy, TEM and TEMD. SiO_2 was introduced as SiO_2-sol and TEOS and it was found the type of precursors influences strongly on the phase formation in the gels studied. The apatite-anorthite glass-ceramics can be obtained from the gels, in which SiO_2 is introduced as TEOS, after heat treatment at 1050°C -1150°C. It has been established that at highest experimental temperature the diffraction peaks of fluorapatite decreased and disappeared and a new phase, gehlenite, was formed.

I. INTRODUCTION

The glass-ceramic materials are perspective for different practical application because they possess many valuable thermal, chemical electrical, magnetic and other physicochemical properties conserving their parameters even at elevated temperatures. During the last years the synthesis of new glass-ceramics for application in medicine and dentistry as bioactive and bioinert materials has been successfully developed (1 - 12). Usually in this kind of glass-ceramics present bioactive crystalline phases (fluorapatite, fluormica or calcium phosphates) and some another phases providing better mechanical or optical properties (vollastonite, anorthite, diopside, leucite, alumina zircona). The bioglass-ceramics in the $CaAI_2Si_2O_8$ - $Ca_5(PO_4)_3F$, $CaMgSi_2O_6$ - $Ca_5(PO_4)_3F$ and $CaAI_2Si_2O_8$ - $CaMgSi_2O_6$ - $Ca_5(PO_4)_3F$ have been successfully obtained by sinter- crystallization of glass powders with different dispersity (13,14).

Recently R. Hill and D. Wood studying ionomer glasses (15, 16) have been established that some of these glasses are with suitable crystallization ability, physicochemical and technological properties for obtaining of glass-ceramics for dental crowns (17, 18). The main crystalline phases in this kind of glass-ceramics are fluorapatite and mullite. M. Dimitrova - Lucacs has been investigated the synthesis of apatite -mullite glass-ceramics using hydroxyapatite as raw material and received glass-ceramic materials with high flexural strengths and fracture toughness (19).

It is well known that sol-gel method for synthesis of glasses and glass- ceramics gives advantages in comparison to the traditional melting technology: lower synthesis temperature, higher homogeneity and purity, possibility to synthesize materials of new composition and obtaining the glass-ceramics by direct crystallization of gels without melting.

B. Samuneva, Y. Dimitriev et al. have synthesized by sol-gel technology glass-ceramic materials in the MgO - Al_2O_3 - SiO_2, CaO - Al_2O_3 - SiO_2, ZnO - ZrO_2 - SiO_2 and ZrO_2 - TiO_2 - SiO_2 systems with homogeneous microstructure and high thermal, chemical and mechanical properties (20 - 25).

By direct crystallization of gels and gel-glasses in the CaO-ZnO- Al_2O_3 - P_2O_5 system have been obtained bioglass-ceramics with main crystalline phases $Ca(PO_3)_2$ and $Ca_2P_2O_7$ (26, 27). The amorphous powders have been sintered as glass-ceramic materials by isostatic pressing and thermal treatment at 500 °C- 600 °C. This glass-ceramics shows higher bioactivity then hydroxyapatite in the initial stage after the implantation.

The main purpose of the present work is to investigate the structural evolution in gels of the SiO_2 - P_2O_5 - Al_2O_3 - CaO - F system during their thermal treatment for synthesis of apatite - anorthite glass-ceramics.

II. EXPERIMENTAL

For the synthesis of gels of the composition 1,5 SiO_2.0,5 P_2O_5.1 Al_2O_3.1CaO. 0,5CaF_2 marked as a glass C in (17), were used in appropriate amounts the following precursors: SiO_2-sol (laboratory obtained (26)), TEOS, $AI(NO_3)_3.9H_2O$,$Ca(NO_3)_2.4H_2O$, $(NH_4)_3PO_4.3H_2O$ and CaF_2. Gels which were obtained by different precursors of SiO_2 were investigated. The samples investigated are characterized as follows:

sample 1- glass C, TEOS, CaF_2 before gelling;
sample 2 - glass C, TEOS, CaF_2 after gelling;
sample 3 - glass C, SiO_2 - sol, before gelling;
sample 4 - glass C, SiO_2 - sol, CaF_2 after gelling;
sample 5 - anorthite, SiO_2 - sol;
sample 6 - anorthite, TEOS.

The manner of the component mixing, gel formation and thermal treatment are shown at scheme 1. The phase formation after thermal treatment in the 950-1250 °C temperature range was followed by means of the X - ray diffraction analysis (Diffractometer DRON- UM1, CuK_α radiation), IR - spectroscopy (Spectrometer SPECORD M80), transmission electron microscopy (TEM) and transmission micro-diffraction (TEMD) (Electron microscope EM-400, PHILIPS).

III. RESULTS AND DISCUSSION

The gels of the composition 1,5 SiO_2.0,5 P_2O_5.1 Al_2O_3.1CaO. 0,5 CaF_2 were prepared and thermally treated according to scheme 1 and the results of X - ray study on the phase formation in thermal treated gels (samples 1 and 2, obtained using TEOS) are presented in Figs. 1 and 3. From the X - ray diffraction data it is shown that at 950°C in two samples are formed anorthite and fluorapatite crystalline phase and still CaF_2 is presented. With the increase in the temperature up to 1050°C CaF_2 vanishes and in the same time fluorapatite and anorthite are the main crystalline phase, but mullite also presents. It is established that the fluorapatite X- ray peaks decrease at elevated temperatures.

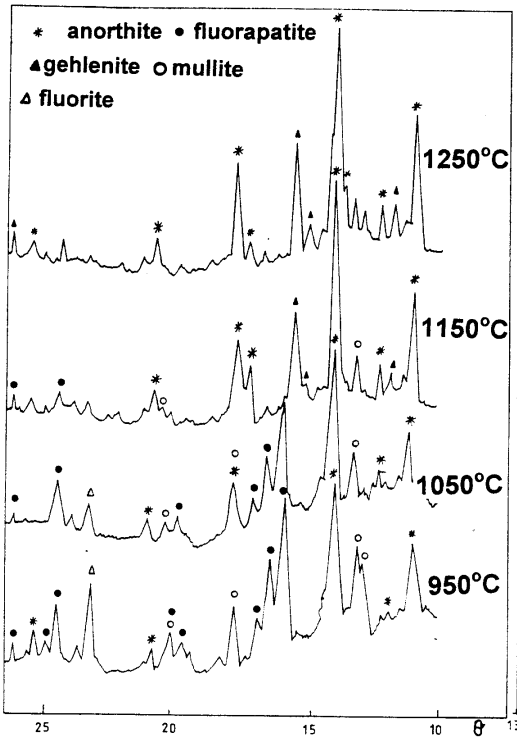

Fig.1. X - ray diffraction patterns of sample 1.

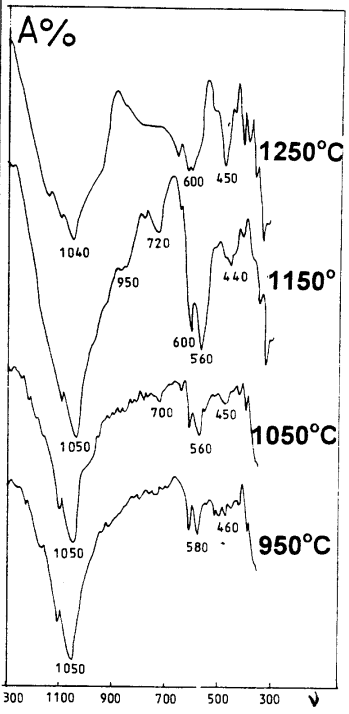

Fig. 2. IR-spectrum of sample 1.

The vanishing of fluorapatite is observed at 1150°C for the sample 1 where the CaF_2 is added before the gelling. For the sample 2, where the CaF_2 is added after the gelling, this process is established at 1250 °C. In the both cases with the disappearance of the fluorapatite the phase gehlenite appears. In this way the final products at the crystallization of the gels described at 1250 °C contain anorthite, gehlenite and small quantities of mullite. In this way the sol-gel glass-ceramics containing fluorapatite and anorthite can be synthesized after thermal treatment of the gels, prepared by TEOS, at 1050 °C (for sample 1) and at 1150 °C (for sample 2). In the case where it is starting from SiO_2-sol and CaF_2 is added before or after gelling (sample 3 and 4) the phase formation is going on by following way: at 950 °C mainly crystallizes fluorapatite, mullite and anorthite with a presence of pure CaF_2. At 1050 °C the diffraction patterns are almost the same but with the increase in the temperature (1250 °C) gehlenite, mullite, fluorapatite and anorthite are presented. For the both samples it is established that the amount of the fluorapatite decrease at elevated temperature. It is interesting that at lower temperatures 950 -1050 °C the quantity of the crystalline phase is higher in the gels, obtained by scheme, according which CaF_2 is added to the gel batch before the gelling temperature (sample 3).

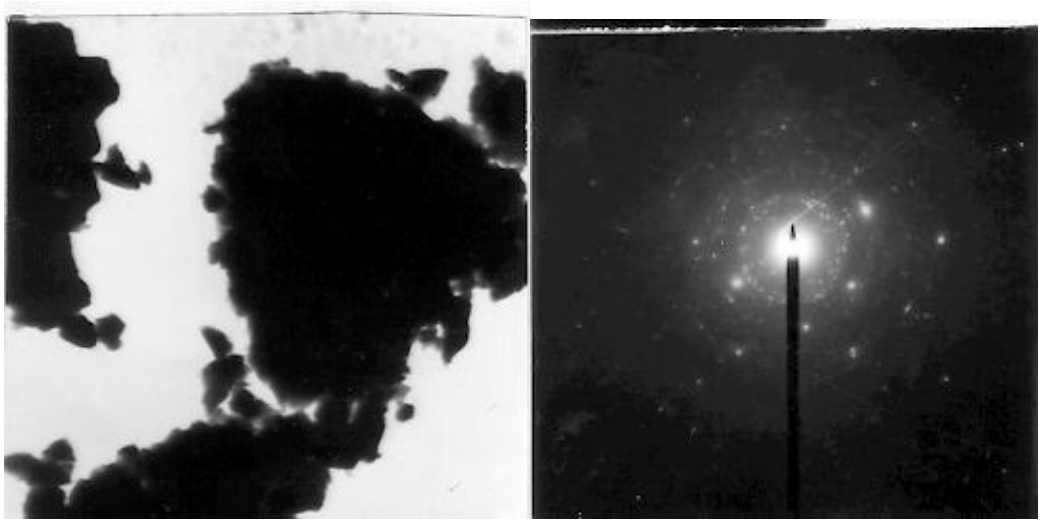

Fig. 5. Electron micrograph and electron diffraction of sample 6.

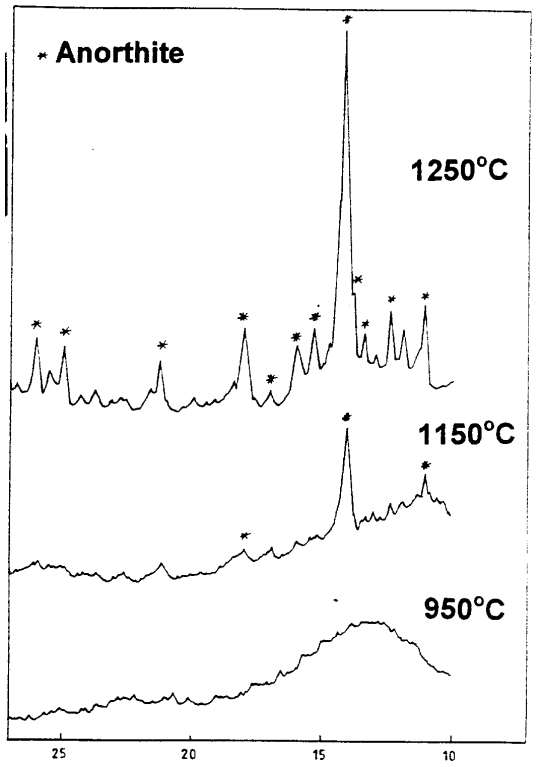

Fig. 6. X - ray diffraction pattern of sample 6.

The spectra at 1250 °C show multiphased nature of the compositions with dominant participation of silicate structures. This is in agreement with the X - ray diffraction data published above.

The pure sol-gel anorthite has been synthesized when TEOS was used as SiO_2 precursors. The X-ray diffraction patterns of thermal treated anorthite gels are given in Fig. 5. It can be seen that till 950 °C the gels are in amorphous state and at 1250 °C can be obtained crystalline material with only one phase - anorthite. The electron micrograph and electron diffraction of this sample

are presented in Fig. 6. it is established that the crystallization process is developed, the size of the crystals is under 0.1 μm and the aggregation tendency is observed.

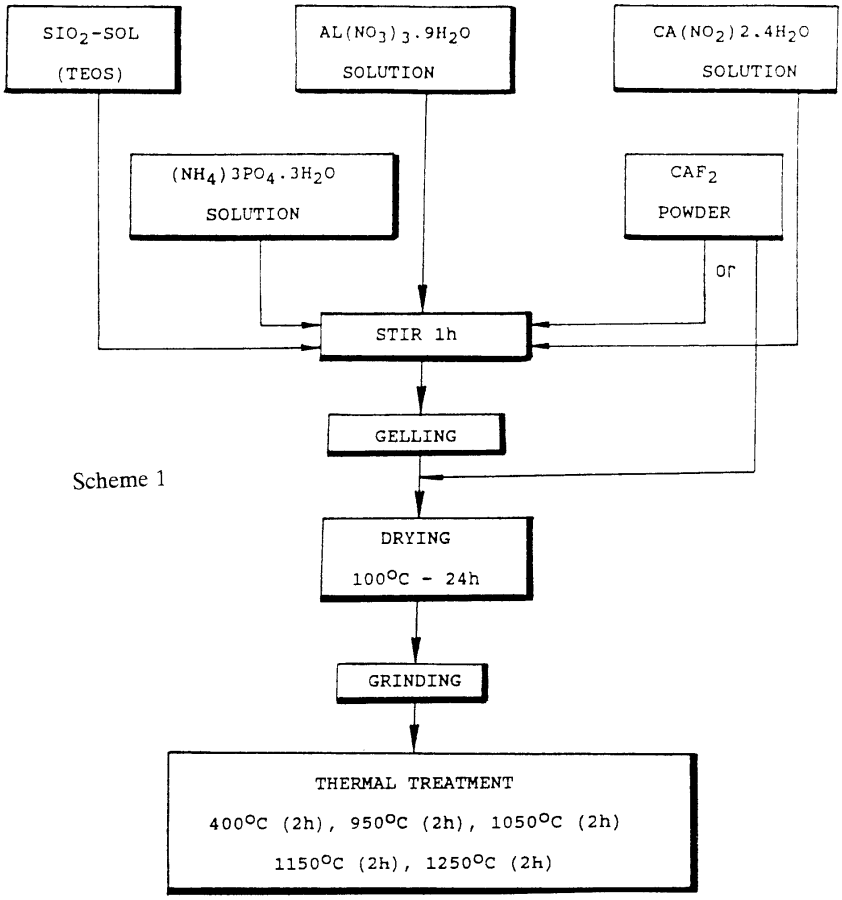

Scheme 1

VI. CONCLUSION

The structural evolution in the gels of the SiO_2 - P_2O_5 - Al_2O_3 - CaO - F system, thermal treated in 950 -1250 °C temperature range using X - ray diffraction analysis, IR- spectroscopy, TEM and TEMD has been investigated. It was found that fluorapatite- anorthite glass-ceramics can be synthesized after thermal treatment of gels of 1,5 SiO_2.0,5 P_2O_5.1 Al_2O_3.1 CaO. 0,5 CaF_2 composition, obtained by TEOS as SiO_2-precursors (1050 °C -1150 °C). Above these temperatures the fluorapatite disappears and a new crystalline phase is formed gehlenite.

Acknowledgment :

We would like to acknowledge the financial support from the EU under the COPERNICUS Project N° ERB3512PL940583 Contract N° CIPA - CT94-0145.

REFERENCES

1. W. McCracken, D. Clark, L. Hench, J. A. Ceram. Soc. Bull.,61(1982)1218.

2. T. Kokubo, Bioceramics,12(1991)155.
3. C.Othsuki, T. Kokubo, T. Yamamuro, J. Non-Cryst. Solids,143(1992)84.
4. Y. Abe, M. Hosoe, T. Kasuga, J. Amer. Seram. Soc.,65(1982)189.
5. P. Christel, A. Klein, Y. Abe, H. Hosono, K. de Groot, Bioceramics,8(1987)23.
6. W. Vogel, W. Holland, Angew. Chem.,99(1987)541.
7. T. Kokubo, Glastech. Ber. Glass Sci. Technol.,67C(1994)105.
8. T. Kokubo, Proc. XIII Int. Congr. Glass, Beijing,1995, v.1,3.
9. W.Vogel, W. Holand, K. Nauman, J. Non-Crist. Solids,80(1986)34.
10. W. Holand, M.Frank, M. Schweiger, V.Rheinberger, Proc. XIII Congress on Glass, Beijing,5(1995)133.
11. M. Dimitrova - Lukacs, Zs.Suba, Z. Miklos, J. Mink, P. Lukacs, Bioceramics, 8(1995)403.;
12. M. Dimitrova - Lukacs, P. Lukacs, I. Sajo, L. Lendvey, A. Juhasz, J. Sasvari, Silicates Industriels,1- 2(1996).15.
13. R. Tairov, D. Tuliaganov, A. Ismatov, Steklo I keramika,3(1991)21.
14. D. Tuliaganov, R. Hodakovskaya, Steklo i keramika,5(1991)27.
15. D. Wood, R. Hill, Biomaterials,12(1991)164.
16. D. Wood, R. Hill, Clinical Materials 7(1991)301.
17. R. Hill, M. Patel, D. Wood in: "Bioceramics", v.4, Ed. W. Bonfield, G. Hastings and K. Tanner (Butterworth Heinemann, London,1991, p.79.
18. R. Hill, C. Goat, D. Wood, J. Amer. Ceram. Soc.,75(1992)778.
19. M. Dimitrova-Lukacs, L. Gillemot, Third Euro-Ceramic, v.3,179,1993, Spain.
20. Anorthite glass - ceramics, Bulg. Patent N^{o} 42893/08.12.1986.
21. Cordierite glass - ceramics, Bulg. Patent N^{o} 43914I08.12.1986.
22. Glass - ceramics in the SiO_2- ZrO_2- ZnO system, Bulg Patent No 44265/ 16.02.1987.
23. B. Samuneva, Y. Dimitriev, Y. Ivanova, V. Dimitrov, P. Djambaski,10 Ibausil, Weimar (1988), Tagungsbericht, Sektion 4,288.
24. B. Samuneva, Y. Dimitriev, V. Dimitrov, Y. Ivanova, E. Kashchieva, P. Djambaski, Proc, XI Inter. Congress on Glass, Leningrad, v.2a(1989)26.
25. B. Samuneva, V. Dimitrov, E. Kashchieva, V. Chernev, P. Hinkov, Glasstech. Ber. Glass Sci .Technol.67C(1994)440.
26. Y. Ivanova, E. Spasova, Y. Dimitriev, B. Samuneva, E. Kashchieva, J. Sol-Gel Sci. Technol.,2(1994)819.
27. E. Spasova, Y.dimitriev, V.Dimitrov, Y.Ivanova, Proc. XI Conf.on Glass and Ceramics, Varna`93,Acad.Publ. Haus, Sofia (1994)130.
28. R.Zinuk et al, IR-spectroscopy in Inorganic Technology, Leningrad, Chimija, 1983.
29. K.Okada, Y.Otsuka, J. Am. Ceram. Soc.,69(1986)652.

SYNTHESIS OF MULLITE GLASS-CERAMICS BY SOL-TECHNOLOGY

Y. Dimitriev, B. Samuneva, D. Wood*,
E. Kashchieva, and E. Gattef

University of Chemical Technology and Metallurgy, Bulgaria
*Leeds Dental Institute, United Kingdom

Abstract

The mullite is important for many industrial applications because of its low thermal expansion coefficient, low dielectric constant, good thermal and chemical stability. A special interest are some polyphase glass-ceramics containing mullite for dental applications. To prevent the difficulties of conventional melting methods of glass production the sol-gel technology is used for the synthesis of this material. A simple technological scheme is developed with the introduction of appropriate precursors for the obtaining of amorphous material and glass-ceramic containing mullite as a predominate phase.

1. INTRODUCTION

The mullite is important for many industrial applications because of its useful technological properties as ceramics, glasses glass-ceramics and composites [1, 2]. Due to the availability of a great number of chemical precursors for aluminium and silicon mullite has become an example in the synthesis by various methods [3]. The progress in sol-gel processing is very useful in this connection especially to prevent the difficulties of conventional melting methods. It has also advantages for the preparation of ultrafine pure mullite powder. A large number of gels and xerogels were made for the first time in the system Al_2O_3-SiO_2 by Roy et al [4]. They also obtained the so called diphase xerogels. After that the problem about gel-formation of mullite is discussed in several review papers [5-8]. For the successful application of sol-gel technique it is very important to know the evolution process of the system from a starting solution to gel, gel-glass transition and gel-crystal transition. The mechanism of the transformation is possibly different depending on the precursors, thermal treatment regime and additives used. Great care has to be taken to achieve a true coopolimerisation of the material. Comparing different combinations of precursors essential conclusion are made by Fukuoka et al [9J for the microstructure, phase formations and properties of the obtained materials. Special attention on the role of aluminium nitrate in combination with tetraetoxysilane is paid in the latest experiments of Jaymes et al [10,11] presented a complete picture for the structural evolution of the mullite gel with increasing of the temperature using NMR-spectroscopy and DTA. The crystallisation of the amorphous mullite precursors is possible to follow two routes: direct formation of orthorhombic mullite at about 980^{o}C, or

two-stage process. The latter includes crystallisation of an alumina-rich spinel and transformation to mullite at above 1200°C. It is shown that the chemical homogeneity determines the crystallisation mechanism. That is why the synthesis conditions of heating by which it is possible to suppress the phase separation are very important [8].

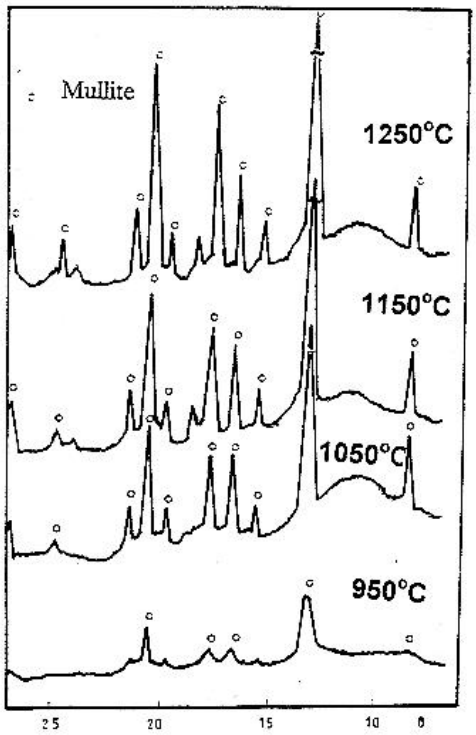

Fig.1. X - ray phase analysis of heat treated mullite from gel.

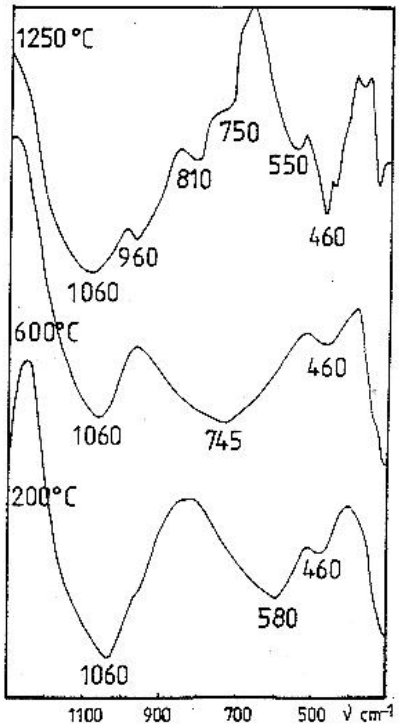

Fig. 3. IR spectra of heat treated pure mullite gel.

The synthesis of polyphase glass-ceramics containing mullite for dental applications [12] puts forward some special requirements for the precursors and the dimensions of the crystals. It would be very useful if in the batches for the melting of the manycomponent compositions takes part pure amorphous mullite or partially crystallised powder with nano-scale size mullite particles. The purpose of the present paper is to propose a simple scheme for the synthesis of mullite from aluminium nitride and TEOS with appropriate technological properties.

II. EXPERIMENTAL

The stoichiometrical composition, corresponding to the mullite and other combinations were synthesised according to the following scheme. $Si(OC_2H_5)_4$ (TEOS) and aluminium nonahydrate, $Al(NO_3)_3.9H_2O$ were used as starting materials. The salt was dissolved in absolute ethanol and TEOS was added and swirled so as to hydrolyse without gelation catalysts. The gels were dried in an oven at 100°C for 24 hours and then heated in steps: at 400, 600, 800, 950, 1050, 1250°C, for 2 hours. From the results of this

heat-treatment was selected an appropriate regime for obtaining of the fine dispersed mullite powders. For the characterisation of the materials at different steps of the investigation are used X-ray phase analysis (DRON-UM, Cu- Kα radiation), IR-spectroscopy (Spectrometer Specord M-80) and transmission electron microscopy-TEM (Electron microscope EM-490 Philips). X-ray diffraction intensity curves are obtained from amorphous samples in the range $2\theta = 4\text{-}120^{o}$. The scanning rate was $0.5^{o}min^{-1}$ with a pulse height analyser and scintillation detector. The x-ray intensity function was corrected for background, absorption and polarisation. Full details of the data analysis procedures adapted for IBM-PC are described in [13].

III. RESULTS AND DISCUSSION.

Fig. 1 shows the results of X-ray patterns for heat treated gels. Up to 600-700^{o}C the main phase is amorphous. At 900-950 ^{o}C begins the crystallisation of orthorhombic mullite and at about 1250 ^{o}C it is the only crystalline phase, but some amorphous phase exists. If the composition is enriched on SiO_2 a small amount of crystobalite is registered.

The microstructure of heat treated gels is presented in selected typical micrographs at Fig. 2. The observation of the powder particles at high magnification between x15000 and x90000 shows that the material is amorphous at 600°C without nanoscale heterogeneities. Above 800 ^{o}C appear small crystals with an average size about 0.1 μm. At 1250^{o}C the crystallisation is not yet completed, small amorphous regions remains.

IR-spectra of the gels, thermal-treated up to 1250 ^{o}C are presented at Fig. 3. A change in the spectral curves vas established with increasing the temperatures. The spectrum of the gels at 200 ^{o}C is characterised by bands at 1060, 580, and 460 cm^{-1} . The band at 580 cm^{-1} is shifted to the 750 cm^{-1} in the spectrum of the gel, treated at 600° C. The bands at 1060, 810, 750, 550 and 460 cm^{-1} are the main characteristic frequencies in the spectrum of the sample treated at 1250 ^{o}C. The band at 1098 cm^{-1} in the pure amorphous $Si0_2$ [13] is assigned to the anti symmetrical stretching vibrations of SiO_4 groups. The band at 804 cm^{-1} to the symmetrical stretching vibrations and the band at 468 cm^{-1} to the bending vibrations of the same groups. Al^{3+} ions can be present as AlO_4 and AlO_6 groups in the structure of alumosilicate groups. It is known that AlO_4 vibrate in 800-700cm^{-1} range [14,15], while the characteristic absorption bands of AlO_6 groups are in the 600-500 cm^{-1} range [15, 16]. On this basis the it is possible to make some conclusions, concerning the structure of the gels. At low temperature the gels contain polymerised SiO_4 groups (bands at 1060 and 460 cm^{-1}) and AlO_6-units (band at 580 cm^{-1}). The shifting of this maximum from 460 to 745 cm^{-1} with increasing of the temperature until 600° C means that AlO_4 groups are formed in big amount. The material obtained at around this temperature may be regarded as a gel-glass. The IR-spectrum of the crystalline material at 1250°C may be discussed as adsorption bands corresponding to vibration of the units in the crystalline mullite. It contains SiO_4 units (bands at 1060, 810, and 460 cm^{-1}) and simultaneous participation of AlO_4 (750cm^{-1}) and AlO_6 550 cm^{-1} groups. These results are in agreement with another investigations previously published.[17-19]

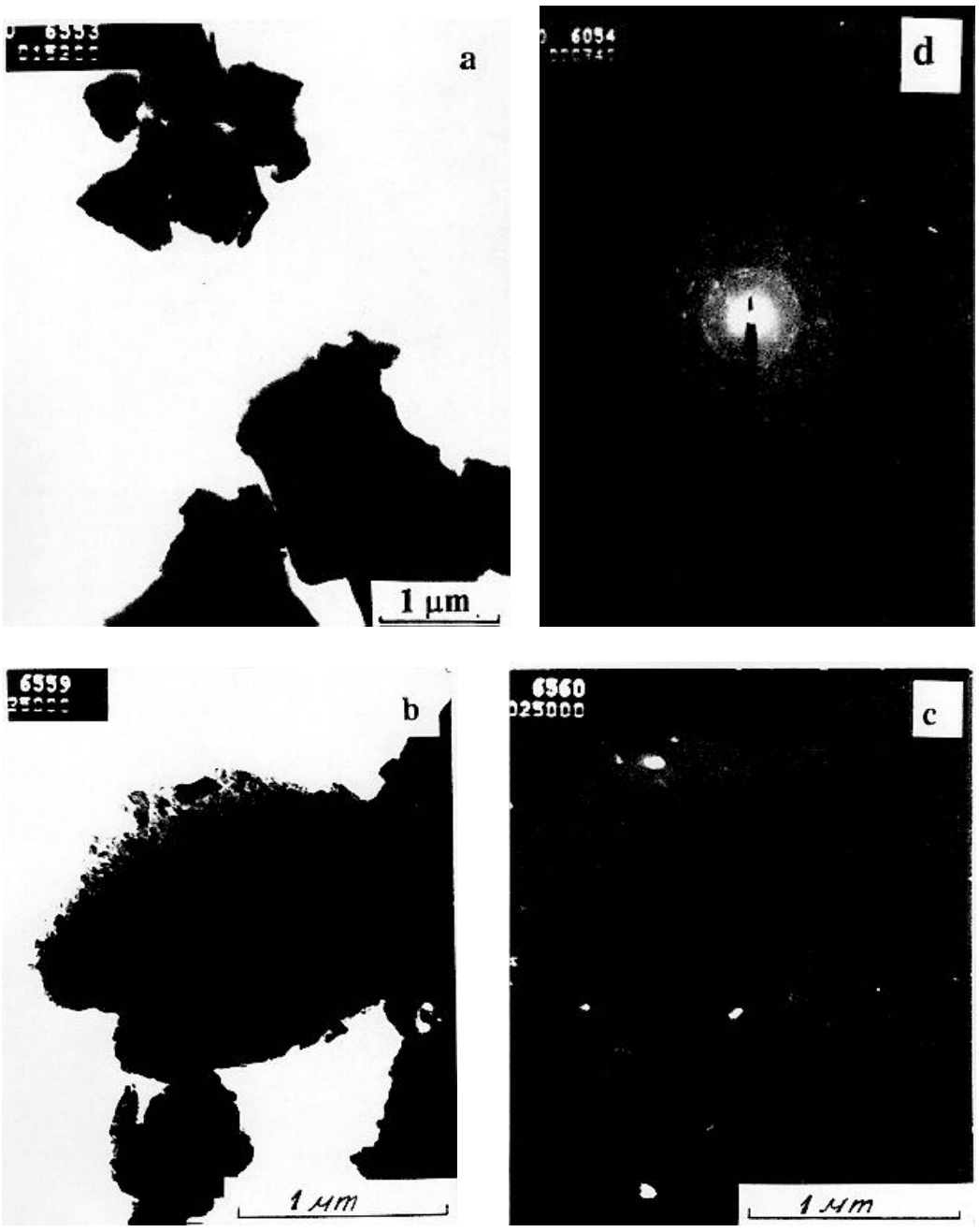

Fig. 2. TEM micrographs of stoichiometric mullite composition: a) TEM of heat treated sample of 600°C - 2 h; b) 1250°C high field; c) 1250°C dark field d) electron diffraction of the same sample heat treated at 1250°C.

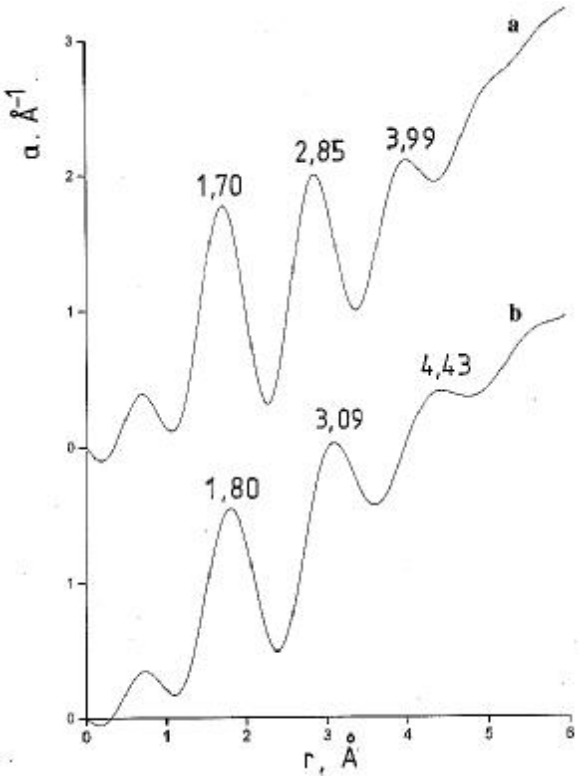

Fig. 4. Total pair correlation function of mullite gel: a) heat treated at 600°C;b) heat treated at 800°C.

To obtain some additional information about short-range order in amorphous gels and gel-glasses x-ray diffraction structural analysis was performed. The results obtained are presented in Fig. 4. The interatomic distance were taken from the total pare correlation functions T(r) since they are more accurate than those from the usual radial distribution function. [21] A well resolved maximum was found in T(r) for all investigated samples which shifts with increasing the heat-treatment temperature to higher values. This maximum is complex and corresponds to the distances in the Si-O and Al-O atomic pairs. [20, 22, 23]. In amorphous Al_2O_3 r_1 (Al-O) is at 1.8Å[22] and may be connected with predominantly octaedrical co-ordination of the aluminium against the oxygen. The slight decrease of r_1 in T(r) of the amorphous mullite gel treated at 600 °C could be interpreted as increasing of the amount of AlO_4 units in the structure. This is in agreement with the infrared spectra of the samples.

4. CONCLUSIONS

By the developed step thermal-treatment regime it was achieved the formation of amorphous mullite gels in which is possible to control the amount of AlO_4 and AlO_6 groups.

After thermal treatment above 1250°C orthorhombic mullite is obtained containing small-scale crystals embedded in amorphous matrix.

ACKNOWLEDGMENTS

This work was financially supported by the COPERNICUS Project No=ERB3512PL940583 Contract No=CIPA-CT94-0145.

REFERENCES

1. Kiyochi Okada, Nozami Otsuka, Ceramic Bull. 70. (1993) 1633.
2. Shigeyuki Somiya, Yoshiro Hirata, Ceramic. Bull. 70 (1991)1624.
3. M. D. Sacks, H. W. Lee, J. A. Pack in: Ceramic Transactions vol. 6, Mullite and Mullite Matrix Composites. Cds. S. Soniya, R. F. Davis and J. A. Pack (American Ceramic Society, Westerville, 0H1990) pp.167-207.
4. D. Hoffman, R. Roy, S. Komarmeni, J. Amer. Ceram. Soc. 67 (1984), 468.
5. S. Sakka, K. Kamiya, J. Non- cryst. Solids 42 (1980) 40.
6. T. Davies, H. Enblem, K. Jones, M. A. Mond, Abd. Rahman, G. K. Sargeant, R. Wakefield. Br. Ceram. Trans. J. 89 (1990) 152.
7. T. Heinrich, F. Raether, J. Non-Cryst. Sol., 147/148 (1992) 152.
8. J. C. Huling, G. Z. Messing, J. Non-Cryst. Solids, 147/148 (1992) 213.
9. M. Fukuoka, Y. Onoda, S. Inoue, K. Wada, A. Nukui, A. Makishita, J. Sol-Gel Sci. and Technol. 1 (1993) 47.
10. I. Jaymes, A. Douy, D. Massiot, J. P. Bushel (in press).
11. I. Jaymes, A. Douy, M. Gervais, Presented at the Sol-Gel Conference Foro' 95.
12. R. G. Hill, M. Patel, D. J. Wood in "Bioceramics" v. 4, Ed. by W. Bonfeld, G. W. Hastings and K. F. Tanner (Butterworth-Heinmann, London,1991) p. 79.
13. N. Zotov, V. Dimitrov, Y. Yanev, Phys. Chem. Miner.16 (1989) 774.
14. T. Plusnina, Infrakrasnie Spektri Silicatov, Moskva, Nauka, (1977).
15. D. Day and G. Rudane, J. Amer. Ceram. Soc. 45, 489 (1962).
16. P. Tarte in Physics of Non-crystalline Solids, Amsterdam, p. 549 (1965).
17. V. Stubicon and R. Roy, Z. Kristallogr,115(1961) 200.
18. M. Saler and J. Alarcon, Bol. Soc. Esp. Ceram., 273 (1994).
19. C. Harrison and Z. Luo, J. Sol-Gel Sci.and Technol, 2, Vidrio 33 (1994) 73.
20. M. Laczka, W. Beier and L. Stoch, Glastech. Ber. 62(1989)320
21. A. C. Wright A. Leadbetter, Phys. Chem. Glasses,17 (1976)114.
22. H. M. Yakovleva, A. D. Fofonov, Inorganic materials (Rus.) 21 (1985) 48.
23. Ph. Colomban, D. J. Johnes, D. Grandjean, A. M. Frank, J. Non-Cryst. Solids, 147/148(1992) 135.
24. M. Lacka, W. Beier, R. Stoch., Glastech. Ber. 62 (1989)320.

TEMPERATURE MODULATED PHOTOACOUSTIC STUDY OF RELAXATION BEHAVIOR*

T. Vassilev and **I. Avramov**
Bulgarian Academy of Sciences, Bulgaria

Abstract

The transition from a configurational frozen glassy state to a metastable liquid state is accompanied by an abrupt change in a number of macroscopic properties like compressibility, thermal expansion coefficient and specific heat. It depends strongly on the measuring time Recently a new technique was developed for measuring the frequency dependence of the specific heat C, subjecting a sample to a small periodically varying temperature oscillations. Up to now, these measurements have not been directly compared to the differential scanning calorimetry (DCS) experiments. In the present paper we are trying to shed more light on the relaxation behavior of glassforming melts by comparing photoacoustic (PA) and DSC data. The relaxation behavior of poly(methyl methacrylate) (PMMA) is derived from PA and differential scanning calorimetry (DCS) measurements. The main conclusions can be summarized as follows: Data, obtained from earlier DSC measurements are well in line with the present PA data. The present results give an experimental evidence that the activation energy for relaxation depends on the structure. It was shown that along with the main or a-transition secondary o b-transition can be detected and studied by the PA temperature measurements.

---

* Full manuscript not available at the time of printing

THE BEHAVIOR OF IR OPTICAL ABSORPTION OF MULTICOMPONENT CERIUM-DOPED g-IRRADIATED GLASSES FOR FIBER LIGHTGUIDES AT 300-840K

Anatolii V. Anan'ev and **Sergei A. Stepanov,**
S.I. Vavilov State Optical Institute, Russia

Abstract

Initial and γ-radiation induced optical absorption in the UV, visible, and near IR spectral ranges and its temperature dependence (300-840 K) at 1.17 eV (1.06 μm) are studied for multicomponent high-purity cerium-doped sodium borosilicate glasses, used in manufacturing of thermal and radiation-resistant high-aperture fiber lightguides.

Low-intensity wide absorption band with a maximum at 2.5 eV is identified in spectra of non-irradiated cerium contained glasses. The band intensity depends on CeO_2 concentration and of iron microimpurities non-linearly. Variations in the absorption coefficient at 1.17 eV with increasing cerium concentration and temperature are established to be due to the 2.5 eV band intensity. The interpretation of the nature of the band is offered.

Temperature relaxations of radiation induced colored centers in the glasses in wide spectral range and its kinetics at 1.17 eV are studied. It is discovered, specifically, that complete relaxation occurs only close to the annealing temperatures.

1. INTRODUCTION

Along with increasing the transparency of glasses for fiber optics, an urgent problem to study is subsequent behavior of fiber-optic elements during their operation under the influence of different external factors, such as ionizing radiation and high temperature.

The objective of this work is to establish absorption dependences in the near IR range on concentrations of cerium and microimpurities, on dose of γ-irradiation and temperature for high-purity multicomponent cerium glasses used in high-aperture fiber lightguides.

2. OBJECTS OF THE STUDY

We studied two compositions of sodium borosilicate glasses of varying cerium dioxide C_{CeO2} concentrations and with different amounts of impurities (Table 1). The amount of iron introduced with CeO_2 did not exceed 3% of the total Fe_2O_3 content in glass. The "core" and "coating" glasses form a matching pair in terms of temperature dependences of their viscosity and coefficient of thermal expansion and in terms of the difference in their refractive indexes; they ensure the aperture of optical fiber, which is equal to 0.5.

Table 1.

	Series I	Series II	Series III
Purpose	For Core		For Coating

Composition	SiO_2, Na_2O, B_2O_3 La_2O_3, BaO, ZrO_2		SiO_2, Na_2O, B_2O_3 Al_2O_3
Concentration of activator and iron admixtures (wt % above 100 %):			
CeO_2	0.2-1.1	0-1.5	0-1.2
Fe_2O_3	$0.5\text{-}10^{-4}$	1.10^{-4}	2.10^{-4}

3. EXPERIMENTAL

Absorption spectra of glasses were measured using optical-quality samples 0.03-10 cm thick. Absorption in the near IR range was determined at 1.17 eV (1.06 μm) by the calorimetric polarization-modulation method [1,2] in the range from 300 K to the lowermost glass annealing temperature (840 K). The glasses were irradiated at γ-unit with a power of 277 R/s at 300 K. All measurements with γ-irradiated glasses were made 24 hours later after irradiation.

4. ABSORPTION OF NON-IRRADIATED GLASSES

4.1. Glass Absorption In the UV and Visible Ranges At 300 K

The UV spectra are formed by short-wave edge of fundamental absorption (at hν≥6 eV) and by the intensive bands of Ce^{4+} (5 eV) and Ce^{3+} (4 eV) ions absorption. The typical absorption spectrum in the 1.6-3.3 eV range (Fig.1) consists of well-defined exponential edge of the Ce^{4+} ions wide absorption band (2.9-3.3 eV) and an absorption band in the 1.6-2.8 eV range. If we extrapolate the exponential edge of the Ce^{4+} band to lower-energy range and calculate the difference between experimental spectrum and extrapolated one, this absorption band can be obtain in an explicit form.

The band has a maximum at 2.5 eV and a width of 0.8-1.0 eV. The natural absorption coefficient dependence at 2.0 eV on the cerium concentration $\alpha_{2.0}= f(C_{CeO2})$ where the error is the smallest is essentially nonlinear (Fig.2). Difference between $\alpha_{2.0}$ for glass Series I and II shows that the band intensity also depends on the Fe_2O_3 impurity concentration.

Let us determine the stability of the Ce^{4+}/Ce^{3+} ratio with the CeO_2 concentration. Because of high UV absorption for glasses with $C_{CeO2} > 0.1$ wt %, we can estimate C^{4+}/Ce^{3+} ratio from the $\alpha_{hv}=f(C_{CeO2})$ dependence at the low-energy wing of UV cerium absorption band. Such dependences at hν=3.0-3.5 eV were qualitatively similar and linear, thereby indicating a constant Ce^{4+}/Ce^{3+} ratio in each glass series. As an example, the $\alpha_{3.2}=f(C_{CeO2})$ dependences are presented in Fig.2.

4.2. Glass Absorption In The Near IR Range At 300 K

The dependences of the absorption coefficient at h_ν=1.17 eV (1.06 μm) on the CeO_2 concentration are non-monotonic, with a minimum at C_{CeO2}=0.2-0.4 wt % (Fig.3). It is natural to assume that this behavior is due to several factors. One of them is the action of cerium: as a strong oxidant, this ion converts some bivalent iron ions in glass into Fe^{3+}, and the intensity of the Fe^{2+} absorption band at 1.1 eV decreases. The magnitude of $\alpha_{1.17}$ in glasses with small CeO_2 contents (up to 0.4 wt %) is in a fairly good agreement with the amount of iron impurities. The wide 2.5 eV band extends into the near IR range of the spectrum by its low-energy wing, thereby raising absorption at 1.17 eV. This process begins to prevail for C_{CeO2}>0.4 wt %. For glasses with CeO_2 content over 0.8 wt %, we observe a good correlation between the absorption at 1.17 eV (Fig 3) and the intensity of the band at 2.5 eV (Fig.2).

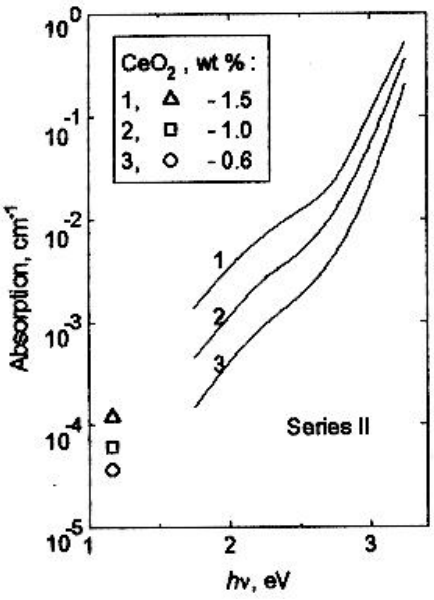

Fig 1

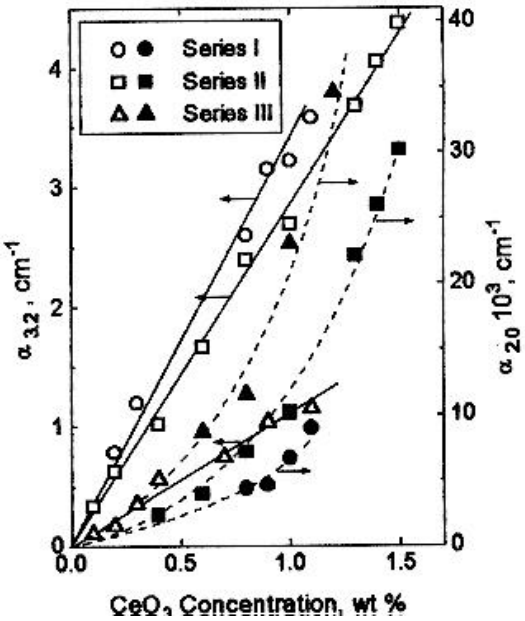

Fig 2

4.3. Temperature Dependences Of Glass Absorption In The Near IR Range

The increase of the absorption at 1.17 eV with temperature and CeO_2 concentration is characteristic of all cerium glasses. Some temperature dependences for Series II glasses are shown in Fig.4.

We carried out special experiments with Fe-dopped free cerium glasses and showed that the run of temperature curves was qualitatively the same in all the ceriumless and iron-containing glasses, and the absorption depended only slightly on the temperature (Fig.4, ceriumless glass). These fact are due to low temperature shift coefficient of the bivalent iron absorption band.

We can explain the nature of temperature dependences $\alpha_{1.17}(T)$ by the 2.5 eV band temperature shifting to low-energy part of the spectrum. Such behavior is characteristically for the most intrinsic and extrinsic absorption bands in glass.

4.4. Nature Of The Absorption Band At 2.5 eV

So far as the Ce^{4+}/Ce^{3+} ratio is invariable in all cerium-activated glasses the nonlinear CeO_2 concentration dependence of 2.5 eV band intensity is not caused by absorption of Ce^{3+} or Ce^{4+} ions.

The analysis of spectroscopic parameters of the 2.5 eV band and of the transition-metal and other lanthanoid absorption bands showed that non of these ions could form the experimental absorption spectrum in the range of 2.5 eV. Hence, we should search for a different cause of the 2.5 eV band.

Nonlinear concentration dependences of absorption band intensities (i.e., the deviations from the Beer Iaw) can be due not only changes in the valence or coordination states of the absorbing ions, but also to exchange interactions of ions in aggregated groups, such as associates or clusters. Spectroscopically, the interactions of ions in clusters is displayed by a sharp increase in the absorbing ability of color ions, by nonlinear dependence of the band intensity on activator content, by new absorption bands, etc. In this case, the intensity of

absorption depends on the concentration of cluster-forming ions in glass and, if different kinds of ions are present in the cluster, on their relative concentrations [3].

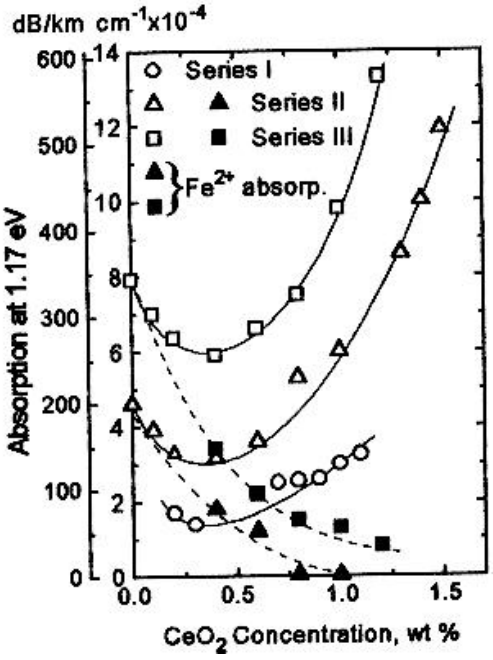

Fig.3

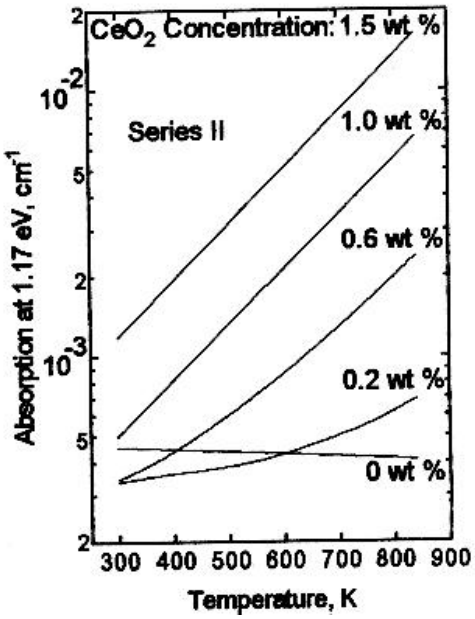

Fig.4

The concentration of ions required for the formation of clusters and for exchange interaction between ions can vary over a very wide range. This range depends on many factors, including the nature of interacting ions, the type of glass-forming element and modifier, the alkali content, and the redox conditions of synthesis. For example, according to [4], "cluster-type associates" of the Fe^{3+} emerge when the Fe_2O_3 concentration is as low as ~10^{-2} wt %.

Modifiers can thus form their own structures (clusters). In our case, when the intensity of the 2.5 eV band increases with cerium and Fe_2O_3 impurity concentrations, and the first dependence is essentially nonlinear, we can assume that certain associated cluster-type groups are formed by interacting ions of cerium and iron impurity.

Results of [5-7] also indicate that an absorption band in the visible spectral range is present in cerium-activated glasses. For example, an intensive band with a maximum at 2.15 eV and width of about 0.5 eV was observed in [7] for magnesium borate glasses containing CeF_3 and Na_2O; it was attributed to intervalence transition in the Ce^{3+}-Ce^{4+} pair.

5. ABSORPTION OF g-IRRADIATED GLASSES

5.1. Absorption Of g-Irradiated Glasses In The Near IR Range At 300 K

Radiation-induced absorption (RIA) spectra of glasses in the UV and visible ranges have complex structure. RIA at 1.17 eV consists of several part. Radiation excharge of iron impurity ions Fe^{3+} causes the RIA at 1.1 eV of $(Fe^{3+})^-$ centers. Typical for alkali-borosilicate glasses intrinsic hole radiation color centers (RCC) are due to RIA centered at 0.89 eV [5] and at 2.0-2.2 eV.

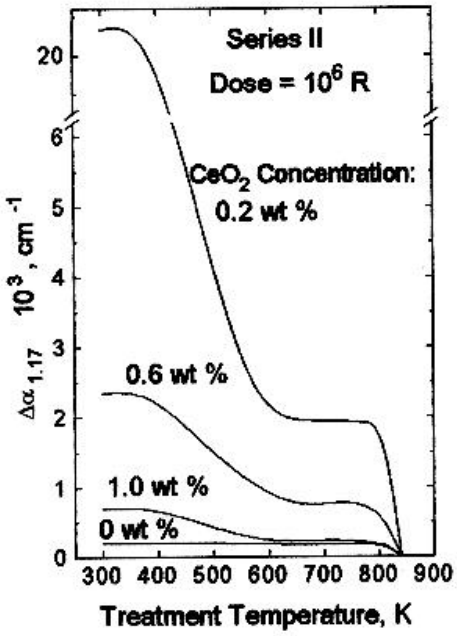

Fig.5: Dependence of the RIA at 1.17 eV on the treatment temperature.

Cerium ions play a role of protectors in relation to captured electrons and holes induced by γ-radiation. Thereby, RIA is decreases as CeO_2 concentration increases.

We also showed that the run of concentration dependences of RIA at 1.17 eV and at 2.0 eV is diversely. This is conditioned by the fact that the Ce^{4+} ions suppress the $(Fe^{3+})^-$ centers more efficiently than the Ce^{3+} ions do hole RCC. These facts are due to the distinction between the Ce^{3+} and Ce^{4+} ions nearest environment.

5.2. Thermostimulated Relaxation Of Radiation Color Centers

The temperature action upon by γ-irradiated glasses offers the RIA change at the total spectrum range. Thermostimulated relaxation (TSR) process in cerium containing glasses has two well-defined stages at 370-470 K and 790-840 K (Fig.5).

The first TSR process in all glasses is caused by intrinsic hole RCC discoloration. Thermostable in the 500-790 K temperature range RIA at 1.17 eV is due to $(Fe^{3+})^-$ centers absorption of which as for Fe^{2+} ions is nearly constant of the temperature. The magnitude of this thermostable RIA depends on glass iron impurity concentration. It increases from glass Series I to Series III.

RCC are nearly complete relaxed at temperatures about 550 K RIA in ceriumless glasses. The second TSR process in cerium-activated glasses is only close to the annealing temperatures (at about 840 K). Such behavior of the TSR at 790-840 K is due to $(Ce^{3+})^+$-$(Fe^{3+})^-$ centers relaxation. The analysis of UV RIA spectra after the thermal treatment up to 670 K in glasses with 0.1 wt % CeO_2 confirmed this fact.

The temperature dependences of absorption at 1.17 eV during the heating process of γ-irradiated Series II glasses (dose 10^6 R, heating speed 0.13 K/s) are shown in Fig.6. The temperature curves for initial glasses are added for comparison.

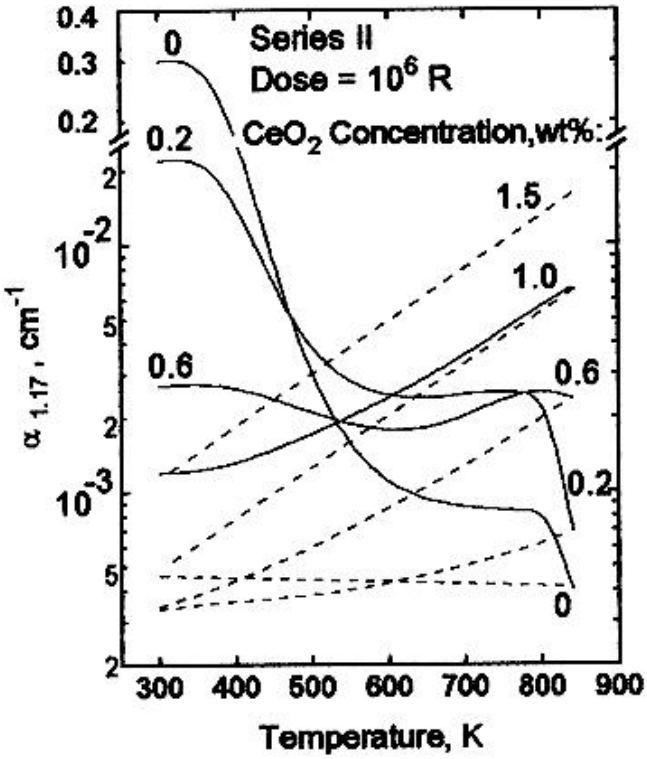

Fig.6. Solid lines-glasses after g-irradiation. Dash Lines-non-irradiated glasses.

Similar experiments were carried out for various doses of radiation in the range of 10^4 to 10^7 R. Received data allow to mark out the cerium concentration range at which the temperature and radiation induced absorption in glasses is minimum.

6. CONCLUSION

1. An absorption band with a maximum at 2.5 eV and with a width of 0.8-1.0 eV is identified in the visible spectrum range in the cerium-activated glasses. The band is assumed to be a result of exchange interaction between cerium and iron microimpurities in associated cluster-type groups containing both types of ions.

2. The absorption of the glasses at 1.17 eV ($\alpha_{1.17}$) at 300 K is determined by two factors: the absorption of the Fe^{2+} and the long-wave wing of the band with a maximum at 2.5 eV. In the former case, $\alpha_{1.17}$ decreases with increasing cerium content, because of Fe^{2+} oxidation by cerium (at $C_{CeO_2} \leq 0.4$ wt %); in the latter case, $\alpha_{1.17}$ increases because of rapidly growing intensity of the 2.5 eV band (at $C_{CeO2} > 0.4$ wt %). The latter intensity also depends on amount of iron impurities.

3. The absorption at 1.17 eV in the cerium-dopped glasses increases with the temperature raising. The reason is that the long-wave edge of the 2.5 eV band is thermical shifted to the low-energy range. The absorption of free cerium glasses depends on temperature a little.

4. Radiation-induced absorption at 1.17 eV at 300 K is due to electron impurity centers $(Fe^{3+})^-$ and influence of intrinsic hole RCC absorption.

5. Thermostimulated relaxation process in cerium containing glasses have two stages at 370-470 K and 790-840 K. Intrinsic hole RCC relax at 370-470 K. Thermostable at 500-790

K RIA at 1.17 eV is due to $(Fe^{3+})^-$ centers absorption. Complete relaxation occurs only close to the annealing temperatures.

6. Data have received allow to make a choice of CeO_2 concentration in glasses for temperatures and/or doses of γ-radiation which result in the lightguides are taken to be used. In any case it should be to decrease to iron impurities containing in glass because of its influence not only on Fe^{2+} ions and $(Fe^{3+})^-$ radiation centers concentrations but on the 2.5 eV band intensity as well.

REFERENCES

[1] Anan'ev, A.V., Peculiarities of Measuring Small Absorption Losses in Optic Materials by the Polarization-Modulation Method, Opt.-Mekh. Prom-st'., 1991, no.12, pp.9-13.

[2] Anan'ev, A.V., and Moskin, N.A., A Polarization Method of Measuring Small Light Absorption Using a Continuous Wave Laser, Opt.-Mekh. Prom-st'., 1989, no.2, pp.2-4.

[3] Zarubina, T.V., Mokeeva, G.A., and Stepanov, S.A., The Influence of Pairwise Interactions between Transition Mn^{2+} and Fe^{3+} Ions on Spectral-Luminescent Properties of Glasses, 4 Vsesouyznyi Simposium "Opticheskie i Spektral'nye Svoistva Stekol" (4th All-Union Symposium on optical and Spectral Properties of Glass), Riga, 1977, pp.60, 61.

[4] Nemilov, S.V. and Zhilin, A.A., Temperature Dependence of the Absorption Edge in Inorganic Glasses with Iron Impurities, Zh. Prikl. Spektr., 1974, vol.120, no.2, pp.268- 274.

[5] Glebov, L.B., Dokuchaev, V.G., and Petrovskii, G.T., The Influence Of Cerium on the Change of Absorption in Sodium-Calcium Silicate High-Purity Glasses in the 0.8-1.6 eV Range under the Action of γ-Radiation, Fiz. Khim. Stekla, 1987, vol.13, no.1, pp.123-126.

[6] Allen, G.G. and Hush, N.S., Intervalence-Transfer Absorption, Pt. I: Qualitative Evidence for Intervalence Absorption in Inorganic Systems in Solution and in the Solid State, Progress Inorg. Chem. 1967, vol. 12, no.3, pp.308-313.

[7] Kraevskii, S.L., Burkov, V.I., and Solinov, V.F., The Use of Magnetooptical Characteristics of Glasses for the Isolation of Intervalence Transition Bands in Absorption Spectra, Fiz. Khim. Stekla, 1986, vol.12, no.3, pp.308-313.

THE EFFECT OF Ta^+ ION-IMPLANTATION ON THE ELECTRIC CONDUCTIVITY OF Li_20-La_20_3-Ta_20_5-$Si0_2$ ELECTRODE GLASSES

Wang Chengyu and **Yang Shibiao**
Dalian Institute of Light Industy, China

Abstract

The samples of Li_20-La_20_3-Ta_20_5-$Si0_2$ glass were implanted tantalum ions at fluences of 5 x 10^{16}, 1 x 10^{17} and 2 x 10^{17} ions/cm^2 by using 50 KeV MEVVA IV implanted machine. The electric conductivity of implanted and unimplanted samples were measured by LCR conduction apparatus. After implantation the activation energy of ionic conduction tends to decrease and the value of activation energy correlated with implanted fluence. The electric conductivity of implanted samples is higher than that of unimplanted samples. It is also showed that the characteristic temperature of conduction $T_{k\text{-}100}$ of implanted samples decreased slightly with increasing fluences. The mechanism of conduction for implanted glass was also discussed.

1. INTRODUCTION

Ion implantation affects the properties of glass, such as hardness, refractive index, optical absorption, nonlinear optics, superconduction, magnetism, weathering, crystallization and nucleation etc. [1-6]. The surface of glass electrode should satisfy the requirement of a low or moderate electrical resistance, the participation in ion-exchange and a higher ion migration; On the other hand, lower ion migration is required to contact the demand of chemical durability in acid or alkali solution. These contradictory requirements bring about difficulties in the design of suitable glass compositions. When the electrical conductivity is improved, the chemical durability is decreased at the same time for the higher content of alkali oxides. To solve this problem we applied ion implantation method. By implanting different kinds of ions respectively, we improved the chemical durability of glass, and achieve the expected electric properties [7]. It is same the other way around. In this woke, we have investigated the dependence of electric properties on dose rate for implanted Ta^+ glasses.

2. EXPERIMENTAL

The glass compositions used in his research are outlined in Table 1. The glass batches were prepared from analytical reagent grade quartz, lithium carbonate, lanthanum sesquioxide and tantalum pentoxide. Premixed batches were melted by using a platinum crucible in an electric furnace at temperature ranging between 1300 ^oC and 1350 ^oC depending on the glass composition. The molten glass was cast into plates then annealed at 525^oC and allowed to cool normally to room temperature. The samples were ground and polished, then cut into 12 x 12 x 2 mm pieces from the glass plates. the tantalum ions were implanted in the samples at dose of 5 x

10^{16}, 1 x 10^{17}, 2 x 10^{17} ions/cm^2, using 60 KeV MEVVA-10 implantation machine at room temperature.

Table 1 Chemical composition of glass samples (mol%)

Glass No.	Li_2O	La_2O_3	Ta_2O_5	SiO_2
1	27	7	-	66
2	27	7	2	64
3	28	5.5	-	66.5
4	28	5.5	2	64.5
5	29	7	2	62

The electric resistance was measured by an Intelligence LCR type ZL5 resistor, with a range of 10^2 -10^8 Ω. Before the measurement of resistance, the paralleled surface of samples were coated with silver, which area has a breadth of 50 mm. Conductivity (σ) values of samples were calculated as follows:

σ = thickness/(resistance x area)

Over a temperature range from 200 to 380^{o}C, the activation energy of conduction is determined by the Arrhenius equation:

$\sigma = A \exp(-E/RT)$

Where A is the pre-exponential factor, which here is 1.01, E is the activation energy for ionic conduction, R is the gas constant and T is the absolute temperature.

3. RESULTS AND DISCUSSION

The dependence of electrical conductivity on temperature and dose rate for implanted and unimplanted samples are shown in Fig.1 and 2 respectively. It can be seen clearly that the electrical conductivity of implanted glasses increased very little but became more pronounced at temperature below 533K.

The relation between activation energy for ionic conduction and implanted dose rate are given in Fig.3. Samples No.2, No.3 and No.5 contain Li_20 27, 28, 29 (mol%) respectively. The activation energy for ionic conduction is decreased with increasing Li_20 content in as much as Li^+ is the charge-transporting cation in glass. Fig.3 also shows that activation energy is reduced with the raise of dose rate. This result is similar to that shown in Fig.1.

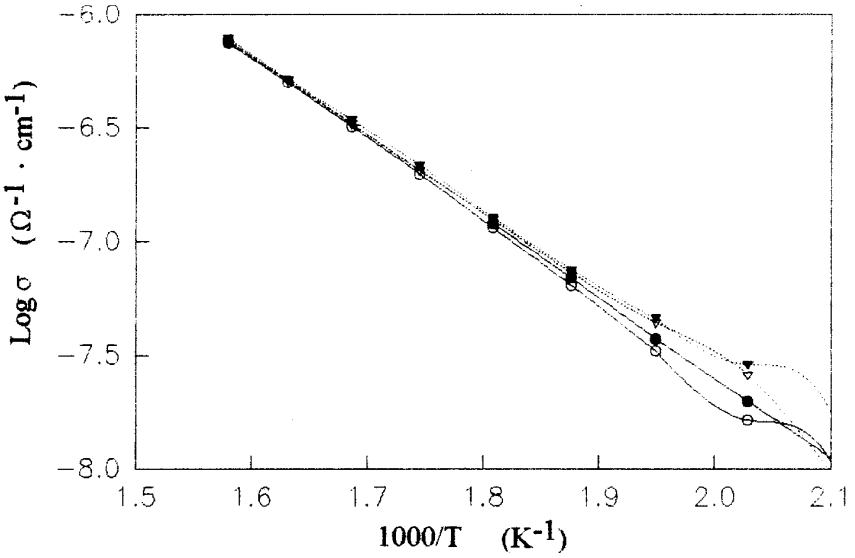

Fig.1 Dependence of electric conductivity on temperature for implanted and unimplanted glasses. ¡ unimplanted, I implanted 5 x 10^{16} ions/cm^2, Ñ implanted 1 x 10^{17} ions/cm^2, – implanted 2 x 10^{17} ions/cm^2

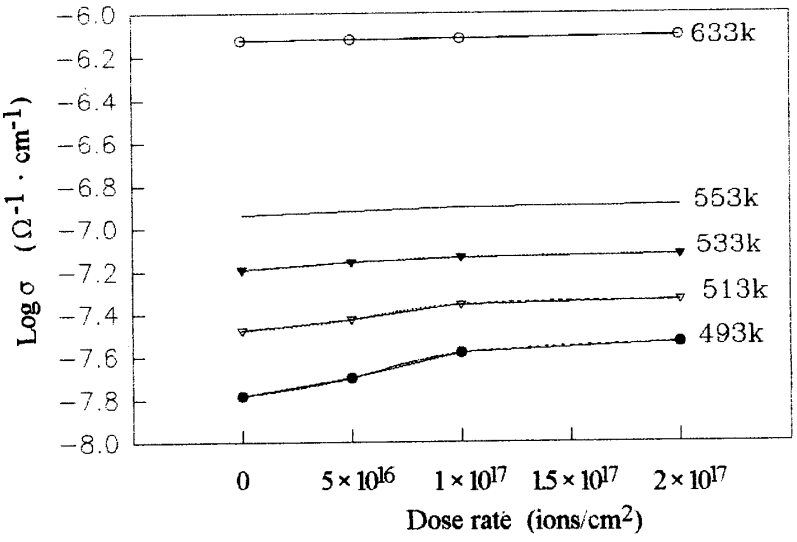

Fig.2 Change of electric conductivity with dose rate at various temperatures

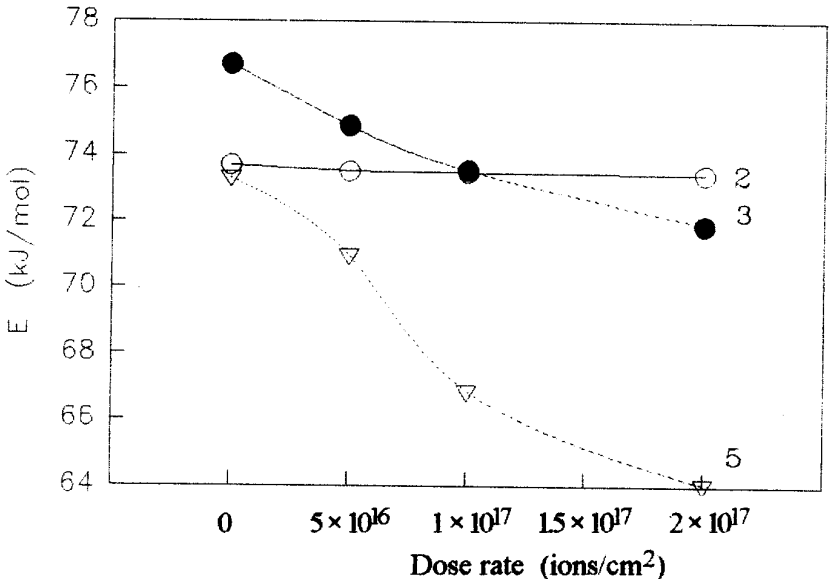

Fig.3 Relation between activation energy and dose rate for implanted glasses

The variation of $T_{k\text{-}100}$ with Ta^{+} ions implanted dose rate of various samples is represented in Fig.4. In this figure, replacement of $Si0_2$ by La_20_3 or Ta_20_5 lowered $T_{k\text{-}100}$, in respect that $Si0_2$ is not conductive participant but a network former, La^{3+} and Ta^{5+} act as cations in holes of network which weaken the bonding strength of structure thus enhance the mobility of Li^{+} as charge-transporting cation. This may also be seen from Fig.4, where increasing the implanted dose rate in samples also decrease $T_{k\text{-}100}$. These curves are in agreement with the results of electric conductivity after implantation.

It is well known that ion-implantation will case irradiation damage. Arnold [8] suggests that structure bonds are broken by irradiation for implanted glass, relax the network or expanse the net, enhance diffusion of light ions. We think that this theory explaining the reason of increasing of electrical conductivity after Ta+ ion implantation is reasonable. The high implantation energy (50KeV) and large dose rate {above 5 X 10^{16} ions/cm2) are enough to produce irradiation-damage of Si-O bond. So migration of charge carriers is advanced, consequently activation energy for ionic conduction is decreased, and meantime $T_{k\text{-}100}$ is reduced.

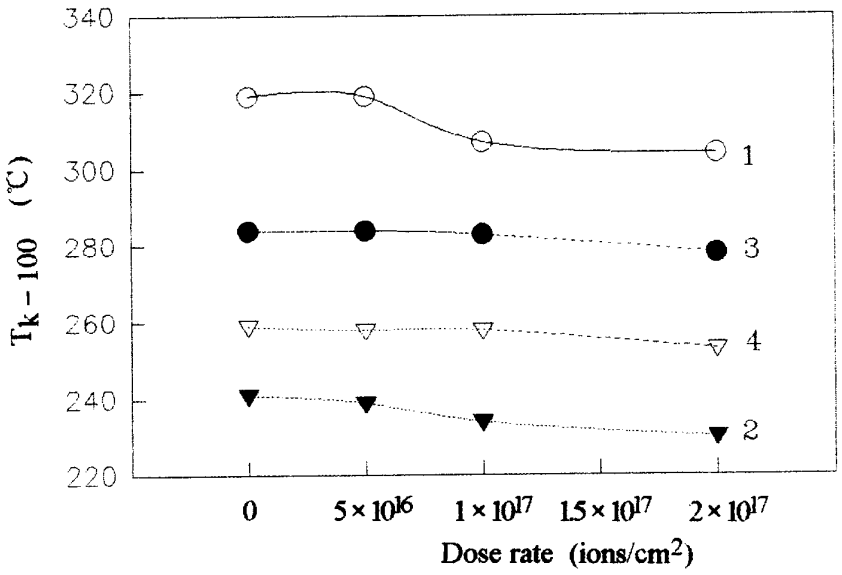

Fig.4. Variation of T_{k-100} with dose rate for implanted glasses.

4. CONCLUSION

The conductivity is improved to a different extent after replacing $Si0_2$ by La_20_3 or Ta_20_5. The irradiation-damage of glass structure bonds occurred after Ta^+ ions were implanted in Li_20-La_20_3-$5i0_2$ and Li_20-La_20_3-Ta_20_5-$5i0_2$ glass, which enhance the diffusion of Li+ and improve the electrical conductivity. Therefore, it is unnecessary to increase the content of Li_20 and other alkali oxide in glass composition to promote conductivity.

REFERENCES

1. G. W. Arnold. J. Appl. Phys, 46, (1975), 4446
2. Wang Chengyu, Tao Ying, Wang Shuchuan. J. Non-Cryst. Solids, 52,(1982),589
3. Wang Chengyu, Wang Bo. J. Non-Cryst. Solids, 123, (1990), 432
5. Nang Chengyu, Chen Min. Diffusion and Defect Data, 53-B4, (1987), 483
6. Nang Chengyu, Hu Yingjie. Glastech. Ber. 68C1, (1995), 549
7.Wang Chengyu, Zuo Zhongge, Jiang Yanyan. Proc.17th. Int.Cong.Glass, 3, (1995, Beijing), 79
9. W.Amold, R. K. Brow, D.R. Myers. J. Non-Cryst. Solids, 124, (1990), 234

THE IMPACT OF COATED GLASS ON TURKEY'S SKYLINE

Yücel AKYÜREK
Camtas Düzcam Pazarlama A.S., SISECAM, TURKEY

Ahmet CANSEVER
Çayirova Cam Sanayi A.S., SISECAM, TURKEY

Abstract

Turkish public has come to terms first time with the value of insulation in glass in 1970's when Þiþecam introduced the Double Glazing units into architectural use. The insulation is achieved through the static and dehydrated air space encapsulated within two panes of glass. Now with the spectrum of production of the new off-line coater the value of the coating has been added to the benefits of Double Glazing Units as an insulator both against the excessive solar gains and against the loss of heat from the interiors to the exterior.

Our product range, depending on the type of coated glass can reduce solar gains up to 1/4 of uncoated glass on the average and decrease the heat flow from interiors to the exterior to 2/3 of the uncoated Double Glazing Units. Our products can easily meet the most demanding specifications of any customer for any purpose anywhere. And the performance levels offered are not a luxury but a blessing for our economy and for the ecology of the World..

Savings in energy consumptions through better insulation help save the world's fossil reserves and decrease the emission of harmful gases to the world's atmosphere, such as CO_2.

THE COMMERCIAL "URBANSCAPE"

The need to build efficient living and working spaces on valuable urban land, developments in structural engineering, improvements in metallurgy and the achievements in mass production and processing of high quality float glass in the 20th century made possible the use of Glass as a building element which envelope the structures, mediating the internal conditions with that of the exterior, while providing light and vision.

"The glass tower" is becoming more and more prominent with the silhouette of large cities of Turkey. The typically glazed building is a reinforced concrete structure with recessed columns and cantilevered floor spaces. The spandrels are internal parapet walls cladded with glass similar in appearance to the glass used in vision areas.

The new glazed tower contradicts the current fabric of building clusters with "worn out looking" facades and undecided heights usually 10 to 15 stories. Glass with its basic

and acquired qualities, challenges all other facade materials such as RC concrete, brick + plaster, marble, granite and opaque industrial panels.

Glass assemblies are thin and light allowing more living space and imposing less loads onto the structure. Continuous ribbons of windows across the elevation provide vision to greater building depths. Glass surfaces are much easier to clean where most of the buildings with other facade materials completed only ten months ago would look ten years old due to the effects of air pollution and mud formed by airborne dust mixing with rain.

QUALITIES OF GLASS

Glass today is able to offer UV, light, solar gains, heat, vision and noise control and protection against theft and assault. Success with glass as the exclusive facade element owes a lot to its qualities acquired through further processing, such as heat treatment, lamination and IG assemblage, but most of all to functional coatings applied onto its surface.

Without going any further, we can immediately conclude that curtain walling would not be possible unless we make use of reflective properties of glass to conceal the individual building elements to achieve uniformity. Nor would it be possible to put up with huge summer solar gains and winter heat losses through the "continuos window" without the climate control assets invested in coatings.

Þiþecam is able to offer since the beginning of 1995, a wide range of reflective solar control products yielding hundreds of solutions through cross breeding nine different coatings with an average of three densities on various substrates of different tints and thicknesses. The new "off-line" hard and soft coatings of Þiþecam, originated in joint venture with and based on the technology provided by **Interpane** features a number of outstanding advantages over the **Aura Reflecta** ® which is another coated product of Þiþecam, and over other "on-line" (pyrolitic) coated products around the world. The advantages which are typical to its kind include flexibility in provision of a wide range of performances, thicknesses, color and versatility in adoption to "custom tailored solutions".

With Þiþecam's **Ipasol (TR)** coatings on clear for instance, it is possible to achieve shading coefficients as low as 0.14 in D/G assemblies with clear inner pane and 0.12 with low-E coated inner pane which is 5.79 times and 6.75 times more energy efficient respectively when compared to uncoated D/G units with 0.81 shading coefficient **(IAS 108)**. The interesting contribution of low-E coatings to the improvement of solar control properties of glass is illustrated on drawing.

CONTRIBUTION OF LOW-E COATINGS ON THE IMPROVEMENT OF SOLAR CONTROL PROPERTIES OF GLASS

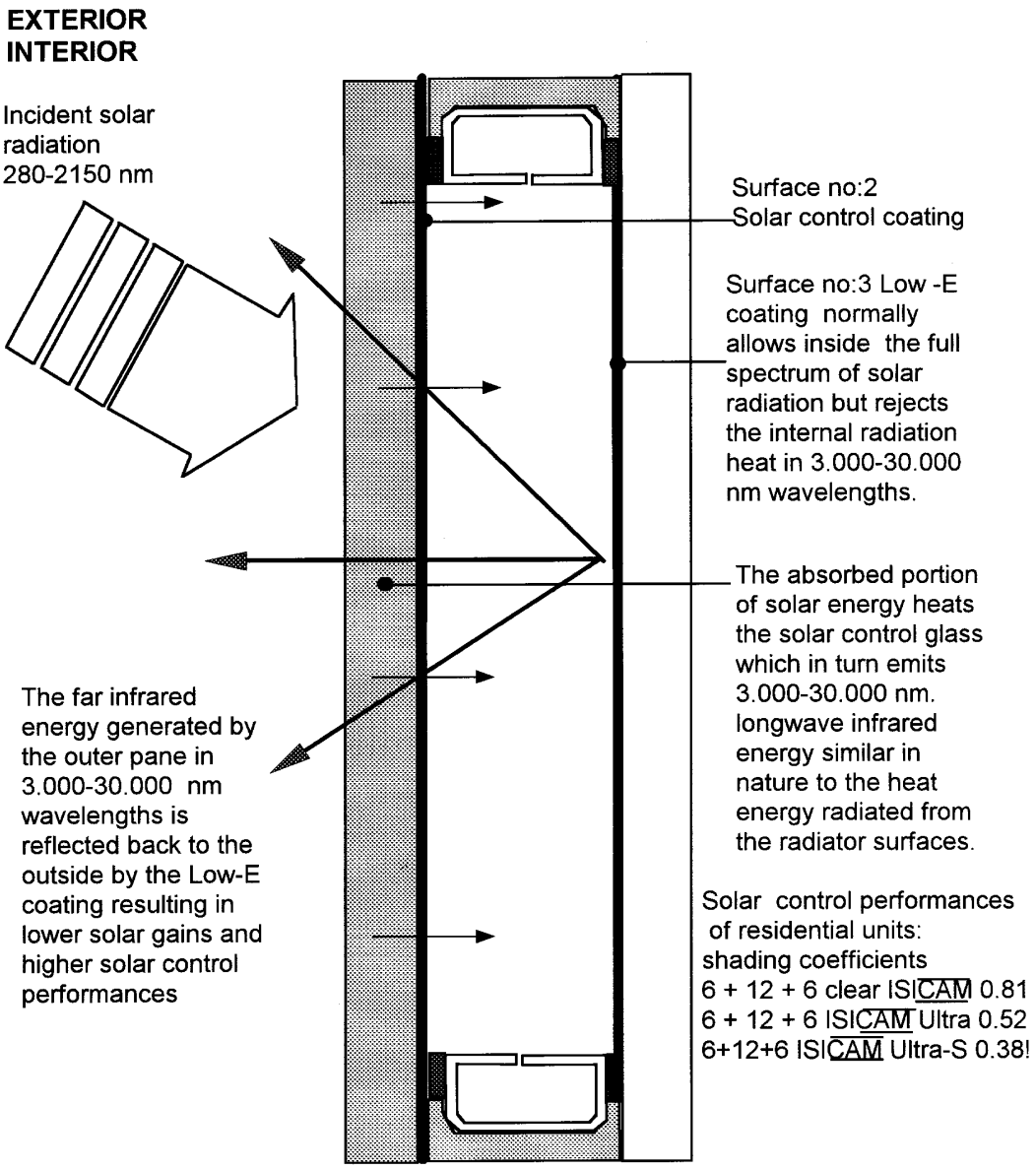

IPASOL (TR), **Aura Reflecta**, **Helio** solar control coatings can be combined within the same ISICAM units with **IPLUS (TR)** Low-E coatings to achieve the desired multifunctional performance objectives.

ISICAM ULTRA-S designates the low-reflectance multifunctional solution mainly intended for residential use.

THE RESIDENTIAL SCENE

Unlike most of the countries of north where only winter heating loads are predominantly important, excessive summer heat is an additional problem with houses in our geography. On the other hand, control of solar radiant heat in houses through coatings with high reflectance is not a widely accepted solution. The mirror like effect is reversed at night time due to higher illumination levels of the interior, hindering visibility to outside. To overcome this problem the **IIN 143** low reflectance coating has been developed to provide a reasonable degree of solar control with only 10 % light reflectance. The **Isýcam Ultra** ® IG units incorporating IIN 143 coatings are capable of providing a shading coefficient of **0.52** with uncoated clear inner pane and **0.38** with low-E coated inner pane (**Isýcam Ultra-S**), providing **56 %** and **114 %** respective improvements in reduction of cooling loads through windows when compared to uncoated clear D/G units. The above performance values offer valuable gains in initial costs and in energy consumption with houses utilizing mechanical cooling in southern provinces of Turkey which is now becoming increasingly popular. For houses without A/C the benefits can be measured in terms of improved levels of comfort against summer heat.

Isýcam-S ® insulating units with low-E is another important commodity introduced to the Turkish market which utilizes the benefits of Þiþecam high performance coatings. k values air filled **1.8 W/m^{2}K** and argon filled **1.4 W/m^{2}K** are possible with 12 mm airspace dual units. Normally Isýcam-S can be regarded as the ideal material for the highlands of East and for the Central Anatolian plateau where the winters can be severe. The climate of the coastal areas of north also make worthwhile the use of Isýcam-S. However Isýcam-S can be uncomfortable at the coastal areas of south and west in summer if not used in combination with solar control glass or measures. Such warmer areas really deserve Isýcam Ultra or Isýcam Ultra-S.

COATING PROCESS OF ÞÝÞECAM OFF LINE COATINGS

Þiþecam's large area vacuum coating line which makes use of **Magnetron Cathode Sputtering Process** is capable to deposit ultra thin films of superior optical qualities onto the glass surface to improve its spectrophotometric and thermal properties.

The Magnetron Cathode Sputtering (**MCS**) Process is carried out in a series of cathode chambers, one of which is shown in the diagram schematically. The glass substrate is conveyed into the cathode chamber which houses the target (the metal plate of the material to be deposited onto the glass substrate) bolted to the cathodes. A controlled amount of gas (argon, argon/oxygen, argon/nitrogen) is fed into the cathode chamber, a negative charge to the cathode and a positive charge to the anode is applied resulting in glow discharge-plasma (positive gas ions+electrons) within the magnetic field created by permanent magnets behind the target. This plasma creates positive argon ions which are attracted to the negatively charged target, bombarding the target with such a strong impact that the atoms from the target are torn away (= sputtered) and deposited atom-by-atom onto the glass substrate in the form of "ultra thin films" (0.00004-0.00015mm.)

having highly uniform thickness. The free electrons, being concentrated by the magnetic field, produce new argon ions and are collected by the anodes.

Sputtering types:

a.) Metallic Sputtering : The target material and the film material deposited on the glass substrate are identical, or

b.) Reactive Sputtering : Oxygen or nitrogen is injected into the plasma in addition to argon. The process allows the deposition of metal oxide or metal nitride films on the glass substrate.

The major materials deposited are Tin, Silver, Chromium, Nickel Chromium and Titanium.

The full range of Solar Control and Climate Control (Low-E) products fulfill or exceed the requirements of prEN 1096-1, CEN Standard for Coated Glass.

Quality is produced by well trained Þiþecam Team, who are highly capable to drive and maintain the fully automated systems of coating line. Tracking the 'pane-by-pane' product quality is achieved by advanced on line spectrophotometric measuring system.

The production activities are substantially supported by the Research Center of Þiþecam on the project basis, by developing new coatings and determining the product performances.

Coatings can be incorporated with clear, tinted pyrolitically coated, laminated, tempered glass substrates.

Nominal annual production capacity is 1.200.000 m^2.

The thickness of the glass substrates may vary within the range of 2.5-12mm.

Max. coated glass size is 3.21 x 6.00 m. Jumbos.

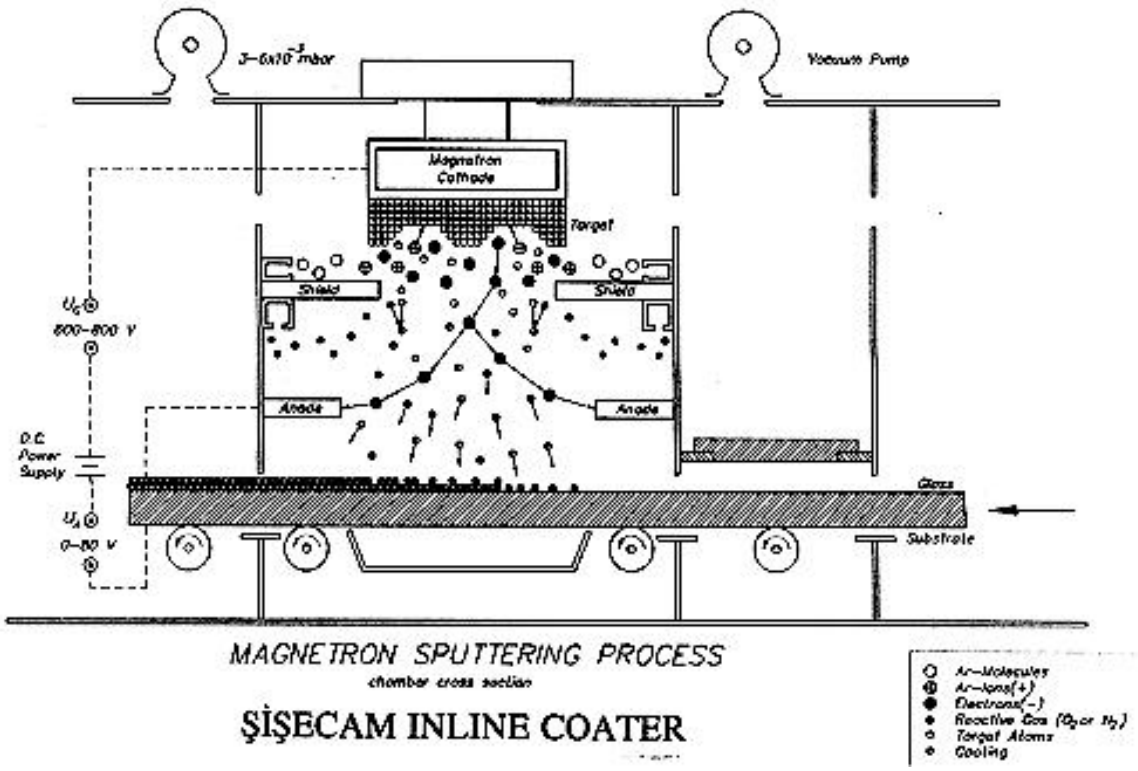

THE ECONOMICAL AND ECOLOGICAL GAINS

Savings in energy consumption and consequently in emission of harmful gases to the atmosphere is on top of the World's ecological agenda. This has been further emphasized on the Habitat II Conference held in Istanbul on June 1996. Insulation with glass should be one of the major concerns of glass industry today. Utilizing the below general formula which is widely accepted for the assessment of energy savings in heating :

$$\frac{\text{Degree days x U value differential W/m}^2\text{K x 3600 sec/h x 24 h/day x 0.000239 Joule/kcal x 1.19Lt/kg}}{\text{0.80 (burning efficiency) x 9700 kcal/kg fuel oil thermal value}}$$

We can conclude that:

Selecting **conventional D/G units** instead of monolithic glass will save

21.5 Lt fuel oil / year / m^2 glazing in **Istanbul**
29.0 Lt fuel oil / year / m^2 glazing in **Ankara**
46.0 Lt fuel oil / year / m^2 glazing in **Erzurum**

Selecting standard Low-E units instead of monolithic glass will save

28.7 Lt fuel oil / year / m^2 glazing in **Istanbul**
38.7 Lt fuel oil l year / m^2 glazing in **Ankara**
61.5 Lt fuel oil / year / m^2 glazing in **Erzurum**

Based on 20 °C indoor temperatures and start up at 15 °C outdoor temperature, Istanbul degree days 2263; Ankara DD 3058; and Erzurum DD 4856.
Source for Degree Days : Prof. Dr. Alpin K. Daðsöz, Istanbul Technical Univ.1995.

A study carried out by National Research Center (Tübitak - MAM) in partnership with Türk - Ytong suggests that the heating energy consumption on an average Istanbul house is **2 times higher** when compared to German houses; **2.5** times to American; **3** times to Danish and **3.6** times to Swedish houses when theoretically compared in exactly similar conditions.

Cooling should be more important because it is generally estimated that cooling costs are approximately 4 times higher than heating.

The economical and ecological benefits to be expected from the whole venture is largely dependent on effective campaigns carried out to educate the designers, contractor and consumers and to the degree of public response received.

THE NATURE OF LIQUID IMMISCIBILITY IN ALKALI BOROSILICATE SYSTEMS*

I.G. POLYAKOVA
Institute of Silicate Chemistry of Russian Academy of Science, Russia

Abstract

The alkali borosilicate systems are the only ternary systems having the critical point located not in binary system but in ternary region. A systematic investigation of liquid immiscibility in sodium, potassium and rubidium borosilicate systems (NBS, KBS and RBS, respectively) was carried out using differential thermal analysis. It was demonstrated that immiscibility regions of this systems have lower temperature boundaries. Isothermal curves of lower surfaces were constructed, upper surfaces locations were refined, three-phase region was found to exist in NBS system. With the reasonable confidence we can say that there are "anionic" and "cationic" characteristic properties of alkali borosilicate immiscibility. The reasons of such regularities and the very fact of the immiscibility existence in ternary systems can not be understood without significant widening of the work content.

The systematic investigation of alkali borosilicate systems was undertaken. The phase equilibrium in KBS and RBS systems were studied and their phase diagrams were constructed. The ‘property-composition’ diagram of NBS, KBS, RBS glasses investigated by us and taken from literature, demonstrate resemblence to each other and to the liquidus surfaces of KBS and RBS systems. In the neighborhood of composition $R_2O.B_2O_3.4SiO_2$ (in KBS system it is known as boroleucite). All glass properties diagrams have maxima connected with boroleucite structure groups formation in melts. The existence of "the boroleucite anomaly" not only explains extrema on "composition-property" diagrams of alkali borosilicate glasses but also is the factor causing liquid phase separation in alkali borosilicate systems.

---

* Full manuscript not available at the time of printing

THE PERSISTENT SPECTRAL HOLE-BURNING IN GLASSES WITH SEMICONDUCTOR NANOCRYSTALS

Alexei Diikov and **Alexander Dotsenko**
S.I.Vavilov State Optical Institute, Russia

Lev Zimin
Institute of Physics ANB, Belarus

Abstract

The persistent spectral hole-burning was observed in exciton bands of CdSe and CuCl nanocrystals doped in glass matrices. The peculiarities of hole-burning are explained on the base of photophysical model of persistent spectral hole burning. The burned holes show the distinct phonon structure which can be attributed to the vibrations on the semiconductor/dielectric boundary. The phonon structure in the z_3 exciton band of CuCl nanocrystal in borosilicate glass matrix is characterized by phonon energy 0.001 eV and calculated Debye-Waller factor $\alpha < 0.5$.

INTRODUCTION

The non-linear optical properties of semiconductor microcrystals in dielectric matrix (SMDM) were detected rather long ago. Last time SMDM attracted an additional interest because of the theory prediction of the non-linear optical property enhancement due to size effect [1]. Besides size, the high microcrystal symmetry is the essential condition of the "giant" optical non-linearity of SMDM. Therefore, the words '"quantum dots, zero dimension structures, etc." became main key words of the recent year publication works. However, the legitimacy of the quantum dot approach in reference to real SMDM is questionable.

The recent investigations [2,3] show an unsoundness of zero dimensional approach in reference to the semiconductor nanocrystal optical nonlinearities. It turned out that just a configuration of the nanocrystal/dielectric environment system determines the non-linear optical response in the many spectral hole-burning experiments. New for semiconductor nanocrystals, so-called persistent spectral hole-burning (PSHB) pretends to be the one of the main model of their optical properties even at room temperature and at short-lived processes. New approach has an advantage of PSHB high resolution spectroscopy and permits to get the new possibilities for investigation of SMDM in glasses.

To clarify the role of nanocrystal/dielectric boundary on the process of hole burning of SMDM in glass matrices we investigate the non-linear optical response in these systems and analyse phonon structure of burning hole.

EXPERIMENTAL SETUP AND RESULTS OF MEASUREMENTS

The samples were; CdSe and CuCl microcrystals doped into glass matrices on the base of GeO_2 and SiO_2-B_2O_3 respectively. The measurements were carried out with a narrow band dye laser as a pump beam source and a dye cell as a probe beam spectrally broad source. The both light sources were pumped by Q-switched Nd^{3+} :YAG laser. The pulse duration was 5 ns and the maximum repetition rate was 30 Hz. Additionally the special chopper is used to provide the second time delay between pump and probe beams. The chopper blocked in turn pump and probe beams. Optical spectra was recorded with an optical multichannel analyser combined with a monochromator. The average size of semiconductor microcrystals was estimated by small-angle X-ray scattering measurements.

Under the usual pump-probe method, when the both pump and probe beams pass through the sample simultaneously, the well known nonlinear response has been recorded. The samples showed the high nonlinear sensitivity, sharp the spectral burned holes and increasing absorption of neighboring off-resonance spectral regions (fig.1 (b)).

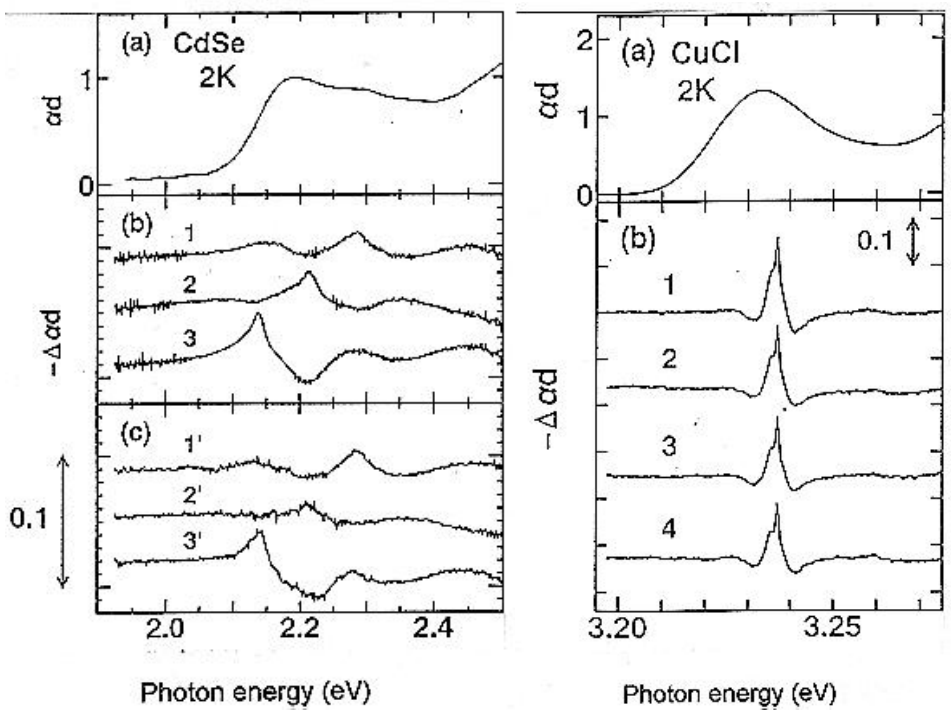

Fig.1. Linear (a) and differential absorption (b, c) spectra of the CdSe microcrystals embedded in GeO_2 glass. The average radius is 2.4 nm. The spectra (b) and (c) were measured for time delays of 0 and 33 ms, respectively. The pump photon energies corresponding to spectra 1 (1'), 2(2') and 3(3') are 2.287 eV, 2.214 eV and 2.138 eV respectively.

Fig. 2. Linear (a) and differential absorption (b) spectra of the CuCl microcrystals embedded in borosilicate glass. The average radius is 2.5 nm. The delay times corresponding to spectra 1, 2, 3 and 4 are 0 s, 0.1 s, 0.5 s and 1.4 s respectively. Pump photon energy is 3.237 eV.

On the fig 1 (c) is shown the differential absorption spectra recorded with the chopper under 33 ms delay between pump and probe beams. It almost completely reproduce those in fig. 1 (b). The further investigation showed that spectral burned holes were stable at low tempera with life times from 1.5 s for CdSe to hours for CuCl. The hole formation is accompanied by the growth of one or two antiholes in the neighboring off-resonance spectral region (fig.1). Therewith the burned

holes show the distinct phonon structure that can clearly see in the long-lived differential absorption spectra of CuCl samples (fig. 2).

These results show clearly an unsoundness of the generally accepted approach of the quantum dot optical non-linearities for the present media. Instead, so-called persistent spectral hole-burning (PSHB) phenomenon seems to be a suitable candidate for explaining these results [4].

MICROSCOPIC MODEL AND ANALYSIS OF EXPERIMENTAL RESULTS

As distinct from the high-symmetry quantum dot model, PSHB uses the concept of the microcrystal-matrix configuration. PSHB model assumes an additional inhomogeneous broadening even for an ensemble of the same microcrystals due to the existence of more than one energetically inequivalent ground states of the total microcrystal-matrix system. The spectrally narrow laser irradiation change the ground state configuration by the transition through the excited state (fig. 3). This changing of configuration leads to the decrease of the ground state population of the resonant transition. Also the neighboring off-resonance states population is increased (so-called photophysical model). Photophysical bleaching is accompanied by the absorption increase at the neighboring frequencies, which is not the absorption from the excited states but so-called antiholes. Decay time of PSHB is mainly due to the relaxation among the ground states, but not the relaxation of excited states. The full decay time of non-linear response depends on the excited state relaxation and the relaxation among ground states. In order to PSHB phenomenon appreciably manifests itself, the relaxation among the ground states should be slower the decay rate of any excited state. It can be seen that the antihole depth value depends on their spectral position in the absorption spectrum (fig. 1). The antiholes are the deepest near the absorption peak and at the high-energy side of it, where absorption is fairly large. The antihole on the low-energy side of the burned hole becomes small as the pump photon energy decreases. The antihole disappears if coincides with the transparency area. According to the photophysical persistent hole-burning approach, the main behavior is clearly understood [4]. The antihole depth correlates with the ground state density and, therefore, the spectral area of the antihole is restricted by the absorption band.

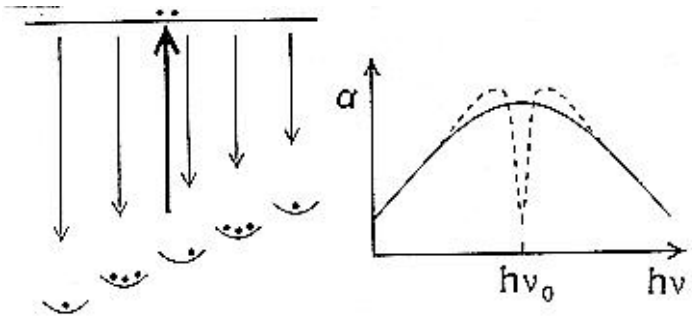

Fig. 3. Schematic representation of photophysical mechanism of persistent hole-burning phenomenon. The ground state levels are represented as the potential energy wells for the explanation of the origin of persistency. Absorption spectrum before (solid line) and after (dashed line) the excitation by spectrally narrow laser beam.

To understand the photophysical mechanism of PSHB is necessary to determine the factor which allow to stabilize electronic system in new configuration (fig. 3). Obviously in this process

must participate electron and lattice systems. The information about electron-phonon interaction can be received from the shape of burning hole. For that reason we investigate the distinct phonon structure of persistent burned hole in the z_3 exciton band of CuCl nanocrystals (fig. 2) and calculate the Debye-Waller factor. The line shape function of one absorption center can be expressed as: $I(\omega-\omega')=\alpha\bullet\delta(\omega-\omega')\bullet(1-\alpha)\cdot p(\omega-(\omega'+\Delta))$, where $h\omega'$ is the energy of zero phonon transition; δ, p are normalized zero phonon line and phonon wing; Δ is phonon energy; α is the Debye-Waller factor which is determined by electron-phonon coupling strength S, $\alpha = \exp(-S)$. Taking into account the distribution $N(\omega)$ of absorbed centers on absorbed frequency ω we can write the following expression for the burned hole shape after irradiation time t at laser frequency ω_1 (5):

$$H_t(\omega) = \int_{-\infty}^{+\infty} N(\omega')\bullet\exp(-ct\bullet I(\omega_\ell-\omega''))\bullet I(\omega-\omega')d\omega', \qquad (1)$$

where c depends from laser intensity and matrix element of electron transition. To compare the results of calculation with experiment is more convenient to consider the differential spectra HD as the difference between absorption spectra without laser excitation and H_t (absorption spectra after laser radiation).

$$HD_t(\omega) = \int_{-\infty}^{+\infty} N(\omega)\bullet(1 - \exp(-ct\bullet I(\omega-\omega'))\bullet I(\omega-\omega')d\omega', \qquad (2)$$

In the limit of saturation (shape of the hole does not change during irradiation} and assumptions that δ and p line shapes are approximated by Gaussian and $N(\omega)$ is constant in the spectral region from hole to antihole, we can rewrite (2) in the following form: HD=

$$\begin{aligned} &= N\bullet\big[\alpha\bullet[F((\omega_\ell + 3\Gamma_0 - \omega)/\Gamma_0) - F((\omega_\ell - 3\Gamma_0 - \omega)/\Gamma_0)] + \\ &+ (\alpha - 1)\bullet[F((\omega_\ell + 3\Gamma_0 - \omega + \Delta)/\Gamma_1) - F((\omega_\ell - 3\Gamma_0 - \omega + \Delta)/\Gamma_1)] + \\ &+ \alpha\bullet[F((\omega_\ell + 3\Gamma_1 - \omega - \Delta)/\Gamma_0) - F((\omega_\ell - 3\Gamma_1 - \omega - \Delta)/\Gamma_0)] + \\ &+ (\alpha - 1)\bullet[F((\omega_\ell + 3\Gamma_1 - \omega)/\Gamma_1) - F((\omega_\ell - 3\Gamma_1 - \omega)/\Gamma_1)]\big], \\ &F(x) = 1/2\bullet\mathrm{erf}(x/\sqrt{2}), \end{aligned} \qquad (3)$$

where Γ_0 and Γ_1 are the widths of the zero phonon line and phonon wing, The 3Γ in (3) is connected with the fact that Gaussian takes noticeable meaning only in region from -3Γ to $+3\Gamma$. The first and the last terms in (3) determine the central peak of burned hole (fig. 4).

The second term determines the phonon wing and the third determines the pseudo phonon wing. In the assumption that peaks are not overlapped we have the following relative intensities in maxima:

$$\begin{array}{ll} 1, & \omega = \omega_\ell \\ \alpha_1 & \omega = \omega_\ell - \Delta \\ (\alpha - 1)\bullet F(3\Gamma_0/\Gamma_1), & \omega = \omega_\ell + \Delta \end{array} \quad (4)$$

The estimations fulfilled with using (4) showed that the Debye-Waller factor reached the meaning $\alpha < 0.5$ ($S > 0.6$) for CuCl nanocrystals in borosilicate glass. The difference in energy between phonon line and phonon wing is 0.001 eV. This low energy phonon differs from phonons of bulk CuCl crystal (TO = 0.021 eV, LO = 0.026 eV) and can be attributed to vibration on the boundary of CuCl nanocrystals and the host matrix. The noticeable electron-phonon coupling means that exciton formation is accompanied by deformation of the atomic lattice. Such deformation can be explained in the assumption that exciton interacts with local states of defects on the nanocrystal/glass boundary.

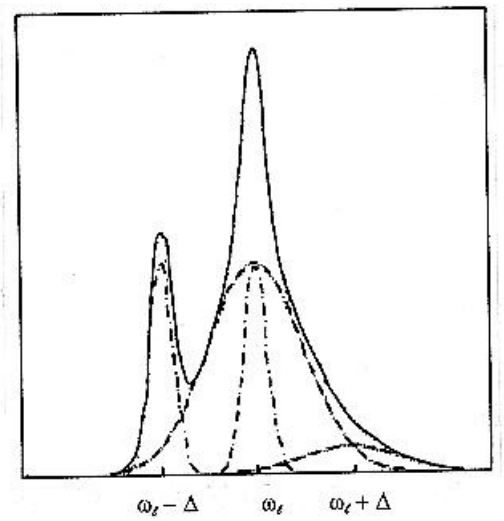

Fig.4. The structure of burned hole. The left peak is pseudo phonon wing, which consists from zero phonon lines burned through their phonon wings. The central peak consists from burned zero phonon lines and phonon wings of zero phonon lines of left peak. The right peak is the phonon wing burned through zero phonon lines of central peak. D is the phonon energy; $h\omega_l$ is the pump photon energy.

CONCLUSION

We have demonstrated the persistent spectral hole-burning phenomenon in semiconductor microcrystals doped into dielectric matrix, specially, the photophysical mechanism of hole-burning. The differential absorption spectra of CdSe and CuCl microcrystals measured by pump-and-probe method keep the burned hole at least more then one second at liquid helium temperature. In all cases, the positive part of differential absorption spectrum, indicating the bleaching around the pump frequency, is accompanied by darkening of one or two spectral parts. These spectral parts are conserved for a long time too and are not caused by the generation of new (multipartical) states. The shape of burning hole is determined by low energy phonons on the nanocrystal/glass boundary.

The experimental results showed that the general accepted model of quantum dots can not be used directly even as a rough approximation for many cases of semiconductor microcrystal laser spectroscopy. PSHB phenomenon detected in semiconductor nanocrystals in glasses on the one hand gives new instrument for semiconductor structure investigations and on the other hand proposes a new class of media for an application-oriented investigations.

REFERENCES

1. E.Hanamura, Phys. Rev. B37, (1988) 1273.
2. L.Zimin, K.Naoe, S.Okamoto, T.Kawazoe, Y.Masumoto, Physical Society of Japan. 3, (1994), 28.
3. Y.Masumoto, L.Zimin, K.Naoe, S.Okamoto, T.Arai., Mateial Science and Engineering. B27, (1994), L5-L9.
4. W.E.Moerner (ed.). Persistent Spectral Hole-Burning: Sience and Applications, Springer, Berlin.1988.

THE POLYMORPHOUS STRUCTURE AND PROPERTIES OF THE GLASSFORMING SiO_2*

V.S. Minaev and **R.V.Galiulin****
Research Institute of Material Science and Technology, Russia
**Russian Academy of Sciences, Russia

Abstract

According to polymorphous-crystalloid concept of non-crystalline substance structure [1,2], coexistence of various crystalline-polymorphous modifications (PM) of SiO_2 causes appearance of ultra-dispersive(films, dehydrated gel) and glassforming silica (v-SiO_2). The last one is formed of liquid or solid ultra-dispersive SiO_2 by polymorphous polymerization of crystalloids-nuclei (fragments) of crystal structure of various PMs, which have no translation symmetry of crystal. Unification of such crystalloids results in altermation of near-and intermediate-range orders, in alternation of different (on their value) interbond and dihedral angles, which are inherent to crystalloids of quartz, tridymite, crystobalite and other PMs, and it leads to formation of glassforming SiO_2 disordered network.

Difference of structural characteristics and properties of v-SiO_2 formed of one source material by various methods is directly connected with PM mutual transformation under the influence of external effects. Correlation of interval of interbond angle values of Si-O-Si (120-180 degrees) and some properties of glasses (e.g. density, refractive index) with interval of values of corresponding characteristics for different SiO_2 PMs has been observed.

---

* Full manuscript not available at the time of printing

THE PROPERTIES OF THE GLASSES IN THE $CaO-BaO-Na_2O-K_2O-SiO_2$ SYSTEM

Peter Òimurka and ***Marek** LiÓka

LR CRYSTAL, Slovakia
*Institute of Inorganic Chemistry of SAS, Slovakia

Abstract

The viscosity, liquidus and transformation temperatures, refractive index, and the water resistance are reported for 15 glass samples of the title glass system. Using the non-linear regression analysis, the temperature and compositional dependence of viscosity was expressed by the mixed polynomial (of the individual oxides mole fractions) representation of the A, B and T_0 coefficients of the Vogel Fulcher Tammann equation. The compositional dependences of the other properties studied were described by the mixed polynomials in both the weight and mole fractions of individual oxides. The obtained results were used in two ways i) the glass composition optimisation with respect to the lowering of the stemware glass production cost; ii) the structural role of the individual oxides estimation based on theirs influence on the studied properties.

I. INTRODUCTION

The scope of the present work resulted from the need of the stemware glass chemical composition optimisation. Thus the aim was to determine the weight fractions of the CaO, BaO, Na_2O, K_2O, SiO_2 oxides in the glass batch. The series of 15 glass compositions resulting from the simplex scheme was proposed. The following ranges of individual oxides weight fractions were chosen: 5-10% CaO, 3.5-8.5% BaO, 10.5-15.5% Na_2O, 3.5-8.5% K_2O, and 72.5% SiO_2. Despite the viscosity curve the other properties relevant to the stemware glass production are the liquidus and transformation temperatures, refractive index, and the water resistance. The prerequisite condition to solve this problem is the knowledge of the compositional dependence of all the above mentioned properties.

The technological needs directed the optimisation to be done in the weight fractions of individual glass components. Although this requirement is quite acceptable the mole fractions were used in the case of viscosity, where the usage of non-physical units (e.g. weight fractions) results in enormous complexity of the approximation polynomials used for the description of A, B and T_0 compositional dependence. On the other hand some structural information may be extracted only from the functional dependencies expressed in the mole fractions of individual oxides. That is why, the polynomials describing the property-composition relationships are presented twice in this work. However, between these two representation there is no one to one correspondence. The best possible interpolation is required in the "technological" representation. Thus maximum value of the Fisher's F statistics (inversely proportional to the residual sum of

squares) was the only criterion for choosing the optimal polynomials in this case. In the second case only the statistically significant terms can be considered to prevent the artificial corruption of structural implications. Of course, all the means of the advanced statistics have to be used to confirm the significance of the regression model proposed in this case.

II. EXPERIMENTAL

Batches were prepared from the industrial raw materials commonly used for the glass batch preparation - the glass sand, lime stone, potash, soda ash, and barium carbonate. The antimony oxide, sodium chloride, sodium sulphate, and sodium nitrate were added in analogy with the industrial glass melting. The constant amounts of these minorite components were not explicitely considered in the regression models. The glass batches were melted in ambient atmosphere in a superkanthal furnace at 1500^{o}C in a Pt-10%Rh crucible. Homogeneity was ensured by hand mixing of the glass melt. Each melt was poured from the crucible onto the stainless steel plate. The glass samples were then tempered in a muffle furnace for twenty minutes at 520^{o}C, then the furnace was switched
off and the samples remained there until reaching the room temperature. The chemical composition was determined after the samples were decomposed by the HF and H_2SO_4 solution by the atomic absorption spectroscopy (Na_2O, K_2O, CaO) and by the gravimetry (BaO as $BaSO_4$). The obtained chemical compositions are summarized in Tab.l.

The low temperature viscosities between 10^{7}-10^{12} dPa.s were determined from the axial deformation rate measured by thermo-mechanical analyzer (Netzsch TMA-402). The viscosities between 100-$10^{6.5}$ dPa.s were measured by concentric cylinder rotation viscometer. The liquidus temperature was determined by keeping the sample of coarsely ground glass in a Pt-30%Rh boat in a gradient furnace for 24 hours. The temperature at which the first crystal appeared in the sample was the liquidus temperature. The transformation temperature was determined from the dilatometric cooling curve measured by the TMA 402 with the cooling rate of 5^{o}C/min. The refractive index was measured on
polished glass samples by the Abbe refractometer using the monobromnaphtalene as immersion liquid. The water resistance was quantified according to CSN 70 0531 (e.g. ISO R719).

Table I: Chemical compositions of the glass samples investigated.

Glass	w(CaO)/%	w(BaO)/%	$w(Na_2O)/\%$	$w(K_2O)/\%$	$w(SiO_2)/\%$
1	9.80	3.63	10.37	3.83	72.37
2	4.98	8.47	10.51	3.71	72.33
3	4.96	3.53	10.57	8.59	72.35
4	5.06	3.76	15.28	3.76	72.14
5	7.48	5.67	10.20	3.60	73.05
6	7.29	3.42	10.28	5.97	73.04
7	7.31	3.47	12.60	3.65	72.97
8	5.06	5.99	10.31	6.03	72.61
9	5.06	5.94	12.66	3.75	72.59
10	5.02	3.42	12.36	6.06	73.14
11	6.60	5.03	10.65	5.28	72.44
12	6.54	5.00	12.24	3.58	72.64
13	6.37	3.41	12.18	5.26	72.78
14	4.99	5.24	12.20	5.35	72.22
15	6.28	4.88	11.68	4.82	72.34

The experimental results are briefly summarized in theTab.II

Table II.: Experimental results: T_g - glass transformation temperature, T_l -liquidus temperature, n_D - refractivity index, W_R - water resistance, and A, B, T_0 coefficients of Fulcher Vogel Tammann viscosity equation.

Glass	$T_g/^0C$	$T_l/^0C$	n_D	W_R/ml 0.01MHCI	A	B/K	T_0/K
1	544	994	1.5212	0.54	-1.962	4529	254
2	506	1118	1.5152	0.58	-1.997	4991	189
3	488	869	1.5145	1.61	-1.634	4413	209
4	502	876	1.5105	1.76	-1.623	4265	214
5	547	1087	1.5163	0.55	-1.964	5040	201
6	551	892	1.5142	0.72	-1.813	4629	224
7	515	979	1.5153	0.79	-1.968	4684	216
8	504	956	1.5123	0.89	-1.799	4913	178
9	512	1030	1.5132	0.96	-1.689	4593	199
10	488	884	1.5103	1.81	-1.808	4589	197
11	522	1004	1.5133	0.54	-1.892	4895	205
12	522	1018	1.5154	0.67	-1.930	4667	220
13	521	848	1.5124	0.83	-1.877	4523	224
14	494	989	1.5116	1.18	-1.784	7440	193
15	520	910	1.5156	0.79	-2.004	4683	210

III. TECHNOLOGICAL APPLICATION

Using the standard least squares method the following relationships were found for individual studied properties:

$$\mathbf{Tg}\ /^{o}C = 805 - 3.429\ w(Na_2O)\ w(K_2O) - 23.22\ w(BaO) - 29.39\ w(CaO) + 4.293\ w(CaO) + w(K_2O) + 2.382\ w(CaO)\ w(BaO) \quad (1)$$

$$\mathbf{T_l}\ /^{o}C = 1775 - 49.94\ w(Na_2O) + 16.81\ w(CaO) - 11.361\ w(CaO)\ w(K_2O) \quad (2)$$

$$\mathbf{n_D} = 1.4566 + (5.808\ w(K_2O) - 0.335\ w(BaO)\ w(K_2O) + 0.322\ w(BaO)\ w(Na_2O) + 5.525\ w(CaO) - 0.508\ w(CaO)\ w(K_2O)).10^{-3} \quad (3)$$

$$\mathbf{W_R}/ml = 11.78 - 0.0541\ w(K_2O) - 1.2313\ w(BaO) + 0.03319\ [w(BaO)]^2 - 2.0115\ w(CaO) + 0.11437\ w(CaO)\ w(BaO) + 0.09021\ [w(CaO)]^2 \quad (4)$$

$$\log(\eta/d\ Pa.s) = A + B / (T - T_O) \quad (5)$$

$$\mathbf{A} = -14.721 + 54.41\ x(CaO) + 51.95\ x(BaO) + 49.34\ x(Na_2O) + 72.58\ x(K_2O) \quad (6)$$

$$\mathbf{B}/K = 24756.1 - 86687\ x(CaO) - 69935\ x(BaO) - 78722\ x(Na_2O) - 108444\ x(K_2O) \quad (7)$$

$$\mathbf{T_0}/K = -863.5 + 6504\ x(CaO) + 5100\ x(BaO) + 4914\ x(Na_2O) + 6828\ x(K_2O) \quad (8)$$

where x are the mole fractions of individual oxides, and T is the thermo-dynamic temperature.

The equations (1-8) were used in the optimisation of stemware glass composition. By proposal of the new glass composition the batch cost was lowered of about 9%, melting temperature was lowered of about $10^{o}C$, while the key properties determining the glass quality were maintained at the same level, or slightly improved.

IV. STRUCTURAL IMPLICATIONS

Using the standard least squares method the following relationships were found for the property-composition dependences in the mole fractions representation:

$$Tg^{o}C = 3270 - 88121\ [x(K_2O)]^2 - 49041\ x(Na_2O) + 142599\ x(Na_2O)\ x(K_2O) + 137153\ [x(Na_2O)]^2 + 68474\ x(BaO) - 649541\ x(BaO)\ x(K_2O) - 681390\ [x(BaO)]^2 - 11568\ x(CaO) + 154050\ x(CaO)\ x(Na_2O) - 332188\ x(CaO)\ x(BaO) \quad (9)$$

$$\mathbf{T_l}\ /^{o}C = 2001 - 5902\ x(Na_2O) - 154203\ x(CaO)\ x(K_2O) \quad (10)$$

$$\mathbf{n_D} = 1.5093 + 0.9578\ [x(CaO)]^2 \quad (11)$$

$$\mathbf{W_R}/\text{ml} = 6.75 - 49.1\ x(BaO) - 109.4\ x(CaO) + 546\ [x(CaO)]^2 \qquad (12)$$

From the structural point of view, the studied glass system consists of only one network-forming oxide (SiO_2), while the other glass components are the typical network-modifiers. In analogy with the theory of thermodynamic partial molar quantities the influence of each glass component may be rationalized in two ways. First, the partial derivative d(i) of the respective physical quantity y with respect to mole fractions of oxide i (i≡CaO, BaO, Na_2O, and K_2O) reflects the effect of equimolar substitution of oxide i for SiO_2. Second, the "partial molar quantities" V(i) reflect the contributions of all the oxides to the quantity y in the following manner:

$$y = x(CaO)\ V(CaO) + x(BaO)\ V(BaO) + x(Na_2O)\ V(Na_2O) + \\ + x(K_2O)\ V(K_2O) + x(SiO_2)\ V(SiO_2) \qquad (13)$$

All the mentioned quantities calculated for the composition of the glass No.15 (the glass situated in the center of the studied glass compositional region) are summarized in the Tab.III.

Table III.: The partial molar contributions V of individual oxides to various properties (see Eq.13), and the partial derivatives d of the approximations polynomials of these properties.

	$\mathbf{T_g}/^0\mathbf{C}$	$\mathbf{T_l}/^0\mathbf{C}$	$\mathbf{n_D}$	$\mathbf{W_R}/\mathbf{ml}$
V (CaO)	817	-2619	1.6396	-28.3
V (BaO)	-2464	2352	1.5045	-45.1
V (Na_2O)	-254	-3551	1.5045	4.0
V (K_2O)	-1018	-8528	1.5045	4.0
V (SiO_2)	757	2352	1.5045	4.0
d (CaO)	61	-4970	0.1352	-32.3
d (BaO)	-3221	0	0	-49.1
d (Na_2O)	-1011	-5902	0	0
d (K_2O)	-1774	-10879	0	0

For all the properties studied, the significant differences between the glass modifying oxides may be deduced from the values presented in Table III. More detailed discussion of the obtained results will be the part of the poster presentation.

THE QUANTITATIVE ASSESSMENT OF GLASS CRYSTALLIZATION TENDENCY BASED ON DTA DATA*

E.V. Tokareva and **I.G. Polyakova**
Institute of Silicate Chemistry of Russian Academy of Sciences, Russia

Abstract

The attempts to use differential thermal analysis (DTA) data for quick evaluation of glass crystallization tendency have already been made before, however they can not be accepted as successful ones because crystallization temperature (Tcr) dependencies of suggested coefficients were nonlinear. We suggest a coefficient Kox varying linearly from 1 to 0 as Tcr shifts from glass transition temperature to melting temperature. Kcr gives the quantitative assessment of the glass crystallization tendency and after additional investigations it can be calculated for each of the phases crystallizing during the DTA process, enabling us to make some quantitative evaluation of structure crystal-likeness.

The potentialities of the strategy suggested are illustrated by the example of the part of binary potassium borate system. It is shown that over the interval from $K_2O.\ 2B_2O_3$ to $5K_2O.\ 19\ B_2O_3$ (approximately 13 mol.%) five structure types alternate, anticrystal structure caused by eutectic interactions in melt being perceived over relatively wide composition region. Kcr calculated for the part of rubidium borate system $R_2O.\ 2B_2O_3$-$R_2O.\ 4B_2O_3$ points to the fact that anticrystal structure prevails even in the glass of composition, corresponding to the congruently melting compound $R_2O.3B_2O_3$.

"Kcr-composition" diagrams of ternary potassium and rubidium borosilicate systems are constructed for the wide composition regions adjacent to the binary alkali borate systems. The diagrams demonstrate anticrystal structure regions ($K_{cr=0}$) surrounding ternary eutectics, while within these regions there exist "islands" having $K_{cr}\neq0$. The last ones correspond to metastable or unstable on heating phases realizing eutectic interactions in solid state.

---

* Full manuscript not available at the time of printing

THE QUANTUM CHEMICAL STUDY OF THE FLUOROSILICATE GLASSES

L.N. Ignatieva and **A.Yu. Beloliptsev**
Russian Academy of Sciences, Russia

Abstract

The behavior of F ion in series of silicate systems modeling glassforming groups have been studied. The factors leading to distortion of SiO_4 tetrahedral polyhedra in F-doped systems were discussed. The connected by bridging bonds distorted tetrahedra of SiO_3F exist in F-doped glasses. The weak Si-F bond is a possible reason of ionic conductivity.

1. INTRODUCTION

The properties and structures of the fluorosilicate glasses have been the subject of several recent investigations [1-3]. These glasses exhibit high fluorine ion conductivity. Gao and Gu marked the low refractive index and better ability of forming bulk body glass at the presence of F ions [4]. The structural behavior of the fluorine in silicate gels and glasses was studied by IR and Raman spectroscopy [4], where authors supposed that fluorine ion in the silica network exists in the formation of SiO_3F tetrahedron. The spectroscopic study is a well-established technique to obtain information on groups formed in glasses. However this information is not always correct, since bands in spectra of glasses are very broad. It makes troubles for interpretation. Moreover, it could be interesting to analyze the mechanism of processes that take place in silicate glasses at fluorine ion presence.

This paper presents the results of quantum chemical analysis to F behavior in series of the silicate systems with purpose to understand the role of fluorine ion in the structure of fluorosilicate glasses.

2. RESULTS AND DISCUSSION

The calculation of SiO_4^{4-}, SiO_3F^{3-}, $SiO_2F_2^{2-}$, $SiOF_3$-, SiF_4 systems were carried out in the frame of Hartree-Fock-Routhaan approach by ab initio method. The complete optimization of geometrical parameters has been fulfilled, the frequencies of fundamental vibrations have been calculated.

We found that calculated results are very close to experimental length, valence angle and frequency of fundamental vibration of Si-F bond of SiF_4 system [5,6]. It shows correctness of our calculations.

The obtained results are listed in tables 1,2,3. The considered models are shown in figure 1.

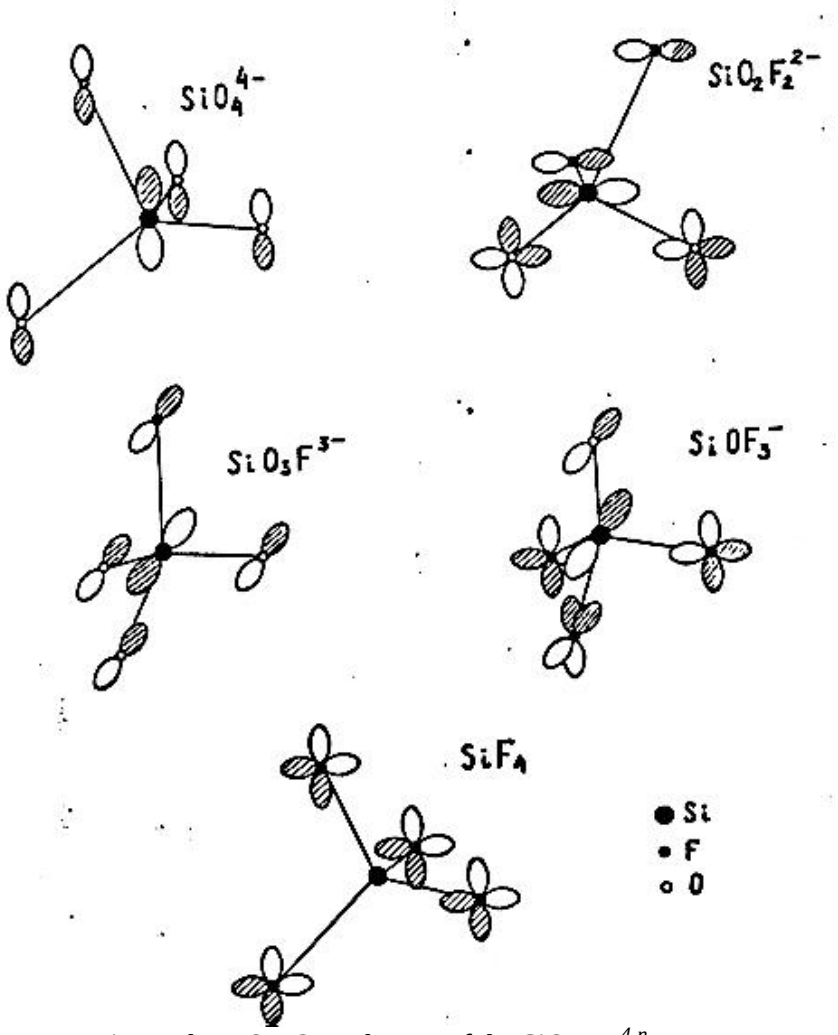

Fig.1. The HOMO's schemes of the $SiO_{4-n}F_n^{4-n}$ systems.

Table 1. The geometrical parameter of SiO_nF_n.

	SiO_4^{4-}	SiO_3F^{3-}	$SiO_2F_2^{2-}$	$SiOF_3$-	SiF_4	
1(Si-O)	1.79	1.68	1.61	1.63		A
1(Si-F)		1.80	1.69	1.63	1.58 exp.1.56	A
θ(O-Si-O)	109	116	1128			o
θ(O-Si-F)		101	107	118		o
θ(O-Si-F)			92	99	109 exp.109	o

Table 2. The effective charges (Q) and HOMO's composition (a) of systems SiO_nF_m.

	SiO_4^{4-}	SiO_3F^{3-}	$SiO_2F_2^{2-}$	$SiOF_3$-	SiF_4
Q(Si)	0.19	0.51	0.77	1.07	1.39
Q(O)	-1.05	-0.97	-0.86	-0.77	
O(F)		-0.61	-0.53	-0.44	-0.34
$\alpha(3p_{Si})$	-0.23	-0.18	-0.15	-0.17	-0.08
α(2po)	0.45	0.51	0.55	-0.91	
$\alpha(2p_F)$		0.05	0.05	0.13	0.34

The substitution of one oxygen atom by fluorine one in SiO_4^{4-}, as it is seen from tables 1 and 2, changes geometrical and electronic structure of the system. In comparison with tetrahedron SiO_4^{4-}, the system of SeO_3F^{3-} is deformed much. Such deformation one can explain from analysis of electron structure systems. The equilibrium configuration of SiO_4^{4-} ion is ensued by interaction of 3s and 3p Si atom orbitals with 2p AO oxygen. It was shown repeatedly [7] that high occupied molecular orbital (HOMO) causes configuration of system mainly. The HOMO of SiO_4^{4-} (Fig.1, tabl.2) is week bonding molecular orbital consisted of 2p AO of oxygen and 3p AO of silicon. The HOMO of SiO_3F^{3-} has more ligand character than HOMO of SiO_4^{4-}. The interaction of 3p(Si)-2p(F) brings some untibonding to this orbital. The increase of O-Si-O angle promotes better 3p(Si)-2p(O) overlapping. It compensates weakness of 3p(Si)-2p(O) interaction and stabilisates Si-O bonds in SiO_3F^{3-} ion. So Si-O bonds are shorter in SiO_3F^{3-} ion than in SiO_4^{4-} one.

We observe the same situation in $SiO_2F_2^{2-}$. The HOMO of it has more ligand character than one of SiO_3F^{3-}. Untibonding brought from two F atoms is compensated by 3p(Si)-2P(O) bonding interaction that becomes stronger due to increase of O-Si-O angle.

The HOMO of $SiOF_3$- is untibonding due to significant contribution of 3p(Si)-2p(F). The system needs decrease untibonding therefore it changes angles of O-Si-F and F-Si-F.

The HOMO of SiF_4 is ligand orbital. It is nonbonding orbital. The system of SiF_4 is stable to dissociation to fragments. It exists as isolated molecule and does not form network. So SiF_4 appears nothing in the glass structure.

On contrary SiO_4^{4-} is unstable as any multicharged ion. It dissociates to fragments of SiO_3^{2-} + O^{2-} with dissociate energy -100 kkal/moll. The forming of bridging bonds of Si-O-Si between tetrahedra of SiO_4^{4-} increases positive charge of Si more than order and decreases excess of oxygen negative charge. It stabilisates system. So structure of silicate glass is formed as the network in which tetrahedra of SiO_4^{4-} are connected by oxygen bridging bonds [8].

Table 3. The overlap populations of silicate and fluorosilicate systems.

	SiO_4^{4-}	SiO_3F^{3-}	$Si_2O_7^{6-}$	$Si_2O_6F_m^{5-}$	$Si_2O_6F_{nm}^{5-}$

$Si\text{-}O_{nm}$	0.500	0.510	0.525	0.550	0.524
$Si\text{-}O_{m}$			0.374		0.278 0.446
$Si\text{-}F_{nm}$		0.202			0.176
$Si\text{-}F_{m}$				0.142	

The substitution of one oxygen by fluorine in SiO_4^{4-} decreases charge of system but it stays unstable. The isolated SiO_3F^{3-} dissociates to SiO_3^{2-} and F-Dissociate energy is equal to -140 kkal/moll. The charge on oxygen is high so SiO_3F^{3-} keeps ability to form bridges. The distorted tetrahedral SiO_3F^{3-} are connected and form network of glass. The calculated frequency of Si-F fundamental vibration is equal to 931 cm^{-1}. It is well compared to 935 cm^{-1}, found in spectra F-doped glasses [4] and confirms presence of tetrahedral SiO_3F^{3-} group in gels and glasses doped by F.

The energy of $Si_2O_6F^{5-}$ system in which bridging oxygen is substituted by fluorine is higher 8 kkal/moll only than one with substituted nonbridging oxygen. It suggests that both ways of substitution can be realized at fluorination. The bridging bond of Si-F-Si is very weak On break of this bond SiO_3F^{3-} ion as it was shown above, dissociates and realizes F- ion. It is conceivable reason for ionic conductivity observed in F-doped silicate glasses.

The substitution of more than one oxygen by fluorine ion forms $SiOF_3$- ion. According to calculations this ion is high stability. It can exist as isolated one and it needs not to connect with neighboring ions, because of the charges on fluorines are small. It is impossible appearance of this group in glass structures.

This work was supported by Grant of RFFR No 95-0308821a.

REFERENCES

[1] J.Coon and J.CShelly, J.Am.Ceram.Soc. 73, (1990) 379
[2] Y.Wang, M.Kobayashi, A.Osaka, Y.Miura, K.Takahashi, J.Am.Ceram.Soc. 71 (1988) 864.
[3] V.N.Sanin and B.G.Varshal, Fizika and Khimia Stekla 21, N3, (1995) 241
[4] S.Gao and Z.Gu, Proc.of the Japan-Russia-China Int.Seminar on the Structure and Formation of Glasses, 1992, p.140.
[5] K.S.Amstrong and R.J.Clark, j.Chem.Soc.Farad.Trans., 72 (1976) 11
[6] K.Nakamoto, infrared Spectra of Inorganic and Coordination Compounds (in Russian), M., Mir, 1966. p.161
[7] L.N.Ignatieva, A.Yu.Beloliptsev, V.I.Sergienko, Zhurn.of Strukt.Khim.32 (1991)N6, 21
[8] A.West, Chemistry of Solids (in Russian) 2, M, M, 1988, p.192

THE STRUCTURAL STATES OF ADMIXED Fe IONS IN LEAD-CONTAINING GLASSES*

A.A. Zhilin
S. I. Vavilov State Optical Institute, Russia

Abstract

The structural states of Fe ions in the concentration range from $1*10^{-4}$ to 1 wt% of Fe_2O_3 were studied in glasses with compositions of lead metasilicate and lead metagermanate by the complex of spectroscopic methods.

On the basis of the analysis of results of:

1. Fe absorption spectra;
2. the temperature dependence of a long-wave "tail" of the UV charge transfer band for Fe^{3+};
3. the g-factor positions and intensities in EPR spectra;
4. the parameters of Mössbauer spectra

the conclusion was drawn that in those glasses Fe ions are present, mainly, as Fe^{3+} ions.

It was found that Fe ions are separated in a glass structure when the Fe_2O_3 content does not exceed 10^{-2} wt%. There is no exchange interaction between them. When the Fe_2O_3 content is higher than 5.10^{-2}, clusters of Fe ions appear having bonds of a (Fe^{3+} - O - Fe^{3+}) type. In those clusters Fe ions are bound by the exchange interactions. The cluster composition is variable and it depends on the Fe_2O_3 content in the glass. Amorphous clusters can play a part of nucleator of a new Fe-containing phase as the Fe_2O_3 content increases. That phase can be observed by X-ray diffraction analysis if the Fe_2O_3 content is higher than 2 wt%.

---

* Full manuscript not available at the time of printing

TO QUESTION ABOUT PHYSICO-CHEMICAL ANALYSIS OF GLASSY SYSTEMS

Valery A. FUNTIKOV

Kaliningrad State University, Russia

Abstract

The new approach to the physico-chemical analysis of glassy systems is offered on basis of eutectoidal model of a glass formation. The eutectoidal model has allowed to generalize that even the ideal glass should be microheterogeneous. From here follows that the physico-chemical analysis of glassy systems is the variety of the physico-chemical analysis of heterogeneous systems. This conclusion permits correctly to analyse diagrams the composition - the property of the glassy systems.

I. INTRODUCTION

The researchers use usually representations about a homogeneous structure of a glass. For this reason the physico-chemical analysis of glassy systems is considered as the physico-chemical analysis of liquid systems. Our approach to the physico-chemical analysis of glassy systems is offered on basis of a microheterogeneous structure of ideal glasses.

II. THEORETICAL MODEL

We have offered the theoretical approach, based on the electronic configuration model of glass formation and eutectoidal model of glassy state of the substance (1-4). Glasses can be considered as the ultradispersed eutectics according to these models even if a glass has a elemental compound. Besides glasses is actually the solid lyophilic colloid with particles that it is possible to name as pseudo-phases (5). These particles can be considered in the quality of nucleuses of quasi-crystals and crystals.

We shall consider some rules of the approach offered by us. In more detail it is stated in the articles (1-4). In the case of the chalcogens and chalcogenides the structural-configuration equilibrium between low-molecular and high-molecular clusters, in our hypothesis, leads to glass formation. The examples of the equations of such equilibriums are shown on fig. 1.

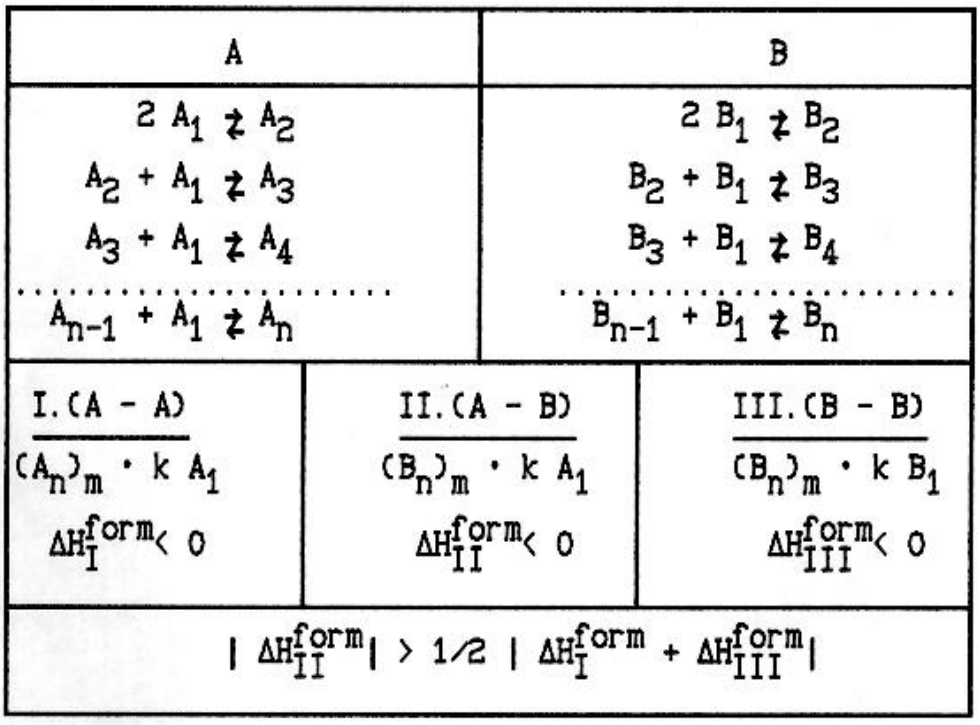

Fig.1. Structural-configurational equilibria in melts of binary systems A-B, leading up eutectoidal interactions and glass formation (DH^{form} - heats of a formation solvates $(A_n)_m \cdot k A_1$, $(B_n)_m \cdot k A_1$ и $(B_n)_m \cdot k B_1$).

The offered model permits to generalize that the availability of a large number the inner reactions and the appropriate chemical equilibriums promotes to the glass formation in case of elementary substances and their compounds. The interaction between the clusters of a different degree of a polyregularity in a melt is dominated in case of the glass forming elementary substances and steady compounds. The peritectic and unstable distectic compounds are promoted to the glass formation if the products of them a disintegration in a melt are capable to enter among themselves or with other components to eutectic interaction.

The electronic-configurational model of the glass formation, topological model of formation of the glass structure, results of application X-ray under small and average angles, electronic-microscopic data, thermodynamical accounts and a information about quasi-crystalline phases are used for the confirmation of a truth of the eutectoidal approach to a structure of the glasses and them melts. The integrated enthalpy diagram of the different states of the substance (gases, melts, amorphous films, glasses, quasi-crystalline phases, crystalline metastable and stable phases) is offered.

The transitions are shown between melts and stable crystals and on the contrary on fig.2,3. It is visible, that these transitions are different ways. The transitions from the melts to glasses, metastable crystals and stable crystals are unequilibriumal transitions. The relaxation of equilibriums has no time to occur, therefore the nucleuses of the metastable phases are frozen in a glass. Then metastable and then stable phases are

crystallizing for a annealing of glasses. On the contrary the transition of stable crystals in melt does occur on a equilibriumal way. Such histerezis permits to realize a nature of the occurrences of a microgeterogeneous structure of glasses and to offer a way of analysis of a diagrams "compound - property".

The eutectoidal model has allowed to generalize that even the ideal glass should be microheterogeneous. From here follows that the physico-chemical analysis of glassy systems is the variety of the physico-chemical analysis of heterogeneous systems. This conclusion permits correctly to analyse diagrams the composition - the property of the glassy systems.

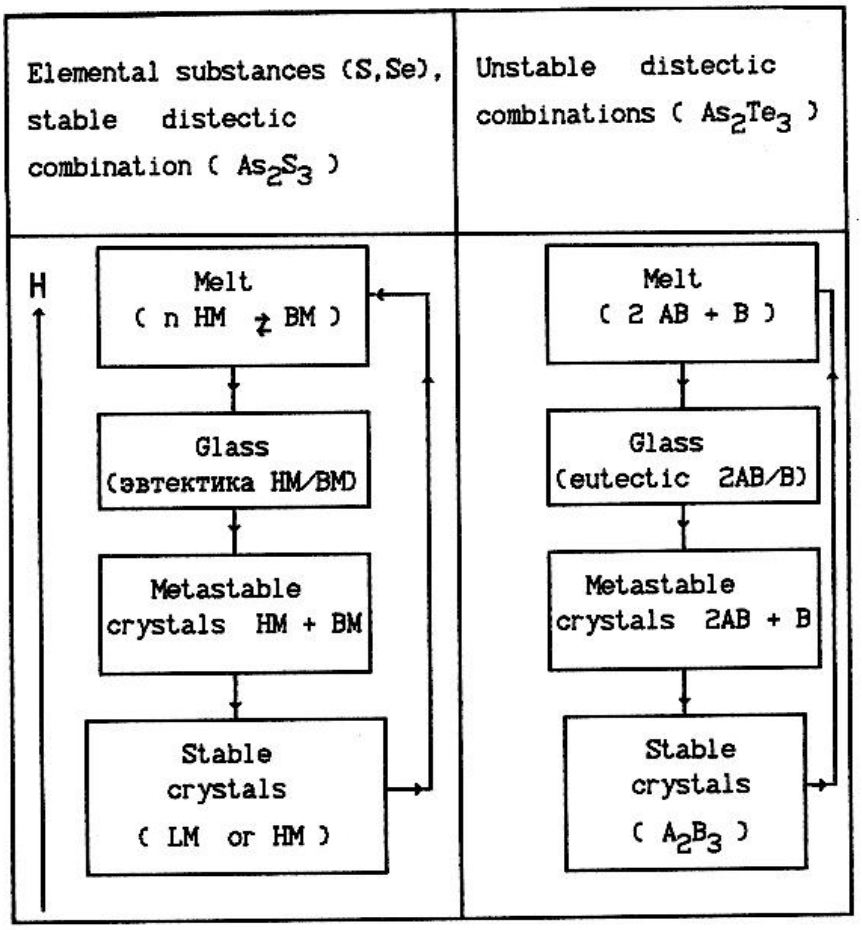

Fig.2. The enthalpy (H) diagram of different states of elemental substances and distectic combinations (LM and HM - low-molecular and high-molecular particles).

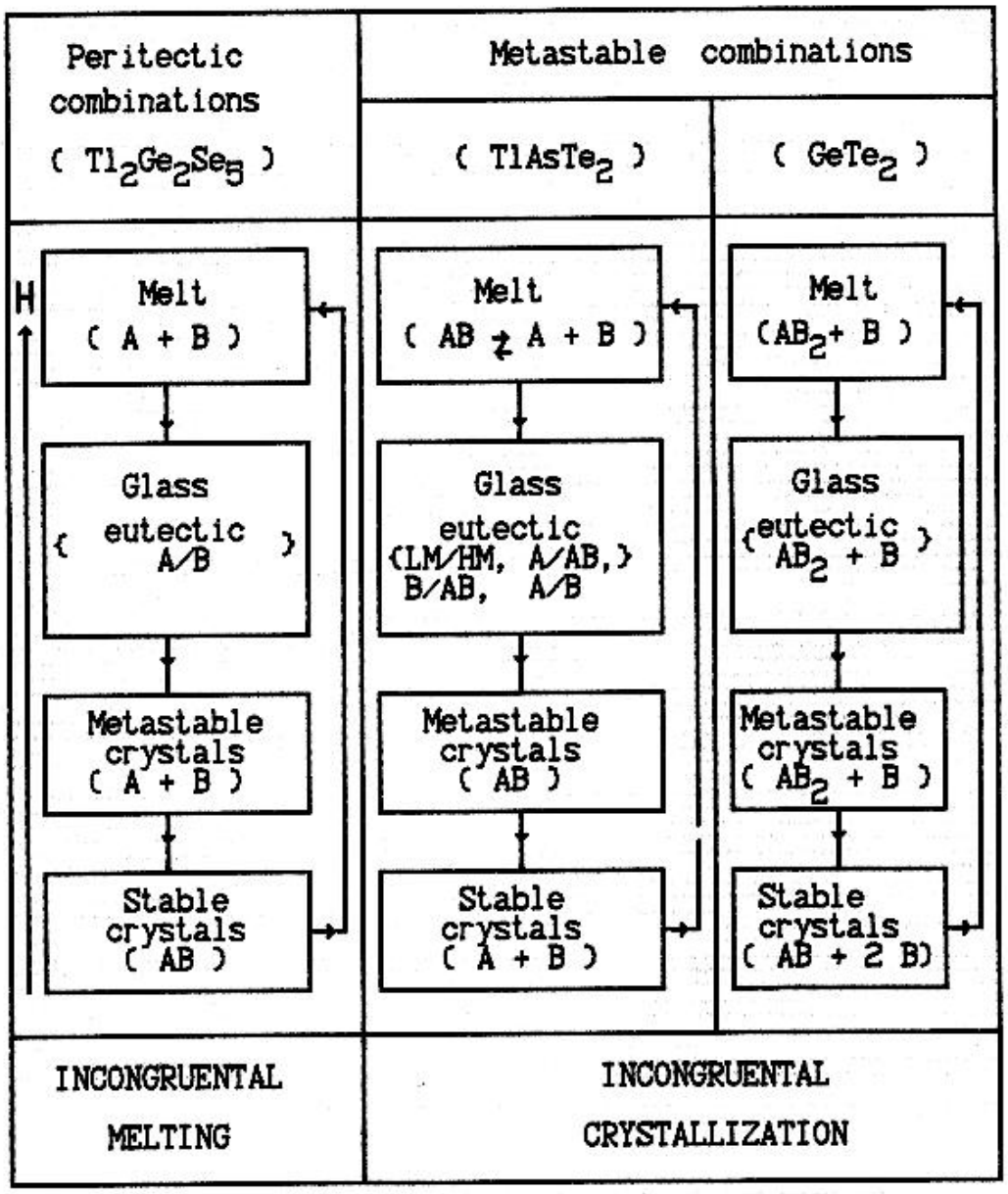

Fig.3. The enthalpy (H) diagram of different states of peritectic and metastable combinations (LM and HM - low-molecular and high-molecular particles).

III. RESUME

It is shown, that glasses can be considered as the quasi-heterogeneous systems from a position of a eutectoidal model. The ideal glass is a multicomponent eutectic, in that number of components compare with possible general number of the structural elements of a near order. In this connection the special points on graphs of a dependence "composition - property" of glassy systems should answer as chemical combinations, as

shift of a type of a heterogeneity of glasses. It is shown, that the physico-chemical analysis of glassy systems follows to consider as the physico-chemical analysis of quasi-heterogeneous systems.

REFERENCES

1. Funtikov V.A., The Electronic Configuration Model of Glass Formation, Proc. Intern. Conf. 'Non-crystalline semiconductors', 89, Uzhgorod, USSR,1989, V.1, pp.58-60.
2. Funtikov V. A., Eutectoidal Model of Glassy State of the Substance, Proc. of XVII Intern. Congress on Glass, Beijing, China, 1995, V.2, pp.256-261.
3. Funtikov V. A., On the Structure of Chalcogenide Glasses, Glass Physics and Chemistry, V.19, No.2,1993, pp.111-115.
4. Funtikov V. A., Electron Configurations of Atoms as a Factor Affecting Glass Formation in Elemental Substances and Their Alloys, Glass Physics and Chemistry, V.20, No.6,1994, pp.492-496.
5. Poryi-Coshitz E.A., The development of structural researches of glasses during last five years, In: Glassy state, Leningrad "Science", 1983, pp.5-10.

TO QUESTION ABOUT ROLE OF TECHNOLOGICAL HELIUM IN INCREASE OF SILICA GEL-GLASSES LIGHT TRANSMISSION*

Malashkevich G.E.[1], Poddenezhny E.N.[2], Melnichenko I.M.[2], Plyusch B.V.[2], Neroda I.Yu.[2], Mudryi A.V.[1]

[1]Academy of Sciences of Belarus
[2]Gomel State University, Belarus

Abstract

It is known that the vitrification of gel-glasses in atmosphere of helium increases them light transmission. It is supposed that such effect is reached as a result of reduction of light scattering because of high diffusion of the gas seized by closed pores [1] and promotion of destruction of defect bonds because of superposition of helium atoms oscillations with the oscillations of matrix structure elements [2]. In the present work we obtained the evidences in favor of that the role of technological helium is more complicated than it is supposed. In particular, with the help of mass-spectrometric investigation is discovered that in similar glasses there are atoms of helium bonded with a matrix and the energy of such bond is not less than 1 eV. But the concentration of the atoms is small and does not exceeds 10^{13} atoms/cm^3. The obtained results permit us in a new fashion to look at the formation of silica gel-glasses structure and role of helium in the increase of their light transmission.

[1] Susa K.,Matsuyama I., Satoh M.-Kotai Butsuri, 1985, v.20, N0.6, p.399.
[2] Poddenezhny E.N., Melnichenko I.M.,Plusch B.V.,Neroda I.yu.,Malashkevich G.E.- J.Advanc.Mater.(in press)

---

* Full manuscript not available at the time of printing

TOPOLOGICAL MODEL OF FORMATION OF STRUCTURE OF GLASSES

Valery A. FUNTIKOV

Kaliningrad State University, Russia

Abstract

The report states the topological approach to the analysis of processes of the formation of the structure in glasses. Our theoretical approach is based that in extreme small volumes of a space for the formation of the continuous ordered structure permit, all possible elements of the symmetry with first on infinite orders. According to our topological model just the large power-generating barrier of the transition from microscopic particles, having infinite set elements of the symmetry, in the crystalline state with the 1imited symmetry and permits to substance to pass in the glassy state from the melt and in the amorphous film from a vapour.

I. INTRODUCTION

The main defect of many structural models of the glassy state of substance consists that in them predominate crystallographic or the formal topological approach. It is developed most, obviously in a crystallite concept, offered Frankenheim (1). The initial crystallite concept is not used. It is possible to discover the increase of attention to purely geometrical and topological aspects of the formation of a structure in glasses. The boundary between geometry and topology is almost elusive. In the case of glassy substances is excluded a formation of ideal geometrical figures, therefore characteristic types of connectedness of atoms have a preference. Phillips has applied the topological approach for the analysis of opportunity of a formation of a grid of a glass for the first time instead of geometrical approach. From this position it is shown that a grid of glass is formed not casually. Phillips considers, that for optimization of the tendency of substance to a formation of glass it is necessary to optimize dimensions of different clusters, that will correspond to mechanical stability of a glass (2). The last condition is possible if

$$N_c N_t = N_c N_d \,, \qquad (1)$$

where N_c is middle number of atoms in a cluster; N_t is number of force communications on the atom; Nd is dimensionality of space; $N_c N_d$ - dimensionality of configurational space, describing a situation of atoms. Phillips has shown, that in systems As-S(Se) connections $As_2S(Se)_3$ of mechanical and chemical stability have on the combinations $As_2S(Se)_3$. Unfortunately, results of calculations differ from experimental results. It follows from that the maximum of the ability to a formation of glass correspond

in given systems not on the combinations $As_2S(Se)_3$, and on eutectic alloys. The eutectic alloys very difficultly crystallize.

II. THEORETICAL MODEL

We offered eutectoidal model of a formation of a structures in glasses (3). The eutectoidal model of the structure of glasses is offered that is based on the Smits's idea about pseudobinary systems (4). All glasses, including elementary glasses, are analysed as a variety of eutectics, formed by the interaction among themselves of "pseudophases". "Pseudophase" is the equivalent of the nucleus of the ordered particle that appear in the supercooling melt. According to our eutectoidpal model even the ideal glass is non-uniformly and can be submitted as the ensemble of sticking microspheres.

The eutectoidal model requires the elucidation of the gear formation of a middle order in glasses. With this purpose we offer topological model of a structure of glassy substances, based on following hypothesises:

1) The elemental structural elements of glassy alloys, responsible for a formation of glasses and being centres of glassy nucleuses, arise in the closed space, homomorphous to sphere S^3, and have in limiting geometrical space R^3 the uncrystallographical axes of a symmetry L_5, L_7, L_8. . . L_∞.

2) The belonging of a dominating structural elements of glasses to closed space lead up to the impossibility of formation of a unbroken glassy grid.

3) In case of weak interactions the ideal structural elements of glasses correspond to structural elements, that are homomorphous to the icocahedron, in case of strong interactions - to the dodecahedron.

4) The equilibrium is established between clusters with the crystallografical and uncrystallografical axes of a symmetry. The structural elements with any axis of symmetry should exist in glassy alloys by this reason.

5) The crystallization of the glasses is accompanying by a transition in final the stable condition through set of stages, in that in the beginning icocahedronal (for metals) or dodecahedronal (for semicoductors and dielectrics) quasicrystals and then metastable and stable crystals are formed.

We are entered the following concepts of nucleouses of a crystallization and vitrification. The clusters, possessed to closed a spherical space S and to the homomorphous geometrical structural elements with the axes of a symmetry $L_{1\text{-}4,6}$, we shall identify with nucleouses of a crystallization. The clusters, possessed to closed a spherical space S and to t,he homomorphous geometrical structural elements with the axes of a symmetry $L_{5,\ 7,\ 8,\ 9,\ .\ .\ ,\infty}$,we shall identify with nucleouses of a vitrification. The set of clusters in a melt W it is possible to separation on two subsets: 1) W - a subset of nucleouses of a crystallization, 2) W - subset nucleouses of a vitrification. Obviously, a transiton from closed space S in a open space R in the case nucleouses of a crystallization can occur continuously without a rupture of a structure, and in the case nucleouses of a vitrification can take place only with a rupture of a structure.

Equilibriums exist at a temperature of a synthesis :

$$2A \Leftrightarrow A_2,\ A_2 + A \Leftrightarrow A_3,\ A_3 + A \Leftrightarrow A_4,\ .\ .\ .,\ A_{n-1} + A \Leftrightarrow A_n. \qquad (2)$$

In a general kind:

$$A_n + A_m \Leftrightarrow A_{n+m} \cdot . . , A_n + A_k \Leftrightarrow A_{n+k} \cdot . . , A_k + A_m \Leftrightarrow A_{k+m}, \quad (3)$$

In quality the most important for the vitrification equilibriums it is possible to allocate equilibriums between clusters with the crystallographic and uncrystallographic axes of a symmetry, that is between nucleouses af a crystallization and vitrification:

$$A_n^{\text{КрИСТ}} \Leftrightarrow A_n^{\text{СТеКп}} \quad (4)$$

The higher the propensity of a melt to glassformation and than closer it temperature to optimum temperature of synthesis of a glass, the closer the share of nucleouses of a vitrification to a maximum. In our opinion, such type two kinds of clusters exist in liquids of any structure, but in case of easily crystallizing liquids power barrier to transition anticrystalline clusters in crystalline clusters extremely is small and crystallization occur easily. The balance (4) can displace to the right in a case of a reduction of dimensions of clusters in a melt. The vitrification is possible by the cooling of melts only by a condition, that a relaxation of a equilibrium (4) to the left practically will be impossible at the expense of high of a power barrier and by the large diversity of nucleouses of a vitrification.

According to our topological model just the large power-generating barrier of the transition from microscopic particles, having infinite set elements of the symmetry, in the crystalline state with the limited symmetry and permits to substance to pass in the glassy state from the melt and in the amorphous film from a vapour. The transitions of glasses and amorphous films in the crystalline state must pass through a stage of the formation quasicrystals. From topological model follows, that such quasicrystals should have axis of symmetry of fifth order and the icosahedral structure in case of metal alloys and the dodecahedral structure in case of semi-conductors and dielectrics. In structure of all glasses the structural elements, having in utmost geometrical variant by all elements of the symmetry of icosahedron and dodecahedron ($6L_5 10L_3 15L_2 15PC$), should dominate. The given conclusions are confirmed by the experimental reception of the quasicrystals at a tempering of metal glasses. It is possible to predict, that such the phases should occur at a tempering of the semiconductor and dielectric glasses. From topological model follows, that even the ideal glass non-uniformly and can be submitted as the ensemble of sticking spheres. The direct experimental confirmation of it consists in a supervision by means of the electronic microscope the many-range structure at typical of one-component glasses after their chemical etching.

The schematic graphs of a dependence of a free Gibbs energy from dimensions are showed on fig.1.

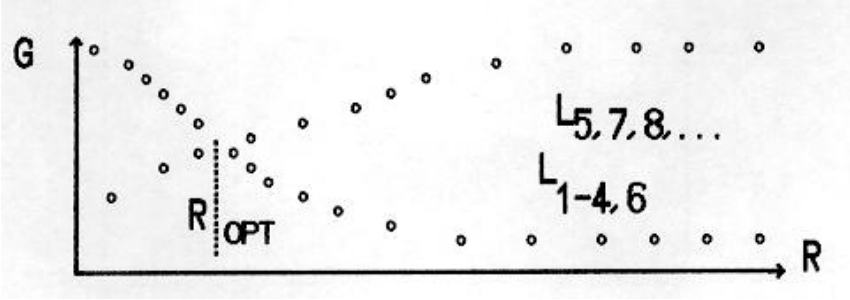

Figure 1

Proceeding of our concept, it is possible to make conclusions about the structural elements of a middle order in glasses. Most easily it is illustrated on covalent chalcogenide glasses. The structural elements of a medium - range order for As, S and As_2S_3 in non-crystalline alloys are shown on fig.2.

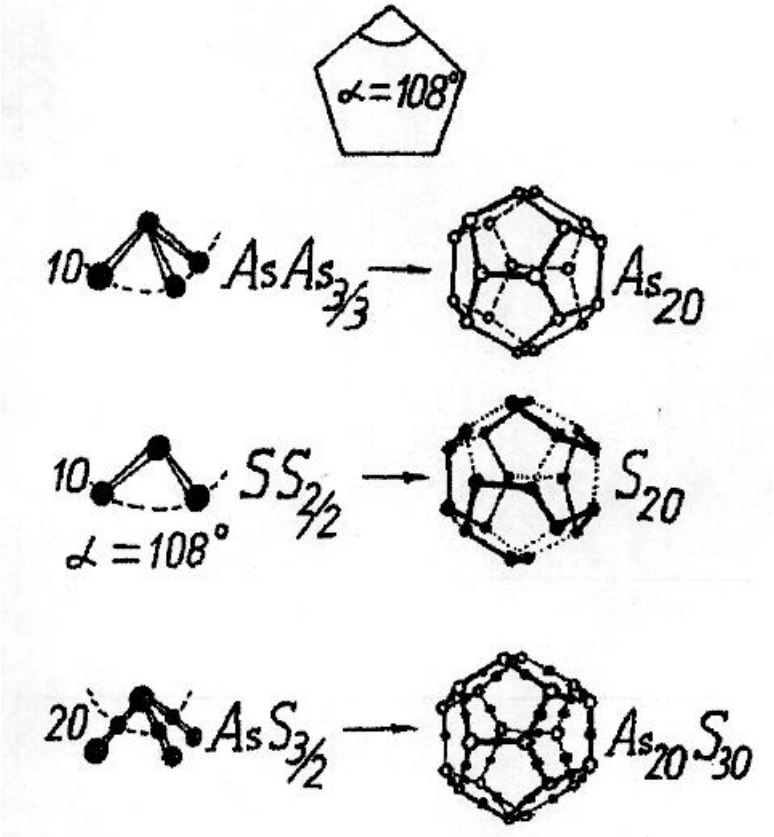

Fig.2. The structural elements of near- and medium - range orders of As, S and As_2S_3 in a non-crystalline alloys.

The predominance in glasses such of structural elements should lead up to a many-range structure with a spherical symmetry, that develop in oecurrenee at the glasses of a shell fracture by them destruction.

III. RESUME

The t,opological approach to the description a structure of glasses is offered, according to that in extreme small volumes of a space for the formation of the continuous ordered structure permit all possible elements of the symmetry with first on infinite orders. The concept of nucleouses of a vitrification are entered, possessed to closed a spherical space S and to the homomorphous geometrical structural elements with the uncrystallographic axes of a symmetry $L_{5,7,8,9...\infty}$ The higher the propensity of a melt to glassformation and the closer it temperature to optimum temperature of synthesis of a glass, the closer the share of nucleouses of a vitrification to a maximum. From a position of our topological approach a microheerogeneity is not only a feature of a real glasses, but should be included and in concept of a ideal glass.

REFERENCES

1. Frankenheim M. L. Die Lehre von der Cohasion, umafassend die Elastizitat der Gase, die Elastizitat und Coharenz der flussigen und festen Korper, und die Krystallkunde. Breslau: A. Schulz und Komp.,1835.502 S.
2. Phillips J. C. Topology of covalent non-crystalline solids II: medium - range order in chalcogenide alloys and A-Si(Ge). ii J.of Non-Cryst,. Solids. 1981. V.43. P.37-77.
3. Funtikov V. A. Eutectoidal model of glassy state of the substance. // Proceedings of XVII International Congress on Glass. Beijing, China, 1995. Vol. 2. P.256-261.
4. Smits A. Die Theorie der Allotropie. Leipzig: Barth, 1921.
5. Sokolovskaya E. M., Guzei L. S. Chemistry of Metats. Moscow: MGU's Publishing House,1986.

TRANSITION-METAL IONS BEHAVIOR IN THE COURSE OF LIQUID PHASE SEPARATION AND PHASE TRANSFORMATIONS IN GLASSES OF $R_2O(RO)$-Al_2O_3-SiO_2-TiO_2 SYSTEMS*

O. S. Dymshits, A. A. Zhilin, T. I. Chuvaeva
S. I. Vavilov State Optical Institute, Russia

Abstract

Transition-metal ions added in small amounts to glasses inclined to liquid phase separation can act as color indicators of structural transformations of these glasses.

In a present study, NiO and CoO were doped to glasses of $R_2O(RO)$-Al_2O_3-SiO_2-TiO_2 system, were R_2O=Li_2O and RO=MgO, ZnO. In the glasses under study the Al_2O_3 content was equal or exceeded the , LiO (RO) content. The glasses of the three systems were heat treated in the temperature ranges of liquid phase separation. On the basis of data obtained from optical absorption spectra, Raman spectra and X-ray diffraction analysis, it was found that:

1. In all the initial glasses Ni (II) and Co (II) acquire octahedral and tetrahedral coordination, the octahedral coordination being dominant.

2. In the course of liquid phase separation Ni (II) and Co (II) ions enter the aluminotitania amorphous phase, by doing so, they stabilize the aluminotitania phase.

Precipitation of TiO_2-containing crystalline phases slow down. In that phase Ni (II) ions acquire octahedral coordination. Increase in a ligand field strength indicates the change in the second coordination sphere of Ni (II) ions. To the contrary, Co (II) ions acquire tetrahedral coordination in this phase. These transformations in amorphous phases lately lead to precipitation of the inverse Ni-spinel and normal Co-spine.

It was found that if the concentration of NiO or CoO exceeds 1.5 wt%, transition metal ions significantly modify the process of precipitation of alumina-containing phase and TiO_2-phase.

---

* Full manuscript not available at the time of printing

TRANSITION FROM THE HETEROGENEOUS TO THE HOMOGENEOUS NUCLEATION IN SOME SILICATE AND PHOSPHATE GLASSES

G.A.Sycheva
Institute of Silicate Chemistry of Russian Academy of Sciences, Russia

Abstract

The kinetics of transition from the heterogeneous (catalyzed) to the homogeneous (spontaneous) volume nucleation in silicate and phosphate glasses was studied. The nucleation catalysis proceeds by the photosensitive mechanism, by introducing an insoluble impurity, by shifting the glass composition to the side of increasing Li_2O content (autocatalysis) in silicate glasses and by passing the water vapor in phosphate glasses.

1. INTRODUCTION

It is known /1/ that the nucleation rate of crystals can be increased by decreasing: 1) the glass viscosity (as a result of introducing water in the glass), 2) the surface energy at the nucleus-glass interface (owing to the water concentration on this interface, 3) the effective surface energy at heterogeneous nucleation of the crystals of one phase on those of the other, the latter being either one of the main phases (lithium metasilicate crystals) or the impurity phase (platinum or gold or silver particles in the photosensitive glasses).

In the present work the comparison between the regularities of homogeneous and heterogeneous crystal nucleation and transition from the heterogeneous to the homogeneous nucleation has been studied on an example of the Li_2O-SiO_2 and R_2O-ZnO-P_2O_5 systems. The nucleation catalysis proceeds through silver, gold and platinum particles obtained for photosensitive glasses by adding Ag or Au with subsequent X-ray irradiation of the glass at room temperature; by displace of composition of glass to the region there metasilicate crystals nucleated; and by passing the water vapors through the primary melts for several time.

II. EXPERIMENTAL

Glass synthesis. Silicate glasses. The batch to be conventionally melted and the sol-gel batch (glasses 3a and 4a) was prepared according to the procedure proposed in /2/. It cannot be too highly stressed that the kinetic curves of the lithium disilicate crystal nucleation that occurs through both homogeneous and heterogeneous mechanisms for glasses synthesized by conventional melting and by melting from the batch prepared by the sol-gel are identical.

Glass synthesis. Phosphate glasses. Glasses were melted at 1050, 1100 and 1170^{o}C. Water was introduced by passing the water vapors through the primary melts $2.Al_2O_3$ $6.7K_2O$ $6.7Li_2O$ $6.6Na_2O$ $45.ZnO$ $33.P_2O_5$ for several times. Water content of glass samples turned out to range from about 0.06 to 0.63 mol%. As was shown in /3/ there are the dependences of water content in glasses on melting temperature, on melting

time and on the rate of blowing water vapor through glass melt. Fig.1,a illustrate the dependences of water content on melting time (the rate of blowing water vapor is 250 ml/h).

Procedure for the study of the kinetics of crystallization in glasses. The stationary rate of crystal nucleation, I_{st} and the time of nonstationary nucleation, τ., are the basic parameters that describe the kinetics of crystal nucleation in glasses. Parameter I_{st} is directly determined experimentally, and the time of non-stationary nucleation is estimated using the induction period t_{ind}. The optical microscopic development technique was used to determine the parameters under consideration. The basic idea of technique is that the crystals nucleated in the course of heat treatment at a low temperature to a size visible in optical microscope. The optimum development temperature corresponded to the exothermic peak observed in the DTA curve. After the nucleated crystals develop at the development temperature T_d (see Tabl 1), the microsectiones of the samples, which were polished and etched in a hydrofluoric acid, were examined in an optical microscope. The number of crystal traces, N_s, was counted on a microsection of area S, and their diameters D_1 and D_2 were measured. The ratio of spherulite diameters was approximately 1.6-2.25. The number of crystals, n, nucleated per unit volume was determined both by the following relationship: $n=N_s/(SD_{av})$, where $Dav=(D_1+D_2)/2$, and by formula (1)

$$n = \frac{N_s}{D_{min} \cdot K\ (D_{min}/D_{max})},$$

there

$$K = \frac{1}{2} \cdot \left[q + \frac{\ln(q+\sqrt{q^2-1})}{\sqrt{q^2-1}} \right], \qquad \text{(I)}$$

$q=D_{min}/D_{max}$, D_{min}, D_{max} - minimum and maximum diameters of spherulite traces /4/. $I_{st}=dn/dt$.

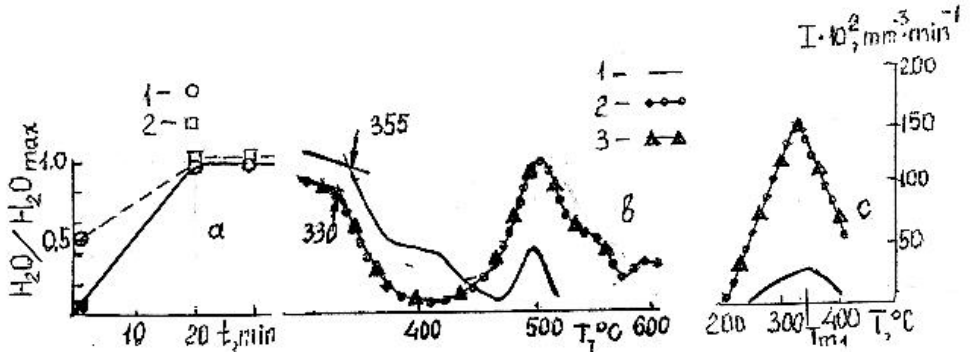

Fig.1 Water content as a function of melting time at T=1100°C for glass 15 : 1 - without Ar-drying, 2 - with Ar-drying 12 minutes (a); DTA curves for glass 15. Conditions: the heating rate of 10 K/min, the value of suspension - 1g, the DTA sensitivity - 1/5, Al_2O_3 as the standard, the platinum crucible (b); graphs of stationary nucleation rate I_{st} for - glass 15, plotted against the temperature for glass 15 : 1 - melting time 10 min, 2 - melting time 20 min, 3 - melting time 30 min (c).

Procedure for the study of the heterogeneous crystallization kinetics in photosensitive glasses. The photosensitive glass samples intended for the study of the kinetics of heterogeneous crystallization had two well-polished surfaces, which were perpendicular to one another. One of the faces was irradiated, and another one was used for measuring the number of particles nucleated at a depth x of the sample. The layers lying at different depths received various radiation doses in the course of irradiation. This was taken into consideration in counting the number of nucleated crystals. After irradiation the glasses 2*,4*,4*a, were kept for a different time, t, at the temperature T at which the crystals nucleated. They then developed at the development temperature T_d (see Table). As a result, the time dependencies could be constructed for the number of crystals nucleated per unit volume, n(T,t), using the method described above, and the rates of heterogeneous (I_{het}) and homogeneous (I_{hom}) nucleation, could be calculated (Table).

In the case of study of transition from the heterogeneous to the homogeneous nucleation in the photosensitive glasses (No.2*,4*,4*a) the temperatures T were chosen to be rather high so that the time of non -stationary nucleation could be neglected but the nucleation rate be rather great. At he curves of stationary nucleation I(T,t) obtained for glasses 2*,4*,4*a these temperatures lie above the temperature of the maximum of nucleation rate whose position was the same for both heterogeneous (on silver particles) and homogeneous nucleation although the values of nucleation rates differed sharply.

III. RESULTS AND DISCUSSION

The influence of X-ray irradiation on the nucleation rate depends on the doze of irradiation obtained by a given glass volume, i.e. it depends on the distance x of the glass layer from the surface on which the X-rays fall. Given in figure 2 (curves 1-10) are the kinetic curves n(t) (the argument T in n(T,t) is omitted) for the nucleation of L2S crystals in the glass No.2* in ten glass layers on depths corresponding to the abcissas of the points indicated in the figure (a). The calculation of n(t) in the layer was made along the face of the glass plate splice. Analogous curves for the nucleation of L2S crystals in glass 4*,4*a (curves 12-14) are shown in figure 2 for free various depths x (both conventional melting and the sol-gel) for the points indicated in the figure (b). The curves n(t) have the form of two intersecting straight lines. Behind the curvature the curves n(t), 1-10, (Fig.2) grow to be almost parallel to the abscissa axis as the rate of homogeneous nucleation is very small (in the figure, curves 1-10, the values of n(t) are indicated for $t \leq 8h$ and $t \geq 48h$). The values of heterogeneous nucleation rate before the curvature and the ones of homogeneous nucleation rate (which coincide with the former behind the curvature) are indicated in Table. Figure 2(a,b) shows the dependencies of the value of logarithm $n=n_s$ in the point of curvature (intersection of extrapolated straight lines) on the layer thickness x. The values of In n_s lie on the straight lines. This result as well as results shown in figure 2 (curves 1-10 and 12-14) can be understood in a sense that the point of curvature corresponds to the exhaustion of silver particles catalyzing the nucleation whose number is proportional to the irradiation doze decreasing in proportion to exp ($-\mu x$) (μ is the absorption coefficient of x-rays) with decreasing depth x. In this case the silver (or gold) particles can be regarded as an imitation of subcritical nuclei of lithium disilicate or metasilicate. The problem on the heterogeneous nucleation in this case can be regarded as the one on statistical joining (and disjoining) of the structural units of

lithium disilicate to the silver (or gold) particles imitating subcritical crystal nuclei, i.e. one can consider the heterogeneous nucleation by analogy with homogeneous nucleation - using the Frenkel scheme /5/. As a result, the nonstationary and stationary heterogeneous types of nucleation can be spoken of as homogeneous nucleation, the stationary nucleation giving the linear growth n(t) with time. However, the barrier on the way of the critical nucleus formation appears to be lowered at the expense of subcritical nuclei already formed (silver, or gold, or platinum particles; platinum particles are nucleating additions without irradiation) which leads to the increase of nucleation rate.

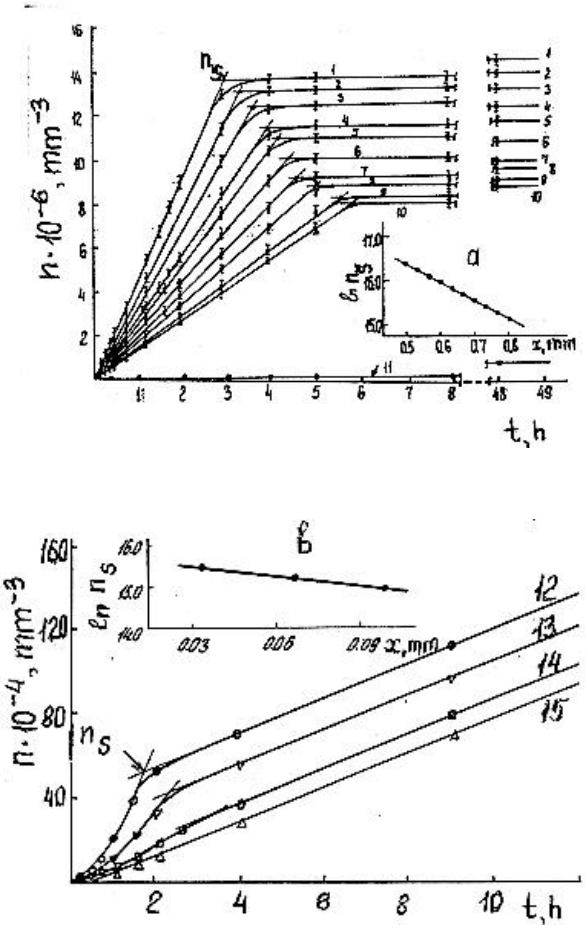

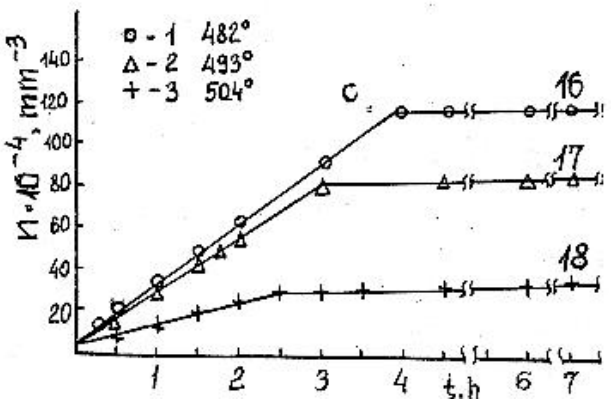

Fig.2. The crystallization kinetic of disilicate crystals in glass 2(1-11), glass 4*, 4a*(12-15) and in glass 8(16-18). 1-10, 12-14-heterogeneous nucleation on the different layers x, mm: 0.50(1), 0.53(2), 0.57(3), 0.60(4), 0.63(5), 0.67(6), 0.70(7), 0.73(8), 0.77(9), 0.80(10), 0.77(12), 0.80(13), 0.83(14); 11 and 15 -homogeneous nucleation. a,b - dependences of ln n_s from x for glasses 2*(a) and 4*,4a*(b). c - the transition from heterogeneous to the homogeneous nucleation for glass 8.*

Table

No		**$I_{st}(T_m).10^{-3}mm^{-3}\ min^{-1}$**	
	Li_2O	**I_{hom}**	**I_{het}**
1	23.40	0.08	
2*	23.40		74.07
3,3a	33.50	0.15	
4*4a*	33.50		60.27
5	33.85	0.28	
6	34.73	0.30	
7	36.20		1.85
8	37.00		4.30
9	37.98		5.60
10	39.00		270.00
11	41.15		512.22
12	44.11		520.00
13	33.50+Au		45.0
14	33.50+Pt		68.00
15	$R_2OZnOP_2O_5$		
15	$+H_2O$ 10min		
15	$+H_2O$ 20min		
15	$+H_2O$ 30min		

*-with 0.03 mas. % Ag_2O

No	T_m, °C	T_d, °C
1,2	470	600
3-6	460	620
7,8	480	620
9,10	480	560
11,12	480	540
13	460	600
14	490	600

Let us consider the data on influence of other phase particles on the nucleation of lithium disilicate "spherulites" in glasses 4-12 (Table). The nucleation rate increases as much as 3000 times (from glass 4 to glass 12). This increase is due to the rapidly growing influence of the heterogeneous nucleation of lithium disilicate on the crystals of lithium metasilicate. In the glasses 7-12, then lithium disilicate crystals nucleate on lithium metasilicate crystals, the acceleration of the disilicate nucleation being promoted by the closeness of unit cell parameters of lithium disilicate (a=5.807, b=14.52, c=4.773A) and lithium metasilicate (a=9.39, c=5.92A, ASTM data). Then the crystals of lithium metasilicate are exhaust, the n(t) curve grows parallel to the n(t) curve for the homogeneous nucleation of lithium disilicate (Fig 2,c).

Phosphate glasses. The lowering of T_g with an increase of the water content may be equivalent to the lowering of viscosity. Glass transition temperatures T_g of phosphate glasses, determined from the thermal expansion curves, are shown as a function of the water content in Fig.1,b. The T_g decreases with increasing water content and increases with decreasing one. Fig.1,c shows graphs relating I_{st} to the temperature for glass 15. With the increase of water content the temperature of the nucleation rate maximum T_m shifts to the lower temperature; the value of $I_{st}(T_m)$ increases as many as six times, and decreases with the decreasing of water content also. The influence of water content on the nucleation rate is not only reduced to the decrease of viscosity. The value can decrease owing to the increase of water concentration (groups OH) on the nucleus surface. Such an increase of water concentration can decrease the glass viscosity in vicinity of the nucleus. This will lead to the increase of I_{st} as well. If concentration of OH-groups is exhaust the I_{st} stop to increase.

REFERENCES

[1] Kalinina AM, Fokin VM, Sycheva GA et al,In: Indian Ceram Soc 1 (1986), 366-373.

[2] Boiko GG, Sycheva GA, Valyuk LG, Fiz Khim Stek 21 (1) (1995), 45-52.

[3] Sycheva GA, Kostyreva TG, Poljakova IG, Proc. XVII Intl. Congr. on Glass 2 (1995), 426-432.

[4] DeHoff RT, Rhines FN, Transactions of the metallurgical society of aime 221 (1961), 975-982.

[5] Frenkel JI, Proc. M-L, 3 (1959), 383 p.

USE OF CHEMICAL EQUIVALENT FOR ESTIMATION OF CHEMICAL STABILITY OF GLASSES

Valery A. FUNTIKOV

Kaliningrad State University, Russia

Abstract

For the first time the chemical equivalent is used for research of glasses. The chemical equivalent was investigated in relation to exchange and oxidizing-reducing reactions of the chemical etching of the chalcogenide glasses. The new method is entered and it is named "equivalent-measurement".

I. INTRODUCTION

The information about a chemical equivalent of glasses is completely away. For the first time the systematic research of the chemical equivalent glassy of chalcogenide alloys of systems A^{IV}-B^{V}-C^{VI}, A^{I}-B^{IV}-C^{VI}, A^{III}-B^{IV}-C^{VI}, A^{I}-B^{V}-C^{VI}, A^{III}-B^{V}-C^{VI} is carried out. The chemical equivalent was determined on a relation to exchange and oxidizing-reducing reactions of the chemical etching of the glasses. The dependence of the chemical equivalent from a structure of the glasses was analysed for the glassy alloys of systems investigated. The gears of the chemical etching of the low- and high-resistance glassy chalcogenide alloys are offerred. For these glasses theoretical significances of the chemical equivalent were calculated. The compositions of glasses were determined on the concentration triangle with different gears of the etching. The experimental results and calculations are testifing about the microheterogeneous structure of the glassy alloys investigated. It is shown that the chemical equivalent of glasses on relation to reactions of them etching in solutions of the alkalies and the oxidizers is possible to be used for the physico-chemical analysis of the corresponding glassy systems.

II. EXPERIMENTAL RESULTS

In this report our method is illustrated on example of a vitreous system Ge-Se in relation to a reaction of the interaction with 1m solution of KOH. The sizes of a molar weight of a chemical equivalent (CE) is calculated under the formula (1):

$$CE = \frac{\Delta m}{(V_o - V_1) \cdot N}$$

where Δm is a loss of a weight of a sample; V_o is a volume of a titrant, used on a titration of a part of a solvent, in which will be dissolve a glass; V_1 is a volume of a titrant, used on a titration of a part of a solvent, remaining after a chemical etching in it of a glass; N is a bulk concentration of a titrant (equivalent on 1itre). In the figure the graphs are showed of a dependence of

experimental size and theoretical sizes of CE of glasses of a system Ge-Se in relation to 1m KOH.

III. DISCUSSION

It is offered three theoretical gears of a chemical etching for finding out of a veritable gear of the etching of glasses (CE_I^{theor}, CE_{II}^{theor}, CE_{III}^{theor}).

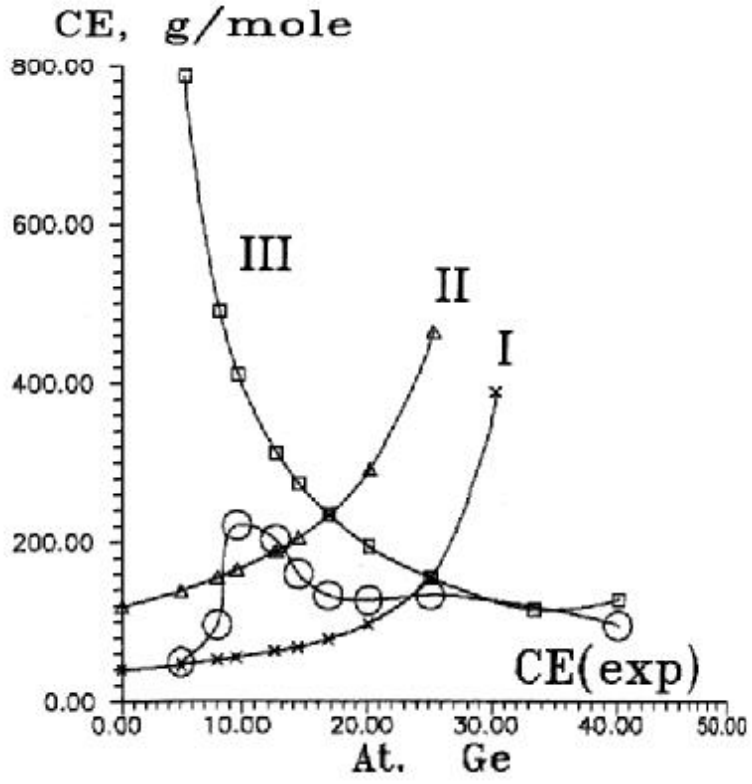

***Figure**. The dependence of the experimental CE^{exper} theoretical CE_I^{theor} CE_{II}^{theor} CE_{III}^{theor} a molar weight of a chemical equivalent, of glasses of a system Ge-Se from a composition of glasses.*

I. $GeSe_x = GeSe_{2\downarrow} + (x-2)Se$

$3Se + 6OH^- = 2Se^{2-} + SeO_3^{2-} + 3H_2O$

$CE_I^{theor} = M_{стекла} / 2 \cdot (x-2)$

II. $GeSe_x = GeSe_{2\downarrow} + (x-2)Se$

$9Se + 6OH^- = 2Se_4^{2-} + SeO_3^{2-} + 3H_2O$

$CE_{II}^{theor} = 1.5 \cdot M_{стекла} / (x-2)$

III. $GeSe_x + 2KOH = K_2GeOSe_2 + (x-2)Se_{\downarrow} + H_2O$

$CE_{III}^{theor} = M_{стекла} / 2$

Obviously, in the field of 10 aT. % Ge a eutectic is showed, appropriate to metastable and stable diagrams of a state of a systems Ge-Se. The structural elements of a selenium are dissolved up to a eutectical composition (0 - 10 at. %Ge). The fragments of $GeSe_2$ are dissolved after a eutectical composition (> 10 at. % Ge).

IV. RESUME

It is shown, that the chemical equivalent of glasses in relation to reactions them etching in different solvents can be used for a valuation of the features a structure of glasses. The results of experiments and calculations testify about a microheterogeneous structure of investigated glasses. Obviously, in the field of 10 aT. % Ge a eutectic is shown, appropriate to metastable and stable diagrams of a state of a systems Ge-Se.